Zoosystematics and Evolution

100 (**4**) 2024

PENSOFT

MUSEUM FÜR NATURKUNDE BERLIN

Zoosystematics and Evolution
A Bulletin of Zoology since 1898

Publisher

PENSOFT

Zoosystematics and Evolution

2024. Volume 100. 4 Issue

ISSN: 1435-1935 (print), 1860-0743 (online)
Abbreviated keys title: Zoosyst. Evol.

In Focus

The cover picture shows shells of *Lannanaia kokensis* sp. nov. – the inner side of the right valve, the outer side of the left valve, and the dorsal view of both valves.

See paper of **Jeratthitikul E, Sutcharit C, Prasankok P:** Two new genera and three new species of exceptionally rare and endemic freshwater mussels (Bivalvia, Unionidae) from the Mekong Basin

Cover design
Pensoft

Zoosystematics and Evolution
A Bulletin of Zoology since 1898

Content of volume **100** (**4**) 2024

Abstract & Indexing Information

Biological Abstracts® (Thompson ISI)
BIOSIS Previews® (Thompson ISI)
Cambridge Scientific Abstracts (CSA/CIG)
Web of Science® (Thompson ISI)
Zoological Record™ (Thompson ISI)

Zoosystematics and Evolution
A Bulletin of Zoology since 1898

Content of volume **100** (**4**) 2024

Zoosyst. Evol. 100 (4) 2024, 1191–1200 | DOI 10.3897/zse.100.131019

PENSOFT

für Natur MUSEUM FÜR NATURKUNDE BERLIN

Description of a new freshwater mussel species of *Plethlophus*, Simpson, 1900 (Bivalvia, Unionidae) from Guangdong, China

Yu-Ting Dai[1*], Zhong-Guang Chen[1*], Cheng-Lin Hu[1], Shan Ouyang[1], Xiao-Chen Huang[1], Xiao-Ping Wu[1]

1 *School of Life Sciences, Nanchang University, Nanchang 330031, China*

https://zoobank.org/C9F1030C-0564-4960-9378-38D9848ACE05

Corresponding authors: Xiao-Chen Huang (xiaochenhuang@hotmail.com, xchuang@ncu.edu.cn); Xiao-Ping Wu (xpwu@ncu.edu.cn)

Academic editor: Matthias Glaubrecht ♦ **Received** 2 July 2024 ♦ **Accepted** 5 August 2024 ♦ **Published** 28 August 2024

Abstract

The Pearl River Basin, China's second-largest freshwater basin, hosts a significant diversity of species and a highly endemic freshwater mussel fauna. In this study, a new species from the Liuxi River in Guangzhou, Guangdong, China, *Plethlophus guangzhouensis* **sp. nov.**, is described based on morphological diagnostic features and molecular phylogenetics. The glochidia shells of the new species are subtriangular, medium-sized, and have a styliform hook on the ventral angle of each valve. Phylogenetic analyses based on the *COI* and *28S* rRNA gene fragments indicated that *Plethlophus guangzhouensis* **sp. nov.** is the sister to *Plethlophus tenuis* + *Plethlophus reinianus*. The pairwise uncorrected *COI p*-distance analysis demonstrated genetic distances ranging from 5.27% (between *P. guangzhouensis* **sp. nov.** and *P. tenuis*) to 11.06% (between *P. guangzhouensis* **sp. nov.** and *P. honglinhensis*). Our findings suggest a significant underestimation of the diversity of freshwater mussel species in Guangdong. Further field collections and systematic studies are necessary to fully explore the biodiversity of this region. Furthermore, integrative classification methods and genetic research are essential for informing the development of effective conservation strategies.

Key Words

conservation, glochidia, molecular systematics, morphological characters, taxonomy

Introduction

Freshwater bivalves (Bivalvia, Unionidae) are well-known for providing important ecosystem functions and services, including nutrient cycling, habitat structure, substrate and food web modification, and serving as environmental monitors (Vaughn 2018). Furthermore, their stable biogeography, characterized by low dispersal and restriction to freshwater habitats, makes them invaluable for elucidating past geological and hydrological events (Zieritz et al. 2021). The life cycle of Unionidae is unique, involving parasitic larvae (glochidia) that must attach to vertebrate hosts, primarily freshwater fish, before becoming sessile adults. This distinctive life cycle has likely contributed significantly to the rapid diversification of this group (Barnhart et al. 2008). However, freshwater mussels represent one of the most threatened faunal groups on a global scale (Böhm et al. 2021), as they are highly impacted by human activities, climate change, and water loss (Aldridge et al. 2022). In recent decades, freshwater mussels have experienced a significant decline, with both species loss and reductions in abundance (Karatayev et al. 2012; Vaughn 2018). This highlights the importance of further research into their diversity, distribution, and evolution.

China exhibits both high species diversity and a highly endemic mussel fauna (Zieritz et al. 2018; Liu et al.

* These authors contributed equally to this paper.

2022). Nevertheless, field investigations and studies of freshwater bivalves in China exhibit a geographic bias, with the majority of research concentrated in the middle and lower reaches of the Yangtze River (Liu et al. 2022; Wu et al. 2022). In recent years, an expanding body of research has revealed that the Pearl River Basin, China's second-largest freshwater basin, hosts numerous previously unidentified and distinct species (Dai et al. 2023). For example, several new species have recently been discovered in the Guangxi Zhuang Autonomous Region, situated along the Pearl River Basin, including *Postolata guangxiensis* Dai, Huang, Guo & Wu, 2023; *Pseudocuneopsis yangshuoensis* Wu & Liu, 2023; *P. wuana* Liu & Wu, 2023; and *P. longjiangensis* Liu & Wu, 2024 (Dai et al. 2023; Dai et al. 2024; Liu et al. 2024). This observation prompted the hypothesis that Guangdong Province, another significant region through which the Pearl River Basin flows, may also be rich in unique species. However, there is a paucity of mussel diversity surveys and studies in Guangdong, particularly over the past decade (Liu and Duan 1991; Hu 2005; He and Zhuang 2013; Zhang et al. 2013; Dong et al. 2017).

Plethlophus Simpson, 1900, belongs to the Unioninae Rafinesque, 1820, in the family Unionidae Rafinesque, 1820. This genus was established by Simpson (1900) as a subgenus of *Cristaria* Schumacher, 1817, with *Cristaria* (*Plethlophus*) *discoidea* (Lea, 1834) (by original designation) designated as the type species. Đặng et al. (1980) elevated *Plethlophus* to the generic level and included three species: *Plethlophus swinhoei* (Adams, 1866), *Plethlophus inangulatus* (Haas, 1910a), and *Plethlophus discoideus* (Lea, 1834). All of these are considered synonyms of *Cristaria tenuis* (He & Zhuang, 2013). Based on the *COI* + *28S* rRNA phylogenies, the species *Cristaria tenuis* (Griffith & Pidgeon, 1833) has been recently reassigned to *Plethlophus* and separated from *Cristaria* (Lopes-Lima et al. 2017). Lopes-Lima et al. (2020) considered *Plethlophus reinianus* (Martens, 1875) to be a valid species based on the analysis of *COI* and *28S* rRNA gene fragments. Recently, Bogan et al. (2023) summarized the taxonomy and diversity of Anodontini in Vietnam, identifying a new species, *Plethlophus honglinhensis* Bogan, Do, Froufe & Lopes-Lima, 2023, based on molecular and morphological evidence. Currently, the genus is recognized to comprise three valid species: *Plethlophus tenuis* (Griffith & Pidgeon, 1833), *Plethlophus reinianus* (Martens, 1875), and *Plethlophus honglinhensis* Bogan, Do, Froufe & Lopes-Lima, 2023. *Plethlophus tenuis* has been recorded as widespread in southeastern Asia, ranging from the Yangtze River south to Cambodia (Bogan et al. 2023). In contrast, the distribution of *P. reinianus* and *P. honglinhensis* is more restricted, with *P. reinianus* endemic to southern Japan and *P. honglinhensis* found exclusively in a coastal basin south of Hanoi, Vietnam (Lopes-Lima et al. 2020; Bogan et al. 2023).

In this study, we discovered a distinct species of freshwater mussel in the Liuxi River, Guangzhou, China. After examining the shell morphology of this unique species, as well as referring to the literature (e.g., Heude 1875, 1877a, 1877b, 1878, 1879, 1880a, 1880b, 1881, 1883, 1885; Simpson 1900, 1914; Haas 1969; Brandt 1974; Liu et al. 1979; He and Zhuang 2013) and MUSSELp online database (see http://mussel-project.uwsp.edu), we were unable to match it to any of the recorded species. Subsequently, a new species of *Plethlophus* was described based on a combination of morphological characters and the *COI* + *28S* rRNA gene phylogenies. We provide morphological descriptions, glochidia descriptions, localities, and photographs for this new species.

Materials and methods

Specimen sampling, identification, and deposition

In January 2021, a total of 10 specimens were collected from the Liuxi River (23°32'02"N, 113°35'03"E) in Guangzhou City, Guangdong, China (Figs 1, 2). A digital vernier caliper with an accuracy of ± 0.01 mm was used to measure the length, height, and width of the type series of the new taxa. Live specimens were euthanized with 100% ethanol and then separated into soft tissue and shells. The adductor muscle was used for subsequent DNA extraction. The remaining soft parts were preserved at −80 °C. All voucher specimens were deposited in the Museum of Biology, Nanchang University (NCUMB), China.

Scanning electron microscopy of glochidia

The glochidial mass was stored in 96% ethanol and subsequently washed with deionized water. It was then transferred into a 5% NaOH solution and allowed to rest for approximately two hours to remove any residual tissue. Following the deionized water wash, the glochidia were observed under an optical microscope to ascertain their cleanliness and the integrity of their shells. The sample preparation process was completed using anhydrous ethanol for storage purposes. Prior to scanning electron microscopy, the samples were dried in a clean environment for a minimum of eight hours, after which their surfaces were sprayed with gold. Subsequently, the samples were subjected to examination via scanning electron microscopy (SEM) (Quanta 200FEG03040702, USA) (Shu and Wu 2005b; Sayenko et al. 2023).

Molecular phylogenetic analyses

The Qiagen Genomic DNA kit (Qiagen, Hilden, Germany) was employed to extract total genomic DNA from the excised tissue following the instructions provided by the manufacturer. The quality and concentration of the DNA

Figure 1. Distribution map of *Pletholophus guangzhouensis* sp. nov.

were checked using 1% agarose gel electrophoresis and NanoDrop 2000 (Thermo Scientific, USA). We amplified and sequenced fragments from the mitochondrial cytochrome *c* oxidase subunit-I gene (*COI*) (LCO22me2 + HCO700dy2) (Walker et al. 2007) and the nuclear *28S* ribosomal RNA gene (28S) (D23F + D4RB) (Park and Foighil 2000). The polymerase chain reaction (PCR) was conducted using a 25 µL mixture of 2 × Taq Plus Master MixII (Vazyme, China) (12.5 µL), ddH_2O (9.5 µL), 10 µM primers (1 µL each), and genomic DNA (1 µL, about 100 ng/µL). Thermal cycling was started at 98 °C for 10 s, followed by 35 cycles of 94 °C for 1 min, annealing at 50 °C for 1 min, extension at 72 °C for 1 min, and then a final extension at 72 °C for 7 min. The PCR products were sequenced commercially by Sangon Biotech (Shanghai, China). The newly obtained sequences have been deposited in GenBank, and their accession numbers are provided in Table 1.

Two datasets were constructed in this study: (i) the *COI* dataset (11 sequences; 600 bp); and (ii) the *COI* + *28S* rRNA dataset (67 sequences; 1,009 bp) (Table 1).

All PCGs were codon-aligned by MUSCLE ver. 3.6 (https://www.drive5.com/muscle/; Edgar 2004) implemented in MEGA ver. 10.1.6 (http://www.megasoftware.net; Kumar et al. 2018), whereas *28S* rRNA were aligned in MAFFT ver. 7 (https://mafft.cbrc.jp/alignment/software/; Katoh et al. 2019) using the Q-INS-i algorithm. We used Gblocks ver. 0.91b (http://gensoft.pasteur.fr/docs/gblocks/0.91b/; Castresana 2000) to exclude ambiguous areas of the alignment for each gene. DnaSP ver. 6 (http://www.ub.edu/dnasp/; Rozas et al. 2017) was used to calculate the number of haplotypes. The best-fit model for each gene and gene partition was calculated by PartitionFinder2 ver. 2.3.4 (Lanfear et al. 2017), based on the corrected Akaike Information Criterion (AICc) and using a heuristic search algorithm. The program proposed the division of the concatenated dataset into three partitions, comprising partitions for the *28S* gene and each of the three codon positions of the *COI* gene. The best-fit model was determined to be GTR + I + G for the first and third codon positions of *COI*, GTR for the second position of *COI*, and GTR + G for *28S*.

Maximum-likelihood (ML) analyses were performed in IQ-TREE (Nguyen et al. 2015) with the ML + rapid bootstrapping method and 10,000 replicates. Bayesian inference (BI) analyses were conducted in MrBayes (Ronquist et al. 2012). Four simultaneous runs with four independent Markov Chain Monte Carlo (MCMC) algorithms were implemented for 10 million generations, and trees were sampled every 1000 generations with a burn-in of 25%. The convergence was checked with the average standard deviation of split frequencies < 0.01 and the potential scale reduction factor (PSRF) ~ 1.

Inter- and intra-specific distances based on the *COI* dataset were calculated in MEGA X using the uncorrected *p*-distance. Standard error estimates were obtained by 1000 bootstrapping replicates.

Table 1. List of sequences used in phylogenetic analyses. (*) Sequenced from this study.

Taxon	*COI*	*28S* rRNA	Country
UNIONIDAE Rafinesque, 1820			
Unioninae Rafinesque, 1820			
Cristariini Lopes-Lima, Bogan, & Froufe, 2017			
Amuranodonta kijaensis Moskvicheva, 1973	MK574204	MK574473	Russia
Anemina arcaeformis (Heude, 1877)	MG462936	MG595463	China
Beringiana beringiana (Middendorff, 1851)	MT020557	MT020799	Japan
Beringiana japonica (Clessin, 1874)	MT020576	MT020803	Japan
Beringiana fukuharai San, Hattori & Kondo, 2020	MT020567	MT020801	Japan
Beringiana gosannensis San, Hattori & Kondo, 2020	MT020584	MT020802	Japan
Buldowskia flavotincta (Martens, 1905)	MT020537	MT020804	South Korea
Buldowskia suifunica (Lindholm, 1925)	MK574190	MK574460	Russia
Buldowskia iwakawai (Suzuki, 1939)	MT020523	MT020806	Japan
Buldowskia kamiyai San, Hattori & Kondo, 2020	MT020525	MT020808	Japan
Buldowskia shadini (Moskvicheva, 1973)	MK574197	MK574467	Russia
Cristaria bellua (Morelet, 1866)	ON704642	ON695893	Laos
Cristaria clessini (Kobelt, 1879)	MT020592	MT020810	Japan
Cristaria plicata (Leach, 1814)	MG462956	MG595484	China
Cristaria truncata Dang, Thai & Pham, 1980	OP491287	OP499826	Vietnam
Plethlophus honglinhensis Bogan, Do, Froufe & Lopes-Lima, 2023	OR912962	OR913009	Vietnam
Plethlophus reinianus (Martens, 1875)	MT020603	n/a	Japan
Plethlophus tenuis (Griffith & Pidgeon, 1833)	KX822658	KX822614	Vietnam
Plethlophus tenuis (Griffith & Pidgeon, 1833)	MT020599	LC519084	Japan
Plethlophus tenuis (Griffith & Pidgeon, 1833)	MT020600	LC519085	Japan
Plethlophus tenuis (Griffith & Pidgeon, 1833)	MT020601	KX822614	Japan
Plethlophus tenuis (Griffith & Pidgeon, 1833)	MT020602	KX822614	Japan
Plethlophus guangzhouensis Dai, Chen, Huang & Wu, sp. nov.*	PP945818	PP956591	China
Plethlophus guangzhouensis Dai, Chen, Huang & Wu, sp. nov.*	PP945819	PP956591	China
Plethlophus guangzhouensis Dai, Chen, Huang & Wu, sp. nov.*	PP945820	PP956591	China
Plethlophus guangzhouensis Dai, Chen, Huang & Wu, sp. nov.*	PP945821	PP956591	China
Sinanodonta angula (Tchang, Li & Liu, 1965)	MG463053	MG595580	China
Sinanodonta calipygos (Kobelt, 1879)	MT020623	MT020833	Japan
Sinanodonta lauta (Martens, 1877)	MT020616	MT020834	Japan
Sinanodonta lucida (Heude, 1877)	MG463066	MG595589	China
Sinanodonta schrenkii (Lea, 1870)	MT020618	MT020837	South Korea
Sinanodonta tumens (Haas, 1910)	MT020622	MT020838	Japan
Sinanodonta pacifica (Heude, 1878)	MG463052	MG595599	China
Sinanodonta woodiana (Lea, 1834)	MG463080	MG595608	China
Parreysiinae Henderson, 1935			
Scabies crispata (Gould, 1843)	MG288632	MG552824	Thailand
Trapezidens exolescens (Gould, 1843)	KX230532	KX230559	Thailand
MARGARITIFERIDAE Henderson, 1929			
Gibbosula laosensis (Lea, 1863)	JX497731	KT343741	Laos
Margaritifera margaritifera (Linnaeus, 1758)	KX550089	KX550093	Russia

Results

Molecular analyses

Four *COI* haplotypes and one *28S* haplotype were identified in the 10 sequenced specimens from Guangzhou, Guangdong. The *COI* dataset had an aligned length of 600 characters, with 95 variable sites and 42 parsimony informative sites. The *COI* + *28S* dataset, which had undergone trimming and concatenation, consisted of 1,009 characters, comprising 600 bp of *COI* and 409 bp of *28S*. There were 383 variable sites and 307 parsimony informative sites.

The ML and BI trees based on the *COI* + *28S* dataset exhibited largely congruent topologies, except for two nodes containing polytomies in the BI tree (Fig. 3). In both trees, *Plethlophus* Simpson, 1900, occupied a distinct position in the subfamily Unioninae and was the sister group with *Sinanodonta* + *Beringiana* (BS/BPP = 98/1.0) (Fig. 3). Within *Plethlophus*, specimens from Guangzhou, Guangdong, represent a distinct taxon and were recovered as sisters to *Plethlophus tenuis* + *Plethlophus reinianus*, with high nodal support (BS/BPP = 98/1). The pairwise uncorrected *COI p*-distance analysis demonstrated genetic distances ranging from 5.27% (between this species and *P. tenuis*) to 11.06% (between this species and *P. honglinhensis*) (Table 2). This species shared a closer relationship with *P. tenuis*. It occupies a unique phylogenetic position and displays distinctive morphological characteristics (Fig. 3; Table 3), which are described herein as *Plethlophus guangzhouensis* sp. nov. Moreover, our results resolved the phylogenetic relationship within *Plethlophus* as (*P. honglinhensis* + (*P. guangzhouensis* sp. nov. + (*P. tenuis* + *P. reinianus*))).

Table 2. Average intraspecific (bold) and interspecific uncorrected *p*-distance (% ± S.E.) for *COI* sequences of species in *Plethol-ophus* Simpson, 1900.

Taxa	1	2	3	4
1. *P. guangzhouensis* sp. nov.	**0.42 ± 0.18**			
2. *P. tenuis*	5.27 ± 0.89	**0.67 ± 0.20**		
3. *P. reinianus*	5.30 ± 0.93	5.68 ± 0.93	**n/c**	
4. *P. honglinhensis*	11.06 ± 1.32	10.75 ± 1.25	11.52 ± 1.32	**n/c**

Table 3. Analyzed conchological characters of *Plethollophus* species. Characteristic descriptions of *P. tenuis*, *P. reinianus*, and *P. honglinhensis* are referenced from published works (Simpson 1900; Haas 1969; He and Zhuang 2013; Bogan et al. 2023) and the MUSSELp online database.

Conchological features	*P. guangzhouensis*	*P. honglinhensis*	*P. reinianus*	*P. tenuis*
Shell shape	Oval	Slightly rectangular to elongate oval	Elliptical or slightly rhomboid	Evenly elliptical
Shell thickness	Thin	Thin	Rather thin	Thin but strong
Shell color	Greenish-yellow in young individuals, darkish-brown in old individuals	Brown to black	Greenish or brownish	Yellowish-green
Umbo	1/4 of shell length, compressed, as high as hinge line	1/3 of shell length, inflated, not elevated above the dorsal margin	1/3 of shell length, compressed, as heigh as hinge line	1/3 of shell length, compressed, as heigh as hinge line
Umbo cavity	Rather shallow, open	Shallow, open	Rather shallow, open	Shallow, open
Posterior ridge	Developed	Prominent but not sharp	Developed	Almost wanting
Surface sculpture	Fine and dense growth lines; two faint ridge on the posterior dorsal; a few elegant, feebly rays	Growth lines	Three faint darker ridges; on the posterior slope with a few slight plications; finer growth lines	Feebly rayed throughout; finer growth lines
Pseudocardinal teeth	Reduced to mere raised threads	One long, thin lamellar tooth	Linear pseudocardinal incach valve	Wanting or reduced to mere raised threads
Lateral teeth	One tooth on both valves, long and narrow	Right valve with a long, narrow lateral tooth; left valve with a straight and well developed tooth	Anterior tooth well developed, posterior tooth reduced	One tooth, high and triangular
Nacre colour	Bluish-white, iridescent	White, becoming bluish-iridescent toward the posterior margin	One tooth on both valves, slender Bluish-white	One tooth on both valves scarcely developed Bluish-white, iridescent behind

Taxonomy

Family Unionidae Rafinesque, 1820
Subfamily Unioninae Rafinesque, 1820
Tribe Cristariini Lopes-Lima, Bogan & Froufe, 2017

Genus *Plethollophus* Simpson, 1900

Type species. *Plethollophus tenuis* (Griffith & Pidgeon, 1833)

Plethollophus guangzhouensis Dai, Chen, Huang & Wu, sp. nov.

https://zoobank.org/E435D35E-CE14-4F27-A726-6346AA0ECF3A
Fig. 2

Material examined. ***Holotype*** China • ♀; Guangdong, Guangzhou City, Conghua District, Liuxi River; 23°32'02"N, 113°35'03"E; 9 January 2021; leg. local people; ex. Y. T. Dai & L. Guo; 24_NCU_XPWU_PGU01. ***Paratypes*** China • 9 shells; same collection data as for the holotype; specimen vouchers are shown in Table 4.

Diagnosis. Periostracum greenish-yellow in young individuals, darkish-brown in old individuals; with fine and dense growth lines and two faint ridges on the posterior dorsal; periostracum often painted with a few elegant, feebly rays. Hinge undeveloped. Beak cavities shallow, open. In both valves, only one peudocardinal and lateral tooth. Peudocardinal teeth reduced to mere raised threads, lateral teeth long and narrow. Nacre bluish-white, iridescent. Glochidia hooked, subtriangular in shape, medium size, shell length less than shell height. The surface of glochidia have deep and dense small holes.

Shell description. Shell medium-sized, not inflated, thin but strong. Length 34.47–51.19 mm, width 6.55–16.21 mm, height 22.86–33.76 mm (Table 4). Shell ovoid, anterior rounded, short, posterior long and wide, slightly obtuse angle, posterior ridge developed. Umbo not prominent, compressed, as high as dorsal margin, located at 1/4 of the dorsal margin, and often eroded. Dorsal margin straight, rear end curved down-wards,

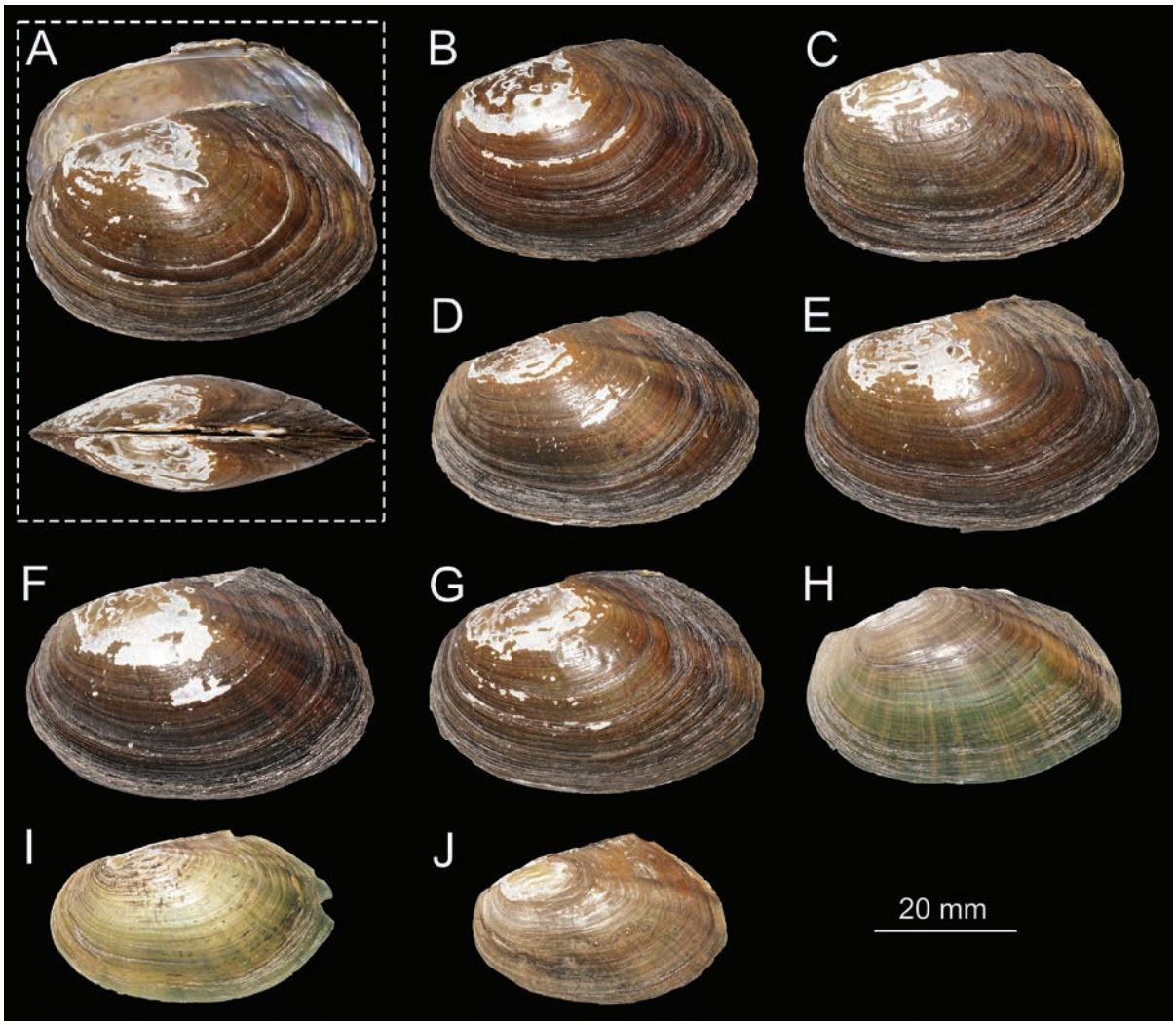

Figure 2. The shell morphology of *Plethlophus guangzhouensis* sp. nov. **A.** holotype; **B–J.** paratypes.

with a low wing behind; ventral margin weakly curved. Periostracum greenish-yellow in young individuals, darkish-brown in old individuals; with fine and dense growth lines and two faint ridges on the posterior dorsal; periostracum often painted with a few elegant, feebly rays. Lines arranged in irregular concentric circles. Hinge undeveloped. Beak cavities shallow, open. In both valves, only one peudocardinal and lateral tooth. Peudocardinal teeth reduced to mere raised threads, and lateral teeth long and narrow. Mantle attachment scars on the edge of shells obvious. Both anterior adductor muscle scars and posterior adductor muscle scars shallow, irregularly crescent-shaped. Nacre bluish-white, iridescent.

Glochidia morphology description. Glochidial shells typically anodontin hooked shells and subtriangular in shape, with the ventral angle slightly protruding dorsally. Medium size, length 0.226 ± 0.003 mm, height 0.247 ± 0.015, shell length less than shell height. The ventral angle of each glochidia valve with an anchor-shaped styliform hook. The hook covered by lanceolate macrospines arranged in 2–3 diagonal rows near the ventral terminus and reduced to a single row distally. Microspines and micropoints cover the entire ventral terminus and less than one-third of the hook lateral lobes. The fossae on the shell surface deep and dense, with distinct small holes.

Etymology. The name of this species is derived from Guangzhou City, in which its type locality is located. For the common name of *Plethlophus guangzhouensis*, we recommend "Guangzhou micro tooth mussel" (English) and "Guang Zhou Wei Chi Bang" (广州微齿蚌) (Chinese).

Table 4. Shell measurements of *Plethlophus guangzhouensis* sp. nov. Measurements are in millimeters (mm).

Status of specimen	Specimen voucher	Shell length	Shell width	Shell height
Holotype	24_NCU_XPWU_PGU01	50.86	15.51	26.72
Paratype	24_NCU_XPWU_PGU02	50.56	15.42	33.76
Paratype	24_NCU_XPWU_PGU03	45.71	11.96	29.87
Paratype	24_NCU_XPWU_PGU04	49.32	15.41	33.11
Paratype	24_NCU_XPWU_PGU05	48.85	15.70	32.54
Paratype	24_NCU_XPWU_PGU06	51.19	16.21	33.22
Paratype	24_NCU_XPWU_PGU07	48.95	15.19	32.38
Paratype	24_NCU_XPWU_PGU08	47.46	14.98	31.02
Paratype	24_NCU_XPWU_PGU09	40.87	11.58	23.98
Paratype	24_NCU_XPWU_PGU10	34.47	6.55	22.86

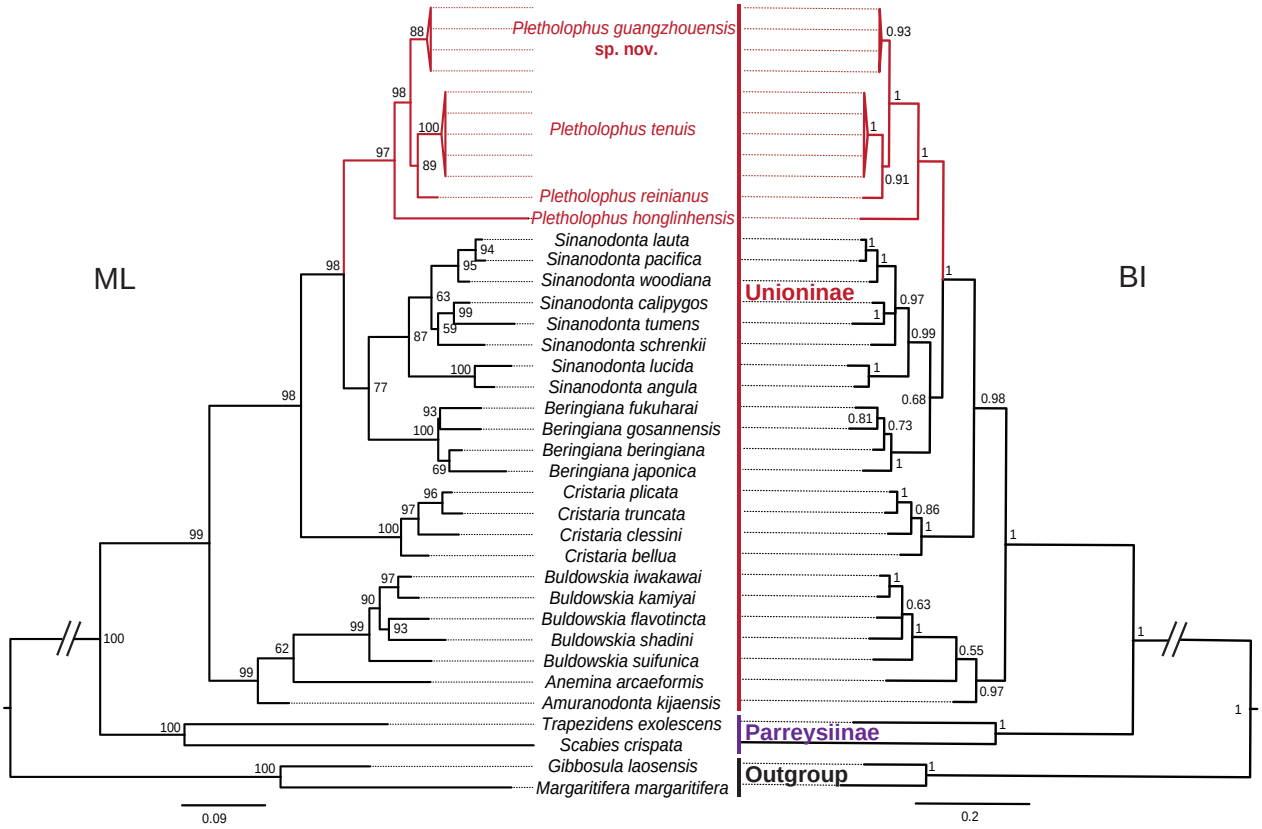

Figure 3. Maximum likelihood (ML) and Bayesian inference (BI) trees of Unionidae based on the *COI + 28S* dataset. *Gibbosula laosensis* and *Margaritifera margaritifera* from the family Margaritiferidae were used as outgroups. Support values above the branches are the posterior probability and bootstrap support, respectively.

Distribution. The species is endemic to the Liuxi River, located in Conghua District, Guangzhou City, Guangdong Province.

Discussion

Our morphological and molecular analyses provide compelling evidence that the freshwater mussels from Guangzhou, Guangdong, represent a new species of *Plethlophus* within the tribe Cristariini of the subfamily Unioninae. Species belonging to the Cristariini exhibit high levels of cryptic diversity, rendering it challenging to distinguish them based solely on morphological characteristics (He and Zhuang 2013; Lopes-Lima et al. 2020; Bogan et al. 2023). Our study has once again highlighted the importance of utilizing an integrative approach in generic classification. In our phylogenetic trees, *Plethlophus guangzhou* sp. nov. formed a well-supported clade in *Plethlophus* and has large genetic distances from its congeneric species, supporting it as a distinct species (uncorrected *COI p*-distance = 5.27% ~ 11.06%; Table 2). The phylogenetic relationships of genera in the Cristariini align with previous studies in most topologies (Lopes-Lima et al. 2020; Bogan et al. 2023). Our *COI + 28S* phylogenies showed the position of *Buldowskia*, *Anemina*, and *Amuranodonta* at the base of Cristariini (Fig. 3). Nevertheless, previous studies have inferred from the *COI + 28S* dataset that *Cristaria* was placed at the base of the clade in Cristariini (Lopes-Lima et al. 2020; Bogan et al. 2023). The incongruencies between topologies are likely due to incomplete lineage sorting, insufficient taxon sampling, and varying rates of genome evolution and mutation (Perkins et al. 2017). To resolve the intergeneric relationships within this tribe, it is recommended that more comprehensive taxon sampling and an increased number of informative loci be utilized.

The morphologic analysis is in alignment with the molecular data. *Plethlophus* is distinguished from other genera in Cristariini by its slender pseudocardinal teeth. For example, *Sinanodonta* lacks any evidence of hinge teeth, while *Cristaria* typically possesses only well-developed lateral teeth (Simpson 1914; Bogan et al. 2023). The new species, *Plethlophus guangzhou* sp. nov., can be distinguished from its congeneric species by its oval shell shape, weakly curved ventral margin, faint rays, and two faint ridges on the posterior dorsal (Fig. 2; Table 3). *Plethlophus tenuis* is taller and has a more rounded ventral margin compared to other species within *Plethlophus*. In contrast, *P. honglinhensis* possesses a more elongated shell. Therefore, *P. tenuis* and *P. honglinhensis* can be readily distinguished from their congeneric species based on shell morphology. *Plethlophus guangzhou* sp. nov. is morphologically similar to *P. reinianus* but can be distinguished

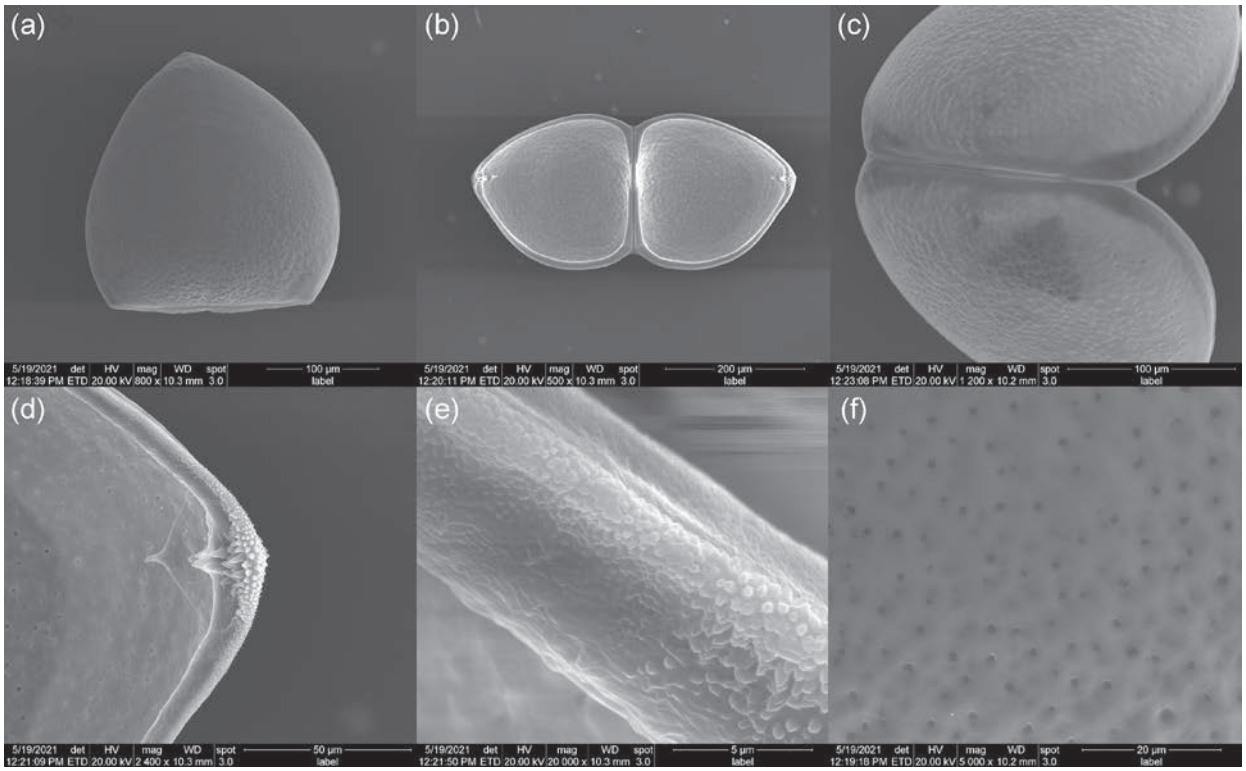

Figure 4. SEM microphotographs of *Plethlophus guangzhouensis* sp. nov. glochidia. **A.** Closed valves of glochidia; **B.** Open valves of glochidia; **C.** Hinge of glochidia; **D.** Hook of glochidia; **E.** Microspines on the ventral margin of glochidia; **F.** Pores on exterior glochidial valve surfaces.

by its more developed pseudocardinal teeth and the presence of two faint ridges (versus reduced pseudocardinal teeth and three faint darker ridges in *P. reinianus*).

In this study, we provide morphological descriptions of the glochidia of *Plethlophus guangzhou* sp. nov., which have proven useful for interpreting the phylogenetic relationships among freshwater mussels (Hoggarth 2000; Sayenko 2006; Sayenko et al. 2020). The glochidia shells of *P. guangzhou* are subtriangular, medium-sized, and have a styliform hook on the ventral angle of each valve (Fig. 4). These characteristics are consistent with those observed in the majority of species within the subfamily Unioninae (Wu et al. 1999a, 1999b; Ćmiel et al. 2021; Sayenko et al. 2023). The majority of Margaritiferidae species, as well as the Ambleminae and Gonideinae within the Unionidae, lack hooks (Shu and Wu 2005a; Xu et al. 2013; Wu et al. 2018; Vikhrev et al. 2019;Ćmiel et al. 2021). Furthermore, the glochidia of Margaritiferidae are notably small and semicircular, as observed in *Margaritifera dahurica* (Ćmiel et al. 2021) and *Gibbosula rochechouartii* (unpublished data from our laboratory). The size of glochidia can aid in taxonomic classification (Ćmiel et al. 2021), while their shape (including aspects such as symmetry and vertical/horizontal elongation) provides valuable taxonomic characteristics that can be utilized in the reconstruction of paleoenvironments (Pfeiffer and Graf 2015; Chernyshev et al. 2020). Given the plasticity of freshwater mussel shells, it is increasingly necessary to incorporate glochidia morphology and anatomical characters into mussel taxonomic studies.

In light of the ongoing global biodiversity loss, the assessment and monitoring of species, along with the detection of new species, are of paramount significance (Dai et al. 2024). The discovery of the new freshwater mussel taxon serves to confirm the high diversity and endemic nature of the mussel fauna in Guangdong. Nevertheless, the high levels of urbanization in the area may result in significant habitat loss for the mussels, thereby threatening their survival. Integrative classification methods and genetic research will inform the development of effective conservation strategies, enabling management based on a more accurate understanding of the unique evolutionary relationships of imperiled freshwater organisms.

Acknowledgments

We are grateful to Prof. Matthias Glaubrecht as well as two reviewers, Dr. Arthur Bogan and Dr. Ivan N. Bolotov, for their helpful comments. This study was supported by the National Natural Science Foundation of China (No. 32100354 and No. 31772412) and the Jiangxi Provincial Natural Science Foundation (No. 20232BAB205067).

References

Đặng N, Thái T, Pham V (1980) Identification of freshwater invertebrates of North Vietnam. Hanoi. Sciences and Technology Publishing Co, Vietnam.

Aldridge DC, Ollard IS, Bespalaya YV, Bolotov IN, Douda K, Geist J, Haag WR, Klunzinger MW, Lopes-Lima M, Mlambo MC, Riccardi N, Sousa R, Strayer DL, Torres SH, Vaughn CC, Zajac T, Zieritz A (2022) Freshwater mussel conservation: A global horizon scan of emerging threats and opportunities. Global Change Biology 29(3): 575–589. https://doi.org/10.1111/gcb.16510

Barnhart MC, Haag WR, Roston WN (2008) Adaptations to host infection and larval parasitism in Unionoida. Journal of the North American Benthological Society 27(2): 370–394. https://doi.org/10.1899/07-093.1

Bogan AE, Do VT, Froufe E, Lopes-Lima M (2023) The Anodontini of Vietnam (Mollusca: Bivalvia: Unionidae: Unioninae) with the description of a new species. Diversity 15(6): 710. https://doi.org/10.3390/d15060710

Böhm M, Dewhurst-Richman NI, Seddon M, Ledger SE, Albrecht C, Allen D, Bogan AE, Cordeiro J, Cummings KS, Cuttelod A (2021) The conservation status of the world's freshwater molluscs. Hydrobiologia 848(12): 3231–3254. https://doi.org/10.1007/s10750-020-04385-w

Brandt RAM (1974) The non-marine aquatic Mollusca of Thailand. Archiv für Molluskenkunde 105: 1–423.

Castresana J (2000) Selection of conserved blocks from multiple alignments for their use in phylogenetic analysis. Molecular biology and evolution 17(4): 540–552. https://doi.org/10.1093/oxfordjournals.molbev.a026334

Chernyshev AV, Sayenko EM, Bogatov VV (2020) Superspecific Taxonomy of the Far Eastern Unionids (Bivalvia, Unionidae): Review and Analysis. Biology Bulletin 47(3): 267–275. https://doi.org/10.1134/S1062359020010045

Ćmiel AM, Dolega J, Aldridge DC, Lipinska A, Tang F, Zajac K, Lopes-Lima M, Zajac T (2021) The size and shape of parasitic larvae of naiads (Unionidae) are not dependent on female size. Scientific Reports 11(1): 23755. https://doi.org/10.1038/s41598-021-03143-9

Dai YT, Huang XC, Wu CHZ, Chen ZG, Guo L, Shu FY, Ouyang S, Wu XP (2023) Multilocus and mitogenomic phylogenetic analyses reveal a new genus and species of freshwater mussel (Bivalvia: Unionidae) from Guangxi, China. Invertebrate Systematics 37(2): 152–166. https://doi.org/10.1071/IS22048

Dai YT, Chen ZG, Peng KJ, Ouyang S, Huang XC, Wu XP (2024) Revisiting the genus *Pseudocuneopsis* (Bivalvia, Unionidae): Morphology, mitochondrial phylogenomics, and the description of a new species. Zoologica Scripta 53 (3): 323–337. https://doi.org/10.1111/zsc.12647

Dong XX, Xing YM, Shu FY (2017) A Preliminary Study on Species and Distributions of Freshwater Mollusca in Zhongshan City, South China. Journal of Qufu Normal University 43(1): 76–80.

Edgar RC (2004) MUSCLE: multiple sequence alignment with high accuracy and high throughput. Nucleic Acids Research 32(5): 1792–1797. https://doi.org/10.1093/nar/gkh340

Haas F (1969) Superfamilia Unionacea. Walter de Gruyter, Germany.

He J, Zhuang Z (2013) The Freshwater Bivalves of China. ConchBooks, Germany.

Heude PM (1875) Conchyliologie fluviatile de la province de Nanking et de la Chine centrale. Premier Fascicule. Librairie F. Savy, France. https://doi.org/10.5962/bhl.title.14450

Heude PM (1877a) Conchyliologie fluviatile de la province de Nanking et de la Chine centrale. Deuxième Fascicule. Librairie F. Savy, France.

Heude PM (1877b) Conchyliologie fluviatile de la province de Nanking et de la Chine centrale. Troisième Fascicule. Librairie F. Savy, France.

Heude PM (1878) Conchyliologie fluviatile de la province de Nanking et de la Chine centrale. Quatrième Fascicule. Librairie F. Savy, France.

Heude PM (1879) Conchyliologie fluviatile de la province de Nanking et de la Chine centrale. Cinquième Fascicule. Librairie F. Savy, France.

Heude PM (1880a) Conchyliologie fluviatile de la province de Nanking et de la Chine centrale. Sixième Fascicule. Librairie F. Savy, France.

Heude PM (1880b) Conchyliologie fluviatile de la province de Nanking et de la Chine centrale. Dixième Fascicule. Librairie F. Savy, France.

Heude PM (1881) Conchyliologie fluviatile de la province de Nanking et de la Chine centrale. Septième Fascicule. Librairie F. Savy, France.

Heude PM (1883) Conchyliologie fluviatile de la province de Nanking et de la Chine centrale. Huitième Fascicule. Librairie F. Savy, France.

Heude PM (1885) Conchyliologie fluviatile de la province de Nanking et de la Chine centrale. Neuvième Fascicule. Librairie F. Savy, France.

Hoggarth M (2000) Descriptions of some of the glochidia of the Unionidae (Mollusca: Bivalvia). Malacologia 41(1): 1–118.

Hu ZQ (2005) Geographical Distribution of Endemic Species of Chinese Freshwater Bivalves. Chinese Journal of Zoology 40: 80–83.

Karatayev AY, Miller TD, Burlakova LE (2012) Long-term changes in unionid assemblages in the Rio Grande, one of the World's top 10 rivers at risk. Aquatic Conservation: Marine and Freshwater Ecosystems 22(2): 206–219. https://doi.org/10.1002/aqc.2226

Katoh K, Rozewicki J, Yamada KD (2019) MAFFT online service: multiple sequence alignment, interactive sequence choice and visualization. Briefings in Bioinformatics 20(4): 1160–1166. https://doi.org/10.1093/bib/bbx108

Kumar S, Stecher G, Li M, Knyaz C, Tamura K (2018) MEGA X: Molecular evolutionary genetics analysis across computing platforms. Molecular Biology and Evolution 35(6): 1547–1549. https://doi.org/10.1093/molbev/msy096

Lanfear R, Frandsen PB, Wright AM, Senfeld T, Calcott B (2017) PartitionFinder 2: New Methods for Selecting Partitioned Models of Evolution for Molecular and Morphological Phylogenetic Analyses. Molecular Biology and Evolution 34(3): 772–773. https://doi.org/10.1093/molbev/msw260

Liu YY, Duan YH (1991) Two new species of freshwater mussel of the genus *Scabies* from China. Acta Zootaxonomica Sinica 16(3): 278–281.

Liu YY, Zhang WZ, Wang YX, Wang EY (1979) Economic fauna of China: Freshwater mollusc. Science Press, China.

Liu XJ, Liu YY, Wu RW, Zanatta DT, Lopes-Lima M, Goncalves DV, Bogan AE, Ouyang S, Wu XP (2022) Systematics, distribution, biology, and conservation of freshwater mussels (Bivalvia: Unionida) in China. Aquatic Conservation: Marine and Freshwater Ecosystems 32(5): 859–895. https://doi.org/10.1002/aqc.3799

Liu L, Zhang L, Hou K, Ning L, Wu R (2024) Addition to the known diversity of Chinese freshwater mussels: integrative description of a new species of *Postolata* Dai et al., 2023 (Bivalvia, Unionidae, Gonideinae). Zoosystematics and Evolution 100(3): 769–778. https://doi.org/10.3897/zse.100.126069

Lopes-Lima M, Froufe E, Do VT, Ghamizi M, Mock KE, Kebapçı Ü, Klishko O, Kovitvadhi S, Kovitvadhi U, Paulo OS, Pfeiffer JM III, Raley M, Riccardi N, Şereflişan H, Sousa R, Teixeira A, Varandas S, Wu X, Zanatta DT, Zieritz A, Bogan AE (2017) Phylogeny of the most species-rich freshwater bivalve family (Bivalvia: Unionida: Unionidae): defining modern subfamilies and tribes. Molecular Phylogenetics and Evolution 106: 174–191. https://doi.org/10.1016/j.ympev.2016.08.021

Lopes-Lima M, Hattori A, Kondo T, Hee Lee J, Ki Kim S, Shirai A, Hayashi H, Usui T, Sakuma K, Toriya T, Sunamura Y, Ishikawa H, Hoshino N, Kusano Y, Kumaki H, Utsugi Y, Yabe S, Yoshinari Y, Hiruma H, Tanaka A, Sao K, Ueda T, Sano I, Miyazaki JI, Gonçalves DV, Klishko OK, Konopleva ES, Vikhrev IV, Kondakov AV, Yu Gofarov M, Bolotov IN, Sayenko EM, Soroka M, Zieritz A, Bogan AE, Froufe E (2020) Freshwater mussels (Bivalvia: Unionidae) from the rising sun (Far East Asia): phylogeny, systematics, and distribution. Molecular Phylogenetics and Evolution 146: 106755. https://doi.org/10.1016/j.ympev.2020.106755

Nguyen LT, Schmidt HA, von Haeseler A, Minh BQ (2015) IQ-TREE: a fast and effective stochastic algorithm for estimating maximum-likelihood phylogenies. Molecular Biology and Evolution 32(1): 268–74. https://doi.org/10.1093/molbev/msu300

Park JK, Foighil DÓ (2000) Sphaeriid and Corbiculid Clams Represent Separate Heterodont Bivalve Radiations into Freshwater Environments. Molecular Phylogenetics and Evolution 14(1): 75–88. https://doi.org/10.1006/mpev.1999.0691

Perkins MA, Johnson NA, Gangloff MM (2017) Molecular systematics of the critically-endangered North American spinymussels (Unionidae: Elliptio and Pleurobema) and description of *Parvaspina* gen. nov. Conservation Genetics 18(4): 745–757. https://doi.org/10.1007/s10592-017-0924-z

Pfeiffer JMI, Graf DL (2015) Evolution of bilaterally asymmetrical larvae in freshwater mussels (Bivalvia: Unionoida: Unionidae). Zoological Journal of the Linnean Society 175(2): 307–318. https://doi.org/10.1111/zoj.12282

Ronquist F, Teslenko M, van der Mark P, Ayres DL, Darling A, Hohna S, Larget B, Liu L, Suchard MA, Huelsenbeck JP (2012) MrBayes 3.2: efficient Bayesian phylogenetic inference and model choice across a large model space. Systematic Biology 61(3): 539–542. https://doi.org/10.1093/sysbio/sys029

Rozas J, Ferrer-Mata A, Sanchez-DelBarrio JC, Guirao-Rico S, Librado P, Ramos-Onsins SE, Sanchez-Gracia A (2017) DnaSP 6: DNA Sequence Polymorphism Analysis of Large Data Sets. Molecular Biology and Evolution 34(12): 3299–3302. https://doi.org/10.1093/molbev/msx248

Sayenko E (2006) Morphology of glochidia (Bivalvia: Unionidae: anodontinae, pseudanodontinae) of Russia. Dalnauka. Vladivostok, PrimoryeTerritory, Russia.

Sayenko EM, Soroka M, Akiyama YB, Uechi T, Ito K, Kondo M (2020) Taxonomic status of genera *Nodularia*, Middendorffinaia and Inversiunio (Bivalvia: Unionidae) from South-East Asia: morphometric, genetic and GenBank data. Systematics and Biodiversity 19(1): 54–73. https://doi.org/10.1080/14772000.2020.1844817

Sayenko EM, Nikischenko VE, Dyachuk VA (2023) Morphological description of the glochidia of *Buldowskia suifunica* (Bivalvia: Unionidae): External and internal structures and organ systems. Scientific Reports 13(1): 19777. https://doi.org/10.1038/s41598-023-46894-3

Shu FY, Wu XP (2005a) A comparative observation on glochidial morphology of two unionid species (unionidae). Shandong Science 18(1): 14–15.

Shu FY, Wu XP (2005b) Observation on Shell Surface of Glochidia of Two Freshwater Mussel Species (Unionidae) by SEM. Life Science Research 9(1): 73–76.

Simpson CT (1900) Synopsis of the Naiades: or pearly fresh-water mussels. US Government Printing Office, USA. https://doi.org/10.5962/bhl.title.935

Simpson CT (1914) Descriptive Catalogue Of The Naiades, Or Pearly Freshwater Mussels. Bryant Walker, USA. https://doi.org/10.5962/bhl.title.10910

Vaughn CC (2018) Ecosystem services provided by freshwater mussels. Hydrobiologia 810(1): 15–27. https://doi.org/10.1007/s10750-017-3139-x

Vikhrev IV, Makhrov AA, Artamonova VS, Ermolenko AV, Gofarov MY, Kabakov MB, Kondakov AV, Chukhchin DG, Lyubas AA, Bolotov IN (2019) Fish hosts, glochidia features and life cycle of the endemic freshwater pearl mussel *Margaritifera dahurica* from the Amur Basin. Scientific Reports 9(1): 8300. https://doi.org/10.1038/s41598-019-44752-9

Walker JM, Bogan AE, Bonfiglio EA, Campbell DC, Christian AD, Curole JP, Harris JL, Wojtecki RJ, Hoeh WR (2007) Primers for amplifying the hypervariable, male-transmitted COII-COI junction region in amblemine freshwater mussels (Bivalvia: Unionoidea: Ambleminae). Molecular Ecology Notes 7(3): 489–491. https://doi.org/10.1111/j.1471-8286.2006.01630.x

Wu XP, Liang Y, Wang H (1999a) A comparative study on glochidial morphology of Unionidae (Bivalvia)-I. *Unio douglasiae, Cuneopsis pisciulus, Acuticosta chinensis* and *Acuticosta ovata*. Acta Hydrobiologica Sinica 23: 145–149. https://doi.org/10.3724/issn1000-3207-1999-2-141-1

Wu XP, Liang Y, Wang H, Ouyang S (1999b) Morphological characters of glochidia of Unionidae and their taxonomic significance. Acta Hydrobiologica Sinica 23: 139–147. https://doi.org/10.3724/issn1000-3207-1999-2-141-1

Wu RW, Chen TH, Zanatta DT, Ouyang S, Wu XP (2018) Reproductive traits of nine freshwater mussel species (Mollusca: Unionidae) from Poyang Lake, China. Journal of Molluscan Studies 84(3): 324–332. https://doi.org/10.1093/mollus/eyy016

Wu XP, Dai YT, Yin N, Shu FY, Chen ZG, Guo L, Zhou CH, Ouyang S, Huang XC (2022) Mitogenomic phylogeny resolves *Cuneopsis* (Bivalvia: Unionidae) as polyphyletic: The description of two new genera and a new species. Zoologica Scripta 51(2): 173–184. https://doi.org/10.1111/zsc.12527

Xu L, Wu XP, Ling C, Ouyang S, Xie GL (2013) Reproductive traits and glochidium Morphology of *Lamprotula leai* (Gray). Journal of Nanchang University 37(3): 263–265.

Zhang MH, Xie GL, Xu L, Liu YY, Wu XP (2013) New Records of a Genus and a Species of Unionidae from China (*Pilsbryoconcha compressa* von Martens, 1860). Life Science Research 17(6): 499–501.

Zieritz A, Bogan AE, Froufe E, Klishko O, Kondo T, Kovitvadhi U, Kovitvadhi S, Lee JH, Lopes-Lima M, Pfeiffer JM, Sousa R, Van Do T, Vikhrev I, Zanatta DT (2018) Diversity, biogeography and conservation of freshwater mussels (Bivalvia: Unionida) in East and Southeast Asia. Hydrobiologia 810: 29–44. https://doi.org/10.1007/s10750-017-3104-8

Zieritz A, Froufe E, Bolotov I, Gonçalves DV, Aldridge DC, Bogan AE, Gan HM, Gomes-Dos-Santos A, Sousa R, Teixeira A (2021) Mitogenomic phylogeny and fossil-calibrated mutation rates for all F-and M-type mtDNA genes of the largest freshwater mussel family, the Unionidae (Bivalvia). Zoological Journal of the Linnean Society 193(3): 1088–1107. https://doi.org/10.1093/zoolinnean/zlaa153

Zoosyst. Evol. 100 (4) 2024, 1201–1209 | DOI 10.3897/zse.100.130676

PENSOFT

für Natur MUSEUM FÜR NATURKUNDE BERLIN

A new species of *Petraeomastus* Möllendorff, 1901, with an atypical shell morphology from the Lancangjiang River Valley in southwest China (Gastropoda, Stylommatophora, Enidae)

Zhong-Guang Chen[1*], Yu-Ting Dai[1*], Xiao-Ping Wu[1], Jiao Jiang[2], Shan Ouyang[1]

1 *School of Life Sciences, Nanchang University, Nanchang 330031, China*

2 *Zhejiang Museum of Natural History, Hangzhou, Zhejiang 310012, China*

https://zoobank.org/997FDAB6-DF4D-45C3-A53C-29C1B01D709E

Corresponding authors: Jiao Jiang (149152414@qq.com); Shan Ouyang (ouys1963@qq.com)

Academic editor: Frank Köhler ♦ **Received** 27 June 2024 ♦ **Accepted** 6 August 2024 ♦ **Published** 29 August 2024

Abstract

Our study contains the first molecular phylogeny of Chinese enids based on the mitochondrial markers cytochrome oxidase c (*COI*) and 16S rRNA (*16S*). We have sequenced 19 species belonging to 10 out of the 12 currently accepted genera. A new species, *Petraeomastus limenghuai* Chen, Dai, Wu & Ouyang, **sp. nov.**, is described from the Lancangjiang River Valley in southwest China based on comparative morphology and molecular phylogeny. The currently accepted classification of Chinese enids relies largely on shell morphology and is deemed to require systematic revision.

Key Words

Biodiversity, dry-hot river valley, land snails, phylogeny, taxonomy

Introduction

Enidae Woodward, 1913, encompasses small to large species from Eurasia, northern Africa, and northern Australia (Wu 2018). China represents a diversity hotspot of the family, harboring about 185 described species and subspecies (Heude 1882, 1885; Ancey 1883, 1884; Hilber 1883; Möllendorff 1901; Annandale 1923; Yen 1938, 1939; Chen and Zhang 2000, 2001; Wu and Wu 2009; Wu and Zheng 2009; Wu and Gao 2010; Zhang et al. 2010; Wang and Wu 2012; Wu and Fang 2012; Wu and Xu 2012; Fang and Wu 2013; Wang and Wu 2013; Wu and Xu 2013; Wu 2018; Chen 2020; Chen et al. 2024a, 2024b). To date, all taxonomic studies have been based exclusively on morphology, with no molecular genetic data being available (Wu 2018; Chen 2020; Chen et al. 2024a, 2024b). Several Chinese genera as currently delineated exhibit overlapping morphological characteristics, hampering an unambiguous classification. The distribution of Enidae in China is highly uneven, with most species restricted to dry-hot sections of several river valleys in the southwest (Wu 2018), including the Bailongjiang River Valley, the Fujiang River Valley, the Minjiang River Valley, the Daduhe River Valley, the Jinshajiang River Valley, and the Lancangjiang River Valley. Among these valleys, the Lancangjiang River Valley is one of the most remote and poorly studied. There has been almost no subsequent study after several species were described from here in the late 19th to early 20th centuries (Heude 1882; Ancey 1883; Hilber 1883; Ancey 1884; Heude 1885; Annandale 1923). The species composition of a large section of the Lancangjiang River Valley is still unclear.

* These authors contributed equally to this work.

During land snail surveys in 2023, we discovered a group of enid specimens with ribbed shells from the Lancangjiang River Valley that did not resemble any known species and were challenging to place in any genus. Based on a combination of comparative morphology and molecular phylogenetic analysis, we describe these snails as a new species of the genus *Petraeomastus* Möllendorff, 1901. The discovery contributes to our understanding of the morphological variations within *Petraeomastus* in China, suggesting that further exploration of the species diversity of Enidae in the Lancangjiang River Valley may yield additional insights. Furthermore, the significant morphological variation within the same genus and the similar morphology between different genera indicate that the current taxonomic classification of Chinese Enidae may be problematic, requiring an integrative, systematic revision.

Materials and methods

Specimens were collected from southern China in 2023. Living specimens were initially frozen at -20 °C for 12 hours and subsequently thawed at room temperature for 12 hours to facilitate the extraction of soft parts. The soft parts were then fixed with 70% ethanol. Empty shells were cleaned, dried, and preserved at 4 °C. Soft parts were transferred from 70% alcohol to 10% alcohol and softened at 4 °C for 5 hours before dissection. Photographs were taken by camera and edited in Adobe Photoshop CC 2015 (Adobe, San Jose, US). Maps were made in ArcGIS Pro (Esri, Redlands, US).

Genomic DNA was extracted from foot tissues preserved in 70% ethanol using a TIANamp Marine Animals DNA Kit (Tiangen Biotech, China). The quality and concentration of the DNA were checked using 1% agarose gel electrophoresis and NanoDrop 2000 (Thermo Scientific, USA). Partial cytochrome c oxidase subunit 1 (*COI*) and 16S ribosomal RNA (*16S*) were amplified and sequenced for molecular phylogenetic analyses. Polymerase chain reaction (PCR) systems, conditions, and primer pairs are listed in Table 1. Sequences were aligned using MEGA v. 6.0 (Tamura et al. 2013) and checked manually. The accession numbers of other species and newly obtained sequences are given in Table 2.

Phylogenies reconstructed by the dataset combined two genes using maximum likelihood (ML) and Bayesian inference (BI). *Camaena detianensis* Zhou & Lin, 2016, *Pupilla muscorum* (Linnaeus, 1758), and *Achatinella sowerbyana* Pfeiffer, 1855, were used as the outgroups for rooting the trees. ML analyses were performed in IQ-TREE v. 1.6.12 (Minh et al. 2013) using the Ultrafast bootstrap approach (Minh et al. 2013) with 10,000 iterations. The most appropriate model of sequence evolution (GTR+I+G) was selected under PartitionFinder2 v. 1.1 (Lanfear et al. 2017). Bayesian inference (BI) analysis was conducted in MrBayes v. 3.2.6 (Ronquist et al. 2012). The most appropriate model of sequence evolution (GTR+I+G) was selected under ModelFinder (Kalyaanamoorthy et al. 2017). Four simultaneous runs with four independent Markov Chain Monte Carlo (MCMC) algorithms were implemented for 10 million generations, and trees were sampled every 10,000 generations with a burn-in of 25%. The convergence was checked with the average standard deviation of split frequencies <0.01 and the potential scale reduction factor (PSRF) ~ 1. Trees were visualized in FigTree v.1.4.3 (http://tree.bio.ed.ac.uk/software/figtree/).

Abbreviations

NCU_XPWU Laboratory of Xiao-Ping Wu, Nanchang University (Nanchang, Jiangxi, China), **ZMNH** Zhejiang Museum of Natural History (Hangzhou, Zhejiang, China), **At** atrium, **AR** retractor muscle of the appendicular branch, **A-1** most proximal section of penial appendix, **A-2** penial appendix section between and thicker than A-1 and A-3, usually bulb-shaped, **A-3** section of the penial appendix connecting proximally A-2 and distally A-4, **A-4** thinnest part of the penial appendix between A-5 and A-3, **A-5** distal part of the penial appendix, more or less swollen, **BC** bursa copulatrix, **BCD** bursa copulatrix duct, **D** diverticle of the bursa copulatrix duct, **Ep** epiphallus, **EpC** epiphallic caecum, **Fl** flagellum, **FO** free oviduct, **P** penis, **PC** penial caecum, **PR** retractor muscle of the penial branch, **Va** vagina, **VD** vas deferens.

Results

Phylogenetic analyses

The sequence dataset consisting of 30 *COI* and 34 *16S* sequences from 19 species, including three outgroup taxa, was employed for phylogenetic analyses (Table 2). The alignments of the *COI* and *16S* genes had lengths of 666 and 437 characters, respectively. Within these alignments, 289 and 231 sites were variable, and 274 and 221 sites were parsimony informative. The Bayesian and Maximum Likelihood analyses produced largely consistent phylogenies (Fig. 1). The genus *Pupinidius* Möllendorff, 1901, is a polyphyletic group, comprising three distinct

Table 1. Primer pairs and PCR conditions used in the analyses of the *COI* and *16S* genes.

Genes	Primer pairs	Reaction systems	Cycling conditions	Reference
COI	LCO1490: GGTCAACAAATCATAAAGATATTGG HCO2198: TAAACTTCAGGGTGACCAAAAAATCA	12.5 µl 2 × Taq Plus Master Mix II (Vazyme, Nanjing, China), 1 µl template DNA, 1 µl of each pair of primers, 9.5 µl ddH2O	94 °C: 2 min; 94 °C: 10 s, 50 °C: 60 s, 72 °C: 1 min, 35 cycles; 72 °C: 10 min	Folmer et al. 1994
16S	16SA: CGGCCGCCTGTTTATCAAAAACAT 16SB: GGAGCTCCGGTTTGAACTCAGATC	12.5 µl 2 × Taq Plus Master Mix II (Vazyme, Nanjing, China), 1 µl template DNA, 1 µl of each pair of primers, 9.5 µl ddH2O	94 °C: 2 min; 94 °C: 10 s, 50 °C: 60 s, 72 °C: 1 min, 35 cycles; 72 °C: 10 min	Páll-Gergely et al. 2019

Table 2. Genbank accession numbers of sequences used in this paper.

Species	Locality	CO1	16S	References
Petraeomastus limenghuai sp. nov. 1	Rumei, Mangkang, Xizang, China, 29°36'39"N, 98°21'1"E	PP945840	PP956541	This study
Petraeomastus limenghuai sp. nov. 2	Rumei, Mangkang, Xizang, China, 29°36'39"N, 98°21'1"E	PP945841	PP956542	This study
Petraeomastus limenghuai sp. nov. 3	Rumei, Mangkang, Xizang, China, 29°36'39"N, 98°21'1"E	PP945842	PP956543	This study
Petraeomastus limenghuai sp. nov. 4	Rumei, Mangkang, Xizang, China, 29°36'39"N, 98°21'1"E	PP945843	PP956544	This study
P. gredleri 1	Rumei, Mangkang, Xizang, China, 29°36'39"N, 98°21'1"E	PP945844	PP956545	This study
P. gredleri 2	Rumei, Mangkang, Xizang, China, 29°36'39"N, 98°21'1"E	PP945845	PP956546	This study
P. heudeanus 1	Rumei, Mangkang, Xizang, China, 29°36'39"N, 98°21'1"E	PP945846	PP956547	This study
P. heudeanus 2	Rumei, Mangkang, Xizang, China, 29°36'39"N, 98°21'1"E	PP945847	PP956548	This study
Serina ser 1	Wenxian, Gansu, China, 33°10'33"N, 105°0'8"E	PP945822	PP956524	This study
Serina ser 2	Wenxian, Gansu, China, 33°10'33"N, 105°0'8"E	PP945823	PP956525	This study
S. schileykoi	Wudu, Gansu, China, 33°25'9"N, 104°48'44"E	PP945826	PP956528	This study
S. sp. 1	Wudu, Gansu, China, 33°25'9"N, 104°48'44"E	PP945824	PP956526	This study
S. sp. 2	Wudu, Gansu, China, 33°25'9"N, 104°48'44"E	PP945825	PP956527	This study
Pupinidius pupinidius 1	Wudu, Gansu, China, 33°25'9"N, 104°48'44"E	PP945829	PP956531	This study
Pupinidius pupinidius 2	Wudu, Gansu, China, 33°25'9"N, 104°48'44"E	PP945830	PP956532	This study
Pu. pupinella 1	Wudu, Gansu, China, 33°25'9"N, 104°48'44"E	PP945827	PP956529	This study
Pu. pupinella 2	Wudu, Gansu, China, 33°25'9"N, 104°48'44"E	PP945828	PP956530	This study
Pu. sp.	Wudu, Gansu, China, 33°25'9"N, 104°48'44"E	PP945831	PP956533	This study
Pu. melinostoma 1	Wenxian, Gansu, China, 33°10'33"N, 105°0'8"E	PP945832	PP956552	This study
Pu. melinostoma 2	Wenxian, Gansu, China, 33°10'33"N, 105°0'8"E	PP945833	PP956553	This study
Pu. porrectus 1	Danba, Ganzu, China, 30°51'11"N, 101°49'27"E	PP945848	PP956549	This study
Pu. porrectus 2	Danba, Ganzu, China, 30°51'11"N, 101°49'27"E	PP945849	PP956550	This study
Subzebrinus dolichostoma	Wenxian, Gansu, China, 33°10'33"N, 105°0'8"E	PP945832	PP956534	This study
Su. beresowskii	Jiuzhaigou, Sichuan, China, 33°15'51"N, 104°14'6"E	PP945833		This study
Clausiliopsis szechenyi 1	Wudu, Gansu, China, 33°25'9"N, 104°48'44"E		PP956554	This study
Clausiliopsis szechenyi 2	Wudu, Gansu, China, 33°25'9"N, 104°48'44"E		PP956555	This study
Turanena microconus 1	Diebu, Gansu, China, 33°58'10"N, 103°31'8"E	PP945834	PP956535	This study
Turanena microconus 2	Diebu, Gansu, China, 33°58'10"N, 103°31'8"E	PP945835	PP956536	This study
Pupopsis pupopsis 1	Wudu, Gansu, China, 33°25'9"N, 104°48'44"E	PP945836	PP956537	This study
Pupopsis pupopsis 2	Wudu, Gansu, China, 33°25'9"N, 104°48'44"E	PP945837	PP956538	This study
Mirus cantori 1	Nanjing, Jiangsu, China, 32°4'13"N, 118°51'9"E	PP945838	PP956539	This study
Mirus cantori 2	Nanjing, Jiangsu, China, 32°4'13"N, 118°51'9"E	PP945839	PP956540	This study
M. frinianus	Jiangxi, China	MT767366	MT767366	Unpublished
Dolichena miranda 1	Maoxian, Sichuan, China, 31°46'26"N, 103°46'45"E		PP956556	This study
Dolichena miranda 2	Maoxian, Sichuan, China, 31°46'26"N, 103°46'45"E		PP956557	This study
Holcauchen sulcatus	Wudu, Gansu, China, 33°25'9"N, 104°48'44"E	PP945850	PP956551	This study
Achatinella sowerbyana	Hawaii	KX356680	KX356680	Price et al. (2016)
Pupilla muscorum	Sweden	KC185404	KC185404	Unpublished
Camaena detianensis	Chongzuo, Guangxi, China	KX345076	KX345081	Ai et al. (2016)

clades. The specimens with ribbed shells from the Lancangjiang River Valley were strongly supported as a sister taxon of *Petraeomastus gredleri* (Hilber, 1883) and form a monophyletic group with *Petraeomastus heudeanus* (Ancey, 1883), which is the type species of the genus. We describe these specimens as a new species here. The genetic distances of *COI* sequences between the new species and other congeners ranged from 20.5% to 23.0%.

Systematics

Family Enidae Woodward, 1903
Subfamily Eninae Woodward, 1903

Genus *Petraeomastus* Möllendorff, 1901

Type species. *Buliminus heudeanus* Ancey, 1883, by original designation.

Petraeomastus limenghuai Chen, Dai, Wu & Ouyang, sp. nov.

https://zoobank.org/EB5041F9-7ECA-4AB0-B209-52FA3249CC3F

Figs 2A, 3

Type. ***Holotype*.** 24_NCU_XPWU_AN351, Rumei Town [如美镇], Mangkang County [芒康县], Changdu City [昌都市], Xizang Autonomous Region [西藏自治区], China, 29°36'20"N, 98°20'40"E, 2838 m a.s.l., leg. Zhong-Guang Chen, Meng-Hua Li & Jin-Sheng Mou, August 2023.

***Paratypes*:** n = 12, 24_NCU_XPWU_AN352–65; n = 2, ZMNH-LB-240003–04, other information same as holotype.

Diagnosis. Shell turreted (vs. cylindrical to conical in all congeners), teleoconch ribbed (vs. smooth in all congeners). Flagellum long. Diverticle unexpanded.

Description. Shell turreted, apex gradually pointed; most swollen at body whorl, dextral, medium-sized,

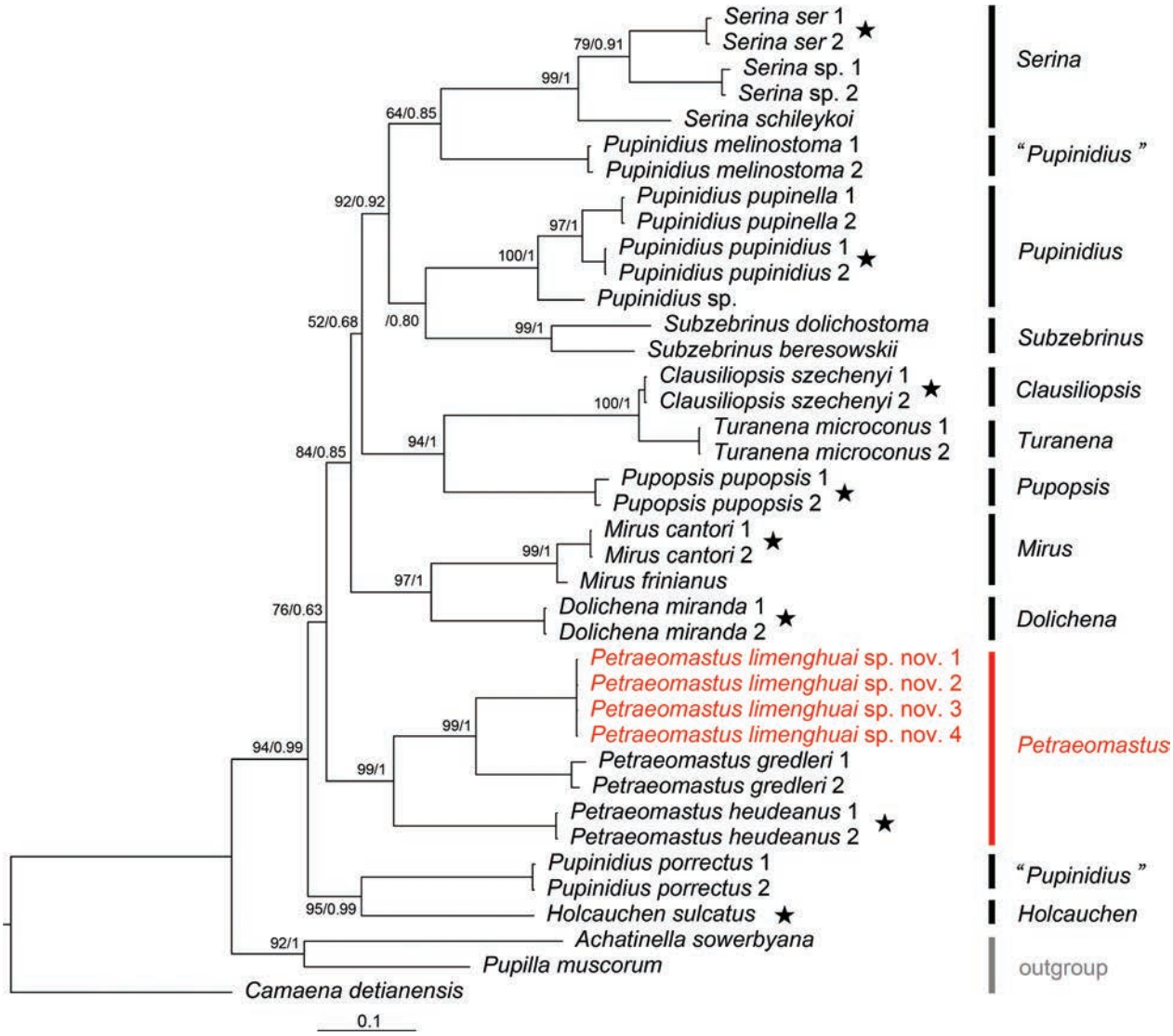

Figure 1. Maximum likelihood tree and Bayesian inference tree inferred from *COI* and*16S* gene sequences. Bootstrap supports/posterior probabilities are shown on the left/right of nodes on the tree if they are greater than 50%. Stars show the type species of the genera.

thick, solid, opaque, sub-glossy, not speckled, not spirally grooved; 8.0–8.5 whorls. Whorls rather flattened, not shouldered. Protoconch smooth, polished. Post-nuclear teleoconch ribbed. Growth lines indistinct. Suture rather deep, with an indistinct narrow band beneath it. Body whorl gradually ascending towards aperture, rounded at periphery. Aperture flat, truncate-ovate, oblique, without tooth, with shallow slightly out angular tubercle, completely adnate to body whorl. Peristome connected, with a shallow channel at upper insertion; white, thickened, expanded, not reflexed. Parietal callus distinct. Columellar margin reflexed. Umbilicus narrowly open. Shell multicoloured, post-nuclear teleoconch with light brown backgroud and white ribs; apex region light brown.

Genitalia. Vas deferens relative short, slightly swollen distally; entering epiphallus apically with distinct demarcation. Epiphallus long; cylindrical; rather straight; externally smooth. Epiphallic caecum present; blunt apically; located near vas deferens entrance. Flagellum long; tubular; proximally normal; with tip pointed. Penis with terminal entrance of epiphallus; clavate; uniformly thickness. Penial caecum absent. Penial appendix long; branched off from penis at some distance from atrium; divided into sections including A-1+A-2, A-3 and A-4+A-5. A-1 and A-2 fused. A-2 and A-3 not fused. Boundary between A-4 and A-5 indistinct. A-5 long; convoluted. Appendicular retractor and penial retractor long; biramous; attaching to penis middle part and to A-2 of penial appendix; with penial retractor arms arising from diaphragm closed to each other. Additional retractor other than penial or appendicular absent. Muscular band connecting vagina and epiphallus absent. Atrium short; without retractor. Free oviduct longer than vagina. Vagina short; not swollen; straight; unpigmented. Bursa copulatrix duct short; proximally straight. Bursa copulatrix ovoid, with stalk; without apical ligament; normal in size; with short neck; well defined. Diverticle normally present; longer than bursa copulatrix; unexpanded. Bursa copulatrix and diverticle distinguishable; forked more distally from their base.

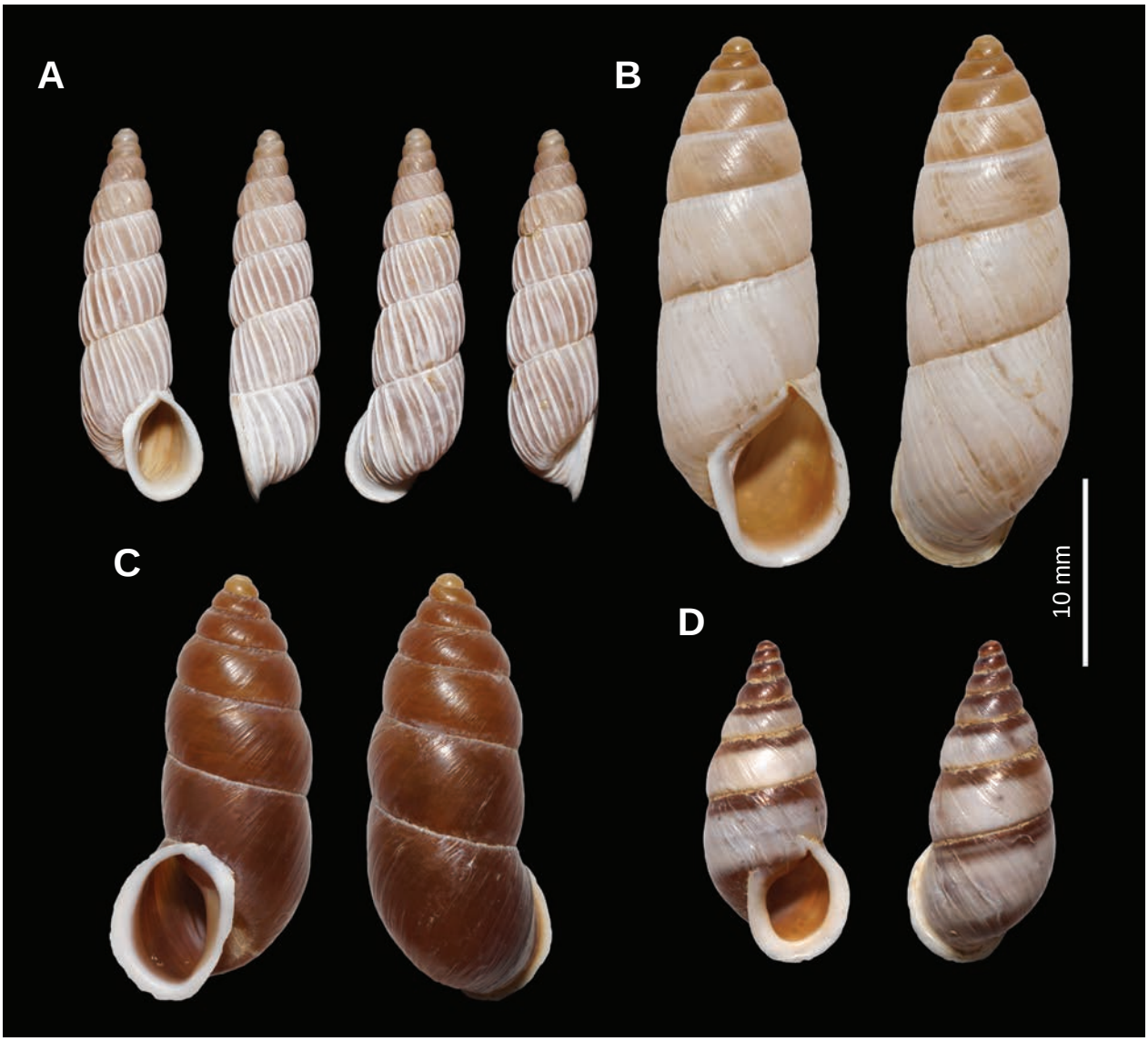

Figure 2. *Petraeomastus limenghuai* sp. nov. and three congeners with typical shell morphology. **A.** Holotype of *Petraeomastus limenghuai* sp. nov.; **B.** *P. heudeanus*; **C.** *P. neumayri*; **D.** *P. xerampelinus*.

Measurements. Holotype: shell height 20.6 mm, width 6.7 mm; aperture height 6.4 mm, width 4.7 mm. Paratypes: shell height 19.8–21.2 mm, width 6.0–7.0 mm; aperture height 6.0–6.6 mm, width 4.2–4.9 mm.

Etymology. The species is named after Meng-Hua Li, who first discovered the new species and assisted in field surveys.

Vernacular name. 黎氏鸟唇螺.

Distribution and ecology. Known from the type locality only (Figs 4, 5). Living on branches of bushes alongside *P. heudeanus* (Fig. 5). Although the two species are sympatric, it has been observed that *Petraeomastus limenghuai* sp. nov. is more common on the shady slopes, while *P. heudeanus* is more common on the sunny slopes. The distribution of *Petraeomastus limenghuai* sp. nov. is limited to the middle part of the valley within a few hundred meters and does not extend to the alpine meadows in the upper part. Only two empty shells were discovered at the lower part of the valley, which may have fallen from their original position. In contrast, *P. heudeanus* is widely distributed in the middle and lower parts of the valley, with numerous individuals observed in close proximity to the river channel.

Discussion

Only four enid species in China have a ribbed shell: *Clausiliopsis clathratus* (Möllendorff, 1901), *Clausiliopsis senckenbergianus* Yen, 1939, *Holcauchen multicostatus* Chen, Xie, Wang & Wu, 2024, and *Serina xirong* Chen, Dai, Wu & Ouyang, 2024 (Möllendorff 1901; Yen 1939; Wu 2018; Chen et al. 2024a, 2024b). *Petraeomastus limenghuai* sp. nov. can be distinguished from *C. clathratus* and *C. senckenbergianus* by absence of a tooth (vs. the presence of a parietal tooth). It resembles *H. multicostatus* and *S. xirong*, which also lack a tooth, but differs from them by having stronger ribs and a larger

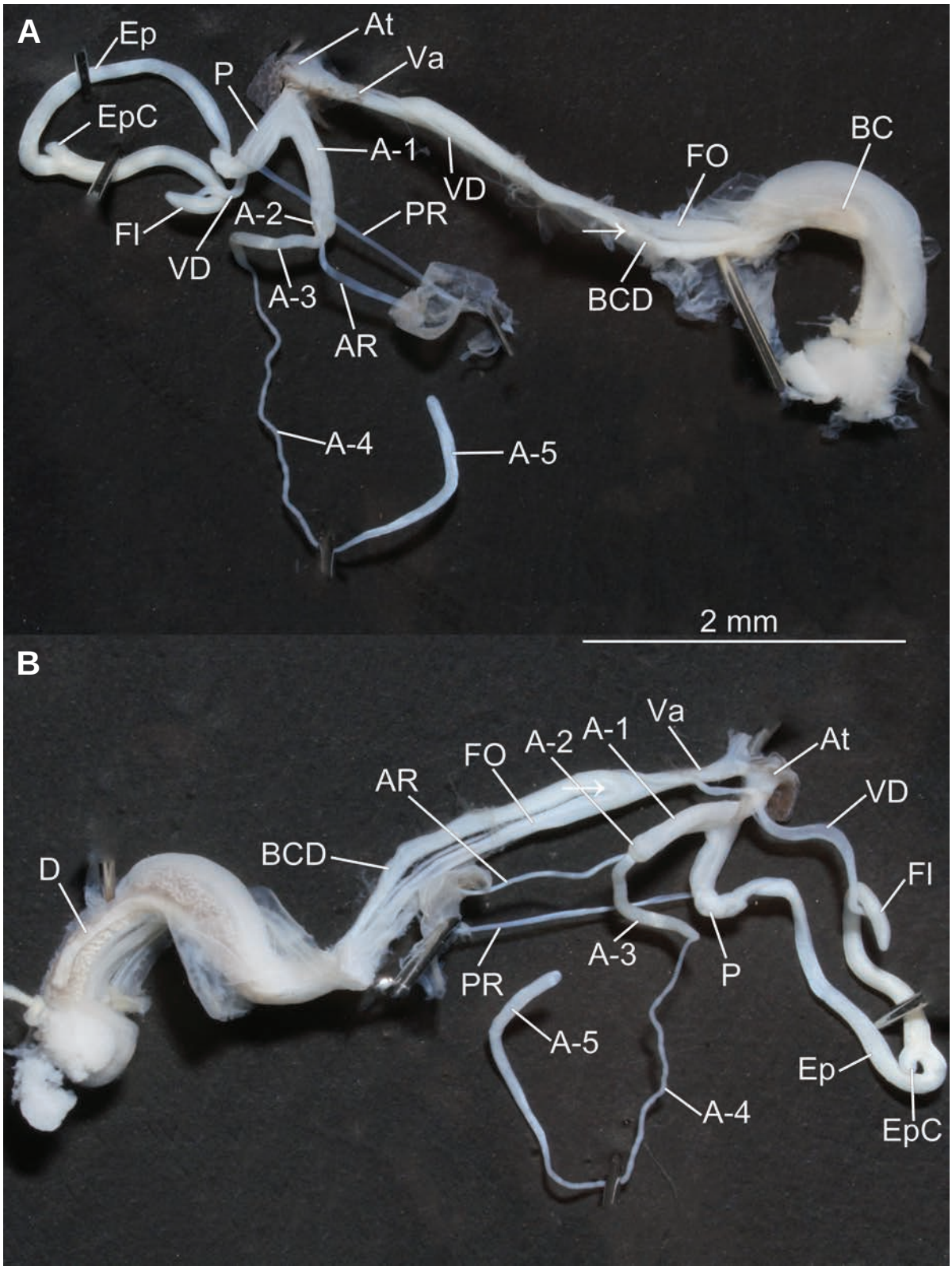

Figure 3. Genitalia of *Petraeomastus limenghuai* sp. nov. from both sides. Arrows show the forks.

shell (height 19.8–21.2 mm vs. 8.3–10.5 mm in *H. multicostatus* and 9.7–11.0 mm in *S. xirong*). It further differs from *H. multicostatus* by having a more pointed shell and from *S. xirong* by having sparser ribs. Within the genus, the new species differs from congeners by the ribbed shell (vs. smooth in all congeners), the long flagellum (vs. short in *P. breviculus*, *P. heudeanus*, and *P. platychilus*), and the unexpanded diverticle (vs. diverticle absent in *P. breviculus*; expanded in *P. heudeanus*, *P. moellendorffi*, *P. mucronatus*, *P. platychilus*, and *P. semifartus*).

The shell morphology of *Petraeomastus limenghuai* sp. nov. is so unique that it is difficult to place it in any genus based on shell morphology alone. It also lacks diagnostic characteristics in its reproductive anatomy. Wu (2018)

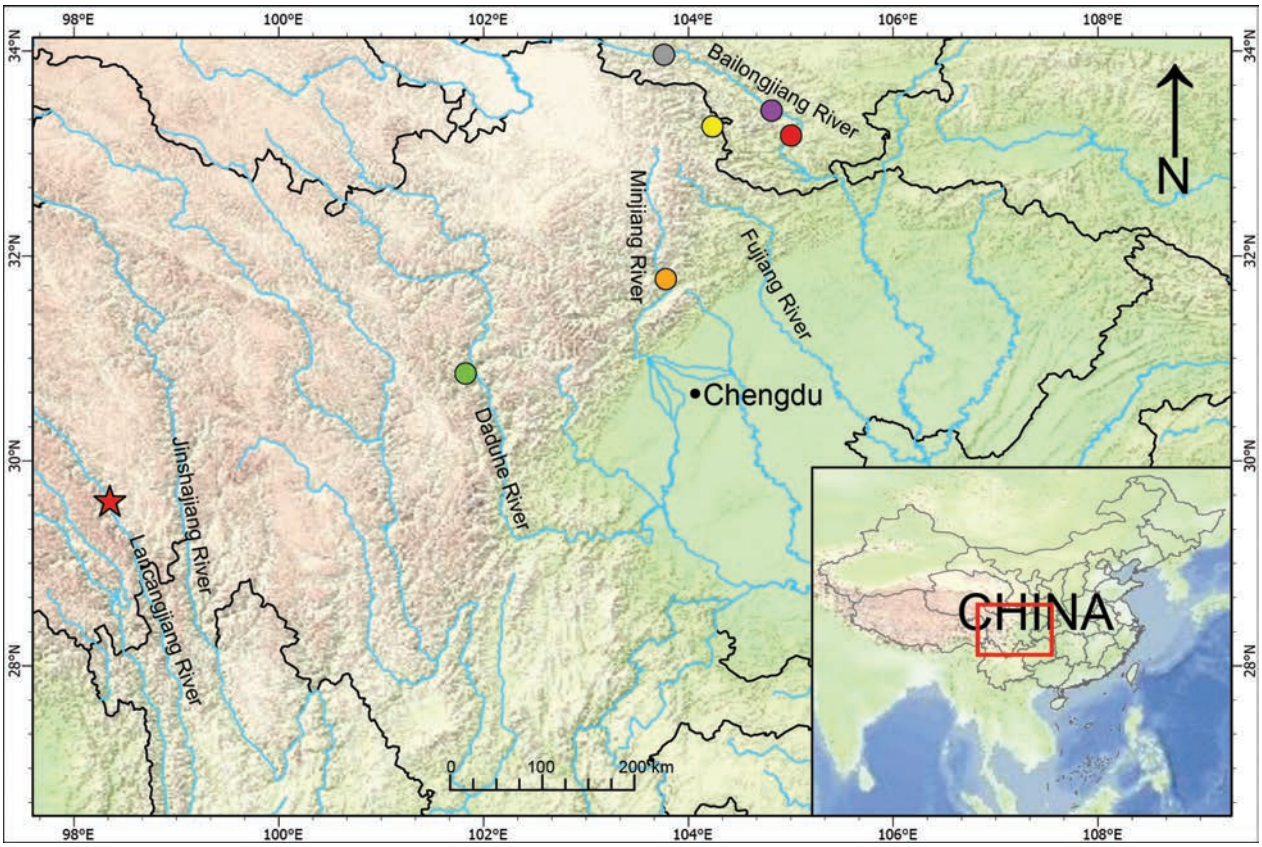

Figure 4. Six dry-hot river valleys and the sample localities in them. **Star.** Rumei; **green point.** Danba; **orange point.** Maoxian; **yellow point.** Jiuzhaigou; **purple point.** Wudu; **red point.** Wenxian; **gray point.** Diebu.

Figure 5. Habitat of *Petraeomastus limenghuai* sp. nov. **A, B.** The Lancangjiang River Valley at Rumei; **C, D.** *Petraeomastus limenghuai* sp. nov. in life.

proposed that the penial pilaster is a relatively stable character in different genera, but we failed to dissect it because it was too thin (< 0.2 mm). However, the molecular phylogeny strongly supported placement in *Petraeomastus* (bootstrap supports = 99, posterior probabilities = 1). All known species of *Petraeomastus* have a broad, cylindrical to conical, and smooth shell (Fig. 2B–D), which is significantly different from that of *Petraeomastus limenghuai* sp. nov. The shell morphology of land snails is frequently influenced by environmental selection, and the characters play a pivotal role in regulating the water and heat budget, thereby preventing desiccation (Cowie and Jones 1985; Chiba 2004; Pfenninger et al. 2005; Giokas et al. 2014). Considering that all Chinese Enidae with ribbed shells are distributed in the dry-hot river valleys (Möllendorff 1901; Yen 1939; Wu 2018; Chen et al. 2024a, 2024b), the special character that evolved independently in four genera may have been developed to adapt to the extremely dry and hot environment. The ribs on the shell could increase its surface area and may promote heat dissipation. Giokas et al. (2014) found that the ribbed shells in *Albinaria* Vest, 1867, retain more water on their shell surface, and the smooth shells exhibit lower water permeability. A similar phenomenon may also occur in Chinese Enidae, although further statistical study is required to confirm it. Currently, the proportion of known Chinese enid species with a ribbed shell is very low. Further comprehensive surveys of several dry-hot river valleys in southwest China might reveal additional species of Enidae with ribbed shells.

Although 10 out of 12 genera of Enidae in China were included in this study, only 19 out of 185 species and subspecies were included. More comprehensive sampling is needed in future research. Currently, the taxonomy of enid genera in China is primarily based on shell morphology (Wu 2018). However, the shell morphology of land snails is frequently influenced by environmental factors (Cowie and Jones 1985; Chiba 2004; Pfenninger et al. 2005; Giokas et al. 2014) and is not stable. Some genital diagnostic characters of Chinese Enidae have been summarized (Wu 2018), but there is overlap between different genera in several characteristics. Currently, the diagnostic characters of Chinese Enidae are insufficiently defined at the genus level, as there is considerable overlap in characters among different genera. This presents a significant challenge in reliably distinguishing some genera from each other. The three clades of *Pupinidius*, which render the genus nonmonophyletic in the molecular phylogenies, exhibit a high similarity in shell morphology. Upon examination of a substantial number of specimens of the three clades, it is challenging to identify any reliable diagnostic characters that distinguish them, both in terms of shell and genitalia. As a rock-dwelling group, the similar morphology between the three clades of *Pupinidius* may be attributed to convergent evolution due to similar environments. The inconsistency between the morphological characters and the molecular phylogenies also occurred in the new species described in this study and is possible to be prevalent in Chinese Enidae. The currently accepted classification of Chinese enids, which relies largely on shell morphology, may be problematic and is deemed to be in need of systematic revision.

Acknowledgements

We thank Menghua Li (Sichuan Agricultural University), Jinsheng Mou (China Agricultural University, Sichuan Agricultural University), Kaichen Ouyang (Kunming), and Shiyang Feng (Sichuan Agricultural University) for assistance in collecting specimens; Frank Köhler, Ruud Bank, and Aydin Örstan for their valuable comments on the manuscript. This study was supported by the National Natural Science Foundation of China under Grant No. 32360132, No. 31772412, the research project of the Zhejiang Natural History Museum under Grant No. 2024001, and the Biodiversity Monitoring Project of Xixi National Wetland Park of Hangzhou.

References

Ai HM, Lin JH, Wang P, Zhou WC, Hwang CC (2016) Descriptions of two new species of the genus *Camaena* from guangxi, China (Gastropoda, Stylommatophora, Camaenidae). Zookeys 634(2): 29–45. https://doi.org/10.3897/zookeys.634.10236

Ancey CMF (1883) Sur les mollusques des parties centrales de l'Asie (Chine et Thibet). Il Naturalista Siciliano 2: 141–143, 163–168, 209–211, 266–270.

Ancey CMF (1884) Contributions à la Faune malacologique Indo-Thibétaine. Annales de Malacologie 1(4): 381–397.

Annandale TN (1923) Zoological results of the Percy Sladen Trust expedition to Yunnan under the leadership professor J. W. Gregory, F. R. S. (1922). Land molluscs. Journal of the Asiatic Society of Bengal 19: 385–422.

Chen ZY (2020) A conical new species of *Pupopsis* Gredler, 1898 from China (Gastropoda: Stylommatophora: Enidae). Folia Malacologica 28(2): 132–134. https://doi.org/10.12657/folmal.028.010

Chen DN, Zhang GQ (2000) A new species of the genus *Holcauchen* from China (Gastropoda: Stylommatophora: Enida). Acta Zootaxonomica Sinica 25(4): 369–372.

Chen DN, Zhang GQ (2001) Five new species of land snails from the Tibet Autonomous Region (Gastropoda: Mesogastropoda, Stylommatophora). Acta Zootaxonomica Sinica 26(1): 11–17.

Chen ZG, Dai YT, Xie GL, Wang P, Jiang J, Ouyang S, Wu XP (2024a) Two new species of enid land snail from Sichuan, China (Stylommatophora: Enidae). Journal of Conchology 45(1): 19–23. https://doi.org/10.61733/jconch/4503

Chen ZG, Hu HF, Dai YT, Wang P, Jiang J, Wu XP, Ouyang S (2024b) Two new enid land snails from Jiuzhaigou County, Sichuan Province, China (Gastropoda: Stylommatophora: Enidae). Animal Taxonomy and Ecology 70(2): 201–207. https://doi.org/10.1556/1777.2024.00026

Chiba S (2004) Ecological and morphological patterns in communities of land snails of the genus *Mandarina* from the Bonin Islands. Journal of Evolutionary Biology 17(1): 131–143. https://doi.org/10.1046/j.1420-9101.2004.00639.x

Cowie RH, Jones JS (1985) Climatic selection on body color in Cepaea. Heredity 55: 261–267. https://doi.org/10.1038/hdy.1985.100

Fang YX, Wu M (2013) A new species of the genus *Serina* from south Gansu, China (Stylommatophora, Enoidea). Acta Zootaxonomica Sinica 38(1): 33–37.

Folmer O, Black M, Hoeh W, Lutz, R, Vrijenhoek R (1994) DNA primers for amplification of mitochondrial cytochrome c oxidase subunit I from diverse metazoan invertebrates. Molecular Marine Biology and Biotechnology 3: 294–299.

Giokas S, Páll-Gergely B, Mettouris O (2014) Nonrandom variation of morphological traits across environmental gradients in a land snail. Evolutionary Ecology 28: 323–340. https://doi.org/10.1007/s10682-013-9676-5

Heude PM (1882) Notes sur les mollusques terrestres de la vallée du Fleuve Bleu. Mémoires Concernant L'Histoire Naturelle de L'Empire Chinois (1): 1–84. https://doi.org/10.5962/bhl.title.50365

Heude PM (1885) Notes sur les mollusques terrestres de la vallée du Fleuve Bleu. Mémoires Concernant L'Histoire Naturelle de L'Empire Chinois (2): 89–132.

Hilber V (1883) Recente und im Löss gefundene Landschnecken aus China. II. SB. Akademie der Wissenschaften in Wien 88: 1349–1392[, 3 pls]. https://doi.org/10.5962/bhl.title.10607

Kalyaanamoorthy S, Minh BQ, Wong TKF, Haeseler A von, Jermiin LS (2017) Modelfinder: Fast model selection for accurate phylogenetic estimates. Nature Methods 14: 587–589. https://doi.org/10.1038/nmeth.4285

Lanfear R, Frandsen PB, Wright AM, Senfeld T, Calcott B (2017) Partitionfinder 2: New methods for selecting partitioned models of evolution for molecular and morphological phylogenetic analyses. Molecular Biology and Evolution 34: 772–773. https://doi.org/10.1093/molbev/msw260

Minh BQ, Nguyen MAT, Haeseler v A (2013) Ultrafast approximation for phylogenetic bootstrap. Molecular Biology and Evolution 30: 1188–1195. https://doi.org/10.1093/molbev/mst024

Möllendorff OF von (1901) Binnen-Mollusken aus Westchina und Centralasien. II. Annuaire du Musée Zoologique de l'Académie Impériale des St.-Petersburg, 6: 299–404[, Taf. XII–XVII].

Páll-Gergely B, Hunyadi A, Chen ZY, Lyu ZT (2019) A review of the genus *Coccoglypta* Pilsbry, 1895 (Gastropoda: Pulmonata: Camaenidae). Zoosystema 41(29): 595–608. https://doi.org/10.5252/zoosystema2019v41a29

Pfenninger M, Hrabakova M, Steinke D, Depraz A (2005) Why do snails have hairs? A Bayesian inference of character evolution. BMC Evolutionary Biology 5(1): 59. https://doi.org/10.1186/1471-2148-5-59

Price MR, Forsman ZH, Knapp I, Toonen RJ, Hadfield MG (2016) The complete mitochondrial genome of *Achatinella sowerbyana* (Gastropoda: Pulmonata: Stylommatophora: Achatinellidae). Mitochondrial DNA Part B 1(1): 666–668. https://doi.org/10.1080/23802359.2016.1219631

Ronquist F, Teslenko M, van der Mark P, Ayres DL, Darling A, Höhna S, Larget B, Liu L, Suchard MA, Huelsenbeck J (2012) Mrbayes 3.2: Efficient bayesian phylogenetic inference and model choice across a large model space. Systematic Biology 61: 539–542. https://doi.org/10.1093/sysbio/sys029

Tamura K, Stecher G, Peterson D, Filipski A, Kumar S (2013) MEGA6: Molecular evolutionary genetics analysis version 6.0. Molecular Biology and Evolution 30: 2725–2729. https://doi.org/10.1093/molbev/mst197

Wang DB, Wu M (2012) A new species of the genus *Holcauchen* from south Gansu, China (Stylommatophora, Enoidae). Acta Zootaxonomica Sinica 37(4): 718–721.

Wang SY, Wu M (2013) A new species of *Petraeomastus* from Gansu, China (Stylommatophora, Enoidae) Acta Zootaxonomica Sinica 38(1): 38–39.

Wu M (2018) Mollusca, Gastropoda: Enoidea. Fauna Sinica, Invertebrata Vol. 58. Science Press, China, 298 pp.

Wu M, Fang YX (2012) A new species of the *Holcauchen* from north Sichuan, China (Stylommatophora, Enoidae). Acta Zootaxonomica Sinica 37(3): 546–549.

Wu M, Gao LH (2010) A review of the genus *Pupopsis* Gredler, 1898 (Gastropoda: Stylommatophora: Enidae), with the descriptions of eight new species from China. Zootaxa 2725: 1–27. https://doi.org/10.11646/zootaxa.2725.1.1

Wu M, Wu Q (2009) A study of the type species of *Clausiliopsis* Möllendorff (Gastropoda, Stylommatophora: Enidae), with the description of a new species. Journal of Conchology 40(1): 91–98. https://doi.org/10.11646/zootaxa.2053.1.1

Wu M, Xu M (2012) A new *Subzebrinus* species from south Gansu, China (Stylommatophora, Enoidae). Acta Zootaxonomica Sinica 37(3): 542–545.

Wu M, Xu Q (2013) *Serina* Gredler (Gastropoda, Stylommatophora: Enidae), the continuous-peristomed mountain snails endemic to the eastern slope of the Qinghai-Xizang Plateau. Zootaxa 3620: 43–66. https://doi.org/10.11646/zootaxa.3620.1.2

Wu M, Zheng W (2009) A review of Chinese *Pupinidius* Moellendorff (Gastropoda, Stylommatophora: Enidae), with the description of a new species. Zootaxa 2053: 1–31. https://doi.org/10.11646/zootaxa.2053.1.1

Yen TC (1938) Notes on the gastropod fauna of Szechwan Province. Mitteilungen aus dem Zoolog. Museum in Berlin 23: 438–457[, 1 Taf].

Yen TC (1939) Die chinesischen Land- und Süßwasser-Gastropoden des Natur-Museums Senckenberg. Abhandlungen der Senckenbergischen Naturforschenden Gesellschaft 444: 1–234[, pls. 1–16].

Zhang WH, Chen DN, Zhou WC (2010) A new species of the genus *Subzebrinus* Westerlund 1887 from China (Pulmonata, Stylommatophora, Enidae). Acta Zootaxonomica Sinica 35(4): 863–864.

Zoosyst. Evol. 100 (4) 2024, 1211–1230 | DOI 10.3897/zse.100.129089

PENSOFT

für Natur MUSEUM FÜR NATURKUNDE BERLIN

A new species of *Thermocyclops* Kiefer, 1927 (Crustacea, Copepoda, Cyclopoida, Cyclopidae) from temporary habitats, with a discussion on the diversity and distribution of the genus in Thailand

Thanida Saetang[1], Kamonwan Koompoot[2], Santi Watiroyram[3], Supiyanit Maiphae[1,4]

1 *Animal Systematics and Ecology Speciality Research Unit (ASESRU), Department of Zoology, Faculty of Science, Kasetsart University, Bangkok 10900, Thailand*

2 *Diversity of Family Zingibeaceae and Vascular Plant of Its Applications Research Unit, Walai Rukhavej Botanical Research Institute, Mahasarakham University, Kantarawichai District, Maha Sarakham 44150, Thailand*

3 *Division of Biology, Faculty of Science, Nakhon Phanom University, Nakhon Phanom 48000, Thailand*

4 *Biodiversity Center Kasetsart University (BDCKU), Kasetsart University, Bangkok 10900, Thailand*

https://zoobank.org/C526568E-EBE2-46E5-A58A-D54C2ACCC04F

Corresponding author: Supiyanit Maiphae (supiyanit.m@ku.ac.th)

Academic editor: Kay Van Damme ♦ **Received** 5 June 2024 ♦ **Accepted** 16 August 2024 ♦ **Published** 2 September 2024

Abstract

Thermocyclops Kiefer, 1927, is a genus of Cyclopidae, one of the most diverse families among cyclopoids. To date, 13 species of this genus have been recorded in Thailand. Through intensive sampling of rice fields in central Thailand and temporary waters in northeastern Thailand, one new species, *Thermocyclops oryzae* **sp. nov.**, was discovered. This new species is clearly distinguished from other *Thermocyclops* by the presence of a serrated lobe on the posterior surface of the medial expansion of the basipodite of the fourth swimming leg. Moreover, it can be distinguished from its congeners by (i) ornamentation on the genital double-somite, succeeding two urosomites and caudal ramus; (ii) the length and width ratio of the caudal ramus; (iii) the length ratio of the innermost terminal seta (VI) and the outermost terminal seta (III); (iv) the number of setae on the second endopodal segment of the antenna; (v) projection and ornamentation on the intercoxal sclerites of the first to fourth swimming legs; (vi) the surface ornamentation of the medial margin of the basipodite of the first to fourth swimming legs; and (vii) the relative length of two apical spines of the third endopodal segment of the fourth swimming leg. The present discovery increases the number of species in this genus in Thailand to 14. A pictorial key to all species is proposed, and their ecologies and distributions within Thailand are updated and discussed.

Key Words

Diversity, habitat preference, niche heterogeneity, temporary habitat, Thailand, *Thermocyclops oryzae* sp. nov.

Introduction

A total of 170 copepod species have been found in freshwater habitats in Thailand (Saetang et al. 2020; Sanoamuang and Dabseepai 2021; Saetang and Maiphae 2023). Cyclopidae is one of the most diverse families of cyclopoids. Approximately 66 valid species of *Thermocyclops* Kiefer, 1927, have been recorded worldwide (Walter and Boxshall 2024), 13 of which have been found in Thailand (Sanoamuang 1999; Wongrat and Pipatcharoenchai 2003; Alekseev and Sanoamuang 2006; Proongkiat 2006; Wansuang and Sanoamuang 2006; Chittapun et al. 2009; Koompoot 2010; Watiroyram 2012; Boonyanusith 2013; Karanovic et al. 2017; Maiphae et al. 2023; Soe and Sanoamuang 2023). Most of these species are widely distributed, while a few have a restricted distribution. The latter group includes two recently described species in Thailand that are restricted to caves: *T. parahastatus* Karanovic, Koomput & Sanoamuang, 2017 and *T. thailandensis* Karanovic, Koomput & Sanoamuang, 2017.

However, more species can be expected, particularly in special habitats that are less explored than lakes, such as caves and temporary water bodies. This is a general fact in tropical zooplankton, where considerable diversity remains to be explored (Brendonck et al. 2022). Rice fields are an example of temporary habitats that provide a unique form of complex temporary habitats (Edirisinghe and Bambaradeniya 2006). They encompass the different characteristics of each phase through which organisms pass during a cultivation cycle. Water levels and dry periods in rice fields are important features of transient aquatic ecosystems that affect not only the diversity and community structures of species but also the life histories of microscopic animals (Edirisinghe and Bambaradeniya 2006; Watanabe 2019). Moreover, rice fields are dynamic and undergo rapid physical, chemical, and biological changes. The heterogeneous composition of rice fields provides various niches for microscopic animals and contributes to their richness and biodiversity (Bambaradeniya et al. 2004). As reported in previous studies, copepods are often among the first groups of zooplankton to arrive and dominate in sampled ponds (Frisch and Green 2007). The rapid dispersal and dominance of certain cyclopoid copepods during early colonization are due to their rapid individual development and ability to store sperm. Given that cyclopoid copepods can survive periods of drought in the sediment of temporary ponds, initial and early colonization by cyclopoids is likely to have a significant effect on propagule banks and future plankton communities when such ponds refill (Frisch and Green 2007).

The present study investigates the diversity of this genus in temporary habitats, including rice fields, temporary canals, and temporary ponds. In a prior survey of five rice fields in central Thailand, 22 samples were collected, and a total of 9 species of this genus were found (Maiphae et al. 2023). Among them, an undescribed species of *Thermocyclops* was found that exhibited clear morphological differences from known species. Moreover, this unknown *Thermocyclops* was also discovered in zooplankton samples collected from seven temporary habitats in northeast Thailand. Therefore, the present study proposes one new species of *Thermocyclops* and provides detailed descriptions and illustrations of both females and males. In addition, a pictorial key to identify *Thermocyclops* species found in Thailand was proposed, the present diversity of the genus was updated, and its distribution in Thailand was discussed.

Materials and methods

Twenty-two samples were qualitatively collected between November 2022 and January 2024 from five rice fields in Suphan Buri Province, Central Thailand, using a plankton net with a 60 µm mesh. They were immediately preserved in 70% ethanol. Environmental variables, including pH, water temperature, conductivity, salinity, total dissolved solids, dissolved oxygen, and chlorophyll, were measured using a calibrated YSI EXO Multiparameter Sonde and YSI EXO Handheld Display 599150. In addition, specimens of the new species collected from six temporary roadside canals and one temporary pond in northeastern Thailand between May and July 2022 were examined.

All adult males and females were sorted using an Olympus SZ40 stereo microscope. Each specimen was dissected and mounted on a slide in glycerin, which was then sealed using nail varnish.

The specimens' morphological characteristics were examined and identified using an Olympus CH2 compound microscope. Drawings of complete and dissected specimens were made by using a camera lucida connected to the microscope. The final versions of the drawings were made using Adobe Illustrator 2024 software (version 28.2). Specimens for digital photographs were taken using an Olympus BX51 compound microscope with an Olympus DP21 digital camera system. Specimens for scanning electron microscopy (SEM) were dehydrated in graded ethanol concentrations and then transferred to pure isoamyl acetate. The specimens were subjected to the critical point drying process, mounted on stubs, coated with gold, and examined with a scanning electron microscope (LEO 1450 VP).

The specimens were identified to the species level in accordance with Ishida (2002), Mirabdullayev et al. (2003), and Hołyńska (2006). The descriptive terminology proposed by Huys and Boxshall (1991) was adopted. The abbreviations used in the text and figures are as follows: **A1** = antennule, **ae** = aesthetasc, **s** = spine, **A2** = antenna, **P1–P6** = first to sixth swimming legs, **ENP1 (2, 3) =** first (second and third) segment of endopod, **EXP1 (2, 3)** = first (second and third) segment of exopod, **G.S.** = genital double-somite.

All materials were deposited in the reference collection of the Princess Maha Chakri Sirindhorn National History Museum, Prince of Songkla University, Songkhla, Thailand.

Results

Systematics

Order CYCLOPOIDA Burmeister, 1834
Family CYCLOPIDAE Rafinesque, 1815

Genus *Thermocyclops* Kiefer, 1927

Type species. *Thermocyclops oithonoides* (Sars G.O., 1863).

***Thermocyclops oryzae* sp. nov.**
https://zoobank.org/384503A9-CDF6-4B54-8E62-1A5098C81F5B

Type locality. Central Thailand, Suphan Buri Province, Bang Pla Ma District, Phai Kong Din Subdistrict; 14°19'41.4"N, 100°15'05.5"E; rice field.

Other localities.

(1) Northeastern Thailand, Bueng Kan Province, So Phisai District, Kham Kaeo Subdistrict, Ban Kham Kaeo; 18°05'32.0"N, 103°31'52.3"E; temporary roadside canal; 3 June 2022; leg. S. Watiroyram.
(2) Northeastern Thailand, Sakon Nakhon Province, at the boundary between Ban Muang-In Plaeng District; 17°48'49.0"N, 103°35'19.8"E; temporary roadside canal; 16 May 2022; leg. S. Watiroyram.
(3) Northeastern Thailand, Sakon Nakon Province, Akat Amnuai District, Samakkhi Phatthana Subdistrict, Ban Nong Sam Kha; 17°19'41.5"N, 103°52'38.2"E; temporary roadside canal; 16 June 2022; leg. S. Watiroyram.
(4) Northeastern Thailand, Udon Thani Province, Nam Som District, Ban Yuak Subdistrict, Ban Champa Thong; 17°43'37.8"N, 102°11'20.4"E; temporary roadside canal; 19 June 2022; leg. S. Watiroyram.
(5) Northeastern Thailand, Udon Thani Province, Kumphawapi District, Nong Wa Subdistrict, Ban Nong Wa; 17°01'33.9"N, 102°58'55.8"E; temporary roadside canal; 18 June 2022; leg. S. Watiroyram.
(6) Northeastern Thailand, Ubon Ratchathani Province, Samrong District, Bon Subdistrict, Ban Kho Bon; 15°04'47.2"N, 104°48'00.9"E; temporary roadside canal; 3 May 2022; leg. S. Watiroyram.
(7) northeast Thailand, Ubon Ratchathani Province, Pho Sai District, Lao Ngam Subdistrict, Ban Pong Pao; 15°45'54.7"N, 105°23'33.0"E; temporary pond; 5 May 2022; leg. S. Watiroyram.

Material examined. ***Holotype*****.** • One adult female, dissected and mounted onto two slides, central Thailand, Suphan Buri Province, Bang Pla Ma District, Phai Kong Din Subdistrict, 27 March 2023, leg. T. Saetang and S. Maiphae; PSUZC-PK2010-01 and PSUZC-PK2010-02.

Allotype**.** • One adult male, dissected and mounted onto two slides, collected from the same locality as the holotype: PSUZC-PK2010-03 and PSUZC-PK2010-04.

Paratype**.** • One adult female, dissected and mounted onto two slides, collected from the same locality as the holotype: PSUZC-PK2010-05 and PSUZC-PK2010-6.

Other specimens examined. Ten adult females, collected from those other seven localities and deposited in the collection of the second author (KK); two adult males, collected from the type locality and deposited in the collection of the fourth author (SM).

Differential diagnosis. *Thermocyclops oryzae* sp. nov. differs from congeneric species in the following characters: female, (i) caudal ramus elongate, about 3.5–4.1 times as long as wide, (ii) innermost terminal seta (VI) 1.1–1.3 times as long as outermost terminal seta (III), (iii) second endopodal segment of antenna with 8 setae, (iv) round projections on the distal margin of intercoxal sclerite of P1–P4 with spinules, (v) intercoxal sclerite of P1–P3 ornamented with one intermittent row of spinules on posterior surface, (vi) intercoxal sclerite of P4 ornamented with spinules arranged in two arcs on the anterior surface, and two transverse rows of spinules on the posterior surface, (vii) medial margin of basis of P4 with serrate lobe, (viii) inner apical spine of third endopodal segment of P4 length about 0.9 times as long as outer spine, (ix) exopodal and endopodal segments of P1–P4 with tiny spinules on posterior surface.

Description of the adult female. ***Body*** (Fig. 1A). Total body length measured from anterior margin of rostrum to posterior margin of caudal rami, ranging from 768–990 µm (mean 894 µm, $n = 3$; 990 µm in holotype).

Prosome (Figs 1A, B, 2A, B, 3C) composed of cephalothorax and three free prosomites (second to fourth pedigerous somites). Surface of prosome pitted. Cephalothorax and second pedigerous somites smooth along posterior margin (Figs 2A, B, 3C); third and fourth pedigerous somites coarsely serrated along posterior margin (Figs 1B, 2B arrow).

Urosome (Figs 1C–E, 2C, D, 3D, E, G, 10A) composed of fifth pedigerous somite, genital double-somite, two free urosomites, and anal somite with caudal rami. Fifth pedigerous somite ornamented with two dorsal sensilla and with dense pattern of tiny spinules on dorsal and lateral surface. Genital double-somite about as long as wide, with two dorsal sensilla; dorsal and ventral surfaces with irregular but mostly transverse short striae; coarsely serrated hyaline frill along posterior margin. Lateral arms of seminal receptacle slightly curved posteriorly. Two free urosomites with irregular but mostly transverse short striae dorsally and ventrally and with coarsely serrated hyaline frill along posterior margin. Anal somite with two dorsal sensilla at base of anal operculum; with spinules present along posterior margin on ventral surface; dorsal surface ornamented with tiny spinules; ventral surface unornamented. Caudal rami (Figs 1C–E, 2D, 3F). cylindrical, parallel, about 3.5–4.1 times as long as wide (mean 3.8, $n = 13$; 4.1 in holotype); inner margin without hairs; dorsal and ventral surfaces with dense pattern of tiny spinules. Each ramus with six setae: innermost terminal seta (VI) 1.1–1.3 times as long as outermost terminal seta (III).

Labrum (Figs 4A, 6C) trapezoidal, with nine teeth between two blunt lateral corners, posterior surface ornamented with two rows of long hairs.

A1 (Figs 3A, 4B, C) 17-segmented. Armature formula (number of segment-[number of setae + aesthetasc (ae) + spine (s)]) of each segment as follows: 1-[8], 2-[4], 3-[2], 4-[6], 5-[4], 6-[1+s], 7-[2], 8-[1], 9-[1], 10-[0], 11-[1], 12-[1+ae], 13-[0], 14-[1], 15-[2], 16-[2+ae], 17-[7+ae]. Last two antennular segments bearing hyaline membrane on ventral surface (Fig. 3A).

A2 (Figs 3B, 4D, E, 6A, B) composed of coxa, basis, and three-segmented endopod. Coxa rectangular, unarmed and unornamented. Basis cylindrical, with one outer bipinnate seta and two inner smooth setae along distal corner; anterior surface (Fig. 4D) ornamented with one oblique row of inner spinules along proximal part, one longitudinal row of inner spinules along middle part; posterior surface (Fig. 4E) ornamented with one oblique row of outer and inner spinules along proximal part, one longitudinal row of outer spinules in middle part, field of tiny spinules near base of inner setae, and one longitudinal

row of tiny spinules along inner margin. ENP1 with one inner smooth seta. ENP2 with 7–8 inner smooth setae. ENP3 with seven apical setae. Posterior surface of each endopodal segment ornamented with one longitudinal row of outer spinules.

Mandible (Fig. 5A, B, F) composed of coxa and palp. Coxal gnathobase with eleven chitinized teeth and two pinnate setae; anterior surface ornamented with one row of three spinules. Palp reduced, with one short smooth seta and two plumose setae.

Maxillule (Figs 5C, 6D, F) composed of praecoxa and two-segmented palp, representing one-segmented coxobasis and one-segmented endopod. Praecoxal arthrite with three smooth and one pinnate apical spine. Praecoxa with seven inner elements; one short naked proximalmost seta, one sub-proximal plumose seta, three middle smooth setae,

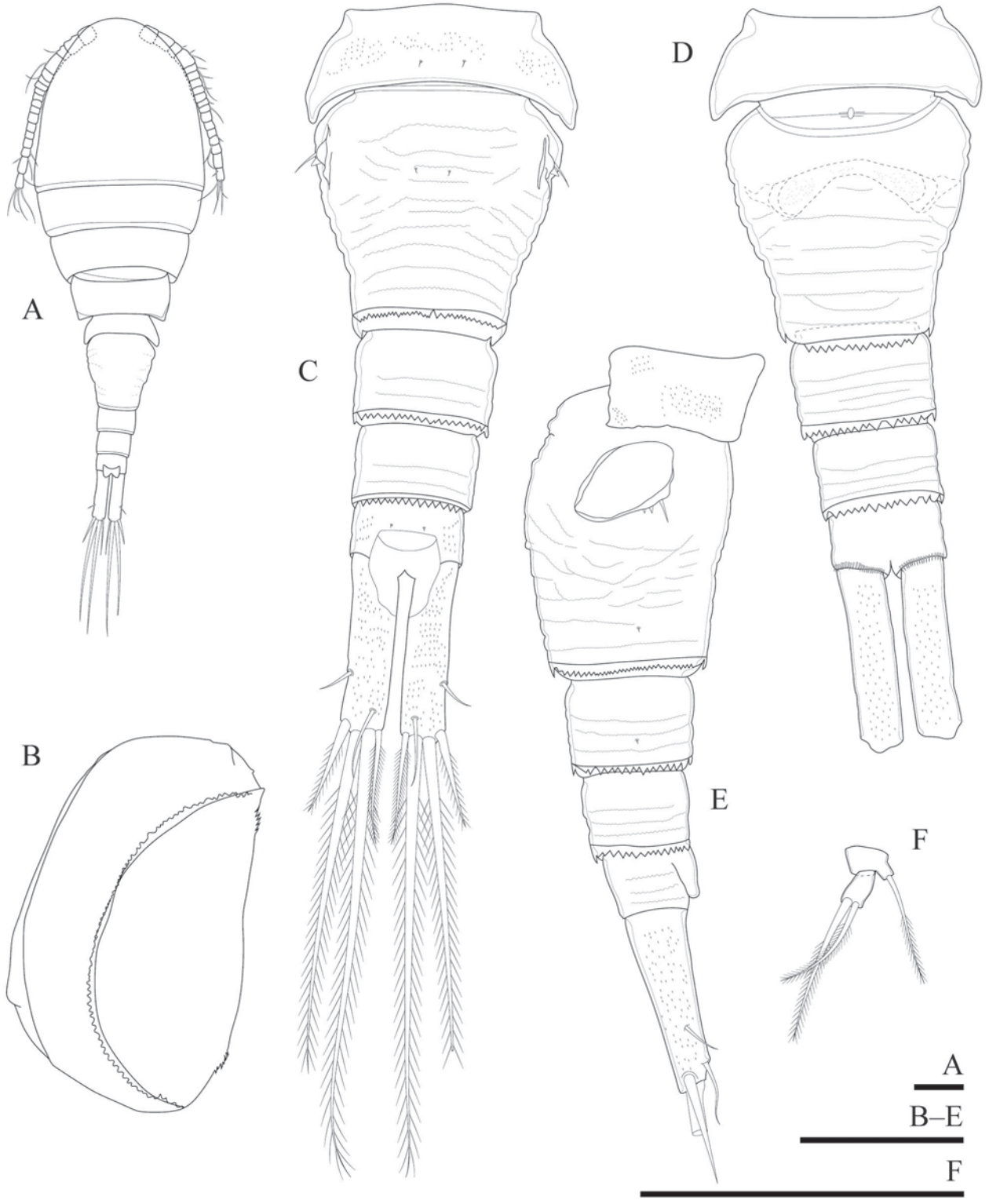

Figure 1. *Thermocyclops oryzae* sp. nov., female holotype. **A.** Habitus, dorsal view; **B.** Fourth pedigerous somite; **C.** Urosome, dorsal view; **D.** Urosome, ventral view; **E.** Urosome, lateral view; **F.** P5. Scale bars: 100 µm.

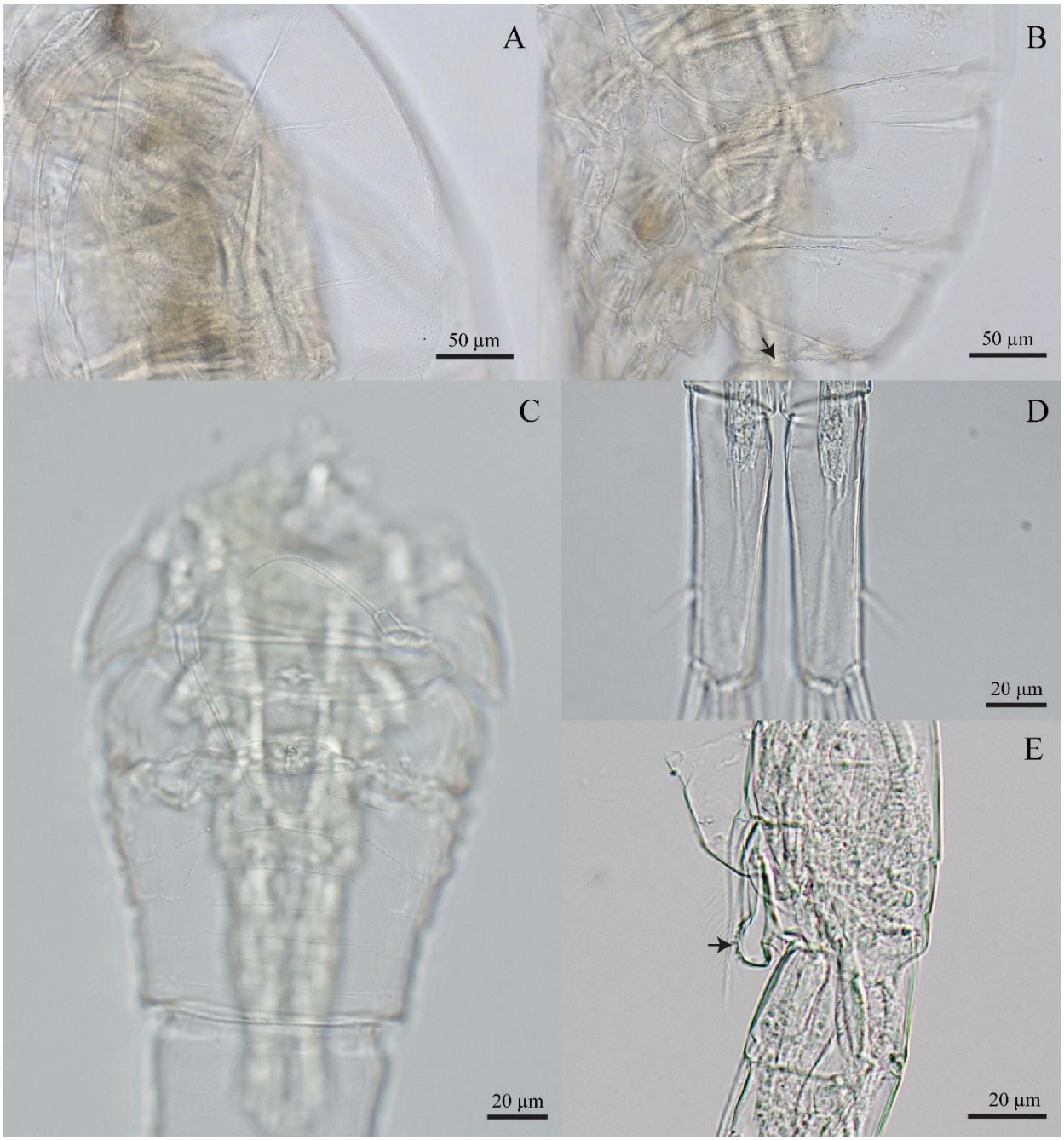

Figure 2. Digital photographs. *Thermocyclops oryzae* sp. nov., female, collected from a type locality. **A.** Cephalothorax, lateral view; **B.** Second to fourth pedigerous somites, lateral view (arrow indicates coarsely serrated posterior margin); **C.** Genital double-somite and P5, ventral view; **D.** Caudal rami, ventral view; **E.** P4 basis, lateral view (arrow indicates serrate lobe).

two distal smooth setae; group of tiny spinules present at base of short naked proximalmost seta. Coxobasis with one spiniform and two smooth setae apically; anterior surface ornamented with tiny spinules. Exopod reduced into one smooth seta near proximal part of coxobasis. Endopod with three apical smooth setae.

Maxilla (Figs 5D, 6E) composed of praecoxa, coxa, basis, and two-segmented endopod. Praecoxal endite with two apical pinnate setae. Coxa with two endites; proximal endite with one apical plumose seta; distal endite with two apical pinnate setae. Basis with claw-like endite and one pinnate seta. ENP1 with two pinnate setae. ENP2 with one pinnate and two smooth setae.

Maxilliped (Fig. 5E) composed of syncoxa, basis, and two-segmented endopod. Syncoxa cylindrical, with three inner pinnate setae; anterior surface ornamented with one group of spinules in middle part of segment. Basis with two inner pinnate setae; long spinules present on medial margin and anterior surface; posterior surface ornamented with two rows of outer spinules. ENP1 with one inner pinnate seta; anterior surface ornamented with one row of inner spinules. ENP2 with one inner pinnate and two inner smooth setae.

P1–**P4** (Figs 2E, 7A–D, 8A–D, 9A–G) composed of intercoxal sclerite, coxa, basis, three-segmented exopod, and three-segmented endopod. Armature formula of P1–P4 as in Table 1.

Table 1. Armature formula of P1–P4 in *Thermocyclops oryzae* sp. nov. (Arabic numerals representing setae and Roman numerals representing spine from outer-inner or outer-apical-inner margins).

Swimming legs	Coxa	Basis	EXP			ENP		
			1	2	3	1	2	3
P1	0–1	1–I	I–1	I–1	II, 2, 2	0–1	0–2	1, I1, 3
P2	0–1	1–0	I–1	I–1	II, I1, 3	0–1	0–2	1, I1, 3
P3	0–1	1–0	I–1	I–1	II, I1, 3	0–1	0–2	1, I1, 3
P4	0–1	1–0	I–1	I–1	II, I1, 3	0–1	0–2	1, II, 2

P1 (Figs 7A, B, 9A, 10B, D). Intercoxal sclerite subquadrate; distal margin with round projection bearing 6-7 spinules; anterior surface unornamented; posterior surface ornamented with one intermittent row of spinules. Coxa with one inner plumose seta; anterior surface ornamented with one longitudinal row of hair-like spinules laterally and three rows of tiny spinules along distal margin; posterior surface ornamented with one oblique row of hair-like spinules near the lateral margin.

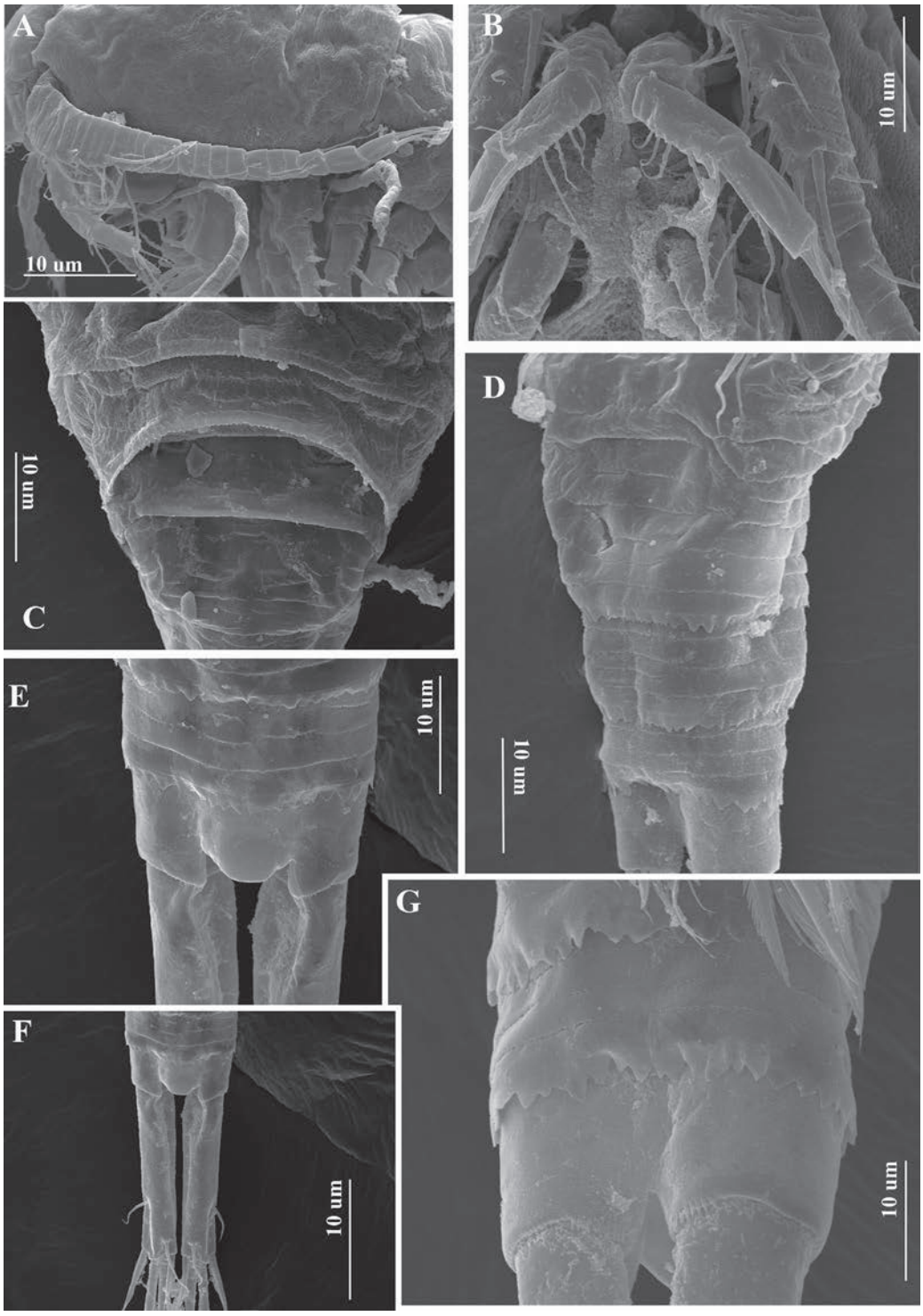

Figure 3. Scanning electron micrographs. *Thermocyclops oryzae* sp. nov., female, was collected from Kumphawapi District, Udon Thani Province, northeastern Thailand. **A.** Antennule and cephalothorax; **B.** Endopodal segments of antenna; **C.** Free prosomites, dorsal view; **D.** Urosomites lateroventral view; **E.** Anal somite, dorsal view; **F.** Caudal rami, dorsal view; **G.** Anal somite, ventral view.

Basis with one outer plumose seta and one inner pinnate spine, distal tip of inner spine reaching middle of ENP2; anterior surface ornamented with two rows of tiny spinules between bases of exopod and endopod, one row of spinules at base of endopod, one row of spinules at base of inner spine, one row of inner tiny spinules along proximal margin of segment, and long setules on median margin of basis. EXP1 with one pinnate outer spine and one inner plumose seta; anterior surface ornamented with one longitudinal row of outer spinules and one longitudinal row of inner setules; one row of tiny spinules at base of outer spine; and one row of spinules along distal margin of segment; posterior surface ornamented with dense pattern of tiny spinules. EXP2 with one pinnate outer spine and one inner plumose seta; anterior surface ornamented as in EXP1. EXP3 with two pinnate outer spines,

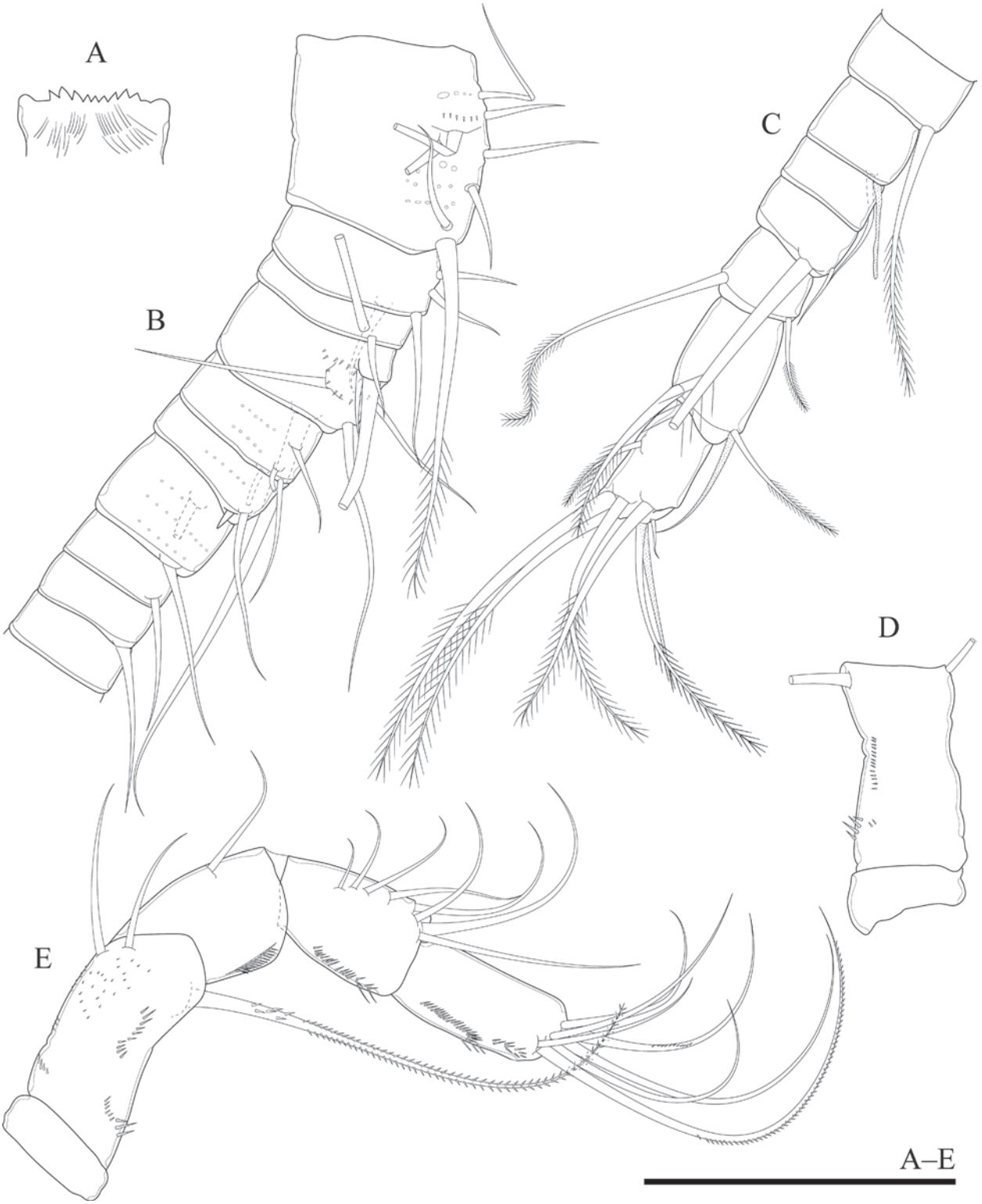

Figure 4. *Thermocyclops oryzae* sp. nov., female holotype. **A.** Labrum; **B.** Antennule, segments 1–10; **C.** Antennule, segments 11–17; **D.** Coxa and basis of antenna, anterior surface; **E.** Antenna, posterior surface. Scale bar: 100 µm.

two apical plumose setae, and two inner plumose setae; anterior surface ornamented as in EXP1 except one row of spinules along distal margin of segment. ENP1 with one inner plumose seta; anterior surface ornamented with one longitudinal row of outer setules and one row of spinules along distal margin of segment; posterior surface ornamented with dense pattern of tiny spinules. ENP2 two inner plumose setae; anterior surface ornamented as in ENP1. ENP3 with one outer plumose seta, two apical elements (outer element: one pinnate spine; inner element: one plumose seta), and three inner plumose setae; anterior surface ornamented as in ENP1.

P2 (Figs 7C, D, 9B, 10C). Intercoxal sclerite subquadrate; distal margin with round projection bearing 4–5 spinules; anterior surface unornamented; posterior surface ornamented with one intermittent row of spinules. Coxa with one inner plumose seta; intermittent longitudinal row of hair-like spinules on lateral margin; two rows of tiny spinules in proximal part; and two rows of tiny spinules along distal margin. Basis with one outer plumose seta; anterior surface ornamented with one row of tiny spinules near outer seta; one row of tiny spinules at base of exopod; one row of tiny spinules between bases of exopod and endopod; and one intermittent row of spinules near base of endopod; posterior surface ornamented with one row of spinules in distal part of medial expansion. EXP1 and EXP2, each with one pinnate outer spine and one inner plumose seta; anterior surface ornamented with one longitudinal row of outer spinules and one longitudinal row of inner setules; one row of tiny spinules at base of outer spine; and one row of spinules along distal margin of segment; posterior surface ornamented with one row of spinules along distal margin of segment, and dense pattern of tiny spinules. EXP3 with two pinnate outer spines, two apical elements (outer element: one pinnate spine; inner element:

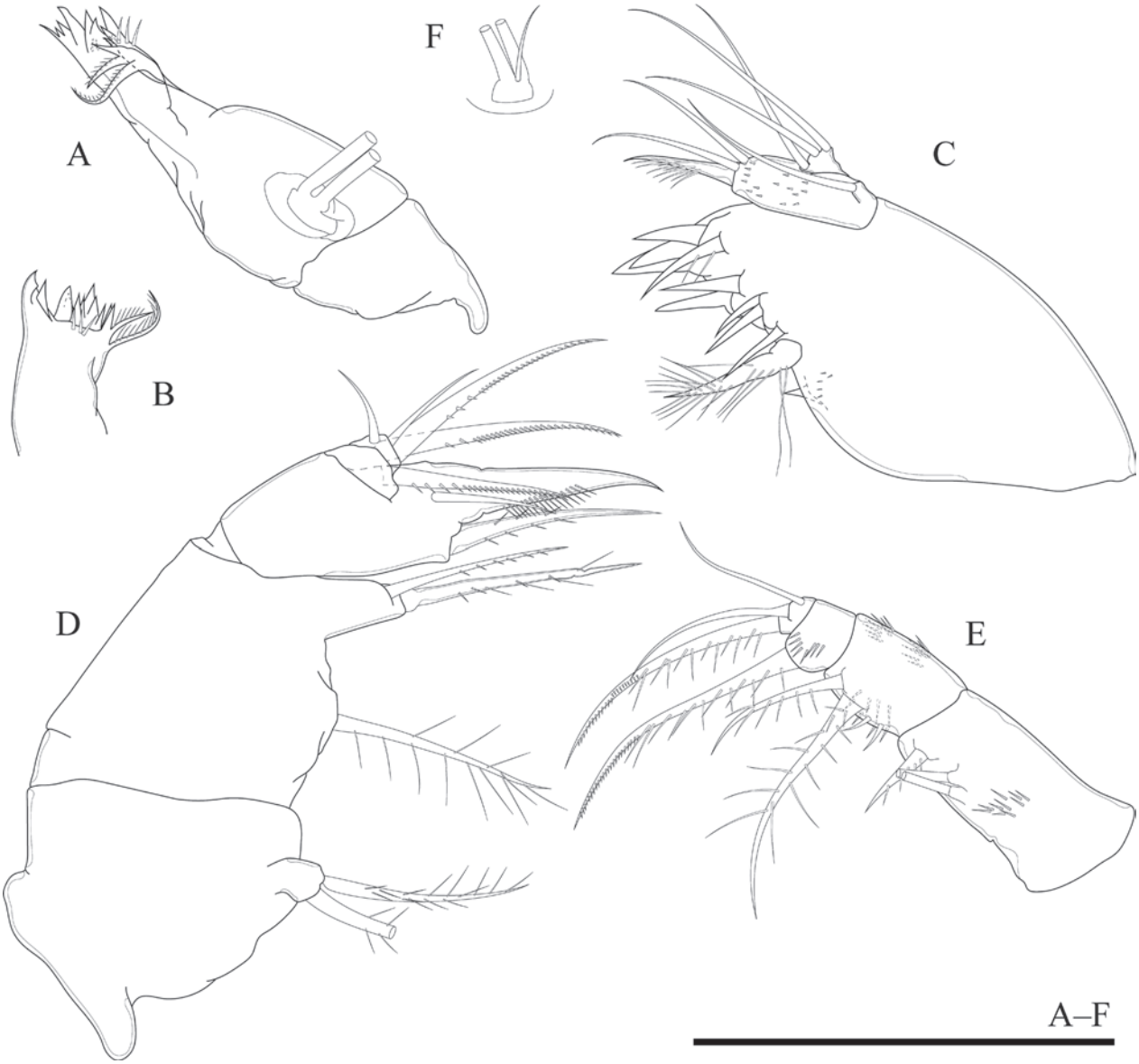

Figure 5. *Thermocyclops oryzae* sp. nov., female holotype. **A.** Mandible; **B.** Cutting edge of mandibular gnathobase; **C.** Maxillule; **D.** Maxilla; **E.** Maxilliped; **F.** Mandibular palp (**F.** Shows the female paratype; other drawings show the holotype). Scale bar: 100 µm.

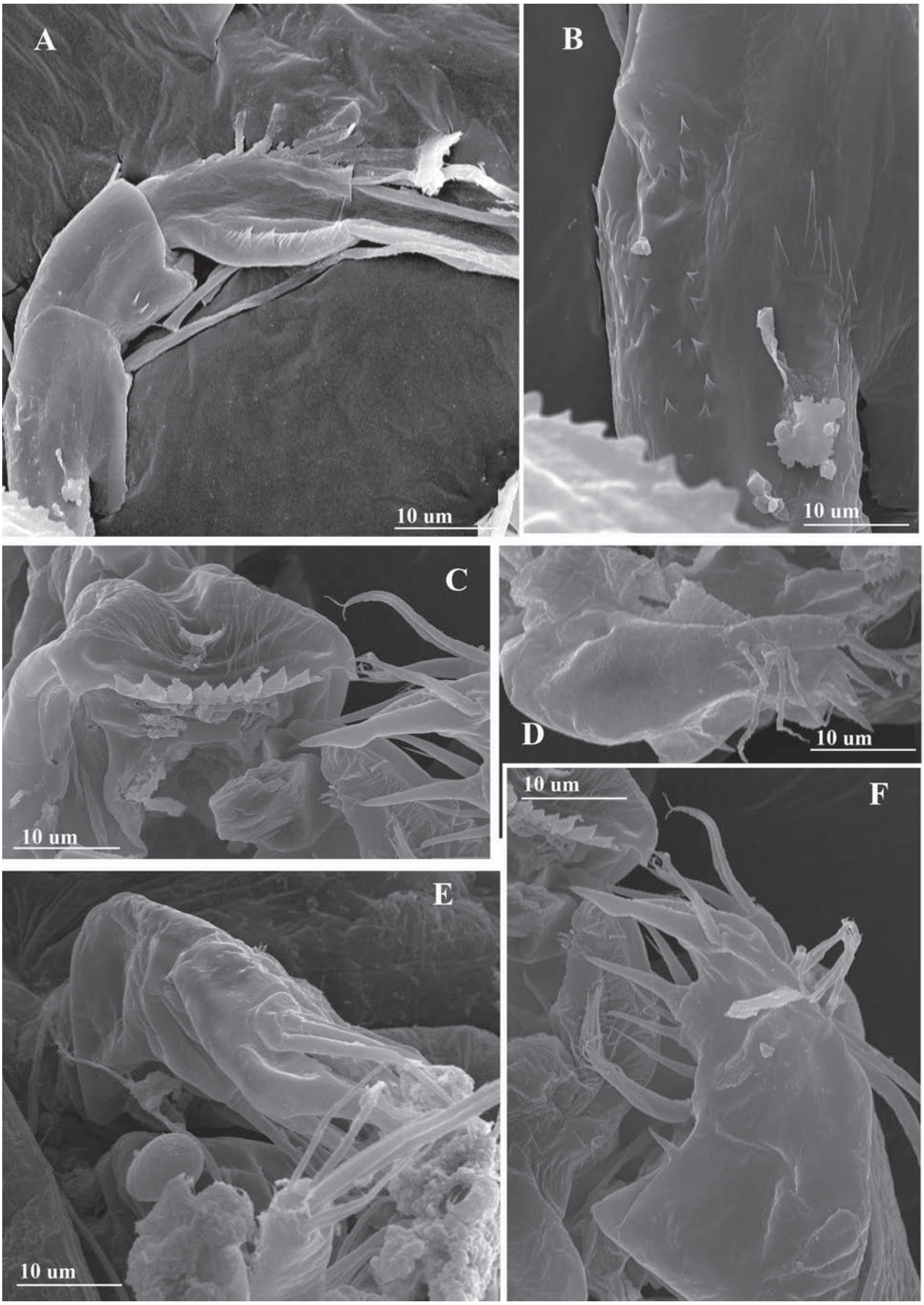

Figure 6. Scanning electron micrographs. *Thermocyclops oryzae* sp. nov., female, was collected from Kumphawapi District, Udon Thani Province, northeastern Thailand. **A.** Basis and endopodal segments of the antenna, posterior surface; **B.** Antennal basis, posterior surface; **C.** Labrum; **D.** Maxillule, anterior surface; **E.** Maxilla; **F.** Maxillule, posterior surface.

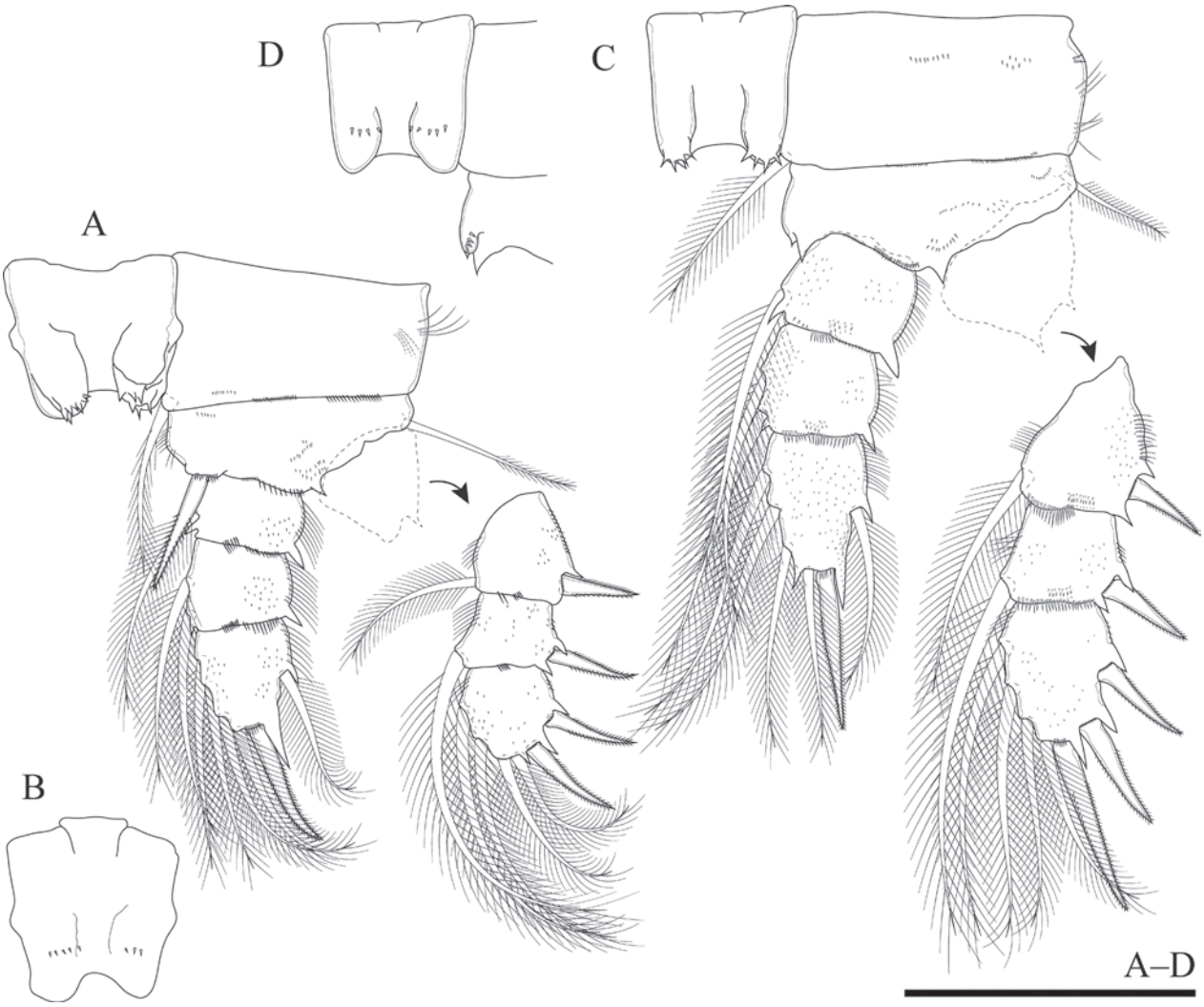

Figure 7. *Thermocyclops oryzae* sp. nov., female holotype. **A.** P1, anterior surface; **B.** Intercoxal sclerite of P1, posterior surface; **C.** P2, anterior surface; **D.** Intercoxal sclerite of P2, posterior surface. The dense pattern of tiny spinules shown in **A, C** is on the posterior surface. Scale bar: 100 µm.

one plumose seta), three inner plumose setae; posterior surface ornamented as in EXP1. ENP1 with one inner plumose seta; anterior surface ornamented with one longitudinal row of outer setules and one row of spinules along distal margin; posterior surface ornamented with one row of spinules along distal margin and dense pattern of tiny spinules. ENP2 two inner plumose setae; anterior and posterior surfaces ornamented as in ENP1. ENP3 with one outer plumose seta, two apical elements (outer element: one pinnate spine; inner element: one plumose seta), three inner plumose setae; anterior surface ornamented with one row of spinules along distal margin; posterior surface ornamented as in ENP1.

P3 (Figs 8A, B, 9C, 10E). Intercoxal sclerite subquadrate; distal margin with round projection bearing 5–6 spinules; anterior surface unornamented; posterior surface ornamented with one intermittent row of spinules. Coxa with one inner plumose seta; anterior surface ornamented with tiny spinules on lateral margin, three rows of tiny spinules along distal margin, and one row of tiny spinules near base of inner seta; posterior surface ornamented with one oblique row of hair-like spinules close to outer margin. Basis with one outer plumose seta. Anterior surface of basis ornamented with one row of tiny spinules between bases of exopod and endopod, one intermittent row of spinules near base of endopod, three rows of tiny spinules close to inner and distal parts of medial expansion (Fig. 8A). Both EXP1–3 and ENP1–3 as in P2.

P4 (Figs 2E, 8C, D, 9D–G, 10F, G). Intercoxal sclerite subquadrate, distal margin with round projection bearing 6 spinules; anterior surface ornamented with one intermittent row of spinules; posterior surface ornamented with two intermittent rows of spinules. Coxa with one inner plumose seta; anterior surface ornamented with one oblique row of tiny spinules in middle of the segment and two rows of tiny spinules along distal margin; posterior surface ornamented with one oblique row of tiny spinules in subproximal part, two oblique rows of spinules close to outer margin, one row of spinules along subdistal margin. Basis with one outer plumose seta; anterior surface ornamented with one row of spinules near base of endopod, one row of inner spinules along subproximal part, and one row of inner

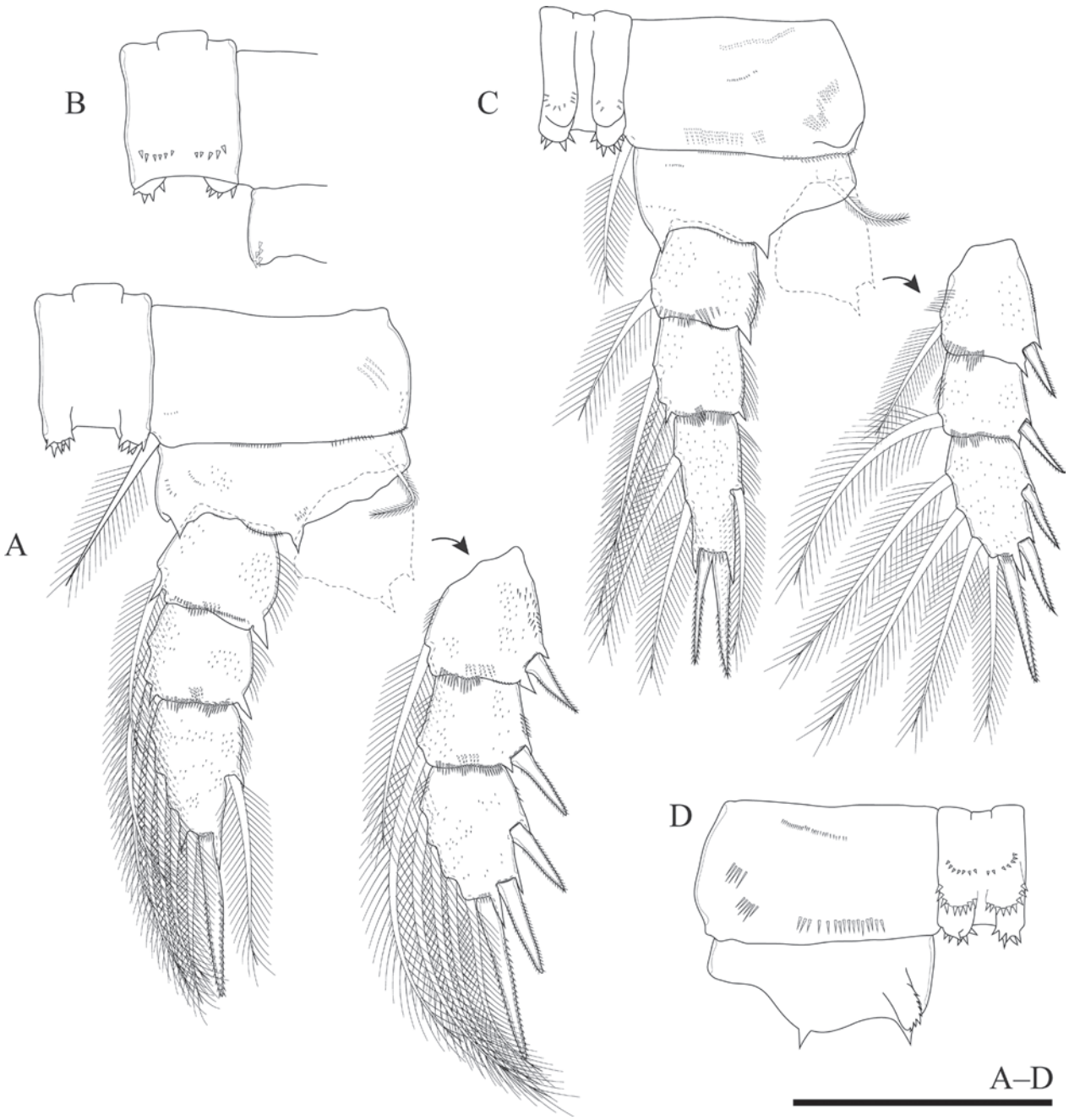

Figure 8. *Thermocyclops oryzae* sp. nov., female holotype. **A.** P3, anterior surface; **B.** Intercoxal sclerite of P3, posterior surface; **C.** P4, anterior surface; **D.** Protopodite of P4, posterior surface. The dense pattern of tiny spinules shown in **A.** and **C.** is on the posterior surface. Scale bar: 100 µm.

spinules along subdistal part; posterior surface ornamented with one distal serrate lobe close to inner margin. EXP1 and EXP2 as in P2, except posterior surface unornamented along distal margin. EXP3 as in P2, except anterior surface without longitudinal row of inner setules. ENP1 and ENP2 as in P2. ENP3 with one outer plumose seta, two apical spines, and two inner plumose setae; inner apical spine about 0.9 times as long as the outer apical spine.

P5 (Figs 1F, 10A) composed of coxobasis and one-segmented exopod. Coxobasis with one outer seta. Exopod with one apical outer smooth seta and one subapical inner pinnate spine; length of the inner apical spine about 1.3 times as long as the outer apical seta.

P6 (Fig. 1C, E) reduced to simple cuticular plate inserted latero-dorsally on genital double-somite, with two subequal smooth spines and one smooth seta; seta about five times as long as spines; surface unornamented.

Description of the adult male. ***Body*** (Fig. 11A). Total body length measured from anterior margin of rostrum to posterior margin of caudal rami, ranging from 686–789 µm (mean 748 µm, $n = 3$, 789 µm in allotype).

Urosome (Figs 11B–D, 12A–C) composed of fifth pedigerous somite, genital somite, three free urosomites, and anal somite with caudal rami. Fifth pedigerous somite ornamented with two dorsal sensilla. Genital somite about 0.8 times as long as wide, with two dorsal sensilla, anterior and posterior surfaces with irregular but mostly

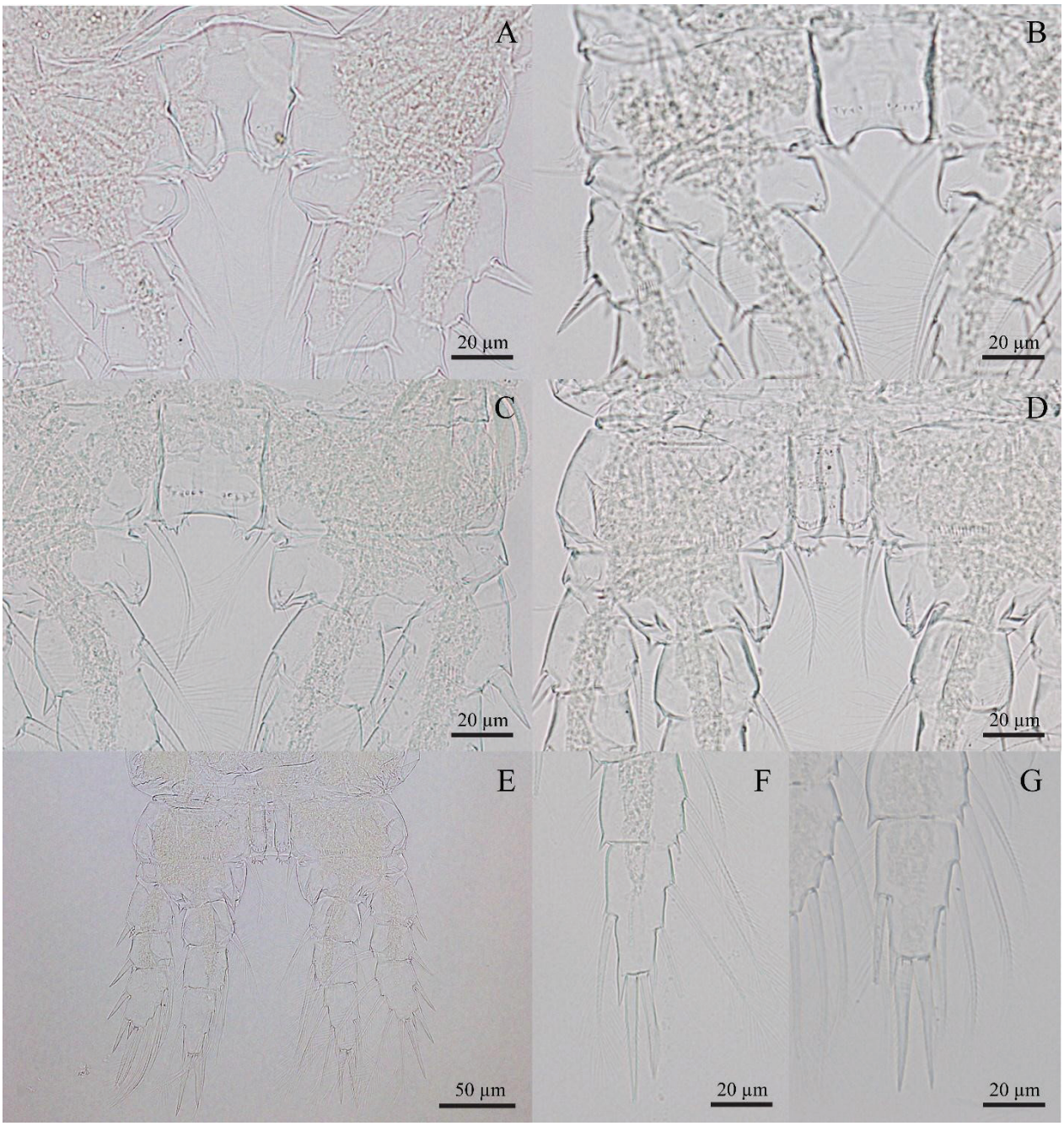

Figure 9. Digital photographs. *Thermocyclops oryzae* sp. nov., female, collected from a type locality. **A.** P1, posterior surface; **B.** P2, posterior surface; **C.** P3, posterior surface; **D, E.** P4, posterior surface; **F, G.** Apical spines of P4 ENP3.

transverse short striae, and with coarsely serrated hyaline frill along posterior margin. Succeeding two urosomites with irregular but mostly transverse striae on both dorsal and ventral surfaces and with coarsely serrated hyaline frill along posterior margin. The fifth urosomite with coarsely serrated hyaline frill along posterior margin. Anal somite with two dorsal sensilla at base of anal operculum; and posterior margin with spinules on both ventral and dorsal surfaces. Caudal rami cylindrical, parallel, about 3.7–3.9 times as long as wide; inner margin without hairs; outer margin ornamented with one transverse row of spinules inserted at distance of 1/3 ramus length measured from anterior margin and at base of outermost terminal seta (III) (Figs 11B–D, 12B, C, arrows). Each ramus with six setae: innermost terminal seta (VI) 1.4–1.5 times as long as outermost terminal seta (III).

A1 (Fig. 13A–D) 17-segmented. Armature formula (number of segment-[number of setae + aesthetasc (ae) + spine (s)]) of each segment as follows: 1-[8+3ae], 2-[4], 3-[2], 4-[1], 5-[1], 6-[2], 7-[1], 8-[2], 9-[1+s], 10-[2], 11-[2], 12-[2], 13-[1+ae], 14-[2+ 1 plate-like modified seta], 15-[1 + 2 plate-like modified setae], 16-[4], 17-[7+ae].

P6 (Fig. 11D) inserted latero-dorsally on genital somite with three smooth setae, length of the outermost seta about 1.4 times as long as the innermost seta, and middle seta about 0.6 times as long as the innermost seta; P6 flap ornamented with two rows of spinules.

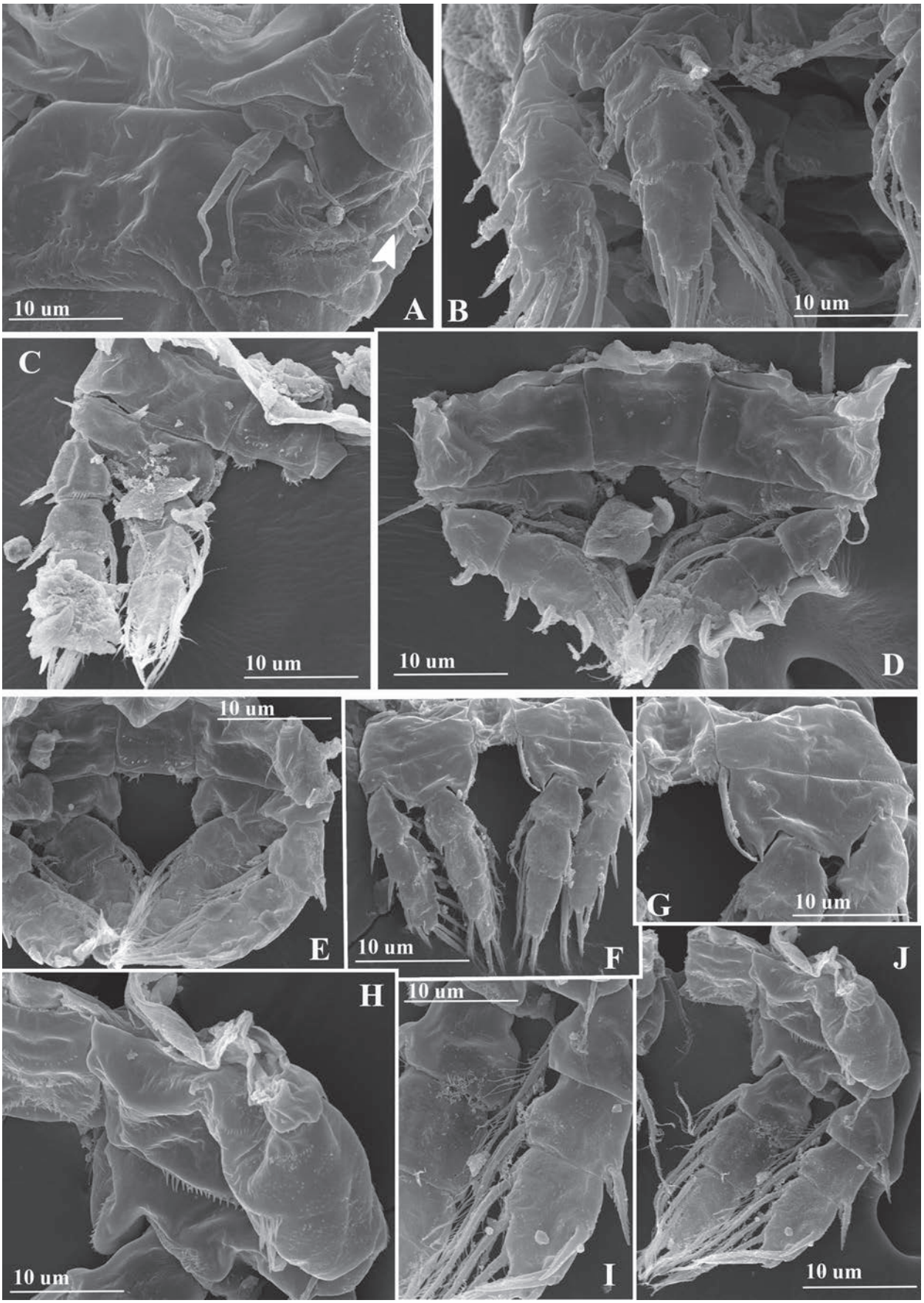

Figure 10. Scanning electron micrographs. *Thermocyclops oryzae* sp. nov., female, was collected from Kumphawapi District, Udon Thani Province, northeastern Thailand. **A.** P5 and pediger 5 (arrow indicates P6); **B.** P1, anterior surface; **C.** P2, posterior surface; **D.** P1, posterior surface; **E.** P3, posterior surface; **F.** P4, anterior surface; **G.** Coxa and basis of P4, anterior surface; **H.** Coxa and basis of P4, posterior surface; **I.** EXP and ENP of P4, posterior surface; **J.** P4, posterior surface.

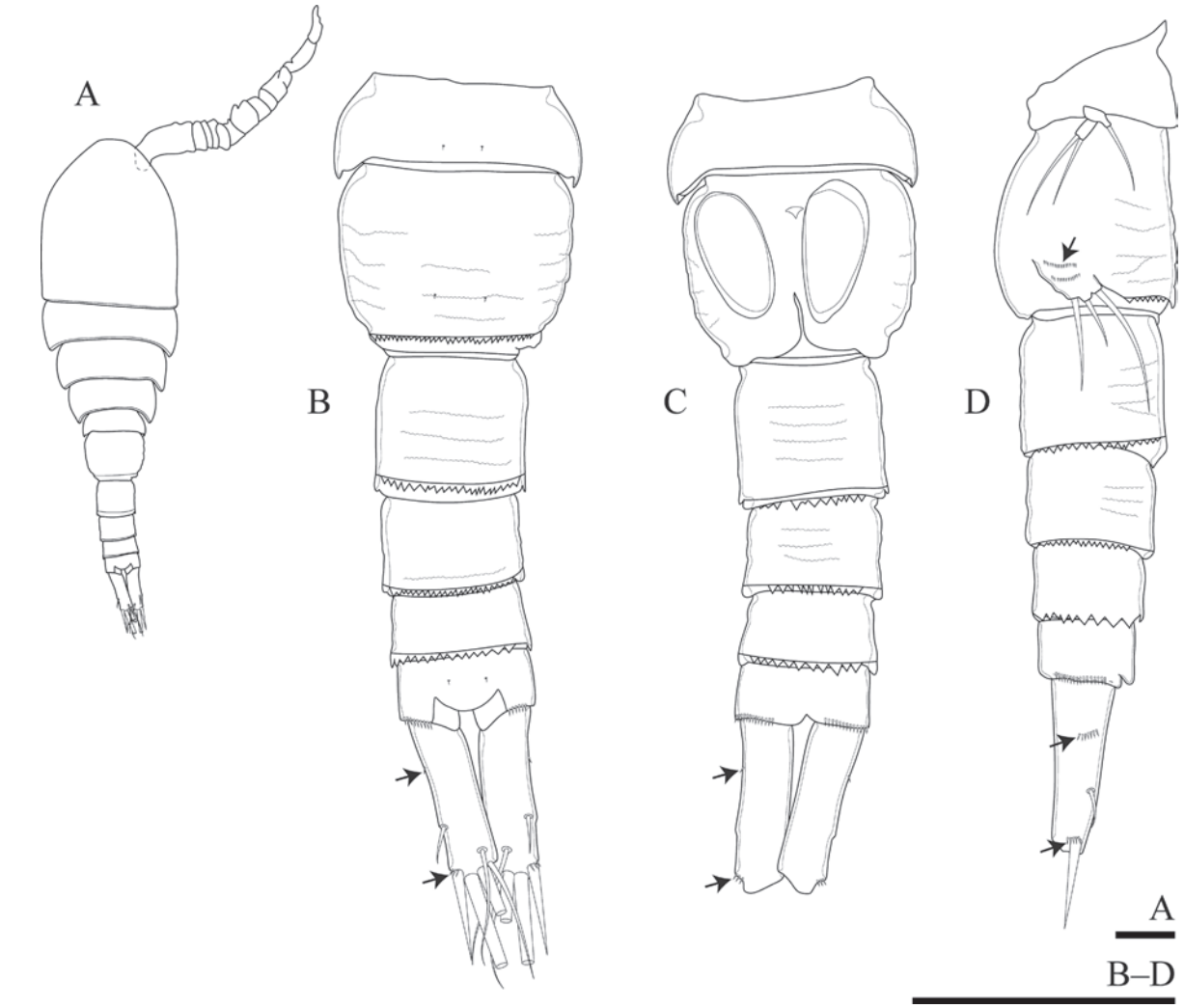

Figure 11. *Thermocyclops oryzae* sp. nov., male allotype. **A.** Habitus, dorsal surface; **B.** Urosome, dorsal surface; **C.** Urosome, ventral surface; **D.** Urosome, lateral surface (arrows indicate rows of spinules on the caudal ramus). Scale bars: 100 µm.

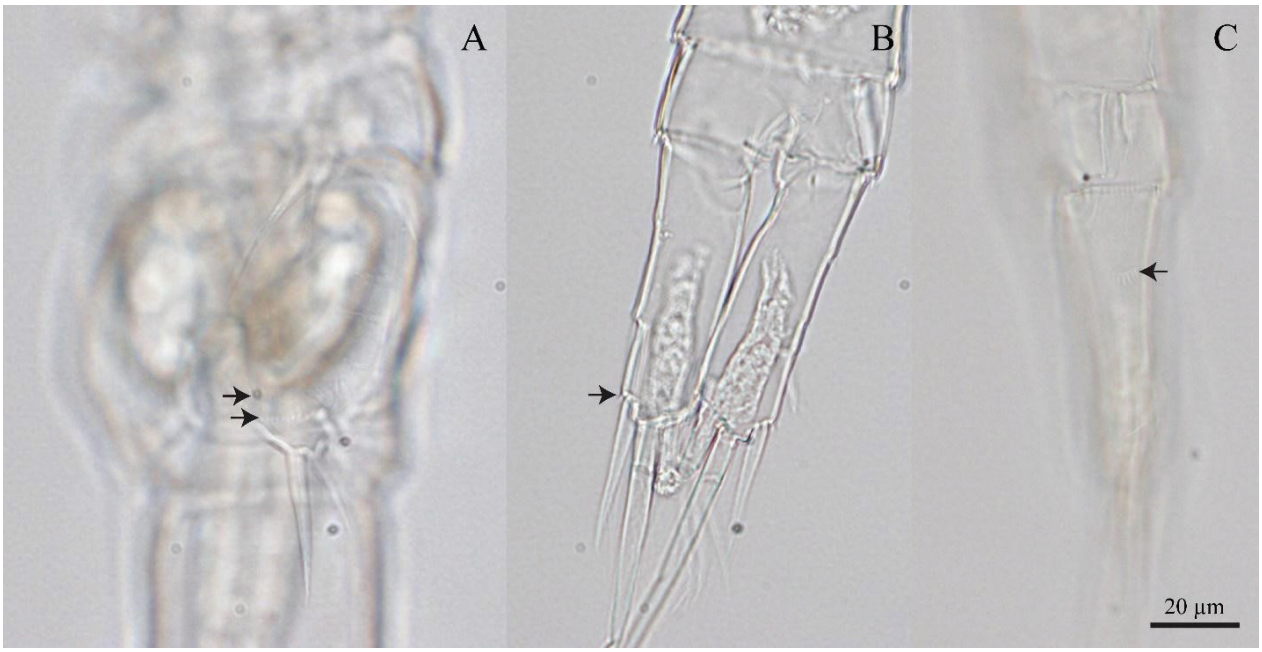

Figure 12. Digital photographs. *Thermocyclops oryzae* sp. nov., male allotype. **A.** P6, lateral surface (arrows indicate two rows of spinules); **B.** Caudal rami, ventral surface (arrow indicates a row of spinules); **C.** Caudal rami, lateral surface (arrow indicates a row of spinules).

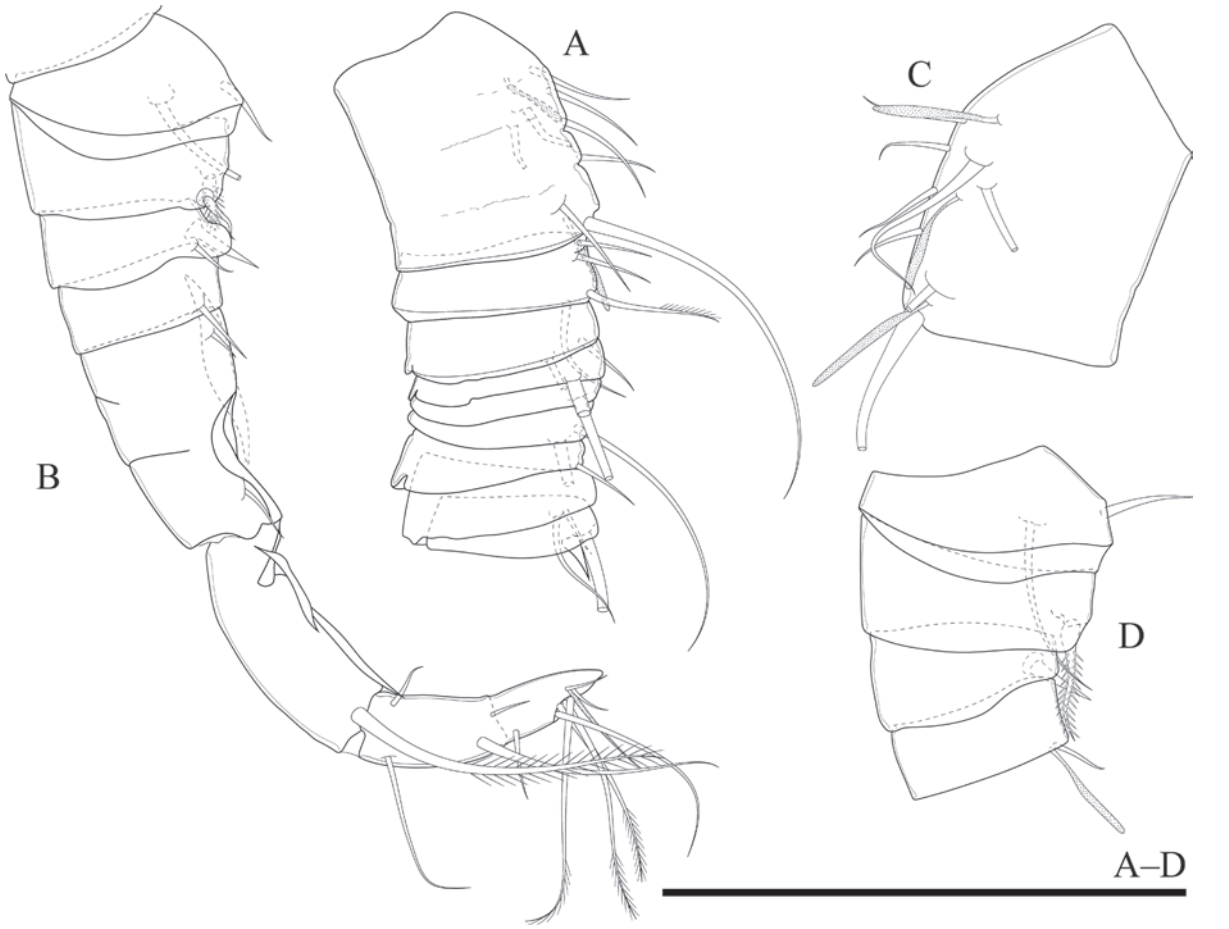

Figure 13. *Thermocyclops oryzae* sp. nov., **A–B** male allotype; **C–D** other specimens collected from type locality. **A.** Antennule, segments 1–9; **B.** Antennule, segments 10–17; **C.** Antennule, segments 1; **D.** Antennule, segments 10–13. Scale bar: 100 µm.

Prosome, A2, labrum, mandible, maxillule, maxilla, maxilliped, P1–P4 (not shown), and P5 (Fig. 11D) same as female.

Variability. Morphological variabilities in female specimens were observed in i) intercoxal sclerite of P1 of specimens from northeast Thailand is naked on the posterior surface ($n = 7$) (Fig. 10D), but one intermittent row of spinules present in specimens from central Thailand ($n = 5$) (Fig. 7B); ii) the inner apical spine of the third endopodal segment of P4 shorter or as long as the outer apical spine (Figs 8C, 9E–G, 10F); and iii) P6 of one specimen from a temporary pond in northeast Thailand has one short spine and one slender seta instead of three elements (Fig. 10A, arrow).

Etymology. The specific name '*oryzae*', which means rice, is derived from the habitat type ("rice") of the type locality".

Co-occurring species. In our samples, the new taxon co-occurred with *Cryptocyclops* sp., *Mesocyclops affinis* Van de Velde, 1987; *M. aspericornis* (Daday, 1906); *M. ogunnus* Onabamiro 1957; *M. thermocyclopoides* Harada, 1931; *Microcyclops* sp., *Thermocyclops crassus* (Fischer, 1853); *T. decipiens* (Kiefer, 1929); *T. operculifer* (Kiefer, 1930); *T. rylovi* (Smirnov, 1928); *T. vermifer* Lindberg, 1935; and *T. wolterecki* Kiefer, 1938.

Distribution and ecology. *Thermocyclops oryzae* sp. nov. is widespread in Thailand, both in the west and northeast. However, it has only been recorded in temporary habitats, including rice fields, temporary roadside canals, and temporary ponds. It was recorded in four out of 22 samples collected from five rice fields in Suphan Buri province during three planting seasons between November 2022 and January 2024. The environmental parameters measured in the studied rice fields were as follows: water temperature ranged from 31.8–36.1 °C, conductivity ranged from 1176.5–1449.9 µs cm-1, salinity ranged from 0.21–0.58 psu, total dissolved solids ranged from 77–676 mg L-1, dissolved oxygen ranged from 7.54–7.54 mg L-1, pH 7.0–7.3, chlorophyll a ranged from 5.31–17.39 µs L-1, and water depth was 10 cm with a substrate of mud. In addition, the temporary canals and temporary pond in the northeast, where this species was found, were not vegetated, but the grass and morning glory (*Ipomoea*) grew near the water's edge.

Pictorial keys to *Thermocyclops* species found in Thailand

The pictorial key of the *Thermocyclops* species found in Thailand is presented in Fig. 14 to facilitate easy and quick identification.

Species diversity and distribution of *Thermocyclops* in Thai water bodies

In Thailand, *Thermocyclops* have been found in various types of freshwater habitats, including rice fields, canals, lakes, and swamps (Sanoamuang 1999; Wongrat and Pipatcharoenchai 2003; Alekseev and Sanoamuang 2006; Proongkiat 2006; Wansuang and Sanoamuang 2006; Chittapun et al. 2009; Koompoot 2010; Watiroyram 2012; Boonyanusith 2013; Karanovic et al. 2017; Maiphae et al. 2023; Soe and Sanoamuang 2023). A total of 14 species have been recorded in Thailand to

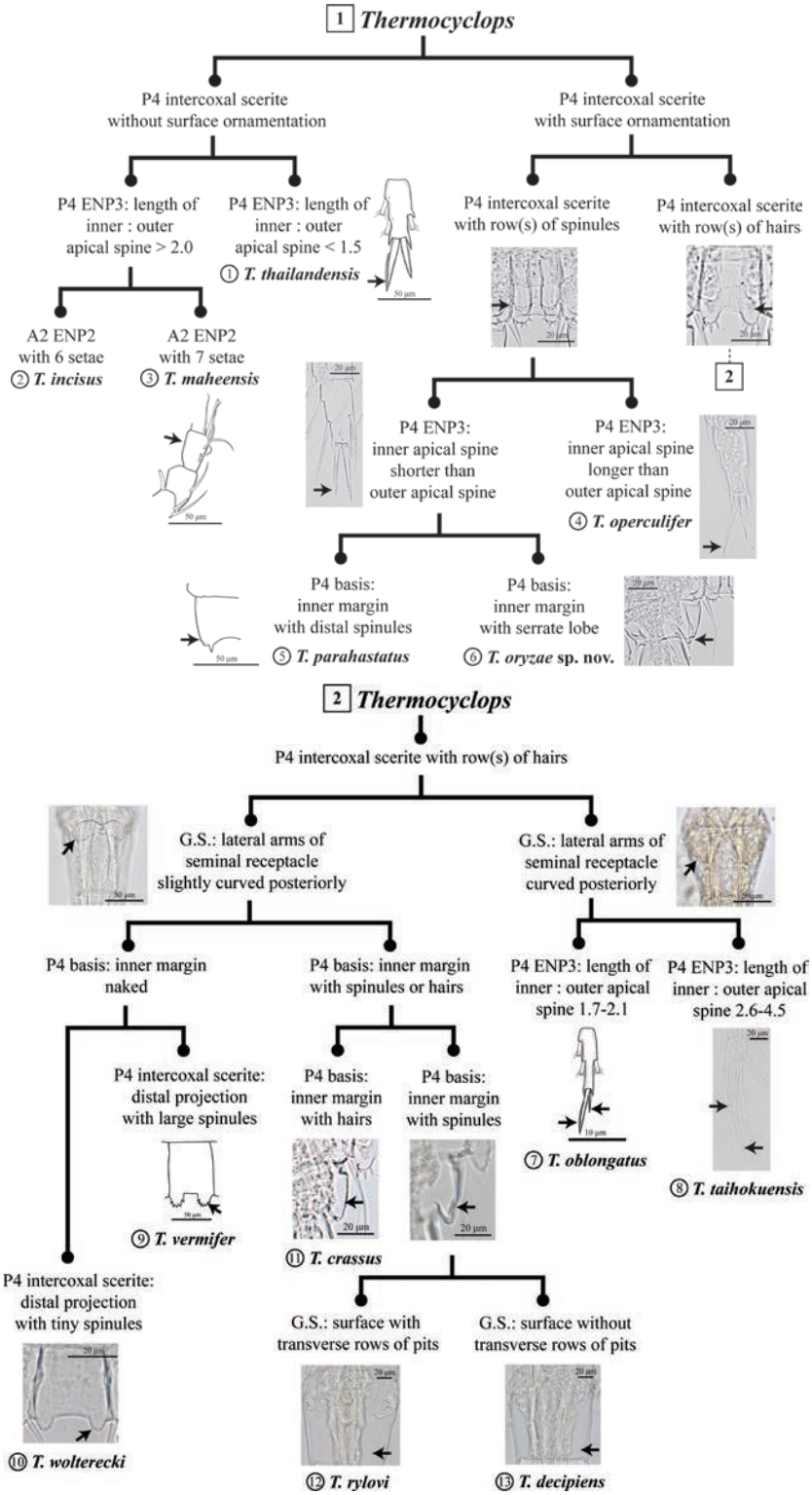

Figure 14. Pictorial key of the adult female of *Thermocyclops* species found in Thailand (*T.* cf. *orientalis* is not included in this figure because its species status needs to be further confirmed; pictures of *T. parahastatus* and *T. thailandensis* were modified from Karanovic et al. 2017; pictures of *T. maheensis* and *T. vermifer* were modified from Chaicharoen et al. 2011; pictures of *T. oblongatus* were modified from Baribwegure et al. 2001).

date: *T. crassus*; *T. decipiens*; *T. incisus* (Kiefer 1932); *T. maheensis* (Lindberg 1941); *T. oblongatus* (G.O. Sars, 1927); *T. operculifer*; *T. rylovi*; and *T. taihokuensis* (Harada 1931); *T. vermifer*; *T. wolterecki*; *T. parahastatus*; and *T. thailandensis*; *T.* cf. *orientalis*; and *T. oryzae* sp. nov. Each species can be found in various types of freshwater habitats, and most can be found in temporary and permanent water bodies (Table 2). In addition, most species are widely distributed in Thailand (Fig. 15), and a few species have a restricted distribution and have been found only in temporary habitats and a few locations.

Discussion

The new species is confirmed to belong to the genus *Thermocyclops* based on the combination of the characteristics described by Mirabdullayev et al. (2003). The morphological characteristics of *Thermocyclops oryzae* sp. nov. are mostly similar to those of *T. crucis* Holynska 2006 (Table 3), but they differ in the following characteristics: in the female, (i) the ratio of length to width of the caudal ramus is 3.6–4.1 (4.1–4.7 in *T. crucis*), (ii) the dorsal and lateral surfaces of the fifth pedigerous somite have tiny spinules (tiny spinules present only laterodorsally in *T. crucis*), (iii) the medial margin of the basis of P1 has hairs (medial spinules and hairs in *T. crucis*), (iv) the posterior surface of the EXP and ENP of P1–P4 is ornamented with tiny spinules (*T. crucis* has no spinules), (v) the intercoxal sclerite of P4 has two rows of spinules (*T. crucis* has three rows), (vi) the inner margin of the base of P4 has a serrate lobe (group of spinules in *T. crucis*); and (vii) the inner apical spine of ENP3 of P4 is 0.9 times as long as the lateral one (1.0 in *T. crucis*) .

With the discovery of this new species, the number of *Thermocyclops* species recorded in Thailand has increased from 13 to 14, accounting for 21% of global *Thermocyclops* species diversity. Based on previous and present research, most *Thermocyclops* species appear to have a wide distribution, and there are two species, *T. crassus* and *T. decipiens*, that are distributed in all regions of the country. However, recent discoveries of *T. parahastatus* and *T. thailandensis* in Thailand (Karanovic et al. 2017), including the present discovery, indicate that cryptic or semiterrestrial habitats may be home to a diverse *Thermocyclops* fauna, especially in temporary habitats. Therefore, further research, particularly on this type of habitat, is needed.

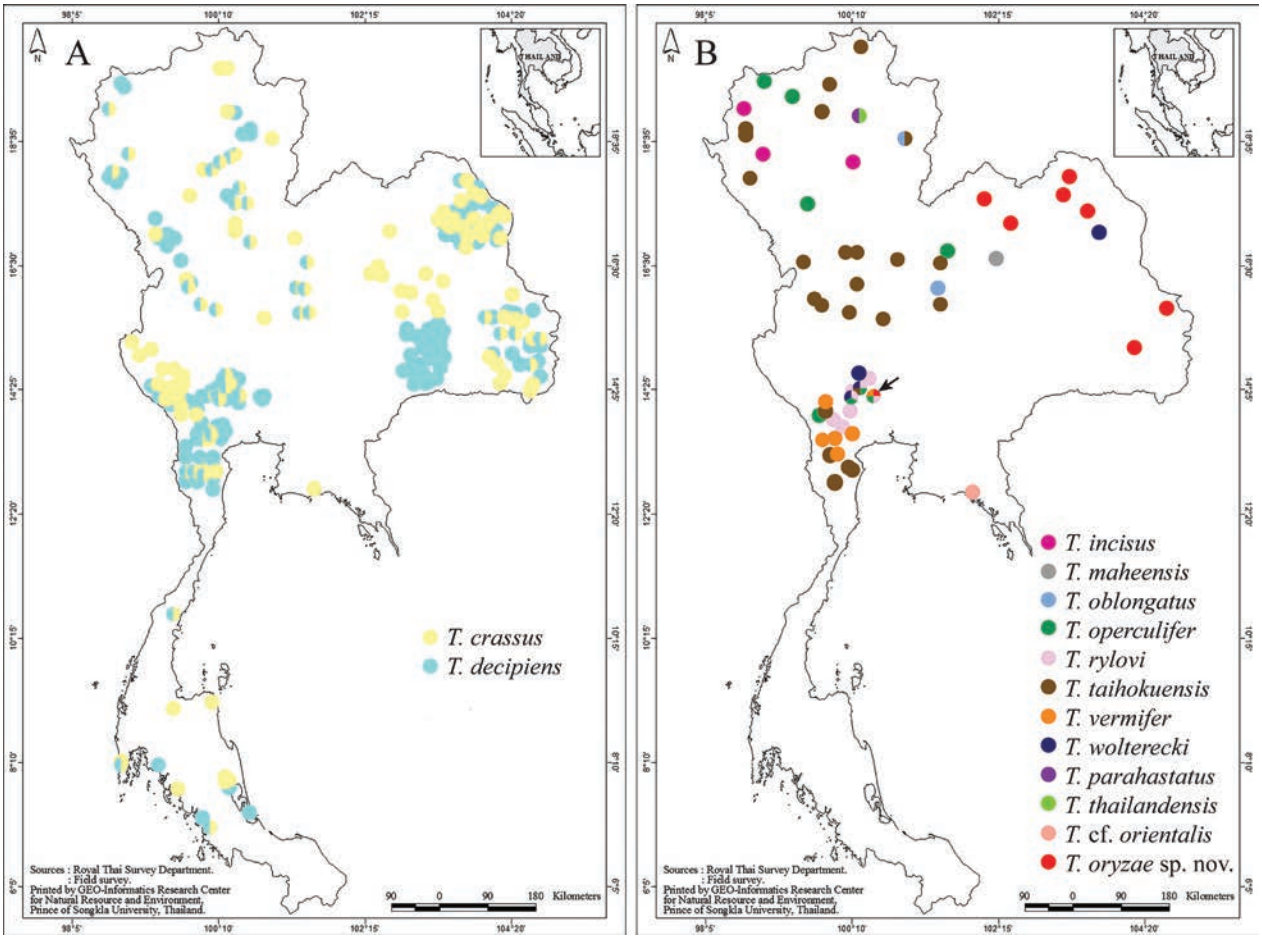

Figure 15. Distribution of *Thermocyclops* species in Thailand. **A.** Species with wide distribution; **B.** Species with restricted distribution (arrow indicates type locality of *T. oryzae* sp. nov.).

Table 2. Co-occurring cyclopoids, habitat information, and general distribution of the *Thermocyclops* species occurring in Thailand.

Species	Co-occurring species in Thai water bodies	Distribution in Thai water bodies	Geographical distribution
1. *T. crassus* (Fischer, 1853)	*Cryptocyclops* sp., *Ectocyclops phaleratus*, *E. polyspinosus*, *Eucyclops euacanthus*, *E. serrulatus*, *Halicyclops* cf. *thermophilus*, *Mesocyclops affinis*, *M. aspericornis*, *M. dissimilis*, *M. ferjemurami*, *M. kayi*, *M. ogunnus*, *M. pilosus*, *M. thermocyclopoides*, *Microcyclops* sp., *Paracyclops fimbriatus*, *Thermocyclops decipiens*, *T. incisus*, *T. oblongatus*, *T. operculifer*, *T. rylovi*, *T. taihokuensis*, *T. vermifer*, *T. wolterecki*, *Tropocyclops prasinus*	Several types of habitats including canal, cave, floodplain, irrigation canal, lake, man-made lake, permanent and temporary pond, reservoir, rice field, river, roadside pond, swamp in central, eastern, northern, northeastern, southern and western Thailand [1, 2, 4, 5, 6, 8, 9, 10, 11, 13, 15, 16, 18, 20, 21, 22].	Americas, Australia, Bangladesh, Cambodia, China, Ethiopia, India, Indonesia, Japan, Philippines, Russia, Uzbekistan, and widely distributed in Europe (Defaye et al. 1987; Defaye 1988; Ueda et al. 1997; Guo 1999; Ishida 2002; Mirabdullayev et al. 2003; Hołyńska 2006; Mirabdullayev and Kuzmetov 2007; Chaicharoen et al. 2011; Lopez et al. 2017; Islam et al. 2022; Stamou et al. 2022; Nowakowski and Sługocki 2024)
2. *T. decipiens* (Kiefer, 1929)	*Cryptocyclops linjanticus*, *Ectocyclops phaleratus*, *Eucyclops arcanus*, *E. serrulatus*, *Halicyclops* cf. *thermophilus*, *Macrocyclops fuscus*, *Mesocyclops affinis*, *M. aspericornis*, *M. ferjemurami*, *M. kayi*, *M. ogunnus*, *M. thermocyclopoides*, *Metacyclops* sp., *Microcyclops* cf. *karvei*, *Paracyclops affinis*, *P. fimbriatus*, *Thermocyclops crassus*, *T. incisus*, *T. operculifer*, *T. rylovi*, *T. taihokuensis*, *T. vermifer*, *T. wolterecki*, *Tropocyclops confinis*, *T. prasinus*	Several types of habitats including canal, cave, floodplain, irrigation canal, lake, peat swamp, permanent and temporary pond, reservoir, rice field, river, roadside canal, swamp in central, northern, northeastern, southern and western Thailand [1, 3, 5, 7, 8, 9, 10, 11, 12, 13, 15, 18, 20, 21, 22].	Circumtropical (Defaye et al. 1987; Defaye 1988; Mirabdullayev et al. 2003; Hołyńska 2006; Chaicharoen et al. 2011; Lopez et al. 2017)
3. *T. incisus* (Kiefer, 1932)	*Ectocyclops phaleratus*, *E. polyspinosus*, *Mesocyclops aspericornis*, *M. thermocyclopoides*, *Paracyclops fimbriatus*, *Thermocyclops crassus*, *T. decipiens*	Pond, reservoir, roadside canal, temporary pond in northern Thailand [10].	Africa: Ghana, Guinea, Mali, Nigeria, Senegal and Uganda (Mirabdullayev et al. 2003)
4. *T. maheensis* (Lindberg, 1941)	*Eucyclops euacanthus*, *Microcyclops rubellus*, *Mesocyclops aspericornis*, *M. thermocyclopoides*, *Thermocyclops rylovi*	River in northeastern Thailand [7].	Cambodia and India (Mirabdullayev et al. 2003; Chaicharoen et al. 2011)
5. *T. oblongatus* (G.O. Sars, 1927)	*Mesocyclops aspericornis*, *M. thermocyclopoides*, *Thermocyclops crassus*, *T. decipiens*, *T. taihokuensis*	Permanent pond and reservoir in central and northern Thailand [10].	Algeria, Angola, Congo, Egypt, Ethiopia, Greece, India, Italy, Kenya, Madagascar, Portugal, Rwanda, South Africa, Tanzania, Tunisia, Uganda and Yemen (Pesce and Pace 1984; Defaye 1988; Mirabdullayev et al. 2003)
6. *T. operculifer* (Kiefer, 1930)	*Cryptocyclops* sp., *Eucyclops serrulatus*, *Mesocyclops affinis*, *M. aspericornis*, *M. kayi*, *M. ogunnus*, *M. thermocyclopoides*, *Microcyclops* sp., *Thermocyclops crassus*, *T. decipiens*, *T. wolterecki*	Cave, irrigation canal, rice field river, roadside canal, temporary pond in central, northern and western Thailand [14, 15, 20, 21, 22].	Australia, Cambodia, Indonesia, Philippines and Vietnam (Defaye et al. 1987; Mirabdullayev et al. 2003; Hołyńska 2006)
7. *T. rylovi* (Smirnov, 1928)	*Cryptocyclops* sp., *Eucyclops euacanthus*, *Microcyclops rubellus*, *Mesocyclops affinis*, *M. aspericornis*, *M. kayi*, *M. thermocyclopoides*, *Thermocyclops crassus*, *T. decipiens*, *T. maheensis*, *T. operculifer*, *T. taihokuensis*, *T. wolterecki*	Canal, permanent and temporary pond, reservoir, rice field, river and swamp in central, northeastern and western Thailand [7, 13, 20, 22].	Afghanistan, Australia, Cambodia, Ethiopia, Kazakhstan, India, Iran, Pakistan, Russia, Tajikistan, Uganda and Uzbekistan (Defaye et al. 1987; Mirabdullayev et al. 2003; Hołyńska 2006; Chaicharoen et al. 2011)
8. *T. taihokuensis* (Harada, 1931)	*Cryptocyclops* sp., *Mesocyclops aspericornis*, *M. kayi*, *M. thermocyclopoides*, *Microcyclops* sp., *Thermocyclops crassus*, *T. decipiens*, *T. rylovi*	Lake, permanent and temporary pond, reservoir, rice field, river, roadside canal, swamp in central, northern and western Thailand [1, 10, 13, 20].	China, Japan, Kazakhstan, Korea, Philippines, Russia, Taiwan, Tajikistan, Uzbekistan and Vietnam (Ueda et al. 1997; Guo 1999; Ishida 2002; Mirabdullayev et al. 2003; Lopez et al. 2017; Lazareva and Zhdanovaa 2023)
9. *T. vermifer* (Lindberg, 1935)	*Cryptocyclops* sp., *Ectocyclops* sp., *Mesocyclops affinis*, *M. aspericornis*, *M. ogunnus*, *M. thermocyclopoides*, *Microcyclops* sp., *Thermocyclops decipiens*, *T. rylovi*	Canal, irrigation canal, rice field, permanent and temporary pond, river in central, northern and western Thailand [13, 20, 21, 22].	Afghanistan, Azerbaijan, Cambodia, China, India, Kazakhstan, Pakistan, Tajikistan, Turkmenistan and Uzbekistan (Guo 1999; Mirabdullayev et al. 2003; Chaicharoen et al. 2011)
10. *T. wolterecki* Kiefer, 1938	*Cryptocyclops linjanticus*, *Eucyclops arcanus*, *E. serrulatus*, *Macrocyclops fuscus*, *Mesocyclops affinis*, *M. aspericornis*, *M. kayi*, *M. ogunnus*, *M. thermocyclopoides*, *Microcyclops* cf. *karvei*, *Paracyclops affinis*, *Thermocyclops crassus*, *T. decipiens*, *T. operculifer*, *T. rylovi*, *Tropocyclops prasinus*	Lake, rice field and roadside canal in central, northern and northeastern Thailand [7, 10, 20, 22].	Cambodia, Papua New Guinea and Philippines (Defaye et al. 1987; Mirabdullayev et al. 2003; Chaicharoen et al. 2011; Lopez et al. 2017)
11. *T. parahastatus* Karanovic, Koomput & Sanoamuang, 2017	*Thermocyclops thailandensis*, *Elaphoidella intermedia*, *Parapseudoleptomesochra phayaoensis*	Cave in northern Thailand [17, 19].	Endemic to Thailand (Karanovic et al. 2017; Koompoot and Sanoamuang 2021)
12. *T. thailandensis* Karanovic, Koomput & Sanoamuang, 2017	*Thermocyclops parahastatus*, *Elaphoidella intermedia*, *Parapseudoleptomesochra phayaoensis*	Cave in northern Thailand [17, 19].	Endemic to Thailand (Karanovic et al. 2017; Koompoot and Sanoamuang 2021)
13. *T.* cf. *orientalis*	No co-occurring species	Peat swamp in eastern Thailand [18].	-
14. *T. oryzae* sp. nov.	*Cryptocyclops* sp., *Mesocyclops affinis*, *M. aspericornis*, *M. ogunnus*, *M. thermocyclopoides*, *Microcyclops* sp., *Thermocyclops crassus*, *T. decipiens*, *T. operculifer*, *T. rylovi*, *T. vermifer*, *T. wolterecki*	Rice field, temporary roadside canal and temporary pond in central and northeastern Thailand [22].	Endemic to Thailand

(1) Sanoamuang 1999; (2) Athibai 2002; (3) Yindee 2002; (4) Lekchan 2003; (5) Tungpunyaporn 2003; (6) Wongrat and Pipatcharoenchai 2003; (7) Alekseev and Sanoamuang 2006; (8) Boonsit 2006; (9) Sanoamuang and Faitakum 2005; (10) Proongkiat 2006; (11) Wansuang and Sanoamuang 2006; (12) Chittapun et al. 2009; (13) Koompoot 2010; (14) Watiroyram 2012; (15) Boonyanusith 2013; (16) Saetang and Maiphae 2015; (17) Karanovic et al. 2017; (18) Maiphae 2017; (19) Koompoot and Sanoamuang 2021; (20) Maiphae et al. 2023; (21) Soe and Sanoamuang 2023 (22) this study.

Table 3. Morphological comparisons between *Thermocyclops oryzae* sp. nov. and the morphologically most similar species, *T. crucis* (character states pertain to females; the main diagnostic character is indicated in bold).

Morphological characters	*Thermocyclops oryzae* sp. nov.	*T. crucis*
Caudal ramus: ratio of L:W	3.6–4.1	4.1–4.7
P1: ornamentation on inner margin of basis	hairs	spinules and hairs
P4: number of spinule rows on posterior surface of intercoxal sclerite	2	3
P4: ornamentation on inner margin of basis	**serrate lobe**	group of spinules
P4: apical spines of ENP3, inner:outer	0.9	1
P1–P4: surface ornamentation of EXP and ENP	tiny spinules	no spinules

Acknowledgements

We would like to thank the editor and the reviewer for their time and effort in reviewing the manuscript. We sincerely appreciate all the valuable comments and suggestions that have helped us improve its quality. We would also like to thank Kasetsart University for research funding through the Biodiversity Center Kasetsart University (BDCKU). This research was approved by the Institutional Animal Care and Use Committee, Kasetsart University, Thailand (approval no. ACKU67-SCI-010).

References

Alekseev VR, Sanoamuang L (2006) Biodiversity of cyclopoida copepods in Thailand with description of *Afrocyclops henrii* sp. n. Arthropoda Selecta 15(4): 277–290.

Athibai S (2002) Distribution of fairy shrimps and zooplankton in temporary water Changwat Khon Kaen and Changwat Udon Thani. Master Thesis, Khon Kaen University, Khon Kaen, Thailand.

Bambaradeniya C, Edirisinghe J, De Silva D, Gunatilleke C, Ranawana K, Wijekoon S (2004) Biodiversity associated with an irrigated rice agroecosystem in Sri Lanka. Biodiversity and Conservation 13: 1715–1753. https://doi.org/10.1023/B:BIOC.0000029331.92656.de

Baribwegure D, Thirion C, Dumont HJ (2001) The integumental pore signature of *Thermocyclops oblongatus* (Sars, 1927) and *Thermocyclops neglectus* (Sars, 1909), with the description of *Thermocyclops africae* new species, and a comparison with *Thermocyclops emini* (Mrázek, 1895). Hydrobiologia 458: 201–220. https://doi.org/10.1023/A:1013193811360

Boonsit B (2006) Species diversity and distribution of calanoid and cyclopoid copepods in Songkhram River Basin. Master Thesis, Khon Kaen University, Khon Kaen, Thailand.

Boonyanusith C (2013) Species diversity and distribution of copepods in caves in the western part of Thailand. PhD Thesis, Khon Kaen University, Khon Kaen, Thailand.

Brendonck L, de Necker L, Dube T, Dalu T, Van Damme K, Pinceel T, Nhiwatiwa T (2022) Chapter 9 - Zooplankton. In: Dalu T, Wasserman RJ (Eds) Fundamentals of Tropical Freshwater Wetlands, Elsevier, 221–271. https://doi.org/10.1016/B978-0-12-822362-8.00004-9

Chaicharoen R, Sanoamuang L, Hołyńska M (2011) A review of the genus *Thermocyclops* (Crustacea, Copepoda, Cyclopoida) in Cambodia. Zoological Studies 50(6): 780–803.

Chittapun S, Pholpunthin P, Sanoamuang L (2009) Diversity and composition of zooplankton in rice fields during a crop cycle at Pathum Thani province, Thailand. Songklanakarin Journal of Science and Technology 31(3): 261–267.

Defaye D (1988) Contribution à la connaissance des Crustacés Copépodes d'Ethiopie. Hydrobiologia 164: 103–147. https://doi.org/10.1007/BF00008454

Defaye D, Dussart BH, Fernando CH, Sarnita AS (1987) On some species of the genus *Thermocyclops* (Crustacea, Copepoda) from the Oriental Region. Canadian Journal of Zoology 65(12): 3144–3153. https://doi.org/10.1139/z87-473

Edirisinghe JP, Bambaradeniya CNB (2006) Rice fields: An ecosystem rich in biodiversity. Journal of the National Science Foundation of Sri Lanka 34: 57–59. https://doi.org/10.4038/jnsfsr.v34i2.2084

Frisch D, Green AJ (2007) Copepods come in first: rapid colonization of new temporary ponds. Fundamental and Applied Limnology 168(4): 289–297. https://doi.org/10.1127/1863-9135/2007/0168-0289

Guo X (1999) The genus *Thermocyclops* Kiefer, 1927 (Copepoda, Cyclopidae) in China. Hydrobiologia 403: 87–95. https://doi.org/10.1023/A:1003761106940

Hołyńska M (2006) On species of the genus *Thermocyclops* (Copepoda, Cyclopidae) occurring in Northern Queensland, Australia. Annales Zoologici 56: 335–364. https://doi.org/10.3161/000345406778700892

Huys R, Boxshall GA (1991) Copepod evolution. The Ray Society, 468 pp.

Ishida T (2002) Illustrated fauna of the freshwater cyclopoid copepods of Japan. Bulletin of the Biogeographical Society of Japan 57: 37–106.

Islam MDS, Azadi MA, Nasiruddin M, Islam MDT (2022) Checklist of zooplankton of the Halda River, Chattogram, Bangladesh. Journal of Bioresource Management 9(1): 110–122.

Karanovic T, Koomput K, Sanoamuang L (2017) Two new *Thermocyclops* species (Copepoda, Cyclopoida) from Thailand, with notes on the genus phylogeny inferred from 18S and ITS sequences. Zoologischer Anzeiger 269: 26–47. https://doi.org/10.1016/j.jcz.2017.07.003

Koompoot K (2010) Species diversity and distribution of calanoid and cyclopoid copepods in Suphanburi, Kanchanaburi, Ratchaburi and Phetchaburi provinces. Master Thesis, Khon Kaen University, Khon Kaen, Thailand.

Koompoot K, Sanoamuang L (2021) *Parapseudoleptomesochra phayaoensis*, a new species of copepod (Copepoda: Harpacticoida: Ameiridae) from a cave in northern Thailand. Invertebrate Zoology 18(1): 1–15. https://doi.org/10.15298/invertzool.18.1.01

Lazareva VI, Zhdanovaa SM (2023) The East Asian Invader *Thermocyclops taihokuensis* (Harada 1931) and the native *Thermocyclops oithonoides* (Sars 1863) (Crustacea, Cyclopoida): A comparative analysis of the morphology of two related species from water bodies of European Russia. Biology Bulletin 50(8): 1826–1837. https://doi.org/10.1134/S1062359023080149

Lekchan S (2003) Distribution of fairy shrimps and zooplankton in temporary waters in Changwat Maha Sarakham and changwat Roi Et. Master Thesis, Khon Kaen University, Khon Kaen, Thailand.

Lopez MLD, Pascual, JAF, Dela Paz ESP, Rizo EZC, Tordesillas DT, Guinto SK, Han B, Dumont HJ, Mamaril AC, Papa RDS (2017) Annotated checklist and insular distribution of freshwater microcrustaceans (Copepoda, Calanoida & Cyclopoida; Cladocera, Anomopoda & Ctenopoda) in the Philippines. Raffles Bulletin of Zoology 65: 623–654.

Maiphae S (2017) Species diversity of meiofauna (rotifers, cladocerans and copepods) in peatswamps, Thailand. KU Research Reports, 44 pp.

Maiphae S, Saetang T, Jantawong N, Wongkamhaeng K, Piyasaengthong N (2023) Diversity of zooplankton in the rice fields in Suphan Buri province, Thailand, with a new record of cyclopoid copepod. Diversity 15: 1054. https://doi.org/10.3390/d15101054

Mirabdullayev IM, Kuzmetov AR (2007) The genus *Thermocyclops* (Crustacea, Copepoda) in Uzbekistan (Central Asia). Internationale Revue der gesamten Hydrobiologie und Hydrographie 82(2): 201–212. https://doi.org/10.1002/iroh.19970820207

Mirabdullayev IM, Reid JW, Ueda H (2003) Genus *Thermocyclops* Kiefer, 1927. In: Ueda H, Reid JW, Dumont HJF. (Eds) Copepoda: Cyclopoida genera *Mesocyclops* and *Thermocyclops*, Guides to the Identification of the Microinvertebrates of the Continental Waters of the World. Backhuys Publishers: Leiden, The Netherlands, 214–302.

Nowakowski K, Sługocki Ł (2024) Contrasting responses of *Thermocyclops crassus* and *T. oithonoides* (Crustacea, Copepoda) to thermal stress. Scientific Reports 14: 7660. https://doi.org/10.1038/s41598-024-58230-4

Pesce GL, Pace R (1984) *Thermocyclops oblongatus* (Sars) (Crustacea, Copepoda): A new cyclopoid for the fauna of India, and zoogeography of the species. Proceedings of the Indian National Science Academy B 50(2): 133–138.

Proongkiat K. 2006. Species diversity and distribution of calanoid and cyclopoid copepods in northern Thailand. PhD Thesis, Khon Kaen University, Khon Kaen, Thailand.

Saetang T, Maiphae S (2015) Species diversity of copepods (calanoid, cyclopoid and harpacticoid) in Thale-Noi, Phatthalung province. Proceeding of the 5th Conference on Taxonomy and Systematics in Thailand (TST) (Thailand), May 2015, 166–176.

Saetang T, Maiphae S (2023) Diversity of the genus *Tropodiaptomus* Kiefer, 1932 (Crustacea, Copepoda, Calanoida, Diaptomidae) in Thailand, with the description of two new species. Zoosystematics and Evolution 99(2): 399–422. https://doi.org/10.3897/zse.99.105511

Saetang T, Sanoamuang L, Maiphae S (2020) A new species of genus *Tropodiaptomus* Kiefer, 1932 (Crustacea, Copepoda, Calanoida, Diaptomidae) from Thailand. Journal of Natural History 54: 2297–2322. https://doi.org/10.1080/00222933.2020.1843726

Sanoamuang L (1999) Species composition and distribution of freshwater Calanoid and Cyclopoid (Copepoda) of north-east Thailand. In: Schram FR, Klein JCV (Eds) Crustaceans and Biodiversity Crisis. Brill Academis Publishers, Leiden, Vol I, 217–230. https://doi.org/10.1163/9789004630543_018

Sanoamuang L, Dabseepai P (2021) Diversity, distribution, and habitat occurrence of the diaptomid copepods (Crustacea, Copepoda, Diaptomidae) in freshwater ecosystems of Thailand. Water 13(17): e2381. https://doi.org/10.3390/w13172381

Sanoamuang S, Faitakum S (2005) Species diversity of cladocerans and copepods in the floodplain of the river Mun, northeast Thailand. KKU Research Journal 10(2): 106–113.

Soe MM, Sanoamuang L (2023) The biodiversity of freshwater copepods in five provinces of northern Thailand. Proceeding of the 7th TICC International Conference 2023 Toward Sustainable Development Goals: Digital Transformation and Beyond (Thailand), February 2023, 177–188.

Stamou G, Kourkoutmani P, Michaloudi E (2022) The Inland Cladocera and Copepoda Fauna in Greece. Diversity 14(11): 997. https://doi.org/10.3390/d14110997

Tungpunyaporn P (2003) Distribution of fairy shrimps and zooplankton in temporary waters in Sakon Nakhon and Nakhon Phanom provinces. Master Thesis, Khon Kaen University, Khon Kaen, Thailand.

Ueda H, Ishida T, Imai JI (1997) Planktonic cyclopoid copepods from small ponds in Kyushu, Japan. II. Subfamily Cyclopinae. Hydrobiologia 356: 61–71. https://doi.org/10.1023/A:1003155710590

Walter TC, Boxshall G. (2024). World of Copepods Database. *Thermocyclops* Kiefer, 1927. [Accessed 01 May 2024] https://www.marinespecies.org/aphia.php?p=taxdetails&id=149770

Wansuang P, Sanoamuang L (2006) Species Diversity of rotifers, cladocerans and copepods in temporary waters in Ubon Ratchathani province. BRT Research Reports, 105–118.

Watanabe T (2019) Paddy Fields as Artificial and Temporal Wetland. Irrigation in Agroecosystems. IntechOpen, 143–157. https://doi.org/10.5772/intechopen.80581

Watiroyram S (2012) Species Diversity and Distribution of Freshwater Copepoda in Caves in Northern Thailand. PhD Thesis, Khon Kaen University, Khon Kaen, Thailand.

Wongrat L, Pipatcharoenchai W (2003) Zooplankton of Kanchanaburi Province, Thailand. Journal of Fisheries and Environment 25: 8–29.

Yindee W (2002) Species diversity and distribution of calanoid and cyclopoid copepods in Surin province. Master Thesis, Khon Kaen University, Khon Kaen.

Zoosyst. Evol. 100 (4) 2024, 1231–1241 | DOI 10.3897/zse.100.128567

PENSOFT

für Natur MUSEUM FÜR NATURKUNDE BERLIN

Tscherskia ningshaanensis: A neglected species based on phylogenetic and taxonomic analysis of *Tscherskia* and *Cansumys* (Cricetidae, Rodentia)

Haijun Jiang[1,2], Xuming Wang[3], Yaohua Yang[1,2], Xuan Pan[4], Shaoying Liu[3], Jiqi Lu[1,2]

1 *School of Life Sciences, Zhengzhou University, Zhengzhou 450001, China*
2 *Institute of Biodiversity and Ecology, Zhengzhou University, Zhengzhou 450001, China*
3 *Sichuan Academy of Forestry, Chengdu 610081, China*
4 *Chengdu Institute of Biology, Chinese Academy of Sciences, Chengdu 610213, China*

https://zoobank.org/45B95842-70FD-4B6C-895F-18E4DDAE0D5F

Corresponding authors: Jiqi Lu (lujq@zzu.edu.cn); Shaoying Liu (shaoyliu@163.com)

Academic editor: Melissa TR Hawkins ♦ **Received** 29 May 2024 ♦ **Accepted** 6 August 2024 ♦ **Published** 2 September 2024

Abstract

The greater long-tailed hamster is primarily distributed in North Korea, Siberia (Russia), and central and northern China, while the Gansu hamster is restricted to southern Gansu Province, China. The genera *Tscherskia* and *Cansumys* have each been considered monotypic. The taxonomic status of these two genera has long been debated, and the specific status of *T. ningshaanensis* has also been contentious. Researchers have variously treated *T. ningshaanensis* as a subspecies of either *T. triton* or *Can. canus*. In this study, we estimated the phylogeny, divergence times, species delimitation, and biogeographical history of *T. ningshaanensis* by using one mitochondrial (*CYT B*) and three nuclear loci (GHR, IRBP, and RAG1) and compared the external and skull morphology variations between *T. ningshaanensis* and *T. triton*. The results showed that: 1) The genus *Cansumys* is a distinct genus in Cricetinae; 2) The notion that the genus *Tscherskia* is a monotypic genus is unsupported, *T. ningshaanensis* and *T. triton* were identified within this genus; and 3) The formation of *T. ningshaanensis* may have been driven by uplift of the Qinling Mountains. We conclude that *T. ningshaanensis* is a valid species within the subfamily Cricetinae.

Key Words

Classification, morphology, Mt. Qinling, phylogeny, Rodentia, *Tscherskia*

Introduction

The greater long-tailed hamster (*Tscherskia triton* de Winton, 1899), family Cricetidae, Order Rodentia, is mainly distributed in North Korea, Siberia (Russia), and central and northern China, including the Provinces of Hebei, Shanxi, Shaanxi, Henan, Anhui, Jiangsu, Shandong, Heilongjiang, Jilin, Liaoning, as well as Inner Mongolia and Beijing (Smith and Xie 2008; Wilson et al. 2017; Wei et al. 2021). Currently, a single species with five subspecies (*T. t. triton*, *T. t. incanus*, *T. t. collinus*, *T. t. fuscipes*, and *T. t. nestor*) has been identified in the genus *Tscherskia* (Smith and Xie 2008; Wilson et al. 2017).

The species-level classification within *Tscherskia* has been controversial to date. In 1899, *Cricetus triton* was first described by de Winton (1899) from Shantung (= Shandong) Province, China. Based on morphological differences, geographical distribution, behavioral, and ecological characteristics, Thomas (1907, 1908) proposed that the classification of *C. triton* be revised from the genus *Cricetus* to *Cricetulus*, with subsequent studies recognizing one species and one subspecies within the genus *Cricetulus*. In 1907, *Cricetulus nestor* was described from Korea (Thomas 1907); and in 1908, *Cricetulus triton incanus* was described from Ko-lan-chow (= Kelan), Shan-si (= Shanxi), and Yen-an-fu (= Yan'an), Shen-si

(= Shaanxi) Provinces (Thomas 1908). Ognev (1914) described *Tscherskia albipes* from eastern Siberia, noting its larger body size and longer tail.

In 1925, two new subspecies were recognized: *Cricetulus triton collinus* from the base of Tai-pei-shan (= Taibaishan), Tsing-ling (= Qinling) Mountains, Shen-si (= Shaanxi) Province; and *Cricetulus triton fuscipes* from Peking, Chili (= Beijing, Hebei) Province (Allen 1925). Kishida (1929) described a new genus, *Asiocricetus*, from Korea, including *Asiocricetus bampensis* and *Asiocricetus yamashinai*. According to early taxonomic studies (e.g., Argyropulo 1933; Ellerman 1941), *Tscherskia* and *Asiocricetus* were regarded as subgenera of the genus *Cricetulus*. Furthermore, *T. albitpes*, *A. bampensis*, and *A. yamashinai* were treated as synonyms of *C. nestor* (Argyropulo 1933). In 1934, *Cricetulus triton meihsienensis* was described by Ho (1934) from Mei-hsi (= Meixian), Shen-si (= Shaanxi) Province, and was subsequently treated as a synonym of *C. t. collinus* (Ho 1934; Wilson et al. 2017). In 1985, *Cricetulus triton ningshaanensis* was described by Song (1985) based on its smaller body size, tail length, and color of tail from Ningshaan, southern Shaanxi Province. Neumann et al. (2006) moved *C. triton* into *T. triton* and treated *Tscherskia* as a monotypic genus based on molecular phylogenetic studies, a view accepted by many researchers (Smith and Xie 2008; Wilson et al. 2017; Wei et al. 2021).

The classification status of Gansu hamster (*Cansumys canus* Allen, 1928) and *C. t. ningshaanensis* has been debated for a long time in China due to the significant morphological (particularly tail length and color) and distributional differences (Wang and Zheng 1973; Chen and Min 1982; Wang and Xu 1992; Gu et al. 2005). *Can. canus* was first described from Choni (= Zhuoni), southern Kansu (= Gansu) Province, China (Allen 1928). Later, Ellerman (1941) treated *Can. canus* as a subspecies of *Cricetulus triton*, a view that was accepted by some researchers (Ellerman and Morrison-Scott 1951; Wang and Zheng 1973). However, *Can. canus* was considered a species placed in *Cricetulus* based on its geographical distribution and tail haircoat (Chen and Min 1982). Ross (1988) supported the idea that *Cansumys* was a valid genus and *Can. canus* a separate species, which was subsequently widely accepted (Corbet and Hill 1992; Musser and Carleton 1993; Pavlinov et al. 1995a). In 1985, *C. t. ningshaanensis* was first described as a subspecies of *C. triton* (Song 1985), but some researchers placed *C. t. ningshaanensis* within *Can. can. ningshaanensis*, supporting *Cansumys* as a valid genus (Wang and Xu 1992; Lu 1997). Yang et al. (2003) claimed *Cansumys* was a separate genus based on karyotype analyses of *Can. can. ningshaanensis* from Ningshaan, Shaanxi Province. Furthermore, Gu et al. (2005) analyzed the external morphology of *Can. canus* and *C. triton* from Zhuoni, southern Gansu Province, and the results supported that *Can. canus* and *C. triton* were two distinct species and that the status of *Can. can. ningshaanensis* warranted further investigation. However, Liao et al. (2007) treated *Can. canus* as a synonym of *C. triton* and *C. t. canus* as a subspecies of *C. triton* based on molecular analysis of specimens from Gansu Province and Ningxia. Since then, there have been no arguments regarding the classification status of *C. triton* and *Can. canus* (Smith and Xie 2008; Wilson et al. 2017; Wei et al. 2021). However, we know little about why *T. t. ningshaanensis* was treated as a synonym of *T. t. incanus* (Wilson et al. 2017; Wei et al. 2021).

In this study, we evaluate specimens from *Tscherskia* and *Cansumys* collected from Gansu, Henan, Shandong, Shanxi, Shaanxi, Heilongjiang, Beijing, and Inner Mongolia Provinces. We compared the external and skull morphologies of these specimens and conducted a combined analysis of the DNA sequences of one mitochondrial and three nuclear genes. Our aims were to infer: 1) the phylogenetic relationship and status of the genera *Tscherskia* and *Cansumys*; 2) the molecular phylogeny among the subspecies of *Tscherskia*; and 3) the taxonomic status of *T. ningshaanensis*.

Materials and methods

Specimen collection and DNA sequencing

We collected tissues from 27 specimens (*Tscherskia* and *Cansumys*) from Gansu, Henan, Shandong, Shanxi, Shaanxi, Heilongjiang Provinces, as well as Inner Mongolia Autonomous Region and Beijing, China (Fig. 1 and Suppl. material 1: table S1). Voucher specimens and liver or muscle tissue are deposited at the Institute of Biodiversity and Ecology (**IBE**), Zhengzhou University, Sichuan Academy of Forestry Sciences (**SAF**), Marine College, Shandong University (**SDU**), and College of Life Sciences, Sichuan Normal University (**SNU**), respectively. The genomic DNA of specimens was extracted from the liver and muscle tissues using a DNA extraction kit (Tiangen DNA Easy Blood and Tissue Kit, Beijing, China). One complete mitochondrial locus [Cytochrome b (*CYT B*)] and partial sequences of three nuclear genes [interphotoreceptor retinoid-binding protein (IRBP), growth hormone receptor (GHR), and recombination activating protein 1(RAG1)] were amplified. Primer pairs were obtained from the literature (Teeling et al. 2000; Galewski et al. 2006; He et al. 2010; Cheng et al. 2017) and are shown in Suppl. material 1: table S2. PCR products were sent to Sangon Biotech Co., Ltd. for sequencing.

Phylogenetic analyses and molecular dating

Phylogenetic analyses

Recovered DNA sequences were assembled and aligned individually using MEGA X (Kumar et al. 2018). Additionally, 49 sequences from 10 species were downloaded from GenBank (Suppl. material 1: table S3). *Lagurus lagurus* was used as the outgroup for all subsequent phylogenetic analyses.

We calculated Bayesian Inference (BI) and maximum likelihood (ML) using BEAST v1.7.4 (Drummond et al. 2012) and W-IQ-TREE (Trifinopoulos et al. 2016),

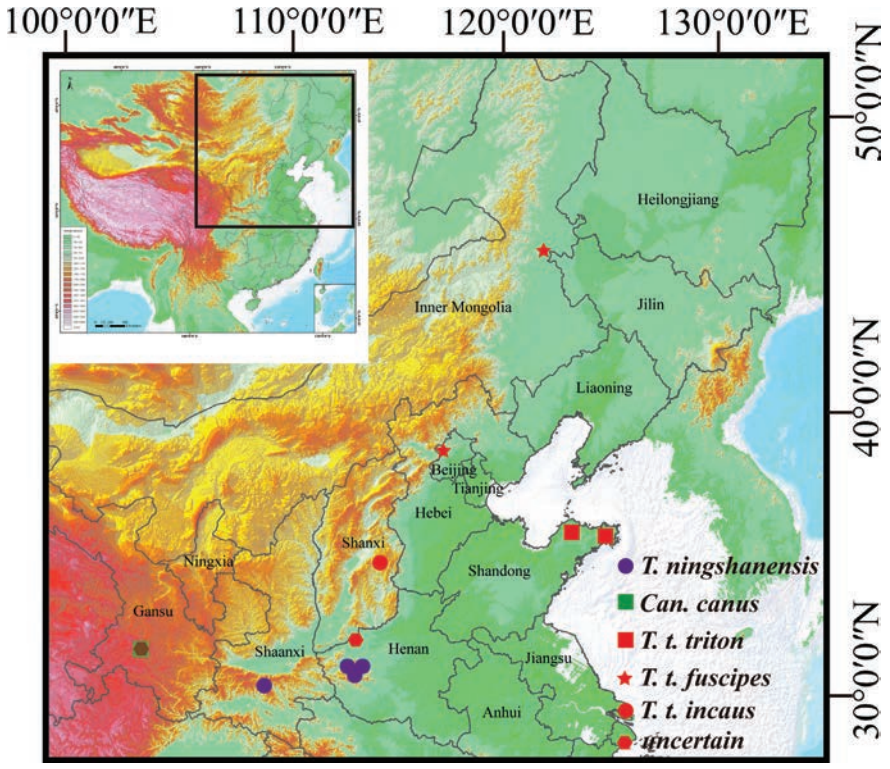

Figure 1. Collection sites of specimens of *Tscherskia* and Cansumys in China.

respectively, based on *CYT B* and nuDNA (GHR + IRBP + RAG1). For the BI analyses, the best-fit evolutionary models for *CYT B* and the three nuclear loci were determined using the Akaike Information Criterion (AIC) implemented in JMODELTEST v2.1.10 (Suppl. material 1: table S4) (Darriba et al. 2012). We employed a relaxed, uncorrelated lognormal clock model, Yule process tree priors, and the default prior distribution of the program for the model parameters. Each analysis was run for 100 million generations, with samples taken every 5,000 generations (Drummond et al. 2012). TRACER v1.7.0 was used to assess the effective sample size (ESS) values (i.e., ESS > 200) (Rambaut et al. 2018). And the first 10% of the trees were treated as burn-in.

For the ML analyses, the prior value of the parameter used was the default value for W-IQ-TREE (Trifinopoulos et al. 2016). We employed ultrafast bootstrap analysis with 1,000 bootstrap replicates, the SH-aLRT branch test with 1,000 iterations, the maximum iterations set to 1,000 iterations, and a minimum correlation coefficient of 0.99.

Species delimitation

Firstly, we calculated the Kimura-2-parameter (K2P) distance between specimens of Cricetinae in this study based on the *CYT B* gene using MEGA X (Kumar et al. 2018). Species trees (*CYT B* + nuDNA combined) were calculated using the *BEAST model in BEAST v1.7.4 (Heled and Drummond 2010; Drummond et al. 2012). Eight lineages were treated as species in the *BEAST based on the results of the K2P distance and phylogenetic analyses. We used the Yule speciation model and the strict clock model for tree construction. Other parameters followed BI settings. Each analysis was run for 100 million generations, with samples taken every 5,000 generations (Drummond et al. 2012).

Secondly, another species delimitation analysis was conducted using the program BPP v3.1 (Camargo et al. 2012; Yang and Rannala 2014). The BPP analyses were performed using dataset1 (*CYT B* + nuDNA combined) and dataset2 (nuDNA combined), respectively. And the best tree topology recovered by BEAST v1.7.4 was used as the guide tree. The validity of our assignment of Cricetinae species was tested in BPP v3.1. The species delimitation analysis only included individuals who possessed both mtDNA and nuDNA data. Two reversible jump Markov chain Monte Carlo (rjMCMC) algorithms for species delimitation (algorithms 0 and 1) were used, respectively. Each rjMCMC was run for 100,000 generations, with sampling every 100 generations following a pre-burn-in of 10,000 generations as determined by TRACER v1.7 (Rambaut et al. 2018).

Divergence-time analyses

Divergence times were estimated based on the three nuclear loci combined (*IRBP* + *GHR* + *RAG1*). The divergence time was estimated using BEAST v1.7.4. The prior for the age of the tree root was based on the results by Steppan et al. (2004) (mean = 19 ma, standard deviation = 1.5), as referenced in Lebedev et al. (2018). We used the Yule Process speciation model and the uncorrelated relaxed clock model for tree construction. The substitution rate model is set according to Bayesian trees. Each analysis was run for 100 million generations, with samples taken every 5,000 generations (Drummond et al. 2012).

Analyses of external morphological and skull features

The external morphological characteristics of specimens (*T. ningshaanensis* and *T. triton*) were compared based on specimens and data from a previous study. Following the original description by Song (1985), we examined *T. ningshaanensis* and compared it with all subspecies of *T. triton*.

A total of 15 specimens (*T. triton*: 7 and *T. ningshaanensis*: 8) were collected. For these specimens, we examined and measured several parameters, including external morphology and 11 craniodental measurements (Yang et al. 2005). External morphological data (including **W**: weight; **HBL**: head and body length; **TL**: tail length; **HL**: hindfoot length; **EL**: ear length) were measured by a digital scale (0.1 g) and measured (1 mm) from the original specimens; craniodental measurements (including **PL**: Profile length; **BL**: Basal length; **SUCL**: Short upper cranium length; **ZB**: Zygomatic breadth; **IOB**: Interorbital breadth; **CH**: Cranial height; **TBL**: tympanic bulla length; **UMRL**: Upper molar row length; **LMRL**: Lower molar row length; **ML**: Mandibular length; **CL**: Condyle length) were taken with digital calipers (0.01 mm). We compared specimens of *Tscherskia* based on measurements of external and skull morphology. Overall similarities between external morphology and skulls were assessed first through principal component analyses (PCA). The PCA was conducted at OriginLab (OriginLab Corporation, version 2024, USA).

Results

Sequence characteristics

We obtained ~3573 bp of sequence for most specimens, partitioned into 1140 bp of mitochondrial sequence (*CYT B* [1140 bp]) and 2433 bp of nuclear sequence (*IRBP* [895 bp], *GHR* [810 bp], and *RAG1* [728 bp]). All new sequences have been deposited in GenBank (accession numbers: *CYT B* PP975895–PP975921, *GHR* PP975932–PP975950, *RAG1* PP975951–PP975969, *IRBP* PP975970–PP975985).

Phylogenetic analyses

The concatenated BI and ML recovered the identical topology; therefore, only the BI tree is presented (Fig. 2). Most of the nodes were strongly supported [i.e., BEAST posterior probabilities (**PP**) ≥ 0.95, SH-aLRT values (**SH**) ≥ 80, ultrafast bootstrap values (**UBS**) (Huelsenbeck and Rannala 2004; Guindon et al. 2010; Minh et al. 2013)], with few exceptions based on combined *CYT B* and nuclear loci (Fig. 2a, b). The BI and ML results strongly supported sister relationships between *T. ningshaanensis* and *T. triton*, and both should be treated as single species, respectively [*T. ningshaanensis* (*CYT B*: **PP** = 1, **SH** = 99.9, **UBS** = 100; nuDNA: **PP** = 1, **SH** = 96.6, **UBS** = 97); *T. triton* (*CYT B*: **PP** = 1, **SH** = 100, **UBS** = 100; nuDNA: **PP** = 1, **SH** = 99.9, **UBS** = 100)] (Fig. 2a, b). The genus *Cansumys* was strongly supported as monophyletic based on *CYT B* (**PP** = 1, **SH** = 100, **UBS** = 100) (Fig. 2a). The BI and ML analyses based on *CYT B* indicate that *T. t. triton* is differentiated from the other subspecies, whereas *T. t. incanus* and *T. t. fuscipes* do not show distinct separation (Fig. 2a). The BI and ML analyses based on nuDNA results do not support the classification as a subspecies of *T. triton* (Fig. 2b). In addition, the species *Phodopus roborovskii* and *Urocricetus kamensis* were placed at the base of Cricetinae in both the analysis of *CYT B* and nuDNA results (*CYT B*: **PP** = 1, **SH** = 83, **UBS** = 85; nuDNA: **PP** = 0.99, **SH** = 97.3, **UBS** = 99) (Fig. 2a, b).

Species delimitation

Calculated K2P distances based on *CYT B* were as follows: between *T. ningshaanensis* and *Can. canus* (25.5%), between *T. ningshaanensis* and *T. triton* (15.1%), and between *Can. canus* and *T. triton* (23.8%) (Table 1). Additionally, BPP analysis results based on dataset1 and dataset2 supported *T. ningshaanensis* and *T. triton* as separate species (**PP** = 1.00), respectively. The BEAST tree analyses recovered the same topology as the BI and ML trees, with sister relationships between *T. ningshaanensis* and *T. triton* also strongly supported (**PP** = 0.99) (Fig. 3a).

Molecular divergence time

Our phylogenetic analyses based on nuDNA revealed highly concordant divergence time estimates (Fig. 3b). The species *Phodopus roborovskii* and *Urocricetus kamensis* were placed at the base of Cricetinae, with the divergence time result estimated to be in the latest Middle Miocene (12.73 Ma). Apart from the split between *T. triton* and *T. ningshaanensis* (3.88 Ma), intra-generic divergence events primarily occurred in the latest Pliocene.

Morphological and skull comparison

All external and skull measurements are provided in Table 2. The mean values of most measurements for *T. ningshaanensis* are smaller than those for *T. triton*, with significant differences in W, HBL, PL, BL, SUCL, ZB, CH, TBL, ML, and CL. However, the sizes of HFL (23.50–27.00, 24.79±1.15 vs 20.00–26.00, 23.24±2.17) and LMRL (5.28–5.41, 5.34±0.05 vs 5.13–5.77, 5.45±0.20) of *T. ningshaanensis* are bigger than those for *T. triton* (Table 2).

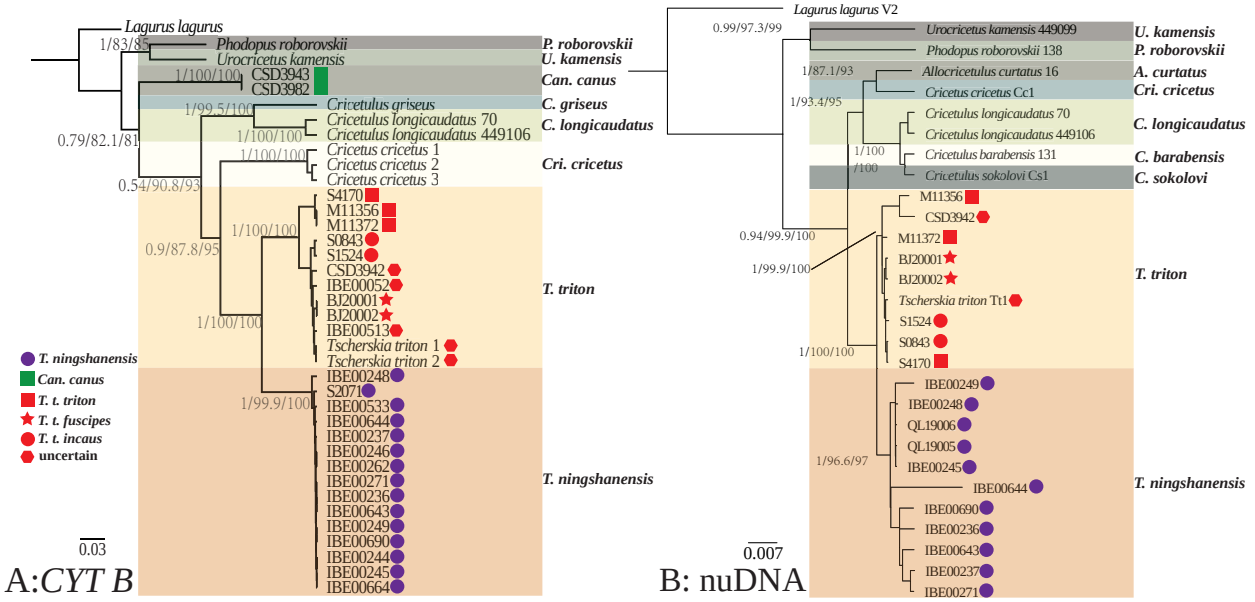

Figure 2. Maximum likelihood and Bayesian inference analysis results based on *CYT B* (**A**) and nuDNA (**B**). Left: BI posterior probabilities; middle: SH-aLRT values; right: ultrafast bootstrap values.

Table 1. K2P distances between species of *Cricetinae* based on the *CYT B* gene.

	Tsc nin	*Cri gri*	*Lag lag*	*Tsc tri*	*Cri cri*	*Pho rob*	*Cri long*	*Uro kam*
Tsc nin								
Cri gri	0.231							
Lag lag	0.269	0.224						
Tsc tri	0.151	0.229	0.258					
Cri cri	0.204	0.188	0.213	0.209				
Pho rob	0.257	0.225	0.222	0.263	0.231			
Cri long	0.236	0.143	0.236	0.223	0.208	0.240		
Uro kam	0.225	0.237	0.220	0.238	0.201	0.198	0.244	
Can can	0.255	0.222	0.221	0.238	0.208	0.212	0.212	0.217

Table 2. Some external and skull measurements (mm) used in PCA analyses of *T. ningshaanensis* and *T. triton*.

Measurement (min, max, mean ± SD)	*T. triton*	*T. ningshaanensis*
W	66.00 – 92.00, 80.67 ± 10.16	37.64 – 93.10, 52.44 ± 19.81
HBL	146.00 – 175.00, 128.00 ± 16.38	112.00 – 155.00, 129.29 ± 16.15
TL	65.00 – 90.00, 77.43 ± 8.28	76.00 – 114.00, 89.71 ± 12.62
HFL	20.00 – 26.00, 23.24 ± 2.17	23.50 – 27.00, 24.79 ± 1.15
EL	18.00 – 22.00, 20.26 ± 1.49	20.00 – 23.00, 21.71 ± 1.04
PL	33.43 – 37.68, 35.79 ± 1.56	29.33 – 37.07, 31.49 ± 2.65
BL	30.42 – 35.30, 32.13 ± 1.79	26.99 – 34.47, 29.03 ± 2.68
SUCL	33.43 – 38.94, 35.97 ± 1.86	30.24 – 37.93, 32.43 ± 2.74
ZB	16.87 – 20.22, 17.99 ± 1.06	15.54 – 19.02, 16.30 ± 1.34
IOB	4.88 – 5.54, 5.18 ± 0.22	4.66 – 5.47, 5.03 ± 0.26
CH	12.83 – 13.38, 13.11 ± 0.20	11.90 – 12.98, 12.31 ± 0.40
TBL	8.62 – 10.94, 10.06 ± 0.79	7.98 – 10.29, 8.63 ± 0.89
UMRL	5.03 – 5.57, 5.27 ± 0.17	4.94 – 5.34, 5.13 ± 0.16
LMRL	5.13 – 5.77, 5.45 ± 0.20	5.28 – 5.41, 5.34 ± 0.05
ML	22.46 – 24.70, 23.69 ± 0.74	19.23 – 25.06, 20.84 ± 2.02
CL	19.08 – 20.70, 19.71 ± 0.64	16.19 – 19.83, 17.18 ± 1.28

Note: W: weight; HBL: head and body length; TL: tail length; HL: hindfoot length; EL: ear length; PL: profile length; BL: basal length; SUCL: short upper cranium length; ZB: zygomatic breadth; IOB: interorbital breadth; CH: cranial height; TBL: tympanic bulla length; UMRL: upper molar row length; LMRL: lower molar row length; ML: mandibular length; CL: condyle length.

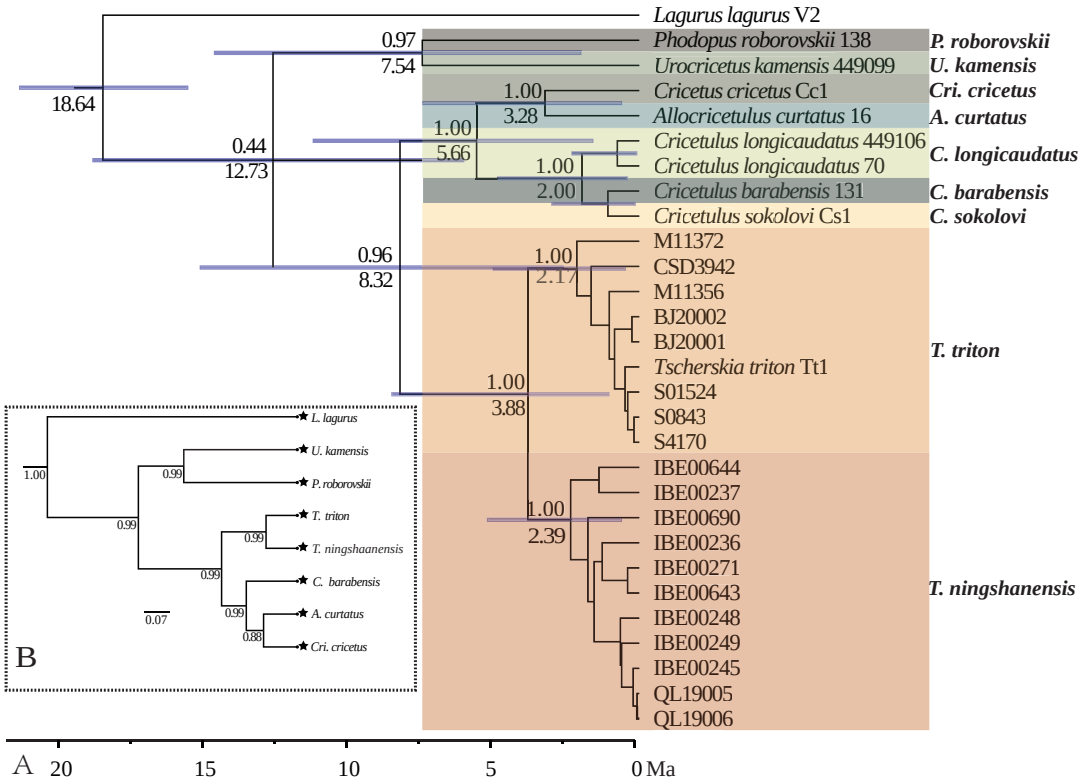

Figure 3. Divergence times estimated (**A**) and species delimitation (**B**) results in this study. a: black stars represents BPP species definition results; numbers of each node represent posterior probabilities (under); b: numbers of each node represent posterior probabilities (upper) and divergence times (under).

The PCA, based on 16 measurements [including external morphology (5) and skull (11) measurements], produced two axes (PC1: 10.20 and PC2: 2.69) with eigenvalues > 2.0, explaining 60.00% and 15.85% of the variance (75.85% total) (Table 3). PC1 was positively correlated with all variables (Table 3). PC2 was strongly correlated with TL and EL, loading > 0.5. The PCA results showed that most specimens of *T. ningshaanensis* and *T. triton* could be distinguished from each other based on 16 $\log_{10}$–transformed variables (Fig. 4).

Table 3. Character loadings, eigenvalues, and percent variance explained on the first two components of a PCA of *T. triton* and *T. ningshaanensis*.

Variables	PC1	PC2
W	0.31	0.02
HBL	0.26	0.00
TL	0.06	0.55
HFL	0.01	0.43
EL	0.02	0.52
PL	0.31	0.03
BL	0.30	0.11
SUCL	0.31	0.10
ZB	0.30	0.05
IOB	0.18	0.21
CH	0.29	–0.14
TBL	0.22	–0.11
UMRL	0.19	0.02
LMRL	0.14	–0.16
ML	0.31	0.03
CL	0.31	–0.05
Eigenvalues	10.20	2.69
Variance explained (%)	60.00	15.85

Discussion

The classification status of *Can. canus* and *T. ningshaanensis* had been extensively discussed in previous studies (Yang et al. 2003; Gu et al. 2005; Liao et al. 2007). The results from this study provide molecular evidence into the classification status of *Can. canus* and *T. ningshaanensis*, encompassing almost all subspecies of *T. triton* found in China (except for *T. t. collinus*). Our phylogenetic and morphological results indicated that the genus *Cansumys* should be treated as a distinct genus, and *T. ningshaanensis* is a distinct species. The genetic distance values among three species based on *CYT B* indicated that *T. ningshaanensis*, *T. triton*, and *Can. canus* are all distinct species (> 11%) (Bradley and Baker 2001). The large genetic distance (20.8% – 25.5%) and phylogenetic analyses based on *CYT B* strongly supported the classification status of *Cansumys* as a distinct genus (**PP** = 1, **SH** = 100, **UBS** = 100, Table 1), which was consistent

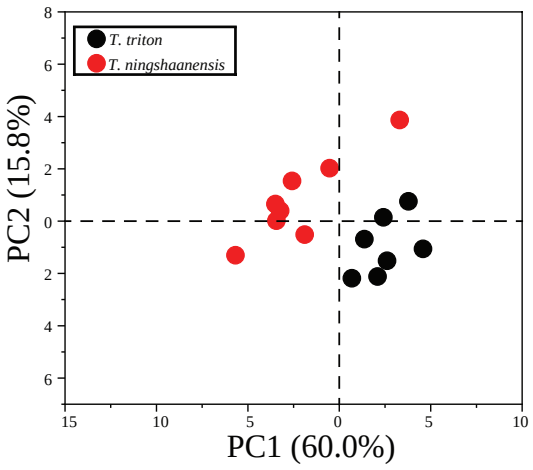

Figure 4. Results of principal component analysis (PCA) of *T. ningshaanensis* and *T. triton*.

with previous research (Smith and Xie 2008; Wilson et al. 2017; Wei et al. 2021). The calculated K2P distances based on *CYT B* of *T. triton* compared with other species of Cricetinae in this study ranged from 15.1% (*T. triton*) to 25.7% (*P. roborovskii*). The results from phylogenetic analyses based on *CYT B* and nuDNA loci strongly supported *T. ningshaanensis* as a separate species (*CYT B*: **PP** = 1, **SH** = 99.9, **UBS** = 100; nuDNA: **PP** = 1, **SH** = 96.6, **UBS** = 97); *T. triton* (*CYT B*: **PP** = 1, **SH** = 100, **UBS** = 100; nuDNA: **PP** =1, **SH** = 99.9, **UBS** = 100)] (Fig. 2a, b). The genus *Cansumys* was strongly supported as monophyletic based on *CYT B* (**PP** = 1, **SH** = 100, **UBS** = 100. Fig. 2a, b). However, the fine-scale subdivision of subspecies of *T. triton* indicates that additional studies are warranted to clarify the status of the described subspecies (Fig. 2a, b).

The growth of the Tibetan Plateau led to the uplift of the Qinling Mountains during the late Miocene to Pliocene (8–4 Ma) (Wang et al. 2011). This rapid uplift contributed to the biodiversity within the Qinling Mountains (Dong et al. 2022). The divergence time between *T. ningshaanensis* and *T. triton* was estimated to be approximately 3.88 million years ago. This divergence time suggested that the formation of *T. ningshaanensis* and *T. triton* was influenced by the uplift of the Qinling Mountains. In Europe, the earliest species of *Tscherskia* (*T. europaeus* and *T. janossyi*) was found at Csarnóta 2 (MN 15, ca. 5–3.5 Ma) in Hungary (Hír 1994; Venczel and Gardner 2005). The earliest known species of *Tscherskia* (*T.* sp.) was found in the Late Pliocene (2.58–3.60 Ma) from the Youhe Formation (ca. 3.40–2.59 Ma) (Yue and Xue 1996; Xie et al. 2021) in Linwei District, Weinan, Shaanxi Province, China. These findings suggested that the species of *Tscherskia* underwent rapid diversification during the late Pliocene (2.58–3.60 Ma). Fossils of *T. t. varians* were found from the late Middle Pleistocene to the Early Pleistocene in China (0.129 Ma–2.58 Ma) (Zheng 1984a, 1984b, 1993; Jin et al. 2009; Xie et al. 2023). This suggested that *T. triton* underwent diversification during the early Pleistocene, which is consistent with the divergence time of *T. triton* estimated in this study.

In addition, we compared the distribution range, external morphology, and skull morphology of *T. ningshaanensis*, *T. triton*, and *Can. canus*. The fact that both *T. triton* and *Can. canus* were found at Muer of Zhuoni, Gansu Province, assisted the conclusion that *T. triton* and *Can. canus* are distinct species. The results of external morphology analyses showed *T. ningshaanensis* and *T. triton* could be distinguished from each other with many distinguishable features. *T. t. triton* (de Winton 1899) has a dorsal coloration that is uniformly drab, with whitish underparts (Suppl. material 2). *T. t. collinus* (Allen 1925) is similar to *T. t. triton* but is much darker with a slightly longer tail. Its dorsal coloration is between drab and mouse gray, with warm buff sides to the head and body. The chin, feet, wrists, and a small median spot on the throat have clear white hairs. The tail is blackish-brown and thinly covered with short, appressed hairs, with many whitish hairs on the lower side. *T. t. fuscipes* (Allen 1925) is similar in general appearance to *T. t. triton* but has ankles and a basal part of the metatarsals that are dusky. Its entire dorsal area is nearly uniformly buffy, with hairs that are entirely black or have a fine black tip. The tail is thinly covered with hairs, dusky above and whitish below. *T. t. incanus* (Thomas 1908) is similar in general appearance to *T. t. triton*, with a white dorsum pedis and dorsal and belly hairs that are pale. *Can. canus* (Allen 1928) has a dorsal surface of the body and tail that is generally gray. The middle of its back has slaty-gray hairs with short whitish tips, interspersed with numerous all-black hairs, and there is a faint wash of buffy color on the sides of the body, while its tail is thickly covered with fine hairs.

In the original description, Song (1985) presented several morphological characters to distinguish it from other subspecies of *T. triton*: 1) smaller body size compared to other subspecies of *T. triton*; 2) entire dorsal surface dark grayish–brown, covered with long black hair, while the ventral grayish–white with the medial part of the body hair being gray and the distal part being whit; 3) center of the chest and feet white, ankles taupe covered with thick haired; 4) long tail, with the tail length nearly 66% of the body length; 5) the tail appears bicolored, with the basal part being grayish-brown and the distal part white, covered with dense hair; 6) white tail percentage, with the white length nearly 40%–60% of the tail; 7) intumescent tail base; and 8) less developed supraorbital ridge (Figs 5, 6). *T. ningshaanensis* and *T. triton* (including four subspecies) can be clearly distinguished from each other based on morphological characteristics (body grayish-brown, long tail with two color rears, 40–60% being white). We believed that the aforementioned evidence supports the conclusion that *T. ningshaanensis* should not be treated as a synonym of *T. t. incanus*.

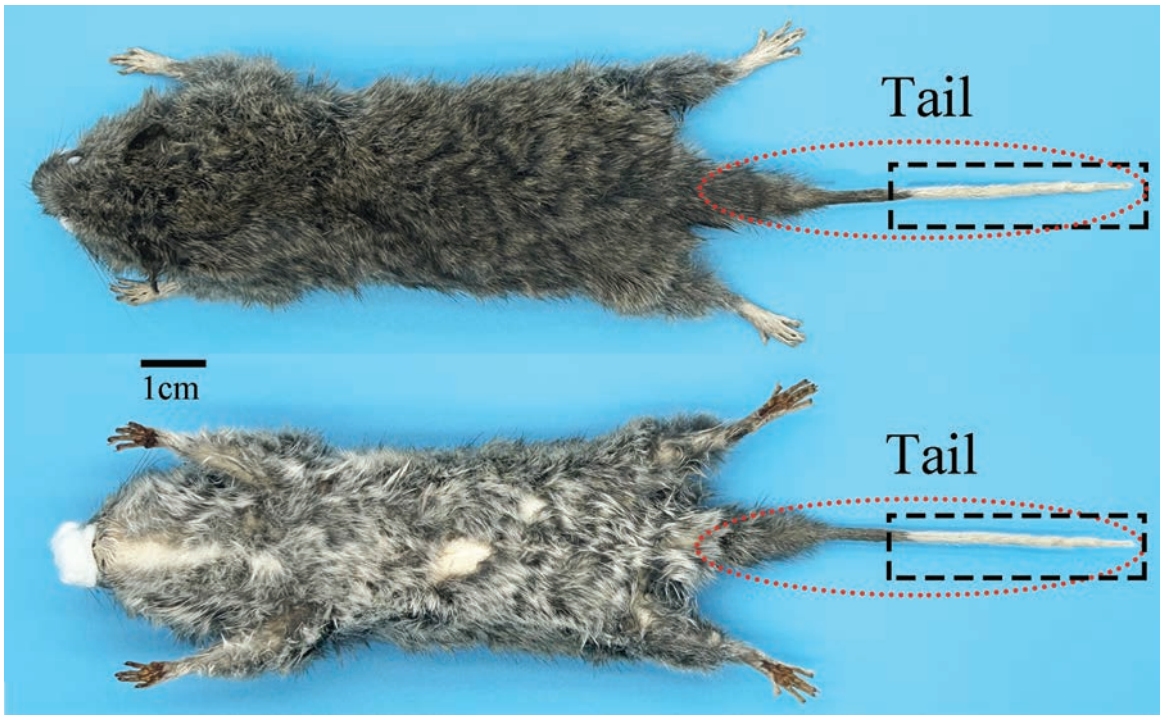

Figure 5. Dorsal and ventral views of *T. ningshaanensis*.

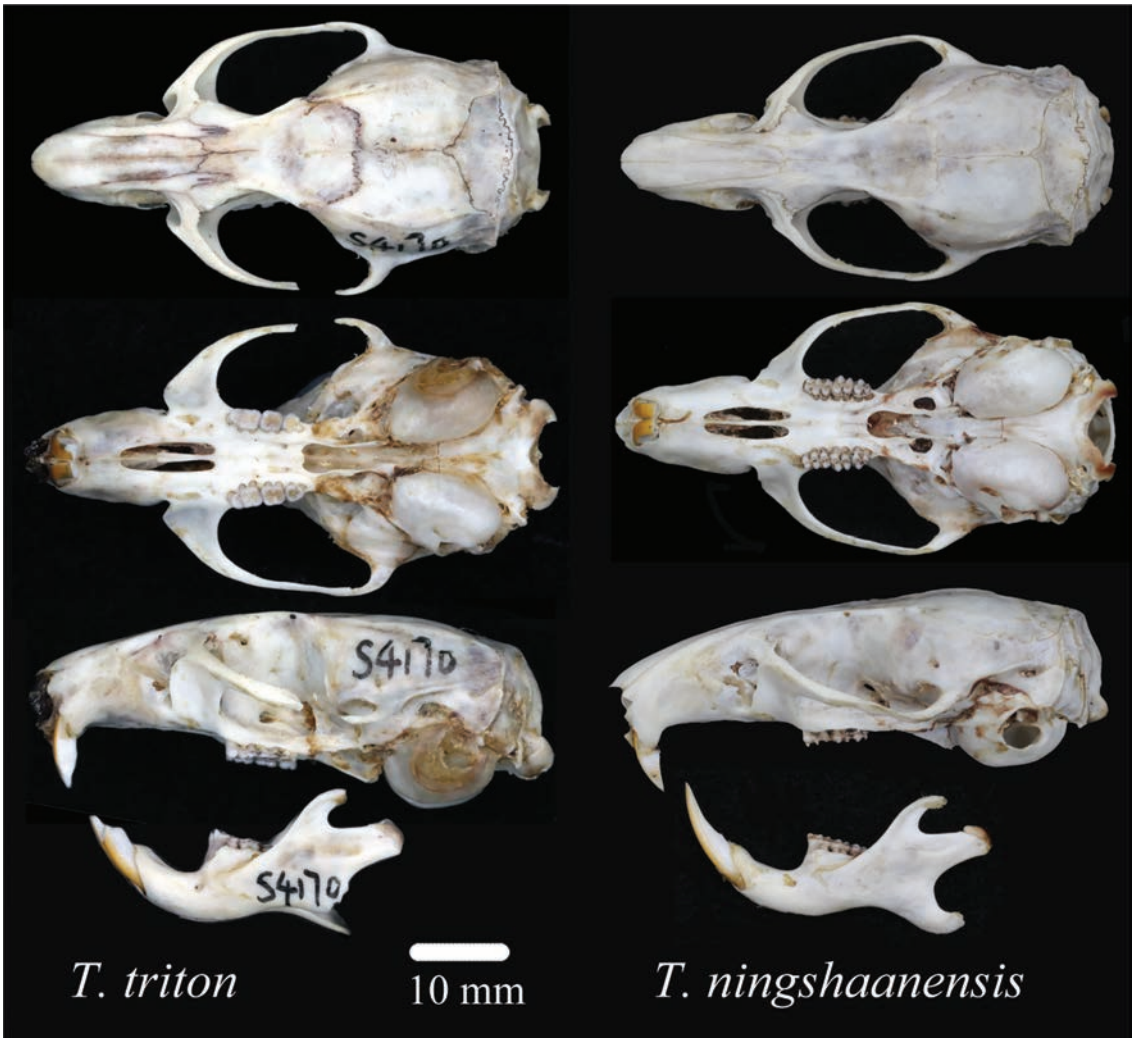

Figure 6. Dorsal, ventral, and lateral views of the skull and lateral views of the mandible, *T. ningshaanensis* and *T. t. triton*.

Conclusions

In this study, we used morphology and molecular phylogeny to investigate the taxonomy, phylogenetic relationships, and evolutionary history of the genera *Tscherskia* and *Cansumys*. The results supported the following conclusions: 1) the genus *Cansumys* is valid and distinct, possibly monotypic as only *Can. canus* is currently described; 2) the genus *Tscherskia* consists of *T. ningshaanensis* and *T. triton*, and *T. ningshaanensis* is not a synonym of *T. t. incanus*; and 3) the uplift of the Qinling Mountains likely facilitated the geographical isolation of ancestral species, further promoting the speciation of *T. ningshaanensis.*

Acknowledgments

Field surveys and collections of specimens follow relevant regulations in China. We thank Prof. Yuchun Li, Marine College, Shandong University, for providing materials for *T. triton* analysis. This research was funded by the Zhengzhou Science and Technology Talent Team Construction Plan (No. 131PLJRC654).

References

Allen GM (1925) Hamsters collected by the American Museum Asiatic Expeditions. American Museum novitates; no. 179. American Museum of Natural History, New York City.

Allen GM (1928) A New Cricetine Genus from China. Journal of Mammalogy 9: 244–246. https://doi.org/10.2307/1373275

Argyropulo A (1933) Die Gattungen und Arten der Hamster (Cricetinae Murray, 1866) der Paläarktik. Zeitschrift für Säugetierkunde 8: 129–149.

Bradley RD, Baker RJ (2001) A Test of the Genetic Species Concept: Cytochrome-b Sequences and Mammals. Journal of Mammalogy 82: 960–973. https://doi.org/10.1644/1545-1542(2001)082<0960:ATOTGS>2.0.CO;2

Camargo A, Morando M, Avila LJ, Sites JW (2012) Species delimitation with abc and other coalescent-based methods: a test of accuracy with simulations and an empirical example with lizards of the *Liolaemus Darwinii* complex (Squamata: Liolaemidae). Evolutionary Anthropology 66: 2834–2849. https://doi.org/10.1111/j.1558-5646.2012.01640.x

Chen FG, Min ZL (1982) Taxonomic review of sevenal speceis in Rondents. Zoological research 3: 369–374.

Cheng F, He K, Chen ZZ, Zhang B, Wan T, Li JT, Zhang BW, Jiang XL (2017) Phylogeny and systematic revision of the genus *Typhlomys* (Rodentia, Platacanthomyidae), with description of a new species. Journal of Mammalogy 98: 731–743. https://doi.org/10.1093/jmammal/gyx016

Corbet GB, Hill. JE (1992) Mammals of the Indomalayan region. A systematic review. Oxford University Press, Oxford.

Darriba D, Taboada GL, Doallo R, Posada D (2012) jModelTest 2: more models, new heuristics and parallel computing. Nature Methods 9: 772–772. https://doi.org/10.1038/nmeth.2109

de Winton W (1899) On Chinese mammals, principally from Western Sechuen, with notes on Chinese squirrels. Proceedings of the Zoological Society of London 67: 572–578. https://doi.org/10.1111/j.1469-7998.1899.tb06875.x

Dong Y, Shi X, Sun S, Sun J, Hui B, He D, Chong F, Yang Z (2022) Co-evolution of the Cenozoic tectonics, geomorphology, environment and ecosystem in the Qinling Mountains and adjacent areas, Central China. Geosystems and Geoenvironment 1: 100032. https://doi.org/10.1016/j.geogeo.2022.100032

Drummond AJ, Suchard MA, Xie D, Rambaut A (2012) Bayesian Phylogenetics with BEAUti and the BEAST 1.7. Molecular Biology and Evolution 29: 1969–1973. https://doi.org/10.1093/molbev/mss075

Ellerman JR (1941) The families and genera of living rodents. Volume II. Muridae. Vol. 2,British Museum, London.

Ellerman JR, Morrison-Scott TCS (1951) Checklist of Palaearctic and Indian mammals, 1758–1946. https://www.biodiversitylibrary.org/bibliography/8602

Galewski T, Tilak M, Sanchez S, Chevret P, Paradis E, Douzery EJP (2006) The evolutionary radiation of Arvicolinae rodents (voles and lemmings): relative contribution of nuclear and mitochondrial DNA phylogenies. BMC Evolutionary Biology 6: 80. https://doi.org/10.1186/1471-2148-6-80

Gu Y, Ma Y, Sun YH (2005) A Rediscussion on the Taxonomic Status of *Cansumys canus*. Chinese Jounal ef Zoology 40: 116–120.

Guindon S, Dufayard JF, Lefort V, Anisimova M, Hordijk W, Gascuel O (2010) New algorithms and methods to estimate maximum-likelihood phylogenies: assessing the performance of PhyML 3.0. Systematic Biology 59: 307–321. https://doi.org/10.1093/sysbio/syq010

He K, Li YJ, Brandley MC, Lin LK, Wang YX, Zhang YP, Jiang XL (2010) A multi-locus phylogeny of Nectogalini shrews and influences of the paleoclimate on speciation and evolution. Molecular Phylogenetics and Evolution 56: 734–746. https://doi.org/10.1016/j.ympev.2010.03.039

Heled J, Drummond AJ (2010) Bayesian inference of species trees from multilocus data. Molecular Biology and Evolution 27: 570–580. https://doi.org/10.1093/molbev/msp274

Hír J (1994) *Cricetinus beremendensis* sp. n. (Rodentia, Mammalia) from the Pliocene fauna of Beremend 15. (S Hungary). Fragmenta Mineralogica et Paleontologica 17: 71–89.

Ho H (1934) A new subspecies of Cricetidae from Shansi. Contributions from the Biological Laboratory of Science Society of China, Naking Zoological Series 10: 288–291.

Huelsenbeck JP, Rannala B (2004) Frequentist Properties of Bayesian Posterior Probabilities of Phylogenetic Trees Under Simple and Complex Substitution Models. Systematic Biology 53: 904–913. https://doi.org/10.1080/10635150490522629

Jin CZ, Zhang YQ, Wei GB, Cui N, Wang Y (2009) Rodentia. In: Jin CZ, Liu JY, eds. Paleolithic Site—The Renzidong Cave, Fanchang, Anhui Province. Science Press, Beijing.

Kishida K (1929) A synopsis of Corean hamsters. In., Lansania, Tokyo 1–160.

Kumar S, Stecher G, Li M, Knyaz C, Tamura K (2018) MEGA X: Molecular Evolutionary Genetics Analysis across Computing Platforms. Molecular Biology and Evolution 35: 1547–1549. https://doi.org/10.1093/molbev/msy096

Lebedev VS, Bannikova AA, Neumann K, Ushakova MV, Ivanova NV, Surov AV (2018) Molecular phylogenetics and taxonomy of dwarf hamsters Milne-Edwards, 1867 (Cricetidae, Rodentia): description

of a new genus and reinstatement of another. Zootaxa 4387: 331–349. https://https://doi.org/10.11646/zootaxa.4387.2.5

Liao J, Xiao Z, Dong Y, Zhang Z, Liu N, Li J (2007) Taxonomic status of Cansumys canus (Allen,1928). Acta Zoologica Sinica 53: 44–53.

Lu JQ (1997) The Study on the Geocraphical Division ofGlires in Henan Province. Journal of Henan Normal University (Natural Science) 25: 68–71. https://doi.org/10.16366/j.cnki.1000-2367.1997.02.017

Minh BQ, Nguyen MA, von Haeseler A (2013) Ultrafast approximation for phylogenetic bootstrap. Molecular Biology and Evolution 30: 1188–1195. https://doi.org/10.1093/molbev/mst024

Musser GG, Carleton. MD (1993) Family Muridae. Pp. 501–755, in: Mammal species of the world, a taxonomic and geographic reference, Second ed. (D. E. Wilson and D. M. Reeder, eds.). Smithsonian Institution Press, Washington D. C xviii.

Neumann K, Michaux J, Lebedev V, Yigit N, Colak E, Ivanova N, Poltoraus A, Surov A, Markov G, Maak S, Neumann S, Gattermann R (2006) Molecular phylogeny of the Cricetinae subfamily based on the mitochondrial cytochrome and 12S rRNA genes and the nuclear vWF gene. Molecular Phylogenetics and Evolution 39: 135–148. https://doi.org/10.1016/j.ympev.2006.01.010

Ognev SI (1914) Die saugetiere aus dem sudlichen Ussurigebiet (the mammals of the southern Ussuri). Journal de la Section Zoologique de la Societe des Amis des Sciences Naturelles, d'Anthropologie et d'ethnographie 2: 101–128.

Pavlinov IY, Yakhontov. EL, Agadzhanyan AK (1995a) Mammals of Eurasia. I. Rodentia. Taxonomic and geographic guide. Vol. 32, Archives of the Zoological Museum, Moscow State University.

Rambaut A, Drummond AJ, Xie D, Baele G, Suchard MA (2018) Posterior Summarization in Bayesian Phylogenetics Using Tracer 1.7. Systematic Biology 67: 901–904. https://doi.org/10.1093/sysbio/syy032

Ross P (1988) The taxonomic status of *Cansumys canus*. Abstracts, Symposium of Asian Pacific Mammalogy. Huirou, Beijing,Peoples Republic of China, 245 pp.

Smith AT, Xie Y (2008) A Guide to the Mammals of China. Princeton University Press, Princeton, New Jersey, 135–144.

Song S (1985) A new subspecies of *Cricetulus triton* from Shananxi, China. Acta Theriological Sinica 5: 137–139.

Steppan SJ, Storz BL, Hoffmann RS (2004) Nuclear DNA phylogeny of the squirrels (Mammalia: Rodentia) and the evolution of arboreality from c-myc and RAG. Molecular Phylogenetics and Evolution 30: 703–719. https://doi.org/10.1016/S1055-7903(03)00204-5

Teeling EC, Scally M, Kao DJ, Romagnoli ML, Springer MS, Stanhope MJ (2000) Molecular evidence regarding the origin of echolocation and flight in bats. Nature 403: 188–192. https://doi.org/10.1038/35003188

Thomas O (1907) The Duke of Bedford's zoological expedition in eastern Asia. V. Second list of mammals from Korea. Proceedings of Zoological Society of London 32: 462–466. https://doi.org/10.1111/j.1469-7998.1907.tb06941.x

Thomas O (1908) *Cricetulus triton incanus* subsp. n. In: Woodward H. Abstract of the proceedings of the zoological society of london 63: 43–46.

Trifinopoulos J, Nguyen L-T, von Haeseler A, Minh BQ (2016) W-IQ-TREE: a fast online phylogenetic tool for maximum likelihood analysis. Nucleic Acids Research 44: 232–235. https://doi.org/10.1093/nar/gkw256

Venczel M, Gardner JD (2005) The geologically youngest albanerpetontid amphibian, from the lower Pliocene of Hungary. Palaeontology 48: 1273–1300. https://doi.org/10.1111/j.1475-4983.2005.00512.x

Wang TZ, Xu WX (1992) Glires (Rondentia and Lagomorpha) fauna of Shaanxi Province. Shaanxi Normal University Press, Xian.

Wang S, Zheng CL (1973) Notes on Chinese Hamsters(Cricetinae). Acta Zoologica Sinica 19: 61–68.

Wang X, Zattin M, Li J, Song C, Peng T, Liu S, Liu B (2011) Eocene to Pliocene exhumation history of the Tianshui-Huicheng region determined by Apatite fission track thermochronology: Implications for evolution of the northeastern Tibetan Plateau margin. Journal of Asian Earth Sciences 42: 97–110. https://doi.org/10.1016/j.jseaes.2011.04.012

Wei F, Yang Q, Wu Y, Jiang X, Liu S, Li B, YANG G, Li M, Zhou J, Li S, Hu Y, Ge D, Li S, YU W, Chen B, Zhang Z, Zhou C, Wu S, Zhang L, Chen Z, Chen S, Deng H, Jiang T, Zhang L, Shi H, Lu X, Li Q, Liu Z, Cui Y, Li Y (2021) Catalogue of mammals in China(2021). Acta Theriological Sinica 41: 487–501. https://doi.org/10.16829/j.slxb.150595

Wilson DE, Mittermeier, RA, Lacher TE (2017) Handbook of the Mammals of the World, Vol. 7: Rodents II. Vol. 7, Lynx Edicions, Barcelona, Spain.

Xie K, Zhang YX, Li YX (2021) Revision to from the Houhecun Fauna and a New Discovery of (Cricetidae, Rodentia) from the Youhe Fauna of Weinan, Shaanxi Province, China. Acta Geologica Sinica-English Edition 95: 1073–1079. https://doi.org/10.1111/1755-6724.14776

Xie K, Zhang YX, Li YX (2023) Large-sized fossil hamsters from the late Middle Pleistocene Locality 2 of Shanyangzhai, China, and discussion on the validity of *Cricetinus* and *C. varians* (Rodentia: Cricetidae). Peerj 11. https://doi.org/10.7717/peerj.15604

Yang ZH, Rannala B (2014) Unguided species delimitation using DNA sequence data from multiple Loci. Molecular Biology and Evolution 31: 3125–3135. https://doi.org/doi:10.1093/molbev/msu279

Yang L, Chen X, Zhao X, Wang J (2003) Karyotype and Classif ication Status of Cansumys canus (Cricetidea, Rodentia). Acta Theriological Sinica 23: 235–238. https://doi.org/10.16829/j.slxb.2003.03.010

Yang QS, Xia L, Ma Y, Feng ZJ, Quan GQ (2005) A guide to the measurement of mammal skull I: Basic measurement. Chinese Journal of Zoology 40: 50–56. https://doi.org/10.13859/j.cjz.2005.03.011

Yue LP, Xue XX (1996) Palaeomagnetism of Chinese Loess. Geology Press, Beijing.

Zheng SH (1984a) Revised determination of the fossil Cricetine (Rodentia, Mammalia) of Choukoutien district. Vertebrata PalAsiatica 22: 179–197. https://doi.org/10.19615/j.cnki.1000-3118.1984.03.002

Zheng SH (1984b) A new species of Kowalskia (Rodentia, Mammalia) of Yinan, Shandong. Vertebrata PalAsiatica 22: 251–260. https://doi.org/10.19615/j.cnki.1000-3118.1984.04.001

Zheng SH (1993) Quaternary rodents of Sichuan-Guizhou area, China. Science Press., Beijing.

Supplementary material 1

Supplamentary information

Authors: Haijun Jiang, Xuming Wang, Yaohua Yang, Xuan Pan, Shaoying Liu, Jiqi Lu

Data type: docx

Explanation note: **table S1.** Sampling localities of genera *Tscherskia* and *Cansumys* in this study. **table S2.** Primers used for PCR and sequencing in this study.**table S3.** Sampling information including localities and GenBank accession numbers for species used in this study. **table S4.** The best molecular evolution model according to the Akaike Information Criterion (AIC) used in phylogenetic reconstructions based on jModeltest v2.10

Link: https://doi.org/10.3897/zse.100.128567.suppl1

Supplementary material 2

Dorsal and ventral views of *T. triton*

Authors: Haijun Jiang, Xuming Wang, Yaohua Yang, Xuan Pan, Shaoying Liu, Jiqi Lu

Data type: psd

Link: https://doi.org/10.3897/zse.100.128567.suppl2

Zoosyst. Evol. 100 (4) 2024, 1243–1257 | DOI 10.3897/zse.100.127169

PENSOFT

MUSEUM FÜR NATURKUNDE BERLIN

Integrative taxonomy reveals a new species of deep-sea squat lobster (Galatheoidea, Munidopsidae) from cold seeps in the Gulf of Mexico

Paula C. Rodríguez-Flores[1,2], Julie W. Ambler[3], Martha S. Nizinski[1,4]

1 *Department of Invertebrate Zoology, National Museum of Natural History, Smithsonian Institution, Washington, DC 23050, USA*

2 *Department of Organismic and Evolutionary Biology, Museum of Comparative Zoology, Harvard University, 26 Oxford St., Cambridge, MA 02138, USA*

3 *Emeritus, Department of Biology, Millersville University, Millersville, PA 17551, USA*

4 *National Systematics Laboratory, NOAA Fisheries, National Museum of Natural History, Smithsonian Institution, Washington, DC 23050, USA*

https://zoobank.org/E15C6ADB-2AB2-4D0C-886F-B2A3AFF3F769

Corresponding author: Paula C. Rodríguez-Flores (rodriguezfloresp@si.edu)

Academic editor: M. Christodoulou ♦ **Received** 11 May 2024 ♦ **Accepted** 2 July 2024 ♦ **Published** 10 September 2024

Abstract

The western Atlantic Ocean harbors a diverse fauna of squat lobsters, particularly in the family Munidopsidae. This study introduces *Munidopsis sedna* **sp. nov.**, a species only found in the Gulf of Mexico and the first species reported to be endemic to cold seeps in the western Atlantic. Our investigation incorporates morphological analyses including micro-CT scanning evidence, multilocus molecular phylogeny, and mtDNA phylogeography, as well as ecological data derived from in situ observations and geographic distribution patterns to substantiate the recognition of the new species. Shallow molecular divergences and multiple morphological differences differentiate the new species from its closest relative, *M. longimanus* (A. Milne-Edwards, 1880). Additionally, we explore the potential scenario for ecological speciation within this newly identified taxon and discuss its significance in the context of conservation efforts in the Gulf of Mexico.

Key Words

Anomura, Atlantic, barcoding, chemosynthetic systems, morphology, nanopore, speciation

Introduction

Squat lobsters, an extremely diverse group of anomuran crustaceans, inhabit broad geographic and bathymetric ranges, occurring circumglobally, primarily in tropical and temperate waters, from the surface to abyssal depths (Schnabel et al. 2011). Commonly found in the deep sea at depths greater than 200 m, many species of squat lobsters occur in vulnerable ecosystems in association with hydrothermal vents, cold seeps, and cold-water corals (e.g., Chevaldonné and Olu 1996; Macpherson and Segonzac 2005; Martin and Haney 2005; Baba et al. 2008). The recent increase in deep-sea exploration has led to the discovery of numerous new species. In fact, many new species are discovered and described every year, especially from unexplored areas in the Pacific Ocean (e.g., Baba 2018; Dong et al. 2021; Rodríguez-Flores and Schnabel 2023, Rodríguez-Flores et al. 2023; Macpherson et al. 2024). Renewed interest and recent work in the Caribbean Sea and the Gulf of Mexico has also revealed new species and species complexes in the western Atlantic Ocean (e.g., Vazquez-Bader et al. 2014; Macpherson et al. 2016; Poupin and Corbari 2016; Baba and Wicksten 2017a, 2017b; Coykendall et al. 2017; Rodríguez-Flores et al. 2018, 2022; Gaytán-Caballero et al. 2022).

While systematic research on squat lobsters is active, ecological research on this group is still in its infancy (Coykendall et al. 2017). Few studies have focused on understanding the natural history and ecology of squat lobsters (Lovrich and Thiel 2011). Multiple species of squat lobster are found closely associated with hydrothermal vents and cold seeps, and some species have special

adaptations for living in these habitats (Williams and van Dover 1983; Baba and de Saint Laurent 1992; Baba and Williams 1998; Desbruyères et al. 2006; Gaytán-Caballero et al. 2022). For instance, *Shinkaia crosnieri* Baba & Williams, 1998, cultivates chemosynthetic bacteria on the body setae (Tsuchida et al. 2011; Watsuji et al. 2017). Additionally, several species of *Munidopsis* Whiteaves, 1874 are found occasionally in chemosynthetic environments, taking advantage of high concentrations of available food (Macpherson and Segonzac 2005; Macpherson et al. 2006). Conversely, some other species in the same genus are suggested to be colonists or vagrants (*sensu* Carney 1994) of seeps and hydrothermal vents rather than restricted to living in these kinds of habitats (Carney 1994; Martin and Haney 2005).

However, little is known about squat lobsters utilizing chemosynthetic habitats, particularly those species considered to be endemic (*sensu* Carney 1994). Probably the most studied vent/cold-seep species are the yeti crabs (*Kiwa* Macpherson, Jones & Segonzac, 2005), which have a high dependence on chemosynthetic ecosystems and multiple adaptations to life in these environments (Macpherson et al. 2005; Goffredi et al. 2008; Thatje et al. 2015). As new vent sites and cold seeps are discovered, new squat lobster species living in these habitats are also discovered (Rodríguez-Flores et al. 2023).

Extreme environments such as hydrocarbon seeps, brine pools, and cold-water coral habitats are broadly distributed throughout the Gulf of Mexico (GoM) on the continental slope at depths ranging from 400 to 3,500 m (Cordes et al. 2009). The chemosynthetic communities consist mainly of mussel beds and tube-worm bushes (e.g., *Bathymodiolus* Kenk & Wilson, 1985, and *Lamellibrachia* Webb, 1969, respectively) and have been extensively researched (Carney 1994; Cordes et al. 2007, 2009, 2010; Fisher et al. 2007). The chemosynthetic communities provide habitat for many other invertebrate taxa, such as polynoid polychaetes, trochid gastropods, alvinocarid shrimps, and squat lobsters (Webb 1969; Kenk and Wilson 1985; Roberts et al. 1990; Fisher et al. 2007). For example, squat lobsters in the genus *Munidopsis* have been detected in abundance on tubeworm aggregations and mussel beds associated with these cold seeps (Carney 1994; Bergquist et al. 2003; Lessard-Pilon et al. 2010). Species of *Munidopsis* living there are an important component of the community and rely completely on chemosynthetic production (MacAvoy et al. 2008a, 2008b). Although extensively studied (Bergquist et al. 2003; Cordes et al. 2010; Coykendall et al. 2017), a species of *Munidopsis* frequently found in association with brine pools and cold seeps in the GoM remained unidentified (Fisher et al. 2007; Lessard-Pilon et al. 2010).

Herein, we describe this new species of squat lobster based on molecular and morphological evidence. The new species is morphologically related to *M. longimanus* (A. Milne-Edwards, 1880) and *M. brevimanus* (A. Milne-Edwards, 1880), known from the Gulf of Mexico and the Caribbean. We therefore compare the material of all these species and highlight the morphological characters distinguishing the new taxa from the other species. Additionally, we highlight ecological observations and discuss a potential scenario of ecological speciation with respect to its closely related and co-occurring sympatric congener, *M. longimanus*.

Materials and methods

Ecological data

Specimens of the new species were collected during several cruises conducted in and around chemosynthetic habitats in the northern GoM (see details below in the Material Examined Section). Histograms of depth distribution were done using Past4 Version 4.16 (https://www.nhm.uio.no/english/research/resources/past/) (Hammer et al. 2001). Maps were generated using the free open-source Geographic Information System QGIS Version 3.34.3 (https://qgis.org/en/site/). Layers of chemosynthetic communities and hydrocarbon seeps in the GoM were downloaded from Sinclair and Shedd (2012) (https://www.ncei.noaa.gov/maps/gulf-data-atlas/atlas.htm).

Morphological examination

We examined a total of 103 lots, including 758 specimens deposited in the following collections: Museum of Comparative Zoology (MCZ), Harvard University, Cambridge, MA; Muséum National d'Histoire Naturelle (MNHN), Paris; Benthic Invertebrate Collection at Scripps Institution of Oceanography (SIO-BIC), San Diego, CA; Field Museum of Natural History (FMNH), Chicago, IL; Voss Marine Invertebrate Collections at the University of Miami (UMML), Miami, FL; Texas Cooperative Wildlife Collection (TCWC) at Texas A&M University, College Station, TX; and National Museum of Natural History (USNM), Smithsonian Institution, Washington, DC. The material examined corresponds to the new species and morphologically related species. We used a Leica MZ 12.5 stereomicroscope coupled with a camera lucida to identify, draw, and dissect the squat lobster specimens. Drawings were digitized using a Wacom Intuos Pro tablet with Adobe Illustrator 2024. The terminology used for the species description follows that of Baba et al. (2011). The size of the specimens is indicated by the postorbital carapace length (PCL). The following morphometric features were examined: rostrum length: straight line distance from the base to the distal tip; rostrum width: straight line distance between the lateral limits of the rostral lobe. Measurements of appendages are taken on the dorsal (pereiopod 1), lateral (antennule, pereiopods 2–4), or ventral (antenna) midlines. Measures of the maxillipeds are taken on the extensor margin. Ranges of morphological and meristic variation are included in the description. Abbreviations used in the description are as

follows: **Mxp** = maxilliped; **P1** = pereiopod 1 (cheliped); **P2–4** = pereiopods 2–4 (walking legs 1–3); **M** = male; **F** = female; **ov.** = ovigerous, **m** = meters, **mm** = millimeters. Holotype measurement values are indicated with brackets. Several specimens were selected for DNA extraction, amplification, and sequencing (see below).

Morphological analyses

Several individuals (N = 13) were photographed on the dorsal view using an Olympus Tough Tg-6 digital camera (Suppl. material 1). A scale was included for reference. A combination of anatomical landmarks and semi-landmarks on the carapace, rostrum, and abdomen were used to compare and analyze features of the new species and its closest relative, *M. longimanus* (A. Milne-Edwards, 1880), using the R package geomorph (Adams and Otárola-Castillo 2013). Morphological information (coordinates in axes X and Y) was then transformed into new coordinates (generalized procrustes analyses) and analyzed and visualized using principal component analyses (PCA).

Micro-Computed Tomography (micro-CT)

Two specimens of both the new species and *M. longimanus* were selected for 3D imaging. The specimens were mounted in 15-mL plastic vials and secured using parafilm and synthetic cotton to minimize their movement during the scanning process. The container was sealed with parafilm.

The micro-CT scans were conducted at the MCZ using a SkyScan 1273 scanner (Bruker MicroCT, Kontich, Belgium). The scanner is supplied with a Hamamatsu 130/300 tungsten X-ray source at 40–130 kV and a flat-panel X-ray detector with 6-megapixel (3072 × 1944). The following scanning parameters were chosen: source current=100 µA, source voltage=75 kV, exposure time=1,000 ms, frames averaged=3–4, rotation step = 0.2, frames acquired over 180°=960, filter=no, binning=no, flat field correction=activated. The scanning time ranged from 50 to 140 min. Reconstruction of the cross-section slides was completed using the software NRecon 1.6.6.0, Bruker MicroCT, Kontich, Belgium. To enhance image contrast and compensate for the ring and streak artifacts, the reconstruction parameters were set to the following: smoothing=no, ring artifact correction=5–11, and beam hardening correction=activated. 3D rendering images and segmentation were performed using Amira software (Thermo Fisher Scientific). Images were edited with Photoshop (Adobe).

DNA extraction, amplification, and sequencing

Tissue subsamples used for molecular analyses were taken from the pereiopod 5, which lacks taxonomic value for squat lobsters. However, for smaller specimens or those with detached legs, another pereiopod was used. Although 55 specimens were selected, most failed to yield usable DNA. We amplified the barcode region of the cytochrome *c* oxidase subunit (COI), the mitochondrial 16S ribosomal RNA, and the nuclear 28S ribosomal RNA following the workflow optimized in previous studies on squat lobsters (e.g., Rodríguez-Flores and Schnabel 2023; Rodríguez-Flores et al. 2023). DNA was extracted with the DNeasy Blood and Tissue Kit (Qiagen), according to the manufacturer's protocol. DNA was amplified via PCR using PuReTaq Ready-To-Go (RTG) PCR Beads (Cytiva) with a combination of primers specifically designed for Galatheoidea and Munidopsidae (Rodríguez-Flores et al. 2022) and universal primers (Folmer et al. 1994; Elbrecht and Leese 2017). Specific primers were designed with Geneious Prime 2023.2.1 Build 2023-07020 11:29 (www.geneious.com) from a matrix including only *Munidopsis* spp. and *Galacantha* spp. samples. A portion of the sequences generated for this study were sequenced using a MinION (Oxford Nanopore Technologies, UK), and the rest were outsourced for Sanger sequencing to Genewiz, Cambridge, UK.

After amplification, we pooled the samples in a single PCR product mix (5–10 µL each) for library preparation and Nanopore sequencing following Rodríguez-Flores et al. (2024). The ligation sequencing kit SQK-LSK109 was used for library prep (Oxford Nanopore Technologies, Oxford, UK) following the Amplicons by ligation of Nanopore protocol as well as amplicon sequencing using Nanopore methodology referenced in recent works (e.g., Srivathsan et al. 2021). The NEBNext Ultra kit (New England BioLabs) was used for DNA repair and end-prep (buffer and enzyme) and adaptor ligation (only ligase). A silica bead clean-up was performed first after the end repair and prep step. A second wash took place after adaptor ligation. The washes were done using magnetic beads, AMPure XP, and PCR Purification Reagent (Applied Biosystems) at 0.8× with 70% ethanol. Amplicon sequencing was performed in a MinION using an expired flow cell stored at 4 °C (FLO-MIN106, expired in 2019), which had 246 pores after QC. The run was 36 h long.

Base calling was done with the software Guppy v6.1.7 (Oxford Nanopore), using the super accuracy algorithm. Demultiplexing was done with ONTbarcoder v0.1.9 (Srivathsan et al. 2021), with read coverage set at a minimum of 5 reads.

Molecular phylogenetic analyses

Phylogenetic relationships were estimated based on a concatenated data set of three molecular markers (COI, 16S, and 28S). Following the phylogenies published by Ahyong et al. (2011) and Rodríguez-Flores et al. (2023), we used two related species, *Munidopsis aspera* and *M. robusta*, as outgroups. These species were chosen as

outgroups because they are the closest relatives to the new species that have molecular data publicly available (Rodríguez-Flores et al. 2018, 2023). Details of specimens sequenced and GenBank accession numbers are provided in Table 1. The mean values of uncorrected pairwise genetic distances (p-distances) for the new species and *M. longimanus* were calculated using MEGA11 (Tamura et al. 2021).

We ran BEAST v2.6.3 (Bouckaert et al. 2014) for the Bayesian inference (BI) analyses. We used a partition scheme by gene with linked trees. The nucleotide substitution models were determined using bModelTest, a Bayesian model test package for BEAST 2 (Bouckaert and Drummond 2017). Parameters were set up using BEAUti v2.6.3 (Bouckaert et al. 2014). A strict molecular clock with a clock rate fixed at 1 was used since the time of divergence of the sequences was not estimated. The tree previously selected was a birth-and-death model. Four Markov Chain Monte Carlo (MCMC) runs were conducted for 1×10^7 generations, sampling trees and parameters every 1,000 generations for the estimation of the posterior probabilities. The initial 25% of the generations were discarded as burn-in. The resulting parameter values and convergence of the chains were checked with Tracer v1.7.1 (Rambaut et al. 2018). A maximum credibility tree was built with TreeAnnotator v2.6.3. Phylogenetic trees were plotted and edited in the interactive Tree of Life (iTOL) annotation tool (Letunic and Bork 2019).

Since specimens from two different localities (the Caribbean Sea and GoM; Table 1) were included in the analyses, haplotype networks, using a parsimony network with the function haploNet, were built with the R package pegas (ver. 1.1, see https://cran.r-project.org/package=pegas; Paradis 2010). Analyses were carried out on the COI matrix on a fragment of 503 pb size with no missing data.

Results

Overall, the present results clearly support the existence of a new species of squat lobster in the GoM. The designation of the new species is supported by phylogenetic evidence, morphometric and morphological differences, and marked ecological differences between the new species and its closest relative, *Munidopsis longimanus*. The mean depth of occurrence for the new species is slightly shallower than that of *M. longimanus*, 479–1070 m *versus* 387–1326 m. Additionally, these two species are found in different habitats, with the new species restricted to cold seeps and salt anomalies (Fig. 1), an association not observed for *M. longimanus*.

Geometric, morphometric, and micro-CT results

Selected landmarks and semi-landmarks are illustrated in Fig. 2. We calculated the morphospace of the carapace and abdomen shape using information from the principal components (PCs). PC1 accounted for 40.55% of the variation among the samples, while PC2 accounted for 17.88%. The PCA results indicated two differentiated clusters corresponding to specimens representing two morphotypes: the new species and *M. longimanus*. The morphotype highlighted differences between the two species, including a more elongated

Table 1. Specimens selected for molecular analyses in this study. Locality and GenBank accession numbers are also provided.

Voucher	Species	Locality	CO1	16S	28S
SIO-BIC C13985-1	*Munidopsis sedna* **sp. nov.**	Gulf of Mexico	PP776025	PP777370	PP777379
SIO-BIC C13985-2	*Munidopsis sedna* **sp. nov.**	Gulf of Mexico	PP776026	PP777371	PP777380
SIO-BIC C13985-3	*Munidopsis sedna* **sp. nov.**	Gulf of Mexico	PP776027	PP777372	PP777381
USNM 1407438	*Munidopsis sedna* **sp. nov.**	Gulf of Mexico	PP776028		
USNM 1407440	*Munidopsis sedna* **sp. nov.**	Gulf of Mexico	PP776029		
USNM 1407439	*Munidopsis sedna* **sp. nov.**	Gulf of Mexico	PP776030		
USNM 1666826_3	*Munidopsis sedna* **sp. nov.**	Gulf of Mexico	PP776031		
USNM 1666823_4	*Munidopsis sedna* **sp. nov.**	Gulf of Mexico	PP776032		
USNM 1666826_4	*Munidopsis sedna* **sp. nov.**	Gulf of Mexico	PP776033		
USNM 1666823_3	*Munidopsis sedna* **sp. nov.**	Gulf of Mexico	PP776034		
USNM 1666808_2	*Munidopsis sedna* **sp. nov.**	Gulf of Mexico	PP776035		
USNM 1407437	*Munidopsis sedna* **sp. nov.**	Gulf of Mexico	PP776036		
USNM 1666807_2	*Munidopsis sedna* **sp. nov.**	Gulf of Mexico	PP776037		
MCZ:IZ 48262	*Munidopsis longimanus*	Trinidad and Tobago	PP776038	PP777373	PP777382
ULLZ10851	*Munidopsis longimanus*	Gulf of Mexico	JN166770	JN166741	
MNHN-IU-2013-18823	*Munidopsis longimanus*	Guadeloupe Island	PP776039	PP777374	
MNHN-IU-2013-19045	*Munidopsis longimanus*	Guadeloupe Island	PP776040	PP777375	PP777383
MNHN-IU-2016-6099	*Munidopsis longimanus*	Guadeloupe Island	PP776041	PP777376	PP777384
MNHN-IU-2016-6101	*Munidopsis longimanus*	Guadeloupe Island	PP776042	PP777377	
MNHN-IU-2016-6104	*Munidopsis longimanus*	Guadeloupe Island	PP776043	PP777378	
SIO-BIC C13951	*Munidopsis aspera*	Costa Rica	ON858114	ON858045	ON858114
MNHN-IU-2013-3367/2550	*Munidopsis robusta*	Guadeloupe Island	MG979485	MG979477	ON858171

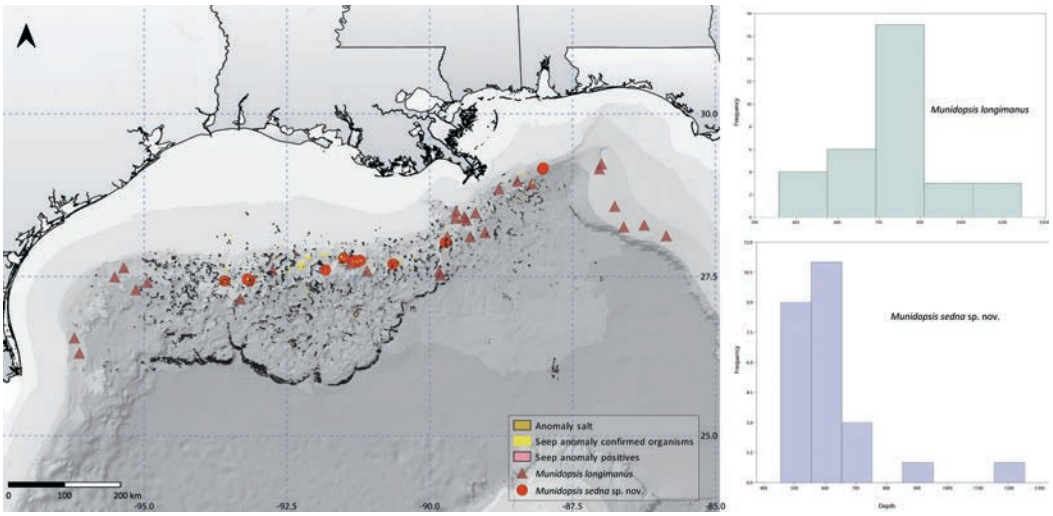

Figure 1. A. Map showing the geographic distribution of the new species and related species in the GoM. The distribution of brine pools and chemosynthetic communities was extracted from Sinclair and Shedd (2012); **B.** Histogram representing the bathymetric distribution of both species.

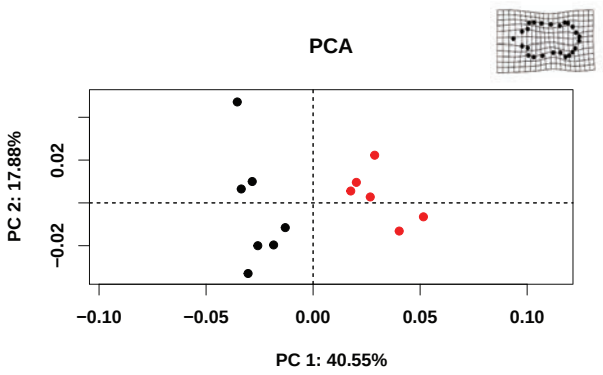

Figure 2. Plot showing PCA results of the analyzed morphospace of both species. Red and black dots represent *Munidopsis sedna* sp. nov. and *Munidopsis longimanus*, respectively.

abdomen for *M. longimanus* and a relatively shorter rostrum for the new species. There was no overlap between the two morphotypes (Fig. 2).

The 3D images resulting from micro-computed tomography showed a clearly distinctive porose tegument with micro-ornamentation in *M. longimanus* that was not present in the new species.

Phylogenetic results

The multilocus BEAST tree recovered two highly supported sister clades (pP = 1) (Fig. 3). The first clade included *Munidopsis longimanus*, occurring in deep waters off Guadalupe, Trinidad and Tobago, and in the GoM.

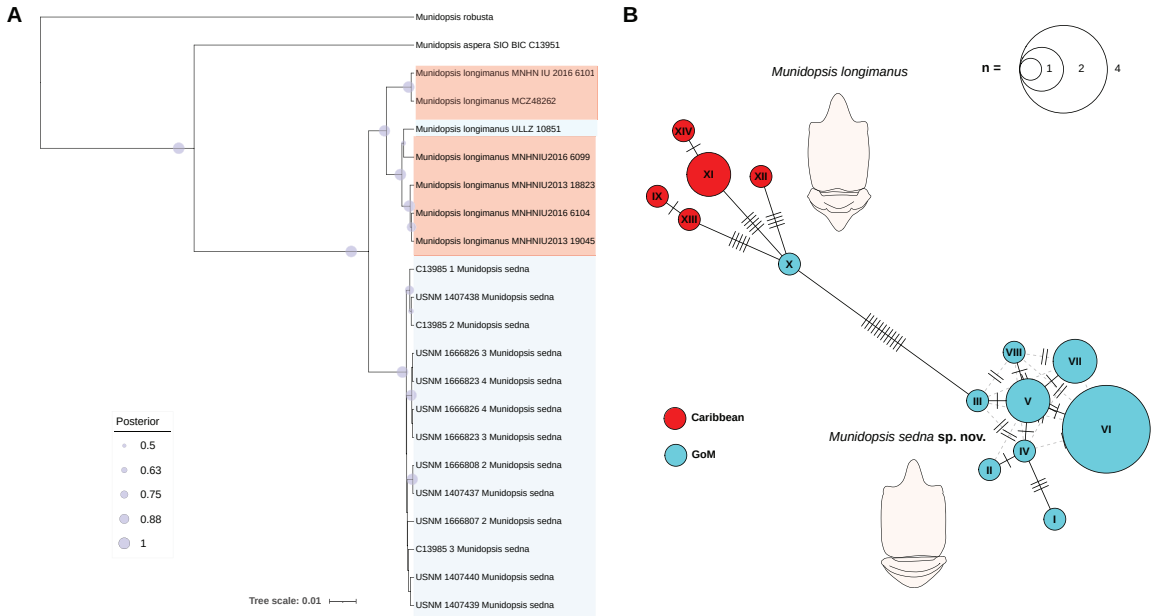

Figure 3. A. Phylogenetic tree resulting from BEAST 2 analyses of the concatenated multilocus matrix (COI, 16S, and 28S). Circles on branches represent the posterior probabilities; **B.** Haplotype network recovered from the analyses of COI data of two species, *Munidopsis longimanus* and *M. sedna* sp. nov. A scale indicates the number of individuals presenting the haplotypes.

The other clade included all specimens of the new species. *Munidopsis aspera* was recovered as a sister species of these two clades; *Munidopsis robusta* was more distantly related. In the COI haplotype network, these two main clades (*M. longimanus* = 6 distinct haplotypes; the new species = 8 distinct haplotypes) are separated by 12 mutational steps. Haplotypes corresponding to *M. longimanus* are grouped in three clusters, all connected by 4–5 mutational steps with the haplotype from the GoM. The network of the new species is represented by a central haplotype connected by 2–3 mutational steps with satellite haplotypes.

The mean genetic p-distances between these two species are 3.25% for the COI, 0.9% for the 16S, and 0.3% for the 28S. Intraspecific mean genetic p-distances were 0.3% for the COI.

Systematics

Superfamily Galatheoidea Samouelle, 1819
Family Munidopsidae Ortmann, 1898
Genus *Munidopsis* Whiteaves, 1874

Munidopsis sedna sp. nov.

https://zoobank.org/5D32B12B-7EC7-495E-A1E8-5BA15E57C8C3

Figs 4, 5, 6A, B, 7

Munidopsis sp. nov. 1: Bergquist et al. (2003), p. 205, 206, 210, 216.

Munidopsis sp.: Fisher et al. (2007), p. 123.

Munidopsis sp. 1: Cordes et al. (2008), p. 781, 783, 786.

Munidopsis sp. (small): Lessard-Pilon et al. (2010), p. 1894, 1885, 1896, 1897.

Material examined. *Holotype*. Gulf of Mexico, United States, Green Canyon, Block 246, 27.6897°N, 90.6450°W, coll. TDI-Brooks International, E. Cordes & C. Fisher, LOPH II, Jason II ROV; Ronald H. Brown R/V, Cruise # RB-10-07, Stn GC 246, sample # MMS-LOPH/II/J2-528/GC246, 17-Oct-2010: M 9.7 mm (USNM 1407437).

***Paratypes*.** Gulf of Mexico, United States, Green Canyon, Block 246, 27.6897°N, 90.6450°W, coll. TDI-Brooks International, E. Cordes & C. Fisher, LOPH II, Jason II ROV; Ronald H. Brown R/V, Cruise # RB-10-07, Stn GC 246, sample # MMS-LOPH/II/J2-528/GC246, 17-Oct-2010: 1 M 7.9 mm (USNM 1407438). —Green Canyon, Block 246, 27.6897°N, 90.6450°W, col. TDI-Brooks International, E. Cordes & C. Fisher, LOPH II Jason II ROV; Ronald H. Brown R/V, Cruise # RB-10-07, Stn GC 246, sample # MMS-LOPH/II/J2-528/GC246, 17-Oct-2010: 1 M 6.9 mm (USNM 1407439) —Green Canyon, Block 246, 27.6897°N, 90.6450°W, coll. TDI-Brooks International, E. Cordes & C. Fisher, LOPH II Jason II ROV; Ronald H. Brown R/V, Cruise # RB-10-07, Stn GC 246, sample # MMS-LOPH/II/J2-528/GC246, 17-Oct-2010: 1 M 8.1 mm (USNM 1407440). —Green Canyon, Block 246, 27.6897°N, 90.6450°W, coll. TDI-Brooks International, E. Cordes & C. Fisher, LOPH II Jason II ROV; Ronald H. Brown R/V, Cruise # RB-10-07, Stn GC 246, sample # MMS-LOPH/II/J2-528/GC246, 17-Oct-2010: 1 M 4.1 mm, 1 F 2.7 mm (USNM 1407474). —Green Canyon 234 27.7461°N, 91.2211°W, coll. C. Fisher, CHEMO, Seward Johnson II R/V; Johnson Sea Link DSR/V, Cruise # 4436, Stn GC 234, sample # CHEMO/JSL/4436, 534 m, 24-Jun-2002, 1 M 10.3 mm (USNM s). —Green Canyon 234, 27.7461°N, 91.2211°W, coll. C. Fisher, CHEMO, Johnson Sea Link DSR/V, Cruise # 4588, Stn GC 234, sample # CHEMO/JSL/4588 534 m, 5-Sep-2003: 34 M 3.3–9.1 mm, 22 ov. F 4.5–7.6 mm, 17 F 3.6–7.2 mm, 7 specimens with rhizocephalan barnacles parasites (USNM 1666805). —Garden Banks 535, 27.4289°N, 93.5897°W, coll. C. Fisher, CHEMO, Johnson Sea Link DSR/V, Cruise # 4583, Stn GB 535, sample # CHEMO/JSL/4583, 575 m, 3-Sep-2003: 4 M 4.5–7.9 mm, 4 ov. F 5.2–9.4 mm, 3F 4.8–8.0 mm, 1 juv 3 mm (USNM 1666806). Bush Hill, Green Canyon, 27.780300°N, 91.5064°W, col. C. Fisher, CHEMO, Johnson Sea Link I DSR/V; Seward Johnson R/V, Cruise #JSL I 1991, sample # JSL 3129, 549 m, 15-Sep-1991:1 M 8.5 mm (USNM 1704816).—180 km south of New Orleans, LA, Gulf of Mexico, Brine Pool NR1 cold seep, 27.7230°N, 91.2750°W, coll. R. Vrijenhoek et al., R/V Seward Johnson I and II, 650 m, 3-Oct-2001: 6 M 7.75–10.11 mm, 7 ov. F 6.72–9.9 mm, 1 F 8.91 mm (SIO-BIC C13985).

Other material. For comparison, additional material of *Munidopsis sedna* sp. nov., *M. longimanus*, and *M. brevimanus* (A. Milne-Edwards, 1880) was examined (see Suppl. material 1).

Etymology. In Inuit mythology, *Sedna* is the goddess of the sea and marine animals, also known as the Mother or Mistress of the Sea. The specific name is substantive in apposition.

Diagnosis. Carapace, excluding rostrum as long as broad, dorsal surface nearly smooth or covered with small granules. Rostrum broadly triangular, not acute at tip, *ca.* one-third carapace length. Frontal margin without delimited orbit, transverse. Cervical grooves distinct. Lateral margins subparallel, without distinct spines. Sternum longer than wide, maximum width at sternites 4 to 6; sternite 3 short and wide, width about half that of sternite 4. Abdomen spineless; telson with 10 plates. Eyes small, movable, and unarmed; cornea small, slightly elongated; peduncle larger than cornea. Antennular article 1 swollen laterally. Basal part of each Mxp 3 not separated by an appreciable gap; merus with 2 acute spines on flexor margin. P1 long and slender, more than twice carapace length, longer than P2. P2–4 moderately stout; extensor margin of articles carinate; propodi not expanded distally; dactyli curved distally; flexor margin with row of 8–12 teeth bearing corneous spinules. Epipods absent from all pereiopods.

Description. *Carapace*: As long as broad, widest at posterior part; convex from side to side. Dorsal surface sparsely covered with small granules or nearly smooth, hepatic and anterior branchial areas with minute granules or smooth. Regions well delineated by furrows, anterior and posterior cervical grooves distinct. Gastric region slightly

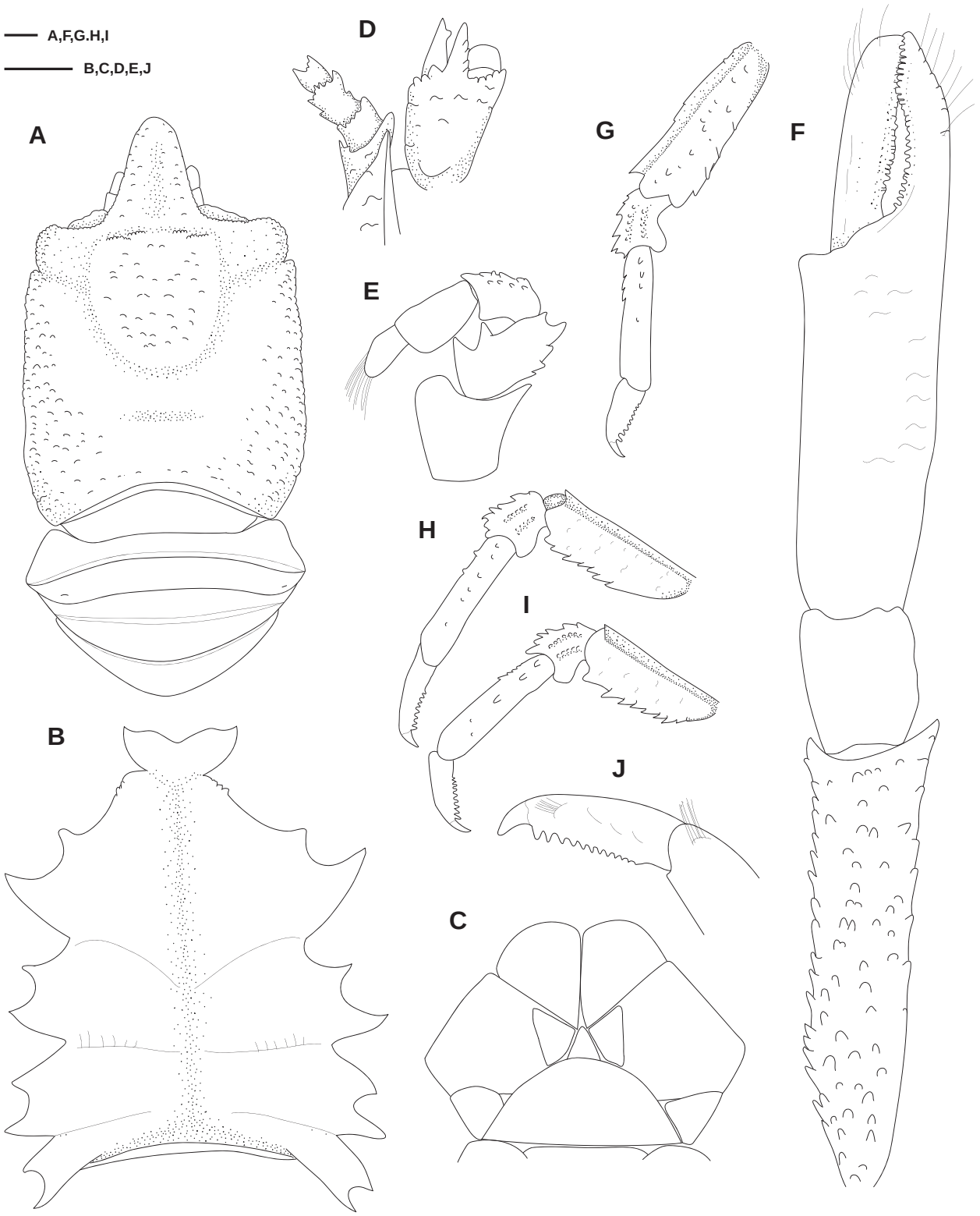

Figure 4. Line drawings of *Munidopsis sedna* sp. nov., Gulf of Mexico, holotype, male 9.7 mm (USNM 1407437). **A.** Carapace and abdomen, dorsal view; **B.** Thoracic sternum, ventral view; **C.** Telson; **D.** Right part of the cephalothorax, ventral view, showing antennular article 1 and antennal peduncle, and anterior part of the pterygostomian flap; **E.** Left Mxp3, lateral view; **F.** Right P1, dorsal view; **G.** Left P2, lateral view; **H.** Left P3, lateral view; **I.** Left P4, lateral view; **J.** Left P2 dactylus, lateral view. Scale bars: 1 mm.

convex. Posterior margin unarmed, dorsally smooth. Rostrum spatulate, horizontally straight, 0.3–[0.4] times carapace length, 0.2–[0.3] times anterior width of carapace, [1.2]–1.9 times as long as wide; dorsal surface concave, with small granules. Frontal margin straight behind ocular peduncle; outer orbital angle not produced, concave; orbit not delimited. Lateral margins straight, no spines; anterolateral angle not produced; blunt, sparsely granulate;

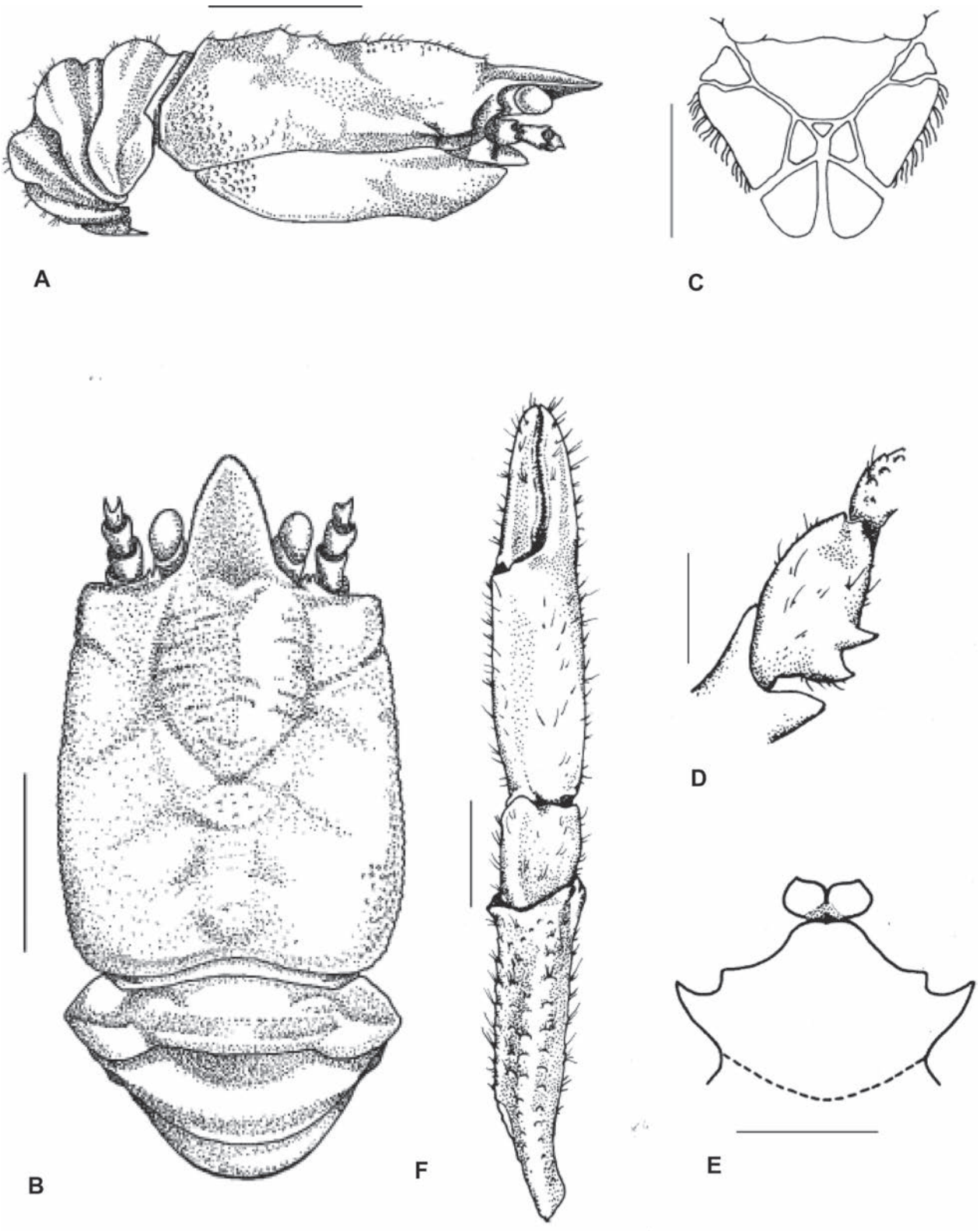

Figure 5. Drawings of *Munidopsis sedna* sp. nov., Gulf of Mexico, paratype, male 8.5 mm (USNM 1704816). **A.** Carapace and abdomen, lateral view; **B.** Carapace and abdomen, dorsal view; **C.** Telson; **D.** Right Mxp3, lateral view; **E.** Sternites 3 and 4, ventral view; **F.** Right P1, dorsal view. Scale bars: 4 mm (**A, B, F**); 2 mm (**C, E**); 1 mm (**D**).

branchial margins granulate; deep notch between hepatic and branchial margins. Epistomial spine absent. Pterygostomian flap surface covered with small granules, anterior margin blunt.

***Sternum*:** Slightly longer than broad, maximum width at sternites 4 to 6. Sternite 3 broad, [3.0] times wider than long, anterolaterally produced and often serrated; anterior margin with broad median notch flanked by 2 lobes.

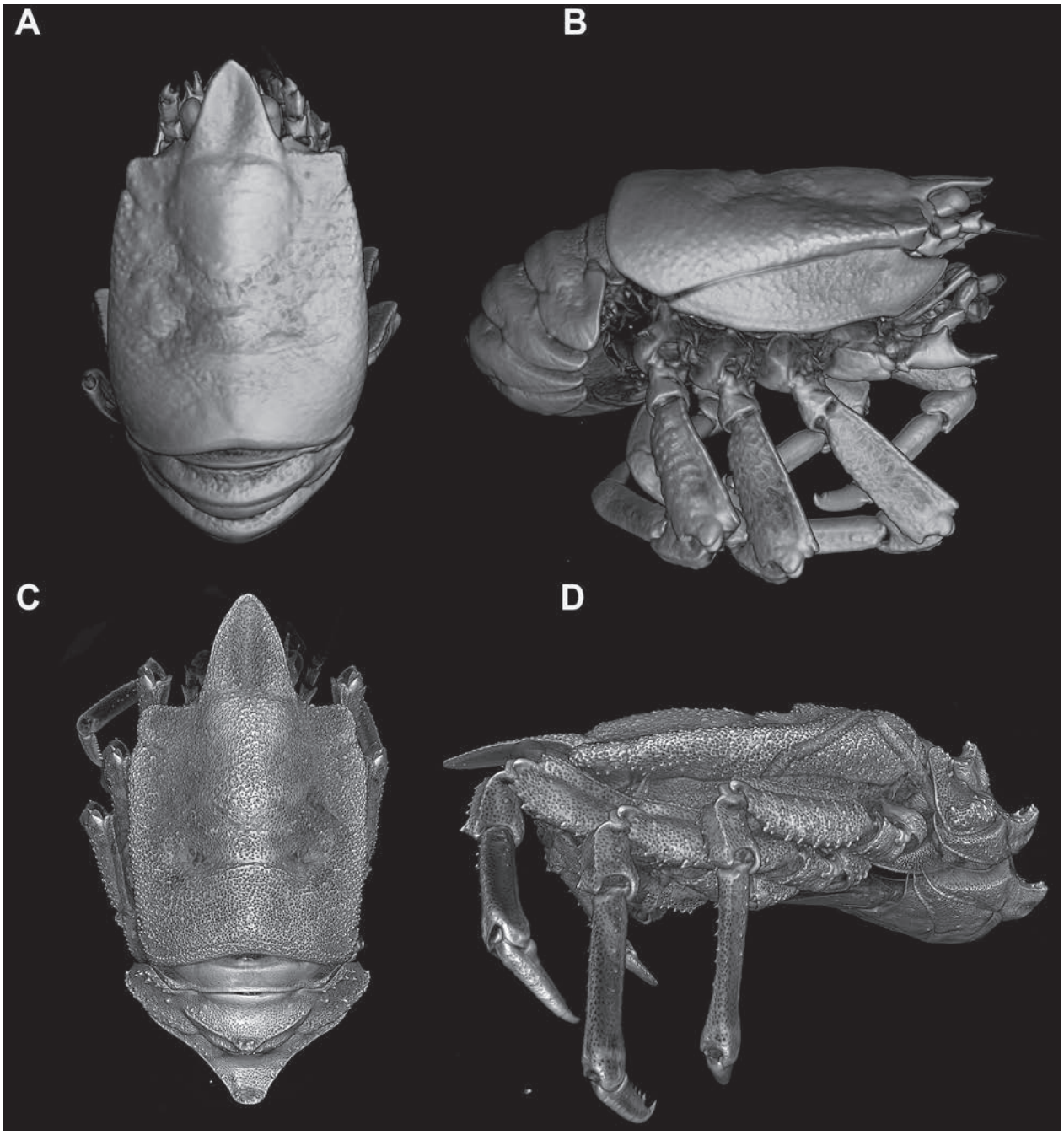

Figure 6. 3D renderings of micro-computed tomography x-ray images. **A, B.** *Munidopsis sedna* sp. nov., Gulf of Mexico, male, paratype (USNM 1666822); **C, D.** *Munidopsis longimanus*, Guadeloupe (MNHN-2013-18823).

Sternite 4 widely elongate anteriorly; anterior margin often serrated; surface depressed in midline, smooth; greatest width [3.3] times that of sternite 3 and [2.1] times length.

***Abdomen*:** Unarmed. Tergites often with small sparse granules on all surfaces; tergites 2–3 each with 1 elevated transverse ridge; tergites 4–6 without ridges; tergite 6 with weakly developed posterolateral lobes and nearly transverse posteromedian margin. Telson composed of 10 plates; [0.7] times as wide as long.

***Eye*:** Eyestalk movable, partially concealed beneath rostrum; peduncle elongated, smooth, [2.7] times as wide as long; cornea ovoid, narrower than peduncle; length [1.3] times that of peduncle.

***Antennule*:** Article 1 of peduncle with dorsolateral and distolateral spines subequal in size; distolateral margin with denticles; distomesial margin with smaller denticles.

***Antenna*:** Peduncle usually not exceeding eye, armed marginally with denticles and granules. Article 1 with small distolateral spine, distomesial angle produced but unarmed. Article 2 unarmed or with minute distomesial and distolateral spine. Article 3 with small distomesial and distolateral spines or with prominent distal denticles. Article 4 unarmed.

***Mxp3*:** Lateral surface with scattered granules. Ischium [1.1] times longer than merus measured on extensor margin; distal extensor margin serrated. Flexor margin of

Figure 7. In situ image of *Munidopsis sedna* sp. nov. in a brine pool in the Gulf of Mexico. Photo courtesy of the BBC.

merus with 2 prominent proximal spines subequal in size and small distal spine; extensor margin with several denticles and small or large distal spine. Carpus with several denticles on dorsal surface.

***P1*:** Slender, 2.4–2.8 (females) and 3.0–[3.7] (males) times longer than PCL, cylindrical. Merus 3.0–[3.6] times as long as carpus, with denticles and granules. Carpus [1.1]–1.5 times longer than broad, unarmed. Palm unarmed, slender, [2.8]–3.0 times longer than carpus, [2.5]–2.8 times as long as broad. Fingers unarmed, smooth, [0.6] –0.7 times longer than palm; opposable margins nearly straight, gaping, distally spoon-shaped; fixed finger without denticulate carina on distolateral margin. Heterochely present in some specimens.

***P2–4*:** Moderately stout, subcylindrical, flattened in cross-section, slightly decreasing in size posteriorly; surfaces with some denticles and granules. P2 merus moderately slender, [0.7] times PCL, nearly [3.5] times longer than high, [1.3] times length of P2 propodus. Meri decreasing in length posteriorly (P3 merus [0.9] length of P2 merus, P4 merus [0.9] length of P3 merus); extensor margin strongly carinate, distal part ending in thick spine; flexor margin with a row of spines. Carpi with spines on each extensor margin, 2 parallel granulate carinas along dorsal side. Propodi 4.5–5.2 times as long as high, flattened in cross-section, with some tubercles proximally on each extensor margin; lateral surface with some small spines on proximal half; flexor margin unarmed. Dactyli moderately slender, 0.5–0.6 times length of propodi; distal claw short, moderately curved distally; flexor margin nearly straight, armed with 8–12 corneous spines.

Epipods absent from pereiopods.

***Eggs*:** About 5–25 rounded eggs of about 1 mm each.

***Coloration*:** Carapace and abdomen orange, white stripe in midline. Eyes light orange. Pereopods orange or light orange, whitish distally.

Distribution. Gulf of Mexico, from 479 to 1,250 m depth.

Habitat. All specimens examined were collected from cold seeps or associated with the seep communities surrounding brine pools.

Genetic data. COI, 16S rRNA, and 28S rRNA (see Table 1).

Remarks. The new species belongs to the *Elasmonotus* group (A. Milne Edwards, 1880), characterized by species having a carapace with a transverse frontal margin, without a delimited orbit, an elongated cornea, and the dorsal surface of the carapace usually smooth. Within the *Elasmonotus* group, *Munidopsis sedna* sp. nov. is morphologically similar to *M. brevimanus* and *M. longimanus*; however, the new species can be distinguished from these other species by the following morphological characters:

- The abdominal tergites 2–4 are smooth and unarmed in *M. sedna*, whereas they are armed with a broad median spine covered with tubercles in *M. longimanus* and *M. brevimanus*.
- The carapace ornamentation is smooth and/or sparsely granulated in the new species, whereas it is highly tuberculate and porose in *M. brevimanus* and *M. longimanus*, respectively.
- The P1 is longer and more slender in the new species than in *M. brevimanus*.
- The abdomen is more elongated in dorsal view in *M. longimanus* and *M. brevimanus* than in the new species, whereas the rostrum is relatively shorter in the new species.

Mayo (1974) discussed the differences between *M. brevimanus* and *M. longimanus* in detail. The main differences between these two species are the relative length of the

P1, which is much shorter and stouter in *M. brevimanus* than in *M. longimanus* (and also in the new species); and the relative length of the median spines on the abdominal tergites 2–4, which are less projected in *M. brevimanus* than in *M. longimanus* (the spines are absent in the new species). Nevertheless, *M. longimanus* females and juveniles seem to have fewer projected abdominal spines (Mayo 1974; this work). The overlap of morphological characters and the general similarity of these two species led of *M. brevimanus* being considered a junior subjective synonym of *M. longimanus* (see A. Milne-Edwards and Bouvier 1894: 283). However, after further examination of the type specimens of the two species and other material, Chace (1942) resurrected *M. brevimanus* as a valid taxon; this taxonomical decision was later confirmed by Mayo (1974).

Discussion

Squat lobsters from hydrothermal vents: endemic vs. colonizers

Deep-sea chemosynthetic ecosystems, such as hydrothermal vents, cold seeps, and woodfalls, support a variety of organisms, whose association with these ecosystems can vary from vagrant to colonist to endemic members of the benthic community (Carney 1994). Squat lobsters are commonly observed, sometimes in high abundances, in these extreme habitats where they play a key role as heterotrophs consuming chemosynthetic products (e.g., Chevaldonné and Olu 1996; MacDonald et al. 2004; Martin and Haney 2005; Macpherson et al. 2006; Baeza 2011; Gaytán-Caballero et al. 2022). To date, several species from the genera *Munidopsis* and *Munida* have been found in association with these habitats (hydrothermal vents and cold seeps) in the Atlantic, primarily along the Mid-Atlantic ridge, but also associated with cold seeps in the GoM (MacDonald et al. 2004; Macpherson and Segonzac 2005; Macpherson et al. 2006; Coykendall et al. 2017; Gaytán-Caballero et al. 2022). Most species collected from nearby cold seeps are likely vagrants since they have been collected in and around other deep-sea habitats (Wenner 1982; Macpherson and Segonzac 2005; Baba et al. 2008; Coykendall et al. 2017; Gaytán-Caballero et al. 2022). However, *Munidopsis sedna* sp. nov., described herein, is the first species of squat lobster considered to be endemic to cold seep habitats in the GoM in particular and the Atlantic in general.

In the Pacific Ocean, several species are known to be endemic to chemosynthetic habitats, including *Munidopsis alvisca* Williams, 1988 from the East Pacific Rise, *M. lauensis* Baba & de Saint Laurent, 1992 from the Lau Basin, and *M. ryukyuensis* Cubelio, Tsuchida & Watanabe, 2007 from hydrothermal vents in the Hatoma Knoll, and recently discovered species inhabiting cold seeps in the East Pacific (Williams 1988; Baba and de Saint Laurent, 1992; Martin and Haney 2005; Cubelio et al. 2007; Rodríguez-Flores et al. 2023). These endemic species may occur in high abundances and with a certain degree of isolation. For example, *M. lentigo* Williams & Van Dover, 1983, is known only from a few vent sites in the Gulf of California. However, a sister species was discovered recently from vent sites off the Galapagos Islands (Rodríguez-Flores et al. 2023). Given that the geographic distance between these two locations is relatively small, an evolutionary scenario of a recent allopatric speciation process is highly probable. This same scenario could also explain the shallow genetic divergences observed between *M. sedna* sp. nov., currently known only from the northern GoM, and its sister species, *M. longimanus*.

Ecological notes

Based on *in situ* observations and collections, the distribution of *Munidopsis sedna* sp. nov. appears to be restricted to cold seep habitats and brine pools in the northern GOM. This species is a common member of the mobile epifauna associated with chemosynthetic invertebrates that colonize GoM cold seeps on the continental slope (MacDonald et al. 1989, 1990a, 1990b). Specifically, *M. sedna* sp. nov. occurs in and around the structurally complex aggregations of vestimentiferan tube worms (*Lamellibrachia luymesi* and *Seepiophila jonesi*) and mussels (*Bathymodiolus childressi*) that not only provide shelter for the squat lobsters but also are other endemic primary consumers such as non-selective grazers, detritivores, and filter feeders (Bergquist et al. 2003, Fisher et al. 2007, Fig. 5). The new squat lobster can be extremely abundant, occurring at densities on the order of tens per square meter. However, the abundance of the species declines at older stages of the seep community succession (Cordes et al. 2009).

Individuals of *M. sedna* sp. nov. are typically observed clinging to the anterior ends of the vestimentiferan tubes (MacDonald et al. 1989) and occupy a similar niche at mytilid assemblages (Fisher et al. 2007, Fig. 5). These squat lobsters may position themselves on the posterior ends of the tubeworms and mussels to feed on exposed tissue. However, Bergquist et al. (2003) did not observe any significant damage to live vestimentiferans caused by non-lethal plume cropping and suggested that direct predation on live vestimentiferan tissue likely represents a minor trophic contribution at these cold seeps. Additionally, isotope analyses confirmed that the new species did not directly consume *B. childressi* (MacAvoy et al. 2008a). Studies on the trophic ecology of *M. sedna* sp. nov. from cold seeps in Green Canyon and Garden Banks Lease areas (540–640 m) suggest that populations of the species from GoM cold seeps rely heavily on small heterotrophic organisms, which feed on material produced by free-living chemosynthetic bacteria (MacAvoy et al. 2008a, b). Thus, this small squat lobster species acts as an important link among macroinvertebrates, fishes and small heterotrophic organisms that feed on the chemoautotrophic bacteria (MacAvoy et al. 2008a, b; Demopoulos et al. 2010).

Species of *Munidopsis* in the Gulf of Mexico

Munidopsis longimanus, the closest relative and sister species to *M. sedna* sp. nov., is widely distributed throughout the GoM and in the Caribbean Sea at depths ranging from 292 to 1281 m (Mayo 1974; Navas et al. 2003; Felder et al. 2009; Baba et al. 2008; Fig. 1). Given the presumed habitat specificity of *M. sedna* sp. nov. to cold seeps, it is possible that divergent natural selection driven by differences between disparate ecological niches (i.e., ecological speciation) contributes to reproductive isolation. In addition to differences in the distribution patterns and habitat utilization between the two species, molecular evidence, including shallow genetic divergences between lineages and the low interspecific genetic distances presented between the sister species, also supports the hypothesis of ecological speciation. However, it would be necessary to gather more evidence, such as an intensive study of the feeding ecology of *M. longimanus* and a more comprehensive taxonomic sampling of *Munidopsis* species from the western Atlantic, to test this hypothesis. So far, the ecological data of *M. longimanus* is scarce and limited to reports that this species has been collected with *Munidopsis platirostris* (A. Milne-Edwards & Bouvier, 1894), a leptostracan, and the limpet *Notocrater youngi* McLean & Harasewych,1995 (A. Milne-Edwards and Bouvier 1894, McLean and Harasewych,1995; Williams et al. 2019).

Most squat lobster species from the western Atlantic are distributed both in the Caribbean and the GoM, and some also occur in the northwestern and southwestern Atlantic (Baba et al. 2008; Felder et al. 2009; Poupin and Corbari 2016). Only six squat lobster species were exclusively found in the GoM: three *Uroptychus*, one *Munida*, and two *Munidopsis* (Baba et al. 2008; Felder et al. 2009; Baba and Wicksten 2015, 2017a, 2017b; Macpherson et al. 2016). *Munidopsis sedna* sp. nov. here described has been known for several years, but its identity has remained a mystery, probably because of the taxonomic problems posed by two closely related species living in the GoM and the Caribbean, *M. longimanus* and *M. brevimanus*. One of the most conspicuous differences between these two species is the length of the chelipeds (P1), which is shorter in *M. brevimanus*. The length of P1 could be a substantial difference that separates species exploiting different resources, as most galatheids, both deposit feeders and predators, use their P1 to capture food and transfer it to the feeding appendages (Nicol 1932). *Munidopsis brevimanus* is a rare species only known with a few records in the Caribbean and the GoM (Mayo 1974; Navas et al. 2003; Felder et al. 2009), and so far, it has not been found sympatrically with the new species.

Conservation perspective

Cold seep and hydrothermal vent sites, often referred to as ”deep islands” of biodiversity, are isolated areas, unstable in time (Vrijenhoek 2010), and are considered vulnerable ecosystems. Given their ephemeral nature and scattered distributions, endemic organisms living in these chemosynthetic habitats show fragmented distributions and isolation, relying on high dispersal capabilities to maintain population connectivity (Vrijenhoek 1997). The fauna endemic to these ecosystems is subject to multiple threats, and if these seeps are massively affected by a catastrophic event (such as a large oil spill), the metapopulation dynamics of organisms associated with this kind of habitat can be severely affected by reducing their possibilities of recolonization, even leading to local or wider geographical-scale complete extinction.

In summary, the new species here presented constitutes a cold-seep endemism only known from a few localities in the GoM. *Munidopsis sedna* sp. nov. has diverged recently from its sister species, which is likely an adaptation to live in the “shallow” cold seeps on the continental shelf in the northern GoM. Its limited distribution pattern and shallow genetic structure suggest stepping-stone dispersal connectivity between nearby cold seeps in the GoM. However, we would need to test this hypothesis with other sources of data, such as rapidly evolving markers that have a resolution at the population scale. This new species is highly vulnerable to extinction threats, given its limited distribution. Therefore, it is critical that we fully characterize and describe the diversity of these fragile deep-sea ecosystems.

Acknowledgments

We thank all the crew, including ROV pilots, navigators, mappers, expedition leaders, and scientists from the numerous expeditions in the Gulf of Mexico where this species was collected, processed, and photographed. We are indebted to Laure Corbari for facilitating the revision of specimens collected during the KARUBENTHOS 2015 expedition. K. Vaughn kindly prepared Fig. 5. Comparative specimens were kindly made available from collections housed at the University of Miami, Texas A&M University, the Field Museum, the Museum of Comparative Zoology (Harvard University), and the Muséum national d’Histoire Naturelle.

The funding for this project was obtained through the Biodiversity Postdoctoral Fellowship program at Harvard University and from the Mesophotic and Deep Benthic Communities (MDBC) project at the Smithsonian National Museum of Natural History.

References

Adams DC, Otárola-Castillo E (2013) Geomorph: An R package for the collection and analysis of geometric morphometric shape data. Methods in Ecology and Evolution 4(4): 393–399. https://doi.org/10.1111/2041-210X.12035

Ahyong ST, Andreakis N, Taylor J (2011) Mitochondrial phylogeny of the deep-sea squat lobsters, Munidopsidae (Galatheoidea). Zo-

ologischer Anzeiger 250(4): 367–377. https://doi.org/10.1016/j.jcz.2011.06.005

Baba K (2018) Chirostylidae of the western and central Pacific: *Uroptychus* and a new genus (Crustacea, Decapoda, Anomura). Tropical Deep-sea Benthos 30. Memoires du Muséum national d'Histoire naturelle 212: 1–612.

Baba K, de Saint Laurent M (1992) Chirostylid and galatheid crustaceans (Decapoda: Anomura) from active thermal vent areas in the southwest Pacific. Scientia Marina 56: 321–332.

Baba K, Wicksten M (2015) *Uroptychus minutus* Benedict, 1902 and a closely related new species (Crustacea, Anomura, Chirostylidae) from the western Atlantic Ocean. Zootaxa 3957(2): 215–225. https://doi.org/10.11646/zootaxa.3957.2.5

Baba K, Wicksten MK (2017a) *Uroptychus atlanticus*, a new species of squat lobster (Crustacea, Decapoda, Anomura, Chirostylidae) from the western Atlantic Ocean. Zootaxa 4227(2): 295–300. https://doi.org/10.11646/zootaxa.4227.2.10

Baba K, Wicksten MK (2017b) *Uroptychus nitidus* (A. Milne-Edwards, 1880) and related species (Crustacea, Decapoda, Anomura, Chirostylidae) from the western Atlantic. Zootaxa 4221(3): 251–290. https://doi.org/10.11646/zootaxa.4221.3.1

Baba K, Williams AB (1998) New Galatheoidea (Crustacea, Decapoda, Anomura) from hydrothermal systems in the West Pacific Ocean Bismarck Archipelago and Okinawa Trough. Zoosystema 20: 143–156.

Baba K, Macpherson E, Poore GCB, Ahyong ST, Bermudez A, Cabezas P, Lin C-W, Nizinski M, Rodrigues C, Schnabel KE (2008) Catalogue of squat lobsters of the world (Crustacea, Decapoda, Anomura families Chirostylidae, Galatheidae and Kiwaidae). Zootaxa 1905(1): 1–220. https://doi.org/10.11646/zootaxa.1905.1.1

Baba K, Ahyong S, Macpherson E (2011) Morphology of marine squat lobsters. In: Poore GCB, Ahyong ST, Taylor J (Eds) The Biology of Squat Lobsters. CSIRO Publishing, Victoria, Australia, 1–37.

Baeza JA (2011) Squat lobsters as symbionts and in chemo–autotrophic environments. In: Poore GCB, Ahyong ST, Taylor J (Eds) The Biology of Squat Lobsters. CSIRO Publishing, Victoria, Australia, 249–270.

Bergquist DC, Ward T, Cordes EE, McNelis T, Howlett S, Kosoff R, Hourdez S, Carney R, Fisher CR (2003) Community structure of vestimentiferan-generated habitat islands from Gulf of Mexico cold seeps. Journal of Experimental Marine Biology and Ecology 289(2): 197–222. https://doi.org/10.1016/S0022-0981(03)00046-7

Bouckaert R, Drummond AJ (2017) bModelTest: Bayesian phylogenetic site model averaging and model comparison. BMC Evolutionary Biology 17.1: 42. https://doi.org/10.1186/s12862-017-0890-6

Bouckaert R, Heled J, Kühnert D, Vaughan T, Wu CH, Xie D, Suchard MA, Rambaut A, Drummond AJ (2014) BEAST 2: A software platform for Bayesian evolutionary analysis. PLoS Computational Biology 10(4): e1003537. https://doi.org/10.1371/journal.pcbi.1003537

Carney RS (1994) Consideration of the oasis analogy for chemosynthetic communities at Gulf of Mexico hydrocarbon vents. Geo-Marine Letters 14(2–3): 149–159. https://doi.org/10.1007/BF01203726

Chace Jr FA (1942) Reports on the scientific results of the Atlantis expeditions to the West Indies, under the joint auspices of the University of Havana and Harvard University. The Anomuran Crustacea I Galatheidea. Torreia 11: 1–106.

Chevaldonné P, Olu K (1996) Occurrence of anomuran crabs (Crustacea: Decapoda) in hydrothermal vent and cold–seep communities: a review. Proceedings of the Biological Society of Washington 109(2): 286–298.

Cordes EE, Carney SL, Hourdez S, Carney RS, Brooks JM, Fisher CR (2007) Cold seeps of the deep Gulf of Mexico: Community structure and biogeographic comparisons to Atlantic equatorial belt seep communities. Deep-sea Research. Part I, Oceanographic Research Papers 54(4): 637–653. https://doi.org/10.1016/j.dsr.2007.01.001

Cordes EE, McGinley MP, Podowski EL, Becker EL, Lessard-Pilon S, Viada ST, Fisher CR (2008) Coral communities of the deep Gulf of Mexico. Deep-sea Research. Part I, Oceanographic Research Papers 55(6): 777–787. https://doi.org/10.1016/j.dsr.2008.03.005

Cordes EE, Bergquist DC, Fisher CR (2009) Macro–ecology of Gulf of Mexico cold seeps. Annual Review of Marine Science 1(1): 143–168. https://doi.org/10.1146/annurev.marine.010908.163912

Cordes EE, Hourdez S, Roberts HH (2010) Unusual habitats and organisms associated with the cold seeps of the Gulf of Mexico. In: Kiel S (Ed.) The Vent and Seep Biota. Topics in Geobiology 33, Springer, Dordrecht, 315–331. https://doi.org/10.1007/978-90-481-9572-5_10

Coykendall DK, Nizinski MS, Morrison CL (2017) A phylogenetic perspective on diversity of Galatheoidea (*Munida*, *Munidopsis*) from cold–water coral and cold seep communities in the western North Atlantic Ocean. Deep-sea Research. Part II, Topical Studies in Oceanography 137: 258–272. https://doi.org/10.1016/j.dsr2.2016.08.014

Cubelio SS, Tsuchida S, Watanabe S (2007) New species of *Munidopsis* (Decapoda, Anomura, Galatheidae) from hydrothermal vent in Okinawa Trough and cold seep in Sagami Bay. Crustacean Research 36(0): 1–14. https://doi.org/10.18353/crustacea.36.0_1

Demopoulos AWJ, Gualtieri D, Kovacs K (2010) Food-web structure of seep sediment macrobenthos from the Gulf of Mexico. Deep-sea Research. Part II, Topical Studies in Oceanography 57(21–23): 1972–1981. https://doi.org/10.1016/j.dsr2.2010.05.011

Desbruyères D, Segonzac M, Bright M (2006) Handbook of deep-sea hydrothermal vent fauna, Second completely revised edition, Linz, Denisia, 18?? 544 pp.

Dong D, Gan Z, Li X (2021) Descriptions of eleven new species of squat lobsters (Crustacea, Anomura) from seamounts around the Yap and Mariana Trenches with notes on DNA barcodes and phylogeny. Zoological Journal of the Linnean Society 192(2): 306–355. https://doi.org/10.1093/zoolinnean/zlab003

Elbrecht V, Leese F (2017) Validation and development of COI metabarcoding primers for freshwater macroinvertebrate bioassessment. Frontiers in Environmental Science 5: 11. https://doi.org/10.3389/fenvs.2017.00011

Felder DL, Álvarez F, Goy JW, Lemaitre R (2009) Decapoda (Crustacea) of the Gulf of Mexico, with comments on the Amphionidacea. In: Felder DL, Camp DK (Eds) Gulf of Mexico Origin, Waters, and Biota, Volume?? 1, Biodiversity: College Station, Tex, Texas AM University Press, 1019–1104.

Fisher C, Roberts H, Cordes E, Bernard B (2007) Cold seeps and associated communities of the Gulf of Mexico. Oceanography 20(4): 118–129. https://doi.org/10.5670/oceanog.2007.12

Folmer O, Black M, Hoeh W, Lutz R, Vrijenhoek R (1994) DNA primers for amplification of mitochondrial cytochrome c oxidase subunit I from diverse metazoan invertebrates. Molecular Marine Biology and Biotechnology 3(5): 294–299.

Gaytán-Caballero A, Escobar-Briones E, Robles R, Macpherson E (2022) *Munidopsis geyeri* and *M. exuta* (Crustacea, Munidopsidae):

A study of two deep-sea, amphi-Atlantic species that co-occur in the southern Gulf of Mexico. Zootaxa 5213(4): 301–335. https://doi.org/10.11646/zootaxa.5213.4.1

Goffredi SK, Jones WJ, Erhlich H, Springer A, Vrijenhoek RC (2008) Epibiotic bacteria associated with the recently discovered Yeti crab, *Kiwa hirsuta*. Environmental Microbiology 10(10): 2623–2634. https://doi.org/10.1111/j.1462-2920.2008.01684.x

Hammer Ø, Harper DAT, Ryan PD (2001) PAST: Paleontological Statistics Software Package for Education and Data Analysis. Palaeontologia Electronica 4(1): 1–9. http://palaeo-electronica.org/2001_1/past/issue1_01.htm

Kenk VC, Wilson BR (1985) A new mussel (Bivalvia, Mytilidae) from hydrothermal vents, in the Galapagos Rift zone. Malacologia 26(1–2): 253–271.

Lessard-Pilon S, Porter MD, Cordes EE, MacDonald I, Fisher CR (2010) Community composition and temporal change at deep Gulf of Mexico cold seeps. Deep-sea Research. Part II, Topical Studies in Oceanography 57(21–23): 1891–1903. https://doi.org/10.1016/j.dsr2.2010.05.012

Letunic I, Bork P (2019) Interactive Tree Of Life (iTOL) v4: Recent updates and new developments. Nucleic Acids Research 47(W1): W256–W259. https://doi.org/10.1093/nar/gkz239

Lovrich GA, Thiel M (2011) Ecology, physiology, feeding and trophic role of squat lobsters. In: Poore GCB, Ahyong ST, Taylor J (Eds) The Biology of Squat Lobsters CSIRO Publishing, Victoria, Australia, 183–222.

MacAvoy SE, Carney RS, Morgan E, Macko SA (2008a) Stable isotope variation among the mussel *Bathymodiolus childressi* and associated heterotrophic fauna at four cold-seep communities in the Gulf of Mexico. Journal of Shellfish Research 27(1): 147–151. https://doi.org/10.2983/0730-8000(2008)27[147:SIVATM]2.0.CO;2

MacAvoy SE, Morgan E, Carney RS, Macko SA (2008b) Chemoautotrophic Production Incorporated by Heterotrophs in Gulf of Mexico Hydrocarbon Seeps: An Examination of Mobile Benthic Predators and Seep Residents. Journal of Shellfish Research 27(1): 153–161. https://doi.org/10.2983/0730-8000(2008)27[153:CPIBHI]2.0.CO;2

MacDonald IR, Boland GS, Baker JS, Brooks JM, Kennicutt MC II, Bidigare RR (1989) Gulf of Mexico chemosynthetic communities II: Spatial distribution of seep organisms and hydrocarbons at Bush Hill. Marine Biology 101: 235–247. https://doi.org/10.1007/BF00391463

MacDonald IR, Guinasso Jr NL, Reilly JF, Brooks JM, Callender WR, Gabrielle SG (1990a) Gulf of Mexico hydrocarbon seep communities: VI Patterns of community structure and habitat. Geo-Marine Letters 10(4): 244–252. https://doi.org/10.1007/BF02431071

MacDonald IR, Reilly JF II, Guinasso Jr NL, Brooks JM, Carney RS, Bryant WA, Bright TJ (1990b) Chemosynthetic mussels at a brine-filled pockmark in the northern. Gulf of Mexico Science 248: 1096–1099. https://doi.org/10.1126/science.248.4959.1096

MacDonald IR, Bohrmann G, Escobar E, Abegg F, Blanchon P, Blinova V, Brückmann W, Drews M, Eisenhauer A, Han X, Heeschen K, Meier F, Mortera C, Naehr T, Orcutt B, Bernard B, Brooks J, De Faragó M (2004) Asphalt volcanism and chemosynthetic life in the Campeche Knolls. Science 304(5673): 999–1002. https://doi.org/10.1126/science.1097154

Macpherson E, Segonzac M (2005) Species of the genus *Munidopsis* (Crustacea, Decapoda, Galatheidae) from the deep Atlantic Ocean, including cold-seep and hydrothermal vent areas. Zootaxa 1095(1): 1–60. https://doi.org/10.11646/zootaxa.1095.1.1

Macpherson E, Jones W, Segonzac M (2005) A new squat lobster family of Galatheoidea (Crustacea, Decapoda, Anomura) from the hydrothermal vents of the Pacific–Antarctic Ridge. Zoosystema 27(4): 709–723.

Macpherson E, Baba K, Segonzac M (2006) Anomura. In: Desbruyères D, Segonzac M, Bright M (Eds) Handbook of deep-sea hydrothermal vent fauna, Second completely revised edition, Linz, Denisia, 434–454.

Macpherson E, Beuck L, Freiwald A (2016) Some species of *Munidopsis* from the Gulf of Mexico, Florida Straits and Caribbean Sea (Decapoda, Munidopsidae), with the description of two new species. Zootaxa 4137(3): 405–416. https://doi.org/10.11646/zootaxa.4137.3.7

Macpherson E, Rodríguez-Flores PC, Machordom A (2024) DNA barcoding and morphology revealed the existence of seven new species of squat lobsters in the family Munididae (Decapoda, Galatheoidea) in the southwestern Pacific. ZooKeys 1188: 91–123. https://doi.org/10.3897/zookeys.1188.114984

Martin JW, Haney TA (2005) Decapod crustaceans from hydrothermal vents and cold seeps: A review through 2005. Zoological Journal of the Linnean Society 145(4): 445–522. https://doi.org/10.1111/j.1096-3642.2005.00178.x

Mayo BS (1974) The systematics and distribution of the deep–sea genus *Munidopsis* (Crustacea, Galatheidae) in the Western Atlantic Ocean. Ph.D. Dissertation, University of Miami, 342 pp.

McLean JH, Harasewych MG (1995) Review of western Atlantic species of cocculinid and pseudococculinid limpets, with descriptions of new species (Gastropoda, Cocculiniformia). Contributions in Science 453: 1–33. https://doi.org/10.5962/p.208088

Milne-Edwards A (1880) Reports on the results of dredging under the supervision of Alexander Agassiz, in the Gulf of Mexico and in the Caribbean Sea,1877, ‘78, ‘79, by the U.S Coast Survey Steamer “Blake”, Lieut.–Commander C.D Sigsbee, U.S.N, and Commander J.R Bartlett, U.S.N commanding. VIII. Études préliminaires sur les Crustacés. Bulletin of the Museum of Comparative Zoology at Harvard College 8(2): 1–68 [pls1–2].

Milne-Edwards A, Bouvier EL (1894) Considérations générales sur la famille des Galathéidés. Annales des Sciences Naturelles, Zoologie, 7e série 16: 191–327. https://doi.org/10.5962/bhl.title.10042

Navas GR, Bermúdez A, Cruz N, Campos NH (2003) Galatéidos (Decapoda, Anomura, Galattheidae) del Caribe colombiano, incluyendo doce primeros registros. Boletin de Investigaciones Marinas y Costeras 32: 183–218. https://doi.org/10.25268/bimc.invemar.2003.32.0.266

Nicol EA (1932) The feeding habits of the Galatheidea. Journal of the Marine Biological Association of the United Kingdom 18(1): 87–106. https://doi.org/10.1017/S0025315400051316

Paradis E (2010) pegas: An R package for population genetics with an integrated–modular approach. Bioinformatics 26(3): 419–420. https://doi.org/10.1093/bioinformatics/btp696

Poupin J, Corbari L (2016) A preliminary assessment of the deep–sea Decapoda collected during the KARUBENTHOS 2015 Expedition to Guadeloupe Island. Zootaxa 4190(1): 1–107. https://doi.org/10.11646/zootaxa.4190.1.1

Rambaut A, Drummond AJ, Xie D, Baele G, Suchard MA (2018) Posterior summarization in Bayesian phylogenetics using Tracer 1.7. Systematic Biology 67(5): 901–904. https://doi.org/10.1093/sysbio/syy032

Roberts HH, Aharon P, Carney R, Larkin J, Sassen R (1990) Sea floor responses to hydrocarbon seeps, Louisiana continental slope. Geo-Marine Letters 10(4): 232–243. https://doi.org/10.1007/BF02431070

Rodríguez-Flores PC, Schnabel KE (2023) New records and species of deep–sea squat lobsters (Galatheoidea, Munidopsidae) from the Hawaiian Archipelago: An integrative approach using micro-CT and barcodes. PeerJ 11: e14956. https://doi.org/10.7717/peerj.14956

Rodríguez-Flores PC, Macpherson E, Machordom A (2018) Three new species of squat lobsters of the genus *Munidopsis* Whiteaves, 1874, from Guadeloupe Island, Caribbean Sea (Crustacea, Decapoda, Munidopsidae). Zootaxa 4422(4): 569–580. https://doi.org/10.11646/zootaxa.4422.4.7

Rodríguez-Flores PC, Macpherson E, Machordom A (2022) New species of deep–sea squat lobsters (Decapoda, Anomura, Galatheoidea) from Guadeloupe, French West Indies, unveiled through integrative taxonomy. Journal of Crustacean Biology 42(1): 1–14. https://doi.org/10.1093/jcbiol/ruab070

Rodríguez-Flores PC, Seid CA, Rouse GW, Giribet G (2023) Cosmopolitan abyssal lineages? A systematic study of East Pacific deep–sea squat lobsters (Decapoda, Galatheoidea, Munidopsidae). Invertebrate Systematics 37(1): 14–60. https://doi.org/10.1071/IS22030

Rodríguez-Flores PC, Torrado H, Combosch D, Giribet G (2024) Diversity of squat lobsters on coral reefs in Guam, Mariana Islands, with the description of two new species and notes on their natural history. Marine Biodiversity 54(4): 57. https://doi.org/10.1007/s12526-024-01446-4

Schnabel KE, Cabezas P, McCallum A, Macpherson E, Ahyong ST, Baba K (2011) Worldwide distribution patterns of squat lobsters. In: Poore GCB, Ahyong ST, Taylor J (Eds) The Biology of Squat Lobsters. CSIRO Publishing, Victoria, Australia, 149–182.

Sinclair J, Shedd W (2012) Petroleum hydrocarbon seeps in deep waters of the central and western Gulf of Mexico. In: Gulf of Mexico Data Atlas [Internet]Stennis Space Center (MS). National Centers for Environmental Information [1 screen]. https://gulfatlas.noaa.gov

Srivathsan A, Lee L, Katoh K, Hartop E, Kutty SN, Wong J, Yeo D, Meier R (2021) ONTbarcoder and MinION barcodes aid biodiversity discovery and identification by everyone, for everyone. BMC Biology 19(1): 217. https://doi.org/10.1186/s12915-021-01141-x

Tamura K, Stecher G, Kumar S (2021) MEGA11: Molecular evolutionary genetics analysis version 11. Molecular Biology and Evolution 38(7): 3022–3027. https://doi.org/10.1093/molbev/msab120

Thatje S, Marsh L, Roterman CN, Mavrogordato MN, Linse K (2015) Adaptations to hydrothermal vent life in *Kiwa tyleri*, a new species of yeti crab from the East Scotia Ridge, Antarctica. PLoS ONE 10(6): e0127621. https://doi.org/10.1371/journal.pone.0127621

Tsuchida, S, Suzuki, Y, Fujiwara, Y, Kawato, M, Uematsu, K, Yamanaka, T, Mizota C, Yamamoto, H (2011) Epibiotic association between filamentous bacteria and the vent–associated galatheid crab, *Shinkaia crosnieri* (Decapoda, Anomura). Journal of the Marine Biological Association of the United Kingdom 91(1): 23–32. https://doi.org/10.1017/S0025315410001827

Vazquez–Bader AR, Gracia A, Lemaitre R (2014) A new species of *Munidopsis* Whiteaves, 1874 (Crustacea, Anomura, Galatheoidea, Munidopsidae) from the Gulf of Mexico and Caribbean Sea. Zootaxa 3821(3): 354–362. https://doi.org/10.11646/zootaxa.3821.3.4

Vrijenhoek RC (1997) Gene flow and genetic diversity in naturally fragmented metapopulations of deep–sea hydrothermal vent animals. The Journal of Heredity 88(4): 285–293. https://doi.org/10.1093/oxfordjournals.jhered.a023106

Vrijenhoek RC (2010) Genetic diversity and connectivity of deep-sea hydrothermal vent metapopulations. Molecular Ecology 19(20): 4391–4411. https://doi.org/10.1111/j.1365-294X.2010.04789.x

Watsuji TO, Tsubaki R, Chen C, Nagai Y, Nakagawa S, Yamamoto M, Nishiura D, Toyofuku T, Takai K (2017) Cultivation mutualism between a deep-sea vent galatheid crab and its chemosynthetic epibionts. Deep-sea Research. Part I, Oceanographic Research Papers 127: 13–20. https://doi.org/10.1016/j.dsr.2017.04.012

Webb M (1969) *Lamellibrachia barhami*, gen. nov. sp. nov. (Pogonophora), from the Northeast Pacific. Bulletin of Marine Science 19(1): 18–47.

Wenner EL (1982) Notes on the Distribution and Biology of Galatheidae and Chirostylidae (Decapoda, Anomura) from the Middle Atlantic Bight. Journal of Crustacean Biology 2(3): 360–377. https://doi.org/10.2307/1548053

Williams AB (1988) New marine decapod crustaceans from waters influenced by hydrothermal discharge, brine, and hydrocarbon seepage. Fish Bulletin 86: 263–287.

Williams AB, van Dover CL (1983) A new species of *Munidopsis* from submarine thermal vents of the East Pacific Rise at 21°N (Anomura, Galatheidae). Proceedings of the Biological Society of Washington 96(3): 481–488.

Williams JD, Boyko CB, Rice ME, Young CM (2019) A report on two large collections of the squat lobster *Munidopsis platirostris* (Decapoda, Anomura, Munidopsidae) from the Caribbean, with notes on their parasites, associates, and reproduction. Journal of Natural History 53(3–4): 159–169. https://doi.org/10.1080/00222933.2019.1582817

Supplementary material 1

Material examined

Authors: Paula C. Rodríguez-Flores, Julie W. Ambler, Martha S. Nizinski

Data type: xlsx

Link: https://doi.org/10.3897/zse.@@.127169.suppl1

Zoosyst. Evol. 100 (4) 2024, 1259–1267 | DOI 10.3897/zse.100.125866

PENSOFT

MUSEUM FÜR NATURKUNDE BERLIN

Description of a new species of the genus *Oreonectes* (Teleostei, Cypriniformes, Nemacheilidae) from Guangxi, China

Jia-Hong Zhong[1], Jian Yang[1], Hao-Lin Mo[1], Wei-Cai Chen[2]

1 *Key Laboratory of Wildlife Evolution and Conservation in Mountain Ecosystem of Guangxi, Nanning Normal University, Nanning 530001, Guangxi, China*

2 *Key Laboratory of Environment Change and Resources Use in Beibu Gulf Ministry of Education, Nanning Normal University, Nanning 530001, Guangxi, China*

https://zoobank.org/29F191C5-30BF-491B-8B59-5EC344BD2584

Corresponding authors: Jian Yang (yj1981yj@163.com); Wei-Cai Chen (chenweicai2003@126.com)

Academic editor: Nicolas Hubert ♦ **Received** 21 April 2024 ♦ **Accepted** 15 August 2024 ♦ **Published** 10 September 2024

Abstract

A new loach species, *Oreonectes zhangi* **sp. nov.**, was identified from Xingye County, Yulin City, Guangxi, China. The species can be distinguished from all other congeners by a combination of the following characters: six branched pelvic-fin rays; a reduced posterior chamber of air-bladder; vertebrae 4 + 32; the tip of the male pelvic fin does not reach the anus. Molecular analyses using the Cyt *b* gene showed that the new species forms a monophyletic group and is closely related to *O. damingshanensis*.

Key Words

Morphology, new species, phylogeny, stream fish, taxonomy

Introduction

The genus *Oreonectes* Günther, 1868, comprises a group of loaches predominantly distributed in southern China (Guangxi, Guangdong, and Hong Kong) and northern Vietnam (Zheng 1981; Zhu and Cao 1987; Zhu 1989; Lan et al. 1995; Kottelat 2001). The genus is characterized by several distinctive features, including closely spaced anterior and posterior nostrils, anterior nostrils with a barbel-like elongation that extends beyond the depth of the nostril tube, a flat head that is wider than it is tall, an incomplete lateral line, and a dorsal fin with six or seven branched rays (Du et al. 2023). Historically, the identification of species within the genus *Oreonectes* has been complicated by their morphological similarities, which have often led to misidentifications. For instance, *Oreonectes platycephalus*, the type species of the genus *Oreonectes* described by Günther in 1868, was previously considered to be widespread throughout the Pearl River Basin and Hong Kong. However, recent studies suggest that *O. platycephalus* may represent a complex of multiple cryptic species (Huang et al. 2020; Yu et al. 2023). Ito (2024) redescribed this species and proved the effectiveness of *O. polystigmus* and *O. damingshanensis*.

Advances in molecular biology and phylogenetics have enabled the effective analysis of genetic materials and genetic differences between species, facilitating a clearer understanding of their evolutionary history and taxonomic status. Luo et al. (2023) recently employed multiple genes to elucidate the phylogeny of cave fish within the Nemacheilidae family, resulting in the description of a new genus, *Karstsinnectes*. Currently, the genus *Oreonectes* comprises seven species: *O. andongensis* Luo, Yang, Du & Luo, 2024; *O. damingshanensis* Yu, Luo, Zhou, Deng & Zhou, 2023; *O. guananensis* Yang, Wei, Lan & Yang, 2011b; *O. guilinensis* Huang, Yang, Wu & Zhao, 2020; *O. luochengensis* Yang, Wu, Wei & Yang, 2011a; *O. platycephalus* Günther, 1868; and *O. polystigmus* Du, Chen & Yang, 2008.

In 2023, 15 specimens were collected from a mountain stream in Yulin City, Guangxi, China (Fig. 1). Analysis of these specimens, including both morphological

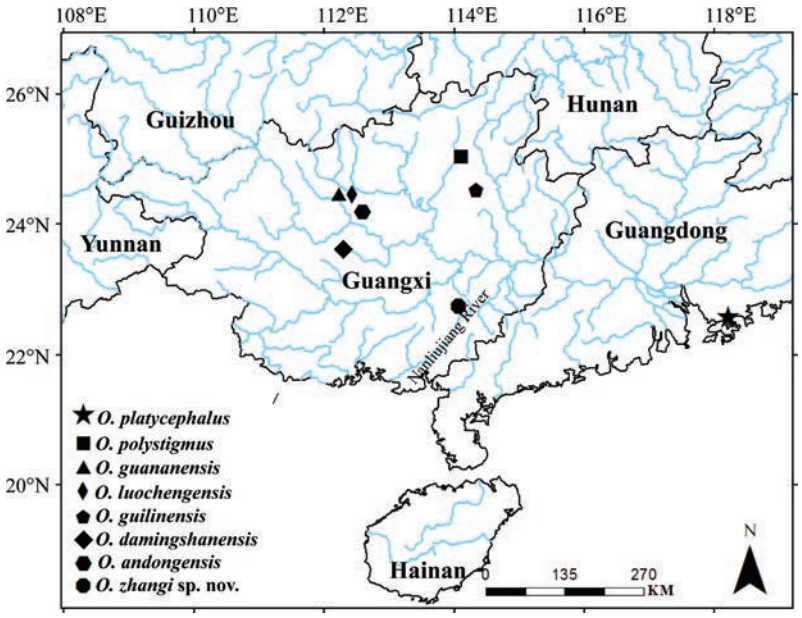

Figure 1. Distributions of *Oreonectes* species.

examination and molecular data from the cytochrome *b* gene (Cyt *b*), revealed significant variations compared to their congeners. Based on these findings, the specimens were identified as a new species within the genus *Oreonectes*, which is described herein.

Materials and methods

Morphological comparisons

In this study, 15 newly collected *Oreonectes* specimens were examined. All measurements and counts follow Kottelat (1990). The specimens were measured point-to-point with a caliper, accurate to 0.1 mm. All measurements were taken on the left side of the specimens. The last two rays of the dorsal and anal fins were counted as one ray, each pair associated with a single pterygiophore. The internal anatomy of the specimens followed the method of Liu and Zheng (2010).

Vertebral counts, including the Weberian apparatus and the last half-centrum, were examined by X-ray images. The caudal skeleton of the new species was studied based on X-ray images, cutting epidermis, and muscle removal. Osteological terminology followed that of Sawada (1982).

Morphological data were analyzed using Microsoft Excel, and statistical analyses were carried out using SPSS v22.0 (SPSS, Inc., Chicago, IL, USA). Principal component analysis (PCA) was utilized to explore morphometric differences between the new species and the similar species. Before analysis, the raw morphometric data were normalized by a logarithmic transformation to minimize the impact of allometry.

Abbreviations used in the study include: **SL**, standard length; **TL**, total length; **HL**, lateral head length; and **NNNU**, Nanning Normal University.

DNA extraction, polymerase chain reaction (PCR), and sequencing

Genomic DNA was extracted from alcohol-preserved pectoral fin tips using a DNA extraction kit from Genenode Biotech (Hubei) Co. Ltd. (China). The mitochondrial Cyt *b* gene was sequenced from three individuals. The forward and reverse primers used were F14724 (5'-GACTTGAAAAACCACCGTTG-3') and R15915 (5'-CTCCGATCTCCGGATTACAAGAC-3'), respectively (Xiao et al. 2001). PCR amplifications were carried out in a 25 μL reaction volume with the following cycling conditions: an initial denaturing step at 95 °C for 5 min, 35 cycles of denaturing at 95 °C for 40 s, annealing at 45 °C for 40 s, and extending at 72 °C for 1 min, followed by a final extension at 72 °C for 10 min. The fragments were sequenced using an ABI Prism 3730 automated DNA sequencer (Applied Biosystems, USA), and the newly obtained sequences were submitted to GenBank.

Phylogenetic analyses

A total of 35 Cyt *b* sequences were used for phylogenetic analysis. In addition to the three new sequences and one *O. damingshanensis* sequence, all the other sequences were obtained from GenBank. *Botia udomritthiruji* Ng 2007 and *Botia lohachata* Chaudhuri 1912 were chosen as outgroups for phylogenetic tree construction. The Cyt *b* sequences were aligned in MEGA v7.0 (Kumar et al. 2016) using the MUSCLE (Edgar 2004) algorithm with default parameters. Both maximum likelihood (ML) and Bayesian inference (BI) methods were used to reconstruct the phylogenetic relationship. ML analysis was run in IQ-TREE 1.6.8 (Nguyen et al. 2015), with the selected F81+F+I+G4 model and 1,000 non-parametric bootstrap replicates. BI was constructed in PhyloSuite v1.2.3. (Xiang et al. 2023), with two independent

runs of 2×10^7 generations and sampling every 1 000 generations. The initial 25% of samples were discarded as burn-in, resulting in a potential scale reduction factor of < 0.01. The best-fit model for BI analyses was determined using the Bayesian information criterion (BIC) in PartitionFinder v2.1.1. (Lanfear et al. 2017), resulting in the selection of the K80 + I + G model. Tree nodes were considered strongly supported with Bayesian posterior probabilities (BPP) ≥ 0.95 and Maximum Likelihood ultrafast bootstrap support (UFB) ≥ 95%. Uncorrected *p*-distances (1 000 replicates) based on the Cyt *b* gene were calculated in MEGA v7.0.

Results

Morphometric analysis

Based on the results of PCA, two principal components of the morphological characters of *Oreonectes zhangi* sp. nov. and *O. damingshanensis* were extracted (Table 1). The first principal component (PC1), which accounted for 67.6% of the variance, was influenced by total length, standard length, prepelvic length, preanus length, lateral head length, and predorsal length; the second principal component (PC2), which accounted for 11.4% of the variance, was influenced by body width at dorsal-fin origin, head depth at nape, and body depth at dorsal-fin origin.

The principal component scatter plot of 30 measurements of *O. damingshanensis* and *O. zhangi* sp. nov. constructed showed that the phenotypic traits of *O. damingshanensis* and *O. zhangi* sp. nov. formed a cluster with fewer overlapping areas (Fig. 2). The samples of the same group are relatively close in the figure, while the samples of different groups are far apart, indicating that the morphological indexes of the same group are similar, while the morphological indexes of different groups have distinct differences. Thus, *Oreonectes zhangi* sp. nov. could be clearly distinguished from *O. damingshanensis* based on morphological characters.

Table 1. Results and percentage of variance explained by principal component analysis.

Morphometric characters	PC1	PC2
Total length	0.22	-0.09
Standard length	0.22	-0.07
Body depth at dorsal-fin origin	0.16	0.31
Body width at dorsal-fin origin	0.12	0.39
Lateral head length	0.21	-0.05
Predorsal length	0.21	-0.13
Dorsal fin length	0.19	-0.22
Dorsal fin base length	0.15	-0.19
Prepelvic length	0.22	-0.08
Pelvic fin length	0.20	-0.01
Pelvic fin base length	0.13	0.29
Preanus length	0.22	-0.05
Preanal length	0.19	-0.20
Anal fin length	0.19	-0.20
Anal fin base length	0.16	-0.14
Prepectoral length	0.19	-0.14
Pectoral fin length	0.20	-0.12
Pectoral fin base length	0.14	0.29
Caudal peduncle length	0.18	-0.18
Caudal peduncle depth	0.18	0.23
Head depth at nape	0.17	0.32
Maximum head width	0.20	0.09
Snout length	0.19	0.04
Outer rostral barber length	0.17	-0.13
Maxillary barber length	0.17	0.04
Inner barber length	0.16	-0.05
Eye diameter	0.08	-0.25
Interorbital width	0.14	0.03
Distance between anterior nostrils	0.19	0.18
Distance between posterior nostril	0.19	0.15
Eigenvalue	20.29	3.42
Contribution ratio (%)	67.6	11.4
Cumulative contribution ratio (%)	67.6	79

Phylogenetic analyses and genetic divergence

BI and ML methods resulted in similar phylogenetic topologies based on the Cyt *b* sequence, consistent with Du et al. (2023). In addition to the outgroups, seven known genera were included in the phylogenetic trees.

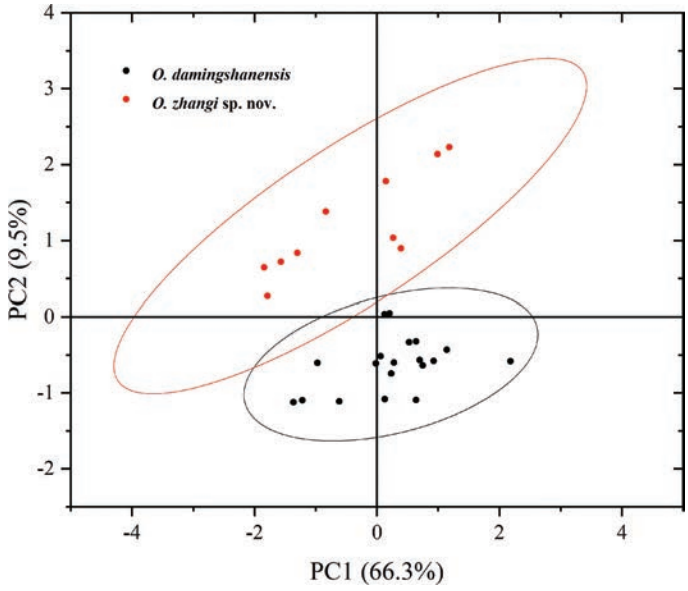

Figure 2. PCA plots of *Oreonectes zhangi* sp. nov. and similar species *O. damingshanensis* based on morphological characters.

The newly collected specimens formed a distinct and well-supported clade with *O. damingshanensis* (BPP = 1; UFB = 95%) (Fig. 3). Uncorrected *p*-distances between the new specimens and other species in *Oreonectes* ranged from 4.6% (for *O. damingshanensis*) to 9.2% (for O. guananensis) (Table 2).

Table 2. Uncorrected *p*-distances (%) between six species of *Oreonectes* based on the mitochondrial Cyt *b* gene.

ID	Species						
1	*Oreonectes zhangi* sp. nov.						
2	*O. andongensis*	7.0%					
3	*O. damingshanensis*	4.6%	6.5%				
4	*O. luochengensis*	7.5%	6.5%	8.0%			
5	*O. guilinensis*	7.4%	7.0%	7.6%	8.2%		
6	*O. guananensis*	9.2%	7.6%	8.9%	5.0%	8.8%	
7	*O. platycephalus*	7.2%	6.7%	7.1%	8.1%	6.7%	8.8%
8	*O. polystigmus*	6.5%	6.0%	6.3%	7.6%	7.5%	8.6%	6.5%

Taxonomic account

Oreonectes zhangi Zhong, Yang & Chen, sp. nov.

https://zoobank.org/73962B24-DB58-41FF-8DBE-0332CAD9635C

Figs 4–10, Tables 3, 4

Materials. ***Holotype*.** • NNNU2023100203 (Fig. 4); 71.1 mm TL, 63.1 mm SL; collected by Jia-Hong Zhong on 2 October 2023; in Mt. Hanshan, Xinye County, Yulin City, Guangxi, China; (22.7364°N, 110.0605°E; elevation 199 m; Fig. 1). ***Paratypes*.** • 14 specimens; NNU2023100201–202, 2023100204–215; were collected by Jia-Hong Zhong from the same locality and at the same time as the holotype.

Etymology. The species was named in honor of the three Zhang brothers, who assisted local residents in locating water during an ancient drought. Following their passing, they were revered as rain deities by the community (Li 2014). We suggest the common Chinese name "张氏岭鳅" (Zhang Shi Ling Qiu).

Comments. *Oreonectes zhangi* sp. nov. is classified within the genus *Oreonectes* based on molecular phylogenetic analyses and genus-specific characteristics, including narrowly separated anterior and posterior nostrils, elongated barbel-like anterior nostrils longer than the depth of the nostril tube (Fig. 5), having an epural in the caudal skeleton (Fig. 7), and a rounded caudal fin with 7 branched dorsal-fin rays. (Du et al. 2023; Ito 2024)

Diagnosis. Comparative data between *Oreonectes zhangi* sp. nov. and all seven known species within the genus *Oreonectes* are provided in Table 3. *Oreonectes zhangi* sp. nov. can be distinguished from *O. guilinensis*, *O. luochengensis*, *O. guananensis*, *O. andongensis*, and *O. polystimus* by the reduced posterior chamber of air-bladder (vs. developed), from *O. platycephalus* by six branched plevic-fin rays (vs. 7), seven branched dorsal-fin rays (vs. 6), from *O. damingshanensis* by six branched pelvic-fin rays (vs. 7), the tip of the male pelvic fin not reaching the anus (vs. exceeding) (Fig. 8), vertebrae 4 + 32 (vs. 4 + 34), head depth at nape (59.6–68.1% HL vs. 46.7–54.6%), body depth at dorsal-fin origin (14.0–16.1% SL vs. 11.1–13.3%).

Description. Morphometric data are given in Tables 3, 4. Body elongated and cylindrical, with insignificant depth decreasing from dorsal-fin origin to caudal-fin base. Head short, head length 18.6–20.2% of standard length, slightly depressed and flattened, width greater than depth (head

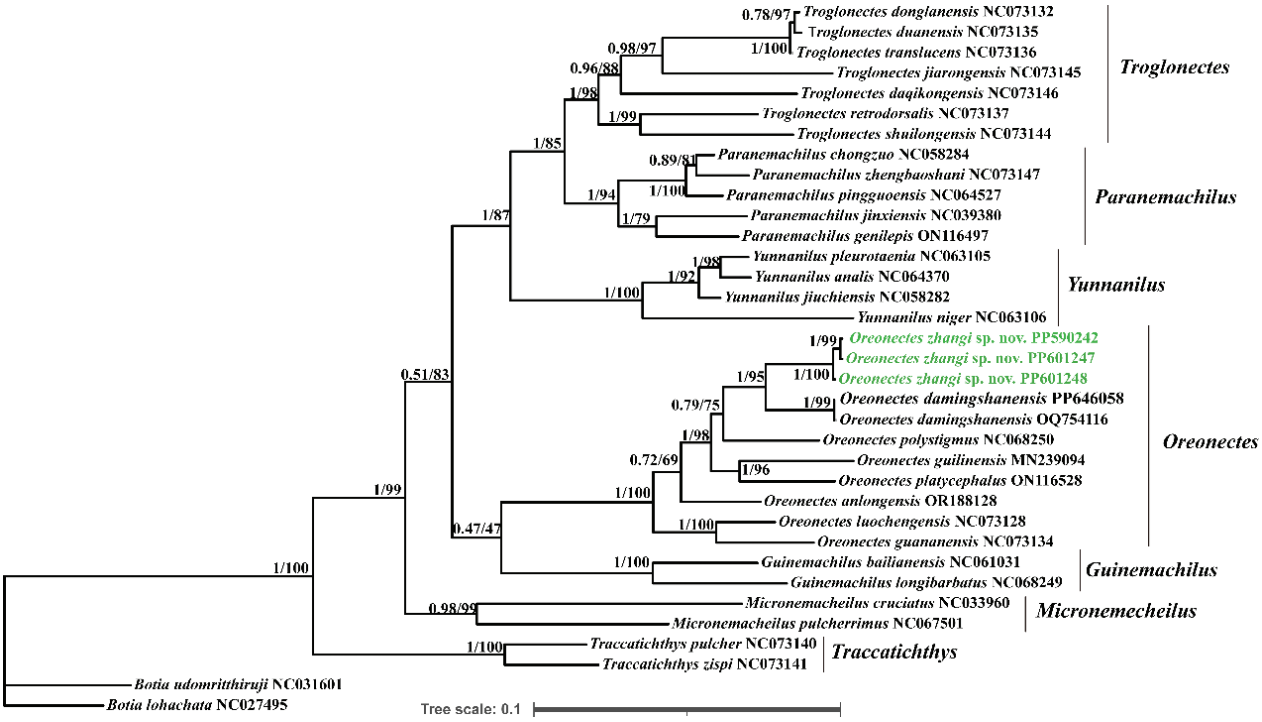

Figure 3. The phylogenetic tree of *Oreonectes* based on the Cyt *b* gene was constructed by Bayesian inference (BI) and maximum likelihood (ML). Node values showed posterior probabilities/bootstrap supports.

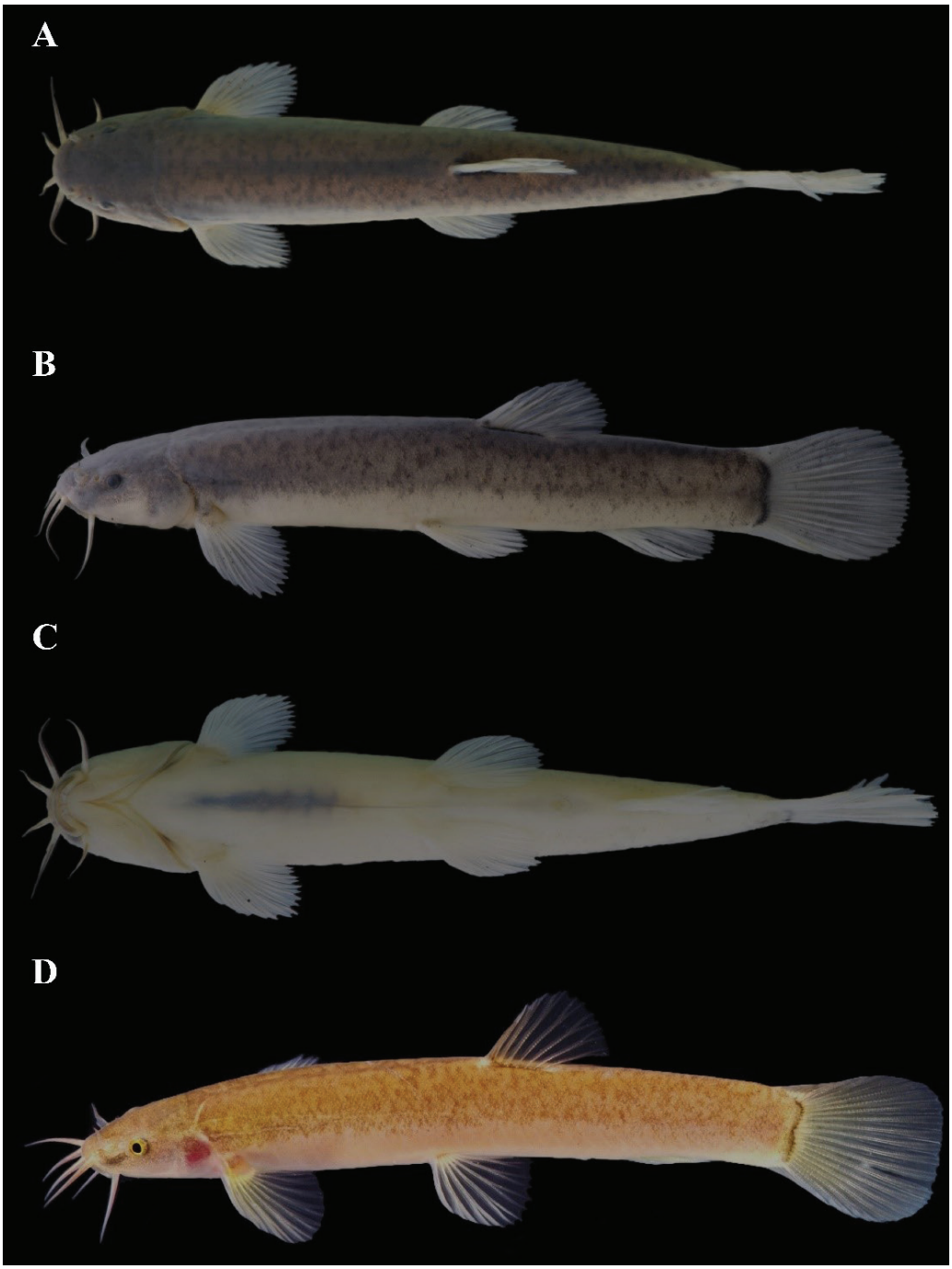

Figure 4. Dorsal, lateral, ventral, and living views of *Oreonectes zhangi* sp. nov. NNNU2023100203, holotype, 71.1 mm TL, 63.1 mm SL.

width/head depth = 1.1–1.5), head depth 59.6–68.1% of head length. Snout round, oblique, and flat, length 38.2–48.8% of head length (HL). Mouth inferior, curved, upper, and lower lips have shallow wrinkles and small spinous processes; lower lip with V-shaped median notch (Fig. 6). Three pairs of barbels, long: inner rostral barbel 35.4–44.1% of HL, extending backward, not reaching anterior margin of eye; outer rostral barbel 49.0–67.6% of HL, extending backward beyond posterior margin of eye. Maxillary barbel 38.4–52.2% of HL, tip not reaching posterior margin of gill cover. Anterior and posterior nostrils are separated by a short distance, 16.8%–36.8% of eye diameter. Anterior nostril tube short, with elongated, short barbel-like tip. Eyes normal, diameter 11.9–17.1% of HL. Gill opening small; gill rakers not developed; nine inner gill rakers on first gill arch (n = 2).

Dorsal-fin rays iii, 7, pectoral-fin rays i, 8–9, pelvic-fin rays i, 6, anal-fin rays iii, 5, branched caudal fin rays 15–16. Dorsal fin short, length 16.7%–21.1% of SL, distal margin round, origin posterior to pelvic-fin insertion, situated slightly posterior to two-thirds distance between snout tip and caudal-fin base. Pectoral fin short, length 15.9%–18.9% of SL. Pelvic fin length 16.1–17.7% of SL; tips of pelvic fin not reaching anus; distance between tips

Figure 5. *Oreonectes zhangi* sp. nov., dorsal view of head., NNNU2023100203, holotype, 63.1 mm SL.

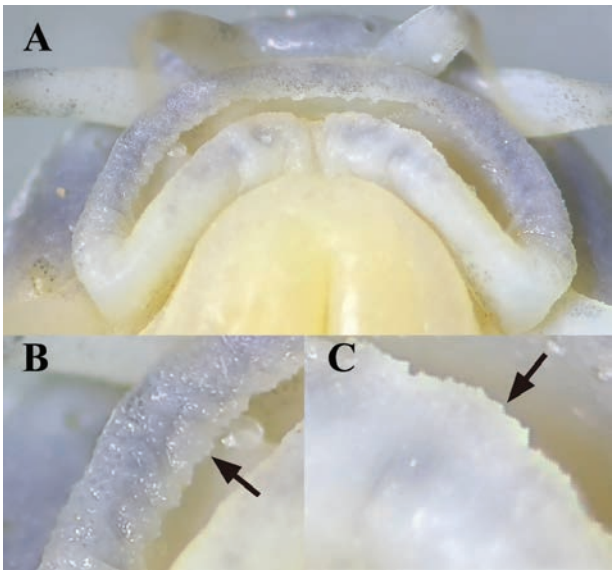

Figure 6. *Oreonectes zhangi* sp. nov., NNNU2023100203, holotype, 71.1 mm TL, 63.1 mm SL. The ventral view of the mouth (**A**) and close-ups of the upper (**B**) and lower (**C**) lips are shown; the black arrow indicates the position of the small spinous processes.

of pelvic fin and anus 0.7 times eye diameter. Anal fin short, length 15.1%–19.5%, origin short distance from anus. Caudal fin rounded, length 13.3%–19.9% of SL, length greater than depth (caudal peduncle length/caudal peduncle depth = 1.1–1.7). vertebrae 4 + 32 (n = 4), having an epural in the caudal skeleton (Fig. 7).

Body completely covered by scales, except head; lateral line incomplete, with 7–13 pores, last one not reaching above tip of pectoral fin; cephalic lateral-line system, with 8 supraorbital pores, 4+9–10 infraorbital pores, three supratemporal canal pores, and 5–8 preoperculo-mandibular canal pores.

U-shaped stomach with straight intestines (Fig. 9). Anterior chamber covered by dumbbell-shaped bony capsule, and posterior chamber reduced, reaching the vertical of the pectoral-fin base (Fig. 10).

Coloration. The body is mainly light yellowish brown in color, with dark brown extending from the front of the eyes to the outer rostral barbel. The base of the caudal fin is black, with each fin showing a light yellow hue. When preserved in 10% formalin, the body color fades to a dark brown shade (Fig. 4B).

Sexual dimorphism. Males have an oval genital papilla located immediately posterior to the anus (Fig. 8B), which is unclear in females (Fig. 4C).

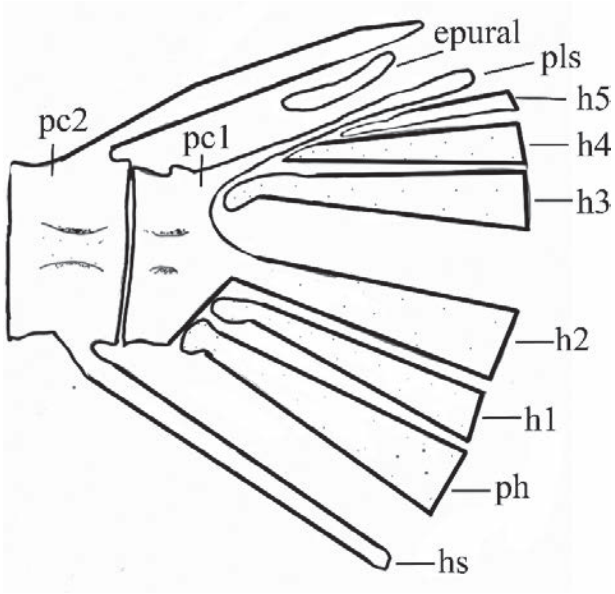

Figure 7. The caudal fin skeleton of *Oreonectes zhangi* sp. nov., NNNU2023100202, paratype, 64.2 mm SL, pc1, first preural centrum; pc2, second preural centrum; h, hypural; hs, haemal spine and arch; ph, parhypural; pls, pleurostylar.

Table 3. *Oreonectes* species and comparison of identifying characteristics between the new species and its congeners.

	Body pigmentation	Dorsal-fin rays	Pectoral-fin rays	Pelvic-fin rays	Anal-fin rays	Caudal-fin rays	Posterior chamber of air-bladder
Oreonectes zhangi sp. nov.	Present	iii, 7	i, 8–9	i, 6	iii, 5	15–16	Reduced
O. damingshanensis	Present	iii, 7	i, 9	i, 7	iii, 5	14–15	Reduced
O. platycephalus	Present	iii, 6	i, 9–11	i, 7	iii, 5	13–15	Reduced
O. guilinensis	Present	ii, 7	i, 10–11	i, 6	iii, 5	13–14	Developed
O. luochengensis	Absent	iii, 7	i, 11–12	i, 7	ii, 5	14–16	Developed
O. guananensis	Present	iii, 7	i, 10–11	i, 7–8	iii, 5	13–17	Developed
O. andongensis	Present	iii, 7	i, 9–10	i, 6	iii, 5	13–14	Developed
O. polystigmus	Present	iii, 6–7	i, 9	i, 6	ii, 5	14–15	Developed

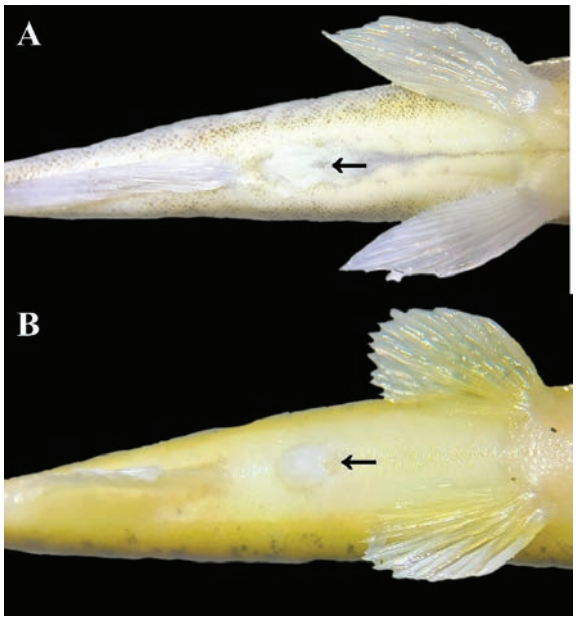

Figure 8. Gonadal structure of *O. damingshanensis* (**A**), NNNU2024052007, 56 mm SL, and *O. zhangi* sp. nov. (**B**), NNNU2023100215, paratype, 43.2 mm SL; the black arrow refers to the position of the anus.

Figure 9. *Oreonectes zhangi* sp. nov., NNNU2023100202, paratype, 64.18 mm SL; digestive tract.

Distribution, habitat, and populations. Based on field investigations, the species is abundant and commonly found in the streams of Mt. Hanshan in Xingye County, Yulin City, and Guangxi, China (Fig. 11). During the day, the species typically seeks shelter in stone crevices and substrates, emerging at night to feed. Exposure to intense light can cause their body color to change from light yellow to dark brown or black. Their diet consists of sediment and tadpoles, including those of Quasipaa spinosa. Interestingly, many pregnant females were collected, even in December. The stream habitats also harbored other species, such as *Schistura fasciolatus*, *Liniparhomaloptera disparis*, and *Rhinogobius similis*.

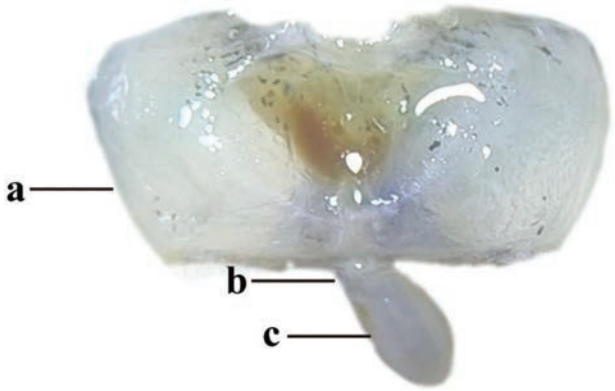

Figure 10. Air-bladder of *Oreonectes zhangi* sp. nov.: a, anterior chamber; b, tube connecting anterior and posterior chambers of the air-bladder; c, posterior chamber.

Discussion

Morphological distinctions between *Oreonectes zhangi* sp. nov. and *O. damingshanensis* included variations in head depth, body depth, number of branched fins, and the shape of genital papillae. Molecular analyses revealed that *Oreonectes zhangi* sp. nov. formed a distinct lineage with *O. damingshanensis*, with an uncorrected *p*-distance of 4.6%. All morphological characters and molecular evidence supported the validity of the new species. *Oreonectes zhangi* sp. nov. is the fourth benthic fish to be identified in surface water systems, similar to *O. damingshanensis*, *O. platycephalus*, and *O. guilinensis*. These fish, inhabiting surface rivers and mountain streams, exhibit sleeker bodies, longer fins and fin bases, and narrower, flatter heads with shorter barbels compared to those species living in underground cave water systems (Yu et al. 2023). Furthermore, except for *O. guilinensis*, the mountain stream-residing species typically possess a reduced air-bladder posterior chamber (Fig. 10, Table 3). Given the shallow water depths usually found in mountain streams, these fish seldom require vertical movement, instead favoring lateral shifts from one location to another (Zhu 1989).

Phylogenetic analysis suggested that the *Oreonectes* group could be divided into two sister groups, with *O. luochengensis* and *O. guananensis* forming one group and *Oreonectes zhangi* sp. nov., *O. polystigmus*, *O. damingshanensis*, *O. guilinensis*, *O. andongensis*, and *O. platycephalus* forming the other.

Comparative material examined

Oreonectes damingshanensis, NNNU2024052001–10, 10 ex, 69.8–85.9 mm, Leping Village, Guling Town, Mashan County, Guangxi, China.

Oreonectes guilinensis, ASIZB208001, holotype, 73.5 mm SL, ASIZB208002–007, paratypes, 6 ex., 52.0–68.3 mm, Shigumen Village, Xingping Town, Yangshuo County, Guilin City, Guangxi.

Table 4. Comparison of measurable traits between *Oreonectes zhangi* sp. nov. and similar species, *O. damingshanensis*. The numbers in parentheses are the mean ± standard deviation (SD).

	***Oreonectes zhangi* sp. nov.**	***O. damingshanensis***
Number of specimens	15	10
TL (mm)	59.8–81.8 (71.0 ± 8.3)	69.8–85.7 (78.9 ± 4.5)
SL (mm)	49.8–67.6 (58.8 ± 7.1)	56–70.6 (65.4 ± 4.6)
Percentage of SL (%)		
Body depth at dorsal-fin origin	14.0–16.1 (14.7 ± 0.7)	11.1–13.3 (12.2 ± 0.7)
Body width at dorsal-fin origin	9.3–12.8 (11.3 ± 1.1)	8.1–10.1 (9.1 ± 0.7)
Lateral head length	18.6–20.2 (19.3 ± 0.7)	18.5–21.2 (19.7 ± 1.1)
Predorsal length	56.2–59.4 (58.0 ± 1.2)	56.8–60.5 (58.3 ±1.1)
Dorsal fin length	16.7–21.1 (17.7 ± 1.4)	16.9–20.7 (18.9 ± 1.3)
Dorsal fin base length	7.2–9.7 (8.7 ± 0.8)	8.2–11.2 (9.5 ± 1.0)
Prepelvic length	48.1–50.8 (49.1 ± 1.0)	48.7–52.6 (50.7 ± 1.1)
Pelvic fin length	16.1–17.7 (16.7 ± 0.7)	14.4–18.3 (15.8 ± 1.2)
Pelvic fin base length	3.9–4.9 (4.3 ± 0.3)	2.8–4.4 (3.5 ± 0.5)
Preanus length	67.4–72.1 (69.3 ± 1.5)	67.0–70.8 (69.2 ± 1.0)
Preanal length	67.7–78.7 (73.8 ± 0.4)	73.8–78.3 (76.0 ± 1.8)
Anal fin length	15.1–19.5 (16.7 ± 1.5)	14.8–20.9 (17.4 ± 1.6)
Anal fin base length	6.6–9.0 (7.4 ± 0.8)	6.9–9.5 (7.8 ± 0.8)
Prepectoral length	18.3–21.2 (19.7 ± 1.1)	17.6–27.7 (21.6 ±2.6)
Pectoral fin length	15.9–18.9 (17.3 ± 0.9)	15.6–19.1 (17.1 ± 1.1)
Pectoral fin base length	4.4–5.3 (4.8 ± 0.3)	3.3–4.6 (3.9 ± 0.4)
Caudal peduncle length	13.3–19.9 (16.1 ± 1.9)	14.3–18.3 (16.3 ± 1.0)
Caudal peduncle depth	11.5–12.5 (11.9 ± 0.3)	9.2–11.8 (10.4 ± 0.8)
Percentage of HL (%)		
Head depth at nape	59.6–68.1 (63.2 ± 2.9)	46.7–54.6 (51.2 ± 2.6)
Maximum head width	70.4–89.3 (82.2 ± 5.3)	71.9–83.2 (76.3 ± 3.7)
Snout length	38.2–48.8 (41.8 ± 3.1)	37.0–44.7 (39.5 ± 2.6)
Outer rostral barber length	49.0–67.6 (57.9 ± 5.2)	50.0–68.2 (56.3 ± 5.6)
Maxillary barber length	38.4–52.2 (46.3 ± 4.7)	37.1–46.4 (41.9 ± 3.6)
Inner barber length	35.4–44.1 (38.8 ± 2.8)	37.1–46.4 (41.9 ± 3.1)
Eye diameter	11.9–17.1 (14.6 ± 1.8)	10.2–17.7 (14.5 ± 2.4)
Interorbital width	29.2–52.5 (44.2 ± 6.7)	39.9–47.5 (43.5 ± 2.2)
Distance between anterior nostrils	25.4–34.4 (31.9 ± 2.8)	25.5–30.6 (28.6 ± 1.8)
Distance between posterior nostril	29.6–41.9 (37.2 ± 3.8)	30.5–34.6 (33.3 ± 1.4)

Figure 11. Habitat of *Oreonectes zhangi* sp. nov.

Oreonectes guananensis, KIZ2010003068–072, paratypes, 5 ex., 51.0–71.9 mm SL, Guan'an Village, Changmei Town, Huanjiang County, Guangxi.

Oreonectes luochengensis, KIZ2010003073, holotype, 71.2 mm SL, NNNU2023080201–2, 2ex, 56.6–70.1 mm, Tianhe Town, Luocheng County, Guangxi, China.

Oreonectes polystigmus, NNNU2024042201–02, 2ex, 47.1–69.8 mm, Dabu Village, Guilin City, Guangxi, China.

Acknowledgments

This research was supported by the Project of Financial Funds of the Ministry of Agriculture and Rural Affairs: Investigation of Fishery Resources and Habitat in the Pearl River Basin and the National Natural Science Foundation of China (Grant No. 32360128). We sincerely thank Dr. Lina Du of Guangxi Normal University and Dr. Chaofang Zhong of Nanning Normal University for their help in this study. We sincerely thank the reviewers and editor for their constructive comments on this article.

References

Du LN, Chen XY, Yang JX (2008) A review of the Nemacheilinae genus *Oreonectes* Günther with descriptions of two new species (Teleostei, Balitoridae). Zootaxa 1729: 23–36. https://doi.org/10.11646/zootaxa.1729.1.3

Du LN, Li SJ, Xu F, Luo T, Luo FG, Yu GH, Zhou J (2023) Clarification of Phylogenetic Relationships among Chinese Nemacheilids with Tube-Shaped Anterior Nostrils, with a Description of a New Genus and Two New Species. Journal of Zoological Systematics and Evolutionary Research 2023: 3600085. https://doi.org/10.1155/2023/3600085

Edgar RC (2004) MUSCLE: multiple sequence alignment with high accuracy and high throughput. Nucleic Acids Research. 32: 1792–1797. https://doi.org/10.1093/nar/gkh340

Günther A (1868) Catalogue of Fishes in the British Museum. Volume 7th. Trustees of the British Museum, London, 512 pp.

Huang JQ, Yang J, Wu ZQ, Zhao YH (2020) *Oreonectes guilinensis* (Teleostei, Cypriniformes, Nemacheilidae), a new loach species from Guangxi, China. Journal of Fish Biology 96: 111–119. https://doi.org/10.1111/jfb.14191

Ito T (2024) *Lefua hoffmanni* Herre, 1932, a junior synonym of *Oreonectes platycephalus* Günther, 1868 (Cypriniformes, Nemacheilidae). Zootaxa 5448(4): 519–530. https://doi.org/10.11646/zootaxa.5448.4.5

Kottelat M (1990) Indochinese Nemacheilines: A Revision of Nemacheiline Loaches (Pisces, Cypriniformes) of Thailand, Burma, Laos, Cambodia and Southern Vietnam. München, United Germany, 262 pp.

Kottelat M (2001) Freshwater Fishes of Northern Vietnam, A Preliminary Check–list of the Fishes Known or Expected to Occur in Northern Vietnam with Comments on Systematics and Nomenclature. Environment and Social Development Sector Unit, East Asia and Pacific Region, the World Bank, 1–261 pp.

Kumar S, Stecher G, Tamura K (2016) MEGA7: Molecular Evolutionary Genetics Analysis Version 7.0 for Bigger Datasets. Molecular Biology and Evolution 33: 1870–1874. https://doi.org/10.1093/molbev/msw054

Lan JH, Yang JX, Chen YR (1995) Two new species of the subfamily Nemacheilinae from Guangxi, China. Acta Zootaxonomica Sinica, 366–372.

Lanfear R, Frandsen PB, Wright AM, Senfeld T, Calcott B (2017) PartitionFinder 2: New Methods for Selecting Partitioned Models of Evolution for Molecular and Morphological Phylogenetic Analyses. Molecular Biology and Evolution 34: 772–773. https://doi.org/10.1093/molbev/msw260

Li LS (2014) On the Cultural Analysis of the Folk Belief Shown in Hanshan Temple Fair in Yulin, Guangxi. Journal of Guangxi Teachers Education University (Philosophy and Social Science Edition) 35(1): 20–22+47.

Liu LY, Zheng GM (2010) Experiments in General Zoology. Higher Education Press, Beijing China, 1–168.

Luo T, Yang Q, Wu L, Wang YL, Zhou JJ, Deng HQ, Xiao N, Zhou J (2023) Phylogenetic relationships of Nemacheilidae cavefish (*Heminoemacheilus*, *Oreonectes*, *Yunnanilus*, *Paranemachilus*, and *Troglonectes*) revealed by analysis of mitochondrial genome and seven nuclear genes. Zoological Research 44: 693–697. https://doi.org/10.24272/j.issn.2095-8137.2022.266

Luo XM, Yang RG, Du LN, Luo FG (2024) A new loach species of the genus *Oreonectes* (Teleostei, Cypriniformes, Nemacheilidae) from Guangxi, China. ZooKeys 1196: 285–301. https://doi.org/10.3897/zookeys.1196.109810

Nguyen LT, Schmidt HA, von Haeseler A, Minh BQ (2015) IQ-TREE: A fast and effective stochastic algorithm for estimating maximum-likelihood phylogenies. Molecular Biology and Evolution 32(1): 268–274. https://doi.org/10.1093/molbev/msu300

Sawada Y (1982) Phylogeny and zoogeography of the superfamily Cobitoidea (Cyprinoidei, Cypriniformes). Memoirs of the Faculty of Fisheries Hokkaido University 28(2): 65–223.

Xiang CY, Gao F, Jakovlić I, Lei HP, Hu Y, Zhang H, Zou H, Wang GT, Zhang D (2023) Using PhyloSuite for molecular phylogeny and tree-based analyses 2: e87. https://doi.org/10.1002/imt2.87

Xiao W, Zhang Y, Liu H (2001) Molecular systematics of *Xenocyprinae* (teleostei: cyprinidae): taxonomy, biogeography, and coevolution of a special group restricted in East Asia. Molecular Phylogenetics and Evolution 18: 163–173. https://doi.org/10.1006/mpev.2000.0879

Yang J, Wu TJ, Wei RF, Yang JX (2011a) A new loach, *Oreonectes luochengensis* sp. nov. (Cypriniformes, Balitoridae) from Guangxi, China, Zoological Research 32: 208–211.

Yang Q, Wei ML, Lan JH, Yang Q (2011b) A New Species of the Genus *Oreonectes* (Balitoridae) from Guangxi,China, Journal of Guangxi Normal University: Natural Science Edition 29: 72–75.

Yu J, Luo T, Lan CT, Zhou JJ, Deng HQ, Xiao N, Zhou J (2023) *Oreonectes damingshanensis* (Cypriniformes, Nemacheilidae), a new species of stream fish from Guangxi, Southwest China. Zookeys 1180: 81–104. https://doi.org/10.3897/zookeys.1180.104645

Zheng PS (1981) Freshwater Fishes Guangxi. Guangxi People's Publishers, Nanning, China, 1–256.

Zhu SQ (1989) The Loaches of the Subfamily Nemacheilinae in China (Cypriniformes, Cobitidae). Jiangsu Science & Technology Publishing House, Nanjing, China, 1–150.

Zhu SQ, Cao WX (1987) The noemacheiline fishes from Guangdong and Guangxi with descriptions of a new genus and three new species (Cypriniformes, Cobitidae). Acta Zootaxonomica Sinica 12: 323–331.

Zoosyst. Evol. 100 (4) 2024, 1269–1286 | DOI 10.3897/zse.100.122874

PENSOFT

für Natur MUSEUM FÜR NATURKUNDE BERLIN

New data on the polyphyletic *Marionina* genus (Annelida, Enchytraeidae): description of three new species from European shore habitats

Tamás Felföldi[1,2], Hajnalka Nagy[1,3], Klára Dózsa-Farkas[4]

1 *Department of Microbiology, ELTE Eötvös Loránd University, H-1117 Budapest, Pázmány Péter sétány 1/C, Hungary*
2 *Institute of Aquatic Ecology, HUN-REN Centre for Ecological Research, H-1113 Budapest, Karolina út 29, Hungary*
3 *Hungarian Natural History Museum, H-1088 Budapest, Baross utca 13, Hungary*
4 *Department of Systematic Zoology and Ecology, ELTE Eötvös Loránd University, H-1117 Budapest, Pázmány Péter sétány 1/C, Hungary*

https://zoobank.org/8DB2BEFF-F7A6-45A5-B9AE-046B735792DD

Corresponding author: Hajnalka Nagy (nhajni6@gmail.com, sparrow@staff.elte.hu)

Academic editor: Greg Rouse ♦ **Received** 12 March 2024 ♦ **Accepted** 18 June 2024 ♦ **Published** 10 September 2024

Abstract

Marionina (Michaelsen in Pfeffer, 1890) is a worldwide distributed genus of small enchytraeids living in mainly aquatic habitats. The genus is polyphyletic, including about 100 species with diverse morphological characters and cryptic lineages; therefore, taxonomic revisions were performed recently, and further actions are needed in the future. In our study, *Marionina* individuals were investigated from decaying seagrass debris collected from seashores in Croatia and Italy using morphological characters and molecular markers involving the COI and H3 genes and the ITS region. Descriptions of two new *Marionina* species, *M. puntaalanensis* **sp. nov.** and *M. orbifera* **sp. nov.**, are presented in this paper, and in addition, the description of a third new *Marionina* species, *M. reicharti* **sp. nov.**, from the shore of the freshwater Lake Balaton (Hungary) is provided here. All three new species are small (2–3.5 mm *in vivo* with less than 30 segments), their clitellum is saddle-shaped, the dorsal anterior blood vessel bifurcation is in III, and the spermatheca is attached to the oesophagus. The main diagnostic features of *M. puntaalanensis* **sp. nov.** are: brain incised posteriorly; dorsal vessel from the clitellar region; two chaetae in all bundles; three pairs of preclitellar nephridia; small subneural glands in XIII–XIV; seminal vesicle absent or small; ectal duct of spermatheca surrounded along the length by glands and one larger. The main features of *M. orbifera* **sp. nov.** are: brain truncate posteriorly; dorsal vessel from the clitellar region; two chaetae in all bundles; two pairs of preclitellar nephridia; subneural glands in XIII–XIV; seminal vesicle well developed; the lumen of the spermathecal ampulla is characteristically full with many spherical sperm rolls. In *M. reicharti* **sp. nov.**: brain incised posteriorly, dorsal vessel origin in XII, maximum five chaetae per bundle, often the middle chaetae slightly smaller than the ental ones, three pairs of preclitellar nephridia, subneural glands absent, spermathecal ampulla globular, ectal duct surrounded along the length by glands, and one large sessile gland at the orifice.

Key Words

Lake Balaton, *Marionina*, Mediterranean Basin, molecular taxonomy, sea and lake shore, species complex

Introduction

We studied the enchytraeid fauna found in the decaying seagrass detritus on the Adriatic and Tyrrhenian coasts between 2019 and 2021 (Nagy et al. 2023). The characteristic enchytraeid fauna of the coastal supralittoral zone consists of relatively large *Enchytraeus* and small-sized *Marionina* species, which are well adapted to the cavity system of the sand grains and the decaying plant biomass. As a result of our research, we described three new *Enchytraeus* species from the *Enchytraeus albidus* species complex recently (Nagy et al. 2023), and we found two *Marionina* species

new to science based on morphological and molecular investigations, which are described in this paper.

Among the specimens collected from the Mediterranean coast, we also found worms morphologically resembling *Marionina spicula* (Leuckart, 1847) (Frey and Leuckart 1847). For comparison, we re-examined specimens identified previously by one of us as *M. spicula* (Dózsa-Farkas 1995). These specimens had been collected from the shore of the shallow freshwater Lake Balaton, Hungary, the largest lake in Central Europe. Applying molecular methods, it turned out that these latter worms represent a third species new to science, genetically different from the Mediterranean *M. spicula*. This species is also described in this paper, and the species comparison includes additional *M. spicula* specimens collected from a Danish seashore. On the other hand, the Mediterranean material of *M. spicula* was heterogeneous at the DNA level, and slight morphological differences further suggested that more than one species was involved. The genetic and morphological diversity of the Mediterranean *M. spicula* is presented and described here, but further evidence is needed to erect them as new species.

Marionina (Michaelsen in Pfeffer, 1890) is a worldwide distributed genus within the family Enchytraeidae, including marine, limnic, and terrestrial small-sized worms. Most of the species live in the marine littoral, supra- or sub-littoral zones, or in salt marshes. The majority of the so-called 'terrestrial' *Marionina* are found only in wet, moist soil, on lake shores, riverbanks, or in swamps, while some species (like *Marionina clavata* Nielsen & Christensen, 1961, and *Marionina communis* Nielsen & Christensen, 1959) are truly terrestrial. Few species occur in the profundal zone of freshwater lakes (Timm 1996; Timm and Vvedenskaya 2006), and one species (*M. spongicola* Rota & Manconi, 2004) lives exclusively in the interior of a sponge in a geothermal lake at a depth of more than 100 m (Rota and Manconi 2004).

Unfortunately, this genus is an artificial assemblage of several unrelated species (Coates 1989; Xie and Rota 2001; Matamoros et al. 2007; Rota et al. 2008; Schmelz and Collado 2010), so the characteristic morphological traits are highly variable between species, e.g., the shape of the chaetae (sigmoid or straight) and their distribution on the body, the shape of the brain, the location of the head pore, the number of the pharyngeal glands, the shape of nephridia, the ratio of pre- and post-septale parts, the origin of the efferent ducts, the location of the anterior bifurcation of the dorsal vessel, the structure of the male copulatory organ, and whether the spermatheca is connected to the oesophagus or not. The heterogeneity was somewhat reduced by the fact that several species were transferred to other genera; e.g., *M. cambrensis* O'Connor, 1963; *M. tubifera* Nielsen & Christensen, 1959; and *M. changbaishanensis* Xie, Liang & Wang, 2000 to *Oconorella* (Rota 1995; Dózsa-Farkas 2002); *M. righiana* Xie & Rota, 2001 to *Xetadrilus* (Schmelz et al. 2011); and *M. riparia* Bretscher, 1899 to *Globulidrilus* (Christensen & Dózsa-Farkas, 2012).

With the introduction of DNA-based studies in the taxonomy and systematics of Enchytraeidae, it was confirmed that the genus is polyphyletic (Erséus et al. 2010; Martinsson et al. 2017); furthermore, notable cryptic diversity has been detected in some species (Matamoros et al. 2012). The revision of the genus has therefore become absolutely necessary. As the initial step of the thorough revision, the type species of this genus, *M. georgiana* (originally *Pachydrilus georgianus* Michaelsen, 1888), has been re-described by Rota et al. (2008) and Schmelz and Collado (2008), providing also the taxonomic history and synonymy of the genus, and Klinth et al. (2022) supplemented the type species with additional characters recently. Molecular studies (Erséus et al. 2010; Klinth et al. 2022) revealed that a large part of the taxonomically problematic *Marionina* genus is not closely related to the type species. These studies also highlighted that further revisions are needed to eliminate the taxonomic problems of the genus and draw attention to the fact that even the morphological characters that could be used in the diagnosis of *Marionina* sensu stricto cannot be defined yet.

In this article, we present the description of three new species currently classified in the *Marionina* genus based on morphological and molecular data, with some remarks on the species *Marionina spicula*.

Materials and methods

Study sites

1. Croatia, Istria, Kale Cove seashore, Adriatic Sea, Kamenjak Peninsula, decaying seagrass (*Zostera*) detritus, 44°51'13.0"N, 13°58'50.5"E, Leg. Júlia Török, 03 Apr 2019, and 05 Sep 2020.
2. Italy, Castiglione seashore, Tyrrhenian Sea, decaying seagrass detritus, 42°45'56.0"N, 10°52'51.0"E, Leg. András Dózsa-Farkas and Kinga Dózsa-Farkas, 13 Dec 2019.
3. Italy, Punta Ala Grosseto, Castiglione della Pescaia, decaying seagrass detritus, 42°46'00.0"N, 10°51'31.0"E, Leg. András Dózsa-Farkas and Kinga Dózsa-Farkas, 24 Sep 2020 and 26 Nov 2020.
4. Hungary, Lake Balaton, Bélatelep, Strand Bátori, lake shore, wet sand between the roots of willow trees, 46°43'51.5"N, 17°31'41.7"E, Leg. György Reichart, 14 Feb 2021. (See details of lakewater characteristics in Somogyi et al. 2020).
5. Denmark, Nivå, seashore, 55°56'29.3"N, 12°31'39.0"E, Leg. Bent Christensen and Klára Dózsa-Farkas, 23 Nov 1999.

Methods of morphological examination

The enchytraeids were extracted by the wet funnel method (O'Connor 1962). Enchytraeids were first investigated and measured alive, then preserved in 70% ethanol.

Some specimens were stained with borax-carmine and then passed through an ethanol (70% to absolute) dehydration series, mounted temporarily in clove oil, and then permanently in Euparal between two coverslips. All important morphological characters were recorded *in vivo*, drawn, and photographed [Axio Imager A2 microscope with differential interference contrast illumination, AxioCam MRc 5 (Zeiss) digital camera, Axiovision software]. The whole-mounted specimens were reinvestigated, measured, and photographed as well. In all micrographs presented in this study, the orientation of specimens is the same: the head is either on the left side or on the top of the picture. Selected material was catalogued with collection numbers, letters for the holotypes ('Ma') and paratypes ('P'), and slide numbers, and was deposited in the collection of the Department of Systematic Zoology and Ecology, ELTE Eötvös Loránd University (Budapest, Hungary).

Methods of molecular analysis

Genomic DNA was extracted from the individuals with the DNeasy Blood & Tissue Kit (Qiagen) according to the instructions given by the manufacturer. Three regions were amplified separately with the PCR method: the mitochondrial cytochrome c oxidase subunit I (COI) gene, the nuclear histone 3 (H3) gene, and the nuclear ribosomal ITS region using the primer pairs HCO2198 (5'-TAA ACT TCA GGG TGA CCA AAA AAT CA-3') and LCO1490 (5'-GGT CAA CAA ATC ATA AAG ATA TTG G-3') (Folmer et al. 1994), H3a-F (5'-ATG GCT CGT ACC AAG CAG ACV GC-3') and H3a-R (5'-ATA TCC TTR GGC ATR ATR GTG AC-3') (Colgan et al. 1998), and ETTS1 (5'-TGC TTA AGT TCA GCG GGT-3') and ETTS2 (5'-TAA CAA GGT TTC CGT AGG TGA A-3') (Kane and Rollinson 1994). If amplification failed in the case of the ITS region, COI, and H3 gene, additional primer sets ITS-5 (5'-GGA AGT AAA AGT CGT AAC AAG G-3') and ITS-4 (5'-TCC TCC GCT TAT TGA TAT GC-3') (White et al. 1990), COI-E^{-} (5'-TAT ACT TCT GGG TGT CCG AAG AAT CA-3') (Bely and Wray 2004), and H3a-new-F (5'- TGG CTC GTA CCA AGC AGA CSG-3') with H3a-new-R (5'-ATG ATG GTG ACG CKY TTG GC-3') (AllGenetics, A Coruña) were applied. PCRs, sequencing reactions, and phylogenetic analyses were conducted as described in detail previously by Dózsa-Farkas et al. (2015). The PCR cycle parameters for ITS-5, ITS-4, and COI-E^{-} were based on Matamoros et al. (2012). Sanger sequencing was performed by the LGC Genomics GmbH (Berlin, Germany), and the construction of maximum likelihood trees, including the search for the best-fit model, was carried out with the MEGA 7 software (Kumar et al. 2016). According to the results of the ModelTest, the following nucleotide substitution models were used for the construction of phylogenetic trees: ITS region: GTR+G+I; COI gene: GTR+G+I; H3 gene: T92+G. In total, 15, 21, and 18 new sequences were obtained from the studied *Marionina* specimens in the cases of ITS, COI, and H3 (Table 1). Unfortunately, we failed to amplify the studied DNA regions from some specimens (e.g., ITS sequences from *Marionina spicula* and H3 sequences from *M. orbifera* sp. n. individuals), which was probably due to the improper hybridization of PCR primer sequences with the extracted genomic DNA. Sequences from other *Marionina* species (Erséus et al. 2010; Matamoros et al. 2012; Felföldi et al. 2020, etc.) were used for comparison. Besides the phylogenetic tree estimations, pairwise genetic distances between the COI, H3, and ITS sequences of the new species and the other investigated *Marionina* species were calculated in MEGA 7.0 using the p-distance method. Gaps and missing data were excluded using pairwise deletions. These settings are based on Martinsson and Erséus (2018). Sequences obtained in this study were deposited in GenBank under the following accession codes: MZ835280–MZ835294 (ITS), MZ750838–MZ750858 (COI), and MZ816248–MZ816265 (H3).

Results

Systematics

Genus *Marionina* (Michaelsen in Pfeffer, 1890)

Marionina puntaalanensis sp. nov.

https://zoobank.org//76F756B7-3F72-4DF4-A731-F769D6BAC2CF

Fig. 1

Type material. ***Holotype*:** Ma. 5, slide No. 3055. ***Type locality*:** (Loc. 3.) Italy, Punta Ala Grosseto, Castiglione della Pescaia, decaying seagrass detritus, 42°46'00.0"N, 10°51'31.0"E, Leg. András Dózsa-Farkas and Kinga Dózsa-Farkas, 24 Sep 2020.

***Paratypes*:** in total, four specimens: P.146.1 slide No. 3022, P.146.2 slide No. 3056, P.146.3 slide No. 3077, P.146.4 slide No. 3192. Same data as for holotype, 24 Sep 2020 and 26 Nov 2020.

Further material examined. Four specimens for DNA analysis, five specimens only *in vivo*.

Diagnosis. (1) Small size (body length 2–2.5 mm, 130–185 μm wide at clitellum, *in vivo*), segment number 19–30; (2) chaetae straight with ental hook, two chaetae in all bundles; (3) clitellum saddle-shaped; (4) first and second pharyngeal glands united dorsally, in V with ventral lobes; the third pair free dorsally with elongated ventral lobes; (5) dorsal vessel from clitellar region, blood colorless, anterior blood vessel bifurcation anteriorly behind the pharynx; (6) three pairs of preclitellar nephridia; (7) coelomocytes disc- or lemon-shaped with granules, 13–20 μm; (8) sperm funnels small, cylindrical, 100–140 μm long *in vivo*, 1.5–2.5 times longer than wide *in vivo*, collar high and narrower than funnel body; (9) spermatozoa 38–43 μm long, heads 15–22 μm *in vivo*; (10) male copulatory organs small and compact; (11) small subneural glands in XIII–XIV; (12) ectal duct of spermatheca surrounded along the length by glands and one larger, 15–27 μm long, sessile gland at orifice. Ampulla oval, 24–40 μm wide and 40–55 μm long *in vivo*.

Table 1. List of specimens used for molecular taxonomic analyses with collection data and GenBank accession numbers. Sequences determined in this study appear in bold. Abbreviations: n. d. = no data.

Species	Specimen ID	Locality	Habitat	Reference	ITS	COI	H3
Marionina puntaalanensis **sp. nov.**	1450	Italy, Castiglione	decaying seagrass detritus	this study	**MZ835280**	**MZ750838**	**MZ816248**
Marionina puntaalanensis **sp. nov.**	1451	Italy, Castiglione	decaying seagrass detritus	this study	**MZ835281**	**MZ750839**	**MZ816249**
Marionina reicharti **sp. nov.**	1360	Hungary, Bélatelep	wet sand between the roots of willow trees	this study	**MZ835282**	-	**MZ816250**
Marionina reicharti **sp. nov.**	1361	Hungary, Bélatelep	wet sand between the roots of willow trees	this study	**MZ835283**	**MZ750840**	**MZ816251**
Marionina reicharti **sp. nov.**	1457	Hungary, Bélatelep	wet sand between the roots of willow trees	this study	**MZ835284**	-	-
Marionina reicharti **sp. nov.**	1465	Hungary, Bélatelep	wet sand between the roots of willow trees	this study	**MZ835285**	**MZ750841**	**MZ816252**
Marionina reicharti **sp. nov.**	1466	Hungary, Bélatelep	wet sand between the roots of willow trees	this study	**MZ835286**	**MZ750842**	**MZ816253**
Marionina orbifera **sp. nov.**	1447	Italy, Castiglione	decaying seagrass detritus	this study	-	**MZ750843**	**MZ816254**
Marionina orbifera **sp. nov.**	1448	Italy, Castiglione	decaying seagrass detritus	this study	**MZ835287**	**MZ750844**	-
Marionina orbifera **sp. nov.**	1449	Italy, Castiglione	decaying seagrass detritus	this study	**MZ835288**	**MZ750845**	-
Marionina aestuum	CE12477	South Georgia Island	intertidal, 4 m up shore from low tide	Klinth et al. 2022	-	MZ393958	MZ394832
Marionina argentea	1193	Korea, Muljangori-oreum Wetland	soil	Felföldi et al. 2020	-	MT425084	MT433804
Marionina argentea	CE807	Sweden, Lerum	near a lake	Erséus et al. 2010	-	GU902092	-
Marionina cf. *argentea*	CE22027	Norway, Hordaland	n. d.	Klinth et al. 2019	-	MN395702	-
Marionina clavata	734	Hungary, Kőszeg Mts.	larch forest	Felföldi et al. 2020	MT428056	-	-
Marionina clavata	1267	Korea, Mt. Gyebangsan	oak forest	Felföldi et al. 2020	MT428057	MT425088	MT433805
Marionina clavata	CE849	Sweden, Lerum	road bank	Erséus et al. 2010; Schmelz et al. 2019	-	GU902097	MN248704
Marionina communis	904	Hungary, Szolnok	under poplar trees	Dózsa-Farkas et al. 2018; Felföldi et al. 2020	MG252215	MG252151	MT433808
Marionina communis	1216	Korea, Mt. Gyebangsan	soil of *Quercus mongolica* forest	Felföldi et al. 2020	-	MT425086	MT433810
Marionina communis	CE811	Sweden, Skara	brown soil	Erséus et al. 2010; Klinth et al. 2017	KU894286	GU902098	KU894216
Marionina cf. *levitheca*	CE1339	Australia, Queensland	beach	Erséus et al. 2010	-	GU902093	-
Marionina cf. *minutissima*	CE843	Sweden, Lerum	near road	Erséus et al. 2010	-	GU902094	-
Marionina filiformis	CE1040	Sweden	coastal waters	Erséus et al. 2010	-	GU902099	-
Marionina fusca	CE12476	South Georgia Island	intertidal, 4 m up shore from low tide	Klinth et al. 2022	-	MZ393959	MZ394834
Marionina nevisensis	CE338	Bahamas, Lee Stocking Island	intertidal sand and rubble at pond outfall	Matamoros et al. 2012	JN799847	JN799911	-
Marionina cf. *nevisensis*	CE260	New Caledonia, Loyalty Islands	beach, marine fine sand with freshwater springs	Erséus et al. 2010; Matamoros et al. 2012	JN799846	GU902095	-
Marionina nothachaeta	LM322	Sweden, Swedish West Coast	intertidal sand	Matamoros et al. 2012	-	JN799950	-
Marionina seminuda	1334	Korea, Mt. Hallasan	soil of *Quercus serrata* copse forest	Felföldi et al. 2020	MT428060	MT425091	MT433811
Marionina southerni	CE674	Sweden, Gotland	coastal waters	Matamoros et al. 2012	JN799849	JN799913	-
Marionina spicula	1338	Croatia, Kale Cove	decaying seagrass (*Zostera*) detritus	this study	-	**MZ750846**	**MZ816255**
Marionina spicula	1339	Croatia, Kale Cove	decaying seagrass (*Zostera*) detritus	this study	-	**MZ750847**	**MZ816256**
Marionina spicula	1341	Croatia, Kale Cove	decaying seagrass (*Zostera*) detritus	this study	-	**MZ750848**	**MZ816257**
Marionina spicula	1366	Croatia, Kale Cove	decaying seagrass (*Zostera*) detritus	this study	**MZ835289**	**MZ750849**	**MZ816258**
Marionina spicula	1377	Croatia, Kale Cove	decaying seagrass (*Zostera*) detritus	this study	**MZ835290**	**MZ750850**	**MZ816259**
Marionina spicula	1378	Croatia, Kale Cove	decaying seagrass (*Zostera*) detritus	this study	-	**MZ750851**	**MZ816260**
Marionina spicula	1381	Croatia, Kale Cove	decaying seagrass (*Zostera*) detritus	this study	-	**MZ750852**	**MZ816261**
Marionina spicula	1441	Croatia, Kale Cove	decaying seagrass (*Zostera*) detritus	this study	-	**MZ750853**	**MZ816262**
Marionina spicula	1442	Croatia, Kale Cove	decaying seagrass (*Zostera*) detritus	this study	**MZ835291**	**MZ750854**	-
Marionina spicula	1443	Croatia, Kale Cove	decaying seagrass (*Zostera*) detritus	this study	-	**MZ750855**	**MZ816263**
Marionina spicula	1444	Croatia, Kale Cove	decaying seagrass (*Zostera*) detritus	this study	**MZ835292**	**MZ750856**	-
Marionina spicula	1445	Croatia, Kale Cove	decaying seagrass (*Zostera*) detritus	this study	**MZ835293**	**MZ750857**	**MZ816264**
Marionina spicula	1446	Croatia, Kale Cove	decaying seagrass (*Zostera*) detritus	this study	**MZ835294**	**MZ750858**	**MZ816265**
Marionina spicula	CE2561	Sweden, Västergötland	upper part of narrow zone of marsh-like vegetation, roots and brown soil	Martinsson et al. 2017; Klinth et al. 2022	-	KX618730	KX644887
Marionina tumulicola	CE571	Australia, South West coast	intertidal sand	Matamoros et al. 2012	-	JN799912	-
Marionina vesiculata	898	Hungary, Kőszeg Mts.	soil	Nagy et al. 2023	MZ835279	MZ750837	MZ816247
Achaeta unibulba (outgroup)	851	Hungary, Kőszeg Mts.	meadow	Dózsa-Farkas and Felföldi 2017	KY583112	KY583130	KY583097

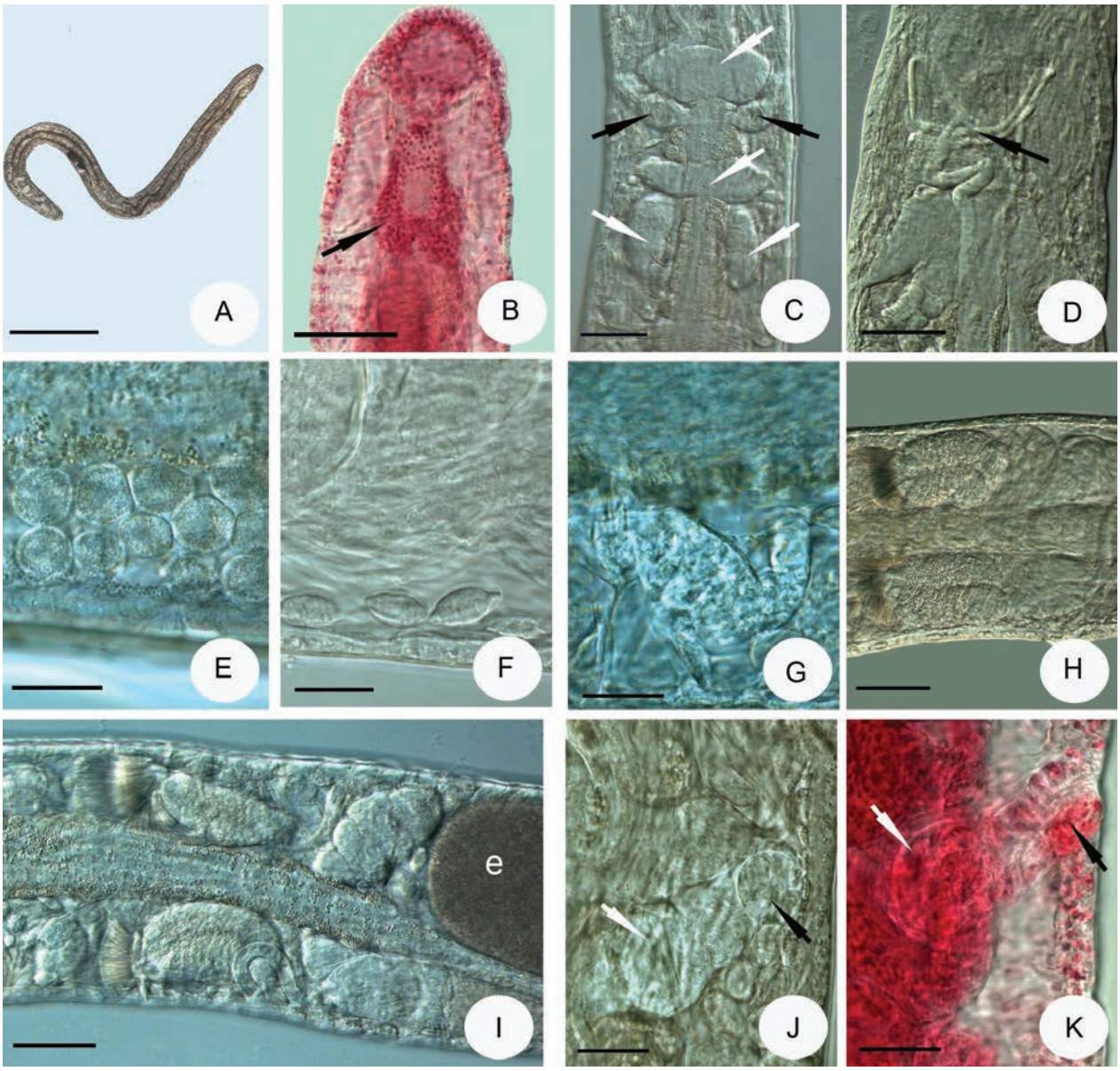

Figure 1. Micrograph of *Marionina puntaalanensis* sp. nov. **A.** Entire specimen; **B.** Brain; **C.** Pharyngeal glands (marked with white arrows; spermathecae marked with black arrows); **D.** Anterior bifurcation of the dorsal vessel in III; **E.** Rounded coelomocytes; **F.** Lemon-shaped coelomocytes; **G.** Preclitellar nephridium; **H, I.** Sperm funnels (e = egg); **J, K.** Spermathecae (ectal glands marked with black arrows, ampullae marked with white arrows). **A, C–J.** *in vivo*, **B, K.** fixed, stained. Scale bars: 500 µm (**A**); 50 µm (**B–D, F, H–J**); 20 µm (**E, G, K**).

Description. Small species (Fig. 1A), holotype 1.9 mm long, 80 µm wide at VIII and 107 µm at clitellum (fixed), segment number 21. Body length of paratypes 2.0–2.5 mm, width 120–180 µm at VIII and 130–185 µm at clitellum, *in vivo*, length of fixed specimens 1.5–2.7 mm, width 80–165 µm at VIII and 105–165 at clitellum, segment number 19–30. Chaetae straight with ental hook. Chaetal formula: 2 - 2: 2 - 2 (in one specimen from Castiglione della Pescaia, three chaetae were in one ventral bundle). The chaetae equal in size within the bundles; in the ventral bundles a little longer than in the lateral ones. 15–20 µm in preclitellar segments and 19–20 µm at the posterior end of the body. Clitellum saddle-shaped in XII-1/2 XIII, gland cells squarish, arranged in transverse rows, midventrally absent. Head pore at 0/I, no dorsal pores. Epidermal gland cells inconspicuous *in vivo*. Thickness of body wall about 18–20 µm, and cuticle thin <1 µm.

Brain (Fig. 1B) ca. 50–60 µm long (fixed), slightly longer than wide, incised posteriorly. Pharynx and postpharyngeal bulbs well developed. Prostomial ganglia absent. In the ventral nerve cord, perikarya continuous. First and second pharyngeal glands compact and united dorsally, in V with ventral lobes; the third pair free dorsally with elongate but stout ventral lobes (Fig. 1C). Chloragocytes from IV forming a denser layer from VI, about 15–20 µm long *in vivo*, filled with refractive globules. Transition between oesophagus and intestine gradual; oesophageal appendage and intestinal diverticula absent. Midgut pars tumida not seen. Dorsal vessel from clitellar region,

blood colorless. The dorsal anterior blood vessel bifurcation in III (Fig. 1D). All coelomocytes nucleated oval, disc-shaped (Fig. 1E) or lemon-shaped (Fig. 1F) with granules, 13–20 µm long *in vivo* and 10–18 µm, fixed. Three pairs of preclitellar nephridia in 6/7–8/9, preseptal part consisting of funnel and coils of canals, postseptal part elongate, about two times as long as preseptal part, efferent duct terminal (Fig. 1G); the first postclitellar pair at 13/14 (mostly seven postclitellar pairs). Seminal vesicle absent or small, paired. Sperm funnels small, cylindrical, 100–140 µm long *in vivo*, 40–75 µm when fixed, and about 1.5–2.5 times longer than wide *in vivo* (1.5–2 times, when fixed), collar high and narrower than funnel body (Fig. 1, I). Spermatozoa 38–43 µm long, heads 15–22 µm *in vivo* and 20–32 µm long and heads 10–13 µm, when fixed. Sperm ducts short, about four times longer than the funnel, coiled into a loose spiral, diameter 7–10 µm *in vivo* and 4–5 µm, when fixed. Male copulatory organs small and compact, 25–36 µm long, 23–40 µm wide, and 15–30 µm high *in vivo* (22–30 µm long, 20–27 µm wide, and 25–30 µm high, when fixed). Small subneural glands in XIII–XIV (in one specimen absent). Ectal duct of spermatheca 24–38 µm long, surrounded along the length by glands and one larger, 15–27 µm long, sessile gland at orifice. Ampulla oval, 24–40 µm wide and 40–55 µm long *in vivo* (20–30 µm wide, 25–35 µm long, fixed), in the lumen with some sperm (Fig. 1J, K). Ampulla attached with a short ental duct to the oesophagus. One or two mature eggs at a time.

Etymology. The new species is named after the Punta Ala beach, where it was found.

Distribution and habitat. Known from Loc. 3 and Loc. 2., the intertidal zone is near Punta Ala (Grosseto) and Castiglione della Pescaia, Italy, in the decaying seagrass detritus.

Differential diagnosis. Among the mostly intertidal small *Marionina* species with two chaetae in all chaetal bundles and without sperm rings in spermathecae, eight species are similar to the new species: *M. istriae* Giere, 1974; *M. miniampullacea* Shurova, 1978; *M. magnifica* Shurova, 1978; *M. mica* Finogenova, 1972; *M. aberrans* Finogenova, 1973; *M. elgonensis* Černosvitov, 1938; *M. neroutsensis* Coates, 1980; and *M. mesopsamma* Lasserre, 1964. The main differences are as follows: *M. istriae* is larger (body length 7–10 mm, segment number 38–43 vs. body length 2–2.5 mm, segment number 19–30), the chaetae are larger (65 µm long vs. 15–20 µm long), and a larger ectal gland is absent. *M. miniampullacea* is also larger (body length 4–5 mm), the chaetae are also larger (50 µm long), the dorsal vessel origin is in VII, and there is a rosette of glands at the orifice of the spermathecal duct. *M. magnifica* is larger (body length 4–5 mm), sometimes 3–4 chaetae occur, the chaetae are larger (40–50 µm long), and a larger ectal gland absent. *M. mica* has three ventral lobes of the pharyngeal glands in IV, V, and VI; the third pair is connected dorsally (vs. only in V; the third pair free); the dorsal vessel origin is in VIII; and the anterior blood vessel bifurcation is prostomial (also known as lumbricillinae-type). In *M. aberrans*, the cuticle is thick (2.5 µm vs. <1 µm), there is a large rosette of ectal glands, the preseptal part of the nephridia consists only of the funnel, and the sperm duct is long (vs. short). *M. elgonensis* is similarly small, but the ectal gland of the spermathecal ectal duct is absent. In *M. neroutsensis*, all pharyngeal glands are without ventral lobes; the ectal glands of spermathecae are absent, but a seminal vesicle is present (vs. absent). *M. mesopsamma* is larger (6 mm long), has a seminal vesicle, has only two pairs of preclitellar nephridia, and the spermathecae are free.

Marionina orbifera sp. nov.

https://zoobank.org/56E26433-75D8-4311-9838-B3ECA58BA1BE

Fig. 2

Type material. ***Holotype*:** Ma. 6, slide No. 3081. ***Type locality*:** (Loc. 3.) Italy, Punta Ala Grosseto, Castiglione della Pescaia, decaying seagrass detritus, 42°46'00.0"N, 10°51'31.0"E, Leg. András Dózsa-Farkas and Kinga Dózsa-Farkas, 24 Sep 2020.

***Paratypes*:** in total, 15 specimens: P.147.1 slide No. 3027, P.147.2 slide No. 3049 (two specimens), P.147.3 slide No. 3050 (two specimens), P.147.4 slide No. 3053 (two specimens), P.147.5 slide No. 3058, P.147.6 slide No. 3060, P.147.7 slide No. 3071, P.147.8 slide No. 3072, P.147.9 slide No. 3074, P.147.10 slide No. 3075, P.147.11 slide No. 3079, P.147.12 slide No. 3080. Same data as for holotype.

Further material examined. 20 specimens (10 only *in vivo*).

Diagnosis. (1) Small size (body length 2.3–3.3 mm, 130–220 µm wide at clitellum, *in vivo*, segment number 17–22); (2) chaetae straight with ental hook, two chaetae per bundle, slightly longer at the posterior end of the body; (3) clitellum saddle-shaped; (4) brain truncate posteriorly; (5) first and secondary pharyngeal glands united dorsally with small ventral lobes; the third pair elongate, free dorsally; (6) dorsal vessel from clitellar region, blood colorless. The dorsal anterior blood vessel bifurcation anteriorly behind the pharynx; (7) two pairs of preclitellar nephridia; (8) coelomocytes oval or disc-shaped with granules, 14–22 µm long *in vivo*; (9) seminal vesicle well developed; (10) sperm funnel 1.5–3 times longer than wide *in vivo*, collar high and narrower than funnel body, spermatozoa 44–60 µm long, heads 20–25 µm *in vivo*; (11) male copulatory organ small and compact, 30–40 µm long *in vivo*; (12) small subneural glands are in XIII–XIV; (13) ectal duct of spermatheca short, surrounded by glands. Ampulla spherical, diameter 40–55 µm *in vivo*, the lumen characteristically full of many spherical sperm rolls. Ampulla attached to the oesophagus; (14) 1–3 mature eggs at a time.

Description. Small species, holotype 2.1 mm long, 134 µm wide at VIII and 150 µm at clitellum (fixed), segment number 21. Body length 2.3–3.4 mm, width

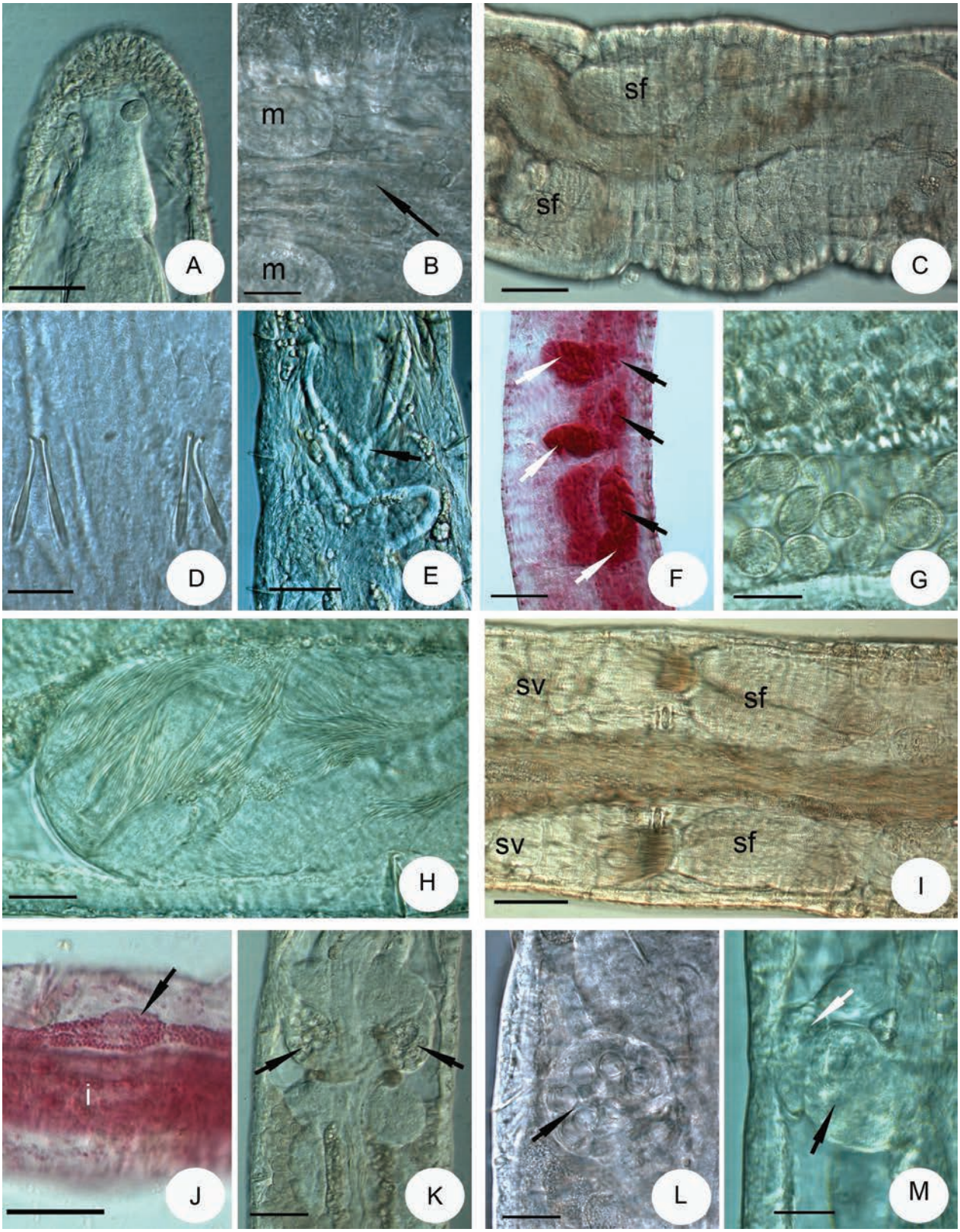

Figure 2. Micrograph of *Marionina orbifera* sp. nov. **A.** Brain; **B.** Clitellar glands absent ventrally (the male copulatory glands = m); **C.** Clitellum (sperm funnels = sf); **D.** Chaetae at the body end; **E.** Anterior bifurcation of the dorsal vessel in III; **F.** Pharyngeal glands, lateral view (primer pharyngeal gland pairs marked with white arrows, ventral lobes marked with black arrows); **G.** Coelomocytes; **H.** Large seminal vesicle; **I.** Sperm funnels (sperm funnels = sf, seminal vesicle = sv); **J.** Subneural gland in XIV; **K–M.** Spermathecae (the sperm rolls in the ampullae marked with black arrows, the glands at the ectal duct marked with white arrows). **A–E, G–I, K–M.** *In vivo*; **F, J.** Fixed, stained. Scale bars: 50 μm (**A, C, E, F, I, J, K**); 20 μm (**B, D, G, H, L, M**).

110–188 µm at VIII and 130–220 µm at clitellum, *in vivo*, length of fixed specimens 1.1–2.1 mm, width 118–160 µm at VIII and 125–180 µm at clitellum, segment number 17–24. Chaetae straight with ental hook. Chaetal formula: 2 - 2: 2 - 2 (in one case, three chaetae were in one ventral bundle of the segment III). The chaetae are equal in size within the bundles, a little longer in the ventral bundles than in the lateral ones. Chaetae are 20–30 × 2.2 µm in preclitellar segments and 28–35 × 2.8–3 µm at the posterior end of the body (Fig. 2D). Clitellum saddle shaped in XII-1/2 XIII, gland cells squarish, arranged in about 16–17 transverse rows (Fig. 2C), midventrally absent (Fig. 2B). Head pore at 0/I, no dorsal pores. Epidermal gland cells inconspicuous *in vivo*. Thickness of body wall about 15–16 µm, and cuticle thin (1 µm).

Brain (Fig. 2A) ca. 80 µm long (fix.) slightly longer than wide, truncate posteriorly. Pharynx well developed. Prostomial glanglia absent. In the ventral nerve cord, perikarya continuous. First and secondary pharyngeal glands compact and united dorsally, with small ventral lobes; the third pair elongate and free dorsally (Fig. 2F). Chloragocytes from IV forming a denser layer from VI, about 17–30 µm long *in vivo*, filled with refractive globules. Transition between oesophagus and intestine gradual; oesophageal appendage and intestinal diverticula absent. Midgut pars tumida not seen. Dorsal vessel origin from clitellar region; blood colorless. The dorsal anterior blood vessel bifurcation in III (Fig. 2E). All coelomocytes nucleated oval or disc-shaped with granules, 14–22 µm long *in vivo* (Fig. 2G) and 8–10 µm fixed. Two pairs of preclitellar nephridia in 7/8 and 8/9, preseptal part consisting of funnel and coils of canal, postseptal part elongate, about four times as long as preseptal part, efferent duct terminal. The first postclitellar pair of nephridia at 13/14. Seminal vesicle well developed, paired, extending anteriorly to X or IX and posteriorly to XII–XIII (Fig. 2H). Sperm funnels cylindrical, 85–140 µm long *in vivo*, 60–100 µm, fixed, and about 1.2–3 times longer than wide, collar high, and narrower than funnel body (Fig. 2C, I). Spermatozoa 44–60 µm long (in two specimens they were 80–87 µm long), heads 20–25 µm *in vivo* (Fig. 2I), (23–28 µm and 10–15 µm, respectively, when fixed). Sperm ducts short, coiled into a loose spiral, diameter 5–7 µm, *in vivo*. Male copulatory organs small and compact (Fig. 2B), 30–40 µm long, 20–35 µm wide, and 15–30 µm high, *in vivo* (25–38 µm long, 18–25 µm wide, and 20–30 µm high, when fixed). Small subneural glands in XIII–XIV (Fig. 2J). The ectal duct of spermatheca short, 20–35 µm long, surrounded along the length by glands, somewhat larger entally, no distinct rosette around the orifice (Fig. 2M). Ampulla spherical, diameter 40–55 µm *in vivo* (33–40 µm, fixed), the lumen filled with many spherical sperm rolls (Fig. 2K–M). Ampulla attached with a short ental duct to the oesophagus. 1–3 mature eggs at a time.

Etymology. The species is named after the characteristic sperm rolls („orb") in the spermatheca [orbifera = orb-bearing (Latin)].

Distribution and habitat. Known from the type locality, decaying seagrass detritus.

Differential diagnosis. Among the intertidal small *Marionina* species, nine species (*M. sjaelandica* Nielsen & Christensen, 1961, *M. levitheca* Erséus, 1990, *M. coatesae* Erséus, 1990, *M. swedmarki* Lasserre & Erséus, 1976, *M. vancouverensis* Coates, 1980, *M. limpida* Shurova, 1979, *M. cana* Marcus, 1965, *M. transunita* Coates, 1990, *M. southerni* (Černosvitov, 1937) and the new species are characterized by spherical sperm rolls in the spermathecal ampulla. The main differences are as follows: The spermathecae of *M. sjaelandica* and *M. coatesae* are similar to the new species; more sperm rolls are in the spermathecae, but not in the cavity, but embedded in the walls of the ampulla. Both species have more segments (segment number 24–27 in *M. sjaelandica*, 27–31 in *M. coatesae*, vs. 18–24 segments in the new species). *M. levitheca* is larger (segment number 38–41), the sperm rolls are arranged in distinct globular cavities scattered in the wall, and there are no glands at the ectal duct of the spermatheca. In *M. swedmarki*, the spermathecal orifice has a conspicuous gland-rosette. *M. vancouverensis* has a maximum of six chaetae per bundle (vs. only two in the new species). *M. limpida* is larger (6–8 mm long, vs. 2.3–3.3 mm), the subneural glands are only in XIII (vs. XIV–XV), the sperm funnel and sperm duct are longer, and the brain is incised posteriorly. In *M. cana*, the sperm rolls are in the walls of the ampulla, the ectal duct is not glandular, and the dorsal vessel origin is in IX, not in the clitellar region; moreover, the brain is incised posteriorly. *M. transunita* is also larger (with segment numbers 26–40), and the two spermathecae are connected entally. *M. southerni* is 8–10 mm long with 28–36 segments; the coelomocytes are black in transmitted light; and the spermatheca has many sessile diverticula.

Marionina reicharti sp. nov.

https://zoobank.org/BA81E0DD-F3A6-4480-B2ED-9A9F523D9B5D

Figs 3–4

Marionina spicula (Leuckart, 1847). Dózsa-Farkas 1995, 125–126, 128, 130.

Type material. *Holotype*: Ma. 7, slide No. 3128. ***Type locality*:** (Loc. 4) Hungary, Lake Balaton, Bélatelep, Strand Bátori, lake shore, wet sand between the roots of willow trees, 46°43'51.5"N, 17°31'41.7"E, Leg. György Reichart, 14 Feb 2021.

***Paratypes*:** In total, 22 (20 adult and 2 subadult) specimens: P.148.1 slide No. 3116 (three specimens), P.148.2 slide No. 3117 (three specimens), P.148.3 slide No. 3122 (two specimens), P.148.4 slide No. 3123 (four specimens), P.148.5 slide No. 3124 (two specimens), P.148.6 slide No. 3126 (two specimens), P.148.7 slide No. 3127, P.148.8 slide No. 3129 (two specimens), and P.148.9 slide No. 3130 (three specimens). Same data as for holotype.

Further material examined. 19 specimens (10 investigated only *in vivo*) + three specimens for DNA analysis.

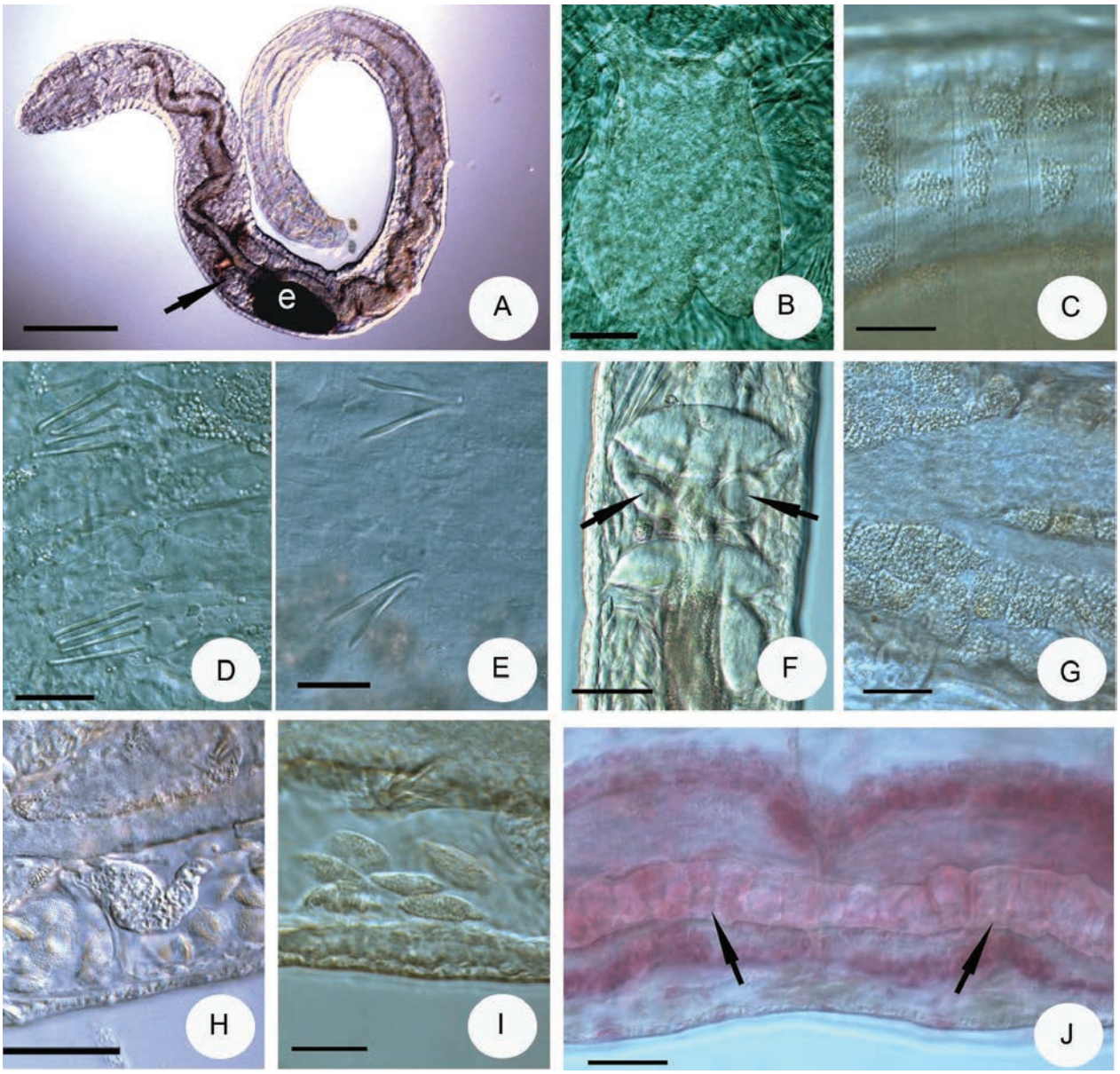

Figure 3. Micrograph of *Marionina reicharti* sp. nov. **A.** Entire specimen (e = egg); **B.** Brain; **C.** Clitellar glands, dorsal view; **D.** Chaetae, anterior bifurcation of the dorsal vessel in III, ventral view; **E.** Chaetae posteriorly; **F.** Pharyngeal glands (spermathecae marked with arrows); **G.** Chloragogen cells; **H.** Preclitellar nephridium; **I.** Coelomocytes; **J.** Pars tumida of midgut in XX–XXI. **A–I.** *In vivo*; **J.** Fixed, stained. Scale bars: 200 µm (**A**); 50 µm (**F–H**); 20 µm (**B–E, G, I, J**).

Diagnosis. (1) Small size (body length 2–3.3 mm, 137–190 µm wide at clitellum, *in vivo*), segment number 19–29; (2) maximum five chaetae per bundle, chaetae straight with ental hook and mostly not equal in size; (3) clitellum saddle-shaped; (4) first and second pairs of pharyngeal glands compact and united dorsally without ventral lobes; the third pair free and elongated; (5) transition between oesophagus and intestine gradual, midgut pars tumida in XVIII–XXII, extending over 3–4 segment lengths; (6) dorsal vessel origin in XII, blood colorless, the dorsal anterior blood vessel bifurcation anteriorly behind the pharynx; (7) three pairs of preclitellar nephridia; (8) coelomocytes nucleated oval or lemon-shaped with fine granules, 15–24 µm long *in vivo*; (9) seminal vesicle absent; sperm morulae occur in all segments; (10) sperm funnel 1.5–3 times longer than wide *in vivo*, collar high and narrower than funnel body; spermatozoa 46–70 µm long, heads 20–30 µm *in vivo*; (11) male copulatory organ oval or bean-shaped and compact, 33–47 µm long *in vivo*; (12) ectal duct of spermatheca surrounded by glands, wider proximally; one larger sessile gland at orifice; ampulla globular, diameter 29–40 µm *in vivo* with some sperm-threads or sperm bundle in it; ampulla attached to oesophagus.

Description. Small species (Fig. 3A), holotype 2.5 mm long, 115 µm wide at VIII and 138 µm at clitellum (fixed), segment number 28. Body length 2.0–3.3 mm, width 130–160 µm at VIII and 137–190 µm at clitellum *in vivo*, length of fixed specimens 1.5–2.5 mm, width 90–135 µm at VIII and 115–160 µm at clitellum,

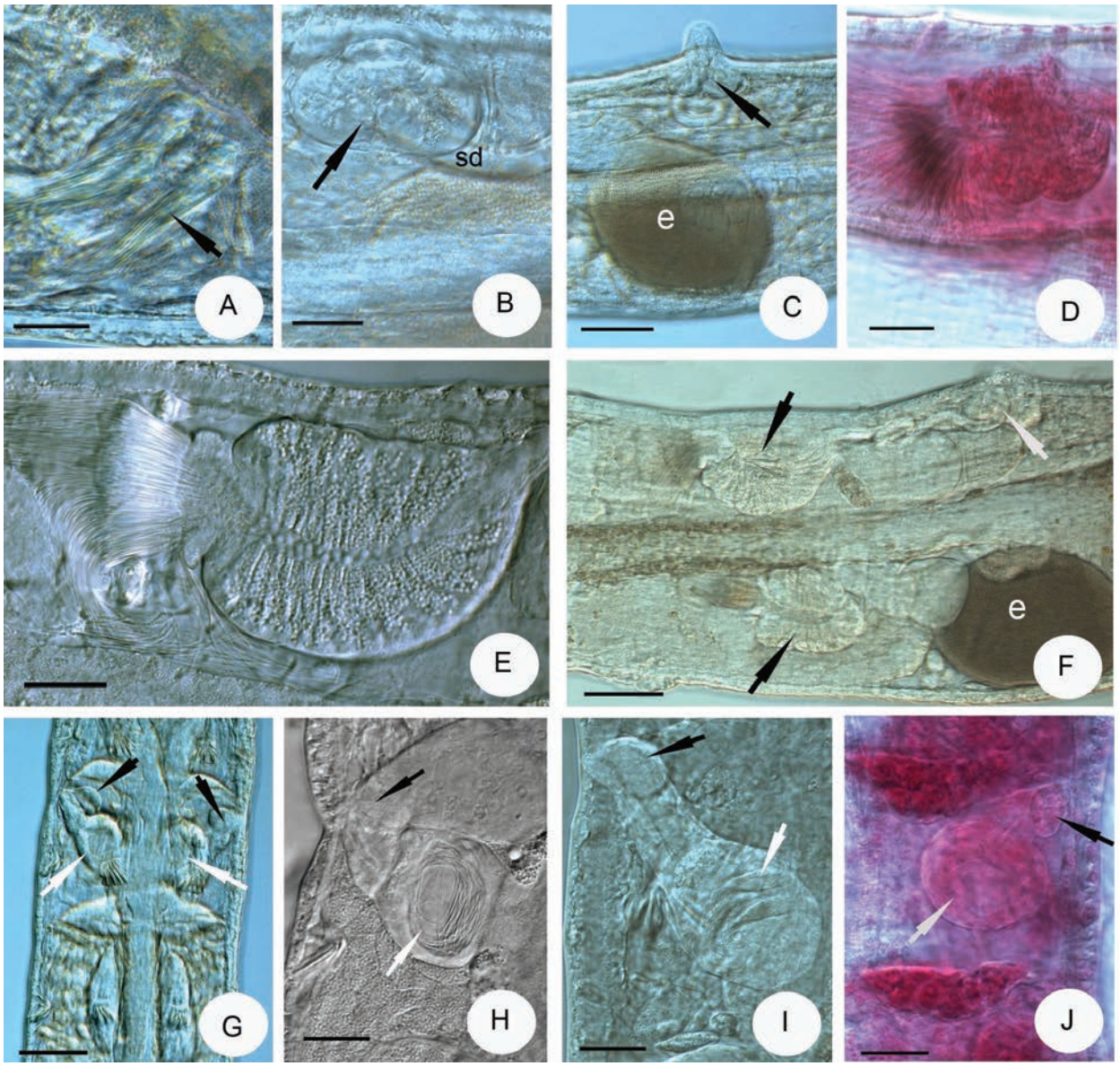

Figure 4. Micrograph of *Marionina reicharti* sp. nov. **A.** Sperm bundles in the coelom; **B, C.** Male copulatory organs (e = egg, sd = sperm duct); **D–F.** Sperm funnels (male copulatory organs marked with a white arrow); **G–J.** Spermathecae (ectal glands marked with black arrows, ampulla marked with white arrows, in **H.** Sperm thread in ampulla, in **I.** Sperm bundles in ampulla). **A–C, E–I.** *In vivo*; **D, J.** Fixed, stained. Scale bars: 50 µm (**C, F, G**); 20 µm (**A, B, D, E, H–J**).

segment number 19–29. Chaetae straight with ental hook (Fig. 3D, E). Chaetal formula: 2.3,(4) - 2.3: (3)4.5,(6) - 2.3,(4). The chaetae are not exactly equal in size within the bundles; often the middle chaetae slightly smaller than the ental ones, e.g., in the ventral preclitellar bundles, 20–19.5–18–20 µm or 25–22–20.4–24.2 µm long and 1.6–1.9 µm wide. The ventral chaetae slightly longer than lateral ones. At the posterior end of the body, chaetae are 21–27 µm long. Clitellum saddle-shaped in XII-1/2 XIII, gland cells squarish, arranged in about 15–18 transverse rows (Fig. 3C), midventrally absent. Head pore not seen, no dorsal pores. Epidermal gland cells inconspicuous *in vivo*. Thickness of body wall about 10–13 µm; cuticle thin (<1 µm).

Brain (Fig. 3B) ca. 47–51 µm long (fixed), slightly longer than wide, incised posteriorly. Prostomial glanglia absent. In the ventral nerve cord, perikarya continuous. First and second pair of pharyngeal glands compact and united dorsally without ventral lobes; the third pair free and elongate (Figs 3F, 4G). Chloragocytes from IV forming a denser layer from VI, about 8–12 µm long *in vivo*, filled with refractive globules (Fig. 3G). Transition between oesophagus and intestine gradual; oesophageal appendage and intestinal diverticula absent. Midgut pars tumida in XVIII–XXII, extending over 3–4 segment lengths (Fig. 3J). Dorsal vessel from XII, blood colorless. The dorsal anterior blood vessel bifurcation in III. All coelomocytes nucleated oval or lemon-shaped with fine granules, 15–24 µm long *in vivo* (Fig. 3I) and 8–10 µm, fixed. Three pairs of preclitellar nephridia in 6/7–8/9, preseptal part consisting of funnel and coils of canal, postseptal part elongate, about 1.7–3 times longer than the preseptal part,

efferent duct terminal (Fig. 3H). Seminal vesicle absent, sperm morulae and sperm bundles may occur in all segments (Fig. 4A). Sperm funnels cylindrical, 60–95 µm long *in vivo*, 40–70 µm, fixed, and about 1.5–3 times longer than wide *in vivo* (1.2–2 times, when fixed), collar high, and narrower than funnel body (Fig. 4D–F). Spermatozoa 46–70 µm long, heads 20–30 µm *in vivo*, 30–50 µm long, heads 10–22 µm, when fixed. Sperm ducts short, about 2.5–3.5 times longer than the funnel, coiled into a loose spiral, diameter 7–9 µm, *in vivo*. Male copulatory organ oval or mostly bean-shaped and compact (Fig. 4B, C, F), 33–47 µm long, 18–26 µm wide, and 18–26 µm high, *in vivo* (30–40 µm long, 21–28 µm wide, and 18–25 µm high, when fixed). Subneural glands absent. Ectal duct of spermatheca, 26–38 µm long, surrounded along the length by glands, 14–18 µm wide proximally and 10–14 µm wide distally *in vivo* (20–23 µm long, 14–20 µm wide proximally, and 12–16 µm wide distally, when fixed). One larger, 15–22 µm long, sessile gland at orifice *in vivo* (15–20 µm, fixed) (Fig. 4G–J). Ampulla globular, diameter 29–40 µm *in vivo* (25–40 µm, fixed), lumen with some sperm-threads (Fig. 4H) or 1–3 sperm bundles (Fig. 4I). Ampulla attached with a short ental duct to the oesophagus. One or two mature eggs at a time (Fig. 4C, F).

Etymology. The new species is named in the honor of György Reichart, who collected the sample with this species.

Distribution and habitat. Known from the lake shore of Lake Balaton at Bélatelep, Strand Bátori, Hungary, in wet sand between the roots of willow trees (Loc. 4). Earlier, they were identified as *Marionina spicula* (Leuckart, 1847) at four stations of the Lake Balaton (between Fűzfő and Alsóörs, Balatonberény, and Bélatelep) in a fauna investigation in 1990–1992 (Dózsa-Farkas 1995). Unfortunately, these specimens were lost.

Remarks on the studied specimens. Some small enchytraeid worms during the former study of Lake Balaton shore fauna were identified as *Marionina spicula* (Dózsa-Farkas 1995); therefore, the question was raised if they really belonged to this species known typically from marine habitats. However, in two papers (Lafont and Juget 1976; Rodriquez 1986), the species was observed along rivers without a detailed morphological description, and its euryhalinity was also reported previously (Giere 1971). This initiated our study with a freshly collected sample from the shore of Lake Balaton, combining DNA sequencing with morphological investigation. Since some specimens fitting the description of *M. spicula* (Nielsen and Christensen 1959) were detected in the Adriatic shore samples (collected in 2019), those specimens were also included in our comparison. Furthermore, specimens collected from a Danish seashore in 1999 (site 5) were also studied, but unfortunately, we were not able to obtain DNA sequences from them due to their fixation in Bouin's fluid. The results of the molecular analysis revealed that the DNA sequences of the Hungarian specimens (Lake Balaton) differ from those of the individuals collected by us from the Adriatic seashore (site 1, Table 1) and from the single DNA sequence of *M. spicula* in NCBI GenBank (see details below), so there is support at the DNA level that the Balaton specimens belong to a new species.

Differential diagnosis. Our species comparison is based on Nielsen and Christensen (1959), and it includes observations on living individuals collected in Denmark on the Nivå coast in 1999 (site 5) and reinvestigated (as fixed material) in this study. The morphological differences are as follows: *M. reicharti* sp. nov. is smaller (2–3.3 mm length vs. 4–5 mm length in *M. spicula* in Denmark, *in vivo*, 1.5–2.5 mm length vs. 2.1–2.6 mm length, fixed), segment number 19–29 vs. 27–30. Sperm funnel slightly shorter (40–70 µm long vs. 67–90 µm, fixed), the spermatozoa are longer in the new species (30–50 µm, heads 11–22 µm vs. 20–38 µm, heads 10–17 µm in *M. spicula*). The ectal duct of the spermatheca is longer in Danish *M. spicula* specimens and proximally wider (20–50 µm long and 16–50 µm wide vs. 20–23 µm long and 14–20 µm wide in the new species). Origin of the dorsal vessel from segment XII vs. from XIII in Danish *M. spicula* specimens.

Keeping in mind that the Mediterranean *M. spicula* specimens studied here may belong to a different species, and since the origin of *M. spicula* specimen CE2561 is from Sweden (see additional details below), we performed a morphological comparison of Mediterranean *M. spicula* with the new species: *M. reicharti* sp. nov. is smaller and has in general fewer segments: length 3 mm, width 137–190 µm at clitellum *in vivo*, 19–29 segments (vs. 3–7 mm, 200–430 µm, 21–39 segments, respectively). The maximum number of ventral chaetae is lower, 5–6 (vs. 7–8). The clitellum is saddle shaped (vs. ring-shaped, glands absent only between the male openings). The spermatozoa are 46–70 µm long, heads 20–30 µm *in vivo* (vs. 60–120 µm long and 30–43 µm), the male copulatory organ is also smaller, 33–47 µm long, 18–26 µm wide, 18–26 µm high (vs. 45–70 × 45–60 × 35–50 µm). Furthermore, the size of the spermatheca is different: ectal duct 26–38 long, ectal gland 15–22 µm long, diameter of ampulla 29–40 µm *in vivo* (vs. 35–51 µm, 30–40 µm and 40–63 µm, respectively). The coelomocytes and the size of sperm funnels are not comparable, because these traits in the specimens of *M. spicula* collected at the Adriatic seashore are very variable (a sign of that possibly *M. spicula* is a species complex).

Morphological notes on the *Marionina spicula* (Leuckart, 1847) specimens of the Adriatic seashore

Figs 5–6

Material examined. About 50 specimens were investigated *in vivo*, slides were made from 28 specimens, and 11 specimens were used for DNA analysis. *Collecting site*: (Loc. 1) Croatia, Istria, Kale Cove seashore, Adriatic Sea, Kamenjak Peninsula, decaying seagrass (*Zostera*) detritus, 44°51'13.0"N, 13°58'50.5"E, Leg. Júlia Török, 03 Apr 2019, and 05 Sep 2020.

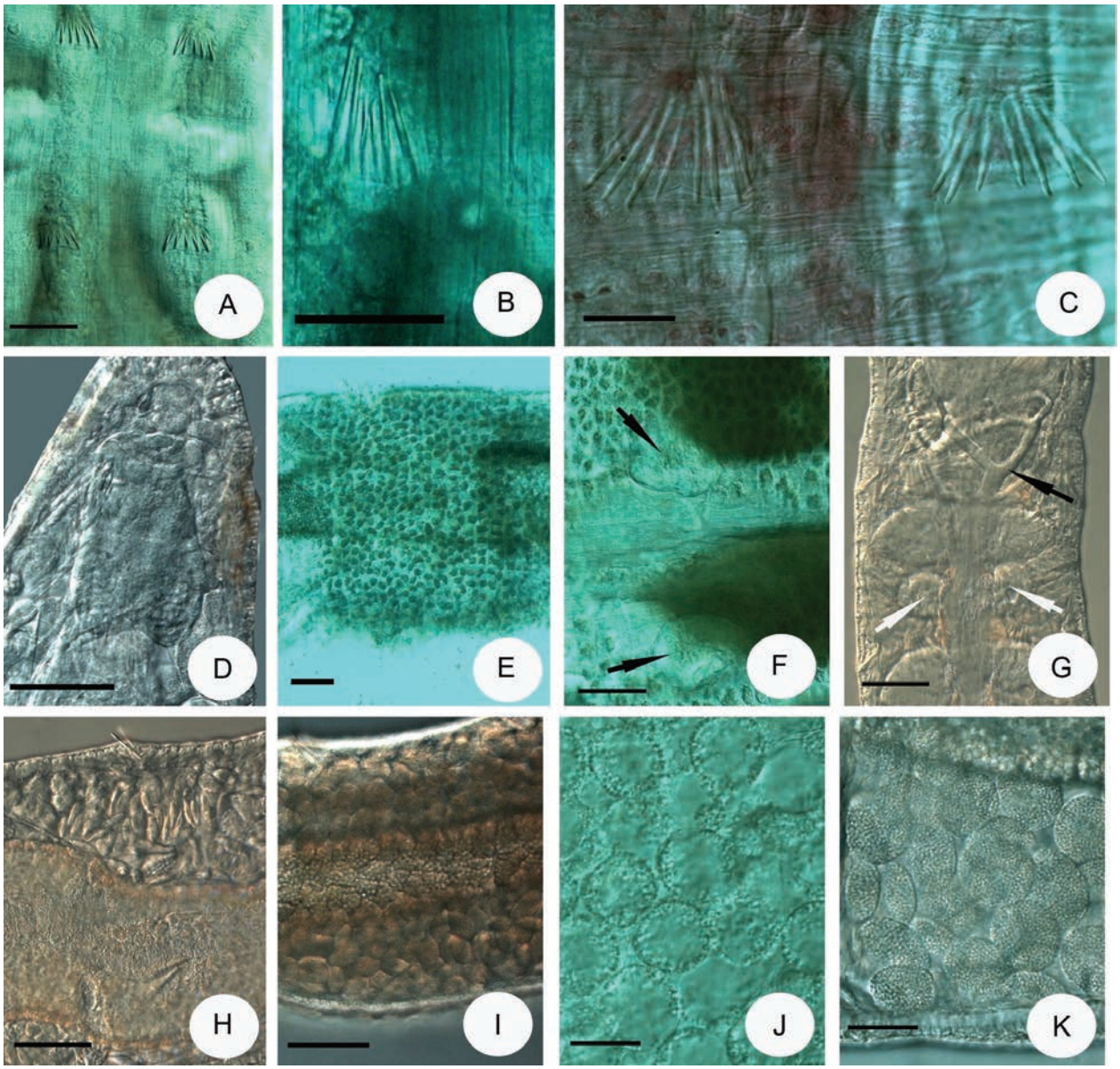

Figure 5. Micrograph of *Marionina spicula*. **A.** Chaetae maximum 5 in a ventral bundle; **B.** The inner chaetae shorter; **C.** Chaetae maximum 7-8 in a ventral bundle. A, B, and C from different specimens; **D.** Brain; **E.** Clitellar glands, dorsal view; **F.** Clitellar glands absent between the male copulatory organs; **G.** Anterior bifurcation of the dorsal vessel in III (spermathecae marked with white arrows); **H.** Lighter coelomocytes; **I.** Dark coelomocytes; **J.** Coelomocytes with fewer granules; **K.** Coelomocytes full with granules. All pictures are *in vivo*. Scale bars: 50 μm.

Description of new material. Small worms, body length 3–7 mm, width 200–430 μm at clitellum *in vivo*; length of fixed specimens 1.9–3.6 mm, width 170–320 μm at clitellum, segment number 21–39. Chaetae straight with ental hook. Chaetal formula variable: 2-5 - 4-2: 4-8 - 6-2. The chaetae unequal in size within the bundles. Mostly the chaetae towards the midlines of the body are shorter than the lateral ones, or the chaetae in the middle of the bundles are shorter (Fig. 5A–C). Clitellum ring-shaped in XII-1/2 XIII, gland cells arranged in irregular transverse rows (Fig. 5E), between the male openings absent (Fig. 5F). Head pore at the middle of prostomium, no dorsal pores. Epidermal gland cells inconspicuous *in vivo*.

Brain (Fig. 5D) 62–87 μm long (fixed), 1.5 times longer than wide, incised posteriorly. Pharynx and postpharyngeal bulbs well developed. Prostomial ganglia absent. In the ventral nerve cord, perikarya continuous. First and secondary pharyngeal glands compact and united dorsally; the third pair free (Figs 5G, 6F). Chloragocytes from IV forming a denser layer from VI, about 15–20 μm long *in vivo*, filled with refractive globules. Transition between oesophagus and intestine gradual; oesophageal appendages and intestinal diverticula absent. Midgut pars tumida not seen. Dorsal vessel from XII, blood colorless. The dorsal anterior blood vessel bifurcation in III, pharyngeal (Fig. 5G). Coelomocytes variable (Fig. 5H–K), nucleated, disc-shaped with gray granules; in some specimens, the coelo-

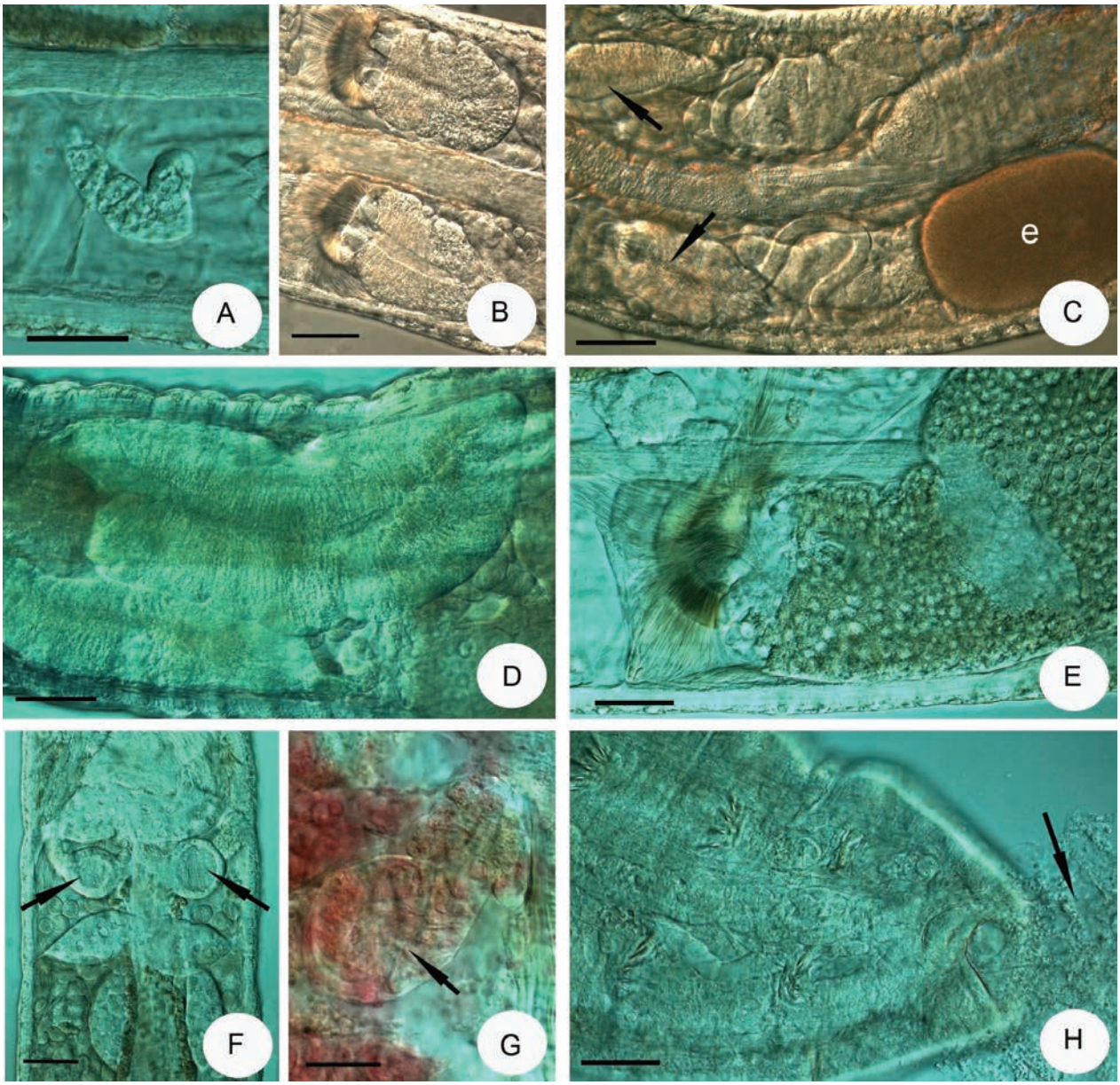

Figure 6. Micrograph of *Marionina spicula*. **A.** Nephridium; **B.** Shorther sperm funnels; **C.** Shorther sperm funnels (marked with arrows) with a short sperm duct (e = egg); **D, E.** Large sperm funnels; **F–G.** Spermathecae (ampullae marked with arrows); **H.** Body-end with ejected sticky mucus. **A–F, H.** *in vivo*, **G.** fixed, stained. Scale bars: 50 µm (**A–F, H**); 20 µm (**G**).

mocytes are with few granules (Fig. 5J), so they are pale in the coelom. In other specimens, the coelomocytes are filled with granules (Fig. 5K), and the coelomocytes are in such large numbers that they fill the entire coelom and are dark gray in transmitted light (Fig. 5I), 15–24 µm long *in vivo*, and 15–17 µm, fixed. Three pairs of preclitellar nephridia in 6/7–8/9, preseptal part consisting of funnel and coils of canal, postseptal part elongate, about 2–2.5 times longer than the preseptal part, efferent duct terminal (Fig. 6A). Seminal vesicle absent. Sperm funnels cylindrical, very variable; they can be about 110–150 µm long and 1.7–2.4 times longer than wide (Fig. 6B, C); in other specimens, they are very large, 170–300 µm long and 3–4.5 times longer than wide *in vivo* (Fig. 6D, E), collar 10–25 µm high and narrower than funnel body. Spermatozoa 60–120 µm long, heads 30–43 µm *in vivo*. Sperm ducts short, about three times longer than the funnel, diameter 10–13 µm, *in vivo* (Fig. 6C). Male copulatory organs compact (Fig. 5F), 45–70 µm long, 45–60 µm wide, and 35–50 µm high *in vivo* (32–58 µm long, 30–53 µm wide, and 28–40 µm high, when fixed). Ectal duct of spermatheca 35–51 µm long, surrounded along the length by glands and one larger, 30–40 µm long, sessile gland at orifice. Ampulla rounded (diameter 40–63 µm wide *in vivo*, 35–53 µm, fixed), sometimes with a rather thick wall (6–14 µm) in the lumen with sperm (Fig. 6F, G). Ampulla attached with a short ental duct to the oesophagus. One or occasionally two mature eggs at a time (Fig. 6C). In this species, as already pointed out by Giere (1971), it is often observed that the coelomic fluid, released through the anus, attaches itself to the grains of sand (Fig. 6H).

Results of molecular analysis

Results of the phylogenetic analyses confirmed that *M. puntaalanensis* sp. nov., *M. orbifera* sp. nov., and *M. reicharti* sp. nov. are genetically separated from the other (sequenced) *Marionina* species because their sequences formed distinct lineages on the phylogenetic trees. The Adriatic specimens, which we identified as *M. spicula*, fall into three separate lineages (Figs 7–9). In all trees, Mediterranean *M. spicula* appears as a heterogeneous group, and specimens from this species form consistently three clades (four, if CE2561 is included, a specimen from the Swedish coast) with various bootstrap support. *M. reicharti* sp. nov. is very similar morphologically to *M. spicula* as conceived by Nielsen and Christensen (1959), but in the trees based on ITS and H3, it is sister to one of the Mediterranean "*M. spicula*" clades. In the COI phylogenetic tree, on the other hand, it appears as the sister group of *M. puntaalanensis* sp. nov. It should be noted that in Fig. 8. —a tree based on the COI sequences of all identified *Marionina* species currently available in GenBank —reference sequences from species that are currently considered to belong to *Marionina* sensu stricto (namely, *M. aestuum* and *M. fusca*) (Klinth et al. 2022) form a clade separate from those species that were described in this study.

The results of the distance analyses supported the phylogenetic investigations. The p-distances between the ITS sequences of the three new species and the other *Marionina* species are 15.8–45.6%, the COI distances between them are 17–25.5%, and the H3 distances between them are 2.1–17.7%. The distances between the ITS sequences of *M. reicharti* sp. nov. and *M. spicula* are 15.8–26%, the COI distances between them are 17–18.7%, and the H3 distances between them are 2.9–4.8%. The ITS distances between the three Croatian *M. spicula* clades are 13.4–20.8%, the COI distances between them are 15.4–17.3%, and the H3 distances between them are 1.1–3.2%. The specimen *M. spicula* CE2561, probably from Sweden, formed a fourth clade since it separated from *M. spicula* individuals collected in Croatia. The COI distances between *M. spicula* CE2561 and the three Croatian *M. spicula* clades are 15.8–17.3%, and the H3 distances between them are 4.1–5%. The ITS distances could not be compared between them because the whole ITS sequence (containing ITS1, 5.8S rDNA, and ITS2) for *M. spicula* CE2561 is currently not available in the GenBank database. The above-presented results suggest that *M. spicula* is a complex of at least four species.

Discussion

As a result of our research on the supralittoral zone of the Mediterranean seashores, we described two species new to science (*Marionina puntaalanensis* sp. nov. and *M. orbifera* sp. nov.) from the Tyrrhenian coast. The distinctive morphological characters served as the basis of the description of these two new species, and their assignment was confirmed with DNA sequence analyses based on the ITS region and the COI and H3 genes.

In the case of the *Marionina spicula* (Leuckart, 1847) specimens found in Adriatic coastal samples, we have shown that they are probably members of a species complex. Morphological differences were detected among the specimens, and the DNA sequences also formed several clades on the phylogenetic trees based on all three studied DNA regions; furthermore, the genetic distances among

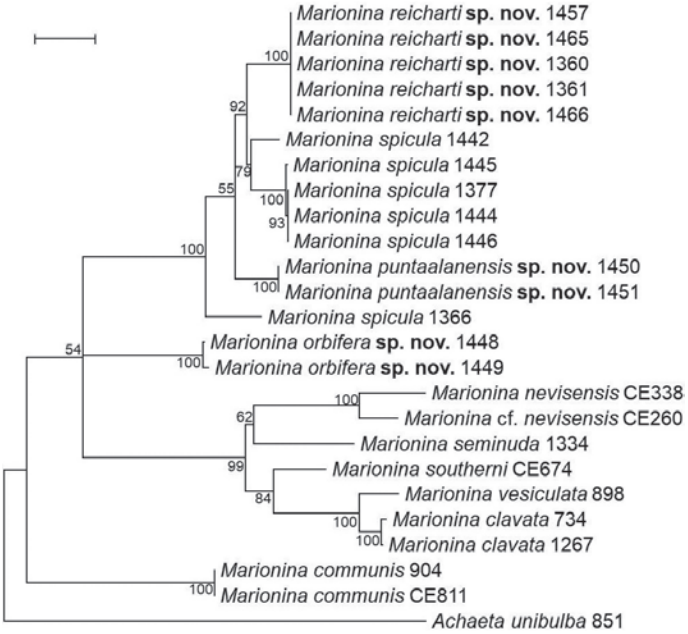

Figure 7. Maximum likelihood (ML) tree of the ITS region for *Marionina* species, based on 854 nucleotide positions using the General Time Reversible substitution model. Bootstrap values greater than 50 are shown at the nodes. Accession codes of sequences with collection information are given in Table 1. Scale bar: 0.2 substitutions per nucleotide.

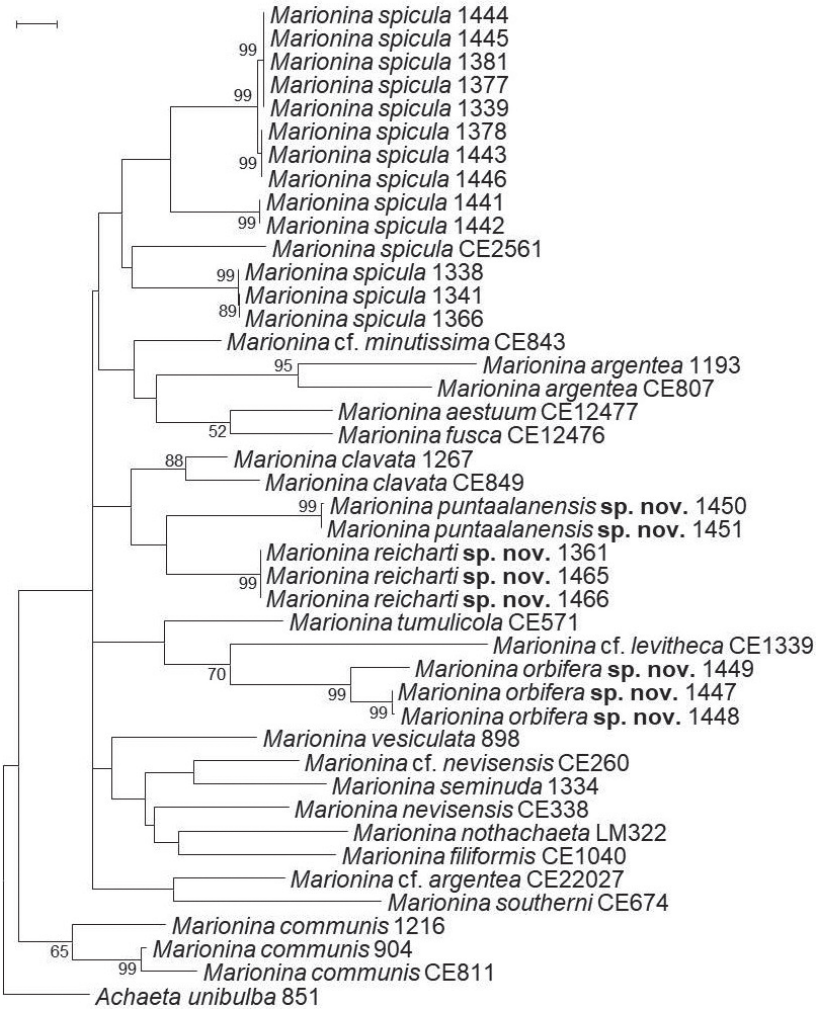

Figure 8. Maximum likelihood (ML) tree of the COI gene for *Marionina* species, based on 517 nucleotide positions using the General Time Reversible substitution model. Bootstrap values greater than 50 are shown at the nodes. Accession codes of sequences with collection information are given in Table 1. Scale bar: 0.1 substitutions per nucleotide.

the detected *Marionina spicula* clades were comparable to the interspecific differences of the other *Marionina* species included in this study. However, we were not able to assign this variability to distinct new species. The observed morphological differences included, for example, the maximum number of chaetae (which in some cases was only 4–5; in other cases, it was 7–8 chaetae per ventral bundle), the size of the sperm funnel (besides the type of "two times longer than wide," there were very large sperm funnels, which were 3–4.5 times longer than wide), and the granularity of coelomocytes (sometimes the coelomocytes were less granulated, but in other cases the coelomocytes were filled with dark grey granules). In cases where coelomocytes with dark granules filled the coelom of the worm in large numbers, it resulted in the internal organs of the animal being difficult to study in transmitted light, which hindered the comprehensive morphological characterization. Furthermore, since, after the completion of the microscopic studies, whole specimens were used for the molecular study due to the small size (few mm) of the animals, the subsequent re-investigation of the worms belonging to different clades was unfortunately not possible to search for further distinctive morphological characters. To circumvent this problem, several additional samples were collected from the same location at the Adriatic coast later, but no living specimens were found in them, most probably because the seagrass detritus was removed from the beach to fulfill the requirements of tourists, and this inhibited the survival of the worms. It was reported (Giere 1971) that coelomic fluid released from the anus helps the individuals of *M. spicula* attach to sand particles (this was also observed by us), and this contributes to their adaptation to the sea wave-generated shore habitat consisting of a mixture of sand and decaying plant material. However, after studying the fixed specimens collected from the Danish coast in 1999, it could be concluded that they fully fit the description given by Nielsen and Christensen (1959). On the other hand, Danish individuals differed from the specimens collected by us from the Adriatic seashore since the Danish individuals have a maximum of only 4–5 chaetae in a bundle and the diameter of the spermathecal ampulla is smaller (25–32 vs. 25–55 μm in Adriatic specimens). Taken all together, further studies are required on the *M. spicula* species complex, which

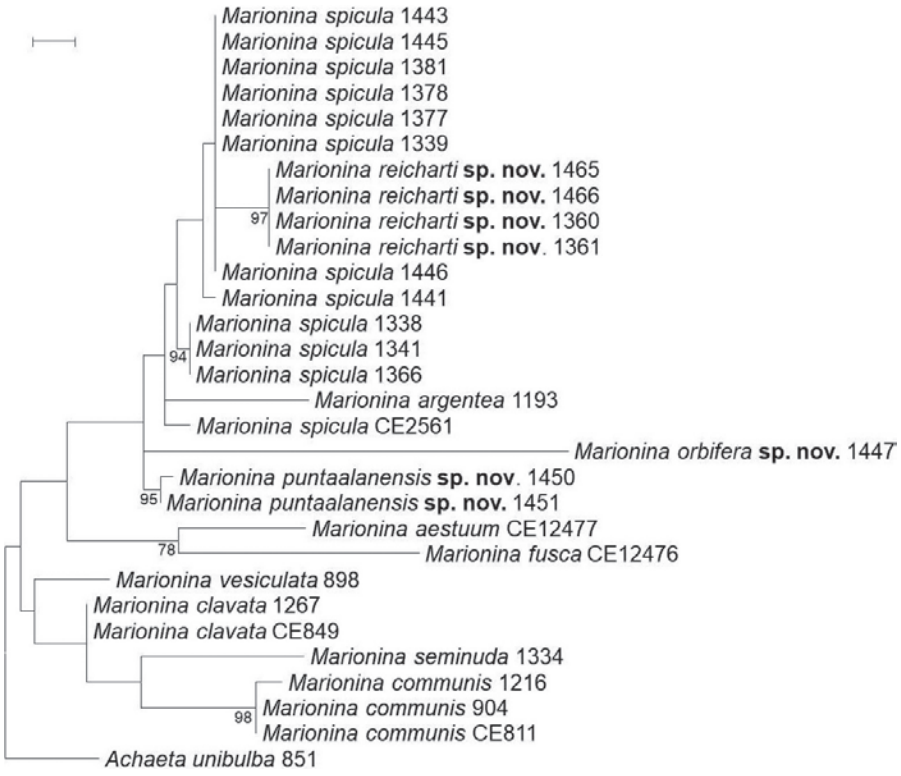

Figure 9. Maximum likelihood (ML) tree of the H3 gene for *Marionina* species, based on 201 nucleotide positions using the Tamura 3-parameter substitution model. Bootstrap values greater than 50 are shown at the nodes. Accession codes of sequences with collection information are given in Table 1. Scale bar: 0.02 substitutions per nucleotide.

should include more specimens from the North and Baltic Seas and a comparison of the morphological variations reported in the literature. A systematic revision of *Marionina spicula* "sensu lato" is beyond the scope of this paper. However, it should be noted that enchytraeid species having a wide geographic distribution similarly to *M. spicula* (e.g., *Enchytraeus albidus*; Collado et al. 2012; Erséus et al. 2019; Nagy et al. 2023) represent a species complex.

Nevertheless, on the way of resolving the problematic issues related to this heterogenous group, we examined specimens previously designated as *M. spicula* from the littoral zone of Lake Balaton in this study, and we described them as a new species (*M. reicharti* sp. nov.) based on the morphological and molecular results. With the species described here, the number of *Marionina* species is increasing from 101 to 104. Summarizing the recent changes within the genus, 94 accepted species were reported in the checklist of Schmelz and Collado (2012), and seven new species (*M. deminuta* Rota, 2013, *M. fusca* Klinth, Rota & Erséus, 2022, *M. mimula* Rota, 2013, *M. mendax* Rota, 2013, *M. naso* Timm, 2012, *M. nothachaeta* Matamoros, Rota & Erséus, 2012, and *Marionina sambugarae* Schmelz, 2015) were described since then by others (Martin et al. 2015; Schmelz and Collado 2015; Klinth et al. 2022), and three new species (two marine and one freshwater) were described in this study.

All three species new to science belong to *Marionina* sensu lato (Klinth et al. 2022), but we hope that our results based on comparative morphological and molecular data will aid the revision of the genus in the future.

Acknowledgements

H. N. was supported by the ÚNKP-20-4 New National Excellence Program of the Ministry for Innovation and Technology from the source of the National Research, Development, and Innovation Fund, Hungary (grant no. ÚNKP-20-4-I-ELTE-281).

The authors are thankful to András Dózsa-Farkas and Kinga Dózsa-Farkas, Dr. Júlia Török, and György Reichart for collecting samples and for the reviewers for their valuable suggestions.

References

Bely AE, Wray GA (2004) Molecular phylogeny of naidid worms (Annelida: Clitellata) based on cytochrome oxidase I. Molecular Phylogenetics and Evolution 30(1): 50–63. https://doi.org/10.1016/S1055-7903(03)00180-5

Bretscher K (1899) Beitrag zur Kenntnis der Oligochaeten-Fauna der Schweiz. Revue Suisse de Zoologie 3(2): 369–426. https://doi.org/10.5962/bhl.part.82518

Černosvitov L (1937) System der Enchytraeiden. Bulletin de l'Association suisse pour les Recherches scientifiques a Prague 5: 263–294.

Černosvitov L (1938) Mission scientifique de l'Omo. Oligochaeta Mèmoires du Muséum National d'Histoire Naturelle 4: 255–318.

Christensen B, Dózsa-Farkas K (2012) A new genus *Globulidrilus* and three new enchytraeid species (Oligochaeta: Enchytraeidae) from Seoraksan National Park (Korea). Journal of Natural History 46(45–46): 2769–2785. https://doi.org/10.1080/00222933.2012.737038

Coates KA (1980) New marine species of *Marionina* and *Enchytraeus* (Oligochaeta, Enchytraeidae) from British Columbia. Canadian Journal of Zoology 58(7): 1306–1317. https://doi.org/10.1139/z80-182

Coates KA (1989) Phylogeny and origins of Enchytraeidae. Hydrobiologia 180(1): 17–33. https://doi.org/10.1007/BF00027534

Coates KA (1990) Marine Enchytraeidae (Oligochaeta, Annelida) of the Albany area, Western Australia. In: Wells FE, Walker DI, Kirkman H, Lethbridge R (Eds) Proceedings of the Third International Marine Biological Workshop: The marine flora and fauna of Albany, Western Australia. Western Australia Museum, Perth, 13–41.

Colgan DJ, McLauchlan AA, Wilson GDF, Livingston SP, Edgecombe GD, Macaranas J, Cassis G, Gray MR (1998) Histone H3 and U2 snRNA DNA sequences and arthropod molecular evolution. Australian Journal of Zoology 46(5): 419–437. https://doi.org/10.1071/ZO98048

Collado R, Hass-Cordes E, Schmelz RM (2012) Microtaxonomy of fragmenting *Enchytraeus* species using molecular markers, with a comment on species complexes in enchytraeids. Turkish Journal of Zoology 36: 85–94. https://doi.org/10.3906/zoo-1002-70

Dózsa-Farkas K (1995) Enchytraeid fauna of the shore of Lake Balaton. In: Mishra PC (Ed.) Advances in Ecology and Enviromental Sciences, Ashish Pub. House, New Delhi: Chapter 8: 117–131.

Dózsa-Farkas K (2002) Notes on the genus *Oconnorella* Rota, 1995. - Natura Jutlandica 2, Proceeding of the 4th International Symposium on Enchytraeidae, Mols Laboratory, Denmark, 2–4 June 2000: 86–90.

Dózsa-Farkas K, Felföldi T (2017) Comparative morphological and molecular taxonomic study of six *Achaeta* species (Clitellata: Enchytraeidae) with the description of a new *Achaeta* species from Kőszeg Mountains, Hungary. Zootaxa 4273(2): 177–194. https://doi.org/10.11646/zootaxa.4273.2.2

Dózsa-Farkas K, Felföldi T, Hong Y (2015) New enchytraeid species (Enchytraeidae, Oligochaeta) from Korea. Zootaxa 4006(1): 171–197. https://doi.org/10.11646/zootaxa.4006.1.9

Dózsa-Farkas K, Felföldi T, Nagy H, Hong Y (2018) New enchytraeid species from Mount Hallasan (Jeju Island, Korea). Zootaxa 4496(1): 337–381. https://doi.org/10.11646/zootaxa.4496.1.27

Erséus C, Daoyuan S, Yanling L, Bin S (1990) Marine Oligochaeta of Jiaozhou Bay, Yellow Sea coast of China. Hydrobiologia 202(1–2): 107–124. https://doi.org/10.1007/BF02208131

Erséus C, Rota E, Matamoros L, De Wit P (2010) Molecular phylogeny of Enchytraeidae (Annelida, Clitellata). Molecular Phylogenetics and Evolution 57(2): 849–858. https://doi.org/10.1016/j.ympev.2010.07.005

Erséus C, Klinth MJ, Rota E, De Wit P, Gustafsson DR, Martinsson S (2019) The popular model annelid *Enchytraeus albidus* is only one species in a complex of seashore white worms (Clitellata, Enchytraeidae). Organisms, Diversity & Evolution 19(2): 105–133. https://doi.org/10.1007/s13127-019-00402-6

Felföldi T, Dózsa-Farkas K, Nagy H, Hong Y (2020) Three new enchytraeid species (Enchytraeidae, Annelida) from mountain soils of Korea and ten species new for the country. Zootaxa 4896: 001–045. https://doi.org/10.11646/zootaxa.4896.1.1

Finogenova NP (1972) New species of Oligochaeta from Dnjepr and Bug Firth and Black Sea and revision of some species. Trudy Zoologicheskogo Intstituta (Akademiya Nauk SSSR) Leningrad 52: 94–116.

Finogenova NP (1973) New species of Oligochaeta from the Caspian Sea. Zoologicheskij Zhurnal Moscow 52: 121–124.

Folmer O, Black M, Hoeh W, Lutz R, Vrijenhoek R (1994) DNA primers for amplification of mitochondrial cytochrome c oxidase subunit I from diverse metazoan invertebrates. Molecular Marine Biology and Biotechnology 3: 294–299.

Frey H, Leuckart R (1847) Beiträge zur Kenntnis wirbelloser Thiere mit besonderer Berücksichtigung der Fauna des norddeutschen Meeres. Vieweg, Braunschweig. https://doi.org/10.5962/bhl.title.2128

Giere O (1971) *Marionina spicula* - ein ökologisch und morphologisch spezialisierter mariner Enchytraeide (Oligochaeta). Helgoländer Wissenschaftliche Meeresuntersuchungen 22(3–4): 350–361. https://doi.org/10.1007/BF01611123

Giere O (1974) *Marionina istriae* n. sp., ein mariner Enchytraeide (Oligochaeta) aus dem mediterranen Hygropsammal. Helgoländer Wissenschaftliche Meeresuntersuchungen 26(3–4): 359–369. https://doi.org/10.1007/BF01627620

Kane RA, Rollinson D (1994) Repetitive sequences in the ribosomal DNA internal transcribed spacer of *Schistosoma haematobium, Schistosoma intercalatum* and *Schistosoma mattheii*. Molecular and Biochemical Parasitology 63(1): 153–156. https://doi.org/10.1016/0166-6851(94)90018-3

Klinth MJ, Martinsson S, Erséus C (2017) Phylogeny and species delimitation of North European *Lumbricillus* (Clitellata, Enchytraeidae). Zoologica Scripta 46(1): 96–110. https://doi.org/10.1111/zsc.12187

Klinth MJ, Kreiling A-K, Erséus C (2019) Investigating the Clitellata (Annelida) of Icelandic springs with alternative barcodes. Fauna Norvegica 39: 119–132. https://doi.org/10.5324/fn.v39i0.3043

Klinth MJ, Rota E, Martinsson S, Prantoni AL, Erséus C (2022) New insights into the systematics of *Lumbricillus* and *Marionina* (Clitellata: Enchytraeidae) inferred from Southern Hemisphere samples, including three new species. Zoological Journal of the Linnean Society 194(4): 1103–1133. https://doi.org/10.1093/zoolinnean/zlab073

Kumar S, Stecher G, Tamura K (2016) MEGA7: Molecular Evolutionary Genetics Analysis version 7.0 for bigger datasets. Molecular Biology and Evolution 33(7): 1870–1874. https://doi.org/10.1093/molbev/msw054

Lafont M, Juget J (1976) Les oligochetes du Rhone. I. Releves faunistiques generaux. Annales de Limnologie 12(3): 253–268. https://doi.org/10.1051/limn/1976015

Lasserre P (1964) Notes sur quelques oligochètes Enchytraeidae, présents dans les plages du Bassin d'Areachon. Procès verbaux de la Société Linnéenne de Bordeaux 101: 87–91.

Lasserre P, Erséus C (1976) Oligochètes marins des Bermudes, Nouvelles espgéces et remarques sur la distribution geograhique de quelques Tubificidae et Enchytraeidae. Cahiers de Biologie Marine 17: 447–462.

Marcus E (1965) Naidomorpha aus brasilianischem Brackwasser. Beiträge zur Neotropischen Fauna 4(2): 61–83. https://doi.org/10.1080/01650526509360380

Martin P, Schmelz RM, Dole-Olivier M-J (2015) Groundwater oligochaetes (Annelida, Clitellata) from the Mercantour National Park (France), with the descriptions of one new genus and two new stygobiont species. Zoosystema 37(4): 551–569. https://doi.org/10.5252/z2015n4a2

Martinsson S, Erséus C (2018) Cryptic diversity in supposedly species-poor genera of Enchytraeidae (Annelida: Clitellata). Zoological Journal of the Linnean Society 183(4): 749–762. https://doi.org/10.1093/zoolinnean/zlx084

Martinsson S, Dózsa-Farkas K, Rota E, Erséus C (2017) Placing the forgotten: on the positions of *Euenchytraeus* and *Chamaedrilus* in an updated enchytraeid phylogeny (Clitellata: Enchytraeidae). Invertebrate Systematics 31(1): 85–90. https://doi.org/10.1071/IS16042

Matamoros L, Yildiz S, Erséus C (2007) A new species within the genus *Marionina* (Enchytraeidae: Annelida: Clitellata) from the southern Black Sea. Marine Biology Research 3(6): 397–402. https://doi.org/10.1080/17451000701694844

Matamoros L, Rota E, Erséus C (2012) Cryptic diversity among the achaetous *Marionina* (Annelida, Clitellata, Enchytraeidae). Systematics and Biodiversity 10(4): 509–525. https://doi.org/10.1080/14772000.2012.723640

Michaelsen W (1888) Die Oligochaeten von Süd-Georgien nach der Ausbeute der Deutschen Station von 1882–1883. Jahrbuch der Hamburgischen Wissenschaftlichen Anstalten 5: 53–73.

Michaelsen W (1889) Oligochaeten des Naturhistorischen Museums in Hamburg. I. Jahrbuch der Hamburgischen Wissenschaftlichen Anstalten 6: 1–17.

Nagy H, Dózsa-Farkas K, Felföldi T (2023) New insights into the *Enchytraeus albidus* complex (Annelida, Enchytraeidae), with the description of three new species from seashores in Italy and Croatia. European Journal of Taxonomy 870: 107–145. https://doi.org/10.5852/ejt.2023.870.2123

Nielsen CO, Christensen B (1959) The Enchytraeidae. Critical revision and taxonomy of European species (studies on Enchytraeidae VII). Natura Jutlandica 8–9: 1–160.

Nielsen CO, Christensen B (1961) The Enchytraeidae. Critical revision and taxonomy of European species. Supplement 1. Natura Jutlandica 10: 1–23.

O'Connor FB (1962) The extraction of Enchytraeidae from soil. In: Murphy PW (Ed.) Progress in Soil Zoology. Butterworths Publishers, London, 279–285.

O'Connor FB (1963) *Marionina cambrensis* sp. nov.: A new enchytraeid worm (Oligochaeta) from North Wales. The Annals and Magaine of Natural History, including Zoology. Botany and Geology London 6(13): 761–766. https://doi.org/10.1080/00222936308651427

Pfeffer G (1890) Die niedere Thierwelt des antarktischen Ufergebietes. Die internationale Polarforschung 1882–1883. Die Deutschen Expeditionen und ihre Ergebnisse (5) 2(17): 455–574.

Rodriquez P (1986) Nuevos resultados acerca de la fauna de oligoquetos acuáticos del País Vasco y cuenca alta del Ebro. 2. Enchytraeidae. Munibe. Ciencias Naturales 38: 81–87.

Rota E (1995) Italian Enchytraeidae. I. Bollettino di Zoologia 62(2): 183–231. https://doi.org/10.1080/11250009509356067

Rota E (2013) How many lookalikes has *Marionina argentea* (Michaelsen, 1889) (Annelida: Clitellata: Enchytraeidae)? Three new species described from morphological evidence. Zoologischer Anzeiger 252(1): 123–137. https://doi.org/10.1016/j.jcz.2012.05.001

Rota E, Manconi R (2004) Taxonomy and Ecology of Sponge-Associate *Marionina* spp. (Clitellata: Enchytraeidae) from the Horomatangi Geothermal System of Lake Taupo, New Zealand. International Review of Hydrobiology 89(1): 58–67. https://doi.org/10.1002/iroh.200310695

Rota E, Matamoros L, Erséus C (2008) In search of *Marionina* (Clitellata, Enchytraeidae): A taxonomic history of the genus and redescription of the type species *Pachydrilus georgianus* Michaelsen, 1888. The Italian Journal of Zoology 75(4): 417–436. https://doi.org/10.1080/11250000801930433

Schmelz RM, Collado R (2008) A type-based redescription of *Pachydrilus georgianus* Michaelsen, 1888, the type species of *Marionina* Michaelsen, 1890, with comments on *Christensenidrilus* Dózsa-Farkas & Convey, 1998 (Enchytraeidae, "Oligochaeta", Annelida). Verhandlungen des Naturwissenschaftlichen Vereins in Hamburg 44: 7–22.

Schmelz RM, Collado R (2010) A guide to European terrestrial and freshwater species of Enchytraeidae (Oligochaeta). Soil Organisms 82(1): 1–176.

Schmelz RM, Collado R (2012) An updated checklist of currently accepted species of Enchytraeidae (Oligochaeta, Annelida). Newsletter on Enchytraeidae 12: 67–87.

Schmelz RM, Collado R (2015) Checklist of taxa of Enchytraeidae (Oligochaeta): An update. Soil Organisms 87: 149–152.

Schmelz RM, Collado R, Römbke J (2011) Mata Atlântica enchytraeids (Enchytraeidae, Oligochaeta), Description of a new genus *Xetadrilus* gen. nov., with three new species, and four new species of *Guaranidrilus* Černosvitov. Zootaxa 2838: 1–29. https://doi.org/10.11646/zootaxa.2838.1.1

Schmelz RM, Klinth MJ, Chalkia C, Anastasiadou P, Vavoulidou E (2019) *Enchytraeus demutatus* sp. nov. (Enchytraeidae, Oligochaeta) has characters hitherto unrecorded in the genus. Soil Organisms 91: 87–96. https://doi.org/10.25674/so91iss3pp87

Shurova NM (1978) The intertidal oligochaetes from the eastern coast of Kamchatka, In: Litoral Beringova moray iyugo-vost Kamchatki Moscow, 98–106. [in Russian with English summary]

Shurova NM (1979) Enchytraeids (Oligochaeta) of the far-east seas of the USSR. In: Studies on the pelagic and groundinhabiting organisms of the Far East seas, Vladivostok, 75–89.

Somogyi B, Felföldi T, Tóth LG, Bernát G, Vörös L (2020) Photoautotrophic picoplankton - a review on their occurrence, role and diversity in Lake Balaton. Biologia Futura 71(4): 371–382. https://doi.org/10.1007/s42977-020-00030-8

Timm T (1996) Oligochaeta of Lake Taimyr: A preliminary survey. Hydrobiologia 334(1–3): 89–95. https://doi.org/10.1007/BF00017357

Timm T (2012) Estonian Enchytraeidae 4. Sublittoral Enchytraeidae (Annelida, Oligochaeta) in the eastern Baltic Sea. Estonian Journal of Ecology 61(3): 157–172. https://doi.org/10.3176/eco.2012.3.01

Timm T, Vvedenskaya TL (2006) Oligochaeta (Annelida) of Lake Kurilskoe, Kamchatka Peninsula. Species Diversity 11(3): 225–244. https://doi.org/10.12782/specdiv.11.225

White TJ, Bruns T, Lee S, Taylor J (1990) Amplification and direct sequencing of fungal ribosomal RNA genes for phylogenetics. In: Innis MA, Gelfand DH, Sninsky JJ, White TJ (Eds) PCR Protocols: A Guide to Methods and Applications. Academy Press, San Diego, 315–322. https://doi.org/10.1016/B978-0-12-372180-8.50042-1

Xie ZC, Rota E (2001) Four new terrestrial species of *Marionina* (Clitellata, Enchytraeidae) from China and re-examination of *M. hoffbaueri* Möller. Journal of Natural History 35(10): 1417–1431. https://doi.org/10.1080/002229301317067610

Xie ZC, Liang YL, Wang HZ (2000) A new species of *Marionina* (Oligochaeta: Annelida: Enchytraeidae). Acta Zootaxonomica Sinica 25: 143–146. [in Chinese with English abstract]

Zoosyst. Evol. 100 (4) 2024, 1287–1296 | DOI 10.3897/zse.100.128885

PENSOFT

MUSEUM FÜR NATURKUNDE BERLIN

Grassland expansions promoted global diversification of the *Pardosa* wolf spiders during the late Cenozoic (Araneae, Lycosidae)

Lijuan Liu[1*], Dan Fu[1*], Yufa Luo[1]

1 *Key Laboratory of Wetland Biodiversity of the Jianhu Basin of Shaoxing, School of Life and Environmental Sciences, Shaoxing University, Shaoxing 312000, China*

https://zoobank.org/31218D24-E11F-4419-9AC5-027DEC73115E

Corresponding author: Yufa Luo (lyf223@126.com)

Academic editor: Danilo Harms ♦ **Received** 3 June 2024 ♦ **Accepted** 12 August 2024 ♦ **Published** 11 September 2024

Abstract

The spiders in the genus *Pardosa* C.L. Koch, 1847, are a young lineage of the family Lycosidae Sundevall, 1833, that exhibit high species diversity and widespread distribution. *Pardosa* is abundant in open and disturbed environments. In fact, most of its species live in grasslands, and the few that live in forests switched habitats relatively recently. The genus markedly prefers grasslands with a broad range of climates. Thus, its origin and diversification were probably associated with grassland expansions during the late Cenozoic. To test this hypothesis, we developed a global phylogenetic hypothesis that helps reconstruct the biogeographic patterns of the genus *Pardosa* using three nuclear (18S, ITS2, and *H3*) and four mitochondrial (12S, 16S, *NADH1*, and *COI*) loci. Our phylogenetic analyses cover 133 (125 described and 8 as yet undescribed) grassland species of *Pardosa* using *Trochosa ruricola* (De Geer, 1778) and *Lycosa coelestis* L. Koch, 1878, as outgroups. The results show that our selection of species in the genus is divided into four major clades: Clade I includes only *P. crassipalpis* Purcell, 1903, from South Africa; Clade II consists of a north-east African group (2 species) and a south-east Asian group (21 species); Clade III contains only *P. sutherlandi* (Gravely, 1924) from SE Asia; and Clade IV includes five species groups from Asia, Europe, and the Americas. The spiders of the genus probably originated in southern Africa or southern and eastern (SE) Asia at the Middle Miocene Climatic Optimum, about 19.40–14.18 Ma, and then expanded northwards to North America via the Bering Strait, as well as southwards to north-east Africa via the Arabian Peninsula, and westwards to Europe via western Asia between about 10.59 and 5.28 Ma. At least three exchanges occurred between North America and SE Asia, and at least two between Europe and North America. The biogeography of *Pardosa* in the past 14.18 Ma, associated with the evolution of grasses, suggested a late Cenozoic diversification of the genus as grasslands expanded.

Key Words

Biogeography, co-evolution, grasses, phylogenetics, species distribution

Introduction

Plants in the family Poaceae, usually called grasses, are composed of more than 12 thousand species (Govaerts et al. 2021). They originated during the late Cretaceous (about 100 million years ago, Ma; Gallaher et al. 2022) and currently cover over 25% of all land on Earth, comprising 35% of the subtropics and tropics. Grasses also occur in all terrestrial habitats with a broad range of climates, from cold to hot and arid to wet. Climate, soils, fire, and herbivory shaped global grassy systems, including the C3 and C4 photosynthesis groups (Linder et al. 2018; Schubert et al. 2019; Strömberg and Staver 2022). The C3 grasses developed the tolerance needed to survive

* These authors contributed equally to this work.

in colder climates (Schubert et al. 2019); the C4 grasses, evolutionarily derived from the C3 grasses, can prosper in hot and dry areas (Linder et al. 2018). Grassy biomes (>20 Ma; Strömberg and Staver 2022), associated with open-canopy habitats, harbor many spiders of the family Lycosidae Sundevall, 1833 (wolf spiders; Piacentini and Ramírez 2019). They interact ecologically with a diverse part of the lycosid fauna, both above and below ground; genera with representatives occurring in grasslands include *Pardosa* C. L. Koch, 1847; *Lycosa* Latreille, 1804, *Trochosa* C. L. Koch, 1847; and *Hippasa* Simon, 1885. These lycosids rely on native grasses as a substrate to live on and to forage on grass-eating insects.

Based on the remarkable abundance of wolf spiders in open habitats and in the fossil record (Wunderlich 2004a), the retention of the third tarsal claw, and the conservative morphology, Jocqué and Alderweireldt (2005) proposed that Lycosidae had a relatively recent origin and had co-evolved with grasslands and, by extension, all types of open habitats. Recently, a dated phylogenetic analysis (Piacentini and Ramírez 2019) inferred that the family appeared before the expansion of grasslands and diversified (about 50 Ma) with the reduction of tropical forests and the advance of open habitats. However, the linkages between the temporal-spatial diversification of Lycosidae, especially its most diverse genus *Pardosa* (based on the number of described species), and grassland expansions have not been specifically tested.

Pardosa wolf spiders inhabit nearly all terrestrial habitats worldwide and currently comprise 532 species (World Spider Catalog 2024). They are free-roaming predators that can disperse over short distances; the spiderlings of some species have been reported to disperse by ballooning on silken threads (e.g., Richter 1970; Greenstone 1982). They are abundant in grasslands and all types of open habitats, such as wetlands, stream banks, floodplains, glades, open deserts, farmlands, and human settlements (Jocqué and Alderweireldt 2005). The marked preference for grasslands contributed to their diversification and successful expansions when the arid and grasslands extended over the globe. Previous studies indicated that *Pardosa* diversified between about 14 and 10 Ma (Piacentini and Ramírez 2019), and most of its species are remarkably distributed in the four areas with different grassland environments and grassy (C3 and C4) evolutionary histories: (1) North America, NA; (2) eastern and southern Africa, EA; (3) central, eastern, and southern Asia, CA; and (4) the region surrounding the Mediterranean Sea, RM. (Fig. 1; Suppl. material 1: table S1; e.g., Vogel 1964, 1970, 2004; Hänggi et al. 1995; Ivanov et al. 2023). Therefore, *Pardosa* is a particularly appropriate animal group to test the hypothesis of a diversification of specific lycosid lineages as grasslands expanded. However, the genus lacks a comprehensive phylogenetic hypothesis, and thus its lineage compositions, phylogenetic relationships, and geographical distribution remain unclear.

Spiders of the genus *Pardosa* have been proposed as effective biological control agents for pests in agricultural systems globally. As the biodiversity and ecological prominence of *Pardosa* spiders are increasingly recognized, there is a demand for illumination of their biogeographical patterns and diversification mechanisms for the purposes of protection and ecological management. The purpose of this study was to produce a robust phylogenetic hypothesis to elucidate the relationship of *Pardosa* grassland lineages based on a global sample of species using three nuclear (18S, ITS2, and *H3*) and four mitochondrial (12S, 16S, *NADH1*, and *COI*) loci. Furthermore, we explored the origin, diversification timeline, and global expansion history using a dated phylogenetic tree and tested the co-evolution between *Pardosa* spiders and grasslands.

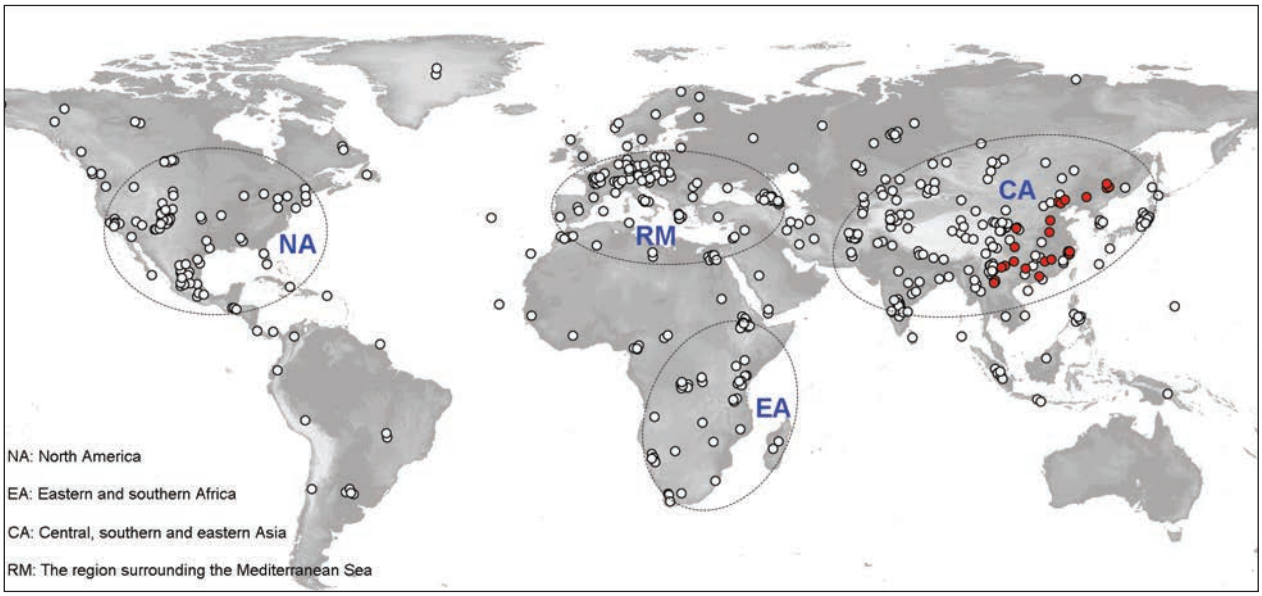

Figure 1. The major distributional areas of *Pardosa* spiders and the main biomes across the globe. White spots indicate the probable type localities of all known *Pardosa* species; red spots indicate the sample localities of *Pardosa* spiders sequenced in this study.

Materials and methods

Sampling and sequence analyses

We collected 27 *Pardosa* grassland species across China between 2018 and 2024 (Fig. 1; Suppl. material 1: table S1). They were fixed in absolute ethanol and stored at -20 °C prior to analysis. Voucher specimens were deposited at Shaoxing University, Shaoxing, China. TIANamp genomic DNA kits were used to extract DNA. Sequences of nuclear (18S, ITS2, and *H3*) and mitochondrial (12S, 16S, *COI*, and *NADH1*) loci were amplified using seven pairs of primers (Suppl. material 1: table S2). Sequencing was performed utilizing BigDye technology on an ABI 3730 automated sequencer (Applied Biosystems, Forter City, CA, USA). BioEdit (Hall 1999) and SEQUENCHER v4.1.2. (Gene Codes, USA) were applied to sequence quality checking and editing. New sequences were submitted to GenBank (Suppl. material 1: table S1). Additional sequences of the *Pardosa* grassland species from North America, Europe, East Asia, and Africa were taken from Zehethofer and Sturmbauer (1998), Muster and Berendonk (2006), Murphy et al. (2006), Piacentini and Ramírez (2019), and Roslin et al. (2022), as well as GenBank and BOLDSYSTEM (Suppl. material 1: table S1). Alignments of genes were generated using Clustal X (Jeanmougin et al. 1998). Sequences of the seven genes were merged to perform phylogenetic analyses, divergence time estimates, and biogeographical reconstructions. The data matrix will be submitted to the Dryad database (online at http://datadryad.org/).

Phylogenetic analyses

Phylogenetic relationships among the sampled *Pardosa* species were inferred using both the maximum likelihood and Bayesian inference approaches. The wolf spiders *Trochosa ruricola* (De Geer, 1778) and *Lycosa coelestis* L. Koch, 1878, were used as outgroups. Maximum likelihood analyses were implemented using the fast online phylogenetic tool W-IQ-TREE (Trifinopoulos et al. 2016). The optimal substitution model for each gene partition (TIM2+F+I+G4 for 12S, 16S, *NADH1*, and *COI*; K2P+I for 18S; K2P+R2 for *H3*; and K2P+I for ITS2) was estimated simultaneously using the greedy algorithm in ModelFinder (Kalyaanamoorthy et al. 2017) with the Bayesian information criterion and the FreeRate heterogeneity. We set the perturbation strength (*p*) and the number of iterations since the last best tree was found (*c*) to 0.3 and 1000, respectively. The SH-aLRT (Guindon et al. 2010) and the ultrafast bootstrap (UFBoot; Minh et al. 2013) were used to assess the support of the branching patterns estimated in the phylogeny with 0.99 of the minimum correlation coefficient and 1,000 of the maximum number of iterations. Bayesian analyses were performed with MrBayes 3.2.1. The best-fitting substitution models were selected by jModelTest under the Bayesian information criterion (Suppl. material 1: table S3; Posada 2008). The Markov Chain Monte Carlo (MCMC) chain was run for 150 million generations using parameters unlinked among partitions and sampled every 100 generations. We used Tracer v1.5 (Rambaut and Drummond 2009) to monitor the mixing of the MCMC chains. A burn-in sample of 375,000 trees was discarded, and a 50% majority rule consensus tree was computed with the remaining trees.

Divergence time estimation

An uncorrelated lognormal relaxed molecular clock model was used to estimate divergence time in BEAST v1.8.1 (Drummond and Rambaut 2007). The birth-death speciation process was chosen as the tree prior. Partitioned strategies (Brandley et al. 2005) were incorporated in BEAST analyses, and each gene was used as a separate partition. For each partition, the specific model of evolution was recommended by jModelTest (GTR+I+G for 12S, 16S, *NADH1*, and *COI*; HKY+G for 18S, ITS2, and *H3*). We ran the MCMC for 50 million generations and sampled every 1000 generations. The maximum clade credibility tree was computed using TreeAnnotator v1.8.0 based on the remaining trees, after discarding the first 25% of the yielded trees as burn-in. Tracer v1.5 was used to determine convergence and measure the effective sample size (>200) for all parameters. We dated the tree of all globally sampled *Pardosa* species. For the molecular clock analysis, we used the minimum ages based on fossils of Lycosidae (15 Ma; Iturralde-Vinent and MacPhee 1996; Penney 2001), Oxyopidae (43 Ma; Wunderlich 2004b; Magalhaes et al. 2020), Thomisidae (43 Ma; Wunderlich 2004c; Magalhaes et al. 2020), and Selenopidae (53 Ma; Penney 2006; Magalhaes et al. 2020) as calibration points (Suppl. material 1: table S4; Renner 2005; Donoghue and Benton 2007). The Agelenidae, Thomisidae, Oxyopidae, Psechridae, Trechaleidae, Selenopidae, and some Lycosidae species were used as outgroups. Their gene sequences were available from our study and GenBank (Suppl. material 1: table S1).

Biogeographical reconstruction

The biogeographical history of *Pardosa* was reconstructed in RASP v3.0 (Yu et al. 2010, 2015) using the Bayesian binary MCMC analysis (BBM; Sanmartín et al. 2001), the statistical dispersal-vicariance analysis (S-DIVA; Yu et al. 2010), and the dispersal-extinction-cladogenesis analysis (DEC; Ree and Smith 2008). We set two areas for the maximum number of ancestral states at each node. The fossil-calibrated trees obtained from BEAST analysis, from which the outgroups were trimmed, were used for biogeographic reconstruction. The distributional data of *Pardosa* species were available from previous literature, GenBank, and information from our samples. Based on the current distribution and the phylogeny of *Pardosa* as well as geographic divisions and climate, we defined five geographic

areas occupied by the genus: southern Africa, north-east Africa, West Asia+Europe/Palearctic, southern and eastern (SE) Asia/Orient, and North America/Nearctic.

Results

Phylogeny of *Pardosa*

The concatenated data set was composed of 2694 nucleotides (12S: 237 bp; 16S: 309 bp; 18S: 529 bp; *COI*: 611 bp; *H3*: 383 bp; ITS2: 195 bp; and *NADH1*: 530 bp) with 133 (125 described and 8 as yet undescribed) terminals within the *Pardosa* grassland lineages covering most of their distribution ranges. Maximum likelihood analyses indicate that *Pardosa* consists of four clades (Fig. 2; Suppl. material 1: fig. S1). Clades I and III only include *P. crassipalpis* Purcell, 1903, from South Africa and *P. sutherlandi* (Gravely, 1924) from SE Asia, respectively; Clade II is composed of the north-east African group (*P. injucunda* (O. Pickard-Cambridge, 1876) and *P. naevia* (L. Koch, 1875)) and the SE Asian group (21 species); Clade IV contains five species groups from Asia, Europe, and the Americas. The *californica* group (CAG) and the

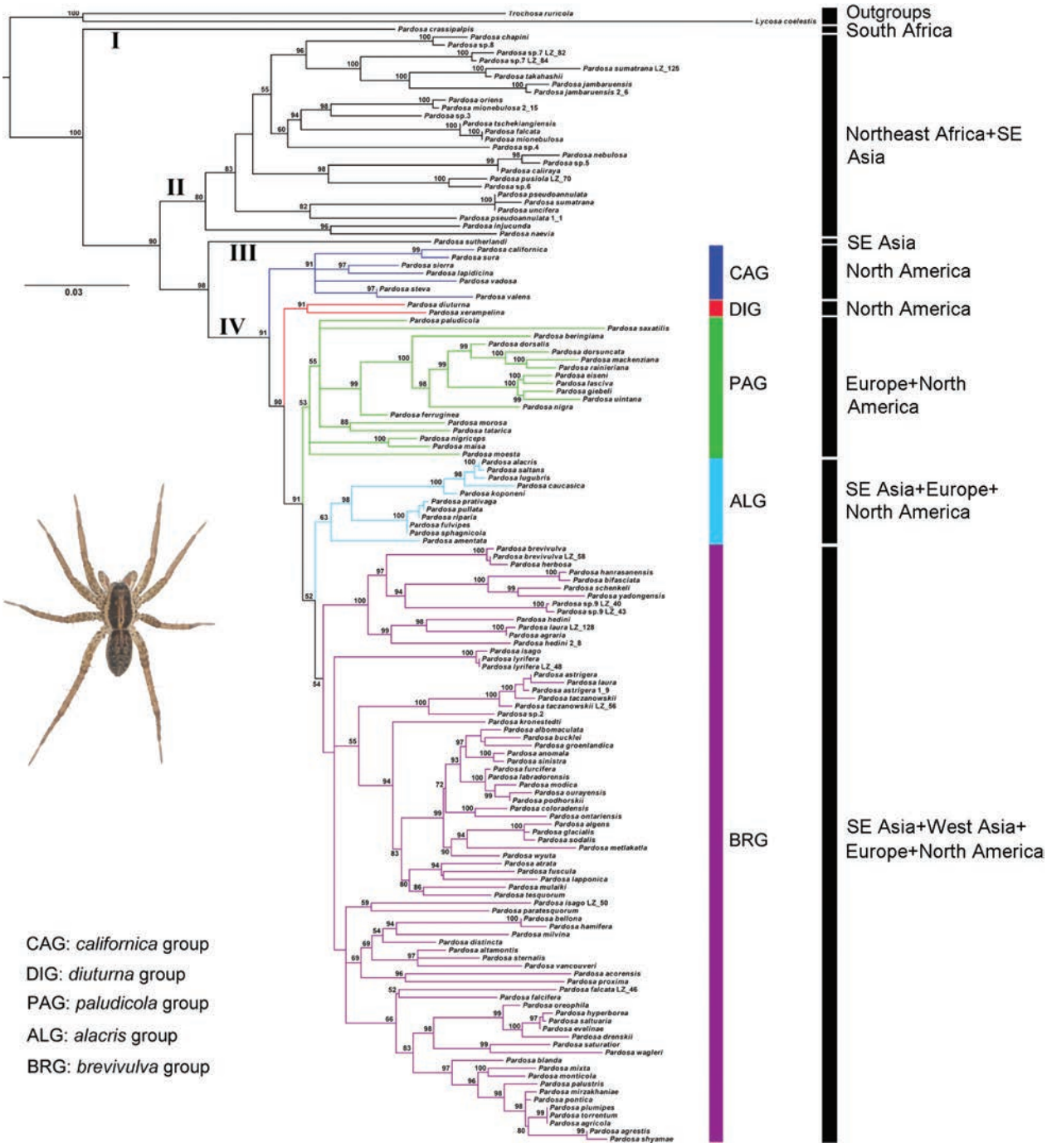

Figure 2. Phylogenetic tree of 133 *Pardosa* species reconstructed using the maximum likelihood method. The numbers at the nodes represent bootstrap support values from the maximum likelihood analyses.

diuturnal group (DIG) comprise 7 and 2 *Pardosa* species from North America, respectively; the *paludicola* group (PAG) is comprised of 18 species from Europe and North America; the *alacris* group (ALG) includes 11 species from SE Asia, Europe, and North America; and the *brevivulva* group (BRG) consists of 95 species from SE Asia, West Asia, Europe, and North America. Bayesian analyses suggest that all sampled African species (*P. crassipalpis*, *P. injucunda*, and *P. naevia*) constitute Clade I with a low posterior probability (only 0.62), and the phylogenetic relationships among most species/groups within Clade IV are unclear (Suppl. material 1: fig. S2).

Divergence time

The fossil-calibrated phylogeny is shown in Fig. 3. The recent ancestor of *Pardosa* probably appeared during the early Miocene, approximately 19.40 Ma (95% credibility interval, CI: 24.72–14.47 Ma). The divergence of the South African *P. crassipalpis* (Clade I) from the species of the clades (II–IV) was predicted to have occurred around 14.18 Ma (95% CI: 18.19–10.74 Ma). Thus, *Pardosa* wolf spiders originated probably at about 19.40–14.18 Ma (the Middle Miocene Climatic Optimum, MMCO). Within Clade II, the *Pardosa* species from north-east Africa diverged from those from SE Asia around 9.64 Ma. The split between the SE Asian *P. sutherlandi* (Clade III) and the taxa of Clade IV from Asia, Europe, and the Americas started about 12.59 Ma. Clade IV first diversified during the late Miocene, approximately 8.82 Ma (95% CI: 10.77–8.73 Ma), and then split into distinct species groups during the Miocene. The North American *diuturna* group (DIG) diverged from the *nigriceps* group (PABG) about 8.17 Ma. Diversification of the widespread species group (PABG) started around 7.77 Ma.

Biogeography

The BBM analysis (Fig. 4) inferred the two possible ancestral ranges occurring during the middle Miocene for *Pardosa*: (1) southern Africa (the marginal probability, MP: 0.6616); and (2) SE Asia/Orient (MP: 0.2391). The inference from S-DIVA (Suppl. material 1: fig. S3a) favored southern Africa+SE Asia (MP: 0.6534), SE Asia+north-east Africa (MP: 0.2066), and southern Africa+North America/Nearctic (MP: 0.0586) as the most likely ancestral areas of the genus, whereas southern Africa+SE Asia was preferred under DEC (Suppl. material 1: fig. S3b). The evolutionary routes of *Pardosa* inferred from the BBM (Fig. 4), S-DIVA (Suppl. material 1: fig. S3a), and DEC (Suppl. material 1: fig. S3b) were generally concordant. The ancestral reconstructions suggest that SE Asia is an important dispersal center for *Pardosa*, with dispersal from SE Asia to North America, north-east Africa, and Europe at around 10.59, 9.64, and 5.28 Ma, respectively. The three intercolonial evens between South-east Asia and North America were observed during the period of about 10.59–5.31 Ma. The inter-colony dispersal between Europe and North America occurred between 5.48 and 2.80 Ma.

Discussion

A detailed exploration of the evolutionary history of *Pardosa* requires a robust phylogenetic framework (Graybeal 1998; Zwickl and Hillis 2002). Current knowledge of the evolutionary relationships among *Pardosa* species is based on assessments of morphological similarity or phylogenetic analyses of lycosids, including very few species of *Pardosa* (e.g., Zehethofer and Sturmbauer 1998; Vink et al. 2002; Muster and Berendonk 2006; Murphy et al. 2006; Piacentini and Ramírez 2019; Roslin et al. 2022). This study first comprehensively addresses the phylogeny of global grassland species of *Pardosa* using multiple nuclear and mitochondrial markers. The topology of the maximum likelihood tree (Fig. 2) is similar to that of the dated tree (Fig. 3) and provides a well-supported hypothesis for the relationships among the major clades/groups of *Pardosa* within our dataset. The biogeographic histories of *Pardosa* suggest that the evolution of this genus was strongly affected by grassland expansions resulting from historic climatic and environmental shifts. These findings mirror other studies highlighting the vital role of the evolution of grasslands in lycosid biogeography (Jocqué and Alderweireldt 2005; Piacentini and Ramírez 2019).

Lycosidae appeared about 33.80 Ma, after the Eocene-Oligocene extinction event, but well before the grassland expansions. *Pardosa* (Pardosinae) diverged from the clade (*Lycosa+Trochosa*) around 19.40 Ma, which is consistent with the age (25–16 Ma) obtained in the phylogenetic analysis of Piacentini and Ramírez (2019). The initial diversification of *Pardosa* spiders was about 14.18 Ma, coinciding with the Middle Miocene Climatic Optimum (17–14 Ma). The time (19.40–14.18 Ma) when *Pardosa* appeared is much later than the original age (55 Ma; Strömberg 2011) of C4 grasses with the hot and dry tolerance (Linder et al. 2018), and the age (30 Ma) when in colder climates, C3 open-habitat grasses developed the tolerance needed to survive frosts (Schubert et al. 2019), but coincides with the time (the late Cenozoic) when open-habitat grasses began to become ecologically dominant (Strömberg and Staver 2022). Four major clades of *Pardosa* emerged during the middle to late Miocene, between 14.81 and 8.82 Ma. This pattern coincides with the rapid expansion of open-habitat grasses and the retreat of tropical forests due to the cooling and aridification climate and the low CO_2 conditions, as well as fire and herbivory activities after the MMCO (Zachos et al. 2001; Strömberg and Staver 2022). Our results support the idea that *Pardosa* is a young lineage of wolf spiders that became vagrant and diversified during the Miocene, when the grasslands expanded. In the past 8 Ma, including the

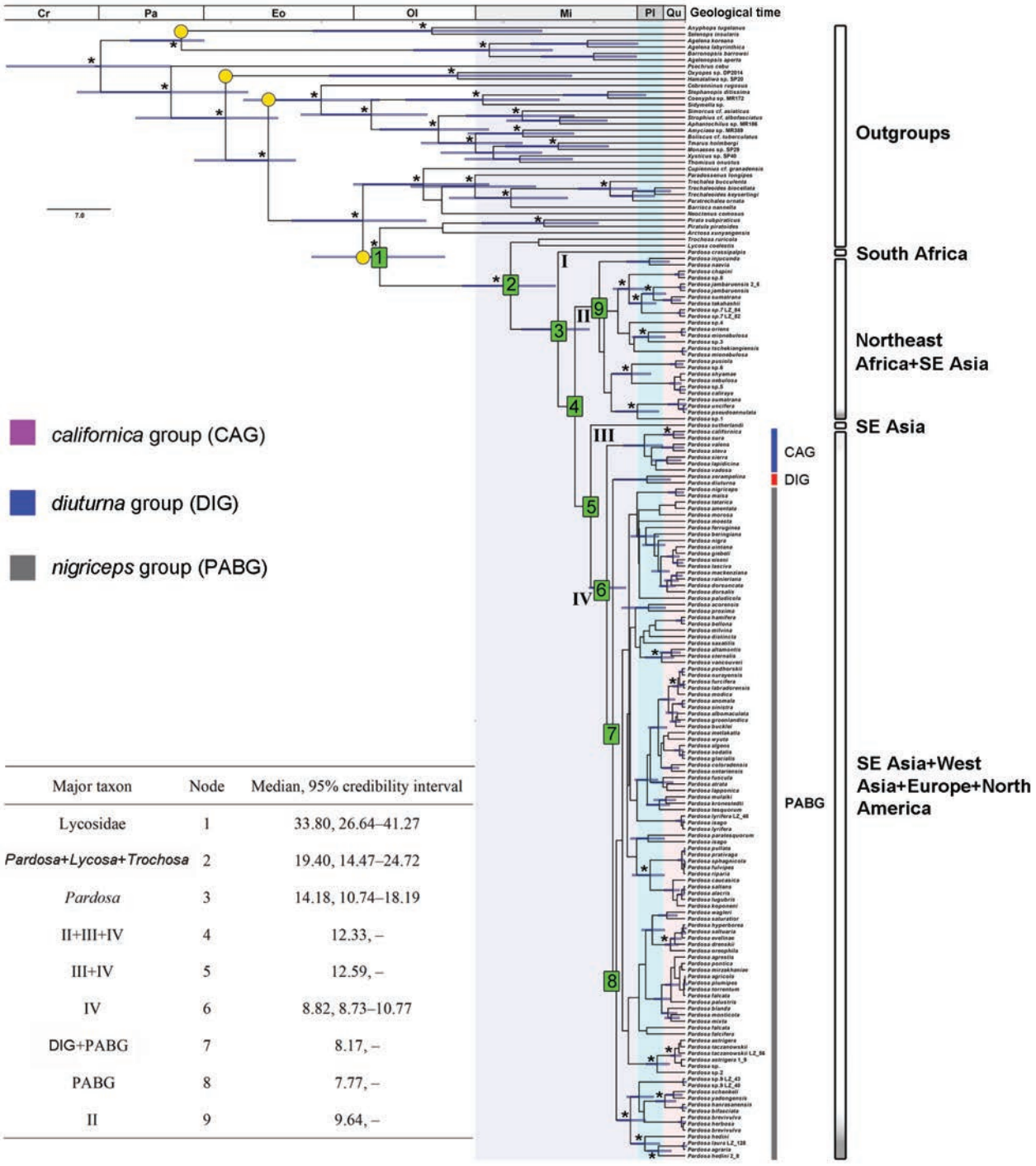

Major taxon	Node	Median, 95% credibility interval
Lycosidae	1	33.80, 26.64–41.27
Pardosa+Lycosa+Trochosa	2	19.40, 14.47–24.72
Pardosa	3	14.18, 10.74–18.19
II+III+IV	4	12.33, –
III+IV	5	12.59, –
IV	6	8.82, 8.73–10.77
DIG+PABG	7	8.17, –
PABG	8	7.77, –
II	9	9.64, –

Figure 3. A dated, fossil-calibrated phylogeny of *Pardosa* species estimated in BEAST. Yellow dots mark the four fossil calibration nodes. "*" indicates stable branches with Bayesian support >0.90. Ma, millions of years ago. Qu, Quaternary; Pl, Pliocene; Mi, Miocene; Ol, Oligocene; Eo, Eocene; Pa, Palaeocene; Cr, Cretaceous; Ju, Jurassic.

global Ice Age (2.6 Ma onward), climatic cooling further accelerated, and grasslands extended as the forests retreated and the open and arid environments expanded. At this time, *Pardosa* spiders rapidly diversified, currently representing the most abundant lycosid genus and being dominant in grasslands and some open environments.

Our ancestral reconstructions suggested that the *Pardosa* spiders originated in southern Africa or SE Asia/Orient during the middle Miocene, likely evolving concurrently with the spread of grasses and the diversification of herbivores (~17 Ma; Charles-Dominique et al. 2016; Strömberg and Staver 2022), followed by the geographic expansions from middle altitudes of SE Asia to high altitudes, and then to North America via the Bering Strait, as well as to north-east Africa southwards via the Arabian Peninsula, and to Europe westwards via West Asia between about 10.59 and 5.28 Ma. This dispersal

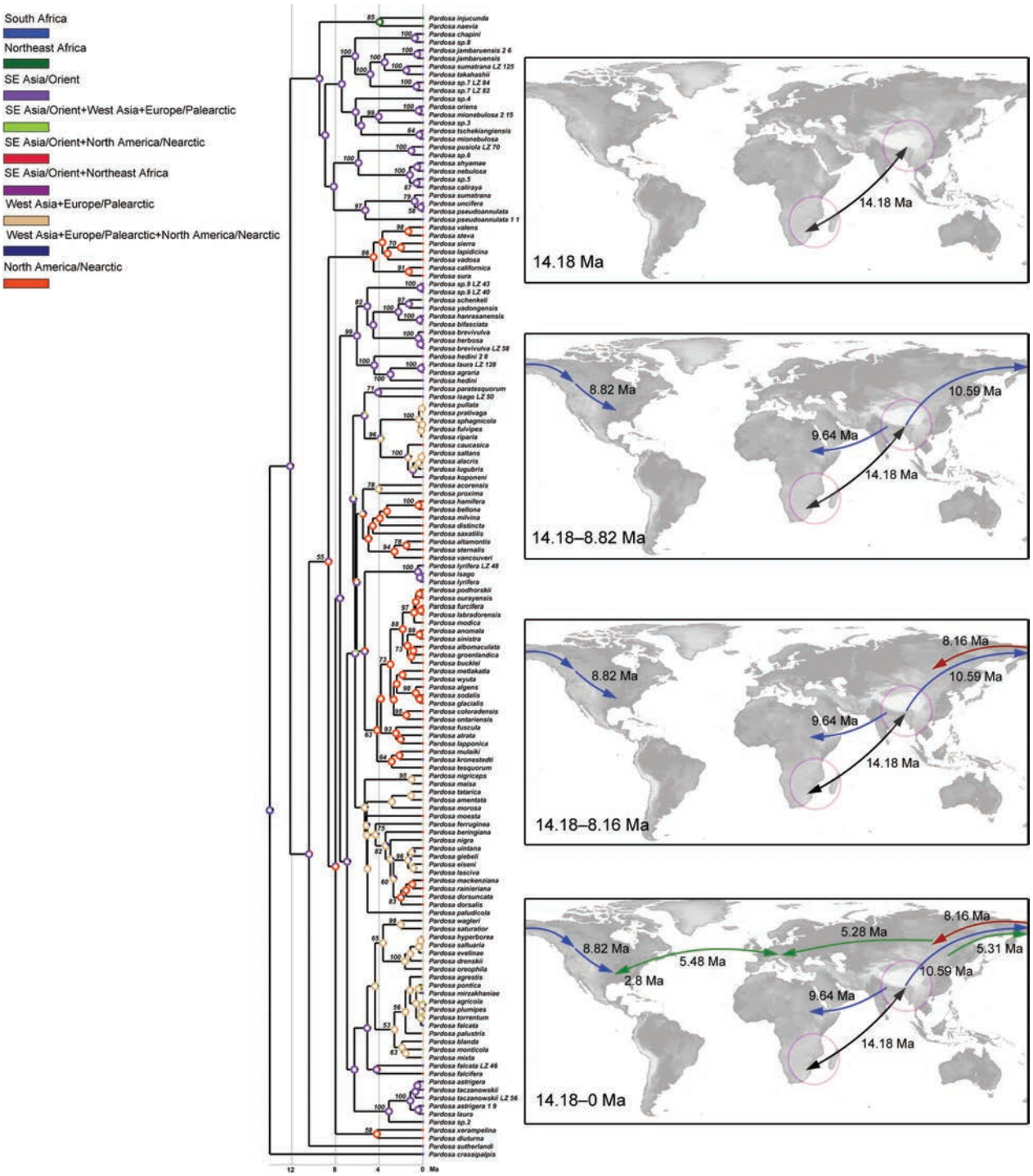

Figure 4. Biogeography of *Pardosa* and potential global dispersion routes (arrows). Reconstruction using Bayesian binary MCMC (BBM) in RASP v3.0. The colors of pie wedges at each node represent geographical areas inferred to have been occupied by ancestral taxa. Pink circles in the maps indicate the possible ancestral ranges occurring during the middle Miocene for *Pardosa*. The numbers at the nodes represent support.

pattern is likely associated with the continent-specific trajectories of grasses (Karp et al. 2021; Kukla et al. 2022). For example, the subtropical C3 open-habitat grasses first spread to the colder regions (Kukla et al. 2022). In the time (about 10–6 Ma), the tropical open-habitat C4 grasses expanded to form grasslands and savannas at low to mid-latitudes (Karp et al. 2021; Lu et al. 2020), and the frost-tolerant grasses spread to higher latitudes. During around 10.59 to 5.31 Ma, multiple exchanges (at least three times) for the spiders occurred between North America and South-east Asia. The *Pardosa* exchanges also appeared between Europe and North America during around 5.48 to 2.80 Ma. These results indicated that intercolony dispersals were associated with grassland extensions and retreats resulting from climatic shifts such as historical glaciations.

The strong dispersal capacity and adaptability to complex climates and disturbed environments (Richter 1970; Greenstone 1982; Samu and Szinetár 2002; Jocqué and Alderweireldt 2005; Woolley et al. 2016) led to a world-wide distribution of *Pardosa* spiders that were dominant in open habitats within only about 15 Ma. Frequent ballooning and cursorial dispersal confer their high mobility and area expansion (e.g., Richter 1970; Greenstone 1982). Our findings indicate that the long-distance overwater dispersal and subsequent range expansions of *Pardosa* spiders occurred between South-east Asia and southern Africa and between North America and Europe. Furthermore, the marked preference of *Pardosa* wolf spiders for disturbed habitats, such as clearings in grasslands or forested areas (Jocqué and Alderweireldt 2005), made them especially successful when arid and open habitats, including grasslands, extended over the globe during the late Cenozoic.

Future directions

This study generated hypotheses regarding the origin and dispersal of *Pardosa* grassland lineages and suggested that grassland expansions drove its global diversification during the late Cenozoic using the nuclear 18S, ITS2, and *H3* and mitochondrial 12S, 16S, *COI*, and *NADH1* loci. Sampling is the process of choosing a subset of a target lineage that will serve as its representative. In this paper, the total sampling specimens for grassland species and some regions are on the low side. However, we hope our study can aid in strategic resampling, reflecting known lineage divergences from grasslands. Moreover, the taxonomic revisions of *Pardosa* need to be made in advance.

Acknowledgements

The manuscript benefited greatly from comments by Danilo Harms (Hamburg, Germany), Volker W. Framenau (Balcatta, Western Australia, Australia), Yanfeng Tong (Shen-yang, China), and one anonymous referee. We thank Ying Cheng and Haodong Chen (Shao-xing, China) for their help in collecting the materials. This study was supported by the National Natural Sciences Foundation of China (NSFC-32170463, 31860602, 31660611) and the Zhejiang Provincial Natural Science Foundation of China (LTGN24C140006).

References

Brandley MC, Schmitz A, Reeder TW (2005) Partitioned Bayesian analyses, partition choice and the phylogenetic relationships of scincid lizards. Systematic Biology 54: 373–390. https://doi.org/10.1080/10635150590946808

Charles-Dominique T, Davies TJ, Hempson GP, Bond WJ (2016) Spiny plants, mammal browsers, and the origin of African savannas. Proceedings of the National Academy of Sciences 113: E5572. https://doi.org/10.1073/pnas.1607493113

Donoghue PCJ, Benton MJ (2007) Rocks and clocks: calibrating the tree of life using fossils and molecules. Trends in Ecology and Evolution 22: 424–431. https://doi.org/10.1016/j.tree.2007.05.005

Drummond AJ, Rambaut A (2007) Beast: Bayesian evolutionary analysis by sampling trees. BMC Evolution Biology 7: 214–221. https://doi.org/10.1186/1471-2148-7-214

Gallaher TJ, Peterson PM, Soreng RJ (2022) Grasses through space and time: An overview of the biogeographical and macroevolutionary history of Poaceae. Journal of Systematics and Evolution 60: 522–569. https://doi.org/10.1111/jse.12857

Govaerts R, Nic Lughadha E, Black N, Turner R, Paton A (2021) The world checklist of vascular plants, a continuously updated resource for exploring global plant diversity. Scientific Data 8: 215. https://doi.org/10.1038/s41597-021-00997-6

Graybeal A (1998) Is it better to add taxa or characters to a difficult phylogenetic problem? Systematic Biology 47(1): 9–17. https://doi.org/10.1080/106351598260996

Greenstone MH (1982) Ballooning frequency and habitat predictability in two wolf spider species (Lycosidae, *Pardosa*). The Florida Entomologist 65: 83–89. https://doi.org/10.2307/3494147

Guindon S, Dufayard JF, Lefort V, Anisimova M, Hordijk W, Gascuel O (2010) New algorithms and methods to estimate maximum-likelihood phylogenies: assessing the performance of PhyML 3.0. Systematic Biology 59: 307–321. https://doi.org/10.1093/sysbio/syq010

Hall TA (1999) BioEdit: a user-friendly biological sequence alignment editor and analysis program for windows 95/98/NT. Nucleic Acids Symposium Series 41: 95–98. https://doi.org/10.1021/bk-1999-0734.ch008

Hänggi A, Stöckli E, Nentwig W (1995) Lebensräume mitteleuropäischer Spinnen. – Charakterisierung der Lebensräume der häufigsten Spinnenarten Mitteleuropas und der mit diesen vergesellschafteten Arten. Neuchâtel: Centre suisse de cartographie de la faune (= Miscnea faun. helvet.) 4: 1–460.

Iturralde-Vinent MA, MacPhee RDE (1996) Age and paleogeographical origin of dominican amber. Science 273: 1850–1852. https://doi.org/10.1126/science.273.5283.1850

Ivanov V, Blagoev G, Danflous S, Gajdoš P, Høye TT, Lee KM, Marusik Y, Mielec CL, Muster C, Pétillon J, Spelda J, Mutanen M, Esposito L (2023) Across mountains and ocean: species delimitation and historical connectivity in Holarctic and Arctic-Alpine wolf spiders (Lycosidae, *Pardosa*). Insect Systematics and Diversity 7(5): 1–14. https://doi.org/10.1093/isd/ixad018

Jeanmougin F, Thompson JD, Gouy M, Higgins DG, Gibson TJ (1998) Multiple sequence alignment with Clustal X. Trends in Biochemical Sciences 23(10): 403–405. https://doi.org/10.1016/S0968-0004(98)01285-7

Jocqué R, Alderweireldt M (2005) Lycosidae: the grassland spiders. Acta Zoological Bulgarica Supplement 1: 125–130.

Kalyaanamoorthy S, Minh BQ, Wong TKF, von Haeseler A, Jermiin LS (2017) ModelFinder: fast model selection for accurate phylogenetic estimates. Nature Methods 14(6): 587–589. https://doi.org/10.1038/nmeth.4285

Karp AT, Andrae JW, McInerney FA, Polissar PJ, Freeman KH (2021) Soil carbon loss and weak fire feedbacks during Pliocene C4 grassland expansion in Australia. Geophysical Research Letters 48(2): 1–10. https://doi.org/10.1029/2020GL090964

Kukla T, Rugenstein JKC, Ibarra DE, Winnick MJ, Strömberg CAE, Chamberlain CP (2022) Drier winters drove Cenozoic open habitat expansion in North America. AGU Advances 3(2): e2021AV000566. https://doi.org/10.1029/2021AV000566

Linder H, Lehmann CE, Archibald S, Osborne CP, Richardson DM (2018) Global grass (Poaceae) success underpinned by traits facilitating colonization, persistence and habitat transformation. Biological Reviews 93(2): 1125–1144. https://doi.org/10.1111/brv.12388

Lu J, Algeo TJ, Zhuang G, Yang J, Xiao G, Liu J, Huan J, Xie S (2020) The Early Pliocene global expansion of C4 grasslands: A new organic carbon-isotopic dataset from the north China plain. Palaeogeography, Palaeoclimatology, Palaeoecology 538: 109454. https://doi.org/10.1016/j.palaeo.2019.109454

Magalhaes IL, Azevedo GH, Michalik P, Ramírez MJ (2020) The fossil record of spiders revisited: implications for calibrating trees and evidence for a major faunal turnover since the Mesozoic. Biological Reviews 95: 184–217. https://doi.org/10.1111/brv.12559

Minh BQ, Nguyen MAT, von Haeseler A (2013) Ultrafast approximation for phylogenetic bootstrap. Molecular Biology and Evolution 30: 1188–1195. https://doi.org/10.1093/molbev/mst024

Murphy NP, Framenau VW, Donnellan SC, Harvey MS, Park YC, Austin AD (2006) Phylogenetic reconstruction of the wolf spiders (Araneae, Lycosidae) using sequences from the 12S rRNA, 28S rRNA, and *NADH1* genes: Implications for classification, biogeography, and the evolution of web building behavior. Molecular Phylogenetics and Evolution 38: 583–602. https://doi.org/10.1016/j.ympev.2005.09.004

Muster C, Berendonk TU (2006) Divergence and diversity: lessons from an arctic–alpine distribution (*Pardosa saltuaria* group, Lycosidae). Molecular Ecology 15(10): 2921–2933. https://doi.org/10.1111/j.1365-294X.2006.02989.x

Penney D (2001) Advances in the taxonomy of spiders in Miocene amber from the Dominican Republic (Arthropoda, Araneae). Palaeontology 44: 987–1009. https://doi.org/10.1111/1475-4983.00211

Penney D (2006) The oldest fossil pholcid and selenopid spiders (Araneae) in Lowermost Eocene amber from the Paris Basin, France. Journal of Arachnology 34: 592–598. https://doi.org/10.1636/H05-61.1

Piacentini LN, Ramírez MJ (2019) Hunting the wolf: A molecular phylogeny of the wolf spiders (Araneae, Lycosidae). Molecular Phylogenetics and Evolution 136: 227–240. https://doi.org/10.1016/j.ympev.2019.04.004

Posada D (2008) jModelTest: phylogenetic model averaging. Molecular Biology and Evolution 25: 1253–1256. https://doi.org/10.1093/molbev/msn083

Rambaut A, Drummond AJ (2009) Tracer v1.5. http://beast.bio.ed.ac.uk/Tracer

Ree RH, Smith SA (2008) Maximum likelihood inference of geographic range evolution by dispersal, local extinction, and cladogenesis. Systematic Biology 57(1): 4–14. https://doi.org/10.1080/10635150701883881

Renner SS (2005) Relaxed molecular clocks for dating historical plant dispersal events. Trends in Plant Science 10: 550–558. https://doi.org/10.1016/j.tplants.2005.09.010

Richter CJJ (1970) Aerial dispersal in relation to habitat in eight wolf spider species (*Pardosa*, Araneae, Lycosidae). Oecologia 5: 200–214. https://doi.org/10.1007/BF00344884

Roslin T, Somervuo P, Pentinsaari M, Hebert PDN, Agda J, Ahlroth P, Anttonen P, Aspi J, Blagoev G, Blanco S, Chan D, Clayhills T, deWaard J, deWaard S, Elliot T, Elo R, Haapala S, Helve E, Ilmonen J, Hirvonen P (2022) A molecular-based identification resource for the arthropods of Finland. Molecular Ecology Resources 22(2): 803–822. https://doi.org/10.1111/1755-0998.13510

Samu F, Szinetár C (2002) On the nature of agrobiont spiders. Journal of Arachnology 30: 389–402. https://doi.org/10.1636/0161-8202(2002)030[0389:OTNOAS]2.0.CO;2

Sanmartín I, Enghoff H, Ronquist F (2001) Patterns of animal dispersal, vicariance and diversification in the Holarctic. Biological Journal of the Linnean Society 73(4): 345–390. https://doi.org/10.1006/bijl.2001.0542

Schubert M, Marcussen T, Meseguer AS, Fjellheim S, Jordan G (2019) The grass subfamily Pooideae: The grass subfamily Pooideae: Cretaceous–Palaeocene origin and climate-driven Cenozoic diversification. Global Ecology and Biogeography 28(8): 1168–1182. https://doi.org/10.1111/geb.12923

Strömberg CAE (2011) Evolution of grasses and grassland ecosystems. Annual Review Earth Planetary Sciences 39: 517–544. https://doi.org/10.1146/annurev-earth-040809-152402

Strömberg CAE, Staver AC (2022) The history and challenge of grassy biomes. Science 377(6606): 592–593. https://doi.org/10.1126/science.add1347

Trifinopoulos J, Nguyen LT, von Haeseler A, Minh BQ (2016) W-IQ-TREE: a fast online phylogenetic tool for maximum likelihood analysis. Nucleic Acids Research 44: 232–235. https://doi.org/10.1093/nar/gkw256

Vink CJ, Mitchell AD, Paterson AM (2002) A preliminary molecular analysis of phylogenetic relationships of Australasian wolf spider genera (Araneae, Lycosidae). Journal of Arachnology 30: 227–237. https://doi.org/10.1636/0161-8202(2002)030[0227:APMAOP]2.0.CO;2

Vogel BR (1964) A taxonomic revision of the *distincta* group of the wolf spider genus *Pardosa* in America north of Mexico (Araneida, Lycosidae). Postilla 82: 1–30.

Vogel BR (1970) Taxonomy and morphology of the *sternalis* and *falcifera* species groups of *Pardosa* (Araneida, Lycosidae). Armadillo Papers 3: 1–31.

Vogel BR (2004) A review of the spider genera *Pardosa* and *Acantholycosa* (Araneae, Lycosidae) of the 48 contiguous United States. Journal of Arachnology 32(1): 55–108. https://doi.org/10.1636/H03-8

Woolley C, Thomas CFG, Blackshaw RP, Goodacre SL (2016) Aerial dispersal activity of spiders sampled from farmland in southern England. Journal of Artachnology 44: 347–358. https://doi.org/10.1636/P15-56.1

World Spider Catalog (2024) World Spider Catalog. Version 25.0. Natural History Museum Bern. [online at] http://wsc.nmbe.ch [accessed on May 10, 2024]

Wunderlich J (2004a) Proof of presence of the family Lycosidae (Araneae) in Baltic and Dominican amber. In: Wunderlich J (Ed.) Beiträge zur Araneologie 3: 1557–1558.

Wunderlich J (2004b) Fossil spiders (Araneae) of the family Oxyopidae in Baltic and Dominican amber. Beiträge zur Araneologie 3: 1554–1556.

Wunderlich J (2004c) Fossil crab spiders (Araneae, Thomisidae) in Baltic and Dominican amber. Beiträge zur Araneologie 3: 1747–1760.

Yu Y, Harris AJ, He XJ (2010) S-DIVA (Statistical Dispersal-Vicariance Analysis): a tool for inferring biogeographic histories. Molecular Phylogenetics and Evolution 56(2): 848–850. https://doi.org/10.1016/j.ympev.2010.04.011

Yu Y, Harris AJ, Blair C, He XJ (2015) RASP (Reconstruct Ancestral State in Phylogenies): a tool for historical biogeography. Molecular Phylogenetics and Evolution 87: 46–49. https://doi.org/10.1016/j.ympev.2015.03.008

Zachos J, Pagani M, Sloan L, Thomas E, Billups K (2001) Trends, rhythms, and aberrations in global climate 65 Ma to present. Science 292: 686–693. https://doi.org/10.1126/science.1059412

Zehethofer K, Sturmbauer C (1998) Phylogenetic relationships of Central European wolf spiders (Araneae, Lycosidae) inferred from 12S ribosomal DNA sequences. Molecular Phylogenetics and Evolution 10(3): 391–398. https://doi.org/10.1006/mpev.1998.0536

Zwickl DJ, Hillis DM (2002) Increased taxon sampling greatly reduces phylogenetic error. Systematic Biology 51(4): 588–598. https://doi.org/10.1080/10635150290102339

Supplementary material 1

Supporting information

Authors: Lijuan Liu, Dan Fu, Yufa Luo

Data type: docx

Explanation note: **table S1.** Samples used in this study: taxon name, specimen voucher, sample collection locality, habitat, and GenBank accession numbers. **table S2.** Primer sequences and annealing temperatures used in this study. **table S3.** Parameters of the best-fitting substitution model for each codon base or gene partition selected under the Bayesian information criterion (BIC). **table S4.** The details and assignments of the calibration points used in BEAST analyses. **fig. S1.** Global distribution for the main clades/groups of the *Pardosa* spiders. **fig. S2.** Phylogenetic tree of 133 *Pardosa* species reconstructed using the Bayesian method. The numbers at the nodes represent posterior probabilities. **fig. S3.** Biogeographical reconstruction from statistical dispersal-vicariance analysis (S-DIVA) (a), and dispersal-extinction-cladogenesis (DEC) (b) from RASP v3.0. Colors of pie wedges at each node represent geographical areas inferred to have been occupied by ancestral taxa. The numbers at the nodes represent support.

Link: https://doi.org/10.3897/zse.100.128885.suppl1

Zoosyst. Evol. 100 (4) 2024, 1297–1314 | DOI 10.3897/zse.100.127201

PENSOFT

für Natur MUSEUM FÜR NATURKUNDE BERLIN

Molecular systematics of *Perinereis* and an investigation of the status and relationships of the cultured species *Perinereis wilsoni* Glasby & Hsieh, 2006 (Annelida, Nereididae)

Deyuan Yang[1,2], Sheng Zeng[2], Zhi Wang[3], Yanjie Zhang[4], Dazuo Yang[5], Christopher J. Glasby[6,7], Jiang-Shiou Hwang[1,8], Lizhe Cai[2]

1 *Institute of Marine Biology, National Taiwan Ocean University, Keelung, Taiwan*
2 *College of the Environment and Ecology, Xiamen University, Xiamen 361102, China*
3 *State Key Laboratory of Marine Environmental Science, College of Ocean and Earth Sciences, Xiamen University, Xiamen 361102, China*
4 *School of Life and Health Sciences, Hainan University, Haikou, China*
5 *Key Laboratory of Marine Bio-resource Restoration and Habitat Reparation in Liaoning Province, Dalian Ocean University, Dalian 116023, China*
6 *Natural Sciences, Museum & Art Gallery Northern Territory, PO Box 4646, Darwin, NT 0801, Australia*
7 *Australian Museum Research Institute, 1 William Street, NSW 2010, Sydney, Australia*
8 *Center of Excellence for the Oceans, National Taiwan Ocean University, Keelung, Taiwan*

https://zoobank.org/95987DFE-0752-4899-B07D-BC6C93DC8C60

Corresponding authors: Lizhe Cai (cailizhe@xmu.edu.cn); Jiang-Shiou Hwang (jshwang@mail.ntou.edu.tw); Christopher J. Glasby (chris.glasby@nt.gov.au)

Academic editor: Greg Rouse ♦ **Received** 9 May 2024 ♦ **Accepted** 16 August 2024 ♦ **Published** 13 September 2024

Abstract

In this study, we conducted morphological and molecular analyses of *Perinereis wilsoni*, a species being considered for aquaculture in China. We found this species difficult to identify because of its close morphological similarity to the sympatric *P. mictodonta* and thus sought genetic markers to more easily distinguish it and to investigate its phylogenetic relationship to *P. mictodonta* and other nereidids. For the first time, we sequenced, assembled, and annotated the complete mitochondrial genome, nuclear ribosomal sequences (*18S-ITS1-5.8S-ITS2-28S*), and four nuclear histone genes (*H3-H2A-H2B-H4*) of *P. wilsoni*. Comprehensive bioinformatics methods were employed to assemble the genome-skimming data of *P. wilsoni* to ensure assembly quality. Phylogenetic analyses based on five datasets of the available mitochondrial genomes (32 taxa in Nereididae, including 8 taxa in *Perineris*), using maximum likelihood and Bayesian analyses, provide support for the monophyly of the genus *Perinereis*. In contrast, the *P. nuntia* species group, a subgroup within *Perinereis*, is nonmonophyletic. *Perinereis wilsoni* has a closer phylogenetic relationship with *P. vancauri-ca* and *P. nuntia*. Our study serves as a baseline for future work on the cultivation, reproductive biology, and phylogeny of *P. wilsoni*.

Key Words

Bioinformatic analyses, genome skimming, mitogenomes, *Perinereis*

Introduction

Recently, a local *Perinereis* species intended for large-scale aquaculture in China by the Key Laboratory of Marine Bio-resource Restoration and Habitat Reparation in Liaoning Province, Dalian Ocean University, was identified as *P. wilsoni* Glasby & Hsieh, 2006. The genus *Perinereis* Kinberg, 1865, belongs to the Nereididae. This family comprises over 700 described species and 45 genera (Wilson et al. 2023). Many nereidid species, particularly *Perinereis*, are of significant commercial and ecological importance for fishing bait, aquaculture feed, and wastewater treatment (Palmer 2010; Arias et al. 2013). In China, *Perinereis aibuhitensis* (Grube, 1878) is farmed

and exported worldwide as fish bait, and *Tylorrhynchus heterochetus* (Quatrefages, 1866) is consumed as food by people in Guangdong Province and other Southeast Asian countries (Glasby and Hsieh 2006; Wilson et al. 2023).

Perinereis represents the second-largest genus in Nereididae, with approximately 100 species (Mahcene et al. 2023; Prajapat et al. 2023; Wilson et al. 2023; Teixeira et al. 2024). Bakken and Wilson (2005) conducted a phylogenetic analysis based on morphological evidence, suggesting that *Perinereis* may be polyphyletic. This was supported by subsequent molecular studies (Glasby et al. 2013; Alves et al. 2020; Elgetany et al. 2022). For practical identification purposes, Hutchings et al. (1991) first divided *Perinereis* into three species groups based on the number of pharyngeal Area VI paragnaths and further divided each group based on parapodial characters. The *Perinereis nuntia* species group was characterized by a distinctive arc of bar-shaped paragnaths on area VI (usually numbering 6–14 on each side) (Hutchings et al. 1991; Wilson and Glasby 1993; Glasby and Hsieh 2006). This group has been reviewed by Wilson and Glasby (1993), Glasby and Hsieh (2006), and Villalobos-Guerrero (2019). Currently, it comprises approximately 20 recognized species (Villalobos-Guerrero 2019; Wilson et al. 2023), with the type localities of about 13 species in the Indo-West Pacific. These studies have significantly improved our understanding of this group. However, relying solely on a morphology-based approach may not be sufficient to resolve the taxonomic status of these species because some key taxonomic characters used to distinguish species often overlap, as they show ontogenetic and intraspecific variation (Tosuji et al. 2019; Tosuji et al. 2023). These morphology-defined species need to be re-evaluated using integrated taxonomic methods by taxonomic specialists. Recently, studies based on integrative taxonomy have revealed more new species in Nereididae (see Glasby et al. 2013; Teixeira et al. 2022a; Teixeira et al. 2022b).

Perinereis wilsoni, a member of the *P. nuntia* species group, is morphologically very similar to *Perinereis mictodonta* (Marenzeller, 1879), with no distinct morphological differences, although slight but statistically significant morphometric differences were found with respect to paragnath numbers and the relative length of the dorsal cirri (Glasby and Hsieh 2006). For this reason, these two species were primarily established based on the differences in *ITS* (internal transcribed spacer) genes (Chen et al. 2002; Glasby and Hsieh 2006). Therefore, identifying these two species based solely on morphology presents a significant challenge. To date, only two studies have contributed molecular data: Chen et al. (2002) provided *ITS* genes. Tosuji et al. (2019) provided sequences for both the partial mitochondrial *16S* ribosomal RNA (*16S*) and *ITS* genes. Although Park and Kim (2007) researched *P. wilsoni* using the partial mitochondrial cytochrome oxidase I (*COX1*) gene, these sequences were not made publicly available. Moreover, there are some *COX1* sequences labeled *P. wilsoni* in the NCBI GenBank database, but these sequences remain pending verification.

Given the considerable economic importance of *Perinereis* species, accurate species identification is crucial because correct scientific names can facilitate the linking of subsequent physiological or reproductive studies, thus ensuring the reproducibility of these research efforts (Glasby and Hsieh 2006; Hutchings and Lavesque 2020). Therefore, we have focused on several key questions regarding taxonomy: 1) Is the identification of *P. wilsoni* from Liaoning Province accurate? 2) Which molecular markers are suitable for identifying this species? 3) What is the phylogenetic relationship of *P. wilsoni* to other nereidids?

In this study, we used low-coverage whole genome sequencing, also known as genome skimming (Straub et al. 2012), which has been widely used in polychaete phylogeny studies because it is cost-effective and does not require fresh tissue (Richter et al. 2015; Coissac et al. 2016; Alves et al. 2020; Hektoen et al. 2024). Utilizing this strategy, we provided more molecular information, including high-copy regions: mitochondrial genome (mitogenome), nuclear ribosomal sequences (*18S* rRNA-*ITS1*-*5.8S* rRNA-*ITS2*-*28S* rRNA), and nuclear histone genes (*H3*-*H2A*-*H2B*-*H4*).

Materials and methods

Sample collection, identification, and sequencing

The specimens of *P. wilsoni* were sampled from Dalian, Liaoning Province, China (38.8732°N, 121.6767°E) and identified by Deyuan Yang. All specimens were fixed directly in 95% ethanol. Two specimens with a fully-everted pharynx were used for morphological and molecular studies. They were deposited at Xiamen University (XMU) under voucher numbers 23007-1 and 23007-2, respectively. Specimens were identified based on the key in Glasby and Hsieh (2006). Methods used in the morphological study were followed by Yang et al. (2022). In summary, whole worms were photographed with an Olympus E-M1 Mark II camera with a 60 mm macro lens, detailed structures with a Zeiss Discovery V20 stereomicroscope, and a Nikon 80i compound microscope. Image stacks were obtained using Helicon Focus 7 (https://www.heliconsoft.com/heliconsoft-products/helicon-focus/) and post-processed using Adobe Photoshop. The terminology of nereidid followed Wilson et al. (2023) generally. To better describe areas II, III, and VI of paragnaths, we introduced the notations 'L:R' and 'L:M:R'. 'L:R' is for areas II and VI, and 'L:M:R' to describe the paragnath patch in area III, where 'L' represents the number of paragnaths on the left, 'M' in the middle, and 'R' on the right. For example, for area II, '2:3' signifies 2 paragnaths on the left and 3 on the right; for area III, '3:5,2R:7' signifies 3 paragnaths on the left, a central patch with 5 paragnaths in 2 rows, and 7 paragnaths on the right.

Before DNA extraction, each individual was cleaned with 95% ethanol. To avoid gut contamination, two to seven parapodia were clipped from the specimens. Whole genomic DNA was extracted using the TIANamp Genomic DNA Kit (TIANGEN, Beijing, China). Genome skimming was conducted on the Illumina NovaSeq X Plus with a PE150 strategy. DNA extraction and sequencing were performed at Novogene Bioinformatics Technology Co., Ltd. (Beijing, China). Our initial sequencing effort was to obtain 5 Gb of raw data for each sample. Voucher number 23007-2 was increased to 25 Gb to explore more universal single-copy ortholog genes.

Assembly and annotation of mitochondrial and nuclear sequences

Raw paired-end reads were removed from sequence adapters, and low-quality regions were trimmed using Fastp v.0.23.4 (Chen et al. 2018). The quality of all cleaned reads was checked with FastQC v.0.12.1 (http://www.bioinformatics.babraham.ac.uk/projects/fastqc/), and subsequently, FastQC results were summarized using MultiQC v.1.8 (Ewels et al. 2016) (Suppl. material 1).

To ensure reliable assembly for the present data, various assemblers were used: 1) SPAdes v.3.15.5 (Bankevich et al. 2012), Ray v.2.3.1 (Boisvert et al. 2010), Megahit v.1.2.9 (Li et al. 2015), and IDBA-UD v.1.1.3 (Peng et al. 2012); 2) GetOrganelle v.1.7.6.1 (Jin et al. 2020); 3) MITObim v.1.9 (Hahn et al. 2013) and NovoPlasty v.4.3.1 (Dierckxsens et al. 2017), with *16S* (GenBank accession numbers: LC482188) as the seed; 4) our new assembly pipeline, FastMitoAssembler (original version at https://github.com/suqingdong/FastMitoAssembler). The pipeline implemented in FastMitoAssembler involved the following steps: First, MEANGS v.1.2.1 (Song et al. 2022) was used to obtain and assemble mitochondrial genes, which then served as a seed input for NovoPlasty. Second, the results of NovoPlasty served as a seed input for GetOrganelle. Third, MitoZ v3.6 (Meng et al. 2019) was used for annotation. This workflow was managed using Snakemake (Köster and Rahmann 2012), which can handle large-scale samples with minimal input–only raw data.

For *de novo* assembly results (SPAdes, Megahit, Ray, and IDBA-UD), we used MitoFinder v.1.4 (Allio et al. 2020) to extract mitochondrial contigs (mt contigs) and annotations, using the *Platynereis dumerilii* mitogenome (GenBank: NC 000931) as a reference. Unfortunately, no mt contigs were found from the Ray assembler. If the circularization of a mt contig was not automatically completed by MitoFinder, the circules.py script (https://github.com/chrishah/MITObim/tree/master/misc_scripts) was used to assess the circularization of the contig. After obtaining mitogenomes from various assemblers, Quast v.5.2.0 (Gurevich et al. 2013) was employed for assembly quality evaluation (Suppl. material 2). A BLASTn query against GenBank in the NCBI (NCBI BLAST Analysis, https://BLAST.ncbi.nlm.nih.gov/BLAST.cgi) was also performed to check for contamination in the mitogenomes (Suppl. material 3: table S1). The GC content and read (per-base) coverage depth of mitogenome sequences were calculated using the visualize subcommand in MitoZ v.3.6 with default parameters.

The mitogenome was annotated using MITOS2 (Donath et al. 2019), MitoFinder v.1.4.1, and MitoZ v.3.6. All annotation files (in .gb or .gbf formats) were reordered with COX1 as the start gene using PhyloSuite v.1.2.3 (Zhang et al. 2020). The reordered GenBank format (gb) file was converted to a fasta file and uploaded to GeSeq (https://chlorobox.mpimp-golm.mpg.de/geseq.html) to combine the results of ARWEN v.1.2.3 and tRNAscan-SE v.2.0.7 into a single gb file. This approach allowed us to compare tRNA annotations generated from three common methods (ARWEN, tRNAscan-SE, and MiTFi). All annotations were then loaded into Geneious Prime v.2022.2.2 for manual curation. First, we utilized the MAFFT plugin in Geneious to align these gb files. Then, we checked the coding region annotations with the assistance of the ORFs function based on the invertebrate mitochondrial genetic code table 5. Second, tRNAs were evaluated using the following criteria: tRNAscan-SE was given precedence over ARWEN and MiTFi, while MiTFi had precedence over ARWEN. Thus, if tRNAscan-SE identified a tRNA, its result was chosen. In cases where both MiTFi and ARWEN identified a tRNA, the result from MiTFi was selected. Subsequently, we imported other gb files of *Perinereis* into Geneious to compare each gene and manually edit them.

The boundaries of each gene were determined by the following rules: 1) Protein-coding genes can overlap with each other but cannot overlap with tRNA genes. In Nereididae, only the *ND4* and *ND4L* coding genes are allowed to overlap. 2) The boundaries of mitochondrial rRNA genes (*12S* and *16S*) were defined by flanking genes. 3) The large non-coding region (or putative control region) was determined by the boundaries of neighboring genes and a low GC region.

The CGView Comparison Tool (CCT) (https://github.com/paulstothard/cgview_comparison_tool) (Grant et al. 2012) was employed to compare all accessible mitogenomes of Nereididae in NCBI (as of 15 January 2024) to evaluate the quality of annotations further.

The high-copy nuclear markers (*18S* to *28S* genes and histone genes) were assembled using GetOrganelle v.1.7.6.1. Considering the lack of effective software or pipelines to annotate these genes, we manually annotated nuclear rRNA genes in Geneious using primer pairs to define gene boundaries: 18*SA* and *18SB* (Medlin et al. 1988) for *18S*, *F63*.2 and *R3264.2* (Struck et al. 2006) for *28S*, and *ITS18SFPOLY* and *ITS28SRPOLY* (Nygren et al. 2009) for the *ITS1-5.8S-ITS2* region. After completing one sequence annotation, we utilized the "Transfer annotations" function within Geneious Prime v.2022.2.2 to annotate other sequences. The histone genes were annotated using the same function, with GenBank accession

number X58895 (*Urechis caupo*) as a reference at an 85% similarity threshold. If the number of gene annotations was incomplete in one sequence, we imported the corresponding cleaned sequencing reads into Geneious and reassembled the sequence employing the "map to reference" function in Geneious Prime v.2022.2.2 (mapper: Geneious, fine-tuning: iterate up to 25 times) and then re-annotated it. Once annotations were completed, each gene was extracted for NCBI BLAST analysis. The read (per-base) coverage depth of nuclear genes was calculated using a custom script, which used BWA (Li 2013) and SAMtools (Li et al. 2009).

BUSCO v.5.6 was employed to generate universal single-copy orthologs (USCOs) (Simão et al. 2015) using only the assembly results (contigs) from SPAdes with the following parameters: -l metazoan_odb10, -m genome, --augustus, -c 40. A total of 618 single-copy genes were searched.

Phylogenetic analyses

The phylogenetic analysis utilized two types of datasets: complete or near-complete mitogenomes of Nereididae and DNA barcoding sequences (*COX1*, *16S*, and *ITS*) of *Perinereis*. All publicly available Nereididae mitogenomes from GenBank (as of 15 January 2024), along with two outgroup species (*Craseoschema thyasiricola* NC 060815 and *Leocrates chinensis* NC 066969, belonging to Chrysopetalidae and Hesionidae, respectively), were included in the phylogenetic analysis. The outgroup taxa were selected based on previous hypotheses that Chrysopetalidae and Hesionidae are sister groups to Nereididae (Glasby 1993; Pleijel and Dahlgren 1998; Tilic et al. 2022). To ensure consistent annotation criteria and to correct potential errors in previous annotations of mitogenomes, we re-annotated all available Nereididae mitogenomes using the methods described above. Ultimately, *Platynereis massiliensis* (NC 051996) and *Alitta succinea* (NC 051993) from the Nereididae were excluded from this study (Suppl. material 3: table S2).

To identify potential taxonomically mislabeled sequences in the mitogenomes dataset, we extracted the *COX1* and *16S* genes and conducted NCBI BLAST analysis. The results were downloaded as CSV files. For each sequence, the top 10 matching sequences were sorted based on identity using WEKits v.1.0 (https://github.com/GP-sir/wekits/releases). Next, we retrieved the source information (subjectAcc) for these matched sequences from NCBI. The species identification of each sequence was then manually verified in Microsoft Excel. Specifically, we focused on matched sequences with identity over 97% and checked whether they were supported by reliable taxonomic references (Suppl. material 3: table S3, S4).

All manually curated mitogenomes were imported into PhyloSuite v.1.2.3. The extracted protein-coding genes (PCGs) and two rRNAs (2R) from these sequences were aligned using MAFFT in normal mode. MACSE v.2 (Ranwez et al. 2018) was used to improve the multiple sequence alignment of 13 PCGs in the "refinement strategy." After completing the alignment tasks, each alignment was manually checked in Geneious. Ambiguously aligned regions were removed using Gblocks with the default settings or trimAl v.1.2 (Capella-Gutiérrez et al. 2009) with the automated1 setting (Suppl. material 3: table S5). Five mitogenomic datasets were used in the phylogenetic analyses: (i) 13PCGs: PCGs with all three codon positions; (ii) 13PCGs12: PCGs without 3rd codon positions; (iii) 13PCGs_2R: PCGs dataset plus two rRNA genes; (iv) 13PCG12_2R: PCG12 dataset plus two rRNA genes; and (v) 13PCGsAA: amino acid sequences translated from 13PCGs. The heterogeneity of each dataset was assessed using AliGROOVE v.1.08 (https://github.com/Patrick-Kueck/AliGROOVE) with the default settings.

ModelFinder v.2.2.0 was used to select the best substitution models for each partition of the maximum likelihood (ML) and Bayesian inference (BI) analyses (Suppl. material 3: table S6). ML analysis was carried out in IQ-TREE v.2.2.2 under the edge-linked partition model with 20,000 ultrafast bootstraps. BI analysis was performed using MrBayes v.3.2.7a (Ronquist et al. 2012), with two parallel runs for at least 2,000,000 generations, ensuring the average standard deviation of split frequencies was below 0.01 (Ronquist et al. 2012).

Considering the mitogenomes of *Perinereis* are limited, shorter DNA sequences (DNA barcodes) were also used to explore the phylogenetic position of *Perinereis wilsoni*. All available *Perinereis* genes from NCBI (https://www.ncbi.nlm.nih.gov/nuccore/?term=Perinereis) were downloaded. The *COX1*, *16S*, *18S*, *28S*, *H3*, and *ITS* genes were further extracted because these molecular markers are widely employed in Annelida. To organize the data more efficiently, we used a custom script (Suppl. material 4) to categorize these data based on voucher numbers (treating isolates, clones, strains, and haplotypes as synonymous with voucher numbers). Ultimately, the *COX1*, *16S*, and *ITS* genes were selected for phylogenetic analysis due to their higher representation among taxa, and new sequences from this study were added to explore the phylogenetic position of *Perinereis wilsoni* (Suppl. material 3: table S7). The trees constructed with the *COX1*, *16S*, and *ITS* genes used the same methods as the mitogenome data.

Multiple alignment summary statistics were generated using the alignment summary function in BioKIT (Steenwyk et al. 2022), including the number of taxa (sequences), alignment lengths, number of constant sites, number of parsimony informative sites and variable sites, and the frequency of all character states.

Pairwise tree structure comparison was conducted using the *all.equal.phylo* function in the ape v.5.7.1 package (Paradis and Schliep 2019), and topological differences were assessed using TreeSpace (Jombart et al. 2017), both implemented in R v.4.3.1 (R Core Team 2023). Finally, iTOL v.6 (Letunic and Bork 2021) was used to visualize the trees.

Sequence analyses

Strand asymmetries were calculated using the following formulae (Perna and Kocher 1995): AT-skew = (A - T) / (A + T); GC-skew = (G - C) / (G + C). Codon usage and relative synonymous codon usage (RSCU) of 13 PCGs were computed in PhyloSuite and visualized using the 'ggplot2' package (Wickham 2016) in R v.4.1.3 (R Core Team 2023). DnaSP v.6.0 (Rozas et al. 2017) was used to calculate the non-synonymous (Ka)/synonymous (Ks) substitution rates among the 13 PCGs of Nereididae and the nucleotide diversity (Pi) with a sliding window of 100 bp and a step size of 25 bp. A Ka/Ks ratio < 1 indicates purifying selection, while a ratio > 1 indicates positive selection.

To determine which molecular marker is reliable for accurate species delimitation, all labeled *P. wilsoni* and *P. mictodonta COX1, 16S*, and *ITS* genes in NCBI were used. We used the following criteria: 1) whether the presence of a barcode gap: the minimum interspecific genetic distance is greater than the maximum intraspecific genetic distance; 2) whether each species is recovered as monophyletic; and 3) whether there is a small overlap between intra- and interspecific distances and a large barcode gap, as recommended by dos Santos Vieira et al. (2020). Genetic distances (p-distance and Kimura 2-parameter) over sequence pairs were calculated in MEGA X (Kumar et al. 2018). The heat maps were generated in TBtools v.2.080 (Chen et al. 2020).

Results

Morphological analyses

Perinereis wilsoni Glasby & Hsieh, 2006

Fig. 1A–K

Material examined. • 23007-1 and 23007-2, both collected from Dalian, Liaoning, China (38.87315°N, 121.676671°E), 08 August 2023, preserved in 95% ethanol.

Description. Description based on 23007-1 and 23007-2. 23007-1 complete, 93 chaetigers, 7.0 cm in length, 2.9 mm wide at chaetiger 10 (excluding parapodia); and 4.0 mm wide at chaetiger 10 (including parapodia) (Fig. 1A). 23007-2 complete, 6.5 cm in length, 98 chaetigers, 2.3 mm wide at chaetiger 10 (excluding parapodia), 3.7 mm wide at chaetiger 10 (including parapodia).

Prostomium and anterior dorsum with dark brown pigmentation. Prostomium anterior margin entire, pear-shaped, wider than long, with shallow longitudinal groove in central area. Antennae conical, about one-third length relative to prostomium length. Palps longer than prostomium, biarticulate, with palpophores and palpostyles (Fig. 1A, C, J). Palpophores barrel-shaped, slightly wider basally, palpostyles spherical (or globular). Eyes black (Fig. 1A).

Pharynx fully everted (Fig. 1A, C–F, J–K). Jaws brown, with 7 teeth (based on 23007-1) (Fig. 1B). Tentacular cirri extend back 3–12 setigers; posterodorsal one extending to chaetiger 8–12.

Paragnath counts (Fig. 1C–E, J–K): area I with 1 conical paragnath; area II with 9 or 11 conical paragnaths on left, 11 or 14 conical paragnaths on right (23007-1, II = 9:11; 23007-2, II = 11:14); area III with 14–17 conical paragnaths, central patch with 9–12 in 2 rows, 2–3 laterally on either side (23007-1, III = 3:9,2R:2; 23007-2, III = 2:12,2R:3); area IV with 18–22 conical paragnaths on each side (23007-1, IV = 18:25; 23007-2, III = 22:22), bars absent; area V with 1 conical paragnath; area VI with 3–5 shield-shaped bars on each side (23007-1, VI = 5:3; 23007-2, VI = 5:5); area VII–VIII with 19 conical paragnths in 2 rows.

Notopodia with 2 lobes, prechaetal lobe absent. Dorsal cirri longer than notopodial ligule, about 1.5 times length of the notopodial ligule throughout. Notopodial ligule similar to median ligule throughout. Neuropodial postchaetal lobe rounded, not projecting beyond acicular lobe. Ventral ligule similar in length to acicular ligule in all chaetigers (Fig. 1F, G, I).

Notopodia homogomph spinigers only. Neuropodial heterogomph spinigers present throughout. At chaetiger 10, lower neurochaetae all heterogomph falcigers, upper neurochaetae with heterogomph falcigers, and heterogomph spinigers. At chaetiger 30 and following chaetigers, lower neurochaetae present heterogomph spinigers.

Remarks. *Perinereis wilsoni* was established by Glasby and Hsieh (2006), who provided a comprehensive description and discussion. In this study, we initially identified our specimens as *P. wilsoni* based on the key and description provided by Glasby and Hsieh (2006). Specifically, in *P. wilsoni*, the dorsal cirri are approximately 1.5 times the length of the dorsal notopodial lobe anteriorly and 2–3 times longer posteriorly; Area IV has 29.8 (± 3.6) conical paragnaths, and Area V has 1–3 conical paragnaths, usually in a longitudinal line. In contrast, in *P. mictodonta*, the dorsal cirri are either equal to or only slightly longer than the dorsal notopodial lobe throughout the body; Area IV has 35.3 (± 6.8) conical paragnaths, and Area V has 3 conical paraganths, usually in a triangle arrangement. Our specimens more closely resemble *P. wilsoni*, having dorsal cirri about 1.5 times the length of the dorsal notopodial lobe throughout the body (or only increasing slightly in length posteriorly), Area IV with 18–22 conical paragnaths, and Area V with 1 conical paragnath. However, despite the statistically significant difference in these morphometric characters (see pp. 573, Glasby and Hsieh 2006), the characters all show overlap (see pp. 560 & 572, Glasby and Hsieh 2006), and thus, morphology alone may not be sufficient to distinguish all specimens belonging to *P. wilsoni* and *P. mictodonta*.

The *ITS* genes may presently be the most effective and reliable method for accurately identifying these species, as these sequences were generated from the paratypes of *P. wilsoni* (Chen et al. 2002; Glasby and Hsieh 2006). DNA sequence-based NCBI BLAST and phylogenetic analyses of *ITS* sequences also support our identification (see next sections).

Distribution. Japan; China (based on *ITS* genes). Other records require validation using at least *ITS* data.

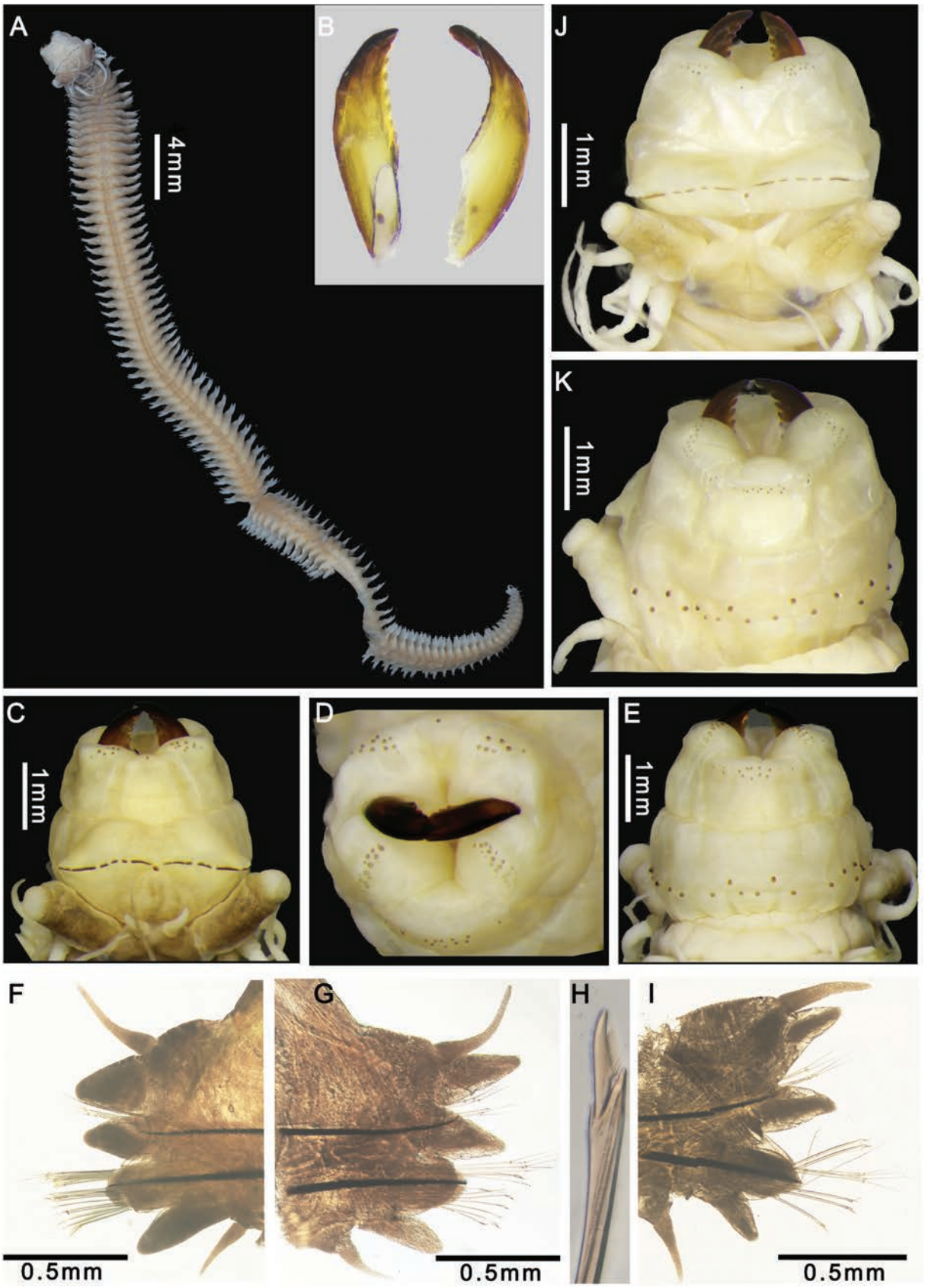

Figure 1. *Perinereis wilsoni* Glasby & Hsieh, 2006; **A–I.** (except **J, K)** 23007-1; **J, K.** 23007-2; **A.** Entire body in dorsal view; **B.** Right jaw, ventral, and dorsal view; **C.** Anterior region with pharynx everted, dorsal view; **D.** Maxillary ring, frontal view; **E.** Anterior end with pharynx everted, ventral view; **F.** Left parapodium, posterior view, chaetiger 10; **G.** Right parapodium, posterior view, chaetiger 30; **H.** Sub-acicular neuropodial heterogomph falciger, chaetiger 30; **I.** Right parapodium, posterior view, chaetiger 80; **J.** Anterior view with pharynx everted, dorsal view; **K.** Anterior view with pharynx everted, ventral view. All photos were taken by Deyuan Yang.

Characteristics of the *Perinereis wilsoni* mitochondrial genome and nuclear genes

The mitogenomes (23007-1 and 23007-2) generated from various assemblers yielded consistent results, except for the Ray assembler. They are 15,817 bp with an average coverage depth of 315×, and read mapping is 0.09% (Suppl. material 2). The genomes contain 13 protein-coding genes (PCGs), two ribosomal RNA (rRNA) genes, 22 transfer RNA (tRNA) genes, and one putative control region measuring 1160 bp. All genes are distributed on the heavy (H-) strand, similar to other Nereidinae species (Fig. 2A, Suppl. material 3: table S8). The nucleotide identity of 13 PCGs between *P. wilsoni* and the other 31 Nereididae species showed that the other species of *Perinereis* and *Neanthes acuminata* (OQ729916) have a high nucleotide identity with *P. wilsoni* (Fig. 2D).

The NCBI BLAST results of the mitogenome revealed that the sequence identity with the published *16S* sequences of *P. wilsoni* (LC482171–LC482183, Tosuji et al. 2019) ranged from 98.34% to 99.52%. However, the NCBI BLAST results for the full-length *16S* indicated over 98% sequence identity with both *P. mictodonta* (e.g., LC482161–LC482168, Tosuji et al. 2019) and *P. wilsoni* (e.g., LC482171–LC482183, Tosuji et al. 2019). These results show that the *16S* marker is not suitable for distinguishing these two species.

The nuclear rRNA contigs for the two specimens (23007-1 and 23007-2) yielded 10,983 bp and 10,820 bp with average coverages of 218.3× and 306×, respectively. Both results contained the full *18S*, *ITS1*, *5.8S*, *ITS2*, and *28S* regions, with gene lengths of 1,849 bp, 358 bp, 160 bp, 305 bp, and 3,840 bp, respectively (Fig. 2B). The nuclear histone genes for both specimens were 6,399 bp, with coverage depths of 1,547.5× and 2,620×, respectively, incorporating complete sequences of *H3* (411 bp), *H2A* (375 bp), *H2B* (372 bp), and *H4* (312 bp) genes (Fig. 2C).

The NCBI BLAST analysis of nuclear rRNA and histone genes showed that the *18S* sequence had over 99% sequence identity with eight species belonging to five genera, indicating that *18S* may not be suitable for species identification: 91.43% for *28S* with *Alitta virens* (OW028578); 98.48%-98.54% for *ITS* with *P. wilsoni* (AF332158–AF332162, Chen et al. 2002); 96%-98% for *H3* genes with *Perinereis* sp. A ZW-2022 (OL546356), *P. aibuhitensis* (MW622055), and *P. suluana* (JX443591); approximately 92% for *H2A* and *H2B* with *A. virens* (OW028584), *P. dumerilii* (X53330); and 89.4% for *H4* (Suppl. material 3: table S1).

Mitochondrial genes and codon usage

The mitochondrial genes in *P. wilsoni* exhibit a high A + T content of 64.6% (34.3% T and 30.3% A) and lower levels of C and G at 21.6% and 13.8%, respectively (Suppl. material 3: table S8). AT-skew and GC-skew are negative for the mitogenome (-0.062 and -0.221) and PCGs except for *COX2* (-0.084 and -0.250), and AT-skew is positive for tRNAs and rRNAs (0.041 and 0.043) (Suppl. material 3: table S8). The mitogenome is compact, with a total of three gene overlaps ranging in length from 2 to 7 bp. There are 12 gene spacers (259 bp in total) from 1 bp to 78 bp. All 13 PCGs start with the ATG codon and stop with T, TAA, or TAG (Suppl. material 3: table S9). A total of 22 tRNA genes with lengths ranging from 53 to 68 bp were identified in the mitogenome of *P. wilsoni*.

The most frequently utilized amino acids in the mitogenome of *P. wilsoni* are *Leu* (14.83%), *Ile* (9.94%), *Ser* (8.60%), and *Ala* (7.84%). The least common amino acids are *Cys* (1.01%), *Arg* (1.78%), *Asp* (1.78%), and *Gln* (1.94%) (Fig. 3, Suppl. material 3: table S10). Relative synonymous codon usage (RSCU) values for the 13 PCGs showed that UCU (*Ser*) and UUA (*Leu*) are the two most frequent codons, whereas UGG (*Trp*) and CCG (*Pro*) have the lowest frequencies (Fig. 3).

Phylogenetic analyses and genetic distances

Summary statistics for multiple alignments of various datasets are available in Suppl. material 3: table S11. The heterogeneity analysis of five mitogenome datasets revealed that datasets excluding the third codon position (13PCGs12, 13PCGs12_2R) exhibited lower heterogeneity compared to those including the third codon position (13PCGs, 13PCGs_2R). The lowest heterogeneity was observed in the 13PCGsAA dataset (see Suppl. material 5).

A total of ten ML and BI trees were inferred from five mitogenome datasets of Nereididae (see Suppl. material 6). These trees exhibit eight different topologies based on pairwise tree comparisons, indicating the significant influence of the chosen mitogenomic dataset and tree-building method on the inferred phylogenetic relationships. In general, ML and BI trees inferred from the same dataset are generally consistent, except for some obvious differences observed in the 13PCGs_2R and 13PCGs12_2R datasets (see Suppl. material 6). In the 13PCGs12 dataset, we could not re-root the ML and BI trees using the outgroup, which was excluded from TreeSpace analysis. The remaining eight trees were clustered into four groups, representing four types of trees (see Fig. 4B–F). The most common topology is depicted in Fig. 4A, D.

Phylogenetic analyses based on five datasets of the available mitochondrial genomes (32 taxa in Nereididae, including 8 taxa in *Perinereis*) provide support for the monophyly of the genus *Perinereis*. *Perinereis* was either sister to the genus *Nereis* and the species *Cheilonereis cyclurus* (MF538532) (Fig. 4C, E, F) or sister to the genera *Platynereis*, *Hediste*, *Alitta*, *Nectoneanthes*, and the species *Laeonereis culveri* (KU992689) (Fig. 4D). In all trees, *P. wilsoni* was sister to *P. vancaurica* and *P. nuntia* with high nodal support values (BS ≥ 94%, PP = 1) (Fig. 4 and Suppl. material 6). The *P. nuntia* species group was found not to be monophyletic. Specifically, *P. linea* (NC 063944), *P. aibuhitensis* (NC 023943), and *P. vancaurica* (ON611802) have two or three paragnaths on Area VI of the pharynx,

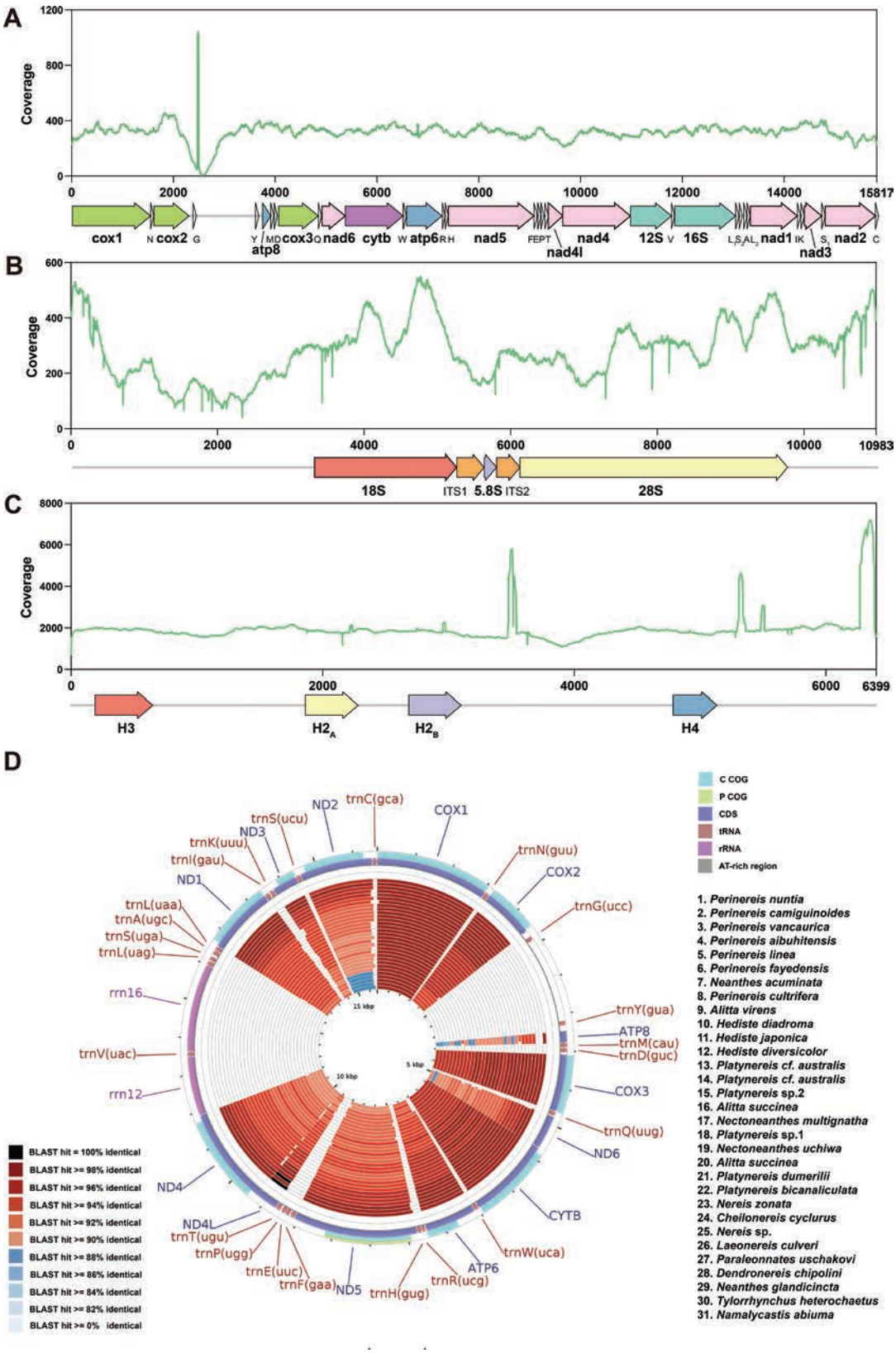

Figure 2. The gene map of *Perinereis wilsoni* (23007-1), 23007-2, is the same as 23007-1 but only shows one; **A.** Mitogenome; **B.** Nuclear rRNA cluster; **C.** And histone genes; **D.** CCT (CGView Comparison Tool) map and sequence identity compare the mitogenome between *P. wilsoni* and the other nereidids. **A–C.** The green lines depict the distribution of coverage depth; **D.** Starting from the outermost ring, the feature rings depict: 1. COG (Clusters of Orthologous Groups of Proteins) functional categories for forward strand coding sequences; 2. Forward strand sequence features; 3. The remaining rings show regions of sequence similarity detected by BLAST comparisons between CDS translations from the reference genome and 31 comparison genomes. BLAST identities are organized from high to low, with higher values closer to the outer ring.

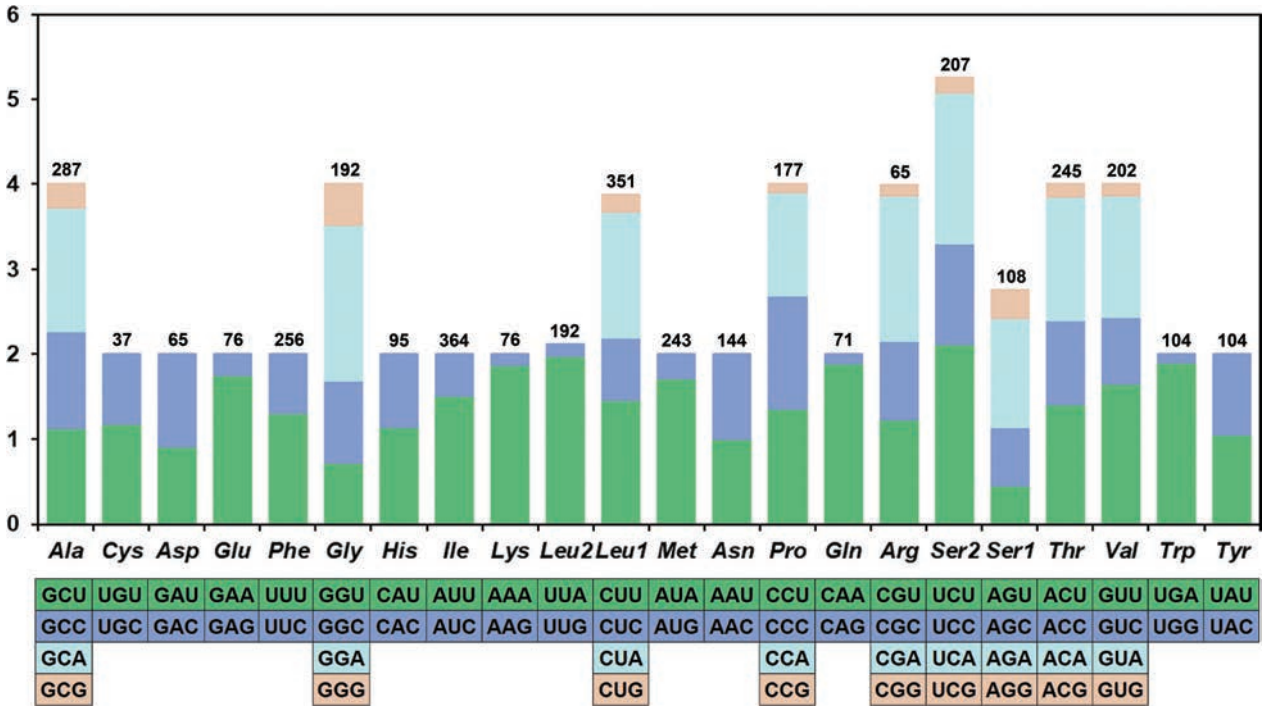

Figure 3. The relative synonymous codon usage (RSCU) in the mitogenome of *Perinereis wilsoni*. The numbers on the bars represent amino acid composition.

which belong to *Perinereis* Group 2 (Hutchings et al. 1991); all other *Perinereis* species (except *Perinereis cultrifera*) in the trees belong to the *P. nuntia* group. Yet, the species of Group 2 were nested within the *P. nuntia* group.

Phylogenetic trees (ML and BI) based on *COX1* genes recovered that *P. wilsoni* (23007-1, 23007-2) have a closer relationship with *P. mictodonta* (KC800632, KC800630, KC800628), with nodal support values (BS = 83%, PP = 0.94). All taxa labeled *P. wilsoni* and *P. mictodonta* did not each form a monophyletic group, respectively; instead, they were divided into five distinct clades. This suggests the potential of cryptic species present within *P. wilsoni* and *P. mictodonta* or that the specimens were sampled from geographically distant localities with some degree of isolation. These five clades were also supported by genetic distances, which have a distinct barcode gap from each other (Fig. 5A, D, and Suppl. material 7). The phylogenetic trees (ML and BI) based on *16S* genes suggested that *P. wilsoni* and *P. mictodonta* were each not monophyletic (Fig. 5B, E, and Suppl. material 8). Genetic distances also showed that the sequences of *P. wilsoni* and *P. mictodonta* had no barcode gap (Fig. 5B). The phylogenetic trees (ML and BI) based on *ITS* genes supported *P. wilsoni* as a sister to *P. mictodonta* (BS = 96%, PP = 1). Although *P. wilsoni* and *P. mictodonta* formed a monophyletic cluster with each other, the genetic distance analyses showed that these two species have no distinct barcode gap (Fig. 5C, F, and Suppl. material 9). Based on the dos Santos Vieira et al. (2020) methodology, optimal markers were selected based on an overlap criterion of less than 20%. However, the overlap between *P. wilsoni* and *P. mictodonta* exceeded 35%, indicating that *COX1*, *16S*, and *ITS* genes are not optimal molecular markers (Fig. 5A–C).

The positions of *Paraleonnates uschakovi* (NC 032361) and *Laeonereis culveri* (KU992689) are unstable, jumping across different phylogenies (Fig. 4, Suppl. material 6). *Laeonereis culveri* (KU992689) is closer to *P. uschakovi* (NC 032361) in four trees (13PCGs_2R_ML, 13PCGs12_ML, 13PCGs12_2R_ML, and 13PCGsAA_BI in Suppl. material 6), all with high nodal support. In contrast, in six other trees, *L. culveri* (KU992689) is more closely related to the genera *Hediste*, *Alitta*, and *Nectoneanthes*, also with high nodal support, except in the 13PCGs12_ML and 13PCGs12_BI trees (Fig. 4, Suppl. material 6). *Paraleonnates uschakovi* is closer to the subfamilies Gymnonereidinae, Dendronereinae, and Nereidinae (8 of 10 trees), with low nodal support in ML trees but with high nodal support in BI trees. In 13PCGs12_ML and 13PCGs12_BI trees, *P. uschakovi* was clustered with the outgroup, all with low nodal support (Suppl. material 6).

There are two primary types of mitochondrial gene order in the known mitochondrial genomes of Nereididae, except for *L. culveri* (KU992689). The first type of gene order is observed in the subfamilies Gymnonereidinae, Dendronereinae, and *P. uschakovi*. The second type is found in the subfamily Nereidinae, except for *L. culveri* (see Fig. 4).

Nucleotide diversity and evolutionary rate analyses

The nucleotide diversity (Pi) analysis was conducted using concatenated alignments of 13 PCGs and

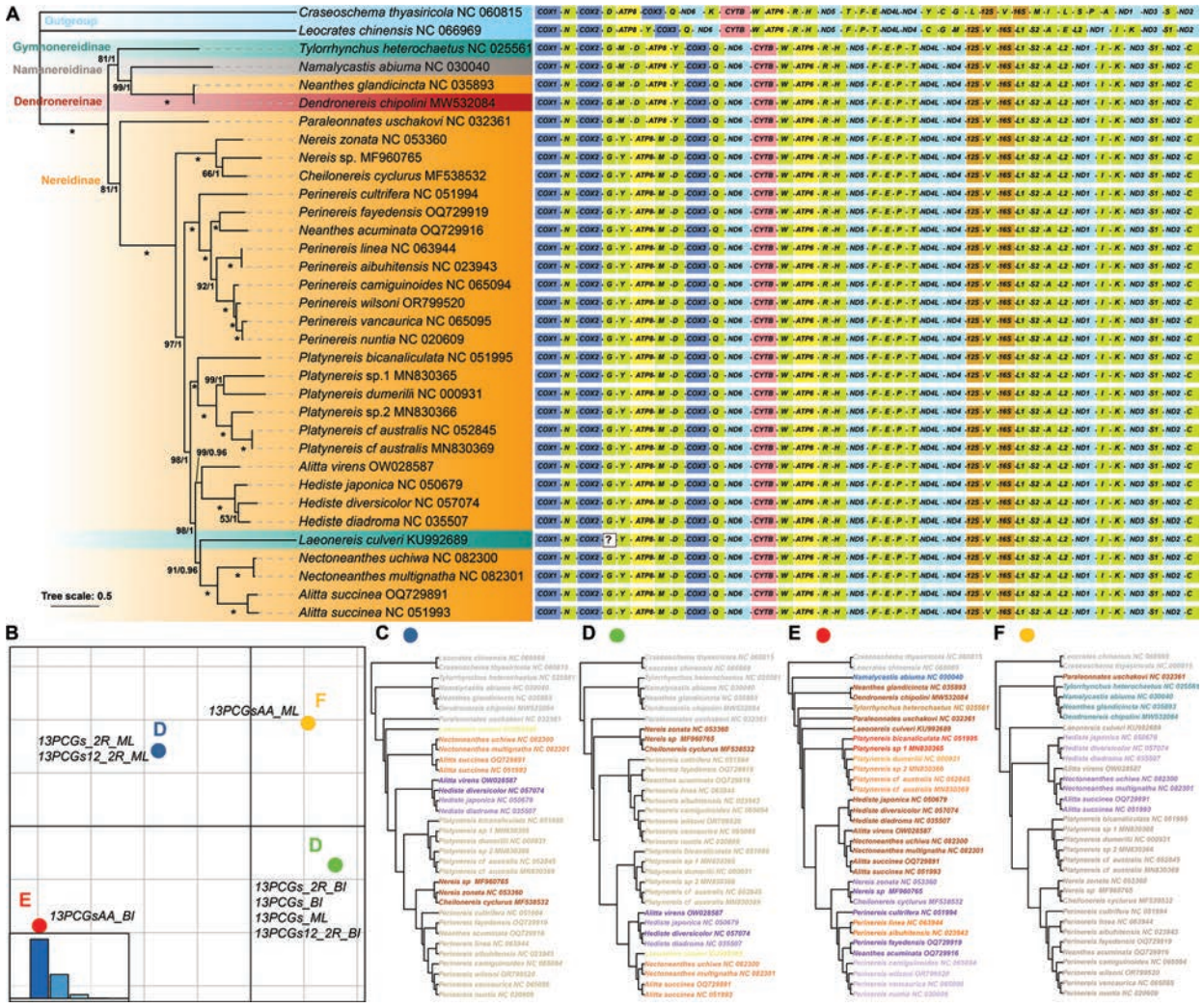

Figure 4. An analysis of phylogenies from five mitogenome datasets. **A.** Maximum likelihood (ML) and Bayesian inference (BI) tree of Nereididae based on the dataset 13PCGs. The GenBank accession numbers used are listed after the species names. The scale bar (0.5) corresponds to the estimated number of substitutions per site. Numbers at nodes are statistical support values for ML bootstrap support. Asterisks denote 100% bootstrap support. "-" indicates no support value. Color-coded clades are four subfamilies within Nereididae. The gene order is shown to the right. "?" indicates the deletion of a gene; **B.** A two-dimensional MDS plot of eight trees (excluding 13PCGs12_ML and 13PCGs12_BI), colored by different clusters. **C–F.** For each cluster identified in **B**., a representative tree was selected. **Note:** *Neanthes glandicincta* (NC 035893) is an incorrectly identified taxon, which should be the genus *Dendronereis*. *Neanthes acuminata* (OQ729916) and *Perinereis fayedensis* (OQ729919) should be *Perinereis suezensis* and *Perinereis damietta*, respectively. *Perinereis aibuhitensis* (NC 023943) should be *Perinereis linea* (NC 063944).

two rRNAs of 32 Nereididae species. The sequence variation ratio exhibits variable nucleotide diversity between the Nereididae, with Pi values for the 100 bp windows ranging from 0.061 to 0.563 (Fig. 6A). *COX1* (Pi = 0.211), *COX3* (0.235), *CYTB* (0.238), and *COX2* (0.239) exhibit a comparatively low sequence variability, whereas *ATP8* (0.405), *ND2* (0.386), and *ND6* (0.378) have a comparatively high sequence variability. This is corroborated by the non-synonymous/synonymous (Ka/Ks) ratio analysis, which shows that *COX1* (Ka/Ks = 0.036), *COX3* (0.038), *CYTB* (0.053), and *COX2* (0.065) are evolving comparatively slowly, whereas *ATP8* (0.270), *ND2* (0.196), and *ND6* (0.173) are evolving comparatively fast (Fig. 6B). All genes are under purifying selection.

Discussion

The taxonomic status of *Perinereis wilsoni*

Before discussing this topic, it is crucial to specify the species concept employed in this study. Despite approximately 30 species concepts having been proposed (Hong 2020), the scientific community has not reached a consensus on defining a species. Our study adopts the Gen-morph species concept, initially proposed by Deyuan Hong (Hong 2020), which requires at least two each of independent morphological characteristics and genetic markers for species definition. According to this concept, morphological characters include quantitative morphological features that have been shown to be statistically different between species.

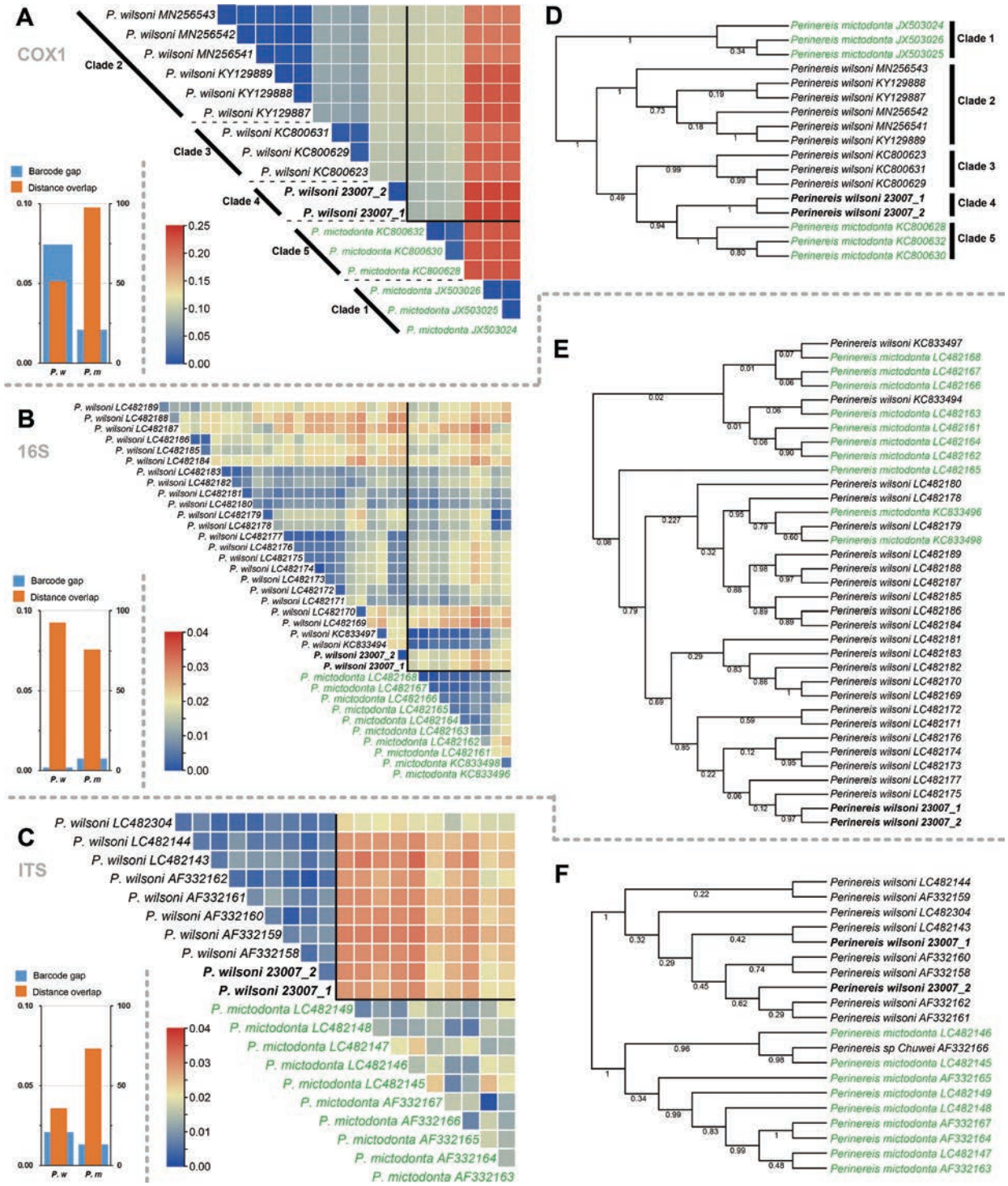

Figure 5. The heatmap of *COX1* **A**, *16S* **B.**, and *ITS* **C.** p-distance for *Perinereis wilsoni* and *P. mictodonta*, with the barcode gap and distance overlap of them on the left. Bayesian inference (BI) phylogenetic trees for the two species, based on sequences of *COX1* **D**, *16S* **E**, and *ITS* **F**, are excerpted from Suppl. materials 7–9. Sequences from *P. wilsoni* are depicted in black, those from *P. mictodonta* in green, with sequences from this study highlighted in bold.

Perinereis wilsoni and *P. mictodonta* were initially established as separate species based on statistically validated morphometric differences and the results of the *ITS* genes (Glasby and Hsieh 2006). Subsequent studies by Park and Kim (2007) and Tosuji et al. (2019) demonstrated that *COX1*, *16S*, and *ITS* genes can distinguish these two species, respectively. However, the *COX1* sequences used in Park and Kim (2007) have not been made publicly available. Moreover, their study relied solely on morphological characteristics for species identification and did not validate these identifications with *ITS* gene analysis, casting doubt on the reliability of their findings. Our re-analysis of sequences from (Tosuji et al. 2019) showed that the *16S* was insufficient to distinguish the

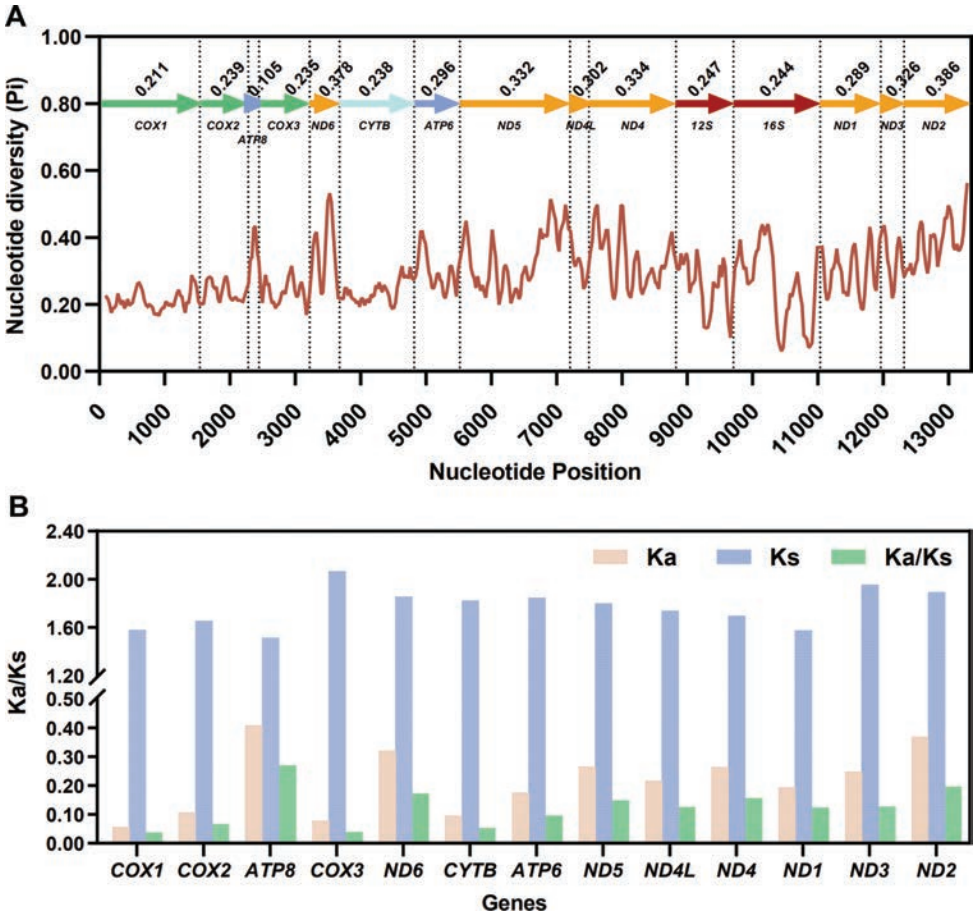

Figure 6. Nucleotide diversity analysis: **A.** Of 13 PCGs + two rRNAs and Ka/Ks rates; **B.** Of 13 PCGs based on 32 Nereididae species. The Pi values for the 13 PCGs + two rRNAs are shown on the graph. The red line represents the value of nucleotide diversity (Pi) (window size = 100 bp, step size = 20 bp). The pink, purple, and green columns represent the values of Ka, Ks, and Ka/Ks, respectively.

two species. To date, only *ITS* genes have proven effective in distinguishing *P. wilsoni* and *P. mictodonta* (Chen et al. 2002; Glasby and Hsieh 2006; Tosuji et al. 2019). Considering the Gen-morph species concept, *P. wilsoni* may not be a "good" species until a second genetic marker (and a more optimal one than *ITS*; see below) can be found. Therefore, comprehensive specimen sampling from various geographical locations is still required to assess its taxonomic status thoroughly (Deyuan Yang et al. in preparation).

Which molecular markers suit *Perinereis wilsoni* Glasby & Hsieh, 2006 identification?

Partial mitochondrial genes, like *COX1* and *16S*, and nuclear genes, like *18S*, *28S*, *ITS*, and *H3*, are widely used in Nereididae for species discovery and phylogenetic studies (Glasby et al. 2013; Elgetany et al. 2022; Teixeira et al. 2022a; Teixeira et al. 2022b; Teixeira et al. 2024). Among these genes, the *18S* and *28S* genes are typically used in higher-taxon phylogenetic analyses. A comprehensive assessment of the effectiveness of these molecular markers in differentiating species, both closely and distantly related across various genera and families, remains limited (Halanych and Janosik 2006).

Given that species within the *P. nuntia* complex are morphologically similar and not easily distinguishable based on morphology alone, molecular-based identification can offer a faster and more reliable method for species identification when reliable molecular references are available. Our analyses were unable to confirm the discriminative capability of the *COX1* gene between *P. wilsoni* and *P. mictodonta*, as the sequences sourced from public databases were not linked to morphological and *ITS* gene data, thus limiting our further study. Additionally, the *16S* gene was proven to be insufficient to distinguish these two species. Although *ITS* genes have been found effective in distinguishing cryptic species (Chen et al. 2002; Pleijel et al. 2009; Nygren and Pleijel 2011; Nygren 2014), they may not be the optimal molecular marker in distinguishing *P. wilsoni* and *P. mictodonta* due to the lack of a distinctive barcoding gap between these two species. Furthermore, there are only a few available sequences of Polychaeta *ITS* genes in the public database, possibly due to difficulties in amplifying these sequences by PCR. We found that the primer sets *ITS18SFPOLY* and *ITS28SRPOLY* (Nygren et al. 2009) may be more effective than the one provided by Chen et al. (2002) for amplifying *ITS* genes in *Perinereis*.

With advances in sequencing technologies, high-throughput sequencing (HTS) is more efficient than PCR-based Sanger sequencing in obtaining molecular markers. Recently,

some new molecular markers have been proposed, such as nearly universal single-copy nuclear protein-coding genes (Eberle et al. 2020) and organelle genomes (Margaryan et al. 2021). In this paper, we found the genome-skimming approach makes it easier to explore the mitogenome, complete nuclear ribosomal DNA (*18S-ITS1-5.8S-ITS2-28S*), and complete histone genes. However, it is more difficult to explore universal single-copy nuclear protein-coding genes, even with sequencing data increased to 25 Gb.

The phylogeny of *Perinereis* and the systematic position of *Perinereis wilsoni*

Currently, a robust phylogenetic backbone of the genus *Perinereis*, based on phylogenomic methods and extensive taxon sampling encompassing major species in all five informal grouping schemes proposed by Hutchings et al. (1991), is still lacking. Traditionally, the genus *Perinereis* has been considered polyphyletic (Bakken and Wilson 2005; Glasby et al. 2013; Alves et al. 2020; Elgetany et al. 2022). However, this view is largely based on morphological evidence or a limited number of loci and/or may include assembly errors in their datasets. In this study, although our curated mitogenome datasets support the monophyly of the genus *Perinereis*, the dataset includes only 8 species, whereas the genus currently comprises 103 species (Prajapat et al. 2024). Furthermore, morphological diversity within the genus has been unevenly sampled. Hutchings et al. (1991) proposed an informal grouping scheme with five groups. Our mitogenome dataset includes Group 1A, represented by 1 taxon (*P. cultrifera*); Group 2A, represented by 4 taxa (*P. linea*, *P. aibuhitensis* (should be *P. linea*), *P. camiguinoides*, and *P. vancuarica*); and Group 3A, represented by 4 taxa (*P. fayedensis*, *N. acuminata* (=*P. suezensis*), *P. wilsoni*, and *P. nuntia*). However, Groups 1B and 3B are not represented. To confidently establish the monophyly of the genus, future analyses should include multiple representatives from each of these informal morphological groupings.

Based on the available mitogenome datasets, *Perinereis wilsoni* is a sister group to *P. vancaurica* and *P. nuntia*, with high nodal support in all phylogenetic trees. In contrast, single-gene phylogenetic trees suggest that *P. wilsoni* is more closely related to *P. mictodonta*, with low nodal support. Although including more taxa, single-gene trees do not provide sufficient resolution in phylogeny. In summary, the phylogenetic relationships of *P. wilsoni* remain poorly understood due to the limited number of *Perinereis* species or other Nereididae for which genomic data are available.

The phylogeny of Nereididae

A deep discussion of the phylogeny of Nereididae is beyond the scope of our current work. Here, we provide a brief discussion. The positions of *P. uschakovi* and *L. culveri* (KU992689) were observed to be unstable in the trees, inferred from different mitogenome datasets in this study.

In detail, *L. culveri* always nested within the subfamily Nereidinae, which was also found in previous studies using different datasets, such as *COX1*, *16S*, and *18S* (Wang et al. 2021; Alves et al. 2023; Villalobos-Guerrero et al. 2024), as well as mitogenome datasets (Alves et al. 2020). *L. culveri* is also a sister group to the Gymnonereidinae, Dendronereinae, and Nereidinae subfamilies, along with *P. uschakovi* (this study; Villalobos-Guerrero et al. 2024). *P. uschakovi* was always found as a sister group to other subfamilies (Alves et al. 2020; Wang et al. 2021; Alves et al. 2023; Villalobos-Guerrero et al. 2024; this study). However, it occasionally grouped with the outgroup *Craseoschema thyasiricola* (NC 060815, see Suppl. material 6: 13PCGs12_ML tree and 13PCGs12_BI tree) or formed a single clade with the Gymnonereidinae and Dendronereinae subfamilies (see Suppl. material 6: 13PCGsAA_ML tree), which appears to be supported by mitochondrial genome gene order. Alves et al. (2020) also found this situation when removing outgroups. Inspired by a morphological phylogenetic tree proposed by Wu et al. (1981), which is based on the characteristics of pharyngeal armature, we propose a hypothesis that *Paraleonnates* and *Laeonereis* (KU992689) may represent early branching members of Nereidinae. The lack of sufficient data on such taxa may be causing their uncertain placements within the phylogenetic framework.

In this study, we uncovered potential errors in assembly and annotation within GenBank. However, the absence of corresponding Sequence Read Archive (SRA) data in public databases hampers accurate confirmation of these errors. Consequently, we filtered these sequences based solely on our expertise. Therefore, I (Deyuan Yang) advocate for the uploading of original data (raw data) to public databases, such as NCBI. Even if some authors are unwilling to upload their data, various assembly methods should be employed to ensure the accuracy of the assemblies.

Additionally, we emphasize that carefully curated datasets (verifying the taxonomic identification of the species used in the phylogenetic study), especially those from public databases, are crucial before conducting phylogenetic studies, as taxonomic misidentifications can lead to incorrect conclusions. For example, Alves et al. (2020) concluded that Gymnonereidinae was non-monophyletic, a finding that was impacted by the inclusion of an incorrectly identified taxon, *Neanthes glandicincta* (NC 035893), which should have been classified under the genus *Dendronereis* Peters, 1854 (Zhen et al. 2022; this study). Additionally, in this study, if we had not questioned the name *Neanthes acuminata* (OQ729916), we would have concluded that *Perinereis* is non-monophyletic. However, *N. acuminata* should be re-identified as *Perinereis suezensis* (Elgetany et al. 2022).

Author Contribution

D.Y.Y. and S.Z. wrote the manuscript, and S.Z. wrote the part on mitochondrial genes, codon usage, nucleotide diversity, and evolutionary rate analyses. D.Y.Y. and S.Z.

analyzed the data. Z.W., Y.J.Z., and D.Z.Y. participated in the discussion and reviewed the manuscript. C.J.G., J.S.H., and L.Z.C. conceived and designed, supervised the work, and reviewed drafts of the paper. S.Z. and D.Y.Y. contributed equally to this manuscript. All authors have read and agreed to the published version of the manuscript.

Acknowledgments

Many thanks to Yuanzheng Meng for helping us organize and format the literature for this paper. Thanks to Grammarly (https://www.grammarly.com/) for grammar correction while writing the first manuscript and ChatGPT 4.0 for generating some Python and R scripts during this study. Thanks to reviewer Robin Wilson for his constructive comments, especially focused on the phylogeny of the genus *Perinereis*, which have greatly contributed to the revision of our article. This work was supported by the Youth Fund of the National Natural Science Foundation of China (42306107) and the China Postdoctoral Science Foundation (2021M691866).

References

Allio R, Schomaker-Bastos A, Romiguier J, Prosdocimi F, Nabholz B, Delsuc F (2020) MitoFinder: Efficient automated large-scale extraction of mitogenomic data in target enrichment phylogenomics. Molecular Ecology Resources 20(4): 892–905. https://doi.org/10.1111/1755-0998.13160

Alves PR, Halanych KM, Santos CSG (2020) The phylogeny of Nereididae (Annelida) based on mitochondrial genomes. Zoologica Scripta 49(3): 366–378. https://doi.org/10.1111/zsc.12413

Alves PR, Halanych KM, Silva EP, Santos CS (2023) Nereididae (Annelida) phylogeny based on molecular data. Organisms Diversity & Evolution, 1–13. https://doi.org/10.1007/s13127-023-00608-9

Arias A, Richter A, Anadón N, Glasby CJ (2013) Revealing polychaetes invasion patterns: Identification, reproduction and potential risks of the Korean ragworm, *Perinereis linea* (Treadwell), in the Western Mediterranean. Estuarine, Coastal and Shelf Science 131: 117–128. https://doi.org/10.1016/j.ecss.2013.08.017

Bakken T, Wilson RS (2005) Phylogeny of nereidids (Polychaeta, Nereididae) with paragnaths. Zoologica Scripta 34(5): 507–547. https://doi.org/10.1111/j.1463-6409.2005.00200.x

Bankevich A, Nurk S, Antipov D, Gurevich AA, Dvorkin M, Kulikov AS, Lesin VM, Nikolenko SI, Pham S, Prjibelski AD (2012) SPAdes: a new genome assembly algorithm and its applications to single-cell sequencing. Journal of Computational Biology 19(5): 455–477. https://doi.org/10.1089/cmb.2012.0021

Boisvert S, Laviolette F, Corbeil J (2010) Ray: simultaneous assembly of reads from a mix of high-throughput sequencing technologies. Journal of Computational Biology 17(11): 1519–1533. https://doi.org/10.1089/cmb.2009.0238

Capella-Gutiérrez S, Silla-Martínez JM, Gabaldón T (2009) trimAl: a tool for automated alignment trimming in large-scale phylogenetic analyses. Bioinformatics 25(15): 1972–1973. https://doi.org/10.1093/bioinformatics/btp348

Chen CA, Chen C-P, Fan T-Y, Yu J-K, Hsieh H-L (2002) Nucleotide sequences of ribosomal internal transcribed spacers and their utility in distinguishing closely related *Perinereis* polychaets (Annelida; Polychaeta; Nereididae). Marine Biotechnology 4: 17–29. https://doi.org/10.1007/s10126-001-0069-3

Chen S, Zhou Y, Chen Y, Gu J (2018) fastp: an ultra-fast all-in-one FASTQ preprocessor. Bioinformatics 34(17): i884-i890. https://doi.org/10.1093/bioinformatics/bty560

Chen C, Chen H, Zhang Y, Thomas HR, Frank MH, He Y, Xia R (2020) TBtools: an integrative toolkit developed for interactive analyses of big biological data. Molecular Plant 13(8): 1194–1202. https://doi.org/10.1016/j.molp.2020.06.009

Coissac E, Hollingsworth PM, Lavergne S, Taberlet P (2016) From barcodes to genomes: extending the concept of DNA barcoding. Molecular Ecology 25(7): 1423–1428. https://doi.org/10.1111/mec.13549

Dierckxsens N, Mardulyn P, Smits G (2017) NOVOPlasty: de novo assembly of organelle genomes from whole genome data. Nucleic Acids Research 45(4): e18-e18. https://doi.org/10.1093/nar/gkw955

Donath A, Jühling F, Al-Arab M, Bernhart SH, Reinhardt F, Stadler PF, Middendorf M, Bernt M (2019) Improved annotation of protein-coding genes boundaries in metazoan mitochondrial genomes. Nucleic Acids Research 47(20): 10543–10552. https://doi.org/10.1093/nar/gkz833

dos Santos Vieira WA, Bezerra PA, da Silva AC, Veloso JS, Câmara MPS, Doyle VP (2020) Optimal markers for the identification of Colletotrichum species. Molecular Phylogenetics and Evolution 143: 106694. https://doi.org/10.1016/j.ympev.2019.106694

Eberle J, Ahrens D, Mayer C, Niehuis O, Misof B (2020) A plea for standardized nuclear markers in metazoan DNA taxonomy. Trends in Ecology & Evolution 35(4): 336–345. https://doi.org/10.1016/j.tree.2019.12.003

Elgetany AH, Struck TH, Glasby CJ (2022) Three new species of the genus *Perinereis* (Annelida, Nereididae) from Egyptian coasts. ZooKeys 1132: 163–188. https://doi.org/10.3897/zookeys.1132.87629

Ewels P, Magnusson M, Lundin S, Käller M (2016) MultiQC: summarize analysis results for multiple tools and samples in a single report. Bioinformatics 32(19): 3047–3048. https://doi.org/10.1093/bioinformatics/btw354

Glasby CJ (1993) Family revision and cladistic analysis of the Nereidoidea (Polychaeta: Phyllodocida). Invertebrate Systematics 7(6): 1551–1573. https://doi.org/10.1071/IT9931551

Glasby CJ, Hsieh H-L (2006) New species and new records of the *Perinereis nuntia* species group (Nereididae: Polychaeta) from Taiwan and other Indo-West Pacific shores. Zoological Studies 45(4): 553–577. https://zoolstud.sinica.edu.tw/Journals/45.4/553.pdf

Glasby CJ, Wei N-WV, Gibb KS (2013) Cryptic species of Nereididae (Annelida: Polychaeta) on Australian coral reefs. Invertebrate Systematics 27(3): 245–264. https://doi.org/10.1071/IS12031

Grant JR, Arantes AS, Stothard P (2012) Comparing thousands of circular genomes using the CGView Comparison Tool. BMC Genomics 13: 1–8. https://doi.org/10.1186/1471-2164-13-202

Gurevich A, Saveliev V, Vyahhi N, Tesler G (2013) QUAST: quality assessment tool for genome assemblies. Bioinformatics 29(8): 1072–1075. https://doi.org/10.1093/bioinformatics/btt086

Hahn C, Bachmann L, Chevreux B (2013) Reconstructing mitochondrial genomes directly from genomic next-generation sequencing reads—a baiting and iterative mapping approach. Nucleic Acids Research 41(13): e129-e129. https://doi.org/10.1093/nar/gkt371

Halanych KM, Janosik AM (2006) A review of molecular markers used for Annelid phylogenetics. Integrative and Comparative Biology 46(4): 533–543. https://doi.org/10.1093/icb/icj052

Hektoen MM, Bakken T, Ekrem T, Radashevsky VI, Dunshea G (2024) Species delimitation and phylogenetic relationships of the *Prionospio* complex (Annelida, Spionidae) in the Northeast Atlantic. Zoologica Scripta: 358–375. https://doi.org/10.1111/zsc.12648

Hong DY (2020) Gen-morph species concept—A new and integrative species concept for outbreeding organisms. Journal of systematics and evolution 58(5): 725–742. https://doi.org/10.1111/jse.12660

Hutchings P, Lavesque N (2020) I know who you are, but do others know? Why correct scientific names are so important for the biological sciences. Zoosymposia 19: 151–163. https://doi.org/10.11646/zoosymposia.19.1.16

Hutchings P, Reid A, Wilson R (1991) *Perinereis* (Polychaeta, Nereididae) from Australia, with redescriptions of six additional species. Records of the Australian Museum 43(3): 241–274. https://doi.org/10.3853/j.0067-1975.43.1991.47

Jin J-J, Yu W-B, Yang J-B, Song Y, DePamphilis CW, Yi T-S, Li D-Z (2020) GetOrganelle: a fast and versatile toolkit for accurate de novo assembly of organelle genomes. Genome Biology 21: 1–31. https://doi.org/10.1186/s13059-020-02154-5

Jombart T, Kendall M, Almagro-Garcia J, Colijn C (2017) treespace: Statistical exploration of landscapes of phylogenetic trees. Molecular Ecology Resources 17(6): 1385–1392. https://doi.org/10.1111/1755-0998.12676

Köster J, Rahmann S (2012) Snakemake—a scalable bioinformatics workflow engine. Bioinformatics 28(19): 2520–2522. https://doi.org/10.1093/bioinformatics/bts480

Kumar S, Stecher G, Li M, Knyaz C, Tamura K (2018) MEGA X: molecular evolutionary genetics analysis across computing platforms. Molecular Biology and Evolution 35(6): 1547. https://doi.org/10.1093/molbev/msy096

Letunic I, Bork P (2021) Interactive Tree Of Life (iTOL) v5: an online tool for phylogenetic tree display and annotation. Nucleic Acids Research 49(W1): W293-W296. https://doi.org/10.1093/nar/gkab301

Li H (2013) Aligning sequence reads, clone sequences and assembly contigs with BWA-MEM. arXiv preprint arXiv:13033997: https://doi.org/10.48550/arXiv.1303.3997

Li H, Handsaker B, Wysoker A, Fennell T, Ruan J, Homer N, Marth G, Abecasis G, Durbin R, Subgroup GPDP (2009) The sequence alignment/map format and SAMtools. Bioinformatics 25(16): 2078–2079. https://doi.org/10.1093/bioinformatics/btp352

Li D, Liu C-M, Luo R, Sadakane K, Lam T-W (2015) MEGAHIT: an ultra-fast single-node solution for large and complex metagenomics assembly via succinct de Bruijn graph. Bioinformatics 31(10): 1674–1676. https://doi.org/10.1093/bioinformatics/btv033

Mahcene HR, Villalobos-Guerrero TF, Kurt G, Denis F, Daas T (2023) A new species of *Perinereis* Kinberg, 1865 (Annelida: Nereididae) from the Western Mediterranean Sea revealed by morphological and molecular approaches. Mediterranean Marine Science 24(2): 454–460. https://doi.org/10.12681/mms.33969

Margaryan A, Noer CL, Richter SR, Restrup ME, Bülow-Hansen JL, Leerhøi F, Langkjær EMR, Gopalakrishnan S, Carøe C, Gilbert MTP (2021) Mitochondrial genomes of Danish vertebrate species generated for the national DNA reference database, DNAmark. Environmental DNA 3(2): 472–480. https://doi.org/10.1002/edn3.138

Medlin L, Elwood HJ, Stickel S, Sogin ML (1988) The characterization of enzymatically amplified eukaryotic 16S-like rRNA-coding regions. Gene 71(2): 491–499. https://doi.org/10.1016/0378-1119(88)90066-2

Meng G, Li Y, Yang C, Liu S (2019) MitoZ: a toolkit for animal mitochondrial genome assembly, annotation and visualization. Nucleic Acids Research 47(11): e63. https://doi.org/10.1093/nar/gkz173

Nygren A (2014) Cryptic polychaete diversity: a review. Zoologica Scripta 43(2): 172–183. https://doi.org/10.1111/zsc.12044

Nygren A, Pleijel F (2011) From one to ten in a single stroke–resolving the European *Eumida sanguinea* (Phyllodocidae, Annelida) species complex. Molecular Phylogenetics and Evolution 58(1): 132–141. https://doi.org/10.1016/j.ympev.2010.10.010

Nygren A, Eklöf J, Pleijel F (2009) Arctic-boreal sibling species of *Paranaitis* (Polychaeta, Phyllodocidae). Marine Biology Research 5(4): 315–327. https://doi.org/10.1080/17451000802441301

Palmer PJ (2010) Polychaete-assisted sand filters. Aquaculture 306(1–4): 369–377. https://doi.org/10.1016/j.aquaculture.2010.06.011

Paradis E, Schliep K (2019) ape 5.0: an environment for modern phylogenetics and evolutionary analyses in R. Bioinformatics 35(3): 526–528. https://doi.org/10.1093/bioinformatics/bty633

Park T-S, Kim W (2007) A taxonomic study on *Perinereis nuntia* species group (Polychaeta: Nereididae) of Korea. Animal Systematics, Evolution and Diversity 23(1): 75–85. https://doi.org/10.5635/KJSZ.2007.23.1.075

Peng Y, Leung HC, Yiu S-M, Chin FY (2012) IDBA-UD: a de novo assembler for single-cell and metagenomic sequencing data with highly uneven depth. Bioinformatics 28(11): 1420–1428. https://doi.org/10.1093/bioinformatics/bts174

Perna NT, Kocher TD (1995) Patterns of nucleotide composition at fourfold degenerate sites of animal mitochondrial genomes. Journal of molecular evolution 41: 353–358. https://doi.org/10.1007/BF01215182

Pleijel F, Dahlgren T (1998) Position and delineation of Chrysopetalidae and Hesionidae (Annelida, Polychaeta, Phyllodocida). Cladistics 14(2): 129–150. https://doi.org/10.1111/j.1096-0031.1998.tb00327.x

Pleijel F, Rouse G, Nygren A (2009) Five colour morphs and three new species of *Gyptis* (Hesionidae, Annelida) under a jetty in Edithburgh, South Australia. Zoologica Scripta 38(1): 89–99. https://doi.org/10.1111/j.1463-6409.2008.00356.x

Prajapat V, Villalobos-Guerrero TF, Vachhrajani KD (2023) A new species of *Perinereis* Kinberg, 1865 (Annelida: Nereididae) and invalidation of two congeners from Western India. Zootaxa 5330(3): 398–412. https://doi.org/10.11646/zootaxa.5330.3.4

Prajapat V, Villalobos-Guerrero TF, Vachhrajani KD (2024) Two new species of *Perinereis* Kinberg, 1865 (Annelida: Nereididae) from the rocky shore of Maharashtra, India, including notes and an identification key to Group 1. European Journal of Taxonomy 935: 256–282. https://doi.org/10.5852/ejt.2024.935.2561

R Core Team (2023) R: A language and environment for statistical computing. R Foundation for Statistical Computing, Vienna, Austria. https://www.R-project.org/

Ranwez V, Douzery EJ, Cambon C, Chantret N, Delsuc F (2018) MACSE v2: toolkit for the alignment of coding sequences accounting for frameshifts and stop codons. Molecular Biology and Evolution 35(10): 2582–2584. https://doi.org/10.1093/molbev/msy159

Richter S, Schwarz F, Hering L, Böggemann M, Bleidorn C (2015) The utility of genome skimming for phylogenomic analyses as demonstrated for glycerid relationships (Annelida, Glyceridae). Genome Biology and Evolution 7(12): 3443–3462. https://doi.org/10.1093/gbe/evv224

Ronquist F, Teslenko M, Van Der Mark P, Ayres DL, Darling A, Höhna S, Larget B, Liu L, Suchard MA, Huelsenbeck JP (2012) MrBayes 3.2: efficient Bayesian phylogenetic inference and model choice across a large model space. Systematic Biology 61(3): 539–542. https://doi.org/10.1093/sysbio/sys029

Rozas J, Ferrer-Mata A, Sánchez-DelBarrio JC, Guirao-Rico S, Librado P, Ramos-Onsins SE, Sánchez-Gracia A (2017) DnaSP 6: DNA sequence polymorphism analysis of large data sets. Molecular Biology and Evolution 34(12): 3299–3302. https://doi.org/10.1093/molbev/msx248

Simão FA, Waterhouse RM, Ioannidis P, Kriventseva EV, Zdobnov EM (2015) BUSCO: assessing genome assembly and annotation completeness with single-copy orthologs. Bioinformatics 31(19): 3210–3212. https://doi.org/10.1093/bioinformatics/btv351

Song M-H, Yan C, Li J-T (2022) MEANGS: an efficient seed-free tool for de novo assembling animal mitochondrial genome using whole genome NGS data. Briefings in Bioinformatics 23(1): bbab538. https://doi.org/10.1093/bib/bbab538

Steenwyk JL, Buida III TJ, Gonçalves C, Goltz DC, Morales G, Mead ME, LaBella AL, Chavez CM, Schmitz JE, Hadjifrangiskou M (2022) BioKIT: a versatile toolkit for processing and analyzing diverse types of sequence data. Genetics 221(3): iyac079. https://doi.org/10.1093/genetics/iyac079

Straub SC, Parks M, Weitemier K, Fishbein M, Cronn RC, Liston A (2012) Navigating the tip of the genomic iceberg: Next-generation sequencing for plant systematics. American Journal of Botany 99(2): 349–364. https://doi.org/10.3732/ajb.1100335

Struck TH, Purschke G, Halanych KM (2006) Phylogeny of Eunicida (Annelida) and exploring data congruence using a partition addition bootstrap alteration (PABA) approach. Systematic Biology 55(1): 1–20. https://doi.org/10.1080/10635150500354910

Teixeira MA, Bakken T, Vieira PE, Langeneck J, Sampieri BR, Kasapidis P, Ravara A, Nygren A, Costa FO (2022a) The curious and intricate case of the European *Hediste diversicolor* (Annelida, Nereididae) species complex, with description of two new species. Systematics and Biodiversity 20(1): 1–39. https://doi.org/10.1080/14772000.2022.2116124

Teixeira MA, Langeneck J, Vieira PE, Hernández JC, Sampieri BR, Kasapidis P, Mucciolo S, Bakken T, Ravara A, Nygren A (2022b) Reappraisal of the hyperdiverse *Platynereis dumerilii* (Annelida: Nereididae) species complex in the Northern Atlantic, with the description of two new species. Invertebrate Systematics 36(11): 1017–1061. https://doi.org/10.1071/IS21084

Teixeira MA, Fourreau CJL, Sampere-Valverde J, Carvalho S (2024) Two new records and description of a new *Perinereis* (Annelida, Nereididae) species for the Saudi Arabian Red Sea region. ZooKeys 1196: 331–354. https://doi.org/10.3897/zookeys.1196.115260

Tilic E, Stiller J, Campos E, Pleijel F, Rouse GW (2022) Phylogenomics resolves ambiguous relationships within *Aciculata* (Errantia, Annelida). Molecular Phylogenetics and Evolution 166: 107339. https://doi.org/10.1016/j.ympev.2021.107339

Tosuji H, Nishinosono K, Hsieh H-L, Glasby CJ, Sakaguchi T, Sato M (2019) Molecular evidence of cryptic species diversity in the *Perinereis nuntia* species group (Annelida: Nereididae) with first records of *P. nuntia* and *P. shikueii* in southern Japan. Plankton and Benthos Research 14(4): 287–302. https://doi.org/10.3800/pbr.14.287

Tosuji H, Park T, Goryo Y, Kan K, Abe H, Sato M (2023) Molecular method to identify the morphologically similar four species of the *Perinereis nuntia* species complex (Annelida: Nereididae) based on PCR-RFLP analysis of nuclear ribosomal ITS, with new distributional records of the two forms of *Perinereis shikueii*. Plankton and Benthos Research 18(3): 124–130. https://doi.org/10.3800/pbr.18.124

Villalobos-Guerrero TF (2019) Redescription of two overlooked species of the *Perinereis nuntia* complex and morphological delimitation of *P. nuntia* (Savigny in Lamarck, 1818) from the Red Sea (Annelida, Nereididae). Zoosystema 41(1): 465–496. https://doi.org/10.5252/zoosystema2019v41a24

Villalobos-Guerrero TF, Huč S, Tilic E, Hiley AS, Rouse GW (2024) A remarkable new deep-sea nereidid (Annelida: Nereididae) with gills. PLoS ONE 19(3): e0297961. https://doi.org/10.1371/journal.pone.0297961

Wang Y, Cheng H, Wang C (2021) A new eyeless species of *Nicon* (Annelida: Nereididae) from the deep Northwest Pacific Ocean. Acta Oceanologica Sinica 40(12): 20–26. https://doi.org/10.1007/s13131-021-1886-z

Wickham H (2016) Data Analysis. In: ggplot2: Elegant Graphics for Data Analysis. Springer International Publishing, Cham, 189–201. https://doi.org/10.1007/978-3-319-24277-4_9

Wilson RS, Glasby CJ (1993) A revision of the *Perinereis nuntia* species group (Polychaeta: Nereididae). Records of the Australian Museum 45(3): 253–277. https://doi.org/10.3853/j.0067-1975.45.1993.23

Wilson RS, Glasby CJ, Bakken T (2023) The Nereididae (Annelida)–diagnoses, descriptions, and a key to the genera. ZooKeys 1182: 35–134. https://doi.org/10.3897/zookeys.1182.104258

Wu B, Sun R, Yang D (1981) The Nereidae (Poluchaetous Annelids) of the Chinese Coast. Ocean Press, Beijing, 228 pp.

Yang D, Wu X, Wang Z, Zhao X, Hwang J, Cai L (2022) Redescription of a rarely encountered species *Travisachinensis* Grube, 1869 (Annelida, Travisiidae), including a description of a new species of Travisa from Amoy, China. ZooKeys 1128: 1–17. https://doi.org/10.3897/zookeys.1128.90020

Zhang D, Gao F, Jakovlić I, Zou H, Zhang J, Li WX, Wang GT (2020) PhyloSuite: An integrated and scalable desktop platform for streamlined molecular sequence data management and evolutionary phylogenetics studies. Molecular ecology resources 20(1): 348–355. https://doi.org/10.1111/1755-0998.13096

Zhen W, Wu X, Hao E, Xu W, Deng J, Zhu J, Xu Y (2022) The first complete mitochondrial genome of the genus *Dendronereis*, represented by *D. chipolini* Hsueh, 2019 (Annelida, Nereididae) from Beibu Gulf, China. Mitochondrial DNA Part B 7(2): 393–395. https://doi.org/10.1080/23802359.2022.2040389

Supplementary material 1

The reports from FastQC

Authors: Deyuan Yang, Sheng Zeng, Zhi Wang, Yanjie Zhang, Dazuo Yang, Christopher J. Glasby, Jiang-Shiou Hwang, Lizhe Cai

Data type: pdf

Explanation note: (a) Basic information on clean data, including duplicate reads (%, Dups), average GC content (%, GC), and total sequences (millions, M Seqs). (b) Sequence counts for each sample. Duplicate read counts are an estimate only.

Link: https://doi.org/10.3897/zse.100.127201.suppl1

Supplementary material 2

The report of Quast

Authors: Deyuan Yang, Sheng Zeng, Zhi Wang, Yanjie Zhang, Dazuo Yang, Christopher J. Glasby, Jiang-Shiou Hwang, Lizhe Cai

Data type: pdf

Explanation note: (a) Basic information of various assemblers. (b) The cumulative length of each assembler. All statistics are based on contigs of size >= 500 bp, unless otherwise noted (e.g., "# contigs (>= 0 bp)" and "Total length (>= 0 bp)" include all contigs).

Link: https://doi.org/10.3897/zse.100.127201.suppl2

Supplementary material 3

Additional information

Authors: Deyuan Yang, Sheng Zeng, Zhi Wang, Yanjie Zhang, Dazuo Yang, Christopher J. Glasby, Jiang-Shiou Hwang, Lizhe Cai

Data type: xlsx

Explanation note: **table S1.** The Blast results of mitochondrial gene, *18S*, *28S*, *ITS*, and histone genes (Only 20 sequences are shown). **table S2.** List of 32 species and two outgroups used in this paper. **table S3.** Sequence Information from NCBI BLAST Analysis of the *COX1* Gene. **table S4.** Sequence Information from NCBI BLAST Analysis of the *16S* Gene. **table S5.** Original and Gblock lengths of the PCGs and PCGsAA sequences. **table S6.** Best partitioning schemes and models based on different datasets for maximum likelihood and Bayesian inference analysis. **table S7.** *COI*, *16S*, *18S*, *28S*, *ITS*, and *H3* gene sequences information of *Perinereis*. **table S8.** Nucleotide composition and skewness comparison of different elements of the mitochondrial genomes of *P. wilsoni*. **table S9.** Features of the *P. wilsoni* mitogenome. **table S10.** Codon numbers and relative synonymous codon usage (RSCU) of 13 PCGs in the *P. wilsoni* mitogenome. **table S11.** Summary statistics for multiple alignment of various datasets.

Link: https://doi.org/10.3897/zse.100.127201.suppl3

Supplementary material 4

The Python script for categorizing data

Authors: Deyuan Yang, Sheng Zeng, Zhi Wang, Yanjie Zhang, Dazuo Yang, Christopher J. Glasby, Jiang-Shiou Hwang, Lizhe Cai

Data type: docx

Link: https://doi.org/10.3897/zse.100.127201.suppl4

Supplementary material 5

Heterogeneity of sequence composition of mitochondrial genomes for 5 different data sets

Authors: Deyuan Yang, Sheng Zeng, Zhi Wang, Yanjie Zhang, Dazuo Yang, Christopher J. Glasby, Jiang-Shiou Hwang, Lizhe Cai
Data type: pdf

Link: https://doi.org/10.3897/zse.100.127201.suppl5

Supplementary material 6

10 trees from different datasets and tree-building methods

Authors: Deyuan Yang, Sheng Zeng, Zhi Wang, Yanjie Zhang, Dazuo Yang, Christopher J. Glasby, Jiang-Shiou Hwang, Lizhe Cai
Data type: pdf

Link: https://doi.org/10.3897/zse.100.127201.suppl6

Supplementary material 7

Phylogenetic trees of *Perinereis* based on the *COX1* dataset

Authors: Deyuan Yang, Sheng Zeng, Zhi Wang, Yanjie Zhang, Dazuo Yang, Christopher J. Glasby, Jiang-Shiou Hwang, Lizhe Cai
Data type: pdf
Explanation note: (a) Bayesian inference (BI, left) and (b) maximum likelihood (ML, right) method

Link: https://doi.org/10.3897/zse.100.127201.suppl7

Supplementary material 8

Phylogenetic trees of *Perinereis* based on the *16S* dataset

Authors: Deyuan Yang, Sheng Zeng, Zhi Wang, Yanjie Zhang, Dazuo Yang, Christopher J. Glasby, Jiang-Shiou Hwang, Lizhe Cai
Data type: pdf
Explanation note: (a) Bayesian inference (BI, left) and (b) maximum likelihood (ML, right) methods.

Link: https://doi.org/10.3897/zse.100.127201.suppl8

Supplementary material 9

Phylogenetic trees of *Perinereis* based on the *ITS* dataset

Authors: Deyuan Yang, Sheng Zeng, Zhi Wang, Yanjie Zhang, Dazuo Yang, Christopher J. Glasby, Jiang-Shiou Hwang, Lizhe Cai
Data type: pdf
Explanation note: (a) maximum likelihood (ML, left) and (b) Bayesian inference (BI, right) methods.

Link: https://doi.org/10.3897/zse.100.127201.suppl9

Zoosyst. Evol. 100 (4) 2024, 1315–1331 | DOI 10.3897/zse.100.125466

PENSOFT

für Natur MUSEUM FÜR NATURKUNDE BERLIN

Synonymy, redescription, molecular characterisation, and new distribution data of species of *Stilestrongylus* and *Guerrerostrongylus* (Nematoda, Heligmonellidae) parasitic in sigmodontine rodents from Argentina and Uruguay: a collection-based survey

María Celina Digiani[1,2], Paula Carolina Serrano[1,2]

1 *CONICET-Consejo Nacional de Investigaciones Científicas y Técnicas, La Plata, Argentina*

2 *División Zoología Invertebrados, Facultad de Ciencias Naturales y Museo, Universidad Nacional de La Plata, Paseo del Bosque s/n, 1900 La Plata, Argentina*

https://zoobank.org/DE37DFA9-F0D9-41AD-B021-7F990C241FA3

Corresponding author: María Celina Digiani (mdigiani@fcnym.unlp.edu.ar)

Academic editor: Andreas Schmidt-Rhaesa ♦ **Received** 17 April 2024 ♦ **Accepted** 8 August 2024 ♦ **Published** 24 September 2024

Abstract

In this study, we review the taxonomic status of the parasitic nematodes *Stilestrongylus oryzomysi* and *Guerrerostrongylus uruguayensis* (Heligmonellidae), which had been described only once from sigmodontine rodents from Argentina and Uruguay, respectively. To this aim, we examined 38 complete helminth sets deposited in the Helminthological Collection of the Museo de La Plata (MLP-He), Argentina, including type material of *G. uruguayensis*, *S. oryzomysi*, and a closely related species, *Stilestrongylus azarai*. We also examined voucher rodent specimens deposited in the Mammal Collection of the Museo de La Plata (MLP-Mz) to assess the identity of the symbiotypes and other rodent hosts. Based on these observations, *S. oryzomysi* is proposed as a junior synonym of *S. azarai*; the identity of the symbiotype of *S. oryzomysi* and *Trichofreitasia lenti* (Heligmonellidae) is emended from *Oligoryzomys flavescens* to *Akodon azarae*; *G. uruguayensis* is proposed as a junior synonym of *Guerrerostrongylus zeta*; *S. azarai* is redescribed based on type and voucher material; and the latter species and *G. zeta* are molecularly characterised using the ITS+ gene. We extend the geographic distribution of *S. azarai* to include Uruguay and provide a new host record for *T. lenti* (*A. azarae*, type host species), a new host record for *G. zeta* in Argentina (*O. flavescens*), and the first record of helminths for *Oligoryzomys nigripes* in Uruguay.

Key Words

Akodon azarae, *Guerrerostrongylus uruguayensis*, *Guerrerostrongylus zeta*, integrated collections, ITS+, *Oligoryzomys* spp., *Stilestrongylus azarai*, *Stilestrongylus oryzomysi*, *Trichofreitasia lenti*

Introduction

Heligmonellidae is the most speciose family of the Trichostrongylina (Strongylida), with ca. 350 species distributed worldwide, most of which are parasites of rodents. Within this family, the cosmopolitan Nippostrongylinae includes the largest number of species (ca. 230), with rodents of the superfamily Muroidea as main hosts (Beveridge et al. 2014; Durette-Desset et al. 2017). In South America, muroids are mostly represented by the Sigmodontinae, which includes ca. 380 species (D`Elía and Pardiñas 2015). In Argentina, ca. 29 species of Nippostrongylinae have been described from sigmodontines mainly inhabiting the Río de la Plata Basin region (Durette-Desset and Sutton 1985; Sutton and Durette-Desset 1991; Digiani and Durette-Desset 2003a, 2003b; Digiani et al. 2003; Navone et al. 2009; Digiani and Kinsella 2014; Panisse et al. 2017; Gómez-Muñoz et al. 2020; Serrano et

al. 2021). In particular, four of the latter species were described in 1991 from yellow pygmy rice rats, *Oligoryzomys flavescens* (Waterhouse) (commonly known as "colilargo del Plata"), which were collected at two localities in Argentina and Uruguay, distant ca. 400 km from each other and separated by the Uruguay River. These species are *Stilestrongylus oryzomysi* Sutton & Durette-Desset, 1991; *Trichofreitasia lenti* Sutton & Durette-Desset, 1991, from the Argentinean locality; *Stilestrongylus flavescens* Sutton & Durette-Desset, 1991; and *Guerrerostrongylus uruguayensis* Sutton & Durette-Desset, 1991, from the Uruguayan locality.

Subsequently, *S. flavescens* was reported from its type host species and other sigmodontine rodents in the Río de La Plata Basin region in Argentina (Navone et al. 2009; Hancke and Suárez 2018; Serrano 2024). *Trichofreitasia lenti* was found in different eco-regions in Argentina and Brazil, though never from its type host species (Digiani et al. 2007; Simões et al. 2011, 2012b; Panisse et al. 2017). *Stilestrongylus oryzomysi* and *G. uruguayensis* were not recorded again (see, however, Digiani et al. 2007 for records of *Guerrerostrongylus* spp.), despite the intensive sampling effort used in different studies (Navone et al. 2009; Panisse et al. 2017; Gómez-Muñoz et al. 2020; Serrano et al. 2021). Both species were described from a very small number of specimens, and their differential diagnoses against known species were mainly based either on morphometric characters of soft organs or on unspecific or rather ambiguous morphological features.

Stilestrongylus oryzomysi was differentiated from *S. azarai* Durette-Desset & Sutton, 1985, parasitic in *Akodon azarae* (Fischer) from Buenos Aires province, by having a more posterior excretory pore and a more developed genital cone (Sutton and Durette-Desset 1991). However, the authors only provided measurements of the holotypes and allotypes, and therefore no measurement ranges are available for any of the two species.

The remarkable similarity between *S. azarai* and *S. oryzomysi*, together with the fact that the latter has only been reported in its original description, led us to suspect that the specimens described as *S. oryzomysi* could be an infrequent acquisition of *S. azarai* by *O. flavescens*.

Similarly, *Guerrerostrongylus uruguayensis* was differentiated from *Guerrerostrongylus zeta* (Travassos, 1937), parasitic in various sigmodontines from Brazil (concerning the use of the spelling *zeta*, see Digiani et al. 2024), by its larger body size and a widening of the body just anterior to the tail in females, and by details of the bursal rays in males. However, the diagnostic characters proposed for females are taxonomically unreliable because they may vary with age and reproductive status, whereas those for males are ambiguous and subjected to individual variation. In addition, the description of *G. uruguayensis* did not account for morphometric variability since it was based solely on the holotype and allotype.

Within this framework, the main aim of the present study was to review the taxonomic status of *S. oryzomysi* and *G. uruguayensis* based on type material examination and comparison with closely related species. Additionally, our results allowed us to provide a morphological redescription of *S. azarai* based on type and voucher material, as well as a molecular characterisation of this species and of *G. zeta* based on the internal transcribed spacer (ITS) region. Finally, we shed some light on the host spectrum and geographic distribution of the species concerned.

Materials and methods

Type material examined from the Helminthological Collection of the Museo de La Plata, Argentina (MLP-He)

Stilestrongylus azarai

ARGENTINA • ♂, holotype; Buenos Aires Province, Balcarce; 1977–1978; Sutton leg.; *Akodon azarae*; MLP-He 0687-1• ♀, allotype; same data as for holotype; MLP-He 0687-2 • 6 ♂♂, 6 ♀♀, paratypes; same collection data as for preceding; MLP-He 0687-3.

Stilestrongylus oryzomysi

ARGENTINA • 2 ♂♂, 10 ♀♀, paratypes; Buenos Aires Province, Campana, National Route 12 (RN12) Km 100-101; [34°00'27.432"S, 58°58'29.28"W]; Apr. 1989; Sutton leg.; *Akodon azarae*, MLP-Mz 3076, "*Oryzomys flavescens*, 1914"; MLP-He 1914-3.

Guerrerostrongylus uruguayensis

URUGUAY • ♂, holotype; Artigas Department, Bella Unión, Colonia España; [30°21'52"S, 57°38'34"W]; Jul. 1989; Sutton leg.; "*Oryzomys flavescens*"; MLP-He 2046-1 • ♀, allotype; same data as for holotype; MLP-He 2046-2 • 2 ♂♂ (distal fragments), 3 ♀♀, paratypes; same collection data as for preceding; MLP-He 2046-3.

Type material of *G. zeta* was not examined; instead, data were drawn from two published redescriptions, which included the study of syntypes and voucher specimens housed in the Helminthological Collection of the Instituto Oswaldo Cruz (CHIOC), Rio de Janeiro, Brazil (Simões et al. 2012a) and of voucher specimens from Brazil and Argentina (Misiones province) (Digiani et al. 2012).

Other material examined

Additionally, we examined 35 sets of parasitic intestinal helminths in *A. azarae* and *Oligoryzomys* spp. housed in MLP-He for identification. These were selected because they had been collected from the type localities of *S. azarai*, *S. oryzomysi*, and *G. uruguayensis* and from the same sampling events as the type material of these species. The sets were complete, and the worms remained unidentified. Therefore, each set examined corresponded to an

infracommunity of intestinal helminths of either *A. azarae* or *Oligoryzomys* spp. from each of the localities concerned.

From Locality I (type locality of *S. azarai*): MLP-He 674, 675, 676, 683, 686.

From Locality II (type locality of *S. oryzomysi*): MLP-He 1905, 1906, 1907, 1911, 1913, 1915, 1933, 1940.

From Locality III (type locality of *G. uruguayensis*): MLP-He 2047, 2048, 2049, 2050, 2051, 2052, 2054, 2055, 2056, 2057, 2058, 2059, 2061, 2062, 2063, 2064, 2066, 2067, 2068, 2069, 2070, 2072.

Prevalence (P) and mean intensity of infection (MI) were calculated by host and locality according to Bush et al. (1997). We followed Beveridge et al. (2014) for high-level taxonomy (Order to Subfamily).

Hosts

Hosts from Loc. I (Table 1) were collected and identified by mammalogists of the Museo Municipal Lorenzo Scaglia, Mar del Plata, Buenos Aires province, Argentina. Their viscera were submitted for parasitological examination to the División Zoología Invertebrados (Facultad de Ciencias Naturales y Museo, Universidad Nacional de La Plata) in the framework of an agreement between both institutions in the 1980's. Voucher host specimens of all helminth sets from Loc. II and several sets from Loc. III were deposited in the Mammal Collection of Museo de La Plata (MLP-Mz), thus allowing us to confirm or emend previous host identifications (Tables 2, 3).

Table 1. Helminth sets from Locality I (Balcarce, Argentina, type locality of *Stilestrongylus azarai*). In parentheses, intensity of infection.

Accession N° MLP-He	Host ID	Heligmonellid species	Other intestinal parasites
674	*Akodon azarae*	*Stilestrongylus azarai* (187)	Rictulariidae undet. (3) Cestoda undet. (3) *Trichuris* sp. (23) *Syphacia* sp. (6)
675	*A. azarae*	*S. azarai* (5)	–
676	*A. azarae*	*S. azarai* (14)	*Syphacia* sp. (3)
683	*A. azarae*	*S. azarai* (31)	*Syphacia* sp. (98)
686	*A. azarae*	*S. azarai* (7)	*Syphacia* sp. (15)
687†	*A. azarae*	*S. azarai* (13)	*Trichuris* sp. (44)

†type host of *S. azarai*.

Morphological study

Worms were studied in toto under a light microscope (Leica DM2500 equipped with a drawing attachment). Measurements are provided in micrometres unless stated otherwise, with the range followed by the mean (in parentheses) and the coefficient of variation expressed as a percent value. Transverse body sections were made and mounted for synlophe examination. The sections are oriented with the dorsal side of the worm towards the top of the page and the left side of the worm towards the left of the page.

Table 2. Helminth sets from Locality II (RN 12 Km 100, Campana, Argentina, type locality of *Stilestrongylus oryzomysi*). In parentheses, intensity of infection. The host's identity was confirmed by the re-examination of the voucher specimen. No other taxa were present in the intestine.

Accession N° MLP-He	Host N° in MLP-Mz	Host ID	Heligmonellid species
1905	3072	*Oligoryzomys flavescens*	*Guerrerostrongylus zeta* (10) *Stilestrongylus flavescens* (23)
1906	3090	*O. flavescens*	*G. zeta* (3) *S. flavescens* (76)
1907	3073	*Oligoryzomys nigripes*	*G. zeta* (1) *S. flavescens* (26)
1913	3075	*O. nigripes*	*G. zeta* (1) *S. flavescens* (12) *Stilestrongylus lanfrediae* (1)
1911	3074	*Akodon azarae*	*Stilestrongylus azarai* (93)
1914	3076†	*A. azarae*	*S. azarai* (9) *Trichofreitasia lenti* (16)
1915	3077	*A. azarae*	*S. azarai* (93) *T. lenti* (1)
1933	3078	*A. azarae*	*S. azarai* (13)
1940	3079	*A. azarae*	*S. azarai* (7)

†symbiotype of *S. oryzomysi* and *Trichofreitasia lenti*.

Molecular study

All attempts to obtain DNA from the aged material deposited in the MLP-He were unsuccessful, and DNA had to be extracted from specimens collected in localities other than the type localities (Table 6). These were recovered from *A. azarae* and *Oligoryzomys nigripes* (Olfers) and identified as *S. azarai* and *G. zeta*, respectively, on morphological criteria. The posterior ends of ethanol-fixed males were cut and individually stored in 70% ethanol as voucher specimens (accession numbers MLP-He 8101 to 8104). Genomic DNA was extracted from the remaining part of the body using a commercial kit (Promega) following the manufacturer's instructions. A region of nuclear rDNA including 18S 3'-terminus, ITS1, 5.8S subunit, ITS2, and 28S 5'-terminus (ITS+) was amplified using the primer sets ITS-F (5'-TTG AAC CGG GTA AAA GTC G-3') and ITS-R (5'-TTA GTT TCT TTT CCT CCG CT-3') (Stock et al. 2001), a PCR master mix (Productos Bio-Lógicos, Argentina), and 6 µl of DNA for a final volume of 50 µl under the following PCR conditions: an initial denaturation at 94 °C for 10 min, followed by 45 cycles at 94 °C for 30 s, 54 °C for 40 s, 72 °C for 80 s, and a final extension at 72 °C for 10 min. PCR products were analysed on 1.5% agarose gel electrophoresis, stained with ethidium bromide, and visualised on a UV transilluminator. Amplicons were submitted for sequencing to Macrogen Inc. (South Korea) with the same primers used for amplification.

The obtained sequences ranged between 995 and 1010 bp in length; they were manually edited and compared with those in GenBank using the BLASTn tool (Altschul et al. 1990) to determine their phylogenetic position. Alignments were made with MUSCLE through MEGA v10.2.6 (Kumar et al. 2018) and

Table 3. Helminth sets from Locality III (Bella Unión, Uruguay, type locality of *Guerrerostrongylus uruguayensis*). In parentheses, intensity of infection. In bold, the host's identity was confirmed by a voucher specimen. Otherwise, host identification is based on field notes.

Accession N° MLP-He	Host N° in MLP-Mz	Host ID	Heligmonellid species	Other intestinal parasites
2046	–	"*Oryzomys*" †	*Guerrerostrongylus zeta* (5) *Stilestrongylus flavescens* (57)	
2047	**3080**	***Oligoryzomys nigripes***	*G. zeta* (14) *S. flavescens* (10)	*Syphacia* sp. (1)
2048	**3081**	***Oligoryzomys flavescens***	*G. zeta* (9) *S. flavescens* (16)	–
2049	**3082**	***O. nigripes***	*G. zeta* (7) *S. flavescens* (17)	*Syphacia* sp. (5)
2050	–	No field data	*G. zeta* (19) *S. flavescens* (51)	–
2052	**3083**	***O. nigripes***	*G. zeta* (48) *S. flavescens* (45)	–
2054	–	No field data	*G. zeta* (7) *S. flavescens* (23)	*Strongyloides* sp. (1)
2056	–	"*Oryzomys*"	*G. zeta* (18) *S. flavescens* (5)	*Syphacia* sp. (3)
2057	–	"*Oryzomys*"	*G. zeta* (8)	–
2058	**3084**	***O. nigripes***	*G. zeta* (20) *S. flavescens* (5)	*Syphacia* sp. (7)
2059	–	"colilargo"	*G. zeta* (40) *S. flavescens* (38)	–
2062	–	"*Oryzomys*"	*G. zeta* (13) *S. flavescens* (7)	–
2063	**3085**	***O. nigripes***	*G. zeta* (25) *S. flavescens* (3)	–
2064	**3086**	***O. flavescens***	*G. zeta* (47) *S. flavescens* (12)	*Syphacia* sp. (7)
2067	–	"*Oryzomys*"	*G. zeta* (27) *S. flavescens* (47)	–
2068	**3088**	***O. flavescens***	*G. zeta* (9) *S. flavescens* (20) *Hassastrongylus hoineffae* (1)	–
2069	–	"*Oryzomys*"	*G. zeta* (21) *S. flavescens* (41)	*Syphacia* sp. (3)
2051	–	"*Akodon*"	*S. azarai* (66)	Rictulariidae undet. (2) Cestoda Hymenolepididae (1)
2055	–	"*Akodon*"	*S. azarai* (315)	Physalopteridae undet. (stomach) (1) *Pterygodermatites* sp. (1)
2061	–	"*Akodon*"	*S. azarai* (2)	*Syphacia* sp. (2) Rictulariidae undet. (1)
2066	**3087**	***Akodon azarae***	*S. azarai* (23)	–
2070	**3089**	***A. azarae***	*S. azarai* (67)	*Syphacia* sp. (1)
2072	–	No field data	*S. azarai* (17)	–

†type host of *Guerrerostrongylus uruguayensis* and *Stilestrongylus flavescens*.

further edited with GBlocks (Castresana 2000). The genetic distances were calculated using the p-distance method as implemented in MEGA v10.2.6 with default parameters. The nucleotide substitution model was selected using jModelTest v2.1 based on the best-fitting model indicated by the Bayesian Information Criterion (BIC) (Darriba et al. 2012). Maximum likelihood analysis was performed in MEGA with 1,000 bootstrap replicates. Posterior probabilities of all branches were calculated using Bayesian-based inference as implemented in MrBayes v3.2, and analyses were run for 20,000,000 generations (Ronquist et al. 2012). *Uncinaria lucasi* Stiles, 1901 (Ancylostomatidae) was used as an outgroup. The resulting phylogenetic trees were edited in FigTree v1.4.4.

It is worth mentioning that, despite several attempts, we failed to amplify the mitochondrial cytochrome c oxidase subunit 1 (COI) gene using the primer sets COIintF (5′-TGATTGGTGGTTTTGGTAA-3′) and COIintR (5′-ATAAGTACGAGTATCAATATC-3′) (Casiraghi et al. 2001), LCOI1490 (5'-GGTCAACAAATCATAAAGATATTGG-3'), and HCOI2198 (5'-TAAACTTCAGGGTGACCAAAAAATCA-3') (Folmer et al. 1994).

Results

Morphological study

Order Strongylida (Railliet & Henry, 1913)
Suborder Trichostrongylina (Leiper, 1908, family) Durette-Desset & Chabaud, 1993
Family Heligmonellidae (Skrjabin & Schikhobalova, 1952 tribe) Durette-Desset & Chabaud, 1977
Subfamily Nippostrongylinae Durette-Desset, 1971

Genus *Stilestrongylus* Freitas, Lent & Almeida, 1937

Figs 1, 2, Table 4

Stilestrongylus azarai Durette-Desset & Sutton, 1985

Redescription. Based on type material (see Material and Methods) and 27 voucher specimens from the same sampling event (14 males, 13 females).

General. Worms small to medium-sized, varying from loosely to tightly coiled, usually with 2–3 spires in anterior portion of body.

Head. Observed in two voucher specimens. Rounded buccal opening surrounded by thin ring; 2 amphids;

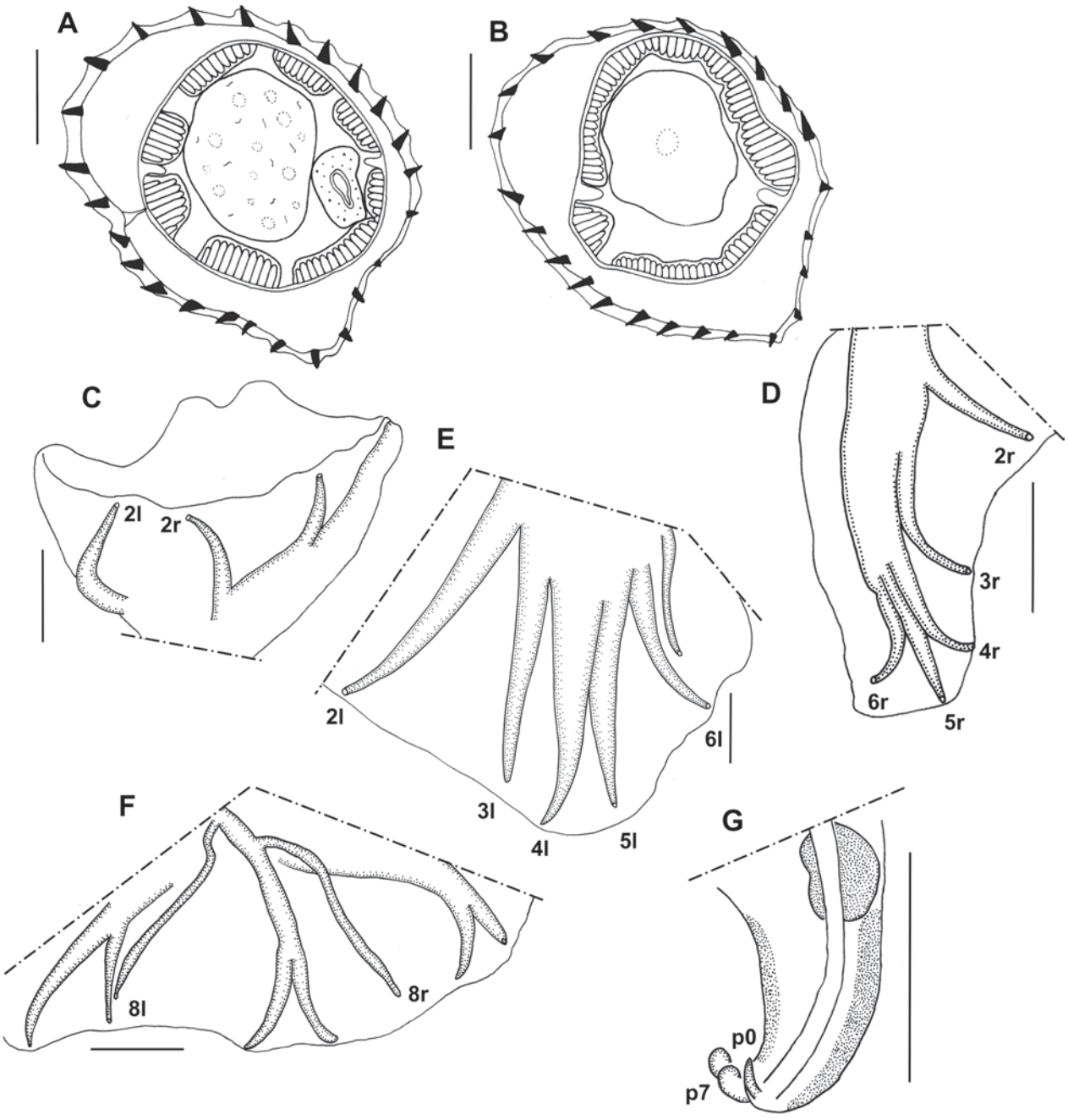

Figure 1. *Stilestrongylus azarai*. **A, B.** Synlophe in transverse section at midbody: **A.** Male; **B.** Female; **C.** Male caudal bursa, ventral view showing papillae 2; **D.** Right lobe of bursa, dorsal view; **E.** Left lobe of bursa, dorsal view; **F.** Dorsal lobe of bursa, dorsal view; **G.** Genital cone, left lateral view. **2l-6l** - left bursal rays 2 to 6; **8l** - left ray 8; **2r-6r** - right bursal rays 2 to 6; **8r** - right ray 8; **p0** - single papilla 0; **p7** - paired papillae 7. Scale bars: 20 µm (**A, B, E**); 50 µm (**C, D, F, G**). **C, G** from paratypes. **A, B**, and **D–F** from other specimens in *A. azarae* from the type locality (Balcarce).

4 externo-labial (2 dorsal, 2 ventral); and 4 cephalic papillae visible; lateral externo-labial papillae probably fused with amphids; each cephalic papilla connected with its contiguous externo-labial papilla by thickening, shaped as arc of circle (see description in Digiani and Durette-Desset 2003c).

Synlophe. Studied in 1 male and 1 female. Identical to that illustrated by Durette-Desset and Sutton (1985). With 25 subequal ridges in both sexes. Double axis of orientation of ridges: right axis inclined at 60° to sagittal axis, left axis at 80°. Twelve dorsal and 13 ventral ridges with respect to axis of orientation (Fig. 1A, B).

Males. Measurements in Table 4. Bursa large, bell-shaped, and dissymmetrical, with dorsal lobe well developed and right lobe markedly larger than left one. Prebursal papillae not observed. Bursa characterised by papillae 2 (ventral) very close (45–50 µm) to each other (Fig. 1C), implying that lobes were studied separately

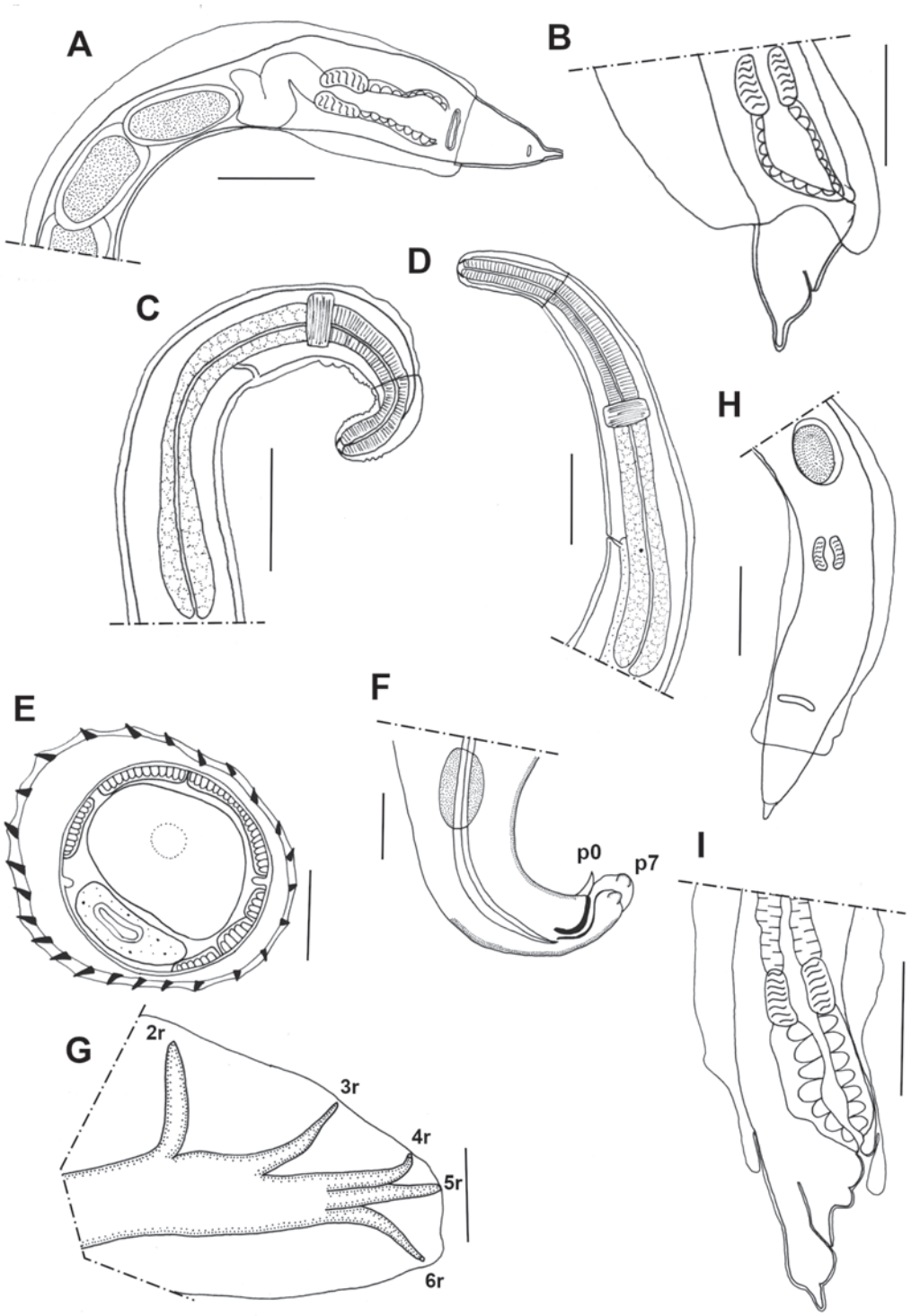

Figure 2. *Stilestrongylus azarai*. **A, B.** Female posterior end: **A.** Ventral view; **B.** Right lateral view; **C, D.** Anterior end: **C.** Curved and wrinkled, right lateral view (male); **D.** Stretched, left lateral view (female); **E.** Female synlophe in transverse section at mid-body; **F, G.** Male: **F.** Genital cone, right lateral view; **G.** Right lobe of caudal bursa, dorsal view; **H, I.** Female, posterior end: **H.** Ventral view; **I.** Right lateral view. **2r-6r** - right bursal rays 2 to 6; **p0** - single papilla 0; **p7** - paired papillae 7. Scale bars: 50 µm (**A–D, G–I**); 20 µm (**E, F**). **A–C** from paratypes of *S. azarai*. **D** from another specimen in *A. azarae* from the type locality (Balcarce). **E, H**, and **I** from a paratype of *S. oryzomysi* from Campana. **F** and **G** from other specimens in *A. azarae* from Campana.

because spreading out the bursa would break them. Right lobe (Fig. 1D): pattern of type 1-4, with ray 2 arising first from long common trunk of rays 3–6. Ray 3 arising at mid-length of common trunk, but distance between papillae 2 and 3 larger than that between papillae 3 and 4. Rays 4–6 diverging nearly at same level at distal quarter of common trunk, forming the characteristic "lateral trident". Ray 6 curved posteriorly, may be slightly longer than rays 4 and 5. Rays 3, 4, 5, and 6 reaching bursal margin. Left lobe (Fig. 1E): pattern of type 2-2-1. Rays 2 and

Table 4. Comparison of measurements of *Stilestrongylus azarai* from Balcarce (type locality), Campana (including paratypes of *Stilestrongylus oryzomysi*), and San Luis City. Measurements are in micrometres, unless otherwise stated.

Locality (Province)	**Balcarce (Buenos Aires)**		**Campana (Buenos Aires)**		**San Luis Capital City (San Luis)**	
Host	***Akodon azarae***		***Akodon azarae***		***Graomys griseoflavus***	
Source	**This work**		**This work**		**Digiani & Durette-Desset (2003c)**	
Body length (mm) (BL)	♂ (n = 23) 2.12–2.75 (2.35) 6%	♀ (n = 19) 2.3–3.8 (3.1) 14.2%	♂ (n = 16) 2.03–3.39 (2.67) 19.4%	♀ (n = 20) 1.88–5.63 (3.33) 40.9%	♂ (n = 10) 3.00–4.00 (3.33)	♀ (n = 10) 4.5–5.7 (5.1)
Body width	50–90 (78) 15%	70–100 (82) 11.4%	50–120 (72) 34.4%	75–130 (106) 19.1%	120–150 (132)	100–140 (120)
Cephalic vesicle length	45–60 (53) 8.4%	55–60 (57) 4.6% (n = 6)	42–60 (54) 10.6%	40–65 (52) 13.5%	55–65 (61)	50–75 (65)
Cephalic vesicle width	18–30 (24) 15.1%	20–28 (25) 11.6% (n = 6)	20–28 (23) 14.4%	14–45 (24) 28.8%	30–40 (33)	35–40 (38)
Oesophagus length (OeL)	230–310 (277) 6.8%	280–330 (298) 5.8%	245–295 (273) 6.7%	210–340 (276) 13.6%	290–310 (300)	320–360 (344)
Nerve ring†	100–135 (113) 9.7% (n = 8)	110–135 (118) 9.8% (n = 5)	110–150 (130) 10.4%	90–170 (124) 14.4%	140–175 (155)	120–170 (150)
Excretory pore† (EP)	170–195 (176) 11% (n = 5)	195–220 (203) 7.1% (n = 3)	185–245 (214) 9.7% (n = 6)	157–250 (197) 16%	220–260 (239)	190–240 (220)
EP/OeL (%)	59.6–70.9 (64) 10.3% (n = 5)	59.1–73.3 (66.6) 10.7% (n = 3)	72.5–83.1 (77.8) 5.1% (n = 6)	61.3–76.9 (69.7) 8.3%	71.0–88.1 (79.2)	54.3–66.7 (61.8)
Deirids†	140–205 (177) 12.9% (n = 10)	195–220 (206) 6.4% (n = 4)	185–245 (219) 9.3% (n = 7)	160–245 (200) 16.2%	220–260 (239)	190–240 (220)
Spicule length (SpL)	310–460 (380) 10.2%	–	290–445 (366) 13.2%	–	440–480 (456)	–
SpL/BL (%)	14.4–18.9 (16.5) 8.7%	–	11.7–16.5 (13.8) 10%	–	11.3–16.0 (13.8)	–
Genital cone length	70–125 (88) 16.3%	–	60–135 (109) 20.7%	–	–	–
Genital cone width	27–50 (40) 16.7%	–	32–50 (42) 14.9%	–	–	–
Vulva‡	–	55–80 (68) 11.6% (n = 9)	–	32–88 (62) 27.5%	–	70–100 (82)
Vestibule length	–	30–65 (48) 22%	–	35–65 (54) 16.3% (n = 9)	–	55–75 (62)
Sphincter length	–	25–30 (27) 7.9%	–	20–30 (28) 12.9%	–	30–40 (38)
Infundibulum length	–	65–85 (77) 8.7% (n = 10)	–	70–80 (78) 6.5% (n = 4)	–	90–110 (104)
Uterus length (UtL)	–	270–880 (460) 31.2%	–	270–1000 (575) 45.4%	–	800–980 (874)
UtL/BL (%)	–	11.2–23.2 (15.5) 22.7%	–	11.3–21.1 (14.8) 22.2%	–	15–19 (17)
Tail length	–	20–35 (28) 16.7% (n = 7)	–	22–45 (34) 25.4% (n = 9)	–	20–25 (23)
Egg number	–	3–24 (9) 61.1%	–	3–12 (7) 42.4%	–	24–43

†distance from apex. ‡distance from posterior extremity.

3 diverging in "V" proximally. Very short common trunk of rays 4–6, with rays 3 and 6 diverging at same level. Rays 4 and 5 diverging last. All rays reach bursal margin. Distance between papillae 2 and 3 slightly larger than that between papillae 5 and 6. Papillae 3, 4, and 5 approximately equidistant from each other. Rays 2 thickest and 6 thinnest. Dorsal lobe well developed, displaced to the left, compensating the reduced size of left lobe. Dorsal ray very long, divided at about its distal quarter into two branches, each one bifurcated distally into two papillae, external rays 9 and internal rays 10. Arising and path of rays 8 markedly dissymmetrical (Fig. 1F). Left ray 8 arising proximally from dorsal ray, nearly at its base; then running close and parallel to left trunk, approaching to and ending near left papilla 6. Right ray 8 arising more distally on dorsal ray, at about its proximal quarter, running between right trunk and dorsal ray, then heading distally towards right ray 6 but ending far from it. Genital cone long, well developed, bulbous at base, strongly curved ventrally in distal part. Distal half of cone with sclerotised walls. Dorsal lip bearing two rounded conspicuous papillae 7; ventral lip with single lappet-shaped papilla 0 (Fig. 1G). Gubernaculum conspicuous. Spicules thin and alate, ending in single sharp tip.

***Females*.** Measurements in Table 4. Reproductive tract monodelphic. Uterus less than 20% of body length; eggs few (3–9). Infundibulum slightly longer than vestibule. Posterior extremity straight or barely curved. Slight cuticular inflation from level of distal uterus up to vulvar aperture. Tail short and stout, ending in mucron (Figs 2A, B). Posterior end moderately retractile.

Voucher material examined. Argentina • 2 ♂♂, 2 ♀♀; Buenos Aires Province, Balcarce; 1977–1978; Sutton leg.; *Akodon azarae*; MLP-He 0674-1 • 3 ♂♂; same collection data as for preceding; MLP-He 0675-1 • 1 ♂, 1 ♀; same collection data as for preceding; MLP-He 0676-1 • 5 ♂♂, 6 ♀♀; same collection data as for preceding; MLP-He 0683-1 • 3 ♂♂, 4 ♀♀; same collection data as for preceding; MLP 0686-1.

Prevalence and mean intensity. P=100% (n=6), MI=42.8 (range 5–187) (Table 1).

Remarks. Worms of the type series showed strong contraction and curvature of the anterior body (Fig. 2C). Indeed, the body portion between the cephalic vesicle and the oesophageal-intestinal junction often appeared considerably wrinkled, hindering measurements of soft organs in this region (Table 4). On the contrary, the posterior body was relaxed, stretched, and easily accessible for measurements. The scarcity of material led us to include additional specimens from other *A. azarae* hosts collected in the same sampling event. We examined a total of five complete helminth sets, all of which were composed of worms assignable to *S. azarai*. Among these, we selected worms with relaxed and stretched anterior ends (Fig. 2D) to take measurements of the proximal part.

Specimens identified as *Stilestrongylus oryzomysi* Sutton & Durette-Desset, 1991

Fig. 2, Table 4

Considerations on the type host species. The rodent with field number 1914, designated as the type host of *S. oryzomysi* and *T. lenti* by Sutton and Durette-Desset (1991), was originally attributed to "*Oryzomys flavescens*" (current name= *Oligoryzomys flavescens*). After re-examination of the voucher (now designated as symbiotype) in MLP-Mz (accession N° 3076), it was found to belong to *A. azarae* (Table 2, Fig. 3). Therefore, *A. azarae* is the actual type host species of *S. oryzomysi*.

Examination of the type series. *Head*. Observed in one female paratype. Identical to that illustrated by Sutton and Durette-Desset (1991).

***Synlophe*.** Based on one female paratype. With 25 subequal ridges, regularly spaced, mostly oriented from right-ventral to left-dorsal quadrant, with axis of orientation inclined at about 60° to sagittal axis. Right-ventral ridges smallest (Fig. 2E).

***Males*.** Proximal part of body loosely coiled. Genital cone long, well developed, strongly curved ventrally in distal part. Distal half of cone with sclerotised walls. Dorsal lip bearing two papillae 7; ventral papilla 0 not observed. Gubernaculum conspicuous. Spicules thin and alate, ending in single sharp tip (Fig. 2F).

***Females*.** Body varying from loosely coiled in 2–3 irregular spirals to tightly coiled in up to 5 spirals. Monodelphic. Uterus less than 20% of body length; eggs few (3–9). Infundibulum longer than vestibule. Posterior extremity mostly straight, sometimes slightly curved ventrally. Cuticular inflation present from level of ovejector up to vulvar aperture. Posterior end retractile into inflation, never completely invaginated. Tail short and stout, ending in mucron (Fig. 2H, I).

Remarks. The worms in the type series of *S. oryzomysi* were relaxed and stretched, and diaphonisation was unnecessary for taking measurements. However, the males showed excessive flattening of the body, hindering the study of the bursa. Additional worms had to be included from the same sampling event due to material scarcity. We examined the complete helminth sets recovered from two *O. flavescens*, two *O. nigripes*, and five *A. azarae*. None of the *Oligoryzomys* spp. harboured worms assignable to *S. oryzomysi*. Instead, they were parasitised by *S. flavescens* (P=100%, MI=34.2) and to a lesser degree, by *Stilestrongylus lanfrediae* Souza, Digiani, Simões, Rodrigues-Silva & Maldonado, 2009 (Table 2). On the other hand, specimens of *A. azarae* were consistently parasitised by worms assignable to *S. azarai* (P=100%, MI=43) (Fig. 2G). Both *A. azarae* and *Oligoryzomys* spp. were also parasitised by nippostrongylines of other genera: two *A. azarae* specimens harboured *T. lenti*, and all *Oligoryzomys* spp. harboured *G. zeta* (P=100%, MI=3.7) (Table 2).

Voucher material examined. Argentina • 11 ♂♂, 10 ♀♀; Buenos Aires Province, Campana, National Route 12 (RN12) Km 100–101; [34°00'27.432"S, 58°58'29.28"W]; Apr. 1989; Sutton leg.; *Akodon azarae*, MLP-Mz 3074; MLP-He 1911-1 • 3 ♂♂; same collection data as for preceding; MLP-Mz 3079; MLP-He 1940-1.

Genus *Guerrerostrongylus* Sutton & Durette-Desset, 1991

Fig. 4, Table 5

Guerrerostrongylus zeta (Travassos, 1937)
Longistriata zeta Travassos, 1937
Hassalstrongylus zeta (Travassos, 1937): Durette-Desset, 1971
Guerrerostrongylus zeta (Travassos, 1937): Sutton & Durette-Desset, 1991

Main diagnostic characters. Body large to very large (males 4.20–8.40, females 5–13.7 mm), uncoiled or coiled irregularly; cephalic vesicle relatively short and stout. Synlophe with numerous (>35) continuous, subequal ridges, oriented from right to left (right, dorsal, and ventral ridges) or perpendicular to body surface (left ridges). Males: 37 to 44 ridges, caudal bursa subsymmetrical, elliptical to rectangular, pattern 2-2-1 tending to 1-3-1, dorsal lobe well developed; rays 6 longest, arising at same level as rays 2; rays 8 arising at proximal 1/4 or

Table 5. Comparison of measurements of *G. zeta* from different sources (including types of *Guerrerostrongylus uruguayensis*). Measurements are in micrometres except otherwise stated.

	Travassos 1937 (description)		Digiani et al. 2012 (redescription, on voucher material)		Simões et al. 2012a (redescription, on syntypes and voucher material)		Werk et al. 2016 (new locality records)		This work	
	♂ (n = ?)	♀ (n = ?)	♂ (n = 23)	♀ (n = 27)	♂ (n = 10)	♀ (n = 10)	♂ (n = 10)	♀ (n = 10)	♂ (n = 22)	♀ (n = 21)
N° of ridges at midbody	?	?	40–44 (n = 4)	35–48 (n = 7)	37 (syntypes, n = 1) 36–42 (vouchers, n = 2)	53 (syntypes, n = 1) 38–42 (vouchers, n = 2)	40–46 (n not specified)		38–53 (n = 4)	40–50 (n = 4)
Body length (mm) (BL)	6400	6800–7300	4.4–8.4 (6.75)	5.5–13.7 (9.17)	4.28–6.90 (5.2)	5.06–12.67 (8.41)	6.6–10.7 (8.5)	10.2–17.9 (14.5)	4.35–8.9 (7.0) 18.3%	4.95–14.9 (9.47) 21.8%
Body width	150	140–150	140–290 (197)	100–290 (197)	80–180	100–320	83–157	157–230	90–250 (176) 24.6%	200–350 (247) 16.1%
Cephalic vesicle length	45–52	45–52	35–70 (56)	35–65 (55)	43–70	40–74	55–64	46–64	40–60 (50) 12.2%	40–70 (49) 17.8%
Cephalic vesicle width	–	32–40 (36)	30–60 (44)	35–60 (43)	20–56	36–67	46–55	46–64	30–70 (47) 23.4%	30–55 (41) 19.6%
Oesophagus length (OeL)	340–470	340–470	345–495 (401)	350–500 (411)	340–716	260–390	369–498	500–672	315–375(348) 8.2% (n = 5)	330–430 (383) 9.9% (n = 6)
Nerve ring†	–	–	190–295 (234)	130–285 (169)	70–233	100–250	182–314	434	120–145 (132) 9.6% (n = 3)	135–210 (178) 21.8% (n = 3)
Excretory pore† (EP)	200	200	250–345 (305))	345–380	229–633	221–402	323–425	455,470	185–225 (203) 9.9% (n = 3)	205–270 (237) 13.7% (n = 3)
EP/OeL (%)	–	–	66–84	75–81 (n = 12)	–	58.8–73.9 (66.1) (n = 5)	–	–	–	58.7–77.1 (66) 14.8% (n = 3)
Deirids†	–	–	250–380 (315)	235–275 (253)	235–327 (267) (n = 4)	200–268 (233) (n = 3)	–	–	230 (n = 1)	330 (n = 1)
Spicule length (SpL)	877	–	750–1420 (1115)	–	580–1160	–	800–1300	–	810–1130 (963) 10.7%	–
SpL/BL (%)	13.7	–	10.6–24.4 (15.5)	–	–	–		–	11.8–18.6 (15) 14.9%	–
Vulva‡	–	112–135	–	112–255 (176)	–	105–233	–	157–277	–	105–145 (130) 10.9% (n = 6)
Uterus length (UtL)	–	–	–	800–1560 (1230)	–	1350–2540	–	–	–	1400–1950 (1622) 14.1%
UtL/BL (%)	–	–	–	9.5–22.4 (16.1)	–	–	–		–	15.4–21.9 (19.2) 11.8% (n = 6)
Tail length	–	43–45	–	40–100 (70)	–	43–97	–	42–61	–	35–60 (49) 18.7% (n = 6)
Egg number	–	–	–	6–50 (28)	–	–	–	>50	–	41–130 (80) 40.1% (n = 6)

†distance from apex. ‡distance from posterior extremity.

1/3 of dorsal trunk. Genital cone moderately developed, telamon V-shaped, spicules long and thin with undulating or winding pattern. Females: 35 to 53 ridges; vestibule as long as infundibulum; uterus ca. 20% of body length; eggs numerous. Posterior extremity straight; tail conical, not retractile. Tail length about 1/3 of distance from vulva to posterior extremity (from Travassos 1937; Digiani et al. 2012; Simões et al. 2012a).

Specimens identified as *Guerrerostrongylus uruguayensis* Sutton & Durette-Desset, 1991

Fig. 4, Table 5

Considerations on the type host species. The rodent with field number 2046, designated as type host of *G. uruguayensis* and *Stilestrongylus flavescens* by Sutton and Durette-Desset (1991), was originally attributed to

Figure 3. *Akodon azarae* MLP-Mz 3076 (field number 1914), symbiotype of *Stilestrongylus oryzomysi* and *Trichofreitasia lenti*.

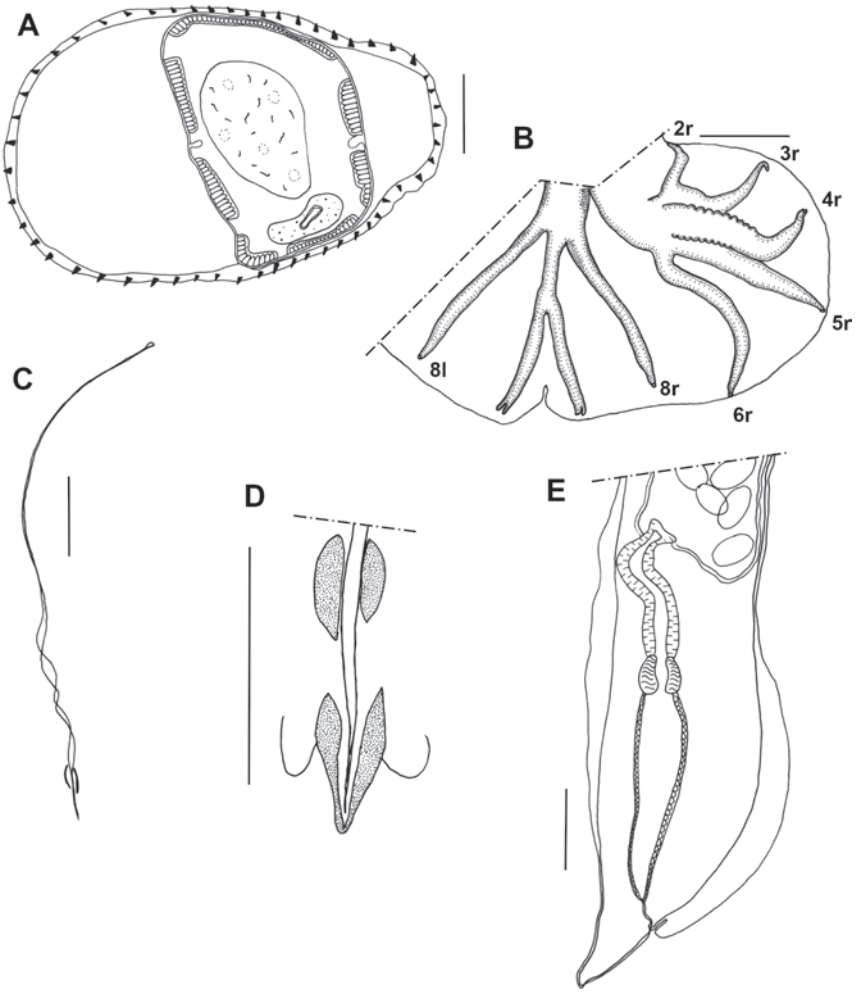

Figure 4. *Guerrerostrongylus zeta*. **A.** Male synlophe in transverse section at midbody; **B.** Male caudal bursa, dorsal view (left lobe omitted); **C.** Spicules, ventral view; **D.** Gubernaculum and genital cone, ventral view; **E.** Female, posterior end, right lateral view. **8l** - left ray 8; **2r-6r** - right bursal rays 2 to 6; **8r** - right ray 8. Scale bars: 50 μm (**A, D**); 100 μm (**B, C, E**). **A, B, D, E** from specimens of *Oligoryzomys nigripes* from Bella Unión. **C** from a paratype of *G. uruguayensis*.

"*Oryzomys flavescens*" (current name= *Oligoryzomys flavescens*). Unfortunately, its specific identity could not be established because no voucher was found in MLP-Mz or in other zoological collections. A symbiotype for these species is therefore lacking.

Examination of the type series. Most of the internal characters of the specimens could not be observed or measured because of their opaque bodies, even after using strong clearing agents. The low number of material prompted us to include more specimens from the same sampling event, and as a result, 16 complete helminth sets from hosts assigned to *Oligoryzomys* spp. were examined. All of them harboured several specimens of *Guerrerostrongylus* sp., which could be studied and measured.

General. Worms large to very large, uncoiled.

Head. Cephalic vesicle short and stout. Apical structures hardly visible. Oral aperture large, triangular, with rounded corners, and surrounded by thick ring. Four externo-labial papillae (dorsal and ventral) observed in one female.

Synlophe. Based on four males and four females. With 38–53 ridges in males (Fig. 4A), 40–50 in females. Ridges continuous, subequal, oriented from right to left (right, dorsal, and ventral ridges), or perpendicular to body surface (left ridges). Two prominent lateral cuticular dilatations, left larger than right one. Synlophe identical to those described by Digiani et al. (2012, figs 3, 4) and (Simões et al. 2012a, figs 4, 5) for *G. zeta*.

Males. Large to very large, uncoiled or coiled irregularly. Bursa subsymmetrical, elliptical, with pattern 2-2-1 tending to 1-3-1. Rays 6 longest, arising at same level as rays 2; rays 8 arising at proximal 1/4 of dorsal trunk. Some specimens show serrated ornamentation on margins of rays 4 or 4–5 and/or thickened bases of dorsal ray and rays 8 (Fig. 4B). Spicules long and thin with undulating pattern (Fig. 4C). Genital cone moderately developed, telamon V-shaped (Fig. 4D).

Females. Large to very large; vestibule as long as infundibulum; uterus ca. 20% of body length; eggs numerous. Posterior extremity straight; tail conical, not retractile. Tail length about 1/3 of distance from vulva to posterior extremity (Fig. 4E).

Voucher material examined. URUGUAY • 1 ♂, 2 ♀♀; Artigas Department, Bella Unión, Colonia España; [30°21'52"S, 57°38'34"W]; Jul. 1989; Sutton leg.; *Oligoryzomys nigripes*, MLP-Mz 3080; MLP He-2047-1 • 3 ♂♂, 2 ♀♀; same data as for preceding; MLP-Mz 3084; MLP-He 2058-1 • 2 ♂♂, 2 ♀ ♀; same collection data as for preceding; "*Oryzomys*"; MLP-He 2056-1 • 4 ♂♂, 5 ♀♀; same data as for preceding; MLP-He 2057-1 • 6 ♂♂, 5 ♀♀; same data as for preceding; "colilargo"; MLP-He 2059-1 • 3 ♂♂, 1 ♀; same data as for preceding; *O. flavescens*, MLP-Mz 3086; MLP-He 2064-1.

Prevalence and mean intensity. P=100% (n=17), MI=19.8 (range 5–48) (Table 3).

Remarks. Some helminth sets from this sampling lacked the voucher host in the mammal collection. Only eight of them could be located, which corresponded to the helminth sets MLP-He 2047, 2049, 2052, 2058, and 2063 (*O. nigripes*); MLP-He 2048, 2064, and 2068 (*O. flavescens*) (Table 3). The hosts of the remaining helminth sets were a priori identified in the field and subsequently labelled as "*Oryzomys* sp." or "colilargo" (Table 3). Whether the identity of these hosts was further confirmed or not, they had helminth assemblages composed of *Guerrerostrongylus* spp. showing the features described above and of *S. flavescens* (P=94.1%, MI=21.2). One specimen identified as *O. flavescens* also harboured *Hassastrongylus hoineffae* (Durette-Desset, 1969). In addition, we examined six *A. azarae* from the same sampling event and found that they were parasitised by *S. azarai* (P=100%, MI=81.7), but not by any species of *Guerrerostrongylus* (Table 3).

Molecular study

Sequences of ITS+ were obtained from three specimens of *G. zeta* (970–973 bp) and one of *S. azarai* (950 bp) (Table 6).

After alignment with MUSCLE, we obtained 1056 positions, which were reduced to 910 using GBLOCKS. GTR+G was selected as the best-fit substitution model using MEGA and MRBAYES. The resulting trees show similar topology except for the position of *Nippostrongylus brasiliensis* (Travassos, 1914).

No genetic divergence is found between the sequences of *G. zeta* specimens (Table 7), which cluster together with *Hassalstrongylus* sp., forming a strongly supported monophyletic clade in both phylogenetic reconstructions (Figs 5, 6). In turn, a clade including these two species and *S. azarai* (South American nippostrongylines) was recovered in both phylogenetic analyses, though with lower support.

Discussion and conclusions

Taxonomic aspects

S. azarai / S. oryzomysi

We found no morphological differences among the type series of *S. oryzomysi*, the specimens of *S. azarai* harboured by *A. azarae* from the same sampling event, and the type series of *S. azarai*. The synlophe of a paratype of *S. oryzomysi* was identical to that of *S. azarai* in fig. IIc of Durette-Desset and Sutton (1985). Details of the ovejector and tail in the female and the bursa and genital cone in the male were identical in both type series. Therefore, we propose to consider the relative distances between papillae 2, 3, and 4 of the right lobe, the pathway of rays 8, and the appearance of the papillae on the genital cone as diagnostic characters of *S. azarai*. Moreover, the cephalic structures and arrangements observed by Sutton and Durette-Desset (1991) in worms from the locality of Campana were also observed in voucher specimens of *S. azarai*.

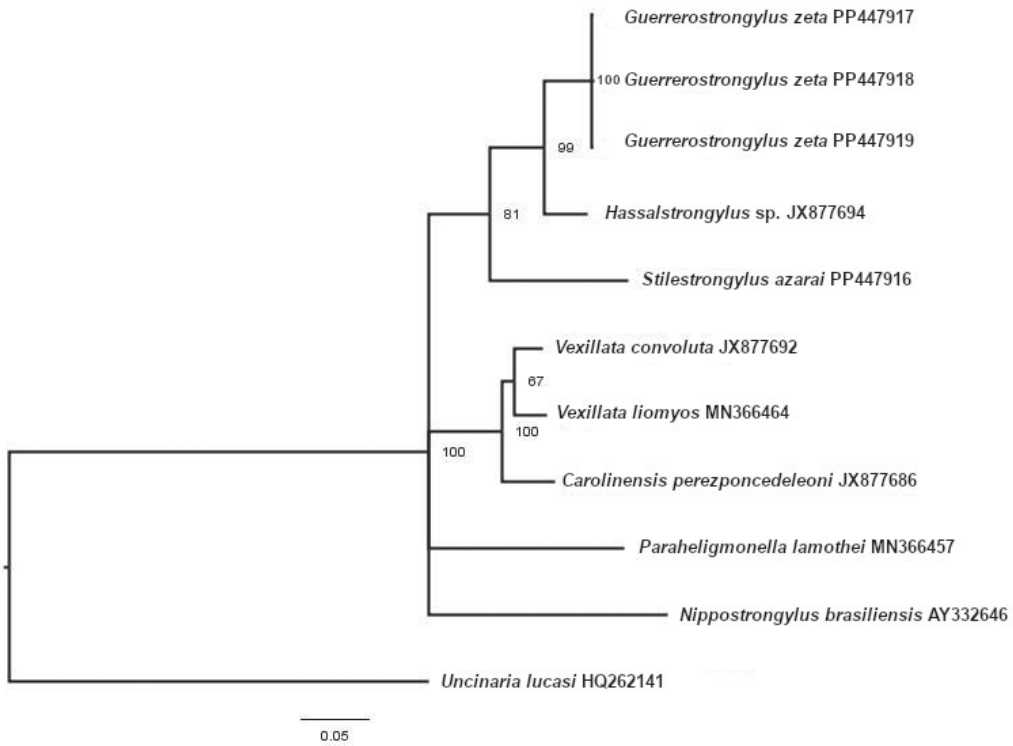

Figure 5. Phylogram resulting from Bayesian inference. The values next to the nodes are posterior probabilities (%). The scale bar represents the number of substitutions per site.

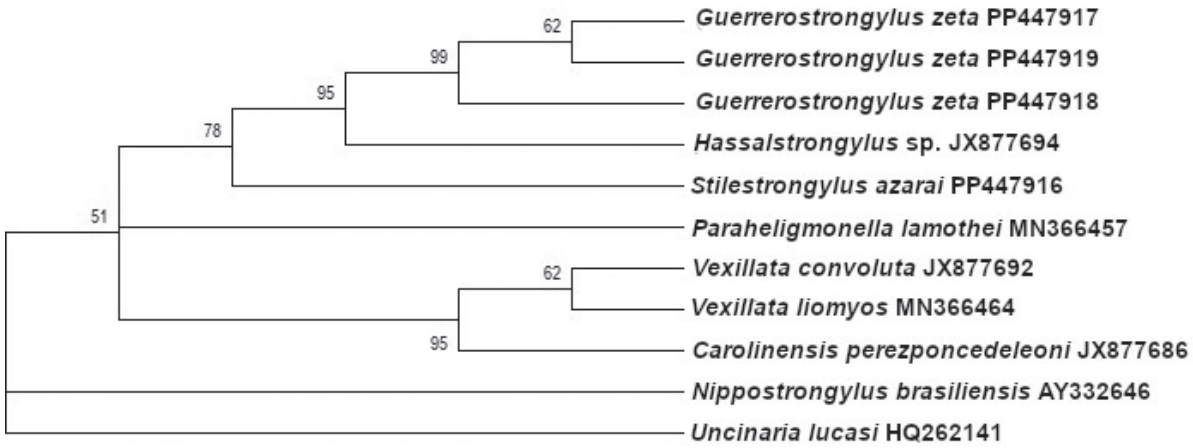

Figure 6. Maximum likelihood bootstrap consensus tree. Values next to the nodes are bootstrap proportions (%).

In regard to morphometry, most of the body length values obtained by us for *S. oryzomysi* were lower than those reported by Sutton and Durette-Desset (1991) (Table 4). *Stilestrongylus oryzomysi* was differentiated from *S. azarai* by the more distal position of the excretory pore (72–74% of the oesophagus length vs. 41–51%) and by the more developed genital cone (90 × 36 μm vs. 80 × 40 μm) (Sutton and Durette-Desset 1991). These characters are of poor diagnostic value in the Trichostrongylina, in which morphometric characters of soft organs may vary even within individual hosts (Durette-Desset et al. 2017). It should be kept in mind that the only measurements reported for both *S. azarai* and *S. oryzomysi* were taken from their holotypes and allotypes, probably accounting for their metric discrepancies. Moreover, the measurements of the anterior organs provided in the original description of *S. azarai* were most likely underestimated because the specimens of the type series were wrinkled. Digiani & Durette-Desset (2003c) also found differences between *S. azarai* specimens parasitising *Graomys griseoflavus* (Waterhouse) from San Luis province, Argentina, and those described in the original description (i.e., larger body measurements, a more distal position of the nerve ring and excretory pore, a larger number of eggs in the uterus) (see Table 4). Notwithstanding these metric discrepancies, the worms from San Luis unequivocally exhibited the diagnostic characters of *S. azarai*. Arc-like structures connecting the cephalic papillae were also present in the helminths of *G. griseoflavus* (figs 26, 33–35 of Digiani and Durette-Desset 2003c).

Table 6. Nematode family and species, host species, collection locality, and GenBank accession number for sequences of ITS+ rDNA used for phylogenetic analysis. In bold, the sequences obtained in this work.

Family	Species	Host	Locality	Accession number
Heligmonellidae	***S. azarai***	***A. azarae***	**Berisso, Buenos Aires province, Argentina**	**PP447916**
	***G. zeta* (1)**	***O. nigripes***	**Campo San Juan, Misiones province, Argentina**	**PP447917**
	***G. zeta* (2)**	***O. nigripes***	**Campo San Juan, Misiones province, Argentina**	**PP447918**
	***G. zeta* (3)**	***O. nigripes***	**Campo San Juan, Misiones province, Argentina**	**PP447919**
	Hassalstrongylus sp.	*Calomys* sp.	Santa Bárbara, Jujuy province, Argentina	JX877694
	Nippostrongylus brasiliensis	Rodents	Brest, France	AY332646
	Carolinensis perezponcedeleoni	*Nyctomys sumichrasti*	Catemaco, Veracruz, Mexico	JX877686
	Paraheligmonella lamothei	*Sylvilagus floridanus*	Chiapas, Mexico	MN366457
Ornithostrongylidae	*Vexillata liomyos*	*Liomys pictus*	Jalisco, Mexico	MN366464
	Vexillata convoluta	*Cratogeomys merriami*	Morelos, Mexico	JX877692
Ancylostomatidae	*Uncinaria lucasi*	*Eumetopias jubatus*	Hazy Island, Southeast AK, USA	HQ262141

Table 7. Genetic divergence among species of Heligmonellidae, estimated through the uncorrected p-distance of the ITS+ rDNA region.

		1	2	3	4	5	6	7	8	9	10	11
1	*Uncinaria lucasi* (outgroup)											
2	*S. azarai*	0.30										
3	*G. zeta* (specimen 1)	0.28	0.13									
4	*G. zeta* (specimen 2)	0.28	0.13	0.00								
5	*G. zeta* (specimen 3)	0.28	0.13	0.00	0.00							
6	*Hassalstrongylus* sp.	0.30	0.13	0.06	0.06	0.06						
7	*Vexillata convoluta*	0.28	0.16	0.14	0.14	0.14	0.14					
8	*Vexillata liomyos*	0.29	0.16	0.15	0.15	0.15	0.14	0.04				
9	*Carolinensis perezponcedeleoni*	0.30	0.16	0.14	0.14	0.14	0.15	0.05	0.06			
10	*Paraheligmonella lamothei*	0.31	0.18	0.17	0.17	0.17	0.17	0.16	0.17	0.17		
11	*Nippostrongylus brasiliensis*	0.33	0.22	0.27	0.27	0.27	0.24	0.21	0.19	0.20	0.24	

In conclusion, both type series appear to be morphologically identical, and after reassigning the symbiotype of *S. oryzomysi* (MLP-Mz 3076) to *A. azarae*, here we propose *S. oryzomysi* as a junior synonym of *Stilestrongylus azarai*.

Stilestrongylus oryzomysi was possibly regarded as a new species because it was described from a host mislabelled as *Oligoryzomys* spp. This assumption is based on the fact that *Oligoryzomys* spp. can be easily distinguished from *A. azarae*, even by non-experts. We believe that this labelling mistake would have been noticed if more hosts from the same sampling were examined at the time of describing the species.

Additionally, since the rodent MLP-Mz 3076 was also the symbiotype of *Trichofreitasia lenti* (Sutton and Durette-Desset 1991), it should be reassigned from *O. flavescens* to *A. azarae*.

G. zeta / *G. uruguayensis*

We found no morphological or metric differences among the type specimens of *G. uruguayensis*, the specimens of *Guerrerostrongylus* harboured by the remaining colilargos from the same sampling, and the specimens of *G. zeta* redescribed by Digiani et al. (2012) and Simões et al. (2012a). Diagnostic characters of *G. zeta*, such as the proportions of the cephalic vesicle, ray pattern of the bursa, details of the genital cone, telamon, and spicules, were observed in all the worms examined from the colilargos from Uruguay. In regard to morphometry, *G. uruguayensis* was differentiated from *G. zeta* by its larger body size. However, the description of *G. uruguayensis* was based only on the holotype and allotype, and it did not account for morphological or morphometric variability. On the other hand, our body length values obtained from the holotype and allotype were lower than those reported by Sutton and Durette-Desset (1991). Additionally, *G. uruguayensis* was differentiated from *G. zeta* by a widening of the body just anterior to the tail in the female; by bursal rays 6 longer than rays 8; by rays 8 arising from the base of the dorsal ray; and by the presence of cuticular ornamentation on rays 4 and 5 in the male (Sutton and Durette-Desset 1991). In females, body size is often related to age and the posterior widening to reproductive status, as gravid specimens bearing numerous eggs in the uterus usually have a widened pre-vulvar region. On the other hand, the bursal characters argued as diagnostic for *G. uruguayensis* are ambiguous and dependent on the degree of spreading of the bursa, or unspecific and subjected to individual variation. The following characters should be dismissed as diagnostic for *G. uruguayensis*: 1) rays 8 arising from the base of the dorsal ray, because all the specimens examined clearly showed a proximal common trunk to rays 8 and the dorsal ray; 2) rays 6 longer

than rays 8, because in the original description of *L. zeta* Travassos (1937) pointed out that rays 6 were the longest; 3) cuticular ornamentation on rays 4 and 5, because it was mostly absent and could be seen on the margins of rays 4 and 5 only in a few males. In addition, males with and without ornamentation coexisted in the same infrapopulation, suggesting that it may be a polymorphic trait or an artefact of fixation.

In conclusion, the comparison of the type series of *G. uruguayensis* against other specimens of *Guerrerostrongylus* from the same sampling event and against all available descriptions of *G. zeta* reported so far confirms that the worms examined herein parasitising *Oligoryzomys* spp. from Uruguay belong to *G. zeta*. This species was originally described as *Longistriata zeta* by Travassos (1937), then transferred to *Hassalstrongylus* by Durette-Desset (1971), and finally to *Guerrerostrongylus* by Sutton and Durette-Desset (1991). The identification of *G. uruguayensis* as a distinct species from that described by Travassos was likely due to the fact that both original descriptions were based on very few specimens, leading to the overestimation of metric differences and morphological variations without specific value. In addition, the description of *G. uruguayensis* was published in 1991, while the synlophe of *G. zeta* remained undescribed until many years later. Further redescriptions of *G. zeta* (Digiani et al. 2012; Simões et al. 2012a) based on paratypes and, especially, on larger sets of voucher specimens provided the description of the synlophe and a range of metric variability broad enough to include Travassos' specimens and the type material of *G. uruguayensis*. Consequently, *G. uruguayensis* is proposed as a junior synonym of *G. zeta*.

The rodent with field number 2046, consigned "*Oryzomys flavescens*" by Sutton and Durette-Desset (1991), is also the type host of *Stilestrongylus flavescens*. Due to the absence of a voucher, the identity of this rodent could not be ratified or rectified (see Table 3), and therefore it must follow the one designated in the original description. Then, the type host species of *S. flavescens* is, according to the current nomenclature, *Oligoryzomys flavescens* (= *Oryzomys flavescens*).

Host range and geographic distribution

The examination of the material has afforded an opportunity to clarify the taxonomic status of two of the examined nippostrongyline species as well as to shed light on the host spectrum and geographic distribution of some others. According to Sutton and Durette-Desset (1991), *O. flavescens* harboured *S. oryzomysi* and *T. lenti* in Argentina, and *S. flavescens* and *G. uruguayensis* in Uruguay. After examining numerous helminth sets, we found not only that this rodent harboured the same nippostrongyline assemblage on both sides of the Uruguay River but also that it was shared with *O. nigripes*. On the other hand, *A. azarae*, which is present in the same sampling localities as above, was strongly parasitised by *S. azarai* and, at least on the Argentinean side and to a lesser degree, by *T. lenti* (see Results and Tables 1, 2). Thus, this study extends the distribution range of *S. azarai* to include Uruguay and reports a new host record for *T. lenti* (*A. azarae*, type host species), a new host record for *G. zeta* in Argentina (*O. flavescens*), and the first record of helminths for *O. nigripes* in Uruguay.

***Stilestrongylus azarai*.** This species seems to be the main component of the helminth community of *A. azarae*. It has been found in most of the rodent's geographic distribution, which ranges from southern Brazil and eastern Paraguay south through Uruguay and central Argentina (Pardiñas et al. 2015). Up to the present, *S. azarai* has been recorded in the Argentinean provinces of Formosa, Chaco, Santa Fe, Entre Ríos, Corrientes, and Buenos Aires, and in Uruguay (Durette-Desset and Sutton 1985; Navone et al. 2009; Miño et al. 2012, 2019; Serrano 2024; this work). It has been rarely found in other hosts, always with relatively low prevalences and intensities of infection, e.g., in *Oligoryzomys fornesi* (Massoia) (P=14%, IM=4, n=7) and *Calomys callosus* (Rengger) (P=33%, IM=1, n=3) both from Chaco province (Serrano 2024). Four out of five *Reithrodon auritus* (Desmarest) from Balcarce (helminth sets housed in the MLP-He) harboured a few *S. azarai* specimens coparasitic with *Stilestrongylus aureus* Durette-Desset & Sutton, 1985 (Digiani pers. obs.). The three latter records were obtained from localities where the respective hosts live in sympatry with *A. azarae*, which is clearly the main host. *Stilestrongylus azarai* was also reported in *Graomys griseoflavus* from San Luis province (P=27.8%, and IM= 16.2, n=18), mainly coparasitic with a species of *Hassalstrongylus* (Digiani and Durette-Desset 2003c). To our knowledge, no other species of *Akodon* have been reported to harbour *S. azarai*. It would be interesting to investigate the role of *Akodon dolores* Thomas as the main host of this parasite in San Luis Province, where it is the only *Akodon* species present (Pardiñas et al. 2015).

On the other hand, *A. azarae* specimens have been rarely found harbouring heligmonellid species other than *S. azarai*, with the exception of *T. lenti*. In Corrientes province, this rodent was reported to be parasitised by *Stilestrongylus stilesi* Freitas, Lent & Almeida, 1937 (P=57%, Gómez-Muñoz et al. 2020) and *Hassalstrongylus dollfusi* (Díaz Ungría, 1963) (P=3.6%, Serrano et al. 2021), neither of which were coparasitic with *S. azarai*.

***Trichofreitasia lenti*.** Although it was not found in the Uruguayan sample, several helminth sets still remain unexamined. Moreover, its presence in Uruguay is expected given the fact that this species has already been reported from different *Akodon* species in Argentina and Brazil (Digiani et al. 2007; Simões et al. 2011, 2012b; Panisse et al. 2017; Cardoso et al. 2018; this work). In Brazil, *T. lenti* has been recorded in other host species, particularly *O. nigripes* (Simões et al. 2011, 2012b; Cardoso et al. 2019; Benatti et al. 2021), but these reports do not include either descriptions or illustrations and may deserve revision. In any case, none of the 22 samples of *Oligoryzomys*

spp. examined in the present survey contained *T. lenti*. Moreover, in another, more extensive survey, Serrano (2024) examined 179 *Oligoryzomys* spp. that were not parasitised by *T. lenti*.

***Guerrerostrongylus zeta*.** Numerous publications have confirmed that the main host of *G. zeta* is *O. nigripes* rather than its type host species, *Nectomys squamipes* (Brants). It was repeatedly reported parasitising *O. nigripes* from Argentina and Brazil (Pinto et al. 1982; Gomes et al. 2003; Simões et al. 2011, 2012a, 2012b; Digiani et al. 2012; Werk et al. 2016; Panisse et al. 2017; Cardoso et al. 2018, 2019; Boullosa et al. 2020; Kersul et al. 2020; Gentile et al. 2022). In Brazil, this species was also recorded in *O. flavescens* (Cardoso et al. 2018), *N. squamipes*, *Cerradomys subflavus* (Wagner), *Galea spixii* (Wagler) (Pinto et al. 1982), *Euryoryzomys russatus* (Wagner), *Akodon cursor* Winge, and *A. montensis* Thomas (Gomes et al. 2003; Simões et al. 2011; Boullosa et al. 2020; Kersul et al. 2020). However, these reports lack descriptions or illustrations. It is possible that at least the worm from *E. russatus* could belong to *Guerrerostrongylus ulysi* Digiani, Notarnicola & Navone, 2012, a species described from *Sooretamys angouya* (Fischer) in Misiones province, Argentina (Digiani et al. 2012) and later found in *E. russatus* in the same province by Panisse et al. (2017).

A special case involves females identified as *Guerrerostrongylus* sp. in *Akodon simulator* Thomas from Tucumán province (northwestern Argentina) (Digiani et al. 2007). These females showed the typical synlophe of *Guerrerostrongylus*, but their opacity precluded the observation of any diagnostic character and thus the identification at the species level. In turn, the males recovered from the same host were identified as *G. uruguayensis* before redescriptions and further reports of *G. zeta* from Argentina were available (Digiani et al. 2007). Although our results suggest that these males would belong to *G. zeta*, the information on their hosts is incomplete and uncertain. Therefore, newly collected material from a larger number of individually identifiable hosts is required for a more accurate identification of *Guerrerostrongylus* spp. associated with *A. simulator*.

Phylogenetic analysis

Despite the wide distribution of South American Nippostrongylinae (SAN) as parasites of sigmodontines, they remain poorly studied from a molecular approach, with only two studies involving molecular phylogenetic reconstructions. Scheibel et al. (2014) mainly focused on the nematode family Viannaiidae and solely included *Hassalstrongylus* sp. as a representative of SAN. Later, Weirich et al. (2016) used a fragment of the mitochondrial gene coding for the large ribosomal subunit RNA (rrnL) to analyse the phylogenetic position of *Guerrerostrongylus marginalis* (Weirich, Catzeflis & Jiménez, 2016), *Hassalstrongylus* sp., and *Stilestrongylus* sp., among other Trichostrongylina. In their phylogenetic tree, these species were clustered in a strongly supported monophyletic clade, though with greater genetic similarity between *Hassalstrongylus* sp. and *Stilestrongylus* sp. In the present study, we confirm, using a nuclear gene, the monophyly of the clade formed by *Stilestrongylus*, *Hassalstrongylus*, and *Guerrerostrongylus*, which are the three most speciose and widely distributed genera of SAN.

In the present study, we provide a significant amount of information on the taxonomy and geographic distribution of three nippostrongyline species obtained from the examination of several lots of material deposited in the Helminthological and Mammal Collections of the Museo de La Plata. Our findings confirm the importance of examining the largest possible number of specimens to describe new taxa and highlight the role of public biological collections as biodiversity repositories.

Acknowledgements

We are grateful to C. Damborenea and V.H. Merlo Alvarez from MLP-He and I. Olivares from MLP-Mz for facilitating access to collection material; to M. Ibañez Shimabukuro and M. Moncada from CEPAVE for molecular laboratory assistance; to M.M. Montes for helping with the phylogenetic analysis; to S. Pietrokovsky for the English revision; and to the three reviewers that helped to improve the first version of the manuscript. Special thanks are due to N. Cazzaniga for helping in the interpretation of the ICZN, to C. Galliari for helping in the identification of the voucher rodents, and to C. Lanzone and E. Soibelzon for providing the rodents harbouring the specimens used for molecular analysis. This research was supported by Agencia I+D+i, Argentina (grant PICT 2019-3535 to MCD) and CONICET, Argentina (grants PIP 2014-0429 and 2010-0006 to MCD). The authors declare that they have no conflict of interest.

References

Altschul SF, Gish W, Miller W, Myers EW, Lipman DJ (1990) Basic local alignment search tool. Journal of Molecular Biology 215: 403–410. https://doi.org/10.1016/S0022-2836(05)80360-2

Benatti D, Andrietti LF, Cândido Jr JF, Vogliotti A, Moraes MFD, Tebaldi JH, Hoppe EGL (2021) Rodent helminths in fragmented Atlantic Forest areas in the western region of the state of Paraná. Revista Brasileira de Parasitologia Veterinária 30: e009521. https://doi.org/10.1590/s1984-29612021058

Beveridge I, Spratt DM, Durette-Desset M-C (2014) Order Strongylida (Railliet & Henry, 1913). In: Schmidt-Rhaesa A (Ed.) Handbook of zoology. Gastrotricha, cycloneuralia and gnathifera. De Gruyter, Germany, 557–612. https://doi.org/10.1515/9783110274257.557

Boullosa RG, Cardoso TS, Costa-Neto SF, Teixeira BR, Freitas TPT, Maldonado Jr A, Gentile R (2020) Helminth community structure of three sigmodontine rodents in the Atlantic Forest, southern Brazil. Oecologia Australis 24: 577–589. https://doi.org/10.4257/oeco.2020.2403.04

Bush AO, Lafferty KD, Lotz JM, Shostak AW (1997) Parasitology meets ecology on its own terms: Margolis et al. revisited. Journal of Parasitology 83: 575–583. https://doi.org/10.2307/3284227

Cardoso TS, Braga CAC, Macabu CE, Simões RO, Costa-Neto SF, Maldonado Jr A, Gentile R, Luque JL (2018) Helminth metacommunity structure of wild rodents in a preserved area of the Atlantic Forest, Southeast Brazil. Revista Brasileira de Parasitologia Veterinária 27: 495–504. https://doi.org/10.1590/s1984-296120180066

Cardoso TS, Macabu CE, Simões RO, Maldonado Jr A, Luque JL, Gentile R (2019) Helminth community structure of two sigmodontine rodents in Serra dos Órgãos National Park, state of Rio de Janeiro, Brazil. Oecologia Australis 23: 301–314. https://doi.org/10.4257/oeco.2019.2302.09

Casiraghi M, Anderson TJC, Bandi C, Bazzocchi C, Genchi C (2001) A phylogenetic analysis of filarial nematodes: comparison with the phylogeny of *Wolbachia* endosymbionts. Parasitology 122: 93–103. https://doi.org/10.1017/S0031182000007149

Castresana J (2000) Selection of Conserved Blocks from Multiple Alignments for Their Use in Phylogenetic Analysis. Molecular Biology and Evolution 17: 540–552. https://doi.org/10.1093/oxfordjournals.molbev.a026334

D'Elía G, Pardiñas U (2015) Subfamily Sigmodontinae Wagner, 1843. In: Patton J, Pardiñas U, D'Elía G (Eds), Mammals of South America Volume 2 Rodents. The University of Chicago Press, 63–685.

Darriba D, Taboada GL, Doallo R, Posada D (2012) jModelTest 2: more models, new heuristics and parallel computing. Nature methods 9: 772–772. https://doi.org/10.1038/nmeth.2109

Digiani MC, Durette-Desset M-C (2003a) *Suttonema delta* n. g., n. sp. (Nematoda: Trichostrongylina: Heligmosomoidea) from *Oxymycterus rufus* (Rodentia: Sigmodontinae) in Argentina. Systematic Parasitology 55: 33–38. https://doi.org/10.1023/A:1023993426975

Digiani MC, Durette-Desset M-C (2003b) Two new species of Nippostrongylinae (Nematoda, Heligmosomoidea, Heligmonellidae) from a sigmodontine rodent in Argentina. Acta Parasitologica 48: 12–18.

Digiani MC, Durette-Desset M-C (2003c) Two new species of Nippostrongylinae (Nematoda: Trichostrongylina: Heligmonellidae) from the grey leaf-eared mouse *Graomys griseoflavus* (Sigmodontinae) in Argentina. Parasite 10: 21–29. https://doi.org/10.1051/parasite/2003101p21

Digiani MC, Kinsella JM (2014) A new genus and species of Heligmonellidae (Nematoda: Trichostrongylina) parasitic in *Delomys dorsalis* (Rodentia: Sigmodontinae) from Misiones, Argentina. Folia Parasitologica 61: 473–478. https://doi.org/10.14411/fp.2014.043

Digiani MC, Sutton CA, Durette-Desset M-C (2003) A new genus of Nippostrongylinae (Nematoda: Heligmonellidae) from the water rat *Scapteromys aquaticus* (Sigmodontinae) in Argentina. Journal of Parasitology 89: 124–132. https://doi.org/10.1645/0022-3395(2003)089[0124:ANGONN]2.0.CO;2

Digiani MC, Navone GT, Durette-Desset M-C (2007) The systematic position of some nippostrongyline nematodes (Trichostrongylina: Heligmosomoidea) parasitic in Argentinean sigmodontine rodents. Systematic Parasitology 67: 87–92. https://doi.org/10.1007/s11230-006-9071-5

Digiani MC, Notarnicola J, Navone GT (2012) The genus *Guerrerostrongylus* (Nematoda: Heligmonellidae) in cricetid rodents from the Atlantic rain forest of Misiones, Argentina: emended description of *Guerrerostrongylus zetta* (Travassos, 1937) and description of a new species. Journal of Parasitology 98: 985–991. https://doi.org/10.1645/GE-3075.1

Digiani MC, Serrano PC, Knoff M, Cazzaniga NJ (2024) The correct original spelling of the specific name of *Guerrerostrongylus zeta* (Travassos, 1937) (Nematoda, Heligmonellidae), parasitic in South American rodents. Systematic Parasitology 101: 59. https://doi.org/10.1007/s11230-024-10180-1

Durette-Desset M-C (1971) Essai de classification des Nématodes Héligmosomes. Corrélation avec la paléobiogéographie des hôtes. Mémoires du Muséum national d'Histoire naturelle 49: 1–126.

Durette-Desset M-C, Sutton CA (1985) Contribución al conocimiento de la fauna parasitológica argentina X, Nematodes (Trichostrongyloidea) en *Akodon azarae azarae* (Fischer) y *Reithrodon auritus* Fischer. Revista del Museo de La Plata 14: 21–33.

Durette-Desset M-C, Digiani MC, Kilani M, Geffard-Kuriyama D (2017) Critical revision of the Heligmonellidae (Nematoda: Trichostrongylina: Heligmosomoidea). Mémoires du Muséum national d'Histoire naturelle, Paris, 290 pp.

Folmer O, Black M, Hoeh W, Lutz R, Vrijenhoek R (1994) DNA primers for amplification of mitochondrial cytochrome c oxidase subunit I from diverse metazoan invertebrates. Molecular Marine Biology and Biotechnology 3: 294–299.

Gentile R, Costa-Neto SF, Cardoso TS, Boullosa R, Macabu CE, Simões RO, Maldonado Jr A (2022) Helminths of small mammals in an Atlantic Forest biological station in Rio de Janeiro, Brazil. Neotropical Helminthology 16: 161–172.

Gomes DC, Cruz RP, Vicente JJ, Pinto RM (2003) Nematode parasites of marsupials and small rodents from the Brazilian Atlantic Forest in the State of Rio de Janeiro, Brazil. Revista Brasileira de Zoologia 20: 699–707. https://doi.org/10.1590/S0101-81752003000400024

Gómez-Muñoz MÁ, Robles MDR, Milano MF, Digiani MC, Notarnicola J, Galliari C, Navone GT (2020) Helminths from Sigmodontinae rodents (Muroidea: Cricetidae) in Humid Chaco ecoregion (Argentina): a list of species, host and geographical distribution. Revista Mexicana de Biodiversidad 25: e913287.

Hancke D, Suárez OV (2018) Structure of parasite communities in urban environments: the case of helminths in synanthropic rodents. Folia Parasitologica 65: 009. https://doi.org/10.14411/fp.2018.009

Kersul MG, Costa NA, Boullosa RG, Silva AAS, Rios ÉO, Munhoz AD, Andrade-Silva BE, Maldonado Jr A, Gentile R, Alvarez MR (2020) Helminth communities of sigmodontine rodents in cocoa agroforestry systems in Brazil. International Journal for Parasitology: Parasites and Wildlife 11: 62–71. https://doi.org/10.1016/j.ijppaw.2019.11.008

Kumar S, Stecher G, Li M, Knyaz C, Tamura K (2018) MEGA X: molecular evolutionary genetics analysis across computing platforms. Molecular biology and evolution 35: 1547–1549. https://doi.org/10.1093/molbev/msy096

Miño MH, Herrera ER, Notarnicola J, Robles MR, Navone GT (2012) Diversity of the helminth community of the Pampean grassland mouse (*Akodon azarae*) on poultry farms in central Argentina. Journal of Helminthology 86: 46–53. https://doi.org/10.1017/S0022149X10000945

Miño MH, Herrera ER, Notarnicola J, Hodara K (2019) Helminth community from Azara's grass mouse (*Akodon azarae*) in three habitats with different land use in farming systems of Argentina. Journal of Helminthology 93: 187–194. https://doi.org/10.1017/S0022149X18000032

Navone GT, Notarnicola J, Nava S, Robles MR, Galliari C, Lareschi M (2009) Arthropods and helminths assemblage in sigmodontine rodents from wetlands of the Rio de la Plata, Argentina. Mastozoología Neotropical 16: 121–133.

Panisse G, Robles MR, Digiani MC, Notarnicola J, Galliari C, Navone GT (2017) Description of the helminth communities of sympatric rodents (Muroidea: Cricetidae) from the Atlantic Forest in northeastern Argentina. Zootaxa 4337: 243–262. https://doi.org/10.11646/zootaxa.4337.2.4

Pardiñas U, Teta P, Alvarado-Serrano DF, Geise L, Jayat JP, Ortiz PR, Gonçalves PR, D'Elía G (2015) Genus *Akodon*. In: Patton J, Pardiñas UF, D'Elía G (Eds) Mammals of South America - Volume 2. The University of Chicago Press, Chicago, Chicago and London, 144–203.

Pinto RM, Kohn A, Fernandes BMM, Mello DA (1982) Nematodes of rodents in Brazil, with description of *Aspidodera vicentei* n. sp. Systematic Parasitology 4: 263–267. https://doi.org/10.1007/BF00009627

Ronquist F, Teslenko M, Van Der Mark P, Ayres DL, Darling A, Höhna S, Larget B, Liu L, Suchard MA, Huelsenbeck JP (2012) MrBayes 3.2: efficient Bayesian phylogenetic inference and model choice across a large model space. Systematic Biology 61: 539–542. https://doi.org/10.1093/sysbio/sys029

Scheibel P, Catzeflis F, Jimenez A (2014) The relationships of marsupial-dwelling Viannaiidae and description of *Travassostrongylus scheibelorum* sp. n. (Trichostrongylina: Heligmosomoidea) from mouse opossums (Didelphidae) from French Guiana. Folia Parasitologica 61: 242–254. https://doi.org/10.14411/fp.2014.032

Serrano PC (2024) Nematodes Trichostrongylina parásitos de roedores sigmodontinos de la Cuenca del Plata argentina: aspectos taxonómicos, ecológicos y patrones de distribución parásito-hospedador. PhD Thesis, Universidad Nacional de La Plata, La Plata, Argentina. https://doi.org/10.35537/10915/168017

Serrano PC, Digiani MC, Gómez-Muñoz MÁ, Notarnicola J, Robles MR, Navone GT (2021) *Hassalstrongylus dollfusi* (Nematoda, Heligmonellidae): rediscovery in native South American rodents, six decades after its description. Parasite 28(80): 1–15. https://doi.org/10.1051/parasite/2021077

Simões RO, Souza JGR, Maldonado Jr A, Luque JL (2011) Variation in the helminth community structure of three sympatric sigmodontine rodents from the coastal Atlantic Forest of Rio de Janeiro, Brazil. Journal of Helminthology 85: 171–178. https://doi.org/10.1017/S0022149X10000398

Simões RO, Santos MM, Maldonado Jr A (2012a) A new heligmonellid (Nematoda: Heligmonellidae) from *Oecomys mamorae* (Rodentia: Sigmodontinae) in the Pantanal and new data on the synlophe of *Guerrerostrongylus zetta* from the Atlantic Forest, Brazil. Journal of Parasitology 98: 801–805. https://doi.org/10.1645/GE-2905.1

Simões RO, Maldonado Jr A, Luque JL (2012b) Helminth communities in three sympatric rodents from the Brazilian Atlantic Forest: contrasting biomass and numerical abundance. Brazilian Journal of Biology 72: 909–914. https://doi.org/10.1590/S1519-69842012000500018

Stock SP, Campbell JF, Nadler SA (2001) Phylogeny of *Steinernema* Travassos, 1927 (Cephalobina: Steinernematidae) inferred from ribosomal DNA sequences and morphological characters. Journal of Parasitology 87: 877–889. https://doi.org/10.2307/3285148

Sutton CA, Durette-Desset M-C (1991) Nippostrongylinae (Nematoda – Trichostrongyloidea) parasites d'*Oryzomys flavescens* en Argentine et en Uruguay. Revue Suisse de Zoologie 98: 535–553. https://doi.org/10.5962/bhl.part.82072

Travassos L (1937) Revisão da família Trichostrongylidae Leiper, 1912. Monographias do Instituto Oswaldo Cruz, Rio de Janeiro, 512 pp.

Weirich J, Catzeflis F, Jimenez A (2016) *Guerrerostrongylus marginalis* n. sp. (Trichostrongyloidea: Heligmonellidae) from the Guianan arboreal mouse (*Oecomys auyantepui*) from French Guiana. Parasite 23. https://doi.org/10.1051/parasite/2016009

Werk DF, Gallas M, Silveira EF, Périco E (2016) New locality records for *Guerrerostrongylus zetta* (Travassos, 1937) Sutton & Durette-Desset, 1991 (Nematoda: Heligmonellidae) parasitizing *Oligoryzomys nigripes* (Olfers, 1818) (Rodentia: Sigmodontinae) from southern Brazil. Check List 12: 1861–1861. https://doi.org/10.15560/12.2.1861

Zoosyst. Evol. 100 (4) 2024, 1333–1345 | DOI 10.3897/zse.100.130929

PENSOFT

für Natur MUSEUM FÜR NATURKUNDE BERLIN

Two new genera and three new species of exceptionally rare and endemic freshwater mussels (Bivalvia, Unionidae) from the Mekong Basin

Ekgachai Jeratthitikul[1], Chirasak Sutcharit[2], Pongpun Prasankok[3]

1 *Animal Systematics and Molecular Ecology Laboratory, Department of Biology, Faculty of Science, Mahidol University, Bangkok 10400, Thailand*

2 *Animal Systematics Research Unit, Department of Biology, Faculty of Science, Chulalongkorn University, Bangkok 10330, Thailand*

3 *School of Biology, Institute of Science, Suranaree University of Technology, Nakhon Ratchasima 30000, Thailand*

https://zoobank.org/4D6C62E4-224B-4AB5-A251-AA7ABEE66D74

Corresponding author: Pongpun Prasankok (prasankok@sut.ac.th)

Academic editor: Matthias Glaubrecht ♦ **Received** 1 July 2024 ♦ **Accepted** 5 September 2024 ♦ **Published** 4 October 2024

Abstract

Two new genera and three new species of freshwater mussels in the tribe Pseudodontini (Bivalvia, Unionidae) are described from the Mekong Basin in Thailand based on an integrative taxonomic study involving morphology and multi-locus phylogenetic analyses (mitochondrial COI and 16S, and nuclear 28S genes). The monotypic genus, *Lannanaia kokensis* **gen. et sp. nov.**, presents unique features of being rather compressed, sub-trigonal in outline with short and high shell, and with a distinct posterior wing. Another new genus, *Isannaia* **gen. nov.**, is characterized by having a thin and moderately inflated shell, with rhomboidal to ovate outline. It includes two lineages that are genetically separated by 3.54% uncorrected COI p-distance, and are herein described as *I. fortunata* **sp. nov.** and *I. occultata* **sp. nov.** Phylogenetic analyses further revealed that these two new genera were nested within a clade of subtribe Pseudodontina, and with pairwise uncorrected COI p-distance to other genera ranging from 11.42 to 15.66%. Based on the present data, *Lannanaia* **gen. nov.** is known only from the Kok River in the north of Thailand, whereas the two species of *Isannaia* **gen. nov.** are restricted to tributaries of the Mekong River in the northeast of Thailand. The discovery of rare and probably endemic freshwater mussels in the Mekong Basin thus again highlights the importance of this region among freshwater biodiversity hotspots of the world.

Key Words

Freshwater mussels, Indochina, Mekong Basin, multi-locus phylogeny, new taxa, Thailand

Introduction

Freshwater mussels in the family Unionidae represent the most diverse group among bivalves that have evolved to live in freshwater environments, with more than 750 extant representatives described worldwide, excluding Antarctica and South America (Graf and Cummings 2021). They are particularly diverse in East Asia, which hosts approximately 40% of all described species (Graf and Cummings 2021). The region is thus considered one of the most important global hotspots of freshwater mussel diversity, alongside North America, due not only to its high species richness but also to the notable endemism (Zieritz et al. 2018; Graf and Cummings 2021), highlighting the need for comprehensive research and conservation efforts. Examples of this endemism include more than one hundred species that are restricted to a single river basin (e.g., Bolotov et al. 2020, 2023; Konopleva et al. 2021; Pfeiffer et al. 2021; Jeratthitikul et al. 2022; Jeratthitikul and Sutcharit 2023; Kongim et al. 2023), as well as cases at the subfamily level, such as Modellnaiinae, which is exclusively distributed in the Mun River, a tributary of the Mekong River Basin in Thailand (Brandt 1974).

The tribe Pseudodontini, which currently contains around 48 extant species in nine genera, has been considered one of the endemic freshwater mussel groups occurring in Southeast Asian limnetic drainage systems (Bolotov et al. 2023, and references therein). Members of this tribe share characteristics such as the presence of V-shaped fossette at the posterior end of the hinge structure on the inner side of the shell and the reduction or absence of lateral teeth (Lopes-Lima et al. 2017). Recent multilocus phylogenetic approaches suggest that Pseudodontini consists of two well-defined clades that are biogeographically separated along the Salween-Mekong border. The subtribe Indopseudodontina is endemic to the western Indochina Subregion from Ayeyarwady to Salween basins, whereas the subtribe Pseudodontina (= Pilsbryoconchina Bolotov, Vikhrev & Tumpeesuwan in Bolotov et al. 2017b) is mainly distributed in the Chao Phraya and Mekong basins, with some taxa found to the east and southeast of the Salween-Mekong border (Bolotov et al. 2023). The Indopseudodontina currently consists of five species in one genus, *Indopseudodon* Prashad, 1922, whereas the Pseudodontina currently comprises 43 species in eight genera (Bolotov et al. 2023). These genera are recovered as well-defined clades in phylogenetic analyses (e.g., Jeratthitikul et al. 2021b; Bolotov et al. 2023; Konopleva et al. 2023).

Many Pseudodontini species exhibit restricted ranges and specialized habitat preferences, making them particularly vulnerable to extinction (i.e., Bolotov et al. 2020, 2023; Jeratthitikul et al. 2021b, 2022; Konopleva et al. 2021, 2023; Jeratthitikul and Sutcharit 2023). This susceptibility mirrors the global trend observed in other unionid species, which have experienced a significant decline in diversity over recent decades (Lopes-Lima et al. 2018; Aldridge et al. 2023).

A recent freshwater mollusc survey along the Mekong River and its tributaries in Thailand has yielded enigmatic specimens that were initially identified as belonging to the Pseudodontini. However, these specimens could not be attributed to any known genera and demonstrated evolutionary distinctiveness through multi-locus phylogenetic analyses. Consequently, they are formally described as two new genera and three new species in this study.

Material and methods

Specimen sampling and morphology examination

Animal use protocol was approved by the Faculty of Science, Mahidol University Animal Care and Use Committee, SCMU-ACUC (MUSC65-013-606).

Specimens of freshwater mussels were collected by hand from three tributaries of the Mekong River in Thailand, including 1) Kok River, Chiang Rai Province, northern Thailand; 2) Thuai River, Nakhon Phanom Province, northeastern Thailand, and 3) Yang Stream in Udon Thani Province, a tributary of Lam Pao River, Chi Basin, northeastern Thailand. Specimens were subjected to euthanization by the two-step method recommended by AVMA (AVMA 2020). In brief, the specimens were put in a container with freshwater, and then 95% (v/v) ethanol was added gradually, starting at a concentration of about 5% (v/v), until the foot and adductor muscles fully relaxed. The anesthetized specimens were subsequently fixed in 70% (v/v) ethanol. Soft bodies were then separated from the shells. Small pieces of foot tissues were cut and preserved in 95% (v/v) ethanol for further molecular analyses. The remaining soft parts were preserved in 70% (v/v) ethanol, while the shells were kept as dry specimens. Holotypes and paratypes of the new taxa are deposited in the Mahidol University Museum of Natural History, Department of Biology, Faculty of Science, Mahidol University, Bangkok, Thailand (**MUMNH**).

Shell morphology was examined based on shell shape, shell outline, shell size, shape and position of the umbo, hinge plate dentition, and muscle attachment scars. Shell dimensions were measured for shell length, height, and width using a digital Vernier caliper (±0.1 mm). Anatomical characteristics of soft parts (i.e., excurrent and incurrent aperture, labial palps, and gills) were also examined under a stereomicroscope.

Molecular analysis

Whole genomic DNA was extracted from the dissected foot tissues using a DNA extraction kit for animal tissue (NucleoSpin Tissue Extraction Kit, Macherey-Nagel, Germany) according to the manufacturer's instructions. Fragments from the mitochondrial cytochrome c oxidase subunit-I gene (COI), the mitochondrial large ribosomal subunit rRNA gene (16S rRNA), and the nuclear 28S large ribosomal subunit rDNA gene (28S rRNA) were amplified and sequenced using primers LoboF1 and LoboR1 for COI (Lobo et al. 2013), 16sar-L-myt and 16Sbr-H-myt for 16S rRNA (Lydeard et al. 1996), and C1 and D2 for 28S rRNA (Jovelin and Justine 2001). Polymerase chain reaction (PCR) was conducted using a T100™ thermal cycler (BIO-RAD) with a final reaction volume of 30 µL (15 µL EmeraldAmp GT PCR Master Mix, 1.5 µL each primer, 10 ng template DNA, and distilled water up to 30 µL total volume). PCR conditions and processes were as follows: 94 °C for 3 min; 35 cycles of 94 °C for 30 s, annealing for 60 s (46 °C for COI and 16S rRNA, and 58 °C for 28S rRNA), 72 °C for 90 s, and a final extension at 72 °C for 5 min. Amplified PCR products were purified using MEGAquick-spinTM plus (Fragment DNA purification kit), and sequenced in both directions by an automated sequencer (ABI prism 3730XL). Contigs of forward and reverse sequences were edited and assembled using MEGA11 v. 11.0.13 (Tamura et al. 2021), and confirmed by visual inspection. The sequences obtained in this study have been uploaded in the GenBank Nucleotide sequence database under accession numbers OR987588–OR987596 for COI, OR987514–OR987522 for 16S rRNA, and OR987523–OR987531 for 28S rRNA (Suppl. material 1).

Phylogenetic analyses

The dataset for phylogenetic analyses includes haplotypes from nine individuals of the new taxa, along with 42 species from all other genera in the tribe Pseudodontini as the ingroup, and some representative taxa from other tribes (i.e., Schepmaniini, Gonideini, Chamberlainiini, Rectidentini, Contradentini, Ctenodesmini, and Lamprotulini) as the outgroup (Suppl. material 1). Apart from the newly obtained sequences in this study, these sequences were from a series of previously published studies that are available on the GenBank database (Huang et al. 2013; Pfeiffer and Graf 2015; Zieritz et al. 2016, 2020, 2021b; Bolotov et al. 2017a, 2017b, 2020, 2023; Lopes-Lima et al. 2017; Jeratthitikul et al. 2019, 2021a, 2021b, 2022; Konopleva et al. 2019, 2021, 2023; Froufe et al. 2020; Jeratthitikul and Sutcharit 2023; Kongim et al. 2023). The sequences were aligned for each gene separately by ClustalW algorithm using MEGA11, and later all three gene alignments were joined into one concatenated data matrix. The final concatenated alignment was divided into five partitions (3 codons of COI + 16S rRNA + 28S rRNA). The best-fit substitution model for each partition was determined using PartitionFinder2 v. 2.3.4 (Lanfear et al. 2017) under the corrected Akaike Information Criterion (AICc). Phylogenetic analyses were performed using the online CIPRES Science Gateway (Miller et al. 2010). The maximum likelihood (ML) phylogenetic tree was reconstructed in IQ-TREE v. 2.2.2.7 (Minh et al. 2020) with 10,000 replicates of ultrafast bootstrap analysis (UFBoot) to assess topology bootstrap support (BS; Hoang et al. 2018). The Bayesian Inference (BI) phylogenetic analysis was performed in MrBayes v. 3.2.7 (Ronquist et al. 2012). Four Monte Carlo Markov Chains of 10,000,000 generations were run with sampling every 1,000 generations. The resulting effective sample sizes were > 200 for all parameters. A clade of obtained phylogenetic trees was considered well supported when the ultrafast BS was ≥ 95% and Bayesian bipartition posterior probability (bpp) was ≥ 0.95 (San Mauro and Agorreta 2010; Hoang et al. 2018).

Genetic distance between pairs of genus/species clades recovered from the phylogenetic analysis was also estimated as uncorrected p-distance of COI gene sequences, using MEGA11.

Results

Phylogenetic analysis and genetic distances

Phylogenetic trees were estimated from a concatenated alignment of 1,935 bp (660 bp of COI, 500 bp of 16S rRNA, and 775 bp of 28S rRNA), and with the best-fit substitution model GTR+I+G for the first codon of COI, 16S rRNA, and 28S rRNA; GTR+I for the second codon of COI; and GTR+G for the third codon of COI. Both ML and BI analyses resulted in a highly congruent tree topology. Therefore, only the best ML tree from IQ-TREE is presented in Fig. 1.

The tree topology showed clear monophyly of the Pseudodontini with high BS and bpp (BS = 100%, bpp = 1). All Pseudodontini genera were recovered as highly supported clades (BS = 98–100%, bpp = 0.99–1). Among these genus-level clades, specimens from the Kok River, northern Thailand, were recovered as a monophyletic clade (BS = 100%, bpp = 1). This clade was nested with the monotypic genus *Songkhlanaia* Konopleva et al., 2023 with high support (BS = 99%, bpp = 0.99), and a deep divergence of 11.42% uncorrected COI p-distance (Table 1). Specimens of the unknown freshwater

Table 1. Mean genetic distances (uncorrected p-distance: %±SD) based on 660 bp COI gene fragment sequences among genera of the tribe Pseudodontini (below diagonal), and between species within each genus (in bold).

	1	2	3	4	5	6	7	8	9	10	11
1. *Lannanaia* **gen. nov.**	**n/a**										
2. *Isannaia* **gen. nov.**	15.40 ± 0.17	**3.08 ± 0.15**									
3. *Namkongnaia*	14.27 ± 0.40	11.77 ± 0.39	**5.38**								
4. *Pseudodon*	14.01 ± 0.77	13.80 ± 0.76	11.04 ± 1.02	**7.03 ± 3.14**							
5. *Bineurus*	13.61 ± 0.47	13.86 ± 0.72	11.58 ± 0.70	11.91 ± 0.59	**4.14 ± 1.25**						
6. *Thaiconcha*	15.66 ± 0.13	14.55 ± 0.36	12.04 ± 0.27	13.44 ± 0.56	11.59 ± 0.52	**3.26 ± 0.67**					
7. *Sundadontina*	13.38 ± 0.95	13.72 ± 0.71	11.79 ± 0.77	12.46 ± 1.01	12.24 ± 1.19	12.96 ± 1.44	**9.92 ± 3.20**				
8. *Nyeinchanconcha*	12.72 ± 0.00	13.49 ± 0.27	11.34 ± 0.08	12.58 ± 0.53	11.13 ± 0.88	12.89 ± 0.40	10.54 ± 0.52	**n/a**			
9. *Pilsbryoconcha*	12.74 ± 0.94	14.21 ± 0.99	12.09 ± 0.80	12.13 ± 1.38	11.41 ± 0.95	12.57 ± 0.95	12.44 ± 1.34	11.54 ± 0.98	**8.98 ± 1.57**		
10. *Songkhlanaia*	11.42 ± 0.00	13.12 ± 0.29	10.28 ± 0.32	11.18 ± 0.56	10.67 ± 0.62	12.67 ± 0.07	11.73 ± 1.56	11.26 ± 0.00	11.17 ± 0.79	**n/a**	
11. *Indopseudodon*	13.76 ± 1.59	15.02 ± 0.66	12.11 ± 0.49	13.07 ± 0.80	12.70 ± 0.96	13.47 ± 0.54	13.31 ± 0.66	12.64 ± 1.12	12.46 ± 0.98	11.72 ± 0.86	**9.29 ± 3.21**

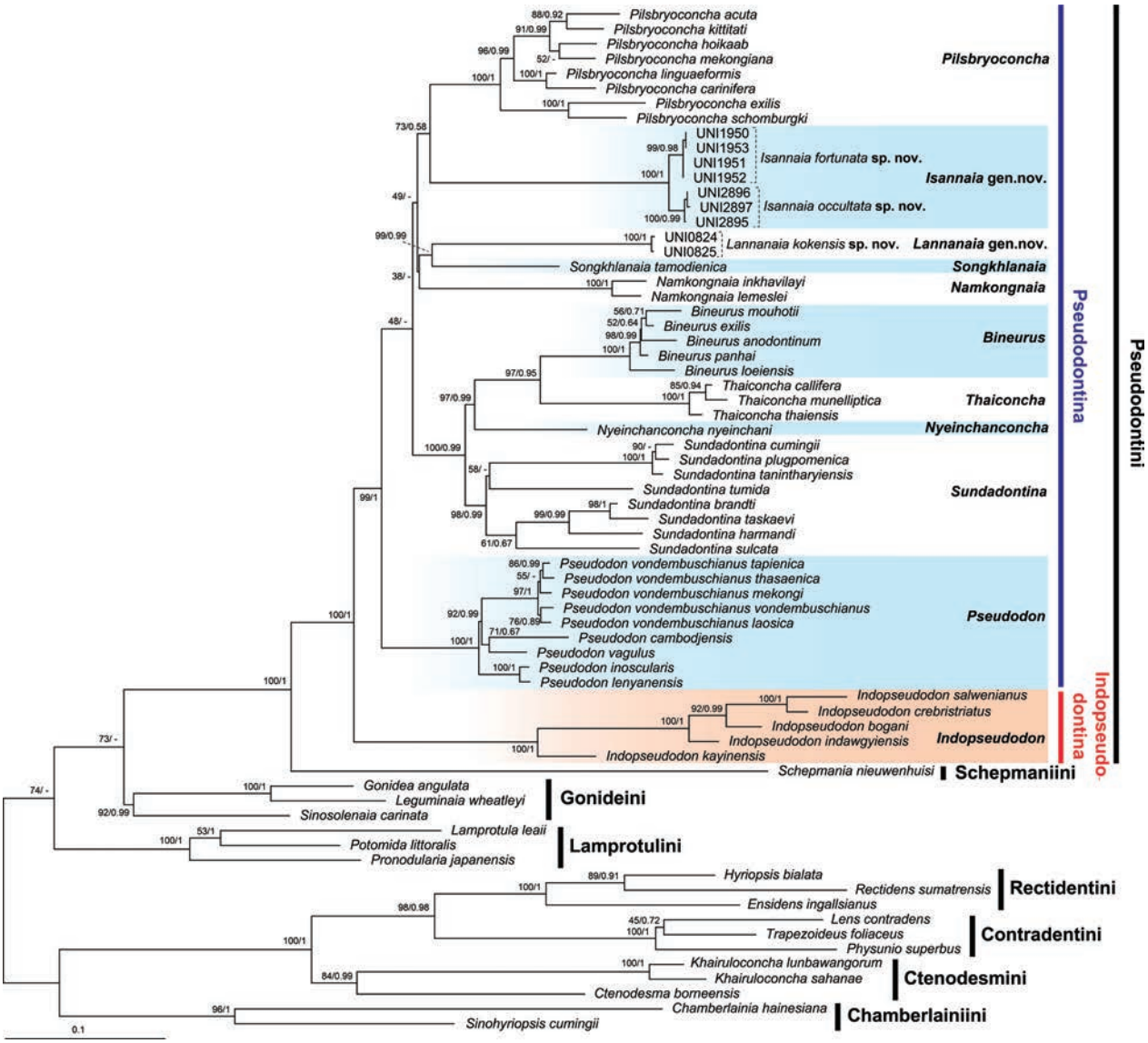

Figure 1. Maximum likelihood (ML) tree of freshwater mussels in subfamily Gonideinae based on 1,935-bp concatenated alignment dataset of COI and 16S rRNA mitochondrial genes, and 28S rRNA nuclear gene. The numbers on nodes represent the bootstrap support (BS) from the ML analysis and the bipartition posterior probability (bpp) from the BI analysis, and are shown as ML/BI. Scale bar indicates the branch length.

mussels from northeastern Thailand were recovered as two well-supported species-level clades (BS = 99–100%, bpp = 0.98–0.99). Each clade contained specimens from a single locality, and differed from each other by 3.54% uncorrected COI p-distance. The two were grouped into a genus-level clade with high support (BS = 100%, bpp = 1), and then nested with the clade of *Pilsbryoconcha* Simpson, 1900, but without significant support (BS = 73%, bpp = 0.58). Nevertheless, in terms of genetic similarity, this group of freshwater mussels from northeastern Thailand showed the closest genetic similarity to *Namkongnaia* Jeratthitikul et al., 2021, with an uncorrected COI p-distance of 11.77%.

These two newly discovered genus-level clades showed unique conchological characteristics distinguishable from other genera in the Pseudodontini (see taxonomic account below). Therefore, they are herein described as *Lannanaia kokensis* gen. et sp. nov. for the clade from northern Thailand and *Isannaia* gen. nov. for the clade from northeastern Thailand. The two species-level clades of the latter genus are described as new species: *I. fortunata* sp. nov. for the clade from the Thuai River and *I. occultata* sp. nov. for the clade from Yang Stream, Chi Basin.

The Pseudodontini is further grouped into two larger clades with high support (BS = 99–100%, bpp = 1), corresponding to the currently accepted subtribe classification (e.g. Bolotov et al. 2023). The clade of the Indopseudodontina contained only one genus, *Indopseudodon*. In contrast, the clade of the Pseudodontina contained ten genera, including the two genera newly described in this study. However, the phylogenetic relationship among genera within the Pseudodontina was still uncertain, except for *Bineurus* Simpson, 1900, *Thaiconcha* Bolotov et al., 2020, *Nyeinchanconcha* Bolotov et al., 2020, and *Sundadontina* Bolotov et al., 2020, which were grouped

into a strongly supported clade (BS = 100%, bpp = 0.99), and a clear sister relationship between *Songkhlanaia* and *Lannanaia* gen. nov. (BS = 99%, bpp = 0.99). Pairwise genetic distances as expressed by uncorrected COI p-distance among genera in Pseudodontina ranged from 10.28% in *Songkhlanaia* versus *Namkongnaia* to 15.66% in *Lannanaia* gen. nov. versus *Thaiconcha*, and with an average of 12.50% (Table 1).

Taxonomic account

Family Unionidae Rafinesque, 1820
Subfamily Gonideinae Ortmann, 1916
Tribe Pseudodontini Frierson, 1927

Subtribe Pseudodontina Frierson, 1927

Remarks. Currently the Pseudodontina is composed of 45 species in ten genera, including the new taxa described herein (Bolotov et al. 2023). These genera are *Bineurus* Simpson, 1900 (5 species), *Isannaia* gen. nov. (2 species), *Lannanaia* gen. nov. (1 species) *Namkongnaia* Jeratthitikul et al., 2021 (2 species), *Nyeinchanconcha* Bolotov et al., 2020 (1 species), *Pilsbryoconcha* Simpson, 1900 (9 species), *Pseudodon* Gould, 1844 (9 species), *Songkhlanaia* Konopleva et al., 2023 (1 species), *Sundadontina* Bolotov et al., 2020 (12 species), and *Thaiconcha* Bolotov et al., 2020 (3 species). *Pseudodon mekongi* (Bolotov et al., 2020) was nested within a clade of *Pseudodon vondembuschianus* (Lea, 1840) in the phylogenetic analysis in this study. Therefore, we recognize it as a subspecies of *P. vondembuschianus*.

Genus *Lannanaia* gen. nov.

https://zoobank.org/6999F44B-DA95-451C-BDAC-E088A0EF84CE

Type species. *Lannanaia kokensis* gen. et sp. nov., by present designation.

Species included. The new genus currently contains only one species, *L. kokensis* sp. nov.

Diagnosis. This new genus is distinguished from other Pseudodontini genera by its compressed, rather short and high shell, with sub-trigonal outline, and distinct posterior wing. The hinge plate is without dentition, or with very rudimentary broad pseudocardinal tooth in each valve, and posterior end of the hinge structure with rather wide V-shaped fossette (Fig. 2). It is also represented as a distinct clade in multi-locus phylogenetic analyses (Fig. 1).

Description. Shell medium-sized, thin, rather short and high, winged, sub-trigonal outline, inequilateral, rather compressed. Anterior margin rounded; posterior margin angulate, somewhat pointed. Umbo tiny, not prominent, eroded. Ligament long, very narrow. Hinge without dentition, or with very rudimentary broad pseudocardinal tooth in each valve; posterior end of the hinge structure with rather wide V-shaped fossette. Anterior adductor muscle scar very shallow, ovate, contiguous with anterior pedal retractor muscle scar, but separated from anterior protractor scar; posterior adductor muscle scar round, very shallow, almost invisible. Pallial line very faint, continuous. Umbo cavity shallow.

Etymology. The generic name "*Lannanaia*" is from the word "*Lanna*", a name of the kingdom located in present-day northern Thailand during the 13th to 18th centuries, and the Greek word "*naiad*" meaning freshwater mussel. The name of this genus thus means "freshwater mussels from Lanna" or "freshwater mussels from northern Thailand". The gender is feminine.

Distribution. Endemic to Kok River, a tributary of the Mekong River in northern Thailand (Fig. 3).

Remarks. The phylogenetic tree generated in this study places *Lannanaia* gen. nov. as a sister group to *Songkhlanaia*, with strong support from both analyses (BS = 100%, bpp = 0.99; Fig. 1), and with a 11.42% p-distance based on the COI gene (Table 1). Both genera share general characteristics of a short shell outline and rather compressed shell. However, *Lannanaia* gen. nov. can be distinguished from *Songkhlanaia* by having a sub-trigonal shell outline and a curved ventral margin (vs a rectangular shell outline and an almost straight ventral margin in *Songkhlanaia*), distinct posterior wing (vs absent posterior wing), and not prominent umbo (vs slightly elevated and easily visible umbo) (Konopleva et al. 2023). In addition, the biogeography of the two genera is also distinct. The monotypic genus *Songkhlanaia* was described from the Songkhla Lake Basin in southern Thailand (Konopleva et al. 2023), while *Lannanaia* gen. nov. is restricted to the Kok River, a tributary of the Mekong River in northern Thailand.

Lannanaia kokensis sp. nov.

https://zoobank.org/873CE4DB-F862-43DF-BFF7-8863B7CBA3C7
Figs 1–3

Type material. ***Holotype*.** Thailand • Chiang Rai Province, Mueang Chiang Rai District, Rop Wiang Subdistrict, Kok River; 19.9131°N, 99.8697°E; E. Jeratthitikul and K. Wisittikoson leg.; MUMNH-UNI0825; shell length 57.2 mm, shell height 40.8 mm, and shell width 14.4 mm. ***Paratype*.** Thailand • 1 shell; same collection data as for holotype; MUMNH-UNI0824.

Description. Shell medium-sized (shell length 57.1–57.2 mm, shell height 40.8–43.8 mm, shell width 14.4–14.8 mm; Table 2), thin, rather short and high (H/L ratio = 0.71–0.77), winged, sub-trigonal outline, inequilateral, rather compressed. Anterior margin rounded; posterior margin angulate, somewhat pointed; ventral margin curved. Dorsal margin straight; anterior low and short, gradually elevated to posterior end; posterior end high and winged. Umbo tiny, not prominent, eroded. Posterior ridge wide and obtuse, not prominent; posterior slope with two fine lines running as curved line from umbo to posterior margin. Periostracum thin, greenish to dark

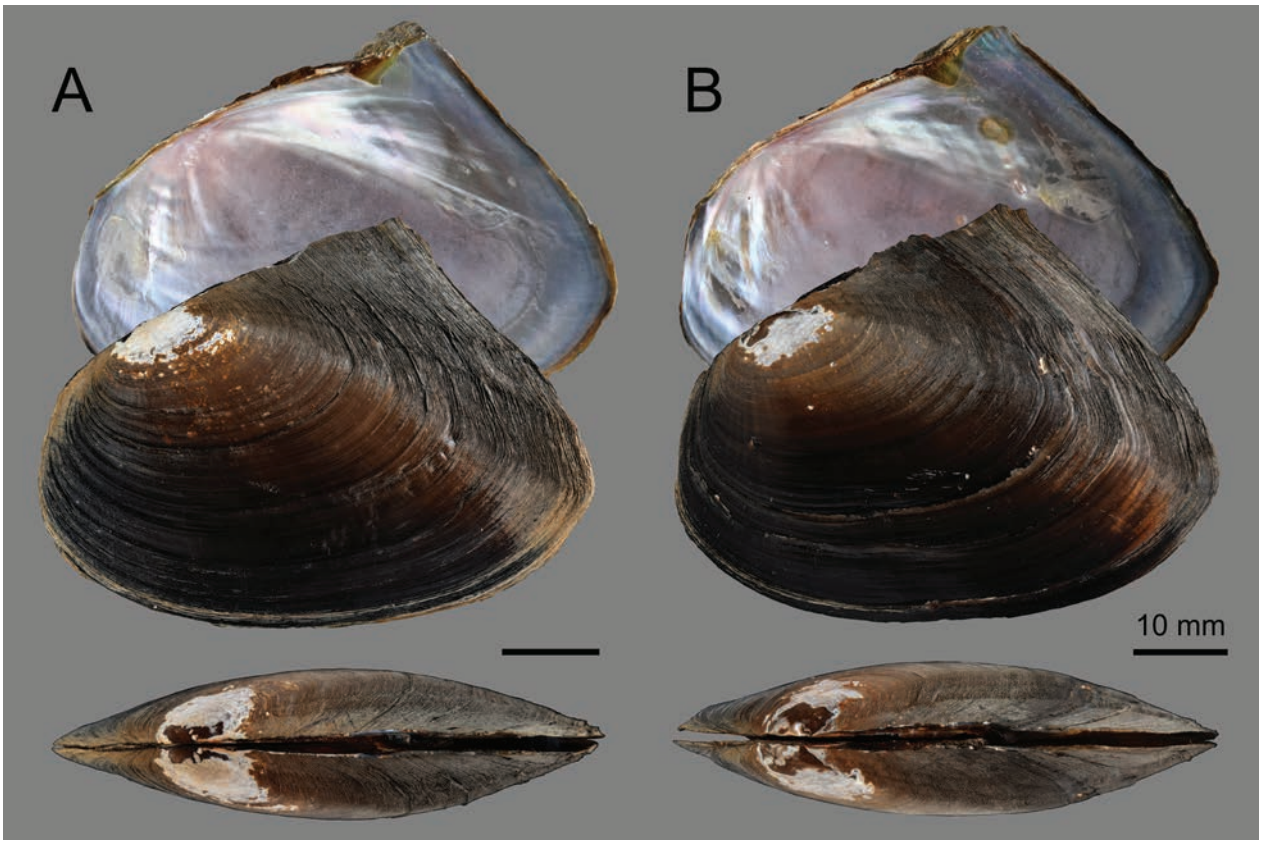

Figure 2. Shells of *Lannanaia kokensis* sp. nov., showing the inner side of the right valve, the outer side of the left valve, and the dorsal view of both valves. **A.** Holotype MUMNH-UNI0825; **B.** Paratype MUMNH-UNI0824. Scale bars: 10 mm.

brown, the eroded part white to coppery-brown. Shell surface with very fine growth lines. Ligament long, very narrow, dark brown. Hinge without dentition, or with very rudimentary broad pseudocardinal tooth in each valve; posterior end of hinge structure with rather broad V-shaped fossette. Anterior adductor muscle scar very shallow, ovate, contiguous with anterior pedal retractor muscle scar, but separated from anterior protractor scar; posterior adductor muscle scar round, very shallow, almost invisible. Pallial line very faint, continuous. Umbo cavity shallow. Nacre blue-whitish.

Exhalant aperture smooth, shorter than inhalant. Inhalant aperture with a row of conical papillae, varying in length. Small epithelial fold divides exhalant and inhalant apertures. Gills elongated and slightly ribbed; outer gills much narrower (about half) than inner gills; anterior margin of inner gills slightly longer than that of outer gills. Labial palps elongate, round at tip. Glochidia unknown.

Etymology. The species name "*kokensis*" refers to the type locality, the Kok River in Chiang Rai Province, northern Thailand.

Distribution. This new species is known only from the type locality.

Remarks. Two living specimens were collected from a small stream that is a tributary to the Kok River, with a muddy bottom. We searched multiple times and locations for this species but failed to find additional specimens. In contrast, *Lens contradens* (Lea, 1838) and *Pilsbryoconcha exilis* (Lea, 1838) were found nearby in high abundance, both living and as empty shells. We assume this new species has a low population density and is possibly endemic to the Kok River Basin.

Genus *Isannaia* gen. nov.

https://zoobank.org/ADD0E6C8-E5BD-4E05-828B-FC89CA662F02

Type species. *Isannaia fortunata* gen. et sp. nov., by present designation.

Species included. The new genus is currently composed of two species, the type species and *I. occultata* sp. nov.

Diagnosis. The new genus is distinguished from other genera in the Pseudodontini by its thin and moderately inflated shell, and with rhomboidal to ovate outline (Fig. 4). The overall shape is somewhat elongated but relatively shorter when compared to those of *Bineurus*, *Pilsbryoconcha* or *Namkongnaia*. The anterior margin is rounded, shouldered, and the posterior margin is truncated to rounded. Its pseudocardinal teeth are rather small, one on each valve, hill-like or triangulate shape, and less developed on the left valve. Its umbo is slightly elevated and the umbo cavity moderately deep. It is also represented as a distinct clade in multi-locus phylogenetic analyses (Fig. 1).

Description. Shell medium-sized, rather thin, rhomboidal to ovate outline, elongate, very inequilateral,

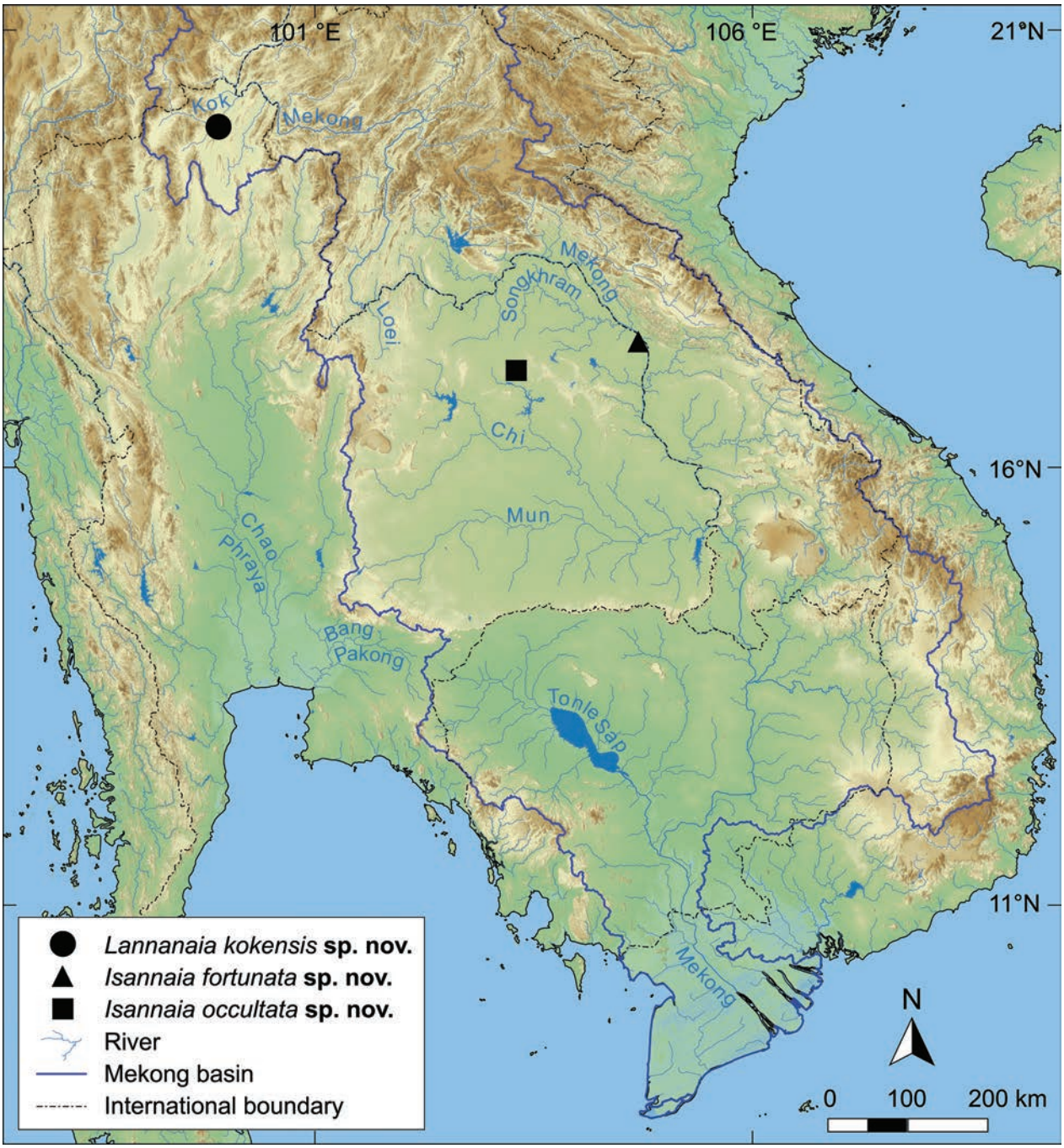

Figure 3. Map showing type localities of the new species: circle *Lannanaia kokensis* sp. nov., triangle *Isannaia fortunata* sp. nov., and square *Isannaia occultata* sp. nov. Map was generated using QGIS v3.24.3 with the outline of Mekong basin from the Freshwater Ecoregions of the World (Abell et al. 2008), river and lake topology from the HydroSHEDS database (https://www.hydrosheds.org), and the map raster data from the NASA EARTHDATA (https://www.earthdata.nasa.gov/).

moderately inflated; anterior margin rounded, shouldered; posterior margin truncated to rounded. Umbo slightly elevated and usually eroded. Ligament very narrow. One shallow hill-like or triangulate pseudocardinal tooth on right valve; left valve with one less developed hill-like to tubercule-like pseudocardinal tooth. End of hinge structure with V-shaped fossette. Anterior adductor muscle scar shallow to well-developed, ovate, contiguous with pedal retractor and anterior protractor muscle scars; posterior adductor muscle scar round, very shallow. Pallial line faint to well-marked, continuous. Umbo cavity moderately deep.

Etymology. The generic name "*Isannaia*" is from the word "*Isan*", the name of the region of northeastern Thailand, and Greek word "*naiad*" meaning freshwater mussel. The name of this genus thus means "freshwater mussels from northeastern Thailand". The gender is feminine.

Distribution. Endemic to tributaries of the Mekong River in northeastern Thailand (Fig. 3).

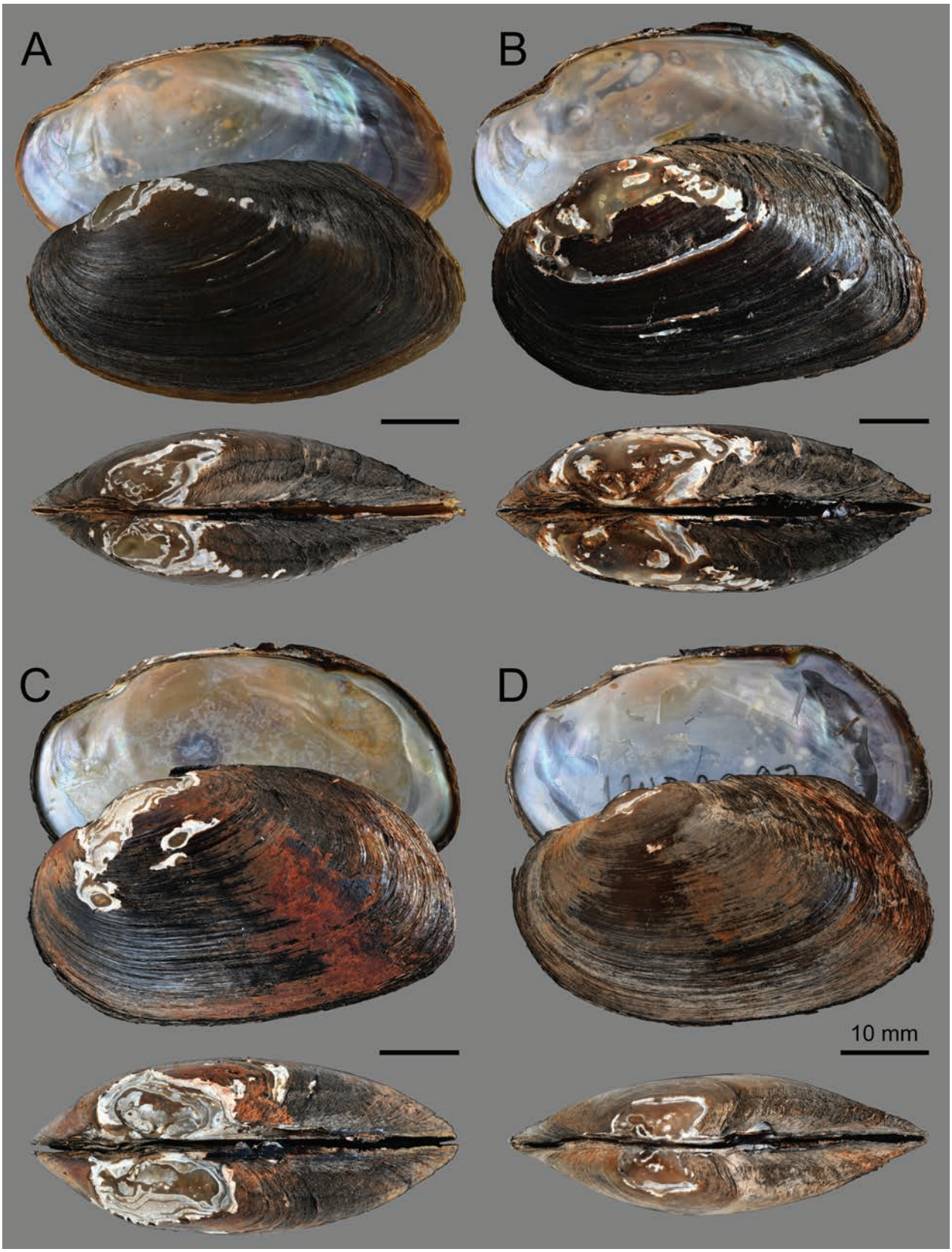

Figure 4. Shells of *Isannaia* gen. nov., showing the inner side of the right valve, the outer side of the left valve, and the dorsal view of both valves. **A.** Holotype (MUMNH-UNI1950) and **B.** Paratype (MUMNH-UNI1952) of *Isannaia fortunata* sp. nov.; **C.** Holotype (MUMNH-UNI2895) and **D.** Paratype (MUMNH-UNI2897) of *Isannaia occultata* sp. nov. Scale bars: 10 mm.

Remarks. Phylogenetic analyses have failed to recover a robustly supported position of *Isannaia* gen. nov. among other Pseudodontina genera. However, in terms of genetic distance, it is nearest to *Namkongnaia*, with a separation of 11.77% p-distance of the COI gene (Table 1). *Isannaia* gen. nov. can be easily distinguished from *Namkongnaia* by having a much shorter shell (Jeratthitikul et al. 2021b).

In general, *Isannaia* gen. nov. bears conchological resemblance to certain species within the *Sundadontina*, such as *S. brandti* Bolotov et al., 2020 or *S. plugpomenica* Konopleva et al., 2023 (Bolotov et al. 2020; Konopleva et al. 2023). Nevertheless, its thin shell with less developed pseudocardinal teeth set it apart from the latter genus, which typically features a thicker and sturdier shell with stout and tubercular-like pseudocardinal teeth (Bolotov et al. 2020).

Isannaia fortunata sp. nov.

https://zoobank.org/B84B9959-FEBF-4AFF-9E9B-B1B965BE8605

Figs 1, 3, 4A, B

Type material. ***Holotype*.** Thailand • Nakhon Phanom Province, Tha Uthen District, Tha Uthen Subdistrict, Thuai River; 17.5621°N, 104.6090°E; E. Jeratthitikul, P. Prasankok, and K. Wisittikoson leg.; MUMNH-UNI1950; shell length 54.13 mm, shell height 29.96 mm, and shell width 14.39 mm. ***Paratypes*.** Thailand • 3 shells; same collection data as for holotype; MUMNH-UNI1951 to UNI1953.

Description. Shell medium-sized (shell length 43.3–61.4 mm, shell height 24.5–35.1 mm, shell width 13.4–18.4 mm; Table 2), rhomboidal, elongate (H/L ratio = 0.55–0.57), rather thin, very inequilateral, moderately inflated. Anterior margin rounded, rather constricted, shouldered; posterior margin truncated, slightly elongate ventrally; ventral margin slightly curved. Dorsal margin slightly curved; anterior low, posterior end slightly higher. Umbo slightly elevated, heavily eroded even in young specimens. Posterior ridge wide and obtuse, not prominent; posterior slope with two faint lines running from umbo to posterior margin. Periostracum thin, brownish-black, eroded part white to coppery-brown. Shell surface with visible growth lines. Ligament long, very narrow, dark brown. One very shallow hill-like or triangulate pseudocardinal tooth on right valve; pseudocardinal tooth on left valve less developed, tubercule-like, or almost absent. Posterior end of hinge structure with small V-shaped fossette. Anterior adductor muscle scar shallow, ovate, contiguous with pedal retractor and anterior protractor muscle scars; posterior adductor muscle scar round, very shallow, almost invisible. Pallial line faint, continuous. Umbo cavity moderately deep, with 1 to 2 tiny muscle scars in the cavity. Nacre blue-whitish with yellowish tint around the umbo cavity.

Exhalant aperture almost smooth, with a row of tiny tubercle-like papillae on edge of aperture, shorter than inhalant. Inhalant aperture with a row of conical papillae, varying in length. Small epithelial fold divides exhalant and inhalant apertures. Gills elongated and slightly ribbed; inner gills slightly wider, and anterior margin of inner gills slightly longer than that of outer gills. Labial palps elongate, slightly curved, pointed at tip. Glochidia unknown.

Etymology. The species name "*fortunata*" is derived from the Latin adjective "*fortunatus*" meaning lucky. This name refers to the fortuitous discovery of this rare freshwater species.

Distribution. This new species is known only from the type locality.

Remarks. This new species is rare and restricted to the Thuai River. Specimens were collected from hard clay along the river bank. It was found sympatrically with several unionid species endemic to Songkhram Basin and nearby tributaries of the Mekong Basin, including *Lens maenamensis* Pfeiffer et al., 2021, *Physunio pellucidus* Pfeiffer et al., 2021, *Ensidens jaculus* (Rochebrune, 1882), *Scabiellus songkramensis* (Kongim et.al., 2015), *Pseudodon cambodjensis* (Petit de la Saussaye, 1865) and *Scabies scobinatus* (Lea, 1856).

Table 2. Shell measurements and GenBank accession numbers for the type series of the new species described in this study. Measurements in millimetres (mm).

Taxa	Status of specimen	Specimen voucher	Shell length	Shell height	Shell width	Genbank accession		
						COI	16S rRNA	28S rRNA
Lannanaia kokensis **sp. nov.**	Holotype	MUMNH-UNI0825	57.2	40.8	14.4	OR987589	OR987515	OR987524
	Paratype	MUMNH-UNI0824	57.1	43.8	14.8	OR987588	OR987514	OR987523
Isannaia fortunata **sp. nov.**	Holotype	MUMNH-UNI1950	54.1	29.9	18.4	OR987590	OR987516	OR987525
	Paratype	MUMNH-UNI1951	45.5	25.6	14.4	OR987591	OR987517	OR987526
	Paratype	MUMNH-UNI1952	61.4	35.1	21.6	OR987592	OR987518	OR987527
	Paratype	MUMNH-UNI1953	43.3	24.5	13.4	OR987593	OR987519	OR987528
Isannaia occultata **sp. nov.**	Holotype	MUMNH-UNI2895	53.8	31.7	20.4	OR987594	OR987520	OR987529
	Paratype	MUMNH-UNI2896	43.8	26.7	13.8	OR987595	OR987521	OR987530
	Paratype	MUMNH-UNI2897	47.9	27.9	14.8	OR987596	OR987522	OR987531

***Isannaia occultata* sp. nov.**

https://zoobank.org/F83569B6-8E5D-43BE-9DD4-4D44C9AD937B

Figs 1, 3, 4C, D

Type material. ***Holotype*.** Thailand • Udon Thani Province, Wang Sam Mo District, Nong Ya Sai Subdistrict, Yang Stream (a tributary of Lam Pao River); 16.9886°N, 103.3638°E; K. Wisittikoson leg.; MUMNH-UNI2895; shell length 53.84 mm, shell height 31.68 mm, and shell width 20.41 mm. ***Paratypes*.** Thailand • 2 shells; same collection data as for holotype; MUMNH-UNI2896, UNI2897.

Diagnosis. This species resembles *I. fortunata* sp. nov., but it can be distinguished by the overall shell shape being more rounded (vs rhomboidal), slightly higher shell (H/L ratio 0.58–0.60 vs 0.55–0.57), wider anterior margin (vs rather constricted), more truncated and rounded posterior margin (vs slightly ventrally elongate), less curved ventral margin (vs curved ventral margin). It also differs in characteristics inside the shell by having higher and more triangulate pseudocardinal tooth on the right valve (vs very shallow and hill-like pseudocardinal tooth), well-developed muscle scars (vs very shallow and sometimes almost invisible), 3 to 5 well-developed muscle scars in the umbo cavity (vs 1 to 2 tiny muscle scars in the umbo cavity), and well-marked pallial line (vs faint pallial line). It can also be distinguished from its congeners by fixed nucleotide substitution positions in the COI gene fragment of base A on the 54th, 114th, 363rd, and 414th; base T on the 90th, 141st, 591st, and 609th; base C on the 57th, and 216th; and base G on 150th, 117th, 192nd, 558th, 480th, 552nd, 627th, 639th, 645th, and 657th.

Description. Shell medium-sized (shell length 43.8–53.8 mm, shell height 26.7–31.7 mm, shell width 13.8–20.4 mm; Table 2), ovate to rectangular, elongate (H/L ratio = 0.58–0.60), rather thin, very inequilateral, moderately inflated. Anterior margin rounded, shouldered; posterior margin truncated to rounded; ventral margin straight to slightly curved. Dorsal margin slightly curved; anterior low, posterior end slightly higher. Umbo slightly elevated, heavily eroded even in young specimens. Posterior ridge wide and obtuse, not prominent; posterior slope with two faint lines running from umbo to posterior margin, invisible in old specimens. Periostracum thin, brown to brownish-black, eroded part white to coppery-brown. Shell surface with visible growth lines. Ligament long, very narrow, dark brown. One hill-like or triangulate pseudocardinal tooth on right valve; pseudocardinal tooth on left valve less developed, hill-like. Posterior end of hinge structure with small V-shaped fossette. Anterior adductor muscle scar well-developed, ovate, contiguous with anterior pedal retractor and anterior protractor muscle scars; posterior adductor muscle scar round, shallow, contiguous with posterior retractor muscle scars; posterior retractor muscle scars triangular. Pallial line well-marked, continuous. Umbo cavity moderately deep, with 3 to 5 muscle scars in cavity. Nacre blue-whitish to yellowish, more yellowish toward the umbo cavity.

Exhalant aperture almost smooth, with a row of tiny tubercle-like papillae on the edge of aperture, similar length with inhalant. Inhalant aperture with a row of very short conical papillae. Small epithelial fold divides exhalant and inhalant apertures. Gills elongated and slightly ribbed; inner gills slightly wider, and anterior margin of inner gills slightly longer than that of outer gills. Labial palps elongate, slightly curved, pointed at tip. Glochidia unknown.

Etymology. The species name "*occultata*" is derived from the Latin adjective "*occultatus*" meaning concealed or hidden, a reference to this new freshwater mussel being hidden in a small stream far from the main river.

Distribution. This new species is known only from the type locality, Yang Stream in Udon Thani Province. Yang Stream is a headwater tributary of the Lam Pao River in the Chi River Basin. The type locality is above the Lam Pao Dam.

Remarks. This new species is rare and difficult to find despite repeated surveys. They were collected from a network of dense tree roots on a clay wall of a small stream. Nearby, there was a community of unionid mussels living in muddy or sandy substrate of the stream bottom, including *Scabies phaselus* (Lea, 1856), *Physunio modelli* Brandt, 1974, *Namkongnaia inkhavilayi* Jeratthitikul et al., 2021, *P. exilis*, *S. brandti*, and *Thaiconcha callifera* (Martens, 1860).

Discussion

Our findings have revealed previously unknown freshwater mussels within the Mekong basin, comprising two distinct genera and three new species. The discovery of new taxa in this study increases the known diversity of the Pseudodontini to eleven genera with 50 extant species. This makes this tribe the most species-rich clade endemic to Southeast Asia, more than in Contradentini (35 species) or Gonideini (27 species), for example (Graf and Cummings 2021; Bolotov et al. 2023). In the past decade, the diversity within this tribe has significantly increased, with several lineages (species and genera) being recently described from Indochina (Bolotov et al. 2020, 2023; Jeratthitikul et al. 2021b, 2022; Konopleva et al. 2021, 2023; Jeratthitikul and Sutcharit 2023). This highlights the unique evolutionary history of the region and underscores the tribe's remarkable diversity.

Both two new genera share shell characteristics with other genera in Pseudodontini by having a V-shaped fossette at the posterior end of the hinge structure, and absence of lateral teeth (Lopes-Lima et al. 2017). However, we cannot confirm another distinctive feature of the tribe which is the presence of a double-looped or W-shaped pattern on the umbonal area (Lopes-Lima et al. 2017), because the umbonal area of all of the examined specimens was extensively eroded, even in young specimens. Similarly, we were unable to examine the glochidia of the new genera since no brooding individuals were collected during this study. However, it is likely that their glochidia exist as an unhooked and semi-elliptical structure, which is the typical shape of glochidia among the Gonideinae (Pfeiffer and Graf 2015; Lopes-Lima et al. 2017).

Molecular phylogenetic analyses further strongly support the inclusion of these two new genera within the subtribe Pseudodontina, with high support values (BS = 99%, bpp = 1). The two new genera possess shell characteristics that fit well with other members of the subtribe, such as fairly thin shells with much reduced or even lacking pseudocardinal teeth (Bolotov et al. 2020, 2023; Konopleva et al. 2021; Jeratthitikul et al. 2022). These shell characteristics make them different from members in the subtribe Indopseudodontina, which generally have thicker shells and possess well-developed knob-like pseudocardinal teeth (Bolotov et al. 2023). However, the phylogenetic relationships among genera within the Pseudodontina in this study, as well as in some previous studies that used similar genetic markers (i.e., a concatenated dataset of COI + 16S rRNA + 28S rRNA), remain largely unclear and still controversial (e.g., Jeratthitikul et al. 2021b; Bolotov et al. 2023; Konopleva et al. 2023). To clarify these relationships, future investigations should incorporate longer nucleotide sequences and additional gene fragments, or utilize more informative molecular markers such as mitogenomic or nuclear genomic data which have been previously successfully employed in the phylogenetic studies of freshwater mussels (Pfeiffer et al. 2019, 2021; Froufe et al. 2020; Zieritz et al. 2021a; Wu et al. 2024).

The three new species described in this study are rare, restricted to small geographic areas, and likely confined to a single drainage. Species with limited ranges are more vulnerable to threats from human activities and climate change compared to widely distributed species (Randklev et al. 2015; da Silva et al. 2023), with some already extinct on a local scale, such as several endemic species in North America (Bogan 1993; Haag and Williams 2014). Urgent conservation efforts are needed. However, essential biological data, such as their geographical distribution, habitat preferences, and fish hosts for their glochidia, remain unknown. Addressing these knowledge gaps is crucial for developing effective conservation strategies and for further understanding freshwater mussel biodiversity in Southeast Asia.

Ethical statement

The animal uses in this study have been approved by the Faculty of Science, Mahidol University Animal Care and Use Committee, SCMU-ACUC (MUSC65-013-606).

Author contributions

EJ and PP developed the concept of the study. All authors collected specimens. EJ performed phylogenetic analyses and prepared taxonomic accounts with input from CS. CS prepared shell images. EJ prepared the manuscript and all illustrations. All authors discussed, gave input and acknowledged the final version of the manuscript.

Acknowledgements

We thank K. Wisittikoson and S. Klomthong for their assistance in collecting samples, and extend our thanks to D.J. Anderson for grammar checking and comments.

This study was financially supported by SUT Research and Development Fund (IRD1-104-66-12-22).

References

Abell R, Thieme ML, Revenga C, Bryer M, Kottelat M, Bogutskaya N, Coad B, Mandrak N, Balderas SC, Bussing W, Stiassny MLJ, Skelton P, Allen GR, Unmack P, Naseka A, Ng R, Sindorf N, Robertson J, Armijo E, Higgins JV, Heibel TJ, Wikramanayake E, Olson D, López HL, Reis RE, Lundberg JG, Sabaj Pérez MH, Petry P (2008) Freshwater ecoregions of the World: A new map of biogeographic units for freshwater biodiversity conservation. BioScience 58: 403–414. https://doi.org/10.1641/B580507

Aldridge DC, Ollard IS, Bespalaya YV, Bolotov IN, Douda K, Geist J, Haag WR, Klunzinger MW, Lopes-Lima M, Mlambo MC, Riccardi N, Sousa R, Strayer DL, Torres SH, Vaughn CC, Zając T, Zieritz A (2023) Freshwater mussel conservation: A global horizon scan of emerging threats and opportunities. Global Change Biology 29: 575–589. https://doi.org/10.1111/gcb.16510

AVMA (2020) AVMA guidelines for the euthanasia of animals. American Veterinary Medical Association.

Bogan AE (1993) Freshwater bivalve extinctions (Mollusca: Unionoida): A search for causes. American Zoologist 33: 599–609. https://doi.org/10.1093/icb/33.6.599

Bolotov IN, Kondakov AV, Vikhrev IV, Aksenova OV, Bespalaya YV, Gofarov MY, Kolosova YS, Konopleva ES, Spitsyn VM, Tanmuangpak K, Tumpeesuwan S (2017a) Ancient river inference explains exceptional oriental freshwater mussel radiations. Scientific Reports 7: 2135. https://doi.org/10.1038/s41598-017-02312-z

Bolotov IN, Vikhrev IV, Kondakov AV, Konopleva ES, Gofarov MY, Aksenova OV, Tumpeesuwan S (2017b) New taxa of freshwater mussels (Unionidae) from a species-rich but overlooked evolutionary hotspot in Southeast Asia. Scientific Reports 7: 11573. https://doi.org/10.1038/s41598-017-11957-9

Bolotov IN, Konopleva ES, Vikhrev IV, Gofarov MY, Lopes-Lima M, Bogan AE, Lunn Z, Chan N, Win T, Aksenova OV, Tomilova AA, Tanmuangpak K, Tumpeesuwan S, Kondakov AV (2020) New freshwater mussel taxa discoveries clarify biogeographic division of Southeast Asia. Scientific Reports 10: 6616. https://doi.org/10.1038/s41598-020-63612-5

Bolotov IN, Konopleva ES, Vikhrev IV, Gofarov MY, Kondakov AV, Lyubas AA, Soboleva AA, Chan N, Lunn Z, Win T, Inkhavilay K (2023) Integrative taxonomic reappraisal and evolutionary biogeography of the most diverse freshwater mussel clade from Southeast Asia (Pseudodontini). Water 15: 3117. https://doi.org/10.3390/w15173117

Brandt RAM (1974) The non-marine aquatic Mollusca of Thailand. Archiv für Molluskenkunde 105: 1–423.

da Silva JP, Sousa R, Gonçalves DV, Miranda R, Reis J, Teixeira A, Varandas S, Lopes-Lima M, Filipe AF (2023) Streams in the Mediterranean Region are not for mussels: Predicting extinctions and range contractions under future climate change. Science of the Total Environment 883: 163689. https://doi.org/10.1016/j.scitotenv.2023.163689

Frierson L (1927) A Classified and Annotated Check List of the North American Naiades. Baylor University Press, Waco, Texas.

Froufe E, Bolotov I, Aldridge DC, Bogan AE, Breton S, Gan HM, Kovitvadhi U, Kovitvadhi S, Riccardi N, Secci-Petretto G, Sousa R, Teixeira A, Varandas S, Zanatta D, Zieritz A, Fonseca MM, Lopes-Lima M (2020) Mesozoic mitogenome rearrangements and freshwater mussel (Bivalvia: Unionoidea) macroevolution. Heredity 124: 182–196. https://doi.org/10.1038/s41437-019-0242-y

Gould AA (1844) Dr. Gould read descritiptions of two *Anodon*, from the river Salwen, in British Burmah, sent him by Rev. F. Mason. Proceedings of the Boston Society of Natural History 1: 160–161.

Graf DL, Cummings KS (2021) A 'big data' approach to global freshwater mussel diversity (Bivalvia: Unionoida), with an updated checklist of genera and species. Journal of Molluscan Studies 87: eyaa034. https://doi.org/10.1093/mollus/eyaa034

Haag WR, Williams JD (2014) Biodiversity on the brink: An assessment of conservation strategies for North American freshwater mussels. Hydrobiologia 735: 45–60. https://doi.org/10.1007/s10750-013-1524-7

Hoang DT, Chernomor O, von Haeseler A, Minh BQ, Vinh LS (2018) UFBoot2: Improving the Ultrafast Bootstrap Approximation. Molecular Biology and Evolution 35: 518–522. https://doi.org/10.1093/molbev/msx281

Huang X-C, Rong J, Liu Y, Zhang M-H, Wan Y, Ouyang S, Zhou C-H, Wu X-P (2013) The complete maternally and paternally inherited mitochondrial genomes of the endangered freshwater mussel *Solenaia carinatus* (Bivalvia: Unionidae) and implications for Unionidae taxonomy. PLOS ONE 8: e84352. https://doi.org/10.1371/journal.pone.0084352

Jeratthitikul E, Sutcharit C (2023) Multi-locus phylogeny reveals a new freshwater mussel in the genus *Bineurus* Simpson, 1900 (Unionidae: Pseudodontini) from Thailand. Tropical Natural History Supplement 7: 173–180.

Jeratthitikul E, Phuangphong S, Sutcharit C, Prasankok P, Kongim B, Panha S (2019) Integrative taxonomy reveals phenotypic plasticity in the freshwater mussel *Contradens contradens* (Bivalvia: Unionidae) in Thailand, with a description of a new species. Systematics and Biodiversity 17: 134–147. https://doi.org/10.1080/14772000.2018.1554607

Jeratthitikul E, Paphatmethin S, Zieritz A, Lopes-Lima M, Ngor PB (2021a) *Hyriopsis panhai*, a new species of freshwater mussel from Thailand (Bivalvia: Unionidae). Raffles Bulletin of Zoology 69: 124–136. https://doi.org/10.26107/RBZ-2021-0011

Jeratthitikul E, Sutcharit C, Ngor PB, Prasankok P (2021b) Molecular phylogeny reveals a new genus of freshwater mussels from the Mekong River Basin (Bivalvia: Unionidae). European Journal of Taxonomy 775: 119–142. https://doi.org/10.5852/ejt.2021.775.1553

Jeratthitikul E, Paphatmethin S, Sutcharit C, Ngor PB, Inkhavilay K, Prasankok P (2022) Phylogeny and biogeography of Indochinese freshwater mussels in the genus *Pilsbryoconcha* Simpson, 1900 (Bivalvia: Unionidae) with descriptions of four new species. Scientific Reports 12: 20458. https://doi.org/10.1038/s41598-022-24844-9

Jovelin R, Justine J-L (2001) Phylogenetic relationships within the polyopisthocotylean monogeneans (Platyhelminthes) inferred from partial 28S rDNA sequences. International Journal for Parasitology 31: 393–401. https://doi.org/10.1016/S0020-7519(01)00114-X

Kongim B, Sutcharit C, Panha S (2015) Cytotaxonomy of unionid freshwater mussels (Unionoida, Unionidae) from northeastern Thailand with description of a new species. ZooKeys 514: 93–110. https://doi.org/10.3897/zookeys.514.8977

Kongim B, Sutcharit C, Jeratthitikul E (2023) Discovery of a new endangered freshwater mussel species in the genus *Chamberlainia* Simpson, 1900 (Bivalvia: Unionidae) from mekong basin. Tropical Natural History Supplement 7: 242–250.

Konopleva ES, Pfeiffer JM, Vikhrev IV, Kondakov AV, Gofarov MY, Aksenova OV, Lunn Z, Chan N, Bolotov IN (2019) A new genus and two new species of freshwater mussels (Unionidae) from western Indochina. Scientific Reports 9: 4106. https://doi.org/10.1038/s41598-019-39365-1

Konopleva ES, Bolotov IN, Pfeiffer JM, Vikhrev IV, Kondakov AV, Gofarov MY, Tomilova AA, Tanmuangpak K, Tumpeesuwan S (2021) New freshwater mussels from two Southeast Asian genera *Bineurus* and *Thaiconcha* (Pseudodontini, Gonideinae, Unionidae). Scientific Reports 11: 8244. https://doi.org/10.1038/s41598-021-87633-w

Konopleva ES, Lheknim V, Sriwoon R, Kondakov AV, Tomilova AA, Gofarov MY, Vikhrev IV, Bolotov IN (2023) Diversity and phylogenetics of freshwater mussels (Unionidae) from southern Thailand with the description of one new genus and five new species-group taxa. Diversity 15: 10. https://doi.org/10.3390/d15010010

Lanfear R, Frandsen PB, Wright AM, Senfeld T, Calcott B (2017) PartitionFinder 2: New methods for selecting partitioned models of evolution for molecular and morphological phylogenetic analyses. Molecular Biology and Evolution 34: 772–773. https://doi.org/10.1093/molbev/msw260

Lea I (1838) Description of new freshwater and land shells. Transactions of the American Philosophical Society 6: 1–154. https://doi.org/10.2307/1005319

Lea I (1840) Descriptions of new fresh water and land shells. Proceedings of the American Philosophical Society 1: 284–289.

Lea I (1856) Description of twenty-five new species of exotic uniones. Proceedings of the Academy of Natural Sciences of Philadelphia 8: 92–95.

Lobo J, Costa PM, Teixeira MAL, Ferreira MSG, Costa MH, Costa FO (2013) Enhanced primers for amplification of DNA barcodes from a broad range of marine metazoans. BMC Ecology 13: 34. https://doi.org/10.1186/1472-6785-13-34

Lopes-Lima M, Froufe E, Do VT, Ghamizi M, Mock KE, Kebapçı Ü, Klishko O, Kovitvadhi S, Kovitvadhi U, Paulo OS, Pfeiffer JM, Raley M, Riccardi N, Şereflişan H, Sousa R, Teixeira A, Varandas S, Wu X, Zanatta DT, Zieritz A, Bogan AE (2017) Phylogeny of the most species-rich freshwater bivalve family (Bivalvia: Unionida: Unionidae): Defining modern subfamilies and tribes. Molecular Phylogenetics and Evolution 106: 174–191. https://doi.org/10.1016/j.ympev.2016.08.021

Lopes-Lima M, Burlakova LE, Karatayev AY, Mehler K, Seddon M, Sousa R (2018) Conservation of freshwater bivalves at the global scale: Diversity, threats and research needs. Hydrobiologia 810: 1–14. https://doi.org/10.1007/s10750-017-3486-7

Lydeard C, Mulvey M, Davis GM (1996) Molecular systematics and evolution of reproductive traits of North American freshwater unionacean mussels (Mollusca: Bivalvia) as inferred from 16S rRNA gene sequences. Philosophical Transactions of the Royal Society of London Series B: Biological Sciences 351: 1593–1603. https://doi.org/10.1098/rstb.1996.0143

Martens EV (1860) On the Mollusca of Siam. Proceedings of the Zoological Society of London 1860: 6–18.

Miller MA, Pfeiffer W, Schwartz T (2010) Creating the CIPRES Science Gateway for inference of large phylogenetic trees. 2010 Gateway Computing Environments Workshop (GCE), 1–8. https://doi.org/10.1109/GCE.2010.5676129

Minh BQ, Schmidt HA, Chernomor O, Schrempf D, Woodhams MD, von Haeseler A, Lanfear R (2020) IQ-TREE 2: New models and efficient methods for phylogenetic inference in the genomic era. Molecular Biology and Evolution 37: 1530–1534. https://doi.org/10.1093/molbev/msaa015

Ortmann AE (1916) The anatomical structure of *Gonidea angulata* (Lea). Nautilus 30: 50–53.

Petit de la Saussaye S (1865) Note sur le genre Monocondylea de d'Orbigny, et description d'une espèce nouvelle. Journal de Conchyliologie 13: 15–19.

Pfeiffer JM, Graf DL (2015) Evolution of bilaterally asymmetrical larvae in freshwater mussels (Bivalvia: Unionoida: Unionidae). Zoological Journal of the Linnean Society 175: 307–318. https://doi.org/10.1111/zoj.12282

Pfeiffer JM, Breinholt JW, Page LM (2019) Unioverse: A phylogenomic resource for reconstructing the evolution of freshwater mussels (Bivalvia, Unionoida). Molecular Phylogenetics and Evolution 137: 114–126. https://doi.org/10.1016/j.ympev.2019.02.016

Pfeiffer JM, Graf DL, Cummings KS, Page LM (2021) Taxonomic revision of a radiation of Southeast Asian freshwater mussels (Unionidae: Gonideinae: Contradentini+Rectidentini). Invertebrate Systematics 35: 394–470. https://doi.org/10.1071/IS20044

Prashad B (1922) A revision of the Burmese Unionidae. Records of the Indian Museum 24: 91–111. https://doi.org/10.26515/rzsi/v24/i1/1922/163472

Rafinesque CS (1820) Monographie des coquilles bivalves fluviatiles de la Riviere Ohio, contenant douze genres et soixante-huit especes. Annales Générales des Sciences Physiques 5(13): 287–322.

Randklev CR, Wang H-H, Groce JE, Grant WE, Robertson S, Wilkins N (2015) Land use relationships for a rare freshwater mussel species endemic to Central Texas. Journal of Fish and Wildlife Management 6: 327–337. https://doi.org/10.3996/012015-JFWM-003

Rochebrune AT (1882) Documents sur la faune malacologique de la Cochinchine et du Cambodge. Bulletin de la Société philomathique de Paris 6: 35–74.

Ronquist F, Teslenko M, van der Mark P, Ayres DL, Darling A, Höhna S, Larget B, Liu L, Suchard MA, Huelsenbeck JP (2012) MrBayes 3.2: Efficient Bayesian phylogenetic inference and model choice across a large model space. Systematic Biology 61: 539–542. https://doi.org/10.1093/sysbio/sys029

San Mauro D, Agorreta A (2010) Molecular systematics: A synthesis of the common methods and the state of knowledge. Cellular and Molecular Biology Letters 15: 311–341. https://doi.org/10.2478/s11658-010-0010-8

Simpson CT (1900) Synopsis of the naiades, or pearly fresh-water mussels. Proceedings of the United States National Museum 22: 501–1044. https://doi.org/10.5479/si.00963801.22-1205.501

Tamura K, Stecher G, Kumar S (2021) MEGA11: Molecular Evolutionary Genetics Analysis Version 11. Molecular Biology and Evolution 38: 3022–3027. https://doi.org/10.1093/molbev/msab120

Wu R, Zhang L, Liu L, Jia J, Liu X (2024) Unraveling the phylogenetic relationships and taxonomic status of a puzzling freshwater mussel genus *Inversidens* (Bivalvia, Unionidae) through multilocus phylogeny and mitochondrial phylogenomics. Journal of Zoological Systematics and Evolutionary Research 2024: 1499508. https://doi.org/10.1155/2024/1499508

Zieritz A, Lopes-Lima M, Bogan AE, Sousa R, Walton S, Rahim KAA, Wilson J-J, Ng P-Y, Froufe E, McGowan S (2016) Factors driving changes in freshwater mussel (Bivalvia, Unionida) diversity and distribution in Peninsular Malaysia. Science of the Total Environment 571: 1069–1078. https://doi.org/10.1016/j.scitotenv.2016.07.098

Zieritz A, Bogan AE, Froufe E, Klishko O, Kondo T, Kovitvadhi U, Kovitvadhi S, Lee JH, Lopes-Lima M, Pfeiffer JM, Sousa R, Van Do T, Vikhrev I, Zanatta DT (2018) Diversity, biogeography and conservation of freshwater mussels (Bivalvia: Unionida) in East and Southeast Asia. Hydrobiologia 810: 29–44. https://doi.org/10.1007/s10750-017-3104-8

Zieritz A, Taha H, Lopes-Lima M, Pfeiffer J, Sing KW, Sulaiman Z, McGowan S, A.Rahim KA (2020) Towards the conservation of Borneo's freshwater mussels: Rediscovery of the endemic *Ctenodesma borneensis* and first record of the non-native *Sinanodonta lauta*. Biodiversity and Conservation 29: 2235–2253. https://doi.org/10.1007/s10531-020-01971-1

Zieritz A, Froufe E, Bolotov I, Gonçalves DV, Aldridge DC, Bogan AE, Gan HM, Gomes-Dos-Santos A, Sousa R, Teixeira A, Varandas S, Zanatta D, Lopes-Lima M (2021a) Mitogenomic phylogeny and fossil-calibrated mutation rates for all F- and M-type mtDNA genes of the largest freshwater mussel family, the Unionidae (Bivalvia). Zoological Journal of the Linnean Society 193: 1088–1107. https://doi.org/10.1093/zoolinnean/zlaa153

Zieritz A, Jainih L, Pfeiffer J, Rahim KAA, Prayogo H, Anwari MS, Fikri AH, Diba F, Taha H, Sulaiman Z, Froufe E, Lopes-Lima M (2021b) A new genus and two new, rare freshwater mussel (Bivalvia: Unionidae) species endemic to Borneo are threatened by ongoing habitat destruction. Aquatic Conservation: Marine and Freshwater Ecosystems 31: 3169–3183. https://doi.org/10.1002/aqc.3695

Supplementary material 1

List of voucher specimens with GenBank accession numbers used in phylogenetic analysis

Authors: Ekgachai Jeratthitikul, Chirasak Sutcharit, Pongpun Prasankok

Data type: docx

Link: https://doi.org/10.3897/zse.100.130929.suppl1

Zoosyst. Evol. 100 (4) 2024, 1347–1360 | DOI 10.3897/zse.100.128717

PENSOFT

MUSEUM FÜR NATURKUNDE BERLIN

Four new species of *Georissa* W. Blanford, 1864 (Gastropoda, Hydrocenidae) from Thailand

Kanyaporn Klongklaew[1], Supattra Poeaim[1], Pongrat Dumrongrojwattana[2]

1 *Department of Biology, School of Science, King Mongkut's Institute of Technology Ladkrabang, Bangkok 10520, Thailand*

2 *Department of Biology, Faculty of Science, Burapha University, Bangsaen, Chonburi 20131, Thailand*

https://zoobank.org/FD4C02D2-01F9-4A4C-817B-F81B27F22A41

Corresponding author: Supattra Poeaim (supattra.poe@kmitl.ac.th)

Academic editor: Frank Köhler ♦ **Received** 31 May 2024 ♦ **Accepted** 19 August 2024 ♦ **Published** 4 October 2024

Abstract

Hydrocenid snails have received little research attention compared to other land snail groups, arguably due to their small size. The present study examines the diversity of hydrocenid snails in limestone hills in central, eastern and southern Thailand. Four new species of *Georissa* W. Blanford, 1864 are described: *G. quinquelirata* **sp. nov.** from central Thailand, *G. sagitta* **sp. nov.** and *G. kohsichangensis* **sp. nov.** from eastern Thailand, and *G. digitinota* **sp. nov.** from southern Thailand. These four new species are distinguished by unique characteristics in their shell, including protoconch sculpture and shell shape, operculum, and radula morphology. A phylogenetic analysis of mitochondrial DNA sequences confirms the distinctiveness of all four species.

Key Words

conchological, Neritimorpha, Southeast Asia, systematics, terrestrial snails

Introduction

Microscopic land snails of the family Hydrocenidae Troschel, 1857 are widely distributed with a range encompassing various Pacific islands, New Zealand, Australia, the Indo-Australian Archipelago, parts of Europe, Asia, Madagascar, and Africa (Egorov 2005). In Asia, hydrocenid snails have been documented in Thailand, Cambodia, Laos, Myanmar, Vietnam, Malaysia, Japan, the Philippines, India, and China (Panha and Burch 2005). Traditionally, the systematic taxonomy of hydrocenids rests primarily on morphological characters. Overall, Hydrocenidae have received little attention in research due to their tiny shell size while the delineation of species is complicated by considerable conchological variation in some species in response to diverse ecological conditions in the their habitats. DNA barcoding holds significant potential to identify cryptic species thereby overcoming the limitations of traditional morphological characters in species identification and delimitation in these micro-snails. DNA barcoding has been useful in identifying a broad spectrum of micro snails, such as in the ellobiids *Zospeum* and *Carychium* (Weigand et al. 2011, 2013), the diplommatinid *Plectostoma concinnum*, the cyclophorid *Alycaeus jagori* (Hendriks et al. 2019), and the gastroscopic *Hypselostoma latispira* (Lipae et al. 2020). However, morphological analyses remain the primary method for distinguishing species despite the challenges posed by the tiny size, conchological variability, and ecological plasticity of hydrocenids. Hence, a combination of molecular and morphology analyses promises to be the best approach for identifying different species within this group.

Georissa is a genus of operculated micro-land snails frequently found in limestone environments. The majority of *Georissa* species have so far been recorded in Malaysia (Schilthuizen et al. 2005, 2012; Haase and Schilthuizen 2007; Phung et al. 2017; Khalik et al. 2018, 2019a, 2019b). Notably, DNA barcoding has proven effective in distinguishing *Georissa* species in Malaysia, as demonstrated in the studies of Khalik et al. (2018, 2019b). These studies reported thirteen scaly species and sixteen non-scaly species from Malaysian Borneo alone.

The cytochrome c oxidase subunit 1 (COI or COX1) gene within mitochondrial DNA served as the predominant and widely utilized DNA barcoding marker in animals, proving to be effective for identification purposes in *Georissa* (Khalik et al. 2018, 2019a, 2019b; Hendriks et al. 2019) and were used in this study. However, other genes such as 16S ribosomal deoxyribonucleic acid (rDNA), 18S rDNA, 28S rDNA, histone 3 (H3) and the aquaporin gene have also been analyzed and successfully delineated in *Georissa* (Kano et al. 2003; Schilthuizen et al. 2005, 2012; Uribe et al. 2016; Colgan and Santos 2018; Khalik et al. 2018, 2019a, 2019b; Hendriks et al. 2019). However, DNA barcoding has not been conducted on *Georissa* in China, Cambodia, Laos, Myanmar, Vietnam, and Thailand. A list of *Georissa* species and their distribution on the mainland in Southeast Asia and China is given in Suppl. material 1.

In Thailand, six species and two subspecies of the genus *Georissa* have been identified (BEDO 2017) and reported through morphological analysis: *G. illex* Benson, 1856, *G. blanfordiana* Stoliczka, 1871, *G. liratula* Stoliczka, 1871, *G. monterosatiana monterosatiana* Godwin-Austin & Nevill, 1879, *G. semisculpta* Godwin-Austen & Nevill, 1879, *G. williamsi* Godwin-Austen, 1889, *G. monterosatiana samuiana* Möllendorff, 1894 (Benson 1856; Stoliczka 1871; Godwin-Austen and Nevill 1879; Godwin-Austen 1889; Möllendorff 1894). This research aimed to present the findings on four new species of hydrocenid snails from Thailand, identified as novel to science based on their shell, operculum, and radula morphology, incorporating DNA barcoding.

Materials and methods

Specimen sampling

The specimens have been received from Asst. Prof. Pongrat Dumrongrojwattana and were collected during fieldwork between July 2019 and February 2023. We surveyed four locations, including Pathawi limestone hill, Uthai Thani Province (15°28'26.9"N, 99°45'25.0"E), Yai Man Cave, Chonburi Province (13°09'08.2"N, 100°48'28.0"E), Khao Maka cave temple, Sa Kaeo Province (13°47'16.6"N, 101°56'53.7"E), and Khao Noi Phothiyan temple, Satun Province (06°45'24.2"N, 100°01'54.2"E) (refer to map in Fig. 1). Hydrocenid specimens were collected through visual searching. We collected both living individuals and empty shells. When collecting empty shells, we picked the operculum from the rock surface to which the shell was attached or from the soil where shells accumulated. Living snails were drowned in water and subsequently preserved in 50% ethanol. These procedures were carried out in the Biology Department, School of Science, at King Mongkut's Institute of Technology Ladkrabang (KMITL) and the Biology Department, Faculty of Science, at Burapha University (BUU).

Morphological studies

The collected specimens were thoroughly cleaned and air-dried. Shell was digitally photographed in standardized views (Callomon 2019). We measured the following shell dimensions (in mm): Shell height (SH), shell width (SW), aperture height (AH), and aperture width (AW) on photographs by using ImageJ version 1.8.0. (Schneider et al. 2012). Taxonomic identifications were carried out by referencing the works of Vermeulen and Whitten (1998) and Panha and Burch (2005). To extract the radula, snails were boiled in 1% (w/v) sodium hydroxide (NaOH) solution in a test tube for 10–20 minutes depending on sample size (modified from Geiger et al. 2007). Subsequently, the radula was extracted under a stereo microscope by using an insect pin No. 0, rinsed with distilled water, and dehydrated in a series of ethanol concentrations (increasing from 10, 30, 50 to 70% for 5 minutes each concentration) (Dumrongrojwattana and Tanmuangpak 2020). Shells, opercula, and radulae were imaged under a scanning electron microscope (SEM). Type specimens were deposited in the Zoological Research Collection of Burapha University (ZRCBUU) in Chon Buri Province, Thailand.

Molecular analysis

Genomic DNA was extracted from representative individuals of different morphotypes by using the GF-1 tissue DNA extraction kit. Preserved snails were rinsed twice in sterilized distilled water before extraction. Partial sequences of the COI gene were amplified by Polymerase Chain Reaction (PCR) using primers the LCO1490 and HCO2198 (Folmer et al. 1994). For PCR protocols and conditions refer to Khalik et al. (2019a). Gel electrophoresis with 1% agarose gel was employed to evaluate the quality and size of the PCR products. DNA sequencing was performed using the Barcode Tag Sequencing (BTSeq) technique, which relies on Next-Generation Sequencing (NGS), at Celemics, Inc., Korea. Twenty-nine sequences were analyzed in this study, including 21 sequences sourced from GenBank and eight from this study. All sequences have been deposited in the GenBank database (https://www.ncbi.nlm.nih.gov/genbank) (Table 1). Bayesian Inference was employed to reconstruct a phylogenetic tree using MrBayes version 3.2.7. (Ronquist et al. 2012). The Effective Sample Size (ESS) values and log-likelihoods were monitored to ensure the analysis reached stationarity. Model selection for the COI gene phylogenetic tree was performed using jModelTest 2 (Darriba et al. 2012), based on the Bayesian Information Criterion (BIC). The Bayesian Inference analysis was conducted with parameters set to 10,000,000 generations, sampling every 1,000 generations, and discarding the first 25% of trees as burn-in. (Pholyotha et al. 2021).

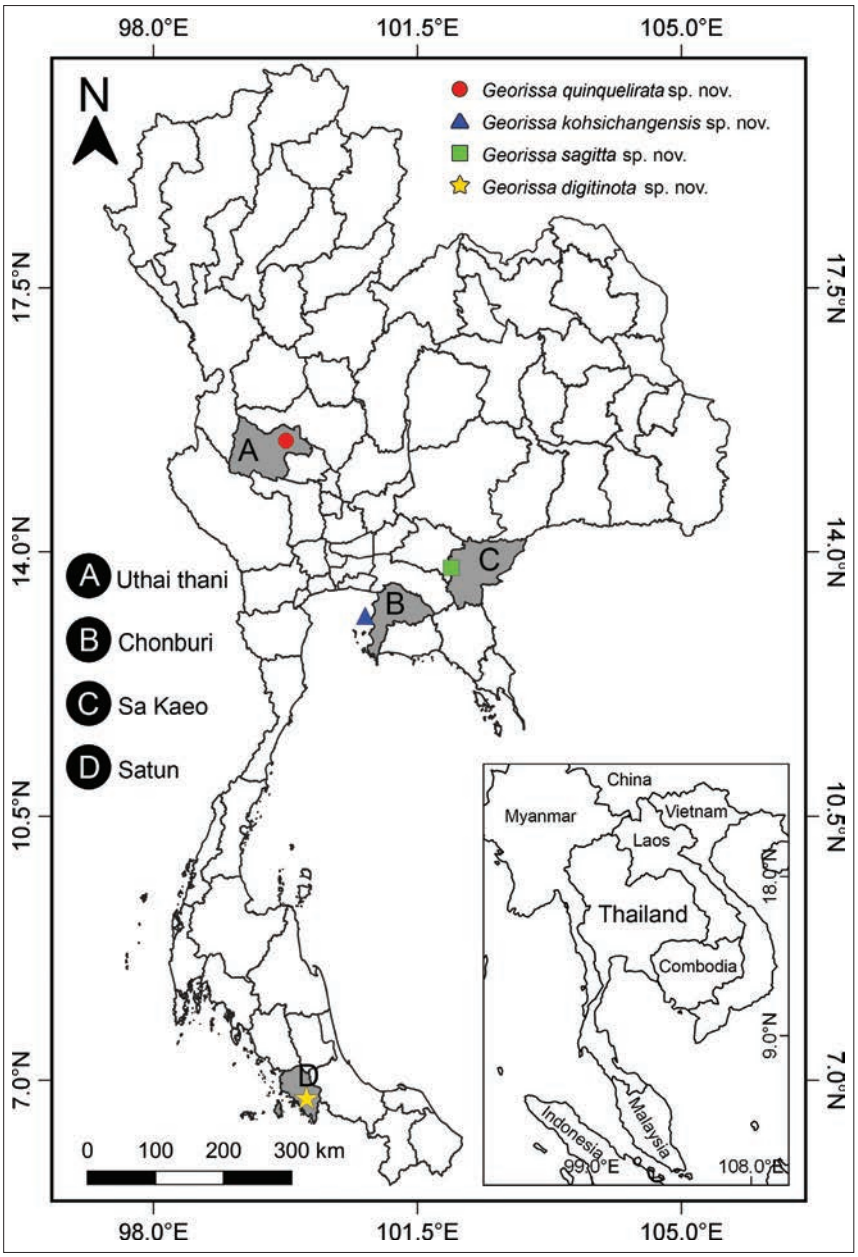

Figure 1. Type localities of *Georissa quinquelirata* sp. nov. (marked with a red circle) in central Thailand, *Georissa kohsichangensis* sp. nov. (marked with a blue triangle), and *Georissa sagitta* sp. nov. (marked with a green square) in eastern Thailand, along with *Georissa digitinota* sp. nov. (marked with a yellow star) in southern Thailand.

Results

Specimen sampling and morphological studies

Hydrocenid snails were found outside the cave, on limestone surfaces, and were particularly abundant on moist surfaces. Based on visual inspection, the shells are tiny, with an average height ranging from 1 to 3 mm. Living snails were orange to brownish. By contrast, deceased snails were white to pale yellow. The shell shape is uniformly round, with spiral cords on the body whorl, the number of which varies among species. Additionally, the aperture is typically round to ovate, the umbilicus is closed, and the white chitinous (corneous) operculum is thin and opaque. Through morphological examination and DNA barcoding, four new *Georissa* species in Thailand were identified, including *G. quinquelirata* sp. nov. from Uthai Thani Province, *G. kohsichangensis* sp. nov. from Chonburi Province, *G. sagitta* sp. nov. from Sa Kaeo Province and *G. digitinota* sp. nov. from Satun Province. The type localities of four new *Georissa* species are displayed in Fig. 1.

Each of the four new *Georissa* species exhibits distinct shell characteristics by first classifying groups based on shell shape. Then, species within each group are distinguished by the number of shell whorls. Further differentiation is made based on shell size for species with the same number of whorls (W). Additionally, the sculpture

Table 1. Sequences used in this study.

No.	Species	Accession number	Reference
1	*Georissa bauensis* isolate B.002	MH033937	Khalik et al. 2018
2	*Georissa bauensis* isolate Q.006	MH033943	Khalik et al. 2018
3	*Georissa hadra* isolate LC.01	MH033896	Khalik et al. 2018
4	*Georissa hadra* isolate LC.03	MH033894	Khalik et al. 2018
5	*Georissa hungerfordi* voucher H.002	MK505430	Khalik et al. 2019b
6	*Georissa hungerfordi* voucher I.002	MK505438	Khalik et al. 2019b
7	*Georissa kinabatanganensis* isolate K.002	MH033958	Khalik et al. 2018
8	*Georissa kinabatanganensis* isolate K.005	MH033960	Khalik et al. 2018
9	*Georissa muluensis* isolate LGG.01	MH033893	Khalik et al. 2018
10	*Georissa muluensis* isolate LGG.03	MH033892	Khalik et al. 2018
11	*Georissa nephrostoma* voucher Knep.001	MK505439	Khalik et al. 2019b
12	*Georissa niahensis* isolate GC.02	MH033880	Khalik et al. 2018
13	*Georissa niahensis* isolate PC.04	MH033954	Khalik et al. 2018
14	*Georissa pachysoma* voucher BSM2.03	MK505441	Khalik et al. 2019b
15	*Georissa pachysoma* voucher BSM2.04	MK505440	Khalik et al. 2019b
16	*Georissa sepulutensis* isolate Sca.002	MH033964	Khalik et al. 2018
17	*Georissa sepulutensis* isolate Sca.004	MH033953	Khalik et al. 2018
18	*Georissa silaburensis* isolate SIG3.03	MH033948	Khalik et al. 2018
19	*Georissa silaburensis* voucher SIG4.04	MK811541	Khalik et al. 2019a
20	*Diplommatina centralis* isolate 4050	HM753339	Webster et al. 2012
21	*Plectostoma concinnum* voucher KPH01588.25	MH254006	Hendriks et al. 2019
22	*Georissa quinquelirata* sp. nov. isolate CPW01.01	PP844569	This study
23	*Georissa quinquelirata* sp. nov. isolate CPW01.03	PP844570	This study
24	*Georissa kohsichangensis* isolate EYM01.03	PP844571	This study
25	*Georissa kohsichangensis* isolate EYM01.04	PP844572	This study
26	*Georissa sagitta* isolate EMK01.01	PP844573	This study
27	*Georissa sagitta* isolate EMK01.02	PP844574	This study
28	*Georissa digitinota* sp. nov. isolate SKN01.04	PP844575	This study
29	*Georissa digitinota* sp. nov. isolate SKN01.05	PP844576	This study

pattern and number of lines on the last body whorl, as well as the shape and surface of the operculum, are used for grouping. These characteristics examined under a stereo microscope, and SEM images were utilized (Figs 2, 4). The shell shape can be categorized into two types: *Georissa sagitta* sp. nov., *G. quinquelirata* sp. nov., and *G. kohsichangensis* sp. nov. have an ovate-conical shape. In particular, *G. kohsichangensis* sp. nov. reveals slight variation whereby the upper half part of the body whorls slopes slightly downward. Conversely, *G. digitinota* sp. nov. has a globose-conical shape (Fig. 2). The species are listed in the order from largest to smallest size as follows: *G. sagitta* sp. nov. (2.4–2.9 mm), *G. digitinota* sp. nov. (2.3–2.7 mm), *G. quinquelirata* sp. nov. (1.9–2.5 mm), and *G. kohsichangensis* sp. nov. (1.7–2.1 mm). Based on the sculpture pattern and the number of lines on the last (or body) whorl, *G. quinquelirata* sp. nov. features a carina-style sculpture with 5–6 prominent cords and weak growth lines between the carinae (Fig. 4A). *Georissa kohsichangensis* sp. nov. and *G. sagitta* sp. nov. exhibit a lirae-style sculpture, with *G. kohsichangensis* having 6–7 cords (Fig. 4E) and *G. sagitta* having 8–9 cords (Fig. 4I). In contrast, *G. digitinota* sp. nov. displays more than 30 prominent striae or spiral lines, which are more frequent than those of the other new species (Fig. 4M). Each new species examined shows a well-incised suture. The protoconch of each species (Fig. 4B, F, J, N) exhibits distinct microscopic sculpture patterns. The microscopic sculpture of the protoconch is wrinkled in *G. quinquelirata* sp. nov. (Fig. 4C), perforated in *G. kohsichangensis* sp. nov. (Fig. 4G), a combination of rounded, ellipsoidal, irregular sculptures and oval indentations in *G. sagitta* sp. nov. (Fig. 4K). In contrast, *G. digitinota* sp. nov. presents an ellipsoidal to irregular sculpture with an oval fingerprint-like indentation (Fig. 4O). All species assessed display a closed umbilicus. The aperture of the shell is observed; *G. quinquelirata* sp. nov., *G. sagitta* sp. nov., and *G. digitinota* sp. nov. are semi-rounded shape while *G. kohsichangensis* sp. nov. is rhombate-shaped. The operculum is paucispiral, featuring a smooth outer with an apophysis, and an arched peg near the base on the inner side the base (Fig. 4D, L, P, H). Regarding the shape of the operculum, *G. quinquelirata* sp. nov., *G. sagitta* sp. nov., and *G. digitinota* sp. nov. display a semi-rounded shape (Fig. 4D, L, P), whereas *G. kohsichangensis* sp. nov. features a rhombate shape (Fig. 4H).

The radula of all examined new species is rhipidoglossate; revealing two long spiral teeth attached to a thin radula plate in the central teeth area on the radula overview (Fig. 5A, E, I, M), characterized by five small central teeth, five rows of lateral teeth, and two rows of marginal teeth. Counting the teeth of the radula from SEM pictures, the central/rachidian teeth are symmetrical and trapezoid in shape, lateral teeth are claw-like alternately long and short denticles; *G. quinquelirata* sp. nov. has 9–13 denticles, *G. kohsichangensis* sp. nov. has 7–11 denticles, *G. sagitta* sp. nov., and *G. digitinota* sp. nov. have 7–13 denticles, each row of lateral teeth decreasing in size from the first lat-

eral tooth toward the 5th lateral tooth and marginal teeth are claw-like equal-sized denticles; *G. quinquelirata* sp. nov., *G. sagitta* sp. nov. and *G. digitinota* sp. nov. have 12–14 denticles, *G. kohsichangensis* sp. nov. has 14–18 denticles. Therefore, the radula formula is 2:5:1+1+1+1+1+1+1:5:2. In describing the radula's central tooth formula, the notation reflects the variation in the appearance and orientation of each tooth. In our case, teeth 1–2 curve to the right, tooth 3 is normal, and teeth 4–5 curve to the left. This notation helps communicate the structure and asymmetry of the radula. However, it is noteworthy that variations exist among specimens in terms of the length or curvature of the teeth. The four newly discovered species are described below in the phylogenetic analysis section.

Phylogenetic analysis

The phylogenetic analysis is based on 29 sequences from 10 species of *Georissa*, including the four new species described herein. Sequences of *Diplommatina centralis* and *Plectostoma concinnum* were used as outgroups to root the tree. All sequences were deposited in GenBank (Table 1). The COI alignment had a length of 600 base pairs. Based on the outcomes from jModelTest 2, the best model selection for constructing a COI gene phylogenetic tree according to the BIC is the General Time Reversible (GTR) model. This model incorporates rate variation across sites using a gamma distribution (G) with the proportion of invariable sites (I). The phylogenetic tree revealed *Georissa* as monophyletic. The new *Georissa* species form two distinct clades. *Georissa quinquelirata* sp. nov., *G. kohsichangensis* sp. nov., and *G. sagitta* sp. nov. are a monophyletic and paraphyletic group with *G. digitinota* sp. nov. *Georissa digitinota* sp. nov. is the sister taxon of the *Georissa* species from Malaysian Borneo (Khalik et al. 2018, 2019a, 2019b) (refer to Fig. 3).

Systematics

Family Hydrocenidae Troschel, 1857
Subfamily Neritimorpha Koken, 1896

Genus *Georissa* Blanford, 1864

Type species. *Georissa pyxis*, Benson 1856, by original designation.

Georissa quinquelirata Klongkaew, Poeaim & Dumrongrojwattana, sp. nov.

https://zoobank.org/70D34F82-2195-4F29-89F2-24C53848CF95
Figs 2A, 4A–D, 5A–D

Type material. ***Holotype*** • ZRCBUU 0900 (Fig. 2A). SH = 2.45 mm, SW = 1.63 mm, AH = 0.80 mm, AW = 0.91 mm, W = 4.25–4.5. ***Paratype*** • ZRCBUU 0901 (Fig. 4A–D) (13 shells); Shell measurements: SH = 1.91–2.36 mm (2.10 ± 0.15 mm), SW = 1.37–1.60 mm (1.46 ± 0.07 mm), AH = 0.71–0.86 mm (0.78 ± 0.06 mm), AW = 0.80–0.92 mm (0.86 ± 0.04 mm), W = 3.75–4.5 (all type material from type locality; 25 February 2023, P. Dumrongrojwattana leg).

Type locality. Thailand, Pathawi limestone hill, Thap Than district, Uthai Thani Province; 15°28'26.9"N, 99°45'25.0"E.

Etymology. The specific designation "*quinquelirata*" indicates the number of lirae on the whorl.

Diagnosis. Shell minute, ovately conical, orangish to brownish, protoconch round to slightly ellipsoid and wrinkled sculpture. Body whorl have about 5–6 prominent carinae, and between carinae have weak growth lines. Aperture semi-rounded. Umbilicus closed. Operculum corneous with apophysis, paucispiral, opaque white, and semi-rounded.

Description. Shell minute, dextral, orangish to brownish, ovately conical with 4.25–4.5 whorls (Fig. 2A). Protoconch orange, about one whorl, round to slightly ellipsoid, covered with wrinkled sculpture (Fig. 4B, C). Teleoconch orange, 3.25–3.5 whorls. Body whorl peripherally rounded, sculptured with 5–6 prominent carinae, weak growth lines between carinae, intersected by weak oblique growth lines. Basal part of body whorl with approximately 9–10 densely spaced spiral cords (Figs 2A, 4A). Suture incised. Aperture semi-rounded. Peristome thin, sharp, unexpanded or thickened, not reflected. Umbilicus closed (Figs 2A, 4A). Operculum paucispiral, nucleus submarginal, corneous, opaque white, semi-rounded, thin, smooth outside surface with apophysis, inside surface with an arched peg arising from base (Fig. 4D).

Radula. Ribbon-like, slender, longer, and delicate towards the outside, rhipidoglossate (Fig. 5A–D). Central tooth five small teeth, trapezoid shape. Lateral teeth five teeth, claw-like, with 9–13 alternately long and short denticles decreasing in size from the first lateral tooth toward the 5th lateral tooth. Marginal teeth two teeth, claw-like, with 12–14 equal-sized denticles. Radula formula 2:5:1+1+1+1+1+1+1:5:2.

Differential diagnosis. *Georissa quinquelirata* sp. nov. resembles *G. hungerfordi* Godwin-Austen, 1889 from Sabah, Borneo, Malaysia, *Georissa hungerfordi* differs in having a less convex body whorl, a smooth sculpture, and more spiral lirae (7–10 lirae instead of 5–6 carinae). This new species is also like *G. liratula* Stolixzka, 1871 from Domotha, Moulmein, but differs in having a more slender shell with fewer spiral lirae.

Georissa kohsichangensis Klongkaew, Poeaim & Dumrongrojwattana, sp. nov.

https://zoobank.org/77F45669-50F9-4FCF-991F-BFC63C7327E7
Figs 2B, 4E–H, 5E–H

Type material. ***Holotype*** • ZRCBUU 0902 (Fig. 2B). SH=2.10mm, SW=1.43mm, AH=0.63mm, AW=0.90mm, W = 4.25–4.5. ***Paratype*** • ZRCBUU 0903 (Fig. 4E–H) (12 shells); Shell measurements: SH = 1.72–2.03 mm

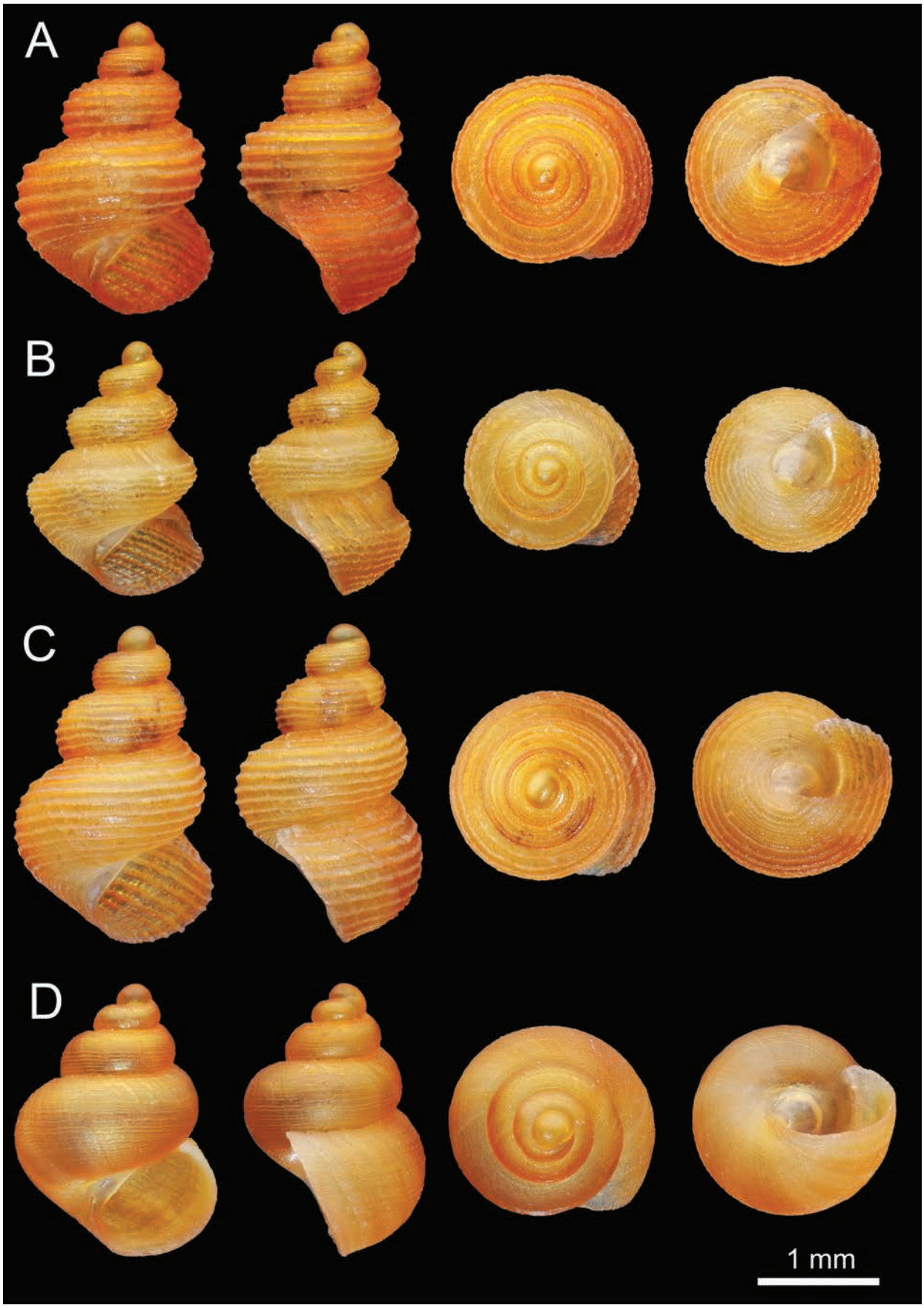

Figure 2. Shell morphology of the new *Georissa* species: **A.** *G. quinquelirata* sp. nov. (Holotype ZRCBUU 0900); **B.** *G. kohsichangensis* sp. nov. (Holotype ZRCBUU 0902); **C.** *G. sagitta* sp. nov. (Holotype ZRCBUU 0904), and **D.** *G. digitinota* sp. nov. (Holotype ZRCBUU 0906).

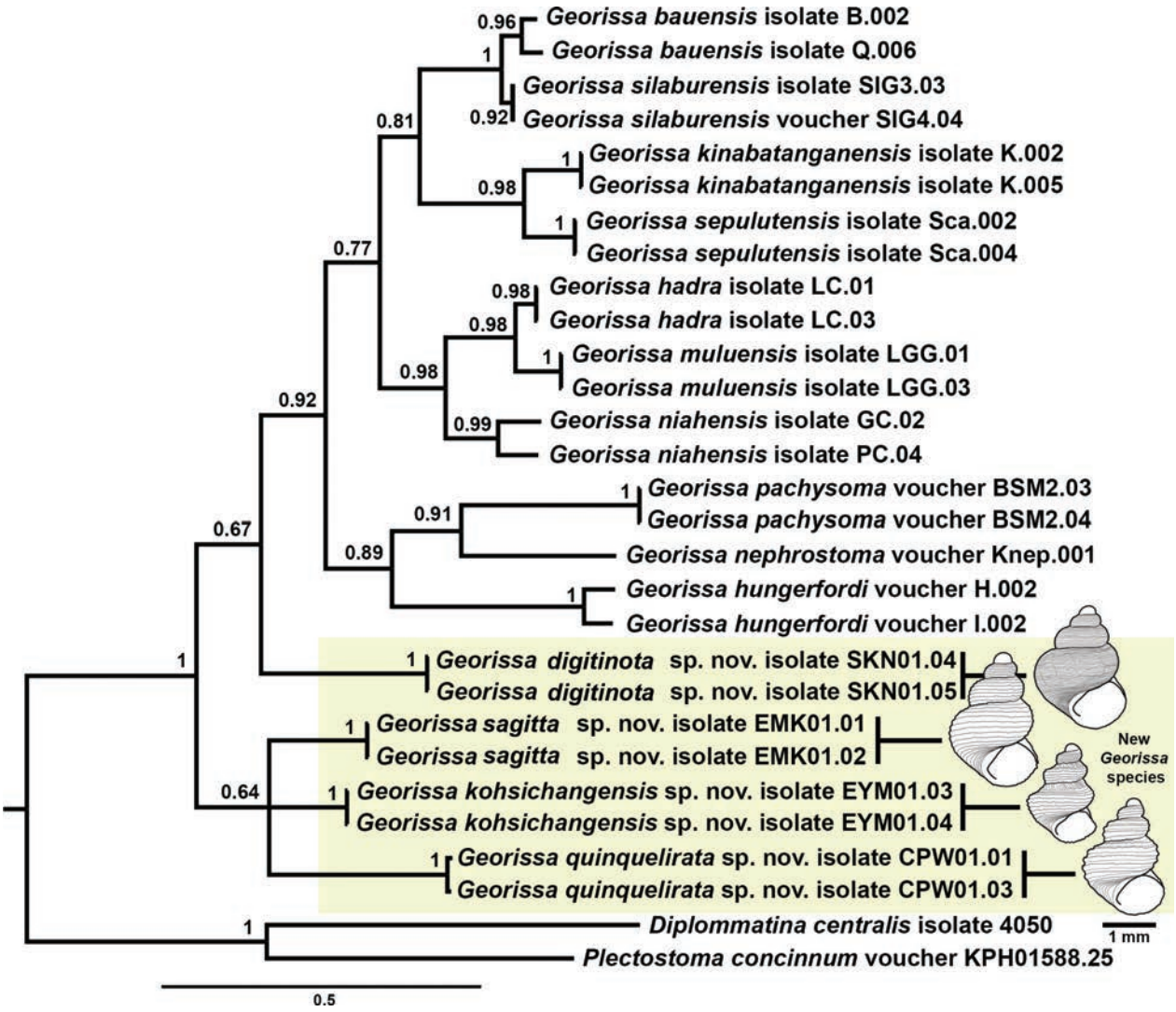

Figure 3. Bayesian inference of phylogenetic analysis (using the GTR+G+I model) with MrBayes for *Georissa*, based on the COI gene. The posterior probability is displayed on each node in the nucleotide sequence.

(1.86 ± 0.10 mm), SW = 1.21–1.42 mm (1.30 ± 0.07 mm), AH = 0.51–0.72 mm (0.62 ± 0.05 mm), AW = 0.75–0.84 mm (0.79 ± 0.03 mm), W = 3.75–4.5 (all type material from type locality; 30 October 2021, P. Dumrongrojwattana leg).

Type locality. Thailand, Yai Man cave, Koh Sichang district, Chonburi Province; 13°09'08.2"N, 100°48'28.0"E.

Etymology. This specific designation "*kohsichangensis*" is a district referring to the type locality.

Diagnosis. Shell minute, ovately conical and the upper half part of the whorls is slightly downward, orangish to brownish, protoconch round to slightly ellipsoid and perforated sculpture. Body whorl with 6–7 spiral lirae. Aperture rhombate. Umbilicus closed. Operculum corneous with apophysis, paucispiral, opaque white, and rhombate.

Description. Shell minute, dextral, orangish to brownish, ovately conical with 4.25–4.5 whorls (Fig. 2B). Protoconch orange, about one whorl, round to slightly ellipsoid, covered with perforated sculpture (Fig. 4F, G). Teleconch orange 3.25–3.5 whorls. The upper half part of the body whorls is slightly downward, sculptured with only strong oblique growth lines, 6–7 prominent lirae, weak oblique growth lines present on the half lower part of the body whorls, more densely spaced spiral cords, ca. 6–8 cords, at the basal part of the body whorl (Fig. 2B, 4E). Suture incised. Aperture rhombate. Peristome thin, sharp, unexpanded or thickened, not reflected. Umbilicus closed. Operculum paucispiral, nucleus submarginal, corneous, opaque white, rhombate shape, thin, smooth outside surface with apophysis, inside surface with an arched peg arising from base (Fig. 4H).

Radula. Ribbon-like, slender, longer and delicate towards the outside, rhipidoglossate (Fig. 5E–H). Central tooth five small teeth, trapezoid shape. Lateral teeth five teeth, claw-like with 7–11 alternately long and short denticles decreasing in size from the first lateral tooth toward the 5th lateral tooth. Marginal teeth two teeth, claw-like with 14–18 equal size denticles. Radula formula 2:5:1+1+1+1+1+1:5:2.

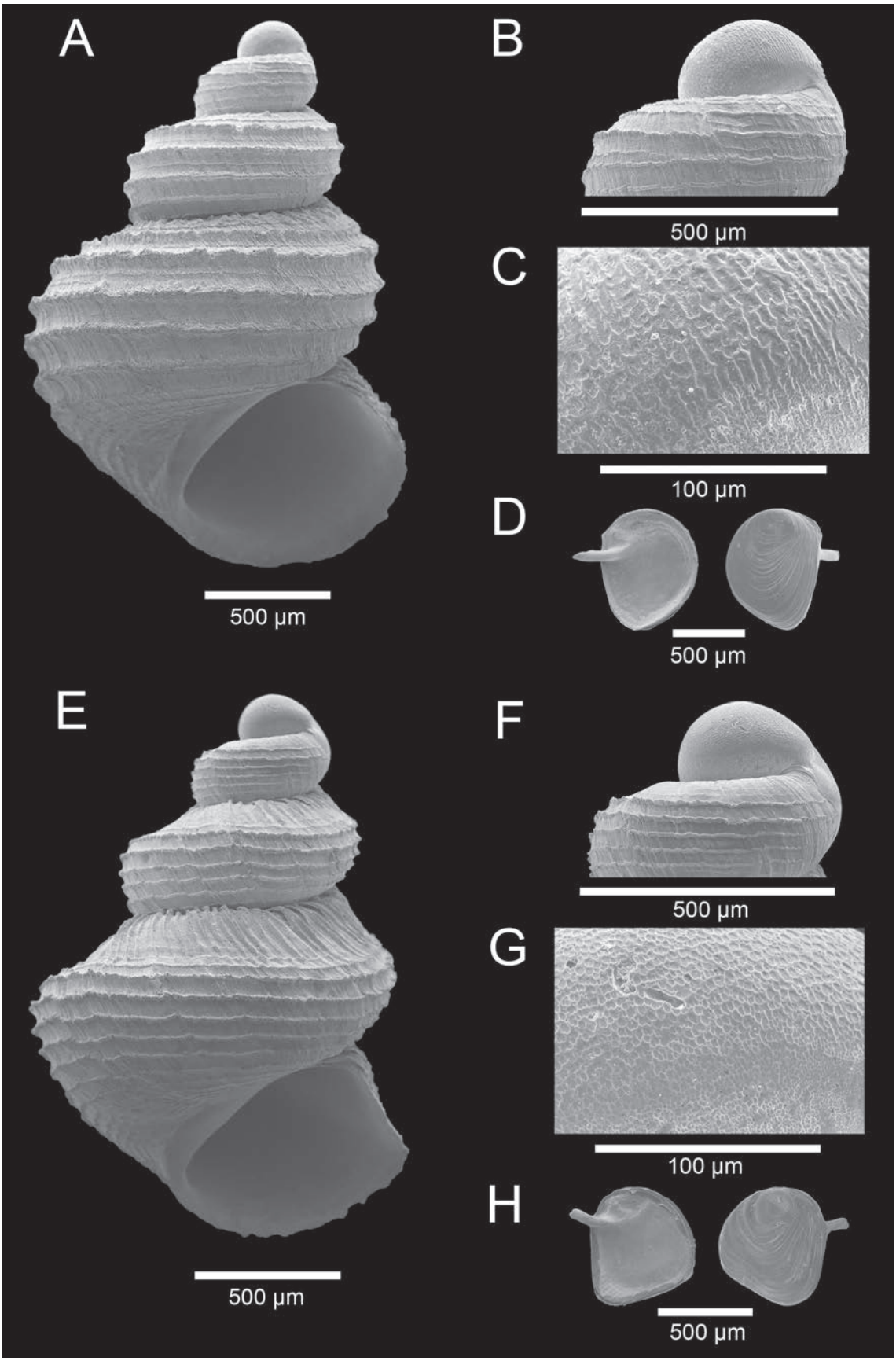

Figure 4. SEM of *Georissa* new species. **A–D.** *G. quinquelirata* sp. nov. (Holotype ZRCBUU 0901); **E–H.** *G. kohsichangensis* sp. nov. (Holotype ZRCBUU 0903); **A, E.** Shell; **B, F.** Protoconch; **C, G.** Sculpture of protoconch; **D, H.** Operculum; **I–L.** *G. sagitta* sp. nov. (Holotype ZRCBUU 0905); **M–P.** *G. digitinota* sp. nov. (Holotype ZRCBUU 0907); **I, M.** Shell; **J, N.** Protoconch; **K, O.** Sculpture of protoconch; **L, P.** Operculum.

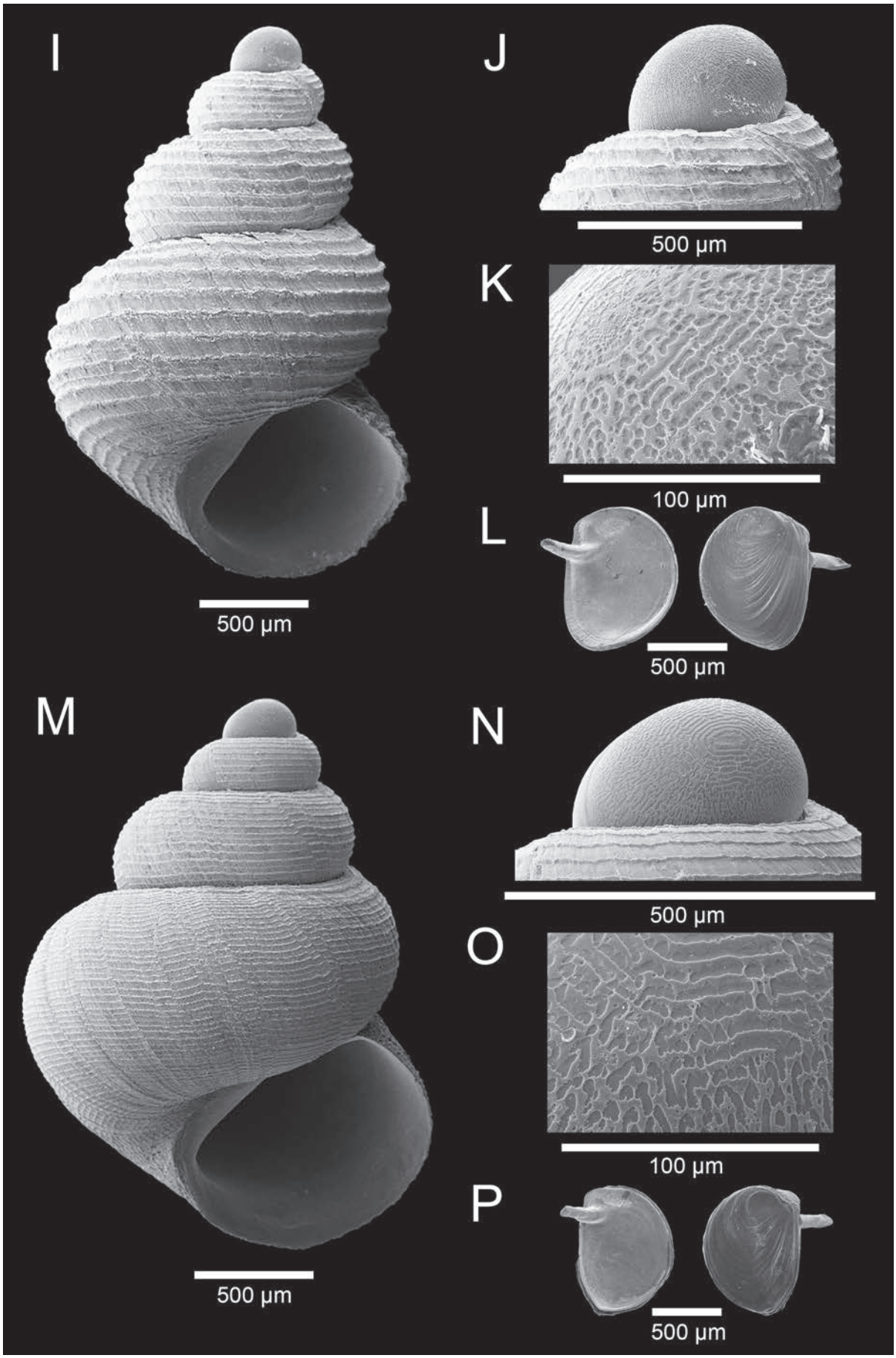

Figure 4. Continued.

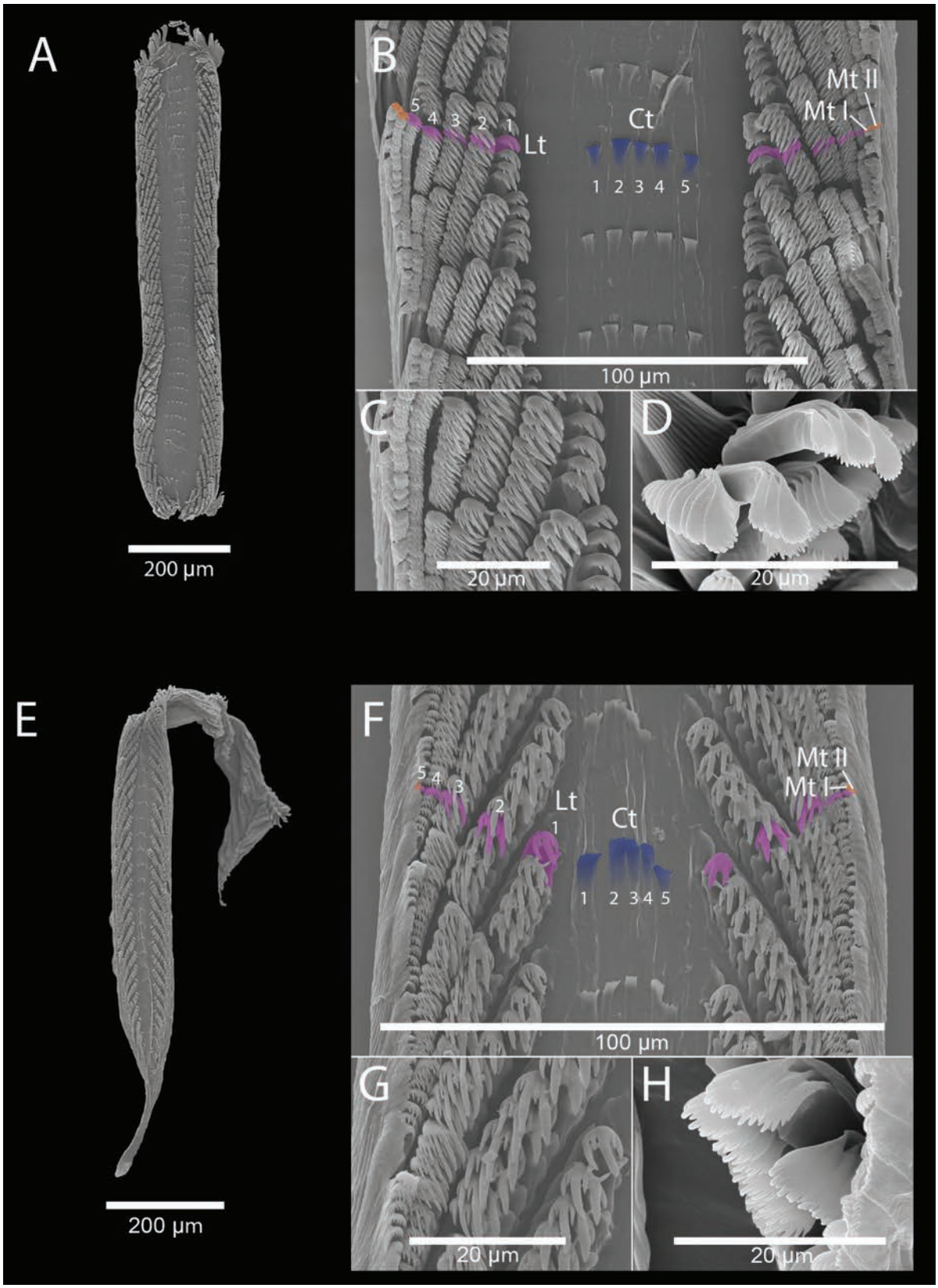

Figure 5. SEM of radula morphology of *Georissa*. **A–D.** *G. quinquelirata* sp. nov.; **E–H.** *G. kohsichangensis* sp. nov.; **A, E.** Radula overview; **B, F.** Radula segment; **C, G.** Lateral teeth (Lt); **D, H.** Marginal teeth (Mt); **I–L.** *G. sagitta* sp. nov. **M–P;** *G. digitinota* sp. nov.; **I, M.** Radula overview; **J, N.** Radula segment; **K, O.** Lateral teeth (Lt); **L, P.** Marginal teeth (Mt). Color highlights show radula position; blue: small central teeth (Ct), purple: lateral teeth, and orange: marginal teeth.

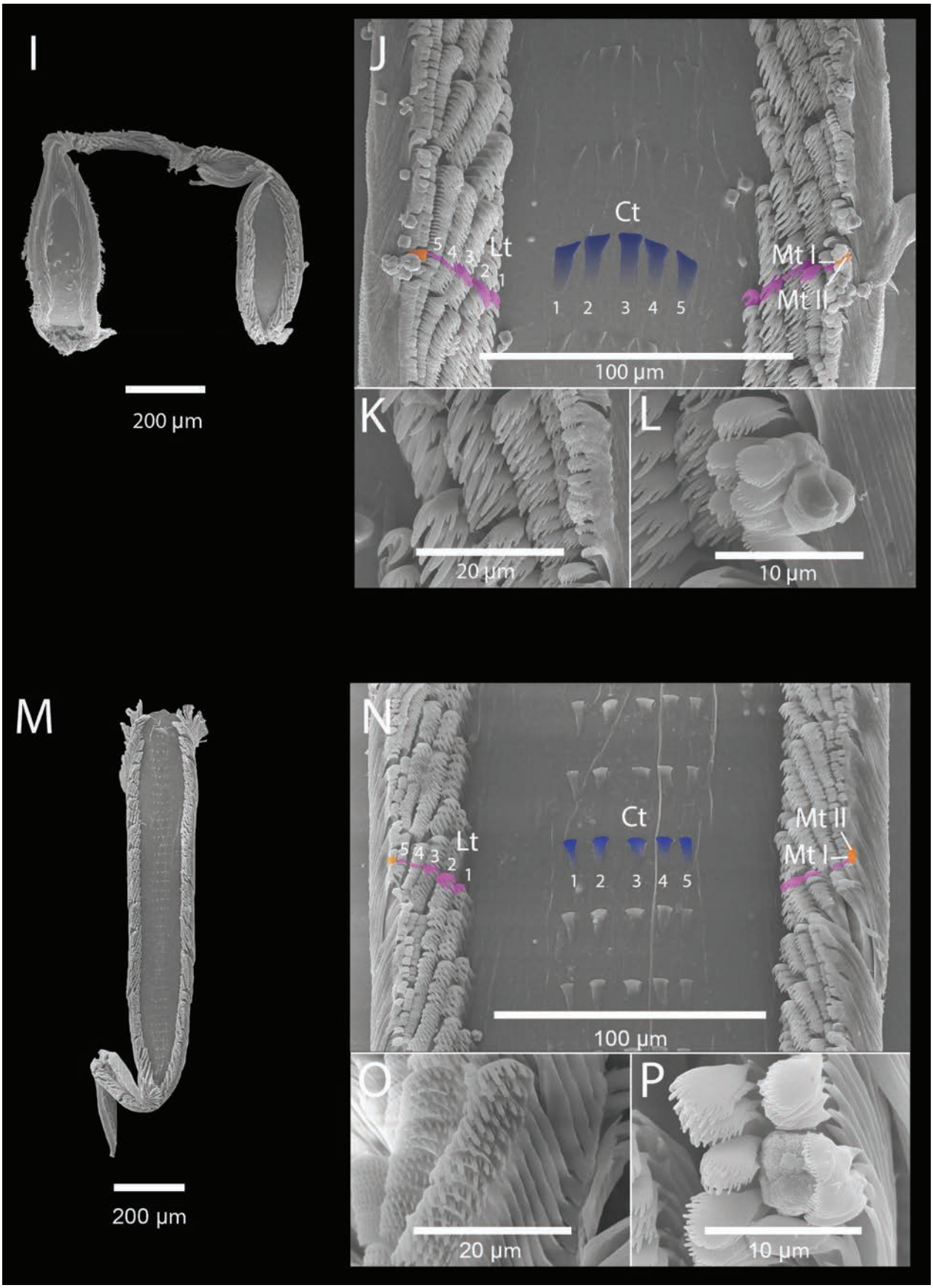

Figure 5. Continued.

Differential diagnosis. *Georissa kohsichangensis* sp. nov. resembles *G. carinata* Sutcharit & Jirapatrasilp, 2020 from Cambodia. *Georissa carinata* differs in having more convex body whorl, a smooth protoconch, and sculptured with thin and uneven growth lines.

Georissa sagitta Klongkaew, Poeaim & Dumrongrojwattana, sp. nov.

https://zoobank.org/965F36E8-E123-496F-A43D-9C2D1B80294F

Figs 2C, 4I–L, 5I–L

Type examined. ***Holotype*** • ZRCBUU 0904 (Fig. 2C); SH = 2.61 mm, SW = 1.63 mm, AH = 0.79 mm, AW = 0.98 mm, W = 4.25–4.5. ***Paratypes*** • ZRCBUU 0905 (Fig. 4I–L) (10 shells); Shell measurements: SH = 2.44–2.88 mm (2.65 ± 0.14 mm), SW = 1.63–1.84 mm (1.70 ± 0.07 mm), AH = 0.79–0.97 mm (0.87 ± 0.05 mm), AW = 0.95–1.09 mm (1.00 ± 0.04 mm), W = 4–4.5 (all type material from type locality; 20 July 2019, P. Dumrongrojwattana leg).

Type locality. Thailand, Khao Maka Cave Temple, Mueang Sakaeo district, Sakaeo Province; 13°47'16.6"N, 101°56'53.7"E.

Etymology. The specific designation "sagitta" for the prominent oval indentation resembling a target in archery.

Diagnosis. Shell minute, ovately conical, orangish, protoconch round to slightly ellipsoid and mix of rounded, ellipsoidal to irregular sculpture with oval indentation. Body whorl peripherally rounded with 8–9 spiral lirae. Aperture semi-rounded. Umbilicus closed. Operculum corneous with apophysis, paucispiral, opaque white, and semi-rounded.

Description. Shell minute, dextral, orangish to brownish, ovately conical with 4.25–4.5 whorls (Fig. 2C). Protoconch orange consists of 1 whorl, round to slightly ellipsoid, covered with mix of rounded, ellipsoidal to irregular sculpture and a large oval indentation present (Figs 4J, 4K). Teleconch orange, consists of 3.25–3.5 whorls. Peripherally rounded, sculptured with 8–9 prominent lirae on the body whorl, crossed with weak oblique growth lines. Basal part of the body whorl, there are more densely spaced spiral cords, approximately 7–8 cords (Figs 2C, 4I). Suture incised. Aperture semi-rounded. Peristome thin, sharp, unexpanded or thickened, not reflected. Umbilicus closed. Operculum paucispiral, nucleus submarginal, corneous, opaque white, semi-rounded, thin, smooth outside surface with apophysis, inside surface with an arched peg arising from base (Fig. 4L).

Radula. Ribbon-like, slender, longer and delicate towards the outside, rhipidoglossate (Fig. 5I–L). Central tooth five small teeth, trapezoid shape. Lateral teeth five teeth, claw-like with 7–13 alternately long and short denticles decreasing in size from the first lateral tooth toward the 5th lateral tooth. Marginal teeth two teeth, claw-like with 12–14 equal size denticles. Radula formula 2:5:1+1+1+1+1+1:5:2.

Differential diagnosis. *Georissa sagitta* sp. nov. resembles *G. monterosatiana* Godwin-Austen & Neville, 1879. *Georissa monterosatiana* differs in having more convex body whorl, smooth protoconch, and more lirae (9–11 instead of 8–9 lirae).

Georissa digitinota Klongkaew, Poeaim & Dumrongrojwattana, sp. nov.

https://zoobank.org/ABD3A8ED-52D0-41C9-85D8-FD5062076E92

Figs 2D, 4M–P, 5M–P

Type examined. ***Holotype*** • ZRCBUU 0906 (Fig. 2D); SH = 2.27 mm, SW = 1.68 mm, AH = 0.85 mm, AW = 1.03 mm, W = 4.25–4.5. ***Paratypes*** • ZRCBUU 0907 (Fig. 4M–P) (9 shells); Shell measurements: SH = 2.34–2.72 mm (2.46 ± 0.12 mm), SW = 1.66–1.86 mm (1.76 ± 0.06 mm), AH = 0.87–1.00 mm (0.93 ± 0.04 mm), AW = 0.96–1.06 mm (1.00 ± 0.04 mm), W = 4–4.5 (all type material from type locality; 24 June 2021, P. Dumrongrojwattana leg).

Type locality. Thailand, Khao Noi Bodhiyan Temple, Mueang Satun district, Satun Province; 06°45'24.2"N, 100°01'54.2"E.

Etymology. The specific designation "digitinota" is for the fingerprints-like sculpture on the protoconch.

Diagnosis. Shell minute, globosely conical, orangish to brownish, protoconch round to slightly ellipsoid and ellipsoidal to irregular sculpture with oval fingerprint-like indentation. Body whorl peripherally rounded with more than 30 spiral lines. Aperture semi-rounded. Umbilicus closed. Operculum corneous with apophysis, paucispiral, opaque white, and semi-rounded.

Description. Shell minute, dextral, orangish to brownish, globosely conical with 4.25–4.5 whorls. Protoconch brownish consists of 1 whorl, round to slightly ellipsoid, covered with ellipsoidal to irregular sculpture and a large oval fingerprint-like indentation present (Fig. 4N, O). Teleconch, orangish to brownish, consists of 3.25–3.5 whorls. Body whorl peripherally rounded, sculptured with more than 30 spiral lines on the body whorl, crossed with very weak oblique growth lines at the basal part of the body whorl (Fig. 4M). Suture incised. Aperture semi-rounded. Peristome thin, sharp, unexpanded or thickened and not reflected. Umbilicus closed. Operculum paucispiral, nucleus submarginal, corneous, opaque white, semi-rounded, thin, smooth outside surface with apophysis, inside surface with an arched peg arising from base (Fig. 4P).

Radula. Ribbon-like, slender, longer and delicate towards the outside, rhipidoglossate (Fig. 5M–P). Central tooth five small teeth, trapezoid shape. Lateral teeth five teeth present, claw-like with 7–13 alternately long and short denticles decreasing in size from the first lateral tooth toward the 5th lateral tooth. Marginal teeth two teeth, claw-like with 12–14 equal-sized denticles. Radula formula 2:5:1+1+1+1+1+1:5: 2.

Differential diagnosis. *Georissa digitinota* sp. nov. resembles *G. monterosatiana* Godwin-Austen & Neville, 1879. *Georissa monterosatiana* differs in having a less convex body whorl, smooth protoconch, and more lirae (9–11 instead of more than 30 spiral lines).

Discussion

The combination of morphological and molecular information supports the distinct separation of the four new *Georissa* species in Thailand; *G. quinquelirata* sp. nov., *G. kohsichangensis* sp. nov., *G. sagitta* sp. nov., and *G. digitinota* sp. nov. However, morphological analysis remains the primary method for distinguishing species. It necessitates the use of specialized equipment for collection and detailed analysis. Their tiny size (1.00–3.00 mm) as *Georissa* in Khalik et al. (2018, 2019b), makes them difficult to detect, collect, and observe, necessitating specialized equipment and techniques.

Several key morphological characteristics are considered. The criteria for classifying each new *Georissa* species based on conchological variability are focusing on shell shape, shell size of height in mm, sculpture pattern of the last (or body) whorl with the number of lines, protoconch sculpture, operculum which has apophysis in ventral view as Neritimorpha snail (Sands et al. 2020), and radula features respectively. The radula teeth of the genus *Georissa* are rhipidoglossate, the radula formula is 2:5:1+1+1+1+1:5:2 and exhibit very similar characteristics. The only notable differences are the number and size of the teeth, which correspond to the size of the *Georissa* snail (Fig. 5). Radula morphology was studied in a research report by Haase and Schilthuizen (2007), focusing on *G. filiasaulae*, a newly discovered species collected from inside a limestone cave in Malaysian Borneo. In their study, they noted the absence of central teeth. However, they encountered difficulty locating these teeth, as they were found only on one side or the other at the time of their study. This is similar to the radula of land micro snails of the genus *Hydrocena*, belonging to the same family, which possesses three small central teeth with a formula represented as ∞1: (1+1+1): 1: ∞ (Egorov 2005).

Molecular analyses were used for the taxon identified and supported morphological evidence such as DNA barcoding and phylogenetic tree (e.g. Khalik et al. 2018, 2019a, 2019b). The phylogenetic analysis indicates that one species, *G. digitinota* sp. nov., bears similarities to other *Georissa* species from Malaysian Borneo due to its similar shape. However, three other species, namely *G. quinquelirata* sp. nov., *G. kohsichangensis* sp. nov., and *G. sagitta* sp. nov., although sharing a similar shape, exhibit slight differences in teleconch sculpture, the number of lirae on the body whorl, and operculum shape. *G. kohsichangensis* sp. nov. has previously been found on Sichang Island and Rin Island in Chonburi Province, which are about 50–60 kilometers on the Google map. Still, this species remains unnamed in the scientific literature (Dumrongrojwattana et al. 2017). When regions are geographically separated, with no spread across limestone hills, it often leads to differentiation between populations in different regions, as isolated groups evolve independently. Additionally, various factors such as historical events, climate, migration patterns, and human activities can influence geographic distribution patterns. Further studies should encompass a broader geographical area and include molecular analysis of Thailand's terrestrial snails, the genus *Georissa*.

Acknowledgments

This research received financial support from KMITL Research and Innovation Services (KRIS) under Grant No. KREF016414. The study has obtained documentary proof of ethical clearance and adhered to the guidelines set by the Animal Care and Use Committee at King Mongkut's Institute of Technology Ladkrabang, as documented in Approval No. ACUC-KMITL-RES/2022/010. The Zoology Laboratory, Faculty of Science, Burapha University, also supported the laboratory for morphological studies. Additionally, we would like to express our deepest appreciation to Asst. Prof. Pongrat Dumrongrojwattana, whose invaluable insights and dedication, despite his passing, significantly influenced the development of this work.

References

BEDO [Biodiversity-Based Economy Development Office] (2017) Land Snails: Checklist of Molluscan Biodiversity in Thailand. BEDO, Bangkok, 300 pp. [in Thai]

Benson WH (1856) Characters of seventeen new forms of the Cyclostomacea from the British Provinces of Burmah, collected by W. Theobald, jun., Esq. Annals and Magazine of Natural History [ser. 2] 17(99): 225–228. https://doi.org/10.1080/00222935608697501

Callomon P (2019) Standard views for imaging mollusk shells. American Malacological Society, 1–19.

Colgan DJ, Santos RP (2018) A phylogenetic classification of gastropod aquaporins. Marine Genomics 38: 59–65. https://doi.org/10.1016/j.margen.2017.12.002

Darriba D, Taboada GL, Doallo R, Posada D (2012) jModelTest 2: more models, new heuristics and parallel computing. Nature Methods 9(8): 772. https://doi.org/10.1038/nmeth.2109

Dumrongrojwattana P, Tanmuangpak K (2020) The terrestrial microsnail genus *Aulacospira* Möllendorff, 1890 (Eupulmonata, Stylommatophora, Hypselostomatidae) in Thailand with key to Thai species. ZooKeys 980(1): 23–42. https://doi.org/10.3897/zookeys.980.54100

Dumrongrojwattana P, Inmadan R, Phanuphong S, Thanamai S (2017) Land microsnails on the islands in Chon Buri Province, Eastern Thailand (Gastropoda: Prosobranchia; Pulmonata). Ramkhamhaeng Research Journal [Science and Technology] 20(2): 19–26. [in Thai]

Egorov RV (2005) Treasure of Russian Shells. Supplement 3. A review of the genera of the recent terrestrial pectinibranch molluscs (synopsis mainly based on published data). Part 1. Neritopsiformes (Hydrocenoidei, Helicinoidei). Moscow, (Colus-Doverie), 57 pp.

Folmer O, Black M, Hoeh W, Lutz R, Vrijenhoek R (1994) DNA primers for amplification of mitochondrial cytochrome c oxidase subunit I from diverse metazoan invertebrates. Molecular Marine Biology and Biotechnology 3(5): 294–299.

Geiger DL, Marsheall BA, Ponder WF, Sasaki T, Warén A (2007) Techniques for collecting, handling, preparing, storing and examining small molluscan specimens. Molluscan Research 27(1): 1–50. https://doi.org/10.11646/MR.27.1.1

Godwin-Austen HH (1889) On a collection of land-shells made in Borneo by Mr. A. Everett with supposed new species. Part I. Cyclostomacae. Proceedings of the Zoological Society of London 57(3): 332–335.

Godwin-Austen HH, Nevill, G (1879) Descriptions of shells from Perak and the Nicobar Islands. Proceedings of the Zoological Society of London 47(4): 734–740. https://doi.org/10.1111/j.1096-3642.1879.tb02710.x

Haase M, Schilthuizen M (2007) A new *Georissa* (Gastropoda: Neritopsina: Hydrocenidae) from a limestone cave in Malaysian Borneo. Journal of Molluscan Studies 73(3): 215–221. https://doi.org/10.1093/mollus/eym020

Hendriks KP, Alciatore G, Schilthuizen M, Etienne RS (2019) Phylogeography of Bornean land snails suggests long-distance dispersal as a cause of endemism. Journal of Biogeography 46: 932–944. https://doi.org/10.1111/jbi.13546

Kano Y, Chiba S, Kase T (2003) Major adaptive radiation in neritopsine gastropods estimated from 28S rRNA sequences and fossil records. Proceedings of the Royal Society B 269(1508): 2457–2465. https://doi.org/10.1098/rspb.2002.2178

Khalik MZ, Bozkurt E, Schilthuizen M (2019a) Morphological parallelism of sympatric cave-dwelling microsnails of the genus *Georissa* at Mount Silabur, Borneo (Gastropoda, Neritimorpha, Hydrocenidae). Journal of Zoological Systematics and Evolutionary Research 53(8): 1–14. https://doi.org/10.1111/jzs.12352

Khalik MZ, Hendriks K, Vermeulen JJ, Schilthuizen M (2018) A molecular and conchological dissection of the "scaly" *Georissa* of Malaysian Borneo (Gastropoda, Neritimorpha, Hydrocenidae). ZooKeys 773: 1–55. https://doi.org/10.3897/zookeys.773.24878

Khalik MZ, Hendriks K, Vermeulen JJ, Schilthuizen M (2019b) Conchological and molecular analysis of the "non-scaly" Bornean *Georissa* with descriptions of three new species (Gastropoda, Neritimorpha, Hydrocenidae). ZooKeys 840: 35–86. https://doi.org/10.3897/zookeys.840.33326

Lipae HB, Estabillo AL, Fontanilla IC, De Chavez EC (2020) A new subspecies of microsnail from Masungi Georeserve, Rizal, Philippines. Philippine Journal of Systematic Biology 14(3): 1–12. https://doi.org/10.26757/pjsb2020c14003

Möllendorff OF von (1894) On a collection of land-shells from the Samui Islands, Gulf of Siam. Proceedings of the Zoological Society of London 1894: 146–156.

Panha S, Burch JB (2005) An introduction to the microsnails of Thailand. Malacological Review 37/38, 155 pp.

Pholyotha A, Sutcharit, C, Tongkerd P, Panha, S (2021). Systematic revision of the limestone karst-restricted land snail genus Aenigmatoconcha (Eupulmonata: Helicarionidae), with description of a new species. European Journal of Taxonomy 767(1): 55–82. https://doi.org/10.5852/ejt.2021.767.1487

Phung CC, Yu FTY, Liew TS (2017) A checklist of land snails from the west coast islands of Sabah, Borneo (Mollusca, Gastropoda). Zookeys 673: 49–104. https://doi.org/10.3897/zookeys.673.12422

Ronquist F, Teslenko M, van der Mark P, Ayres DL, Darling A, Höhna S, Larget B, Liu L, Suchard MA, Huelsenbeck JP (2012) MRBAYES 3.2: Efficient Bayesian phylogenetic inference and model selection across a large model space. Systematic Biology 61(3): 539–542. https://doi.org/10.1093/sysbio/sys029

Sands AF, Glöer P, Gürlek ME, Albrech C, Neubauer TA (2020) A revision of the extant species of *Theodoxus* (Gastropoda, Neritidae) in Asia, with the description of three new species. Zoosystematics and Evolution 96(1): 25–66. https://doi.org/10.3897/zse.96.48312

Schilthuizen M, Rutten EMJ, Haase M (2005) Possible speciation with gene flow in tropical cave snails. Journal of Zoological Systematics and Evolutionary Research 43(2): 133–13. https://doi.org/10.1111/j.1439-0469.2004.00289.x

Schilthuizen M, Rutten EMJ, Haase M (2012) Small-scale genetic structuring in a tropical cave snail and admixture with its above-ground sister species. Biological Journal of The Linnean Society 105(4): 727–740. https://doi.org/10.1111/j.1095-8312.2011.01835.x

Schneider C, Rasband W, Eliceiri K (2012) NIH Image to ImageJ: 25 years of image analysis. Nature Methods 9: 671–675. https://doi.org/10.1038/nmeth.2089

Stoliczka F (1871) Notes on terrestrial Mollusca from the neighborhood of Moulmein (Tenasserim Provinces), with descriptions of new species. The Journal of the Asiatic Society of Bengal, Part II 40(2): 143–177.

Uribe JE, Colgan D, Castro LR, Kano Y, Zardoya R (2016) Phylogenetic relationships among superfamilies of Neritimorpha (Mollusca: Gastropoda). Molecular Phylogenetics and Evolution 104(1): 21–31. https://doi.org/10.1016/j.ympev.2016.07.021

Vermeulen JJ, Whitten T (1998) Fauna Malesiana guide to the land snails of Bali. Backhuys Publishers, Leiden, 135 pp.

Webster NB, Van Dooren TJM, Schilthuizen M (2012) Phylogenetic reconstruction and shell evolution of the Diplommatinidae (Gastropoda: Caenogastropoda). Molecular Phylogenetics and Evolution 63(3): 625–638. https://doi.org/10.1016/j.ympev.2012.02.004

Weigand AM, Jochum A, Pfenninger M, Steinke D, Klussmann-Kolb A (2011) A new approach to an old conundrum - DNA barcoding sheds new light on phenotypic plasticity and morphological stasis in microsnails (Gastropoda, Pulmonata, Carychiidae). Molecular Ecology Resources 11: 255–265.https://doi.org/10.1111/j.1755-0998.2010.02937.x

Weigand AM, Jochum A, Slapnik R, Schnitzler J, Zarza E, Klussmann-Kolb A (2013) Evolution of micro gastropods (Ellobioidea, Carychiidae): integrating taxonomic, phylogenetic and evolutionary hypotheses. BMC Evolutionary Biology 13(1): 1–24. https://doi.org/10.1186/1471-2148-13-18

Supplementary material 1

A list of *Georissa* species and their geographical distribution across the mainland in Southeast Asia and China

Authors: Kanyaporn Klongklaew, Supattra Poeaim, Pongrat Dumrongrojwattana

Data type: docx

Link: https://doi.org/10.3897/zse.100.128717.suppl1

Zoosyst. Evol. 100 (4) 2024, 1361–1373 | DOI 10.3897/zse.100.129398

PENSOFT

für Naturkunde MUSEUM FÜR NATURKUNDE BERLIN

Taxonomic revision of the genus *Micryletta* (Amphibia, Microhylidae), with description of a new species from Thailand

Yu-Yang Cao[1,2*], Chatmongkon Suwannapoom[3*], Felista Kasyoka Kilunda[2,4], Wei Gao[2], Chun-Lian Wu[1], Yun-He Wu[2,5], Jing Che[2,5]

1 *Key Laboratory of Southwest China Wildlife Resources Conservation, China West Normal University, Ministry of Education, 637009, Nanchong, Sichuan, China*

2 *Key Laboratory of Genetic Evolution and Animal Models, and Yunnan Key Laboratory of Biodiversity and Ecological Conservation of Gaoligong Mountain, Kunming Institute of Zoology, Chinese Academy of Sciences, 650223, Kunming, Yunnan, China*

3 *School of Agriculture and Natural Resources, University of Phayao, 56000, Phayao, Thailand*

4 *Kunming College of Life Science, University of the Chinese Academy of Sciences, 650204, Kunming, Yunnan, China*

5 *Southeast Asia Biodiversity Research Institute, Chinese Academy of Sciences, 05282, Yezin, Nay Pyi Taw, Myanmar*

https://zoobank.org/88844296-DDE9-4541-B3A2-177A01139814

Corresponding authors: Jing Che (chej@mail.kiz.ac.cn); Yun-He Wu (wuyunhe@mail.kiz.ac.cn); Chun-Lian Wu (wcl_xj@163.com)

Academic editor: Umilaela Arifin ♦ **Received** 11 June 2024 ♦ **Accepted** 31 August 2024 ♦ **Published** 10 October 2024

Abstract

The genus *Micryletta* is widely distributed in South China and Southeast Asia. Although significant progress has been made in the diversity and taxonomy of this genus over the past few years, the distribution range and taxonomy of some species still remain controversial, especially in *M. inornata* sensu lato. Consequently, limitations at national borders have resulted in a lack of comparative research on species from different countries. To resolve the classification dispute, assess species diversity, and determine the distribution range of *Micryletta*, a series of specimens were collected from the Yunnan Province of China and Thailand during herpetological surveys from 2009 to 2020. Subsequent analyses based on morphological and molecular data revealed a distinct and previously unknown lineage from western Thailand, which we formally describe as a new species. Furthermore, our study confirms that *M.* '*inornata*', previously known from Mengla, Yunnan, was actually *M. menglienica*, and further extends its distribution range to Thailand and Laos. In addition, our findings extend the latitudinal distribution of *M. inornata* and *M. subaraji* northward into southern Thailand. Notably, this study brings the total number of known species in the genus *Micryletta* from 13 to 14, with the count rising from three to six species in Thailand and from one to three in Laos. Our study further confirms that species diversity within the genus *Micryletta* is underestimated and emphasizes the important role that international collaborations play in taxonomy. Intensifying field surveys in other regions (e.g., Myanmar, Vietnam, and Guangxi of China) will be extremely necessary in the future to clarify any taxonomic questions and reevaluate the distribution range of these species.

Key Words

Distribution range, diversity, *Micryletta*, *M. inornata* sensu lato, new species

* These authors contributed equally to this work.

Introduction

South China and Southeast Asia span the Himalaya, Indo-Burma, and Sundaland biodiversity hotspots and host a high diversity of species (Myers et al. 2000). The region's complex evolutionary histories and highly diverse habitats, primarily attributed to the wide variation in landforms, climate, and latitude, are deemed to support the high species diversity (Janssens et al. 2016; Huang et al. 2023). Over the past few years, research on *Sylvirana* (Sheridan and Stuart 2018), *Leptobrachella* (Chen et al. 2021), *Megophrys* (Chen et al. 2017), and *Amolops* (Wang et al. 2020) suggests the presence of cryptic amphibian species diversity within this region. Additionally, some new genera and new species have been discovered in this area (e.g., Wu et al. 2021; Yodthong et al. 2021; Suwannapoom et al. 2022; Matsui et al. 2023). Despite being home to an extensively rich amphibian diversity, southern China and Southeast Asia are also threatened by human activity and global warming (Hughes 2018), which increases the risk of extinction prior to the discovery of new species.

The genus *Micryletta*, originally described by Dubois (1987) to accommodate two previously known species, *M. inornata* (Boulenger, 1890) and *M. steinegeri* (Boulenger, 1909), now includes 13 recognized species (Frost 2024). Among these, nine new species have been described in the last five years (e.g., Das et al. 2019; Liu et al. 2021a; Miller et al. 2021; Poyarkov et al. 2021; Yang and Poyarkov 2021; Sankar et al. 2022). Members of the genus *Micryletta* are widely distributed from southern China to northern Indonesia and eastern India (Frost 2024), with most species only known from their type localities (e.g., Poyarkov et al. 2018, 2021; Munir et al. 2020; Suwannapoom et al. 2020; Yang and Poyarkov 2021; Sankar et al. 2022). National boundaries have posed a challenge to the documentation of species distribution ranges, resulting in paucity of comparative research between different countries.

Moreover, species classification within *Micryletta* has been faced with a long-standing controversy, especially *M. inornata* sensu lato (Liu et al. 2021a). Its morphological similarities with other species of *Micryletta* led *M. inornata* to be historically considered a widespread species that occurred in Sumatra throughout the Malay Peninsula and Indochina. However, a recent study by Alhadi et al. (2019) restricted the distribution of *M. inornata* to the island of Sumatra, resulting in numerous unnamed lineages eventually described as new species by other authors (Das et al. 2019; Munir et al. 2020; Suwannapoom et al. 2020; Liu et al. 2021a; Poyarkov et al. 2021; Yang and Poyarkov 2021). However, *M. inornata* sensu lato is still paraphyletic with a disjunct distribution as it contains undescribed paraphyletic lineages. Among these, lineages from Kanchanaburi in Thailand (Miller et al. 2021), Phongsaly in Laos (Das et al. 2019), and Yunnan and Guangxi in China (Liu et al. 2021a; Yeung et al. 2023) remain uncertain.

To resolve the classification dispute, assess species diversity, and determine the distribution range of *Micryletta*, we sort out a number of specimens from fieldwork collections in southern China and Southeast Asia from 2009 to 2020. Subsequent genetic analyses and morphological comparisons revealed that populations from western Thailand represent a distinct evolutionary lineage that could not be classified into any known taxa; therefore, we identify it as a new species. In addition, we further clarify and update the distribution ranges for *M. menglienica* and *M. subaraji*.

Materials and methods

Sampling

A total of 17 samples were collected from China and Thailand in different seasons (Fig. 1). After euthanasia, liver tissues were stored in 95% ethanol. All specimens were fixed in 10% formalin, then transferred to 75% ethanol, and finally deposited at Kunming Natural History Museum of Zoology, Kunming Institute of Zoology, Chinese Academy of Sciences (KIZ). Research protocols were approved by the Ethics Committee of the Kunming Institute of Zoology, Chinese Academy of Science (IACUC no.: IACUC-OE-2021-07-001).

DNA extraction, PCR amplification, and sequencing

Total genomic DNA was extracted from the liver or muscle tissues using the standard phenol-chloroform extraction protocol (Sambrook et al. 1989). A fragment of the mitochondrial 16S ribosomal RNA gene (16S rRNA) was amplified and sequenced for all samples using primers 16S rRNA-F (CGCCTGTTTAYCAAAAACAT) and 16S rRNA-R (CCGGTYTGAACTCAGATCAYGT) (Kocher et al. 1989). The reaction volume of PCR amplifications was 25 µl, and the reaction procedure was as follows: initial denaturing step at 95 °C for 4 min, 35 cycles of denaturation at 94 °C for 40 s, annealing at 55 °C for 40 s, extension at 72 °C for 1 min, and a final extension at 72 °C for 10 min. The amplified PCR product was purified using a Qiagen PCR purification kit (Watson Biotechnologies, Shanghai, China) and then sequenced in both directions using an ABI 3100 automated sequencer. Sequences generated in this study were assembled and edited using AutoSeqMan (Sun 2018). Sequences were aligned and manually optimized in MEGA 6.0 (Tamura et al. 2013). All the new sequences were submitted to the GenBank. Homologous sequences of the genus *Micryletta* and those of the outgroups *Mysticellus franki*, *Kaloula pulchra*, and *Uperodon systom* were downloaded from the GenBank (Table 1).

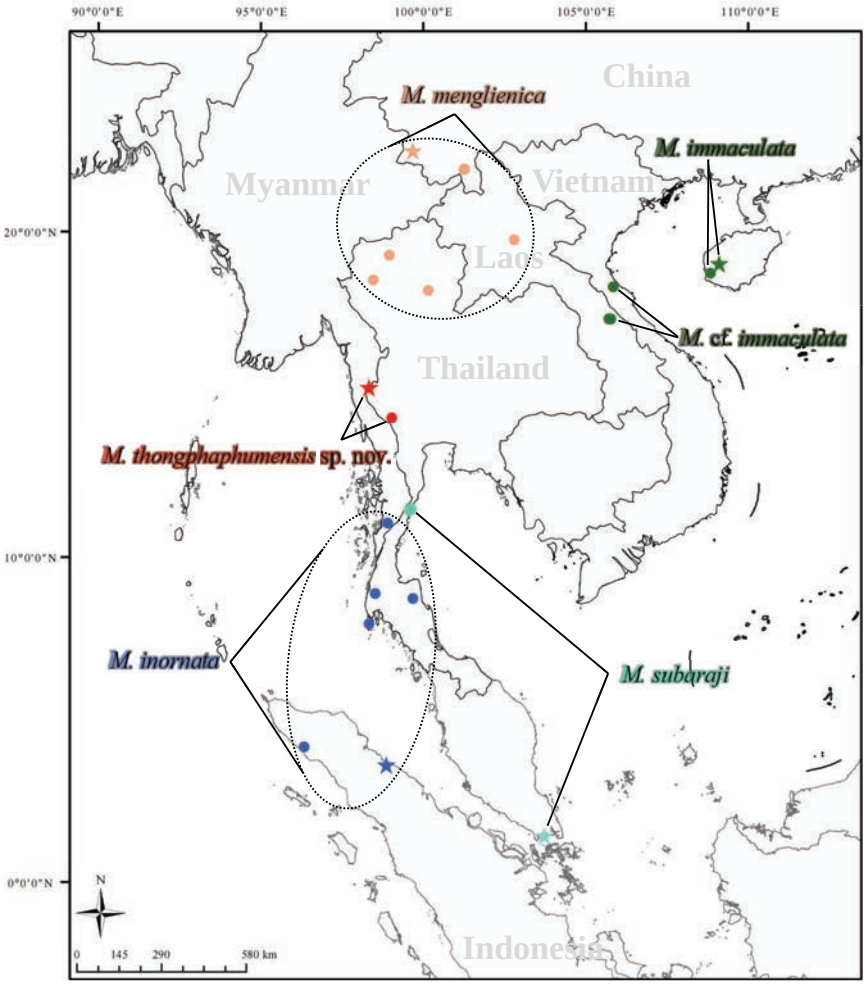

Figure 1. Map showing the distribution of *M. thongphaphumensis* sp. nov., *M. menglienica*, *M. immaculata*, *M. subaraji*, and *M. inornata*. The pentagram represents the type locality of these species. The same color represents the same species.

Molecular analysis

Bayesian inference (BI) and maximum likelihood (ML) methods were used to analyze phylogenetic relationships based on mitochondrial 16S rRNA. The BI analysis and ML analysis were conducted using the MrBayes tool on XSEDE and RAxML-HPC BlackBox in CIPRES Web (Miller et al. 2010). For BI analysis, we ran a jModelTest with Bayesian information criteria on the alignment, resulting in the best-fitting nucleotide substitution model of TIM2ef+I+G (Darriba et al. 2012). The Monte Carlo Markov chain length was run for 10,000,000 generations and sampled every 1,000 generations. The first 30% of the sampled trees were discarded as burn-in after the standard deviation of split frequencies of the two runs was less than a value of 0.01. The remaining trees were used to create a 50% majority rule consensus tree and to estimate Bayesian posterior probabilities. For the ML analysis, we used the proportion of invariable sites estimated from the data and 1,000 bootstrap pseudo replicates. We also computed pairwise comparisons of uncorrected sequence divergence (*p*-distance) for the partial sequences of the 16S rRNA using MEGA 6.0 (Tamura et al. 2013).

Morphology

Only adult specimens were examined for morphometric studies. The sex and maturity of the specimens were determined by identifying secondary sexual characteristics (such as vocal sacs in males and eggs in gravid females) or through gonadal examination using a small lateral or ventral incision. Measurements were taken to the nearest 0.1 mm with digital calipers. The morphometrics and character terminology follow Fei et al. (2009): snout-vent length (**SVL**); head length (**HL**); head width (**HW**); snout length (**SL**); internasal space (**INS**); interorbital space (**IOS**); width of upper eyelid (**UEW**); diameter of eye (**ED**); diameter of tympanum (**TD**); distance from anterior border of tympanum to posterior orbital border (**TYE**); distance from the center of the nostril to the tip of the snout (**SN**); distance from the front of the eye to the center of the nostril (**EN**); internal front of eyes, the shortest distance between the anterior orbital borders of the eyes (**IFE**); internal back of eyes, the shortest distance between the posterior orbital borders of the eyes (**IBE**); forearm length, measured from the elbow to the wrist (**FAL**); hand length (**HAL**); diameter of lower arm (**LAD**); thigh length, from the cloaca to the knee (**THL**); tibia length/shank length,

Table 1. Localities, voucher information, and Genbank accession numbers for all specimens used in molecular analyses of this study. The "*" indicates that the sequences are derived from the holotype or paratype. The "#" indicates that the sequences are derived from the type locality.

ID	Species	Voucher ID	Locality	GenBank No.	References
Ingroup					
1	*M. aishani*#	SDBDU 3920	Subhong, Cachar district, Assam, India	MK889218	Das et al. 2019
2	*M. aishani*	CAS 231509	Kachin State, Myanmar	MW035603	Miller et al. 2021
3	*M. dissimulans**	AUP 01690	Saba Yoi District, Songkhla, Thailand	MT573414	Suwannapoom et al. 2020
4	*M. dissimulans**	AUP 01691	Saba Yoi District, Songkhla, Thailand	MT573415	Suwannapoom et al. 2020
5	*M. dissimulans**	AUP 01696	Saba Yoi District, Songkhla, Thailand	MT573416	Suwannapoom et al. 2020
6	*M. erythropoda*#	ZMMUA4721-1542	Ma Da, Dong Nai, Vietnam	MH756147	Poyarkov et al. 2018
7	*M. erythropoda*#	ZMMUA4721-1533	Ma Da, Dong Nai, Vietnam	MH756146	Poyarkov et al. 2018
8	*M. hekouensis**	KIZ 20210510	Nanxi, Hekou, Yunnan, China	MZ536627	Liu et al. 2021a
9	*M. hekouensis**	KIZ 20210511	Nanxi, Hekou, Yunnan, China	MZ536628	Liu et al. 2021a
10	*M. immaculata**	KFBG 14271	Exianling Nature Reserve, Hainan, China	MW376737	Yang and Poyarkov 2021
11	*M. immaculata**	KFBG 14270	Exianling Nature Reserve, Hainan, China	MW376736	Yang and Poyarkov 2021
12	*M.* cf. *immaculata*	TZ 98110	Chin Xai, Ha Tinh, Vietnam	AF285207	Ziegler 2000
13	*M.* cf. *immaculata*	FMNH 255121(1)	Boualapha, Khammouan, Laos	KC822494	Blackburn et al. 2013
14	*M.* cf. *immaculata*	FMNH 255121(2)	Boualapha, Khammouan, Laos	KC179997	De Sá et al. 2012
15	*M. inornata*	USNM 587625	Lenya National Park, Tanintharyi, Myanmar	MT609033	Miller et al. 2021
16	*M. inornata*	MZB 27242	Suka Makmue, Aceh, Sumatra, Indonesia	LC208138	Alhadi et al. 2017
17	*M. inornata*	KIZ 031299	Kanom District, Phuket, Thailand	PQ208536	This study
18	*M. inornata*	KIZ 025629	Nopphitam, Nakhon Si Thammarat, Thailand	PQ208534	This study
19	*M. inornata*	KIZ 031264	Klong Sok District, Suratthani, Thailand	PQ208535	This study
20	*M. inornata*#	MZB 23948	Deli Serdang, Sumatra, Indonesia	LC208137	Alhadi et al. 2017
21	*M. inornata*#	MZB 23947	Deli Serdang, Sumatra, Indonesia	LC208136	Alhadi et al. 2017
22	*M. inornata*#	MZB 23949	Deli Serdang, Sumatra, Indonesia	LC208135	Alhadi et al. 2017
23	*M. lineata*	CAS 247206	Kawthaung, Tanintharyi, Myanmar	KM509167	Peloso et al. 2016
24	*M. lineata*	KUHE 23858	Ranong, Thailand	AB634695	Matsui et al. 2011b
25	*M. lineata*	USNM 587624	Lenya, Ma Noe Lone, Tanintharyi, Myanmar	MT609052	Miller et al. 2021
26	*M. lineata*	USNM 587911	Nint Tenku, Tanintharyi, Myanmar	MT609036	Miller et al. 2021
27	*M. lineata*	CAS 247200	Tanintharyi, Myanmar	MW042901	Miller et al. 2021
28	*M. melanops*#	ZMMU NAP-01381-5	Bidoup Nui Ba National Park, Lam Dong, Vietnam	MZ474685	Poyarkov et al. 2021
29	*M. melanops**	ZMMU A7583	Bidoup Nui Ba National Park, Lam Dong, Vietnam	MZ474684	Poyarkov et al. 2021
30	*M. menglienica*	K 3246	Ban Sop Chuna, Luangprabang, Laos	KC180027	De Sá et al. 2012
31	*M. menglienica*	K 3068	Doi Chiang Dao, Chiang Mai, Thailand	KR827953	Grosjean et al. 2015
32	*M. menglienica*	KUHE 20497	Mae Yom, Phrae, Thailand	AB598341	Matsui 2011a
33	*M. menglienica*	-	Thailand	AF215375	Vences 1999
34	*M. menglienica*	KFBGF14654	Menglun, Mengla, Yunnan, China	OR053963	Yeung et al. 2023
35	*M. menglienica*	KFBGF14653	Menglun, Mengla, Yunnan, China	OR053962	Yeung et al. 2023
36	*M. menglienica*	KIZ 038313	Menglun, Mengla, Yunan, China	PQ208545	This study
37	*M. menglienica*	KIZ 01554	Menglun, Mengla, Yunan, China	PQ208543	This study
38	*M. menglienica*	KIZ 030759	Chomtong, Ban Laung, Chiang Mai, Thailand	PQ208544	This study
39	*M. menglienica*#	KIZ 20210712	Jingxin, Menglian, Yunnan, China	OK335187	Liu et al. 2021b
40	*M. menglienica*#	KIZ 20210711	Jingxin, Menglian, Yunnan, China	OK335186	Liu et al. 2021b
41	*M. nigromaculata*	DTU 301	Cuc Phuong National Park, Ninh Binh, Vietnam	MH756154	Poyarkov et al. 2018
42	*M. nigromaculata**	ZMMUA5934	Cat Ba National Park, Ninh Binh, Vietnam	MH756150	Poyarkov et al. 2018
43	*M. nigromaculata**	ZMMUA5940	Cat Ba National Park, Ninh Binh, Vietnam	MH756152	Poyarkov et al. 2018
44	*M. nigromaculata**	ZMMUA5942	Cat Ba National Park, Ninh Binh, Vietnam	MH756153	Poyarkov et al. 2018
45	*M. steinegeri*	-	Tainan, Taiwan, China	MW376735	Yang and Poyarkov 2021
46	*M. steinegeri*	ZMMUA5336-3	Kaohsiung, Taiwan, China	MW376734	Yang and Poyarkov 2021
47	*M. subaraji*	KIZ 049448	Ang Thong, Prachuap Khiri Khan, Thailand	PQ208547	This study
48	*M. subaraji*	KIZ 018074	Ang Thong, Prachuap Khiri Khan, Thailand	PQ208546	This study
49	*M. subaraji**	ZRC1.13389	Kranji Marshes, Singapore	ON026066	Sankar et al. 2022
50	*M. subaraji**	ZRC1.13370	Kranji Marshes, Singapore	ON026065	Sankar et al. 2022
51	*M. subaraji**	ZRC1.13369	Kranji Marshes, Singapore	ON026064	Sankar et al. 2022
52	*M. subaraji**	ZRC1.13323	Kranji Marshes, Singapore	ON026063	Sankar et al. 2022
53	*M. sumatrana**	MZB. Amph 30594	Hutan Harapan, Musi Banyuasin, Indonesia	MN727065	Munir et al. 2020
54	*M. thongphaphumensis* sp. nov.	KUHE 35133	Kanchanaburi, Thailand	AB611968	Kurabayashi et al. 2011
55	*M. thongphaphumensis* sp. nov.	KIZ 016771	Sai Yok Noi, Kanchanaburi, Thailand	PQ208541	This study
56	*M. thongphaphumensis* sp. nov.	KIZ 016690	Sai Yok Noi, Kanchanaburi, Thailand	PQ208537	This study
57	*M. thongphaphumensis* sp. nov.	KIZ 016768	Sai Yok Noi, Kanchanaburi, Thailand	PQ208539	This study
58	*M. thongphaphumensis* sp. nov.	KIZ 016763	Sai Yok Noi, Kanchanaburi, Thailand	PQ208538	This study
59	*M. thongphaphumensis* sp. nov.	KIZ 016769	Sai Yok Noi, Kanchanaburi, Thailand	PQ208540	This study
60	*M. thongphaphumensis* sp. nov.	KIZ 024670	Thong Pha Phum, Kanchanaburi, Thailand	PQ208542	This study
Outgroup					
61	*Mysticellus franki**	ZSI/WGRC/V/A/967	Suganthagiri, Wayanad district, Kerala state, India	MK285340	Garg and Biju 2019
62	*Uperodon systoma*	SDBDU 2005.4723	Kunnapattu, Tamil Nadu, India	MG557949	Garg et al. 2018
63	*Kaloula pulchra*	NMNS 3208	China	KC822614	Blackburn et al. 2013

from the knee to the ankle (**TL**); foot length (**FL**); length of inner metatarsal tubercle (**IMT**); first finger length (**FIL**); second finger length (**FIIL**); third finger length (**FIIIL**); fourth finger length (**FIVL**); first toe length (**TIL**); second toe length (**TIIL**); third toe length (**TIIIL**); fourth toe length (**TIVL**); fifth toe length (**TVL**).

Results

The BI and ML analyses obtained similar topologies with relatively high nodal support values for most terminal nodes, differing mainly at nodes identified as weakly supported or collapsed (Fig. 2). Our phylogenetic result shows that the monophyly of the genus *Micryletta* was strongly supported (BPP = 1.00; BS = 89; Fig. 2). In addition, phylogenetic analyses showed that our newly collected *Micryletta* specimens were recovered as four major clades (Fig. 2).

The first clade: seven samples (four samples from northern Thailand, two samples from Xishuangbanna, Yunnan, China, and one sample from Laos) clustered with the specimens (including the topotypic specimens) of *M. menglienica* with weak support (Fig. 2, clade I). The genetic distance of this clade was found to be very small, ranging from 0.0 to 1.0% (Suppl. material 1). Therefore, we considered them to be conspecific with *M. menglienica*.

The second clade: the population of *M.* cf. *inornata* from Kanchanaburi in Thailand, represented a distinct phylogenetic lineage with strong support (BPP = 1.00; BS = 100, clade II), which differed notably from topotypic specimens of *M. inornata* sensu stricto from Indonesia (Fig. 2). The interspecific genetic distance between the Kanchanaburi population and the other species of the genus *Micryletta* ranged from 2.8% (*M. hekouensis*) to 12.8% (*M. sumatrana*) (Table 2). It is comparable to the divergences among the nearest neighbor genetic distances of this group,

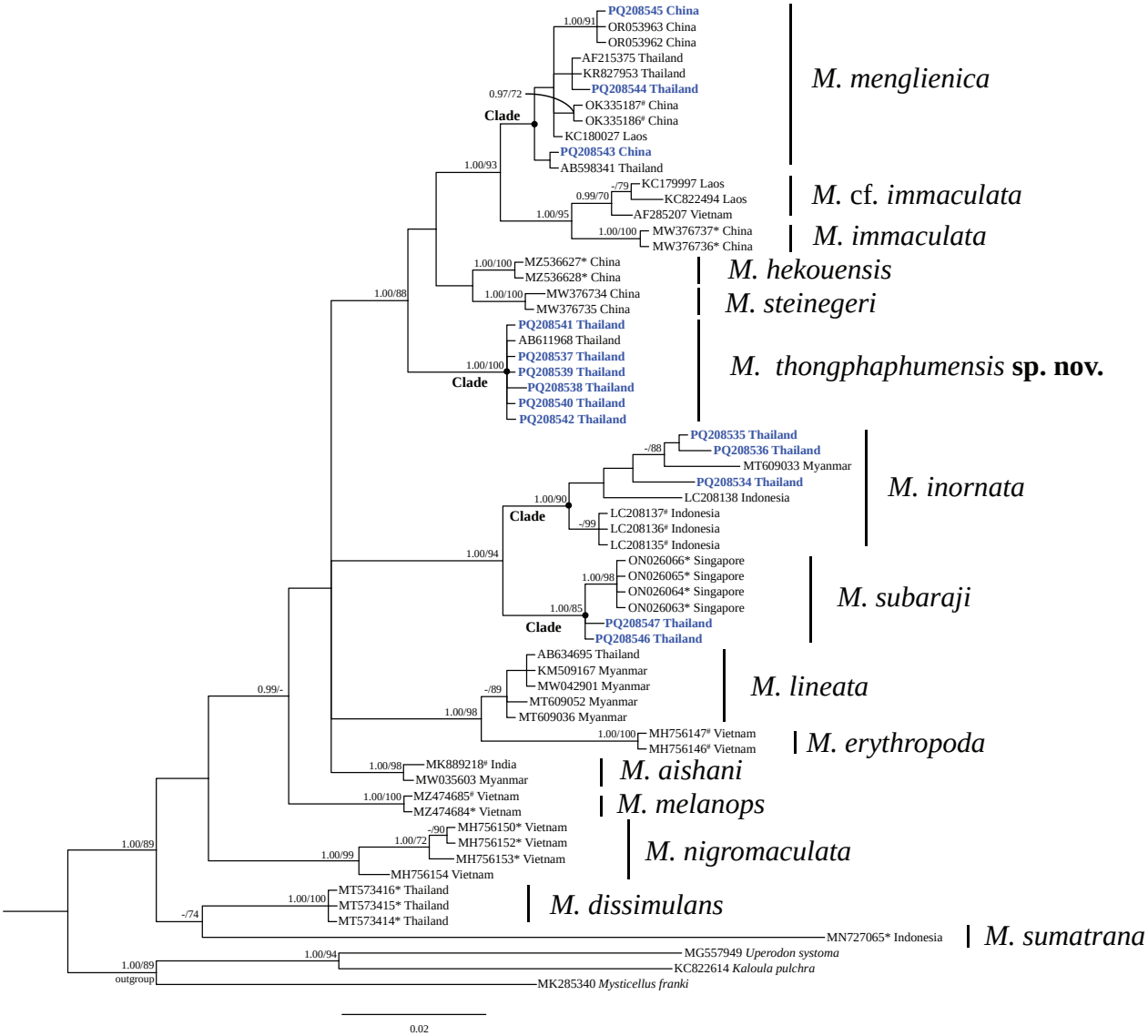

Figure 2. Phylogram of *Micryletta* based on mitochondrial 16S rRNA gene. Bayesian posterior probabilities (BPP) from BI analyses and bootstrap supports (BS) from ML analyses are listed beside the nodes. The symbol '-' represents a value below 0.95/70. '*' denotes the holotype or paratype. '#' denotes the specimen from the type locality. Blue bold text indicates newly generated data.

Table 2. Mean uncorrected *p*-distances (%) of 16S sequences among *Micryletta* species (below the diagonal) and standard error estimates (above the diagonal). The ingroup mean uncorrected *p*-distances are shown on the diagonal in bold.

ID	Species	1	2	3	4	5	6	7	8	9	10	11	12	13	14	15
1	*M. aishani*	**0.2**	0.8	0.9	0.9	0.8	0.9	1.0	0.8	0.7	0.8	0.8	1.0	0.8	0.9	1.4
2	*M.* cf. *immaculata*	3.9	**0.5**	1.1	1.0	0.7	0.5	1.1	0.8	0.9	1.0	0.6	1.1	0.7	1.1	1.5
3	*M. dissimulans*	4.4	6.2	**0.0**	1.2	1.0	1.1	1.0	1.1	1.0	1.0	1.0	1.0	1.0	1.0	1.4
4	*M. erythropoda*	4.7	5.9	7.4	**0.0**	0.9	1.0	1.1	1.0	0.7	1.0	1.0	1.1	1.0	1.0	1.6
5	*M. hekouensis*	3.2	2.7	5.0	5.0	**0.0**	0.8	1.0	0.7	0.8	0.9	0.6	1.1	0.5	1.0	1.5
6	*M. immaculata*	4.8	1.7	6.4	6.8	3.1	**0.0**	1.2	0.8	1.0	1.0	0.6	1.2	0.7	1.1	1.5
7	*M. inornata*	5.2	7.1	5.9	7.6	5.7	7.4	**1.6**	1.0	1.0	1.0	1.1	1.1	1.0	0.6	1.5
8	*M. thongphaphumensis* sp. nov.	3.5	4.0	6.0	5.7	2.8	4.4	6.1	**1.3**	0.8	0.9	0.7	1.1	0.7	1.0	1.6
9	*M. lineata*	3.4	4.4	5.9	2.7	3.6	5.3	6.3	4.2	**0.2**	0.9	0.9	1.0	0.8	1.0	1.5
10	*M. melanops*	3.1	5.0	5.0	5.4	3.7	5.4	5.6	4.2	4.2	**0.0**	0.9	1.0	0.9	0.9	1.5
11	*M. menglienica*	3.5	2.1	5.3	6.0	2.3	2.4	6.6	3.4	4.6	4.4	**0.5**	1.0	0.6	1.0	1.5
12	*M. nigromaculata*	5.0	7.1	5.6	7.9	6.2	7.4	6.8	6.6	5.9	5.1	6.4	**0.9**	1.0	1.1	1.2
13	*M. steinegeri*	3.5	3.1	4.8	5.7	1.3	3.0	5.6	3.1	4.3	4.4	2.2	5.8	**0.2**	1.0	1.4
14	*M. subaraji*	4.6	6.5	5.8	6.7	5.4	7.0	3.0	5.8	5.4	5.0	6.1	6.3	5.4	**0.3**	1.6
15	*M. sumatrana*	10.8	12.3	9.9	14.0	11.4	12.5	12.9	12.8	12.2	11.2	11.7	9.6	10.8	13.3	-

which varied from 1.3% (*M. steinegeri* and *M. hekouensis*) to 14.0% (*M. sumatrana* and *M. erythropoda*) for 16S rRNA (Table 2). Morphologically, the Kanchanaburi population of *M.* cf. *inornata* differs in a number of taxonomically important diagnostic characters from other congeners, including *M. inornata* from Indonesia. Thus, both molecular and morphological analyses clearly indicate that this population represents a separately evolving lineage and an undescribed species, which we describe below.

The third clade: three samples from Surat Thani, Phuket, and Nakhon Si Thammarat in Thailand clustered with *M. inornata* sensu stricto from Indonesia and Myanmar (BPP = 1.00; BS = 90; Fig. 2, clade III). The mean intraspecific genetic distance of *M. inornata* sensu stricto is 1.6% (Table 2), ranging from 0.0–2.8% (Suppl. material 1).

The fourth clade: two specimens from Prachuap Khiri Khan in Thailand were grouped with type specimens of *M. subaraji* with strongly supported (BPP = 1.00; BS = 85; Fig. 2, clade IV). The uncorrected *p*-distance between the newly-discovered populations from Prachuap Khiri Khan Province and the topotypic *M. subaraji* (Kranji Marshes, Singapore) was very small, ranging from 0.0–0.6% (Suppl. material 1), indicating that they represent the same taxon.

Taxonomic account

Micryletta thongphaphumensis Cao, Suwannapoom, Kilunda, Wu & Che, sp. nov.

https://zoobank.org/6BE93CBC-4833-46E9-A9B2-176804292322

Figs 3–5

Micryletta inornata., Kurabayashi et al. 2011.

Etymology. The specific name is a Latinized toponymic adjective in neuter gender derived from ‘‘Thong Pha Phum’’ in reference to the type locality Thong Pha Phum District in Kanchanaburi Province, Thailand.

Suggested common name. We propose “Thong Pha Phum Paddy Frog” as the common English name.

Type material. ***Holotype*** (Figs 3, 4) • KIZ 024670, adult male from Thong Pha Phum District in Kanchanaburi Province, Thailand (15°11'52.72"N, 98°19'29.71"E; 242 m a.s.l.), collected by Chatmongkon Suwannapoom, Jing Che, Fang Yan, and Wei Gao on 5 August 2013.

Paratypes (Fig. 5) • KIZ 016763, KIZ 016768, KIZ 016771, and KIZ 016690, four adult females from Sai Yok Noi Waterfall in Kanchanaburi Province, Thailand (14°14'19"N, 99°03'30"E; 182 m a.s.l.), collected by Zhi-Yong Yuan and Chatmongkon Suwannapoom on 4 August 2014. KIZ 016769 adult male, with the same collection information as females.

Referred specimens. One adult female KIZ 016762 and two adult males, KIZ 016764 and KIZ 016770, from the same location as paratypes.

Diagnosis. *Micryletta thongphaphumensis* sp. nov. is assigned to the genus *Micryletta* based on the following combination of morphological traits: small body size; absence of vomerine teeth; tympanum small and externally visible; subarticular tubercles on fingers and toes prominent; three well-developed metacarpal tubercles; absence of webbing between fingers and toes (Dubois 1987; Fei et al. 2009). The new species differs from its congeners by a combination of the following characters: medium-sized within the genus (SVL 21.3–25.6 mm in males, n = 5; 24.4–29.7 mm in females, n = 4; Table 3); snout truncate in dorsal view; tympanum distinct; supratympanic fold absent; a black streak extending from tip of the snout to crotch; upper lip white; tibiotarsal articulation adpressed limb reaching level of tympanum; lack of webbing between fingers and toes; relative finger lengths: I < II < IV < III; relative toe lengths: I < II < V < III < IV; outer metatarsal tubercle absent; ventral skin of body and limbs smooth; brown marbling patterns on dorsal limbs; dorsal orange-brown with black spots (Fig. 4).

Description of the holotype (Fig. 4, Table 3). Adult male, body size small (SVL = 25.6 mm), elongated oval-shaped; head wider than long (HW/HL = 1.2); canthus rostralis distinct, rounded; loreal region slightly concave; top of head relatively flat; snout slightly projecting beyond lower jaw, truncate in dorsal view, and bluntly

Figure 3. Adult male holotype (KIZ 024670) of *Micryletta thongphaphumensis* sp. nov. in life. **A.** Dorsal view; **B.** Lateral view of left side; **C.** Lateral view of right side. Photos by Jing Che.

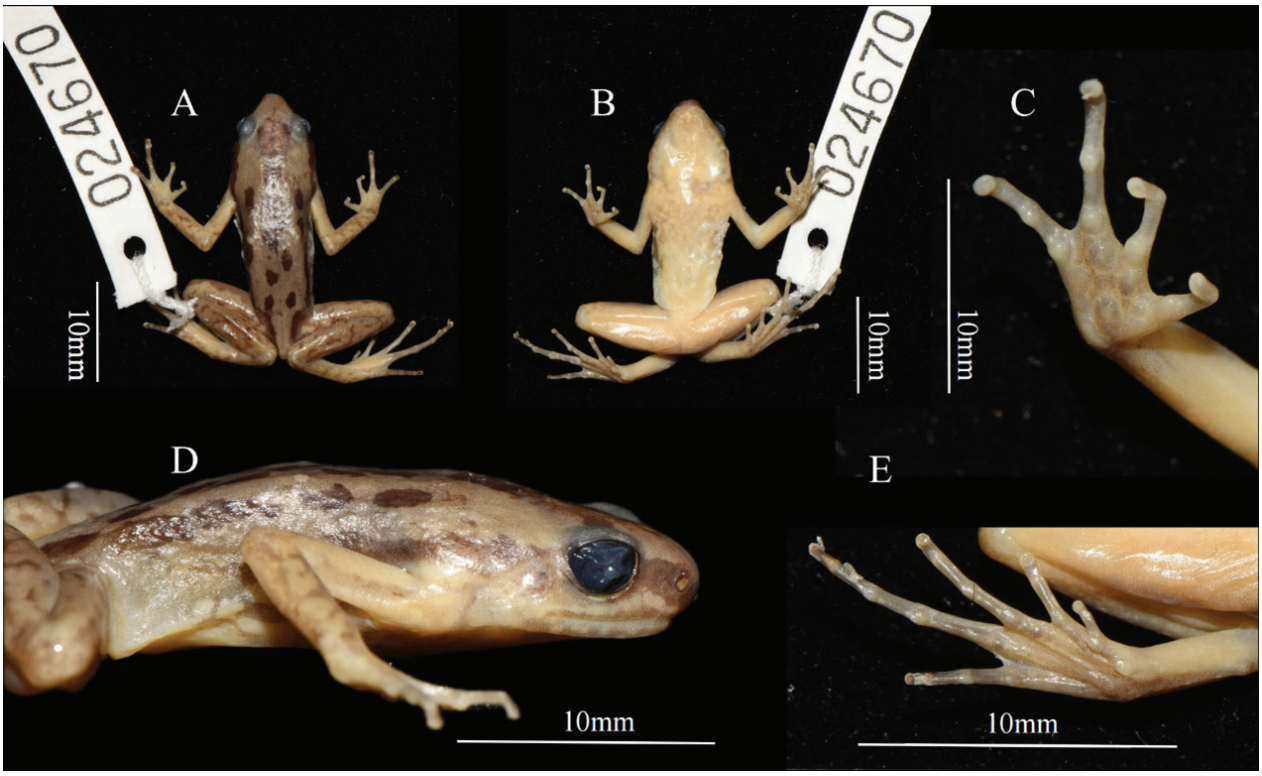

Figure 4. Adult male holotype (KIZ 024670) of *Micryletta thongphaphumensis* sp. nov. in preservative. **A.** Dorsal view; **B.** Ventral view; **C.** Volar view of right hand; **D.** Lateral view of head; **E.** Plantar view of right foot. Photos by Yu-Yang Cao.

rounded in profile; snout length longer than diameter of eye (SL/ED = 1.3); nostril round, closer to tip of snout than to eye (SN/EN = 0.6); internarial distance greater than upper eyelid width (INS/UEW = 1.6), and shorter than interorbital distance (INS/IOS = 0.5); upper eyelid width roughly equal one-third of interorbital distance (UEW/IOS = 0.3) and half of diameter of eye (UEW/ED = 0.5); eyes medium in size (ED/HL = 0.4); vomerine teeth absent; opening of vocal sac long cleft; tongue oval, with no notch at posterior tip; tympanum distinct, small (TD = 0.9 mm) and rounded; diameter of tympanum shorter than diameter of eye (TD/ED = 0.4); interorbital distance between anterior margins of eyes closer than that of posterior margins (IFE/IBE = 0.6); supratympanic fold absent.

Forelimbs slender and long, hand slightly longer than forearm length (HAL/FAL = 1.1); relative finger lengths: I < II < IV < III (FIL = 2.5 mm, FIIL = 3.4 mm, FIIIL = 6.1 mm, FIVL = 4.6 mm); tips of fingers round and not expanded to disks; subarticular tubercle on fingers rounded and prominent, subarticular tubercle formula: 1, 1, 2, 2; nuptial pad absent; webbing between fingers absent; three well-developed metacarpal tubercles at the base of outer three fingers, inner one rounded and smallest, outer metacarpal tubercle elongated, medial metacarpal tubercle large, oval and prominent.

Hindlimbs slender, tibia length shorter than half of snout-vent length (TL/SVL = 0.4), tibia length slightly shorter than foot length (TL/FL = 0.9); heels slightly overlapped when thighs are positioned at right angles to the body;

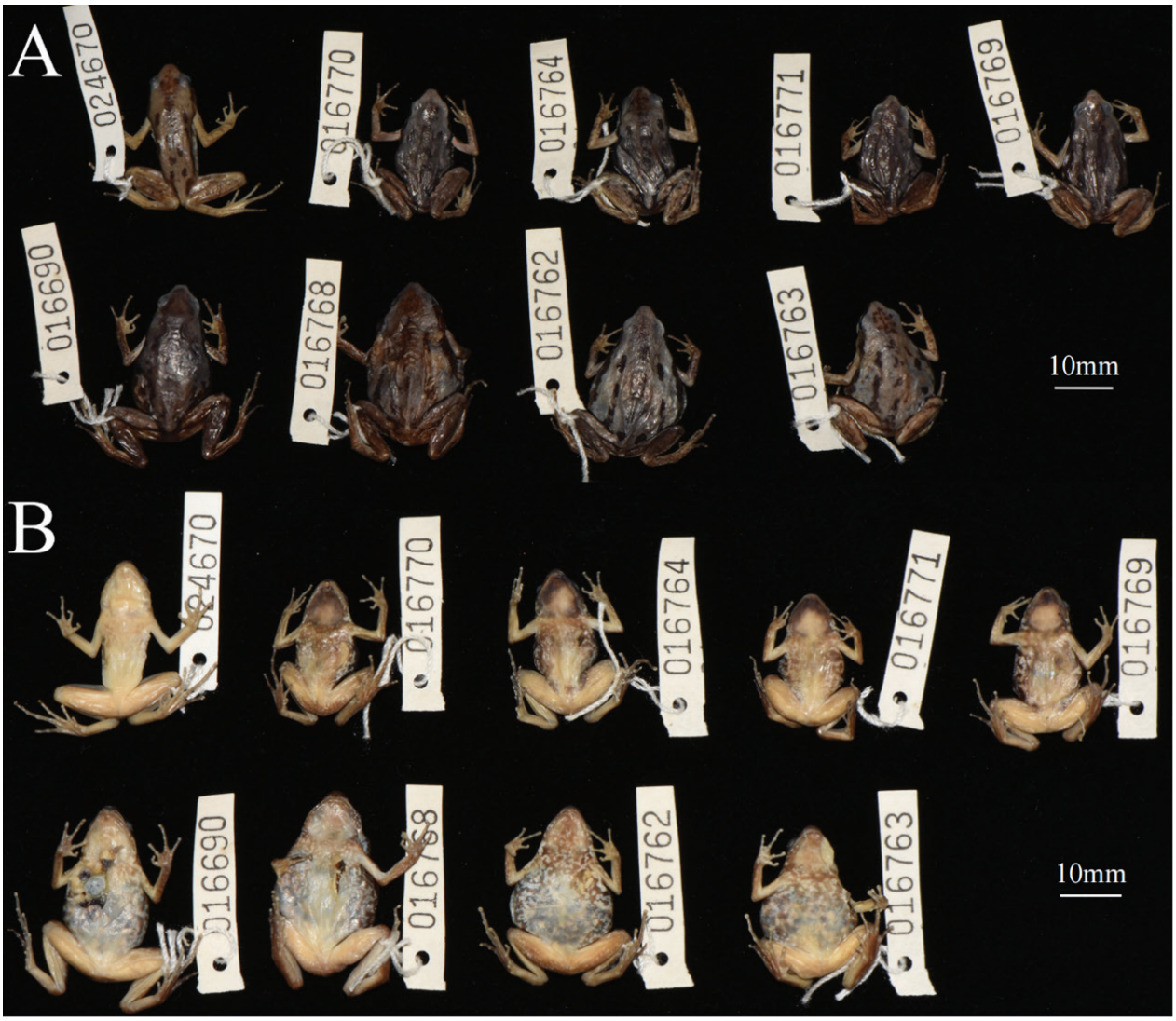

Figure 5. Type series and referred specimens of *Micryletta thongphaphumensis* sp. nov. from Kanchanaburi province in preservative **A.** Dorsal view; **B.** Ventral view. Photos by Yu-Yang Cao.

tibiotarsal articulation adpressed limb reaching level of tympanum; tips of toes round and not expanded to disks; subarticular tubercles on toes rounded and prominent, formula: 1, 1, 2, 3, 2; relative toe lengths: I < II < V < III < IV (TIL = 2.4 mm, TIIL = 4.7 mm, TIIIL = 8.3 mm, TIVL = 11.2 mm, TVL = 6.6 mm); three small supernumerary tubercles at base of toes II–IV, smaller than proximal subarticular tubercles; inner metatarsal tubercle oval and distinct (IMT = 0.9 mm); outer metatarsal tubercle absent; webbing between toes absent.

Dorsum skin of body and limbs smooth without small tubercles; dorsolateral fold absent; ventral surface of throat, belly, forelimbs, and hindlimbs smooth; upper eyelid lacking tubercles; dorsal skin of body sparsely granular in life; vent area smooth.

Color of holotype in life (Fig. 3). Dorsum skin of body orange-brown with some scattered blackish black spots elongate; lateral sides of dorsum with brownish black stripes from snout to groin; subtle longitudinal median line present on dorsum; upper lip white, extending up to the anterior forelimb; lower lip puce with white mottling along the margins; dorsal surface of forearms orange-brown without brown marbling patterns; dorsal surface of hindlimbs orange-brown without dark transverse bands, brown marbling patterns clearly, extending to dorsal of fifth toe; finger and toes I–IV gray-brown with white mottling; groin, anterior and posterior parts of thigh, and lateral surfaces of shank and tarsus brown with a few fuzzy white spots; irregular white and brown spots on chest and lateral belly; iris bicolored, with upper third bronze and lower two-thirds dark brown.

Color of holotype in preservative (Fig. 4). Colors considerably faded; dorsum skin of body grey-brown with blackish black spots; the pattern generally remains unchanged; subtle longitudinal median line fuzzy on dorsum; upper lip, belly, and white spots turned to light grey.

Variation and sexual dimorphism (Fig. 5). The body sizes of males are smaller than females generally, although there is overlap in the ranges of values (male SVL 21.3–25.6 mm, female SVL 24.4–29.7 mm); translucent skin on belly through which the large bicolored white and black eggs are visible; dark-brown spots markings variable in density from few to many and most somewhat elongate rather than round; the shapes of spots varied; subtle longitudinal median line clear or fuzzy on dorsum.

Table 3. Measurements (in mm) of *Micryletta thongphaphumensis* sp. nov. from Thailand. Abbreviations are defined in Methods.

	KIZ 024670	KIZ 016769	KIZ 016771	KIZ 016763	KIZ 016768	KIZ 016690	KIZ 016770	KIZ 016764	KIZ 016762
	Holotype	Paratype	Paratype	Paratype	Paratype	Paratype	Referred specimen	Referred specimen	Referred specimen
Gender	Male	Male	Female	Female	Female	Female	Male	Male	Female
SVL	25.6	23.5	21.3	24.4	29.7	28.1	22.3	23.7	27.3
HL	6.6	6.9	6.6	6.6	6.8	6.5	6.4	6.7	6.9
HW	8.1	7.2	7.5	7.7	8.9	8.0	7.4	8.1	8.2
HW/HL	1.2	1.0	1.1	1.2	1.3	1.2	1.2	1.2	1.2
SL	3.3	3.4	3.0	3.4	3.2	2.9	3.1	3.2	3.3
INS	2.1	2.1	1.6	2.2	2.1	2.1	2.1	2.0	2.2
IOS	4.5	3.5	3.4	3.8	3.9	3.7	3.8	3.6	3.8
INS/IOS	0.5	0.6	0.5	0.6	0.5	0.6	0.6	0.6	0.6
UEW	1.3	1.4	1.1	1.2	1.1	1.4	1.2	1.2	1.2
INS/UEW	1.6	1.5	1.5	1.8	1.9	1.5	1.8	1.7	1.8
UEW/IOS	0.3	0.4	0.3	0.3	0.3	0.4	0.3	0.3	0.3
ED	2.5	2.0	2.0	2.5	2.1	2.6	2.4	2.0	2.7
UEW/ED	0.5	0.7	0.6	0.5	0.5	0.5	0.5	0.6	0.4
ED/HL	0.4	0.3	0.3	0.4	0.3	0.4	0.4	0.3	0.4
SL/ED	1.3	1.7	1.5	1.4	1.5	1.1	1.3	1.6	1.2
TD	0.9	1.2	1.2	1.4	1.3	1.5	1.1	1.0	1.2
TD/ED	0.4	0.6	0.6	0.6	0.6	0.6	0.5	0.5	0.4
TYE	0.9	0.6	0.4	0.6	0.6	0.6	0.6	0.6	0.7
SN	1.1	0.9	1.0	1.0	1.1	0.7	1.0	1.1	1.2
EN	2.0	1.9	2.1	2.1	1.9	2.2	1.8	2.1	2.3
SN/EN	0.6	0.5	0.5	0.5	0.6	0.3	0.6	0.5	0.5
IFE	4.0	4.2	4.0	4.1	4.8	4.7	3.8	4.2	4.3
IBE	6.6	6.6	6.1	6.8	7.3	6.6	6.1	6.4	6.8
IFE/IBE	0.6	0.6	0.7	0.6	0.7	0.7	0.6	0.7	0.6
FAL	6.7	6.1	5.7	6.5	6.4	6.6	6.3	6.1	6.5
HAL	7.2	6.2	6.0	6.2	7.4	7.2	6.4	6.0	7.0
HAL/FAL	1.1	1.0	1.0	1.0	1.1	1.1	1.0	1.0	1.1
LAD	1.4	1.3	1.6	1.4	1.9	1.6	1.4	1.7	1.7
THL	11.0	10.1	9.7	11.9	12.4	12.0	11.0	11.0	11.9
TL	11.4	10.7	10.0	11.0	12.5	11.9	11.3	11.1	11.5
TL/SVL	0.4	0.5	0.5	0.5	0.4	0.4	0.5	0.5	0.4
FL	12.9	11.9	10.7	11.7	14.0	13.1	11.9	12.8	12.0
TL/FL	0.9	0.9	0.9	0.9	0.9	0.9	0.9	0.9	1.0
IMT	0.9	0.6	0.5	0.6	0.9	0.8	0.8	0.7	0.9
FIL	2.5	2.2	2.0	2.5	2.6	2.1	2.1	2.0	2.3
FIIL	3.4	2.9	2.5	3.3	3.6	3.9	3.0	3.2	2.9
FIIIL	6.1	5.0	4.8	5.7	5.9	5.9	5.3	5.4	5.5
FIVL	4.6	4.0	2.8	3.6	4.5	4.0	3.4	3.9	3.9
TIL	2.4	2.6	1.7	2.0	2.1	2.4	2.0	2.3	2.1
TIIL	4.7	4.3	4.0	4.3	4.8	4.8	4.3	4.3	4.5
TIIIL	8.3	7.6	6.8	7.1	8.1	8.1	6.8	7.1	7.2
TIVL	11.2	10.2	9.7	9.9	11.3	11.2	10.1	10.2	11.1
TVL	6.6	6.2	5.4	5.6	6.4	6.3	5.5	5.5	6.2

Distribution and ecology. *Micryletta thongphaphumensis* sp. nov. is currently known from the Thong Pha Phum District and Sai Yok Noi in Kanchanaburi Province, Thailand (Fig. 1). Considering that the region borders Myanmar, it is speculated that this species may also be present in Myanmar. Eggs were visible in the females we collected, thus indicating that August is the breeding season for this species. Other frog species were observed at the same location, including *Microhyla mukhlesuri*, *M. heymonsi*, *Hylarana nigrovittata*, *Occidozyga martensii*, *Limnonectes jarujini*, and *Fejervarya limnocharis*.

Morphological comparison. We compared *Micryletta thongphaphumensis* sp. nov. to all other recognized species of the genus *Micryletta* (Tarkhnishvili 1994; Poyarkov et al. 2018, 2021; Alhadi et al. 2019; Das et al. 2019; Munir et al. 2020; Suwannapoom et al. 2020; Liu et al. 2021a, b; Miller et al. 2021; Yang and Poyarkov 2021; Sankar et al. 2022).

Micryletta thongphaphumensis sp. nov. differs from *M. hekouensis* by its supratympanic fold absent (vs. supratympanic fold distinct); dorsum of upper arms and dorsum of body orange-brown with brown marbling patterns in life (vs. dorsum of upper arms golden, dorsum of hindlimbs solid black with brownish black stripes); tibiotarsal articulation adpressed limb reaching level of tympanum (vs. reaching front of eye); dermal ridges absent (vs. dermal ridges present under 2nd to 4th toes but indistinct).

Micryletta thongphaphumensis sp. nov. differs from *M. steinegeri* by snout length slightly longer than diameter of eye (vs. snout length shorter than diameter of eye); webbing between fingers and toes absent (vs. rudimentary webbing between toes); second finger shorter than fourth finger, relative finger lengths: I < II < IV < III (vs. second finger longer than fourth finger, relative finger lengths: I < IV < II < III); supratympanic fold absent (vs. distinct).

Micryletta thongphaphumensis sp. nov. differs from *M. immaculata* by dorsum orange-brown in life (vs. dorsum bronze brown to reddish brown); black stripes extending from tip of snout to crotch and dark brown spots on dorsum obvious (vs. dark brown spots and stripes on dorsum and flank absent); white stripes on upper lips present (vs. irregular white spots along upper lips present); supratympanic fold absent (vs. distinct and lower margin of supratympanic fold black); webbing between toes absent (vs. webbing between toes basal and poorly developed).

Micryletta thongphaphumensis sp. nov. differs from *M. menglienica* by supratympanic fold absent (vs. distinct); dermal ridges absent (vs. dermal ridges present under 2nd to 4th toes but indistinct); dorsum of forelimbs and body orange-brown in life (vs. dorsum of forelimbs light yellow, dorsum of hindlimbs the same color as dorsum of body); ventral side of head and chest brown (vs. ventral side of head and chest greyish brown or purple grey); tibiotarsal articulation adpressed limb reaching level of tympanum (vs. reaching eye or between eye and tympanum).

Micryletta thongphaphumensis sp. nov. differs from *M. aishani* by white stripes on upper lips (vs. ash-grey mottling along the margins of the upper lips); dorsum orange-brown with many large or small scattered blackish black spots in life (vs. dorsum reddish-brown with few scattered blackish-brown spots on posterior parts of the back and near the groin); tibiotarsal articulation adpressed limb reaching level of tympanum (vs. reaching up to the level of armpit); lateral sides of dorsum with brownish black stripes from snout to groin (vs. blackish-brown streak extending from snout to lower abdomen); fifth toe longer than second toe, relative toes lengths: I < II < V < III < IV (vs. fifth toe shorter than second toe, relative toe lengths: I < V < II < III < IV).

Micryletta thongphaphumensis sp. nov. differs from *M. sumatrana* by tibiotarsal articulation adpressed limb reaching level of tympanum (vs. tibiotarsal articulation reaching front of eye); upper lip white (vs. cream spots between lip and axilla); supratympanic fold absent (vs. supratympanic fold thick, rounded, glandular, curving from posterior corner of the eye to shoulder); brown marbling patterns on tibia and tarsal (vs. complete and incomplete dark brown cross bands on tibia and tarsus); dorsum orange-brown with large or small scattered blackish black spots (vs. dorsal coloration of body golden brown with some irregular dark spots and dark thin vertebrae line).

Micryletta thongphaphumensis sp. nov. differs from *M. erythropoda* by the outer metatarsal tubercle absent (vs. presence of an outer metatarsal tubercle); orange-brown dorsum in life (vs. brick-reddish dorsum); webbing between toes absent (vs. toes with rudimentary web); second finger shorter than fourth (vs. second finger equal to fourth).

Micryletta thongphaphumensis sp. nov. differs from *M. inornata* by tibiotarsal articulation adpressed limb reaching level of tympanum (vs. reaching the eye); dorsum orange-brown with large or small scattered blackish spots (vs. dorsum brownish-grey with a silver tinge and irregular blackish-brown blotches of variable size); lateral sides of dorsum with continuous brownish black stripes from snout to groin (vs. presence of a discontinuous lateral blackish-brown streak from the tip of the snout to near the groin); throat brown with irregular fuzzy white spots (vs. throat light reddish-grey without prominent spots); dorsal of limbs with black marbling patterns (vs. dorsal of limbs with irregular golden yellow spots).

Micryletta thongphaphumensis sp. nov. differs from *M. dissimulans* by hand wider than long (vs. head longer than wide); snout length longer than diameter of eye (vs. diameter of eye equal to snout length); dorsal orange-brown with black spots (vs. dorsal shagreened with irregular-shaped brown blotches edged in beige, no black spots on dorsum); without large black spot behind eye (vs. large black spot behind eye); lateral sides of dorsum with brownish black stripes from snout to groin (vs. two large black blotches in axillary and inguinal areas on each side); white patches on lips (vs. absent).

Micryletta thongphaphumensis sp. nov. differs from *M. subaraji* by tympanum distinct (vs. hidden); dorsum orange-brown with black spots in life (vs. greyish brown); upper eyelid width equals one-third of interorbital distance UEW/IOS = 0.3 (vs. UEW/IOS = 0.7); internarial distance equals half of interorbital distance INS/IOS = 0.5 (vs. INS/IOS = 0.8).

Micryletta thongphaphumensis sp. nov. differs from *M. menlanops* by tibiotarsal articulation adpressed limb reaching level of tympanum (vs. reaching eye); supratympanic fold absent (vs. present); webbing between fingers and toes absent (vs. toe webbing rudimentary between toes II–III and III–IV); dorsum orange-brown with large black spots in life (vs. dorsal pale dark brown with small reddish speckles); dorsal surfaces of limbs orange-brown with brown marbling patterns (vs. dark brown with orange-red speckles); fifth toe longer than second toe, relative toes lengths: I < II < V < III < IV (vs. fifth toe shorter than second toe, relative toe lengths: I < V < II < III < IV); white patches on lips (vs. absent); iris bicoloured, with upper third bronze and lower two-thirds brownish black (vs. iris uniform black).

Micryletta thongphaphumensis sp. nov. differs from *M. nigromaculata* by tibiotarsal articulation adpressed limb reaching level of tympanum (vs. reaching eye); supratympanic fold absent (vs. present); dorsum light brown to orange-brown with large black spots (vs. dorsum with dark-brown irregular hourglass-shaped pattern edged with orange); white patches on lips (vs. absent); lateral sides of dorsum with brownish black stripes from snout to groin (vs. a large black blotch in inguinal area on each side).

Micryletta thongphaphumensis sp. nov. differs from *M. lineata* by second finger longer than fourth finger, relative finger lengths: I < II < IV < III (vs. second finger equal to fourth finger, relative finger lengths: I < IV = II < III); fifth toe longer than third toe, relative toes lengths: I < II < V < III < IV (vs. fifth toe equal to third toe, relative toes lengths: I < II < V = III < IV); ventral side of body smooth (vs. chest and abdomen with large flat abutting tubercles); tympanum diameter about one-third that diameter of eye (vs. about two-thirds).

Discussion

In this study, we explored the diversity, distribution, and classification of *Micryletta* by integrating our long-term fieldwork and published data. Our study supported the monophyly of *Micryletta*, consistent with previous studies by Sankar et al. (2022), Liu et al. (2021a), and Munir et al. (2020). Our study further clarified the classification controversy and distribution range of *M. inornata* sensu lato as follows:

The distribution range of *M. menglienica*

Micryletta menglienica was reported as *Kalophrynus menglienicus*, according to the original publication by Yang and Su (1980). Liu et al. (2021b) transferred the species to *Micryletta* based on both 16S rRNA and morphological analysis. Previously, this species was known only from the type locality (Menglian, Yunnan in China) and northern Vietnam (Frost 2024). In addition, the taxonomic status of *M.* '*inornata*' recorded in Mengla of Yunnan and Guangxi, China, was also controversial (Liu et al. 2021a; Yeung et al. 2023). Among these, Yeung et al. (2023) indicated that *M.* '*inornata*' from Mengla, Yunnan, was actually *M. menglienica*. Our study agrees with the findings by Yeung et al. (2023) and further extends the distribution range to Thailand and Laos for the first time. Therefore, *M. menglienica* is currently found in Yunnan province, China, Laos, Vietnam, and Thailand, with a potential occurrence in Myanmar. However, the support value of the *M. menglienica* lineage was low, possibly due to limited loci. Moreover, the *M.* cf. *inornata* from Guangxi, China, remains unknown. Future studies should employ multiple nuclear markers using phylogenomic approaches combined with extensive sampling to resolve this question.

The distribution range of *M. inornata*

Micryletta inornata is currently confirmed to be distributed in Sumatra, Indonesia, and southern Myanmar, but distribution records from the uplands of Thailand, Cambodia, China, and Vietnam require further verification (Frost 2024). Our study confirms the distribution of this species in Thailand for the first time. In addition, our study confirms that *M.* cf. *inornata* from Kanchanaburi, Thailand, is a new species based on molecular and morphological evidence, herein described as *M. thongphaphumensis* sp. nov. However, our study did not confirm the existence of this species in other areas (e.g., Yaephy, Tanintharyi in Myanmar) with questionable distribution. Therefore, future collaborative research among herpetologists from different countries is necessary to employ more extensive sampling across the range of *M. inornata* and further clarify its distribution.

The distribution range of *M. immaculata*

Micryletta immaculata was reported by Yang and Poyarkov (2021) and is only known from Hainan Island, China. Our study shows that populations from central Laos and central Vietnam formed a monophyletic lineage, which was the sister taxon to the type specimens of *M. immaculata*. The uncorrected genetic *p*-distances between the two clades are 1.7%, which is higher than the minimum interspecific genetic distance (*M. steinegeri* and *M. hekouensis*, Table 2). However, due to the absence of specimens from central Laos and central Vietnam, we could not determine whether this lineage represents an undescribed species or *M. immaculata*. We agree with Sankar et al. (2022) and consider the lineage from Vietnam and Laos as *M.* cf. *immaculata* provisionally. Although the Gulf of Tonkin acts as a geographical barrier isolating northern Vietnam and Hainan Island, China, they occur in the same zoogeographic region. Both regions still share some species, such as *Odorrana nasuta*, *Theloderma corticale*, *Rhacophorus rhodopus*, and *Rohanixalus hansenae* (Frost 2024). We recommend strengthening fieldwork surveys in the Indochina Peninsula paired with the integration of population genomics and acoustic data in order to clarify the taxonomic status of the lineage from Laos and Vietnam.

The distribution range of *M. subaraji*

Micryletta subaraji was reported by Sankar et al. (2022) and is only known from Kranji Marshes in Singapore. Our study indicates that specimens collected from Thap Sakae and Prachuap Khiri Khan in Thailand are *M. subaraji*. This is the first recorded instance of *M. subaraji* in Thailand, thus extending its latitudinal distribution northward for more than 1000 km to southern Thailand. Given that Malaysia is located between Thailand and Singapore, we presume that this species might also be present there. Future studies should conduct thorough investigations of *Micryletta* species in Malaysia to confirm the distribution of *M. subaraji*.

Acknowledgments

This work was supported by the National Key R&D Program of China (2022YFC2602500), the Second Tibetan Plateau Scientific Expedition and Research (STEP) program (Grant No. 2019QZKK0501), Science and Technology Basic Resources Investigation Program of China (2021FY100200); National Natural Science Foundation of China (NSFC 32100371); Major Science and Technique Programs in Yunnan Province (202102AA310055), the Key R & D program of Yunnan Province (202103AC100003, 202303AH310055), Yunnan Applied Basic Research Projects (No. 202301AT070312, 202301AT070431), Yunnan Revitalization Talent Support Program Yunling Scholar Project; China's Biodiversity Observation Network (Sino-BON), the Animal Branch

of the Germplasm Bank of Wild Species, CAS (Large Research Infrastructure Funding); the Plant Genetic Conservation Project under the Royal Initiative of Her Royal Highness Princess Maha Chakri Sirindhorn, University of Phayao and the Thailand Science Research and Innovation Fund and the University of Phayao (Unit of Excellence 2025 on Aquatic animals biodiversity assessment (Phase I)). Specimen collection protocols were approved by the Institutional Ethical Committee of Animal Experimentation of the University of Phayao (certificate number UP-AE59-01-04-0022 issued to Chatmongkon Suwannapoom) and the Institute of Animal for Scientific Purposes Development Thailand (No. U1-01205-2558). We thank Jie-Qiong Jin, Wen-Jie Dong, Chen-Qi Lu, Fang Yan, Zhi-Yong Yuan, Ke Jiang, Jin-Min Chen, Parinya Pawangkhant, and Zhong-Xiong Fu for helping with collecting samples in the field.

References

Alhadi F, Hamidy A, Farajallah, Ach A, Munir M, Atmaja VY, Garg S, Biju SD, Smith EN (2019) Rediscovery of *Micryletta inornata* (Boulenger, 1890) from Sumatra: redescription, molecular identity, and taxonomic implications. Zootaxa 4613: 111–126. https://doi.org/10.11646/zootaxa.4613.1.5

Blackburn DC, Siler CD, Diesmos AC, McGuire JA, Cannatella DC, Brown RM (2013) An adaptive radiation of frogs in a southeast Asian island archipelago. Evolution International Journal of Organic Evolution 67(9): 2631–2646. https://doi.org/10.1111/evo.12145

Boulenger GA (1890) List of the reptiles, batrachians, and freshwater fishes collected by Professor Moesch and Mr. Iversen in the district of Deli, Sumatria. Proceedings of the Zoological Society of London 1890: 30–39.

Boulenger GA (1909) Descriptions of four new frogs and a new snake discovered by Mr. H. Sauter in Formosa. Annals and Magazine of Natural History Series 84(24): 492–495. https://doi.org/10.1080/00222930908692704

Chen JM, Zhou WW, Poyarkov NA, Stuart BL, Brown RM, Lathrop A, Wang YY, Yuan ZY, Jiang K, Hou M, Chen HM, Suwannapoom C, Nguyen SN, Duong TV, Papenfuss TJ, Murphy RW, Zhang YP, Che J (2017) A novel multilocus phylogenetic estimation reveals unrecognized diversity in Asian horned toads, genus *Megophrys* sensu lato (Anura: Megophryidae). Molecular Phylogenetics and Evolution 106: 28–43. https://doi.org/10.1016/j.ympev.2016.09.004

Chen JM, Suwannapoom C, Wu YH, Poyarkov NA, Xu K, Pawangkhanant P, Che J (2021) Integrative taxonomy reveals a new species of *Leptobrachella* (Anura: Megophryidae) from the mountains of northern Thailand. Zootaxa 5052(2), 41–64. https://doi.org/10.11646/zootaxa.5052.2.2

Darriba D, Taboada GL, Doallo R, Posada D (2012) jModelTest 2: More models, new heuristics and parallel computing. Nature Methods 9(8): e772. https://doi.org/10.1038/nmeth.2109

Das A, Garg S, Hamidy A, Smith EN, Biju SD (2019) A new species of *Micryletta* frog (Microhylidae) from Northeast India. PeerJ 2019: e7012. https://doi.org/10.7717/peerj.7012

De Sá RO, Streicher JW, Sekonyela R, Forlani MC, Loader SP, Greenbaum E, Richards S, Haddad CF (2012) Molecular phylogeny of microhylid frogs (Anura: Microhylidae) with emphasis on relationships among New World genera. BMC Evolutionary Biology 12: 1–21. https://doi.org/10.1186/1471-2148-12-241

Dubois A (1987) Miscelanea taxinomica batrachologica, II. Alytes 6: 1–9.

Fei L, Hu SQ, Ye CY, Huang YZ (2009) Fauna Sinica. Amphibia. Vol. 2. Anura. Science Press, Chinese Academy of Science, Beijing, 957 pp. [in Chinese]

Frost DR (2024) Amphibian species of the world: an online reference. Version 6.2. American Museum of Natural History, New York, USA. https://doi.org/10.5531/db.vz.0001 [Accessed on 12 Jan. 2024]

Garg S, Biju SD (2019) New microhylid frog genus from Peninsular India with Southeast Asian affinity suggests multiple Cenozoic biotic exchanges between India and Eurasia. Scientific Reports 9(1): 1906. https://doi.org/10.1038/s41598-018-38133-x

Garg S, Senevirathne G, Wijayathilaka N, Phuge S, Deuti K, Manamendra-Arachchi K, Meegaskumbura M, Biju S (2018) An integrative taxonomic review of the South Asian microhylid genus *Uperodon*. Zootaxa 4384(1): 1–88. https://doi.org/10.11646/zootaxa.4384.1.1

Grosjean S, Ohler A, Chuaynkern Y, Cruaud C, Hassanin A (2015) Improving biodiversity assessment of anuran amphibians using DNA barcoding of tadpoles Case studies from Southeast Asia. Comptes Rendus Biologies 338(5): 351–361. https://doi.org/10.1016/j.crvi.2015.03.015

Huang JF, Li SQ, Xu R, Peng YQ (2023) East-West genetic differentiation across the Indo-Burma hotspot: evidence from two closely related dioecious figs. BMC Plant Biology 23(1): 321–341. https://doi.org/10.1186/s12870-023-04324-6

Hughes AC (2018) Have Indo-Malaysian forests reached the end of the road? Biological Conservation 223: 129–137. https://doi.org/10.1016/j.biocon.2018.04.029

Janssens SB, Vandelook F, De Langhe E, Verstraete B, Smets E, Vandenhouwe I, Swennen R (2016) Evolutionary dynamics and biogeography of Musaceae reveal a correlation between the diversification of the banana family and the geological and climatic history of Southeast Asia. The New phytologist 210(4): 1453–1465. https://doi.org/10.1111/nph.13856

Kocher TD, Thomas WK, Meyer A, Edwards SV, Pääbo S, Villablanca FX, Wilson AC (1989) Dynamics of mitochondrial DNA evolution in animals: amplification and sequencing with conserved primers. Proceedings of the National Academy of Sciences 86(16): 6196–6200. https://doi.org/10.1073/pnas.86.16.6196

Kurabayashi A, Matsui M, Belabut DM, Yong HS, Ahmad N, Sudin A, Kuramoto M, Hamidy A, Sumida M (2011) From Antarctica or Asia? New colonization scenario for Australian-New Guinean narrow mouth toads suggested from the findings on a mysterious genus *Gastrophrynoides*. BMC Evolutionary Biology 11: 1–12. https://doi.org/10.1186/1471-2148-11-175

Liu S, Hou M, Mo M, Rao D (2021a) A new species of *Micryletta* Dubois, 1987 (Anura, Microhylidae) from Yunnan Province, China. Herpetozoa 34: 131–140. https://doi.org/10.3897/herpetozoa.32.e69755

Liu S, Yang B, Wang Q, Hou M (2021b) Taxonomic reassessment of the poorly known microhylid, *Kalophrynus menglienicus* Yang & Su, 1980. Herpetozoa 34(34): 223–232. https://doi.org/10.3897/herpetozoa.34.e72627

Matsui M (2011a) Taxonomic revision of one of the Old World's smallest frogs, with description of a new Bornean *Microhyla* (Amphibia, Microhylidae). Zootaxa 2814(1): 33–49. https://doi.org/10.11646/zootaxa.2814.1.3

Matsui M, Hamidy A, Belabut DM, Ahmad N, Panha S, Sudin A, Nishikawa K (2011b) Systematic relationships of Oriental tiny frogs of the family Microhylidae (Amphibia, Anura) as revealed by mtDNA genealogy. Molecular phylogenetics and evolution 61(1): 167–176. https://doi.org/10.1016/j.ympev.2011.05.015

Matsui M, Panha S, Eto K (2023) Two new species of *Leptobrachella* from Northern Thailand (Amphibia, Anura, Megophryidae). Current Herpetology 42(1): 83–97. https://doi.org/10.5358/hsj.42.83

Miller MA, Pfeiffer W, Schwartz T (2010) Creating the CIPRES Science Gateway for inference of large phylogenetic trees. Gateway Computing Environments Workshop (GCE), 1–8. https://doi.org/10.1109/GCE.2010.5676129

Miller AH, Zug GR, Wogan GOU, Lee JL, Mulcahy DG (2021) Phylogeny, Diversity, and Distribution of *Micryletta* (Anura: Microhylidae) in Myanmar. Ichthyology & Herpetology 109(1): 245–257. https://doi.org/10.1643/h2020100

Munir M, Hamidy A, Matsui M, Kusrini MD, Nishikawa K (2020) A new species of *Micryletta* (Amphibia: Anura) from Sumatra, Indonesia. Zoological Science 37(3): 295–301. https://doi.org/10.2108/zs200006

Myers N, Mittermeier RA, Mittermeier CG, Da Fonseca GA, Kent J (2000) Biodiversity hotspots for conservation priorities. Nature 403(6772): 853–858. https://doi.org/10.1038/35002501

Peloso PLV, Frost DR, Richards SJ, Rodrigues MT, Donnellan S, Matsui M, Raxworthy CJ, Biju SD, Lemmon EM, Lemmon AR, Wheeler WC (2016) The impact of anchored phylogenomics and taxon sampling on phylogenetic inference in narrow-mouthed frogs (Anura, Microhylidae). Cladistics 32(2): 113–140. https://doi.org/10.1111/cla.12118

Poyarkov NA, Nguyen TV, Duong TV, Gorin VA, Yang JH (2018) A new limestone-dwelling species of *Micryletta* (Amphibia: Anura: Microhylidae) from northern Vietnam. PeerJ 6: e5771. https://doi.org/10.7717/peerj.5771

Poyarkov NA, Nguyen TV, Yang J-H, Gorin VA (2021) A new species of *Micryletta* (Amphibia: Anura: Microhylidae) from the Langbian Plateau in southern Vietnam. Zoological Research 42: 726–733. https://doi.org/10.24272/j.issn.2095-8137.2021.228

Sambrook J, Fritsch EF, Maniatis T (1989) Molecular cloning: a laboratory manual. 2nd edn. Cold Spring Harbor Laboratory Press, 1626 pp.

Sankar A, Law IT, Law IS, Shivaram R, Abraham RK, Chan KO (2022) Morphology, phylogeny, and species delimitation of *Micryletta* (Anura: Microhylidae) reveals a new species from Singapore. Vertebrate Zoology 72: 457–467. https://doi.org/10.3897/vz.72.e85020

Sheridan JA, Stuart BL (2018) Hidden species diversity in *Sylvirana nigrovittata* (Amphibia: Ranidae) highlights the importance of taxonomic revisions in biodiversity conservation. PLoS ONE 13(4): e0196242. https://doi.org/10.1371/journal.pone.0196242

Sun YB (2018) FasParser2: a graphical platform for batch manipulation of tremendous amount of sequence data. Bioinformatics 34(14): 2493–2495. https://doi.org/10.1093/bioinformatics/bty126

Suwannapoom C, Nguyen TV, Pawangkhanant P, Gorin VA, Chomdej S, Che J, Poyarkov NA (2020) A new species of *Micryletta* (Amphibia: Microhylidae) from southern Thailand. Zoological Research 41(5): 581–588. https://doi.org/10.24272/j.issn.2095-8137.2020.139

Suwannapoom C, Grismer LL, Pawangkhanant P, Poyarkov NA (2022) A new species of stream toad of the genus *Ansonia* Stoliczka, 1870 (Anura: Bufonidae) from Nakhon Si Thammarat Range in southern Thailand. Zootaxa 5168: 119–136. https://doi.org/10.11646/zootaxa.5168.2.2

Tamura K, Stecher G, Peterson D, Filipski A, Kumar S (2013) MEGA6: Molecular Evolutionary Genetics Analysis version 6.0. Molecular Biology and Evolution 30(12): 2725–2729. https://doi.org/10.1093/molbev/mst197

Tarkhnishvili DN (1994) Amphibian communities of the southern Viet Nam: preliminary data. Journal of the Bengal Natural History Society 13(1):3–62.

Vences M (1999) Phylogenetic studies of ranoid frogs (Amphibia: Anura), with a discussion of the origin and evolution of the vertebrate clades of Madagascar. Herpetology.

Wang K, Bhattarai S, Wu YH, Che J, Siler CD (2020) Resurrection of *Amolops nepalicus* Yang, 1991 (Amphibia: Anura: Ranidae), with Comments on the Record of *A.* cf. *afghanus* in Nepal and China and the Validity of Two Other Junior Synonyms of *A. marmoratus* (Blyth, 1855). Zootaxa 4819(1): 143–158. https://doi.org/10.11646/zootaxa.4819.1.7

Wu YH, Liu XL, Gao W, Wang YF, Li YC, Zhou WW, Yuan ZY, Che J (2021) Description of a new species of Bush frog (Anura: Rhacophoridae: *Raorchestes*) from northwestern Yunnan, China. Zootaxa 4941(2): 239–258. https://doi.org/10.11646/zootaxa.4941.2.5

Yang JH, Poyarkov NA (2021) A new species of the genus *Micryletta* (Anura, Microhylidae) from Hainan Island, China. Zoological Research 42: 234–240. https://doi.org/10.24272/j.issn.2095-8137.2020.333

Yang DT, Su CY (1980) A new species of the family Microhylidae frog from Yunnan. Zoological Research 1: 257–260.

Yeung HY, Zhao J, Yang JH (2023) Confirmation on the occurrence of *Micryletta menglienica* (Yang Su, 1980) (Anura: Microhylidae) in Mengla County, Xishuangbanna Dai Autonomous Prefecture, Yunnan Province, China. Sauria 45(2): 69–75.

Yodthong S, Rujirawan A, Stuart BL, Aowphol A (2021) A new *Limnonectes* (Anura: Dicroglossidae) from Southern Thailand. Animals 11(2): 566–594. https://doi.org/10.3390/ani11020566

Ziegler T (2000) Research on the herpetofauna in a wetland preserve in the south of North Vietnam. Unpublished PhD Thesis, Bonn.

Supplementary material 1

Uncorrected *p*-distance (percentage) 16S rRNA sequences of individuals included in phylogenetic analyses and standard error estimates

Authors: Yu-Yang Cao, Chatmongkon Suwannapoom, Felista Kasyoka Kilunda, Wei Gao, Chun-Lian Wu, Yun-He Wu, Jing Che

Data type: xlsx

Link: https://doi.org/10.3897/zse.100.129398.suppl1

Zoosyst. Evol. 100 (4) 2024, 1375–1385 | DOI 10.3897/zse.100.129520

PENSOFT

für Natur MUSEUM FÜR NATURKUNDE BERLIN

Description of two new species of the genus *Paranemachilus* (Cypriniformes, Nemacheilidae) from Guangxi, China

Hao-Lin Mo[1], Jian Yang[1], Peng Li[1], Li-Na Du[2,3]

1 *Key Laboratory of Wildlife Evolution and Conservation in Mountain Ecosystem of Guangxi, Nanning Normal University, Nanning, 530001, China*

2 *Key Laboratory of Ecology of Rare and Endangered Species and Environmental Protection (Guangxi Normal University), Ministry of Education, Guilin, Guangxi, 541004, China*

3 *Guangxi Key Laboratory of Rare and Endangered Animal Ecology, College of Life Science, Guangxi Normal University, Guilin, Guangxi, 541004, China*

https://zoobank.org/C676AE6A-A1BE-4017-B11F-516593F09A81

Corresponding authors: Jian Yang (yj1981yj@163.com); Li-Na Du (dulina@mailbox.gxnu.edu.cn)

Academic editor: Nicolas Hubert ♦ **Received** 12 June 2024 ♦ **Accepted** 18 September 2024 ♦ **Published** 14 October 2024

Abstract

This study describes two new species within the genus *Paranemachilus*. *Paranemachilus luegvetensis* **sp. nov.** and *Paranemachilus liui* **sp. nov.** can be distinguished from all recognized congeners by a combination of morphological characteristics and substantial genetic divergences. *Paranemachilus luegvetensis* **sp. nov.** is characterized by scaled cheeks; the whole body covered in scales, except for the head; 11–12 branched pectoral fin rays; 4–5 preoperculomandibular canal pores; body depth 13.5%–16.8% of standard length; and preanus length 68.3%–73.9% of standard length. *Paranemachilus liui* **sp. nov.** is characterized by scaled cheeks; the whole body covered in scales except for the head; 11–13 branched pectoral fin rays; 11–15 supraorbital canal pores at the base of the anterior nostrils; 7–9 preoperculomandibular canal pores; preanus length 67.4%–74.3% of standard length; snout length 21.4%–28.7% of lateral head length.

Key Words

cave loach, scaled cheeks, taxonomy, Xijiang River

Introduction

The genus *Paranemachilus* Zhu, 1983, is classified with the family Nemacheilidae of the order Cypriniformes. Despite its type species, *Paranemachilus genilepis* Zhu, 1983, being characterized by scaled cheeks (Zhu, 1983), later described species, such as *Paranemachilus pingguoensis* Gan, 2013, are noted for their scaleless cheeks (Lan et al. 2013). For a long time, no more species were added to the genus *Paranemachilus*. With the help of molecular biology, some species have been re-studied and classified into the genus *Paranemachilus*. Following taxonomic revisions of Yunnanilini using both morphological characteristics and molecular evidence, Du et al. (2021) placed *Yunnanilus jinxiensis* Zhu, Du, Chen & Yang, 2009 into *Paranemachilus*. Luo et al. (2023) subsequently suggested that *Heminoemacheilus* Zhu & Cao, 1987 is a synonym of *Paranemachilus*, placing the type species of *Heminoemacheilus*, i.e., *Heminoemacheilus zhengbaoshani* Zhu & Cao, 1987, into *Paranemachilus*, while *Heminoemacheilus hyalinus* Lan, Yang & Chen, 1996 and *Heminoemacheilus parvus* Zhu & Zhu, 2014 were transferred to the newly established genus *Karstsinnectes* Zhou, Luo, Wang, Zhou & Xiao, 2023. More recently, Du et al. (2023) revised the phylogenetic relationships among Chinese nemacheilids with tube-shaped anterior nostrils and undertook the description of a new species of *Paranemachilus*, *Paranemachilus chongzuo* Du et al., 2023, from Guangxi. Currently, five valid species of *Paranemachilus* are recognized, all of which inhabit underground rivers in Guangxi Province, China. The diagnostic characteristics of the genus include anterior

nostrils tube-like, tip of anterior nostrils with weak barbel-like elongation, barbel length shorter than half of tube depth, anterior and posterior nostrils adjacent, lips without papillae, lateral line incomplete, disappearing behind vertical at end of pectoral fin, and air-bladder lying free in abdominal cavity (Zhu 1983; Zhu and Cao 1987; Lan et al. 2013; Du et al. 2023).

Fieldwork conducted in 2017 and 2023 resulted in the collection of two and nine loach specimens, respectively, in Liuzhou City, Guangxi Province, China. Additionally, in June 2023, eight loach specimens were collected from Wuming County, Nanning City, Guangxi, China. Based on morphological analysis and molecular evidence, these specimens represent two previously undescribed species of *Paranemachilus*, formally described herein as *Paranemachilus liui* sp. nov. and *Paranemachilus luegvetensis* sp. nov.

Materials and methods

All care and use of experimental animals complied with the relevant laws of the Chinese Laboratory of Animal Welfare and Ethics (GB/T 35892-2018). Collection and preservation of specimens followed Li and Gao (2016). Specimens of *Paranemachilus liui* sp. nov. and *Paranemachilus luegvetensis* sp. nov. were euthanized rapidly by an overdose of clove oil anesthetic. Tissue samples were taken from the fins and preserved in anhydrous ethanol. Complete mitochondrial genes of *Paranemachilus luegvetensis* sp. nov. were sequenced by the Nanjing Jisi Huiyuan Biotechnology Company (China) following standard Illumina procedures. The mitochondrial cytochrome b (cytb) gene of *Paranemachilus liui* sp. nov. was sequenced by the Kunming Branch of Beijing Genco Biotechnology Co., Ltd. (China). The polymerase chain reaction (PCR) primer sequence was (5′-GAC TTG AAA AAC CAC CGT TG-3′ and 5′-CTC CGA TCT CCG GAT TAC AAG AC-3′) (Xiao et al. 2001). The MUSCLE was used to align the gene sequence in MEGA v11 with default parameters (Edgar, 2004; Tamura et al. 2021) and subsequently concatenated. Reference sequences of 27 nemacheilid species were retrieved from GenBank to reconstruct phylogenetic trees. The trees were constructed based on Bayesian inference (BI) using MrBayes on XSEDE (v3.2.7a) and the CIPRES Science Gateway (Miller et al. 2010). The analysis involved the Markov Chain Monte Carlo (**MCMC**) method with three heated chains and one cold chain, running for 2000000 generations with sampling every 100 generations under a complex model (GTR+I+G). The first 5000 samples were discarded as burn-in, with the remaining samples then used to generate a majority rule consensus tree.

Mitochondrial cytochrome b gene (cytb) sequencing data for the two new species were submitted to GenBank (Accession No. PP566646, PP566647 for *Paranemachilus luegvetensis* sp. nov.; PP566648, PP566649, PP566650 for *Paranemachilus liui* sp. nov.).

Most counts and morphometric measurements followed Tang et al. (2012), except for dorsal fin length (measured at the last simple dorsal ray) and caudal-peduncle depth (measured at the posterior anal-fin base), taken from the left side of the specimen. Additionally, characteristics of the cephalic lateral line system followed Kottelat (1990). Measurements were made with digital calipers, and data were recorded to the nearest 0.1 mm. The morphometric and meristic data of the two new species in this study have been deposited in the ScienceDB repository (https://www.scidb.cn/s/6ZFzQ3, accessed on 19 May 2024). The type specimens were deposited at the Nanning Normal University (**NNNU**).

Results

Paranemachilus luegvetensis Mo, Yang, Li & Du, sp. nov.

https://zoobank.org/F28EAC7B-6706-4AFB-9071-EF94CEE578AF

Figs 1, 2A, C, Tables 1, 3

Materials. ***Holotype*.** • NNNU230611 (NNNU: Nanning Normal University), 41.2 mm standard length. China: Guangxi, Wuming County, Chuanqian Village, 23°13'25.08"N, 108°26'18.50"E, collected by H.L. Mo and J.H. Zhong in June 2023.

***Paratypes*.** • NNNU230603–230610, 8 ex., 26.1–33.4 mm standard length; same data as for holotype.

Etymology. The name luegvetensis originates from the Zhuang language of the Luoyue Ancient Kingdom, pronounced LOKWET. This kingdom, believed to be located in what is now the Wuming District of Nanning City, Guangxi, China, where the type specimens were collected, is considered the cradle of this ancient civilization. The Luoyue Ancient Kingdom was known for its rich cultural contributions, including rice cultivation, cotton textiles, cliff paintings, witchcraft, Longmu rituals, and jade carving. These cultural elements profoundly influenced not only Chinese and Southeast Asian civilizations but also had significant global impacts. We propose the common Chinese name "骆越异条鳅" (Luo Yue Yi Tiao Qiu).

Diagnosis. Comparative data between *Paranemachilus luegvetensis* sp. nov. and all five known species within the genus *Paranemachilus* are provided in Table 3. *Paranemachilus luegvetensis* sp. nov. differs from all other congeneric species of *Paranemachilus* by cheeks scaled (vs. scaleless in *P. chongzuo*, *P. pingguoensis*, and *P. zhengbaoshani*), 11–12 branched pectoral fin rays (vs. 10 in *P. chongzuo*), 4–5 preoperculomandibular canal pores (vs. zero in *P. chongzuo*, 11–12 in *P. pingguoensis* and *P. zhengbaoshani*, 10 in *P. genilepis*, and 10–11 in *P. jinxiensis*), body depth 13.5%–16.8% of standard length (vs. greater than 18% in *P. jinxiensis* and *P. pingguoensis*), and preanus length 68.3%–73.9% of standard length (vs. greater than 75.3% in *P. chongzuo*, *P. genilepis*, *P. jinxiensis*, *P. pingguoensis*, and *P. zhengbaoshani*).

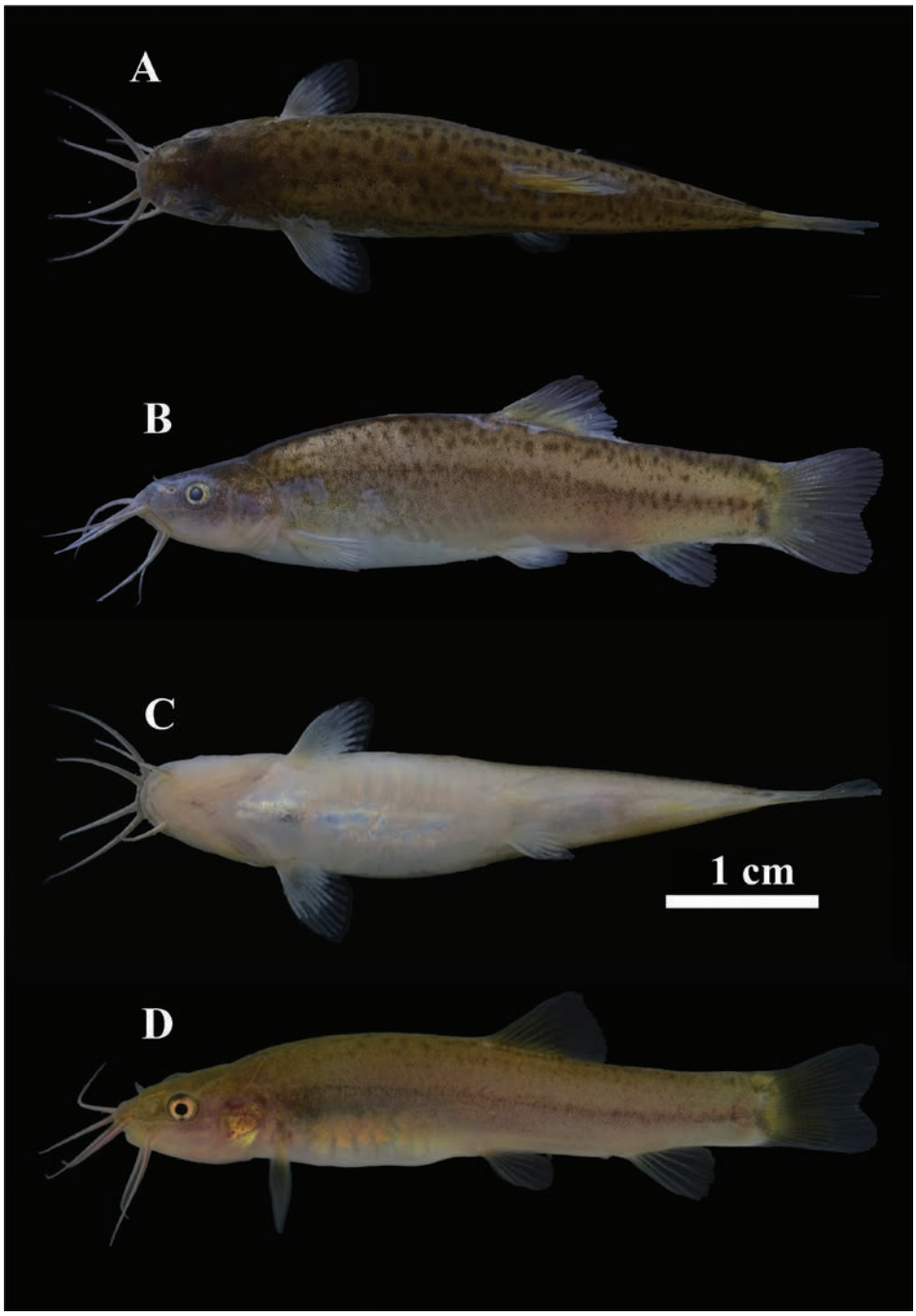

Figure 1. The dorsal (**A**), lateral (**B**), and ventral (**C**) views of *Paranemachilus luegvetensis* sp. nov. NNNU230611, holotype, 41.2 mm standard length. **D.** Living photo of *Paranemachilus luegvetensis* sp. nov., NNNU230611, holotype. Scale bar: 1 cm

Description. The morphometric data of the type specimen of *Paranemachilus luegvetensis* sp. nov. are given in Table 1. Body short, slightly bulging at back. From snout to dorsal-fin origin, body depth increases to maximum, 13.5%–16.8% of standard length, head slightly depressed, flattened, maximum head width greater than deepest head depth, 44.7%–56.5% of head length, snout length 24.5–32.1% of lateral head length, shorter than postorbital length. Mouth inferior, snout obtuse, lips developed and smooth, median of lower lip with V-shaped notch. Anterior and posterior nostrils adjacent; anterior nostrils tube-like, barbel-like elongation of anterior nostrils shorter than half the depth of nostril tube. Cheeks scaled, no reduction in eye size, eye diameter 19.3%–25.3% of head length. Three pairs of barbels: inner rostral barbel extending to posterior margin of eye, outer rostral barbel reaching or exceeding posterior margin of anterior opercular, above posterior operculum, and maxillary barbel above posterior margin of posterior operculum. Dorsal fin with three unbranched and 8–9 branched rays; distal margin cut; origin closer to caudal-fin base than to tip of snout. Pectoral fin with one unbranched and 11–12 branched rays; pectoral fin length 45.7%–61.4% of pelvic-fin insertion; pelvic fin with one unbranched and 6–7 branched rays, inserted below first or

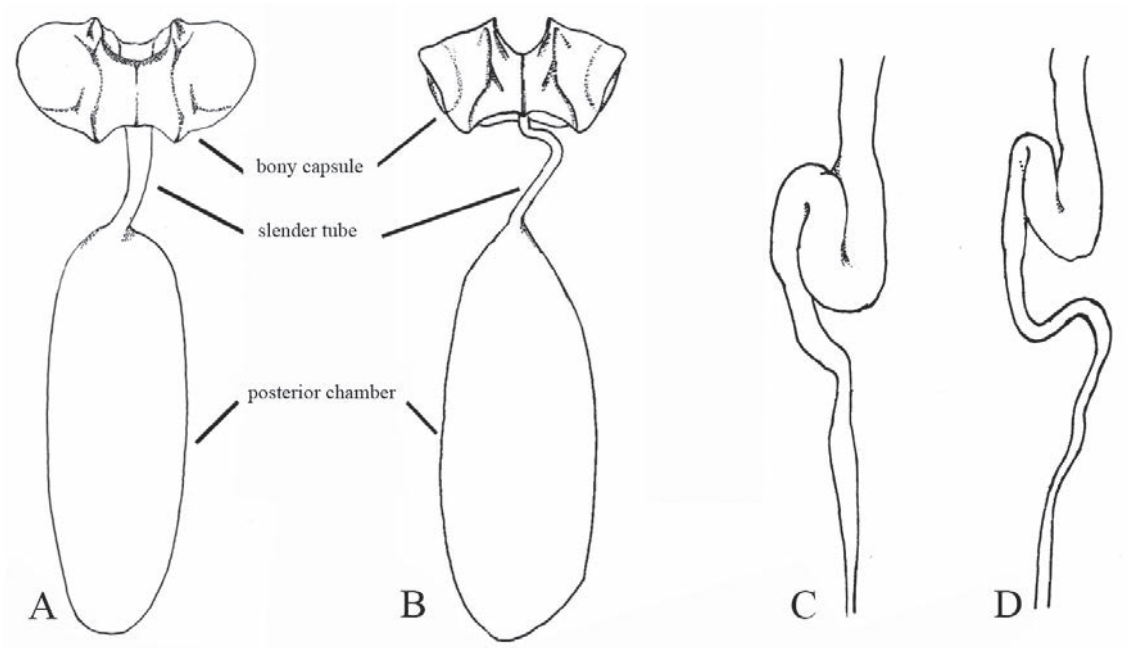

Figure 2. Swim bladder, stomach, and intestine of *Paranemachilus luegvetensis* sp. nov. (**A, C**) and *Paranemachilus liui* sp. nov. (**B, D**).

Table 1. Morphometric characters of *Paranemachilus luegvetensis* sp. nov. and *Paranemachilus liui* sp. nov.

	***Paranemachilus luegvetensis* sp. nov.**		***Paranemachilus liui* sp. nov.**	
	Holotype	**Paratypes (n = 8)**	**Holotype**	**Paratypes (n = 8)**
	NNNU230611	**NNNU230603–10**	**NNNU230710006**	**NNNU230710001–008**
Dorsal fin ray	3, 8	3, 8–9	3, 8	3, 8
Anal fin ray	3, 5	3, 6	3, 5	3, 5
Pectoral fin ray	1, 12	1, 11–12	1, 11	1, 11–13
Pelvic fin ray	1, 6	1, 6–7	1, 7	1, 6–7
Caudal fin ray	2, 17	2, 17–18	2, 17	2, 17
Standard length/mm	41.7	26.1–34.8 (31.6 ± 2.7)	51.4	47.6–61.6 (53.0 ± 4.3)
Body height	8.3	3.7–5.4 (4.7 ± 0.6)	10.0	9.8–12.2 (10.8 ± 1.1)
Maximum body height	9.4	3.8–5.7 (4.9 ± 0.7)	10.4	10.4–14.0 (11.6 ± 0.8)
Body width	6.6	2.2–3.8 (3.2 ± 0.5)	7.0	6.5–8.7 (7.2 ± 0.8)
Maximum body width	7.7	2.6–4.8 (3.8 ± 0.7)	8.7	6.7–9.8 (8.4 ± 1.0)
Body width at anus	4.7	1.3–2.8 (2.0 ± 0.4)	5.2	4.8–6.9 (5.5 ± 0.6)
Predorsal length	22.7	14.0–18.7 (16.9 ± 1.4)	28.9	27.2–33.0 (29.8 ± 1.9)
Dorsal fin length	5.0	3.3–5.9 (4.7 ± 1.0)	5.7	5.5–7.3 (6.2 ± 0.6)
Dorsal fin-base length	5.1	3.1–4.6 (4.0 ± 0.5)	5.9	5.4–7.6 (6.4 ± 0.7)
Prepelvic length	22.7	14.2–19.0 (17.4 ± 1.5)	29.0	26.4–34.8 (29.6 ± 2.4)
Pelvic fin length	5.0	3.6–4.9 (4.2 ± 0.4)	6.1	5.9–8.7 (6.8 ± 0.8)
Pelvic fin base length	1.1	0.6–1.1 (0.9 ± 0.1)	2.0	1.8–2.3 (2.0 ± 0.2)
Preanus length	29.2	17.8–24.6 (22.5 ± 2.1)	36.7	33.9–45.8 (37.4 ± 3.6)
Preanal length	32.2	18.6–26.0(24.0 ± 2.3)	39.2	36.7–48.6 (40.3 ± 3.6)
Anal fin length	5.2	4.3–6.3 (5.5 ± 0.6)	6.5	6.5–9.8 (7.8 ± 1.0)
Anal fin base length	3.1	2.3–2.9 (2.6 ± 0.2)	3.7	3.1–4.6 (3.8 ± 0.4)
Prepectoral length	9.7	7.0–8.6 (7.8 ± 0.6)	12.0	11.3–15.3 (12.4 ± 1.2)
Pectoral fin length	6.4	4.3–5.5 (5.2 ± 0.4)	8.1	7.0–9.8 (8.2 ± 0.9)
Pectoral fin base length	1.5	0.7–1.2 (1.0 ± 0.2)	1.9	1.4–3.0 (1.8 ± 0.5)
Caudal fin length	6.3	5.6–7.8 (6.8 ± 0.6)	9.2	9.1–11.1 (9.9 ± 0.7)
Caudal-peduncle length	5.2	4.5–5.5 (5.0 ± 0.3)	8.2	7.0–9.5 (8.6 ± 0.7)
Caudal-peduncle depth	5.3	2.3–4.0 (3.0 ± 0.6)	6.9	6.9–8.8 (7.8 ± 0.6)
Head length	9.7	7.2–8.7 (8.1 ± 0.6)	12.6	11.7–15.6 (12.9 ± 1.2)
Head height at eye	5.1	2.0–4.1 (3.0 ± 0.6)	5.2	4.5–6.7 (5.7 ± 0.7)
Head height at nape	5.8	3.4–4.4 (4.1 ± 0.3)	6.9	6.9–8.8 (7.5 ± 0.7)
Head width at eye	6.4	3.2–4.8 (4.1 ± 0.5)	8.0	6.1–9.6 (7.4 ± 1.0)
Maximum head width	7.1	3.9–5.7 (5.0 ± 0.5)	9.4	7.3–11.6 (8.9 ± 1.2)
Snout length	2.4	1.8–2.8 (2.3 ± 0.3)	2.7	2.7–4.5 (3.4 ± 0.5)

second unbranched dorsal-fin ray; tip of pelvic fin far from anus. Anal fin with three unbranched and 5–6 branched rays with truncate distal margins; origin halfway between pelvic-fin insertion and caudal-fin base. Caudal fin with 17–18 branched rays; caudal fin forked, upper and lower lobes equivalent.

Cephalic lateral-line canals developed, with 7+18–19 infraorbital canal pores, 15–17 supraorbital canal pores at base of anterior nostrils, 2–4 supratemporal canal pores, and 4–5 preoperculomandibular canal pores. Lateral line incomplete, with 2–6 lateral line pores present before midpoint of pectoral fin, 15–16 inner gill rakers on first gill arch (two specimens).

Stomach "U"-shaped, intestines slightly to back of stomach, curved. Two air-bladder chambers: anterior chamber encased in bony capsule, posterior chamber filling body cavity, and anterior and posterior chambers connected by short, thin, and curved tubes (Fig. 2).

Coloration. Photograph of *Paranemachilus luegvetensis* sp. nov. alive is provided in Fig. 1D. Sides of head and trunk brownish yellow; abaxial surface dark brown; ventral and lateral surfaces of head untextured. Obscure brown longitudinal stripe extending along lateral line to base of caudal fin. Body sides light yellow, except along lateral line; no spots on entire body at capture. Post-feeding, some individuals developed small black spots on side and back above lateral line, with darkened longitudinal stripes on side of body, though basic body color remained unchanged. No spots on fin, fin membrane hyaline. Specimens preserved in 10% formalin appear grayish-white.

Distribution and habitat. The species is known only from a karst cave (108°26'18.4973"N, 23°13'25.0813"E) near Nonghu Tun, Chuanqian Village, Wuming District, Nanning City (Fig. 3). The cave entrance has been artificially enlarged, with the underground river serving as an important source of drinking water and irrigation for local residents. *Paranemachilus luegvetensis* sp. nov. inhabits this silt-based underground river, co-occurring with *Caridina* sp. and *Silurus* sp. The underground river was not swollen at the time of collection, so the specimens were obtained deep within the cave.

Remarks. All collected individuals were initially extremely thin and weak. The holotype, raised in the same tank as other cavefish species for 91 days in an artificial environment. It was fed once every two days and sacrificed on day 91, with prepared specimens showing obvious fat accumulation on its back and sides. The species often migrates from the cave to feed in flooded mountain swales and farmlands during the rainy season, a behavior frequently observed by working locals. In the dry season, the water temperature of the pool is 18–20 °C, and in the rainy season, the temperature of the pool formed outside the outflow of the river can reach 26 °C. Despite its water habitats being contaminated with fertilizers and pesticides, *Paranemachilus luegvetensis* sp. nov. appears to have adapted to these environmental conditions.

Paranemachilus liui Mo, Yang, Li & Du, sp. nov.

https://zoobank.org/62C3991C-CF91-4DF5-B446-029287E5E852

Figs 2B, D, 4, Tables 1, 3

Materials. ***Holotype*.** • NNNU230710006, 51.4 mm standard length, China: Guangxi, Liuzhou County, Youshan Village, 24°15'03.9813"N, 109°25'42.8397"E, collected by H.L. Mo and J.J. Zhou in July 2023.

***Paratypes*.** • NNNU230710001–008, 47.59–61.63 mm standard length; same data as for holotype.

Etymology. The new species is named in honor of Zongyuan Liu, a distinguished official, literary author, and thinker. During his tenure in Liuzhou, Liu significantly promoted the economic and cultural landscape of the region, thereby elevating the quality of life for its residents and earning him deep admiration and respect from the local community. We propose the common Chinese name "柳氏异条鳅" (Liu Shi Yi Tiao Qiu).

Figure 3. Pool or a cave from which *Paranemachilus luegvetensis* sp. nov. type species was collected in Nonghu Tun, Chuanqian Village, Wuming District, Nanning City. Left (15 October 2023), right (10 June 2023).

Diagnosis. Comparative data among *Paranemachilus liui* sp. nov. and all five known species within the genus *Paranemachilus* are provided in Table 3. *Paranemachilus liui* sp. nov. can be distinguished from all other congeneric species of the genus *Paranemachilus* by cheeks scaled (vs. scaleless in *P. chongzuo*, *P. pingguoensis*, and *P. zhengbaoshani*), 11–13 branched pectoral fin rays (vs. 10 in *P. chongzuo*), 7–9 preoperculomandibular canal pores (vs. zero in *P. chongzuo*, 11–12 in *P. pingguoensis* and *P. zhengbaoshani*), preanus length 67.4%–74.3% of standard length (vs. greater than 75.3% in *P. chongzuo*, *P. genilepis*, *P. jinxiensis*, *P. pingguoensis*, and *P. zhengbaoshani*), snout length 21.4%–28.7% of lateral head length (vs. greater than 30.0% in *P. chongzuo*, *P. genilepis*, *P. jinxiensis*, *P. pingguoensis*, and *P. zhengbaoshani*), and 11–15 supraorbital canal pores at base of anterior nostrils (vs. 3 in *P. chongzuo*, 9 in *P. jinxiensis*, and 9–10 in *P. zhengbaoshani* and *P. pingguoensis*).

Description. The morphometric data of the type specimen of *Paranemachilus liui* sp. nov. are given in Table 1. Body elongated, large in size. Maximum body depth occurs before insertion of dorsal fin, body depth 18.7%–23.2% of standard length, head slightly depressed, flattened, maximum head width greater than deepest head depth, head width 49.9%–63.7% head length, snout length 21.4%–28.7% of lateral head length, shorter than postorbital length. Anterior and posterior nostrils adjacent; anterior nostrils tube-like; tip of anterior nostrils with distinct triangular elongation, shorter than half of tube depth. Cheeks scaled, no reduction in eye size, eye diameter 17.3%–21.9% of head length. Mouth inferior, snout obtuse, lips developed and smooth; in most specimens, median of lower lip with V-shaped notch; missing in specimens such as NNNU230710006 (holotype). Three pairs of barbels: inner rostral extending to posterior margin of posterior opercular, outer rostral, and maxillary barbel reaching or exceeding posterior margin of head. Dorsal fin with three unbranched and eight branched rays; distal margin straight; origin closer to caudal-fin base than to tip of snout. Pectoral fin with one unbranched and 11–13 branched rays; pectoral fin length 49.5%–51.8% of pelvic-fin insertion; pelvic fin with one unbranched and 6–7 branched rays, inserted below first or second unbranched dorsal-fin ray; tip of pelvic fin far from anus. Anal fin with three unbranched and five branched rays with truncate distal margins; origin closer to pelvic-fin insertion than to caudal-fin base. Caudal fin with 17 branched rays; caudal fin forked, upper and lower lobes equivalent.

Body completely covered by tiny scales. Cephalic lateral-line canals developed, with 4–6+13–15 infraorbital canal pores, 11–15 supraorbital canal pores at base of anterior nostrils, four supratemporal canal pores, and 7–9 preoperculomandibular canal pores. Lateral line incomplete, with 8–14 lateral line pores present before tip of pectoral fin, 14–16 inner gill rakers on first gill arch (two specimens).

Stomach "U"-shaped, intestines slightly to back of stomach, curved. Two air-bladder chambers: anterior chamber encased in bony capsule, posterior chamber filling body cavity, and anterior and posterior chambers connected by short, thin, and curved tubes (Fig. 2).

Coloration. Photograph of *Paranemachilus liui* sp. nov. specimen in life is provided in Fig. 4D. Dorsal surface dark brown, head and trunk of body yellowish brown, head untextured. Obscure brown longitudinal stripe extending along lateral line to base of caudal fin. Whole body untextured at capture. Post-feeding, some samples developed small black spots on dorsal surface. Fin rays faint yellow, fin membrane hyaline.

Distribution and habitat. Specimens of *Paranemachilus liui* sp. nov. were collected from several caves around Youshan Village, Yifeng District, Liuzhou City, Guangxi Province, China. The type specimen was collected from an underground river in Keyuan Cave (Fig. 5), which sustains a long, narrow, perennially water-filled pool. Near the cave entrance, some water sections are exposed to sunlight, with an average water temperature ranging from 20 to 23 °C. In the same location, we also collected *Yunnanilus bailianensis*, *Typhlocaridina semityphlata*, and an unidentified catfish species. Notably, the vicinity of Keyuan Cave is heavily utilized for farmlands and duck farms, resulting in a significant population from fertilizers and feed in the water where the specimens were found. Despite this, *Paranemachilus liui* sp. nov. appears to have adapted to these environmental conditions.

Phylogenetic analysis. The BI phylogenetic tree (Fig. 6) revealed that the *Paranemachilus* species formed a monophyletic group, sister to the genus *Troglonectes*. *Paranemachilus luegvetensis* sp. nov. and *Paranemachilus liui* sp. nov. formed a well-supported monophyletic group (bootstrap support = 98 and Bayesian posterior probability = 1) with other *Paranemachilus* species, including the type species *P. genilepis*. All samples from Wumin District, Nanning City, Guangxi Zhuang Autonomous Region clustered together in a sister clade to (*P. genilepis* + *Paranemachilus liui* sp. nov.). All samples from Yüfeng District, Liuzhou City, and Guangxi Zhuang Autonomous Region clustered together in a sister clade to *P. genilepis*. The tree topologies are similar to those reported in previous studies [2, 13], with highly consistent and strong support of the monophyly of the genus *Paranemachilus*. Analysis also indicated that the genus could be divided into two major clades, i.e., cheek-scaled group and cheek-scaleless group. The cheek-scaled group contained *P. genilepis*, *P. jinxiensis*, *Paranemachilus liui* sp. nov. and *Paranemachilus luegvetensis* sp. nov., while the cheek-scaleless group contained *P. chongzuo*, *P. pingguoensis*, and *P. zhengbaoshani*.

Mitochondrial differentiation. Comparative analysis of the cytb gene revealed that the two new species could be distinguished from all known *Paranemachilus* species based on distinct molecular differences. The minimum p-distances were 7.92% between *Paranemachilus luegvetensis* sp. nov. and *Paranemachilus liui* sp. nov. and 6.16% between *Paranemachilus liui* sp. nov. and *P. genilepis* (Table 2).

Table 2. Uncorrected pairwise distances among *Paranemachilus* species based on cytb gene.

		1	2	3	4	5	6	7	8	9
1	*Paranemachilus genilepis*									
2	*Paranemachilus jinxiensis*	6.98%								
3	*Paranemachilus pingguoensis*	7.26%	6.70%							
4	NNNU20230710001Liuzhou	6.21%	7.69%	7.10%						
5	NNNU20230710002Liuzhou	6.16%	7.92%	7.04%	0.29%					
6	NNNU20230710003Liuzhou	6.73%	8.19%	7.31%	0.30%	0.88%				
7	Paranemachilus *zhengbaoshani*	9.22%	8.38%	3.63%	7.69%	7.62%	7.89%			
8	NNNU230601.Wuming	9.22%	10.06%	8.94%	8.58%	8.50%	8.77%	8.94%		
9	NNNU230602.Wuming	8.66%	9.50%	8.38%	7.99%	7.92%	8.19%	8.94%	0.56%	
10	*Paranemachilus chongzuo*	6.98%	6.42%	1.40%	6.21%	6.16%	6.43%	3.35%	8.66%	8.10%

Table 3. Comparison of identifying characteristics between the two new species and its congeners of the genus *Paranemachilus*.

	Cheek scales	Pectoral-fin rays	body depth of standard length (%)	Preoperculomandibular canal pores	Supraorbital canal pores
Paranemachilus luegvetensis sp. nov.	Present	i, 11–12	13.5–16.8	4–5	15–17
Paranemachilus liui sp. nov.	Present	i, 11–13	18.7–23.2	7–9	11–15
P. jinxiensis	Present	i, 13–14	21.7–25.6	10–11	9
P. genilepis	Present	i, 11–13	17.8–21.0	10	11–12
P. chongzuo	Absent	i, 10	16.6–17.6	Absent	3
P. zhengbaoshani	Absent	i, 11–12	17.0–20.1	11–12	9–10
P. pingguoensis	Absent	i, 12–13	18.2–21.2	11–12	9–10
	Preanus length of standard length (%)		**Snout length of head length (%)**		**Reference**
Paranemachilus luegvetensis sp. nov.	68.3–73.9		24.5–32.1		This study
Paranemachilus liui sp. nov.	67.4–74.3		21.4–28.7		This study
P. jinxiensis	/		37–41.7		This study
P. genilepis	76–78.5		30–33.5		This study
P. chongzuo	76.7–78		32.5–37		This study
P. zhengbaoshani	75.3–75.8		33–34.6		This study
P. pingguoensis	75.5–78.2		29.1–36.7		This study

Identification Key to Species of *Paranemachilus*

1 Cheeks scaled 2
– Cheeks scaleless 5
2 Body depth 13.5%–16.8% of standard length ..... *Paranemachilus luegvetensis* sp. nov.
– Body depth exceeds 17.8% of standard length 3
3 Snout length 21.4%–28.7% of lateral head length ..... *Paranemachilus liui* sp. nov.
– Snout length exceeds 30.0% of lateral head length 4
4 Caudal peduncle length 88.1%–97.7%, 18 inner gill rakers on first gill arch ..... *P. genilepis*
– Caudal peduncle length 100.0%–130.0%, 14 inner gill rakers on first gill arch ..... *P. jinxiensis*
5 Preoperculomandibular canal pores absent ..... *P. chongzuo*
– Preoperculomandibular canal pores present 6
6 Processus dentiformis on upper lip ..... *P. zhengbaoshani*
– No processus dentiformis on upper lip ..... *P. pingguoensis*

Discussion

The genus *Paranemachilus* can be diagnosed by the following combination of characteristics: anterior nostrils tube-like, tip of anterior nostrils with weak barbel-like elongation, barbel length shorter than half of tube depth, anterior and posterior nostrils adjacent, lips without papillae, lateral line incomplete, disappearing behind vertical at the end of the pectoral fin, and anterior part of the air-bladder lying free in the abdominal cavity (Zhu 1983; Zhu and Cao 1987; Lan et al. 2013; Du et al. 2023). These two new species were assigned to the genus *Paranemachilus* based on the following additional characters: body completely covered by tiny scales, lateral line incomplete,

Figure 4. A–C. dorsal, lateral, and ventral views of *Paranemachilus liui* sp. nov. NNNU230710006, holotype, 51.39 mm standard length. **D** *Paranemachilus liui* sp. nov. NNNU230710006, holotype, live, photo taken on 11 June 2023. Scale bar: 1 cm.

present before the mid-point of the pectoral fin, mouth inferior, snout obtuse, lips developed and smooth, median of lower lip with V-shaped notch, anterior and posterior nostrils adjacent, anterior nostrils tube-like, tip of anterior nostrils with triangular-like elongation, shorter than half of the depth of the nostril tube, stomach "U"-shaped, intestines slightly to the back of the stomach, curved, two air-bladder chambers: anterior chamber encased in a bony capsule, posterior chamber filling the body cavity, and anterior and posterior chamber connected by a slender tube.

The genus *Paranemachilus* Zhu, 1983, was established with *P. genilepis* as the type species (Zhu, 1983), while *Heminoemacheilus* Zhu & Cao, 1987, was established with *H. zhengbaoshani* Zhu & Cao, 1987, as the type species (Zhu and Cao 1987). *Heminoemacheilus zhengbaoshani* differs from *P. genilepis* by having scaleless cheeks (vs. scaled) and an absent postcleithrum (vs. present). *Yunnanilus jinxiensis* Zhu, Du, Chen & Yang, 2009 and *H. zhengbaoshani* were later reclassified as *P. jinxiensis* and *P. zhengbaoshani* in *Paranemachilus* (Du et al. 2021; Luo et al. 2023), with *P. jinxiensis* having scaled cheeks (Du et al. 2023). Similarly, the two new species, *Paranemachilus luegvetensis* sp. nov. and *Paranemachilus liui* sp. nov., also feature scales on their cheeks. Both *P. pingguoensis* and *P. chongzuo* were placed in *Paranemachilus* based on shared characteristics, notably anterior and posterior nostrils adjacent, anterior nostrils tube-like, lateral line incomplete, disappearing behind the vertical at the end of

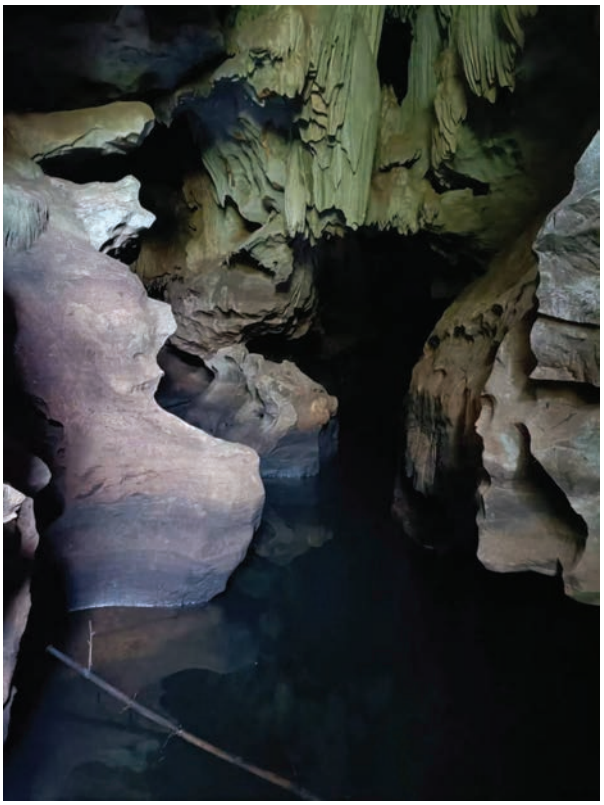

Figure 5. Pool and a cave from which type *Paranemachilus luegvetensis* sp. nov. was collected in Youshan Village, Yufeng District, Liuzhou County.

the pectoral fin, and anterior part of the air-bladder lying free in the abdominal cavity (Zhu 1983; Zhu and Cao 1987; Lan et al. 2013; Du et al. 2023). These classifications are supported by morphological and molecular evidence (Luo et al. 2023). The BI phylogenetic tree constructed during this study (Fig. 6) revealed that *Paranemachilus luegvetensis* sp. nov. and *Paranemachilus liui* sp. nov. clustered together in a sister clade to (*P. genilepis* + *P. jinxiensis*), while *P. pingguoensis*, *P. zhengbaoshani*, and *P. chongzuo* clustered together in another sister clade. These findings suggest that *Paranemachilus* could be divided into two species groups: the cheek-scaled group, including *P. genilepis*, *P. jinxiensis*, *Paranemachilus luegvetensis* sp. nov., and *Paranemachilus liui* sp. nov., and the cheek-scaleless group, including *P. chongzuo*, *P. pingguoensis*, and *P. zhengbaoshani*. However, apart from cheek scales, no additional distinguishing traits have been identified between the two groups. In this study, the phylogenetic tree was constructed based solely on the cytb gene, as only this gene was analyzed. The genus *Heminoemacheilus* is characterized by the absence of a postcleithrum (Zhu and Cao 1987), a feature that has not yet been examined in *P. jinxiensis* and the two new species. Thus, further research is necessary to determine the validity of the *Heminoemacheilus* genus. In this work, we do not consider *Heminoemacheilus* valid; the group with scaleless cheeks was still regarded as *Paranemachilus* when making the identification key.

Freshwater fish continues to be undervalued and overlooked—and thousands of species are heading towards extinction. Due to their exclusive confinement to cave ecosystems, cavefish are highly vulnerable to threats such as habitat degradation, hydrological changes, environmental pollution, resource overexploitation, and non-native species introduction (Lan et al. 2013; Ma, Zhao & Yang, 2019). As noted in Ma et al. (2019), cavefish typically possess morphological adaptations to the extreme conditions of cave environments, such as eye degeneration or loss, reduced pigmentation, and diminished scales.

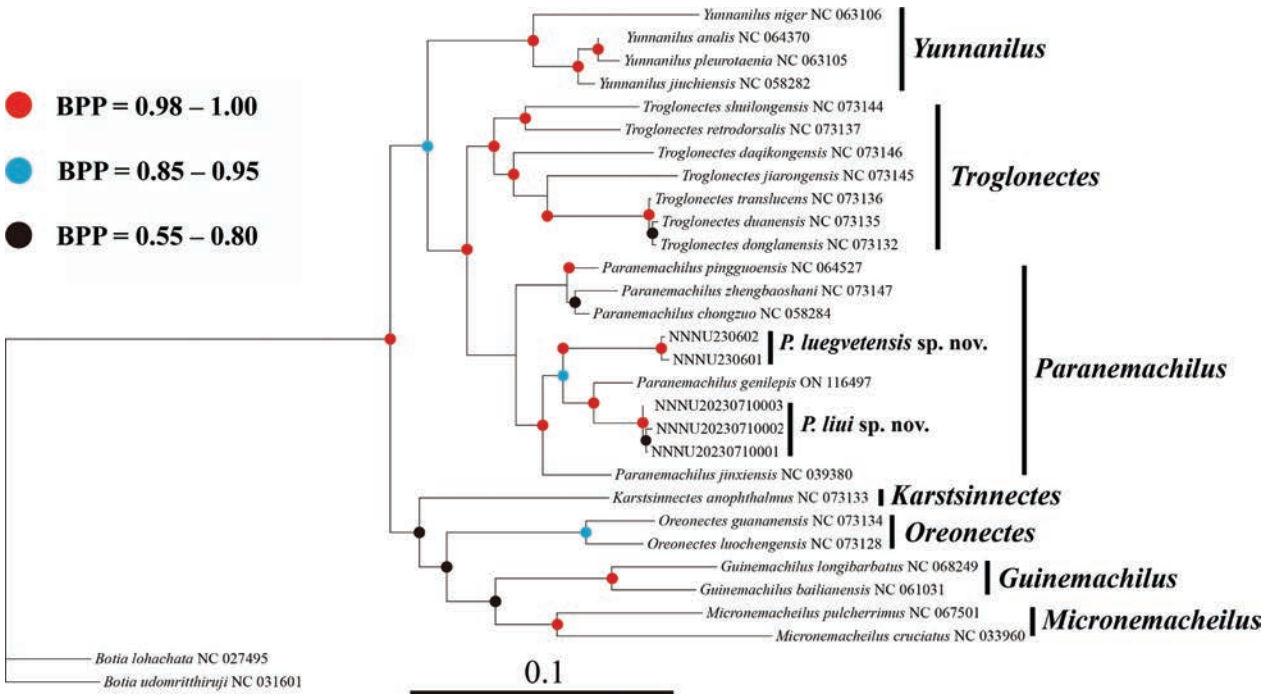

Figure 6. Bayesian phylogeny of cytb lineages of species within the family Nemacheilidae. *Botia* genus was used as an outgroup. Numbers on internode branches are Bayesian posterior probabilities.

These unique features endow cavefish with a distinctive exotic appearance, which often attracts the attention of fish collectors. In contrast, *Paranemachilus liui* sp. nov. and *Paranemachilus luegvetensis* sp. nov. do not exhibit these distinctive phenotypes but demonstrate remarkable adaptability. For instance, *Paranemachilus liui* sp. nov. annually migrates to a cave pond that floods during the rainy season for breeding purposes, despite the pond often being heavily polluted by effluent from nearby sugar factories and duck farms. Furthermore, the cave inhabited by *Paranemachilus luegvetensis* sp. nov. serves as the sole water source for irrigation in the area, subject to unregulated exploitation and intrusion by non-cave species like *Metzia* sp. and *Labeo rohita* due to human activities. Nevertheless, no decline in the populations of the two newly described species has been observed. Notably, the currently known species of *Paranemachilus* found are distributed in scattered areas in western and central Guangxi (Fig. 7), with recorded sites being relatively distant from each other. In Guangxi, where karst landforms are well-developed and underground rivers suitable for *Paranemachilus* survival are widely distributed, it is plausible that additional habitats for this genus exist. This suggests the likely presence of more undescribed *Paranemachilus* species in the region. In our view, the diversity of *Paranemachilus* species in Guangxi may be underestimated, warranting comprehensive and systematic exploration.

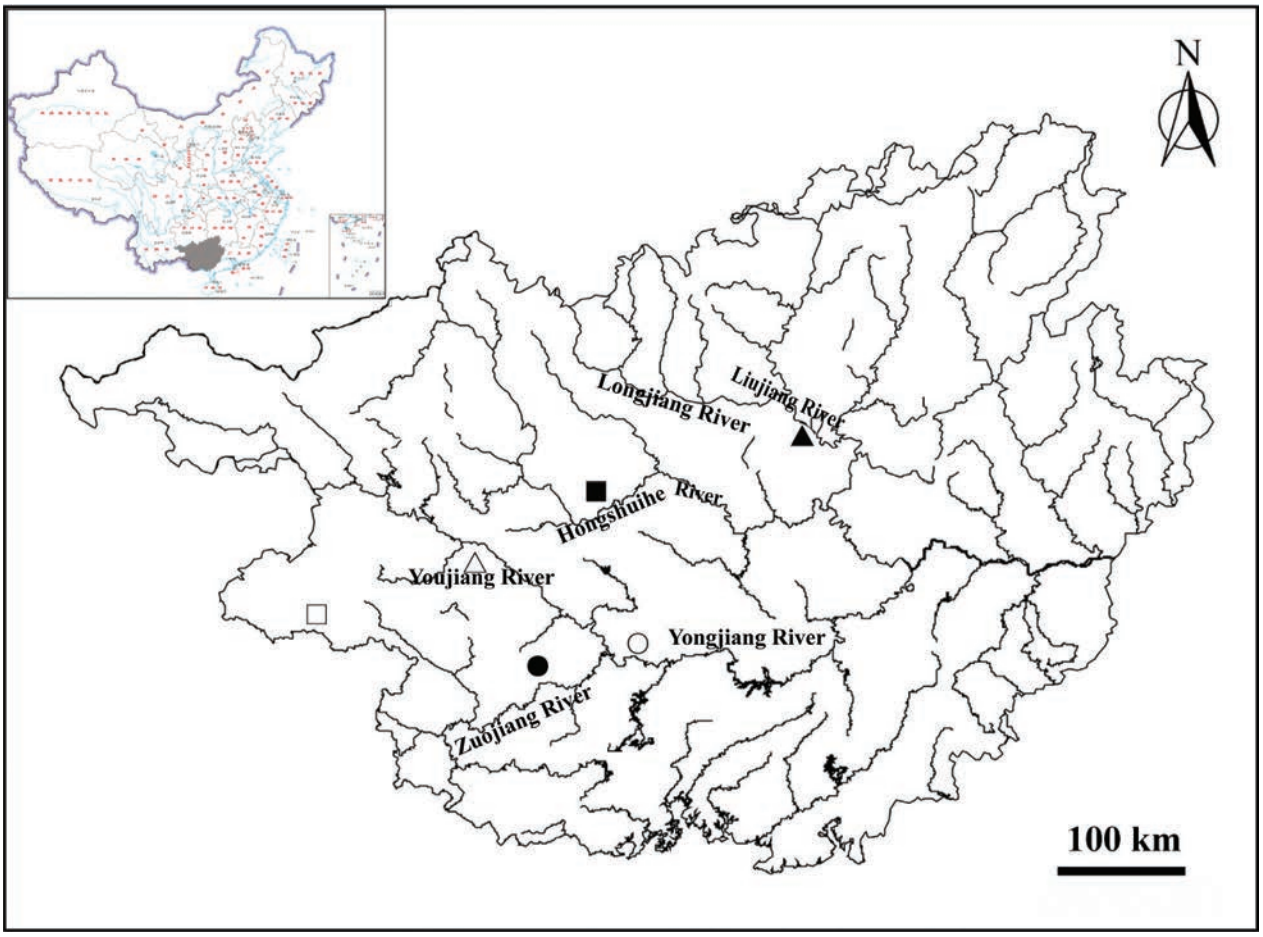

Figure 7. Map showing distribution of *Paranemachilus* species in Guangxi Zhuang Autonomous Region. *P. zhengbaoshani* (black square), *P. jinxiensis* (white square), *P. genilepis* (black dott), *Paranemachilus luegvetensis* sp. nov. (white dott), *Paranemachilus liui* sp. nov. (black triangle), and *P. pingguoensis* (white triangle).

Acknowledgments

We are grateful to J.H. Zhong and D.D. Huang from Nanning Normal University and J.J. Zhou from the Zhejiang Forest Resource Monitoring Center for their help in specimen collection. We are also grateful to Y.J. Wei from the Agricultural Bank of China, Ltd., Liuzhou Branch, for providing part of the funds to support our field research, and C. Watts for English corrections and suggestions. This work was supported by the Project of Financial Funds of the Ministry of Agriculture and Rural Affairs: Investigation of Fishery Resources and Habitat in the Pearl River Basin, Innovation and Entrepreneurship Training Program for College Students (202427060300203), and Guangxi Natural Science Foundation Project (2022GXNSFAA035563).

References

Du LN, Yang J, Min R, Chen XY, Yang JX (2021) A review of the Cypriniform tribe Yunnanilini Prokofiev, 2010 from China, with an emphasis on five genera based on morphologies and complete mitochondrial genomes of some species. Zoological Research 42: 310–334. https://doi.org/10.24272/j.issn.2095-8137.2020.229

Du LN, Li SJ, Xu F, Luo T, Luo FG, Yu GH, Zhou J (2023) Clarification of Phylogenetic Relationships among Chinese Nemacheilids with Tube–Shaped Anterior Nostrils, with a Description of a New Genus and Two New Species. Journal of Zoological Systematics and Evolutionary Research 2023: 3600085. https://doi.org/10.1155/2023/3600085

Edgar RC (2004) MUSCLE: multiple sequence alignment with high accuracy and high throughput. Nucleic Acids Research 32: 1792–1797. https://doi.org/10.1093/nar/gkh340

Kottelat M (1990) Indochinese nemacheilines: A revision of nemacheiline loaches (Pisces, Cypriniformes) of Thailand, Burma, Laos, Cambodia and southern VietNam. Verlag Dr. Friedrich Pfeil, München, 262 pp.

Lan JH, Gan X, Wu TJ, Yang J (2013) Cave Fishes of Guangxi, China; Science Press: Beijing, China, 266 pp.

Li DY, Gao BG (2016) Collection and Preparation of Biological Specimens. Chemical Industry Press, Beijing, 178 pp.

Luo T, Yang Q, Wu Li, Wang YL, Zhou JJ, Deng HQ, Xiao N, Zhou J (2023) Phylogenetic relationships of Nemacheilidae cavefish (Heminoemacheilus, Oreonectes, Yunnanilus, Paranemachilus, and Troglonectes) revealed by analysis of mitochondrial genome and seven nuclear genes. Zoological Research 44: 693–697. https://doi.org/10.24272/j.issn.2095-8137.2022.266

Ma L, Zhao YH, Yang JX (2019) Chapter 28 - Cavefish of China. In: White WB, Culver DC, Pipan T (Eds) Encyclopedia of Caves. 3rd edn. Waltham: Academic Press, 237–254. https://doi.org/10.1016/B978-0-12-814124-3.00027-3

Miller MA, Pfeiffer W, Schwartz T (2010) Creating the CIPRES Science Gateway for inference of large phylogenetic trees. In 2010 Gateway Computing Environments Workshop (GCE), 8 pp., New Orleans, LA, USA, November 2010. https://doi.org/10.1109/GCE.2010.5676129

Tamura K, Stecher G, Kumar S (2021) MEGA 11: Molecular Evolutionary Genetics Analysis Version 11. Molecular Biology and Evolution 38: 3022–3027. https://doi.org/10.1093/molbev/msab120

Tang L, Zhao YH, Zhang CG (2012) A new blind loach, *Oreonectes elongatus* sp. nov. (Cypriniformes, Balitoridae) from Guangxi, China. Environmental Biology of Fishes 93(4): 483–449. https://doi.org/10.1007/s10641-011-9943-7

Xiao WH, Zhang YP, Liu HZ (2001) Molecular systematics of Xenocyprinae (Teleostei, Cyprinidae): taxonomy, biogeography, and coevolution of a special group restricted in East Asia. Molecular Phylogenetics and Evolution 18: 163–173. https://doi.org/10.1006/mpev.2000.0879

Zhu SQ (1983) A new genus and species of Nemachilinae (Pisces, Cobitidae) from China. Acta Zootaxonomica Sina 12: 311–313.

Zhu SQ, Cao WX (1987) The Noemacheiline fishes form Guangdong and Guangxi with descriptions of a new genus and three new species. Acta Zootaxonomica Sina 12: 323–331.

Zhu Y, Du LN, Chen XY, Yang JX (2009) A new nemacheiline loach of genus *Yunnanilus* (Balitoridae) from Guangxi, China—*Yunnanilus jinxiensis*. Zoological Research 30: 195–198. https://doi.org/10.3724/SP.J.1141.2009.02195

Zoosyst. Evol. 100 (4) 2024, 1387–1400 | DOI 10.3897/zse.100.118522

PENSOFT

für Natur MUSEUM FÜR NATURKUNDE BERLIN

The ornate rubbernose pleco (Siluriformes, Loricariidae, *Chaetostoma*), a new species from the Ucayali River Basin, Peru

Vanessa Meza-Vargas[1,2], Jorge L. Ramirez[1,2], Nathan K. Lujan[3,4]

1 *Departamento de Ictiología, Museo de Historia Natural, Universidad Nacional Mayor de San Marcos, Avenida Arenales 1256, Jesus Maria, Lima 14, Peru*

2 *Departamento de Biología Celular y Genética, Facultad de Ciencias Biológicas, Universidad Nacional Mayor de San Marcos, Avenida Germán Amézaga 375, Cercado De Lima, Lima, Peru*

3 *Department of Natural History, Royal Ontario Museum, 100 Queens Park, Toronto, ON M5S 2C6, Canada*

4 *Ecology and Evolutionary Biology Department, University of Toronto, 25 Willcocks St, Toronto, ON M5S 3B2, Canada*

https://zoobank.org/9D3FFC51-0277-4669-B215-23DA5A1D5483

Corresponding author: Vanessa Meza-Vargas (meza.sv@gmail.com)

Academic editor: Nicolas Hubert ♦ **Received** 11 January 2024 ♦ **Accepted** 14 August 2024 ♦ **Published** 18 October 2024

Abstract

A new species in the rubbernose catfish genus *Chaetostoma* is described from the Aguaytia, Pisqui and Palcazu Rivers, which drain the Pampa de Sacramento Region in the Ucayali River drainage of central Peru. The new species is distinguished from congeners, except *C. anomalum*, *C. branickii*, *C. dorsale*, *C. leucomelas*, *C. microps*, *C. nudirostre*, *C. palmeri* and *C. thomsoni* by having distinct, white, variably-shaped spots or vermiculations ½–2× nostril diameter on dark grey to black background on the head (vs. spots absent or black on light-coloured background). The new species is distinguished from *C. anomalum*, *C. branickii*, *C. dorsale*, *C. microps*, *C. nudirostre* and *C. thomsoni* by having highly variable, distinct white spots, vermiculations or bands ½–10× nostril diameter on the body, from *C. leucomelas* by having dorsal and caudal fin indistinctly and variably-patterned with zero to four bands (vs. dorsal and caudal fin consistently having five or more uniform bands) and from *C. palmeri* by having two predorsal plates (vs. three), supraoccipital excrescence present (vs. absent) and pelvic-fin insertion slightly posterior to dorsal-fin insertion (vs. pelvic-fin insertion at middle of dorsal-fin base). Species delimitation analyses of the COI and Cytb genes further support the recognition of this new species.

Key Words

Amazon, Andes, Chaetostoma clade, freshwater, molecular, Neotropical, taxonomy

Introduction

With over 1060 currently valid species, 19% of which (200) were described in the last decade, the suckermouth armoured catfish family Loricariidae is the fifth largest vertebrate family and one of the fastest growing (Fricke et al. 2024). Of the four vertebrate families that are more species-rich (Characidae, Cichlidae, Cyprinidae and Gobiidae), none is growing as quickly or is as geographically restricted as Loricariidae, which naturally occurs only in fresh or estuarine waters from southern Costa Rica to northern Argentina. Within Loricariidae, the rubbernose catfish genus *Chaetostoma* Tschudi 1846 is the third most species-rich genus with 49 valid species (Meza-Vargas et al. 2022), being superseded only by *Hypostomus* (> 150 valid species) and *Ancistrus* (76 valid species) (de Queiroz et al. 2020; Neuhaus et al. 2023). *Chaetostoma* is also the most geographically restricted of these species-rich genera, with 46 species being restricted to flanks of the Andes and Caribbean Coastal mountains from Panama to southern Peru and three species (*C. jegui*, *C. orientale* and *C. vasquezi*) occurring in rivers draining the Guiana or Brazilian shields (Meza-Vargas et al. 2022).

All but one species of *Chaetostoma* (*C. platyrhynchus*) are externally distinguished from most other loricariid genera by having the anterior and anterolateral snout

margins free of plates, with this region instead being covered by a broad band of naked (i.e. unplated) skin, lacking tentacles. Five other loricariid genera also have unplated snout margins (*Ancistrus* Kner, 1854, *Corumbataia* (Britski, 1997), *Paulasquama* Armbruster & Taphorn, 2011, *Soromonichthys* Lujan & Armbruster, 2011 and *Transancistrus* Lujan, Meza-Vargas & Barriga-Salazar, 2015), but only *Ancistrus* and *Transancistrus* are sympatric with *Chaetostoma*. *Chaetostoma* can be easily distinguished from *Ancistrus* by lacking snout tentacles (vs. tentacles present), having at least five longitudinal series of plates at the shallowest part of the caudal peduncle (vs. three) and having eight or more branched dorsal-fin rays (vs. seven). The only *Chaetostoma* with a fully-plated snout (*C. platyrhynchus*) is restricted to the upper Caqueta and Napo drainages of Colombia and Ecuador, respectively; it shares all other traits above with congeners.

Chaetostoma has never undergone a comprehensive species-level taxonomic revision, though Lujan et al. (2015b) reviewed species from the centre of the genus's geographic range in and around Ecuador and provided a multi-locus molecular phylogenetic hypothesis spanning many species and the entire geographic range of the genus. This analysis was recently enlarged and updated by Meza-Vargas et al. (2022). Both studies used combinations of up to 18 external morphological traits including colouration, meristics and morphometrics to distinguish amongst 13 species from rivers draining east of the Andes (cis-Andean), making taxonomy of the cis-Andean distribution of *Chaetostoma* the most well-studied (Salcedo 2006a, 2006b; Salcedo and Ortega 2015; Ballen et al. 2016). Within this distribution, the Huallaga River in central Peru is the epicentre of species diversity, with seven species currently recognised: *C. changae*, *C. daidalmatos*, *C. lexa*, *C. marmorescens*, *C. stroumpoulos*, *C. taczanowskii*, and *C. trimaculineum*. In the much larger Ucayali River drainage, which borders the Huallaga to the east and south, only two species are currently known: *C. lineopunctatum* and *C. loborhynchos*. In this paper, we describe a new, third species for the Ucayali River drainage. Seidel (2011) first reported this species as undescribed in the ornamental aquarium fish literature, simultaneously highlighting the species' considerable colour pattern variation by assigning it three different L-numbers (L455, L456, L457). L-numbers are codes used by the ornamental aquarium fish industry to differentiate amongst and market distinct, often scientifically undescribed colour morphs (Stawikowski 1988).

In scientific literature, the species was first recognised as new by Lujan et al. (2015a), who referred to it as '*Chaetostoma* n.sp. Ucayali' and included it in a multi-locus molecular phylogenetic analysis. This analysis found the new species to be part of a polytomy containing *C. breve*, *C. dermorhynchus*, *C. dorsale*, *C. formosae*, *C. orientale* (then *Chaetostoma* n.sp. Xingu), *C. trimaculineum* and an undescribed species from the Orinoco River Basin. In a re-analysis and expansion of the Lujan et al. (2015c) dataset, Meza-Vargas et al. (2022) found the new species to be sister to *Chaetostoma breve* Regan, 1904, a species whose nomenclature we revisit in light of these phylogenetic results and a large series of more recently collected topotype material for *Chaetostoma branickii* Steindachner, 1881.

Material and methods

Taxon sampling

This study is based mostly on 12 formalin-fixed, 70% ethanol-preserved, museum-catalogued specimens of the undescribed species collected from the Aguaytia River and the Raya and Omaiz Rivers in the Palcazu River drainage (Fig. 1) in August and September 2022 and on 313 specimens of *Chaetostoma branickii* collected in the Marañon River drainage in August 2018 (collection permit: Nº 00680-2022-PRODUCE/DGPCHDI). Specimens were euthanised prior to preservation by overdose of eugenol (clove oil) until ventilation stopped for at least 30 minutes in adherence with an institutional animal use protocol approved by Auburn University (protocol 2018–3354; Lucena et al. (2013)). Institutional codes follow Sabaj (2020).

Gene amplification and sequencing

Genetic samples of fin or muscle tissue were dissected prior to specimen fixation and individually linked to source specimens using unique, matching alphanumeric tags on voucher specimens and cryosafe tubes, then preserved in 95% ethanol. Whole genomic DNA was extracted from tissue subsamples using a salt precipitation protocol (Alijanabi and Martinez 1997). DNA sequence data were obtained for two mitochondrial markers: Cytochrome C oxidase I (COI) and Cytochrome b (CytB). A 658-base region of COI was amplified using the primers ANOSCOIF and ANOSCOIR (Ramirez and Galetti 2015) and a 1150-base region of the mitochondrial CytB gene was amplified using the primers and protocol of Lujan et al. (2015a). Amplified gene regions were sequenced on an ABI 3730 capillary sequencer at the Royal Ontario Museum (Toronto, Canada) or sent for sequencing at Macrogen Inc. (Seoul, South Korea).

Molecular analyses

Sequences for each gene were automatically aligned using Clustal W (Larkin et al. 2007) then manually edited and checked to ensure the absence of internal stop codons. *De novo* CytB sequences were compared with existing data for the *Chaetostoma* Clade from Lujan et al. (2015b) and additional COI sequences were obtained from BOLD (Table 1). Both gene datasets were used to run three species delimitation methods: the General Mixed Yule Co-

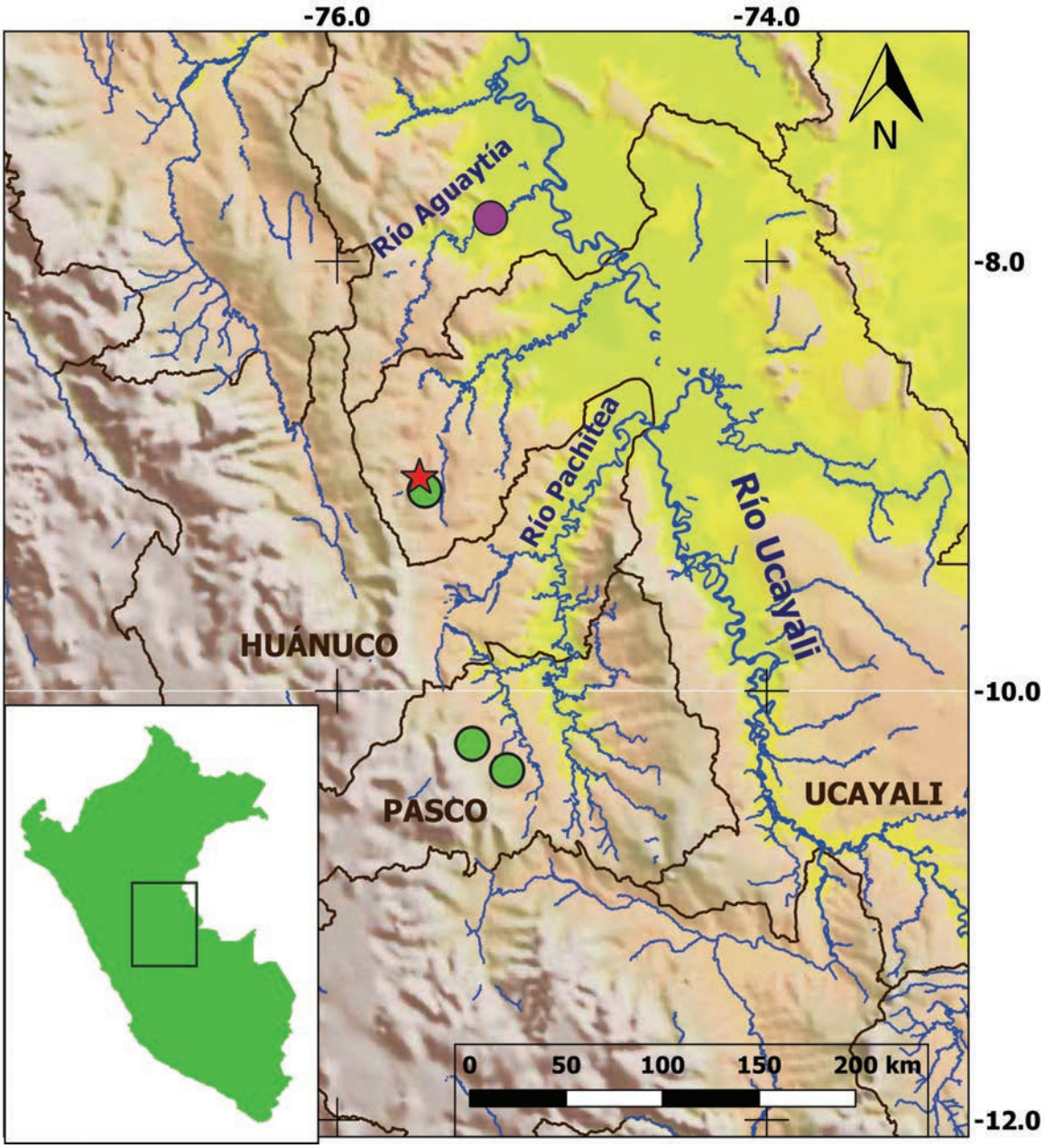

Figure 1. Distribution of *Chaetostoma sacramento* type specimen sample sites along the Pampa del Sacramento in Andean left-bank tributaries of the Ucayali River Basin. Holotype (red star), green dots (paratypes), purple dots (aquarist trade).

alescent model (GMYC) with a single threshold (Pons et al. 2006), the Bayesian implementation of the PTP model (bPTP) (Zhang et al. 2013) and the Assemble Species by Automating Partitioning (ASAP) method (Puillandre et al. 2021). As input for the first two methods, an ultrametric tree was built using BEAST v.2.7.4 (Bouckaert et al. 2014) with a GTR+I molecular evolution model for COI and an HKY+I+G model for CytB, a fast log-normal relaxed clock and a birth-death tree model. The analyses were run for 100 million Markov Chain Monte Carlo (MCMC) generations with the first 10% discarded as burn-in. Convergence of MCMC chains within a stable range and effective sample sizes (ESS) greater than 200 were confirmed in Tracer v.1.6 (Rambaut et al. 2014). The pipeline SPdel (Ramirez et al. 2023) was used to compute and compare all delimitation methods.

Morphological analysis

Morphometric landmarks follow Armbruster (2003) with lateral trunk plate row terminology following Schaefer (1997) and cheek odontode type following Lujan et al. (2015b). Standard length (SL) is expressed in mm and other measurements are expressed as percentages of either standard length or, for subunits of the head, head length. Measurements and counts were taken on the left side of specimens when possible.

Table 1. Tissue samples used in the molecular species delimitation analyses, including GenBank accession number (coI = Cytochrome oxidase subunit I, cytb = cytochrome b), voucher specimen catalogue number, country and drainages of origin. Bold accession numbers = new sequences for this study.

Taxa	Tissues Number	cytb	col	Catalogue Number	Country	Drainage
Chaetostoma anale	T24822	OL303592	–	ROM 107267	Colombia	Orteguasa
Chaetostoma anale	T24946	OL303593	OK514631	ROM 107837	Colombia	Orteguasa
Chaetostoma anale	T24906	OL303604	OK514628	ROM 107811	Colombia	Caqueta
Chaetostoma anale	T24907	OL303605	OK514629	ROM 107811	Colombia	Caqueta
Chaetostoma anomalum	T631	OL303608	–	INHS 55455	Venezuela	Maracaibo
Chaetostoma bifurcum	T13602	KP960196	–	ROM 93687	Ecuador	Esmeraldas
Chaetostoma bifurcum	T13603	OL303609	–	ROM 93687	Ecuador	Esmeraldas
Chaetostoma bifurcum	T13665	OL303610	–	ROM 93721	Ecuador	Guayas
Chaetostoma bifurcum	T13896	OL303611	–	ROM 93787	Ecuador	Santa Rosa
Chaetostoma bifurcum	T13897	OL303612	–	ROM 93787	Ecuador	Santa Rosa
Chaetostoma breve	P6292	KP960190	–	AUM 46515	Peru	Marañon
Chaetostoma breve	PE08208	OL303613	–	MHNG 2712.047	Peru	Huallaga
Chaetostoma breve	PE08213	OL303614	–	MHNG 2712.048	Peru	Huallaga
Chaetostoma breve	PE08648	OL303615	–	MHNG 2712.074	Peru	Huallaga
Chaetostoma breve	PE08673	OL303616	–	MHNG 2712.078	Peru	Huallaga
Chaetostoma breve	P6294	OL303617	–	AUM 46516	Peru	Marañon
Chaetostoma breve	T14360	OL303618	–	ROM 93950	Ecuador	Napo S
Chaetostoma breve	T19715	OL303619	–	ROM 100323	Ecuador	Napo N
Chaetostoma breve	T19716	OL303620	–	ROM 100320	Ecuador	Napo N
Chaetostoma breve	T14224	OL303621	–	ROM 93923	Ecuador	Pastaza
Chaetostoma breve	T14005	OL303622	–	ROM 93848	Ecuador	Santiago
Chaetostoma brevilabiatum	6630	OL303623	–	ANSP 189597	Colombia	Honda
Chaetostoma brevilabiatum	6631	OL303624	–	ANSP 189597	Colombia	Honda
Chaetostoma cf. *anale*	T19707	OL303594	–	ROM 100322	Ecuador	Napo
Chaetostoma cf. *anale*	T19708	OL303595	OK514634	ROM 100322	Ecuador	Napo
Chaetostoma cf. *anale*	T19606	OL303628	OK514632	ROM 100250	Ecuador	Napo
Chaetostoma cf. *anale*	T19647	OL303629	–	ROM 100263	Ecuador	Napo
Chaetostoma cf. *fischeri*	T9034	KP960197	–	STRI 11581	Panama	Tuira
Chaetostoma cf. *lineopunctatum*	CH153	OL303630	–	MUSM 44253	Peru	Huallaga
Chaetostoma cf. *lineopunctatum*	PE08318	OL303631	–	MHNG 2712.057	Peru	Huallaga
Chaetostoma cf. *lineopunctatum*	PE08545	OL303632	–	MHNG 2712.069	Peru	Huallaga
Chaetostoma cf. *loborhynchus*	CH200	OL303633	–	MUSM 44899	Peru	Huallaga
Chaetostoma cf. *loborhynchus*	CH202	OL303634	–	MUSM 44899	Peru	Huallaga
Chaetostoma cf. *loborhynchus*	CH2023	OL303635	–	MUSM 44899	Peru	Huallaga
Chaetostoma cf. *loborhynchus*	CH204	OL303636	–	MUSM 44899	Peru	Huallaga
Chaetostoma changae	PE08442	OL303637	–	MHNG 2712.064	Peru	Huallaga
Chaetostoma changae	PE08543	OL303638	–	MHNG 2712.067	Peru	Huallaga
Chaetostoma chimu	TICT-FCA-07	–	FBCH009-21	–	Colombia	Meta
Chaetostoma chimu	TICT-FCA-223	–	FBCH118-21	–	Colombia	Meta
Chaetostoma chimu	TICT-FCA-148	–	FBCH143-21	–	Colombia	Meta
Chaetostoma daidalmatos	CH140	OL303639	–	MUSM 44845	Peru	Huallaga
Chaetostoma daidalmatos	CH141	OL303640	–	MUSM 44845	Peru	Huallaga
Chaetostoma daidalmatos	PE08191	OL303641	–	MHNG 2712.045	Peru	Huallaga
Chaetostoma daidalmatos	PE08207	OL303642	–	MHNG 2712.051	Peru	Huallaga
Chaetostoma daidalmatos	PE08347	OL303644	–	MHNG 2712.055	Peru	Huallaga
Chaetostoma dermorhynchus	T14258	KP960191	–	ROM 93656	Ecuador	Pastaza
Chaetostoma dermorhynchus	T14287	OL303647	–	ROM 93656	Ecuador	Pastaza
Chaetostoma dermorhynchus	T14293	OL303648	–	ROM 93946	Ecuador	Bobonaza
Chaetostoma dermorhynchus	T14296	OL303649	–	ROM 93946	Ecuador	Bobonaza
Chaetostoma dermorhynchus	T14308	OL303650	–	ROM 93946	Ecuador	Bobonaza
Chaetostoma dorsale	TICT-FCA-08	–	FBCH008-21	–	Colombia	Meta
Chaetostoma dorsale	TICT-FCA-168	–	FBCH078-21	–	Colombia	Meta
Chaetostoma dorsale	TICT-FCA-185	–	FBCH086-21	–	Colombia	Meta
Chaetostoma dorsale	TICT-FCA-244	–	FBCH091-21	–	Colombia	Meta
Chaetostoma fischeri	T9026	KP960195	–	STRI 7604	Panama	Chagres
Chaetostoma fischeri	T9027	OL303651	–	STRI 905	Panama	Bayano

Taxa	Tissues Number	cytb	col	Catalogue Number	Country	Drainage
Chaetostoma fischeri	T9036	OL303652	–	STRI 12274	Panama	Bayano
Chaetostoma fischeri	T9037	OL303653	–	STRI	Panama	Chagres
Chaetostoma fischeri	STRI-01740	–	BSFFA489-07	–	Panama	Tuira
Chaetostoma fischeri	STRI-01732	–	BSFFA490-07	–	Panama	Acla
Chaetostoma fischeri	STRI-01735	–	BSFFA491-07	–	Panama	Bayano
Chaetostoma fischeri	STRI-01754	–	BSFFA492-07	–	Panama	Tuira
Chaetostoma fischeri	STRI-01760	–	BSFFA493-07	–	Panama	Bayano
Chaetostoma fischeri	STRI-07104	–	BSFFA735-07	–	Panama	Chagres
Chaetostoma formosae	T17431	OL303654	–	ROM 95260	Colombia	Meta
Chaetostoma formosae	TICT-FCA-64	–	FBCH052-21	–	Colombia	Meta
Chaetostoma guairense	VZ122	OL303655	–	INHS 34786	Venezuela	Limon
Chaetostoma jegui	Tec63785	OL303596	OK514635	LBP 15478	Brazil	Branco
Chaetostoma jegui	Tec63786	OL303597	OK514636	LBP 15478	Brazil	Branco
Chaetostoma joropo	T17428	OL303656	–	ROM 95259	Colombia	Meta
Chaetostoma joropo	T17429	OL303657	–	ROM 95259	Colombia	Meta
Chaetostoma joropo	TICT-FCA-208	–	FBCH134-21	–	Colombia	Meta
Chaetostoma joropo	TICT-FCA-224	–	FBCH136-21	–	Colombia	Meta
Chaetostoma joropo	TICT-FCA-245	–	FBCH137-21	–	Colombia	Meta
Chaetostoma leucomelas	–	–	CIUA550-20	–	Colombia	Cauca
Chaetostoma leucomelas	–	–	CIUA557-20	–	Colombia	Cauca
Chaetostoma leucomelas	CIUA-7439	–	UDEA074-18	–	Colombia	Cauca
Chaetostoma leucomelas	CIUA-7441	–	UDEA075-18	–	Colombia	Cauca
Chaetostoma leucomelas	CIUA-7482	–	UDEA076-18	–	Colombia	Magdalena
Chaetostoma leucomelas	CIUA-7491	–	UDEA077-18	–	Colombia	Magdalena
Chaetostoma lineopunctatum	P4772	GU569899	EU359409	ANSP 180446	Peru	Urubamba
Chaetostoma lineopunctatum	P4814	GU569913	EU359410	ANSP 180448	Peru	Madre de Dios
Chaetostoma lineopunctatum	PE08047	KP960199	–	MHNG 2712.041	Peru	Ucayali
Chaetostoma lineopunctatum	T10088	OL303658	–	AUM 51166	Peru	Madre de Dios
Chaetostoma lineopunctatum	T10089	OL303659	–	AUM 51166	Peru	Madre de Dios
Chaetostoma loborhynchos	TK70561	KJ947862	–	MUSM 20291	Peru	Tulumayo
Chaetostoma loborhynchos	TK70563	KJ947864	–	MUSM 20291	Peru	Tulumayo
Chaetostoma loborhynchos	TK70579	KJ947865	–	MUSM 20307	Peru	Paucartambo
Chaetostoma loborhynchos	TK70580	KJ947866	–	MUSM 20307	Peru	Paucartambo
Chaetostoma loborhynchos	TK70581	KJ947867	–	MUSM 20307	Peru	Paucartambo
Chaetostoma marmorescens	CH198	KP960194	–	MUSM 44898	Peru	Huallaga
Chaetostoma marmorescens	CH197	OL303660	–	MUSM 44898	Peru	Huallaga
Chaetostoma marmorescens	CH199	OL303661	–	MUSM 44898	Peru	Huallaga
Chaetostoma microps	T14125	KP960189	–	ROM 93895	Ecuador	Santiago
Chaetostoma microps	CH121	OL303662	–	MUSM 44313	Peru	Huallaga
Chaetostoma microps	CH149	OL303665	–	MUSM 44869	Peru	Huallaga
Chaetostoma microps	CH150	OL303666	–	MUSM 44869	Peru	Huallaga
Chaetostoma microps	PE08190	OL303667	–	MHNG 2712.046	Peru	Huallaga
Chaetostoma microps	PE08580	OL303668	–	MHNG 2712.07	Peru	Huallaga
Chaetostoma microps	P6034	OL303669	–	AUM 45518	Peru	Marañon
Chaetostoma microps	T14364	OL303670	–	ROM 93949	Ecuador	Napo S
Chaetostoma microps	MEPN1255	OL303671	–	MEPN 1255	Ecuador	Napo S cave
Chaetostoma microps	MEPN1259	OL303672	–	MEPN 19165	Ecuador	Napo S cave
Chaetostoma microps	ROM 93902	OL303673	–	ROM 93902	Ecuador	Santiago
Chaetostoma microps	T14096	OL303674	–	ROM 93877	Ecuador	Yungantza
Chaetostoma microps	T14097	OL303675	–	ROM 93877	Ecuador	Yungantza
Chaetostoma milesi	JAM1984	OL303677	–	MPUJ	Colombia	Suaza
Chaetostoma milesi	CIUA-8907	–	UDEA079-18	–	Colombia	Magdalena
Chaetostoma milesi	T24605	OL303676	–	ROM 106963	Colombia	Suaza
Chaetostoma milesi	–	–	CIUA680-20	–	Colombia	Magdalena
Chaetostoma nudirostre	T2084	OL303682	–	ANSP 191471	Venezuela	Valencia
Chaetostoma orientale	B1464	OL303679	OK514638	ANSP 199686	Brazil	Xingu
Chaetostoma orientale	B1472	OL303680	OK514639	ANSP 199686	Brazil	Xingu
Chaetostoma orientale	B1487	OL303681	OK514640	ANSP 199686	Brazil	Xingu
Chaetostoma orientale	2606	–	OK514647	INPA-ICT 58146	Brazil	Xingu
Chaetostoma sacramento sp. nov.	PE08121	OL303678	–	MHNG 2712.042	Peru	Ucayali

Taxa	Tissues Number	cytb	col	Catalogue Number	Country	Drainage
Chaetostoma sacramento sp. nov.	LGBBF358	OR875871	OR859576	MUSM 72046	Peru	Ucayali
Chaetostoma sacramento sp. nov.	LGBBF359	OR875872	OR859577	MUSM 72046	Peru	Ucayali
Chaetostoma sacramento sp. nov.	MUSMT1564	–	OR859578	MUSM 71392	Peru	Ucayali
Chaetostoma sacramento sp. nov.	MUSMT1566	–	OR859579	MUSM 71392	Peru	Ucayali
Chaetostoma sp. Apure	T08954	OL303683	–	AUM 54034	Venezuela	Apure
Chaetostoma sp. Apure	T08955	OL303684	–	AUM 54034	Venezuela	Apure
Chaetostoma sp. Apure	T491	OL303685	–	AUM 41073	Venezuela	Apure
Chaetostoma sp. Apure	T621	OL303686	–	INHS 56147	Venezuela	Apure
Chaetostoma sp. CuruaUna	525	OL303599	OK514641	MCP 53005	Brazil	Curua-Una
Chaetostoma sp. L445	T12930	KP960193	–	ROM 94925	Colombia	Meta
Chaetostoma sp. L445	T17424	OL303687	–	ROM 95257	Colombia	Meta
Chaetostoma sp. L445	T17425	OL303688	–	ROM 95257	Colombia	Meta
Chaetostoma sp. Meta	–	–	CIUA698-20	–	Colombia	Cauca
Chaetostoma sp. Meta	–	–	CIUA707-20	–	Colombia	Cauca
Chaetostoma stroumpoulos	CH120	OL303689	–	MUSM 44303	Peru	Huallaga
Chaetostoma stroumpoulos	CH142	OL303691	–	MUSM 44847	Peru	Huallaga
Chaetostoma stroumpoulos	PE08210	OL303693	–	MHNG 2712.049	Peru	Huallaga
Chaetostoma thomsoni	JAM1966	OL303695	–	ICNMHN 17768	Colombia	Chucuri
Chaetostoma thomsoni	–	–	CIUA541-20	–	Colombia	Cauca
Chaetostoma thomsoni	–	–	CIUA542-20	–	Colombia	Cauca
Chaetostoma thomsoni	–	–	CIUA543-20	–	Colombia	Cauca
Chaetostoma thomsoni	–	–	CIUA544-20	–	Colombia	Cauca
Chaetostoma thomsoni	–	–	CIUA545-20	–	Colombia	Cauca
Chaetostoma thomsoni	–	–	CIUA546-20	–	Colombia	Cauca
Chaetostoma thomsoni	–	–	CIUA547-20	–	Colombia	Cauca
Chaetostoma thomsoni	–	–	CIUA553-20	–	Colombia	Cauca
Chaetostoma thomsoni	–	–	CIUA554-20	–	Colombia	Magdalena
Chaetostoma thomsoni	–	–	CIUA559-20	–	Colombia	Cauca
Chaetostoma thomsoni	–	–	CIUA560-20	–	Colombia	Cauca
Chaetostoma thomsoni	–	–	CIUA563-20	–	Colombia	Cauca
Chaetostoma thomsoni	–	–	CIUA565-20	–	Colombia	Cauca
Chaetostoma thomsoni	–	–	CIUA566-20	–	Colombia	Magdalena
Chaetostoma thomsoni	–	–	CIUA570-20	–	Colombia	Cauca
Chaetostoma thomsoni	–	–	CIUA572-20	–	Colombia	Cauca
Chaetostoma thomsoni	–	–	CIUA574-20	–	Colombia	Cauca
Chaetostoma thomsoni	–	–	CIUA576-20	–	Colombia	Cauca
Chaetostoma thomsoni	–	–	CIUA579-20	–	Colombia	Cauca
Chaetostoma thomsoni	–	–	CIUA580-20	–	Colombia	Cauca
Chaetostoma thomsoni	–	–	UDEA080-18	–	Colombia	Cauca
Chaetostoma thomsoni	–	–	UDEA083-18	–	Colombia	Cauca
Chaetostoma thomsoni	–	–	UDEA085-18	–	Colombia	Cauca
Chaetostoma trimaculineum	P6047	OL303696	–	AUM 45524	Peru	Marañon
Chaetostoma trimaculineum	T14136	OL303697	–	ROM 93894	Ecuador	Santiago
Chaetostoma vasquezi	T09945	KP960192	–	AUM 53812	Venezuela	Caura
Chaetostoma vasquezi	V27	OL303698	OK514643	AUM 36555	Venezuela	Caroni
Chaetostoma vasquezi	V28	OL303699	OK514644	AUM 36555	Venezuela	Caroni

Results

Taxonomic accounts

Chaetostoma sacramento sp. nov.

https://zoobank.org/5B9D5C88-4581-4EE0-A529-DABC39FFB914

Fig. 2, Tables 2, 3

Chaetostoma sp. nov. Ucayali: Lujan et al. (2015b) [molecular phylogeny].

Type material. ***Holotype*** • Adult MUSM 72045; 65.1 mm SL; Peru, Ucayali Department, Padre Abad Province, Boqueron District, Shambillo, Amazon Basin, Ucayali River, unnamed left-bank tributary of Aguaytia River; 09°0'29.88"S, 75°37'1.92"W; alt. 365 m; 07 Aug 2022; D. Faustino, J. Chuctaya, C. Nolasco, O. Quispe.

***Paratype*:** All Peru, Amazon – Ucayali River Basin • MHNG 2712.042, 1; 32.2 mm SL; tissues PE08-122, 123, 124; Padre Abad Province, Aguaytia River at mouth of the Boca Yurac River; 11 September 2008; S. Fisch- Muller, R. Covain, P. de Rham, H. Ortega, J. Figuerosa Minaya, J. Sanchez Ramirez • MUSM 71392, 4; 50.5–79.4 mm SL; Pasco Department, Oxapampa Province, Palcazu District, Raya River; 10°22'13.61"S, 75°7'52.90"W;

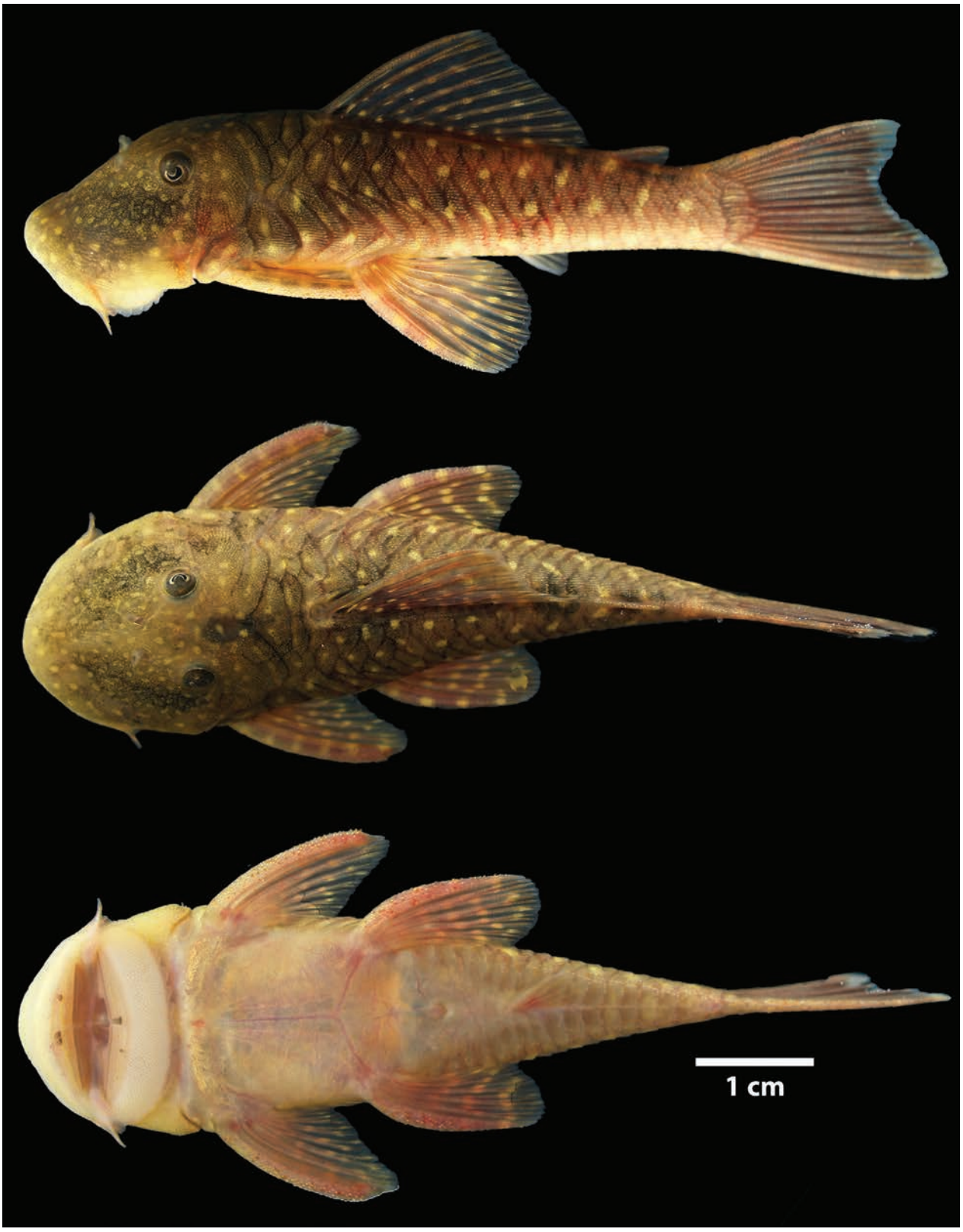

Figure 2. Live holotype of *Chaetostoma sacramento* MUSM 72045, 65.1 cm, collected from the Yamino River, a tributary of the Aguaytía River. Photos by D. Faustino.

7 September 2022; R. Olivera, R. Quispe, J. Arana, M. Paniagua • MUSM 72046, 34; 44.2–12.5 mm SL; Ucayali Department, Padre Abad Province, Padre Abad District, Aguaytia River; 9°4'8.58"S, 75°30'51.48"W; 8 August 2022; D. Faustino, J. Chuctaya, C. Nolasco, R. Quispe • ANSP 182805, 3; 57.8–70.5 mm SL; same data as MUSM 71392 • ROM 114668, 4; 54.3–76.7 mm SL; same data as MUSM 71392.

Genseq-2 COI. GenBank accession number. Obtained from paratypes MUSM 72046 (OR859576 and OR859577) and MUSM 71392 (OR859578 and OR859579).

Genseq-2 CytB. GenBank accession number. Obtained from paratypes MUSM 72046 (OR875871 and OR875872).

Diagnosis. *Chaetostoma sacramento* can be diagnosed from all congeners, except *C. anomalum*, *C. branickii*, *C. dorsale*, *C. leucomelas*, *C. microps*, *C. nudirostre*, *C. palmeri* and *C. thomsoni* by having distinct, white, variably-shaped spots or vermiculations ½–2× nostril diameter on grey to brown background on the head (vs. spots absent or black on light-coloured background). *Chaetostoma sacramento* is distinguished from *C. anomalum*, *C. branickii*, *C. dorsale*, *C. nudirostre* and *C. thomsonii* by having highly variable, small to large distinct white spots, vermiculations or bands on the body (vs. spots, vermiculations or bands absent or black on light-coloured background), from *C. anomalum* by having adipose fin fully formed (vs. rudimentary), from *C. dorsale* by having uniformly brown adipose fin (vs. adipose fin with black spot), from *C. leucomelas* by having golden spots across the dorsal fin rays (vs. light bands), from *C. microps* by having eight branched dorsal-fin rays (vs. nine), from *C. nudirostre* by having curved cheek odontodes (vs. strait), from *C. palmeri* by having two predorsal plates (vs. three), excrescence present (vs. absent) and pelvic-fin insertion slightly posterior of dorsal-fin insertion (vs. pelvic-fin insertion at middle of dorsal-fin base).

Description. Morphometric data in Table 2 and meristic data in Table 3. Snout moderately depressed, dorsal profile of head convex from snout tip to dorsal-fin origin, then straight and gradually descending to adipose fin. Caudal peduncle dorsal profile slightly concave. Ventral profile straight from snout to caudal fin. Body depressed, deepest at dorsal-fin origin, shallowest at caudal peduncle; greatest width at pectoral girdle. Caudal peduncle slightly compressed, roundly triangular in cross-section.

Head wide, anteriorly rounded in dorsal view; snout anterior margin unplated, lacking odontodes and tentacles. Orbit small (5.2–6.6% HL), dorsolaterally positioned, posterior margin aligned with vertical through anterior margin of cleithrum; skull roof flat. Oral disc wide, elliptical, occupying most of head width, lower lip ending just anterior to origin of opercular opening. Oval papillae covering upper lip, roundish papillae covering lower lip; all papillae smaller towards outer lip margins; lower lip margin crenulate. Buccal cavity with digitate papillae present posterior to premaxillary symphysis, one large patch of rugose papillae dorsomedial to each dentary tooth row. Maxillary barbel short (2.5–4.4% HL). Premaxillary tooth row straight, joining contralateral tooth row at 160º angle. Dentary straight, joining contralateral tooth row at 170º angle. Teeth small, villiform, asymmetrically bicuspid. Opercle external border having row of six straight odontodes, odontodes slightly larger than elsewhere on body. Three to five type 3 hypertrophied hook-like evertible cheek odontodes (mode 5), odontodes hooked anteriorly, not reaching cleithrum. Supraoccipital excrescence restricted to vestigial longitudinal unplated patch, keel absent.

Table 2. Morphometrics of *Chaetostoma sacramento*. Morphometric values as percentages of standard length (SL) or head length (HL). H = holotype, SD = standard deviation, (n = 11).

	H	Min	Max	Mean	SD
Standard length (mm)	65.13	50.49	76.74	63.7	–
Percent of standard length					
Head length	33.9	34.6	37.6	36.0	1.0
Predorsal length	43.4	41.9	47.3	45.1	1.5
Head-dorsal length	9.8	8.7	11.1	9.9	0.7
Cleithral width	33.6	29.3	33.4	32.0	1.2
Cleithral widest distance	37.1	34.8	36.5	35.7	0.5
Head-pectoral length	31.2	30.1	34.3	31.8	1.3
Thorax length	21.7	19.2	23.9	21.3	1.2
Pectoral-spine length	36.3	26.2	29.1	28.1	0.9
Abdominal length	25.4	23.0	25.5	24.5	0.7
Pelvic-spine length	25.7	24.8	28.5	26.4	1.0
Postanal length	30.2	29.1	34.8	32.0	1.4
Anal-fin spine length	15.0	8.7	10.4	9.8	0.5
Dorsal-pectoral distance	27.9	28.5	31.0	29.8	0.7
Dorsal spine length	26.7	25.5	29.4	27.8	1.0
Dorsal-pelvic distance	24.0	21.5	24.1	23.1	0.7
Dorsal-fin base length	28.7	25.0	26.4	25.5	0.4
Dorsal-fin base length	26.2	22.8	26.3	23.8	0.9
Dorsal-adipose distance	16.1	13.2	15.6	14.4	0.8
Adipose-spine length	8.2	7.7	9.4	8.2	0.5
Adipose-up. caudal distance	12.2	12.2	17.4	15.1	1.6
Caudal peduncle depth	15.2	12.4	13.9	13.1	0.6
Adipose-low. caudal distance	21.3	21.2	24.8	23.3	1.2
Adipose-anal distance	20.9	18.6	22.4	20.7	1.0
Dorsal-anal distance	17.1	15.6	17.0	16.3	0.5
Pelvic-dorsal distance	28.9	26.9	29.7	27.9	0.9
Percent of head length					
Head-eye length	29.7	10.0	11.1	10.6	0.3
Orbit diameter	14.0	5.2	6.6	5.9	0.4
Snout length	71.4	22.7	24.9	23.6	0.7
Internares width	14.5	4.6	5.7	5.2	0.4
Interorbital width	45.0	13.8	16.1	15.1	0.7
Head depth	71.9	24.7	26.3	25.6	0.5
Head width	95.6	33.3	35.6	34.5	0.9
Mouth length	60.3	21.1	23.5	22.2	0.8
Mouth width	81.3	29.5	33.2	30.9	1.0
Barbel length	12.3	2.5	4.4	3.6	0.6
Dentary tooth cup length	32.0	11.5	13.4	12.3	0.7
Premaxillary tooth cup length	27.1	10.4	11.6	11.0	0.3
Occipital length	54.1	17.9	20.0	19.1	0.8
Caudal peduncle length	24.3	24.5	28.2	26.8	1.3
Opercle length	9.7	3.3	5.0	4.0	0.5
Interbranchial distance	25.9	24.2	26.3	24.9	0.7

Table 3. Meristics of *Chaetostoma sacramento*. H = holotype, SD = standard deviation, (n = 11).

Count	H	Min	Max	Mode	SD
Median plates	24	22	24	23	0.5
Supramedian plates	23	22	24	24	0.7
Inframedian plates	24	24	25	24	0.5
Caudal plates rows	5	5	5	5	0.0
Dorsal-fin branched rays	8	8	8	8	0.0
Pectoral-fin branched rays	6	6	6	6	0.0
Pelvic-fin branched rays	5	5	5	5	0.0
Anal-fin branched rays	4	4	4	4	0.0
Caudal–fin branched rays	14	13	14	14	0.3
Dorsal procurrent caudal–fin rays	4	4	4	4	0.0
Ventral procurrent caudal–fin rays	4	2	4	3	0.6
Dorsal fin base plates	7	7	7	7	0.0
Preadipose plates	6	5	5	5	0.0
Adipose-caudal plates	5	6	6	6	0.0
Infraorbital plates	6	6	6	6	0.0
Left dentary teeth	186	82	214	104	40.3
Left premaxillary teeth	115	63	137	86	19.4
Cheek odontodes	4	3	5	5	0.6

Flanks covered by five longitudinal plate series. Plates absent from abdomen and around dorsal-fin base. Body plates flat or gently curved, lacking keel or ridge. Dorsal-fin base bordered laterally by seven dorsal plates. Medial interdorsal plates five. Dorsal plate series with 20 plates, supramedian with 24, median series with 23, mid-ventral series with 24, ventral series with 19.

Dorsal fin II,8; locking mechanism functional, spinelet *V*-shape, dorsal-fin origin slightly anterior to pelvic-fin origin, last dorsal-fin ray not reaching adipose fin when adpressed. Pectoral-fin rays I,6; pectoral-fin spine reaching first third of pelvic fin when adpressed. Pelvic-fin rays i,5; unbranched rays surpassing anal-fin origin; dorsal skin folds present on proximalmost two-thirds of unbranched pelvic-fin rays. Pectoral-fin spine with thicker odontodes irregularly distributed along entire dorsal, anterior and ventral surface of spine; one aligned row of larger odontodes along posterodorsal margin. Odontodes present on all, but posteriormost branched pectoral- and pelvic-fin rays. Anal-fin rays ii,4, first unbranched ray almost as long as second. Second branched anal-fin ray longest, with remaining rays successively shorter. Caudal fin obliquely forked, lower lobe longer than upper; i,7+7,i. Dorsal procurrent caudal-fin rays four, ventral two to four.

Colour in alcohol. Head and body base colour brown dorsally, yellowish-white ventrally. Head with dense small white dots. In some specimens, scattered white spots on the body may be fused. Supraoccipital excrescence black or grey. Dorsal fin with white scattered spots on brownish base composed of melanophores distributed on rays and membrane. Remaining fins with brownish base composed of scattered melanophores. Tip of unbranched dorsal- and caudal-fin rays whitish in some individuals.

Sexual dimorphism. Males with fleshy dorsal fold on the pelvic-fin leading ray. Males have more distinct, intense and contrasting white patterns on darker brown to black base colour. Females with duller colour patterns on lighter brown to black base colour.

Distribution. *Chaetostoma sacramento* is known exclusively from the Pampa de Sacramento valley east of the eastern cordillera of the Andes in Peru, inhabiting the Negro River, a tributary of the Pisqui River in Loreto Department; the Yamino River, a tributary of the Aguaytia River**;** the Chui River, a tributary of upper San Alejandro River in Ucayali Department; and the Raya River, a left-bank tributary of Iscozacin River in Pasco Department (Fig. 1).

Etymology. The species epithet *sacramento* refers to the plain (pampa) in central Peru between the Huallaga and Ucayali Rivers, approximately delimited by the Pisqui River in the north and Palcazu River in the south. *Chaetostoma sacramento* is currently known exclusively from this region, known as the Pampa de Sacramento, which occupies a valley between Huánuco and Ucayali provinces that is part of the Peruvian subandean belt and surrounds Boqueron del Padre Abad in the Cordillera Azul. The Pampa de Sacramento was first encountered by Europeans on 21 June 1726, by an expedition led by Don Juan Nunez Lobo and was christened Pampa del Sacramento to commemorate the Catholic ceremony of the Corpus Christi. Subsequent Franciscan missionaries highlighted the rich ethnic diversity of this region (IBC 2016). A noun in apposition.

Molecular species delimitation

With 626 total bases and 72 sequences from 12 nominal species, the COI dataset yielded 158 parsimony informative sites (25%). The ASAP species delimitation analysis yielded 20 Molecular Operational Taxonomic units (MOTUs) (score = 2.5), whereas GMYC and bPTP yielded 23 and 22 MOTUs, respectively. These results can be summarised with 22 consensus MOTUs (Fig. 3).

With 1048 total bases and 108 sequences from 24 nominal species, the CytB dataset yielded 355 parsimony informative sites (34%). ASAP (score = 8.0), GMYC and bPTP species delimitation analyses yielded 46, 45, 49 MOTUs, respectively, for a total of 46 consensus MOTUs (Fig. 3).

In all species delimitation analyses of both genes, *Chaetostoma sacramento* was identified as an MOTU distinct from all other examined *Chaetostoma* species. The minimum genetic distance to the nearest species was 6.15% for CytB, with *C. branickii* being the closest species. For COI, the closest species was *C. leucomelas*, with a genetic distance of 4.48%.

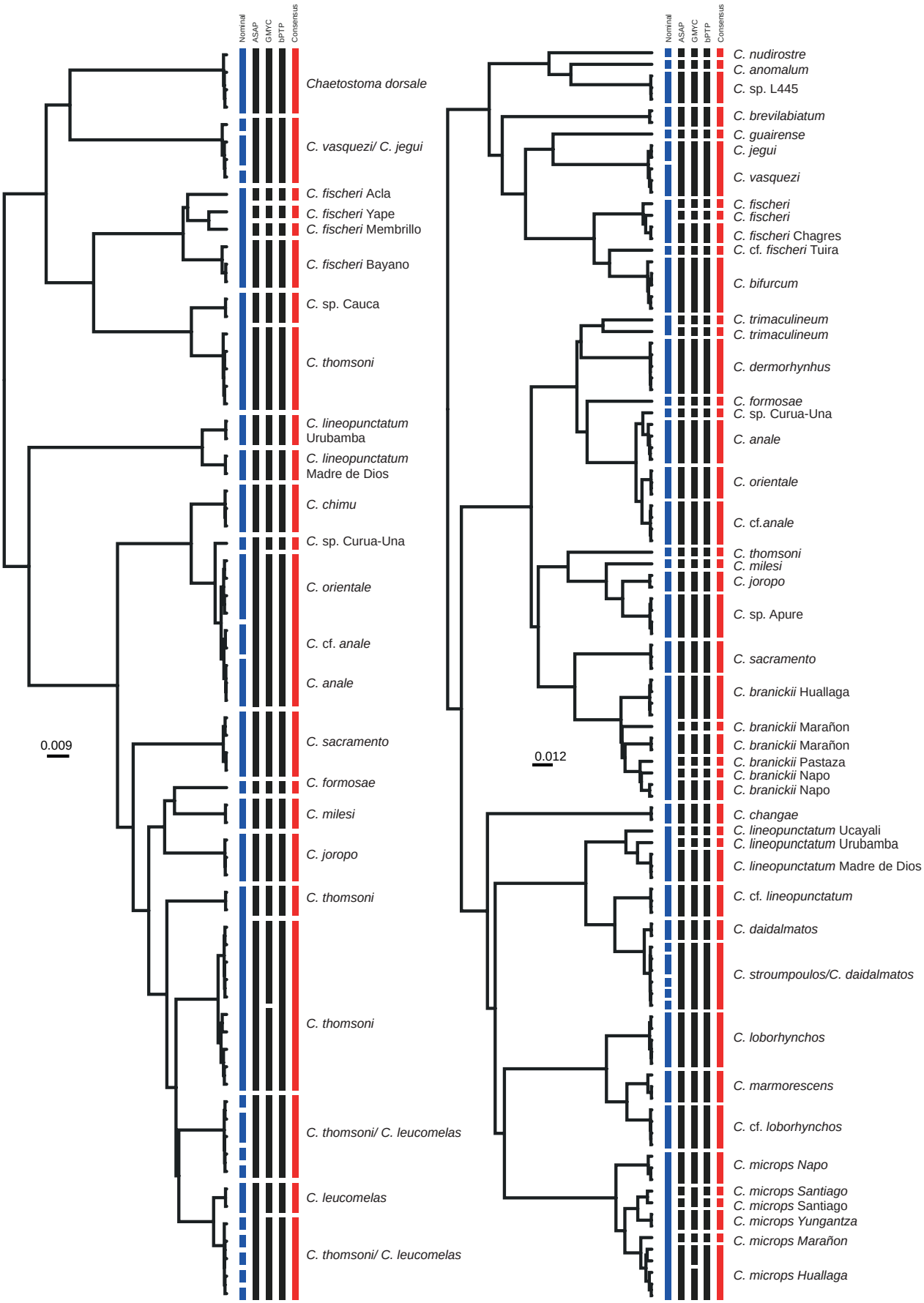

Figure 3. Results of species delimitation analyses, based on COI (left) and CytB (right) gene regions.

Chaetostoma branickii Steindachner 1881

Figs 4, 5

Chaetostoma breve Regan 1904 [synonym]

Diagnosis and description. As for *Chaetostoma breve* in Lujan et al. (2015a).

Comments. Regan (1904) based the description of *Chaetostoma breve* on specimens from the Zamora River in south-eastern Ecuador. Lujan et al. (2015a) re-described *Chaetostoma breve* based on specimens from throughout most of the species' range, from the Napo River in the north (although the species is also now known from more northern Caqueta River headwaters in Colombia; ROM 107831, 107845) to the Marañon River in the south. Lujan et al. (2015a) also generated a multi-locus molecular phylogenetic hypothesis spanning over 24 valid and undescribed species, with *Chaetostoma breve* represented by samples from the Napo, Pastaza, Marañon, Santiago and Huallaga River Basins. Bayesian and Maximum Likelihood analyses found uniformly strong support for monophyly of the entire *Chaetostoma breve* clade (Bayesian posterior probability: 1.00, Maximum Likelihood bootstrap: 100).

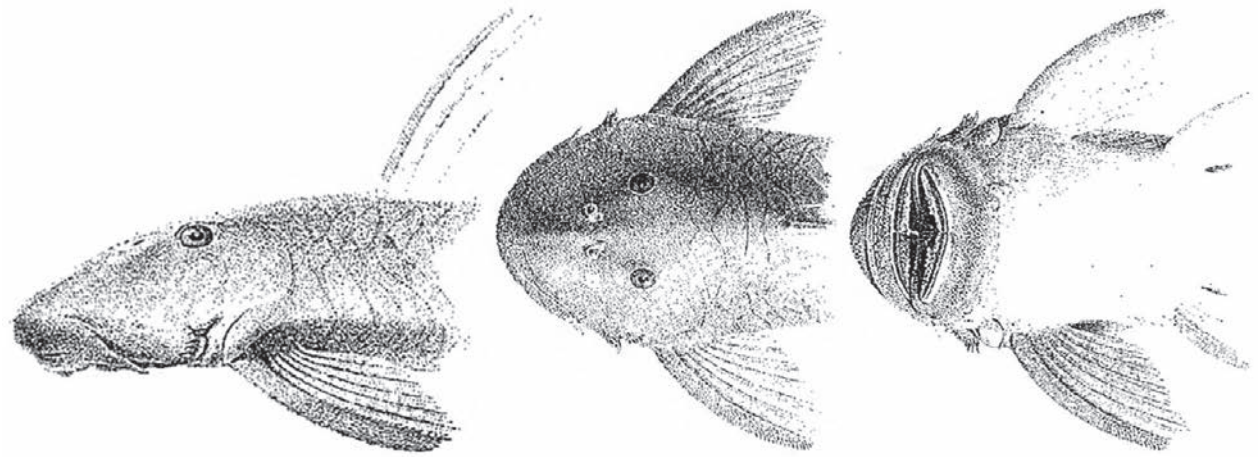

Figure 4. Original illustrations of *Chaetostoma branickii* from Steindachner 1881.

Figure 5. Photo comparison of a nearly 150-year-old preserved syntype of *Chaetostoma branickii* (NMW 47270-71, photos by Mark Sabaj & Kyle Luckenbill, copyright NMW) with a live specimen collected in 2018 from the Marañon River, Cajamarca Province, Peru (ROM 109213, photos by NKL). Scale bars: 1 cm.

Chaetostoma branickii was described by Steindachner (1881), based on specimens from the Chota River near Cajamarca in northern Peru. That portion of the Marañon River Basin was poorly sampled at the time of Lujan et al. (2015c), thus few specimens and no tissues from that specific region were available, making it reasonable to assume that a distinct, endemic species might exist there. Moreover, the syntypes of *Chaetostoma branickii* were in Vienna and not directly accessible to the authors. Lujan et al. (2015c) concluded that *Chaetostoma branickii* might be more closely allied with *Chaetostoma taczanowskii*, which was described by Steindachner (1881), based on specimens from the Huallaga River drainage to the south. To further investigate the validity of *Chaetostoma branickii*, Lujan and colleagues sampled the upper middle Marañon River in 2018, collecting over 540 fresh specimens and 60 tissues of *Chaetostoma*. This new material allowed a more detailed comparison of fresh, nearly topotypic specimens with the specimens on which Lujan et al. (2015a) based their re-description of *Chaetostoma breve* and type images of *Chaetostoma branickii* (Figs 4, 5). Based on this comparison, it has become clear that these are the same species and that *Chaetostoma branickii* should thus be recognised as the senior synonym of *Chaetostoma breve*.

Chaetostoma taczanowskii Steindachner 1882 is another taxonomically ambiguous species from northern Peru, described from the Huallaga River Basin, a southern tributary of the Marañon. Type images of this species suggest that it is also closely related to *Chaetostoma branickii*, if not another junior synonym, but a robust evaluation of the status of this species must await availability of fresh topotypic specimens and tissues.

Discussion

Fourteen *Chaetostoma* species are currently recognised from Peruvian drainages, most of which (12) inhabit the Marañon River Basin, including the Huallaga, Pastaza and Napo Rivers, with only three now described from the Ucayali River Basin: *C. lineopunctatum* from the Pachitea River, *C. loborhynchos* from the Tulumayo Rivers and *C. sacramento*. Until now, the colour pattern described for most species of *Chaetostoma* in Peru comprises black spots on the body and head (*C. daidalmatos*, *C. lineopunctatum*, *C. stroumpoulos*, *C. trimaculineum*) or irregular black spots on the body alone (*C. loborhynchos*, *C. spondylus*). There are also six species described as having uniform or marbled colouration (*C. branickii*, *C. changae*, *C. marmorescens*, *C. lexa* and *C. taczanowskii*). White patterns on a darker base colour are observed in only two species in Peru, *C. dermorhynchus* and *C. microps*, from which *C. sacramento* differs by having distinct and highly variable small to large white spots on the body, head and fins (vs. white spots on only the dorsal fin in C. *dermorhynchus*) and by having eight dorsal-fin branched rays (vs. nine in *C. microps*). Our recognition of *C. sacramento* is further supported by our molecular results, which consistently identify it as a distinct MOTU using the mitochondrial genes COI and CytB. Additionally, our findings demonstrate that *C. dermorhynchus* and *C. microps* each represent a separate MOTU and are phylogenetically distant species to *C. sacramento*, as shown in Lujan et al (2015b).

One of the fundamental criticisms of DNA-based approaches to species delimitation is that such analyses are incapable of distinguishing between genetic structure due to population-level processes and that due to species boundaries (Sukumaran and Knowles 2017). We advocate for a conservative approach in which MOTUs are treated as candidate species to be recognised taxonomically only if they are also morphologically diagnosable. Thus, the combined molecular and morphological evidence supports our recognition of *Chaetostoma sacramento* as a distinct species. Alternatively, the molecular species delimitation analyses consistently subdivided the *Chaetostoma branickii* clade into six MOTUs that we do not recognise as distinct species because of the overall morphologically similarity of these subunits and the strong monophyly of the parent clade. Future research may yet yield morphological characteristics capable of distinguishing these populations, thereby supporting their recognition as distinct species. Such a potentiality would be unlikely to resurrect *Chaetostoma breve*, however, given the very close genetic relationship between individuals from the Santiago (*breve*) and Marañon (*branickii*) river type locality populations, consistent with our decision to recognise *Chaetostoma branickii* as the senior synonym for this species.

Although *Chaetostoma sacramento* has been known in the aquarium fish trade for almost 30 years, it was originally assigned three L-numbers in 2011 (L455, L456 and L457; Seidel (2011)) and is known in the aquarium trade most commonly as L455. Other common aquarium trade names for the species include ‘Tiger *Chaetostoma*’, ‘Tingo Red *Chaetostoma*’ or ‘Ornate *Chaetostoma*’. Specimens on which the present description is based were collected in the San Carlos River, part of the Palcazu River Basin in Yanachaga Chemillen National Park (PNYC) in 2007 and in the Aguaytia River in 2008. According to aquarium fish exporters, this species also occurs in the Negro River, a small tributary of the upper Pisqui River near the Boqueron del Padre Abad and in the Chiu River, a tributary of San Alejandro River (Seidel 2011).

Acknowledgements

We thank Dario Faustino, Junior Chuctaya, Claudia Nolasco, Omar Quispe, Jerry Arana and Miguel Paniagua for field assistance, Raphael Covain at MHNG for sharing specimens and data and Julian Dignall at PlanetCatfish.com for sharing photos, aquarium literature and his thoughts on L455. This work was financed by CONCYTEC through the PROCIENCIA programme within the framework of the contest “Projects for the incorporation of postdoctoral researchers in Peruvian institutions”

according to contract [074-2021] and [PE501084299-2023-PROCIENCIA-BM] within the framework of the call “Interinstitutional Alliances for Doctorate Programs”.

References

Aljanabi SM, Martinez I (1997) Universal and rapid salt-extraction of high-quality genomic DNA for PCR-based techniques. Nucleic acids research 25(22): 4692–4693. https://doi.org/10.1093/nar/25.22.4692

Armbruster JW (2003) *Peckoltia sabaji*, a new species from the Guyana Shield (Siluriformes: Loricariidae). Zootaxa 344: 1–12. https://doi.org/10.11646/zootaxa.344.1.1

Ballen GA, Urbano-Bonilla A, Maldonado-Ocampo JA (2016) Description of a new species of the genus Chaetostoma from the Orinoco River drainage with comments on Chaetostoma milesi Fowler, 1941 (Siluriformes: Loricariidae). Zootaxa 4105(2): 181–197. https://doi.org/10.11646/zootaxa.4105.2.6

Bouckaert R, Heled J, Kühnert D, Vaughan T, Wu CH, Xie D, Suchard M, Rambaut A, Drummond AJ (2014) BEAST 2: a software platform for Bayesian evolutionary analysis. PLoS computational biology 10(4): e1003537. https://doi.org/10.1371/journal.pcbi.1003537

Carvalho TP, Lehmann AP, Reis RE (2008) *Gymnotocinclus anosteos*, a new uniquely-plated genus and species of loricariid catfish (Teleostei: Siluriformes) from the upper rio Tocantins basin, central Brazil. Neotropical Ichthyology 6: 329–338. https://doi.org/10.1590/S1679-62252008000300006

de Queiroz LJ, Cardoso Y, Jacot-des-Combes C, Bahechar IA, Lucena CA, Py-Daniel LR, Soares LM, Nylinder S, Oliveira C, Parente C, Torrente-Vilara G, Covain R, Buckup P, Montoya-Burgos JI (2020) Evolutionary units delimitation and continental multilocus phylogeny of the hyperdiverse catfish genus Hypostomus. Molecular phylogenetics and evolution 145: 106711. https://doi.org/10.1016/j.ympev.2019.106711

Fricke R, Eschmeyer WN, Van der Laan R (2024) Catalog of fishes: genera, species, references. California Academy of Sciences, San Francisco, CA, USA https://researcharchive.calacademy.org/research/ichthyology/catalog/fishcatmain.asp

Instituto Del Bien Común (IBC) (2016) Estudio previo de reconocimiento de las propuestas de reservas indígenas kakataibo norte y sur. “Proyecto de Regularización de Reservas Indígenas en Aislamiento para la Propuesta de Reserva Indígena Kakataibo”.

Larkin MA, Blackshields G, Brown NP, Chenna R, McGettigan PA, McWilliam H, Valentin F, Wallace IM, Wilm A, Lopez R, Thompson JD, Gibson TJ, Higgins DG (2007) Clustal W and Clustal X version 2.0. Bioinformatics 23(21): 2947–2948. https://doi.org/10.1093/bioinformatics/btm404

Lucena CAS, Calegari BB, Pereira EHL, Dallegrave E (2013) O uso de oleo de cravo na eutanasia de peixes. Boletim Sociedade Brasileira de Ictiologia 105: 20–24.

Lujan NK, Armbruster JW, Lovejoy NR, López-Fernández H (2015a) Multilocus molecular phylogeny of the suckermouth armored catfishes (Siluriformes: Loricariidae) with a focus on subfamily Hypostominae. Molecular phylogenetics and evolution 82: 269–288. https://doi.org/10.1016/j.ympev.2014.08.020

Lujan NK, Meza-Vargas V, Astudillo-Clavijo V, Barriga-Salazar R, López-Fernández H (2015b) A multilocus molecular phylogeny for *Chaetostoma* clade genera and species with a review of *Chaetostoma* (Siluriformes: Loricariidae) from the Central Andes. Copeia 103: 664–701. https://doi.org/10.1643/CI-14-194

Lujan NK, Meza-Vargas V, Barriga-Salazar R (2015c) Two new *Chaetostoma* group (Loricariidae: Hypostominae) sister genera from opposite sides of the Andes Mountains in Ecuador, with the description of one new species. Copeia 103(3): 651–663. https://doi.org/10.1643/CI-15-246

Meza-Vargas V, Calegari BB, Lujan NK, Ballen GA, Oyakawa OT, Sousa LM, Reis RE (2022) A New Species of *Chaetostoma* (Siluriformes: Loricariidae) Expands the Distribution of Rubbernose Plecos Eastward into the Lower Amazon Basin of Brazil. Ichthyology & Herpetology 110(2): 364–377. https://doi.org/10.1643/i2021068

Neuhaus EB, Meza-Vargas V, Herrera JR, Lujan NK (2023) A new distinctively striped species of bushynose catfish (Siluriformes: Loricariidae: *Ancistrus*) from the Pachitea River drainage, Pasco, Peru. Journal of Fish Biology 104(4): 969–978. https://doi.org/10.1111/jfb.15637

Pons J, Barraclough TG, Gomez-Zurita J, Cardoso A, Duran DP, Hazell S, Kamoun S, Sumlin WD, Vogler AP (2006) Sequence-based species delimitation for the DNA taxonomy of undescribed insects. Systematic biology 55(4): 595–609. https://doi.org/10.1080/10635150600852011

Puillandre N, Brouillet S, Achaz G (2021) ASAP: assemble species by automatic partitioning. Molecular Ecology Resources 21(2): 609–620. https://doi.org/10.1111/1755-0998.13281

Rambaut A, Suchard MA, Xie D, Drummond AJ (2014) Tracer v1. 6.

Ramirez JL, Galetti Jr PM (2015) DNA barcode and evolutionary relationship within *Laemolyta* Cope 1872 (Characiformes: Anostomidae) through molecular analyses. Molecular Phylogenetics and Evolution 93: 77–82. https://doi.org/10.1016/j.ympev.2015.07.021

Ramirez JL, Valdivia P, Rosas-Puchuri U, Valdivia NL (2023) SPdel: A pipeline to compare and visualize species delimitation methods for single-locus datasets. Molecular Ecology Resources 23(8): 1959–1965. https://doi.org/10.1111/1755-0998.13864

Regan CT (1904) “A monograph of the fishes of the family Loricariidae.” Transactions of the Zoological Society of London 17: 191–350. https://doi.org/10.1111/j.1096-3642.1904.tb00040.x

Sabaj MH (2020) Codes for natural history collections in ichthyology and herpetology. Copeia 108(3): 593–669. https://doi.org/10.1643/ASIHCODONS2020

Salcedo NJ, Ortega H (2015) A new species of *Chaetostoma*, an armored catfish (Siluriformes: Loricariidae), from the río Marañón drainage, Amazon basin, Peru. Neotropical Ichthyology 13(1): 151–156. https://doi.org/10.1590/1982-0224-20140073

Salcedo NJ (2006a) New species of *Chaetostoma* (Siluriformes: Loricariidae) from Central Peru. Copeia 2006(1): 60–67. https://doi.org/10.1643/0045-8511(2006)006[0060:NSOCSL]2.0.CO;2

Salcedo NJ (2006b) Two new species of *Chaetostoma* (Siluriformes: Loricariidae) from the Huallaga River in central Peru. Ichthyological Exploration of Freshwaters 17(3): 207–220. https://doi.org/10.1643/0045-8511(2006)006[0060:NSOCSL]2.0.CO;2

Schaefer SA (1997) The neotropical cascudinhos: systematics and biogeography of the *Otocinclus* catfishes (Siluriformes: Loricariidae). Proceedings of the Academy of Natural Sciences of Philadelphia 148: 1–120.

Seidel I (2011) Gleich drei neue *Chaetostoma*-Arten aus Peru. Neu importiert 2011: 28–29.

Stawikowski R (1988) “Harnischwelse aus südlichen Amazonaszuflüssen.” Die Aquarien- und Terrarienzeitschrift (DATZ) 41: 556–558.

Steindachner F (1881) “Beiträge zur Kenntniss der Flussfische Südamerika’s. II.” Denkschriften der Mathematisch-Naturwissenschaftlichen Classe der Kaiserlichen Akademie der Wissenschaften in Wien 43: 103–146.

Sukumaran J, Knowles L (2017) Multispecies coalescent delimits structure, not species. Proceedings of the National Academy of Sciences 114:1607–1612. https://doi.org/10.1073/pnas.1607921114

Zhang J, Kapli P, Pavlidis P, Stamatakis A (2013) A general species delimitation method with applications to phylogenetic placements. Bioinformatics 29(22): 2869–2876. https://doi.org/10.1093/bioinformatics/btt499

Zoosyst. Evol. 100 (4) 2024, 1401–1417 | DOI 10.3897/zse.100.131971

PENSOFT

für Natur MUSEUM FÜR NATURKUNDE BERLIN

Molecular phylogeny, including a new species of *Anindobothrium* (Cestoda, Rhinebothriidea) from the Southern eagle ray *Myliobatis goodei*, finally solves the taxonomic enigma of *Phyllobothrium myliobatidis*

Guillermina García Facal[1,2], Sebastián Franzese[1,2], Martín Miguel Montes[3], Adriana Menoret[1,2]

1 *Laboratorio de Sistemática y Biología de Parásitos de Organismos Acuáticos (SIBIPOA), Departamento de Biodiversidad y Biología Experimental, Facultad de Ciencias Exactas y Naturales, Universidad de Buenos Aires, Buenos Aires, Argentina*

2 *CONICET-Universidad de Buenos Aires, Instituto de Biodiversidad y Biología Experimental (IBBEA), Buenos Aires, Argentina*

3 *Centro de Estudios Parasitológicos y de Vectores (CEPAVE), Consejo Nacional de Investigaciones Científicas y Técnicas, Universidad Nacional de La Plata (CONICET-UNLP-CICPBA), Boulevard 120 S/N e/60 y 64 (1900), La Plata, Buenos Aires, Argentina*

https://zoobank.org/50A363FC-F02F-4B6A-A0A8-963EC8D5A65C

Corresponding author: Guillermina García Facal (guillefacal@gmail.com)

Academic editor: Tom Artois ♦ **Received** 13 July 2024 ♦ **Accepted** 2 October 2024 ♦ **Published** 18 October 2024

Abstract

During a parasitological survey of tapeworms from *Myliobatis goodei* Garman, 1885 (Myliobatiformes: Myliobatidae) in coastal waters off Argentina in the Southwestern Atlantic, a new rhinebothriidean cestode species, *Anindobothrium danielae* **sp. nov.**, is described using morphological and molecular techniques. This species differs from its congeners by a particular combination of features, including the configuration of the bothridia, the number of marginal loculi, and the number and distribution of testes. Additionally, *Anindobothrium myliobatidis* **comb. nov.** is proposed based on several morphological traits, including the presence of stalked bothridia with marginal loculi and an apical sucker, euapolytic strobila, and postvaginal testes. The diagnosis of the genus *Anindobothrium* Marques, Brooks & Lasso, 2001 is amended to include the features exhibited by these two species; two species subsets are suggested based on the configuration of the bothridia. The presence of *A. danielae* **sp. nov.** and *A. myliobatidis* **comb. nov.** in the studied area not only increases the number of cestodes in *M. goodei* here from eight to ten but also represents the first report of a rhinebothriidean cestode parasitizing stingrays of the family Myliobatidae in the Southwestern Atlantic.

Key Words

Anindobothriidae, description, molecular identification, morphology, Myliobatiformes, Southwest Atlantic, tapeworms

Introduction

The rhinebothriidean cestode genus *Anindobothrium* Marques, Brooks & Lasso, 2001 currently consists of four valid species: *A. anacolum* (Brooks, 1977), *A. carrioni* Trevisan, Primon & Marques, 2017, *A. inexpectatum* Trevisan, Primon & Marques, 2017, and *A. lisae* Marques, Brooks & Lasso, 2001. According to Trevisan et al. (2017), these species are principally characterized by a scolex composed of four stalked bothridia typically longer than wide, with or without longitudinal septa, with apical sucker and marginal loculi, with or without facial loculi; testes numerous arranged in two lateral columns; the presence of postporal testes; a genital pore in the anterior half of the proglottid; and a vitellarium interrupted by terminal genitalia and partial or totally interrupted by ovary.

Members of *Anindobothrium* were found in stingrays of the family Potamotrygonidae (Myliobatiformes) in marine and freshwater environments. Three species were found in potamotrygonids of the marine genus *Styracura* Carvalho,

Loboda & da Silva, 2016, with *A. anacolum* and *A. inexpectatum* from several localities in the Caribbean Sea in Central and South America, and *A. carrioni* from the Tropical Eastern Pacific Ocean in Central America (Trevisan et al. 2017). To date, *A. lisae* Marques, Brooks & Lasso, 2001 was exclusively found in freshwater stingrays of the genus *Potamotrygon* Garman, 1877, in rivers of South America (Marques et al. 2001; Trevisan et al. 2017). Recently, Trevisan et al. (2017), based on the phylogeny of *Anindobothrium*, suggested that the diversification of the genus follows the colonization by their hosts, the marine-derived freshwater stingrays, with an ancestor in rivers of South America after marine incursions in northern latitudes (Fontenelle et al. 2021), which consequently explains the presence of *Anindobothrium* in both environments.

During field trips off the coastal waters off Argentina in the Southwestern Atlantic (SWA), eagle rays of the genus *Myliobatis* Cuvier, 1816 were examined for cestodes. Preliminary studies on the collected specimens based mainly on the morphology of the scolex and the proglottids indicated that these were similar to those exhibited by *A. lisae*. However, an exhaustive morphological study based on entire mature worms, fine histology, and scanning electron microscopy (SEM), in addition to molecular analyses, allowed us to identify a new species of *Anindobothrium*.

Two eagle rays of the genus *Myliobatis* (i.e., *Myliobatis goodei* Garman, 1885 and *Myliobatis ridens* Ruocco, Lucifora, Díaz de Astarloa, Mabragaña & Delpiani, 2012) have been previously reported as hosts for several species of tapeworms in the SWA, being parasitized by nine species of cestodes of the orders Diphyllidea, Lecanicephalidea, "Tetraphyllidea," and Trypanorhyncha, and one of uncertain placement, *Phyllobothrium myliobatidis* Brooks, Mayes & Thorson, 1981 (see Franzese et al. 2023). Furthermore, prior to this study, there are no other records of *Myliobatis* being infected by rhinebothriideans in the SWA.

Of particular interest is *P. myliobatidis*, originally described as a member of the family Phyllobothriidae, included in the polyphyletic order "Tetraphyllidea," parasitizing the Southern eagle ray, *M. goodei*, near the Río de la Plata estuary. *Phyllobothrium myliobatidis* exhibits, among other morphological features, a scolex composed of four bothridia with marginal loculi, a cephalic peduncle, and a genital pore located in the anterior third of proglottid (Brooks et al. 1981). Subsequently, Ruhnke (2011) suggested that this species should be placed in the order Rhinebothriidea since, like *Anindobothrium*, its members also possess bothridial stalks, a diagnostic morphological criterion for the order. Similarities in morphology and host association between *P. myliobatidis* and the specimens recently collected along the SWA cast doubts about its actual generic and ordinal placement. Consequently, in addition to the new species herein described, a new combination is proposed based on morphological characters, and *P. myliobatidis* is transferred to the genus *Anindobothrium* in anticipation of eventual new material to be included in future molecular phylogenetic studies.

Materials and methods

Tapeworms and host collection

Cestodes examined in this study were collected from the spiral intestines of seven individuals of *M. goodei* (Myliobatiformes: Myliobatidae) caught from different localities along the coast of the Argentine Sea. Two specimens were caught off Puerto Quequén, Buenos Aires Province, at 38°53.00'S, 58°27.00'W in July 2001 (assigned unique host number VIPQ-052) and January 2018 (GGPQ-115), and two specimens were caught off Balneario San Cayetano at 38°54.01'S, 59°12.02'W, Buenos Aires Province, in February 2018 (AGPQ-001, AGPQ-024), all by commercial trawlers (Fig. 1). One specimen was caught in San Matías Gulf, Río Negro Province, at 41°11.00'S, 64°03.26'W in March 2011 (PD3-155) and two were caught off Bahía San Blas, Buenos Aires Province, at 40°42.92'S, 62°00.58'W in April 2013 (PD7-512, PD7-514) with bottom trawls on board the RV *Puerto Deseado* (CONICET). Additional five specimens of *M. goodei* were also examined, but no rhinebothriidean cestodes were recovered. Three were caught off Balneario San Cayetano, Buenos Aires Province, at 38°54.01'S, 59°12.02'W in February 2018, and two specimens were caught off Puerto Quequén, Buenos Aires Province, at 38°53.00'S, 58°27.00'W in December 2019 also by commercial trawlers. Cestode specimens included in this study were recovered from the spiral intestines using a stereomicroscope. All tapeworms were removed from the spiral intestine of their respective host and relaxed in seawater. A subset of specimens was fixed in 10% formalin and transferred to 70% ethanol for long-term storage; a total of two specimens were fixed in ethanol and stored at -20 ºC.

Morphological examination of cestodes

The specimens prepared for light microscopy (permanent mounts) were hydrated in a graded ethanol series, stained with Harris' haematoxylin, dehydrated in a graded ethanol series, cleared in methyl salicylate, and mounted in Canada balsam. A single bothridium was removed from the scolex of five tapeworms, observed in glycerine (non-permanent mount), and posteriorly included in the permanent mount.

One bothridium and the terminal portion of three strobilae were embedded in paraffin and serially cross-sectioned at a thickness of 7 micrometers (μm). Histological sections were stained with Harris' haematoxylin, counterstained with eosin, and mounted in Canada balsam. Whole mounts, non-permanent mounts, and histological sections were measured using an Olympus BX 51 compound microscope. Drawings were made with the aid of a drawing tube attached to the Olympus BX 51 compound microscope. All measurements of reproductive structures were taken from mature proglottids in which the vas deferens was not sperm-filled. Measurements are expressed

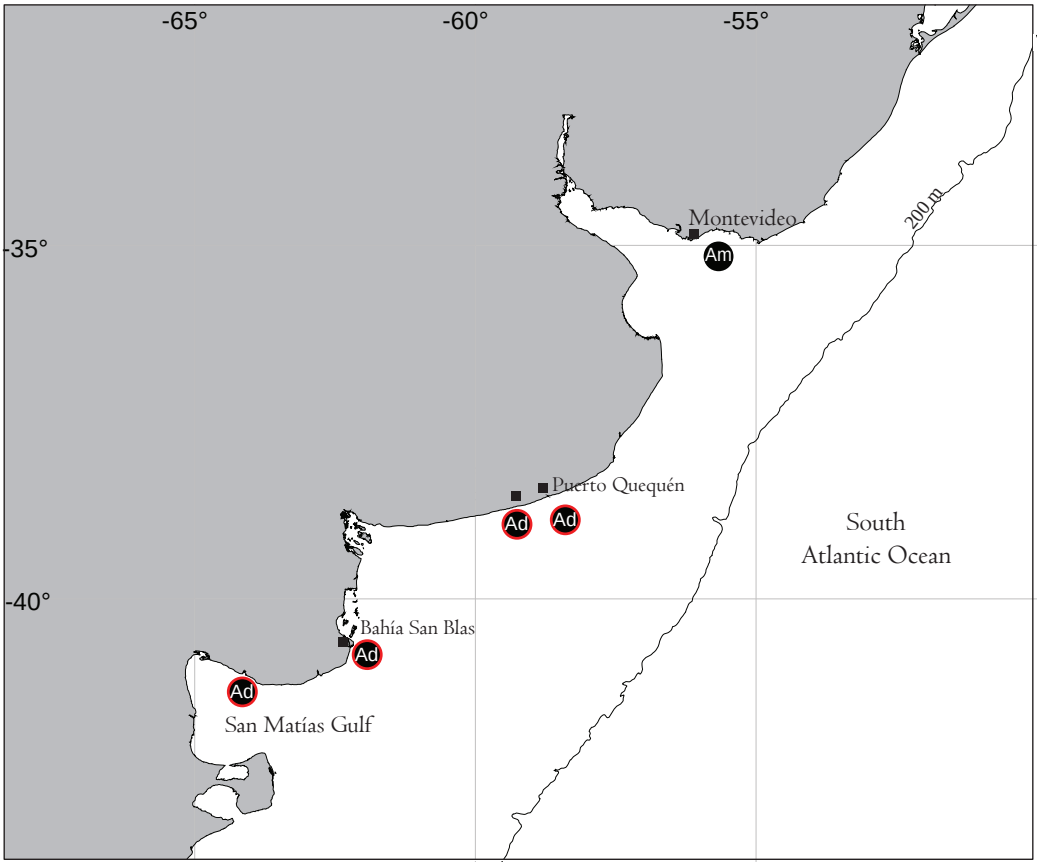

Figure 1. Sampling sites of the southern eagle rays, *Myliobatis goodei*, examined during the present study. Ad, *Anindobothrium danielae* sp. nov.; Am, *Anindobothrium myliobatidis* comb. nov. Red circles, hosts examined in this study; black circles, hosts examined in Brooks et al. (1981).

as the range, followed in parentheses by the mean, standard deviation (when n ≥ 3), and the number of worms from which the measurements were taken (n). All measurements are in µm unless otherwise stated.

Worms prepared for scanning electron microscopy (SEM) were hydrated in a graded ethanol series, post-fixed in 1% osmium tetroxide overnight at room temperature, dehydrated in a graded ethanol series, and dried using hexamethyldisilazane. After drying, the specimens were mounted on stubs with carbon tape, coated with *c.* 40 nm of gold/palladium in a Thermo VG Scientific Polaron SC 7630, and examined in either a Zeiss GeminiSEM 360 or a Carl Zeiss NTS-SUPRA 40 scanning electron microscope.

Molecular methods and phylogenetic analysis

Total genomic DNA was extracted from two cestode specimens using PURO-Genomic DNA produced by PB-L (Productos Bio-Lógicos, Argentina), according to the manufacturer's protocol. The D1–D3 region of the nuclear large subunit ribosomal gene (28S rDNA) was amplified by PCR using the forward primer LSU-5 (5′-TAG GTC GAC CCG CTG AAYTTA AGC A-3′) and the reverse primer 1500R (5′-GCT ATC CTG AGG GAA ACT TCG-3′) (Olson et al. 2003). The reactions were carried out with a Mastercycler thermocycler (Eppendorf) in a 50 µL reaction mixture containing 25 µL of PB-L master mix (Productos Bio-Lógicos, Argentina), 0.4 µM of each forward and reverse primer, and 6 µL of the template DNA. The PCR cycling conditions were: 3 min denaturing at 94 °C; 45 cycles of 30 s at 94 °C, 30 s at 50 °C, 1 min 45 s at 72 °C; followed by a final extension period of 2 min at 72 °C.

Sample sequencing was carried out in a specialized laboratory (Macrogen, Korea). Sequences were assembled using the platform Geneious 5.0.4. In addition to the new sequences reported in the present study, the phylogenetic analysis included known sequences of 29 species of Rhinebothriidea obtained from GenBank, which are representatives of the six families currently included in the order (Ruhnke et al. 2015; Trevisan et al. 2017; Herzog et al. 2023) (Table 1). Additional sequences obtained from GenBank of nine phyllobothriidean species with scolex morphology similar to specimens collected from *M. goodei* (flat or foliose bothridia with marginal loculi) were also included in the phylogenetic analysis (Table 1). Two outgroup species of the orders Litobothriidea and Trypanorhyncha were also included (Table 1). Taxa names, GenBank accession numbers for 28S, voucher accession numbers, host, and sources are given for the 40 species in Table 1.

Table 1. Cestodes included in the phylogenetic analysis.

Cestode species	Host	Order	Rhinebothriidean family	No. GenBank 28S	No. voucher	Source
Dollfusiella tenuispinis (Linton, 1890)*	*Hypanus sabinus*	TR	NA	DQ642796	BMNH 2008.5.21.2	Olson et al. (2010)
Litobothrium amplifica (Kurochkin and Slankis, 1973)*	*Alopias pelagicus*	LI	NA	KF685906	LRP8279	Caira et al. (2014)
Anindobothrium anacolum (Brooks, 1977)	*Styracura schmardae*	RH	Anindobothriidae	MF920345	MZUSP 7778	Trevisan et al. (2017)
Anindobothrium carrioni Trevisan, Primon & Marques, 2017	*Styracura pacifica*	RH	Anindobothriidae	MF920342	MZUSP 7785	Trevisan et al. (2017)
***Anindobothrium danielae* sp. nov.**	***Myliobatis goodei***	**RH**	**Anindobothriidae**	**PQ346666 PQ346665**	**MACN-Pa 801/1 MACN-Pa 801/2**	**Present study**
Anindobothrium inexpectatum Trevisan, Primon & Marques, 2017	*Styracura schmardae*	RH	Anindobothriidae	MF920353	MZUSP 7767	Trevisan et al. (2017)
Anindobothrium lisae Marques, Brooks & Lasso, 2001	*Potamotrygon orbignyi*	RH	Anindobothriidae	MF920362	MZUSP 7782	Trevisan et al. (2017)
Anthocephalum alicae Ruhnke, 1994	*Hypanus americanus*	RH	Anthocephaliidae	KM658205	LRP 8508	Ruhnke et al. (2015)
Anthocephalum healyae Ruhnke, Caira & Cox, 2015	*Neotrygon kuhlii*	RH	Anthocephaliidae	KM658200	LRP 8512	Ruhnke et al. (2015)
Barbeaucestus ralickiae Caira, Healy, Marques & Jensen, 2017	*Taenyura lima*	RH	Anthocephaliidae	FJ177108	LRP3922 (CH35)	Healy et al. (2009)
Barbeaucestus jockuschae Caira, Healy, Marques & Jensen, 2017	*Neotrygon kuhlii*	RH	Anthocephaliidae	FJ177109	LRP3894 (CH3)	Healy et al. (2009)
Divaricobothrium tribelum Caira, Healy, Marques & Jensen, 2017	*Maculabatis* cf. *gerrardi*	RH	Anthocephaliidae	FJ177107	LRP3902 (CH11)	Healy et al. (2009)
Echeneibothrium sp. 1	*Rostroraja velezi*	RH	Echeneibothriidae	FJ177098	LRP4217 (TE94)	Healy et al. (2009)
Echeneibothrium sp. 2	*Raja miraletus*	RH	Echeneibothriidae	KF685876	LRP8312	Caira et al. (2014)
Escherbothrium cielochae Bueno, Trevisan & Caira, 2024	*Urotrygon rogersi*	RH	Escherbothriidae	KM658197	LRP 8519	Ruhnke et al. (2015)
Mixobothrium healyae Herzog, Caira & Jensen, 2023	*Pristis clavata*	RH	Mixobothriidae	FJ177119	LRP4220 (CH26)	Healy et al. (2009)
Mixobothrium carinesmarinei Herzog, Caira & Jensen, 2023	*Pristis pristis*	RH	Mixobothriidae	OQ429320	LRP10963	Herzog et al. (2023)
Mixobothrium bengalense Herzog, Caira & Jensen, 2023	*Glaucostegus obtusus*	RH	Mixobothriidae	OQ429316	LRP10970	Herzog et al. (2023)
Pseudanthobothrium sp.	*Leucoraja erinacea*	RH	Echeneibothriidae	KF685750	LRP8324	Caira et al. (2014)
Rhabdotobothrium anterophallum Campbell, 1975	*Mobula hypostoma*	RH	Rhinebothriidae	AF286961	BMNH 2001.1.31.3-4	Olson et al. (2001)
Rhinebothrium sp.	*Maculabatis pastinacoides*	RH	Rhinebothriidae	FJ177121	LRP3903 (CH12)	Healy et al. (2009)
Rhinebothrium megacanthophallus Healy, 2006	*Urogymnus polylepis*	RH	Rhinebothriidae	FJ177120	LRP3901 (CH10)	Healy et al. (2009)
Rhinebothroides sp.	*Potamotrygon wallacei*	RH	Rhinebothriidae	MF920365	MZUSP 7792	Trevisan et al. (2017)
Rhodobothrium paucitesticulare Mayes & Brooks, 1981	*Rhinoptera bonasus*	RH	Rhinebothriidae	FJ177100	LRP4216 (TE61)	Healy et al. (2009)
Scalithrium sp.	*Hypanus longus*	RH	Rhinebothriidae	KF685878	LRP8333	Caira et al. (2014)
Semiorbiseptum yakiae (Franzese, Montes, Shumabukuro & Arredondo, 2024)	*Sympterygia bonapartii*	RH	Escherbothriidae	OR791403	MACN-Pa 785/4	Franzese et al. (2024)
Spongiobothrium sp.	*Rhynchobatus* cf. *australiae*	RH	Rhinebothriidae	FJ177134	LRP3919 (CH32)	Healy et al. (2009)
Stillabothrium amuletum (Butler, 1987)	*Glaucostegus typus*	RH	Escherbothriidae	FJ177117	LRP 3917 (CH-30)	Healy et al. (2009)
Stillabothrium cadenati (Euzet, 1954)	*Zanobatus schoenleinii*	RH	Escherbothriidae	FJ177110	LRP3924 (CH37)	Healy et al. (2009)
Stillabothrium davidcynthiaorum Daigler & Reyda, 2016	*Brevitrygon walga*	RH	Escherbothriidae	FJ177116	LRP3926 (CH45)	Healy et al. (2009)

Cestode species	Host	Order	Rhinebothriidean family	No. GenBank 28S	No. voucher	Source
Sungaicestus kinabatanganensis (Healy, 2006)	*Urogymnus polylepis*	RH	Anthocephaliidae	FJ177118	LRP3900 (CH9)	Healy et al. (2009)
Chimaerocestos sp.	*Rhinochimaera pacifica*	PH	NA	KF685758 KF685882	LRP8303 LRP8348	Caira et al. (2014)
Rockacestus carvajali Caira, Bueno & Jensen, 2021	*Dipturus chilensis*	PH	NA	MW419973	LRP8913	Caira et al. (2021)
Rockacestus conchai Caira, Bueno & Jensen, 2021	*Bathyraja albomaculata*	PH	NA	MW419959	LRP10324	Caira et al. (2021)
Scyphophyllidium guariticus (Marques, Brooks & Lasso, 2001)	*Paratrygon aiereba*	PH	NA	KF685888	LRP8286	Caira et al. (2014)
Scyphophyllidium janineae (Ruhnke, Healy & Shapero, 2006)	*Hemipristis elongata*	PH	NA	HQ680625	QM G 231309–14	Cutmore et al. (2011)
Scyphophyllidium kirstenae (Ruhnke, Healy & Shapero, 2006)	*Hemigaleus microstoma*	PH	NA	KC505626	LRP7962	Ruhnke and Workman (2013)
Scyphophyllidium orectolobi (Butler, 1987)	*Orectolobus maculatus*	PH	NA	MG008940	–	Cutmore et al. (2017)
Scyphophyllidium randyi (Ruhnke, Caira & Carpenter, 2006)	*Chiloscyllium hasseltii*	PH	NA	KF685767	LRP8318	Caira et al. (2014)
Scyphophyllidium tyleri (Ruhnke, Caira & Carpenter, 2006)	*Chiloscyllium punctatum*	PH	NA	KF685890	LRP8315	Caira et al. (2014)

Outgroup species: LI, Litobothriidea; NA, not apply; PH, Phyllobothriidea; RH, Rhinebothriidea; TR, Trypanorhyncha.

Sequences were aligned using the online version of MAFFT v.7 (Katoh et al. 2019). Ambiguously aligned and hypervariable regions in the 28S dataset were removed with Gblocks online version 0.91b (Talavera and Castresana 2007), according to a secondary structure model, with the parameter settings of a less stringent selection (allowing smaller final blocks, gap positions within the final blocks, and less strict flanking positions).

The substitution model was chosen under the Bayesian Information Criterion (BIC) in Jmodeltest 2.1 (Darriba et al. 2012). The appropriate nucleotide substitution model implemented for the 28S rDNA matrix was GTR+I+G.

The phylogenetic reconstruction was performed using Bayesian Inference (BI) through MrBayes v. 3.2.6 (Ronquist et al. 2012). Phylogenetic trees were constructed using two parallel analyses of Metropolis-Coupled Markov Chain Monte Carlo (MCMC) for 10 million generations each to estimate the posterior probability (PP) distribution. Topologies were sampled every 1,000 generations, and the average standard deviation of split frequencies was observed to be less than 0.01 at the end of the run, as suggested by Ronquist et al. (2012). The robustness of clades was assessed using Bayesian posterior probability (PP), where PP > 0.95 was considered strongly supported. A majority consensus tree with branch lengths was reconstructed for each run after discarding the first 25% of trees sampled as "burn-in." The consensus tree for the 28S gene was visualized in FigTree 1.4.3 (Rambaut, 2014). Additionally, uncorrected p-distances were calculated using MEGA X (Kumar et al. 2018) with the bootstrap method (1000 replicates) and nucleotide substitution (transition + transversions). A uniform rate was applied, and gaps/missing data were considered as complete deletions. The newly generated sequences were submitted to GenBank.

Mapping and geographic sites

Geographic coordinates of type and additional localities of species of *Anindobothrium* are expressed in degrees and minutes. Estimated coordinates were assigned to records of specimens of Brooks et al. (1981) (Fig. 1). The geographic distribution of the *Anindobothrium* species was charted using the PANMAP software v.0.9.6 (Diepenbroek et al. 2002).

Terminology for microtriches, sources of valid zoological names, marine regionalization, and abbreviations of zoological names

Terminology for the morphology of microtriches follows Chervy (2009). Valid cestode names follow Caira et al. (2022). Valid host names follow Froese and Pauly (2024). Marine regionalization follows Spalding et al. (2007). Zoological abbreviations include *A.* for *Anindobothrium* and *An.* for *Anthocephalum*.

Material examined and museum abbreviations

The museum material examined includes light micrographs of the holotype (USNM No. 1371266) and three paratypes (USNM No. 1371267) of *P. myliobatidis* provided by Anna Phillips from the Smithsonian National Museum of Natural

History–Invertebrate Zoology Collection, Washington, D.C., USA. Museum abbreviations are as follows: **BMNH**, History Museum, London, United Kingdom; **LRP**, Lawrence R. Penner Parasitology Collection, Department of Ecology and Evolutionary Biology, University of Connecticut, Storrs, Connecticut, USA; **MACN-Pa**, Museo Argentino de Ciencias Naturales, Colección Parasitológica, Buenos Aires, Argentina; **MLP-He**, Museo de La Plata, Colección de Invertebrados, La Plata, Argentina; **MZUSP**, Museu de Zoologia da Universidade de São Paulo, São Paulo, Brazil; **QM G**, Queensland Museum, Brisbane, Australia.

Results

Order Rhinebothriidea Healy, Caira, Jensen, Webster & Littlewood, 2009
Genus *Anindobothrium* Marques, Brooks & Lasso, 2001

Anindobothrium danielae sp. nov.

https://zoobank.org/68F38AF4-AF06-4F51-BFE4-1B35734CC36F

Figs 2–5

Type material. ***Holotype*** • an entire, mature worm, off Bahía San Blas, Buenos Aires Province, Argentina (40°42.92'S, 62°00.58'W), 23 m, 2 Apr 2013, A. Menoret leg., MACN-Pa No. 798.

Paratypes • Three entire, mature worms, cross-section of 2 attached mature proglottids, same data as preceding, MACN-Pa No. 799/1–5 • Two entire, mature worms, same data as preceding, MLP-He No. 8136 • Six entire, mature worms, off Puerto Quequén, Buenos Aires Province (38°53.00'S, 58°27.00'W), 20 Jul 2001, V. A. Ivanov leg., MACN-Pa Nos. 795/1–2 and 800/1–4 • Two entire, mature worms, same data as preceding, MLP-He No. 8135 • One entire, mature worm, off Puerto Quequén, Buenos Aires Province, Argentina (38°53.00'S, 58°27.00'W), 22 Jan 2018, G. García Facal leg., MACN-Pa No. 796 • Three entire, mature worms, off Balneario San Cayetano, Buenos Aires Province, Argentina (38°54.01'S, 59°12.02'W), 37 m, 20 Feb 2018, G. García Facal & A. Menoret leg., MACN-Pa No. 797/1–3 • Cross-section of 1 scolex, off San Matías Gulf, Rio Negro Province, Argentina (41°11.00'S, 64°03.26'W), 73 m, 20 Mar 2011, A. Menoret & V. A. Ivanov leg., MACN-Pa No. 800.

Description. Based on 23 specimens in total: 18 entire, mature worms, cross-sections of 2 terminal mature proglottids, cross-sections of 1 scolex, and SEM of 2 worms. Worms euapolytic, 9.1–21.5 (14.2 ± 4.1, n = 17) mm long, 22–49 (32 ± 9, n = 17) acraspedote proglottids (Fig. 2A). Scolex 510–1,150 (775 ± 176, n = 17) long, 600–1,625 (1011 ± 309, n = 17) wide, composed of four stalked bothridia (Figs 2B, 3A). Bothridia orbicular-shaped, 272–850 (561 ± 213, n = 7) long, 272–1,000 (729 ± 296, n = 7) wide, with 101–121 (115 ± 10, n = 5) marginal loculi and anterior apical sucker. Apical sucker 40–90 (64 ± 19, n = 6) long, 48–100 (66 ± 21, n = 6) wide (Figs 2B, C, 3A–C). Transverse and longitudinal septa absent. Distal portion of marginal septa formed by marginal muscle bundles; proximal portion formed by radial muscles with proximal fibers ending adjacent to each other (Fig. 2D). Cephalic peduncle 410–1,400 (856 ± 292, n = 18) long, 100–300 (192 ± 63, n = 18) wide.

Apex of scolex proper covered with acicular filitriches (Fig. 3D). Proximal bothridial surface covered with acicular filitriches, cilia present in marginal loculi (Fig. 3F). Distal surface covered with capilliform filitriches and coniform spinitriches (Fig. 3E). Surface of bothridial stalks covered with acicular filitriches. Cephalic peduncle and anterior portion of strobila covered with capilliform filitriches (Fig. 3G).

Immature proglottid, initially wider than long, becoming longer than wide with maturity. Most terminal proglottids and some subterminal proglottids with sperm-filled vas deferens. Mature proglottids without sperm-filled vas deferens 1,080–2,150 (1,491 ± 269, n = 18) long, 315–600 (423 ± 103, n = 18) wide, length to width ratio 2.3–5.3 (3.7 ± 0.9, n = 18): 1 (Figs 2A, 4A). Terminal mature proglottids with sperm-filled vas deferens 1,525–2,675 (2,013 ± 312, n = 15) long, 300–620 (427 ± 107, n = 15) wide, length to width ratio 3.1–6.8 (4.9 ± 1.0, n = 15): 1 (Figs 2A, 4B), mature proglottids 2–7 (4 ± 1, n = 18) in number per worm (Fig. 2A). Gravid proglottids not observed.

Testes round to oval, 52–83 (68 ± 8, n = 17) long, 39–68 (55 ± 8, n = 17) wide, 76–115 (97 ± 11, n = 17) in number, 9–19 (13 ± 3, n = 17) preporal, 24–38 (32 ± 4, n = 17) postporal, 41–64 (51 ± 7, n = 17) aporal, arranged anteroposteriorly in 4 regular columns, 2 layers deep in cross-section; each column extending from anterior margin of proglottid reaching anterior margin of ovary (Figs 4A, B, 5A–C). Cirrus sac pyriform in anterior third of proglottid, bent posteriorly, 103–200 (152 ± 32, n = 17) long, 43–135 (93 ± 26, n = 17) wide, containing coiled cirrus; cirrus covered with spinitriches (Figs 4C, 5C, F). Vas deferens coiled, extending posteriorly at level of cirrus sac to near anterior margin of ovary, entering cirrus sac at anteromedial margin (Figs 4A–C, 5C, F).

Vagina thick-walled, extending anteriorly from ootype, then running along midline of proglottid to anterior margin of cirrus sac, and laterally opening into genital atrium anterior to cirrus, vaginal sphincter present (Figs 4C, 5B, E). Ovary H-shaped in frontal view, poral lobe 185–450 (314 ± 66, n = 17) long, aporal lobe 218–440 (310 ± 61, n = 17) long, 170–380 (266 ± 57, n = 17) wide at isthmus, tetra-lobed in cross-section (Figs 4A, B, 5D). Mehlis' gland posterior to ovarian isthmus, 65–115 (97 ± 16, n = 16) long, 70–120 (90 ± 17, n = 17) wide. Vitellarium follicular; vitelline follicles oval, 10–22 (15 ± 4, n = 16) long, 12–42 (27 ± 7, n = 16) wide, in 2 dorsal and 2 ventral columns on each lateral margin of proglottid, lateral to testes, extending from near anterior margin of proglottid to posterior margin of proglottid, partly interrupted by terminal genitalia and uninterrupted by ovary (Figs 4A–C, 5A–F). Uterus saccate, medial, and ventral, extending from the level of the genital atrium to ovarian isthmus (Fig. 4A–C). Osmoregulatory ducts 4, 1 dorsal,

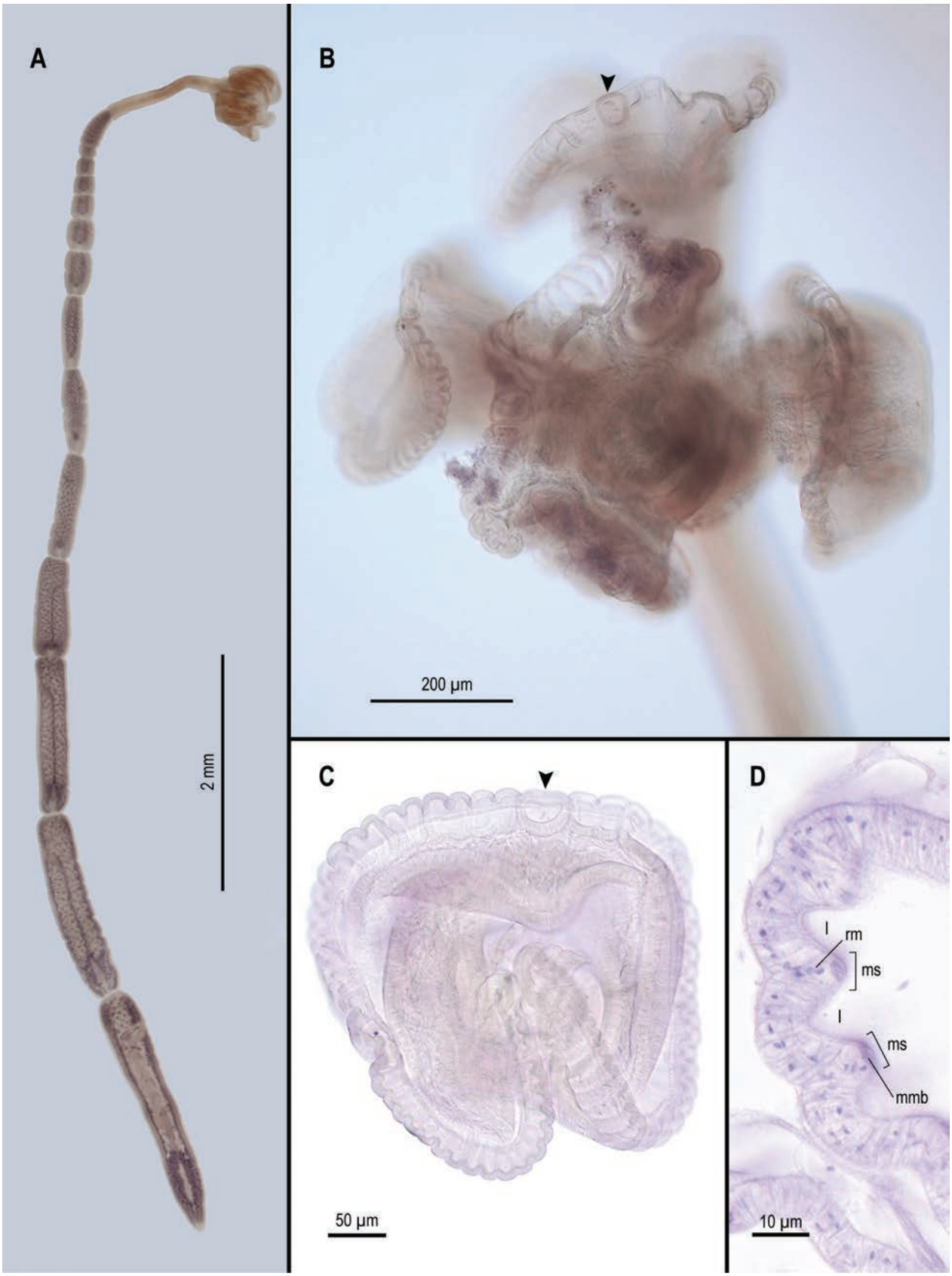

Figure 2. Light micrographs of *Anindobothrium danielae* sp. nov. from *Myliobatis goodei*. **A.** Entire, mature worm (holotype MACN-Pa No. 798); **B.** Scolex (paratype MACN-Pa No. 799/2); **C.** Bothridium (paratype MACN-Pa No. 799/1); **D.** Longitudinal section of bothridium (paratype MACN-Pa No. 800). Abbreviations: l - loculus; mmb - marginal muscle bundles; ms - marginal septum; rm - radial muscle. Arrowhead indicates the apical sucker.

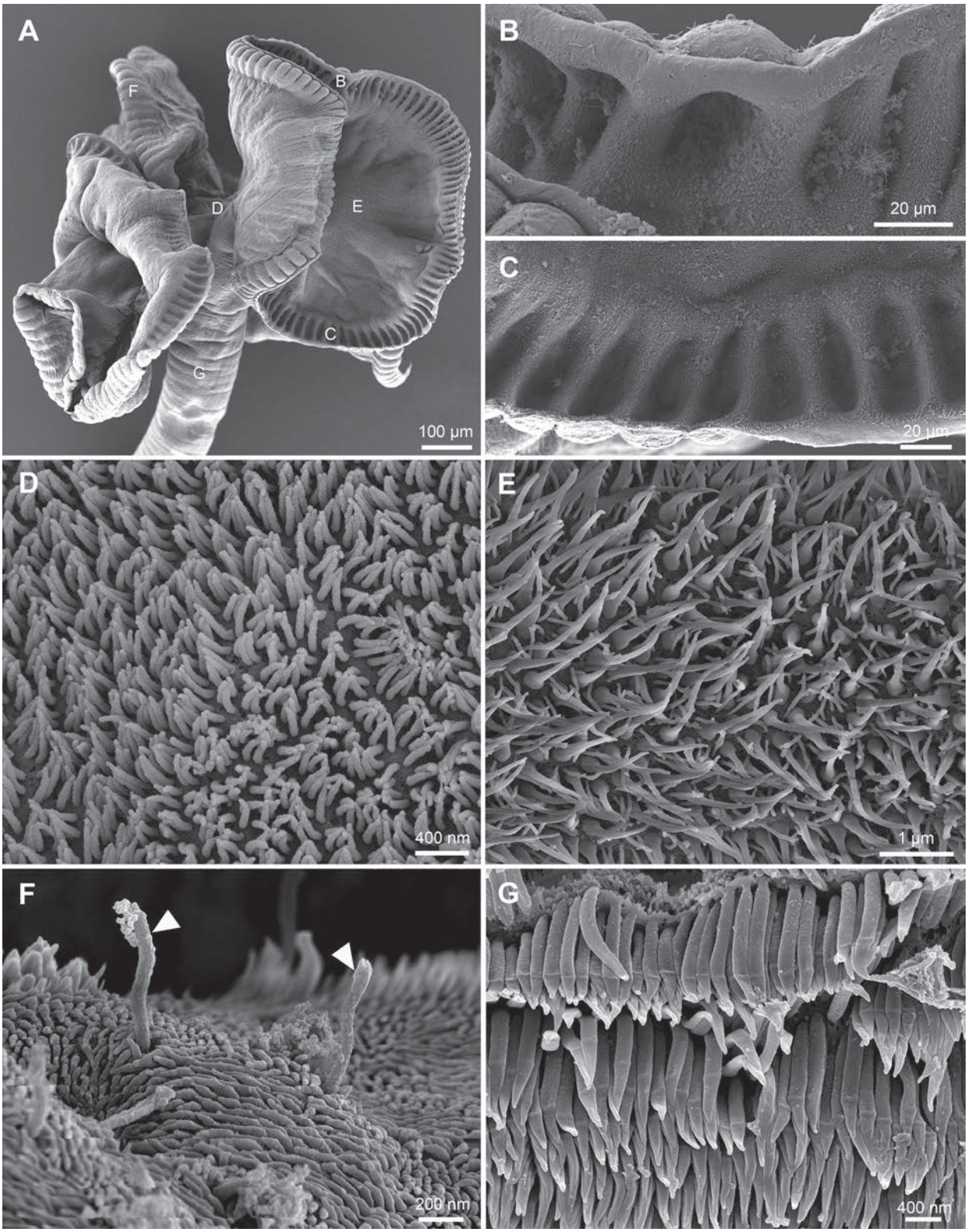

Figure 3. Scanning electron micrographs of *Anindobothrium danielae* sp. nov. from *Myliobatis goodei*. **A.** Scolex, small letters indicate locations of detail shown in **B–G**; **B.** Bothridial apical sucker; **C.** Bothridial marginal loculi; **D.** Detail of apex surface with acicular filitriches; **E.** Detail of distal bothridial surface with capilliform filitriches and coniform spinitriches; **F.** Detail of proximal bothridial surface of marginal loculi with acicular filitriches; arrowheads indicate cilia; **G.** Detail of cephalic peduncle surface with capilliform filitriches.

and 1 ventral pair on each lateral margin of proglottid, dorsal pair larger than ventral pair (Figs 4C, 5A–C).

Host. *Myliobatis goodei* Garman, 1855, Southern eagle ray (Myliobatiformes: Myliobatidae) (type host). Site of infection: spiral intestine. Prevalence of infection: 58% (7 hosts infected out of 12 examined).

Sequence data. GenBank accession numbers PQ346665, PQ346666; 2 hologenophores MACN-Pa No. 801/1-2.

Figure 4. Line drawings of *Anindobothrium danielae* sp. nov. from *Myliobatis goodei*. **A.** Subterminal mature proglottid (holotype MACN-Pa No. 798); **B.** Terminal mature proglottid with sperm-filled vas deferens (holotype MACN-Pa No. 798); **C.** Detail of terminal genitalia of subterminal proglottid, ventral view, (paratype MACN-Pa No. 795/4).

Etymology. This species is named after Daniela Barbieri, the first author's dear friend, in appreciation for her continued support and enthusiasm for science.

Distribution. *Anindobothrium danielae* sp. nov. occurs mainly along coastal waters off Buenos Aires Province, at depths of <100 m in the Warm Temperate SWA Marine Province.

Remarks. *Anindobothrium danielae* sp. nov. can easily be distinguished from *A. anacolum*, *A. carrioni*, and *A. inexpectatum* by the morphology of the bothridia. The new species has orbicular-shaped bothridia without longitudinal and transverse septa, whereas the three congeners exhibit ellipsoid-shaped bothridia with longitudinal and transverse septa (Figs 2C, 3A, 6). *Anindobothrium danielae* sp. nov. is different from *A. anacolum*, *A. carrioni*, *A. inexpectatum*, and *A. lisae* by having more testes per proglottid (76–115 vs. 24–50, 21–31, 23–44, and 30–72, respectively) along with the presence of two rows of testes arranged dorsoventrally instead of one. Furthermore, *A. danielae* sp. nov. possesses similar orbicular-shaped bothridia as *A. lisae* but can be distinguished from the freshwater species by the number of marginal loculi (101–121 vs. 40–58) and ovary length (59–159 vs. 185–450).

Molecular and phylogenetic analysis

The phylogeny obtained in this study placed the two specimens recovered from *M. goodei* as members of the genus *Anindobothrium* (Fig. 7). These specimens were conspecific (no genetic variation) and corresponded to a new species of *Anindobothrium* (Suppl. material 1, Fig. 7).

The genetic distance among 28S sequences varied between 0.00 and 0.31 (Suppl. material 1). Within *Anindobothrium*, there was a large clade, with support of 1.00, constituted by most of the species that comprise the genus (i.e., *A. anacolum*, *A. carrioni*, *A. lisae*, and *A. inexpectatum*), and that parasitize batoids belonging to the family Potamotrygonidae (Fig. 7). The sister taxon of this clade was *A. danielae* sp. nov., with a genetic distance of 0.08 (Suppl. material 1), associated with a new host family for *Anindobothrium* (Myliobatidae) (Fig. 7).

Anindobothrium myliobatidis (Brooks, Mayes & Thorson, 1981), comb. nov.

Fig. 8

Phyllobothrium myliobatidis Brooks, Mayes & Thorson, 1981 (Syn.).

Type material. ***Holotype*** • an entire, mature worm, Río de la Plata estuary near Montevideo, Uruguay, July 1979, T.B. Thorson leg., USNM No. 1371266.

Paratypes • three entire, mature worms, same data as preceding, USNM No. 1371267.

Amended diagnosis. Based on type material (holotype USNM No. 1371266 and 3 paratypes USNM No. 1371267). Worms euapolytic, 10.56–18.48 (14.04 ± 3.67, n = 4) mm long (Fig. 8A), proglottids acraspedote. Scolex 1,012–1,960 (1,385 ± 505, n = 3) long, 1,228–2,015 (1,517 ± 433, n = 3) wide, composed of four stalked bothridia (Fig. 8A, C, E). Bothridia orbicular-shaped, with marginal loculi and anterior apical sucker. Transverse and longitudinal septa absent (Fig. 8C, E). Cephalic peduncle

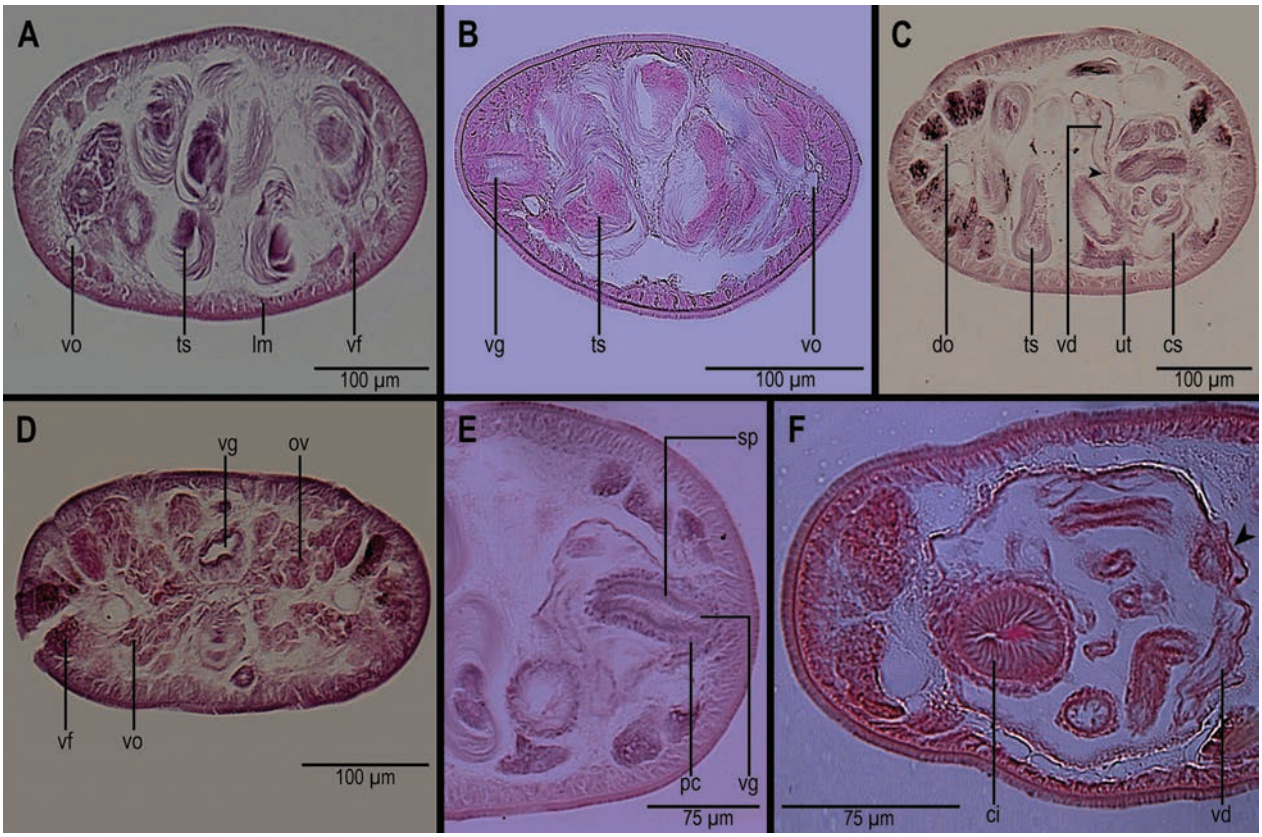

Figure 5. Light micrographs of cross-sections of mature proglottids of *Anindobothrium danielae* sp. nov. from *Myliobatis goodei*. **A.** Testes anterior to the cirrus sac (paratype MACN-Pa No. 799/3); **B.** At the level of the vagina (paratype MACN-Pa No. 799/4); **C.** At the level of the cirrus sac; arrowhead indicates the entrance of the vas deferens to the cirrus sac (paratype MACN-Pa No. 799/3); **D.** At the level of the ovarian isthmus (paratype MACN-Pa No. 799/3); **E.** Detail of the vagina showing vaginal sphincter and pigmented cells (paratype MACN-Pa No. 799/3); **F.** Detail of the cirrus sac showing armed cirrus; arrowhead indicates the entrance of the vas deferens to the cirrus sac (paratype MACN-Pa No. 799/3). Abbreviations: ci -cirrus; cs - cirrus sac; do - dorsal osmoregulatory duct; lm - longitudinal muscle; ov - ovary; pc - pigmented cells; sp - sphincter; ts - testes; ut - uterus; vd - vas deferens; vf - vitelline follicle; vg - vagina; vo - ventral osmoregulatory duct.

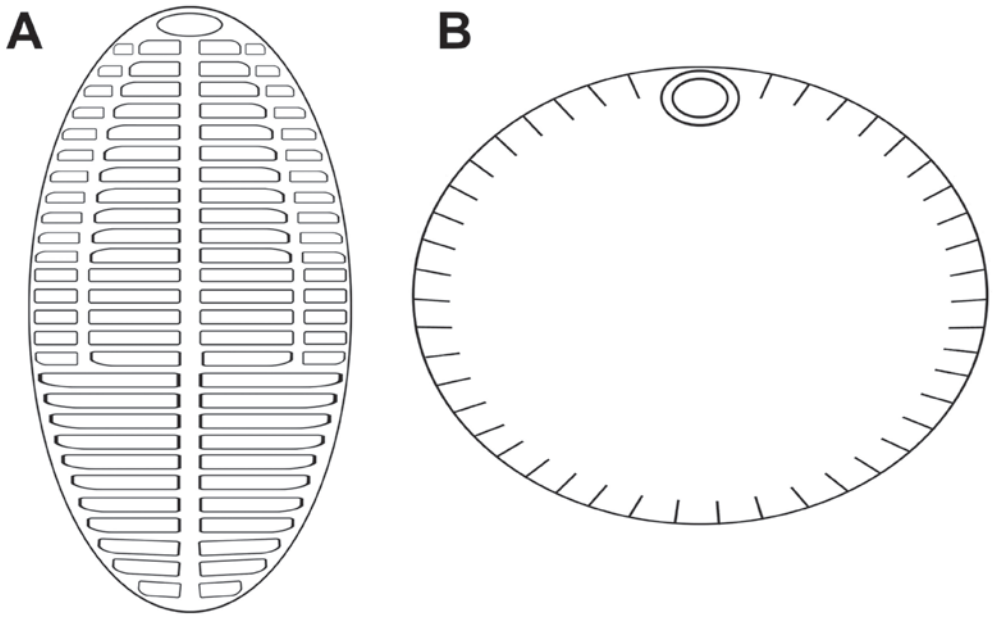

Figure 6. Schematic representation of the bothridia shape in the genus *Anindobothrium*. **A.** Ellipsoid-shaped bothridia, species subset 1: *A. anacolum*, *A. carrioni*, and *A. inexpectatum*; **B.** Orbicular-shaped bothridia, species subset 2: *A. danielae* sp. nov., *A. lisae*, and *A. myliobatidis* comb. nov.

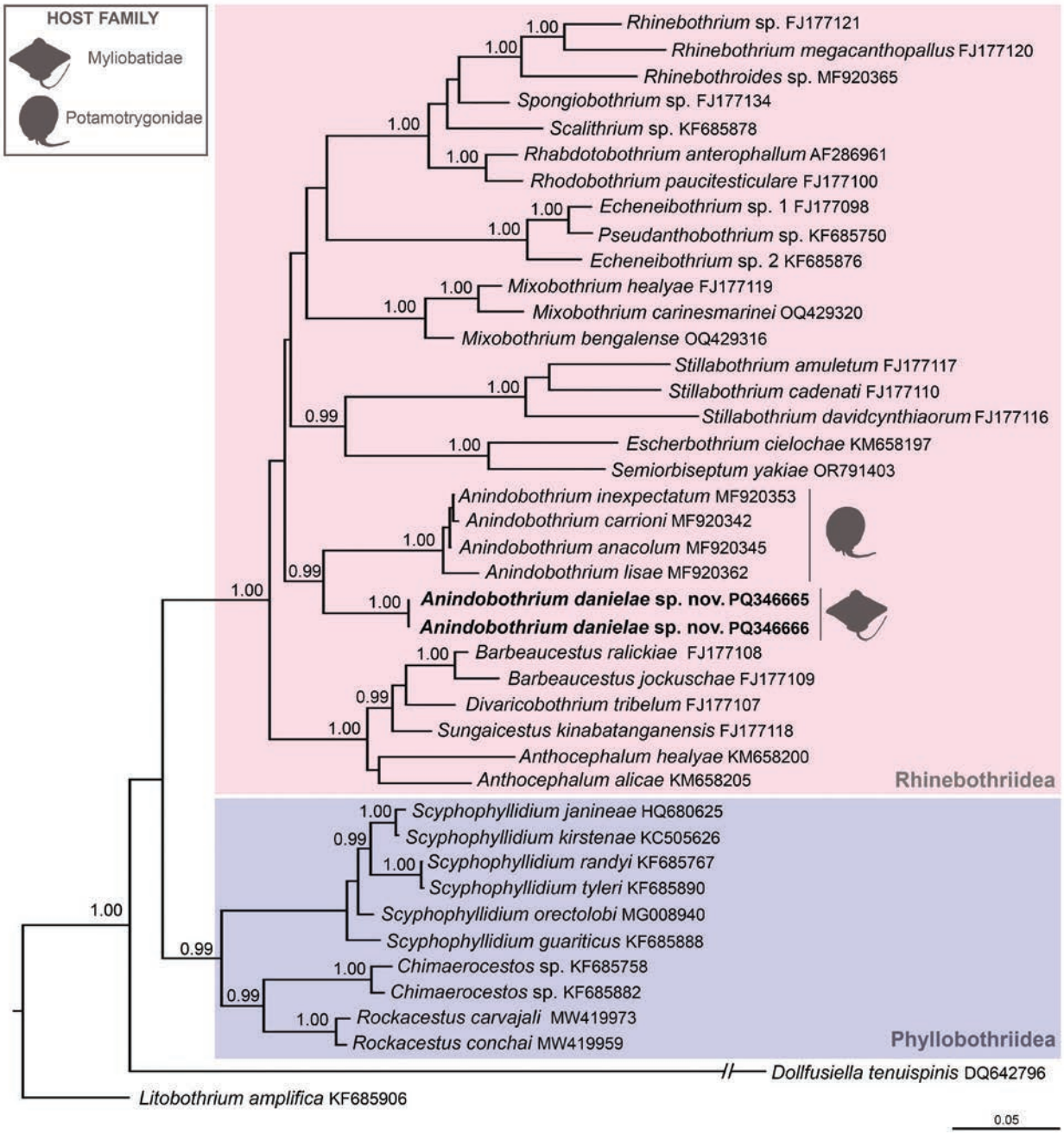

Figure 7. Phylogram resulting from Bayesian inference of the 28S rDNA from the species of cestodes indicated in Table 1. Branch support values indicate posterior probabilities. Taxon labels include cestode species followed by GenBank accession numbers. New sequences are indicated in bold.

present. Immature proglottid, initially wider than long, becoming longer than wide with maturity. Most terminal proglottids and some subterminal proglottids with sperm-filled vas deferens (Fig. 8A, B). Terminal mature proglottids 1,597–2,670 (2,333 ± 564, n = 3) long, 345–412 (387 ± 36, n = 3) wide, length to width ratio 4.6–6.6 (5.7 ± 1.0, n = 3):1. Testes round to oval, arranged anteroposteriorly in several columns, 2 layers deep; each column extending from anterior margin of proglottid reaching anterior margin of ovary (Fig. 8D). Vitellarium follicular; vitelline follicles oval, in 2 dorsal and 2 ventral columns on each lateral margin of proglottid, lateral to testes, extending from near anterior margin of proglottid to posterior margin of proglottid, partly interrupted at level of terminal genitalia, uninterrupted by ovary (Fig. 8A, B, D).

Host. *Myliobatis goodei* Garman, 1855, Southern eagle ray (Myliobatiformes: Myliobatidae). Site of infection: spiral intestine.

Distribution. *Anindobothrium myliobatidis* comb. nov. is known from off the estuary of Río de La Plata near Montevideo, Uruguay, in the Warm Temperate SWA Marine Province.

Remarks. *Phyllobothrium myliobatidis* of Brooks et al. (1981) is herein transferred to *Anindobothrium* on

Figure 8. Light micrographs of *Anindobothrium myliobatidis* comb. nov. from *Myliobatis goodei*. **A.** Entire worm (holotype USNM No. 1371266); **B.** Terminal proglottid (holotype USNM No. 1371266); **C.** Scolex (holotype USNM No. 1371266); arrowhead indicates apical sucker; **D.** Mature proglottid (paratype USNM No. 1371267) showing testes arranged in two layers deep; arrowheads indicate testes in the top layer and circles indicate those in the deeper layer; **E.** Scolex (paratype USNM No. 1371267); arrowhead indicates apical sucker.

the basis of the type material examined in this study. The amended diagnosis includes modifications to accommodate the new observations of the morphological features, such as a scolex consisting of four orbicular-shaped bothridia with marginal loculi and an apical sucker, a terminal proglottid with a sperm-filled vas deferens, a reduced number of testes, and testes distributed in two layers deep (Fig. 8). Additionally, some morphological measurements (i.e., total length of tapeworms, size of the scolex, and terminal proglottids) were provided for the first time. Therefore, *A. myliobatidis* comb. nov. can be distinguished from its congeners as follows: *A. anacolum*, *A. carrioni*,

and *A. inexpectatum* belong to subset 1 by having ellipsoid-shaped bothridia with longitudinal and transverse septa, whereas *A. myliobatidis* comb. nov. belongs to subset 2 by possessing orbicular-shaped bothridia with marginal loculi (Fig. 6A, B). *Anindobothrium myliobatidis* comb. nov. is also different from those three species along with *A. danielae* sp. nov. and *A. lisae* by possessing more proglottids per worm (50–75 vs. 8–33, 20–33, 23–49, 15–39, and 7–24, respectively) and more testes per proglottid (122–150 vs. 24–50, 21–31, 23–44, 76–115, and 30–72, respectively). *Anindobothrium myliobatidis* comb. nov. further differs from *A. danielae* sp. nov. in the number of marginal loculi (83–90 vs. 101–121).

Update of generic diagnosis, valid species, distribution, and hosts of *Anindobothrium*

Worms euapolytic. Ellipsoid-shaped bothridia with longitudinal and transverse septa (species subset 1) (Fig. 6A) or orbicular-shaped bothridia only with marginal loculi (species subset 2) (Fig. 6B). Microtriches on scolex surfaces include filitriches and gladiate or coniform spinitriches. Testes dorsoventrally distributed in 1–2 layers. Terminal proglottid typically with sperm-filled vas deferens. Vaginal sphincter present. Vitelline follicles partly or fully interrupted by terminal genitalia, interrupted or uninterrupted by ovary.

Type species. *Anindobothrium anacolum* (Brooks, 1977).

Additional species. *Anindobothrium carrioni* Trevisan, Primon & Marques, 2017, *Anindobothrium danielae* sp. nov., *Anindobothrium inexpectatum* Trevisan, Primon & Marques, 2017, *Anindobothrium lisae* Marques, Brooks & Lasso, 2001, and *Anindobothrium myliobatidis* (Brooks, Mayes & Thorson, 1981), comb. nov.

Geographic distribution. Marine realms including Tropical Eastern Pacific, Tropical Atlantic, and Temperate South America; also covering freshwater rivers in South America.

Hosts. Stingrays of the families Myliobatidae and Potamotrygonidae.

Discussion

The study of the rhinebothriidean specimens from *Myliobatis* caught along the coast of Argentina has led to the identification of a new species. *Anindobothrium danielae* sp. nov. parasitizes *M. goodei* in waters off Bahía San Blas and other localities off Buenos Aires Province in the SWA. This species is unique in a combination of morphological features, including the bothridial shape and loculi configuration; the number of marginal loculi, proglottids, and testes; and the distribution of testes. In addition, molecular support is also provided to recognize *A. danielae* sp. nov. as a new member of the genus *Anindobothrium*.

The examination of the type material of *A. myliobatidis* comb. nov. allowed us to verify the presence of four stalked orbicular-shaped bothridia, with marginal loculi and apical sucker, and proglottids with sperm-filled vas deferens, among other characters, providing an appropriate generic and ordinal placement for this species from the Southern eagle ray. Previously, Ruhnke (2011) treated this species as *incertae sedis* under the name *P. myliobatidis*, noting that its morphological features were not consistent with the generic diagnosis of *Phyllobothrium* (e.g., bothridia not foliose and posteriorly bifid), and, in fact, he suggested it was potentially a member of *Anthocephalum* Linton, 1890, a genus of the order Rhinebothriidea. The presence of bothridial stalks, marginal loculi, and a posteriorly recurved cirrus sac indicated a potential relationship between *P. myliobatidis* and *Anthocephalum*. However, the genital pore position in the anterior third of the proglottid and the apparent lack of apical sucker raised doubts about the generic placement at the time (Ruhnke 2011).

The presence of *A. danielae* sp. nov. and *A. myliobatidis* comb. nov. in *M. goodei* in the studied area not only allowed us to redefine the diagnosis of *Anindobothrium* but also to extend the geographical distribution of the genus to include coastal waters off Argentina in the SWA.

Morphology

Two subsets of members of *Anindobothrium* can be considered based on the morphology of the bothridia. *Anindobothrium anacolum*, *A. carrioni*, and *A. inexpectatum* have bothridia ellipsoid-shaped (longer than wide) characterized by a distal surface with longitudinal and transverse septa (subset 1), whereas *A. danielae* sp. nov., *A. lisae*, and *A. myliobatidis* comb. nov. are characterized by orbicular-shaped bothridia (wider than long) with only marginal loculi lacking transverse and longitudinal septa (subset 2) (Fig. 6). Additionally, the presence of an apical sucker is only evident in the species belonging to subset 2, in which it is typically rounded in shape and highly muscular, being easily distinguished from the remaining surface of the bothridia. (Figs 2B, C, 3B, 8C, E in this study; see fig. 10A, B in Trevisan et al. 2017).

In contrast, the species of *Anindobothrium* from subset 1, despite being described as having an apical sucker by Trevisan et al. (2017), appear to have an anteriormost loculus rather than an apical sucker *sensu* Caira et al. (1999), who essentially defined these structures based on the shape of their posterior margin, being straight for the first and rounded for the latter. Also, Bueno (2018) considered the apical suckers typically highly muscular and round in shape and the loculi weakly muscular and generally oblong. Thus, *A. carrioni* is, in fact, characterized by an anteriormost loculus as it is weakly muscular and oblong (see fig. 13A in Trevisan et al. 2017), while the remaining species of subset 1 seem to exhibit a weak musculature delimiting an anteriormost loculus (see figs 7A, 11A in Trevisan et al. 2017). Therefore, these two bothridial structures should be defined following objective criteria such as the musculature arrangement or the thickness of the muscular wall, as suggested by Franzese and Ivanov

(2020) and Franzese et al. (2022), given that the shape of the posterior margin in both structures could be altered by fixation and processing methods. It would be important to study the muscular configuration of the anterior portion of the bothridia of the species of *Anindobothrium* to verify if the presence of the anteriormost loculus is only restricted to the species of subset 1 and the apical sucker is only present in species of subset 2.

The detailed study of the muscular morphology of the marginal septa of *A. danielae* sp. nov. is herein presented and is the first to be carried out within the genus. The disposition of the musculature in this type of septa has previously been studied in two species of Rhinebothriidea: *Anthocephalum duszynskii* Ruhnke, 1994, and *Echeneibothrium williamsi* Carvajal & Dailey, 1975 (see Healy 2006a; Franzese et al. 2022). *Anindobothrium danielae* sp. nov. shows the same muscular morphology of the marginal septa and a similar configuration of the marginal loculi than *An. duszynskii* (distal portion of septa with marginal muscle bundles and underlying radial muscles with proximal fibers ending adjacent to each other and small and numerous marginal loculi), differing from *E. williamsi* (distal portion of septa with marginal muscle bundles and underlying parallel radial muscles, and larger and less numerous marginal loculi), making it difficult to know if these loculi are homologous structures among the three species. It would be interesting to study the muscular morphology of the marginal septa among the species of *Anindobothrium* of subset 2, as well as in other rhinebothriideans with similar bothridial configuration, as in the case of members of *Alveobothrium* Boudaya, Neifar & Euzet, 2018, *Anthocephalum*, *Biotobothrium* Tan, Zhou & Yang, 2009, *Cairaeanthus* Kornyushin & Polyakova, 2012, and *Clydonobothrium* Euzet, 1959 (see Franzese and Ivanov 2020).

The tegumental study revealed that *A. danielae* sp. nov. has filitriches covering all the studied surfaces and coniform spinitriches only restricted to the distal bothridial surface. In contrast, in the four species previously described (i.e., *A. anacolum*, *A. carrioni*, *A. inexpectatum*, and *A. lisae*), the proximal surface is covered with both acicular filitriches and gladiate spinitriches. Also, the distal bothridial surface of *A. anacolum*, *A. inexpectatum*, and *A. carrioni* was described by having gladiate spinitriches and filitriches (see Trevisan et al. 2017). However, these species seem to have coniform spinitriches as they are like a cone with round bases (see figs 8F, G, 12F, G, 14F in Trevisan et al. 2017), such as those exhibited by *A. danielae* sp. nov. (see Fig. 3E). Therefore, the scolex surface of *Anindobothrium* is essentially characterized by having filitriches on the entire surface, with gladiate spinitriches covering the proximal bothridial surface and gladiate or coniform spinitriches in the distal bothridial surface.

The surface of the scolex of *A. danielae* sp. nov. also exhibits cilia (Fig. 3F). These structures with sensory functions have been detected in the scolex of several genera of rhinebothriideans including *Anthocephalum*, *Crassuseptum* Eyring, Healy & Reyda, 2012; *Echeneibothrium* van Beneden, 1850; *Rhinebothrium* Linton, 1890; and *Stillabothrium* Healy & Reyda, 2016 (Healy 2006b; Eyring et al. 2012; Reyda et al. 2016; Herzog and Jensen 2018; Franzese et al. 2022). Although Trevisan et al. (2017) did not mention the presence of cilia in any of the species of *Anindobothrium*, the distal bothridial surface of *A. lisae* is covered with spinitriches and cilia (see fig. 10F in Trevisan et al. 2017). Therefore, it would be interesting to verify if the third species of subset 2, *A. myliobatidis* comb. nov., also exhibits the microthrix pattern known so far, with spinitriches, coniform spinitriches, and cilia.

The tapeworms of *Anindobothrium* were considered apolytic by Trevisan et al. (2017), but this term has been used with subtle differences in different works (Franzese and Ivanov 2018). According to Caira et al. (1999), cestodes that retain mature proglottids in the strobila but never gravid proglottids are euapolytic. Since all known species of *Anindobothrium* have strobila with mature terminal proglottids, we consider that the genus is represented by euapolytic tapeworms.

In most species of *Anindobothrium*, the terminal proglottid has a voluminous vas deferens filled with sperm, testes restricted to the anterior portion of the proglottid with most of them already degenerated, and the vitelline follicles increasing in size, thickening the lateral bands, being quite different from the subterminal proglottid (Figs 4A, B). The exception to these observations is *A. lisae*, in which the terminal proglottid exhibits a vas deferens less voluminous and vitelline follicles smaller, delimiting narrower lateral bands, resembling the subterminal proglottid of their congeners.

The testes are arranged dorsoventrally in one layer in most species of *Anindobothrium*, while in *A. danielae* sp. nov. and *A. myliobatidis* comb. nov. they are distributed into two layers (Figs 4A, B, 5A–C, and Fig. 8D, respectively). The presence of a distinct seminal vesicle was included in the diagnosis of the *Anindobothrium* by Marques et al. (2001), but this feature was not mentioned in the amended diagnosis of the genus by Trevisan et al. (2017), not even in any of the species these authors discussed. We could not verify the presence of a seminal vesicle in the type material of *A. myliobatidis* comb. nov. due to the poor magnification of the images, nor was this character mentioned in the original description. So far, *A. danielae* sp. nov. is the only species in which the absence of this structure was effectively verified, based on whole mounts and cross-sections of several proglottids. Therefore, we include the testes arranged in 1–2 layers as a feature of the genus, but we do not consider the presence of a distinct seminal vesicle a diagnostic character of *Anindobothrium*.

Phylogeny

The molecular analysis based on 28S rDNA data unequivocally placed the two specimens recovered from *M. goodei* as members of the genus *Anindobothrium* (Fig. 7). The genetic distances observed concerning the rest of

the species of the genus (Suppl. material 1) have allowed us to corroborate our morphological studies in which we considered these specimens as representatives of a new species of the genus.

Additionally, our phylogenetic hypothesis for *Anindobothrium* mirrors the phylogeny of their hosts (see Naylor et al. 2012), similar to the results of previous studies (Trevisan et al. 2017). However, our results suggest that there was no single codivergence event in the split between marine and freshwater lineages of *Anindobothrium* as proposed by Trevisan et al. (2017). Instead, there probably could have been a previous codivergence event that gave rise to a clade of marine species of *Anindobothrium* present in Myliobatidae and a sister group including marine and freshwater species parasitizing batoids of the family Potamotrygonidae (Fig. 7). Within the latter clade, the same codivergence referred by Trevisan et al. (2017) was observed in the present study, with the only freshwater species (*A. lisae*) as sister to a clade composed of the remaining species of *Anindobothrium* from marine potamotrygonids (i.e., *A. anacolum*, *A. carrioni*, and *A. inexpectatum*) (Fig. 7). However, we could not corroborate the grouping of species by oceans observed by Trevisan et al. (2017) (see fig. 16 in Trevisan et al. 2017), since in our study species distributed in different oceans (i.e., *A. carrioni*, *A. inexpectatum*) appeared as part of the same clade (Fig. 7).

The inclusion of molecular sequences of *A. myliobatidis* comb. nov. in future phylogenetic analyses is needed to verify the codivergence hypothesis proposed in the present study but also to validate the new combination herein considered, which was based on morphological characters only.

Host-parasite association and distribution

Prior to this study, the marine species of *Anindobothrium* were restricted to stingrays of the genus *Styracura*. *Styracura schmardae* (Werner, 1941), registered at the Caribbean Sea in the Tropical Atlantic, was found parasitized by *A. anacolum* and *A. inexpectatum*, whereas *S. pacifica* (Beebe & Tee-Van, 1941) off the Tropical Eastern Pacific was found infected with *A. carrioni*. Therefore, the presence of *A. danielae* sp. nov. and *A. myliobatidis* comb. nov. in the Southern eagle ray from off the Argentinean coast in Temperate South America represents the first report of batoids of the genus *Myliobatis* found parasitized by tapeworms of *Anindobothrium*.

To date, seven species of eagle stingrays of the genus *Myliobatis* have been reported from coastal waters of South America: *M. californica* Gill, 1865; *M. chilensis* Philippi, 1892; *M. longirostris* Apple & Fitch, 1964; and *M. peruvianus* Garman, 1913, from the Pacific; and *M. freminvillei* Lesueur, 1824; *M. goodei*, and *M. ridens* from the Atlantic (Bustamante et al. 2014; Cornejo et al. 2015; Calle-Morán and Béarez 2020; Froese and Pauly 2024). Among them, *M. goodei* hosts the greatest cestode species richness, including diphyllideans, lecanicephalideans, "tetraphyllideans," trypanorhynchs, and the rhinebothriideans herein treated. Although *M. californica*, *M. longirostris*, and *M. freminvillei* have been reported as hosts of cestodes in North America (Mexico and USA) (see Caira et al. 2022), it appears that most species of *Myliobatis* in surrounding South American waters have not been surveyed for tapeworms. Particularly, we have not had the opportunity to study specimens of *M. freminvillei* so far, and only two individuals of *M. ridens* were examined prior to this study (Menoret et al. 2017). Given the great diversity of cestodes found in the Southern eagle ray in the studied area, we estimate that other species of *Myliobatis* can also be suitable hosts for new species of cestodes of the coasts of South America.

Finally, the results obtained in the present study allowed us to increase the number of species of *Anindobothrium* from eight to ten globally and to expand our knowledge of the rhinebothriideans and batoids of the family Myliobatidae association in the Southern Hemisphere.

Acknowledgments

We thank Gustavo Chiaramonte, who made laboratory facilities at the Estación Hidrobiológica Quequén, Museo Argentino de Ciencias Naturales-CONICET, available to us, and Sebastián Polimeni for fishing the Southern eagle rays at Puerto Quequén, Buenos Aires Province, Argentina. We also thank the Consejo Nacional de Investigaciones Científicas y Técnicas (CONICET) for giving us the chance to work on board the research vessel "Puerto Deseado." Special thanks are due to Anna Phillips from the Smithsonian National Museum of Natural History—Department of Invertebrate Zoology, Washington, D.C., USA, for providing us with digital micrographs of type material. This work was supported by the Consejo Nacional de Investigaciones Científicas y Técnicas (CONICET) [grant numbers PIP 11220200101713CO, PIP 11220210100134CO] and Fondo para la Investigación Científica y Tecnológica (FONCyT) [grant numbers PICT-2021-I-INVI-00341, PICT-2020-SERIE A-01531, PICT-2020-SERIE A-00660, PICT-2016-3672]. This study was conducted under collecting permits No. 39 and No. 260 from the Dirección Provincial de Pesca-Ministerio de Asuntos Agrarios de la Provincia de Buenos Aires, Argentina.

References

Brooks DR, Mayes MA, Thorson TB (1981) Cestode parasites in *Myliobatis goodei* Garman (Myliobatiformes, Myliobatidae) from Río de la Plata, Uruguay, with a summary of cestodes collected from South American elasmobranchs during 1975–1979. Proceedings of the Biological Society of Washington 93: 239–1252. https://biostor.org/reference/73890

Bueno VM (2018) Skate tapeworms revisited: a modern approach. Doctoral Dissertation, University of Connecticut, Storrs, USA.

Bustamante C, Vargas-Caro C, Bennett MB (2014) Biogeographic patterns in the cartilaginous fauna (Pisces, Elasmobranchii and Holocephali) in the southeast Pacific Ocean. PeerJ 2: e416. https://doi.org/10.7717/peerj.416

Caira JN, Jensen K, Healy CJ (1999) On the phylogenetic relationships among tetraphyllidean, lecanicephalidean and diphyllidean tapeworm genera. Systematic Parasitology 42: 77–151. https://doi.org/10.1023/A:1006192603349

Caira JN, Jensen K, Waeschenbach A, Olson PD, Littlewood DTJ (2014) Orders out of chaos–molecular phylogenetics reveals the complexity of shark and stingray tapeworm relationships. International Journal for Parasitology 44: 55–73. https://doi.org/10.1016/j.ijpara.2013.10.004

Caira JN, Bueno V, Jensen K (2021) Emerging global novelty in phyllobothriidean tapeworms (Cestoda, Phyllobothriidea) from sharks and skates (Elasmobranchii). Zoological Journal of the Linnean Society 193: 1336–1363. https://doi.org/10.1093/zoolinnean/zlaa185

Caira JN, Jensen K, Barbeau E (2022) Global cestode database, v.2022. https://tapewormdb.uconn.edu

Calle-Morán MD, Béarez P (2020) Updated checklist of marine cartilaginous fishes from continental and insular Ecuador (Tropical Eastern Pacific Ocean). Cybium 44: 239–250. https://doi.org/10.26028/cybium/2020-443-004

Chervy L (2009) Unified terminology for cestode microtriches: a proposal from the international workshops on cestode systematics in 2002–2008. Folia Parasitologica 56: 199–230. https://doi.org/10.14411/fp.2009.025

Cornejo R, Vélez-Zuazo X, González-Pestana A, Kouri C, Mucientes G (2015) An updated checklist of chondrichthyes from the southeast Pacific off Peru. Check List 11: 1809–1809. https://doi.org/10.15560/11.6.1809

Cutmore SC, Theiss SM, Bennett MB (2011) A new phyllobothriid genus and species from the snaggletooth shark, *Hemipristis elongata* (Carcharhiniformes, Hemigaleidae), from Moreton Bay, Australia. Folia Parasitologica 58: 187–196. https://doi.org/10.14411/fp.2011.019

Cutmore SC, Bennett MB, Miller TL, Cribb TH (2017) Patterns of specificity and diversity in species of *Paraorygmatobothrium* Ruhnke, 1994 (Cestoda, Phyllobothriidae) in Moreton Bay, Queensland, Australia, with the description of four new species. Systematic Parasitology 94: 941–970. https://doi.org/10.1007/s11230-017-9759-8

Darriba D, Taboada GL, Doallo R, Posada DJ (2012) JModelTest 2: more models, new heuristics and parallel computing. Nature Methods 9: 772. https://doi.org/10.1038/nmeth.2109

Diepenbroek M, Grobe H, Reinke M, Schindler U, Schlitzer R, Sieger R, Wefer G (2002): PANGAEA – An information system for environmental sciences. Computers & Geosciences 28: 1201–1210. https://doi.org/10.1016/S0098-3004(02)00039-0

Eyring K, Healy CJ, Reyda FB (2012) A new genus and species of cestode (Rhinebothriidea) from *Mobula kuhlii* (Rajiformes, Mobulidae) from Malaysian Borneo. Journal of Parasitology 98: 584–591. https://doi.org/10.1645/GE-2913.1

Fontenelle JP, Marques FPL, Kolmann MA, Lovejoy NR (2021) Biogeography of the neotropical freshwater stingrays (Myliobatiformes, Potamotrygoninae) reveals effects of continent scale paleogeographic change and drainage evolution. Journal of Biogeography 48: 1406–1419. https://doi.org/10.1111/jbi.14086

Franzese S, Ivanov VA (2018) Hyperapolytic species of *Acanthobothrium* (Cestoda, Onchoproteocephalidea) from batoids off Argentina. Parasitology International 67: 431–443. https://doi.org/10.1016/j.parint.2018.04.001

Franzese S, Ivanov VA (2020) A new genus of Rhinebothriidea from species of *Psammobatis* (Rajiformes, Arhynchobatidae) off Argentina. Zootaxa 4803: 355–372. https://doi.org/10.11646/zootaxa.4803.2.7

Franzese S, Mutti LD, Tropea C, Ivanov VA (2022) Morphological study of members of the genus *Echeneibothrium* (Cestoda, Rhinebothriidea, Echeneibothriidae) from rajiform skates of the Argentine Sea and analysis of the phylogenetic relationships within the family Echeneibothriidae. Zoologischer Anzeiger 299: 1–20. https://doi.org/10.1016/j.jcz.2022.05.002

Franzese S, García Facal G, Menoret A (2023) Tapeworms (Platyhelminthes, Cestoda) from marine chondrichthyans of the Southwestern Atlantic Ocean, and the sub-Antarctic and Antarctic islands: a checklist. ZooKeys 1163: 78–119. https://doi.org/10.3897/zookeys.1163.100485

Franzese S, Montes MM, Shimabukuro MI, Arredondo NJ (2024) Description of a new genus of Escherbothriidae (Cestoda: Rhinebothriidea) in species of *Sympterygia* (Rajiformes, Arhynchobatidae) from South America based on morphological and molecular evidence, with an amended diagnosis of the family. Zoologischer Anzeiger 308: 35–47. https://doi.org/10.1016/j.jcz.2023.11.002

Froese R, Pauly D (2024) FishBase. World Wide Web electronic publication. http://www.fishbase.org [Accessed 1 September 2023]

Healy CJ (2006a) A revision of selected Tetraphyllidea (Cestoda): *Caulobothrium*, *Rhabdotobothrium*, *Rhinebothrium*, *Scalithrium*, and *Spongiobothrium*. Doctoral Dissertation, University of Connecticut, Storrs, USA.

Healy CJ (2006b) Three new species of *Rhinebothrium* (Cestoda, Tetraphyllidea) from the freshwater whipray, *Himantura chaophraya*, in Malaysian Borneo. Journal of Parasitology 92: 364–374. https://doi.org/10.1645/GE-560R.1

Healy CJ, Caira JN, Jensen K, Webster BL, Littlewood DT (2009) Proposal for a new tapeworm order, Rhinebothriidea. International Journal for Parasitology 39: 497–511. https://doi.org/10.1016/j.ijpara.2008.09.002

Herzog KS, Jensen K (2018) Five new species of the tapeworm genus *Anthocephalum* (Rhinebothriidea, Anthocephaliidae) parasitizing a single species of indo-pacific stingray and a revised diagnosis of the genus. Journal of Parasitology 104: 505–522. https://doi.org/10.1645/18-53

Herzog KS, Caira JN, Kar PK, Jensen K (2023) Novelty and phylogenetic affinities of a new family of tapeworms (Cestoda, Rhinebothriidea) from endangered sawfish and guitarfish. International Journal for Parasitology 53: 347–362. https://doi.org/10.1016/j.ijpara.2023.02.007

Katoh K, Rozewicki J, Yamada KD (2019) MAFFT online service: multiple sequence alignment, interactive sequence choice and visualization. Briefings in Bioinformatics 20: 1160–1166. https://doi.org/10.1093/bib/bbx108

Kumar S, Stecher G, Li M (2018) Mega X: molecular evolutionary genetics analysis across computing platforms. Molecular Biology and Evolution 35: 1547–1549. https://doi.org/10.1093/molbev/msy096

Marques FP, Brooks DR, Lasso CA (2001) *Anindobothrium* n. gen. (Eucestoda, Tetraphyllidea) inhabiting marine and freshwater potamotrygonid stingrays. Journal of Parasitology 87: 666–672. https://doi.org/10.1645/0022-3395(2001)087[0666:ANGETI]2.0.CO;2

Menoret A, Mutti LD, Ivanov VA (2017) New species of *Aberrapex* Jensen, 2001 (Cestoda, Lecanicephalidea) from eagle rays of the genus *Myliobatis* Cuvier (Myliobatiformes, Myliobatidae) from off Argentina. Folia Parasitologica 64: 009. https://doi.org/10.14411/fp.2017.009

Naylor GJP, Caira JN, Jensen K, Rosana KAM, Straube N, Lakner C (2012) Elasmobranch phylogeny: a mitochondrial estimate based on 595 species. In: Carrier JC, Musick JA, Heithaus MR (Eds) Biology of Sharks and Their Relatives. CRC Press, Taylor & Francis Group, Florida, 31–56. https://doi.org/10.1201/b11867-4

Olson PD, Littlewood DTJ, Bray RA, Mariaux J (2001) Interrelationships and evolution of the tapeworms (Platyhelminthes, Cestoda). Molecular Phylogenetics and Evolution 19: 443–467. https://doi.org/10.1006/mpev.2001.0930

Olson PD, Cribb TH, Tkach VV, Bray RA, Littlewood DTJ (2003) Phylogeny and classification of the Digenea (Platyhelminthes, Trematoda). International Journal for Parasitology 33: 733–755. https://doi.org/10.1016/S0020-7519(03)00049-3

Olson PD, Caira JN, Jensen K, Overstreet RM, Palm HW, Beveridge I (2010) Evolution of the trypanorhynch tapeworms: parasite phylogeny supports independent lineages of sharks and rays. International Journal for Parasitology 40: 223–242. https://doi.org/10.1016/j.ijpara.2009.07.012

Rambaut A (2014) FigTree v1.4.4. (version 1.4.4) [software]. http://tree.bio.ed.ac.uk

Reyda FB, Healy CJ, Haslach AR, Ruhnke TR, Aprill TL, Bergman MP, Daigler AL, Dedrick EA, Delgado I, Forti KS, Herzog KS, Russel RS, Willsey DD (2016) A new genus of rhinebothriidean cestodes from batoid elasmobranchs, with the description of five new species and two new combinations. Folia Parasitologica 63: 038. https://doi.org/10.14411/fp.2016.038.

Ronquist F, Teslenkovan M, van der Mark P, Ayres DL, Darling A, Hönna S, Larget B, Liu L, Suchard MA, Huelsenbeck JP (2012) MrBayes 3.2: efficient Bayesian phylogenetic inference and model choice across large model space. Systematic Biology 61: 539–542. https://doi.org/10.1093/sysbio/sys029

Ruhnke TR (2011) Tapeworms of Elasmobranchs (Part III): A monograph on the Phyllobothriidae. Bulletin of the University of Nebraska State Museum, Lincoln, 208 pp.

Ruhnke TR, Workman RE (2013) Two new species and a new phyllobothriid cestode genus from sharks of the genus *Negaprion* Whitley (Carcharhiniformes). Systematic Parasitology 85: 37–48. https://doi.org/10.1007/s11230-013-9411-1.

Ruhnke TR, Caira JN, Cox A (2015) The cestode order Rhinebothriidea no longer family-less: a molecular phylogenetic investigation with erection of two new families and description of eight new species of *Anthocephalum*. Zootaxa 3904: 51–81. https://doi.org/10.11646/zootaxa.3904.1.3

Spalding MD, Fox HE, Allen GR, Davidson N, Ferdaña ZA, Finlayson M, Halpern BS, Jorge MA, Lombana A, Lourie SA, Martin KD, McManus E, Molnar J, Recchia CA, Robertson J (2007) Marine ecoregions of the world: a bioregionalization of coastal and shelf areas. BioScience 57: 573–583. https://doi.org/10.1641/B570707

Talavera G, Castresana J (2007) Improvement of phylogenies after removing divergent and ambiguously aligned blocks from protein sequence alignments. Systematic Biology 56: 564–577. https://doi.org/10.1080/10635150701472164

Trevisan B, Primon JF, Marques FP (2017) Systematics and diversification of *Anindobothrium* Marques, F. Brooks & Lasso, 2001 (Eucestoda, Rhinebothriidea). PLOS ONE 12: e0184632. https://doi.org/10.1371/journal.pone.0184632

Supplementary material 1

Genetic divergence estimated through uncorrected p-distance of the 28S rDNA

Authors: Guillermina García Facal, Sebastián Franzese, Martín Miguel Montes, Adriana Menoret

Data type: xlsx

Link: https://doi.org/10.3897/zse.100.131971.suppl1

Zoosyst. Evol. 100 (4) 2024, 1419–1429 | DOI 10.3897/zse.100.135217

PENSOFT

MUSEUM FÜR NATURKUNDE BERLIN

Molecular phylogeny reveals a new genus and species of freshwater mussel (Bivalvia, Unionidae, Gonideinae) from Jiangxi, China

Yu-Ting Dai[1], Zhong-Guang Chen[1], Yu-Zhuo Cheng[1], Xiao-Chen Huang[1], Shan Ouyang[1], Feng-Yue Shu[2], Xiao-Ping Wu[1]

1 *School of Life Sciences, Nanchang University, Nanchang 330031, China*

2 *College of Life Sciences, Qufu Normal University, Qufu 273165, China*

https://zoobank.org/6BD143C1-F9E5-4685-9B80-857CDDB788AD

Corresponding authors: Feng-Yue Shu (shfyue01@163.com); Xiao-Ping Wu (xpwu@ncu.edu.cn)

Academic editor: Matthias Glaubrecht ♦ **Received** 21 August 2024 ♦ **Accepted** 1 October 2024 ♦ **Published** 22 October 2024

Abstract

Freshwater mussels of the tribe Gonideini (Bivalvia: Unionidae: Gonideinae) constitute one of the most taxonomically diverse groups and serve as keystone species in riverine and lacustrine ecosystems across East Asia. A new genus and species of Gonideini (Bivalvia: Unionidae) is described from Jiangxi, China, as *Pseudopostolata angula* **gen. et sp. nov.** based on an integrative analysis of shell morphology and molecular data. The validity of the new genus and species is supported by distinct conchological features: a short, rounded anterior; a long, wide posterior; a slightly downward-curved dorsal margin; and a distinctly obtuse angle at the center of the posterior margin. The multi-locus (*COI* + *16S* rRNA + *28S* rRNA) phylogeny showed that the species formed a monophyletic group in the tribe Gonideini of the subfamily Gonideinae. *Pseudopostolata angula* **gen. et sp. nov.** is identified as the sister group to a clade comprising the genera *Postolata*, *Cosmopseudodon*, *Obovalis*, *Ptychorhynchus*, *Parvasolenaia*, and *Koreosolenaia*. We emphasize the significant morphological convergence in freshwater mussels, particularly within Gonideini, highlighting the necessity of an integrated taxonomic approach for accurate generic classification of this group.

Key Words

Gonideini, molecular systematics, morphological characters, taxonomy

Introduction

The Unionida, a group of freshwater mussels, is the most species-diverse among the freshwater bivalve, comprising approximately 192 genera and 958 of the more than 1,200 existing species (Graf and Cummings 2021). North America, as well as eastern and southeastern Asia, represent two major hotspots of unionid bivalve diversity (Haag 2012; Zieritz et al. 2018). Recent research efforts have concentrated on the Unionida fauna of China, encompassing extensive specimen collection and DNA sequencing. These endeavors have led to a notable expansion in the documented diversity of Unionida species in the region, along with the identification of numerous new taxa (Wu et al. 2022, 2023, 2024; Chen et al. 2023; Dai et al. 2023, 2024a, 2024b; Liu et al. 2024). The majority of these taxonomic changes were from Southern China. This indicates that the diversity of species in South China may be significantly underestimated, particularly in creeks that have not been previously studied (Dai et al. 2023). Many freshwater mussel populations have rapidly declined because of different factors such as pollution, water quality degradation, habitat destruction or alteration, and invasive species (Haag 2012; Aldridge et al. 2022; Sousa et al. 2022). Consequently, research and conservation efforts for this community are receiving greater attention, underscoring the imperative to describe species diversity and systematics in previously unstudied areas (Huang et al. 2019; Chen et al. 2023; Dai et al. 2023; Zieritz et al. 2024).

Gonideini Ortmann, 1916, within the subfamily Gonideinae of the family Unionidae, represents one of the most taxonomically diverse groups of freshwater mussels in East Asia. At least 12 genera of 33 valid species are recognized, with more than half distributed in China (MUSSEL Project Database, see http://mussel-project.uwsp.edu/). Notably, *Postolata* Dai, Huang, Guo & Wu, 2023 is endemic to China. Gonideini species are distinguished by their trapezoidal to rectangular shells, the absence or presence of only vestigial hinge teeth, and a tetragenous brooding type (Lopes-Lima et al. 2017; Froufe et al. 2020). Nevertheless, the shell morphology exhibits significant phenotypic plasticity and convergence, making it difficult to classify based solely on morphological traits reliably (Zieritz and Aldride 2009; Inoue et al. 2013). This is particularly pronounced in Gonideini. In the tribe Gonideini, the four species of the genus *Sinosolenaia*, except *Sinosolenaia carinata* (Heude, 1877), exhibit a high degree of convergence. Moreover, the morphology of *Ptychorhynchus* Simpson, 1900, *Postolata* Dai, Huang, Guo, and Wu, and *Obovalis* Simpson, 1900, displays notable similarities (Dai et al. 2023). An integrative approach, encompassing both morphological and molecular characterization, is a relatively straightforward and precise method for classifying freshwater mussels (Smith et al. 2019; Bolotov et al. 2020a, 2023).

In the present study, we found a unique freshwater mussel species from Wujiang River, Ji'an City, China. Morphological and molecular evidence supported these loach specimens as a new genus and a new species in the tribe Gonideini of the subfamily Gonideinae. Hence, the new genus and species *Pseudopostolata angula* gen. et sp. nov. are described herein. Furthermore, the phylogenetic relationships within Gonideini are discussed.

Materials and methods

Specimen sampling, identification, and deposition

In December 2023, eight specimens were collected from the Wujiang River (27°03'37"N, 115°42'17"E) in Ji'an City, Jiangxi Province, China (Figs 1, 2, 4). A digital vernier caliper with an accuracy of ± 0.01 mm was used to measure the length, height, and width of the type series for the new taxa. Live specimens were euthanized with 100% ethanol and then separated into soft tissue and shell. The adductor muscle was used for DNA extraction, while the remaining soft tissue was preserved at −80 °C. All voucher specimens were deposited in the Museum of Biology, Nanchang University (NCUMB), China.

Molecular phylogenetic analyses

The Qiagen Genomic DNA Kit (Qiagen, Hilden, Germany) was employed to extract total genomic DNA from the excised tissue following the instructions provided by the manufacturer. The quality and concentration of the DNA were checked on 1% agarose gel electrophoresis and NanoDrop 2000 (Thermo Scientific, USA).

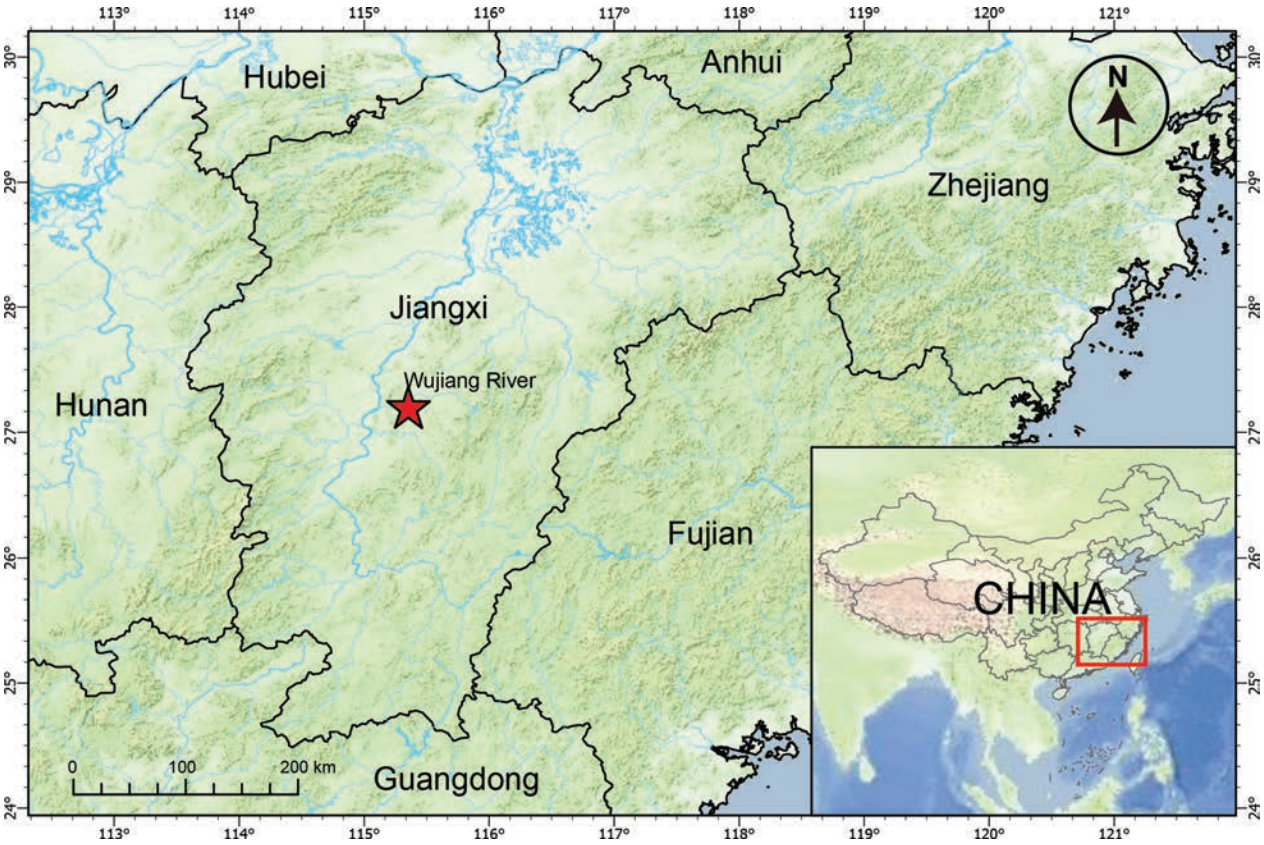

Figure 1. Distribution map of *Pseudopostolata angula* gen. et sp. nov.

Figure 2. The type locality and shell morphology of *Pseudopostolata angula* gen. et sp. nov. **A, B.** General view of the type locality, Wujiang River, Ji'an City, Jiangxi Province, China; **C, D.** Shell morphology of *Pseudopostolata angula*.

We amplified and sequenced fragments from the mitochondrial cytochrome c oxidase subunit-I gene (*COI*) (LCO22me2 + HCO700dy2) (Walker et al. 2007), *16S* small ribosomal RNA gene (*16S*) (16sar-L-myt + 16sbr-H-myt) (Bolotov et al. 2018), and nuclear *28S* ribosomal RNA gene (*28S*) (D23F + D4RB) (Park and Foighil 2000). The polymerase chain reaction (PCR) was conducted using a 25 µL mixture of 2 × Taq Plus Master MixII (Vazyme, China) (12.5 µL), ddH2O (9.5 µL), 10 µM primers (1 µL each), and genomic DNA (1 µL, about 100 ng/µL). Thermal cycling was started at 98 °C for 10 s, followed by 35 cycles of 94 °C for 1 min, annealing at 50 °C for 1 min, extension at 72 °C for 1 min, and then a final extension at 72 °C for 7 min. The PCR products were sequenced commercially by Sangon Biotech (Shanghai, China). The newly obtained sequences have been deposited in GenBank (Tables 1, 2).

Two datasets were constructed in this study: (i) the *COI* dataset (46 sequences; 600 bp) (Table 1); (ii) the three-gene dataset (containing *COI*, *16S*, and 28S; 60 sequences; 1,482 bp) (Table 2).

Table 1. List of sequences used in genetic distances (*, sequenced in this study).

Species	*COI* GenBank accession no.	Locality
Pseudopostolata angula **gen. et sp. nov.**	PQ189757*	China: Jiangxi, Ji'an, Wujiang River
Pseudopostolata angula **gen. et sp. nov.**	PQ189758*	China: Jiangxi, Ji'an, Wujiang River
Obovalis omiensis	MT020684	Japan
Obovalis omiensis	LC518995	Japan: Gifu
Obovalis omiensis	LC518996	Japan: Kyoto
Obovalis omiensis	LC518997	Japan: Shiga
Ptychorhynchus pfisteri	MG463036	China: Jiangxi, Gan River
Ptychorhynchus pfisteri	MG463034	China: Jiangxi, Gan River
Ptychorhynchus pfisteri	MG463035	China: Hunan, Xiangyin
Ptychorhynchus pfisteri	MG933729	Dongting Lake, China
Ptychorhynchus pfisteri	MG933730	Dongting Lake, China
Ptychorhynchus pfisteri	KY067440	China
Parvasolenaia rivularis	MG463100	China: Jiangxi, Gan River
Parvasolenaia rivularis	MG463101	China: Jiangxi, Gan River
Parvasolenaia rivularis	MG463098	China: Jiangxi, Gan River
Parvasolenaia rivularis	MG463103	China: Jiangxi, Gan River
Parvasolenaia rivularis	MG463102	China: Jiangxi, Gan River
Parvasolenaia rivularis	MG463099	China: Jiangxi, Gan River
Parvasolenaia rivularis	MG463104	China: Jiangxi, Gan River
Koreosolenaia sitgyensis	MT020682	South Korea
Koreosolenaia sitgyensis	MT020683	South Korea
Postolata guangxiensis	OP009379	China: Guangxi, Guilin, Luo Qing River
Postolata guangxiensis	OP009380	China: Guangxi, Guilin, Luo Qing River
Postolata guangxiensis	OP009381	China: Guangxi, Guilin, Luo Qing River
Postolata guangxiensis	OP009382	China: Guangxi, Guilin, Luo Qing River
Postolata guangxiensis	OP009383	China: Guangxi, Guilin, Luo Qing River
Postolata guangxiensis	OP009384	China: Guangxi, Guilin, Luo Qing River
Postolata guangxiensis	OP009385	China: Guangxi, Guilin, Luo Qing River
Postolata longjiangensis	PP786557*	China: Guangxi, Hechi, Longjiang River
Postolata longjiangensis	PP786557*	China: Guangxi, Hechi, Longjiang River
Cosmopseudodon wenshanensis	PP079444	China: Yunnan, Wenshan, Panlong River
Cosmopseudodon wenshanensis	PP079445	China: Yunnan, Wenshan, Panlong River
Cosmopseudodon wenshanensis	PP079446	China: Yunnan, Wenshan, Panlong River
Cosmopseudodon wenshanensis	PP079447	China: Yunnan, Wenshan, Panlong River
Cosmopseudodon wenshanensis	PP079448	China: Yunnan, Wenshan, Panlong River
Cosmopseudodon wenshanensis	PP079449	China: Yunnan, Wenshan, Panlong River
Cosmopseudodon wenshanensis	PP079450	China: Yunnan, Wenshan, Panlong River
Cosmopseudodon wenshanensis	PP079451	China: Yunnan, Wenshan, Panlong River
Cosmopseudodon resupinatus	PP079436	China: Guangxi, Hechi, Taohua River
Cosmopseudodon resupinatus	PP079437	China: Guangxi, Hechi, Taohua River
Cosmopseudodon resupinatus	PP079438	China: Guangxi, Hechi, Taohua River
Cosmopseudodon resupinatus	PP079439	China: Guangxi, Hechi, Taohua River
Cosmopseudodon resupinatus	PP079440	*China: Guangxi, Hechi, Taohua River*
Cosmopseudodon resupinatus	PP079441	*China: Guangxi, Hechi, Taohua River*
Cosmopseudodon resupinatus	PP079442	*China: Guangxi, Hechi, Taohua River*
Cosmopseudodon resupinatus	PP079443	*China: Guangxi, Hechi, Taohua River*

The *COI* sequences were codon-aligned by MUSCLE ver. 3.6 (Edgar 2004) implemented in MEGA ver. 10.1.6 (Kumar et al. 2018), whereas *16S* rRNA and *28S* rRNA were aligned in MAFFT ver. 7 (Katoh et al. 2019) using the Q-INS-i algorithm. We used Gblocks ver. 0.91b (Castresana 2000) to exclude ambiguous areas of the alignment for each gene. DnaSP ver. 6 (Rozas et al. 2017) was used to calculate the number of haplotypes. The best-fit model for each gene and gene partition was calculated by PartitionFinder2 ver. 2.3.4 (Lanfear et al. 2017), based on the corrected Akaike Information Criterion (AICc) and using a heuristic search algorithm. The program proposed the division of the concatenated dataset into four partitions, comprising partitions for the *16S* and *28S* genes and each of the three codon positions of the *COI* gene. The best-fit model was determined to be GTR + I + G for the first and second codon positions of *COI*, as well as for *16S* and *28S*, while GTR + G was selected for the third position of *COI*.

Inter- and intra-specific distances based on the *COI* dataset were calculated in MEGA X using the uncorrected *p*-distance. Standard error estimates were obtained by 1000 bootstrapping replicates.

Maximum likelihood (ML) analyses were performed in raxmlGUI ver. 2.0 (Edler et al. 2020) with the ML + rapid bootstrapping method and 1000 replicates. Bayesian inference (BI) analyses were conducted in MrBayes ver. 3.2.6 (Ronquist et al. 2012). Four simultaneous runs with four independent Markov Chain Monte Carlo (MCMC) were implemented for 10 million generations, and trees were sampled every 1000 generations with a burn-in of 25%. The convergence was checked with the average standard deviation of split frequencies < 0.01 and the potential scale reduction factor (PSRF) ~ 1.

Results

Phylogenetic analyses

A total of two *COI* haplotypes, one *16S* haplotype, and two *28S* haplotypes were identified in the eight sequenced specimens from Ji'an, Jiangxi. The *COI* dataset had an aligned length of 600 characters, with 164 variable sites and 162 parsimony informative sites. After trimming and concatenation, the three-gene dataset consisted of 1,482 characters, including 603 bp from *COI*, 467 bp from *16S*, and 412 bp from *28S*. This combined dataset contained 600 variable sites and 538 parsimony-informative sites.

The ML and BI trees based on the three-gene dataset exhibited largely congruent topologies, except for the phylogenetic relationships within Lamprotulini (Fig. 3). Both the ML and BI trees display a node with polytomies in the tribe Gonideini due to low nodal support. In our multilocus phylogenetic analysis, all eight recognized tribes within the subfamily Gonideinae were recovered as monophyletic groups. Specimens from Jiangxi formed a robust monophyletic clade (BS/BPP = 97/1.00) in the tribe Gonideini that did not belong to any previously known species or

Table 2. List of sequences used in multi-locus phylogenetic analyses (*, sequenced in this study).

Taxon	*COI*	*16S* rRNA	*28S* rRNA
UNIONIDAE Rafinesque, 1820			
Gonodeinae Ortmann, 1916			
Gonideini Ortmann, 1916			
Obovalis omiensis	MT020684	LC223994	MT020830
Obovalis omiensis	LC518995	LC223994	MT020830
Obovalis omiensis	LC518996	LC223995	LC519064
Obovalis omiensis	LC518997	LC519045	LC519065
Ptychorhynchus pfisteri	MG463036	KY067440	MG595564
Ptychorhynchus pfisteri	MG463034	KY067440	MG595563
Ptychorhynchus pfisteri	MG463035	KY067440	MG595562
Parvasolenaia rivularis	MG463100	KX966393	MG595626
Sinosolenaia carinata	MG463087	NC_023250	MG595616
Sinosolenaia oleivora	MG463090	NC_022701	MG595617
Sinosolenaia iridinea	MG463091	MT477834	MG595618
Sinosolenaia recognita	MG463092	KY561653	MG595619
Leguminaia wheatleyi	MN402614	MN396725	MN396721
Microcondylaea bonellii	KX822652	KT966473	KX822609
Gonidea angulata	MN402615	MN396726	MN396722
Koreosolenaia sitgyensis	MT020682	GQ451859	MT020817
Postolata guangxiensis	OP009379	OP020466	OP020470
Postolata guangxiensis	OP009380	OP020467	OP020470
Postolata guangxiensis	OP009381	OP020468	OP020470
Postolata guangxiensis	OP009382	OP020469	OP020471
Postolata guangxiensis	OP009383	OP020467	OP020472
Postolata guangxiensis	OP009384	OP020468	OP020470
Postolata guangxiensis	OP009385	OP020469	OP020471
*Postolata longjiangensis**	PP786557	PP786405	PP786407
*Postolata longjiangensis**	PP786557	PP786406	PP786407
*Postolata longjiangensis**	PP786558	PP786405	PP786407
*Postolata longjiangensis**	PP786558	PP786406	PP786407
Pseudopostolata angula **gen. et sp. nov.***	PQ189757	PQ201945	PQ201943
Pseudopostolata angula **gen. et sp. nov.***	PQ189757	PQ201945	PQ201944
Pseudopostolata angula **gen. et sp. nov.***	PQ189758	PQ201945	PQ201943
Pseudopostolata angula **gen. et sp. nov.***	PQ189758	PQ201945	PQ201944
Cosmopseudodon resupinatus	PP079436	PP079964	PP080006
Cosmopseudodon wenshanensis	PP079444	PP079972	PP080014
Pseudodontni Frierson, 1927			
Pseudodon mekongi	KX865861	KX865632	KX865733
Pseudodon vondembuschianus	KP795029	KP795052	MZ684028
Pseudodon cambodjensis	KP795028	NC_044112	KP795011
Bineurus loeiensis	KX865879	KX865650	KX865750
Bineurus mouhotii	KX865876	KX865647	KX865747
Sundadontina tanintharyiensis	MN275057	MN307248	MN307189
Sundadontina brandti	MN275058	MN307249	MN307190
Pilsbryoconcha exilis	KP795024	NC_044124	KP795007
Pilsbryoconcha compressa	KX865875	KX865646	KX865746
Thaiconcha callifera	KX865862	KX865633	KX865734
Thaiconcha munelliptica	MN275063	MN307252	MN307193
Nyeinchanconcha nyeinchani	KP795025	KP795050	KP795008
Lamprotulini Modell, 1942			
Lamprotula caveata	MG462991	NC_030336	MG595518
Lamprotula leaii	MN402616	MN396727	MN396723
Potomida littoralis	MN402617	MN396728	MN396724
Pronodularia japanensis	KX822659	AB055625	KX822615
Chamberlainiini Bogan, Froufe & Lopes-Lima in Lopes-Lima et al., 2017			
Sinohyriopsis schlegelii	MT020706	EF507846	MT020836
Sinohyriopsis cumingii	MG463086	NC011763	MG595613
Chamberlainia hainesiana	KX822635	NC_044110	KX822592
Rectidentini Modell, 1942			
Hyriopsis bialata	KX051274	MT993644	MT993697
Ensidens ingallsianus	MT993541	MT993687	MT993739
Contradentini Modell, 1942			
Lens contradens	MG581991	MT993693	MT993745
Lens comptus	KX865928	KX865682	KX865799
Physunio superbus	MG582020	MT993689	MT993741
Schepmaniini Lopes-Lima, Pfeiffer & Zieritz, 2021			
Schepmania sp.	MZ678755	MZ684082	MZ684035
Ctenodesmini Pfeiffer, Zieritz, Rahim & Lopes-Lima, 2021			
Khairuloconcha lunbawangorum	MN900790	MZ684078	MN902294
Khairuloconcha sahanae	MZ678752	MZ684079	MZ684024
Unioninae Rafinesque, 1820			
Anemina arcaeformis	NC_026674	NC_026674	MG595457
Cristaria plicata	NC_012716	NC_012716	MG595484
Sinanodonta woodiana	HQ283346	HQ283346	MG595604
MARGARITIFERIDAE Henderson, 1929			
Gibbosula laosensis	JX497731	KC845943	KT343741
Margaritifera margaritifera	KX550089	KX550091	KX550093

genera in the subfamily Gonideinae (Fig. 3). This species was identified as the sister group to the focal clade comprising the genera *Postolata*, *Cosmopseudodon*, *Obovalis*, *Ptychorhynchus*, *Parvasolenaia*, and *Koreosolenaia*. In this clade of Gonideini, the pairwise uncorrected *COI p*-distance ranged from 11.69% (between this species and *Ptychorhynchus pfisteri* (Heude, 1874)) to 13.58% (between this species and *Koreosolenaia sitgyensis* Lee, Kim, Lopes-Lima & Bogan, 2020)) (Table 3), providing compelling evidence for the founding of the new genus (Jeratthitikul et al. 2021; Wu et al. 2022; Dai et al. 2023). Furthermore, this species shows unique morphological characteristics distinguishable from other genera. Therefore, it is described herein as *Pseudopostolata angula* gen. et sp. nov.

Taxonomy

Family Unionidae Rafinesque, 1820
Subfamily Gonideinae Ortmann, 1916
Tribe Gonideini Ortmann, 1916

Genus *Pseudopostolata* Dai, Chen, Huang & Wu, gen. nov.

https://zoobank.org/4B4557A9-93D2-408E-AC1B-12CF9BDA2D2F
Figs 2C, D, 4

Type species. *Pseudopostolata angula* Chen, Dai, Huang & Wu, sp. nov.

Diagnosis. Shell medium size, moderately thick, flat, long, glossy, black without any color rays. Anterior rounded, short, posterior long, and wide. Dorsal margin slightly curved downwards and truncated behind, with a distinct obtuse angle in the middle of posterior margin. Shell surface with a low secondary posterior ridge end in the angle on the posterior margin. Both left and right valves with one or two pseudocardinal teeth.

Etymology. The specific name *pseudopostolata* is made from the Latin *pseudo* for false and *postolata* for a unionid genus, alluding to their similar shell morphology.

Vernacular name. 'Pseudorear-wide mussel genus' (English) and 'Ni Hou Ju Bang Shu' (拟后矩蚌属) (Chinese).

Distribution. Wujiang River in the Yongfeng section of Jiangxi Province, China.

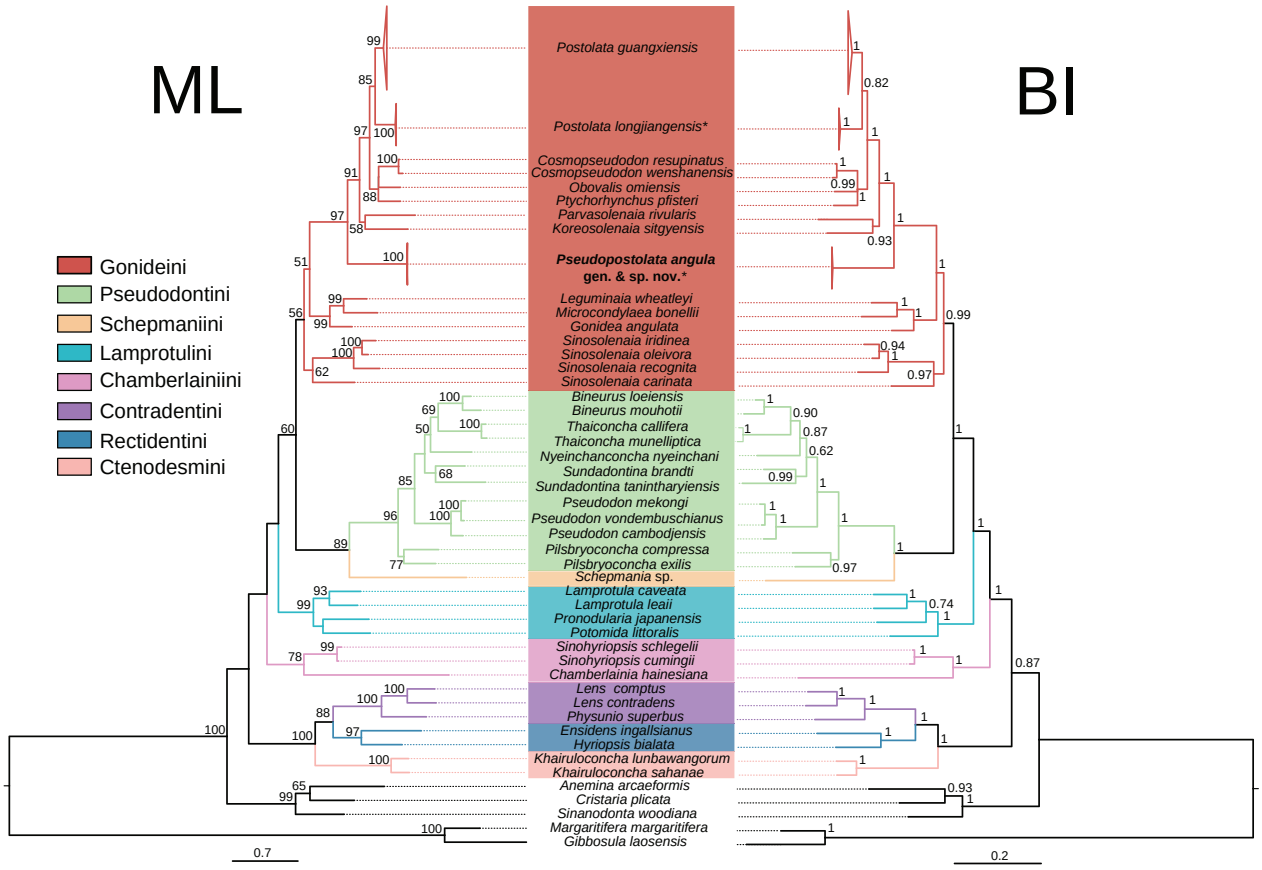

Figure 3. Maximum likelihood (ML) and Bayesian inference (BI) trees of Unionidae based on the three-gene dataset. *Gibbosula laosensis* and *Margaritifera margaritifera* from the family Margaritiferidae were used as outgroup taxa. Maximum likelihood bootstrap support less than 50% or Bayesian posterior probability less than 0.5 were not shown. Taxa marked with an asterisk (*) were sequenced in this study.

Remarks. The new genus belongs to the tribe Gonideini of the subfamily Gonideinae, which currently consists of only one species. The new genus exhibits morphological similarities with *Postolata guangxiensis* Dai, Huang, Guo & Wu, 2023. However, it differs in terms of its elongated shell and the more distinct angle on the posterior margin.

Pseudopostolata angula Chen, Dai, Huang & Wu, sp. nov.

https://zoobank.org/B1F2A547-13E7-47CF-A80B-FF54B9404AB5

Figs 2C, D, 4

Material examined. ***Holotype*** • 24_NCU_XPWU_PA01, Wujiang River [乌江], Yongfeng County [永丰县], Ji'an City [吉安市], Jiangxi Province [江西省], China, 27°03'37"N, 115°42'17"E, collected by Zhong-Guang Chen in December 2023; ***Paratypes*** China • 7 shells; same collection data as for holotype; specimen vouchers were shown in Table 4.

Diagnosis. See the diagnosis of the genus.

Description. Shell medium size, moderately thick, flat, long, glossy. Length 52.16–84.18 mm, width 16.80–25.95 mm, height 32.40–49.53 mm (Table 4). Anterior rounded, short, posterior long, and wide. Dorsal margin slightly curved downwards and truncated in behind, with a distinct obtuse angle in the middle of posterior margin; ventral margin weakly curved. Umbo inflated, below or even with the hinge line, located at 1/3 of the dorsal margin, and often eroded. Periostracum black with thin growth lines. Posterior slope with a low secondary posterior ridge end in the angle on the posterior margin. Growth lines arranged in irregular concentric circles. Hinge long. Ligament short and strong. Beak cavities shallow, open. Mantle attachment scars on the pallial line obvious. Anterior adductor muscle scars irregularly oval, deep, rough; posterior adductor muscle scars long, oval, smooth. Anterior retractor muscle scar deep; posterior adduster muscle scar shallow, Located obliquely above posterior adductor muscle scars. Left valve with one or two pseudocardinal teeth; anterior tooth elevated pyramidal or degenerated; posterior tooth thick and pyramidal. Right valve also with one or two pseudocardinal teeth; anterior tooth small or elevated pyramidal; posterior tooth low triangular or degenerated. Lateral teeth of both valves long and thick. Nacre light orangish.

Etymology. The specific name *angula* is made from the Latin *angula* for angled, alluding to the angle on the posterior margin of this species.

Vernacular name. 'Angulated pseudorear-wide mussel' (English) and Ju Jiao Ni Hou Ju Bang (具角拟后矩蚌) (Chinese).

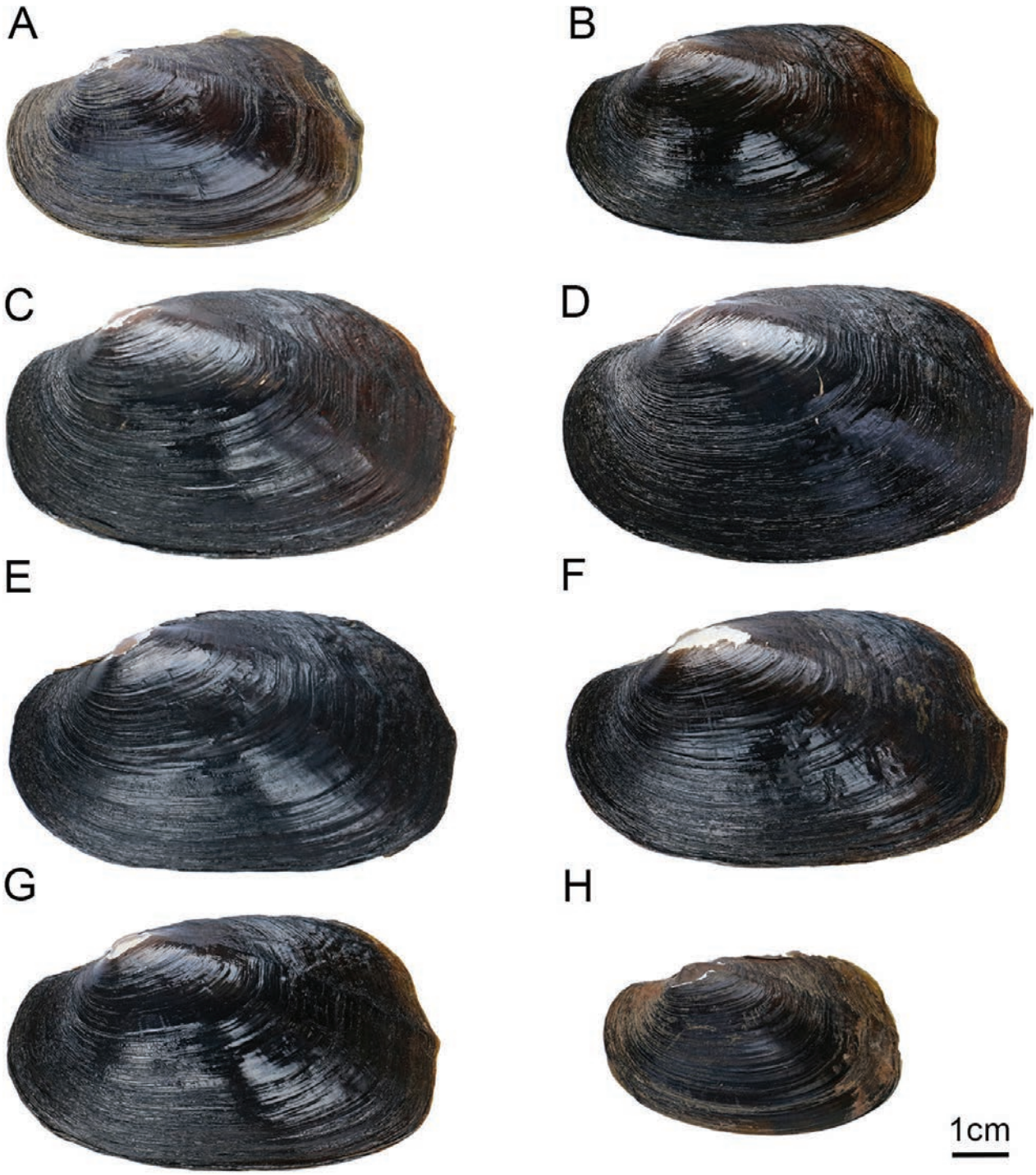

Figure 4. Eight specimens of *Pseudopostolata angula* gen. et sp. nov. were collected from the Wujiang River in Ji'an City, Jiangxi, China. A is the holotype; A-H responds to specimen vouchers: 24_NCU_XPWU_PA01- 24_NCU_XPWU_PH08.

Distribution. *Pseudopostolata angula* sp. nov. is only known from the type locality (Fig. 1).

Habitat. This new species was found to occur in the muddy or pebbly substrate of the river together with *Diaurora aurorea* (Heude, 1883), *Lanceolaria triformis* (Heude, 1877), *Lamprotula caveata* (Heude, 1877), *Nodularia douglasiae* (Gray, 1833) and *Pseudocuneopsis yangshuoensis* Wu & Liu, 2023 (Fig. 2A, B). It is the occasional species in the habitat, accounting for 5% of the total density of freshwater mussels.

Discussion

This study integrates morphological and molecular analyses to describe a new genus and species within the Gonideini tribe, which is endemic to the Wujiang River, Jiangxi, China. The newly described genus and species, *Pseudopostolata angula* gen. et sp. nov., shares morphological features typical of Gonideini, including an irregularly rectangular shell (Lopes-Lima et al. 2017; Froufe et al. 2020; Dai et al. 2023). Given the similarities in shell shape, including

Table 3. Average intraspecific (bold) and interspecific uncorrected *p*-distance (% ± S.E.) for *COI* sequences of species in Gonideini.

Taxa	1	2	3	4	5	6	7	8	9
1. *Pseudopostolata angula* **gen. et sp. nov.**	**0.17 ± 0.17**								
2. *Postolata guangxiensis*	12.01 ± 1.31	**0.59 ± 0.20**							
3. *Postolata longjiangensis*	12.33 ± 1.32	7.94 ± 1.10	**0.17 ± 0.17**						
4. *Cosmopseudodon wenshanensis*	12.92 ± 1.40	10.64 ± 1.28	11.08 ± 1.31	**0 ± 0**					
5. *Cosmopseudodon resupinatus*	13.35 ± 1.42	11.41 ± 1.27	11.35 ± 1.31	1.94 ± 0.55	**0.09 ± 0.09**				
6. *Koreosolenaia sitgyensis*	13.58 ± 1.40	12.14 ± 1.34	12.50 ± 1.39	11.50 ± 1.29	11.50 ± 1.29	0.17 ± 0.16			
7. *Obovalis omiensis*	12.38 ± 1.33	9.76 ± 1.17	10.67 ± 1.21	10.25 ± 1.23	10.44 ± 1.20	12.96 ± 1.35	1.61 ± 0.36		
8. *Parvasolenaia rivularis*	12.11 ± 1.29	11.71 ± 1.25	12.65 ± 1.35	11.40 ± 1.33	11.65 ± 1.35	11.08 ± 1.24	12.48 ± 1.27	1.23 ± 0.27	
9. *Ptychorhynchus pfisteri*	11.69 ± 1.31	10.43 ± 1.26	11.53 ± 1.33	8.56 ± 1.14	8.60 ± 1.12	11.61 ± 1.30	9.22 ± 1.16	10.23 ± 1.23	0.59 ± 0.19

Table 4. Shell measurements of *Pseudopostolata angula* gen. et sp. nov. Measurements in millimeters (mm).

Status of specimen	Specimen voucher	Shell length	Shell width	Shell height
Holotype	24_NCU_XPWU_PA01	63.29	19.05	37.77
Paratype	24_NCU_XPWU_PA02	52.16	16.80	32.40
Paratype	24_NCU_XPWU_PA03	84.18	25.95	49.16
Paratype	24_NCU_XPWU_PA04	83.55	24.92	49.53
Paratype	24_NCU_XPWU_PA05	80.64	25.38	46.28
Paratype	24_NCU_XPWU_PA06	75.27	22.15	45.68
Paratype	24_NCU_XPWU_PA07	76.67	22.6	45.19
Paratype	24_NCU_XPWU_PA08	62.94	19.31	37.60

a short, rounded anterior and a broad, elongated posterior, this species could easily be mistaken for belonging to the genus *Postolata* Dai, Huang, Guo & Wu, 2023 (Dai et al. 2023). However, further morphological examination revealed distinct characteristics specific to this species. The new genus differs from other genera in Gonideini by its slightly curved dorsal margin, truncated posteriorly with a distinct obtuse angle in the middle of the posterior margin (Fig. 2C, D, Table 5). Additionally, this species exhibits two types of pseudocardinal teeth, which is unique within Gonideini. The first type has two pseudocardinal teeth on both valves; in the left valve, the anterior pseudocardinal tooth is taller than the posterior one, while in the right valve, the anterior pseudocardinal tooth is smaller (Fig. 2C). The second type has a single tall triangular-conical pseudocardinal tooth on both valves; in the left valve, the anterior pseudocardinal tooth is reduced, and in the right valve, the posterior pseudocardinal tooth is reduced (Fig. 2D). The new genus is further distinguished from *Postolata* by its light orange-hued nacre, in contrast to the white nacre of *Postolata*, as well as by its longer shell (Table 5). Given the high prevalence of endemism among freshwater mussels, their taxonomic classification is closely tied to their geographic distribution (Bolotov et al. 2020b; Konopleva et al. 2023). The majority of Gonideini species are found in China, primarily in the Yangtze River Basin, with a few species also present in the Guangxi and Hainan regions (Graf and Cummings 2021; Liu et al. 2024). *Pseudopostolata angula* and *Postolata* are distributed across distinct geographical drainages. The former is endemic to the Yangtze River basin, while the latter, comprising two species (*Postolata guangxiensis* Dai, Huang, Guo & Wu, 2023 and *Postolata longjiangensis* Liu & Wu, 2024), is found in the Pearl River basin (Guangxi) (Dai et al. 2023; Liu et al. 2024). This distinct distribution facilitates a clear differentiation between the two genera.

Five genera within Gonideini, including *Pseudopostolata*, *Postolata*, *Cosmopseudodon*, *Obovalis*, and *Ptychorhynchus*, exhibit a high degree of convergence, with similarities in shell size, shape, and thickness (Table 4). For instance, *Ptychorhynchus murinum* (Heude, 1883) shares a similar shell shape with *Postolata longjiangensis* Liu & Wu, 2024. However, the absence of molecular data for *Ptychorhynchus murinum* precludes a molecular comparison between the two species. Morphologically, *Postolata longjiangensis* is distinguished by fine and dense growth lines on the posterior dorsal, a feature that clearly differentiates it from *Ptychorhynchus murinum*. Additionally, their distinct distributions—*Ptychorhynchus murinum* in the Yangtze River basin and *Postolata longjiangensis* in the Pearl River basin (Guangxi)—further support their differentiation (Graf and Cummings 2021; Liu et al. 2024). Consequently, accurate species identification requires not only useful distinguishing characteristics but also consideration of their distribution, habitat, and a combination of molecular data (Pieri et al. 2018; Jeratthitikul et al. 2022; Bolotov et al. 2023; Dai et al. 2024b).

The use of molecular data for DNA taxonomy has shown great promise in expediting the process of species discovery (Huang et al. 2019; Chen et al. 2023). The molecular data results are consistent with morphological analysis. In our multi-locus trees, *Pseudopostolata angula* formed a well-supported monophyletic clade in the tribe Gonideini that did not belong to any previously known species or genera (Fig. 3, Table 3). Furthermore, the considerable genetic divergence from other genera lends additional support to its classification as a distinct genus. (Jeratthitikul et al. 2021; Wu et al. 2022; Dai et al. 2023). The phylogenetic relationships of genera in the focal clade of Gonideini align with previous studies based on *COI* + *16S* rRNA + *28S* rRNA phylogenies (Dai et al. 2023; Liu et al. 2024), although our analysis did not recover the sister relationship between *Ptychorhynchus pfisteri* (Heude, 1874) and *Obovalis omiensis* (Heimburg, 1884) (Fig. 3). Moreover, the phylogenetic analysis revealed that *Parvasolenaia rivularis* (Heude, 1877) is sister to *Koreosolenaia sitgyensis* Lee, Kim, Lopes-Lima & Bogan, 2020, which contradicts the *COI* + *ND1* + *16S* rRNA + *18S* rRNA + *28S* rRNA phylogeny (Wu et al. 2024). The observed discrepancies between topologies are likely attributable to factors such as incomplete lineage sorting, insufficient taxon sampling, and varying rates of genome evolution and mutation (Perkins et al.

Table 5. Analyzed conchological characters of *Pseudopostolata*, *Postolata*, *Cosmopseudodon*, *Ptychorhynchus*, *Obovalis*, *Parvasolenaia*, and *Koreosolenaia*.

Conchological features	*Pseudopostolata*	*Postolata*	*Cosmopseudodon*	*Obovalis*	*Ptychorhynchus*
Shell shape	Irregularly rectangular	Irregularly rectangular	Elongate elliptical	Elongate oval	Elongate elliptical
Shell thickness	Moderately thick	Moderately thick	Moderately thick	Thin	Thin-medium
Umbo	Moderately inflated	Inflated	Moderately inflated	Moderately inflated	Low and flat
Posterior margin	With a distinct obtuse angle in the middle of posterior margin	Almost perpendicular to ventral margin	Weakly curved	Weakly curved	Weakly curved
Surface sculpture	With a low secondary posterior ridge end in the angle on the posterior margin	One sulcus near the posterior dorsal margin	Covered with multiple curved wrinkles and one sulcus	Coarse nodules	Posterior slope sculptured with strong ridges
Pseudocardinal teeth of the left valve	One or two thick and pyramidal teeth	Anterior tooth small, posterior tooth thick and pyramidal	One tooth, thick and Obtuse	One tooth, pyramidal	Two teeth, rather stumpy and roughened
Pseudocardinal teeth of the left valve	One or two thick and pyramidal teeth	Anterior tooth well developed, posterior tooth reduced	One tooth, thick and Obtuse	One tooth, high and triangular	One tooth, blunt
Lateral teeth	One tooth on both valves, long and thick	One tooth on both valves, small and short	One tooth on both valves, weakly developed and short	One tooth on both valves, small and short	1~2 granulous teeth on the left and slightly split up teeth on the right
Nacre colour	Light orangish	White	Bluish-white with an orange umbo pocket	Bluish-white	White

2017). The recognition of higher-level taxa based on poorly supported topologies can give rise to instability in classification systems (Pfeiffer et al. 2019). Phylogenomic analysis will be needed to provide a more robust understanding of the intergeneric relationships within this tribe.

Acknowledgments

This study was supported by the National Natural Science Foundation of China (No. 32360132, No. 32100354) and the Jiangxi Provincial Natural Science Foundation (No. 20232BAB205067).

References

Aldridge DC, Ollard IS, Bespalaya YV, Bolotov IN, Douda K, Geist J, Haag WR, Klunzinger MW, Lopes-Lima M, Mlambo MC, Riccardi N, Sousa R, Strayer DL, Torres SH, Vaughn CC, Zajac T, Zieritz A (2022) Freshwater mussel conservation: A global horizon scan of emerging threats and opportunities. Global Change Biology 29(3): 575–589. https://doi.org/10.1111/gcb.16510

Bolotov IN, Vikhrev IV, Lopes-Lima M, Lunn Z, Chan N, Win T, Aksenova OV, Gofarov MY, Kondakov AV, Konopleva ES, Tumpeesuwan S (2018) Discovery of *Novaculina myanmarensis* sp. nov. (Bivalvia, Pharidae, Pharellinae) closes the freshwater razor clams range disjunction in Southeast Asia. Scientific Reports 8(1): 16325. https://doi.org/10.1038/s41467-018-05133-4

Bolotov IN, Kondakov AV, Konopleva ES, Vikhrev IV, Aksenova OV, Aksenov AS, Bespalaya YV, Borovskoy AV, Danilov PP, Dvoryankin GA, Gofarov MY, Kabakov MB, Klishko OK, Kolosova YS, Lyubas AA, Novoselov AP, Palatov DM, Savvinov GN, Solomonov NM, Spitsyn VM, Sokolova SE, Tomilova AA, Froufe E, Bogan AE, Lopes-Lima M, Makhrov AA, Vinarski MV (2020a) Integrative taxonomy, biogeography and conservation of freshwater mussels (Unionidae) in Russia. Scientific Reports 10(1): 3072. https://doi.org/10.1038/s41598-020-59867-7

Bolotov IN, Konopleva ES, Vikhrev IV, Gofarov MY, Lopes-Lima M, Bogan AE, Lunn Z, Chan N, Win T, Aksenova OV, Tomilova AA, Tanmuangpak K, Tumpeesuwan S, Kondakov AV (2020b) New freshwater mussel taxa discoveries clarify biogeographic division of Southeast Asia. Scientific Reports 10(1): 6616. https://doi.org/10.1038/s41598-020-63612-5

Bolotov IN, Konopleva ES, Vikhrev IV, Gofarov MY, Kondakov AV, Lyubas AA, Soboleva AA, Chan N, Lunn Z, Win T, Inkhavilay K (2023) Integrative Taxonomic Reappraisal and Evolutionary Biogeography of the Most Diverse Freshwater Mussel Clade from Southeast Asia (Pseudodontini). Water 15(17): 3117. https://doi.org/10.3390/w15173117

Castresana J (2000) Selection of conserved blocks from multiple alignments for their use in phylogenetic analysis. Molecular biology and evolution 17(4): 540–552. https://doi.org/10.1093/oxfordjournals.molbev.a026334

Chen ZG, Dai YT, Ouyang S, Huang XC, Wu XP (2023) Unveiling the identity of Diaurora Cockerell, 1903 (Bivalvia, Unionidae): morphology, molecular phylogenetics, and the description of a new species. ZooKeys 1173: 131–144. https://doi.org/10.3897/zookeys.1173.106148

Dai YT, Huang XC, Wu CHZ, Chen ZG, Guo L, Shu FY, Ouyang S, Wu XP (2023) Multilocus and mitogenomic phylogenetic analyses reveal a new genus and species of freshwater mussel (Bivalvia, Unionidae) from Guangxi, China. Invertebrate Systematics 37(2): 152–166. https://doi.org/10.1071/is22048

Dai YT, Chen ZG, Hu CL, Ning PF, Ouyang S, Huang XC, Wu XP, Giribet G (2024a) Taxonomic reassessment of *Scabies* (Bivalvia, Unionidae) species in China based on multilocus and mitogenomic phylogenetic analyses. Invertebrate Systematics 38(6): IS24020. https://doi.org/10.1071/is24020

Dai YT, Chen ZG, Peng KJ, Ouyang S, Huang XC, Wu XP (2024b) Revisiting the genus *Pseudocuneopsis* (Bivalvia, Unionidae): Morphology, mitochondrial phylogenomics, and the description of a new species. Zoologica Scripta 53(3): 323–337. https://doi.org/10.1111/zsc.12647

Edgar RC (2004) MUSCLE: multiple sequence alignment with high accuracy and high throughput. Nucleic Acids Research 32(5): 1792–1797. https://doi.org/10.1093/nar/gkh340

Edler D, Klein J, Antonelli A, Silvestro D, Matschiner M (2020) raxmlGUI 2.0: A graphical interface and toolkit for phylogenetic analyses using RAxML. Methods in Ecology and Evolution 12(2): 373–377. https://doi.org/10.1111/2041-210x.13512

Froufe E, Bolotov I, Aldridge DC, Bogan AE, Breton S, Gan HM, Kovitvadhi U, Kovitvadhi S, Riccardi N, Secci-Petretto G, Sousa

R, Teixeira A, Varandas S, Zanatta D, Zieritz A, Fonseca MM, Lopes-Lima M (2020) Mesozoic mitogenome rearrangements and freshwater mussel (Bivalvia, Unionoidea) macroevolution. Heredity 124(1): 182–196. https://doi.org/10.1038/s41437-019-0242-y

Graf DL, Cummings KS (2021) A 'big data' approach to global freshwater mussel diversity (Bivalvia, Unionoida), with an updated checklist of genera and species. Journal of Molluscan Studies 87(1): eyaa034. https://doi.org/10.1093/mollus/eyaa034

Haag WR (2012) North American freshwater mussels: natural history, ecology, and conservation. Cambridge University Press, UK. https://doi.org/10.1017/CBO9781139048217

Huang XC, Su JH, Ouyang JX, Ouyang S, Zhou CH, Wu XP (2019) Towards a global phylogeny of freshwater mussels (Bivalvia, Unionida): Species delimitation of Chinese taxa, mitochondrial phylogenomics, and diversification patterns. Molecular Phylogenetics and Evolution 130: 45–59. https://doi.org/10.1016/j.ympev.2018.09.019

Inoue K, Hayes DM, Harris JL, Christian AD (2013) Phylogenetic and morphometric analyses reveal ecophenotypic plasticity in freshwater mussels Obovaria jacksoniana and Villosa arkansasensis (Bivalvia, Unionidae). Ecology and Evolution 3(8): 2670–2683. https://doi.org/10.1002/ece3.649

Jeratthitikul E, Sutcharit C, Ngor PB, Prasankok P (2021) Molecular phylogeny reveals a new genus of freshwater mussels from the Mekong River Basin (Bivalvia, Unionidae). European Journal of Taxonomy 775: 119–142. https://doi.org/10.5852/ejt.2021.775.1553

Jeratthitikul E, Paphatmethin S, Sutcharit C, Ngor PB, Inkhavilay K, Prasankok P (2022) Phylogeny and biogeography of Indochinese freshwater mussels in the genus *Pilsbryoconcha* Simpson, 1900 (Bivalvia, Unionidae) with descriptions of four new species. Scientific Reports 12(1): 20458. https://doi.org/10.1038/s41598-022-24844-9

Katoh K, Rozewicki J, Yamada KD (2019) MAFFT online service: multiple sequence alignment, interactive sequence choice and visualization. Briefings in Bioinformatics 20(4): 1160–1166. https://doi.org/10.1093/bib/bbx108

Konopleva ES, Bolotov IN, Vikhrev IV, Inkhavilay K, Gofarov MY, Kondakov AV, Tomilova AA, Chapurina YE, Van Do T, Pfeiffer JM, Lopes-Lima M, Bogan AE (2023) A freshwater mussel species reflects a Miocene stream capture between the Mekong Basin and East Asian rivers. Zoosystematics and Evolution 99(1): 29–43. https://doi.org/10.3897/zse.99.90784

Kumar S, Stecher G, Li M, Knyaz C, Tamura K (2018) MEGA X: Molecular evolutionary genetics analysis across computing platforms. Molecular Biology and Evolution 35(6): 1547–1549. https://doi.org/10.1093/molbev/msy096

Lanfear R, Frandsen PB, Wright AM, Senfeld T, Calcott B (2017) PartitionFinder 2: New Methods for Selecting Partitioned Models of Evolution for Molecular and Morphological Phylogenetic Analyses. Molecular Biology and Evolution 34(3): 772–773. https://doi.org/10.1093/molbev/msw260

Liu L, Zhang L, Hou K, Ning L, Wu R (2024) Addition to the known diversity of Chinese freshwater mussels: integrative description of a new species of *Postolata* Dai et al., 2023 (Bivalvia, Unionidae, Gonideinae). Zoosystematics and Evolution 100(3): 769–778. https://doi.org/10.3897/zse.100.126069

Lopes-Lima M, Froufe E, Do VT, Ghamizi M, Mock KE, Kebapci Ü, Klishko O, Kovitvadhi S, Kovitvadhi U, Paulo OS, Pfeiffer JM, Raley M, Riccardi N, Şereflişan H, Sousa R, Teixeira A, Varandas S, Wu XP, Zanatta DT, Zieritz A, Bogan AE (2017) Phylogeny of the most species-rich freshwater bivalve family (Bivalvia, Unionida, Unionidae): Defining modern subfamilies and tribes. Molecular Phylogenetics and Evolution 106: 174–191. https://doi.org/10.1016/j.ympev.2016.08.021

Park JK, Foighil DÓ (2000) Sphaeriid and Corbiculid Clams Represent Separate Heterodont Bivalve Radiations into Freshwater Environments. Molecular Phylogenetics and Evolution 14(1): 75–88. https://doi.org/10.1006/mpev.1999.0691

Perkins MA, Johnson NA, Gangloff MM (2017) Molecular systematics of the critically-endangered North American spinymussels (Unionidae, Elliptio and Pleurobema) and description of *Parvaspina* gen. nov. Conservation Genetics 18(4): 745–757. https://doi.org/10.1007/s10592-017-0924-z

Pfeiffer JM, Breinholt JW, Page LM (2019) Unioverse: A phylogenomic resource for reconstructing the evolution of freshwater mussels (Bivalvia, Unionoida). Molecular Phylogenetics and Evolution 137: 114–126. https://doi.org/10.1016/j.ympev.2019.02.016

Pieri AM, Inoue K, Johnson NA, Smith CH, Harris JL, Robertson C, Randklev CR (2018) Molecular and morphometric analyses reveal cryptic diversity within freshwater mussels (Bivalvia, Unionidae) of the western Gulf coastal drainages of the USA. Biological Journal of the Linnean Society 124(2): 261–277. https://doi.org/10.1093/biolinnean/bly046

Ronquist F, Teslenko M, van der Mark P, Ayres DL, Darling A, Hohna S, Larget B, Liu L, Suchard MA, Huelsenbeck JP (2012) MrBayes 3.2: efficient Bayesian phylogenetic inference and model choice across a large model space. Systematic Biology 61(3): 539–542. https://doi.org/10.1093/sysbio/sys029

Rozas J, Ferrer-Mata A, Sanchez-DelBarrio JC, Guirao-Rico S, Librado P, Ramos-Onsins SE, Sanchez-Gracia A (2017) DnaSP 6: DNA Sequence Polymorphism Analysis of Large Data Sets. Molecular Biology and Evolution 34(12): 3299–3302. https://doi.org/10.1093/molbev/msx248

Smith CH, Johnson NA, Inoue K, Doyle RD, Randklev CR (2019) Integrative taxonomy reveals a new species of freshwater mussel, Potamilus streckersoni sp. nov. (Bivalvia, Unionidae): implications for conservation and management. Systematics and Biodiversity 17(4): 331–348. https://doi.org/10.1080/14772000.2019.1607615

Sousa R, Zając T, Halabowski D, Aksenova OV, Bespalaya YV, Carvalho F, Castro P, Douda K, da Silva JP, Ferreira-Rodríguez N, Geist J, Gumpinger C, Labecka AM, Lajtner J, Lewin I, Lopes-Lima M, Meira A, Nakamura K, Nogueira JG, Ondina P, Ożgo M, Reis J, Riccardi N, Shumka S, Son MO, Teixeira A, Thielen F, Urbańska M, Varandas S, Wengström N, Zając K, Zieritz A, Aldridge DC (2022) A roadmap for the conservation of freshwater mussels in Europe. Conservation Biology 37(2): e13994. https://doi.org/10.1111/cobi.13994

Walker JM, Bogan AE, Bonfiglio EA, Campbell DC, Christian AD, Curole JP, Harris JL, Wojtecki RJ, Hoeh WR (2007) Primers for amplifying the hypervariable, male-transmitted COII-COI junction region in amblemine freshwater mussels (Bivalvia, Unionoidea, Ambleminae). Molecular Ecology Notes 7(3): 489–491. https://doi.org/10.1111/j.1471-8286.2006.01630.x

Wu XP, Dai YT, Yin N, Shu FY, Chen ZG, Guo L, Zhou CH, Ouyang S, Huang XC (2022) Mitogenomic phylogeny resolves *Cuneopsis* (Bivalvia, Unionidae) as polyphyletic: The description of two new genera and a new species. Zoologica Scripta 51(2): 173–184. https://doi.org/10.1111/zsc.12527

Wu RW, Liu LL, Zhang LP, Jia JL, Jin DD, Wu XP, Liu XJ (2023) New species of the genus *Pseudocuneopsis* Huang, Dai, Chen & Wu, 2022 (Bivalvia, Unionidae) from Guangxi Province, China. ZooKeys 1166: 261–270. https://doi.org/10.3897/zookeys.1166.104150

Wu R, Liu L, Zhang L, Bogan AE, Niu G, Jin D, Wu X, Liu X (2024) Taxonomic revision of two species in the genus *Ptychorhynchus* Simpson, 1900 (Bivalvia, Unionidae, Gonideinae), with description of a new species. Invertebrate Systematics 38: IS24014. https://doi.org/10.1071/IS24014

Zieritz A, Aldride D (2009) Identification of ecophenotypic trends within three European freshwater mussel species (Bivalvia, Unionoida) using traditional and modern morphometric techniques. Biological Journal of the Linnean Society 98(4): 814–825. https://doi.org/10.1111/j.1095-8312.2009.01329.x

Zieritz A, Bogan AE, Froufe E, Klishko O, Kondo T, Kovitvadhi U, Kovitvadhi S, Lee JH, Lopes-Lima M, Pfeiffer JM, Sousa R, Van Do T, Vikhrev I, Zanatta DT (2018) Diversity, biogeography and conservation of freshwater mussels (Bivalvia, Unionida) in East and Southeast Asia. Hydrobiologia 810: 29–44. https://doi.org/10.1007/s10750-017-3104-8

Zieritz A, Pfeiffer J, Rahim KAA, Prayogo H, Anwari MS, Diba F, Froufe E, Blackwell T, Hartikainen H, Lopes-Lima M (2024) High endemic freshwater mussel (Bivalvia, Unionida) diversity in western Borneo, with description of three new species. Zoological Journal of the Linnean Society 201(3): zlae076. https://doi.org/10.1093/zoolinnean/zlae076

Zoosyst. Evol. 100 (4) 2024, 1431–1442 | DOI 10.3897/zse.100.130288

PENSOFT

für Natur MUSEUM FÜR NATURKUNDE BERLIN

An update on the genus *Ischiomysis* with a description of *I. proincisa* sp. nov. (Crustacea, Mysida) from a sublittoral marine cave in the Gulf of Guinea (tropical E-Atlantic)

Karl J. Wittmann[1], Peter Wirtz[2]

1 *Department of Environmental Health, Medical University of Vienna, Kinderspitalgasse 15, A-1090 Vienna, Austria*

2 *CCMAR—Center of Marine Sciences, University of Algarve, Campus de Gambelas, 8005-139, Faro, Portugal*

https://zoobank.org/07A629AB-C1D1-45F3-995C-F114D8493685

Corresponding author: Karl J. Wittmann (karl.wittmann@meduniwien.ac.at)

Academic editor: Luiz F. Andrade ♦ **Received** 23 June 2024 ♦ **Accepted** 12 September 2024 ♦ **Published** 24 October 2024

Abstract

Ischiomysis proincisa **sp. nov.** is described from a comparatively large, semi-dark marine cave in sublittoral waters off the small island Ilhéu das Rolas, directly south of São Tomé Island in the Gulf of Guinea. As striking features, the new species is distinguished from both its congeners by an anteriorly incised rostrum in both sexes and by two versus only one modified flagellate spine on the ischium of the eighth thoracic endopod in males. The new species is sympatric yet ecologically remote from the congener *I. telmatactiphila*, which is associated with the sea anemone *Telmatactis cricoides* in brighter habitats. New records and morphological notes are given for *I. telmatactiphila* and *I. peterwirtzi*. An updated definition of the genus *Ischiomysis* and a key to its three species are given.

Key Words

Association with *Telmatactis cricoides*, equatorial E-Atlantic, first description, São Tomé Island, symbiotic species, troglophilic species

Introduction

Very large eyes, red body color (as in Fig. 2), freely swimming and forming small swarms as in the here first described mysid or even forming large swarms—such mysid life-form types can be encountered in small recesses, including empty mollusk shells, etc., up to very large caves. Detailed studies by Wittmann (1978) and Riera et al. (1991) on *Hemimysis speluncola* Ledoyer, 1963, *H. margalefi* Alcaraz, Riera & Gili, 1986, and *Sirielella gracilipes* H. Nouvel, 1942, in Mediterranean marine caves showed that these mysids seek shelter in dimly lit to dark zones during daytime and widely distribute over the sea floor for feeding and reproduction during the night. In the morning, they again seek shelter, often not returning to the same microhabitat. Part of the *S. gracilipes* population may remain in the phytal zone, hiding among algae. In analogy, many pelagic mysid species show diurnal vertical migration between euphotic, dysphotic, and aphotic zones (review in Mauchline 1980).

Mysids of the genus *Ischiomysis* Wittmann, 2013, were detected and described late in the taxonomic literature. This is probably because of the still early state of exploration of shallow coastal waters in the tropical E-Atlantic, whereas offshore waters were well-explored by great oceanographic expeditions such as the DIVA-1 expedition to the Angola Basin (Wittmann 2020). Both previously known species of *Ischiomysis* are associated with the club-tipped anemone *Telmatactis cricoides* (Duchassaing de Fonbressin, 1850), where they are easily spotted and sampled by divers. A photo (published by Wittmann 2013: Fig. 4) taken by Lisandro de Almeida

shows undetermined mysids with a similar habitus and red-orange body aggregated over the oral disc of a *T. cricoides* from the Island of Trindade in the tropical W-Atlantic, 1160 km off the coast of Brazil. Samples of this species are eagerly awaiting to determine its taxonomic affiliation, potentially with the genus *Ischiomysis*. That mysid and the present description of a new cave-dwelling species are an impetus to strengthen efforts in exploring the coastal fauna of the tropical Atlantic.

Materials and methods

Mysids were collected with diver-operated hand nets from the club-tipped anemone *Telmatactis cricoides* and in marine caves of São Tomé and São Vicente islands in the tropical E-Atlantic. Laboratory methods, definitions, and units of measurement as in Wittmann (2024). Expansion on slides makes the carapace appear wider but no longer compared with its shape *in loco*. Statolith diameters are measured as geometric means of apparent length and width in dorsal view. Artificial digital coloring of objects (by the camera system of the microscope) in Figs 4, 9 serves to visualize poorly contrasting details. Terminology as outlined by Wittmann (2024). Wilson (1989) defined "whip setae" (Fig. 7R) based on the basal part (handle) bearing a thin flagellum (cord) separated in the present context by an articulation, suture, or at least by an optically dense section upon standard microscopy. Wittmann et al. (2021) proposed to restrict the term "subrostral" to frontal processes between the rostrum and ocular symphysis and to use "epi-antennular" and "hypo-antennular" for frontal processes immediately above and below the antennular trunk (Fig. 5A), respectively. The hypo-antennular processes should not be confounded with a (here not treated) potential frontal process off the clypeus. The dorsal lobe (Fig. 5C) behind the distal margin of the terminal segment of the antennular trunk is termed the "disto-median lobe". Larval stages are distinguished according to Wittmann (1981).

Abbreviations and repository

BL body length measured from anterior margin of carapace to terminus of telson without spines
NHMW Natural History Museum of Vienna (repository)

Results

Systematics

Subfamily Heteromysinae Norman, 1892
Tribe Heteromysini Norman, 1892

Genus *Ischiomysis* Wittmann, 2013

Ischiomysis Wittmann, 2013: 489–492; San Vicente and Monniot 2014: 333, 340; Wittmann et al. 2014: 231, 309, 341; Wittmann and Wirtz 2017: 147; Daneliya 2021: 3, 6–7; Mees and Meland 2024: AphiaID 723169.

Short diagnosis. Shortened and updated from Wittmann (2013). Heteromysini with normal eyes, eyestalks without spiniform extension, no ocular papilla. Flagellate spine opposed by a large smooth seta on disto-mesial corner of terminal segment of antennular trunk; no modified spines (setae) on basal and middle segments. Appendix masculina short, with tuft of setae. Antennal scale well developed, with apical segment. Carapace (not counting rostrum) and mouthparts are normal. Thoracic sternites 2–8 without median processes in both sexes. Endopods 1–8 with distinct claw at apex. Third endopod specialized as gnathopod by forming a moderately strong subchela; carpus enlarged, not subdivided, armed with several flagellate spines. Fourth endopod with several weakly modified setae on carpopropodus and with apically bifid claw in both sexes. Endopod 8 only in males with a strong spiniform extension of praeischium and with 1–2 modified flagellate spine on ischium. Pleopods entire, reduced to small setose plates in both sexes; no spines or teeth. Uropods normal, with setae all around, no spine. Telson with spines on lateral margins; distinct apical cleft with spine-like laminae, no setae.

Species inventory. *I. peterwirtzi* Wittmann, 2013, from sublittoral rock recesses up to large marine caves, mostly observed associated with the club-tipped anemone *Telmatactis cricoides* but also distant from anemones at São Vicente Island and the small nearby island Ilhéu dos Pássaros in the Cape Verde archipelago, tropical E-Atlantic.

I. telmatactiphila Wittmann, 2013, close to *T. cricoides* in well-lit rock recesses at São Tomé Island and the small nearby islet Ilhéu de Santana, Gulf of Guinea, tropical E-Atlantic.

I. proincisa sp. nov. from a large semi-dark sublittoral cave at the coast of Rolas Island, close to São Tomé Island, in the Gulf of Guinea, tropical E-Atlantic.

Key to the species of the genus *Ischiomysis* (updated from Wittmann and Wirtz 2017)

1 Rostrum apically incised in both sexes; two flagellate spines on ischium of endopod 8 in males..... *I. proincisa* sp. nov.
– Rostrum entire in both sexes; only one flagellate spine on ischium of endopod 8 in males..... 2
2 Carapace anteriorly produced into a well-projecting triangular rostrum with rounded apex; exopod of uropods reaches with 18–25% of its length beyond telson; cleft of telson with spine-like laminae along basal 45–55% of its margins .... *I. telmatactiphila*
– Carapace with short rostrum forming a terminally rounded blunt angle; exopod of uropods reaches with 39–56% of its length beyond telson; cleft of telson with spine-like laminae along basal 80–86% of its margins .....*I. peterwirtzi*

Ischiomysis telmatactiphila Wittmann, 2013

Fig. 1

Ischiomysis telmatactiphila Wittmann, 2013: 492–497, 503–505, figs 1–3; San Vicente and Monniot 2014: tab. 1; Wittmann et al. 2014: 349, figs 18, 20; Bhaduri and Crowther 2016: tab. 1; Wittmann and Wirtz 2017: 132, 148; Saito et al. 2018: tab. 2; Wittmann and Ariani 2019: suppl.; Mees and Meland 2024: AphiaID 723174.

Material. São Tomé • 10 ♀♀ ad. (BL 4.2–5.4 mm), 6 ♂♂ ad. (BL 3.8–4.7 mm), 2 ♀♀ subad.; E-Atlantic, Gulf of Guinea, small islet Ilhéu de Santana; 0.2417°N, 6.7587°E; 15 m depth; 4 Feb. 2017; P. Wirtz leg.; well-lit fissure in exposed rock in front of the "Santana Tunnel", mysids above mouth disk of *Telmatactis cricoides* in crevice.

Note. The present record at the Ilhéu de Santana is the first after the first description. It extends the known distribution by 31 km air route across São Tomé Island or by >48 km waterway around São Tomé, respectively. Fig. 1 shows a dense swarm of this mysid species spread over the oral disc of *T. cricoides*. Additional mysid swarms were found closely associated with five other *Telmatactis* (above the oral disk and around the column of the anemone) in well-lit fissures of exposed rock in the Santana Bay at 0.2462°N, 6.7461°E. So far, no records of this species were made distant from anemones.

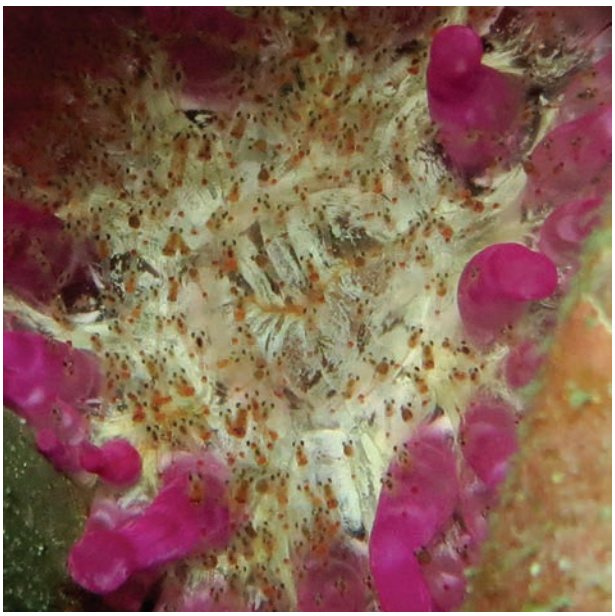

Figure 1. *Ischiomysis telmatactiphila* aggregated over the oral disk of *Telmatactis cricoides* in Santana Bay; photo P. Wirtz.

Ischiomysis peterwirtzi Wittmann, 2013

Figs 2, 3

Ischiomysis peterwirtzi Wittmann, 2013: 497–505, figs 5–6; San Vicente and Monniot 2014: tab. 1; Wittmann et al. 2014: 277, 349; Wittmann and Griffiths 2017: 40; Wittmann and Wirtz 2017: 132, 145, 148; Saito et al. 2018: tab. 2; Wittmann and Chevaldonné 2021: tab. 1, suppl.; Wittmann 2023: tab. S1; Mees and Meland 2024: AphiaID 723175.

Material. São Vicente • 6 ♀♀ ad. (BL 4.2–4.8 mm), 3 ♂♂ ad. (BL 4.1–4.4 mm), 2 ♀♀ subad.; E-Atlantic, Cape Verde archipelago, off Mindelo, small island Ilhéu dos Pássaros; 16.91147°N, 25.01181°W; 17 m depth; 26 Aug. 2015; P. Wirtz leg.; mysids around the basis of *Telmatactis cricoides* at foot of large stone • 3 ♂♂ ad. (BL 4.5–4.7 mm), 3 imm., 1 juv.; São Vicente, marine cave Furna da Rosa; 16.8500°N, 25.0833°W; 16 m depth; 5 April 2022; P. Wirtz leg.

Note. Cornea black in freshly caught specimens, eyestalks vary between transparent, opaque, and light red, cephalothorax and tail fan all over deeply red, pleon transparent to light red (ex-situ photo in Fig. 2), not considering colors of the content of foregut and intestine, in part visible through the (semi)-transparent body. The present records at the Ilhéu dos Pássaros and the cave Furna da Rosa are the first and second after the first description, respectively. They extend the known distribution by only 11 km to the NE. Swarms associated with *T. cricoides* (Fig. 3) as well

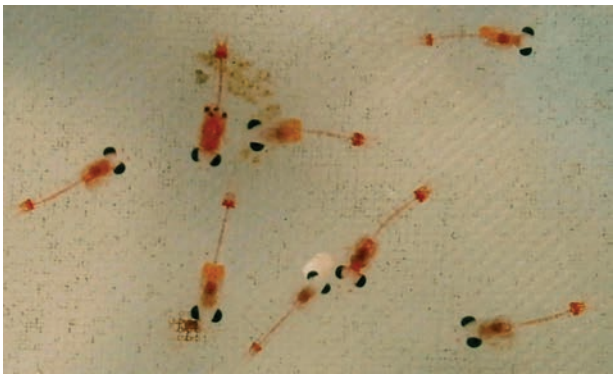

Figure 2. *Ex-situ* photo of living *Ischiomysis peterwirtzi* from small island Ilhéu dos Pássaros; photo P. Wirtz.

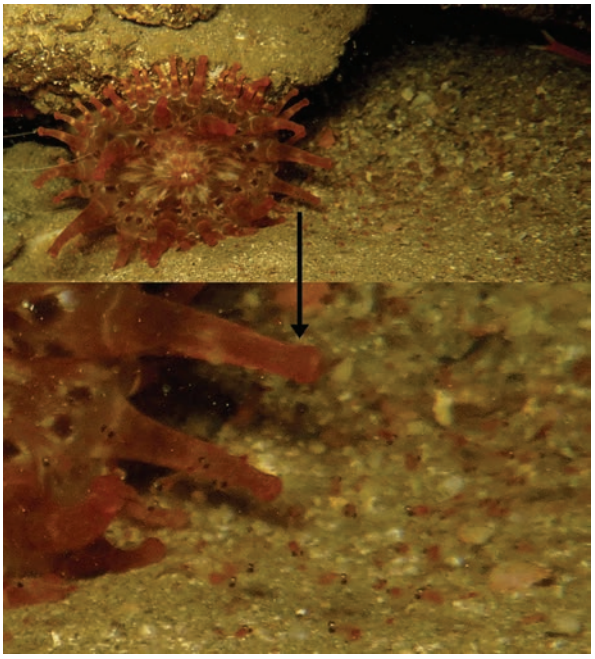

Figure 3. *Ischiomysis peterwirtzi* associated with *Telmatactis cricoides* in the marine cave Furna da Rosa; detail shows a swarm of this mysid species over sand and a small number of specimens over tentacles of the anemone; photo P. Wirtz.

as swarms distant from anemones were found in the large cave Furna da Rosa. Additional swarms were observed in five more submarine caves at São Vicente.

Ischiomysis proincisa sp. nov.

https://zoobank.org/88373DD6-43B0-4198-89ED-12344B6F3717

Figs 4–9

Type material. São Tomé • Holotype adult ♂ (BL 4.2 mm, NHMW-CR-30447), paratypes, 1 ♂ ad. (BL 3.7 mm), 1 ♂ subad., 1 ♀ subad., 2 imm., 1 juv. (NHMW-CR-30448); E-Atlantic, Gulf of Guinea, Ilhéu das Rolas (= small island crossed by the equator), off Ponta das Furnas (= cape); 0.0091°S, 6.5110°E; 19 m depth; 28 Aug. 2002, 9:50–10:10 local time; K.J. Wittmann leg.; V-shaped (i.e. two branches) semi-dark marine cave with three diveable entrances, from small mysid swarms in darker lateral recesses, diver operated hand net • Paratypes, 3 ♀♀ ad. (BL 4.0–4.3 mm), 13 ♂♂ ad. (BL 3.8–4.6 mm), 4 ♀♀ subad., 7 imm., 7 juv. (NHMW-CR-30448); 17 m depth; 22 Aug. 2002, 15:23–15:50 local time; remaining data as for holotype.

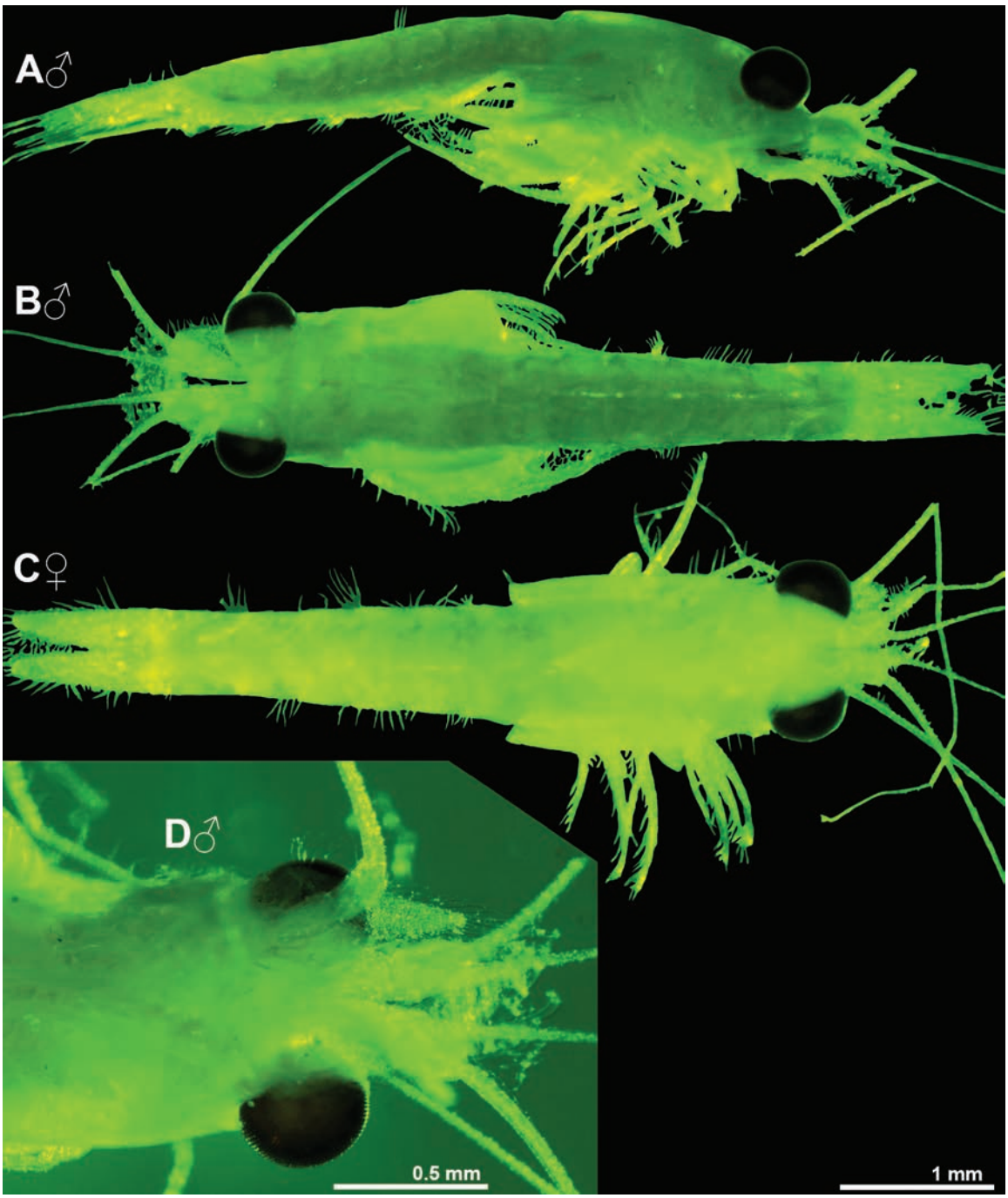

Figure 4. Habitus of *Ischiomysis proincisa* sp. nov.; holotype adult ♂ (BL 3.9 mm, **A, B, D**) and paratype adult ♀ (4.2 mm, **C**); **A, B.** Holotype *in toto*, lateral (A) and dorsal (B); **C.** Paratype *in toto*, dorsal; **D.** Cephalic region of holotype, ventral. **A–D.** Photos of fixed specimens, objects artificially separated from background, green coloring of objects artificial.

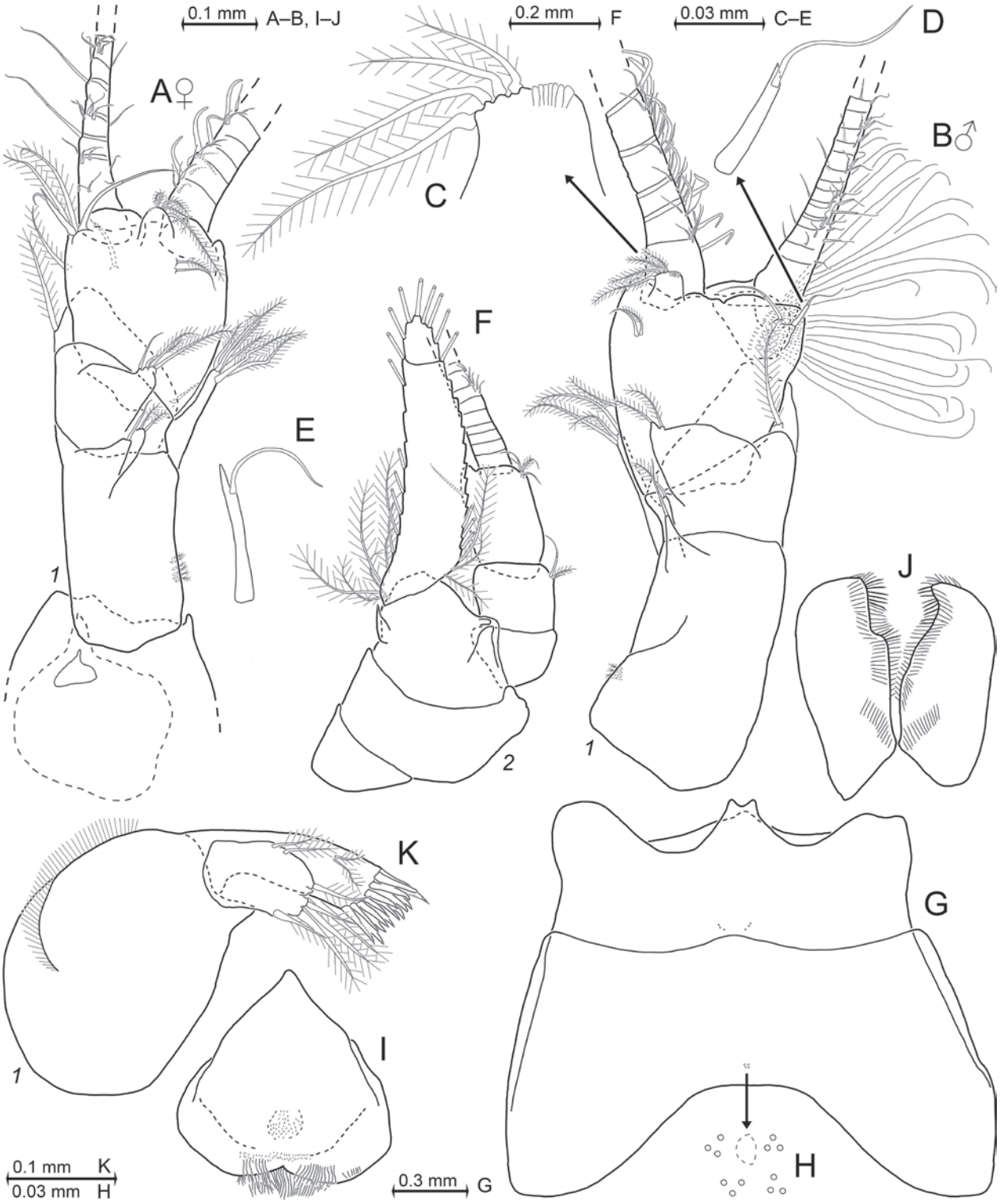

Figure 5. *Ischiomysis proincisa* sp. nov., paratypes adult ♀ (BL 4.3 mm, **A, E, I**) and adult ♂ (BL 4.5 mm, **B–D, F–H, J–K**); **A.** Right female antennula with associated processes from the frons, dorsal; **B.** Left male antennula, dorsal; details of the terminal segment of the trunk show the disto-median lobe (**C**) and the disto-mesial flagellate spine (**D**); **E.** Disto-mesial flagellate spine from left female antennula, dorsal; **F.** Antenna with antennal gland, dorsal, many setae omitted from the antennal scale; **G.** Carapace expanded on slide; **H.** Detail of (**G**) showing posterior pore group, pore diameters not to scale; **I.** Labrum, aboral face; **J.** Labium, frontal face; **K.** Maxillula, caudal.

Etymology. The species name is a Latin adjective with feminine ending, formed from the adjective *incisa* (incised) prefixed by the adverb *pro* (anteriorly), referring to the apically incised rostrum.

Type locality. Off cape Ponta das Furnas, 0.0091°S, 6.5110°E, in 17–19 m depth inside semi-dark marine cave. Each branch of the V-shaped cave is about 30 m long and open on both ends.

Diagnosis. Based on adults of both sexes. Large calotte-shaped cornea (Fig. 4) occupies distal 2/3 of eye surface (half eye length in dorsal view); cornea diameter is 28–35% carapace length. Rostrum trapezoid, anteriorly incised (Fig. 5G), about as long as the terminal segment of the antennular trunk. Only the terminal segment of the antennular trunk near disto-mesial edge with obliquely forwards oriented subapically flagellate spine with handle ending in a tooth-like projection (Fig. 5D); this spine opposed by a large smooth whip seta. Appendix masculina short though well developed, densely setose. Antennal scale (Fig. 5F) with small terminal segment separated by a not always distinct suture; scale reaching to the terminal margin of the antennular trunk; scale overreaching the antennal peduncle by 1/2 up to 2/3 of its length. Scale weakly bent laterally, slender; length is 4–5 times maximum width. Labrum (Fig. 5I) with distally narrowly rounded, roughly triangular rostral protrusion. Both sexes with small median lobe on thoracic sternite 1, no median processes on sterna 2–8 (Fig. 6E). Carpopropodus of thoracic endopods 1–8 with 2, 2, 2, 2, 3, 3, 3, and 3 segments (Fig. 6F, I, K, and Fig. 7L, P). Length of carpopropodus 3 is 4.0–4.5 times maximum width; carpus and propodus separated by a distinct suture (Fig. 7A, C). Carpus with 4 flagellate spines on distal fourth of its mesial margin in males (Fig. 7B) versus 5 spines on distal third in females (Fig. 7D). Propodus without spines. Carpopropodus of endopod 4 (Fig. 6K) with several simple smooth setae and 2–3 unilaterally barbed setae in two variants (Fig. 6L, M); claw almost straight, smooth, with bifid tip (Fig. 7G). Endopod 8 only in males with modified flagellate spine (Fig. 7M) on the outer margin of the ischium at one third ischium length from basis and an additional flagellate spine (Fig. 7N) basally on the inner margin; praeischium with a strong spiniform extension (Fig. 7O). Marsupium with large oostegite on thoracopods 7–8 plus a rudimentary plate on thoracopod 6. Penes tubular, terminally lobate (Fig. 6E); length without lobes is 3.5 times width; penes half as long as ischium of endopod 8. Pleopods (Fig. 8E–K) rudimentary, unsegmented, setose in both sexes, no spines. Uropods (Fig. 9A) setose all around, no spines. Exopod extends 14–27% its length beyond endopod and 28–44% beyond telson. Telson (Fig. 9B) length is 1.8–2.1 times maximum width and 1.0–1.2 times pleonite 6. Lateral margins with 13–18 spines only on distal half, not counting the apical spines. Telson with V-shaped narrow apical cleft penetrating 39–42% telson length; cleft with total of 30–37 spine-like laminae along basal 45–53% of its margins. Terminal lobes of telson each with two spines among which the disto-lateral spine is 14–15% telson length; the disto-mesial spine 0.3–0.4 times length of the disto-lateral spine. Telson with total of 31–37 spines.

Description. All features of the diagnosis. General appearance robust. Body red *in vivo*, length 3.7–4.6 mm in adult males (n = 15) and 4.0–4.3 mm in adult females (n = 3). Cephalothorax represents 28–33% body length, pleon without telson 51–56%, telson 11–12%, carapace without rostrum 20–26%, and rostrum 4–5%.

Eyes (Fig. 4). Eyestalks and cornea dorsoventrally compressed by a factor of 1.2. Cornea diameter twice the length of the apical segment of the antennular trunk. Eyestalks finely hispid by minute scales. Organ of Bellonci ellipsoidal, length 1/6 cornea diameter.

Carapace (Fig. 5G, H). The rostrum forms a distinct horizontal plate covering part of eyestalks. It reaches to 2/3 antero-posterior extension of normal-oriented eyestalks. Disto-lateral edges of the carapace well-rounded, anteriorly slightly produced. Posterior margin leaves the ultimate 1–1.5 thoracomere mid-dorsally exposed. As in many species of Mysidae, two characteristic groups of pores present on the midline of the carapace. The anterior group (Fig. 5G) is shortly in front of the cervical sulcus and comprises 6–10 pores with <1 μm diameter in symmetrical paramedian arrangement. The posterior pore group (Fig. 5G, H) is shortly in front of the posterior margin of the carapace; this group consists of 10–12 pores with about 2 μm diameter surrounding a larger but indistinct, rounded structure. Except for the here stated structures, carapace with smooth outer surface.

Antennulae (Fig. 5A–E). The trunk extends half its length beyond normal-oriented eyes. Measured along dorsal midline, the basal segment is 46–51% trunk length, median 18–20%, and terminal 30–34%. Basal segment of the antennular trunk (Fig. 5A, B) with two setose dorsal lobes (apophyses) near distal margin, in addition with a disto-lateral lobe; median and terminal segments each with one setose dorsal lobe near distal margin. Basal segment on basal half of its lateral face with 3–5 minute setae. The large barbed seta arising from the inner distal corner of the median segment not extending beyond the terminal segment in both sexes. The flagellum of the spine at the terminal segment of the antennular trunk inserts more apically in the male (Fig. 5D) compared to the female (Fig. 5E); this dimorphism also found in the congener *I. telmatactiphila*. Epi-antennular process (solid line in Fig. 5A) subtriangular with small, rostral, acute projection; hypo-antennular process (dashed line in Fig. 5A) subcircular with blunt subtriangular rostral projection.

Antennae (Fig. 5F). Sympod dorsally with terminally rounded, tongue-like process. Disto-lateral edge of sympod with tooth-like process. Sympod caudally with bulbous lobe containing end sac of antennal gland. Antennal scale setose all around. Apical segment, if distinct, contributes 11–16% to total scale length. Peduncle 0.7–0.8 times scale length but extending to only about half scale length due to its more caudal insertion. Basal segment is 24–29% the length of the peduncle, second is 27–31%, and third is 44–46%.

Primary mouthparts (Fig. 5I, J and Fig. 6A–C). Labrum (Fig. 5I) weakly cuticularized, densely covered by short, stiff bristles. Paragnaths (Fig. 5J) with moderately stiff bristles, no tooth-like bristles. Mandibular palp three-segmented (Fig. 6A). Its proximal segment without setae, 8–12% length of palp. Median segment: 63–65% palp length. Its length 3.0–3.7 times maximum width. Its lateral margin almost all along with 8–9 smooth setae, an additional basally barbed seta in distal-most position.

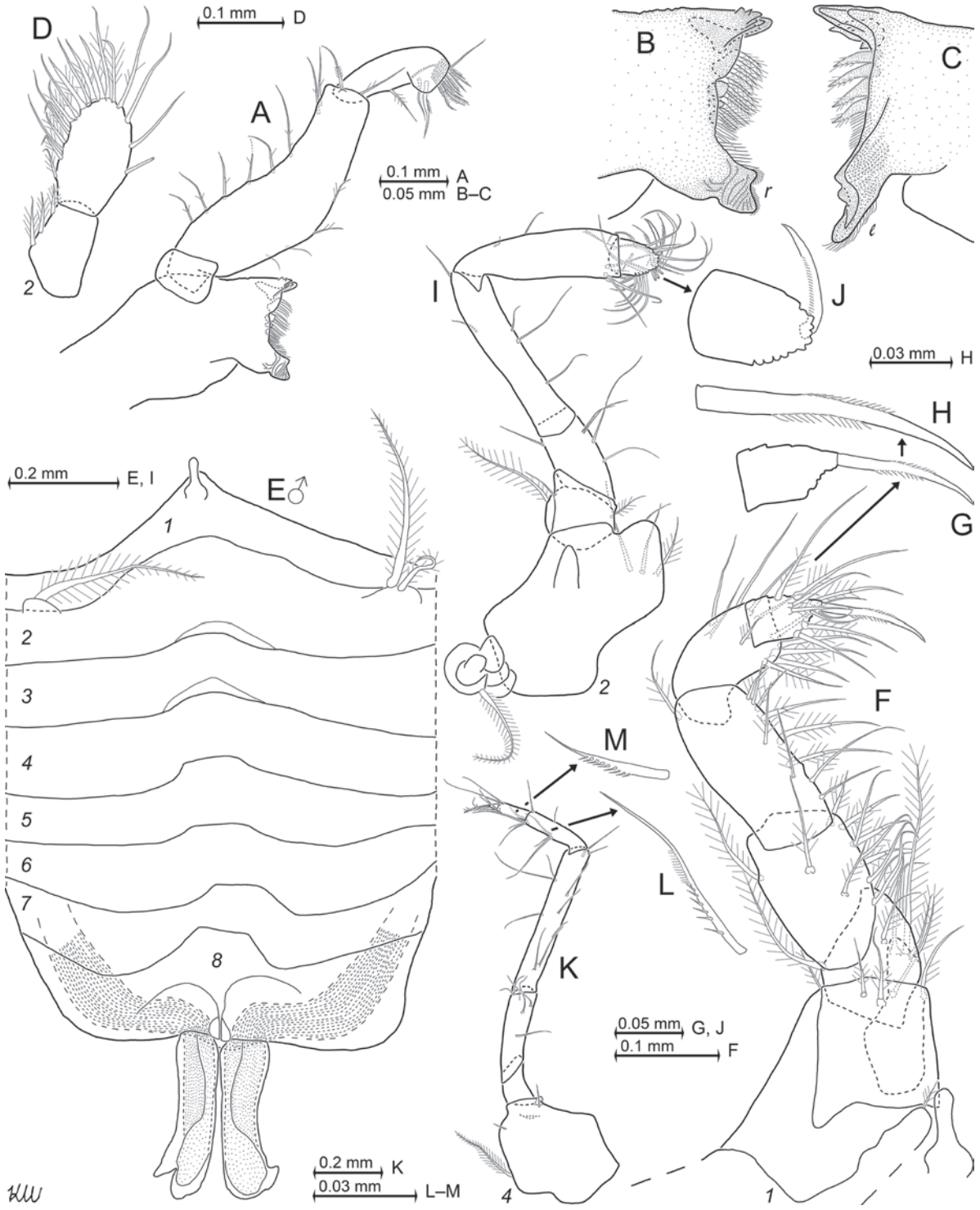

Figure 6. *Ischiomysis proincisa* sp. nov.; paratypes adult ♀ (BL 4.3 mm, **A–D**) and adult ♂ (BL 4.5 mm, **E–M**); **A.** Right mandible with palpus, caudal; **B, C.** Masticatory parts of right (**B**) and left (**C**) mandibles, caudal; **D.** Maxillary palp, rostral; **E.** Thoracic sternites 1–8 with penes, ventral; **F.** Thoracic endopod 1 with part of coxa, caudal; **G.** Detail of (F) showing dactylus 1 with claw, setae omitted; **H.** Secondary detail of (F) showing claw 1; **I.** Thoracic endopod 2, rostral; **J.** Detail of (I) showing dactylus 2 with claw, setae omitted; **K.** Thoracic endopod 4 with basis (sympod), rostral; **L, M.** Details of (K) showing modified setae of the carpus (**L**) and the propodus (**M**).

Mesial margin with 4–6 smooth setae distributed with mostly large interspaces. Terminal segment 27–28% palp length. Its mesial margin bare except for some setae near apex; distal half of lateral margin densely setose. Pars molaris with well-developed though comparatively small grinding surface in both mandibles. Left mandible (Fig. 6C) with pars incisiva bearing three teeth, digitus mobilis with two teeth, pars centralis with four basally thick, spiny teeth. Right mandible (Fig. 6B) with pars incisiva bearing 4–5 teeth, digitus mobilis with two teeth; pars

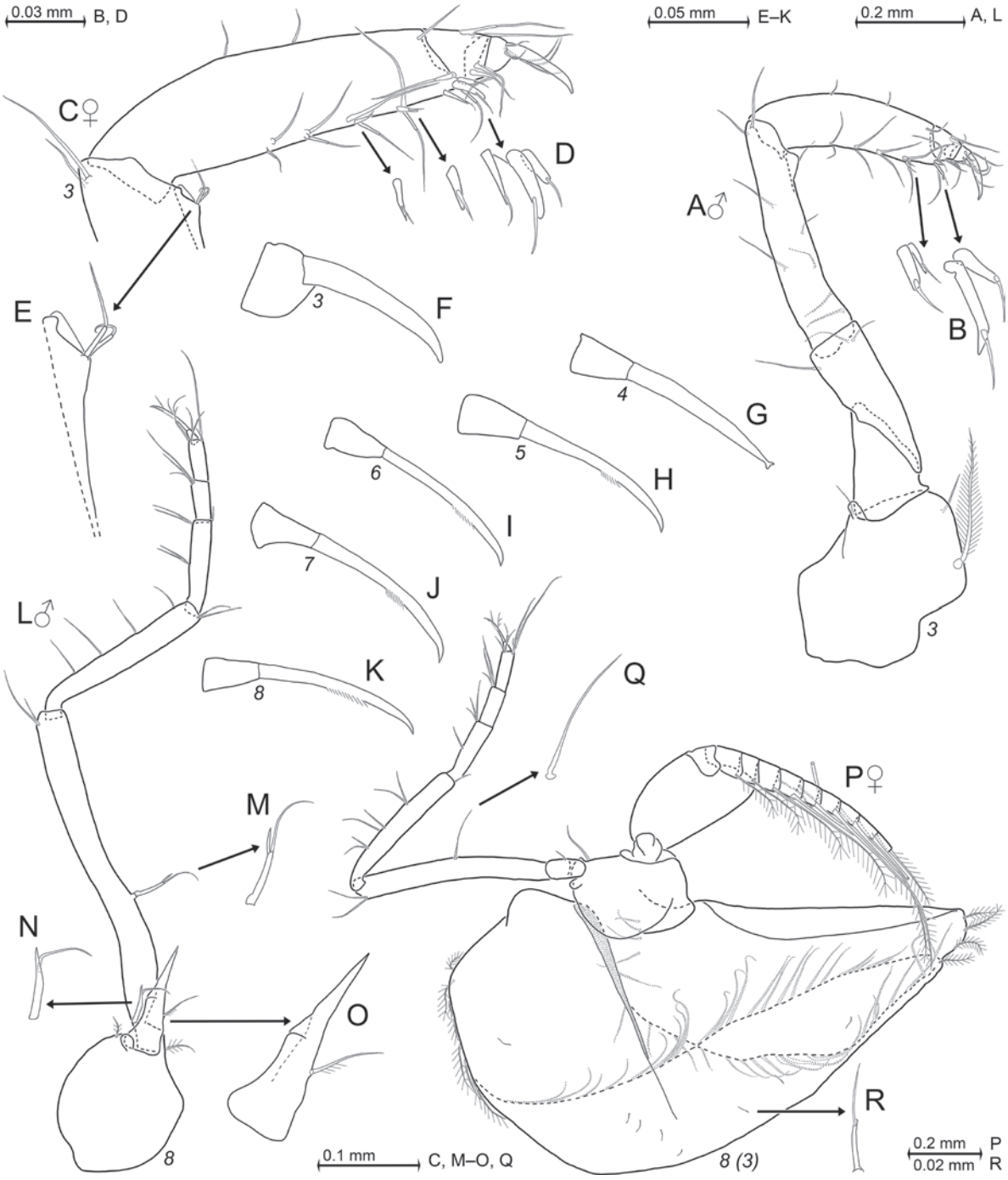

Figure 7. Thoracopods 3–8 in *Ischiomysis proincisa* sp. nov.; paratypes adult ♂ (BL 4.5 mm, **A, B, G–O**) and adult ♀ (BL 4.3 mm, **C–F, P–R**); **A.** Male thoracic endopod 3, rostral; details (**B**) show the flagellate spines of the carpus; **C.** Tarsus and distal portion of the merus in female thoracic endopod 3, rostral; details show the flagellate spines of the carpus (**D**) and the disto-mesial carina of the merus (**E**); **F–K.** Series of dactyli 3–8 with claw, setae omitted; **L.** Male thoracic endopod 8, caudal; details show the flagellate spines (**M, N**) of the ischium and the modified praeischium (**O**) with large tooth-like projection; **P.** Female thoracopod 8 with outer face of oostegite 3, lateral; details show a normal smooth seta (**Q**) of the ischium and a subapically flagellate whip seta (**R**) from the outer face of the oostegite.

centralis with 3–4 separate bases each bearing numerous slender spines that are bilaterally armed with stiff bristles. Bases decreasing in size and numbers of spines orally.

Foregut (Fig. 8A–D). Lateralia anteriorly with group of slender, apically coronate spines (Fig. 8A) with small denticles along distal <2/3 of the shaft. Lateralia more caudally with shorter, apically pronged spines (Fig. 8B) bearing small denticles along >2/3. Lateralia on each side of the foregut more caudally with cluster of 6–7 weakly, in part indistinctly serrated spines (Fig. 8C) of varying size. Dorsolateral infoldings each with cluster of three strong rugose spines (Fig. 8D).

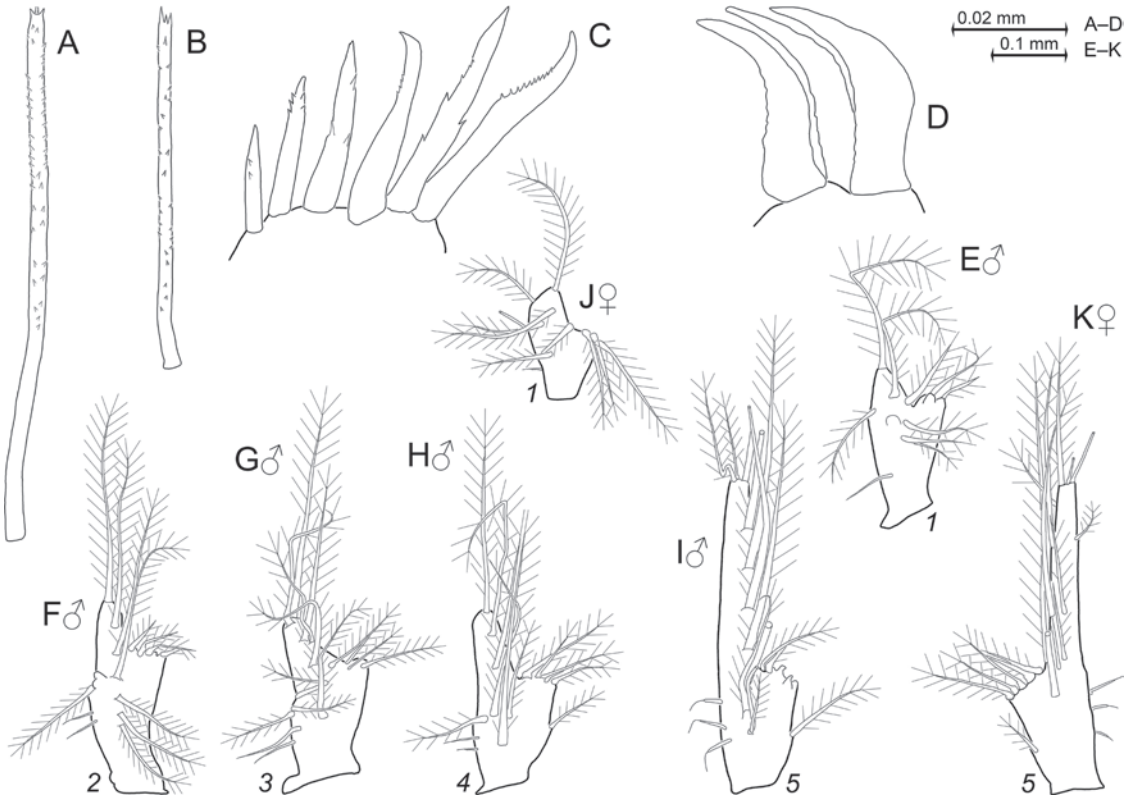

Figure 8. Spines of the foregut and pleopods in *Ischiomysis proincisa* sp. nov.; paratypes adult ♂ (BL 4.5 mm, **A–I**) and adult ♀ (BL 4.3 mm, **J, K**); **A–D.** Modified spines of the foregut in dorsal view, from the anterior (**A, B**) and posterior (**C**) parts of the lateralia and from dorsolateral infolding (**D**); **E–I.** Series of right male pleopods 1–5, lateral = rostral face; **J.** Right female pleopod 1, lateral; **K.** Left female pleopod 5, lateral.

Maxillula (Fig. 5K). Distal segment terminally with series of 10–11 strong spines, among which the two most peripheral spines are largest and subapically serrated, whereas the spines in between are weakly or not serrated. This segment subterminally with two short setae bearing long barbs on their distal 2/3; no pores detected near these setae. These setae not reaching the basis of the spines. Only two short setae also found in the congener *I. telmatactiphila*, whereas most Mysidae species show more and longer setae of that kind. Endite of the maxillula terminally with three large spiny setae accompanied by three shorter setae of that kind, caudal face with two small barbed setae.

Maxilla (Fig. 6D) with terminal segment of palp 1.6–1.8 times longer than wide and 1.3–1.6 times length of the basal segment. Terminal segment with densely setose mesial margin; only 3–4 setae along distal 2/3 of the lateral margin, no spines. Basal segment with three basally thick, barbed setae.

Thoracic sternites (Fig. 6E). Sternite 1 with small, about linguiform anterior lobe. Sternites 2–8 without median processes in both sexes. Sternite 2 with 1–3 barbed setae on intersegmental joint with thoracopod 2. Penes distally ending in 4 lobes, no setae.

Thoracopods in general (Fig. 6F–M and Fig. 7). Basal plate (Fig. 7P) of exopods expanded, length 1.5–1.9 times maximum width. Lateral margin of the plates ends in a broadly rounded corner. Flagellum of exopods 1–8 with 8, 9, 9, 9, 9, 9, 9, and 9 segments (Fig. 7P), respectively. Thoracopod 1 with large, leaf-like, smooth epipod. Basis (fused with sympod) of endopod 2 (Fig. 6I) with comparatively large lappet-like apophysis on rostral face; this apophysis small in endopods 3–8 (Fig. 6K and Fig. 7A, L, P); no such apophysis in endopod 1. Ischium shorter than merus in endopods 1–4 (Fig. 6F, I, K, and Fig. 7A), but longer than merus in endopods 5–8 (Fig. 7L, P). Thoracic endopods 1–2 each with dactylus (Fig. 6G, J) larger than that of endopods 3–8 (Fig. 7F–K); dactylus 3 (Fig. 7F) wider but not longer than dactyli 4–8 (Fig. 7G–K). Dactylus 1 with slender, weakly bent claw which is bilaterally "serrated" by stiff bristles along median portions (Fig. 6G, H). Claw 2 unilaterally rugose along proximal 2/3 (Fig. 6J). Claw 3 strong, somewhat bent, smooth (Fig. 7F). For claw 4, see "Diagnosis". Claws 5–8 weakly bent, "serrated" in subapical portions (Fig. 7H–K). Combined praeischium plus ischium of endopod 2 (Fig. 6I) are 0.6 times merus length, carpopropodus plus dactylus 1.1 times merus. Dactylus 2 very large, with dense brush formed by large numbers of normal setae and 6–10 modified setae, the latter apically bent, bearing double series of stiff barbs along proximal 2/3 to 3/4.

Gnathopods (Fig. 7A–F). Thoracic endopod 3 forms a powerful subchela. Basis with much shorter endite (Fig. 7A), if any, compared to that (Fig. 6I) of endopod 2. Ischium of endopod 3 is 2.6–3.0 times as long as wide; merus 4.5–5.1 times as long as wide and 1.4–1.6 times length of ischium. Ischium and merus strong, with smooth

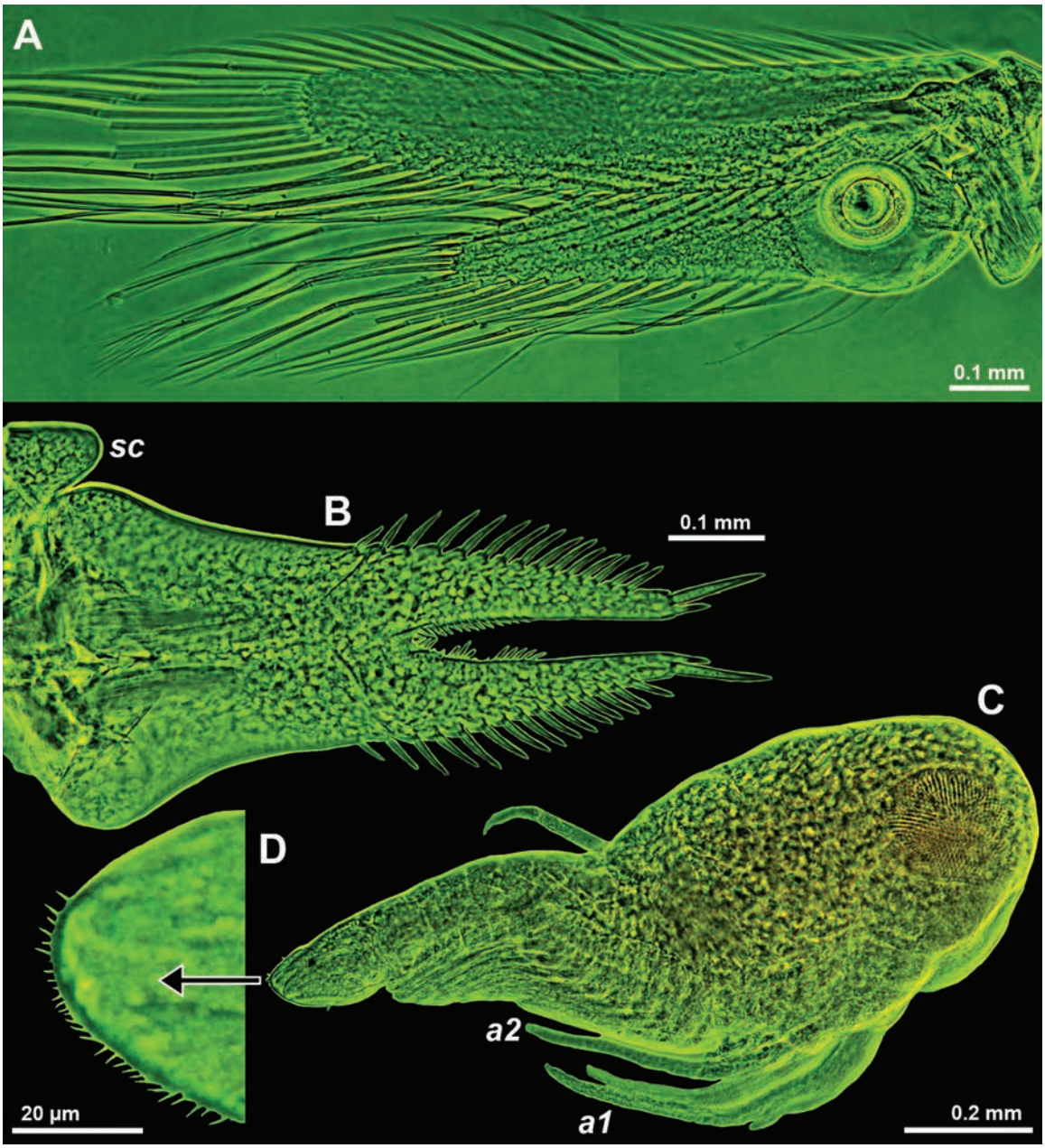

Figure 9. *Ischiomysis proincisa* sp. nov.; paratype adult ♂ (BL 4.5 mm, **A, B**) and nauplioid larvae (**C, D**); **A.** Uropods, ventral; **B.** Telson and right scutellum paracaudale (*sc*), ventral; **C.** Nauplioid larva at substage N4, lateral; lower case labels indicate antennula (*a1*) and antenna (*a2*); **D.** Tip of pleon in another nauplioid specimen. Panel (**A**) combined from two photos; **A–D.** Green coloring of objects artificial; **B–D.** Objects artificially separated from background.

setae only. Disto-mesial edge of merus with short longitudinal ridge bearing two setae (Fig. 7E). Carpopropodus as long as 0.8–0.9 times merus and 1.2–1.3 times ischium. Length of carpus 3.4–3.5 times maximum width.

Marsupium (Fig. 7P, R). Ultimate (third) oostegite rolled inwards to form two widely communicating sub-chambers. Its rostral and ventral margins with dense series of barbed (plumose) setae; inside with 5–9 microserrated setae close to the insertion on thoracic sympod 8; ventral half of oostegite 3 with about 7–10 small whip setae (Fig. 7R) loosely scattered over the outer surface.

Pleon (Fig. 8E–K). Pleomeres 1–5 measure 0.7–0.9, 0.6–0.8, 0.7–0.9, 0.6–0.9, and 0.7–0.8 times the length of pleomere 6, respectively; in other words, pleomere 6 is always shorter than combined pleomeres 4–5. Length without setae increases in series of pleopod 1, followed by subequal pleopods 2–4, and then by the much longer and slender pleopod 5. Pleopods 1–5 (Fig. 8E–K) mainly with plumose or barbed setae, but there are 1–3 smooth seta only in subbasal position on the outer margin; the latter setae clearly representing whip setae in pleopod 5 of both sexes. Pleopods 1–5 show no other types of setae, no extraordinarily long setae, no spines or teeth.

Tail fan (Fig. 9A, B). Scutellum paracaudale (labeled "*sc*" in Fig. 9B) forms a well-rounded shield covering the basolateral edge of the telson. Exopod of uropods (Fig. 9A): 4.9–5.6 times longer than broad, inner margin convex, outer margin very slightly concave, almost

Table 1. Morphological comparison between the species of *Ischiomysis*.

Characters	*I. peterwirtzi* Wittmann, 2013	*I. telmatactiphila* Wittmann, 2013	*I. proincisa* sp. nov.
BL (mm) of females	4.2–5.6	4.2–5.4	4.0–4.3
BL (mm) of males	3.5–5.1	3.5–4.7	3.7–4.6
Rostrum	short, widely rounded	triangular, apex narrowly rounded	trapezoid, anteriorly incised
Handle of flagellate spines on antennular trunk and on carpus of thoracic endopod 3	without distal projection	with tooth-like projection	with tooth-like projection
No. flagellate spines on carpus of thoracic endopod 3 in females	3	5	5
No. flagellate spines on carpus of thoracic endopod 3 in males	2	4	4
No. flagellate spines on ischium of thoracic endopod 8 in males	1	1	2
Ratio of penis length to width (without lobes)	2	3	3–4
Exopod of uropods reaches X% of its length beyond telson	39–56%	18–25%	28–44%
Ratio of telson length to maximum width	1.6–1.7	1.9–2.2	1.8–2.1
Ratio of bare portion to total length of lateral margins of telson	0.5–0.6	0.5	0.5
No. spines on each lateral margin of telson	5–7	11–14	13–18
Apical cleft penetrates X% telson length	27–34%	34–37%	39–42%
Telson cleft with laminae along basal X% of its margins	80–86%	45–55%	45–53%
Distribution	São Vicente and nearby island, Cape Verde archipelago, E-Atlantic	São Tomé and nearby island, Gulf of Guinea, E-Atlantic	Small island close to São Tomé, Gulf of Guinea, E-Atlantic
Microdistribution	Swarms associated with *Telmatactis cricoides*, also found distant from anemones inside marine cave	Swarms closely associated with *Telmatactis cricoides*	Small swarms in dimly-lit marine cave, no anemones detected
Depth (m)	8–17	15–46	17–19

straight, 1.2–1.4 times the length of endopod. Statoliths composed of fluorite; shape discoid, diameter 60–136 µm, maximum thickness 27–60 µm, statolith formula 2 + 3 + (5–7) + (1–2) + (4–5) = 15–19 (n = 12). Telson (Fig. 9B) shaped as in *I. telmatactiphila*, length is 1.1 times endopod of uropod and 0.8–0.9 times exopod of uropod. Spines on lateral margins continuously increase in size from half-length to 3/4-length of lateral margins and then decrease weakly in size distally. Laminae of the cleft are shorter than the pair of disto-mesial spines flanking the cleft. For additional details, see "Diagnosis."

Nauplioid larvae (Fig. 9C, D) with three pairs of free naupliar appendages. Apical portions of antennulae, antennae, and abdomen with minute hairs.

Discussion

The new species clearly belongs to the genus *Ischiomysis* by modified setae of the carpopropodus and apically bifid claw of thoracic endopod 4 in both sexes, as well as by modified praeischium and subapically flagellate spines on the ischium of endopod 8 in males. It differs from both so far known congeners by apically incised rostrum in both sexes, by two versus only one flagellate spine on the ischium of endopod 8 in males, and by additional characters outlined in Table 1.

Due to the short distance (only 37 km air route and >40 km waterways) between the type locality of *I. telmatactiphila* at the coast of the Island of São Tomé and that of *I. proincisa* sp. nov. off the only 2-km distant, much smaller Ilhéu das Rolas, these two species are considered sympatric. The third species of this genus, *I. peterwirtzi* from the Cape Verde Islands, is geographically and also morphologically "remote" from both its congeners by the handle of the flagellate spines on the antennular peduncle and on the carpus of thoracic endopod 3 not ending in a spiniform projection, by carpus 3 bearing fewer flagellate spines, by lateral margins of the telson on average with longer bare portion, and telson cleft shorter and with longer portion lined by laminae. The allopatric *I. telmatactiphila* and *I. peterwirtzi* share an association (less close in *I. peterwirtzi*) with the club-tipped anemone *Telmatactis cricoides*, whereas the two sympatric species are ecologically more remote due to the anemone association of *I. telmatactiphila* in well-lit habitats versus *I. proincisa* sp. nov. dwelling in a comparatively large semi-dark cave without anemones.

An incised anterior margin of the carapace is rare but not exceptional within the Mysidae. It is also known from *Neomysis ilyapai* Holmquist, 1957, belonging to the subfamily Mysinae, phylogenetically remote from the present new species, which belongs to the Heteromysinae. The former species is endemic to the coasts of Chile. A slightly depressed mid-anterior margin of the carapace is found in *N. rayii* (Murdoch, 1885) from the N-Pacific and Arctic seas and in *N. czerniavskii* Derzhavin, 1913, from the NW- and N-Pacific.

Acknowledgements

The Centro de Ciencias do Mar, University of the Algarve, co-financed several trips of the second author to São Tomé and to the Cape Verde Islands. This study received Portuguese national funds through FCT—Foundation for Science and Technology—through projects UIDB/04326/2020, UIDP/04326/2020, and LA/P/0101/2020.

References

Alcaraz M, Riera T, Gili JM (1986) *Hemimysis margalefi* sp. nov. (Mysidacea) from a submarine cave of Mallorca Island, western Mediterranean. Crustaceana 50(2): 199–203. https://doi.org/10.1163/156854086X00214

Bhaduri RN, Crowther AL (2016) Association of the mysid *Idiomysis inermis* with the sea anemone *Stichodactyla haddoni* in Moreton Bay. Marine Biodiversity 46: 707–711. https://doi.org/10.1007/s12526-015-0408-7

Daneliya ME (2021) On the mysid crustacean genus *Heteromysis* (Mysidae: Heteromysinae) of the Tasman Sea, with notes on the Tribe Heteromysini. Records of the Australian Museum 73: 1–50. https://doi.org/10.3853/j.2201-4349.73.2021.1737

Derzhavin AN (1913) Neue Mysiden von der Küste der Halbinsel Kamtschatka. Zoologischer Anzeiger 43: 197–204. https://www.zobodat.at/pdf/ZoologischerAnzeiger_43_0197-0204.pdf

Duchassaing de Fonbressin P (1850) Animaux Radiaires des Antilles. Plon Frères, Paris, 35 pp.

Holmquist C (1957) Mysidacea of Chile. Reports of the Lund University Chile Expedition 1948–1949. Lunds Univeristets Årsskrift, N.F. Adv. 2, 53(6): 1–53.

Ledoyer M (1963) *Hemimysis speluncola* n.sp. Mysidacé nouvelle des grottes sous-marines obscures. Recueil des Travaux de la Station Marine d'Endoume 30: 77–81.

Mauchline J (1980) The biology of mysids and euphausiids. In: Blaxter JHS, Russell FS, Young M (Eds) Advances in Marine Biology, Academic Press, London, Vol. 18, 1–677.

Mees J, Meland K [Eds] (2024) World List of Lophogastrida, Stygiomysida and Mysida. In: World Register of Marine Species. Instant Web Publishing. https://www.marinespecies.org/aphia.php?p=taxdetails&id=1379689

Murdoch J (1885) Description of seven new species of Crustacea and one worm from Arctic Alaska. Proceedings of the United States National Museum 7: 518–522. https://doi.org/10.5479/si.00963801.459.518

Norman AM (1892) On British Mysidae, a family of Crustacea Schizopoda. Annals and Magazine of Natural History, ser. 6, 10(56): 143–166. https://doi.org/10.1080/00222939208677385

Nouvel H (1942) Diagnoses préliminaires de Mysidacés nouveaux provenant des campagnes du Prince Albert 1er de Monaco. Bulletin de l'Institut Océanographique de Monaco 831: 1–12. www.vliz.be/imisdocs/publications/261362.pdf

Riera T, Zabala M, Peñuelas J (1991) Mysids from a submarine cave emerge each night to feed. Scientia Marina 55: 605–609. https://diposit.ub.edu/dspace/bitstream/2445/32435/1/121050.pdf

Saito N, Hoshino O, Fukuoka K (2018) First record of *Pleurerythrops secundus* (Crustacea, Mysida) in association with benthic hydroids (Cnidaria, Hydrozoa) in shallow water of Izu-Ohshima, Pacific coast of central Japan. Crustacean Research 47: 137–143. https://doi.org/10.18353/crustacea.47.0_137

San Vicente C, Monniot F (2014) The ascidian-associated mysid *Corellamysis eltanina* gen.nov., sp.nov. (Mysida, Mysidae, Heteromysinae): a new symbiotic relationship from the Southern Ocean. Zootaxa 3780(2): 323–346. https://doi.org/10.11646/zootaxa.3780.2.6

Wilson GDF (1989) A systematic revision of the deep-sea subfamily Lipomerinae of the isopod crustacean family Munnopsidae. Bulletin of the Scripps Institution of Oceanography 27: 1–138.

Wittmann KJ (1978) Biotop- und Standortbindung mediterraner Mysidacea. Doctoral thesis, Univ. Vienna, 1–211.

Wittmann KJ (1981) Comparative biology and morphology of marsupial development in *Leptomysis* and other Mediterranean Mysidacea (Crustacea). Journal of experimental marine Biology and Ecology 52: 243–270. https://doi.org/10.1016/0022-0981(81)90040-X

Wittmann KJ (2013) Mysids associated with sea anemones from the tropical Atlantic: descriptions of *Ischiomysis* new genus, and two new species in this taxon (Mysida: Mysidae: Heteromysinae). Crustaceana 86: 487–506. https://doi.org/10.1163/15685403-00003166

Wittmann KJ (2020) Lophogastrida and Mysida (Crustacea) of the "DIVA-1" deep-sea expedition to the Angola Basin (SE-Atlantic). European Journal of Taxonomy 628: 1–43. https://doi.org/10.5852/ejt.2020.628

Wittmann KJ (2023) Evidence and modification of non-visual eyestalk organs in troglobiont Mysida and Stygiomysida (Crustacea). Arthropoda 1(4): 432–450[, suppl.]. https://doi.org/10.3390/arthropoda1040019

Wittmann KJ (2024) Mysidae (Crustacea: Mysida) from sponges in sublittoral waters of Lizard Island (Indo-Pacific: Coral Sea), with description of *Heteromysis kaufersteinae* sp. nov., first record of *H. domusmaris* from nature, and range extension in *Anchialina lobata*. Crustacean Research 53: 97–111. https://doi.org/10.18353/crustacea.53.0_97

Wittmann KJ, Ariani AP (2019) Amazonia versus Pontocaspis: a key to understanding the mineral composition of mysid statoliths (Crustacea: Mysida). Biogeographia – The Journal of Integrative Biogeography 34: 1–15. https://doi.org/10.21426/B634142438

Wittmann KJ, Chevaldonné P (2021) First report of the order Mysida (Crustacea) in Antarctic marine ice caves, with description of a new species of *Pseudomma* and investigations on the taxonomy, morphology and life habits of *Mysidetes* species. ZooKeys 1079: 145–227. https://doi.org/10.3897/zookeys.1079.76412

Wittmann KJ, Griffiths CL (2017) Three new species of *Heteromysis* (Mysida, Mysidae, Heteromysini) from the Cape Peninsula, South Africa, with first documentation of a mysid-cephalopod association. ZooKeys 685: 15–47. https://doi.org/10.3897/zookeys.685.13890

Wittmann KJ, Wirtz P (2017) *Heteromysis sabelliphila* sp. nov. (Mysida: Mysidae: Heteromysinae) in facultative association with sabellids from the Cape Verde Islands (subtropical N.E. Atlantic). Crustaceana 90: 131–151. https://doi.org/10.1163/15685403-00003624

Wittmann KJ, Ariani AP, Lagardère J-P (2014) Chapter 54. Orders Lophogastrida Boas, 1883, Stygiomysida Tchindonova, 1981, and Mysida Boas, 1883 (also known collectively as Mysidacea). In: von Vaupel Klein JC, Charmantier-Daures M, Schram FR (Eds) Treatise on Zoology - Anatomy, Taxonomy, Biology. The Crustacea. Revised and updated, as well as extended from the Traité de Zoologie, Koninklijke Brill NV, Leiden, Vol. 4 Part B: 189–396. https://doi.org/10.1163/9789004264939_006

Wittmann KJ, Abed-Navandi D, Dubois M, Chevaldonné P (2021) Three new species of *Heteromysis* (Crustacea: Mysida) from coral reef aquaria in Florida and Central Europe. Zootaxa 4980: 490–520. https://doi.org/10.11646/zootaxa.4980.3.3

Zoosyst. Evol. 100 (4) 2024, 1443–1457 | DOI 10.3897/zse.100.126666

PENSOFT

für Natur MUSEUM FÜR NATURKUNDE BERLIN

Evolutionary ecology of the North Atlantic Talitridae (Crustacea, Amphipoda): A review

David J. Wildish[1]

1 *Huntsman Marine Science Centre, St. Andrews, New Brunswick, E5B 2L7, Canada*

https://zoobank.org/AF4B76F6-3F54-4E11-9870-834249B8053D

Corresponding author: David J. Wildish (talitridnb@gmail.com)

Academic editor: Luiz F. Andrade ♦ **Received** 4 May 2024 ♦ **Accepted** 30 September 2024 ♦ **Published** 24 October 2024

Abstract

Four primary estuarine/marine ecotopes recognized in the North Atlantic continental littoral and continental terrestrial margins give rise to the following ecotypes: wrack generalists (=beach-hoppers), psammophilic talitrids (=sandburrowing-hoppers), palustral talitrids (=salt marsh-hoppers), and xylophagous talitrids (=driftwood hoppers). On the European continent, there are freshwater riverine and lacustrine talitrids. In addition, there are a few terrestrial ecotypes in the Northeast Atlantic Islands: rainforest leaflitter talitrids and one troglobiont (=cave-hopper). Wrack generalist species are phenotypically plastic and can live in one or more secondary ecotopes. It is hypothesized herein that switching on/off appropriate genes by cellular mechanisms (epigenesis) occurs during the microevolution of Talitridae. The generalist/specialist continuum concept supports our understanding of both the ecology and microevolution of talitrids. Microevolutionary characteristics of wrack generalists are that they exhibit the most phenotypic variability and occurrences of epigenesis, have the most extensive zoogeographic range, and have the lowest speciation potential and endemism rate. Examples where epigenesis may be part of the microevolutionary process include low/high salinity and hypogean/epigean combined switches giving rise to sibling (sister) species pairs. Current views of the phylogeny of the Talitridae based on either morphological characters used in taxonomy or molecular genetic methods are still under development. Molecular genetic methods show promise of providing a scientifically reproducible phylogeny and temporal history of talitrids (macroevolution), but insufficient coverage of genera within talitrids and of related groups is available to do so yet.

Key Words

Generalist/specialist continuum, micro-/macro-evolution, primary and secondary talitrid ecotypes, sibling species pairs, Talitridae

Introduction

The Talitridae (talitrids) are a family within the Amphipoda, which in 2018 consisted of 80 genera and 512 species worldwide (Tykarska et al. 2019), with new genera and species being added annually. Many of the new talitrid species described do not contain adequate ecological descriptions of the type locality (Lowry and Myers 2019).

Talitrids are found in many ecotopes (=ecological habitats or niches) from marine and estuarine to freshwater to terrestrial (Hurley 1968; Friend and Richardson 1986; Wildish 1988). A current summary of the established ecotopes occupied by talitrids on the shores of the Atlantic Ocean is shown in Table 1. This is a preliminary list because only a few talitrids, mostly in the temperate North Atlantic, have been adequately studied from an ecological perspective. As further ecological studies, notably on southern hemisphere terrestrial species, are completed, further ecotopes will be added to a world list expanded from Table 1.

Evolutionary studies of talitrids include changes that occur at very different temporal and spatial scales. Both scales are continuous, making it difficult to characterize the particular evolutionary changes of concern. Here I consider microevolution to result from a limited number of environmental factors and genetic or epigenetic changes in one or a few species. By contrast, macroevolution involves all species within the family Talitridae from

their origin millions of years ago from an amphipod stem group to their radiation to most parts of the world today.

This presentation is an update and expansion of a review dealing only with xylophagous talitrids (Wildish 2017). The expansion includes new ecological discoveries and microevolutionary findings concerning Talitridae in all ecotopes of the North Atlantic coastal region. This includes the Gulf of Mexico and the Mediterranean Sea, Atlantic islands, and the terrestrial ecotopes of the Northeast Atlantic islands (Azores, Madeira, and Canaries Archipelagos).

Primary and secondary ecotopes

In ecology, we require an accurate descriptive nomenclature for each talitrid ecotype (a talitrid species occupying and adapted to a particular ecotope) recognized so that it is possible to refer each species to an ecotope within a given ecosystem (Table 1). For this reason, the term "semi-terrestrial" as occasionally used in the literature for marine intertidal talitrids (e.g., Hupalo and Grabowski 2018) is inadmissible in ecology because there is no ecosystem to which it is referable. Thus, wrack generalists (as here defined) are never "semi-terrestrial" and are more accurately described in an ecological sense as 'amphibious' because they live in both damp air in the intertidal zone and sometimes in seawater (at high tide and occasionally during passive seawater dispersal). Table 1 considers only primary ecotypes and represents a work in progress, as it is expected that many more ecotopes and ecotypes remain to be discovered and described from other parts of the world. Primary ecotopes are ones in which a given species is usually found and to which it has evolved characteristic adaptations. It is contrasted with one or more secondary ecotopes, in each of which the same species is less commonly found and lacks some of the characteristic adaptations of the primary ecotype (Wildish and Robinson 2016a).

The most studied ocean system concerning talitrid ecology is the coastal North Atlantic, inclusive of the Gulf of Mexico and the Mediterranean Sea, with a species and ecotype list given by Wildish and Chang (2017). This list is summarized in Table 2. It does not include the northeast Atlantic Island talitrids; they are dealt with separately below. There is disagreement regarding the zoogeography of *Orchestia gammarellus* (Pallas, 1766) in the northwest Atlantic (Canada and Iceland), with Myers and Lowry (2020) suggesting that it is a new species despite the molecular genetic evidence of Henzler and Ingolfsson (2008) that it is the same species on both sides of the North Atlantic. Wildish and McDonald (2023) have proposed a natural, passive dispersal hypothesis to account for the presence of *O. gammarellus* in post-glacial Iceland and Canada. The other amphi-Atlantic species of Table 2 are *Platorchestia exter* Myers & Lowry, 2023, and *P. oliveirae* Myers & Lowry, 2023. These two species are the dominant wrack generalists of the coastal northwest Atlantic with a zoogeographic range from Brazil to Newfoundland. *Platorchestia exter* occupies the northerly part and *P. oliveirae* the more southerly part of this range, with the separation occurring somewhere in, or north of, Florida. It has been hypothesized (Wildish and Chang 2017) that both species reached the northeast Atlantic coast recently either by natural, passive rafting carried by Gulf Stream currents or by synanthropy. Preliminary molecular genetic evidence that the European *Platorchestia* are the same species as those from North America is available (Radulovici 2012; Hupalo and Grabowski 2018).

It was discovered by field observations in 2015 that *P. exter* could occupy a secondary ecotope: stranded driftwood (Wildish and Robinson 2016a) when specimens were found occupying this habitat in a driftwood depository in the Bay of Fundy. This study also confirmed that *P. exter* could be cultured solely on driftwood as food for at least six months. Driftwood acclimation, which involves ingesting rotting driftwood, resulted in reduced growth and shorter adult total body lengths (Table 3).

Table 1. Primary talitrid ecotopes with names for the presently known ecotypes of the North Atlantic region. Based on Friend and Richardson (1986), Wildish (1988), Wildish (2017), Lowry and Myers (2019), and Myers (2022) with species names conforming to WoRMS (Horton et al. 2023), accessed in 2023.

Ecosystem	Primary Ecotope	Ecotype Name	Common Name	Example
Marine/Estuarine	Eulittoral wrack	Wrack generalist	Beach-hopper	*Orchestia mediterranea*
	Supralittoral wrack	Wrack generalist	Beach-hopper	*Orchestia gammarellus*
	Eulittoral salt marsh	Palustral	Salt-marsh-hopper	*Uhlorchestia uhleri*
	Supralittoral salt marsh	Palustral	Salt-marsh-hopper	*Speziorchestia grillus*
	Supralittoral mangrove	Mangal	Mangrove-hopper	*Chelorchestia forceps*
	Supralittoral sand-burrowing	Psammophile	Sand burrowing-hopper	*Americorchestia longicornis*
	Supralittoral driftwood	Xylophage	Driftwood-hopper	*Macarorchestia roffensis*
Freshwater	Plant drift-riverine	Riverine	Riverine-hopper	*Cryptorchestia cavimana*
	Plant drift-lacustrine	Lacustrine	Lacustrine-hopper	*Cryptorchestia garbinii*
	Non-tidal freshwater marsh	Freshwater palustral	Freshwater marsh-hopper	–
Terrestrial	Evergreen rainforest floor	Rain forest leaflitter	Leaf litter-hopper	*Palmorchestia epigaea*
	Soil- burrowing	Fossorial	Soil-hopper	–
	Marine caves	Troglobiont	Cave-hopper	*Palmorchestia hypogaea*
	Arboreal rainforest	Rain forest bryophile	Moss-hopper	–

Table 2. Primary ecotypes of marine/estuarine Talitridae. Comparing the coastal northwest Atlantic/Gulf of Mexico talitrids with those from the coastal northeast Atlantic/Mediterranean Sea. From Wildish and Chang (2017), all species names included below are given in Table 1 of this reference.

Primary ecotype	Numbers of Species		Number of shared species	Name of shared species
	NW Atlantic/ Gulf of Mexico	NE Atlantic/ Mediterranean		
Wrack Generalists	9	8	3	*O. gammarellus P. exter P. oliveirae*
Psammophiles	5	6	0	–
Palustrals	9	0	0	–
Xylophages	0	5	0	–
Troglobiont	0	1	0	–
Mangal	1	0	0	–

Table 3. Total body length (mm) of *P. exter* under various acclimation conditions (A to C). A Naturally acclimated to driftwood, collected in September 2014 and cultured for 6 months over winter in driftwood, from Wildish and Robinson (2016a). B Experimentally acclimated (~3 months) in culture with driftwood and collected from Haggerty's Beach in the summer of 2015. C Experimentally acclimated (~3 months) in culture with wrack (control) and collected from Indian Point in the summer of 2015. B and C from Wildish and Robinson (2016b).

Acclimation Conditions	Ecotope	Mean	Standard Deviation	N	Maximum	Minimum
A	Secondary	9.1	1.8	126	13.5	5.8
B	Secondary	11.5	1.7	32	15.9	6.3
C (Control)	Primary	12.7	1.8	42	16.6	6.3

In the control culture, treatment C of Table 3, total body length is significantly greater than in treatment A by t-test ($t = 11.225$, $df = 167$, $p < 0.001$), and C is also greater than B ($t = -2.952$, $df = 73$, $p < 0.005$). It was experimentally shown that slower growth rates were linked to lower standard metabolic rates (Wildish and Robinson 2018), suggesting that aged driftwood was more difficult to digest than aged macroalgal wrack. Experimental demonstration that *P. exter* can readily reverse the acclimation process from driftwood to wrack or vice versa has been obtained (Wildish and Robinson 2018). The mechanisms that produce dwarf morphs within *P. exter* because of a diet switch to driftwood remain unknown but could involve some form of phenotypic plasticity (see below).

Dwarf secondary ecotypic morphs have also been recognized in two other wrack generalists. The eulittoral wrack generalist *Orchestia mediterranea* A. Costa 1857 was found in a floating piece of driftwood that beached in the tidal Swale, Kent, England, containing 16 specimens (Wildish 2018 and references therein). The dwarf specimens of *O. mediterranea* were originally described as a new xylophagous specialist species, but the genetic data showed this was not the case (Wildish 2018). It is possible that *O. gammarellus* can also exist in a secondary driftwood ecotope (Wildish 2017). Thus, at least three species of secondary ecotype dwarf morphs associated with xylophagy have been identified and the primary ecotype of each is a wrack generalist, suggesting that this may be a general feature of this ecotype.

Orchestia gammarellus is also reported to live in European salt marshes (Sprung and Machado 2000; Dias and Sprung 2003; Schrama et al. 2015) rather than in the supralittoral drift line of beaches (primary ecotope), and this may be a further example of a secondary palustral ecotype. As far as I am aware, the morphological, physiological, and behavioral changes associated with a palustral ecotope for *O. gammarellus* have not been investigated. However, a change of diet from decaying macroalgae to decaying lignivorous salt marsh grasses is involved.

The generalist/specialist continuum

A generalist/specialist continuum within Talitridae was introduced by Wildish and Radulovici (2019) to help understand the ecological and evolutionary characteristics of this family. The generalist group of species are those capable of living in more than one ecotope and consuming a varied diet range. They contrast with specialist groups that live in a single ecotope and consume a singular diet.

Specific examples of primary ecotypes currently known from the North Atlantic coastal region are listed below in the same continuum order (generalist to specialist) shown in Table 4:

- # 1. Wrack generalists include *P. exter*, *P. oliveirae*, and *O. gammarellus*, which occur on both northeast and northwest Atlantic coasts. Wrack generalists limited to the northwest Atlantic coast are *Mexorchestia carpenteri carpenteri*, *M. c. radulovici-ae*, *Tethorchestia antillensis*, and *Platorchestia* sp. (identified genetically by Radulovici 2012). Limited to the northeast Atlantic coast are *Orchestia mediterranea*, *O. aestuarensis*, *O. montagui*, *O. xylino*, and *Speziorchestia stephensi*.
- # 2. Up to 7 genetically defined palustral species currently included within *Speziorchestia grillus* are confined to the northwest Atlantic coast.

- # 3. Different species of psammophilic talitrids occur on each side of the Atlantic: northwest: *Americorchestia longicornis*, *A. megalophthalma*, *A. heardi*, *A. salomani*, and *A. barbarae*; on the northeast: *Talitrus saltator*, *Deshayesorchestia deshayesii*, *Sardorchestia pelecaniformis*, *Britorchestia brito*, *B. ugolini*, and *Africorchestia spinifera*.
- # 4. Five species of xylophagous talitrids occur on the northeast Atlantic coast only: *Macarorchestia microphthalma*, *M. remyi*, *M. pavesiae*, *M. roffensis*, and *M. martini.*
- # 5. A single troglobiont in the northeastern Atlantic islands: *Palmorchestia hypogea.*

Of the five ecotopes in Table 4, the most variable one is the marine/estuarine supralittoral wrack zone. Wrack includes a wide range of different species of green, brown, and red macroalgae, driftwood (from natural tree fall and human discards), and may contain or be dominated by angiosperm leaf litter, including seagrasses such as *Zostera* sp. and *Posidonia* sp. Over the full range of a given wrack generalist species, for example, *O. gammarellus* from northern Africa to Norway, the composition of wrack is zoogeographically highly variable. In addition, each item of plant detritus in wrack may be at a different stage of the decay cycle. The amount of wrack at a given location varies temporally depending on tidal conditions (predictable) and wind effects (random and unpredictable). Thus, offshore winds may carry wrack and driftwood away as flotsam, while onshore winds may deposit new sources of wrack and driftwood. Because of the high degree of environmental variability, it is not surprising that species belonging to the wrack generalist ecotype are phenotypically plastic, e.g., in *P. exter* (as *P. platensis*, Stock 1996; LeCroy 2011), rendering morphological classification difficult.

Psammophilic talitrids (# 2 Table 4) are limited to sandy beaches into which they can make temporary burrows for residence during daylight hours. There are five species on the northwest Atlantic and six on the northeast Atlantic coasts. There is some evidence that psammophiles are selective feeders, choosing particular macroalgal species from wrack on which to feed. An example is *Talitrus saltator* in France, which prefers *Fucus serratus* over other wrack species (Adin and Riera 2003). At another location in Spain, *T. saltator* preferred two different species of brown (phaeophycete) seaweed wrack: *Sargassum muticum* and *Gongolaria baccata* (Olabarria et al. 2009). Such results suggest that availability (of a phaeophycete) within the local wrack determines the food choice. Most authors stress the importance of wrack aging (microbial decomposition) in food choice, thought to be because of increased nutritional value (Lastra et al. 2015) or the decomposition of grazer deterrent chemicals (phlorotannins) in brown macroalgae (Pennings et al. 2000).

Of the palustral ecotype (# 3 Table 4), there are possibly seven species on the northwest Atlantic coast, whereas in the northeast Atlantic, there are none. However, *O. gammarellus* may be present in salt marshes of the northeast Atlantic as a secondary palustral ecotype (see above, although experimental support that it is consuming seagrass leaf litter is lacking). Food available to salt marsh hoppers includes a range of salt marsh angiosperm plants, sometimes with the addition of marine macroalgae thrown into the marsh by storm winds or in flooding seawater. As far as I know, no studies on digestive physiology are available for talitrids where the primary ecotope is a salt marsh.

There are five known species of specialist xylophagous talitrids (# 4 Table 4) found only on the northeast Atlantic coast. They are obligate feeders on rotting driftwood. Recently, a new species of xylophagous talitrid was discovered in Thailand by Wongkamhaeng et al. (2022). It is the first driftwood hopper discovered outside the northeast Atlantic/Mediterranean region and is likely an example of convergent evolution.

The single species of cavernicolus talitrid (# 5 Table 4) occurs only in the northeastern Atlantic Islands, and its feeding habits have not been studied (as is true of all other troglobiontic talitrids so far discovered).

Table 4. Marine/estuarine talitrid ecotopes of the North Atlantic coastal region in continuum order. The most generalist is #1, and #5 is the most specialist. Note that #5 is technically a terrestrial taxon.

Biological Characteristic	Continuum order				
	1	2	3	4	5
Ecotype	Wrack generalist	Psammophile	Palustral	Xylophage	Troglobiont
Size: Total body length, mm	> 15	> 15	> 15, < 15	< 15	< 15
Ecotope Variability	Highest	→	→	→	Lowest
Passive Dispersal	Best	→	→	→	Worst
Reproductive Potential	Maximum	→	→	→	Minimum
Standard Metabolic rate	Highest	→	→	→	Lowest
Dorsal Epidermal Pigment Patterns	Present	→	→	→	Absent
Behavioural Activity pattern	Nocturnally active	→	→	→	Random activity
Predation Risk	High	→	→	→	Low
Random Escape Response	Most	→	→	→	Least

Microevolution in contemporary talitrids

Mechanisms of microevolution

A modern understanding of Neo-Darwinian evolution must consider both genetic and epigenetic mechanisms (Jablonka and Lamb 2014).

Speciation involving sexual or natural selection of genetic change may occur in the following ways:

- Allopatric, where some form of barrier divides a breeding population into two parts such that the barrier prevents interbreeding between the separated populations. Liu et al. (2018) studied psammophilic hoppers with molecular genetic methods and showed that populations separated by a land bridge evolved independently on either side of the bridge.
- Sympatric, where genetic change occurs within the same population and the genetic variants are naturally selected and evolve reproductive isolation mechanisms that prevent interbreeding with the parent population. Wrack generalists found on Gulf of Mexico shores, such as *Mexicorchestia carpenteri carpenteri* Wildish & LeCroy, 2014, and *Tethorchestia antillensis* Bousfield, 1984, may have evolved from a common ancestor in this way.
- Peripatric evolution occurs when an isolated peripheral population is formed on an oceanic island by immigrants from the continental mainland. On the island, they evolve to become reproductively isolated from the parent, producing a new sister species. An example is from the Azores archipelago, where the xylophagous *Marcarorchestia martini* Stock, 1989, evolved from a mainland ancestor of *Macarorchestia* sp., which arrived as an immigrant on the island of Terceira in a floating driftwood log (Stock 1989; Wildish 2017).
- Parapatric evolution occurs when a smaller population becomes partially isolated from the main population at the edge of its zoogeographic range, then becomes genetically differentiated and a new species. A possible example is *Orchestia aestuarensis* Wildish, 1987, which is limited in distribution to an isolated mesohaline section of lowland estuaries at the edge of the range of its sister (parent) species, *O. mediterranea* A. Costa, 1857 (but see below).

Microevolution involving epigenetically derived alternative phenotypes (polyphenism or polymorphism) occurs as a result of the following (West-Eberhard 1989, 2005):

- Allelic-switch, in which the alternative phenotype chosen by the individual depends on one or more alleles present on one or more switch genes.
- Combined allelic switch, in which the alternative phenotype is switched on or off by a combination of allelic and environmental stimuli.

The non-genetic cellular controls that switch genes on or off in epigenesis (epimutation) include DNA methylation, histone modification, and non-coding RNA action (Bossdorf et al. 2008). I know only one talitrid study of epigenetic variation (Baldanzi et al. 2017). It concerned the psammophilic talitrid, *Capeorchestia capensis* (Dana, 1853) and looked for differences in DNA methylation among geographically separate populations in South Africa, which were loosely linked to different temperature regimes.

Future work on epigenesis in Talitridae should be focused on wrack generalist hoppers (Table 4) because this ecotype experiences the most environmental variability. Some specific areas where epigenetic studies utilizing ecological genetic techniques might be fruitful are suggested in the following sections.

Biological interactions

Talitrids interact with many different species (intraspecific interactions are excluded) from viruses and bacteria to mammals and birds (Wildish 1988). All types of interspecific interaction can be found among talitrids, but here predation by other species is the only one considered. The chief predators of wrack generalists and psammophilic talitrids are birds, particularly many species of shorebirds that forage intertidally, such as seagulls, starlings, and crows, but less commonly mice and the blue fox (Wildish 1988). During dispersion wrack, generalists have also been found in the stomachs of inshore fish, indicating that they have been predated during passive dispersal at sea (Gibson and Robb 1996; Laffaille et al. 1999).

Wrack generalists and psammophiles remain hidden during the day, the former in and under wrack piles cast up by recent high tides and the latter in temporary supralittoral burrows made in the sand above the recent wrack so they remain in contact with moisture. Endogenous diel rhythms with maximum activity at night have been found in many species of wrack generalists and sand-burrowing hoppers (Wildish et al. 2021). In the latter study, xylophagous-acclimated *Platorchestia exter* Myers & Lowry (2023), living in a secondary ecotope (its primary ecotype is a wrack generalist), lost its endogenous diel rhythm. This finding could be of use in understanding control mechanisms in talitrid locomotory activity. The locomotor activity rhythm study of Wildish et al. (2021) was the first comparative study of talitrids that included most of the ecotopes of the North Atlantic. Thus, the marine eulittoral hyalid (proposed stem group of the talitrids according to Bousfield 1984) had a circatidal rhythm; the palustral *Speziorchestia grillus* Bosc, 1802; and the marine xylophagous *Macarorchestia remyi* (Schellenberg, 1950), both lacked an endogenous rhythm, and activity was random. These findings are consistent with the adaptive value of endogenous rhythms and diurnal cryptic behavior. This includes hiding in wrack or burrows during

daylight to avoid bird predators, which use vision to capture talitrid prey and are only active by day. An additional benefit of cryptic behavior during daylight is that talitrids avoid the high temperatures and desiccation caused by sunlight. The fact that permanently cryptic ecotypes, such as xylophagous and troglobiontic talitrids, have lost diel activity (Table 4), implies that the maintenance of this behavior is physiologically costly.

Foraging birds in the supralittoral attempt to capture wrack generalists and sand-burrowing hoppers, the former by disturbing the wrack and the latter by probing burrows. The typical response of wrack generalists to disturbance of their habitat is random jumping in all directions at once. This group response may confuse the predator and serve to limit the predator's success in capturing individual talitrids. The escape response is continued until each talitrid can find a hiding place that is both humid and dark. This is an area of talitrid research where future experimental studies might be focused on the behavioral interactions of predators and prey. The intensity and duration of the escape response decrease along the generalist-specialist continuum (Table 4). For palustral talitrids, the main predators are foraging fish (Vince et al. 1976). The presently known palustral talitrids associated with the northwestern Atlantic coastline are *Speziorchestia grillus* (Bosc, 1802), *Uhlorchestia uhleri* (Shoemaker, 1930), and *U. spartinophila* Bousfield & Heard, 1986 (although genetic evidence of Radulovici (2012) suggests that *S. grillus* could be divisible into up to seven new species). Kneib (1982) showed by field experiments that the zonation patterns, with *S. grillus* occupying the high marsh and *U. spartinophila* lower in the marsh, were controlled by tidal inundation patterns. This mirrors the findings of intertidal zonation patterns of talitrids, such as *Orchestia mediterranea* controlled by tidal levels on the northeastern Atlantic coast (Wildish 1988). Availability of palustral talitrids to the main fish predator, *Fundulus* sp., decreases at higher tidal levels, so that *U. spartinophila* was more vulnerable to predation than *S. grillus*. Nevertheless, *U. spartinophila* has one more behavioral adaptive strategy to avoid fish predation: it can climb the *Spartina* stems and hide in the axils (Covi and Kneib 1995). Little is known about the biotic interactions of both xylophagous and troglobiontic talitrids. Since the former spend most of the day in burrows and cracks in decaying wood and the latter spend their lives in caves (Table 4), they are unlikely to encounter bird or fish predators. Further study is needed to discover the nature of the biotic relationships they have with other invertebrates with which they share their habitat.

Another adaptive strategy to reduce predation on wrack generalists and sand-burrowing hoppers is for the talitrids to produce epidermal pigments, which are hypothesized (Wildish and LeCroy 2014) to provide camouflage as protection from visual bird predators. In *Mexorchestia* sp., the habitat backgrounds in Florida vary from white sand for populations living under digging pellets of fiddler crabs where wrack was absent to hiding within copious banks of wrack where the background was dark. This sets up selective pressure by bird predation in opposite directions depending on the type of background; thus, on white sand, selection favors a non-pigmented body pattern, whereas on a wrack background, a highly pigmented pattern is selected (Wildish and LeCroy 2014). The nature of the ultimate polyphenic control of dorsal pigment patterns is unknown. In general, the likelihood of finding epidermal pigment patterns decreases along the generalist-specialist continuum (Table 4), until in xylophagous and troglobiontic talitrids the epidermal pigments are absent.

Low salinity

Marine talitrids can penetrate estuaries and other bodies of water with reduced salinities, such as the Baltic Sea (Persson 2001). In an English lowland estuary, it was shown that two *Orchestia* spp. penetrating from the seawater end had very different salinity limits (Wildish 1970a, 1970b). Thus, *O. gammarellus* was found at salinities down to 5% of full-strength seawater, versus a lower limit of 52% for *O. mediterranea*. Beyond the saline limit for *O. mediterranea*, a second, closely related sibling species, *O. aestuarensis*, was found upstream of the salinity limit of *O. mediterranea* in the Medway estuary, where mesohaline salinities ranged from 31 to 52% of full-strength seawater (Wildish and Radulovici 2020). *Orchestia gammarellus* uses a different strategy for penetrating estuaries than *O. mediterranea.* Thus, eggs of *O. gammarellus* grown in vitro were killed at < 40% seawater, but if the eggs were allowed to mature in the living female marsupium (= brood pouch) at culture salinities down to 10%, they survived and successfully developed (Morritt and Stevenson 1993). The explanation for this result provided by Morritt and Spicer (1998) was that the female was able to control the osmotic concentration of the marsupial fluid so that development continued despite the lethality of ambient seawater to the eggs. By contrast, cultured adult females carrying young in the brood pouch of *O. mediterranea* in diluted seawater (42% full-strength seawater) increased the intermoult period, dropped more dead eggs, and caused selective female mortality (Wildish 1970a). All of these effects in dilute seawater resulted in reduced population fertility for *O. mediterranea.*

The response of *O. mediterranea* when confronted with dilute seawater < 52% seawater is to produce a polymorphic form with minor morphological differences (Table 5) and a better ability to tolerate dilute seawater (down to 31% seawater in the Medway estuary). The mechanism controlling the appearance of the mesohaline form is unknown, although Wildish and Radulovici (2020) have proposed two mechanisms to account for this involving either epigenesis or regular speciation. The first

Table 5. Biological comparisons of a sister species pair of *Orchestia*. Data from Wildish (1987) and Pavesi et al. (2014).

Biological Characteristic		Sibling Species Pair	
General	**Specific**	***O. mediterranea***	***O. aestuarensis***
Ecotope		Marine/ Estuarine	Estuarine only
Salinity	% Full-strength seawater	>52%	<52%
Morphology	Male P2 palm	Sinuous	Notched
	General spination	More	Less
	Female P2 basis	Anterior hump	No anterior hump
	Female P2 propodus	Larger	Smaller
	Dorsal pigment pattern	No mid-dorsal holes	2 mid-dorsal holes/segment
Genetics	Mitochondrial CO1 K2P	11%	
	Nuclear 18S K2P	0.33%	
	Nuclear 28S K2P	0.15%	

involves epigenesis, in which a polymorphic allele, or set of alleles, is carried within the euryhaline form and initiated by the low salinity conditions to produce the mesohaline form. After the initial epigenesis switch gene(s) are established, they become linked by genetic assimilation with an ability to breed at reduced salinity and the morphological changes shown in Table 5. The second alternative hypothesis is that the mesohaline form evolves by regular parapatric speciation.

The genetic findings (Pavesi et al. 2014) for the mitochondrial CO1 gene for all *Orchestia* populations studied suggest that the average K2P difference of 22% is two times greater than for the values between *O. mediterranea* and *O. aestuarensis* (Table 5). Coupled with the small genetic differences for nuclear genes, this suggests that *O. aestuarensis* recently diverged from *O. mediterranea*. Further experimental studies are needed to test the alternative low salinity switch hypotheses. It is considered that regular speciation mechanisms are an unlikely explanation to account for the appearance of *O. aestuarensis* in estuaries because the morphologies between estuaries are so similar (and this would not be the case if *O. aestuarensis* arose de novo in each estuary).

If the low salinity switch hypothesis proves to be supported, it would explain the geographical distribution conundrum of *O. aestuarensis*: how does it get to the isolated position in the mesohaline section of an estuary by passive dispersal? It is unlikely that it could be passively distributed from one estuary to another to reach the mesohaline part of the estuary. If the low salinity switch hypothesis is supported for *O. aestuarensis*, the answer is that the appropriate silent genes are carried there within the body of its sibling, *O. mediterranea*, utilizing the passive dispersal mechanisms of the latter. The low salinity then acts as a switch, turning on the genes for the mesohaline phenotype.

Dwarfness

Three talitrids have been shown to have natural populations living in a driftwood secondary ecotope: *P. exter* (Wildish and Robinson 2016a), *O. mediterranea* (Wildish et al. 2012), and *O. gammarellus* (Wildish 2017). All three can sometimes be found feeding on decaying driftwood, and this diet results in slower growth and dwarf morphology, although the only one where this has been experimentally verified is in *P. exter* (Wildish 2017).

Besides these wrack generalist taxa living in a secondary ecotope, there is one genus, *Macarorchestia* Stock, 1989, where driftwood is the primary ecotope. *Macarorchestia* currently has five specialist xylophagous species, which all appear to be obligate feeders on driftwood (Wildish 2017), although this has yet to be checked experimentally in three (*microphthalma*, *pavesiae*, *martini*) of the five *Macarorchestia* spps. Xylophagous specialist adaptations were reviewed in Wildish (2017) and include dwarfism, small eye size, females larger than males, and lack of dorsal pigment patterns. An experimental investigation of the ultimate causes of dwarfism in talitrids utilized *P. exter* acclimated to a driftwood diet (Wildish and Robinson 2016b). Two of the hypotheses: (1) dwarfism evolved to allow talitrids to live in and negotiate the small burrows made by gribbles (Isopoda, Limnoridae) after driftwood reaches the sea, and (2) driftwood was poor quality food, forcing reduced metabolism, growth, and adult maximum size, were both supported by the behavioral and physiological experiments undertaken. A powerful support for hypothesis (1) was that there is evidence that the *Macarorchestia* species form a series of declining sizes from *M. microphthalma* (largest) to *M. martini* (smallest) and that the serial dwarfism displayed by this xylophagous genus allows successively smaller species to occupy a greater percentage of gribble burrows because of their smaller size (Wildish and Robinson 2016b).

The underlying physiology of dwarfism in the xylophagous specialist genus *Macarorchestia* is contrary to the metabolic theory of Kingsolver and Huey (2008), according to which most Talitridae develop slower, mature slower, and achieve larger final body sizes the further they are from the equator (Wildish et al. 2011). Xylophagous populations reach smaller adult sizes not as a result of warmer temperature regimes but by adapting to living in ever smaller spaces.

Molecular genetic methods and talitrid microevolution

Modern molecular genetic methods utilize DNA markers, such as microsatellites, restriction fragment length polymorphisms, and DNA sequence data (Monsen-Collar and Dolcemascolo 2010). The development of polymerase chain reaction (PCR) methods has made it possible to use smaller amounts of genetic material in the analysis. The results of such studies could be used to determine:

- The amount of genetic variation within a population or species
- The degree of relatedness among populations/species (of use in taxonomy)
- Determine the evolutionary history of species and higher taxa (of use in evolutionary studies)
- If enough taxa are included, it can be used to construct phylogenies and estimate geological divergence times from a common ancestor.

To determine the amount of genetic variation within talitrid species, the earliest molecular genetic methods utilized allozyme electrophoresis. The results are summarized by Pavesi and Ketmaier (2013), and their review includes a list of 12 species each with an estimate of genetic diversity within each population sampled. The genetic structure of a population indicates the multiple factors affecting the genetic input it receives from immigrants arriving after dispersal and thus includes those that influence dispersal success between isolated 'island' populations (Wildish 2012). All of the wrack generalists included in Pavesi and Ketmaier (2013): *O. gammarellus*, *O. mediterranea*, *O. montagui*, and *P. exter* have low levels of genetic diversity, supporting the view that passive dispersal is high and/or that the distances between occupied ecotopes (or 'islands') are small. One anomalous species, *Speziorchestia stephensi*, is a wrack generalist but has a high level of genetic diversity. Apart from one riverine/lacustrine species, all the other talitrids were specialists (three psammophiles and one each of a xylophage, a troglobiont, and a rain forest leaflitter species) with a high level of genetic diversity. The results outlined by Pavesi and Ketmaier (2013) for wrack generalists, with the exception of *O. montagui* and *S. stephensi*, have a wider zoogeographic distribution outside the Mediterranean Sea along the northeast Atlantic coast. These results largely support the lineal 'island' theory of dispersal proposed by Wildish (2012).

With the mtDNA cytochrome oxidase I gene (CO1), Ketmaier et al. (2010) showed that in the psammophile *Talitrus saltator*, the degree of genetic diversity increased with decreasing shoreline erosion along the same beach. *Talitrus saltator* subpopulations had the least genetic diversity if the sandy beach sample location underwent irregular erosion events. Presumably this was because, at this location on the sandy beach, more talitrids were lost by storm events and received more fresh immigrants following storms and onshore winds. In another study using the CO1 gene and three Mediterranean populations of the xylophagous talitrid, *Macarorchestia remyi*, a deep split in genetic diversity between populations from the Adriatic and Tyrrhenian Seas was found (Pavesi et al. 2011). This is consistent with this xylophagous talitrid having low dispersal capability (Table 4). On further examination of individuals from both Adriatic and Tyrrhenian populations, small morphological differences were found, and a new species was described for the Tyrrhenian population (Wildish 2014).

Baldanzi et al. (2016) measured the genetic diversity with the CO1 gene of another psammophile, *Capeorchestia capensis*, distributed around the tip of South Africa. Eight locations were sampled along a coastal stretch of ~ 2500 km in a region where the Atlantic and Indian Oceans join. Like the Mediterranean sandhoppers described above, they also found deep genetic diversity, including three main haplogroups. Each of these was described as an evolutionary significant unit, loosely linked to the temperature regimes of the biogeographic provinces of South Africa. However, examination of the same populations of *C. capensis* by conventional morphological taxonomic methods (Lowry and Baldanzi 2016) found no differences between the three evolutionary significant units. Baldanzi et al. (2016) suggest that *C. capensis* at the southern tip of Africa has undergone cryptic speciation in forming a species complex. Subsequently, Baldanzi et al. (2017) found evidence in the same populations of indications of epigenetic variation among populations of *C. capensis* with the methylation-sensitive amplified polymorphism method.

Talitrid colonization of the North Atlantic Oceanic Islands

There are many islands present in the North Atlantic (International Hydrographic Organization 1953), of which only a few have been investigated to determine talitrid biodiversity. According to the influential model of island biogeography of MacArthur and Wilson (1967) and subsequent studies in insects (Peck and Finston 1993), the following factors might influence island occurrence by talitrids: island area, ecotope diversity on the island, the marine distance from the continental mainland, as well as island age. Factors affecting talitrid dispersal to oceanic islands include: emigration frequency from the donor population, the size of the donor population, and the dispersal capability of the transport raft (dependent on ocean current direction), including raft longevity (Wildish 2012).

As far as I am aware, only two oceanic islands have been studied sufficiently well to provide even a species list for the Talitridae occupying them. They are La Palma in the Canaries Archipelago in the eastern, and Bermuda in the western, North Atlantic.

La Palma in the Canaries Archipelago

The Canaries Archipelago is the closest of the northeast Atlantic islands to a continental land mass, with La Palma 445 km from North Africa. La Palma is semi-tropical (29°N) with a land area of 708 km^2, and although the Canaries is one of the older volcanic island chains in the northeast Atlantic at 20.5 MYA (Wildish 2012), La Palma was formed only 1.8 MYA. It has a diverse flora depending on altitude; thus, at 500–1400 m a laurel cloud forest is present. At lower altitudes from sea level upwards to 500 m are the endemic Canary Island pine forests. At altitudes greater than 1400 m, shrubs and heathland dominate (Aguilar et al. 2010).

Talitrid geographic distribution data for the islands of the Canaries Archipelago is spotty and almost certainly incomplete. Perhaps the best studied for talitrids is La Palma, due largely to the fieldwork of Jan Stock. Shown in Table 6 is the limited data available for the whole Archipelago.

The two *Talitroides* species are aliens, probably introduced synanthropically and limited to cultivated lands at lower altitudes. The three wrack generalists of Table 6 could be recent immigrants, arriving either by natural passive wrack rafting or by some form of synanthropy (Wildish 2012). The presence of a sandhopper on some of the Canary Islands suggests that *T. saltator* arrived relatively recently by synanthropy or was able to wrack raft from the mainland. The most interesting group is the five terrestrial leaf litter hoppers. The authors describing them suggested that they are individual island endemics, although much more comprehensive sampling is needed for all of the Canaries Archipelago islands before this claim can be substantiated. All five of the terrestrial species identified in Table 6 live in forest leaf litter, although their zoogeographic distribution on the islands of discovery remains unknown (apart from the two *Palmorchestia* spps). What is clear is that they are terrestrial species that evolved on the islands, where they are now found from marine ancestors that were naturally dispersed from the continental mainland.

Villacorta et al. (2008) present a field sampling and molecular genetic study of the two *Palmorchestia* species discovered by Stock and Martin (1988) and Stock (1990). Twelve localities were sampled throughout the island for a total of 89 individuals sequenced for the cytochrome oxidase mtDNA region (alignment length of 761 bp). Stock (1990) and Villacorta et al. (2008) both hypothesized that *Palmorchestia* originated from a supralittoral ancestor that migrated to a contiguous, ancient laurel forest leaf litter environment to become a terrestrial landhopper. During periods of drought on La Palma, the landhopper sought refuge in the lava tubes and caves that permeate the island and provide constant high humidity, where it became acclimated as a cavehopper. A more plausible alternative hypothesis is that the ancestor was a supralittoral driftwood hopper that arrived at a cave mouth opening in the supralittoral. The new immigrant first became acclimated to the cave environment before spreading throughout the island in the extensive lava tubes (Wildish 2012). *Palmorchestia* colonized a secondary ecotope, the contiguous humid laurel forest leaf litter at higher altitudes on La Palma. During periods of drought, leaf litter populations retreated to the cave environment, still carrying the dormant genes necessary for cave life. Wildish (2012) originally suggested a form of parapatric speciation to explain the driftwood ancestor hypothesis, but a more plausible explanation is that epigenetically derived alternative phenotypes within *Palmorchestia* populations occur on La Palma in response to the two contiguous ecotopes (hypogean and epigean). The driftwood hypothesis requires that *P. hypogaea* has an older origin than *P. epigaea* and that both are sister species and can partially interbreed. Inconclusive evidence in support of the driftwood ancestor hypothesis for *Palmorchestia* includes:

- Estimates of phylogenetic age suggest that *P. hypogaea* has an older common ancestor than *P. epigaea* (table 2 in Villacorta et al. 2008).
- The driftwood hypothesis does not require the laurel forest to be at sea level.
- The driftwood hypothesis does explain how *Palmorchestia* could reach both the northern and

Table 6. Talitrid fauna of islands in the Canary Archipelago, from Wildish (2012). Based on published systematic data to 1990. Generic names are corrected according to WoRMS (Horton et al. 2023) accessed in 2023.

Species names from WoRMS accessed 2023	Ecotype	Islands	Island Endemic
Insularorchestia monodi (Mateus, Mateus & Afonso,1986)	Wrack generalist	Many	No
Orchestia gammarellus (Pallas, 1766)	Wrack generalist	Many	No
Orchestia mediterranea A. Costa, 1857	Wrack generalist	Many	No
Talitrus saltator (Montagu, 1808)	Psammophile	Many	No
Cryptorchestia canariensis Dahl, 1950	Terrestrial	Gran Canaria	Yes
Canariorchestia gomeri Stock, 1989	Terrestrial	La Gomera	Yes
Speziorchestia guancha Stock & Boxshall, 1989	Terrestrial	Tenerife	Yes
Cryptorchesta stocki Ruffo, 1990	Terrestrial	Gran Canaria	Yes
Palmorchestia hypogaea Stock & Martin,1988.	Troglobiont	La Palma	Yes
Palmorchestia epigaea Stock, 1990	Terrestrial	La Palma	Yes
Talitroides topitotum (Burt, 1934)	Terrestrial	Many	No
Talitroides alluaudi (Chevreux, 1896)	Terrestrial	Many	No

southern ends of the island by active and passive dispersal within lava tubes.
- There is a precedent for a driftwood hopper, *Macarorchestia remyi*, being present in an Italian cave opening in the supralittoral of the island of Corsica (Schellenberg 1950).
- Both *Macarorchestia* and *Palmorchestia* species are small, with the ovigerous female larger than the adult male in both genera.

In a review of the troglobiontic insects of the Galapagos Islands, Peck and Finston (1993) describe many cases of eyeless cave and eyed epigean sister species (e.g., beetles), which are found in close but not overlapping geographic proximity. Peck and Finston (1993) hypothesize that the insect hypogean/epigean sister pairs arose by parapatric evolution, but it could involve epigenesis as explained above.

Bermuda

The volcanic eruptions that formed Bermuda first began some 110 MYA and ended some 30 MYA. The present-day Bermudian archipelago has a land surface area of only 53 km^2, and the nearest continental landmass is in North Carolina, U.S.A., some 1020 km distant (Wildish et al. 2016). Fluctuations in sea level during the Pleistocene led to extinctions of the terrestrial and littoral fauna, the last of which occurred at 0.4 MYA, when most of Bermuda was below sea level (Olson et al. 2006). Thus, faunal recolonization of Bermuda occurred relatively recently (< 0.4 MYA). A comprehensive survey of the supralittoral talitrid fauna (excluding palustral and most terrestrial ecotopes) revealed that only 5 talitrid species were present in 2014. The list shown in Table 7 excludes the one synanthropically introduced terrestrial, leaf-litter species. There are no endemics consistent with the short time (< 0.4 MYA) available for colonization and lack of ecotope variability on the island. Wrack generalists may reach Bermuda by natural rafting, but the picture is obscured because of synanthropic dispersal in modern times. Despite the availability of sandy beaches, no psammophilic talitrids were found on Bermuda (Wildish et al. 2016), consistent with their poorer dispersal ability (Table 4).

Macroevolution and the origin of the Talitridae

The following types of macroevolution might occur during a study of the phylogeny of talitrids:

- Divergence: a once interbreeding population splits into two or more species, and the new species becomes more dissimilar with time. Many of the wrack generalist talitrids may have originated by divergent evolution.
- Convergence: occurs when two species from different genetic backgrounds occupy the same or similar ecotope and, by adaptative processes, come to show the same phenotypic characteristics. An example is the troglobiontic talitrids, in which all species so far recognized have lost eyes and epidermal pigment patterns.
- Parallel evolution: occurs when two species from genetically different ancestor lines develop similar phenotypic traits when occupying the same ecotope. An example would be the behavioral escape response of jumping in random directions to confuse avian predators shown by co-occurring *Platorchestia oliveirae* and *Mexorchestia carpenteri carpenteri* in the Gulf of Mexico wrack (Wildish and LeCroy 2014).
- Coevolution: when two often radically different species influence each other's evolution to the benefit of both. An example is the wrack generalist *Orchestia montagui* feeding on wrack from *Posidonia* sp., which maintains a lignivorous bacterial species in the hepatopancreas capable of metabolizing the food that the talitrid eats (Abdelrhman et al. 2017). In return, the talitrid provides a suitable culture environment for the bacterium, which is rare or absent in the general environment.

A comprehensive fossil record for the Talitridae is absent. Currently, only three talitrid fossils have been discovered, two in Mexican amber (Bousfield and Poinar 1994; Hegna et al. 2020), the other from Dominican Republic amber (Bousfield and Poinar 1995), and all from 26–38 MYA. They were terrestrial species and are currently uninformative about their evolutionary history.

Table 7. Supralittoral talitrids of the Bermuda archipelago in 2014 (Wildish et al. 2016). BOLD = Barcode of Life Data System, available at www.boldsystems.org. WG = wrack generalist, T = terrestrial leaf litter hopper. 21 of 23 stations are occupied by talitrids.

Species names from WoRMS accessed 2024	BOLD	Ecotype	Number of stations occupied Total = 23	Percentage commonness
Platorchestia oliveirae Myers & Lowry, 2023	AAB3402	WG	12	52
Platorchestia exter Myers & Lowry, 2023	AAA2949	WG	4	17
Mexorchestia carpenteri carpenteri Wildish & LeCroy, 2014	AAC1491	WG	2	9
Tethorchestia antillensis Bousfield, 1984	–	WG	1	4
Talitroides alluaudi (Chevreux, 1896)	ACH9326	T	2	9

In classical taxonomy, a sufficient number of morphological characters must be chosen to distinguish between closely related populations and a subjective decision made by the taxonomist as to what constitutes a new species (Myers 1997). Such characters have also been used to infer the phylogeny of the Talitroidea. Thus, Bousfield (1982) used a phenetic analysis to do so within the Talitroidea, recognizing the problem of homoplasy and ecological overlap but apparently not correcting for them in his data matrix. More recently, Myers and Lowry (2020) have used a morphological cladistic analysis of the talitroids and determined for each character state whether the relationship was synapomorphic or homoplastic. A total of 46-character states were used in the analysis by Myers and Lowry (2020), of which 16 were zoogeographic in nature. Not surprisingly, there was little agreement between the two methods. A central problem with morphological reconstructions of amphipod phylogeny is that individual taxonomists use both a different number and quality of input data (morphological character states). Thus, in Bousefield's (1982) phenetic analysis, 60 character states were included, involving some overlap with those used by Myers and Lowry (2020). The quality of the input data in the latter study was clearly higher than in the former.

No equivalent molecular-genetic method has been attempted to determine the phylogeny of the Talitroidea. The input data for such a study would be drawn from the genetic material found in each eukaryote cell. This method does offer one advantage over the morphological ones discussed above: it can be used to estimate the time that elapsed when a common ancestor branched into two clades using the molecular clock approach (Ho and Duchêne 2014). Smaller-scale phylogenies of Lake Baikal amphipods (Macdonald et al. 2005), world-wide species of *Gammarus* (Hou et al. 2007), and Ponto-Caspian amphipods (Mamos et al. 2021) have been based on molecular genetic data. A first attempt at a phylogeny of the Amphipoda (including Talitroidea) using a dataset containing representative species from approximately one-half of the known families of Amphipoda was published by Copilaș-Ciocianu et al. (2019). Four common genetic markers (mitochondrial CO1, nuclear ribosomal RNA subunits 28S and 18S, and nuclear histone H3) were used, and divergence time estimates for the Talitroidea were 40–72 MYA, depending on which of three calibration methods were used. This preliminary result is supportive of the more recent origin (70–110 MYA) of the Talitridae suggested by Bousfield (1984).

Ideally, we would test a data set common between a morphological cladistic analysis and one where molecular genetic data was available from the same taxa. Unfortunately, no such study has been attempted, and we must conclude that both methods are still under development and that such a test is premature. Thought experiments suggest that for the morphological cladistic analysis it must yield results that are similar when performed by different taxonomists who may be using different numbers and quality of morphological character states. Similarly, for molecular genetic input data, we would expect the same results if different molecular geneticists ran the analysis and chose different types of input data (mitochondrial or nuclear genes). For both approaches, independent scientists producing similar results would be a good indicator that they had achieved a reproducible scientific method.

In the North Atlantic, apart from the three amphi-Atlantic talitrid species of Table 2, all remaining 41 species are not shared between the northwestern and northeastern Atlantic coastlines. This is interpreted as circumstantial evidence of vicariance, in this case, the formation of the North Atlantic Ocean by the spreading apart of tectonic plates (Bousfield 1984; Myers 2022), which separated the North American and Eurasian continents. Thereafter, when the last land bridge between North America and Eurasia was severed at ~ 50 MYA (Atlantic Geoscience Society 2001), the fauna, including talitrids, evolved independently on the two separated continents.

One common route of land colonization by Talitridae has been demonstrated using knowledge of geological events in the Pacific Ocean (e.g., temporal patterns of sea level rise) and molecular genetic methods (Yang et al. 2013; Liu et al. 2022). The mechanism involved marine supralittoral talitrids in East Asia, which were carried inland by marine incursions when global sea level was high at 10–17 MYA.

Discussion

Armed with the methods available to study ecology and microevolution, including field experimental ecological genetics (Ford 1975) coupled with modern molecular genetic methods and the new field of epigenetic evolution to explore, the student of these topics can make important discoveries with talitrids as the target. Both study areas are a good fit for young students of the Amphipoda keen to make fundamental discoveries with field biology methods. This is because so little has been achieved yet in either the ecology or evolution of the Talitridae. Another bonus for the aspiring talitrid student is that it will take you to interesting sampling locations.

We have seen in this review that the wrack generalist talitrids found in the Atlantic coastal region occupy an environment that offers the most variability: wrack, driftwood, salt marshes, and intertidal caves. Importantly, these are contemporary marine/estuarine ecotopes where each is adjacent or contiguous to each other and not solely dependent on passive dispersion to cross environmental boundaries. Passive mechanisms are thought to enable long-range dispersal (Wildish 2012). On the other hand, specialists occupy a single ecotope and have phenotypic adaptations specifically to it. The ecotopes of specialists become rarer as the continuum order becomes more specialized. Thus, caves that adjoin the marine intertidal are

uncommon and far apart, rendering passive dispersal to and from them virtually impossible. These results emphasize the primacy of the environment in shaping the talitrid species that exist today.

Whether all wrack generalists share the ability to respond to the different ecotopes available remains to be demonstrated with those species not yet studied ecologically. A pertinent question is whether specialist ecotypes share the phenotypical plasticity characteristic given the experimental or natural opportunity to do so. The *Palmorchestia* example studied by Villacorta et al. (2008) suggests that the specialist does retain phenotypical plasticity to respond to contiguous biotopes (cave to subtropical forest leaf litter) in response to an undetermined environmental switch. Specialist ecotypes generally experience less environmental variability than generalists.

An important realization from this review is that the initial stages of talitrid microevolution may be controlled by epigenetic mechanisms in response to specific environmental factors and aided by switch genes. Two of the best examples given above may qualify as involving epigenesis. The first is the sibling pair *O. mediterranea/O. aestuarensis*, where the environmental cue is low salinity (Wildish and Radulovici 2020), and the second is the hypogaean/epigean sibling pair of *Palmorchestia* spp., with the environmental switch undetermined. Sibling pairs of hypogaean/epigean species are found in many other invertebrates, such as insects (Peck and Finston 1993), and the existence of sister species pairs could be a general indicator that epigenetic mechanisms were involved in their formation. If epigenesis is involved in microevolution in the formation of cryptic species complexes (Baldanzi et al. 2016, 2017), it has implications for morphological systematics as currently practiced in the Talitridae (Myers and Lowry 2020, 2023). As we have seen, wrack generalist talitrids are biologically vagile, including in their morphology in responding to the ecotope variability that they meet throughout their zoogeographic range. Such a situation poses a problem for the biological species concept (Mayr 1942) and the morphological systematics of talitrids. Part of the solution involves the introduction of molecular genetic methods into the routine practice of systematics (Coleman and Radulovici 2020), as well as increased field sampling to discover new talitrids.

For variation in dorsal pigment patterns used as camouflage protection against avian predators, the genetic variation brought about by sexual reproduction, including crossing over during meiosis (Jablonka and Lamb 2014), may be key. Here, natural selection by bird predation at the population level can determine which pigment patterns survive against the background ecotope in which a population lives. For talitrid dwarfness, two environmental drivers have been identified. The first involves wrack generalists, such as *Platorchestia exter*, who, if they adopt driftwood as food, have a reduced standard metabolic rate, slower growth, and final body size, and if the usual wrack diet is offered, metabolism and growth rate are restored (Wildish and Robinson 2016a). The second case involves obligate driftwood-living talitrids of the genus *Macarorchestia.* The five species of this genus form a series of decreasing sizes, with the leading hypothesis being that they were adapting to gribble burrow hole diameters in driftwood (Wildish and Robinson 2016b).

Is it better to become a specialist or remain a generalist, that is, to specialize or not to specialize? The question is rhetorical and does not imply that the talitrid has a choice. The business end of the matter is the individual and population undergoing natural selection in response to the environmental limiting factors it has to face. The latter include those environmental limits involved in passive dispersal mechanisms of talitrids. Comparing the wrack generalist with the troglobiont (Table 4), the main difference between them is that there are many more individual locations available for the former than the latter. This results from the larger zoogeographic range of wrack generalists and therefore more nuanced ecotope variations to which it is exposed. The collateral effects that follow (Table 8) are that phenotypic variation is higher, the zoogeographic range is larger, speciation potential is lower, and endemism is lower in wrack generalists than in talitrid specialists. This implies the primacy of environmental variability in determining whether to speciate or not to speciate.

Table 8. Marine/estuarine ecotypes of the North Atlantic coastal region in continuum order and their evolutionary characteristics.

Evolutionary Characteristic	Continuum order				
	1	2	3	4	5
	Wrack generalist	**Psammophile**	**Palustral**	**Xylophage**	**Troglobiont**
Phenotypic Variability	Most	→	→	→	Least
Occurrence of Epigenetics	Most Likely	→	→	→	Least Likely
Zoogeographic Range	Greatest	→	→	→	Smallest
Speciation Potential	Low	→	→	→	High
Degree of Endemism	Lowest	→	→	→	Highest

Acknowledgements

The following are thanked for reviewing earlier versions: John McDonald, Gerhard Pohle, and Davide Asnicar. Alan Myers and Luiz de Andrade improved a later version.

References

Abdelrhman KFA, Bacci G, Nistri A, Mengoni A, Ugolini A (2017) Diet and gut microbiota of two supralittoral amphipods *Orchestia montagui* and *Talitrus saltator* living in different microhabitats Estuarine Coastal and Shelf Science 197: 119–125. https://doi.org/10.1016/j.ecss.2017.08.016

Adin R, Riera P (2003) Preferential food source utilization among stranded macroalgae by *Talitrus saltator* (Amphipoda, Talitridae): a stable isotopes study in the northern coast of Brittany (France). Estuarine, Coastal and Shelf Science 56: 91–98. https://doi.org/10.1016/S0272-7714(02)00124-5

Aguilar dA, González-González M-J, Garzón-Machado RV, Pizarro-Hernández B (2010) Actual and potential natural vegetation on the Canary Islands and its conservation status. Biodiversity & Conservation, 19: 3089–3140. https://doi.org/10.1007/s10531-010-9881-2

Atlantic Geoscience Society (2001) The Last Billion Years. A Geological History of the Maritime Provinces of Canada. Atlantic Geological Society Special Pub. No. 15, Nimbus Publ., Halifax, 212 pp.

Baldanzi S, Gouws G, Barker NP, Fratini S (2016) Molecular evidence of distinct evolutionary units in the sandhopper *Talorchestia capensis* (Amphipoda, Talitridae) along South African coasts. Hydrobiologia 779: 35–46. https://doi.org/10.1007/s10750-016-2797-4

Baldanzi S, Watson R, McQuaid CD, Gouws G, Porri F (2017) Epigenetic variation among natural populations of the South African sandhopper *Talorchestia capensis*. Evololutinary Ecology 31: 77–91. https://doi.org/10.1007/s10682-016-9877-9

Bossdorf O, Richards CL, Pigliucci M (2008) Epigenetics for ecologists. Ecology Letters 11: 106–115. https://doi.org/10.1111/j.1461-0248.2007.01130.x

Bousfield EL (1982) The amphipod superfamily Talitroidea in the northeastern Pacific Region. I. Family Talitridae: systematics and distributional ecology. Publications in Biological Oceanography No. 11, 73 pp.

Bousfield EL (1984) Recent advances in the systematics and biogeography of landhoppers (Amphipoda: Talitridae) of the Indo-Pacific region. In: Radovsky F J, Raven P H, Sohmer SH (Eds) Biogeography of the tropical Pacific. Proceedings of a Symposium, Bishop Museum Special Publication No 72: 171–210.

Bousfield EL, Poinar GO (1994) A new terrestrial amphipod for Tertiary amber deposits of Chiapas Province, southern Mexico. Historical Biology 7: 105–114. https://doi.org/10.1080/10292389409380448

Bousfield EL, Poinar GO (1995) New terrestrial amphipod from the Tertiary amber deposits of the Dominican Republic. Journal of Crustacean Biology 15: 746–755. https://doi.org/10.2307/1548823

Coleman CO, Radulovici AE (2020) Challenges for the future: talents, databases and knowledge growth. Megataxa 1: 28–34. https://doi.org/10.11646/megataxa.1.1.5

Copilaş-Ciocianu D, Borko Š, Fišer C (2019) The late blooming amphipods: global change promoted post-Jurassic ecological radiation despite Palaezoic origin. Molecular Phylogenetics and Evolution 143: 106664. https://doi.org/10.1016/j.ympev.2019.106664

Covi MP, Kneib RT (1995) Intertidal distribution, population dynamics and production of the amphipod *Uhlorchestia spartinophila* in a Georgia, USA, salt marsh. Marine Biology 121: 447–455. https://doi.org/10.1007/BF00349453

Dias N, Sprung M (2003) Population dynamics and production of the amphipod *Orchestia gammarellus* (Talitridae) in a Ria Formosa salt marsh (southern Portugal). Crustaceana 76: 1123–1141. https://doi.org/10.1163/156854003322753448

Ford EB (1975) Ecological genetics. Fourth Edition. Chapman & Hall, London, 442 pp. https://doi.org/10.1007/978-94-009-5825-8

Friend JA, Richardson AMM (1986) Biology of terrestrial amphipods. Annual Reviews of Entomology 31: 25–48. https://doi.org/10.1146/annurev.en.31.010186.000325

Gibson RN, Robb L (1996) Piscine predation on juvenile fishes on a Scottish sandy beach. Journal of Fish Biology 49: 120–138. https://doi.org/10.1111/j.1095-8649.1996.tb00009.x

Hegna TA, Lazo-Wasem EA, Serrano-Sanchez MdL, Barraganan R, Vega FJ (2020) A new fossil talitrid amphipod from the lower early Miocene Chiapas amber documented with micro CT scanning. Journal of South American Earth Sciences https://doi.org/10.1016/j.jsames.2019.102462

Henzler CM, Ingolfsson A (2008) The biogeography of the beach-flea, *Orchestia gammarellus* (Crustacea, Amphipoda, Talitridae) in the North Atlantic with special reference to Iceland: A morphometric and genetic study. Zoologica Scripta 37: 57–70. https://doi.org/10.1111/j.1463-6409.2007.00307.x

Ho SYW, Duchêne S (2014) Molecular clock methods for estimating evolutionary rates and timescales. Molecular Ecology 23: 5947–5965. https://doi.org/10.1111/mec.12953

Horton T, Lowry J, De Broyer C, Bellan-Santini D, Copilas-Ciocianu D, Corbari L, Costello MJ, Daneliya M, Dauvin J-C, Fišer C, Gasca R, Grabowski M, Guerra-García JM, Hendrycks E, Hughes L, Jaume D, Jazdzewski K, Kim Y-H, King R, Krapp-Schickel T, LeCroy S, Lörz A-N, Mamos T, Senna AR, Serejo C, Souza-Filho JF, Tandberg AH, Thomas JD, Thurston M, Vader W, Väinölä R, Valls Domedel G, Vonk R, White K, Zeidler W (2023) World Amphipoda Database. Accessed through World Register of Marine Species, on December, 2023.

Hou Z, Fu J, Li S (2007) A molecular phylogeny of the genus *Gammarus* (Crustacea: Amphipoda) based on mitochondrial and nuclear gene sequences. Molecular Phylogenetics and Evolution 45: 596–611. https://doi.org/10.1016/j.ympev.2007.06.006

Hupalo K, Grabowski M (2018) A first insight into transatlantic population genetic structure of the beach flea, *Platorchestia platensis* (Krøyer, 1845). BioInvasions Records 7: 165–170. https://doi.org/10.3391/bir.2018.7.2.08

Hurley DE (1968) Transition from water to land in Amphipod Crustaceans. American Zoologist 8: 327–353. https://doi.org/10.1093/icb/8.3.327

International Hydrographic Organization (1953) Limits of Oceans and Seas. Third Edition. Imp. Monégasque, Monte-Carlo, 43 pp. https://iho.int/uploads/user/pubs/standards/s-23/S-23_Ed3_1953_EN.pdf

Jablonka E, Lamb MJ (2014) Evolution in four dimensions: Genetic, epigenetic, behavioral, and symbolic variation in the history of life. Revised Edition, MIT Press Cambridge, Massachusetts, 462 pp. https://doi.org/10.7551/mitpress/9689.001.0001

Ketmaier V, De Matthaeis E, Fannini L, Rossano C, Scapini F (2010) Variation of genetic and behavioural traits in the sandhopper *Talitrus saltator* (Crustacea, Amphipoda) along a dynamic sand beach. Ethology, Ecology & Evolution 22: 17–35 https://doi.org/10.1080/03949370903515919

Kingsolver JG, Huey RB (2008) Size, temperature, and fitness: three rules. Evolutionary Ecology Research 10: 251–268.

Kneib RT (1982) Habitat preference, predation, and the intertidal distribution of gammaridean amphipods in a North Carolina salt marsh. Journal Experimental Marine Biology and Ecology 59: 219–230. https://doi.org/10.1016/0022-0981(82)90117-4

Laffaille P, Feunten E, Lefeure J-C (1999) Competition alimentaire entre deux especes de gobies *Pomatoschius lozanoi* et *P. minutus* (Pallas), dans un marais sale macrotidal. Comptes Rendu de l'Academie des Sciences - Series III - Sciences de la Vie 322: 1231–1235. https://doi.org/10.1016/S0764-4469(00)86656-1

Lastra M, Lopez J, Neves G (2015) Algal decay, temperature and body size influencing trophic behaviour of wrack consumers in sandy beaches. Marine Biology 162: 221–233. https://doi.org/10.1007/s00227-014-2562-z

LeCroy SE (2011) An illustrated identification guide to the nearshore marine and estuarine gammaridean Amphipoda of Florida. Vol. 5. Family Talitridae Bulycheva, 1957. State of Florida, Department of Environmental Protection, Talahassee, Florida, 739–763.

Liu H, Li S, Ugolini A, Momtazi F, Hou Z (2018) Tethyan closure drove tropical marine biodiversity: vicariant diversification of intertidal crustaceans. Journal of Biogeography 45: 9419–9451. https://doi.org/10.1111/jbi.13183

Liu H, Tong Y, Zheng Y, Li S, Hou Z (2022) Sea-land transition drove terrestrial amphipod diversification in East Asia, with a description of a new species. Zoological Jou rnal of the Linnean Society 196: 940–958. https://doi.org/10.1093/zoolinnean/zlab119

Lowry JK, Baldanzi S (2016) New talitrids from South Africa (Amphipoda, Senticaudata, Talitroidea, Talitridae) with notes on their ecology. Zootaxa 4144: 151–174. https://doi.org/10.11646/zootaxa.4144.2.1

Lowry JK, Myers AA (2019) New genera of Talitridae in the revised superfamily Talitroidea Bulycheva 1957 (Crustacea, Amphipoda, Senticaudata). Zootaxa 4553: 11–00. https://doi.org/10.11646/zootaxa.4553.1.1

MacArthur R, Wilson EO (1967) The theory island biogeography. Monographs in Population Biology, Princeton University Press, Princeton, 220 pp.

Macdonald KS, Yampolsky L, Duffy JE (2005) Molecular and morphological evolution of the amphipod radiation of Lake Baikal. Molecular Phylogenetics and Evolution 35: 3233–3243. https://doi.org/10.1016/j.ympev.2005.01.013

Mamos T, Grabowski M, Rewicz T, Bojko J, Strapagiel D, Burzynski A (2021) Mitochondrial genomes, phylogenetic associations, and SNP recovery for the key invasive Ponto-Caspian amphipods in Europe. International Journal of Molecular Science 22(19): 10300. https://doi.org/10.3390/ijms221910300

Mayr E (1942) Systematics and the origin of species from the viewpoint of a zoologist. Columbia University Press, New York, 334 pp.

Monsen-Collar KJ, Dolcemascolo P (2010) Using molecular techniques to answer ecological questions. Nature Education Knowledge 3(10): 1.

Morritt D, Spicer JI (1998) The physiological ecology of talitrid amphipods: an update. Canadian Journal of Zoology 76: 1965–1982. https://doi.org/10.1139/z98-168

Morritt D, Stevenson TDI (1993) Factors influencing breeding initiation in the beachflea *Orchestia gammarellus* (Pallas) (Crustacea: Amphipoda). Journal of Experimental Marine Biology and Ecology 165: 191–208. https://doi.org/10.1016/0022-0981(93)90105-W

Myers AA (1997) Biogeographic barriers and the development of marine biodiversity. Estuarine and Coastal Shelf Science 44: 241–248. https://doi.org/10.1006/ecss.1996.0216

Myers AA (2022) The conquest of land by the Amphipoda (Senticaudata, Talitroidea) explained by global tectonics and vicariance. Zootaxa 5214: 224–234. https://doi.org/10.11646/zootaxa.5214.2.4

Myers AA, Lowry JK (2020) A revision of the genus *Orchestia* Leach, 1814 with the reinstatement of *O. inaequalipes* (K.H. Barnard, 1951), the designations of a neotype for *Orchestia gammarellus* (Pallas, 1776) and the description of three new species (Crustacea: Amphipoda: Talitridae: Talitrinae) Zootaxa 4808: 201–250. https://doi.org/10.11646/zootaxa.4808.2.1

Myers AA, Lowry JK (2023) The beach-hopper genus *Platorchestia* (Crustacea: Amphipoda: Talitridae) on Atlantic coasts and on those of associated Seas. Records of the Australian Museum 75: 485–505. https://doi.org/10.3853/j.2201-4349.75.2023.1887

Olabarria C, Incera M, Garrido J, Rodil I, Rossi F (2009) Intraspecific diet shift in *Talitrus saltator* inhabiting exposed sandy beaches. Estuarine Coastal and Shelf Science 84: 282–288. https://doi.org/10.1016/j.ecss.2009.06.021

Olson SL, Hearty PJ, Pregill GK (2006) Geological constraints on evolution and survival in endemic reptiles in Bermuda. Journal of Herpetology 40: 394–398. https://doi.org/10.1670/0022-1511(2006)40[394:GCOEAS]2.0.CO;2

Pavesi L, Ketmaier V (2013) Patterns of genetic structuring and levels of differentiation in supralittoral talitrid amphipods: an overview. Crustaceana 86: 890–907. https://doi.org/10.1163/15685403-00003212

Pavesi L, De Matthaeis E, Tiedemann R, Ketmaier V (2011) Temporal population genetics and COI phylogeography of the sandhopper *Macarorchestia remyi* (Amphipoda: Talitridae). Zoological Studies 50(2): 220–229.

Pavesi L, Wildish DJ, Gasson P, Lowe M, Ketmaier V (2014) Further morphological and molecular studies of driftwood hoppers (Crustacea: Amphipoda: Talitridae) from Mediterranean/north-east Atlantic coastlines. Journal of Natural History 49: 1047–1071. https://doi.org/10.1080/00222933.2014.974708

Peck SB, Finston TL (1993) Galapagos Islands troglobites: the question of tropical troglobites, parapatric distributions with eyed-sister species, and their origin by parapatric speciation. Mémoires de Biospéologie 20: 193–197.

Pennings SC, Carefoot TH, Zimmer M, Danko JP, Ziegler A (2000) Feeding preferences of supralittoral isopods and amphipods. Canadian Journal of Zoology 78: 1918–1929. https://doi.org/10.1139/z00-143

Persson L-E (2001) Dispersal of *Platorchestia platensis* (Krøyer) (Amphipoda: Talitridae) along Swedish coasts: a slow but successful process. Estuarine, Coastal and Shelf Science 52: 201–210. https://doi.org/10.1006/ecss.2000.0735

Radulovici A (2012) A tale of two diversity levels inferred from DNA barcoding of selected North Atlantic crustaceans. Ph. D. Thesis, Université du Québec á Rimouski, Quebec. 245 pp.

Schellenberg A (1950) Subterrane Amphipoden korsikanischer Biotope. Archiv für Hydrobiologie 44: 325–330.

Schrama M, van Boheemen LA, Olff H, Berg MP (2015) How the litter-feeding bioturbator *Orchestia gammarellus* promotes late-successional salt marsh vegetation. Journal of Ecology 103: 9159–9124. https://doi.org/10.1111/1365-2745.12418

Sprung M, Machado M (2000) Distinct life histories of peracarid crustaceans in a Ria Formosa salt marsh (S. Portugal). Wetlands Ecology and Management 8: 105–115. https://doi.org/10.1023/A:1008484216971

Stock JH (1989) Landhoppers (Amphipoda, Talitridae) of the genus *Orchestia* of the Canary Islands. Bulletin du Muséum National d'Histoire Naturelle 11: 659–668. https://doi.org/10.5962/p.288288

Stock JH (1990) A new forest-hopper (Amphipoda, Talitridae) from La Palma, Canary Islands. Vieraea 18: 919–918.

Stock JH (1996) The genus *Platorchestia* (Crustacea, Amphipoda) on the mid-Atlantic islands, with description of a new species from Saint Helena. Miscellania Zoologica 19: 149–157.

Stock JH, Martin JM (1988) A new cavehopper (Amphipoda: Talitridae) from lava tubes in La Palma, Canary Islands. Journal of Natural History 22: 1121–1133. https://doi.org/10.1080/00222938800770701

Tykarska MB, Janas U, Brzana R (2019) Distribution and abundance of Talitridae in the southern Baltic Sea – twelve years after the first record of *Platorchestia platensis* (Krøyer, 1845) in 2005. Oceanological and Hydrobiological Studies 48: 66–75. https://doi.org/10.1515/ohs-2019-0007

Villacorta C, Jaume D, Oromí P, Juan C (2008) Under the volcano: phylogeography and evolution of the cave-dwelling *Palmorchestia hypogaea* (Amphipoda, Crustacea) at La Palma (Canary Islands). BMC Biology 6: 7. https://doi.org/10.1186/1741-7007-6-7

Vince S, Valiela I, Backus N, Teal JM (1976) Predation by the salt marsh killifish *Fundulus heteroclitus* (L.) in relation to prey size and habitat structure; consequences for prey distribution and abundance. Journal of Experimental Marine Biology and Ecology 23: 2552–2566. https://doi.org/10.1016/0022-0981(76)90024-1

West-Eberhard MJ (1989) Phenotypic plasticity and the origins of diversity. Annual Review of Ecology and Systematics 20: 249278. https://doi.org/10.1146/annurev.es.20.110189.001341

West-Eberhard MJ (2005) Developmental plasticity and the origin of species differences. The Proceedings of the National Academy of Sciences 102, Suppl.1: 6543–6549. https://doi.org/10.1073/pnas.0501844102

Wildish DJ (1970a) Polymorphism in *Orchestia mediterranea* A. Costa. Crustaceana 19: 113–118. https://doi.org/10.1163/156854070X00446

Wildish DJ (1970b) Some factors affecting the distribution of *Orchestia* Leach in estuaries. Journal of Experimental Marine Biology and Ecology 5: 276–284. https://doi.org/10.1016/0022-0981(70)90007-9

Wildish DJ (1987) Estuarine species of *Orchestia* (Crustacea: Amphipoda: Talitoidea) from Britain. Journal of the Marine Biological Association of the United Kingdom 67: 571–583. https://doi.org/10.1017/S0025315400027302

Wildish DJ (1988) Ecology and natural history of aquatic Talitroidea. Canadian Journal of Zoology 66: 23402–24359. https://doi.org/10.1139/z88-349

Wildish DJ (2012) Long distance dispersal and evolution of talitrids (Crustacea: Amphipoda: Talitridae) in the northeast Atlantic islands. Journal of Natural History 46: 2677–2700. https://doi.org/10.1080/00222933.2012.717971

Wildish DJ (2014) New genus and two new species of driftwood hoppers (Crustacea, Amphipoda, Talitridae) from northeast Atlantic and Mediterranean coastal regions. Zoosystematics and Evolution 90: 133–146. https://doi.org/10.3897/zse.90.8410

Wildish DJ (2017) Evolutionary ecology of driftwood talitrids: a review. Zoosystematics and Evolution 93: 353–361. https://doi.org/10.3897/zse.93.12582

Wildish DJ (2018) *Neotenorchestia* Wildish, 2014 is a junior synonym of *Orchestia* Leach, 1814. Zoosytems and Evolution 94: 545–546. https://doi.org/10.3897/zse.94.28876

Wildish DJ, Chang BD (2017) Is long-distance dispersal of talitrids (Amphipoda) in the North Atlantic feasible? Crustaceana 90: 207–224. https://doi.org/10.1163/15685403-00003636

Wildish DJ, LeCroy SE (2014) *Mexorchestia*: a new genus of talitrid amphipod (Crustacea, Amphipoda, Talitridae) from the Gulf of Mexico and Caribbean Sea, with a description of a new species and two new subspecies. Zootaxa 3856: 555–577. https://doi.org/10.11646/zootaxa.3856.4.5

Wildish DJ, McDonald JH (2023) Possible causes of amphi-Atlantic distribution of *Orchestia gammarellus* (Pallas, 1776) (Crustacea, Amphipoda, Talitridae) in the North Atlantic: a review. Zoosystematics and Evolution 99: 55–62. https://doi.org/10.3897/zse.99.95980

Wildish DJ, Radulovici AE (2019) Zoogeography and evolutionary ecology of the genus *Platorchestia* (Crustacea, Amphipoda, Talitridae). Journal of Natural History 53: 2413–2435. https://doi.org/10.1080/00222933.2019.1704463

Wildish DJ, Radulovici AE (2020) Amphipods in estuaries: the low salinity switch hypothesis. Zoosystematics and Evolution 96: 797–805. https://doi.org/10.3897/zse.96.55896

Wildish DJ, Robinson SMC (2016a) A new secondary ecotope for talitrids: driftwood in the Bay of Fundy. Crustaceana 39: 737–757. https://doi.org/10.1163/15685403-00003557

Wildish DJ, Robinson SMC (2016b) Ultimate cause(s) of dwarfism in Invertebrates: the case of driftwood talitrids. Evolutionary Ecology Research 17: 685–698.

Wildish DJ, Robinson SMC (2018) Effect of diet on oxygen uptake rate in the talitrid amphipod *Platorchestia platensis.* Marine and Freshwater Behaviour and Physiology 51: 293–294. https://doi.org/10.1080/10236244.2019.1567267

Wildish DJ, Kraft A, Pohle GW, LeCroy SE (2011) Variation in body size of two species of supralittoral talitrids (Amphipoda, Talitroidea) from the Gulf of Mexico and Atlantic coasts of North America. Crustaceana 84: 1243–1250. https://doi.org/10.1163/156854011X587504

Wildish DJ, Pavesi L, Ketmaier V (2012) Talitrid amphipods (Crustacea: Amphipoda: Talitridae) and the driftwood ecological niche: a morphological and molecular study. Journal of Natural History 46: 2677–2700. https://doi.org/10.1080/00222933.2012.717971

Wildish DJ, Smith R, Loeza-Quintana T, Radulovici AE, Adamowicz SJ (2016) Diversity and dispersal history of the talitrids (Crustacea: Amphipoda: Talitridae) of Bermuda. Journal of Natural History 49: 1047–1071. https://doi.org/10.1080/00222933.2016.1180719

Wildish DJ, Robinson SMC, Black M (2021) Locomotor activity rhythms of North Atlantic coastal talitroids. Marine and Freshwater Behaviour and Physiology 54: 181–202. https://doi.org/10.1080/10236244.2021.1993737

Wongkamhaeng K, Dumrongrojwattana P, Sumitrakij R, Keetapithchayakul TS (2022) *Thailandorchestia rhizophila* sp. nov., a new genus and species of driftwood hopper (Crustacea, Amphipoda, Protorchestiidae) from Thailand. Zookeys 1099: 139–153. https://doi.org/10.3897/zookeys.1099.82949

Yang L, Hou Z, Li S (2013) Marine incursions into East Asia: a forgotten driving force of biodiversity. Proceedings of the Royal Society B 280: 20122892. https://doi.org/10.1098/rspb.2012.2892

Zoosyst. Evol. 100 (4) 2024, 1459–1471 | DOI 10.3897/zse.100.120872

PENSOFT

MUSEUM FÜR NATURKUNDE BERLIN

DNA sequencing of topotypes helps delineate species distributions in the *Ischnocnema verrucosa* complex (Anura, Brachycephalidae)

Diego J. Santana[1], João Victor A. Lacerda[2], Priscila S. Carvalho[1], Manuella Folly[3], Bruno Bove da Costa[4†], Iuri Ribeiro Dias[5], Luiz Fernando Carmo[3], Henrique C. Costa[6], Donald B. Shepard[7], Clarissa Canedo[3,8]

1 *Instituto de Biociências, Universidade Federal de Mato Grosso do Sul, 79070-900, Campo Grande, MS, Brazil*
2 *Instituto Nacional da Mata Atlântica, 29650-000, Santa Teresa, Espírito Santo, Brazil*
3 *Departamento de Vertebrados, Museu Nacional, Universidade Federal do Rio de Janeiro, Quinta da Boa Vista, 20940-040, Rio de Janeiro, RJ, Brazil*
4 *Departamento de Zoologia, Instituto de Biologia, Universidade Federal do Rio de Janeiro, Avenida Brigadeiro Trompowski, 21941-902, Rio de Janeiro, RJ, Brazil*
5 *Departamento de Ciências Biológicas, Universidade Estadual de Santa Cruz, 45662-900, Ilhéus, BA, Brazil*
6 *Departamento de Zoologia, Instituto de Ciências Biológicas, Universidade Federal de Juiz de Fora, 36036-900, Juiz de Fora, MG, Brazil*
7 *Department of Biological Sciences, University of Arkansas, Fayetteville, Arkansas, 72701, USA*
8 *Departamento de Zoologia, Instituto de Biologia, Universidade do Estado do Rio de Janeiro, 20550-900, Rio de Janeiro, RJ, Brazil*

https://zoobank.org/6F5B592F-5473-4470-B678-3A8B58D5D477

Corresponding author: Diego J. Santana (jose.santana@ufms.br)

Academic editor: Pedro Taucce ♦ **Received** 14 February 2024 ♦ **Accepted** 8 October 2024 ♦ **Published** 31 October 2024

Abstract

As many new evolutionary lineages are being discovered and formally named, sequencing topotypes when holotypes are not available becomes essential for taxonomy. This study uses a DNA-taxonomy approach to sequence new populations of the *Ischnocnema verrucosa* species complex (Brazilian Wart Frogs) from different locations, including, for the first time, individuals from the type localities. Phylogenetic analysis of the mitochondrial *16S* gene recovered a monophyletic *Ischnocnema verrucosa* species series composed of three main clades. The most recent common ancestor was estimated to be 33.76 million years ago, and diversification within the three main clades occurred primarily during the Miocene. We delimited eight species-level lineages with high levels of sequence divergence (7% to 16%). Our study highlights the importance of DNA taxonomy and the necessity of protecting and sequencing topotypes in taxonomic studies. Our study also contributes to the conservation and understanding of the genus *Ischnocnema* and the biodiversity of the Brazilian Atlantic Forest region.

Key Words

Brazilian Atlantic Forest, DNA taxonomy, Eocene, Miocene, phylogeny, taxonomy, type locality

Introduction

In the last 300 years, taxonomists have served the purpose of describing, classifying, and naming organisms based, exceptionally, on morphological characters (Linnaeus 1750; Haeckel 1866; Hennig 1966). At present, integrative taxonomic approaches incorporating molecular data have revolutionized the field of biodiversity research, providing a powerful tool for uncovering cryptic diversity (Padial et al. 2010; Pilgrim and Darling 2010). This

† In Memoriam.

is particularly important because cryptic diversity, which refers to distinct species erroneously classified under one species name due to morphological similarities, is a significant contributor to the Linnean shortfall, where the number of known species falls short of the actual number of existing species (Hortal et al. 2015; Fišer et al. 2018; Struck et al. 2018). This has implications for our understanding of global biodiversity, highlighting the need for continued efforts to uncover and document new species.

In recent years, many species previously thought to be a single taxon have been revealed to be species complexes (e.g., Suatoni et al. 2006; Guimarães et al. 2022; Moraes et al. 2022; Araujo-Vieira et al. 2023; Brunes et al. 2023), with potential candidate species or known nominal species having small distributions and being under threat (Gehara et al. 2013). This trend is particularly frequent in anurans in several ecoregions across the globe (Hasan et al. 2012; Guarnizo et al. 2015; Cryer et al. 2019). The Neotropics harbor the largest amphibian diversity in the world, and many new species continue to be discovered, especially in tropical forest ecoregions such as the Amazon and Brazilian Atlantic Forest (Moura et al. 2018; Vacher et al. 2020).

The Brazilian Atlantic Forest (BAF), a biodiversity hotspot (Ribeiro et al. 2011), is characterized by a complex topography that has driven amphibian diversification (Paz et al. 2021). Among the many anuran groups that have evolved in the BAF, direct-developing frogs of the genus *Ischnocnema* Reinhardt & Lütken, 1862 are strongly associated with the biome (Hedges et al. 2008; Canedo and Haddad 2012). This genus comprises 39 species (Frost 2024), six of which have been described using integrative taxonomic approaches with molecular data (Brusquetti et al. 2013; Taucce et al. 2018a, 2018b, 2019; Silva-Soares et al. 2021), but many identified species complexes remain unresolved taxonomically (Gehara et al. 2013, 2017; Thomé et al. 2020; Oswald et al. 2023). If the nomenclatural history of a taxon is not assessed properly, the number of taxonomic inconsistencies tends to increase (e.g., Tobias et al. 2010; Mângia et al. 2014; Yodthong et al. 2019; Mângia et al. 2020), and even the resolutions and descriptions may not be effectively implemented from a nomenclatural standpoint (Leaché and Fujita 2010; Lourenço et al. 2015; Guayasamin and Trueb 2020). The act of naming species removes independent lineages from anonymity and highlights their evolutionary historical importance (Hillis 2007; Vences et al. 2013), while also improving the evaluation of conservation status (Mace 2004).

A lack of type specimens can create problems for taxonomic decision-making, just as the difficulty (and still high cost) of sequencing genetic material from century-old, fluid-preserved specimens brings challenges for proper nomenclature of cryptic species (Bell et al. 2020). However, this bias can often be overcome through the collection of recent topotypes, that is, new specimens collected from the type locality, which provide genetic material (Cacciali et al. 2017; Murphy et al. 2017). Over the last two decades, several molecular studies have focused on the brachycephalid frog genus *Ischnocnema*, defining and redelimiting the genus and its main clades, which currently include the *I. guentheri*, *I. lactea*, *I. parva*, *I. verrucosa*, and *I. venancioi* species series (*sensu* Hedges et al. 2008) (Canedo and Haddad 2012; Taucce et al. 2018b). The *Ischnocnema verrucosa* series comprises eight species (Canedo and Haddad 2012; Taucce et al. 2018b): *I. abdita* Canedo & Pimenta, 2010; *I. bolbodactyla* (Lutz, 1925); *I. juipoca* (Sazima & Cardoso, 1978); *I. karst* Canedo, Targino, Leite, & Haddad, 2012; *I. octavioi* (Bokermann, 1965); *I. penaxavantinho* Giaretta, Toffoli, & Oliveira, 2007; *I. surda* Canedo, Pimenta, Leite, & Caramaschi, 2010; and *I. verrucosa* (Reinhardt & Lütken, 1862). The placements of *I. surda* and *I. karst* in this group are not verified by genetic data because tissue samples were not available (Canedo and Haddad 2012).

Within the *I. verrucosa* species series, there is an unresolved taxonomic puzzle regarding *Ischnocnema verrucosa*, *I. octavioi*, and *I. surda*, three very similar-looking species (Fig. 1) not easily distinguished from each other (Canedo et al. 2010; Dantas and Ferreira 2010; Silva et al. 2013; Holer et al. 2017; Araújo et al. 2023). *Ischnocnema verrucosa* was described as *Leiuperus verrucosus* from 'Omegnen af Byen Juiz de Fora i Minas Geraes (altsaa fra Urskovsregionen)' (Reinhardt and Lütken 1862), i.e., 'the surroundings of the municipality of Juiz de Fora, state of Minas Gerais (from the primeval forest region)'. Currently, its distribution includes localities in the Brazilian states of Espírito Santo, Minas Gerais (Caramaschi and Canedo 2006; Silva et al. 2013), and Bahia (Orrico 2010; Freitas et al. 2011; Rojas-Padilla et al. 2020; Bastos and Zina 2022). *Ischnocnema octavioi* was described from the Tijuca Mountains in the state of Rio de Janeiro, Brazil (Bokermann 1965); currently, it is recorded in the Brazilian states of São Paulo (Holer et al. 2017), Espírito Santo (Dantas and Ferreira 2010), and Rio de Janeiro (Vrcibradic et al. 2008). Canedo et al. (2010) could not diagnose *I. octavioi* and *I. verrucosa* using morphological features. Finally, *I. surda* was described from Estação Ecológica do Tripuí, in the municipality of Ouro Preto, in the state of Minas Gerais, and shortly after its distribution was expanded to include other localities of this state (Silva et al. 2013; Lacerda et al. 2014). Silva et al. (2013) suggest clinal variation in the diagnostic characteristic between *I. surda* and *I. verrucosa*, indicating the need for studies to better elucidate the taxonomic identity of both species. Furthermore, topotype specimens of *I. verrucosa* and *I. octavioi* have never been included in molecular analyses, and populations identified as *I. verrucosa* have not been recovered as monophyletic (Canedo and Haddad 2012). Thus, whether species diversity is correctly delimited has not been adequately evaluated. Here, we use a DNA-taxonomy approach with new populations of the *Ischnocnema verrucosa* species complex from different locations, including, for the first time, individuals from the type localities of *I. verrucosa* and *I. octavioi* and individuals from the same municipality, close to the type locality of *I. surda*. We demonstrate the importance of sampling topotypes to accurately delineate distributions and properly name species in these complexes.

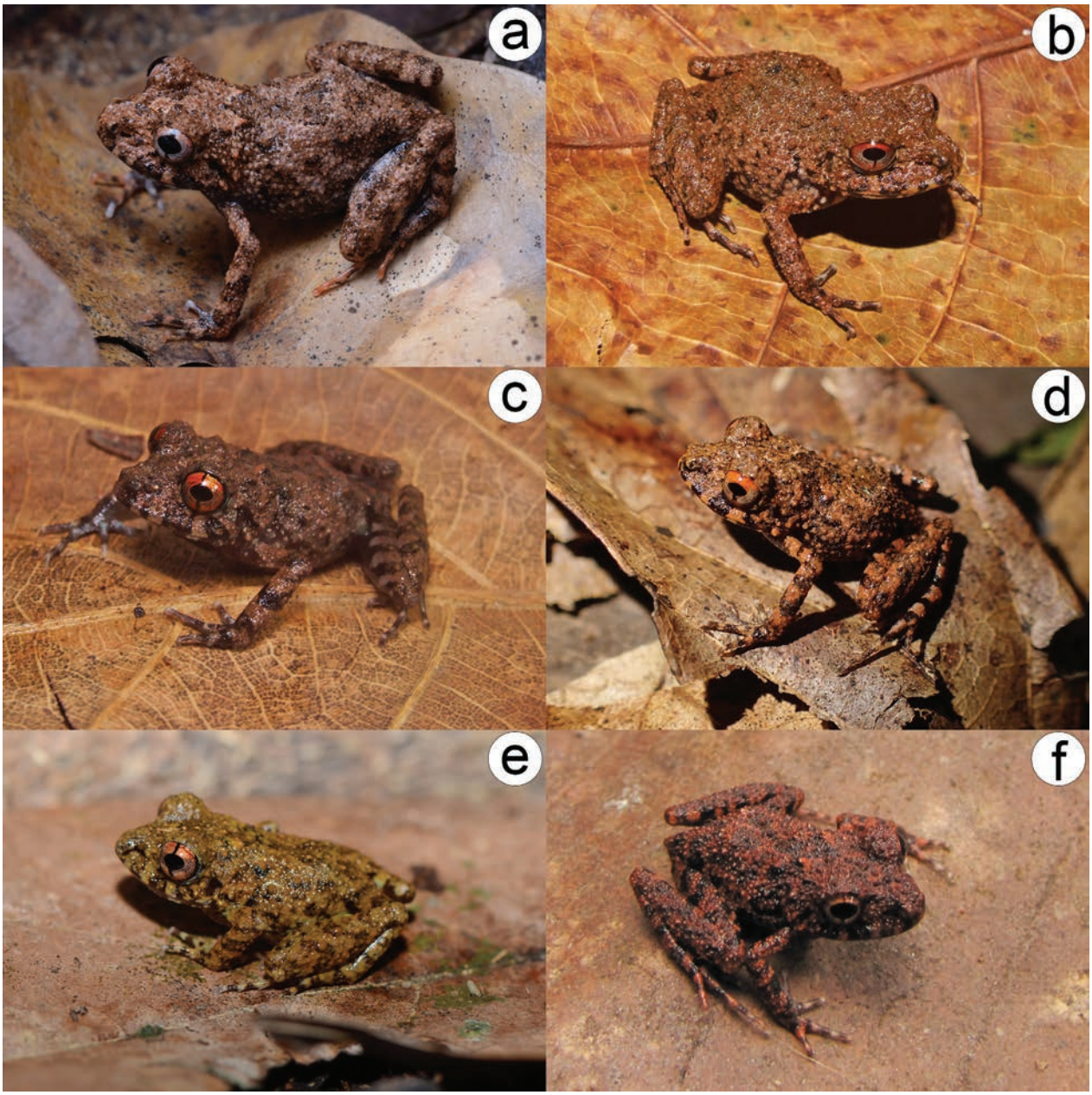

Figure 1. Live specimens in the *Ischnocnema verrucosa* species complex. **a.** Topotype of *Ischnocnema verrucosa* (MAP6749) from Parque Natural Municipal da Lajinha, municipality of Juiz de Fora, state of Minas Gerais; **b.** *I. verrucosa* (MZUESC8829) from Serra Bonita, municipality of Camacan, state of Bahia; **c.** *I. verrucosa* (MZUESC23730) from municipality of Wenceslau Guimarães, state of Bahia; **d.** *I.* aff. *verrucosa* (unvouchered specimen) from municipality of Santa Teresa, state of Espírito Santo; **e.** Topotype of *I. octavioi* (MNRJ94357) from Parque Nacional da Tijuca, municipality of Rio de Janeiro, state of Rio de Janeiro; and **f.** *I. surda* (UFMG-A17166) from municipality of Ouro Preto, state of Minas Gerais. (Photos by D.J. Santana [**a**], H.C. Costa [**f**], P.H. Pinna [**e**], I. Dias [**b, c**], J.V.A. Lacerda [**d**]).

Materials and methods

Whole genomic DNA was extracted from muscle or liver tissues of 11 specimens from the *Ischnocnema verrucosa* series using a Qiagen DNeasy kit (Valencia, California, USA) following the manufacturer's protocol. Next, we amplified a fragment of the mitochondrial *16S* gene using primers 16Sar and 16Sbr (Palumbi et al. 2002) or 16S-AR and 16S-Wilk2 (Wilkinson et al. 1996). Reactions contained 10 µl of GoTaq(R) G2 Green Master Mix, 6 µl of H_2O, 1 µl of each primer (10 µM), and 2 µl of template DNA (≥ 2 ng/µl). The PCR protocol was configured with one initial phase of 94 °C for 3 min, followed by 35 cycles of 94 °C for 20 s, 50 °C for 20 s, and 72 °C for 40 s, with a final extension phase of 72 °C for 5 min. Purification of PCR products and DNA sequencing were performed by Eurofins Genomics Inc. (Louisville, Kentucky, USA) and Centro de Pesquisa Sobre o Genoma Humano e Células Tronco (Universidade de São Paulo, Brazil).

We combined our newly generated *16S* sequences with all comparable *16S* sequences of the *Ischnocnema verrucosa* series available on GenBank. In addition, we downloaded from GenBank one *16S* sequence for each *Ischnocnema* species series and one *Brachycephalus* for use as outgroups, following Taucce et al. (2018b). Chromatogram sequences were visualized in Chromas and Geneious v.9.0.5 (Biomatters Ltd., Auckland, New Zealand). We aligned the *16S* gene fragments using MAFFT (Katoh et al. 2002) implemented in Geneious v.9.0.5 with the algorithm set as auto, which selects an appropriate strategy from L-INS-i, FFT-NS-I, and FFT-NS-2. The final alignment comprised 39 sequences of a 560 base-pair (bp) fragment of the mitochondrial *16S* gene. All GenBank accession numbers and genetic vouchers used here are listed in Table 1.

Table 1. Species, GenBank accession numbers for sequence data, specimen voucher numbers, collecting locality information, GPS coordinates, and references for all samples included in molecular analyses. * Topotypes.

Species	Genbank Accession	Voucher	Locality	Latitude, Longitute	Reference	Lineage
Brachycephalus nodoterga	KJ649783	IB6311	Ilha de São Sebastião, SP	-23.827, -45.373	Clemente-Carvalho et al. (2016)	Outgroup
*I. abdita**	JX267471	MNRJ34903	Santa Teresa, ES	-19.919, -40.619	Canedo and Haddad (2012)	*I. abdita*
I. abdita	JX267472	MTR12625	Caparao, MG	-20.524, -41.906	Canedo and Haddad (2012)	*I. abdita*
I. abdita	KY646094	MZUFV15919	Espera Feliz, MG	-20.651, -41.908	Rocha et al. (2017)	*I. abdita*
I. abdita	KY646095	MZUFV15920	Espera Feliz, MG	-20.651, -41.908	Rocha et al. (2017)	*I. abdita*
I. abdita	KY646096	MZUFV15922	Espera Feliz, MG	-20.651, -41.908	Rocha et al. (2017)	*I. abdita*
I. abdita	KY646097	MZUFV15923	Espera Feliz, MG	-20.651, -41.908	Rocha et al. (2017)	*I. abdita*
I. abdita	MN450228	TLFT 2831	Ibitirama, Parque Nacional do Caparao ES	-20.502, -41.722	Zornosa-Torres et al. (2020)	*I. abdita*
I. bolbodactyla	JX267476	CFBH5785	Paraty, RJ	-23.219, -44.716	Canedo and Haddad (2012)	*I. bolbodactyla*
I. cf. *penaxavantinho*	JX267298	CFBH10230	Grao Mogol, MG	-16.565, -42.893	Canedo and Haddad (2012)	*I.* cf. *penaxavantinho*
I. guentheri	EF493533	NA	Estacao Ecologica de Juréia, SP	-24.530, -47.189	Heinicke et al. (2007)	*I. guentheri*
I. juipoca	DQ283093	CFBH4450	Poços de Caldas, MG	-21.785, -46.561	Frost et al. (2006)	*I. juipoca*
I. juipoca	JX267348	CFBH19697	Caieiras, SP	-23.362, -46.746	Canedo and Haddad (2012)	*I. juipoca*
I. juipoca	JX267349	CFBH9904	Campos de Jordao, SP	-22.740, -45.594	Canedo and Haddad (2012)	*I. juipoca*
I. juipoca	JX267373	AFlab#0963	Poços de Caldas, MG	-21.785, -46.561	Canedo and Haddad (2012)	*I. juipoca*
I. juipoca	JX267511	AFlab#0969	Poços de Caldas, MG	-21.785, -46.561	Canedo and Haddad (2012)	*I. juipoca*
I. juipoca	JX267512	MCLfield#0122	Estacao Biologica de Boraceia, Salesopolis, SP	-23.636, -45.946	Canedo and Haddad (2012)	*I. juipoca*
I. juipoca	JX267513	MCLfield#0069	Estacao Biologica de Boraceia, Salesopolis, SP	-23.636, -45.946	Canedo and Haddad (2012)	*I. juipoca*
I. lactea	JX267308	MTR10435	Paranapiacaba, Santo Andre, SP	-23.777, -46.299	Canedo and Haddad (2012)	*I. lactea*
I. octavioi	JX267312	MNRJ48752	Reserva Biologica Uniao, RJ	-22.378, -42.118	Canedo and Haddad (2012)	*I. verrucosa*
I. octavioi	JX267322	MNRJ42488	Parque Estadual do Desengano, Santa Maria Madalena, RJ	-21.904, -41.949	Canedo and Haddad (2012)	*I. verrucosa*
I. octavioi	JX267521	MNRJ62328	Reserva Ecológica de Guapiaçu, Cachoeira de Macacu, RJ	-22.449, -42.776	Canedo and Haddad (2012)	*I. verrucosa*
I. octavioi	MN450229	MN450229	Alto Caparao, Parque Nacional do Caparao, MG	-20.446, -41.847	Zornosa-Torres et al. (2020)	*I. verrucosa*
*I. octavioi**	PQ456291	MNRJ93604*	Parque Nacional da Tijuca, Rio de Janeiro, RJ	-22.950, -43.286	Present work	*I. octavioi*
I. octavioi	PQ456292	MNRJ92356	Parque Arqueológico e Ambiental de São João Marcos, Rio Claro, RJ	-22.800, -44.029	Present work	*I. octavioi*
I. octavioi	PQ456293	MNRJ92360	Parque Arqueológico e Ambiental de São João Marcos, Rio Claro, RJ	-22.800, -44.029	Present work	*I. octavioi*
I. parva	EF493532	NA	NA	NA, NA	Heinicke et al. (2007)	Outgroup
I. surda	PQ456283	UFMG-A17166	Samarco, Ouro Preto, MG	-20.188, -43.509	Present work	*I. surda*
I. surda	PQ456284	MNRJ77811	Reserva Particular do Patrimônio Natural Serra do Caraça, MG	-20.133, -43.500	Present work	*I. surda*
I. venancioi	JX267321	MNRJ44564	Parque Nacional da Serra dos Órgãos, RJ	-22.485, -43.067	Canedo and Haddad (2012)	Outgroup
I. verrucosa	JX267383	MNRJ34900	Santa Teresa, ES	-19.919, -40.619	Canedo and Haddad (2012)	*I.* aff. *verrucosa*
I. verrucosa	JX267537	MNRJ34899	Santa Teresa, ES	-19.919, -40.619	Canedo and Haddad (2012)	*I.* aff. *verrucosa*
I. verrucosa	JX267538	CFBH23685	RPPN Serra Bonita, Camacan, BA	-15.397, -39.572	Canedo and Haddad (2012)	*I. verrucosa*
*I. verrucosa**	PQ456285	MAP6749*	Parque Natural Municipal da Lajinha, Juiz de Fora, MG	-21.792, -43.366	Present work	*I. verrucosa*
*I. verrucosa**	PQ456286	MAP6751*	Parque Natural Municipal da Lajinha, Juiz de Fora, MG	-21.792, -43.366	Present work	*I. verrucosa*
*I. verrucosa**	PQ456287	MAP6750*	Parque Natural Municipal da Lajinha, Juiz de Fora, MG	-21.792, -43.366	Present work	*I. verrucosa*
I. verrucosa	PQ456288	MZUESC23732	Parque Nacional da Serra das Lontras, Arataca, BA	-15.262, -39.414	Present work	*I. verrucosa*
I. verrucosa	PQ456289	MZUESC15886	Serra do Mandim, Itarantim, BA	-15.654, -40.060	Present work	*I. verrucosa*
I. verrucosa	PQ456290	MZUESC23731	Estação Ecológica Wenceslau Guimarães, BA	-13.687, -39.478	Present work	*I. verrucosa*

We performed Bayesian phylogenetic inference in BEAST v.2.7.4 (Bouckaert et al. 2019) for 100 million generations, sampling every 10,000 steps, using a Yule Process tree prior and a relaxed-clock model rate of 0.006 substitutions/site/million years (Gehara et al. 2017) with uniform distribution. Additionally, we set a prior with all individuals belonging to the genus *Ischnocnema* as monophyletic. We used the default settings for all the other priors. We used the model-averaging method by running the analysis with bModelTest (Bouckaert and Drummond 2017). We performed two independent runs to check for convergence. We checked for stationarity by visually inspecting trace plots and ensuring all effective sample size values were > 200 in Tracer v.1.7.1 (Rambaut et al. 2018). The first 10% of sampled genealogies were discarded as burn-in, and the maximum clade credibility tree with median node ages was calculated with TreeAnnotator v.2.7.4 (Bouckaert et al. 2019).

We conducted the Generalized Mixed Yule Coalescent (GMYC; Pons et al. 2006; Fujisawa and Barraclough 2013) and the multi-rate Poisson Tree Processes (mPTP; Kapli et al. 2017) delimitation analyses. To perform these analyses, based on the topologies, we created a new alignment using unique haplotypes. To remove identical sequences, we used the Biostrings package (Pagès et al. 2024) in R. This reduced alignment had 32 sequences (including the same outgroups) with the same 560 bp. For both analyses, we used as input the tree obtained in a Bayesian analysis in BEAST with the same parameters mentioned earlier. We performed GMYC in R v.4.1.1 (R Core Team 2021) using the package *splits* v.1.0-20 (Ezard et al. 2017) and mPTP species delimitation analysis on the mPTP webserver (https://mptp.h-its.org/). Finally, we performed Assemble Species by Automatic Partitioning (ASAP; Puillandre et al. 2021), which is a distance-based method. We performed the ASAP delimitation on the webserver (https://bioinfo.mnhn.fr/abi/public/asap/asapweb), considering a simple distance model to compute the distances between samples and default parameters. We retained the delimitation scheme supported by the lowest ASAP score (Puillandre et al. 2021). Finally, we defined the lineages based on the combined evidence from these three delimitation methods, considering congruence of results when at least two of three agreed (Moraes et al. 2022). Lastly, we calculated pairwise-sequence divergences (uncorrected *p*-distances) among species/individuals using MEGA v.10.1.1 (Kumar et al. 2018), with pairwise deletion for gaps.

Results

Our gene tree recovered the *Ischnocnema verrucosa* species series as monophyletic (PP = 0.94), comprising eight lineages: *Ischnocnema* cf. *penaxavantinho*, *I. juipoca*, *I. bolbodactyla*, *I. abdita*, *I. verrucosa*, *I. octavioi*, *I. surda*, and *I.* aff. *verrucosa* (Fig. 2). The initial divergences at the base of the tree gave rise to three main clades. The first clade (PP = 1.0), composed of *I.* cf. *penaxavantinho* and *I. juipoca*, is the sister group of the other two clades. The second clade (PP = 1.0), composed of *I. bolbodactyla* and *I. abdita*, is the sister group of the third clade (PP = 1.0), which is composed of species in the *I. verrucosa* complex: *I. verrucosa*, *I. octavioi*, *I. surda*, and one allied lineage that we call here, *I.* aff. *verrucosa*. Additionally, populations from Reserva Biológica União (RJ), Parque Estadual do Desengano (RJ), Reserva Ecológica de Guapiaçu (RJ), and Parque Nacional do Caparaó (MG), previously identified as *I. octavioi*, were revealed to be *I. verrucosa*.

The most recent common ancestor (MRCA) of the *Ischnocnema verrucosa* species series was estimated to be 33.76 million years ago (mya; HPD 95%: 26.18–42.01) at the end of the Eocene, when the last common ancestor of *I.* cf. *penaxavantinho* and *I. juipoca* separated from the last common ancestor of the other two clades. Soon after, in the Oligocene, around 28.53 mya (HPD 95%: 26.18–42.01), the MRCA of the other two clades diverged. Finally, the *Ischnocnema verrucosa* species complex diversified throughout the Miocene with the divergence between *I. octavioi* from the others in the early Miocene, around 21.25 mya (HPD 95%: 16.5–26.51), and then, right after this separation, the lineage we called *I.* aff. *verrucosa* diverged from *I. surda*–*I. verrucosa* in the early Miocene around 20.38 mya (HPD 95%: 14.88–24.21). Finally, the most recent lineages, *I. verrucosa* and *I. surda*, diverged in the Miocene, around 16.28 mya (HPD 95%: 11.93–19.84).

The mPTP (Score Null Model: -178.0243) and ASAP (asap score: 4.00; threshold distance: 0.075) species delimitation methods recovered the same eight lineages for the *I. verrucosa* series, while the GMYC split the series into 12 lineages (confidence interval: 10–13; likelihood ratio test: 16.604; result of the LR test: < 0.001) (Fig. 2). The *p*-distances between lineages within the *I. verrucosa* complex show high levels of sequence divergence, ranging from 10% between *I. surda* and *I. verrucosa* to 13.1% between *I.* aff. *verrucosa* and *I. octavioi* (Table 2).

Table 2. Average pairwise uncorrected (*p*-distance) sequence divergence between different lineages within the *Ischnocnema verrucosa* species series. Data in bold on the diagonal are intraspecific divergences. n/c = Not Calculated.

	Lineage	1	2	3	4	5	6	7	8
1	*I. surda*	**0.004**							
2	*I. verrucosa*	0.100	**0.059**						
3	*I.* aff. *verrucosa*	0.128	0.111	**<0.001**					
4	*I. bolbodactyla*	0.148	0.136	0.158	**n/c**				
5	*I. abdita*	0.127	0.109	0.123	0.079	**0.004**			
6	*I.* cf. *penaxavantinho*	0.133	0.144	0.140	0.140	0.124	**n/c**		
7	*I. juipoca*	0.151	0.151	0.140	0.153	0.150	0.088	**0.007**	
8	*I. octavioi*	0.129	0.129	0.131	0.153	0.137	0.145	0.164	**0.012**

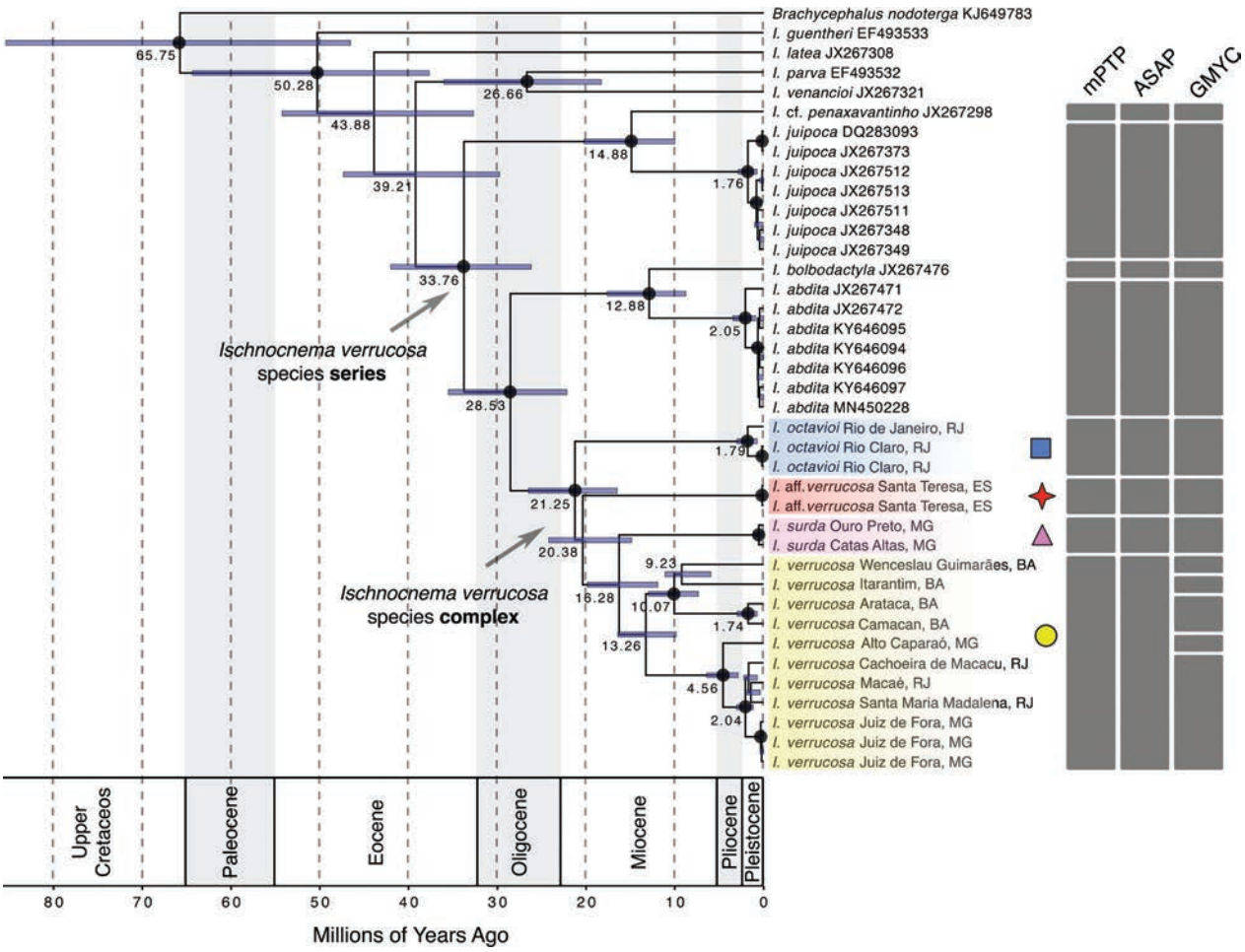

Figure 2. Bayesian chronogram for the *Ischnocnema verrucosa* series based on analysis of the mitochondrial *16S* gene. Circles on nodes denote significant posterior probability (pp = 0.95–1.0). Median ages in millions of years are shown on nodes, and 95% HPDs of node ages are indicated by horizontal blue bars. Vertical gray bars on the right represent the species delimited by GMYC (Generalized Mixed Yule Coalescent), mPTP (multi-rate Poisson Tree Processes), and Assemble Species by Automatic Partitioning (ASAP).

Discussion

In the present study on phylogenetic relationships of the *Ischnocnema verrucosa* species series, we found eight species-level lineages distributed in three main clades, with the most recent common ancestor estimated to have lived 33.76 mya (Fig. 2). The lineages were identified based on the congruence of two of the three species delimitation methods, revealing high levels of genetic divergence. Our study also identified diversification events, many of which originated in the Oligocene and Miocene, with some lineages experiencing diversification during the Pliocene. The estimated divergence times for the *Ischnocnema verrucosa* species complex suggest an ancient and gradual diversification. While mitochondrial data can sometimes overestimate divergence times (Duchêne et al. 2014), our results align with the broad timelines observed in other Terrarana (Gehara et al. 2017; Condez et al. 2020; Mônico et al. 2024). The ancient divergences indicate that the complex underwent significant diversification during a period of climatic shifts and landscape changes in the Brazilian Atlantic Forest (BAF) (Brown et al. 2020). Within Brachycephalidae, *Ischnocnema* has a complex evolutionary history (Heinicke et al. 2007; Canedo and Haddad 2012; Taucce et al. 2018a, 2018b), and many new species have recently been discovered (e.g., Taucce et al. 2018a; 2018b, 2019; Silva-Soares et al. 2021). Therefore, our finding of at least eight evolutionary lineages within the *I. verrucosa* series is expected.

Canedo and Haddad (2012) presented the first well-sampled, multi-locus phylogeny of *Ischnocnema*, finding the same relationships that we recovered in our tree. The authors also found *I. verrucosa* to be paraphyletic, but they did not indicate which group should be named as the nominal species as there was no topotype sampled. Nevertheless, this was an early indication of cryptic diversity within the *I. verrucosa* complex. In a later phylogeny of the Terrarana clade with emphasis on *Ischnocnema* (Taucce et al. 2018b), the topology of the *I. verrucosa* species series was the same as previously reported. However, the dataset used was also the same, with fewer samples of *I. verrucosa*, which disregarded its paraphyly. Here, using only the mitochondrial *16S* gene, a common marker for species identification and delimitation (Vences et al. 2012; Lyra et al. 2017; Koroi-

va and Santana 2022), we found the same topology for the main clades with high support, confirming the paraphyly of *I. verrucosa* and *I. octavioi*. In order to properly name the populations, we re-identified them based on our tree topology and the species delimitation methods, which yielded one candidate species (*I.* aff. *verrucosa*) in addition to the nominal ones.

In this study, we employed three delimitation methods, GMYC (General Mixed Yule-Coalescent), mPTP (multi-rate Poisson Tree Processes), and ASAP (Assemble Species by Automatic Partitioning), to analyze the species boundaries within the *Ischnocnema verrucosa* complex. While such methods have their strengths (Dellicour and Flot 2018), they also come with inherent limitations. The GMYC method, although effective in distinguishing between speciation and intraspecific variation, can sometimes oversplit (Dellicour and Flot 2018), particularly in cases of recent divergence or incomplete lineage sorting. On the other hand, the mPTP method, a more accurate implementation of PTP (Kapli et al. 2017), tends to be more conservative. Finally, ASAP is a distance-based method that tends to yield good results under a broad range of speciation conditions (Dellicour and Flot 2018; Puillandre et al. 2021). Future studies could benefit from integrating additional data types, such as bioacoustics and morphology, and using high-throughput sequencing to obtain a more comprehensive understanding of species boundaries.

Despite the names used to identify samples, the taxonomic complexity in the *Ischnocnema verrucosa* species complex has always been attributed to their conservative external morphology, which hampers the diagnosis of species (Canedo et al. 2010; Silva et al. 2013; Holer et al. 2017; Araújo et al. 2023). Therefore, finding distinct characters to better diagnose evolutionary lineages would help to resolve taxonomic issues. Since morphological characteristics alone have proven to be confusing for species identification, it is crucial to prioritize bioacoustics, osteological, and even ecological differences when describing new species (Carvalho and Giaretta 2013; Martins and Giaretta 2013; Hamdan et al. 2024). In today's taxonomic world, we are racing against time to describe new species before they disappear (Moura and Jetz 2021). Therefore, adopting integrative methods for delimiting species is essential for accurately describing new taxa (Fujita et al. 2012).

Ischnocnema verrucosa complex is endemic to the BAF, and it is found in the mountain ranges of Serra do Mar, Serra da Mantiqueira, southern Serra do Espinhaço, eastern Minas Gerais in the Rio Doce valley, and southern Bahia (Fig. 3). This distribution pattern is common among many amphibian groups, with closely related species or divergent populations of the same species occurring in distinct mountain ranges in southeastern Brazil (Cruz and Feio 2007; Cassini et al. 2013; Magalhães et al. 2020). Certain geographic congruences are observed in the phylogenetic relationships of lineages. Two samples of *I. verrucosa* from the Serra da Mantiqueira form a well-supported clade with samples from three other localities in Serra do Mar. Additionally, along the coastal mountains of the BAF in the states of Rio de Janeiro, Espírito Santo, and southern Bahia, the diversification of lineages within the *I. verrucosa* complex mainly occurred during the Miocene. Model-based analyses revealed population diversification and cryptic species in the *Ischnocnema parva* complex in the BAF (Gehara et al. 2017). Divergences between high-altitude lineages may indicate an influence of climatic cycles and mountains in diversification of *I. parva* (Gehara et al. 2017) and *I. verrucosa* species complexes.

Cryptic diversity appears to be common within *Ischnocnema* (Oswald et al. 2023); however, describing new species without evaluating topotypes of the closest-related species is problematic. Our work included, for the first time, samples of individuals from the type localities of the two nominal species within the *I. verrucosa* complex (*I. verrucosa* and *I. octavioi*) and populations attributed to *I. surda* close to its type locality. An important case to highlight is the population from the municipality of Santa Teresa, in the state of Espírito Santo, previously identified as *I. verrucosa* (see Rödder et al. 2007; Almeida et al. 2011; Canedo and Haddad 2012; Ferreira et al. 2019). The advertisement call of this population was recently described (Araújo et al. 2023). However, our samples from the municipality of Santa Teresa were recovered as a different species (named *I.* aff. *verrucosa*) (Figs 1, 2). Consequently, the advertisement call of the nominal population of *I. verrucosa* and the other lineages in the complex remain undescribed for more than 160 years. Nonetheless, there is a synonym for *I. verrucosa* from the municipality of Colatina, Espírito Santo state, *Eupsophus versus* Gorham, 1966 (a replacement name for the homonym *Eupsophus verrucosus* Miranda-Ribeiro, 1937). Our findings challenge the notion that geographic distance is the most effective criterion for delineating named species. Despite the proximity (~45 km) of the populations in Santa Teresa, we refrain from assigning the name *Eupsophus versus* to them. Vocalizations may prove critical for resolving taxonomic questions in these complexes still without morphological diagnosis, as demonstrated for the related species *I. oea* (Heyer, 1984), *I. garciai* Taucce, Canedo, & Haddad, 2018, and *I. feioi* Taucce, Canedo, & Haddad, 2018 (Taucce et al. 2018b), or even for the *I. guentheri* complex, which, although unnamed mainly because of sympatry of lineages, has candidate species with acoustic diagnoses (Gehara et al. 2013).

We emphasize that including samples from the type localities of the two named species in the *I. verrucosa* complex was crucial for defining to which evolutionary lineages these names correspond. In some other groups, potential new species have been and are frequently revealed, but no taxonomic decision can be made because of the troublesome taxonomic history of the type specimen or because the type locality is unknown or imprecise, leaving the group unresolved (e.g., Cassini et al. 2010). In the case of the *I. verrucosa* complex,

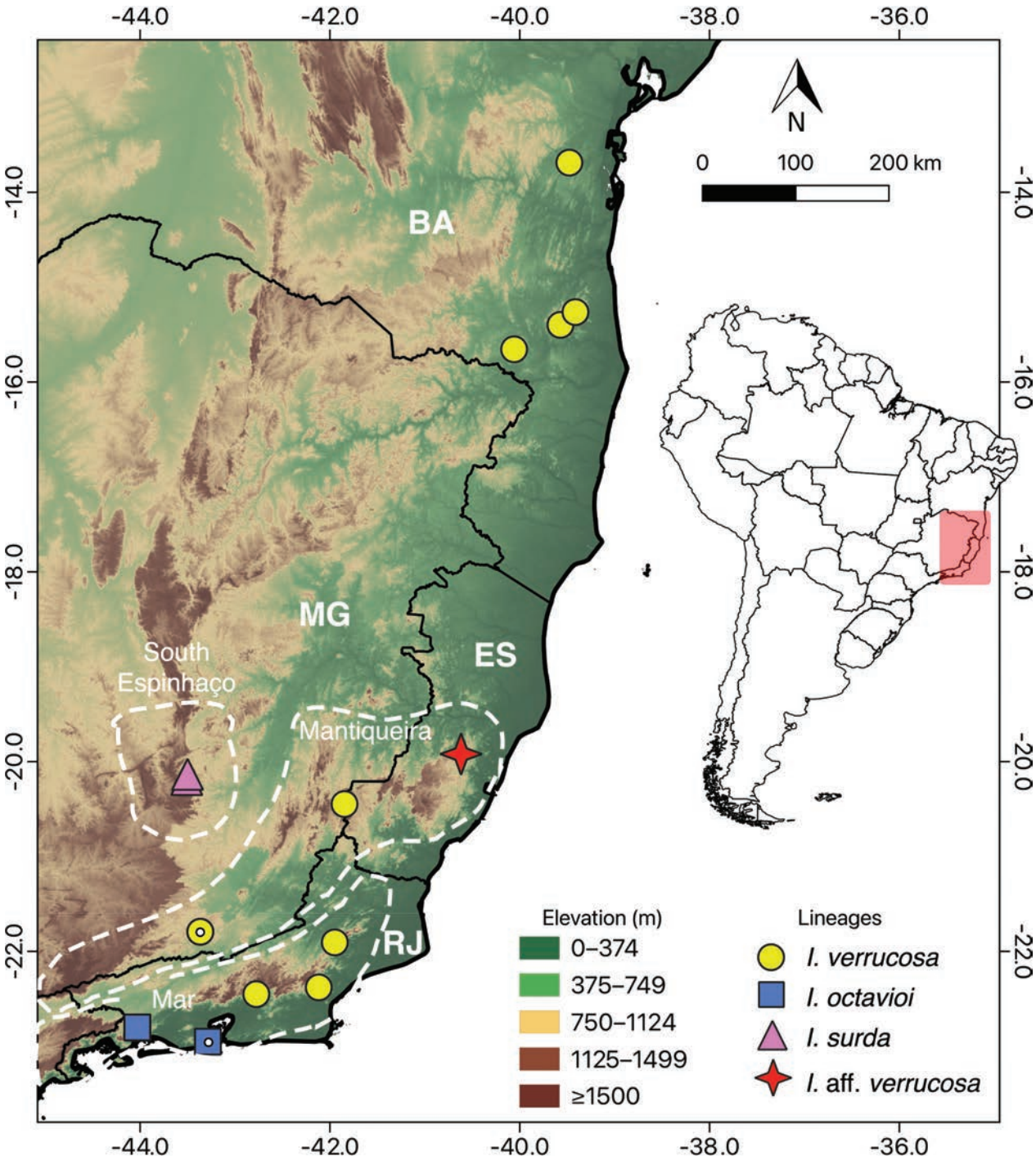

Figure 3. Geographic locations of samples of the *Ischnocnema verrucosa* complex used in this study. White dots on symbols indicate type localities. White dashed areas correspond to the mountain complexes.

I. surda occurs in the southern region of the Espinhaço mountain range, specifically within the Iron Quadrangle (Quadrilátero Ferrífero), also cited for the northern Mantiqueira range and across the Rio Doce valley (Silva et al. 2013). Unfortunately, we were unable to include samples from the formerly cited populations in our analysis. Consequently, in relation to the distribution of *I. surda*, we are refraining from definitively stating its precise geographic distribution. *Ischnocnema octavioi* occurs in the portion closest to the coast of the Serra do Mar, in the south of Rio de Janeiro state. *Ischnocnema verrucosa* occurs in the Serra da Mantiqueira, Serra do Mar (in the Serra dos Órgãos portion), and southern Bahia, making it the species with the broadest distribution of the complex. However, genetic divergence within *I. verrucosa* is high (5.9%; Table 2), higher than the average *16S* divergence usually found among anuran species (Fouquet et al. 2007; Vences et al. 2012; Lyra et al. 2017; Koroiva and Santana 2022). Nonetheless, our value is consistent with previous studies on the genus *Ischnocnema*. For instance, Gehara et al. (2013) reported a *16S p*-distance of 6% between lineages of *I. guentheri*, while Taucce et al. (2018a) found a 7.3% distance between lineages of *Ischnocnema*.

One possible limitation of our work and similar attempts relates to the sampling scope and the possibility of sympatry between cryptic lineages. Sympatry between cryptic lineages of *Ischnocnema* is known from previous studies (Gehara et al. 2013, 2017; Taucce et al. 2018b; Thomé et al. 2020; Oswald et al. 2023). Our sampling, for example, in the municipality of Juiz de Fora was restricted to a single area (Parque Natural Municipal de Lajinha), which may not fully represent the species' diversity in the region. Without extensive sampling at various points in the municipality, there remains doubt as to whether our samples accurately represent the nominal species. While we did not find any sympatric species in our samples, the possibility of their presence cannot be ruled out, as has been documented in other *Ischnocnema* complexes. Future research should aim to include broader sampling across different localities to reveal potential sympatric species.

Taxonomy, particularly when employing molecular approaches, plays a crucial role in identifying key areas for research and conservation efforts since it highlights the presence of endemic species and/or high-diversity hotspots (Baker et al. 2003; Frankham 2010; Gehara et al. 2013). Given the current biodiversity crisis and its increasingly accelerated loss, more support for taxonomy studies should be considered. Recently, the IUCN Red List of Threatened Species was re-evaluated, and *I. verrucosa* and *I. surda* were listed as Least Concern (LC), based on their wide geographic ranges (IUCN SSC Amphibian Specialist Group, Instituto Boitatá de Etnobiologia e Conservação da Fauna 2023a, 2023b). However, *I. surda* was sampled only in the southern Espinhaço, a region heavily impacted by mining activities and home to other threatened species (e.g., Bastos et al. 2023; Santana et al. 2024). It is crucial to search for new populations of *I. surda* to gauge the urgency of conservation efforts needed for this species, especially if it is confirmed that it occurs solely in this region. It is common to find microendemic species in Brachycephalidae frogs (Gehara et al. 2013; Pie et al. 2013; Thomé et al. 2020; Taucce et al. 2022), and small distributions are associated with increased extinction risk because they make species more prone to negative effects of habitat loss (Ficetola et al. 2014), climate change (Li et al. 2013), wildfires (Anjos et al. 2021), and emerging diseases (Kilpatrick et al. 2010). However, facing historical taxonomic difficulties, such as in the *I. verrucosa* species complex, we emphasize the importance of using a molecular delimitation approach that includes samples from type localities of these populations before using these occurrences to delimit species, delineate distributions, and revise taxonomy, all of which will aid in future evaluations of species' conservation status.

Acknowledgments

We thank Fundação de Amparo à Pesquisa do Estado de Minas Gerais (FAPEMIG process APQ-02302-21) and the Institutional Program of Internationalization sponsored by Coordination for the Improvement of Higher Education Personnel (Capes-PrInt 41/2017 – Process 88881.311897/2018–01) for financial support. DJS (CNPq 311284/2023-0; CNPq 402012/2022-4), IRD (CNPq 315362/2021-9), JVAL (CNPq 301349/2023-1, 300766/2024-6), and LFC (CNPq 141577/2023-1) thank the Conselho Nacional de Desenvolvimento Científico e Tecnológico (CNPq) for research fellowships. DBS thanks Dr. Johnny Armstrong, the James C. Jeffery, M.D. Professorship, and the School of Biological Sciences at Louisiana Tech University for financial support. CC thanks Fundação de Amparo à Pesquisa do Estado do Rio de Janeiro (FAPERJ processes E-26/010.100643/2018, 010.100954/2018, 211.154/2019, 210.297/2021, 211.231/2021) for financial support. We dedicate this work to the memory of our dear friend and co-author, B.B. Costa, who sadly passed away during the course of this research. His invaluable contributions and collaboration were fundamental to this study, and his presence is greatly missed. We want to thank two anonymous reviewers and the editor, Pedro Taucce, for their valuable suggestions

References

Almeida AP, Gasparini JL, Peloso PLV (2011) Frogs of the state of Espírito Santo, southeastern Brazil – The need for looking at the coldspots. CheckList 7: 542–560. https://doi.org/10.15560/7.4.542

Anjos AG, Solé M, Benchimol M (2021) Fire effects on anurans: what we know so far?. Forest Ecology and Management 495: 119338. https://doi.org/10.1016/j.foreco.2021.119338

Araújo AP, Ferreira RB, Canedo C, Zocca C, Lacerda JVA (2023) After 160 years of 'silence': the advertisement call of the frog *Ischnocnema verrucosa*. Herpetological Bulletin 163: 31–34. https://doi.org/10.33256/hb163.3134

Araujo-Vieira K, Lourenço ACC, Lacerda JVA, Lyra ML, Blotto BL, Ron SR, Baldo D, Pereyra MO, Suárez-Mayorga ÁM, Baêta D, Ferreira RB, Barrio-Amorós CL, Borteiro C, Brandão RA, Brasileiro CA, Donnelly MA, Dubeux MJM, Köhler J, Kolenc F, Fortes Leite FS, MacIel NM, Nunes I, Orrico VGD, Peloso P, Pezzuti TL, Reichle S, Rojas-Runjaic FJM, Da Silva HR, Sturaro MJ, Langone JA, Garcia PCA, Rodrigues MT, Frost DR, Wheeler WC, Grant T, Pombal JP, Haddad CFB, Faivovich J (2023) Treefrog Diversity in the Neotropics: Phylogenetic Relationships of Scinaxini (Anura: Hylidae: Hylinae). South American Journal of Herpetology 27: 1–143. https://doi.org/10.2994/SAJH-D-22-00038.1

Baker C, Dalebout M, Lavery S, Ross H (2003) www.DNA-surveillance: applied molecular taxonomy for species conservation and discovery. Trends in Ecology and Evolution 18: 271–272. https://doi.org/10.1016/S0169-5347(03)00101-0

Bastos DFO, Zina J (2022) Amphibian fauna in an ecotonal and mountainous area in south-central Bahia State, northeastern Brazil. Herpetology Notes 15: 365–376.

Bastos RP, Martins MR, Bataus YSL, Côrtes LG, Uhlig VM, Almeida APL, Canedo C, Caramaschi U, Costa COR, Ferrante L, Ferreira RB, Garcia PCA, Gasparini JL, Hepp F, Moraes RL, Leite FSF, Martins IA, Nascimento LB, Santana DJ, Filho ISNS, Soares TS, Toledo LF (2023) *Sphaenorhynchus canga* Araujo-Vieira, Lacerda, Pezzuti, Leite, Assis & Cruz, 2015. Sistema de Avaliação do Risco

de Extinção da Biodiversidade - SALVE. [Acesso em: 08 de fev. de 2024] https://doi.org/10.37002/salve.ficha.21923

Bell RC, Mulcahy DG, Gotte SW, Maley AJ, Mendoza C, Steffensen G, Barron JC, Hyman O, Flint W, Wynn A, Mcdiarmid RW, Mcleod DS (2020) The Type Locality Project: collecting genomic-quality, topotypic vouchers and training the next generation of specimen-based researchers. Systematics and Biodiversity 18: 557–572. https://doi.org/10.1080/14772000.2020.1769224

Bokermann WCA (1965) A new *Eleutherodactylus* from southeastern Brazil. Copeia 1965: 440–441. https://doi.org/10.2307/1440993

Bouckaert RR, Drummond AJ (2017) bModelTest: Bayesian phylogenetic site model averaging and model comparison. BMC evolutionary biology 17: 1–11. https://doi.org/10.1186/s12862-017-0890-6

Bouckaert R, Vaughan TG, Barido-Sottani J, Duchêne S, Fourment M, Gavryushkina A, Heled J, Jones G, Kühnert D, De Maio N, Matschiner M, Mendes FK, Müller NF, Ogilvie HA, Du Plessis L, Popinga A, Rambaut A, Rasmussen D, Siveroni I, Suchard MA, Wu CH, Xie D, Zhang C, Stadler T, Drummond AJ (2019) BEAST 2.5: An advanced software platform for Bayesian evolutionary analysis. PLoS Computational Biology 15: e1006650. https://doi.org/10.1371/journal.pcbi.1006650

Brown J, Paz A, Reginato M, Amaro R, Assis C, Lyra M, Caddah M, Aguirre-Santoro J, d'Horta F, Raposo do Amaral F, Goldenberg R, Silva-Brandão K, Freitas A, Rodrigues M, Michelangeli F, Miyaki C; Carnaval A (2020). Seeing the forest through many trees: multi-taxon patterns of phylogenetic diversity in the Atlantic Forest hotspot. Diversity and Distributions 26: 1160–1176. https://doi.org/10.1111/ddi.13116

Brunes TO, Pinto FCS, Taucce PPG, Santos MTT, Nascimento LB, Carvalho DC, Oliveira G, Vasconcelos S, Leite FSF (2023) Traditional taxonomy underestimates the number of species of *Bokermannohyla* (Amphibia: Anura: Hylidae) diverging in the mountains of southeastern Brazil since the Miocene. Systematics and Biodiversity 21. https://doi.org/10.1080/14772000.2022.2156001

Brusquetti F, Thomé MTC, Canedo C, Condez TH, Haddad CFB (2013) A new species of *Ischnocnema parva* species series (Anura, Brachycephalidae) from northern state of Rio de Janeiro, Brazil. Herpetologica 69: 175–185. https://doi.org/10.1655/HERPETOLOGICA-D-12-00050

Cacciali P, Morando M, Medina CD, Köhler G, Motte M, Avila LJ (2017) Taxonomic analysis of Paraguayan samples of *Homonota fasciata* Duméril & Bibron (1836) with the revalidation of *Homonota horrida* Burmeister (1861) (Reptilia: Squamata: Phyllodactylidae) and the description of a new species. PeerJ 5: e3523. https://doi.org/10.7717/peerj.3523

Canedo C, Haddad CFB (2012) Phylogenetic relationships within anuran clade Terrarana, with emphasis on the placement of Brazilian Atlantic rainforest frogs genus *Ischnocnema* (Anura: Brachycephalidae). Molecular Phylogenetics and Evolution 65: 610–620. https://doi.org/10.1016/j.ympev.2012.07.016

Canedo C, Pimenta BVS, Leite FSF, Caramaschi U (2010) New species of *Ischnocnema* (Anura: Brachycephalidae) from the State of Minas Gerais, southeastern Brazil, with comments on the *I. verrucosa* species series. Copeia 2010: 629–634. https://doi.org/10.1643/CH-09-159

Caramaschi U, Canedo C (2006) Reassessment of the taxonomic status of the genera *Ischnocnema* Reinhardt and Lütken, 1862 and *Oreobates* Jiménez-de-la-Espada, 1872, with notes on the synonymy of *Leiuperus verrucosus* Reinhardt and Lütken, 1862 (Anura: Leptodactylidae). Zootaxa, 1116: 43–54. https://doi.org/10.11646/zootaxa.1116.1.3

Carvalho TR de Giaretta AA (2013) Taxonomic circumscription of *Adenomera martinezi* (Bokermann, 1956) (Anura: Leptodactylidae: Leptodactylinae) with the recognition of a new cryptic taxon through a bioacoustic approach. Zootaxa 3701: 207–237. https://doi.org/10.11646/zootaxa.3701.2.5

Cassini CS, Cruz CAG, Caramaschi U (2010) Taxonomic review of *Physalaemus olfersii* (Lichtenstein & Martens, 1856) with revalidation of *Physalaemus lateristriga* (Steindachner, 1864) and description of two new related species (Anura: Leiuperidae). Zootaxa 2491(1): 1–33. https://doi.org/10.11646/zootaxa.2491.1.1

Cassini CS, Orrico VGD, Dias IR, Solé M, Haddad CFB (2013) Phenotypic variation of *Leptodactylus cupreus* Caramaschi, São-Pedro and Feio, 2008 (Anura, Leptodactylidae). Zootaxa 3616: 73–84. https://doi.org/10.11646/zootaxa.3616.1.6

Clemente-Carvalho RBG, Perez SI, Tonhatti CH, Condez TH, Sawaya RJ, Haddad CFB, Reis SF (2016) Boundaries of morphological and molecular variation and the distribution of a miniaturized froglet, *Brachycephalus nodoterga* (Anura: Brachycephalidae). Journal of Herpetology 50: 169–178. https://doi.org/10.1670/14-119

Condez TH, Haddad CF, Zamudio KR (2020) Historical biogeography and multi-trait evolution in miniature toadlets of the genus *Brachycephalus* (Anura: Brachycephalidae). Biological Journal of the Linnean Society 129(3): 664–686. https://doi.org/10.1093/biolinnean/blz200

Cruz CAG, Feio RN (2007) Endemismos em anfíbios em áreas de altitude na Mata Atlântica no sudeste do Brasil. In: Nascimento LB, Oliveira ME (Eds) Herpetologia no Brasil II. Belo Horizonte, Sociedade Brasileira de Herpetologia, Belo Horizonte, 117–126.

Cryer J, Wynne F, Price SJ, Puschendorf R (2019) Cryptic diversity in *Lithobates warszewitschii* (Amphibia, Anura, Ranidae). ZooKeys 838: 49–69. https://doi.org/10.3897/zookeys.838.29635

Dantas RB, Ferreira RB (2010) Geographic distribution: *Ischnocnema octavioi*. Herpetological Review 41: 103–104.

Dellicour S, Flot JF (2018) The hitchhiker's guide to single-locus species delimitation. Molecular Ecology Resources 18(6): 1234–1246. https://doi.org/10.1111/1755-0998.12908

Duchêne S, Lanfear R, Ho SY (2014) The impact of calibration and clock-model choice on molecular estimates of divergence times. Molecular Phylogenetics and Evolution 78: 277–289. https://doi.org/10.1016/j.ympev.2014.05.032

Ezard T, Fujisawa T, Barraclough T (2017) Splits: species' limits by threshold statistics. R package version 1.0-19/r52.

Ferreira RB, Mônico AT, Silva ET, Lirio FCF, Zocca C, Mageski MM, Tonini JFR, Beard KH, Duca C, Silva-Soares T (2019) Amphibians of Santa Teresa, Brazil: the hotspot further evaluated. ZooKeys 857: 139–162. https://doi.org/10.3897/zookeys.857.30302

Ficetola GF, Rondinini C, Bonardi A, Baisero D, Padoa-Schioppa E (2014) Habitat availability for amphibians and extinction threat: A global analysis. Diversity and Distributions 21: 302–311. https://doi.org/10.1111/ddi.12296

Fišer C, Robinson CT, Malard F (2018) Cryptic species as a window into the paradigm shift of the species concept. Molecular Ecology 27(3): 613–635. https://doi.org/10.1111/mec.14486

Fouquet A, Gilles A, Vences M, Marty C, Blanc M, Gemmell NJ (2007) Underestimation of species richness in neotropical frogs revealed by mtDNA analyses. PLoS One 2: 1–10. https://doi.org/10.1371/journal.pone.0001109

Frankham R (2010) Challenges and opportunities of genetic approaches to biological conservation. Biological Conservation 143: 1919–1927. https://doi.org/10.1016/j.biocon.2010.05.011

Freitas MA, Souza BH, Fonseca PM (2011) Geographic distribution: *Ischnocnema verrucosa*. Herpetological Review 42: 385.

Frost DR, Grant T, Faivovich J, Bain RH, Haas A, Haddad CFB, de Sá RO, Channing A, Wilkinson M, Donnellan SC, Raxworthy CJ, Campbell JA, Blotto BL, Moler P, Drewes RC, Nussbaum RA, Lynch JD, Green DM, Wheeler WC (2006) The amphibian tree of life. Bulletin of the American Museum of natural History 297: 1–291.Frost DR (2024) Amphibian Species of the World: an Online Reference. Version 6.2. American Museum of Natural History, New York, USA. [Accessed at 07/26/2024] https://doi.org/10.1206/0003-0090(2006)297[0001:TATOL]2.0.CO;2

Frost DR (2024) Amphibian Species of the World: an Online Reference. Version 6.2 (Oct 15th, 2024). American Museum of Natural History, New York, USA. https://doi.org/10.5531/db.vz.0001

Fujisawa T, Barraclough TG (2013) Delimiting species using single-locus data and the generalized mixed yule coalescent approach: A revised method and evaluation on simulated data sets. Systematic Biology 62: 707–724. https://doi.org/10.1093/sysbio/syt033

Fujita MK, Leaché AD, Burbrink FT, McGuire JA, Moritz C (2012) Coalescent-based species delimitation in an integrative taxonomy. Trends in Ecology and Evolution 27: 480–488. https://doi.org/10.1016/j.tree.2012.04.012

Gehara M, Canedo C, Haddad CFB, Vences M (2013) From widespread to microendemic: Molecular and acoustic analyses show that *Ischnocnema guentheri* (Amphibia: Brachycephalidae) is endemic to Rio de Janeiro, Brazil. Conservation Genetics 14: 973–982. https://doi.org/10.1007/s10592-013-0488-5

Gehara M, Barth A, Oliveira EF de, Costa MA, Haddad CFB, Vences M (2017) Model-based analyses reveal insular population diversification and cryptic frog species in the *Ischnocnema parva* complex in the Atlantic Forest of Brazil. Molecular Phylogenetics and Evolution 112: 68–78. https://doi.org/10.1016/j.ympev.2017.04.007

Guarnizo CE, Paz A, Munoz-Ortiz A, Flechas SV, Mendez-Narvaez J, Crawford AJ (2015) DNA barcoding survey of anurans across the Eastern Cordillera of Colombia and the impact of the Andes on cryptic diversity. PLoS ONE 10: e0127312. https://doi.org/10.1371/journal.pone.0127312

Guayasamin JM, Trueb L (2020) Zoological nomenclature: Suggestions to increase stability and facilitate the naming of clades. Zootaxa 4820: 186–194. https://doi.org/10.11646/zootaxa.4820.1.10

Guimarães KLA, Lima MP, Santana DJ, Souza MFB, Barbosa RS, Rodrigues LRR (2022) DNA barcoding and phylogeography of the *Hoplias malabaricus* species complex. Scientific Reports 12: 5288. https://doi.org/10.1038/s41598-022-09121-z

Haeckel E (1866) Generelle Morphologie der Organismen: Allgemeine Grundzüge der organischen Formen-Wissenschaft, mechanisch begründet durch die von Charles Darwin reformirte Descendenz-Theorie. https://doi.org/10.5962/bhl.title.3953

Hamdan B, Bonatto SL, Rödder D, Seixas VC, Santos RMF, Santana DJ, Machado LG, Kleiz-Ferreira JM, de Freitas MA, Gonzalez RC, Cavalcante T, de Souza MB, Régis CB, Fernandes DS, Fernandes-Ferreira H, Zingali RB (2024) When a name changes everything: Taxonomy and conservation of the Atlantic Bushmaster *Lachesis* Daudin, 1803 (Serpentes: Viperidae: Crotalinae). Systematics and Biodiversity 22(1): 2366215. https://doi.org/10.1080/14772000.2024.2366215

Hasan M, Islam MM, Khan MMR, Alam MS, Kurabayashi A, Igawa T, Kuramoto M, Sumida, M (2012) Cryptic anuran biodiversity in Bangladesh revealed by mitochondrial 16S rRNA gene sequences. Zoological science 29: 162–172. https://doi.org/10.2108/zsj.29.162

Hedges SB, Duellman WE, Heinicke MP (2008) New World direct-developing frogs (Anura: Terrarana): Molecular phylogeny, classification, biogeography, and conservation. Zootaxa 1737: 1–182. https://doi.org/10.11646/zootaxa.1737.1.1

Heinicke MP, Duellman WE, Hedges SB (2007) Major Caribbean and Central American frog faunas originated by ancient oceanic dispersal. Proceedings of the National Academy of Sciences 104: 10092–10097. https://doi.org/10.1073/pnas.0611051104

Hennig W (1966) Phylogenetic Systematics. Urbana: University of Illinois Press.

Hillis DM (2007) Constraints in naming parts of the Tree of Life. Molecular Phylogenetics and Evolution 42: 331–338. https://doi.org/10.1016/j.ympev.2006.08.001

Holer T, Sýkorovský D, Hejcmanová P (2017) First record of *Ischnocnema octavioi* (Bokermann, 1965) from São Paulo State, Brazil. Check List 13: 2126. https://doi.org/10.15560/13.3.2126

Hortal J, De Bello F, Diniz-Filho JAF, Lewinsohn TM, Lobo JM, Ladle RJ (2015) Seven Shortfalls that Beset Large-Scale Knowledge of Biodiversity. Annual Review of Ecology, Evolution, and Systematics 46: 523–549. https://doi.org/10.1146/annurev-ecolsys-112414-054400

IUCN SSC Amphibian Specialist Group, Instituto Boitatá de Etnobiologia e Conservação da Fauna (2023a) *Ischnocnema verrucosa*. The IUCN Red List of Threatened Species 2023: e. T57109A172224520. https://doi.org/10.2305/IUCN.UK.2023-1.RLTS.T57109A172224520.en. [Accessed on 19 January 2024]

IUCN SSC Amphibian Specialist Group, Instituto Boitatá de Etnobiologia e Conservação da Fauna (2023b) *Ischnocnema surda*. The IUCN Red List of Threatened Species 2023: e. T78518211A86254584. https://doi.org/10.2305/IUCN.UK.2023-1.RLTS.T78518211A86254584.en. [Accessed on 19 January 2024]

Kapli T, Lutteropp S, Zhang J, Kobert K, Pavlidis P, Stamatakis A, Flouri T (2017) Multi-rate Poisson tree processes for single-locus species delimitation under maximum likelihood and Markov chain Monte Carlo. Bioinformatics 33(11):1630–1638. doi:https://doi.org/10.1093/bioinformatics/btx025

Katoh K, Misawa K, Kuma KI, Miyata T (2002) MAFFT: A novel method for rapid multiple sequence alignment based on fast Fourier transform. Nucleic Acids Research 30: 3059-3066. https://doi.org/10.1093/nar/gkf436

Kilpatrick AM, Briggs CJ, Daszak P (2010) The ecology and impact of chytridiomycosis: an emerging disease of amphibians. Trends in Ecology and Evolution 25: 109–118. https://doi.org/10.1016/j.tree.2009.07.011

Koroiva R, Santana DJ (2022) Evaluation of partial 12S rRNA, 16S rRNA, COI and Cytb gene sequence datasets for potential single DNA barcode for hylids (Anura: Hylidae). Anais da Academia Brasileira de Ciencias 94: e20200825. https://doi.org/10.1590/0001-3765202220200825

Kumar S, Stecher G, Li M, Knyaz C, Tamura K (2018) MEGA X: Molecular evolutionary genetics analysis across computing platforms. Molecular Biology and Evolution 35: 1547–1549. https://doi.org/10.1093/molbev/msy096

Lacerda JVA, Dayrell JS, Pires DMV, Feio RN (2014) Anfíbios da Mata do Paraíso. In: Lima GS, Ribeiro GA, Gonçalves W, Martins SV, Almeida MP (Eds) Ecologia de Mata Atlântica. Estudos ecológicos na Mata do Paraíso. Supremo, Viçosa, 133–152.

Leaché AD, Fujita MK (2010) Bayesian species delimitation in West African forest geckos (*Hemidactylus fasciatus*). Proceedings of the Royal Society B: Biological Sciences 277: 3071–3077. https://doi.org/10.1098/rspb.2010.0662

Li Y, Cohen JM, Rohr JR (2013) Review and synthesis of the effects of climate change on amphibians. Integrative Zoology 8: 145–161. https://doi.org/10.1111/1749-4877.12001

Linnaeus C (1750) Species plantarum. Stockholm, Sweden: Impensis Laurentii Salvii.

Lourenço LB, Targueta CP, Baldo D, Nascimento J, Garcia PCA, Andrade GV., Haddad CFB, Recco-Pimentel SM (2015) Phylogeny of frogs from the genus *Physalaemus* (Anura, Leptodactylidae) inferred from mitochondrial and nuclear gene sequences. Molecular Phylogenetics and Evolution 92: 204–216. https://doi.org/10.1016/j.ympev.2015.06.011

Lyra ML, Haddad CFB, de Azeredo-Espin AML (2017) Meeting the challenge of DNA barcoding Neotropical amphibians: polymerase chain reaction optimization and new COI primers. Molecular Ecology Resources 17: 966–980. https://doi.org/10.1111/1755-0998.12648

Mace GM. (2004). The role of taxonomy in species conservation. Philosophical Transactions of the Royal Society of London. Series B: Biological Sciences, 359(1444), 711-719. https://doi.org/10.1098/rstb.2003.1454

Magalhães F de M, Lyra ML, de Carvalho TR, Baldo D, Brusquetti F, Burella P, Colli GR, Gehara MC, Giaretta AA, Haddad CFB, Langone JA, López JA, Napoli MF, Santana DJ, de Sá RO, Garda AA (2020) Taxonomic Review of South American Butter Frogs: Phylogeny, Biogeographic Patterns, and Species Delimitation in the *Leptodactylus latrans* Species Group (Anura: Leptodactylidae). Herpetological Monographs 34: 131–177. https://doi.org/10.1655/0733-1347-31.4.131

Mângia S, Santana DJ, Cruz CAG, Feio RN (2014) Taxonomic review of *Proceratophrys melanopogon* (Miranda-Ribeiro, 1926) with description of four new species (Amphibia, Anura, Odontophrynidae). Boletim do Museu Nacional, 531: 1–33.

Mângia S, Oliveira EF, Santana DJ, Koroiva R, Paiva F, Garda AA (2020) Revising the taxonomy of *Proceratophrys* Miranda-Ribeiro, 1920 (Anura: Odontophrynidae) from the Brazilian semiarid Caatinga: Morphology, calls and molecules support a single widespread species. Journal of Zoological Systematics and Evolutionary Research 58: 1151–1172. https://doi.org/10.1111/jzs.12365

Martins LB, Giaretta AA (2013) Morphological and acoustic characterization of *Proceratophrys goyana* (Lissamphibia: Anura: Odontophrynidae), with the description of a sympatric and related new species. Zootaxa 3750: 301–320. https://doi.org/10.11646/zootaxa.3750.4.1

Mônico AT, Koch ED, Ferrão M, Fernandes IY, Marques GMG, Chaparro JC, Rodrigues MT, Lima AP, Fouquet A (2024) The small and inconspicuous majority: Revealing the megadiversity and historical biogeography of the *Pristimantis unistrigatus* species group (Anura, Strabomantidae). Molecular Phylogenetics and Evolution 201: 108203. https://doi.org/10.1016/j.ympev.2024.108203

Moraes LJCL, Werneck FP, Réjaud A, Rodrigues MT, Prates I, Glaw F, Kok PJR, Ron SR, Chaparro JC, Osorno-Muñoz M (2022) Diversification of tiny toads (Bufonidae: *Amazophrynella*) sheds light on ancient landscape dynamism in Amazonia. Biological Journal of the Linnean Society 136: 75–91. https://doi.org/10.1093/biolinnean/blac006

Moura MR, Jetz W (2021) Shortfalls and opportunities in terrestrial vertebrate species discovery. Nature Ecology & Evolution 5: 631–639. https://doi.org/10.1038/s41559-021-01411-5

Moura MR, Costa HC, Peixoto MA, Carvalho ALG, Santana DJ, Vasconcelos HL (2018) Geographical and socioeconomic determinants of species discovery trends in a biodiversity hotspot. Biological Conservation 220: 237–244. https://doi.org/10.1016/j.biocon.2018.01.024

Murphy JC, Lehtinen RM, Charles SP, Wasserman D, Anton T, Brennan PJ (2017) Amphibian and Reptile Conservation Cryptic multicolored lizards in the *Polychrus marmoratus* Group (Squamata: Sauria: Polychrotidae) and the status of *Leiolepis auduboni* Hallowell. https://openworks.wooster.edu/facpub

Orrico V (2010) Amphibia, Anura, Brachycephalidae, *Ischnocnema verrucosa* Reinhardt and Lütken, 1862: distribution extension to northeastern Brazil. Check List 6(2): 246–247. https://doi.org/10.15560/6.2.246

Oswald CB, de Magalhães RF, Garcia PCA, Santos FR, Neckel-Oliveira S (2023) Integrative species delimitation helps to find the hidden diversity of the leaf-litter frog *Ischnocnema manezinho* (Garcia, 1996) (Anura, Brachycephalidae), endemic to the southern Atlantic Forest. PeerJ 11: e15393. https://doi.org/10.7717/peerj.15393

Padial JM, Miralles A, De la Riva I, Vences M (2010) The integrative future of taxonomy. Frontiers in Zoology 7: 16. https://doi.org/10.1186/1742-9994-7-16

Pagès H, Aboyoun P, Gentleman R, DebRoy S (2024). Biostrings: Efficient manipulation of biological strings. R package version 2.72.1. https://bioconductor.org/packages/Biostrings

Palumbi S, Martin A, Romano S, McMillan WO, Stice L, Grabowski G (2002) The Simple Fool's Guide to PCR, Version 2.0. University of Hawaii, USA.

Paz A, Brown JL, Cordeiro CLO, Aguirre-Santoro J, Assis C, Amaro RC, Raposo do Amaral F, Bochorny T, Bacci LF, Caddah MK, d'Horta F, Kaehler M, Lyra M, Grohmann CH, Reginato M, Silva-Brandão KL, Freitas AVL, Goldenberg R, Lohmann LG, Michelangeli FA, Miyaki C, Rodrigues MT, Silva TS, Carnaval AC (2021) Environmental correlates of taxonomic and phylogenetic diversity in the Atlantic Forest. Journal of Biogeography 48: 1377–1391. https://doi.org/10.1111/jbi.14083

Pie MR, Meyer ALS, Firkowski CR, Ribeiro LF, Bornschein MR (2013) Understanding the mechanisms underlying the distribution of microendemic montane frogs (*Brachycephalus* spp., Terrarana: Brachycephalidae) in the Brazilian Atlantic Rainforest. Ecological Modelling 250: 165–176. https://doi.org/10.1016/j.ecolmodel.2012.10.019

Pilgrim EM, Darling JA (2010) Genetic diversity in two introduced biofouling amphipods (*Ampithoe valida* & *Jassa marmorata*) along the Pacific North American coast: investigation into molecular identification and cryptic diversity. Diversity & Distributions 16: 827–839. https://doi.org/10.1111/j.1472-4642.2010.00681.x

Pons J, Barraclough TG, Gomez-Zurita J, Cardoso A, Duran DP, Hazell S, Kamoun S, Sumlin WD, Vogler AP (2006) Sequence-based species delimitation for the DNA taxonomy of undescribed insects. Systematic Biology 55: 595–609. https://doi.org/10.1080/10635150600852011

Puillandre N, Brouillet S, Achaz G (2021) ASAP: assemble species by automatic partitioning. Molecular Ecology Resources 21(2): 609–620. https://doi.org/10.1111/1755-0998.13281

R Core Team (2021) A language and environment for statistical computing.

Rambaut A, Drummond AJ, Xie D, Baele G, Suchard MA (2018) Posterior summarization in Bayesian phylogenetics using Tracer 1.7. Systematic Biology 67: 901–904. https://doi.org/10.1093/sysbio/syy032

Reinhardt J, Lütken C (1862) Bidrag til Kundskab om Brasiliens Padder og Krybdyr. Videnskabelige Meddelelser forening i Kjobenhavn 3: 143–242.

Ribeiro MC, Martensen AC, Metzger JP, Tabarelli M, Scarano F, Fortin MJ (2011) The Brazilian Atlantic Forest: A Shrinking Biodiversity Hotspot. In: Zachos F, Habel J (Eds) Biodiversity Hotspots. Springer, Berlin Heidelberg, 405–434. https://doi.org/10.1007/978-3-642-20992-5_21.

Rocha PC, Lacerda JVA, Magalhães RF, Canedo C, Pimenta BVS, Heitor RC, Garcia PCA (2017) Call variation and vocalizations of the stealthy litter frog *Ischnocnema abdita* (Anura: Brachycephalidae). Acta Herpetologica 12: 37–48.

Rödder D, Teixeira RL, Ferreira RB, Dantas RB, Pertel W, Guarniere GJ (2007) Anuran hotspots: the municipality of Santa Teresa, Espírito Santo, southeastern Brazil. Salamandra 43: 91–110.

Rojas-Padilla O, Menezes VQ, Dias IR, Argôlo AJS, Solé M, Orrico VGD (2020) Amphibians and reptiles of Parque Nacional da Serra das Lontras: An important center of endemism within the Atlantic forest in southern Bahia, Brazil. ZooKeys 2020: 159–185. https://doi.org/10.3897/zookeys.1002.53988

Santana DJ, Yves A, Pereira EA, Carvalho PS, Lima LM, Costa HC, Shepard DB (2024). DNA barcoding reveals a new population of the threatened Atlantic Forest frog *Sphaenorhynchus canga*. Journal of Threatened Taxa 16: 25040–25048. https://doi.org/10.11609/jott.8694.16.4.25040-25048

Silva ET, Santos PS, Coelho HL, Viana RS, Heitor RC, Garcia PCA (2013) New records of *Ischnocnema verrucosa* Reinhart and Lütken, 1862 and *I. surda* Canedo, Pimenta, Leite and Caramaschi, 2010 (Anura, Brachycephalidae) in Minas Gerais State, Brazil. Check List 9: 1062–1066. https://doi.org/10.15560/9.5.1062

Silva-Soares T, Ferreira RB, Ornellas IS, Zocca CZ, Caramaschi U, Cruz CAG (2021) A new species of *Ischnocnema* (Anura: Brachycephalidae) from the mountainous region of Atlantic Forest, southeastern Brazil, with a new phylogeny and diagnose for *Ischnocnema parva* series. Zootaxa 5082: 201–222. https://doi.org/10.11646/zootaxa.5082.3.1

Struck TH, Feder JL, Bendiksby M, Birkeland S, Cerca J, Gusarov VI, Kistenich S, Larsson K-H, Liow LH, Nowak MD (2018) Finding evolutionary processes hidden in cryptic species. Trends in Ecology & Evolution 33: 153–163. https://doi.org/10.1016/j.tree.2017.11.007

Suatoni E, Vicario S, Rice S, Snell T, Caccone A (2006) An analysis of species boundaries and biogeographic patterns in a cryptic species complex: the rotifer—*Brachionus plicatilis*. Molecular phylogenetics and evolution 41: 86–98. https://doi.org/10.1016/j.ympev.2006.04.025

Taucce PPG, Canedo C, Haddad CFB (2018a) Two New Species of *Ischnocnema* (Anura: Brachycephalidae) from Southeastern Brazil and their Phylogenetic Position within the *I. guentheri* Series. Herpetological Monographs 32: 1–21. https://doi.org/10.1655/HERPMONOGRAPHS-D-16-00014.1

Taucce PPG, Canedo C, Parreiras JS, Drummond LO, Nogueira-Costa P, Haddad CFB (2018b) Molecular phylogeny of *Ischnocnema* (Anura: Brachycephalidae) with the redefinition of its series and the description of two new species. Molecular Phylogenetics and Evolution 128: 123–146. https://doi.org/10.1016/j.ympev.2018.06.042

Taucce PPG, Zaidan BF, Zaher H, Garcia PCA (2019) A new species of *Ischnocnema* Reinhardt and Lütken, 1862 (Anura: Brachycephalidae) of the *I. lactea* species series from southeastern Brazil. Zootaxa 4706: 531–545. https://doi.org/10.11646/zootaxa.4706.4.3

Taucce PPG, Costa-Campos CE, Carvalho TR, Michalski F (2022) Anurans (Amphibia: Anura) of the Brazilian state of Amapá, eastern Amazonia: species diversity and knowledge gaps. European Journal of Taxonomy 836: 96–130. https://doi.org/10.5852/ejt.2022.836.1919

Thomé MTC, Lyra ML, Lemes P, Teixeira LS, Carnaval AC, Haddad CFB, Canedo C (2020) Outstanding diversity and microendemism in a clade of rare Atlantic Forest montane frogs. Molecular Phylogenetics and Evolution 149: 106813. https://doi.org/10.1016/j.ympev.2020.106813

Tobias JA, Seddon N, Spottiswoode CN, Pilgrim JD, Fishpool LDC, Collar NJ (2010) Quantitative criteria for species delimitation. Ibis 152: 724–746. https://doi.org/10.1111/j.1474-919X.2010.01051.x

Vacher JP, Chave J, Ficetola FG, Sommeria-Klein G, Tao S, Thébaud C, Blanc M, Camacho A, Cassimiro J, Colston TJ, Dewynter M, Ernst R, Gaucher P, Gomes JO, Jairam R, Kok PJR, Lima JD, Martinez Q, Marty C, Noonan BP, Nunes PMS, Ouboter P, Recoder R, Rodrigues MT, Snyder A, Marques-Souza S, Fouquet A (2020) Large-scale DNA-based survey of frogs in Amazonia suggests a vast underestimation of species richness and endemism. Journal of Biogeography 47: 1781–1791. https://doi.org/10.1111/jbi.13847

Vences M, Nagy ZT, Sonet G, Verheyen E (2012) DNA barcoding amphibians and reptiles. In: Methods in Molecular Biology. Springer: 79–107. https://doi.org/10.1007/978-1-61779-591-6_5

Vences M, Guayasamin JM, Miralles A, De La Riva I (2013) To name or not to name: Criteria to promote economy of change in Linnaean classification schemes. Zootaxa 3636: 201–244. https://doi.org/10.11646/zootaxa.3636.2.1

Vrcibradic D, Almeida-Gomes M, Van Sluys M, Rocha CFD (2008) Amphibia, Anura, *Hylodes charadranaetes*, *Ischnocnema octavioi*, and *Euparkerella cochranae*: distribution extension. Check List 4: 103–106. https://doi.org/10.15560/4.2.103

Wilkinson JA, Matsui M, Terachi T (1996) Geographic variation in a Japanese tree frog (*Rhacophorus arboreus*) revealed by PCR-aided restriction site analysis of mtDNA. Journal of Herpetology 30: 418–423. https://doi.org/10.2307/1565184

Yodthong S, Stuart BL, Aowphol A (2019) Species delimitation of crab-eating frogs (*Fejervarya cancrivora* complex) clarifies taxonomy and geographic distributions in mainland Southeast Asia. ZooKeys 883: 119–153. https://doi.org/10.3897/zookeys.883.37544

Zornosa-Torres C, Augusto-Alves G, Lyra ML, Silva-Júnior JC, Garcia PCA, Leite F, Verdade V, Rodrigues MT, Gasparini JL, Haddad CFB, Toledo LF (2020) Anurans of the Caparaó National Park and surroundings, southeast Brazil. Biota Neotropica 20(3): e20190882. https://doi.org/10.1590/1676-0611-bn-2019-0882

Zoosyst. Evol. 100 (4) 2024, 1473–1486 | DOI 10.3897/zse.100.133964

PENSOFT

MUSEUM FÜR NATURKUNDE BERLIN

Evolutionary history of Chinese karst loaches (Nemacheilidae, *Karstsinnectes*): new insights from mitochondrial-based genomes and description of a new species from Guangxi, China

Tao Luo[1,2,3*], Fang-Wei Luo[1*], Chang-Ting Lan[4], Ming-Yuan Xiao[4], Jia-Jun Zhou[5], Mei Liao[1], Ning Xiao[6], Jiang Zhou[1]

1 *School of Karst Science, Guizhou Normal University, Guiyang, China*
2 *School of Life Sciences, Yunnan University, Kunming, China*
3 *Southwest United Graduate School, Kunming, China*
4 *School of Life Sciences, Guizhou Normal University, Guiyang, China*
5 *Zhejiang Forest Resource Monitoring Center, Hangzhou, China*
6 *Guiyang Healthcare Vocational University, Guiyang, China*

https://zoobank.org/326B6F9E-E524-422A-8389-570E82341BBD

Corresponding author: Jiang Zhou (zhoujiang@ioz.ac.cn)

Academic editor: Nicolas Hubert ♦ **Received** 5 August 2024 ♦ **Accepted** 10 October 2024 ♦ **Published** 5 November 2024

Abstract

The genus *Karstsinnectes* of blind fishes known as karst loaches from China was established in 2023 during a revision of the genus *Oreonectes* (Nemacheilidae). Six species are recorded in this study and some taxonomic progress has been made; however, the lack of genetic data for some species (e.g., *K. anophthalmus*) may have weakened our current understanding of *Karstsinnectes*. This study reassessed the phylogeny and evolutionary history of *Karstsinnectes* by integrating a combination of previously published and newly sequenced mitochondrial genomic data. A phylogenetic tree was developed that was able to divide *Karstsinnectes* into two clades corresponding to drainages and clarify the phylogenetic position of *K. anophthalmus*. Divergence times show that *Karstsinnectes* originated at the Oligocene/Miocene boundary (~22.37 Mya), with the most recent common ancestor occurring in the early Miocene (~18.87 Mya) and interspecific divergence occurring in the late Miocene. Ancestral area reconstruction suggests that the most recent common ancestor of *Karstsinnectes* most likely inhabited the Hongshui River basin and dispersed into the Zuojiang-Yujiang, Beipanjiang, and Youjiang river basins during the early Miocene (~18.87 Mya), middle Miocene (~12.78 Mya), and late Miocene (~6.71 Mya), respectively. The dispersal under the influence of orogenesis and a monsoon climate drove the speciation and diverse distribution of *Karstsinnectes*. Such findings are important for conservation considering that *Karstsinnectes* strictly inhabits deep caves. Additionally, the taxonomic status of the distributed *Karstsinnectes* population in Leiping Town, Daxin County, Guangxi, China was revised by combining genetic and morphological differences to describe this population as a new species, *Karstsinnectes daxinensis* Luo, Zhou & Zhou, **sp. nov.** The definition of the phylogenetic position of *K. anophthalmus* emphasizes the importance of using type locality material for the identification of cryptic species.

Key Words

Biogeography, blind fishes, *Karstsinnectes anophthalmus*, phylogeny, taxonomy

* Authors contributed equally to this work.

Introduction

Southwest China features rich caves and groundwater resources, which have become the habitat of a large number of cave organisms (Duan et al. 2021; Ma et al. 2023). Chinese karst loaches in the genus *Karstsinnectes* Zhou, Luo, Wang, Zhou & Xiao, 2023 (Cypriniformes, Nemacheilidae) are a strictly troglobitic species that exhibit distinct cave-adapted characters, of which the most distinct is the unpigmented body and with eyes that are absent or highly degenerate (Lan et al. 2013; Zhu and Zhu 2014; Luo et al. 2023; Ge et al. 2024). Few people encounter the species of this genus, mainly because these species usually inhabit deep caves, have a small body size (total length < 70 mm), and have very small populations so that only two to three specimens can be collected in each survey (Lan et al. 2013; Zhu and Zhu 2014; Luo et al. 2023; Ge et al. 2024). This has indirectly contributed to the longstanding taxonomic confusion in the genus. Species of this genus were long placed within the genus *Oreonectes* Günther, 1868, until Luo et al. (2023) classified *Karstsinnectes* as a separate genus based on phylogeny. All of the species of this genus are strictly troglobitic and exhibit distinct cave-adapted characters as described above.

Although the confusing taxonomy of the genus *Karstsinnectes* has been clarified, its diversity and evolutionary history remain largely unknown. For example, the recent description of *K. cehengensis* Luo, Zhao & Zhou, 2024 and *K. longzhouensis* Ge, Du & Zhou, 2024 were based on field surveys as well as morphological and genetic data (Ge et al. 2024; Zhao et al. 2024). The discovery of these two new species may indicate that the diversity of the genus has been underestimated. Additionally, Ge et al. (2024) provided an important addition to their diagnosis and the morphology of species within the genus *Karstsinnectes* by examining additional specimens of the genus. Currently, the genus *Karstsinnectes* encompasses six recognized species that are distributed in karst caves in Guizhou Province and Guangxi Zhuang Autonomous Region, China (Fig. 1). These species include *K. acridorsalis* (Lan, 2013), *K. anophthalmus* (Zheng, 1981), *K. cehengensis*, *K. hyalinus* (Lan, Yang & Chen, 1996), *K. longzhouensis*, and *K. parvus* (Zhu & Zhu, 2014) (Zheng 1981; Lan et al. 1996, 2013; Fricke et al. 2024; Ge et al. 2024; Zhao et al. 2024). Furthermore, in several previous phylogenetic studies, samples of *K. anophthalmus* were not from the type locality (Luo et al. 2023; Ge et al. 2024; Zhao et al. 2024), and therefore, nothing is known about the true phylogenetic position of the species. In addition, despite some progress in phylogeny and classification, unknowns also exist about the origin of the genus and species of *Karstsinnectes*.

Here, to understand the phylogenetic classification and evolutionary history of the genus *Karstsinnectes*, the mitochondrial genome of Chinese karst loaches samples collected from extensive surveys over the past three years were sequenced. Specifically, the objectives of this study were to (1) infer the evolutionary relationships among species and clarify the phylogenetic position of *K. anophthalmus*; (2) identify and describe potential cryptic species; and (3) assess divergence times, reconstruct ancestral distributions, and discuss the historical biogeography of the genus *Karstsinnectes*.

Materials and methods

Taxon sampling, morphological analyses, and skeletal X-ray scanning

A total of 18 *Karstsinnectes* specimens were collected during field surveys from 2019 to 2024, from Guangxi and Guizhou in southwestern China (Fig. 1). The treatment of experimental animals in this study was consistent with the Chinese animal welfare laws (GB/T 35892–2018). All of the specimens used for morphological studies were fixed in a 10% formalin buffer and then transferred to 75% ethanol and stored at the Animal Ecology Laboratory of Guizhou Normal University (GZNU), Guiyang City, Guizhou, China. All of the molecular samples were stored at −80 °C in a refrigerator.

In total, 10 specimens of new species and *K. anophthalmus* were analyzed and measured, following Zhao et al. (2024) who measured 27 kinds of morphological data using digital calipers with an accuracy of 0.1 mm. All of the measurements were taken on the left side of each fish specimen. Morphological data were also collected from the literature for *K. acridorsalis*, *K. hyalinus*, *K. longzhouensis*, and *K. parvus* so that morphological comparisons could be made (Ge et al. 2024).

Given the morphological similarity between the new species and *K. anophthalmus*, statistical analysis was performed of the morphometric data for both species. In order to reduce the impact of allometry, a size-corrected value from the ratio of each character to standard length was calculated for the following morphometric analyses. Principal component analyses with eigenvalues greater than one, the maximum variance method, and simple bivariate scatter plots were used to explore and characterize the morphometric differences (Xu et al. 2023) between the new species and closely related species. One-way analysis of variance was conducted to determine the significance of differences in morphometric characters between the new species and the aforementioned similar species. All of the statistical analyses were performed using SPSS v.21.0 (SPSS, Inc., Chicago, IL, USA), and differences were considered statistically significant at $P < 0.05$.

Skeletal X-ray scanning was performed at the Key Laboratory of Vertebrate Evolution and Human Origins, Institute of Vertebrate Paleontology and Paleoanthropology, Chinese Academy of Sciences, using micro-computed tomography (Siemens Somatom Definition X-ray machine). The skull images were exported from a virtual 3D model which was reconstructed using Volume Graphics Studio 3.0 software.

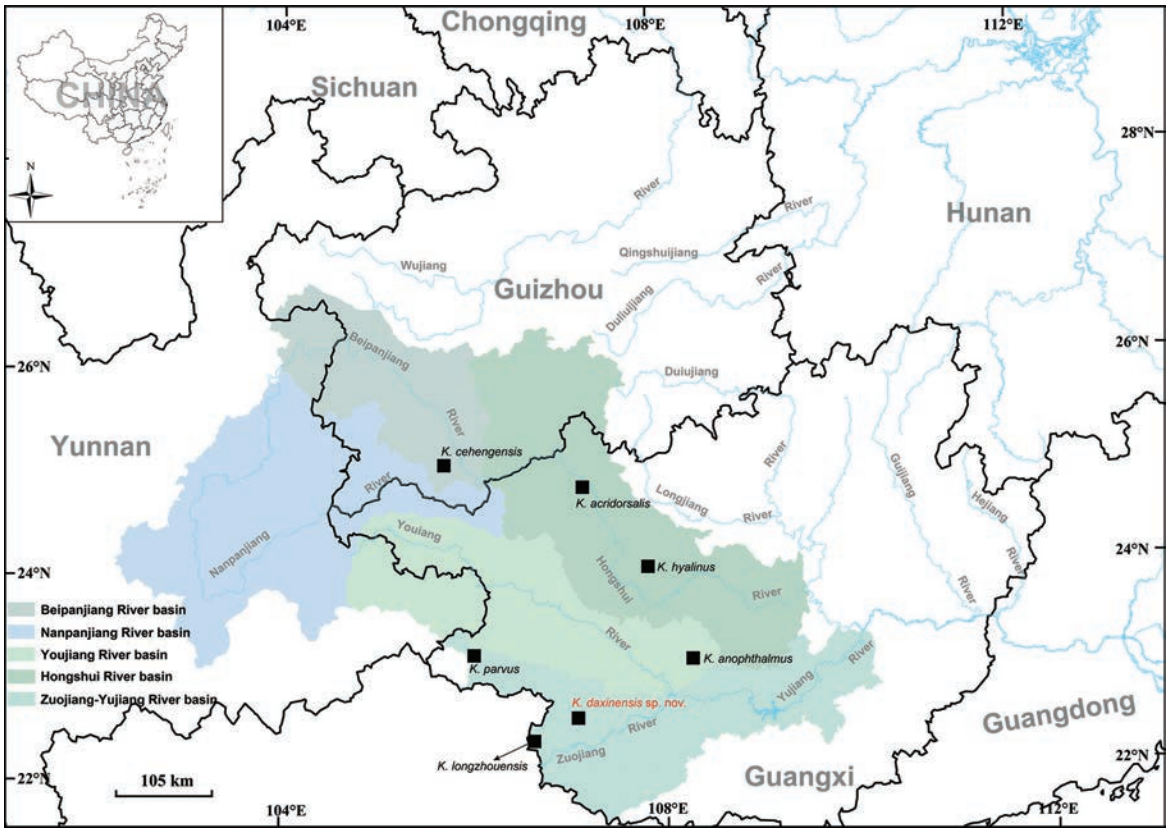

Figure 1. Geographical distribution of recognized species of the genus *Karstsinnectes* in southwestern China.

DNA extraction, sequencing, and mitogenome assembly

Total genomic DNA was extracted from three samples of three species from 95% ethanol-preserved tissues using the cetyltrimethylammonium bromide method. The process of DNA library construction and detection followed Luo et al. (2023) and DNA was sequenced by TSINGKE Biotechnology Co., Ltd. (Chengdu, Sichuan, China) on an Illumina NovaSeq 6000 platform. A total of 36 Gb of raw bases were generated, with each sample generating approximately 12 Gb of raw data. These sequencing data were completed using MitoFinder v.1.4.2 (Allio et al. 2020) for genome assembly and annotation of the mitogenome using *Oreonectes platycephalus* as the reference (accession number: NC_031579). All of the sequences have been deposited in GenBank (Table 1).

Phylogenetic construction and divergence time estimation

In this study, three mitochondrial genomes were newly sequenced while 26 mitochondrial genomes and three Cyt *b* were downloaded from the US National Center for Biotechnology Information. Two datasets were constructed for phylogenetic analysis in this study, where datasets 1 and 2 included the mitogenome and only the Cytochrome *b* (Cyt *b*), respectively. Here, the mitogenome was extracted using PhyloSuite v.1.2.3 (Zhang et al. 2020) for 13 protein coding genes, two rRNAs, and 22 tRNAs for subsequent genetic analysis.

Multiple sequence alignment was performed using MAFFT v.7.4 (Katoh and Standley 2013) within PhyloSuite v.1.2.3 (Zhang et al. 2020) and checked using MEGA v.7.0 (Kumar et al. 2016) to rule out possible errors. In addition, Partitionfinder v.2.1.1 (Lanfear et al. 2017) was used to select the best-fit partitioning and nucleotide substitution model for the two datasets, based on the Bayesian information criterion. In dataset 1, each gene fragment was pre-set as an independent partition. Luo et al. (2023) was referred to for selecting species of *Homaloptera parclitella* as an outgroup (Table 1).

Phylogenetic trees were reconstructed using Bayesian inference (BI) and maximum likelihood (ML) methods based on best-fit partitioning and nucleotide substitution models. Bayesian inference analysis was performed using MrBayes v.3.2.1 (Ronquist et al. 2012). Each BI analysis was run independently using four Markov Chain Monte Carlo chains (three heated chains and one cold chain) starting with a random tree; each chain was run for 2×10^7 generations and sampled every 1000 generations. Convergence of the data runs was confirmed when the average standard deviation of split frequencies was less than 0.01. The ML analysis was performed using IQ-tree v.2.0.4 (Nguyen et al. 2015) based on the best-fit model with 10,000 ultrafast bootstrap (UFB) replicates (Hoang et al. 2018). The ML analysis was performed until a correlation

Table 1. Localities, voucher information, and GenBank numbers for all of the samples used. NA denotes that the data is not available.

ID	Genus	Species	Localities (* type localities)	Voucher	Mitogenome
1	*Karstsinnectes*	*Karstsinnectes anophthalmus*	Xiahuang Village, Chengxiang Town, Wuming County, Guangxi, China*	WY01	PQ159188
2		*Karstsinnectes cehengensis*	Rongdu Town, Ceheng County, Guzihou, China*	GZNU 20230106003	OR936095
3		*Karstsinnectes cehengensis*	Rongdu Town, Ceheng County, Guzihou, China*	GZNU 20230106004	PP155585
4		*Karstsinnectes cehengensis*	Rongdu Town, Ceheng County, Guzihou, China*	GZNU 20230106005	PP155586
5		*Karstsinnectes cehengensis*	Rongdu Town, Ceheng County, Guzihou, China*	GZNU 20230106006	PP155587
6		*Karstsinnectes acridorsalis*	Bamu Town, Tiane County, Guangxi, China*	Tissue ID: GZNU2020	ON116515
7		*Karstsinnectes daxinensis* sp. nov.	Leiping Town, Daxin County, Guangxi, China*	GZNU 2019122201	ON116506
8		*Karstsinnectes daxinensis* sp. nov.	Leiping Town, Daxin County, Guangxi, China*	GZNU 2019011310	ON116513
9		*Karstsinnectes daxinensis* sp. nov.	Leiping Town, Daxin County, Guangxi, China*	GZNU 2019011210	ON148333
10		*Karstsinnectes daxinensis* sp. nov.	Leiping Town, Daxin County, Guangxi, China*	YJ14	PQ159190
11		*Karstsinnectes parvus*	Ande Town, Jingxi City, Guangxi, China*	Tissue ID: JTQ02	ON116520
12		*Karstsinnectes longzhouensis*	Xiadong Town, Longzhou County Guangxi, China*	LD-2023	OR947935
13		*Karstsinnectes longzhouensis*	Xiadong Town, Longzhou County Guangxi, China*	YJ18	PQ159189
14	*Oreonectes*	*Oreonectes damingshanensis*	Daming Mountain, Shanglin County, Guangxi, China*	GZNU 2020112502	ON116496
15		*Oreonectes luochengensis*	Tianhe Town, Luocheng County, Guangxi, China*	GZNU 2020011502	ON116495
16	*Micronemacheilus*	*Micronemacheilus pulcherrimus*	Duan County, Hechi City, Guangxi, China	GZNU20210609004	ON116493
17		*Micronemacheilus cruciatus*	NA	NA	AP012142
18	*Guinemachilus*	*Guinemachilus bailianensis*	Bailian cave, Liuzhou City, Guangxi, China*	GZNU 2020041603	ON116504
19		*Guinemachilus longibarbatus*	Gaoling Town, Duan County, Guangxi, China*	GZNU 2020073104	ON116508
20	*Troglonectes*	*Troglonectes microphthalmus*	Tianhe Town, Luocheng County, Guangxi, China*	GZNU 2020041601	ON116494
21		*Troglonectes shuilongensis*	Shuilong Town, Sandu County, Guizhou, China*	GZNU 2019011201	ON116522
22	*Paranemachilus*	*Paranemachilus pingguoensis*	Changping Town, Fusui County, Guangxi, China*	GZNU 2019122205	ON116500
23		*Paranemachilus genilepis*	Guohua Town, Pingguo County, Guangxi, China*	GZNU 2019122206	ON116497
24	*Yunnanilus*	*Yunnanilus jiuchiensis*	NA	NA	MW532080
25		*Yunnanilus pleurotaenia*	Fuxian Lake, Yuxi City, Yunnan Province, China	Tissue ID: GZNUCW01	ON116531
26	*Eonemachilus*	*Eonemachilus longidorsalis*	Agang Longtan pool, Luoping County, Yunnan, China	NA	NC_062728
27		*Eonemachilus niger*	NA	NA	OM681515
28	*Lefua*	*Lefua costata*	NA	NA	KT943751
29	*Traccatichthys*	*Traccatichthys zispi*	Wangxia Town, Changjiang County, Hainan, China	Tissue ID: HNMLXTQ	ON116518
30	*Triplophysa*	*Triplophysa nasobarbatula*	Dongtang Town, Libo County, Guizhou, China*	GZNU20190114001	ON116529
31	*Barbatula*	Barbatula barbatula			KP715096
32	Balitoridae	Homaloptera parclitella			AP011438

coefficient of at least 0.99 was achieved. Nodes were considered highly supported when the Bayesian posterior probability (BPP) value for the BI analysis was greater than 0.95 and the UFB value for the ML analysis was greater than 95%. Based on dataset 2, genetic distances were calculated using the uncorrected *p*-distance model and 1000 bootstrap replications, in MEGA v.7.0 (Kumar et al. 2016).

Molecular dating and time tree reconstruction was conducted in BEAST v.2.4.7 (Bouckaert et al. 2014), using dataset 1. Considering that the genus *Karstsinnectes* has no known fossil record, two calibration nodes were set up with reference to recent studies (Wang et al. 2016; Hirt et al. 2017): (1) the origin of the family Nemacheilidae dates to 45.5 million years ago (Mya) (95% confidence interval (CI): 36.7–55.8 Mya) (Hirt et al. 2017); (2) the divergence of the genera *Triplophysa* and *Barbatula* occurred at 23.5 Mya (95% CI: 20.5–26.1 Mya) (Wang et al. 2016). The BEAST analysis used an uncorrelated lognormal relaxation clock and a Yule tree prior. The BEAST analysis was run for 200 million generations and sampled every 1000 generations. All of the calibrations used a normal prior, monophyly, and standard deviation values of 2.2. Convergence of the run parameters was checked using Tracer v.1.7.1 (Rambaut et al. 2018) to ensure that the effective sample size of all of the parameters was greater than 200. Three runs were made in total, and the trees were finally merged using LogCombiner v.2.4.7. A maximum clade credibility tree was generated using TreeAnnotator v.2.4.1 (implemented in BEAST) by applying a burn-in of 25%.

Ancestral area reconstruction

Species of the genus *Karstsinnectes* are currently known to be distributed mainly in the Pearl River drainage in southern China (Fig. 1), showing a top-down distribution and can be mapped onto phylogenetic topologies (Zhao et al. 2024). To estimate the origin and dispersal of species in the genus *Karstsinnectes*, the present study conducted biogeographic analyses using the R package BioGeoBEARS (Matzke 2013). Prior to the analysis, six models were estimated using BioGeoBEARS, Dispersal-Extinction-Cladogenesis (DEC), a ML version of Dispersal-Vicariance Analysis (DIVALIKE), Bayesian biogeographical inference model (BAYAREALIKE), each with and without founder-event speciation (+J).

Results

Sequence information, phylogeny, and genetic divergence

In this study, 29 mitogenomes and three Cyt *b* sequences were collected for phylogenetic and genetic analysis. The total length of dataset 1 included 15,664 bases, 9377 conserved sites, 6263 variable sites, and 4993 parsim-informative sites. The total length of dataset 2 was 1140 bp, 871 conserved sites, 6269 variable sites, and 197 parsim-informative sites. The predefined 16 partitions of dataset 1 were suggested by Partitionfinder to be divided into five partitions and the corresponding evolutionary models were GTR+I+G, GTR+I+G, TVM+I+G, TVM+I+G, and HKY+I+G (Table 2).

Phylogenetic analyses highly supported the monophyly of *Karstsinnectes* (BPP/UFB = 1.00/100) and as the sister clade to *Guinemachilus*, *Micronemacheilus*, and *Oreonectes* (Fig. 2, Suppl. material 1). *Karstsinnectes* contains two clades (BPP/UFB = 1.00/100), where Clade I contains *K. acridorsalis* and *K. cehengensis* while Clade II contains *K. parva*, *K. longzhouensis*, *K. anophthalmus*, and a group of four samples *Karstsinnectes* sp. from Daxin County, Guangxi (Fig. 2). Divergence among species of the genus *Karstsinnectes* is highly supported (Suppl. material 1).

Table 2. Best-fit partitioning and evolutionary models used for phylogenetic analysis.

ID	Partition schemes	Length (bp)	Best Model
1	16S	1708	GTR+I+G
2	tRNAs, 12S	2523	GTR+I+G
3	ND2, ND1, ND4, ND5, ATP6, ND3, Cyt *b*	7422	TVM+I+G
4	ATP8, COI, ND4L, COIII, COII	3489	TVM+I+G
5	*ND6*	522	HKY+I+G

Genetic differences within the genus *Karstsinnectes* were assessed using Cyt *b* and ranged from 5.8 to 13.1% (Table 3). Genetic differences between samples from Daxin County, Guangxi, and species within the genus *Karstsinnectes* ranged from 6.9 (vs. *K. anophthalmus*) to 12.8% (vs. *K. acridorsalis*), with the smallest genetic distances being greater than the recognized interspecies difference of 5.8% (*K. longzhouensis* vs. *K. parvus*) (Table 3). Thus, the genetic evidence supports that the geographic population of Daxin County, Guangxi, should be treated as a new undescribed phylogenetic species.

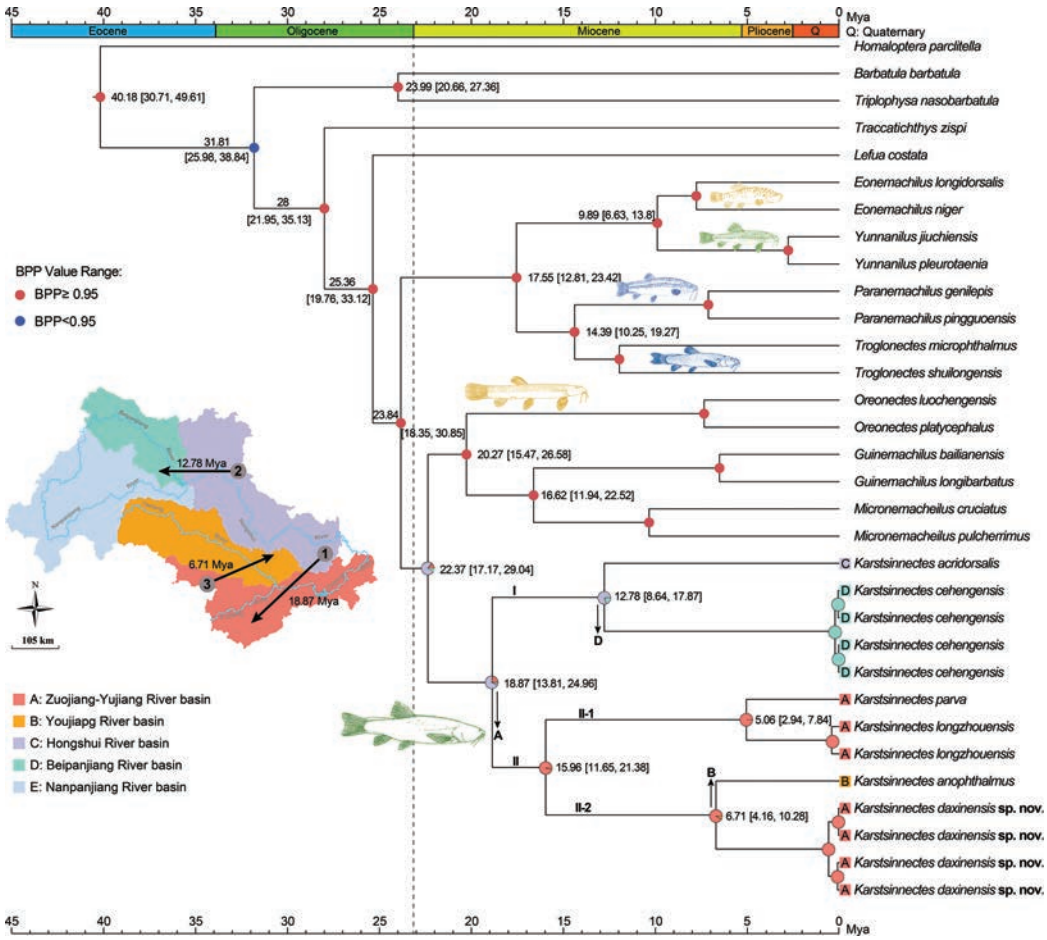

Figure 2. Chronogram and phylogeny of the genus *Karstsinnectes*. Circles at each node indicate Bayesian posterior probabilities (BPP). Colored squares at the tip of *Karstsinnectes* branches indicate species distributions, and the three major clades are marked using Roman numerals (I–II). Divergence times for major clades are marked in parentheses with 95% confidence intervals. Arrows show dispersal events. Species photos from Zhu (1989).

Table 3. Average uncorrected pairwise genetic distances (*p*-distance) among the six currently-known species of the genus *Karstsinnectes* estimated using the mitochondrial Cyt *b*.

ID	Species	1	2	3	4	5
1	*K. daxinensis* sp. nov.					
2	*K. anophthalmus*	6.9%				
3	*K. acridorsalis*	12.8%	12.1%			
4	*K. cehengensis*	10.9%	10.7%	9.4%		
5	*K. longzhouensis*	10.1%	9.6%	12.8%	11.1%	
6	*K. parvus*	10.8%	10.3%	13.1%	11.2%	5.8%

Divergence time and biogeography

The time tree in Fig. 2 shows that the genus *Karstsinnectes* originated at the Oligocene/Miocene boundary, ca. 22.37 Mya (95% CI = 17.17–29.04 Mya), with the most recent common ancestor occurring in the early Miocene, ca. 18.87 Mya (95% CI = 13.81–24.96 Mya). Interspecific divergence occurred from the middle of the Miocene to the early Pliocene (5.06–15.96 Mya), and the divergence of the Daxin population of Guangxi from its sister species *K. anophthalmus* occurred in the late Miocene, ca. 6.71 Mya (95% CI = 4.16–10.28 Mya). Additionally, the time tree provides the origins of other genera in the family Nemacheilidae. For example, the split between *Paranemachilus* and *Troglonectes* occurred ca. 14.39 Mya (95% CI = 10.25–19.27 Mya); the split between *Yunnanilus* and *Eonemachilus* occurred ca. 9.89 Mya (95% CI = 6.63–13.80 Mya); *Oreonectes* originated ca. 20.27 Mya (95% CI = 15.47–26.58 Mya); and the split between *Guinemachilus* and *Micronemacheilus* occurred between about 16.62 Mya (95% CI = 11.94–22.52 Mya) (Fig. 2).

The results of model comparisons used for ancestral area reconstruction within BioGeoBEARS are provided in Table 4. Based on the DEC+J model (Fig. 2, Suppl. material 2, 3), dispersal events may have shaped the current distribution of *Karstsinnectes*. Biogeographical inference based on the best model, DEC+J (AIC weight = 0.53; Table 4), suggests that the most recent common ancestor of extant *Karstsinnectes* likely inhabited the Hongshui River basin and then dispersed southwestward into the Zuojiang-Yujiang and Beipanjiang river basins (Fig. 2). After colonizing the Zuojiang-Yujiang River basin, the genus dispersed eastward into the Youjiang River basin. The BAYAREALIKE+J model (AIC weight = 0.47; Table 4; Suppl. material 4) was second-best and yielded similar results.

Morphological differences

Principal component analysis of the new species and *K. anophthalmus* using 18 measured characters showed that a total of five principal component (PC) factors were extracted based on eigenvalues greater than one. The first three components explained 69.45% of the total variance, with PC1 accounting for 37.97%, PC2 for 17.75%, and PC3 for 13.74% (Table 5). In the scatterplot of PC1 versus PC2, *K. daxinensis* sp. nov. and *K. anophthalmus* formed distinct clusters that were separated on the PC1 axis (Fig. 3). Body depth, caudal peduncle depth, head depth, head width, mouth width, and maxillary barbel length were mainly loading on PC1 (Table 5). Analysis of variance indicated that 40% of the 20 morphometric characters shared by *K. daxinensis* sp. nov. and *K. anophthalmus* were significantly different (Table 6). When compared with *K. anophthalmus*, *K. daxinensis* sp. nov. has a smaller predorsal length (15.1 ± 2.0 vs. 18.9 ± 2.6), prepelvic length (13.8 ± 1.2 vs. 18.1 ± 2.7), head length (5.4 ± 0.5 vs. 7.3 ± 0.9), head depth (2.1 ± 0.4 vs. 3.1 ± 0.5), head width (3.4 ± 0.7 vs. 4.8 ± 0.8), mouth width (1.7 ± 0.2 vs. 2.7 ± 0.4), but for inrostral barbel length, *K. daxinensis* sp. nov. is larger than *K. anophthalmus* (2.2 ± 0.5 vs. 1.3 ± 0.1) (Table 6).

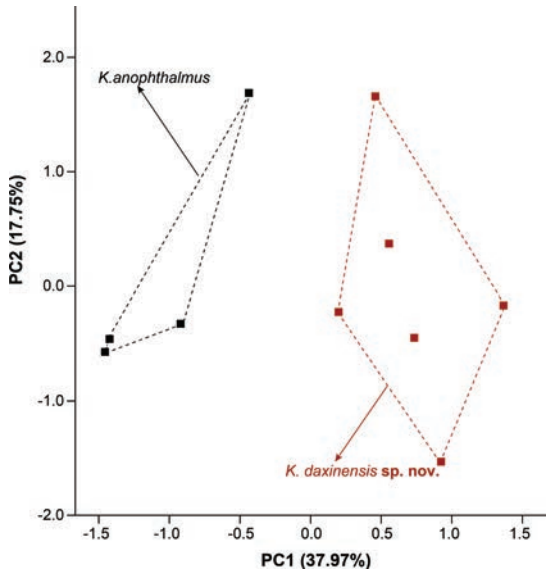

Figure 3. Scatter plots of the 1st and 2nd principal components for *Karstsinnectes daxinensis* sp. nov. and *K. anophthalmus*.

Table 4. Estimated and statistical results for six models (DEC, DIVALIKE, BAYAREALIKE, and their corresponding +J models) using the R package BioGeoBEARS. The model with the maximum AIC model weight is the best model and is indicated using bold. Abbreviations: LnL referred to log-likelihood; *d*, rate of dispersal; *e*, rate of extinction; *j*, likelihood of founder-event speciation at cladogenesis; AIC, Akaike's information criterion.

Model	LnL	Number of parameters	*d*	*e*	*j*	AIC	AIC model weight
DEC	-72.37	2	4.50E-03	9.90E-03	0	148.7	4.00E-10
DEC+J	**-50.37**	**3**	**1.00E-12**	**1.00E-12**	**0.042**	**106.7**	**0.53**
DIVALIKE	-63.76	2	0.0039	1.00E-12	0	131.5	2.20E-06
DIVALIKE+J	-63.76	2	0.0039	1.00E-12	0	131.5	2.20E-06
BAYAREALIKE	-82.37	2	8.10E-03	4.70E-02	0	168.7	1.80E-14
BAYAREALIKE+J	-50.48	3	1.00E-07	1.00E-07	0.041	107	0.47

Table 5. PCA loadings of the five principal components extracted from 18 measured characters of morphometric data for *Karstsinnectes daxinensis* sp. nov. and *K. anophthalmus*.

	PC1	PC2	PC3	PC4	PC5
Standard length	-0.182	-0.865	0.145	0.322	-0.087
Body depth	-0.849	-0.311	-0.061	-0.039	-0.257
Predorsal length	-0.014	0.293	-0.104	0.502	0.699
Dorsal fin length	-0.198	-0.264	0.128	-0.676	0.593
Preanal length	0.447	0.310	-0.706	-0.126	0.303
Analfin length	0.518	0.735	0.157	-0.228	-0.325
Pectoral fin length	0.356	0.443	0.689	-0.100	0.112
Prepelvic length	-0.574	0.665	-0.290	-0.269	-0.219
Pelvic fin length	0.530	-0.137	-0.405	-0.047	-0.371
Caudal peduncle length	0.066	0.299	0.778	-0.330	0.072
Caudal peduncle depth	0.737	-0.079	-0.316	0.293	0.332
Head length	-0.552	0.731	-0.283	0.177	0.130
Head depth	-0.781	0.318	0.241	0.461	-0.031
Head width	-0.711	0.076	0.263	0.440	-0.084
Mouth width	-0.920	0.268	-0.101	0.180	0.103
Outrostral barbel length	0.711	0.002	0.495	0.446	0.141
Inrostral barbel length	0.767	0.295	-0.063	0.412	-0.387
Maxillary barbel length	0.963	0.075	0.041	0.092	-0.014
Eigenvalues	0.314	2.854	0.608	1.51	0.71
Percentage of total variance	37.967	17.746	13.736	11.163	9.058
Cumulative percentage	37.967	55.714	69.449	80.612	89.670

Taxonomic account

***Karstsinnectes daxinensis* Luo, Zhou & Zhou, sp. nov.**

https://zoobank.org/BA75B4CD-0B3E-4EC6-AD2A-CB8556244BA7

Suppl. material 5, Figs 4, 5

Chresonymy. *Oreonectes anophthalmus*: Wang, 2022 (Leiping Town, Daxin County, Guangxi, China). *Karstsinnectes anophthalmus*: Luo et al. 2023, 2024; Yu et al. 2023; Ge et al. 2024; Zhao et al. 2024 (Leiping Town, Daxin County, Guangxi, China).

Holotype. GZNU20200427002, 30.8 mm total length, 27.5 mm standard length (SL), collected by Tao Luo on April 27, 2020, in Leiping Town, Daxin County, Chongzuo City, Guangxi Zhuang Autonomous Region, China (22.64141996°N, 107.1030802°E; ca. 155 m a.s.l.).

Paratypes. Five specimens from the same locality as the holotype: GZNU20200427001, GZNU20200427006, GZNU20200427003–427005, collected by Tao Luo on April 27, 2020.

Etymology. The specific epithet "*daxinensis*" refers to the type locality of the new species: Leiping Town, Daxin County, Chongzuo City, Guangxi, China. We propose the English common name "Daxin Chinese Karst Loach" and Chinese common name "Dà Xīn Zhōng Huá Kā Qiū (大新中华喀鳅)."

Diagnosis. *Karstsinnectes daxinensis* sp. nov. can be distinguished from all of the other congeners by the following combination of characters: (1) body naked and without pigmentation; (2) eyes absent; (3) dorsal-fin rays iii-7, pectoral-fin rays i-10–11, pelvic-fin rays i-5, anal-fin rays iii-5, caudal fin truncated with 13–14 branched caudal-fin rays; (4) pelvic fins slightly long, length 9.5–13.2% of SL, tip reaching the anus; (5) high and wide head (depth 6.3–9.8% of SL; wide 10.0–14.8% of SL), narrow mouth (width 6.2–7.9% of SL), long inrostral barbel length (length 7.2–12.7% of SL), and long maxillary barbel length (length 11.3–13.1% of SL).

Description. Morphological data of all of the specimens of *Karstsinnectes daxinensis* sp. nov. were collected in this study are provided in Table 6 and Suppl. material 5.

Body elongated and cylindrical, anterior portion gradually raised from upper eye to dorsal-fin base, posterior portion gradually compressed from dorsal fin to caudal-fin base, with deepest body depth anterior to dorsal-fin origin, deepest body depth 9.1–10.4% of SL. Dorsal profile of forehead and predorsal profile convex, concave from dorsal-fin origin to anterior margin of upper caudal adipose keel. Ventral profile flat. Head short, length 18.9–23.6% of SL, slightly depressed and flattened, width greater than depth (head depth/head length = 29.2–42.6%). Snout short and lightly blunt. Mouth inferior, snout tip truncated, upper and lower lips smooth, lower lip with a V-shaped median notch.

Three pairs of barbels: inrostral barbels short, length 7.2–12.7% of SL, tip not reaching to corner of the mouth; outrostral barbel long, length 9.4–12.7% of SL, tip reaching to posterior margin of the eye. Maxillary barbel slightly developed, length 11.3–13.1% of SL, tip not reaching to anterior margin of operculum. Anterior and posterior nostrils adjacent. Anterior nostril tube long, truncated, without elongated long barbel-like tip. Eyes absent. Gill rakers not developed, 9–10 gill rakers on first gill arch (n = 2).

Dorsal-fin rays iii-7, pectoral-fin rays i-10–11, pelvic-fin rays i-5, anal-fin rays iii-5, and with 13–14 branched caudal-fin rays. Dorsal fin short, length 12.7–17.2% of SL, distally margin truncated, origin slightly posterior to pelvic-fin insertion, first branched ray longest, tip of dorsal fin slight beyond to vertical of anus. Pectoral fin slightly developed, length 12.8–14.8% of SL, tip not beyond midpoint between origins of pectoral and pelvic fins. Pelvic fin slightly long, length 9.5–13.2% of SL, distally margin oval, vertically aligned with first unbranched ray of dorsal fin, tip of pelvic fin reaching the anus. Anal fin slightly long, length 11.7–16.8% of SL, tip not reaching to caudal-fin base. Caudal fin truncated, upper lobe is equal in length to lower one, tip pointed, caudal peduncle length 13.2–16.8% of SL, caudal peduncle depth 7.4–10.4% of body depth, with not developed adipose crests along both dorsal and ventral sides. Total vertebrae: 4 + 31 (n = 1) (Fig. 4D).

Body naked, smooth, and scaleless. Cephalic lateral line system developed. Lateral line and head sensory pores absent. Two chambers of air-bladder, anterior chamber dumbbell-shaped and membranous, open on both sides and posteriorly (Fig. 4E), and posterior chamber slight developed, slightly filling body cavity, connected with anterior chamber by short tube.

Coloration. In cave water bodies when living, body semi-translucent and pale pink, without skin pigment, and all of the fins hyaline (Fig. 5). After fixation in 7% formalin solution, the body color was yellowish white, thorax and gills light brown color, transparent on all of the fins (Fig. 4A–C).

Table 6. Morphometric statistics and results of analysis of variance from *Karstsinnectes daxinensis* sp. nov. and *K. anophthalmus*. Abbreviations: *Kd*, *K. daxinensis* sp. nov.; *Ka*, *K. anophthalmus*. NA denotes that the data is not available.

	***K. daxinensis* sp. nov. (n = 6)**		***K. anophthalmus* (n = 4)**		***P*-value from ANOVA**
	Range	**Mean ± SD**	**Range**	**Mean ± SD**	***Kd* vs. *Ka***
Total length	26.4–32.3	29.1 ± 2.9	30.5–42.8	36.5 ± 5.1	0.055
Standard length	22.1–27.8	25.0 ± 2.8	25.3–36.9	31.4 ± 4.8	0.055
Body depth	2.4–3.2	2.9 ± 0.4	2.8–5.3	4.2 ± 1.1	0.054
Body width	1.9–2.9	2.3 ± 0.5	NA	NA	NA
Predorsal length	12.6–17.9	15.1 ± 2.0	15.8–22.0	18.9 ± 2.6	0.033
Dorsal fin base length	1.8–2.6	2.3 ± 0.3	NA	NA	NA
Dorsal fin length	2.9–4.6	3.9 ± 0.7	4.1–6.0	5.3 ± 0.8	0.055
Preanal length	16.8–20.3	18.8 ± 1.6	19.3–25.1	23.0 ± 2.6	0.055
Anal fin base length	1.3–1.9	1.6 ± 0.2	NA	NA	NA
Anal fin length	2.7–3.7	3.3 ± 0.4	3.5–4.2	3.7 ± 0.3	0.240
Prepectoral length	4.1–5.7	4.8 ± 0.7	NA	NA	NA
Pectoral fin base length	0.7–1.4	1.0 ± 0.3	NA	NA	NA
Pectoral fin length	2.9–4.1	3.5 ± 0.6	3.9–4.8	4.3 ± 0.4	0.055
Prepelvic length	12.3–15.0	13.8 ± 1.2	14.8–21.2	18.1 ± 2.7	0.033
Pelvic fin base length	0.6–0.9	0.8 ± 0.1	NA	NA	NA
Pelvic fin length	2.3–3.0	2.7 ± 0.3	1.4–3.0	2.6 ± 0.8	0.285
Caudal peduncle length	3.0–4.6	3.8 ± 0.7	4.1–6.3	4.8 ± 1.0	0.136
Caudal peduncle depth	1.6–2.4	2.2 ± 0.3	1.7–2.7	2.1 ± 0.4	0.670
Head length	4.8–6.0	5.4 ± 0.5	6.2–8.4	7.3 ± 0.9	0.011
Head depth	1.4–2.5	2.1 ± 0.4	2.6–3.7	3.1 ± 0.5	0.010
Head width	2.2–4.0	3.4 ± 0.7	3.7–5.5	4.8 ± 0.8	0.033
Upper jaw length	0.9–1.5	1.2 ± 0.2	NA	NA	NA
Lower jaw length	0.8–1.1	1.0 ± 0.1	NA	NA	NA
Mouth width	1.4–1.9	1.7 ± 0.2	2.2–3.2	2.7 ± 0.4	0.011
Outrostral barbel length	2.1–3.5	2.8 ± 0.6	2.1–3.1	2.6 ± 0.4	0.394
Inrostral barbel length	1.6–2.8	2.2 ± 0.5	1.1–1.3	1.3 ± 0.1	0.011
Maxillary barbel length	2.6–3.6	3.1 ± 0.4	2.3–2.6	2.5 ± 0.1	0.087

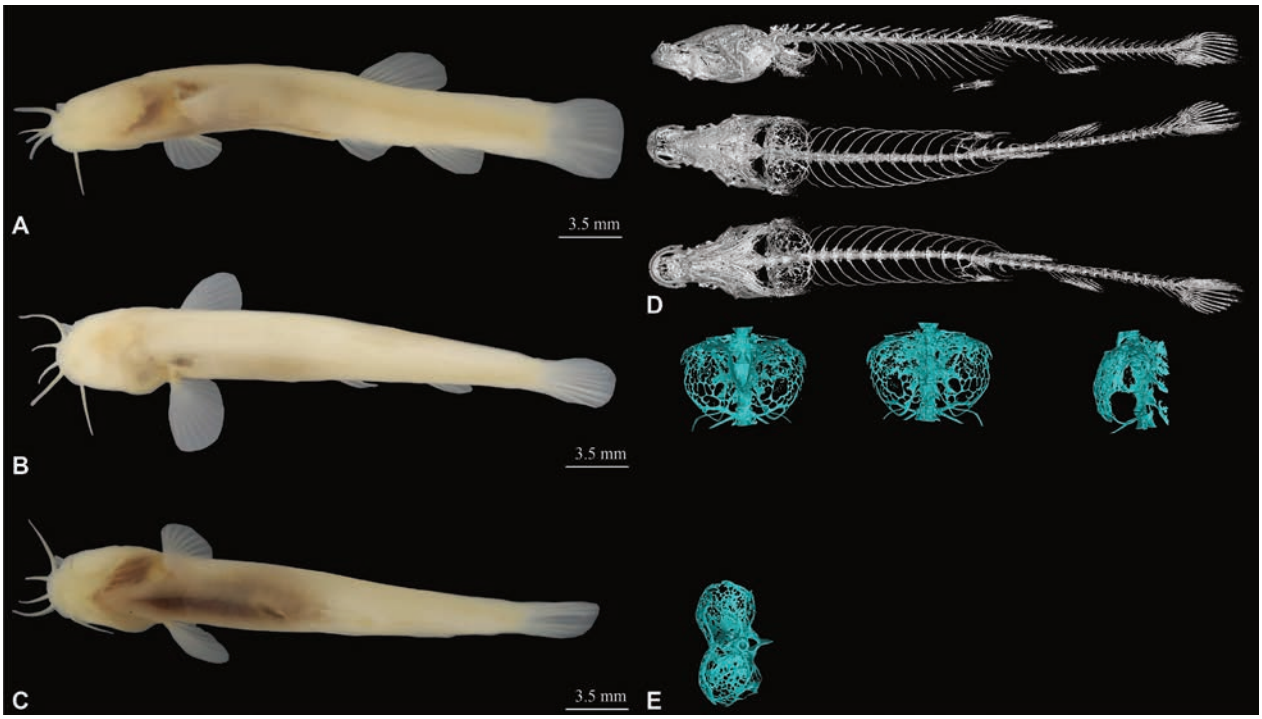

Figure 4. *Karstsinnectes daxinensis* sp. nov., GZNU20200427002, holotype, 27.5 mm standard length; Zuojiang River basin, Leiping Town, Daxin County, Guangxi, China. **A**. Lateral view; **B**. Dorsal view; **C**. Ventral view; **D**. Micro-computed tomography of lateral, dorsal, and ventral views of body; **E**. Ventral, dorsal, lateral, and from above views of air bladder posterior chamber based on micro-computed tomography.

Comparisons. Morphological data of *K. daxinensis* sp. nov. with the six known species within genus *Karstsinnectes* are given in Table 7.

Karstsinnectes daxinensis sp. nov. can be distinguished from *K. cehengensis*, *K. acridorsalis*, *K. parvus*, *K. hyalinus*, and *K. longzhouensis* by caudal fin truncated

Table 7. Comparison of the diagnostic characters of the new species described here, *Karstsinnectes daxinensis* sp. nov., with those selected for the six other known species of the genus *Karstsinnectes*. Modified from Zhao et al. (2024). Abbreviations: *K. an*, *K. anophthalmus*; *K. ce*, *K. cehengensis*; *K. ac*, *K. acridorsalis*; *K. pa*, *K. parvus*; *K. hy*, *K. hyalinus*; and *K. lo*, *K. longzhouensis*.

	***K. daxinensis* sp. nov.**	***K. an***	***K. ce***	***K.ac***	***K. pa***	***K. hy***	***K. lo***
Caudal fin	Truncated	Truncated	Forked	Forked	Forked	Forked	Forked
Eyes	Absent	Absent	Reduced	Absent	Absent	Absent	Absent
Scales	Absent	Absent	Absent	Absent	Absent	Present (tiny scales)	Absent
Lateral line	Absent	Absent	Incomplete	Absent	Present	Absent	Present
Dorsal-fin rays	iii, 7	iii, 7	iii, 7	iii, 8–9	iii, 9	ii, 9	iii, 9
Anal-fin rays	iii, 5	ii, 5	iii, 5	ii, 5	iii, 5	ii, 4	iii, 5
Pectoral-fin rays	i, 10–11	i, 10–12	ii, 11–12	i, 10	i, 10	i, 11	i, 10/12
Pelvic-fin rays	i, 5	i, 4–5	i, 7	i, 5	i, 6	i, 5	i, 5
Caudal-fin rays	13–14	12–13	14	13–14	12–13	11–12	13–14
Gill rakers	9–10	8–9	9	9	11	12	11–12
Dorsal-fin rays tip	Slightly beyond to anal-fin insertion	Far beyond to anal-fin insertion	Reaching to anal-fin insertion	Far beyond to anal-fin insertion	Far beyond to anal-fin insertion	Reaching to anal-fin insertion	Far beyond to anal-fin insertion
Dorsal fin origin	Slightly posterior to pelvic-fin origin	Posterior to pelvic-fin origin	Slightly posterior to pelvic-fin origin	Posterior to pelvic-fin origin	Anterior to pelvic-fin origin	Slightly anterior to pelvic-fin origin	Anterior to pelvic-fin origin
Pelvic fin tip	Reaching the anus	Not reaching the anus	Not reaching the anus	Not reaching the anus	Exceeding anus	Reaching the anus	Reaching the anus
Distribution	Zuojiang River	Youjiang River	Beipanjiang River	Hongshui River	Youjiang River	Hongshui River	Zuojiang River
Source	This study	Lan et al. 2013	Zhao et al. 2024	Lan et al. 2013; Ge et al. 2024	Zhu and Zhu, 2014; Ge et al. 2024	Lan et al. 1996; Ge et al. 2024	Ge et al. 2024

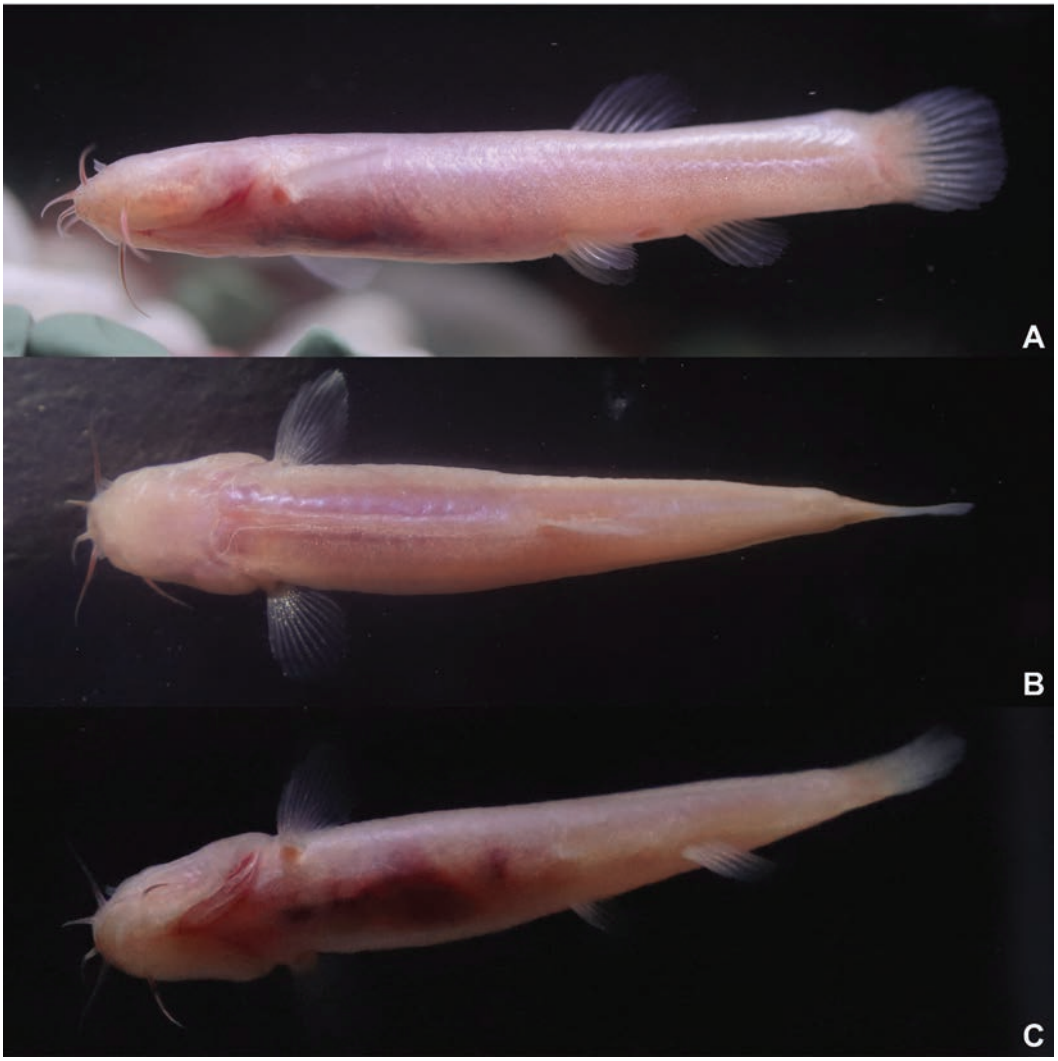

Figure 5. Lateral, dorsal, ventral views of *Karstsinnectes daxinensis* sp. nov. In living.

(vs. forked). The new species can be further distinguished from *K. cehengensis* by eye absent (vs. reduced); and from *K. cehengensis*, *K. parvus*, and *K. longzhouensis* by lateral line absent (vs. present).

Morphologically and genetically, *K. daxinensis* sp. nov. is closest to *K. anophthalmus*, but can still be distinguished by some morphological characters. *Karstsinnectes daxinensis* sp. nov. different from *K. anophthalmus* by tip of pelvic fin reaching the anus (vs. not reaching the anus) (Fig. 6), three unbranched pelvic-fin rays (vs. two), narrow mouth (6.2–7.9% of SL vs. 8.7–8.8% of SL), long inrostral barbel length (7.2–12.7% of SL vs. 3.4–5.3% of SL), and long maxillary barbel length (11.3–13.1% of SL vs. 7.1–10.0% of SL).

Distribution. At present, this new species *K. daxinensis* sp. nov. has only been discovered in the type locality and nearby caves within the Zuojiang River basin (Fig. 1).

Discussion

The genus *Karstsinnectes*, a group of truly blind fishes, has only six species which have all been described in the last 40 years, indicating that the genus has a low level of species diversity which may be a result of the lack of thorough field surveys. We have comprehensively reconstructed the phylogenetic and evolutionary history of *Karstsinnectes* for the first time by integrating the mitochondrial genome. Phylogenic analysis revealed that *Karstsinnectes* can be divided into two clades and follows an intriguing pattern in which phylogeny corresponds to geographical distribution. The divergence time and ancestral area reconstruction suggest that the genus *Karstsinnectes* originated at the Oligocene/Miocene boundary at ~22.37 Mya (~17.17–29.04 Mya), with the most recent common ancestor found

Figure 6. Morphological comparison of *Karstsinnectes daxinensis* sp. nov. (**A**) and *K. anophthalmus* (**B, C**). This mainly shows the relative locations at the tip of the pelvic fin and the anus separating these two species. Photo **A** by Tao Luo, Photos **B, C** by Mr. Jia-Jun Zhou and Mr. Jia-Hu Lan.

to occur ~18.87 Mya, and that dispersal events have shaped the current distribution pattern of diversity in the genus *Karstsinnectes*.

Paleogeoclimatic events and the formation of karst landscapes drove the origin and dispersal of *Karstsinnectes*. Dispersal played an important role within the evolution of *Karstsinnectes*. Ancestral area reconstruction results suggest that the most recent common ancestor of *Karstsinnectes* species most likely inhabited the Hongshui River basin, then dispersed to the Zuojiang-Yujiang (18.87 Mya) and Beipanjiang (~12.78 Mya) river basins. At ~6.71 Mya, the ancestor of Clade II-2 dispersed to the Youjiang River basin from the Zuojiang-Yujiang River basin. These dispersal events suggest that the formation of the modern conditions between the Beipanjiang and Hongshui rivers, between the Hongshui and Zuojiang-Yujiang rivers, and between the basins of the Zuojiang-Yujiang and Youjiang rivers dates back to at least the middle to late Miocene (~6.71–18.87 Mya). Notably, these basins are situated on the right side of the Ailao Shan-Red River shear zone. Geological and phylogenetic evidence has shown that at least two rapid orogenic events occurred in the Ailao Shan-Red River shear zone, first during the late Eocene-early Miocene (16–35 Mya) and second in the late Miocene (5–11 Ma) (Leloup et al. 2001; Gilley et al. 2003; Li et al. 2024). Geological evidence also suggests that several accelerations of uplift of the Qinghai-Xizang Plateau occurred (An et al. 2006), with the most dramatic one occurring at 15–25 Mya (Ding et al. 2017, 2022). Additionally, the uplift of the Qinghai-Xizang Plateau caused a rapid shift in the climate of East Asia to a monsoon-dominated pattern (Wu et al. 2022); the large amounts of rainfall brought about by intensification of the monsoon (Farnsworth et al. 2019) provided an additional impetus for the dispersal and speciation of *Karstsinnectes*. As a result of these paleogeoclimatic events, during the Miocene, the landforms of southwestern China were reorganized above and below ground, including high mountains, valleys, rivers, and caves (He et al. 2023; Lu et al. 2023). During the same period, dramatic orogeny and rainfall also accelerated the formation of karst caves and upstream drainage systems of the Pearl River (Che and Yu 1985; Zhang et al. 2023), e.g., the Beipanjiang, Hongshui, Zuojiang, and Youjiang rivers, which is consistent with palaeogeological evidence (Zhang et al. 2023). Subterranean caves and rivers generated by paleogeoclimatic events created ecological conditions that allowed for the dispersal and formation of cave fishes. Together, these appear to be consistent with our estimates of divergence times based on DNA data and with spatial and temporal changes in the diversification of other cave-dwelling fishes (Wen et al. 2022), suggesting the possibility that orogeny, cave formation, and monsoon winds have played a role in facilitating the formation and dispersal of cave species.

The diversity of *Karstsinnectes* needs to be further assessed using a combination of field surveys along with genetic and morphological analysis. Based on morphological characters, specimens of *Karstsinnectes* from Daxin, Guangxi, were previously treated as *K. anophthalmus* (Luo et al. 2023; Yu et al. 2023; Ge et al. 2024; Zhao et al. 2024), but were not compared with *K. anophthalmus* from the type locality. Previous studies have noted morphological differences between the Daxin population and *K. anophthalmus*, but lacked data to support separating them taxonomically (Ge et al. 2024). Genetically, the genetic distance between the new species and *K. anophthalmus* from the type locality was 6.9%, which was greater than that between other species of the same genus, e.g., *K. longzhouensis* and *K. parvus* had a genetic distance of 5.8% (Table 3), genetically supporting the validity of the new species. *Karstsinnectes daxinensis* sp. nov. and *K. anophthalmus* are also morphologically distinguishable (see Comparisons). This work has emphasized that the use of type locality data is very important for the correct identification of cryptic species. Additionally, the longer branch lengths, the older divergence times, and the discontinuity in distribution suggest that there may be undiscovered populations, e.g., only *K. anophthalmus* occurs in the Youjiang River basin (Fig. 1), which needs to be further explored with new field surveys.

Key to species of *Karstsinnectes*, from southwest China (modified from Zhao et al. 2024; Ge et al. 2024).

1	Eyes reduced, two unbranched pectoral-fin rays	*K. cehengensis*
–	Eyes absent, single unbranched pectoral-fin rays	2
2	Caudal fin truncated	3
–	Caudal fin forked	4
3	Three unbranched anal-fin rays, tip of pelvic fin reaching the anus	*Karstsinnectes daxinensis* sp. nov.
–	Two unbranched anal-fin rays, tip of pelvic fin not reaching the anus	*K. anophthalmus*
4	Body covered by tiny scales	*K. hyalinus*
–	Body scaleless	5
5	Lateral line absent	*K. acridorsalis*
–	Lateral line absent	6
6	Pectoral fin with 10 branched rays, five branched pelvic fin rays	*K. parvus*
–	Pectoral fin with 11 or 12 branched rays, six branched pelvic fin rays	*K. longzhouensis*

Acknowledgments

We thank Jing Yu, Ya-Li Wang, and Xu Yang for their help during the sample collection. We thank Prof. Li-Na Du and Mr. Jia-Hu Lan for providing the morphometric data and photos of *K. anophthalmus*. We thank Dr. Jing-Song Shi for his help with the CT scan of the bones. Finally, we thank LetPub (www.letpub.com.cn) for its linguistic assistance during the preparation of this manuscript. This study was supported by the programs of the Diversity and Distribution Survey of Chiroptera species in China (2021FY100302), the Guizhou Province Top Discipline Construction Program Project (Qianjiao Keyan Fa [2019] 125), and the Guizhou Normal University Academic Emerging Talent Fund Project (Qianshi Xin Miao [2021]).

References

Allio R, Schomaker-Bastos A, Romiguier J, Prosdocimi F, Nabholz B, Delsuc F (2020) MitoFinder: Efficient automated large-scale extraction of mitogenomic data in target enrichment phylogenomics. Molecular Ecology Resources 20(4): 892–905. https://doi.org/10.1111/1755-0998.13160

An Z, Zhang P, Wang E, Wang S, Qiang X, Li L, Song Y, Chang H, Liu X, Zhou W, Liu W, Cao J, Li X, Shen J, Liu Y, Ai L (2006) Changes of the monsoon-arid environment in China and growth of the Tibetan Plateau since the Miocene. Quaternary Sciences 26(5): 678–693.

Bouckaert R, Heled J, Kühnert D, Vaughan T, Wu C-H, Xie D, Suchard MA, Rambaut A, Drummond AJ (2014) BEAST 2: A Software Platform for Bayesian Evolutionary Analysis. PLoS Computational Biology 10(4): e1003537. https://doi.org/10.1371/journal.pcbi.1003537

Che YT, Yu JZ (1985) Karst in China. Beijing: Science Press, 88–95. [in Chinese]

Ding L, Spicer RA, Yang J, Xu Q, Cai F, Li S, Lai Q, Wang H, Spicer TEV, Yue Y, Shukla A, Srivastava G, Khan MA, Bera S, Mehrotra R (2017) Quantifying the rise of the Himalaya orogen and implications for the South Asian monsoon. Geology 45(3): 215–218. https://doi.org/10.1130/G38583.1

Ding L, Kapp P, Cai F, Garzione CN, Xiong Z, Wang H, Wang C (2022) Timing and mechanisms of Tibetan Plateau uplift. Nature Reviews Earth & Environment 3(10): 652–667. https://doi.org/10.1038/s43017-022-00318-4

Duan YF, Li M, Xu KW, Zhang L, Zhang LB (2021) Protect China's karst cave habitats. Science 374(6568): 699–699. https://doi.org/10.1126/science.abm5389

Farnsworth A, Lunt DJ, Robinson SA, Valdes PJ, Roberts WH, Clift PD, Markwick P, Su T, Wrobel N, Pancost RD (2019) Past East Asian monsoon evolution controlled by paleogeography, not CO_2. Science Advances 5(10): eaax1697. https://doi.org/10.1126/sciadv.aax1697

Fricke R, Eschmeyer WN, Van der Laan R (eds) (2024) Catalog of fishes: genera, species, references. California Academy of Sciences, San Francisco. http://researcharchive.calacademy.org/research/ichthyology/catalog/fishcatmain.asp. [Electronic version accessed 8 August 2024]

Ge JY, Nong ZQ, Yang J, Du LN, Zhou JJ (2024) Taxonomic revision of the cavefish genus *Karstsinnectes* (Cypriniformes, Nemacheilidae), with a description of a new species from Guangxi Province, China. Zoosystematics and Evolution 100(2): 663−673. https://doi.org/10.3897/zse.100.118061

Gilley LD, Harrison TM, Leloup PH, Ryerson FJ, Lovera OM, Wang JH (2003) Direct dating of left-lateral deformation along the Red River shear zone, China and Vietnam. Journal of Geophysical Research: Solid Earth 108(B2): 2127. https://doi.org/10.1029/2001JB001726

Günther A (1868) Catalogue of the fishes in the British museum. Trustees of the British Museum, London.

He J, Garzanti E, Jiang T, Barbarano M, Liu E, Chen S, Liao Y, Li X, Wang H (2023). Evolution of eastern Asia river systems reconstructed by the mineralogy and detrital-zircon geochronology of modern Red River and coastal Vietnam river sand. Earth-Science Reviews 245: 104572. https://doi.org/10.1016/j.earscirev.2023.104572

Hirt MV, Arratia G, Chen WJ, Mayden RL, Tang KL, Wood RM, Simons AM (2017) Effects of gene choice, base composition and rate heterogeneity on inference and estimates of divergence times in cypriniform fishes. Biological Journal of the Linnean Society 121(2): 319−339. https://doi.org/10.1093/biolinnean/blw045

Hoang DT, Chernomor O, von Haeseler A, Minh BQ, Vinh LS (2018) UFBoot2: Improving the ultrafast bootstrap approximation. Molecular Biology and Evolution 35(2): 518–522. https://doi.org/10.1093/molbev/msx281

Katoh K, Standley D M (2013) MAFFT multiple sequence alignment software version 7: improvements in performance and usability. Molecular Biology and Evolution 30(4): 772–780. https://doi.org/10.1093/molbev/mst010

Kumar S, Stecher G, Tamura K (2016) MEGA7: Molecular evolutionary genetics analysis version 7.0 for bigger datasets. Molecular Biology and Evolution 33(7): 1870–1874. https://doi.org/10.1093/molbev/msw054

Lan JH, Yang JX, Chen YR (1996) One new species of cavefish from Guangxi (Cypriniformes: Cobitidae). Zoological Research 17(2): 109–112.

Lan JH, Gan X, Wu TJ, Yang J (2013) Cave Fishes of Guangxi, China. Beijing: Science Press, 68–98. [in Chinese]

Lanfear R, Frandsen PB, Wright AM, Senfeld T, Calcott B (2017) PartitionFinder 2: New methods for selecting partitioned models of evolution for molecular and morphological phylogenetic analyses. Molecular Biology and Evolution 34(3): 772–773. https://doi.org/10.1093/molbev/msw260

Leloup PH, Arnaud N, Lacassin R, Kienast JR, Harrison TM, Trong TP, Replumaz A, Tapponnier, P (2001) New constraints on the structure, thermochronology, and timing of the Ailao Shan-Red River shear zone, SE Asia. Journal of Geophysical Research: Solid Earth 106(B4): 6683–6732. https://doi.org/10.1029/2000JB900322

Li XQ, Peng HW, Xiang KL, Xiang XG, Jabbour F, Ortiz RDC, Soltis PS, Wang W (2024) Phylogenetic evidence clarifies the history of the extrusion of Indochina. Proceedings of the National Academy of Sciences of the United States of America 121(35): e2322527121. https://doi.org/10.1073/pnas.2322527121

Lu H, Feng H, Lyu H, Wang H, Zhang X, Zhang H, Wang X, Li Y (2023) Formation and evolution of the Asian landscape during the Cenozoic. The Innovation Geoscience 1(2): 100020. https://doi.org/10.59717/j.xinn-geo.2023.100020

Luo T, Yang Q, Wu L, Wang YL, Zhou JJ, Deng HQ, Xiao N, Zhou J (2023) Phylogenetic relationships of cavefishes of the Nemacheilidae (*Heminoemacheilus*, *Oreonectes*, *Yunnanilus*, *Paranemachilus*,

and *Troglonectes*) revealed by phylogenetic analysis of mitochondrial genome and seven nuclear genes. Zoological Research 44(4): 693–697. https://doi.org/10.24272/j.issn.2095-8137.2022.266

Ma L, Yang JX, Lei FK, Xu MZ, Zhao YH, Jeffery WR (2023) Protection and exploration of the scientific potential of Chinese cavefish. Zoological Research 44(4): 675–677. https://doi.org/10.24272/j.issn.2095-8137.2022.484

Matzke NJ (2013) Probabilistic historical biogeography: new models for founder-event speciation, imperfect detection, and fossils allow improved accuracy and model-testing. Frontiers of Biogeography 5(4): 242–248. https://doi.org/10.21425/F55419694

Nguyen LT, Schmidt HA, Von HA, Minh BQ (2015) IQ-TREE: A fast and effective stochastic algorithm for estimating maximum-likelihood phylogenies. Molecular Biology and Evolution 32(1): 268–274. https://doi.org/10.1093/molbev/msu300

Rambaut A, Drummond AJ, Xie D, Baele G, Suchard MA (2018) Posterior summarization in Bayesian phylogenetics using Tracer 1.7. Systematic Biology 67(5): 901–904. https://doi.org/10.1093/sysbio/syy032

Ronquist F, Teslenko M, Van DMP, Ayres DL, Darling A, Höhna S, Larget B, Liu L, Suchard MA, Huelsenbeck JP (2012) MrBayes 3.2: Efficient Bayesian phylogenetic inference and model choicem across a large model space. Systematic Biology 61(3): 539–542. https://doi.org/10.1093/sysbio/sys029

Wang Y, Shen Y, Feng C, Zhao K, Song Z, Zhang Y, Yang L, He S (2016) Mitogenomic perspectives on the origin of Tibetan loaches and their adaptation to high altitude. Scientific Reports 6(1): 29690. https://doi.org/10.1038/srep29690

Wang YL (2022) Systematic taxonomy of the genus *Oreonectes* and *Troglonectes* (Master's thesis). Guizhou Normal University, Guiyang. [in Chinese]

Wen H, Luo T, Wang Y, Wang S, Liu T, Xiao N, Zhou J (2022) Molecular phylogeny and historical biogeography of the cave fish genus *Sinocyclocheilus* (Cypriniformes: Cyprinidae) in southwest China. Integrative Zoology 17(2): 311−325. https://doi.org/10.1111/1749-4877.12624

Wu F, Fang X, Yang Y, Dupont-Nivet G, Nie J, Fluteau F, Zhang T, Han W (2022) Reorganization of Asian climate in relation to Tibetan Plateau uplift. Nature Reviews Earth & Environment 3(10): 684−700. https://doi.org/10.1038/s43017-022-00331-7

Xu C, Luo T, Zhou JJ, Wu L, Zhao XR, Yang HF, Xiao N, Zhou J (2023) *Sinocyclocheilus longicornus* (Cypriniformes, Cyprinidae), a new species of microphthalmic hypogean fish from Guizhou, Southwest China. ZooKeys 1141: 1–28. https://doi.org/10.3897/zookeys.1141.91501

Yu J, Luo T, Lan C-T, Zhou J-J, Deng H-Q, Xiao N, Zhou J (2023) *Oreonectes damingshanensis* (Cypriniformes, Nemacheilidae), a new species of stream fish from Guangxi, Southwest China. ZooKeys 1180: 81–104. https://doi.org/10.3897/zookeys.1180.104645

Zhang D, Gao F, Jakovlić I, Zou H, Zhang J, Li WX, Wang GT (2020) PhyloSuite: An integrated and scalable desktop platform for streamlined molecular sequence data management and evolutionary phylogenetics studies. Molecular Ecology Resources 20(1): 348–355. https://doi.org/10.1111/1755-0998.13096

Zhang Z, Daly JS, Tian Y, Lei C, Sun X, Badenszki E, Qin Y, Hu J (2023) Late Oligocene formation of the Pearl River triggered by the opening of the South China Sea. Geophysical Research Letters 50(8): e2023GL103049. https://doi.org/10.1029/2023GL103049

Zhao X, Lan C, Luo T, Yu J, Zhou J, Xiao N, Zhou J (2024) *Karstsinnectes cehengensis* (Cypriniformes: Nemacheilidae), a new species of cave fish from Guizhou, China. Zoological Systematics 49(2): 101–115. https://doi.org/10.11865/zs.2024204

Zheng BS (1981) Freshwater fishes of Guangxi Province. Nanning: Guangxi People's Publishers, 162–163. [in Chinese]

Zhu SQ (1989) The loaches of the subfamily Nemacheilinae in China (Cypriniformes: Cobitidae). Nanjing: Jiangsu Science and Technology Publishing House, 10–25. [in Chinese]

Zhu Y, Zhu DG (2014) Description of a new species of the genus *Heminoemacheilus* (Teleostei: Balitoridae) in Guangxi, China. Journal of Guangdong Ocean University 34(6): 18–21.

Supplementary material 1

Phylogenetic tree based on mitochondrial genomes

Authors: Tao Luo, Fang-Wei Luo, Chang-Ting Lan, Ming-Yuan Xiao, Jia-Jun Zhou, Mei Liao, Ning Xiao, Jiang Zhou

Data type: png

Explanation note: In this phylogenetic tree, Bayesian posterior probabilities (BPP) from BI analyses/ultrafast bootstrap supports (UFB) from maximum likelihood analyses were noted beside nodes. The scale bar represents 0.05 nucleotide substitutions per site.

Link: https://doi.org/10.3897/zse.100.133964.suppl1

Supplementary material 2

Raw details of reconstruction of the ancestral area of *Karstsinnectes* at the species level using the R package BioGeoBEARS (DEC+J model)

Authors: Tao Luo, Fang-Wei Luo, Chang-Ting Lan, Ming-Yuan Xiao, Jia-Jun Zhou, Mei Liao, Ning Xiao, Jiang Zhou

Data type: png

Explanation note: The pie chart shows the probability of the most likely distribution.

Link: https://doi.org/10.3897/zse.100.133964.suppl2

Supplementary material 3

Raw details of reconstruction of the ancestral area of *Karstsinnectes* level using the R package BioGeoBEARS (DEC+J model)

Authors: Tao Luo, Fang-Wei Luo, Chang-Ting Lan, Ming-Yuan Xiao, Jia-Jun Zhou, Mei Liao, Ning Xiao, Jiang Zhou

Data type: png

Explanation note: The rectangular box shows the most likely distribution.

Link: https://doi.org/10.3897/zse.100.133964.suppl3

Supplementary material 4

Raw details of reconstruction of the ancestral area of *Karstsinnectes* at the species level using the R package BioGeoBEARS (BAYAREALIKE+J model)

Authors: Tao Luo, Fang-Wei Luo, Chang-Ting Lan, Ming-Yuan Xiao, Jia-Jun Zhou, Mei Liao, Ning Xiao, Jiang Zhou

Data type: png

Explanation note: The pie chart shows the probability of the most likely distribution.

Link: https://doi.org/10.3897/zse.100.133964.suppl4

Supplementary material 5

Raw measurement data used for morphological analysis

Authors: Tao Luo, Fang-Wei Luo, Chang-Ting Lan, Ming-Yuan Xiao, Jia-Jun Zhou, Mei Liao, Ning Xiao, Jiang Zhou

Data type: docx

Link: https://doi.org/10.3897/zse.100.133964.suppl5

Zoosyst. Evol. 100 (4) 2024, 1487–1513 | DOI 10.3897/zse.100.128211

PENSOFT

MUSEUM FÜR NATURKUNDE BERLIN

Acotylea (Platyhelminthes, Polycladida) from the southern and western Iberian Peninsula, with the description of five new species

Patricia Pérez-García[1], Filipa Gouveia[2], Gonçalo Calado[2,3], Carolina Noreña[4], Juan Lucas Cervera[1,5]

1 *Departamento de Biología, Facultad de Ciencias del Mar y Ambientales, Campus de Excelencia Internacional del Mar (CEI MAR), Av. República Saharahui, s/n, Ap. 40. 11510, Puerto Real (Cádiz), Spain*

2 *EPCV-Departamento de Ciências da Vida, Universidade Lusófona, Campo Grande, 376, 1749-024 Lisboa, Portugal*

3 *MARE - Centro de Ciências do Mar e do Ambiente (FCT/NOVA), Campus de Caparica, Caparica, Portugal*

4 *Departamento de Biodiversidad and Biología Evolutiva, Museo Nacional de Ciencias Naturales (CSIC), C/Jose Gutiérrez Abascal 2, Ap. 28006, Madrid, Spain*

5 *Instituto Universitario de Investigación Marina (INMAR), Campus de Excelencia Internacional del Mar (CEI·MAR), Universidad de Cádiz, Av. República Saharahui, s/n, Ap. 40. 11510, Puerto Real (Cádiz), Spain*

https://zoobank.org/C47F14AC-1C3E-43AC-9645-D5FBC843AA7A

Corresponding author: Patricia Pérez-García (patricia.perezgarcia@uca.es)

Academic editor: Tom Artois ♦ **Received** 23 May 2024 ♦ **Accepted** 12 September 2024 ♦ **Published** 7 November 2024

Abstract

Most of the European polyclad species were described after material was collected from the Gulf of Naples, Italy, which was compiled in the renowned monograph of Arnold Lang in 1884. On the other hand, little is known about the diversity of flatworms in the Iberian Peninsula, with 49 recorded species, which are mainly registered in the northern coast of Spain. Moreover, polyclads in Portugal have never been studied before. In our study, specimens of 13 species of acotylean flatworms were collected from the southern and western Atlantic coasts of the Iberian Peninsula. All of the species included here are well documented with colour pictures and histological sections. The geographical distribution of the known species has been updated. Five of the collected species are new to science: *Stylochus erytheius* **sp. nov.**, *S. marimarensis* **sp. nov.**, *Plehnia cascaisensis* **sp. nov.**, *Izmira lusitanica* **sp. nov.**, and *Emprosthopharynx onubensis* **sp. nov.**

Key Words

Anatomy, biodiversity, marine flatworms, Portugal, Spain

Introduction

The Iberian Peninsula has an exceptional geographic position and is well known for having a great variety of habitats and high species richness (Molina-Venegas et al. 2015). However, it has been estimated that the overall number of marine invertebrate species in this area is still unknown, especially considering the punctually studied taxa such as marine flatworms (Aguado et al. 2011). The Iberian Peninsula is a region of high interest for biodiversity due to the convergence of two different water masses (the Atlantic Ocean and Mediterranean Sea), the resulting environmental changes (Farina et al. 2003; Templado et al. 2021), and the strategic location of the Strait of Gibraltar. These factors have led to the emergence of a hotspot for endemism and the migration of non-native species from other areas in the region.

In this context, a study of Polycladida (Rhabditophora, Platyhelminthyes) from the southern coast of Spain and Portugal was conducted. Polycladida is a group of free-living worms with 1033 species described worldwide (Tyler et al. 2006–2024). They are almost exclusively marine and inhabit a wide range of environments, including seagrass meadows and sandy bottoms, as well as the deep sea (Quiroga et al. 2006, 2008; Oya and Kajihara 2018). Several scientific reports covering the

polyclads found in the Iberian Peninsula have been published in the last decade (Gammoudi and Tekaya 2012; Noreña et al. 2014, 2015; Marquina et al. 2014a, 2014b; Rodríguez et al. 2017; Pérez-García et al. 2019). These reports recorded 49 species of polyclads, which are mainly located on the northern coasts of Spain. In contrast, reports of marine flatworms on the coasts of Portugal are rare, except for reports of *Leptoplana tremellaris* (Müller OF, 1773) (Saldanha 1974) and some records by naturalists (e.g., iNaturalist [www.inaturalist.org]).

The main goal of this study is to provide a comprehensive geographical record of acotylean flatworms identified on the southern and western coasts of the Iberian Peninsula. In addition, we update the geographical distribution of the known species and improve taxonomical knowledge on these species within the coastal areas of the Iberian Peninsula.

Methods

Study area

The coastal geology of Cadiz and Algeciras is mainly composed of sedimentary rocks, which have been shaped by tectonic activity and erosion. On the other hand, Portugal's coast has a diverse geological history that includes sedimentary, igneous, and metamorphic rocks. These geological differences have an impact on the coastal morphology and substrate composition, leading to distinct landscapes. Cadiz and Algeciras have rugged coastlines characterised by rocky cliffs and sandy beaches, which are influenced by the nearby Strait of Gibraltar. Portugal's coastline has cliffs and sandy beaches as well, but it also has pronounced estuaries, lagoons, and tidal flats that provide unique habitats. The coast of this region is distinguished by its extensive seagrass meadows and salt marshes, which support a wide range of aquatic and bird species. However, both regions face environmental challenges such as coastal erosion, pollution, habitat loss, climate change, high population densities, land use patterns, and management strategies (Micallef and Rangel-Buitrago 2019; Morales 2022).

For this study, polyclads were collected at seventeen stations. Of these, sixteen are from the southern and southwestern Iberian Peninsula (Fig. 1, Table 1), and one from northern Portugal. These stations are located along the coasts of Algeciras, Cadiz, and Portugal and share some similar characteristics. However, they also have some unique differences, which are outlined in the descriptions of the different species. The numbers of the stations are referred to from north to south:

Station 1, Praia de Gondarém, Oporto (41°9'22.31"N, 8°40'53.70"W);
Station 2, Praia do Baleal, Peniche (39°22'21.1"N, 9°20'26.4"W);
Station 3, Cascais (38°40'59.32"N, 9°25'55.59"W);
Station 4, Area Marinha Protegida das Avencas, Parede (38°41'35"N, 9°22'03"W);
Station 5, Troia, Grândola (38°29'16.8"N, 8°53'18.1"W);
Station 6, Praia de Alpertuche, Arrabida (38°28'01.8"N, 8°59'25.1"W);
Station 7, Sagres (37°0'44.43"N, 8°55'47.29"W);
Station 8, Praia da Luz, Lagos (37°5'6.32"N, 8°43'6.23"W);
Station 9, Ria Formosa, Faro (37°0'30.40"N, 7°59'39.57"W);
Station 10, El Portil, Huelva (37°12'33.72"N, 7°3'17.50"W);
Station 11, La Caleta Beach, Cádiz (36°31'55.50"N, 6°18'26.45"W);
Station 12, Santa Maria del Mar Beach, Cádiz (36°31'18.53"N, 6°12'18.17"W);
Station 13, El Chato Beach, Cádiz (36°28'48.89"N, 6°15'57.79"W);
Station 14, Sancti Petri Beach, Chiclana (36°22'52.69"N, 6°12'18.17"W);
Station 15, Tarifa (36°0'42.59"N, 5°35'54.54"W);
Station 16, Punta Carnero, Algeciras (36°11'10.16"N, 6°15'56.65"W);
Station 17, La Ballenera Beach, Algeciras (36°5'17.81"N, 5°26'30.77"W).

The material was collected over a long period of time, extending from July 2013 to July 2019.

Most of the polyclads were found under rocks intertidally (0.1–0.8 m deep) and were removed from the rocky substrate by the application of a paintbrush. The flatworms were photographed in situ when possible. Most flatworms from Cádiz (Spain) and Algarve (Portugal) were found camouflaged through calcareous rodophytes, mainly *Ellisolandia elongata* (J. Ellis and Solander) K.R. Hind and G.W. Saunders 2013 and lush phaeophytes such as *Halopteris scoparia* (Linnaeus) Sauvageau or *Dictyota dichotoma* (Hudson) J.V. Lamouroux. Nevertheless, some species were observed on stones without benthic fauna or algae.

Morphological study and species identification

The specimens were observed under a stereoscope microscope in glass Petri dishes upon arrival at the laboratory. The specimens were anaesthetised with 7.5% magnesium chloride, measured in length, and then a piece of the lateral body was cut for further molecular analyses and stored in absolute ethanol. The relaxed flatworms were then immersed in Bouin's solution for 30 minutes, stretched for manipulation, and preserved in 70% ethanol (Newman and Cannon 2003).

Acotylean specimens were histologically processed to study their internal morphology after sectioning and staining with the Azan trichrome method (Romeis 1987). The relevant sections were photographed and used to reconstruct their internal anatomy.

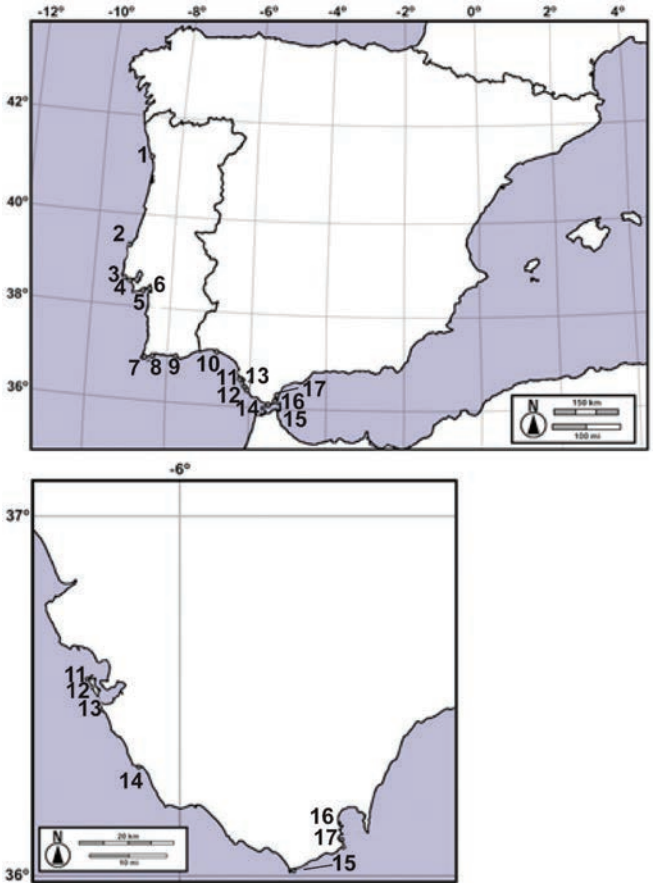

Figure 1. Map of the coasts of the Iberian Peninsula (top) and the province of Cadiz (bottom) showing the sampling locations studied.

Table 1. Species and number of specimens collected at each station. The grey cells correspond to sampling points from Portugal, and the white cells belong to Spain.

Species	Station 1	Station 2	Station 3	Station 4	Station 5	Station 6	Station 7	Station 8	Station 9	Station 10	Station 11	Station 12	Station 13	Station 14	Station 15	Station 16	Station 17	Total of specimens
Stylochus neapolitanus (Delle-Chiaje, 1841–1844)			1								1							2
Stylochus mediterraneus Galleni, 1976											5	1	1					7
Stylochus erytheius sp. nov.											4							4
Stylochus marimarensis sp. nov.												1						1
Plehnia cascaisensis sp. nov.			4															4
Leptoplana mediterranea Bock, 1913	10	3		5							3	4		1				26
Parviplana jeronimoi sp. nov.											3	1						4
Echinoplana celerrima Haswell, 1907							1				1	4						6
Notoplana alcinoi (Schmidt, 1861)											7	3						10
Izmira lusitanica sp. nov.				2														2
Emprosthopharynx onubensis sp. nov.										1								1
Comoplana agilis (Lang, 1884)				1				2			5							8
Phaenoplana caetaria sp. nov.															1	4	5	10
Discocelis tigrina (Blanchard, 1847)				1	1	1		1	1	2	4							11
Total of specimens	1	1	2	4	1	1	1	2	1	2	10	6	1	1	1	1	1	**96**

Species were identified based on internal and external morphological characteristics. Body measurements were taken from live and fixed specimens as well as histological sections. In the description of the new species, the organ measurements refer to a single specimen, the holotype.

The specimens from Spain were deposited in the Invertebrate Collection of the Museo Nacional de Ciencias Naturales de Madrid (**MNCN**), Spain. The specimens from Portugal were deposited in the Invertebrate Collection of the Museu Nacional de História Natural e da Ciência of Lisbon (**MNHNC**), Portugal.

Results

A total of 96 specimens had been identified throughout this study. Their presence in each locality is shown in Table 1.

Systematic description

Suborder ACOTYLEA Lang, 1884
Superfamily STYLOCHOIDEA Poche, 1926
Family STYLOCHIDAE Stimpson, 1857
Genus *Stylochus* Ehrenberg, 1851

***Stylochus neapolitanus* Lang, 1884**

Fig. 2

Planaria neapolitana Delle Chiaje, 1841–1844.

Material examined. • MNCN 4.01/3281 to 3334, Station 11, 23 February 2015, 28 mm long, sagittaly sectioned into 54 slides. All of the measurements from the description refer to this specimen.

The specimen from Station 3 was damaged during transport to the laboratory. However, it could be photographed in situ. This information has been added to the material as a comment.

Description. *Stylochus neapolitanus* from Cadiz agrees with the original description of the species by Lang 1884.

Body shape elongated, with pointed anterior and rounded posterior end, 28 mm long alive. Dorsal surface with dark brown background colour with scattered whitish and greenish spots (Fig. 2A), larger at the margins and smaller in the body centre. An orange band surrounds the margins. Ventral whitish (Fig. 2B). Nuchal tentacles conical, white, and with remarkable orange spots on the tips.

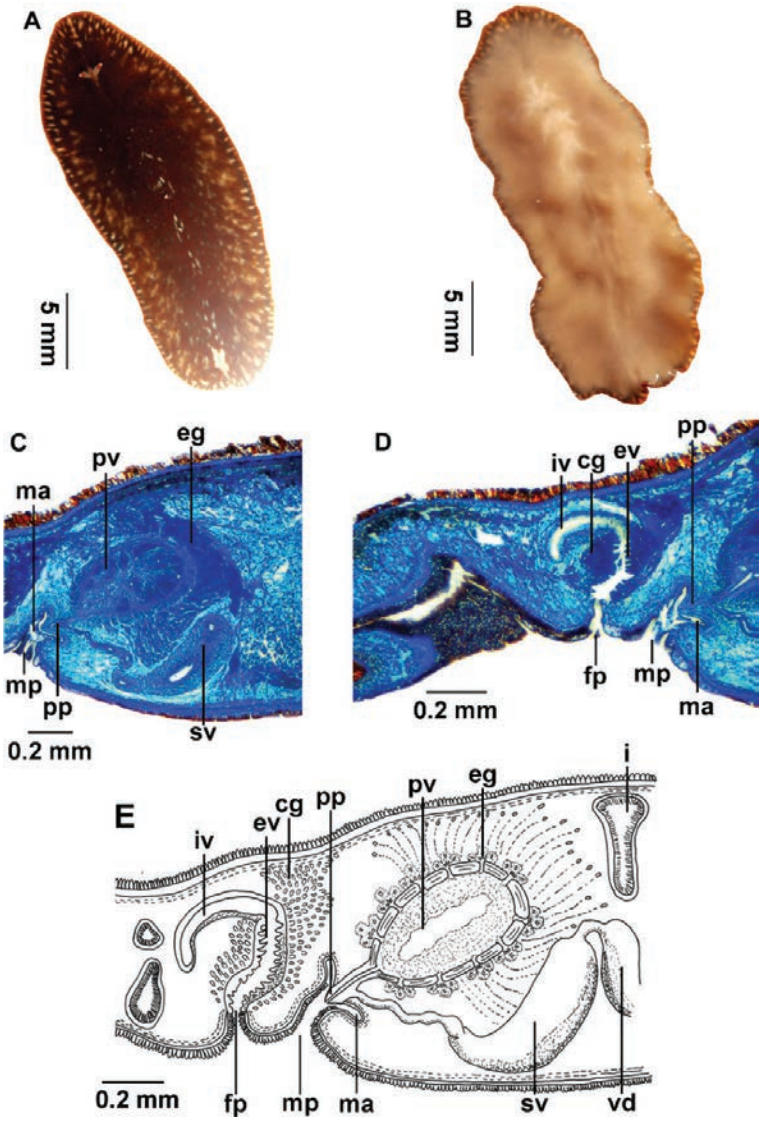

Figure 2. *Stylochus neapolitanus* (MNCN 4.01/3281 to 3334). Histological sections are postero-anteriorly oriented: **A.** Dorsal view of a living specimen; **B.** Ventral view; **C.** Histological section of the male copulatory organs; **D.** Histological section of the female apparatus; **E**. Sagittal reconstruction of the reproductive system. Abbreviations: cg, cemental glands; eg, extravesicular glands; ev, external vagina; fp, female pore; i, intestine; iv, internal vagina; ma, male atrium; mp, male pore; pp, penis papilla; pv, prostatic vesicle; sv, seminal vesicle; vd, vas deferens.

Tentacular eyes at the base and on the tentacles. Cerebral eyes between tentacles. Marginal eyes present only in the anterior margin. Pharynx ruffled, with well-developed lateral branches (Fig. 2B). Oral pore at the centre of the pharynx. Male and female pores separated (0.2 mm) and located near the posterior end.

Reproductive system. Male copulatory apparatus with a true seminal vesicle, an oval prostatic vesicle, and a small penis papilla. Elongated seminal vesicle 0.7 mm in length. Free prostatic vesicle surrounded by extravesicular glands. Short penis papilla housed in a small atrium. Sperm and prostatic ducts join medially. Female apparatus consists of a folded external vagina and a smooth internal vagina (Fig. 2D, E). Well-developed cement gland surrounds the external vagina. Internal vagina extends backwards, receiving the oviducts at the end. Lang's vesicle absent.

Biology. This species was found among samples of the alga *Dictyota dichotoma* (Phaeophyceae, Ochrophyta) collected from rocky substrates in intertidal areas. Previously, it was also collected in substrate covered by the green algae *Caulerpa prolifera* (Forsskal) J. V. Lamouroux 1809 (Chlorophyta, Caulerpaceae) (Marquina et al. 2014a) or on the bottom surface of barges and lamellibranch empty shells (Noreña et al. 2015).

Distribution. *Stylochus neapolitanus* was recorded in Sicily, Naples (Lang 1884), Cape Verde (Laidlaw 1906), Senegal (Palombi 1939), Catalonia (Novell 2001, Murcia (Marquina et al. 2014a), Galicia (Noreña et al. 2015), and Sidi Ifni (Cuadrado et al. 2021). This is the first report of *S. neapolitanus* in Andalusia.

Stylochus mediterraneus Galleni, 1976

Fig. 3

Stylochus (Imogine) *mediterraneus* Galleni, 1976.
Imogine mediterranea (Galleni, 1976) Jennings & Newman, 1996.

Material examined. • MNCN 4.01/3448 to 3463, Station 11, 29 April 2014, 14 mm long, sagittal sectioned into 16 slides; • MNCN 4.01/3521 to 3560, Station 11, 19 April 2015, 30 mm long, sagittal sectioned into 40 slides (all the measurements from the description refer to this last specimen); • MNCN 4.01/3957, Station 11, 30 November 2017, 12 mm long; • MNCN 4.01/3959, Station 11, 19 May 2016, 32 mm long; • MNCN 4.01/3960, Station 11, 2 February 2018, 28 mm long; • MNCN 4.01/3561 to 3630, Station 12, 2 March 2014, live and fixed specimen, no histological processed; Station 13, 15 June 2015, 42 mm long, sagittal sectioned into 70 slides.

Description. Thick worm with oval shape and variable length, 42 mm long (26.33 ± 11.41 mm). Dorsal side brownish with brown pale spots scattered along the whole surface (Fig. 3A). A few dark spots are also present, more numerous in the body margin. Margins white, with dark spots. Ventral side pale or cream (Fig. 3B). Nuchal retractile tentacles present. Tentacular eyes present at the base and on the tips of the tentacles (Fig. 3C). Cerebral eyes arranged in two clusters between the tentacles. Frontal eyes present, scattering to the anterior margin. Marginal eyes around the entire body edge. Pharynx ruffled, anterior located with numerous lateral branches (Fig. 3B). Oral pore anteriorly positioned in the central part of the pharynx. Gonopores separated but close together (0.2 mm), located in the last third of the body.

Reproductive system. Male system with spermiducal bulbs, anchor-shaped seminal vesicle, polyglandular prostatic vesicle, and short penis papilla (Fig. 3G). Spermiducal bulbs enter separately into the tripartite seminal vesicle. Seminal vesicle horizontal (Fig. 3D), located just behind the prostatic vesicle. Prostatic vesicle elongated (0.74 mm long), with a well-developed muscular wall (0.05 mm) and crossed by numerous extravesicular glands (Fig. 3E, G). In the middle section, the prostatic and seminal ducts together form the ejaculatory duct (Fig. 3G). Penis papilla short-housed in a ciliated male atrium (Fig. 3E).

Female pore close to the male pore, leading to a slightly folded external vagina (Fig. 3F, G). Distal part of the external vagina internally folded (Fig. 3F, G). Smooth internal vagina, in which the paired oviducts are received. Lang's vesicle absent.

Remarks. The features of the specimens studied herein match Galleni's (1976) description for specimens found on the Tuscany coast (Italy), except for the structure of the female complex, in which the presence of folds within the vagina externa is not mentioned. However, Gammoudi et al. (2009) also noted the horizontal orientation of the penis papilla, the ciliated or non-ciliated atrium, and the dilatations in the external vagina in specimens from Tunisia and not for the populations from Tuscany (Galleni 1976).

Biology. The specimens were observed under rocks in the intertidal zone and among brown algae *Halopteris scoparia* (Ochrophyta). In other studies, this species and its egg masses were found in cultures of *Mytilus galloprovincialis* (Mollusca, Bivalvia) (Gammoudi et al. 2009).

Distribution. This species was reported in several localities of the Mediterranean Sea, such as Croatia (Bytinski-Salz 1935, as *Stylochus pilidium*); Livorno, Marina di Pisa, and Punta Bianca, Italy (Galleni 1976); Liguria, Italy (Wenzel et al. 1992); Temara, Morocco, the Atlantic Ocean (Prudhoe 1989); Tunisia (Gammoudi et al. 2009); and Murcia (Marquina et al. 2014a). Our record is the first for this species on the Atlantic coasts of the Iberian Peninsula and in Andalusia.

Stylochus erytheius sp. nov.

https://zoobank.org/9D19D6CC-7155-41D6-B6DB-39EE6E52F479

Fig. 4

Holotype. • MNCN 4.01/3059 to 3113 and 4336 to 4535, Station 11, 9 October 2014, 71 mm long, sagittal sectioned into 254 slides.

Additional material. • MNCN 4.01/3962, Station 11, 20 April 2015, 35 mm long; • MNCN 4.01/3964, Station 11, 20 April 2015, 37 mm long; • MNCN 4.01/3966, Station 11, 2 February 2018, 120 mm long.

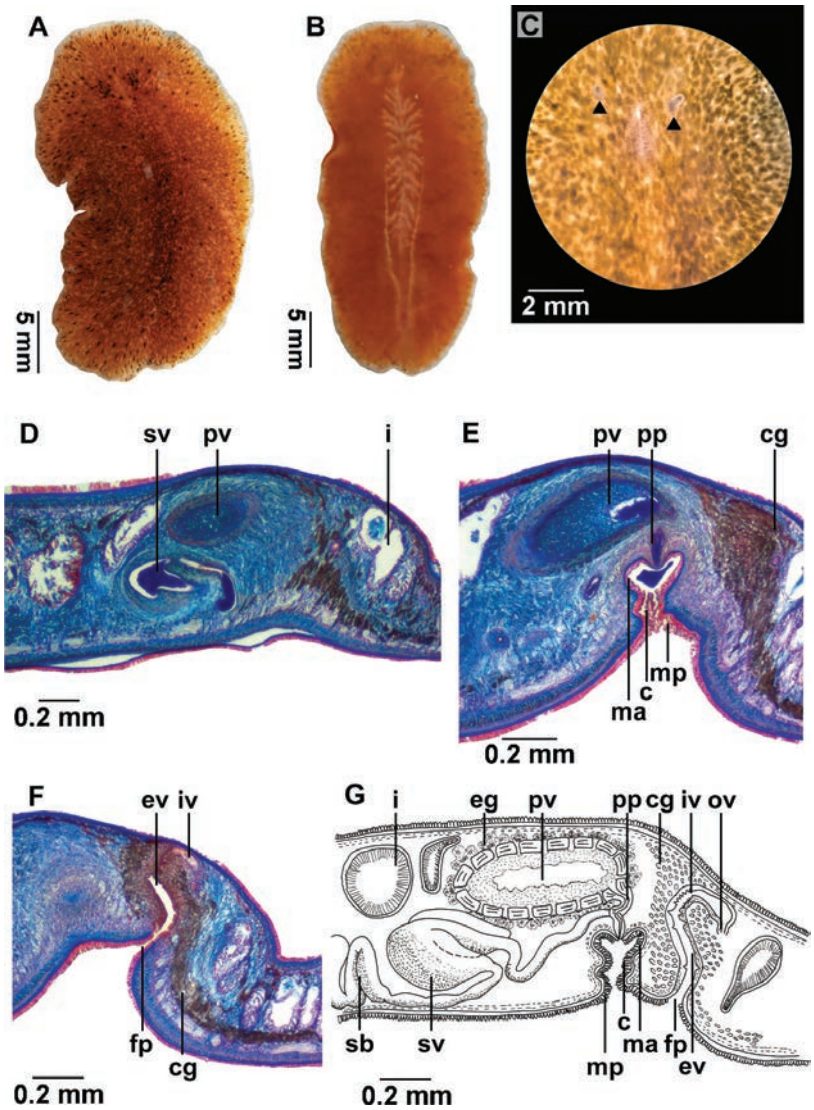

Figure 3. *Stylochus mediterraneus* (MNCN 4.01/3521 to 3560). Histological sections are antero-posteriorly oriented: **A.** Dorsal view of a living specimen; **B.** Ventral view; **C.** Detail of the tentacles and cerebral eyes; **D.** Histological section of the seminal vesicle and part of the prostatic vesicle; **E.** Histological section of the male copulatory organs; **F.** Histological section of the female apparatus; **G.** Sagittal reconstruction of the reproductive system. Abbreviations: c. cilia; cg, cemental glands; eg, extravesicular glands; ev, external vagina; fp, female pore; i, intestine; iv, internal vagina; ma, male atrium; mp, male pore; ov, oviduct; pp, penis papilla; pv, prostatic vesicle; sb, spermiducal bulbs; sv, seminal vesicle.

Diagnosis. Body shape is oval with rounded anterior and posterior ends. Orange-brown dorsal background; numerous dark brown and whitish dots scattered on the dorsal surface; visible line of white dots along the main body axis; ventral surface pale orange; gonopores well-separated; with spermiducal bulbs; opening of the sperm duct distally located; penis papilla short.

Description. Oval-shaped Stylochidae, with rounded anterior and posterior ends, fleshy, 71 mm in length (65.75 ± 39.76 mm) and 63 mm in width. Margins mostly smooth. Background colouration orange-brown, with multiple dark brown and white dots on the dorsal surface (as shown in Fig. 4A). Additionally, a conspicuous line of white dots extends along the central axis of the body. Ventrally pale orange (Fig. 4B). Nuchal conical tentacles transparent, with tentacular eyes at the base and tips (Fig. 4C). Poorly visible cerebral eyes in two scattered clusters between the tentacles. Marginal eyes along the entire body margin. Pharynx ruffled centrally. Oral pore at the centre of the pharynx. Reddish, conspicuous gonopores well-separated (0.6 mm) posteriorly located.

Reproductive system. Male copulatory apparatus comprises spermiducal bulbs, a tripartite seminal vesicle, and a free prostatic vesicle (Fig. 4F). Spermiducal bulbs broad, run ventrally, and then posteriorly, turning dorsally before entering the seminal vesicle. Tripartite seminal vesicle anchor-like shape (Fig. 4D, F), well developed. Prostatic vesicle, large and oval-shaped (1.5 mm long), belongs to the polyglandular ("*djiboutiensis*") type (Faubel 1983). Muscular wall crossed by numerous extravesicular glands. The prostatic duct and the seminal duct join to form the short ejaculatory duct just before entering the

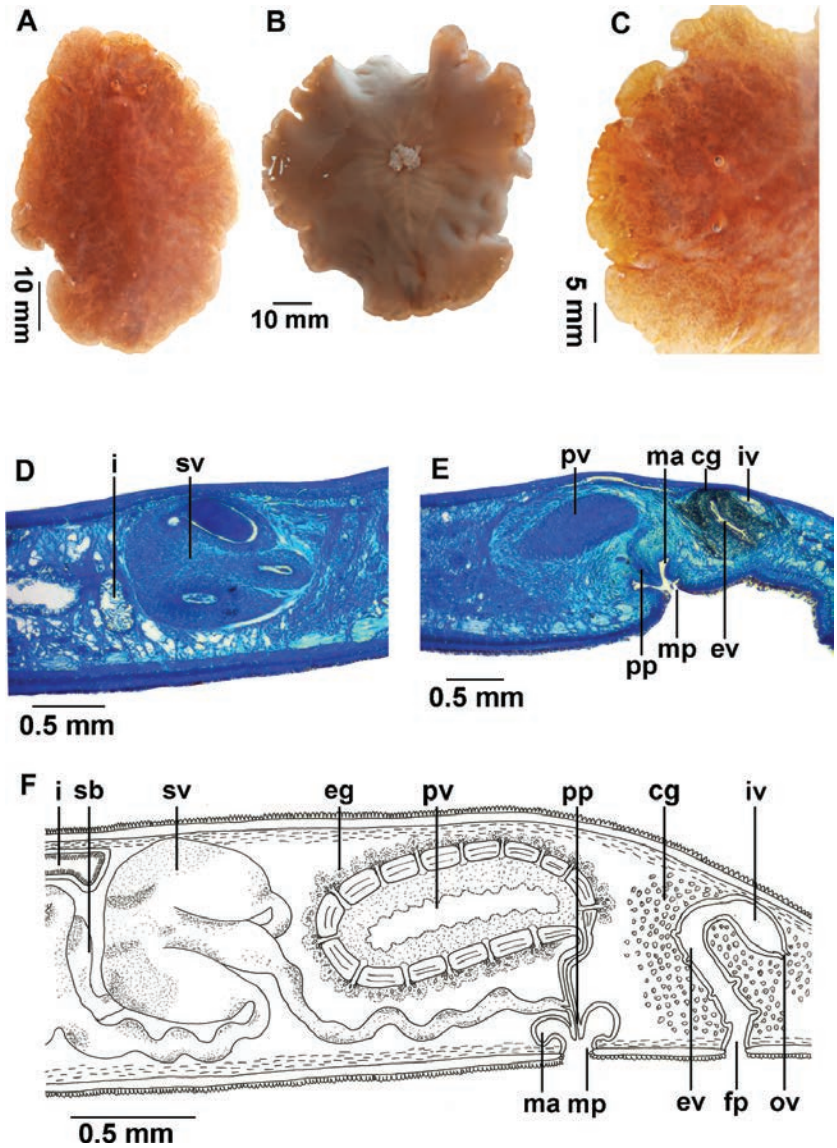

Figure 4. *Stylochus erytheius* sp. nov. (MNCN 4.01/3059 to 3113 and 4336 to 4535). Histological sections are antero-posteriorly oriented: **A.** Dorsal view of a living specimen; **B.** Ventral view; **C.** Detail of the tentacles and cerebral eyes; **D.** Histological section of the seminal vesicle; **E.** Histological section of the male and female copulatory organs; **F.** Sagittal reconstruction of the reproductive system. Abbreviations: cg, cemental glands; eg, extravesicular glands; ev, external vagina; fp, female pore; i, intestine; iv, internal vagina; ma, male atrium; mp, male pore; ov, oviduct; pp, penis papilla; pv, prostatic vesicle; sb, spermiducal bulbs; sv, seminal vesicle.

penis papilla. Penis papilla elongated (0.21 mm), opening into a sinuous male atrium (Fig. 4E).

The female copulatory apparatus simple and inconspicuous, formed by the vagina externa and interna. Without Lang's vesicle. The oviducts open together into the posterior region of the vagina interna. Abundant shell and cement glands open into the vagina externa and distal region of the vagina interna.

Type locality. La Caleta Beach, Cadiz, Spain.

Etymology. Named after Erytheia, a small island where the Phoenicians settled approximately 1100 BC. This area is where the beach of La Caleta is located, the type locality of the new species.

Remarks. A discussion of this species is included together with *S. marimarensis* sp. nov.

Biology. Specimens were collected from rocky substrates under stones in the intertidal zone.

Distribution. This species has only been found in La Caleta, Cadiz, Spain.

Stylochus marimarensis sp. nov.

https://zoobank.org/2A320C66-4963-4B70-A7E6-E7E11C60625F

Fig. 5

Holotype. • MNCN 4.01/2820 to 3058, Station 12, 2 March 2014, 55 mm long, sagittally sectioned into 237 slides.

Diagnosis. Oval-shaped worm with flattened anterior and tapered posterior ends. Pinkish colouration and pale pink spots scattered on the dorsal surface; black spots dis-

persed along the margins and at the base of the tentacles; margins whitish; ventral body pale pink; gonopores separated in last body third; with spermiducal bulbs; opening of the ejaculatory duct medially within the penis papilla; penis papilla elongated; male and female atrium ciliated.

Description. Oval shaped Stylochidae with flattened anterior and tapered posterior ends. Firm corporal thickness. Dorsal pigmentation pinkish, with scattered pale pink spots (Fig. 5A). Whitish margins with some folds and black mottling. Ventral surface pale pink (Fig. 5B). Transparent, conical nuchal tentacles (Fig. 5C) on either side of the cerebral lobes. Tentacular eyes situated at the base and tips of the tentacles. Two elongated clusters of cerebral eyes between the tentacles. Marginal eyes along the body margin, more numerous anteriorly. Pharynx ruffled along central body region. Oral pore medial. Gonopores separated (0.82 mm), reddish pigmented, and near the posterior end.

Reproductive system. Male system with an anchor-shaped seminal vesicle, a polyglandular prostatic vesicle ("*djiboutiensis*" type), and an elongated penis papilla (Fig. 5F). Spermiducal bulbs well-developed (Fig. 5D). Seminal vesicle tripartite (0.55 mm length, 0.65 mm width). Prostatic vesicle elongated, oval-shaped (1 mm long), surrounded by numerous extravesicular glands. Penis papilla elongated (0.22 mm) opening in a ciliated atrium. Seminal and prostatic ducts join medially to form the ejaculatory duct (Fig. 5F).

The female reproductive system is a simple tube divided into the external and internal vagina. Without Lang's vesicle. The oviducts open together in the proximal region of the internal vagina. Abundant shell and cement glands empty into both vaginas. Female atrium shallow and ciliated.

Type locality. Santa Maria del Mar Beach, Cadiz (Spain).

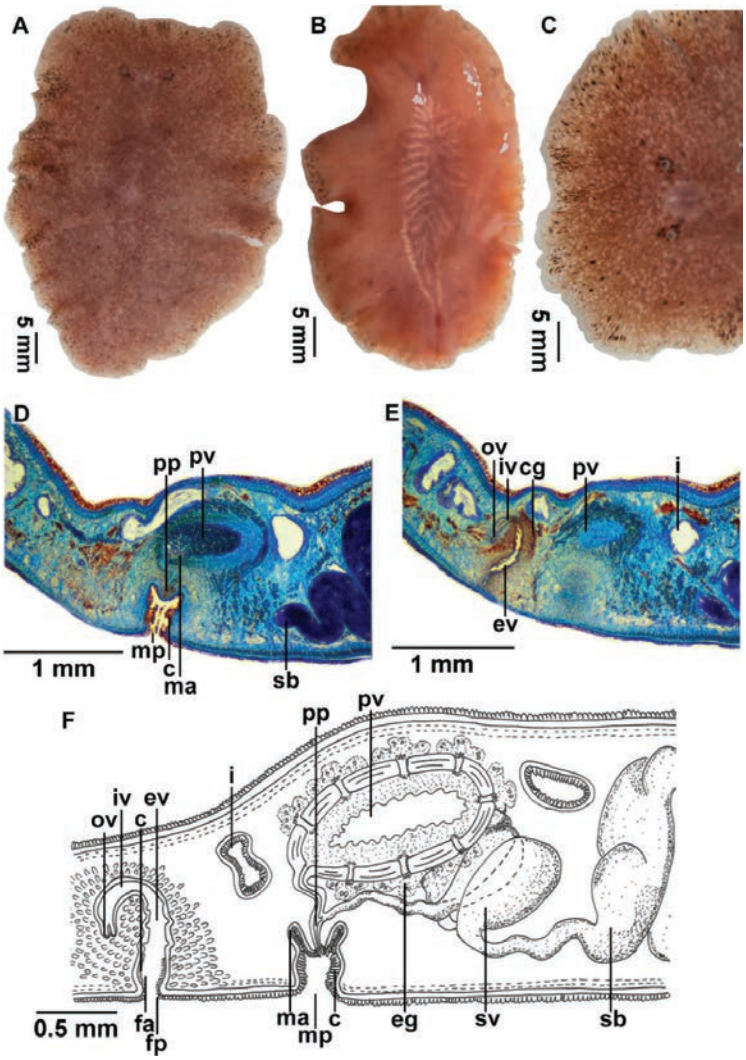

Figure 5. *Stylochus marimarensis* sp. nov. (MNCN 4.01/2820 to 3058). Histological sections are postero-anteriorly oriented: **A.** Dorsal view of a living specimen; **B.** Ventral view; **C.** Detail of the tentacles and cerebral eyes; **D.** Histological section of the male copulatory apparatus; **E.** Histological section of the female copulatory organs; **F.** Sagittal reconstruction of the reproductive system. Abbreviations: c, cilia; cg, cement glands; eg, extravesicular glands; ev, external vagina; fa, female atrium; fp, female pore; i, intestine; iv, internal vagina; ma, male atrium; mp, male pore; ov, oviduct; pp, penis papilla; pv, prostatic vesicle; sb, spermiducal bulbs; sv, seminal vesicle.

Etymology. The name of the new species refers to the type locality, Santa María del Mar.

Biology. Collected under rocks in the intertidal zone. The species was found on a stony bottom interspersed with rocky pools.

Distribution. The only locality where this species was collected is Santa Maria del Mar Beach, Cadiz (Spain).

General discussion of the newly described species of *Stylochus*. Sixty-two accepted *Stylochus* species are distributed worldwide (Tyler et al. 2006–2024) and are distinguished mainly by their colour pattern, eye arrangement, and colour and shape of the tentacles (Jennings and Newman 1996; Bulnes 2010). Nevertheless, additional features allow distinction among these species, such as the opening of the gonopores, together or separately, the junction of the seminal duct with the prostatic duct in the penis papilla, the shape and size of the penis papilla, and the inner outline of the external vagina. All of these characteristics are compared in Table 2 for *Stylochus* spp. distributed in the eastern Atlantic, Mediterranean, and Black Seas.

Stylochus marimarensis sp. nov. differs from other known species of the genus by its pinkish pigmentation with pale pink spots on the dorsal side, bordering whitish margins, and black mottling. The known species in the Mediterranean and eastern Atlantic vary in colour from brown, orange, and white to yellow, but none of them display a continuous white edge, as in *S. marimarensis* sp. nov.

Stylochus spp. distributed out of these territories that share similar pigmentation with *S. marimarensis* sp. nov. are *S. qeshmensis* Maghsoudlou & Momtazi, 2014 and *S. kimae* Jennings & Newman, 1996. *S. qeshmensis* has a rosy brown colour with dark brown spots scattering dorsally except along the margins, white tentacles, and a short penis papilla. Black spots of *S. marimarensis* sp. nov. are distributed within the margins only, and few of them are under the tentacles. This latter presents transparent tentacles and long penis papilla. *S. kimae* has a bright orange-pink colour and several light brown dots, features which are lacking in *S. marimarensis* sp. nov. Both *S. qeshmensis* and *S. kimae* lack spermiducal bulbs, a very prominent character in *S. marimarensis* sp. nov.

Stylochus erytheius sp. nov. has remarkable orange, dark pigmentation and lacks a whitish margin. *S. fafai* also shares an orange colour, displays close but separated gonopores, a reduced penis papilla, and a female system without dilatations. The mottling of *S. mediterraneus* is

Table 2. Comparison among *Stylochus* spp. from the Eastern Atlantic, Mediterranean Sea, and Black Sea.

Species name	Dorsal colour	Junction of the prostatic and seminal ducts	Length of the penis papilla	Distal dilatation of the external vagina	Distribution	References
Stylochus alexandrinus Steinbock, 1937	Not described	Proximal	Short	Without dilatations	Egypt, Italy and Morocco (Atlantic)	Steinböck (1937); Galleni (1976); Prudhoe (1989); Bulnes et al. (2005);
***Stylochus erytheius* sp. nov.**	Orange-brown with dark brown spots and scattered whitish dots	Distal	Long	With dilatations	Spain (Atlantic)	This study
Stylochus fafai (Marquina, Fernandez-Alvarez & Noreña, 2014)	Bright orange with small dark spots	Medial	Short	Without dilatations	Spain (Atlantic)	Marquina et al. (2014b)
***Stylochus marimarensis* sp. nov.**	Pinkish with pale pink spots scattered. Margins whitish with black mottling	Medial	Long	With dilatations	Spain (Atlantic)	This study
Stylochus mediterraneus Galleni, 1976	Brownish with dark brown spots except in the mid-body. A white band is present along the margins	Medial/Distal	Short	With dilatations	Italy, Tunisia, Morocco (Atlantic)	Wenzel et al. (1992); Galleni (1976); Gammoudi et al. (2009); Prudhoe (1989)
Stylochus melihertani (Bulnes, 2010)	Orange-brownish with brownish speckles	Medial	Long	With dilatations	Türkiye	Bulnes (2010)
Stylochus neapolitanus (Delle Chiaje, 1841-1844)	Dark brown background colour interspersed by whitish and greenish mottling. Orange band in the margins	Proximal	Short	Without dilatations	Cape Verde, Italy, Senegal, Spain (Atlantic)	Laidlaw (1903); Bulnes et al. (2005); Palombi (1939); Noreña et al. (2015)
Stylochus pilidium (Goette, 1881)	Pale yellow, with dark and white mottling	Proximal	Short	Without dilatations	Italy, Spain (Mediterranean)	Goette (1881); Marquina et al. (2014a)
Stylochus plessisii Lang, 1884	Greyish-white, with brown spots on the dorsal side and a bold white marginal band interrupted by orange spots	Proximal	Short	Without dilatations	Italy	Lang (1884)
Stylochus stellae (Marquina et al., 2014)	Brownish with dark brown spots	Proximal	Long	Triangular dilatations	Spain (Mediterranean)	Marquina et al. (2014a)
Stylochus tauricus Jacubowa, 1909	Dark yellow with brown margins before the clear borders	Proximal	Short	Without dilatations	Black Sea, Ukraine	Jacubowa (1909)
Stylochus vesiculatus Jacubowa, 1909	Dirty yellow, with dark spots	Proximal	Short	Without dilatations	Black Sea, Ukraine	Jacubowa (1909)

darker than that of *S. marimarensis* sp. nov., and the latter has a more elongated penis papilla than the one observed in *S. mediterraneus*. *S. neapolitanus* presents a bold orange band in the margins, a dark brown background and greenish mottling on the dorsal side, and a reduced penis papilla. All of these features differ from those of the new species. The same occurs with *S. plessisii* since the colour pattern is different, with a whitish colour and black and orange spots. *S. pilidium* bears a yellowish, pale colour and a reduced penis papilla. Finally, *S. stellae* has a brown colour with dark brown spots, with separated gonopores close to each other and a proximal junction of the prostatic and seminal ducts, while *S. marimarensis* sp. nov. displays well-separated gonopores and a medial junction of the ducts.

On the other hand, the species that most resemble *S. erytheius* sp. nov. are *S. fafai* and *S. pilidium*. *S. fafai* shows a similar body shape and pigmentation, but the gonopores are located close together, the penis papilla is reduced, and the external vagina lacks dilatation. The background colour of *S. pilidium* is quite different, showing pale-yellow pigmentation, and the junction of the prostatic and seminal ducts is proximally located; the penis papilla is shorter than that observed in *S. erytheius* sp. nov., and the external vagina lacks dilatation.

Other species that share some similarities with *S. erytheius* are *S. kimae* and *S. rutilis* Yeri and Kaburaki 1918. The most pronounced differences between *S. kimae* and *S. erytheius* are the dorsal pigmentation. This one is brighter and pinkish with light brown mottling in *S. kimae* and orangish with darker brown mottling and white dots in *S. erytheius* sp. nov. Additionally, the junction between the seminal and prostatic ducts occurs proximally in *S. kimae* and distally in *S. erytheius* sp. nov. Conversely, *S. rutilis* displays a reddish orange dorsal colour, with also reddish spots and a red median line. This type of pattern is lacking in *S. erytheius* sp. nov. The marginal eyes are distributed along the anterior margins of *S. rutilis* but encircle the entire body of *S. erytheius* sp. nov. Finally, the gonopores are very close together in *S. rutilis* but distinctly separated in *S. erytheius* sp. nov.

Family PLEHNIIDAE Bock, 1913
Genus *Plehnia* Bock, 1913

Plehnia cascaisensis sp. nov.

https://zoobank.org/21A8A353-8C24-4D6D-AC33-CE4F1C7142B8

Figs 6, 7

Holotype. • MNHNC MB16-000107, Station 3, 29 May 2015 at 28 m depth, 9 mm long fixed, sagittal sectioned into 8 slides.

Additional material. • MNHNC MB16-000108, Station 3, 26 May 2015, at 9.1 m depth, 4 mm long, fixed, and sagittally sectioned into 3 slides. • MNHNC MB16-000109, Station 3, 28 May 2015 at 24 m depth, 6 mm long fixed. • MNHNC MB16-000110, Station 3, 28 May 2015 at 24 m depth, 6 mm long fixed.

Diagnosis. Plehniidae with a yellowish-brown background colour and multiple brown spots scattered on the dorsal surface; pale yellow ventral body; well-separated gonopores; penis papilla characterised by a cap-shaped connective tissue; wide external vagina; and very long internal vagina.

Description. Plehniidae with fleshy and elongated body shape, rounded anteriorly and posteriorly, with high thickness. Length of voucher specimens varies between 4 and 6 mm fixed (average of 6.25 ± 2.06 mm). Ground colouration yellowish-brown with numerous brown spots scattered across the dorsal surface (see Fig. 6A, B). Ventral side pale yellow. Nuchal tentacles present (Fig. 6D). Tentacular eyes arranged in two clusters, located just under the tentacles. Small cerebral eyes in two clusters, extending from the tentacle to the anterior margin (Fig. 6C). Frontal eyes scattered at the anterior body margin. Ruffled pharynx positioned between the second and third regions. Genital pores separated and posterior to the pharyngeal pocket. Ovaries dorsal to the testes.

Reproductive system. Male reproductive complex directed backwards, composed of two spermiducal vesicles, a free prostatic vesicle, and an unarmed penis papilla (Fig. 6E). Vas deferens run ventrally under the vagina and turn backwards once reached the pharynx. Vas deferens expand and distally form spermiducal vesicles. Spermiducal vesicles reach the prostatic vesicle separately and medially (Fig. 7C). Prostatic vesicle large and pear-shaped (0.27 mm high and 0.32 mm wide) with a smooth glandular lining and strong muscular wall (0.12 mm thick). Numerous prostatic glands. Distally, a short penis papilla (0.1 mm long) is housed in a shallow male atrium. Penis papilla surrounded by cap-shaped connective tissue.

Female reproductive systems were large and completely developed in the studied animals (Figs 6F, 7A–C). Wide external vagina (0.08 mm), but not bulbous (Fig. 6F). Narrow, tube-like internal vagina ending in Lang's vesicle. Lang's vesicle is small (Fig. 7B) and oval-shaped (0.07 mm wide). The oviducts open in the distal region of the internal vagina.

Type locality. Cascais, Portugal.

Etymology. The specific name is dedicated to Cascais, the area where the holotype was collected.

Remarks. The presence of a separate opening of the vas deferens into the neck of the prostatic vesicle, the smooth glandular lining, the absence of a seminal vesicle, the long female vagina, and the presence of a well-developed Lang's vesicle allow the inclusion of the specimens in the genus *Plehnia*. *Plehnia* comprises four recognised species: *Plehnia arctica* (Plehn, 1896), *P. ellipsoides* (Girard in Stimpson, 1854), *P. caeca* Hyman, 1953, and *P. ovatus* Kato, 1937.

As shown in Table 3, *Plehnia arctica* and *P. cascaisensis* sp. nov. share only the position of the pharynx. However, many characteristics of *P. arctica* remain unclear due to its insufficient description. Notably, there are differences in size; *P. arctica* is larger and lacks nuchal tentacles, whereas *P. cascaisensis* sp. nov. is smaller and possesses tentacles.

On the other hand, the new species exhibits certain similarities with *P. ellipsoides* (see Table 3), including the

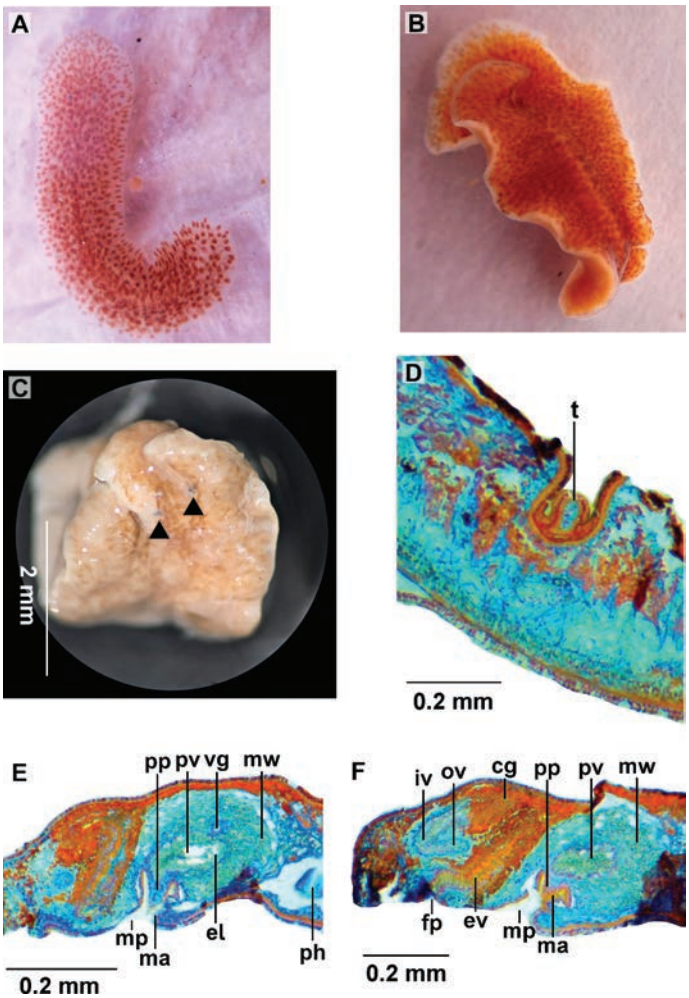

Figure 6. *Plehnia cascaisensis* sp. nov. Histological sections are postero-anteriorly oriented: **A.** Dorsal view of a living specimen (holotype, MNHNC MB16-000107); **B.** Dorsal view of a living specimen (additional material, MB16-000108); **C.** Detail of the eyes (additional material); **D.** Histological section of the tentacle (holotype); **E.** Histological section of the male copulatory organs (holotype); **F.** Histological section of the male and female organs (holotype). Abbreviations: cg, cemental glands; el, epithelial lining; ev, external vagina; fp, female pore; iv, internal vagina; ma, male atrium; mp, male pore; mw, muscular wall; ov, oviduct; ph, pharynx; pp, penis papilla; pv, prostatic vesicle; t, tentacle; vg, vesicular glands.

presence of tentacular, cerebral, and marginal eyespots, as well as similar background colouration. Substantial differences emerge, such as the absence of tentacles in *P. ellipsoides* and the position of the spermiducal vesicles' opening into the prostatic vesicle, which is distally positioned in *P. ellipsoides* and medially positioned in *P. cascaisensis* sp. nov. Additionally, differences in the female reproductive system exist; *P. ellipsoides* has a strong external vagina and an elongated Lang's vesicle, whereas the new species from Cascais has a wide external vagina and a small, rounded Lang's vesicle.

P. cascaisensis sp. nov. and *P. ovatus* are the only *Plehnia* species that share the presence of tentacles and the position of the opening of the spermiducal vesicles into the prostatic vesicle (see Table 3). Nonetheless, *P. ovatus* is smaller and possesses an oval body shape, resembling that of Stylochidae species (see fig. 4 in Kato 1937). In contrast, *P. cascaisensis* sp. nov. is elongated and narrower (Fig. 6A). The dorsal pigmentation also differs, with *P. ovatus* being darkish brown and *P. cascaisensis* sp. nov. being yellowish brown, displaying a spotted pattern. In *P. ovatus*, the prostatic vesicle is elongated, and the penis papilla opens into a large male atrium lined with ciliated cells. In *P. cascaisensis*, the vesicles are rounder and wider, and the penis papilla is contained within a shallow male atrium. The Lang's vesicle in the Japanese species is larger than that in the Iberian species.

P. caeca and *P. cascaisensis* differ externally and within the reproductive system, mainly in the female system. *P. caeca* lacks eyes and tentacles and has an elongated and less muscular prostatic vesicle. *P. caeca* also lacks a Lang's vesicle, and the oviducts empty into the proximal region of the internal vagina. In contrast, *P. cascaisensis* has a well-developed Lang vesicle and oviducts that empty into the distal region of the internal vagina.

All of these differences, as well as the unique characteristics of *P. cascaisensis* sp. nov., such as its spotted dorsal pattern, wide external vagina, and long internal vagina, led us to consider the specimens from Cascais as a distinct species.

Biology. collected in a rocky area covered by a reef of *Sabellaria* Lamarck 1818 (Annelida, Polychaeta).

Distribution. only known from Cascais, Portugal.

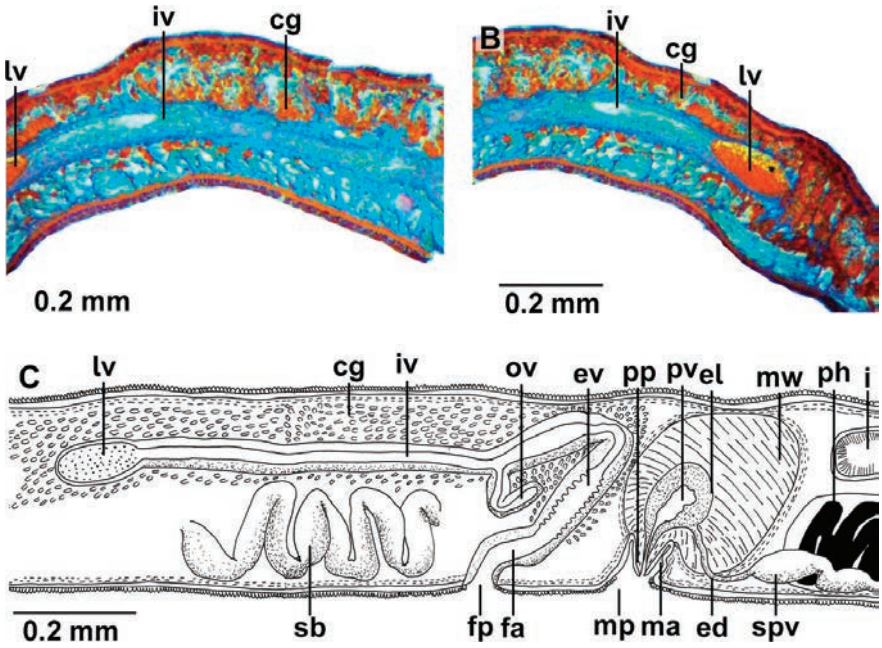

Figure 7. *Plehnia cascaisensis* sp. nov. (holotype, MNHNC MB16-000107). Histological sections are postero-anteriorly oriented: **A.** Histological section of the long internal vagina (holotype); **B.** Histological section of the end of the internal vagina and Lang's vesicle (holotype); **C.** Sagittal reconstruction of the reproductive system (holotype). Abbreviations: cg, cemental glands; ed, ejaculatory duct; el, epithelial lining; ev, external vagina; fp, female pore; i, intestine; iv, internal vagina; lv, Lang's vesicle; ma, male atrium; mp, male pore; mw, muscular wall; ov, oviduct; ph, pharynx; pp, penis papilla; pv, prostatic vesicle; sb, spermiducal bulbs; spv, spermiducal vesicle.

Table 3. Comparison among the species of the genus *Plehnia*.

	Plehnia ellipsoides **(Girard in Stimpson 1854)**	***Plehnia arctica*** **(Plehn, 1896)**	***Plehnia caeca*** **Hyman, 1953**	***Plehnia ovatus*** **(Kato, 1937)**	***Plehnia cascaisensis*** **sp. nov.**
Shape of the body	Elliptical	Oval	Elliptical	Oval	Elongated
Body length	25.4 mm	60 mm	10-14 mm	4.5 mm long (fixed)	9 mm (fixed)
Dorsal colour	Yellowish-brown	-	Whitish-greyish	Darkish brown	Yellowish-brown. Several brown spots scattered
Ventral colour	Grey	-	-	-	Pale yellow
Nuchal tentacles	Absent	Absent	Absent	Present	Present
Tentacular eyes	Present	Not seen	Absent	Present	Present
Cerebral eyes	Present	Not seen	Absent	Present	Present
Marginal eyes	Present	Not seen	Absent	Present	Present
Pharynx	Central	Behind the centre of the body	"…slightly posterior to the central area of the body"	Central	Behind the centre of the body
Genital pores	Separated	Separated	Separated	Separated	Separated
Connection of the spermiducal vesicles with the prostatic vesicle	Distal	Distal	Medial	Medial	Medial
Prostatic vesicle	Large, bulbous	-	Pear-shaped	Large	Pear-shaped
External vagina	Strong	-	Long and vertical	Strong	Wide
Internal vagina	Narrow and long	-	Short and horizontal	Wide	Narrow and very long
Lang's vesicle	Elongated	-	Absent	Large	Small and oval shaped
Distribution	USA, Canada	Norway, Greenland	California (USA)	Japan	Spain
References	Stimpson (1854); Verrill (1893); Hyman (1940)	Plehn (1896); Steinböck (1932)	Hyman 1953	Kato (1937)	This study

Superfamily LEPTOPLANOIDEA Faubel, 1984
Family LEPTOPLANIDAE Stimpson, 1857
Genus *Leptoplana* Ehrenberg, 1831

Leptoplana mediterranea (Bock, 1913)

Fig. 8

Leptoplana tremellaris mediterranea Bock, 1913.

Material examined. • MNHNC MB16-000100, Station 1, 8 September 2016, 24 mm long, sagittal sectioned into 12 slides; • MNHNC MB16-000113, Station 1, 8 September 2016, 24 mm long; • MNHNC MB16-000133, Station 1, 8 September 2016, 24 mm long; • MNHNC MB16-000101, Station 1, 8 September 2016, 22 mm long, sagittally sectioned into 3 slides; • MNHNC MB16-000102, Station 1, 8 September 2016, 23 mm long, sagittally sectioned into 4

slides; • MNHNC MB16-000111, Station 1, 8 September 2016, 18 mm long; • MNHNC MB16-000103, Station 1, 8 September 2016, 25 mm long, sagittally sectioned into 18 slides; • MNHNC MB16-000112, Station 1, 8 September 2016, 20 mm long; • MNHNC MB16-000115, Station 1, 8 September 2016, 21 mm long; • MNHNC MB16-000122, Station 2, 28 October 2018, 17 mm long, sagittally sectioned into 13 slides; • MNHNC MB16-000121, Station 2, 28 October 2018, 17 mm long, sagittally sectioned into 28 slides; • MNHNC MB16-000123, Station 2, 10 November 2018, 14 mm long, sagittally sectioned into 50 slides; • MNHNC MB16-000116, Station 4, 23 February 2019, 23 mm long, sagittally sectioned into 20 slides; • MNHNC MB16-000117, Station 4, 23 February 2019, 28 mm long, sagittally sectioned into 21 slides; • MNHNC MB16-000118, Station 4, 23 February 2019, 19 mm long, sagittally sectioned into 27 slides; • MNHNC MB16-000119, Station 4, 23 February 2019, 13 mm long, sagittally sectioned into 17 slides; • MNHNC MB16-000120, Station 4, 23 February 2019, 18 mm long, sagittally sectioned into 16 slides; • MNCN 4.01/3968 to 3981, Station 11, 10 May 2015, 14 mm long, sagittally sectioned into 13 slides. All of the measurements from the description refer to this specimen; • MNCN 4.01/3382 to 3393, Station 11, 10 May 2015, 11 mm long, sagittally sectioned into 12 slides; • MNCN 4.01/3982, Station 11, 11 April 2016, 11 mm long; • MNCN 4.01/3409 to 3416, Station 12, 6 December 2013, 13 mm long, sagittally sectioned into 8 slides; • MNCN 4.01/3417 to 3428, Station 12, 6 December 2013, 15 mm long, sagittally sectioned into 12 slides; • MNCN 4.01/3429 to 3447, Station 12, 6 December 2013, 17 mm long, sagittally sectioned into 19 slides; • MNCN 4.01/3394 to 3408, Station 12, 6 December 2013, 16 mm long, sagittally sectioned into 15 slides.

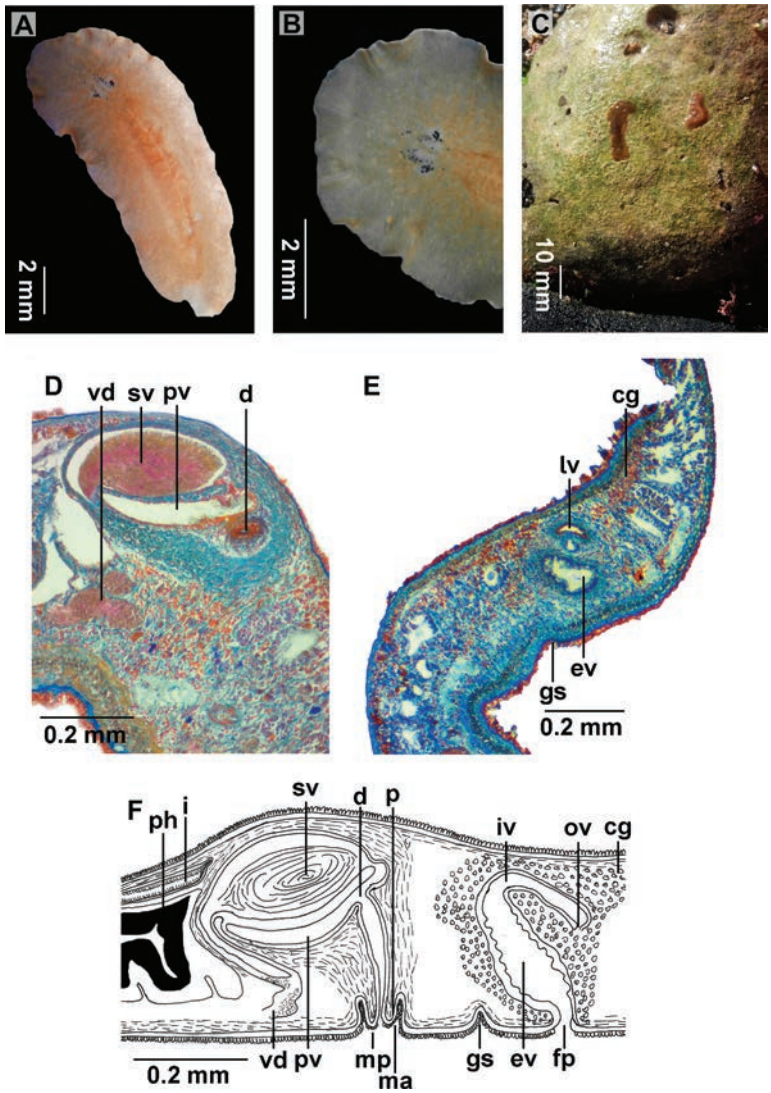

Figure 8. *Leptoplana mediterranea* (MNCN 4.01/3968 to 3981) Histological sections are antero-posteriorly oriented: **A.** Dorsal view of the living specimen; **B.** Detail of the eyes; **C.** Example of the environment where the specimen was found; **D.** Histological section of the male copulatory apparatus; **E.** Histological section of the female copulatory apparatus; **F.** Sagittal reconstruction of the reproductive system. Abbreviations: cg, cemental glands; d, diverticula; ev, external vagina; fp, female pore; gs, genital sucker; i, intestine; iv, internal vagina; ma, male atrium; mp, male pore; ov, oviduct; p, penis; ph, pharynx; pv, prostatic vesicle; sv, seminal vesicle; vd, vas deferens.

Description. Elongated worm, wider in the anterior end and narrower in the posterior end. Length between 11 mm and 31 mm (18.42 ± 4.58 mm). Ground colour of the dorsal surface, beige brownish in the pharynx area (Fig. 8A). Tentacles absent. A whitish colour is observed in the brain area, allowing clear observation of approx. 35 cerebral and 26 tentacular eye clusters (Fig. 8B). Ruffled pharynx between the first and second thirds of the body, mouth opening in the last third. Genital pores separated (approximately 0.33 mm) and located just behind the pharynx.

Reproductive system. Male reproductive system with a true and large seminal vesicle (0.28 mm long × 0.14 mm wide), interpolated prostatic vesicle, and an unarmed penis cirrus, all enclosed in a muscular bulb (Fig. 8F). Vas deferens ventrally positioned, joining together before entering into the seminal vesicle. Seminal vesicle oval-shaped (Fig. 8D). Prostatic vesicle ventrally fastened to the seminal vesicle and separated by an epithelial common wall. Genital sucker located between the male and female pores.

Female complex simple and composed of a wide external vagina and a short and curved internal vagina. Lang's vesicle rudimentary (Fig. 8E, F). Numerous shell glands surround the whole female system.

Remarks. These diagnostic characters are present in the specimens collected during the present study, so this is the first report of the presence of *L. mediterranea* outside the Mediterranean.

Likewise, it is possible that the specimens found by Saldanha (1974) reported as *L. tremellaris* belong to *L. mediterranea* as well since some specimens of *L. mediterranea* were found close to Arrabida. However, this hypothesis needs to be confirmed with histological sections.

Biology. Under rocks (Fig. 8C, present study), but it was also found with *Caulerpa prolifera* (Chlorophyta) (Marquina et al. 2014a).

Distribution. Widely distributed along the Mediterranean coasts, *L. mediterranea* was reported as *L. tremellaris* "forma mediterranea" in Palermo (Grube 1840), Naples (Lang 1884; Palombi 1936), the Gulf of Lyon (Pruvot 1897), Trieste (Micoletzky 1910), Port Said (Palombi 1928), the Adriatic Sea (Steinböck 1933), the Italian coasts (Galleni and Gremigni 1989), and Catalonia (Novell 2001. Tunisia (Gammoudi et al. 2012, 2017); Mar Menor, SE Spain (Marquina et al. 2014a); and the southern plus western Iberian Peninsula (present study). This is the first record of *L. mediterranea* in Oporto (Portugal).

Genus *Parviplana* Hyman, 1953

Parviplana jeronimoi Pérez-García, Noreña & Cervera, 2018

Fig. 9

Material examined. • MNCN 4.01/4263, Station 11, 23 December 2014, 29 mm.

Type locality. La Caleta Beach, Cádiz.

Description. *Parviplana* species with elongated body shapes, dorsal background colour yellow-brown, ventrally pale yellow. Paired cerebral and tentacular eyes. Genital pores separated. Male apparatus with a true seminal vesicle, interpolated and bulb-shaped prostatic vesicle, and massive penis papilla, while the female system shows a vagina bulbosa and a well-developed Lang's vesicle (for more details, see Pérez-García et al. 2019).

Remarks. The genus *Parviplana* comprises four species and is one of the least numerous genera within Polycladida. *Parviplana jeronimoi* is a very common species in Cadiz and Sancti Petri (Chiclana). Nevertheless, this species has not been reported in other localities until now. The other species of the genus are *Parviplana hymani* Faubel, 1983, and *P. lynca* (Du-Bois Reymond Marcus, 1958), which are from the Pacific and West Atlantic Oceans, respectively. Finally, after the Iberian species were described, *P. sodade* was described by Cuadrado et al. (2021) from Cape Verde.

Biology. This species was collected and always observed under stones in the intertidal zone.

Distribution. only known from several localities on the coasts of Cadiz, southern Spain (see Pérez-García et al. 2019).

Family GNESIOCEROTIDAE Du-Bois Reymond Marcus & Marcus, 1966
Genus *Echinoplana* Haswell, 1907

Echinoplana celerrima Haswell, 1907

Fig. 10

Material examined. • MNHNC MB16-000104, Station 7, 13 May 2018, 16 mm long. All the measurements from the description refer to this specimen; • MNCN 4.01/3983, Station 11, 19 February 2015, 9 mm long.

Morphology. Elongated worm, wider in the anterior margin with a blunt end (Fig. 10A). Length between 9 and 16 mm alive (12.5 ± 4.95 mm). Dorsal colour caramel and translucent intestinal branches are easily observed and vary from brown to green. Central part of the body darkish brown. Tentacles absent. Tentacular and cerebral eye clusters present, distributed parallelly and in two long rows (Fig. 10B). Tentacular and cerebral eyes clustered in approximately 32 and 43 eyes, respectively. Pharynx ruffled, located in the second third of the body. Oral pore in the last third of the pharynx.

Reproductive system. Genital pores separated (separated approximately 2.26 mm). Male apparatus (4.3 mm long) characterised by a seminal vesicle, an interpolated prostatic vesicle, and a conspicuous cirrus shown by transparency (Fig. 10C). Female system with a large vagina (2.29 mm), a ductus vaginalis, and Lang's vesicle in its distal region.

Remarks. *Echinoplana celerrima* is the only species of the genus *Echinoplana* described by Haswell (1907) from

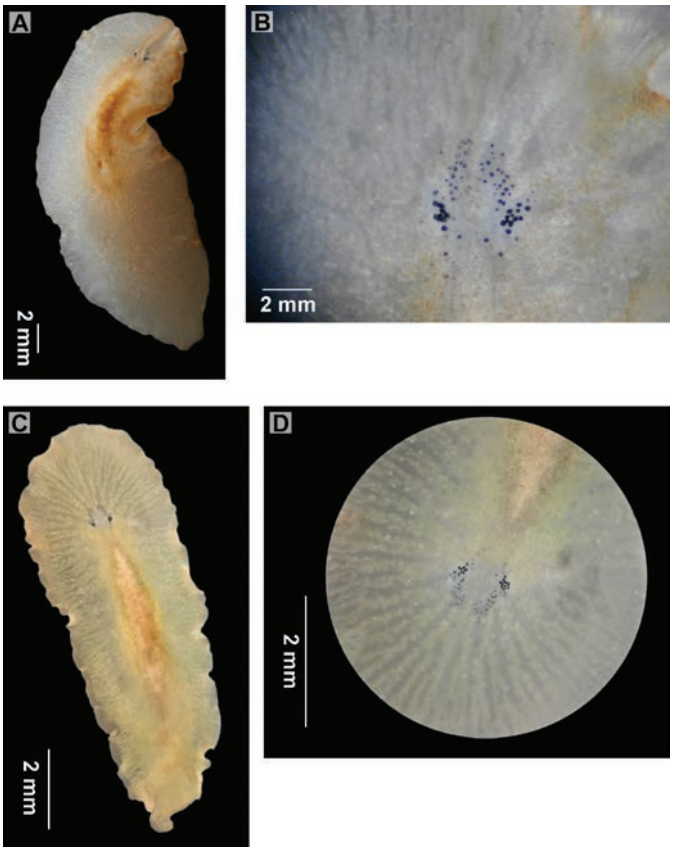

Figure 9. *Parviplana jeronimoi* (MNCN 4.01/4263): **A–C.** Dorsal view of living specimens; **B–D.** Detail of the eyes.

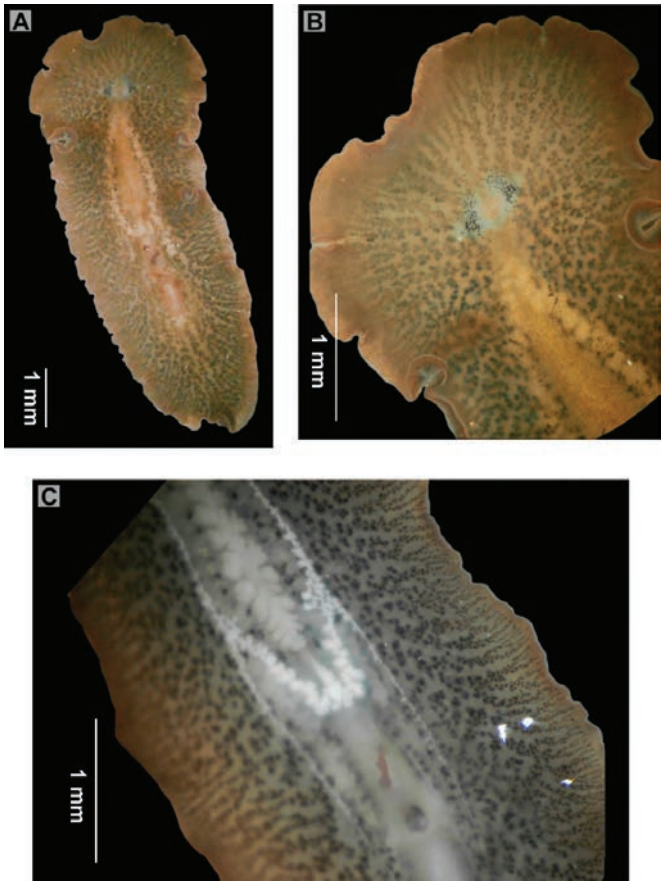

Figure 10. *Echinoplana celerrima* (MNHNC MB16-000120): **A.** Dorsal view of the living specimen; **B.** Detail of the eyes; **C.** Ventral view of the living specimen, showing the male copulatory apparatus.

Port Jackson, Sidney, Australia. After that, Galleni (1978) reported this species in the Port of Livorno, Italy, which was the first record of the species in the Mediterranean. Later, Holleman (2007) reported this species on the Pacific coast on the North Island of New Zealand. *E. celerrima* was also recorded in the lagoon of Tunis (Gammoudi et al. 2009; 2017) and now in the southern Iberian Peninsula (present study). Considering the geographical distance between the specimens from Australia, New Zealand, and the Mediterranean Sea, the contrast of information provided by the morphological characteristics and the DNA analyses (using nuclear and mitochondrial markers) is crucial to elucidating whether the populations belong to the same species.

Biology. In this study, the specimens were collected under stones in the intertidal zone. Furthermore, *Echinoplana celerrima* frequently inhabits areas with human activity, such as harbours (Haswell 1907, Galleni 1978). Hence, the specimen of Sagres was precisely collected in a rocky area attached to a harbour zone, supporting one of the possible scenarios about the dispersion of this species (Prudhoe 1982).

Distribution. As previously explained, *Echinoplana celerrima* is widely distributed on the southeastern coast of Australia (Haswell 1907; Prudhoe 1982; Johnston and Lee 2008; Rodríguez et al. 2021), Livorno, Italy (Galleni 1978), New Zealand (Holleman 2007), Tunisia (Gammoudi et al. 2009, 2017), and Catalonia, Spain (Gammoudi and Tekaya 2012). Our specimens provide the first reports of this species on the North-Atlantic shores of Portugal and Andalusia (Spain).

Family NOTOPLANIDAE Du-Bois Reymond Marcus & Marcus, 1966
Genus *Notoplana* Laidlaw, 1903

Notoplana alcinoi (Schmidt, 1861) Bock, 1913

Fig. 11

Leptoplana alcinoi Schmidt, 1861.
Opisthoporus tergestinus Minot, 1877.

Material examined. • MNCN 4.01/3476 to 3492, Station 11, 29 April 2014, 23 mm long, sagittal sectioned into 17 slides. All of the measurements from the description refer to the following specimens: • MNCN 4.01/3984, Station 11, 19 February 2015, 9 mm long; • MNCN 4.01/3985 to 4007, Station 11, 10 May 2015, 10 mm long, transversally sectioned into 22 slides; • MNCN 4.01/4008, Station 11, 10 May 2015, 22 mm long; • MNCN 4.01/4083, Station 11, 19 May 2016, 23 mm long; • MNCN 4.01/4084, Station 11, 19 May 2016, 16 mm long; • MNCN 4.01/3955, Station 11, 22 March 2019, 16 mm long; • MNCN 4.01/4009 to 4045, Station 12, 21 March 2015, 21 mm long, transversally sectioned into 37 slides; • MNCN 4.01/4046 to 4070, Station 12, 21 March 2015, 16 mm long, sagittally sectioned into 25 slides; and • MNCN 4.01/4071 to 4082, Station 12, 18 April 2015, 11 mm long, sagittally sectioned into 12 slides.

Description. Notoplanidae with elongated and narrow body, very delicate and fragile appearance. Maximum length alive approximately 23 mm (mean 16.7 ± 5.41). Without tentacles. Transparent, whitish background colour, sometimes with a yellowish spot in the pharynx area (Fig. 11A). Visible intestinal branches colouring the dorsal surface with brownish or dark green shades. Paired tentacular and cerebral eye clusters present, with 9 tentacular and 17 cerebral eyes in each cluster (Fig. 11B). Pharynx ruffled, located between the first and second thirds of the body. Mouth opening in the last third of the pharynx. Gonopores separated but very close together (at 0.1 mm distance) behind the pharyngeal cavity (Fig. 11D, E).

Reproductive system. Male copulatory apparatus is composed of a true seminal vesicle, an interpolated prostatic vesicle, and a deep atrium that hosts a stylet (Fig. 11E). Vas deferens enter the seminal vesicle separately. Seminal vesicle elongated, bent in two sections. Prostatic vesicle rounded and large (0.54 mm long and 0.4 mm wide) with five tubular chambers joined to the ejaculatory duct (Fig. 11C, E). One specimen with 8 chambers instead of 5 (see Fig. 11F). Muscular wall of the prostatic vesicle (0.12 mm wide) crossed by numerous extravesicular glands. Penis stylet long (0.6 mm), slender and pointed, and housed in a deep atrium (0.42 mm).

Female copulatory apparatus consists of a smooth external vagina, a narrow internal vagina, and an elongated Lang's vesicle (Fig. 11D, E). Numerous cement glands surround the whole female organs. The external vagina curves dorsally to the posterior end. The common oviduct enters the internal vagina ventrally. Lang's vesicle is large (0.5 mm) and wavy, extending backwards (Fig. 11E).

Remarks. *Notoplana* is one of the most species-rich genera within Polycladida, with 36 accepted species (Tyler et al. 2006–2024). Regarding the Mediterranean Sea and the Atlantic coasts of the Iberian Peninsula, the recorded species of this genus are *N. atomata* (Müller OF, 1776) Bock 1913 and *N. vitrea* (Lang, 1884) Bock 1913 (Novell 2001 Marquina et al. 2014b), which are species from northern and southern Europe, respectively. More recently, *N. alcinoi* was recorded in Tunisia (Gammoudi et al. 2017).

Our identification of *N. alcinoi* was based on the description and the drawings provided by Lang (1884), because the original description (Schmidt 1861) is too brief for comparison. The specimens of *N. alcinoi* from Cádiz and those described by Lang hardly differ, except for the folded external vagina and the large Lang's vesicle in comparison to the smooth external vagina and short Lang's vesicle described by Lang. However, these female features depend on the state of maturation (Litvaitis et al. 2019).

Biology. Collected from rocky substrates in the intertidal zone. The original description mentioned the presence of this species in the algae *Ellisolandia* and *Chondria* (Rhodophyta) environments.

Distribution. This species was reported for the first time in Corfu, Greece (Schmidt 1861) and later in Trieste, Italy (Minot 1876; Micoletzky 1910), Naples, Italy (Lang 1884), Cape Verde (Laidlaw 1906), and Tunisia (Gam-

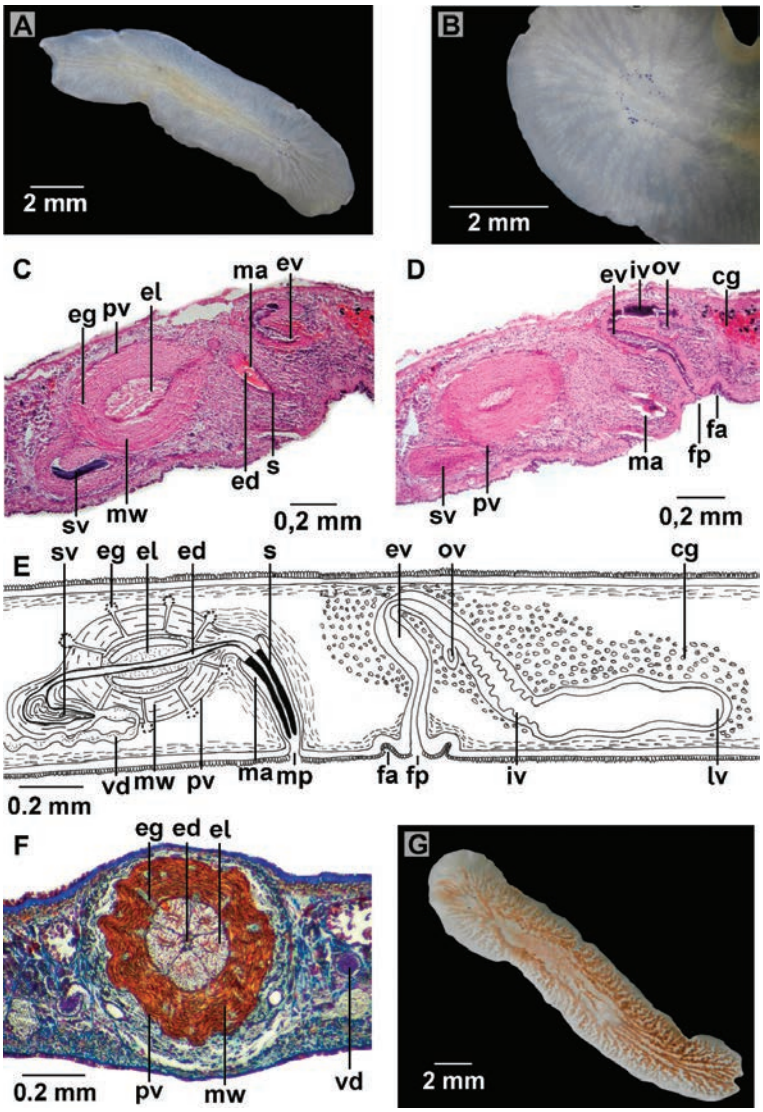

Figure 11. *Notoplana alcinoi* (MNCN 4.01/3476 to 3492). Histological sections are antero-posteriorly oriented: **A.** Dorsal view of the living specimen; **B.** Detail of the eyes; **C.** Histological section of the male copulatory organs; **D.** Histological section of the female copulatory organs; **F.** Transversal section of the prostatic vesicle; **G.** Dorsal view of a living specimen showing a different morphotype (MNCN 4.01/4008). Abbreviations: cg, cemental glands; ed, ejaculatory duct; eg, extravesicular glands; el, epithelial lining; ev, external vagina; fa, female atrium; fp, female pore; i, intestine; iv, internal vagina; lv, Lang's vesicle; ma, male atrium; mp, male pore; mw, muscular wall; ov, oviduct; pv, prostatic vesicle; s, stylet; sv, seminal vesicle; vd, vas deferens.

moudi et al. 2017). The presence of this species in the Iberian Peninsula is reported for the first time.

Family PLEIOPLANIDAE Faubel, 1983
Genus *Izmira* Bulnes, 2010

Izmira lusitanica sp. nov.

https://zoobank.org/00043DB7-4270-48F4-AB2D-BC5533D3094F
Fig. 12

Holotype. • MNHNC MB16-000124, Station 4, 8 December 2018, 21 mm fixed, sagittal sectioned into 16 slides.

Additional material. • MNHNC MB16-000134, Station 4, 9 March 2019, 13 mm, juvenile.

Diagnosis. Pleioplanidae with transparent body; tentacles absent; with cerebral eyes, gonopores separated; small and bean-shaped seminal vesicle; prostatic vesicle oval; elongated penis papilla; female apparatus with a vagina bulbosa.

Description. Body shape elongated and delicate, widened anteriorly and tapered distally. The mature specimen is approximately 21 mm long when alive, while the juvenile specimen is approximately 13 mm in length.

Dorsal surface transparent, brownish-coloured intestinal branches easily observable (Fig. 12A), central longitudinal area lacks pigmentation. Ventral side translucent. Tentacles absent. Paired clusters of tentacular and cerebral eyes present, with approximately 28 tentacular eyes and 42 cerebral eyes in each cluster (Fig. 12B). Pharynx ruffled and centrally located between the second and third fourths of the body, oral pore at the beginning of the last third of the pharynx. Gonopores separated and located between the third and the last fourth of the body.

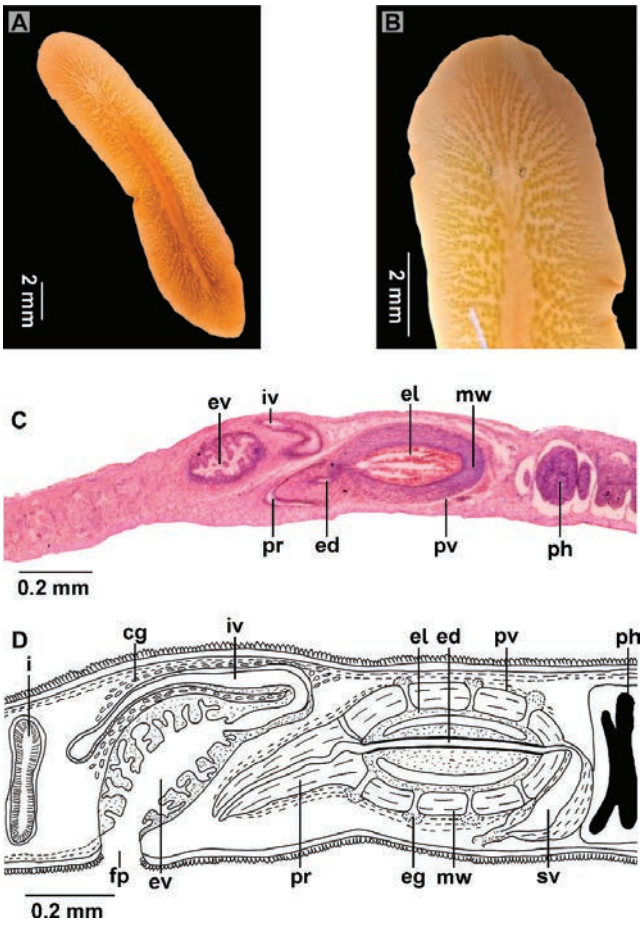

Figure 12. *Izmira lusitanica* sp. nov. (holotype, MNHNC MB16-000124). Histological sections are postero-anteriorly oriented: **A.** Dorsal view of a living specimen; **B.** Detail of the tentacular and cerebral eyes (holotype); **C.** Histological section of the reproductive system (holotype); **D.** Sagittal reconstruction of the reproductive system (holotype). Abbreviations: cg, cemental glands; ed, ejaculatory duct; eg, extravesicular glands; el, epithelial lining; ev, external vagina; fp, female pore; i, intestine; iv, internal vagina; mw, muscular wall; ph, pharynx; pr, penis rod; pv, prostatic vesicle; sv, seminal vesicle.

Reproductive system. Male reproductive organs composed of a true seminal vesicle, an interpolated oval-shaped prostatic vesicle, and a long penis rod. Vas deferens thick, forming spermiducal bulbs that run ventrally and proximally and enter separately into the seminal vesicle. Seminal vesicle bean-shaped and small (0.25 mm) located proximal to the prostatic vesicle (Fig. 12D). Prostatic vesicle well developed (0.5 mm), with chambered epithelial linings (Fig. 12C, D). Ejaculatory duct runs from the proximal to the distal end of the prostatic vesicle. Penis papilla muscular, broad (0.35 mm long; 0.09 mm wide), and conical (Fig. 12C, D). Diameter of the penis papilla decreases from proximal to distal.

Female copulatory apparatus with a wide external vagina (0.21 mm) with several folds and a bulbous vagina (Fig. 12C, D). Internal vagina long and narrow, without Lang's vesicle. Several cement glands surround the internal vagina.

Type locality. Area Marinha Protegida das Avencas, Parede, Cascais, Portugal.

Etymology. The specific name refers to Lusitania, the original Roman name of the region from Portugal where the holotype was collected.

Remarks. The genus *Izmira* was established by Bulnes in 2010 based on specimens from the Aegean Sea. The representatives of this genus are characterised by an oval or elongated body, absence of tentacles, presence of tentacular eyes, absence of cerebral, frontal, or marginal eyes, separated gonopores, a true seminal vesicle, an interpolated "*atomata*" type of prostatic vesicle, a penis rod, and a female reproductive system with a vagina bulbosa and without Lang's vesicle. The species described in the present work shows these features except for the presence of cerebral eyes, which are observable in *I. lusitanica* sp. nov.

The genus *Izmira* comprises only two previously known species: *I. cinari* Bulnes 2010 and *I. turkeyi* Bulnes 2010. *I. lusitanica* sp. nov. shares several characteristics with *I. turkeyi*, including separated gonopores, the presence of spermiducal bulbs, a similar length of the penis rod, and a similar structure of the vagina bulbosa. However, they exhibit notable differences; for instance, the body shape of *I. turkeyi* is oval, whereas that of *I. lusitanica* sp. nov. is elongated; the colouration of *I. turkeyi* tends to be dark, whereas that of *I. lusitanica* sp. nov. is distinctly transparent; and *I. turkeyi* possesses tentacle

knobs, a feature absent in the new species. Furthermore, the presence of cerebral eyes distinguishes the two species; *I. turkeyi* lacks them, whereas *I. lusitanica* sp. nov. has them. Notably, *I. turkeyi* has a seminal vesicle longer than the prostatic vesicle, whereas *I. lusitanica* sp. nov. has a bean-shaped seminal vesicle, smaller than the prostatic vesicle. Moreover, the prostatic vesicle is small and rounded in *I. turkeyi* but large and oval-shaped in the new species. The shape of the penis papilla also differs significantly: in *I. turkeyi*, the penis papilla forms a rounded pouch distally, whereas in *I. lusitanica* sp. nov., it narrows and has a conical shape.

On the other hand, significant differences exist between *I. cinari* and *I. lusitanica*. sp. nov.. *I. cinari* is light brown and darker medially, while *I. lusitanica* sp. nov. is transparent. Cerebral eyes are absent in *I. cinari* but present in *I. lusitanica* sp. nov.. The seminal vesicle in *I. cinari* is longer than the prostatic vesicle, whereas in *I. lusitanica* sp. nov., it is bean-shaped and small. Additionally, the prostatic vesicle is different: rounded in *I. cinari* and large and oval in *I. lusitanica* sp. nov.. The penis papilla of the Turkish species is longer than that of the new species.

These observed differences between the valid *Izmira* species and the unique combination of characteristics observed in *I. lusitanica* sp. nov. led us to consider the specimens from Avencas as a new species. This is the first record of the genus *Izmira* outside the Mediterranean.

Family STYLOCHOPLANIDAE Faubel, 1983
Genus *Emprosthopharynx* Bock, 1913

Emprosthopharynx onubensis sp. nov.

https://zoobank.org/8B51F8D2-5B3B-484A-927C-8B7E6DA4BB32

Fig. 13

Holotype. • MNCN 4.01/2799 to 2819, Station 10, 21 February 2019, 25 mm, sagittal sectioned into 20 slides.

Diagnosis. Elongated oval Stylochoplanidae with yellowish brown colour; tentacles absent; gonopores separated; with spermiducal bulbs and tubular seminal vesicle; interpolated prostatic vesicle pear-shaped, with smooth irregular epithelium; female apparatus with vagina bulbosa; without Lang's vesicle.

Description. Elongated oval body, with few marginal folds. Dorsal colouration yellowish-brown with a translucent appearance and intense pigmentation in the pharyngeal region (Fig. 13A, B). Intestinal branches patent. Ventral side yellowish-brown. Without tentacles. Clusters of tentacular and cerebral eyes located anterior to the brain, with 19 tentacular eyes and 21 cerebral eyes per cluster (Fig. 13C). Few cerebral eyes posterior to the brain. Pharynx ruffled in the first half of the body, and the oral pore in the second third of the pharynx. Gonopores separated (0.9 mm) and positioned immediately behind the pharynx.

Reproductive system. Male copulatory apparatus comprises spermiducal bulbs (Fig. 13D), an interpolated prostatic vesicle encircled by well-developed muscle layers and crossed by extravesicular glands, and a short penis papilla (Fig. 13E, G). Vasa deferentia ventrally and dilated in spermiducal bulbs enter separated into the tubular seminal vesicle (Fig. 13E). Prostatic vesicle elongated and oval, 1 mm in length, with a thick muscular wall (0.18 mm wide). Epithelial lining of the prostatic vesicle well-developed and irregular. Penis papilla short (0.2 mm long) and opens distally into a ciliated male atrium (0.18 mm wide and 0.36 mm deep), including a characteristic diverticulum just before the male pore (Fig. 13E).

The female reproductive system comprises a folded and ciliated external vagina and the vagina bulbosa (Fig. 13F). The external vagina extends dorsally and then curves backwards, forming a narrower internal vagina. Without Lang's vesicle.

Type locality. El Portil, Huelva, Spain.

Etymology. The specific name refers to Onuba, the Latin name of Huelva, the area where the holotype was collected.

Remarks. The genus *Emprosthopharynx* was established by Bock in 1913 and classified within the family Stylochoplanidae. This family is characterised by a simple male copulatory apparatus, a small tubular seminal vesicle, a prostatic vesicle lined with irregular epithelium, and a female reproductive system lacking Lang's vesicle (Fig. 13D).

In Table 4, it is evident that *E. onubensis* sp. nov. exhibits unique characteristics that distinguish it from other species within the genus, leading to the classification of a new species. Its external morphology includes yellow-brown dorsal pigmentation, numerous tentacular (19), and cerebral eyes (21). Furthermore, it shares common features with few species, such as an elongated-oval body shape, a larger body size (more than 20 mm), and a pyriform prostatic vesicle, characters found in *E. rasae* only.

E. onubensis sp. nov. lacks tentacles, but the presence of this structure is not a very distinctive feature within the genus. For example, some species like *E. gracilis* and *E. hancocki* have tentacles, while others such as *E. opisthoporus* and *E. vanhoffeni* have a rudimentary form of tentacle.

Of the nine species currently recognised in the genus (including *E. onubensis* sp.nov.), only *E. opisthoporus*, *E. rasae*, and *E. vanhoffeni* have marginal eyes. The other six species, including *E. onubensis* sp. nov., lack marginal eyes. Usually, the pharynx is centrally located in the *Emprosthopharynx*, but four species (*E. opisthoporus*, *E. rasae*, *E. heroniensis*, and *E. lysiosquillae*) share with *E. onubensis* sp. nov. an anterior pharynx position.

E. onubensis sp. nov. has separate gonopores, a shared feature with *E. pallida*, *E. opisthoporus*, *E. rasae*, and *E. lysiosquillae*. The other species have closely located gonopores. The prostatic vesicle in *E. onubensis* sp. nov. is pyriform, similar to *E. rasae*. In other species, the prostatic vesicle is oval, rounded, or elongated. Despite most species having an oval, rounded, or elongated seminal vesicle, *E. heroniensis* has a pear-shaped seminal vesicle, and *E. lysiosquillae* has a bean-shaped vesicle.

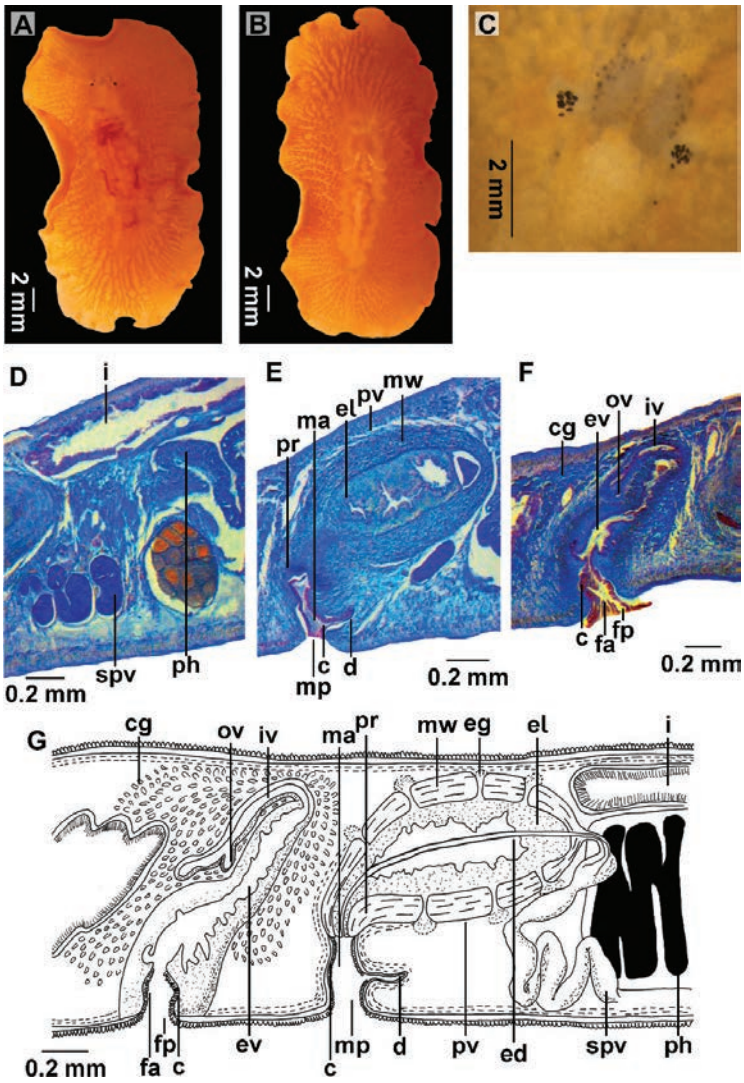

Figure 13. *Emprosthopharynx onubensis* sp. nov. (holotype MNCN 4.01/2799 to 2819). Histological sections are postero-anteriorly oriented: **A.** Dorsal view of a living specimen; **B.** Ventral view; **C.** Detail of the eyes; **D.** Histological section of the spermiducal vesicles; **E.** Histological section of the male copulatory organs; **F.** Histological section of the female organs; **G.** Sagittal reconstruction of the reproductive system. Abbreviations: c, cilia; cg, cemental glands; d, diverticulum; ed, ejaculatory duct; eg, extravesicular glands; el, epithelial lining; ev, external vagina; fa, female atrium; fp, female pore; i, intestine; iv, internal vagina; ma, male atrium; mp, male pore; mw, muscular wall; ov, oviduct; ph, pharynx; pr, penis rod; pv, prostatic vesicle; spv, spermiducal vesicles; sv, seminal vesicle.

Furthermore, *E. onubensis* sp. nov. has a tubular seminal vesicle, a feature shared with *E. vanhoffeni*. The penis papilla of *E. onubensis* sp. nov. is short, like most of the species within the genus. This one is distinguished from the elongated papilla of *E. pallida* and *E. heroniensis* and the pointed papillae of *E. hancocki* and *E. lysiosquillae* as well.

The genus *Emprosthopharynx* is known from the American Pacific coast (e.g., *E. gracilis* and *E. hancocki* are from California), Australia (*E. heroniensis*), Hawaii (*E. rasae*), Ecuador (*E. opisthoporus*), and Japan (*E. lysiosquillae*). On the other hand, E. *pallida* and *E. vanhoffeni* are known from the Cape Verde coast. *E. pallida* is also known from the Italian Mediterranean coast. *E. onubensis* sp. nov. represents the first record for the European and Iberian Atlantic coasts.

Genus *Comoplana* Faubel, 1983

Comoplana agilis (Lang, 1884) Faubel, 1983

Fig. 14

Stylochoplana agilis Lang, 1884.

Material examined. • MNHNC MB16-000125, Station 4, 8 December 2018, 8 mm long; • MNHNC MB16-000126, Station 8, 16 May 2018, 4 mm long; • MNHNC MB16-000127, Station 8, 17 May 2018, 3 mm long; • MNCN 4.01/3631 to 3633, Station 11, 28 October 2015, 4 mm long, sagittally sectioned into 3 slides; • MNCN 4.01/4085, Station 11, 28 October 2015, 4 mm long; and • MNCN 4.01/34634 to 3635, Station 11, 29 October 2015, 6 mm long, sagittally sectioned into 2 slides. All of the

Table 4. Comparison among the species of the genus *Emprosthopharynx*.

	***E. pallida* (Quatrefage, 1845)**	***E. gracilis* (Heath & Mcgregor, 1912)**	***E. opistho-porus* Bock, 1913**	***E. hancocki* (Hyman, 1953)**	***E. rasae* Prudhoe, 1968**	***E. her-oniensis* Beveridge, 2018**	***E. lysiosquillae* Oya, Nakajima & Kajihara, 2022**	***E. vanhoffeni* Bock, 1931**	***E. onubensis* sp. nov.**
Body Shape	Oval, pointed end	Oval,	Oval	Oval	Elongated oval	Oval	Oval	Oval	Elongated oval
Body length	20 mm	7.5 mm	9 mm	6 mm	20 mm	22 mm	2.6-5.8 mm	9.5 mm	25 mm
Dorsal colour	Transparent	Brownish-yellow	Pale yellow	-	Reddish-brown	Pale orange	Whitish	Grey (conserved)	Yellowish brown
Tentacles	Absent	Present	Rudimentary	Present	Absent	Absent	Absent	Rudimentary	Absent
Tentacular eyes per cluster	-	4 eyes	4 eyes	4 eyes	2-4 eyes	10-12 eyes	Absent	5-6	19 eyes
Cerebral eyes `per cluster	-	14 eyes	7 eyes	8 eyes	3-5 eyes	5-8 eyes	2-6 eyes	4 eyes	21 eyes
Marginal eyes	Absent	Absent	Present	Absent	Present	Absent	Submarginal eyes present	Present	Absent
Pharynx	Central	Central	Somewhat anterior	Central	Somewhat anterior	Somewhat posterior	Somewhat anterior	Central	Somewhat anterior
Genital pores	Separated	Close together	Separated	Close together	Separated	Close together	Separated	Close together, in the caudal end	Separated
Prostatic vesicle	Oval	Round-oval	Oval	Cylindrical	Piriform	Elongated	Elongated	Elongated oval	Piriform
Seminal vesicle	Elongated	Oval	Rounded	Elongated	Elongated	Pear shaped	Bean-shaped	Tubular	Tubular
Penis papilla	Long	Short	Short	Pointed	Short	Long	Pointed penis stylet	Short	Short
Distribution	Italy, Cape Verde and Suez Canal	California	Ecuador	California	Hawaii	Australia	Japan	Cape Verde	Spain
References	Quatrefages (1845); Laidlaw (1903); Palombi (1928)	Heath and McGregor (1913); Hyman (1953)	Bock (1913)	Hyman (1953)	Prudhoe (1968)	Beveridge (2018)	Oya et al. 2022	Bock (1931)	This study

measurements from the description refer to this specimen; • MNCN 4.01/4086, Station 11, 19 June 2018, 3 mm long; • MNCN 4.01/4087, Station 11, 19 June 2018, 3 mm long.

Description. small Stylochoplanidae, with lengths varying between 3 mm and 8 mm (4.33 ± 1.66 mm). Body shape elongated much wider in the anterior region and at the blunt posterior end (Fig. 14A). Dorsal colour differs from dark brown to dark green, with white or cream spots along the central longitudinal area. Conspicuous, cylindrical tentacles located at the anterior end to the beginning of body narrowing. Tentacular eyes (approximately 6 eyes per cluster) inside the tentacles and cerebral eyes (16 eyes per cluster) around the base of the tentacles. (Fig. 14B). Pharynx ruffled, located more or less central. Oral pore situated in the posterior part of the pharynx. Genital pores joining in a common atrium (Fig. 14C–E).

Reproductive system. Male copulatory system with true seminal vesicle, interpolated prostatic vesicle, and conical penis papilla (Fig. 14C–E). Vas deferens run ventrally and enter proximally into the seminal vesicle through a common duct. Seminal vesicle voluminous (0.12 mm long and 0.23 mm wide), kidney-shaped, and connected proximally to the prostatic vesicle. A narrow ejaculatory duct runs from the seminal vesicle to the lumen of the prostatic vesicle (Fig. 14D). Prostatic vesicle more or less rounded and well-developed (0.2 mm long and 0.28 mm wide), with a thick muscular wall (0.04 mm) pierced by extravesicular glands. Epithelial lining of the prostatic vesicle smooth. Penis papilla 0.2 mm long, with a sinuous trajectory to the deep and ciliated common atrium.

Female system with a narrow external and internal vagina, Lang's vesicle present (Fig. 14D). External vagina runs dorsally and turns backwards, continuing to the internal vagina, which receives the common oviduct ventrally. Lang's vesicle large, rounded (0.15 mm long and 0.1 mm wide), and lies on the ventral side of the body (Fig. 14C–E).

Biology. Due to its small size and colouration, this species is very cryptic on substrates such as stones or sand. The specimens studied were mainly found on algae such as *Halopteris scoparia*, *Dictyota dichotoma* (Ochrophyta), and *Ellisolandia elongata* (Rodophyta).

Distribution. Widely known from the Mediterranean, this species was reported in Naples, Italy (Lang 1884), the coasts of Catalonia (Novell 2001), and the Atlantic coasts of Europe, such as Galicia (Aguado et al. 2017), the North Sea (Karez 1991; Harms 1993), and the British coasts (Howson and Picton 1997). This is the first report of this species in Portugal and Andalusia.

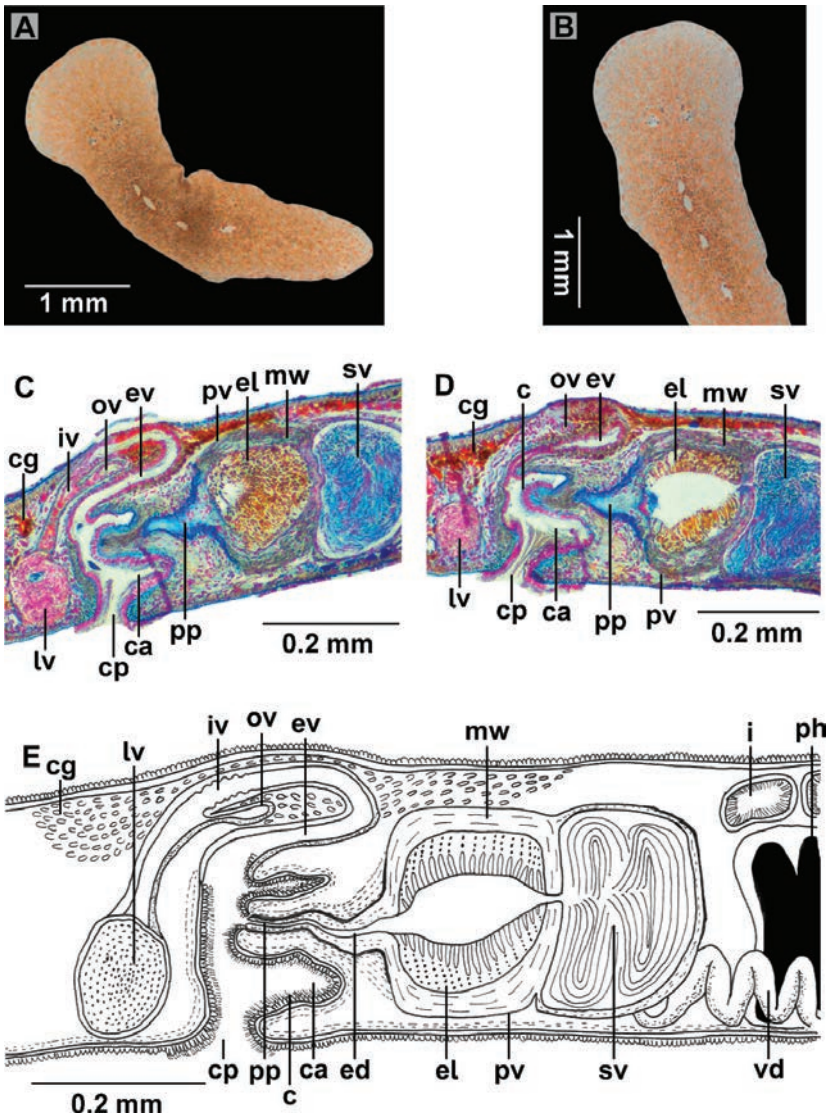

Figure 14. *Comoplana agilis* (MNCN 4.01/34634 to 3635). Histological sections are postero-anteriorly oriented: **A.** Dorsal view of the living specimen; **B.** Detail of the tentacles and eyes; **C, D.** Histological sections of the reproductive system; **E.** Sagittal reconstruction of the reproductive system. Abbreviations: c, cilia; ca, common atrium; cp, common pore; cg, cemental glands; ed, ejaculatory duct; el, epithelial lining; ev, external vagina; i, intestine; iv, internal vagina; lv, Lang's vesicle; mw, muscular wall; ov, oviduct; ph, pharynx; pp, penis papilla; pv, prostatic vesicle; sv, seminal vesicle; vd, vas deferens.

Genus *Phaenoplana* Faubel, 1983

Phaenoplana caetaria Pérez-García, Noreña & Cervera, 2018

Fig. 15

Material examined. Specimen found in the field, Station 16, 19 May 2015, 13 mm; specimen found in the field, Station 16, 19 May 2015, 21 mm; specimen found in the field, Station 17, 19 April 2015, 24 mm.

Type locality. Punta Carnero, Cádiz, Spain.

Description. Stylochoplanidae with elongated body, wider anteriorly, and folded within the margins. Length between 24 mm and 13 mm (19.3 ± 5.69). Colour of the dorsal surface light brown with yellowish spots (Fig. 15A, C). Ventral surface pale brown. Tentacles absent. Tentacular and cerebral eyes arranged in two clusters, with approximately 15 tentacular eyes and 27 cerebral eyes in each cluster (Fig. 15B, D). Pharynx ruffled, positioned slightly anteriorly, between the first and second thirds of the body. Opening of the mouth in the last third of the pharynx. Genital pores separated. Male copulatory apparatus composed of a true seminal vesicle, an interpolated prostatic vesicle, and a penis papilla with a penis rod. Female complex consists of a well-developed external vagina (vagina bulbosa) and reduced Lang's vesicle (for more details, see Pérez-García et al. 2019).

Remarks. After the original description of *Phaenoplana caetaria* (Pérez-García et al., 2019), Oya and Kajihara (2019) described a new species of *Phaenoplana* from Japan (*P. kopepe*), increasing the number of species in this genus to six. In this context, *P. kopepe* is differentiated from *P. caetaria* by the presence of tentacles, a muscular bulb that surrounds the prostatic vesicle, the shaft of the penis, and the male atrium, a character that is missing in *P. caetaria*, which shows instead a very characteristic

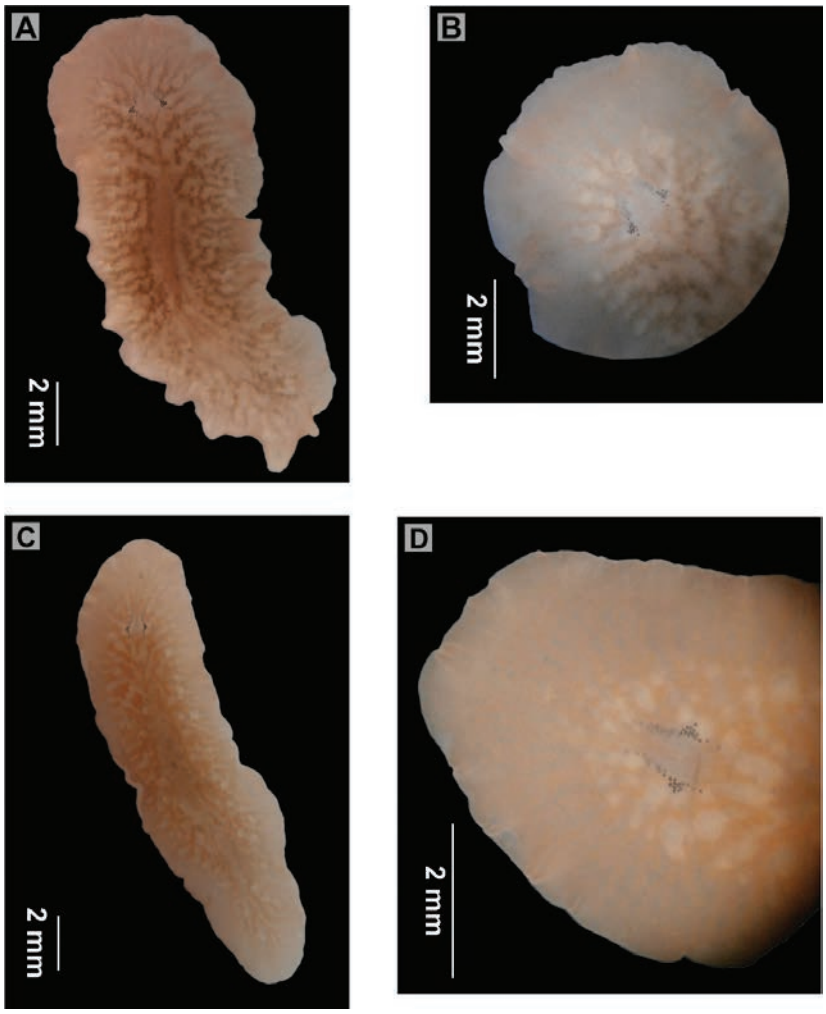

Figure 15. *Phaenoplana caetaria* (Two living specimens of Station 16): **A.** Dorsal view of specimen A; **B.** Detail of the eyes; **C.** Dorsal view of specimen B; **D.** Detail of the eyes.

twisted penis rod. Representatives of *Phaenoplana* have a predominantly Pacific distribution (5 known species) compared to the Mediterranean or Atlantic (two species), although the record of *P. caetaria* shows a clear expansion of the specific distribution of *Phaenoplana*.

Biology. This species is found under stones in the intertidal area of La Ballenera and Punta Carnero Beach, Cadiz, Spain.

Superfamily DISCOCELOIDEA Dittmann, Cuadrado, Aguado, Noreña & Egger, 2019
Family DISCOCELIDAE Laidla, 1903
Genus *Discocelis* Ehrenberg, 1836

Discocelis tigrina (Blanchard, 1847) Lang, 1884

Fig. 16

Polycelis tigrina Blanchard, 1847.
Leptoplana tigrina (Blanchard, 1847) Diesing, 1850.
Elasmodes tigrinus (Blanchard, 1847) Stimpson, 1857.

Material examined. • MNHNC MB16-000128, Station 4, 28 October 2018, 30 mm long; • MNHNC MB16-000129, Station 5, 22 April 2019, 39 mm long; • MNHNC MB16-000130, Station 6, 5 May 2019, 34 mm long; • MNHNC MB16-000131, Station 8, 16 May 2018, 25 mm long; • MNHNC MB16-000132, Station 9, 15 May 2018, 12 mm long; • MNCN 4.01/4088, Station 10, 21 February 2019, 18 mm long; • MNCN 4.01/4089, Station 10, 21 February 2019, 20 mm long; • MNCN 4.01/4090, Station 11, 29 April 2014, 20 mm long; • MNCN 4.01/4091, Station 11, 9 October 2014, 16 mm long; • MNCN 4.01/4092, Station 11, 19 February 2015, 11 mm long.

Description. Living specimens between 11 mm and 39 mm in length (21.45 ± 9.51). Body shape oval, with rounded anterior and posterior ends. Dorsal surface smooth, light brown with many dark brown spots throughout the body, more concentrated in the main axis (Fig. 16A). Ventral face pale brown without spots (Fig. 16B). Without tentacles. Marginal, tentacular, and cerebral eyes present (Fig. 16C). Tentacular clusters with approximately 21 eyes each, and cerebral clusters with 32 eyes each. Pharynx ruffled, centrally positioned, and with deep pharyngeal folds. Oral pore opens at the end of the first third of the pharynx. Male and female systems open into a common genital atrium between the second and the last third of the body.

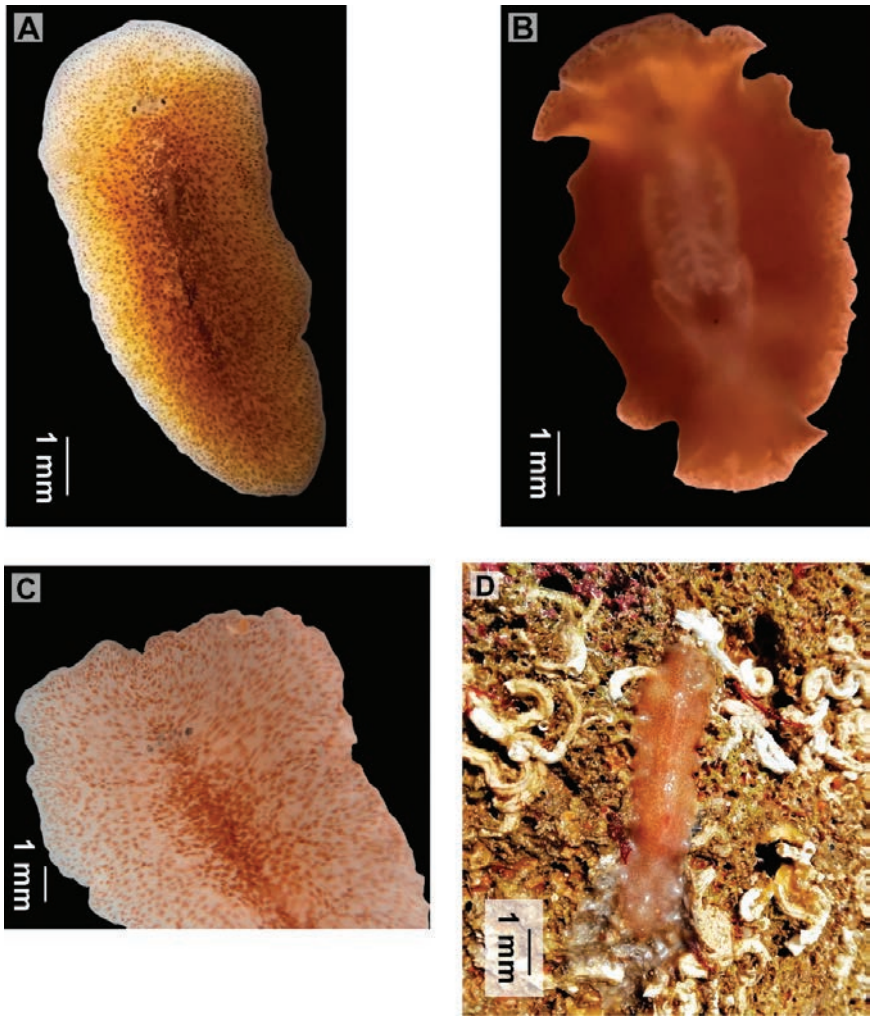

Figure 16. *Discocelis tigrina* (MNHNC MB16-000128): **A.** Dorsal view of the living specimen; **B.** Ventral view; **C.** Detail of the eyes (MNCN 4.01/4089); **D.** Example of the habitat where the specimens were found.

Remarks. The genus *Discocelis* comprises seven accepted species and is considered the genus with the largest number of species within the Discocelidae family. Three of these species exhibit a spotted dorsal pattern: *D. japonica* Yeri & Kabiraki, 1918, *D. pusilla* Kato, 1938, and *D. parvimaculata* Beveridge, 2000. These species are distributed on the Pacific coasts, whereas *D. tigrina* is considered an endemic species of the Mediterranean (Patzner et al. 2005).

Biology. Under stones, living on the rocky shore (Fig. 16D). Sometimes observed among brown algae, *Dictyota dichotoma* (Ochriphyta), and close to meadows of *Caulerpa prolifera* (Chlorophyta) (only in the Ria Formosa environment). It is known that this species frequently appears in association with bivalves (Gammoudi et al. 2017). Indeed, some of the specimens in our study were also found inside the empty shells of mussels. This finding is common within acotylean worms, as they are predators of a wide variety of molluscs (Galleni et al. 1980, Bahia 2016, Gutiérrez et al. 2023); hence, we could assume that this species feeds on them.

Distribution. This species has a wide distribution within the Mediterranean Sea and the Atlantic. The localities where *Discocelis tigrina* was reported are Sicily (Blanchard 1847); the Gulf of Naples (Lang 1884); the Peninsula de Rio de Oro, Western Sahara, and Port-Étienne; Mauritania (Palombi 1939); the coast of Catalonia (Novell 2001 Gammoudi and Tekaya 2012); the Canary Islands (De Vera et al. 2009; Cuadrado et al. 2017); Asturias (Marquina et al. 2014b); Galicia (Noreña et al. 2015); and Tunisia (Gammoudi and Tekaya 2012; Gammoudi et al. 2012; Gammoudi et al. 2017). This is the first record of this species in Portugal (Avencas, Arrabida, Troia, Lagos, and Faro) and Andalusia.

Acknowledgements

We are very thankful to the EMEPC (Estrutura de Missão para a Extensão da Plataforma Continental) and especially to Monica Albuquerque for providing us with the polyclad material from the M@rBis project. This material belongs to the M@rBis collections and was loaned to us through the MUHNAC (Museu Nacional de História Natural e da Ciência, Universidade de Lisboa). Thus, we also thank the museum staff, especially Judite Alves, Al-

exandra Cartaxana, and all of the scientists involved in the samplings carried out for collecting the M@rBis samples. Special thanks to Gonçalo Calado, Filipa Gouveia, and her family, who made this meaningful exchange possible between Portugal and Spain. We are also thankful to the AUIP (Iberoamerican Association of Postgraduate Universities) for providing financial support to the first author and the ERASMUS + Program, both of which are designed to carry out short stays in Lisbon. We are grateful for the GC work, which was funded through the strategic project uidb/04292/2020 and was granted to MARE. Finally, the last phase in the elaboration of this contribution was carried out under the auspices of the project "La Caleta (Cádiz) e intermareales rocosos asociados: una ventana permanente al conocimiento de la biodiversidad marina", funded by Fundación Biodiversidad of the Spanish Ministry of Ecological Transition.

References

Aguado MT, San Martín G, Templado J (2011) La biodiversidad de Invertebrados no Artrópodos en España. In: Biodiversidad. Aproximación a la diversidad botánica y zoológica de España. Memorias Real Sociedad Española de Historia Natural 9: 209–233.

Aguado MT, Noreña C, Alcaraz L, Marquina D, Brusa F, Damborenea C, Almon B, Bleidorn C, Grande C (2017) Phylogeny of Polycladida (Platyhelminthes) based on mtDNA data. Organisms Diversity & Evolution 17(4): 767–778. https://doi.org/10.1007/s13127-017-0344-4

Bahia J (2016) First record of polyclads (Platyhelminthes, Polycladida) associated with *Nodipecten nodosus* (Linnaeus 1758) aquaculture. Marine Biodiversity 46: 911–915. https://doi.org/10.1007/s12526-015-0425-6

Blanchard E (1847) Recherches sur l'organisation des vers. Annales des Sciences Naturelles 8: 271–275. https://doi.org/10.5962/bhl.title.51506

Beveridge I (2018) Three new species of acotylean polyclads (Platyhelminthes) from Queensland, Australia, with the erection of a new genus. Memoirs of the Queensland Museum 61: 143–153. https://doi.org/10.17082/j.2204-1478.61.2018.2017-12

Bock S (1913) Studien über Polycladen. Zoologiska Bidrag fran Uppsala 2: 31–344.

Bock S (1931) Die Polycladen der Deutschen Südpolar-Expedition 1901–1903. Deutsche südpolar-expedition 20(Zool): 259–304. [Berlin]

Bulnes VN (2010) Five new Polycladida (Platyhelminthes: Acotylea) species from the Aegean Sea with remarks on the prostatic structures. Journal of Natural History 44(9): 515–544. https://doi.org/10.1080/00222930903497535

Bulnes VN, Faubel A, Park J-K (2005) Two new marine species from South Korea with remarks on the family Stylochidae (Acotylea, Polycladida, Plathelminthes). Journal of Natural History 39(23): 2089–2107. https://doi.org/10.1080/00222930500081997

Bytinski-Salz H (1935) Un policlado (*Sylochus pilidium* Lang) dannoso ai parchi ostricoli. Thalassia 2(1): 1–24.

Cuadrado D, Moro L, Noreña C (2017) The Polycladida (Platyhelminthes) of the Canary Islands. New genus, species and records. Zootaxa 4312(1): 038–068. https://doi.org/10.11646/zootaxa.4312.1.2

Cuadrado D, Rodríguez J, Moro L, Grande C, Noreña C (2021) Polycladida (Platyhelminthes, Rhabditophora) from Cape Verde and related regions of Macaronesia. European Journal of Taxonomy 736: 1–43. https://doi.org/10.5852/ejt.2021.736.1249

De Vera A, Moro L, Bacallado JJ, Hernández F (2009) Contribución al conocimiento de la biodiversidad de policládidos (Platyhelminthes, Turbellaria) en las Islas Canarias. Revista de la Academia de Ciencias Canarias 20(4): 45–59.

Farina A, Johnson AR, Turner SJ, Belgrano A (2003) "Full" world versus "empty" world paradigm at the time of globalisation. Ecological Economics 45(1): 11–18. https://doi.org/10.1016/S0921-8009(02)00255-0

Faubel A (1983) The Polycladida, Turbellaria. Proposal and stablishment of a new system. Part I. The Acotylea. Mitteilungen aus den Hamburgischen Zoologischen Museum und Institut 80: 17–121.

Faubel A (1984) The Polycladida, Turbellaria. Proposal and establishment of a new system. Part II. The Cotylea. Mitteilungen aus den Hamburgischen Zoologischen Museum und Institut 81: 189–259.

Galleni L (1976) Polyclads of the Tuscan Coasts. II. *Stylochus Alexandrinus* Steinböck and *Stylochus Mediterraneus* n. sp. from the Rocky shores near Pisa and Livorno. Italian Journal of Zoology 43: 1–2, 15–25. https://doi.org/10.1080/11250007609434882

Galleni L (1978) Policladi delle coste toscane. III. *Echinoplana celerrima* Haswell, Planoceridae nuovo per il Mediterraneo e note sul genere. *Echinoplana*. Atti. Atti della Società Toscana de Scienze Naturali di Pisa 85: 139–148.

Galleni L, Gremigni V (1989) Platyhelminthes-Turbellaria. In: Adiyodi KG , Adiyodi RG (Eds) Reproductive biology of invertebrates, Vol. IV, Part A. Fertilization, development and parental care. John Wiley and Sons, New York, 63–89.

Galleni L, Tongiorgi P, Ferrero E, Salghetti U (1980) *Stylochus mediterraneus* (Turbellaria: Polycladida), Predator on the Mussel *Mytilus galloprovincialis*. Marine Biology 55: 317–326. https://doi.org/10.1007/BF00393784

Gammoudi M, Tekaya S (2012) Distribution in the western Mediterranean of some Polyclads (Platyhelminthes). Bulletin de la Societé Zoologique de France 137(1–4): 197–213.

Gammoudi M, Tekaya S, Noreña C (2009) Contribution to the knowledge of Acotylean Polyclads (Platyhelminthes, Polycladida) from Tunisian Coasts. Zootaxa 2195: 43–60. https://doi.org/10.11646/zootaxa.2195.1.3

Gammoudi M, Egger B, Tekaya S, Noreña C (2012) The genus *Leptoplana* (Leptoplanidae, Polycladida) in the Mediterranean basin. Redescription of the species *Leptoplana mediterranea* (Bock 1913) comb. nov. Zootaxa 3178: 45–56. https://doi.org/10.11646/zootaxa.3178.1.4

Gammoudi M, Garbouj M, Egger B, Tekaya S (2017) Updated inventory and distribution of free-living flatworms from Tunisian waters. Zootaxa 4263(1): 120–138. https://doi.org/10.11646/zootaxa.4263.1.5

Girard in Stimpson W (1854) Synopsis of the marine invertebrate of Grand Manan: or the region about the mouth of the Bay of Fundy, New Brunswick. Smithsonian Contributions to Knowledge 4 or 6(5): 1–67. https://doi.org/10.5962/bhl.title.11697

Goette A (1881) Zur Entwicklungsgeschichte der Würmer. Zoologischer Anzeiger 4.

Grube AE (1840) Actinien, Echinodermen und Würmer des adriatischen und Mittelmeers, nach eigenen Sammlungenbeschrieben. Königsberg, 92 pp. https://doi.org/10.5962/bhl.title.10133

Gutiérrez A, Auby I, Gouillieux B, Daffe G, Massé C, Antajan E, Noreña C (2023) A new polyclad flatworm, *Idiostylochus tortuosus* gen. nov., sp. nov. (Platyhelminthes, Polycladida) from France. Can this Foreign Flatworm be Responsible for the Deterioration of Oyster and Mussel Farm? Zoological Studies 62: e15. https://doi.org/10.6620/ZS.2023.62-15

Harms J (1993) Check-list of species (algae, invertebrales and vertebrales) found in the vicinity of the island of Helgoland (North Sea, German Bight) - a review of recent records. Helgoländer Wissenschaftliche Meeresuntersuchungen 41: 1–34. https://doi.org/10.1007/BF02366182

Haswell WA (1907) Observations on Australian polyclads. Transactions of the Linnean Society of London 9: 465–485. https://doi.org/10.1111/j.1096-3642.1907.tb00455.x

Heath H, McGregor EA (1913) New polyclads from Monterey Bay, California. Proceedings of the Academy of Natural Sciences of Philadelphia 64: 455–488.

Holleman J (2007) Some New Zealand Polyclads (Platyhelminthes, Polycladida). Zootaxa 1560(1): 1–17. https://doi.org/10.11646/zootaxa.1560.1.1

Howson CM, Picton BE (1997) The species directory of the marine fauna and flora of the british isles and surrounding seas. Ulster Museum and the marine conservation society, Belfast and Ross-on Wye Ulster museum publication 276: 1–508.

Hyman LH (1940) The polyclad flatworms of the Atlantic Coast of the United States and Canada. Proceedings of the United States National Museum 89: 449–492. https://doi.org/10.5479/si.00963801.89-3101.449

Hyman LH (1953) The polyclad flatworms of the Pacific coast of North America. Bulletin of the American Museum of Natural History 100: 269–391.

Jacubowa L (1909) Die Polycladida der Bucht von Sevastopol. Mémoires Présentés a l'Académie Impériale des Sciences de Saint Pétersbourg par Divers Savans et lus dans ses Assemblées, Série VII 24: 1–32.

Jennings KA, Newman LJ (1996) Two new stylochid flatworms (Platyhelminthes: Polycladida) from the southern Great Barrier Reef, Australia. The Raffles Bulletin of Zoology 44(1): 135–142.

Johnston EL, Lee KM (2008) Brooding behaviour and reproductive success in two species of free-living simultaneous hermaphrodites. Marine Biology 155: 555–561. https://doi.org/10.1007/s00227-008-1056-2

Karez R (1991) Die Besiedlung sublitoraler Rotalgenam Felssockel von Helgoland. Dipl. Arb. Univ. Marburg, 143 pp.

Kato K (1937) Thirteen new Polyclads from Misaki. Japanese Journal of Zoology 7: 347–371.

Laidlaw FF (1903) On the marine fauna of Zanzibar and British East Africa, from collections made by Cyril Crossland in the Years 1901 and 1902. Turbellaria Polycladida. I. The Acotylea. Proceedings of the Zoological Society of London 2(8): 99–113 [+ 1 pl].

Laidlaw FF (1906) On the Marine Fauna of the Cape Verde Islands, from Collections made in 1904 by Mr. C. Crossland. – The Polyclad Turbellaria. Proceedings of the Zoological Society of London 1906: 705–719.

Lang A (1884) Die Polycladen (Seeplanarien) des Golfes von Neapel und der angrenzenden Meeresabschnitte. Eine Monographie. Fauna und Flora des Golfes von Neapel 11. W Engelmann, Leipzig. https://doi.org/10.5962/bhl.title.10545

Litvaitis MK, Bolaños DM, Quiroga SY (2019) Systematic congruence in Polycladida (Platyhelminthes, Rhabditophora): Are DNA and morphology telling the same story? Zoological Journal of the Linnean Society 186: 865–891. https://doi.org/10.1093/zoolinnean/zlz007

Marquina D, Osca D, Rodríguez J, Fernández-Despiau E, Noreña C (2014a) State of knowledge of the Acotylea (Polycladida, Platyhelminthes) from the Mediterranean coasts of Spain: New records and new species. Zootaxa 3780(1): 108–134. https://doi.org/10.11646/zootaxa.3780.1.4

Marquina D, Fernández-Álvarez FA, Noreña C (2014b) Five new records and one new species of Polycladida (Platyhelminthes) for the Cantabrian Coast (North Atlantic) of the Iberian Peninsula. Marine Biological Association of the UK 95(2): 311–322. https://doi.org/10.1017/S0025315414001106

Micallef A, Rangel-Buitrago N (2019) The Management of Coastal Landscapes. In: Rangel-Buitrago N (Ed.) Coastal Scenery. Coastal Research Library, Vol. 26. Springer, Cham. https://doi.org/10.1007/978-3-319-78878-4

Micoletzky H (1910) Die Turbellarienfauna des Golfes von Triest. Arbeiten aus dem Zoologischen Institut der Universität Wien 18: 167–182.

Minot CS (1876) Studien an Turbellarien. Beitrage zur Kenntnis der Plathelminthen. Arbeiten Zool.-Zoot. Inst. Würzburg, III. Bd. Hamburg. Arbeiten aus dem Zoologisch-Zootomischen Institut in Würzburg 3: 405–471.

Molina-Venegas R, Aparicio A, Lavergne S, Arroyo J (2015) The building of a biodiversity hotspot across a land-bridge in the Mediterranean. Proceedings of the Royal Society 28(1813): 20151116. https://doi.org/10.1098/rspb.2015.1116

Morales JA (2022) Coastal geology. Springer textbooks in earth sciences, geography and environment. Springer, Cham, Switzerland, 477–477. https://doi.org/10.1007/978-3-030-96121-3

Newman LJ, Cannon LRG (2003) Marine Flatworms: The World of Polyclads. CSIRO Publishing, Australia. https://doi.org/10.1071/9780643101197

Noreña C, Marquina D, Pérez J, Almon B (2014) First records of Cotylea (Polycladida, Platyhelminthes) for the Atlantic coast of the Iberian Peninsula. Zookeys 404: 1–22. https://doi.org/10.3897/zookeys.404.7122

Noreña C, Rodríguez J, Pérez J, Almon B (2015) New Acotylea (Polycladida, Platyhelminthes) from the east coast of the NorthAtlantic Ocean with special mention of the Iberian littoral. Zootaxa 4039(1): 157–172. https://doi.org/10.11646/zootaxa.4039.1.7

Novell C (2001) Contribution to the knowledge of polyclad Turbellaria of the Catalan coast. PhD Thesis, University of Barcelona, Spain. http://www.tesisenxarxa.net/TESIS_UB/AVAILABLE/TDX-0107104-121621//Tesis.PDF

Oya Y, Kajihara H (2018) A new bathyal species of *Cestoplana* (Polycladida: Cotylea) from the West Pacific Ocean. Marine Biodiversity 49: 905–911. https://doi.org/10.1007/s12526-018-0875-8

Oya Y, Kajihara H (2019) A New Species of *Phaenoplana* (Platyhelminthes: Polycladida) from the Ogasawara Islands. Species Diversity 24: 1–6. https://doi.org/10.12782/specdiv.24.1

Oya Y, Nakajima H, Kajihara H (2022) A new symbiotic relationship between a polyclad flatworm and a mantis shrimps: description of a new species of Emprosthopharynx (Polycladida: Acotylea) associated with Lysiosquilla maculata (Crustacea: Stomatopoda). Marine Biodiversity 52: 46. https://doi.org/10.1007/s12526-022-01288-y.

Palombi A (1928) Report on the Turbellaria (Cambridge Expedition Suez Canal 1924). Transactions of the Zoological Society of London 22(5): 579–631. https://doi.org/10.1111/j.1096-3642.1928.tb00208.x

Palombi A (1936) Policladi liberi e commensali raccolti sulle coste del Sud Africa, della Florida e del Golfe di Napoli. Archivio Zoologico Italiano 23: 1–45.

Palombi A (1939) Turbellaria Policladea. Memoires du Musee royal d'histoire naturelle de Belgique 15(2): 95–114.

Patzner RA, Hofrichter R, Schmidt-Raesa A, Faubel A, Noreña C (2005). Plathelminthes (Platelmintos, gusanos planos). In: El Mar Mediterráneo: fauna, flora y ecología. Volumen II/1, Editorial Omega, 654–656.

Pérez-García P, Noreña C, Cervera JL (2019) Two new acotylean flatworms (Polycladida) of two genera unrecorded in the Eastern Atlantic. Marine Biodiversity 49: 1187–1195. https://doi.org/10.1007/s12526-018-0900-y

Plehn M (1896) Neue Polycladen, gesammelt von Herrn Kapitan Chierchia bei der Erdumschiffung der Korvett Vettor Pisani, von Herrn Prof. Dr. Kukenthal im nordlichem Eismeer und von Herrn Prof Dr. Semon in Java. Jenaische Zeitschrift 30: 137–181.

Prudhoe S (1968) A new polyclad turbellarian associating with a hermit-crab in the Hawaiian Islands. Pacific Science 22: 408–411.

Prudhoe S (1982) Polyc1ad turbellarians from the southern eoasts of Australia. Records of South Australian Museum 18: 361–384.

Prudhoe S (1989) Polyclad turbellarians recorded from African waters. Bulletin of the British Museum of Natural History 55: 47–96.

Pruvot G (1897) Essai sur les Fonds et la Faune de la Manche occidentale (Côtes de Bretagne) comparés à ceux du Golfe du Lion. Archive de Zoologie Expérimentale et Générale 3(5): 19–20, 617–660.

Quatrefages A (1845) Études sur les types inférieurs de l'embranchement des annelés: mémoire sur quelques planairées marines appurtenant aux genres Tricelis (Ehr.), Polycelis (Ehr.), Prosthiostomum (Nob.), Proceros (Nob.), Eolidiceros (Nob.), et Stylochus (Ehr). Annales des Sciences Naturelles 4(3): 326 [or 129–184].

Quiroga SY, Bolaños M, Litvaitis MK (2006) First description of deep-sea polyclad flatworms from the North Pacific: *Anocellidus* n. gen. *profundus* n. sp. (Anocellidae, n. fam.) and *Oligocladus voightae* n. sp. (Euryleptidae). Zootaxa 1317(1): 1–19. https://doi.org/10.11646/zootaxa.1317.1.1

Quiroga SY, Bolaños M, Litvaitis MK (2008) Two new species of flatworms (Platyhelminthes: Polycladida) from the continental slope of the Gulf of Mexico. Journal of the Marine Biological Association of the UK 88(7): 1363–1370. https://doi.org/10.1017/S0025315408002105

Rodríguez J, Grande C, Bulnes NV, Almon B, Perez J, Noreña C (2017) Systematic revision of the family Pleioplanidae Faubel, 1983 (Polycladida, Acotylea): new genus and combinations. European Journal of Taxonomy 264: 1–30. https://doi.org/10.5852/ejt.2017.264

Rodríguez J, Hutchings PA, Williamson JE (2021) Biodiversity o intertidal marine flatworms (Polycladida, Platyhelminthes) in southeastern Australia. Zootaxa 5024(1): 1–63. https://doi.org/10.11646/zootaxa.5024.1.1

Romeis B (1987) Mikroskopische Technik. 17. Neubearb. U. hrsg. Von P. Böck – 17 Auflage – Urban u. Schwarzenberg. München, Wien, Baltimore, 697 pp.

Saldanha L (1974) Estudo do povoamento dos horizontes superiors da rocha litoral da costa da Arrabida (Portugal). Museu e Laboratório Zoológico e Antropológico. Faculdade de Ciências de Lisboa. Arquivos do Museu Bocage V (I), 382 pp.

Schmidt O (1861) Untersuchungen ueber Turbellarien von Corfu und Cephalonia, nebst Nachträgen zu früheren Arbeiten. Zeitschrift für wissenschaftliche Zoologie 11: 1–32.

Steinböck O (1932) Die Turbellarien des arktischen Gebietes. In: Römer & Schaudinn. Fauna Arctica, Jena 6: 295–342.

Steinböck O (1933) Die Turbellarienfauna der Umgebung von Rovigno. Thalassia 1: 1–33.

Steinböck O (1937) The fishery grounds near Alexandria. 14. Turbellaria. Ministry of Commerce and Industry, Egypt; Hydrobiology and Fisheries Directorate. Notes and Memoirs No. 25. Gov. Press, Cairo, 15 pp.

Stimpson W (1854) Synopsis of the marine invertebrate of Grand Manan: or the region about the mouth of the Bay of Fundy, New Brunswick. Smithsonian Contributions to Knowledge 4 or 6(5): 1–67. https://doi.org/10.5962/bhl.title.11697

Templado J, Luque AA, Moreno D, Tierno de Figueroa JM, Sánchez Tocino L, Aguilar R, De la Torriente A (2021) Invertebrates: The Realm of Diversity. In: Báez JC, Vázquez J-T, Caiñas JA, Idrissi MM (Eds) Alboran Sea-Ecosystems and Marine Resources. Springer Nature Switzerland, 359–430 pp. [ISBN 978-3-030-65516-7] https://doi.org/10.1007/978-3-030-65516-7_10

Tyler S, Artois T, Schilling S, Hooge M, Bush LF [Eds] (2006–2024) World list of turbellarian worms: Acoelomorpha, Catenulida, Rhabditophora. http://www.marinespecies.org/turbellarians/

Verrill AE (1893) Marine planarians of New England. Transactions of the Connecticut Academy of Arts and Sciences 8: 459–520 [+ 5 plates (40–44)].

Wenzel C, Ehlers U, Lanfranchi A (1992) The larval protonephridium of *Stylochus mediterraneus* Galleni (Polycladida, Plathelminthes): an ultrastructural analysis. Microfauna Marina 7: 323–340.

Zoosyst. Evol. 100 (4) 2024, 1515–1541 | DOI 10.3897/zse.100.132111

PENSOFT

für Natur MUSEUM FÜR NATURKUNDE BERLIN

A review of the millipede genus *Pseudodesmus* Pocock, 1887 (Diplopoda, Platydesmida, Andrognathidae) from Vietnam, with descriptions of five new species and notes on its phylogeny

Anh D. Nguyen[1,2], Lien T. P. Nguyen[1,2], Zoltán Korsós[3]

1 *Institute of Ecology and Biological Resources, Vietnam Academy of Science and Technology, 18, Hoangquocviet Rd., Caugiay District, Hanoi, Vietnam*

2 *Graduate University of Science and Technology, Vietnam Academy of Science and Technology, 18, Hoangquocviet Rd., Caugiay District, Hanoi, Vietnam*

3 *University of Veterinary Medicine Budapest, István u. 2, 1078 Budapest, Hungary*

https://zoobank.org/B39508EB-6EB2-4CC0-88D8-B3E87BDCED02

Corresponding author: Anh D. Nguyen (ducanh.iebr@gmail.com)

Academic editor: Luiz Felipe Iniesta ♦ **Received** 18 July 2024 ♦ **Accepted** 9 October 2024 ♦ **Published** 7 November 2024

Abstract

The platydesmidan genus *Pseudodesmus* Pocock, 1887 is reviewed within the scope of the Vietnamese fauna. A total of seven species have been recorded in Vietnam including five new species: *Pseudodesmus bidoup* **sp. nov.**, *Pseudodesmus karstomus* **sp. nov.**, *Pseudodesmus ngoclinh* **sp. nov.**, *Pseudodesmus condao* **sp. nov.**, and *Pseudodesmus irregularis* **sp. nov.** Cytochrome c oxidase I barcodes are provided for these species, and their phylogenetic relationship is discussed.

Key Words

Biodiversity, bio-investigation, COI, phylogeny, Southeast Asia, taxonomy

Introduction

Members of the millipede order Platydesmida represent a taxon of ancient millipedes originally distributed in the former supercontinent of Laurasia (Shelley and Golovatch 2011; Moritz and Wesener 2019). Two distinct habitus types are known: a short body with wide paraterga (= paranota) or a very slender, elongated body with very short (or rarely no) paraterga (Wesener 2015). They have a small and pyriform head, and lack ommatidia. Like other colobognath millipedes, platydesmidan males have simple leg-like gonopods (leg pairs 9 and 10). Due to this and their small size, it is difficult to distinguish platydesmidan species based solely on gonopod characters (Shorter et al. 2018). Most species discrimination is from other characters, for example, antenna, head, legs, coloration, and metazonital shape and sculpture.

The order Platydesmida is currently classified into two families, Platydesmidae de Saussure, 1860 and Andrognathidae Cope, 1869, with 69 described species in 14 genera (Shear 2011; Minelli 2014). Two genera of Platydesmidae only occur in the western Hemisphere, whereas Andrognathidae has 12 genera and 36 species in North America, the Mediterranean Europe, and East and Southeast Asia. Of these, *Brachycybe* (Wood 1864) (3/8); *Pseudodesmus* (Pocock 1887) (9/9); *Symphyopleurium* (Attems 1951) (3/3); and *Yamasinaium* (Verhoeff 1939) (3/3) are presently considered as valid genera from East and Southeast Asia (in parentheses, number of species recorded in Asia/total number of species). Seven other Asian genera described earlier (*Bazillozonium* (Verhoeff 1935), *Sumatronium* (Verhoeff 1935), *Trichozonium* (Miyosi 1953), *Yamasinaium* Takashima, 1953, *Yoshimarium* Takashima, 1953, *Zinaceps* (Chamberlin and Wang

1953), and *Zinazonium* (Chamberlin 1945) are all junior synonyms according to Hoffman (1980) .

Another genus, *Sinocybe* (Loomis, 1942) (with only one species, *Sinocybe cooki* (Loomis, 1942), is listed by Hoffman (1980). He also added that he "by no means [is] assured that *Sinocybe* can be distinguished from *Pseudodesmus*" (Hoffman 1980: p. 117). However, later *Sinocybe* was considered a junior synonym of *Brachycybe* Wood, 1864 (Shelley et al. 2005).

Carl (1912) distinguished the two genera *Platydesmus* and *Pseudodesmus* by the following characters. *Platydesmus* has a collum that is distinctly wider than the head, shaped trapezoidally, with the anterior edge emarginated or notched in the middle; tergite regularly arched, without longitudinal rows of enlarged tubercles; wide ventral sterna, with the coxae of the legs therefore very far apart; and last tergite with tubercles on the apical edge. On the contrary, *Pseudodesmus* has a collum that is not or barely wider than the head, shaped like a crescent or semicircle; tergite more or less distinctly flattened in the middle and with one or more longitudinal rows of enlarged tubercles; the ventral plates very narrow between the insertion of the legs; the coxae therefore are very close together and almost contiguous on the midline of the body; and the last tergite has a smooth apical edge, lacking tubercles.

Up to now, nine species belong to the genus *Pseudodesmus* (in chronological order of descriptions):

1. *Pseudodesmus quadrituberculatus* (Tömösváry 1885) from Matang, Sarawak, Borneo, Malaysia (= *Siphonophora quadrituberculata*: Carl 1912; Jeekel 2001);
2. *Pseudodesmus verrucosus* Pocock, 1887 from Perak, Malay Peninsula, Malaysia (type species of the genus);
3. *Pseudodesmus tuberculatus* (Silvestri 1899) from Peninsular Malaysia;
4. *Pseudodesmus nodulosus* (Verhoeff, 1935) from Sumatra, Indonesia (= *Sumatronium nodulosum*: Hoffman 1980);
5. *Pseudodesmus camptotrichus* (Attems, 1938) from Laos (Bolloven, Paklay, Luong Prabang), Vietnam (Phu Yen: Varella Cap; Khanh Hoa: Hon Ba Mt., Nha Trang; Lam Dong: Lang Biang; Da Nang: Ba Na Mt., Hai Van pass; Kien Giang: Nam Du (Poul Condore); Lao Cai: Sapa); (= *Sumatronium camptotrichum*: Hoffman 1980);
6. *Pseudodesmus variegatus* (Attems, 1938) from Laos (Xieng Khoang) and Vietnam (Lang Bian) (= *Sumatronium variegatum*: Hoffman 1980);
7. *Pseudodesmus leeuweni* (Chamberlin, 1945) from Sibolangir, Sumatra, Indonesia (= *Zinanonium leeuweni*: Hoffman 1980);
8. *Pseudodesmus persimilis* (Attems, 1953) from Laos (Paklay, Luong Prabang) (= *Sumatronium persimile*: Hoffman 1980);
9. *Pseudodesmus kelantanicus* (Sinclair 1901) from the Malay Peninsula (= *Platydesmus kelantanicus*: Carl 1912).

Hoffman (1980), Decker (2014), and Wesener (2015) mentioned 9 species of *Pseudodesmus*, but in MilliBase, there are only 8 species listed (Sierwald et al. 2024). There is some uncertainty regarding a ninth species, but we agree with Carl (1912) who considered *Platydesmus kelantanicus* to be a species of *Pseudodesmus* (Carl 1912). From these, only two species were previously reported from Laos and Vietnam: *Pseudodesmus camptotrichus* and *P. variegatus* (Likhitrakarn et al. 2014). However, *P. persimilis*, originally described from Laos, can probably also occur in Vietnam (Attems 1938, 1953).

This paper is devoted to providing a review of the genus *Pseudodesmus* in Vietnam, descriptions of five new species, and notes on its phylogenetic relationships.

Material and methods

Millipede specimens were collected from various parts of Vietnam during expeditions organized by the Institute of Ecology and Biological Resources (IEBR) and Vietnamese-Russian Tropical Center from 2004 to 2024. Specimens were collected by hand from under logs, rocks, barks, and by pitfall traps. All specimens were preserved in 80% ethanol.

Morphological characters were investigated with an Olympus SZX16 stereomicroscope. Gonopods were dissected for morphological examination and photographed. Colour images were taken at various focal planes using a Sony A6000 camera coupled to a SMZ800N Nikon stereomicroscope. UV images were taken using the aforementioned camera-microscope combination with illumination from a Nichia Convoy UV flashlight. Images were focal stacked using Helicon Focus version 7.0 and assembled in Adobe Photoshop CS6.

Gonopods were removed from the body, preserved in series of increasing ethanol concentrations, 90%, 95% and 99% for dehydration in 24 hours, mounted on an aluminum stuff, then coated with gold. Scanning electron microscope (SEM) images were taken using the Prisma E system (ThermoFisher Scientific) at IEBR.

Total genomic DNA was extracted using a Qiagen DNeasy Blood and Tissue Kit. A 680-bp fragment of the mitochondrial gene, cytochrome c oxidase subunit I (COI), was amplified and sequenced using a pair of universal primers, LCO1490 and HCO2198 (Folmer et al. 1994). Polymerase chain reaction (PCR) conditions for amplification of the COI gene follow those of Nguyen et al. (2017) as follows: an initial denaturation at 95 °C for 2 min followed by 36 cycles of 95 °C for 20 sec, 42 °C for 45 sec, and 72 °C for 1 min, and a final extension at 72 °C for 5 min. The successfully amplified PCR products were submitted to First-Base Company (Malaysia) for purification and sequencing. COI sequences were checked and confirmed using a BLASTN 2.6.0+ search (Zhang et al. 2000) and registered for GenBank with unique accession numbers. All confirmed sequences were aligned using multiple sequence alignment with the program ClustalX ver. 2.0 (Larkin et al. 2007). The

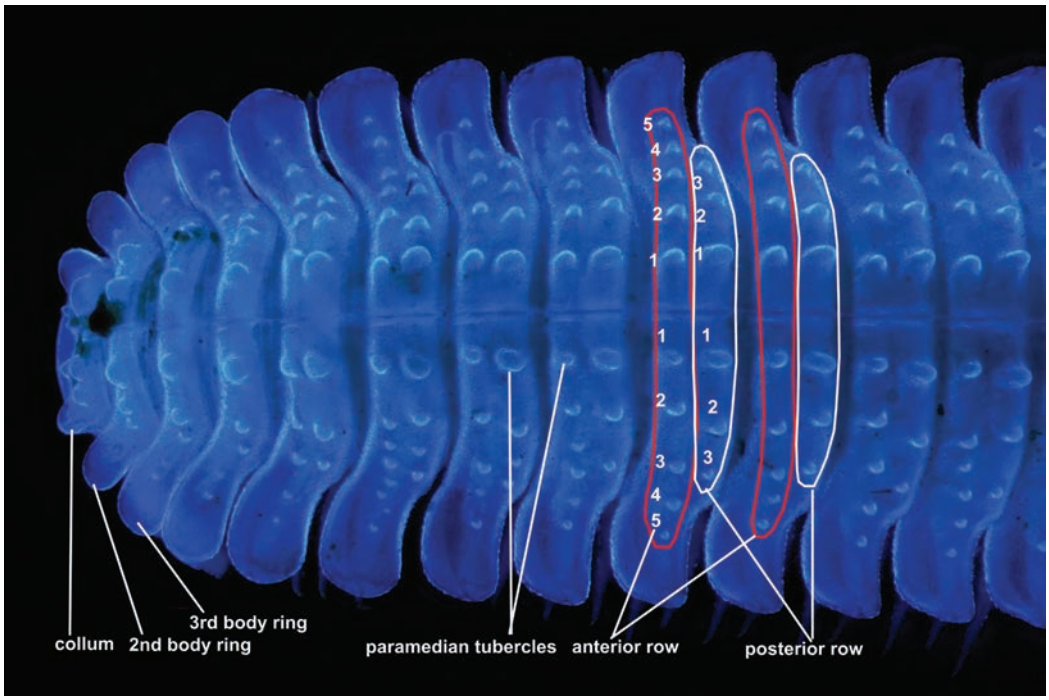

Figure 1. Tubercle notation of *Pseudodesmus bidoup* sp. nov. Numbers refers to tubercles.

genetic distance between platydesmidan samples was calculated using the Kimura 2-parameter model performed in MEGA ver.7.0 (Kumar et al. 2016). A maximum likelihood bootstrap analysis was conducted using the IQTREE server with 1,000 replicates at http://iqtree.cibiv.univie.ac.at/ (Trifinopoulos et al. 2016).

All terminology follows (Mikhaljova et al. 2010). Tubercle notation is shown in Fig. 1. Holotype and paratypes are deposited in IEBR, Hanoi, Vietnam; some are shared with the Department of Zoology, Hungarian Natural History Museum, Budapest, Hungary (HNHM).

Abbreviations

IEBR-Myr = Institute of Ecology and Biological Resources, Myriapod collection; HNHM = Hungarian Natural History Museum, Department of Zoology; NHMW = Naturhistorisches Museum Wien; NP = National Park.

Results

Taxonomy

Order Platydesmida de Saussure, 1860
Family Andrognathidae Cope, 1869
Subfamily Bazillozoniinae Verhoeff, 1935

Genus *Pseudodesmus* Pocock, 1887

Type-species. *Pseudodesmus verrucosus* Pocock, 1887, by original designation. Known only from two female specimens from Perak State, Peninsular Malaysia.

Historical diagnosis. Translated from Latin in Pocock (1887): *Platydesmus* form. With a long body, bearing a series of tubercles above and keels below on each side. With a number of segments numbering greater than seventy; the last segment posteriorly not sharp; the segments, except for the first and last, bearing keels near the lower part of the side, rising close to level, and with a groove along the middle of the back. Each keel, except the first three, has a repugnatorial pore on the lateral margin. The first four segments have two legs each, the others are equipped with two pairs of legs; the last (and possibly the penultimate) lacking legs. The legs consist of six joints; the last joint of the leg is armed with a claw at the tip. The leg-bearing plates are free. The head is bent under the anterior segments, with a convex front; the anterior margin scarcely produced into a snout. Without eyes. Antennae consist of seven articles; located on the sides of the head; the last article being the smallest. The mandibles are hidden. The gnathochilarium is prominent; with large stipes; the jaws and cardines are not conspicuous; there are no lobes on the small, thin lamellae linguales; the mentum is hammer-shaped and large.

According to Wesener (2015), the genus can be recognized by the following characters: “Colour variable. Trunk wide, paraterga strongly elongated. Body length up to 60 mm, with 66–76 body rings. Collum with tubercles. Tergites densely pilose, strongly sculptured, with several smaller and one row of larger tubercles. Larger tubercles sometimes forming a ridge or resembling conic spines”.

Remarks. The genus has been found only in Southeast Asia, but has been poorly studied. Since the description of its last species, *Pseudodesmus persimilis* (Attems, 1953), there has been very little taxonomic information about the genus.

***Pseudodesmus camptotrichus* (Attems, 1938)**

Sumatronium camptotrichum Attems, 1938: p. 303, figs 219–235.

Type material. 26 specimens, including 1 male and 16 females (NHMW-MY2288–2293).

Historical diagnosis. According to Attems (1938, p. 303), the species can be recognized by coloration of earth brown; length 14 mm, width 2 mm, male with 37–42 body rings, female with 35–49 body rings; head almost evenly rounded; collum relatively short, lateral paraterga rounded, anteriad-directed. Metazonites with two rows of 5+5 or 5+4 tubercles on body ring 2, 6–9+6–9 tubercles on the following body rings; the paramedian tubercles the largest, rather elongated.

Records from Vietnam. Khanh Hoa Province (Ba Ngoi; Hon Ba; Po Nagar; Cau Da), Phu Yen Province (Varella), Da Nang Province (Ba Na; Hai Van), Lam Dong Province (Lang Biang), Binh Phuoc Province (Bu Dap), Ba Ria-Vung Tau Province (Con Son isl.) (Attems 1938)(Attems 1938).

***Pseudodesmus variegatus* (Attems, 1938)**

Sumatronium variegatum Attems, 1938: 308, figs 236–243.

Type material. 1 male and 2 juveniles (NHMW-MY2287).

Historical diagnosis. According to Attems (1938: p. 308), the species can be recognized by striking coloration of fairly irregular distribution of black and yellow-brown color; male with 53–56 body rings, length 32 mm, width 5.8 mm; collum scarcely wider than the head; other metazonites densely covered with tiny hairs dorsally on the tubercles and on the underside of paraterga, with 2 transverse rows of shiny tubercles; anterior row of 8–15 + 8–15 tubercles, extending to paraterga; posterior row of 5–7 + 5–7 tubercles present only on metaterga.

Record from Vietnam. Lam Dong Province (Lang Bian).

New species

***Pseudodesmus bidoup* sp. nov.**

https://zoobank.org/0E9D217B-0ED9-41E8-9712-960188EF700A

Figs 2–5

Type material. ***Holotype*.** Vietnam • 1 male; Lam Dong Province, Bi Doup–Nui Ba National Park; 12.11231°N, 108.6627°E; 1,500–1,800 m a.s.l.; 29 April–9 May 2009; Anh D. Nguyen leg; mixed forest; IEBR-Myr 957H.

***Paratypes*.** Vietnam • 1 female, 1 juvenile; same data as for the holotype; IEBR-Myr 957P • 1 female; same data as for the holotype; HNHM • 1 male (41 body rings); Kon Tum Province, Lo Xo pass; 15.23439°N, 107.73386°E; 830 m a.s.l.; 15–19 April 2004; Anh D. Nguyen leg.; secondary forest; pitfall trap; IEBR-Myr 961.

Diagnosis. Head slightly smaller than collum. Collum with two rows of tubercles 1+1(2) smaller and 2+2 larger tubercles. Body smooth, neither setose nor pubescent, midbody rings with two rows of tubercles on metazonites, anterior row longer, extending to about midlength of paraterga, containing 5+5 tubercles; posterior row shorter and extending to base of paraterga, consisting of 3+3 tubercles. Posterior gonopods 6-segmented, distally carrying four apical stylets.

Diagnosis remark. The new species is easily distinguished from *P. camptotrichus* by coloration in alcohol (light yellowish vs earth brown). It also differs from two previously known species, *P. variegatus* and *P. camptotrichus* in having smaller size (number of male body rings: 35 vs 53–56 and 37–42; length: 9.25 mm vs 32 mm and 14 mm; width: 1.63 mm vs 5.8 mm and 2.0 mm, respectively), number of metazonal tubercles (two rows of 5+5 and 3+3 vs two rows of 8–15+8–15 and 5–7+5–7, and two rows of 6+6 to 9+9 each row, respectively).

Description. Male holotype.

Measurements: 35 body rings plus telson; length about 9.25 mm, length of metazona about 0.19 mm, width of metazona about 1.63 mm, width of prozona about 1.25 mm; ratio of width of head and width of collum = 0.93.

Coloration of ethanol-preserved specimen: whole body including legs and antenna light yellowish.

Head almost smooth, not setose, round-shaped. Antenna stout, clavate, *in situ* extending to body ring 4; antennomere 6 > 5 >3 > 4 = 2 > 7=1 in length. Collum with distinct, but small paraterga directed anterolaterad (Figs 2B, 3A); two rows of tubercles on collum: anterior row with 1+1 small tubercles, posterior row with 2+2 large tubercles including larger paramedian ones (Fig. 3A). Body smooth, neither setose nor pubescent. Metatergites elevated medially and slightly declined laterad, so body in cross-section subtriangular. Terga 2–4 with a row of 2–4+2–4 large tubercles including 2+2 tubercles on paraterga (Figs 2B, 3A); other terga with two rows of tubercles, anterior row longer, extending to about midlength of paraterga, containing 5+5 tubercles; posterior row shorter and extending to base of paraterga, consisting of 3–4+3–4 tubercles. Paramedian tubercles considerably larger (Figs 2A–C, 3A, B).

Paraterga slightly curved anteriad on body rings 2–5, lateral margins rounded (Fig. 2A, B); increasingly less so curved the following body rings, slightly curved caudad on body rings 25–27, and strongly curved caudad on body rings 28–31; caudal corners of paraterga increasingly acute on 6–7 posteriormost body rings in front of telson; paraterga of penultimate body ring produced strongly caudad and flanking telson (Figs 2A–C, 3A, B). All margins of paraterga serrated, with tiny setae.

Telson (Figs 2C, 3D) short, caudal margin rounded; epiproct with 2+2 small/tiny tubercles at caudal margin. Paraprocts and hypoproct semi-circular.

Legs slender, shorter than mid-metazonal width, terminating before lateral margins of paraterga. Prefemur = tarsus > femur > postfemur = tibia in length. Claws normal. Coxal sacs present from body rings 3–28 (Fig. 3D).

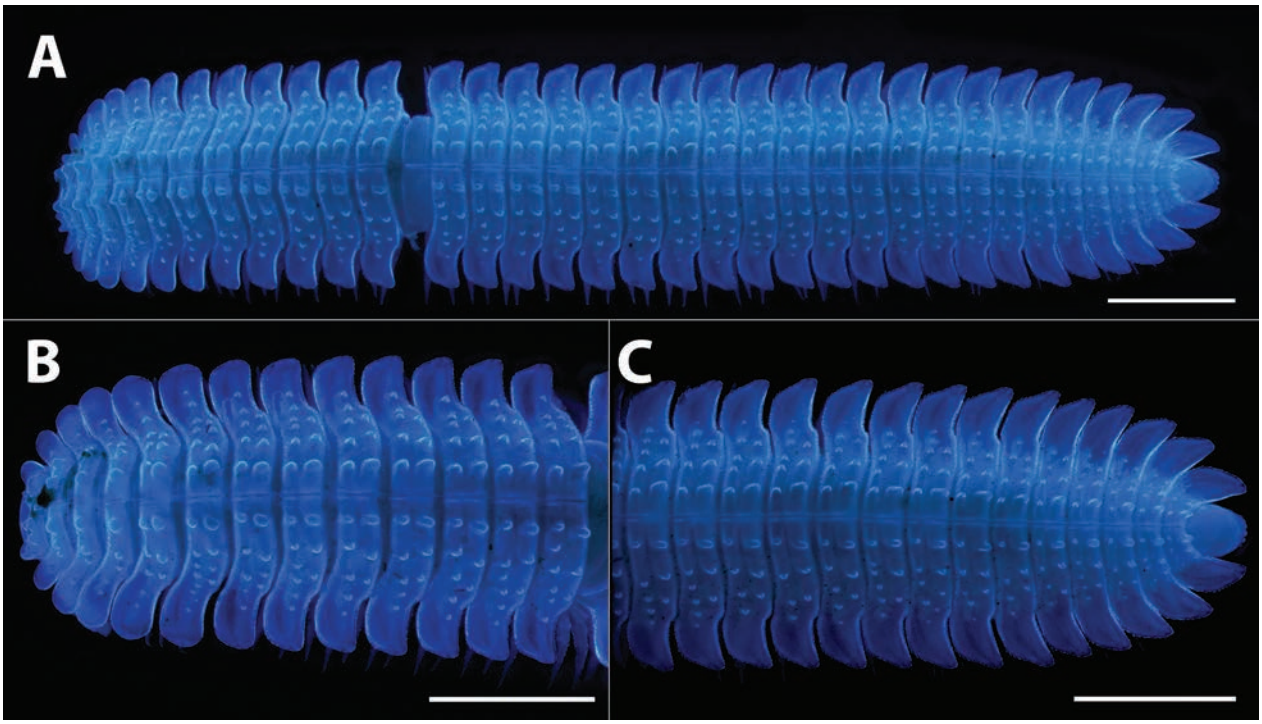

Figure 2. *Pseudodesmus bidoup* sp. nov. Holotype (IEBR-Myr 957), under UV light. **A.** Habitus, dorsal view; **B.** Anterior part of body, dorsal view; **C.** Posterior part of body, dorsal view. Scale bars: 1 mm.

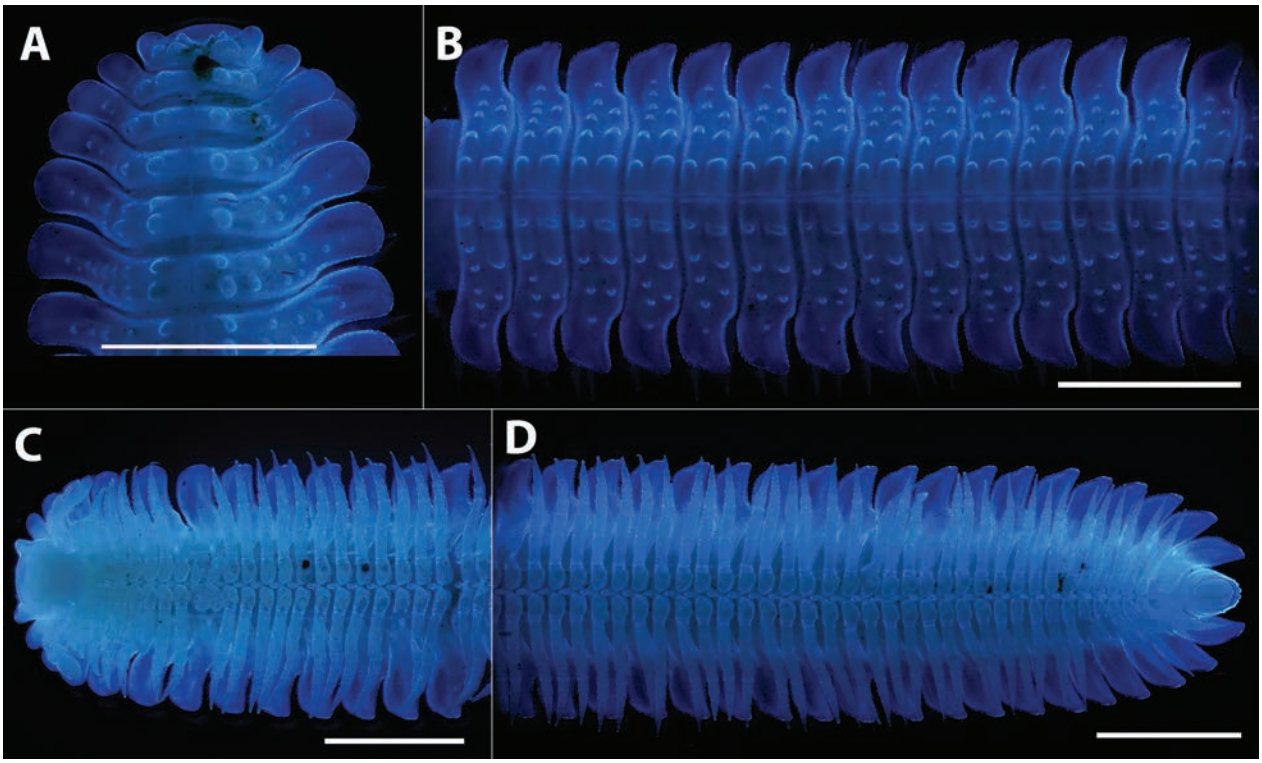

Figure 3. *Pseudodesmus bidoup* sp. nov. Holotype (IEBR-Myr 957), under UV light. **A.** Collum and body rings 2–6, dorsal view; **B.** Midbody body rings, dorsal view; **C.** Anterior part of body, ventral view; **D.** Posterior part of body, ventral view. Scale bars: 1 mm.

Gonopods: Two pairs of gonopods directed anteromesad. Anterior gonopods (Figs 4A, 5A, B) 6-segmented, covered with long setae; coxite broad, basal part sparsely covered with microgranulations; podomere 3 and ultimate podomere (*po6*) longest; ultimate podomere with distal long, thick setae (*mse*). Posterior gonopods (Figs 3B, 4C, D) 6-segmented, covered with sparse long setae; coxite broadly large, basal part sparsely covered with microgranulations; podomeres 2–5 short and stout, somewhat equal in length; ultimate podomere (*po6*) longest, with four apical stylets (*sty*).

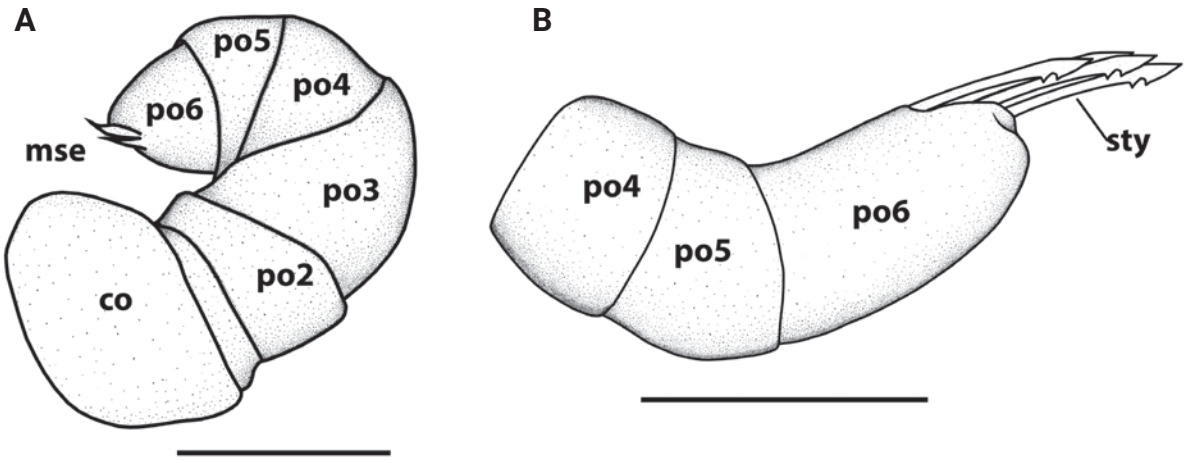

Figure 4. *Pseudodesmus bidoup* sp. nov. Holotype (IEBR-Myr 957). Gonopods. **A.** Right anterior gonopods, anterior view; **B.** Right posterior gonopod, distal part, ventral view. *Abbreviations*: co = coxite = podomere 1; po2 = podomere 2; po3 = podomere 3; po4 = podomere 4; po5 = podomere 5; po6 = podomere 6 (ultimate podomere); mse = macrosetae; sty = stylet. Scale bars: 0.1 mm.

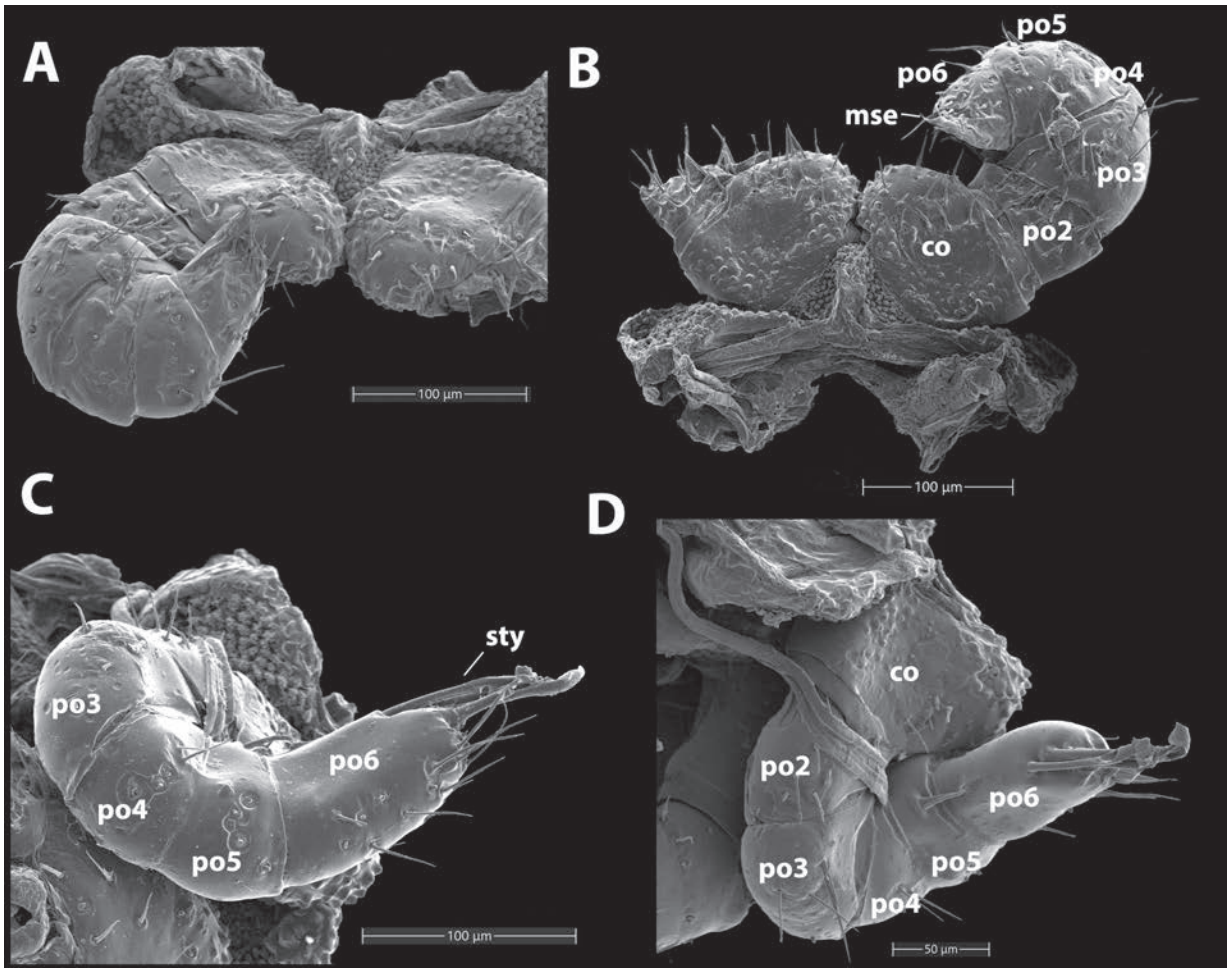

Figure 5. *Pseudodesmus bidoup* sp. nov. Holotype (IEBR-Myr 957). Gonopods. SEM. **A, B.** Right anterior gonopods, ventral view (**A**), anterior view (**B**); **C, D.** Right posterior gonopod, ventral view (**C**), sublateral view (**D**). *Abbreviations*: co = coxite = podomere 1; po2 = podomere 2; po3 = podomere 3; po4 = podomere 4; po5 = podomere 5; po6 = podomere 6 (ultimate podomere); mse = macrosetae; sty = stylet.

Variation. ***Female paratype:*** number of body rings 43–44 plus telson, length ca. 13.75–14.50 mm, length of midbody metazonites about 0.27–0.31 mm, width of midbody metazonite and prozonite ca. 2.25–2.50 mm and 1.56–1.63 mm, respectively; ratio of width of head and width of collum = 0.96. Nonsexual characters as in male.

The male sample IEBR-Myr 961 has strong tubercles, even on the collum, then on every body ring the two (1+1) median posterior tubercles form a strong paramedian crest along the entire body. Anterior tubercles are also the same but smaller. Color is uniformly yellowish, without a dark pattern.

Etymology. Named after the "Bi Doup" mountain, type locality. Noun in apposition.

Distribution. The species has been found in mixed forests and regenerated forests in Kon Tum and Lam Dong provinces, Highlands of Vietnam.

DNA barcoding. Sequencing a fragment of the COI gene failed.

Pseudodesmus ngoclinh sp. nov.

https://zoobank.org/3132C8AB-185A-4282-873E-274B50C0ECC7
Figs 6–10

Material examined. ***Holotype.*** Vietnam • 1 male; Kon Tum Province, Ngoc Linh Mts; 15.07134°N, 107.97158°E; 1,800–1,900 m a.s.l.; 21 Mar.–9 Apr. 2006; Anh D. Nguyen leg.; primary forest, decaying wood, under the bark; IEBR-Myr 986H.

Paratypes. Vietnam • 1 male, 2 females; same data as for the holotype; IEBR-Myr 986P • 2 females; same data as for the holotype; HNHM.

Diagnosis. Head slightly broader than collum. Collum with distinct paraterga directed anterad, with two rows of 1+1 smaller and 2+2 larger tubercles. Body covered with dense minute pubescence. Midbody body rings with two rows of tubercles on metazona, posterior row of 4–5+4–5 tubercles, shorter and extending to base of paraterga; anterior row of 5–10 + 5–10 small tubercles, longer, extending to about midlength of paraterga. Posterior gonopods 6-segmented, with two apical stylets.

Diagnosis remarks. The new species is easily distinguished from *P. camptotrichus* by coloration (yellowish/brownish plus dark spots vs whole earth brown). It also differs from *P. variegatus* and *P. camptotrichus* in having smaller size (length: 11.4 mm vs 32 mm and 14 mm; width: 2.74 mm vs 5.8 mm and 2.0 mm, respestively), number of metazonal tubercles (two rows of 5–10 + 5–10 and 4–5+4–5 vs two rows of 8–15+8–15 and 5–7+5–7, and two rows of 6+6 to 9+9 each row, respectively).

Description. Male holotype.

Measurements: 51 body rings plus telson; length about 11.40 mm, length of midbody metazona about 0.19 mm, width of midbody metazona about 2.74 mm, width of midbody prozona about 1.26 mm; ratio of width of head and width of collum = 1.05.

Coloration of ethanol-preserved specimens: first 6 body rings including collum yellowish in the middle, then most body rings with a light median section, dark spots (on tubercles) irregularly on one side or both sides, dark spots on paraterga, asymmetrically, and almost every body ring different, sometimes repeating 3–4 body rings, last 5–6 body rings uniformly brownish.

Head (Figs 6A, B, F, 7A–D) round-shaped, moderately densely setose. Antenna stout, clavate, *in situ* reaching to body ring 5; antennomere 6 > 5 >3 > 4 = 2 > 7 = 1 in length. Collum with distinct paraterga directed anterad, with two rows: anterior row with 1+1 tubercles, posterior row with 2+2 tubercles, paramedian ones being larger (Figs 6A, 7A, B). Body covered with dense minute pubescence. Slopes of dorsum steep, so body in cross-section subtriangular. Body rings 2–4 with a single row, each of 1+2, 1+1, 3+4 tubercles, respectively (Figs 6A, C, 7A). Midbody body rings with two rows of tubercles on metazona, posterior row of 4–5+4–5 tubercles, shorter and extending to base of paraterga; anterior row of 5–10 + 5–10 small tubercles, longer, extending to about midlength of paraterga. Paramedian tubercles considerably larger, and posterior paramedian tubercles much larger than anterior paramedian ones (Figs 6D, 8A, 8C). The last 6 body rings with only a row of 4+4 tubercles (Figs 6E, 8C).

Paraterga curved strongly anteriad on body rings 2–5, increasingly less so on body rings 6–10 (to body ring 11 on paratype specimens), slightly curved caudad on body ring 11 (to body ring 12 on paratype specimens) and following body rings; caudal curvature of paraterga increasingly clear on 6–7 posteriormost body rings in front of telson; paraterga of penultimate body ring produced strictly caudad and flanking telson (Figs 6E, G, 8C, D). Caudal paratergal margins entire, without notches (Figs 6–8).

Telson (Figs 6C, 8C, D) short, caudal margin rounded; epiproct with 2+2 small/tiny tubercles at caudal margin. Paraprocts and hypoproct semi-circular.

Legs slender, shorter than width of body ring together with paraterga, terminating before lateral paratergal margins. Prefemur = tarsus > femur > postfemur = tibia in length. Claws normal. Coxal sacs present on body rings 3–41 (Figs 6G, 8B).

Gonopods: Two pairs of gonopods directed mesoanteriad. Anterior gonopods (Figs 9A, 10A, B) 6-segmented, covered with long setae; coxite broadly stout, basal part sparsely covered with microgranulations; podomeres 2–5, short and stout; podomere 6 slightly longer than other podomeres, distally carrying macrosetae (*mse*). Posterior gonopods (Figs 9B, 10C, D) 6-segmented, covered with sparse long setae; coxite broad, basal part sparsely covered with microgranulations; podomeres 2–5 short and stout; ultimate podomere (*po6*) longest, with two apical stylets (*sty*).

Variation. ***Male paratype:*** 53 body rings + telson; length about 11.73 mm, length of midbody metazona about 0.21 mm, width of midbody metazona about 2.79 mm, width of midbody prozona about 1.28 mm.

Female paratypes. 48–51 body rings + telson. Length *ca* 12.21–13.52 mm, width of midbody metazona about 2.84–3.02 mm; width of prozona about 1.32 mm; length of metazona about 0.26 mm, average ratio of width of head and width of collum = 1.14. Nonsexual characters as in male.

Etymology. Named after the "Ngoc Linh" Mountain, the type locality. Noun in apposition.

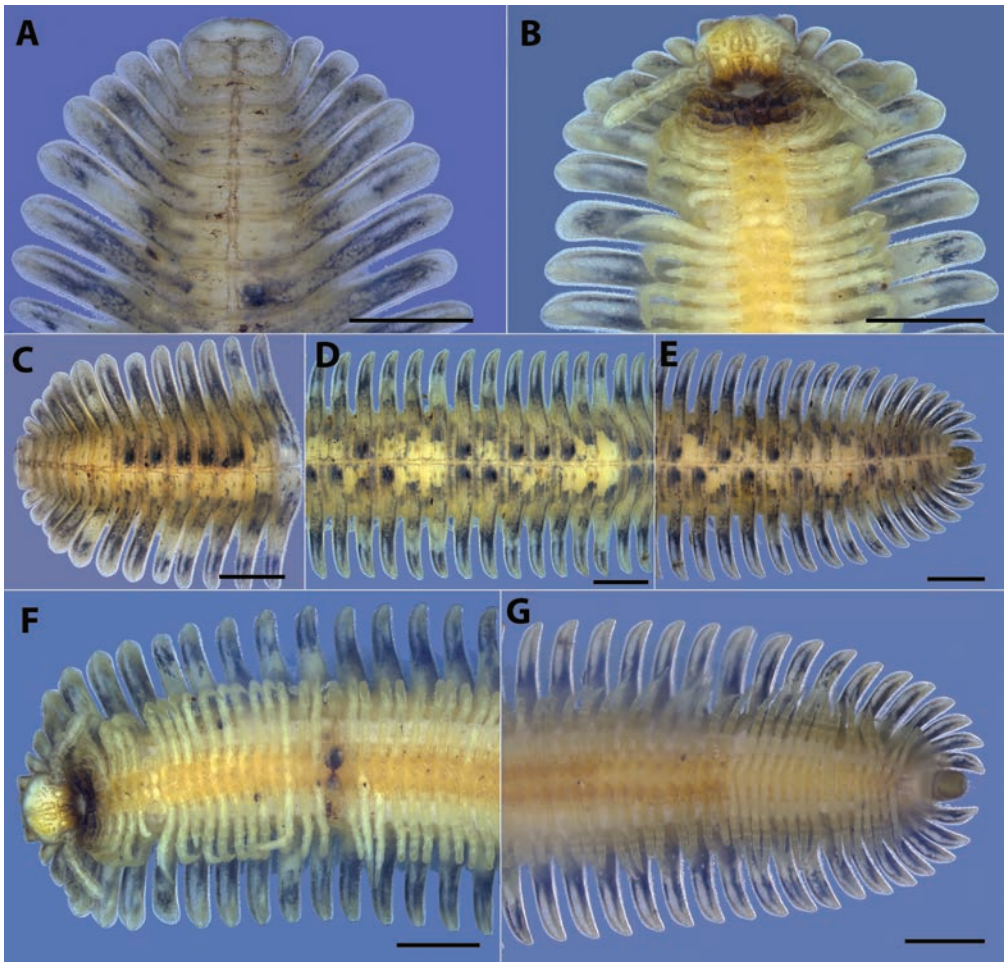

Figure 6. *Pseudodesmus ngoclinh* sp. nov, holotype (IEBR-Myr 986H), under white light. **A–C.** Anterior part of body, dorsal view (**A, C**), ventral view (**B**); **D.** Midbody body rings, ventral view; **E.** Posterior part of body dorsal view; **F.** Anterior half of body, ventral view; **G.** Posterior half of body, ventral view. Scale bars: 1 mm.

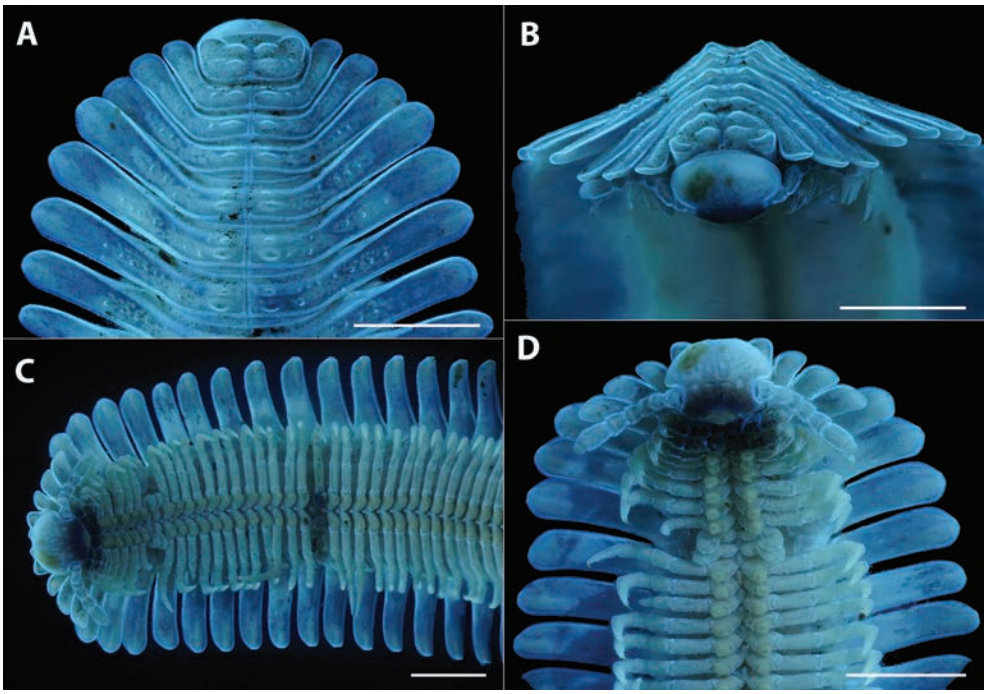

Figure 7. *Pseudodesmus ngoclinh* sp. nov, holotype (IEBR-Myr 986H), under UV light. **A.** Anterior part of body, dorsal view; **B.** Head and collum, anterior view; **C.** Anterior half of body, ventral view; **D.** Anterior part of body, ventral view. Scale bars: 1 mm.

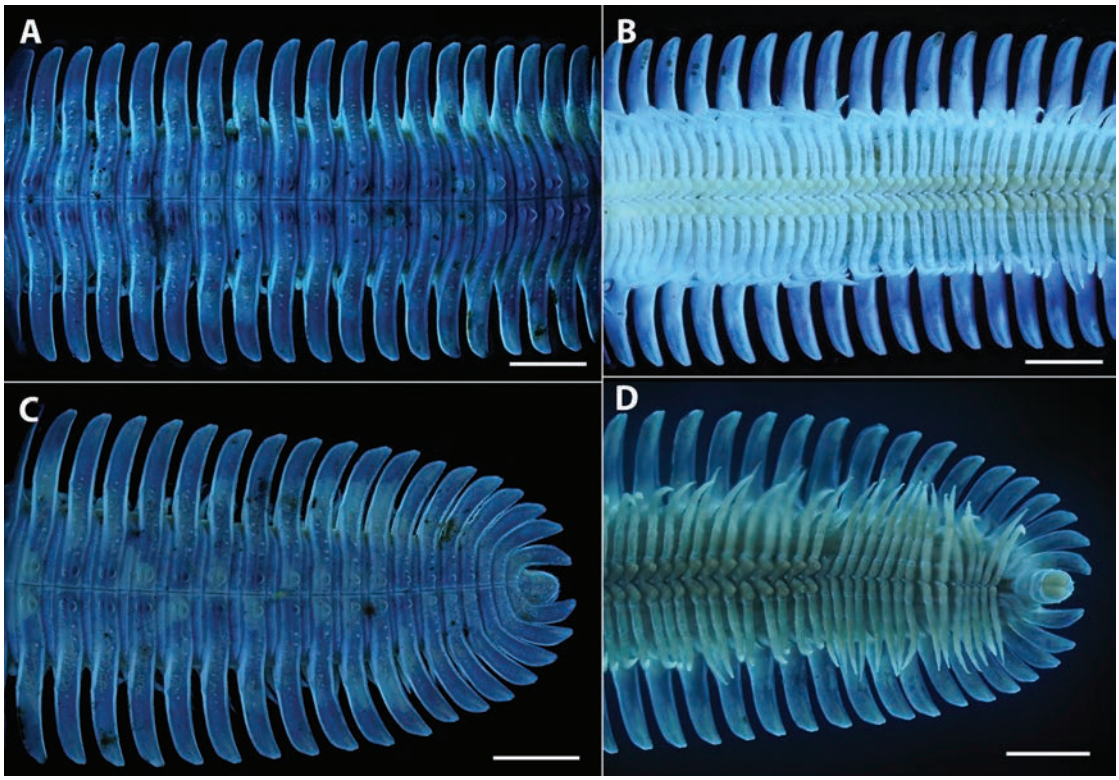

Figure 8. *Pseudodesmus ngoclinh* sp. nov, holotype (IEBR-Myr 986H), under UV light. **A, B.** Midbody body rings, dorsal view (**A**), ventral view (**B**); **C, D.** Posterior half of body, dorsal view (**C**), ventral view (**D**). Scale bars: 1 mm.

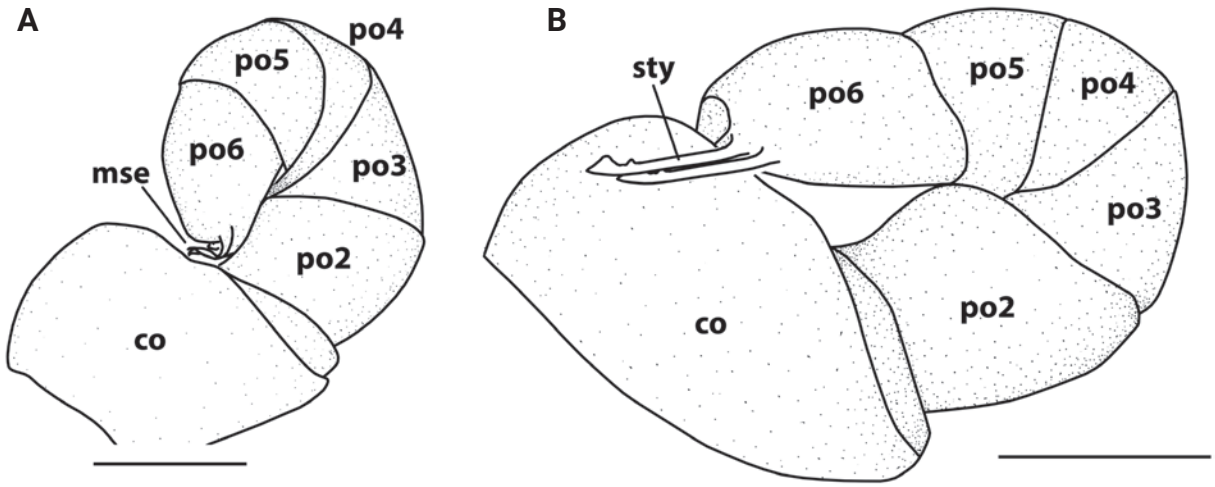

Figure 9. *Pseudodesmus ngoclinh* sp. nov, holotype (IEBR-Myr 986H), gonopods. **A.** Left anterior gonopod, ventral view; **B.** Posterior gonopods, anterior view. *Abbreviations*: co = coxite = podomere 1; po2 = podomere 2; po3 = podomere 3; po4 = podomere 4; po5 = podomere 5; po6 = podomere 6 (ultimate podomere); mse = macrosetae; sty = stylet. Scale bars: 0.1 mm.

Distribution. The species has been found in Ngoc Linh Mts at the high elevation of 1800–1900 m a.s.l. in Kon Tum Province, Vietnam.

DNA barcoding. A fragment of the COI gene is accessioned at NCBI GenBank with the following accession numbers: PQ423222–PQ423223. The new species has a COI gene similarity with Androgna thidae spp. (MF983566 and MF983567) of 89.13% and 89.37% identity, respectively.

Pseudodesmus karstomus sp. nov.

https://zoobank.org/0EE484F0-C29F-439C-B717-5478C9838FEF

Figs 11–14

Material examined. ***Holotype.*** Vietnam • 1 male; Cao Bang Province, Tra Linh District, Quoc Toan commune, Thang Hen Lake, near Ham Huong cave; 22.7588°N, 106.2958°E, 1 Nov. 2021; A.D. Nguyen leg.; IEBR-Myr 959H.

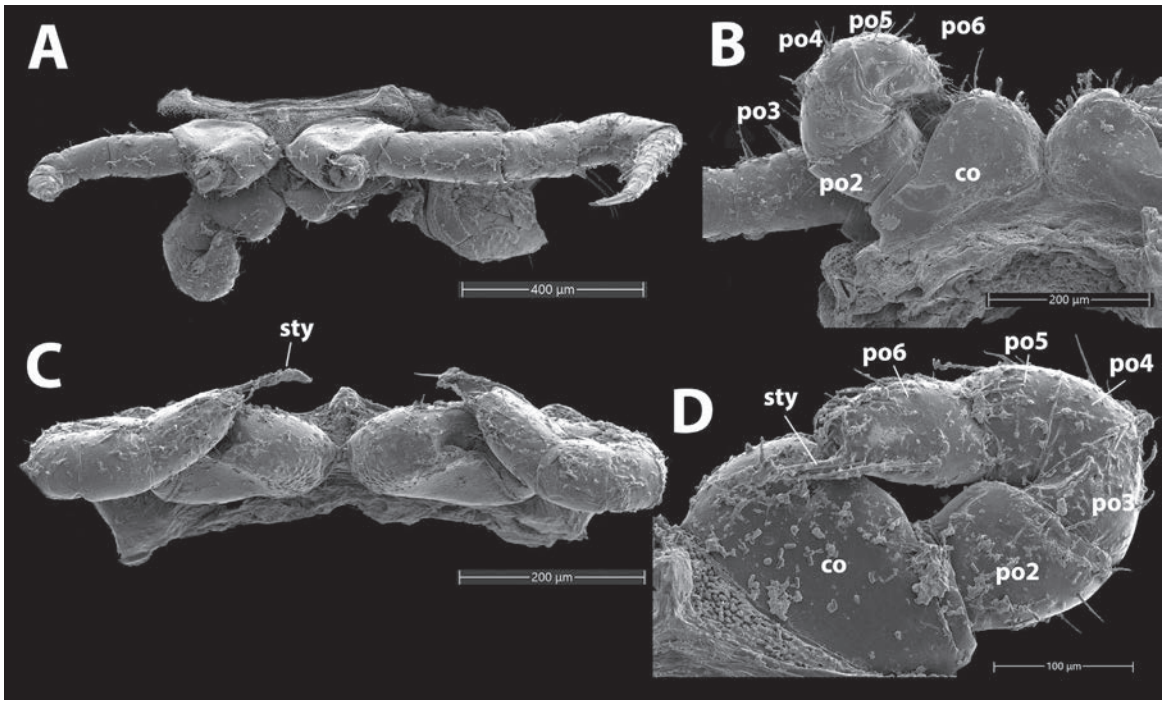

Figure 10. *Pseudodesmus ngoclinh* sp. nov, holotype (IEBR-Myr 986H), gonopods. SEM. **A, B.** Left anterior gonopod, ventral view (**A**), posterior view (**B**); **C, D.** Posterior gonopods, ventral view (**C**), anterior view (**B**). *Abbreviations*: co = coxite = podomere 1; po2 = podomere 2; po3 = podomere 3; po4 = podomere 4; po5 = podomere 5; po6 = podomere 6 (ultimate podomere); mse = macrosetae; sty = stylet.

Paratypes. Vietnam • 1 male, 1 female same data as for the holotype; IEBR-Myr 959P • 1 male; same data as for the holotype; HNHM.

Diagnosis. Terga and base of paraterga marbled yellowish brown with some blackish tubercles on several body rings. Head triangular-shaped, slightly narrower than collum. Collum stout strongly bilobed, anteriorly excavated, with small 2 bumps in the middle, densely setose. Midbody metazonae with two rows of tubercles, anterior row with 7–8+7–8 tubercles, posterior one with 2+2 tubercles. Posterior gonopods 6-segmented, with two apical stylets and two lateroapical stylets.

Diagnosis remarks. The new species is easily distinguished from *P. camptotrichus* by coloration (marbled yellowish brown with some blackish tubercles vs earth brown), larger size (length: 18.64 mm vs 14 mm; width: 2.74 mm vs 2.0 mm), number of metazonal tubercles (two rows of 7–8+7–8 and 2+2 tubercles vs two rows of 6+6 to 9+9 each row).

It also differs from *P. variegatus* in having smaller size (length: 18.64 mm vs 32.0 mm; width: 2.74 mm vs 5.8 mm), number of metazonal tubercles (two rows of 7–8+7–8 and 2+2 tubercles vs two rows of 8–15+8–15 and 5–7+5–7).

Pseudodesmus karstomus sp. nov. is differentiated from two above new species, *P. bidoup* sp.nov. and *P. ngoclinh* sp.nov in body size and number of gonopod stylets. It shares with *P. bidoup* sp.nov. a posterior gonopod with four distal stylets, but two species are distinguished by body size (length: 18.62 mm vs 9.25 mm; width: 4.05 mm vs 1.63 mm). *Pseudodesmus karstomus* is also larger than *P. ngoclinh* (length: 18.62 mm vs 11.4 mm; width: 4.05 mm vs 2.74 mm), and having more distal stylets in posterior gonopod (four vs two).

Description. Male holotype.

Measurements: 61 body rings plus telson, length about 18.64 mm, length of midbody metazona ca. 0.29 mm, width of midbody metazona ca. 4.05 mm, width of midbody prozona ca. 1.35 mm; ratio of width of head and width of collum = 0.98.

Coloration of ethanol-preserved specimens: Terga and base of paraterga marbled yellowish brown with some blackish tubercles on several body rings. Collum and first 4 body rings yellow, 5th weakly brownish, then increasing color pattern: 6–10th light in the middle and brownish at the base of paraterga, 11–12th dark brown in the middle and light borwn at the base of paraterga; then the same pattern repeated as 4 light+3 brown, 5 light+3 brown, 5 light+3 brown, 5 light+3 brown, 3 light+2 brown, 2 light+2 light brown, 3 light in the middle and brownish at the base of paraterga, then the ultimate 3 body rings plus telson and light yellow (Fig. 11A–C). Paraterga paler in preserved specimens, but pinkish in alive specimens.

Head (Figs 11D, E, 12D, E) somewhat smooth, triangular-shaped. Antenna short, somewhat stout, *in situ* extending to body ring 5; antennomere 6 > 5 >3 > 4 = 2 > 7 = 1 in length. Collum (Figs 11D, E, 12D, E) stout strongly bilobed, anteriorly excavated, with two small bumps in the middle, densely setose. Paraterga very tiny, somewhat like lateral keels, caudal margin similar lateral keels.

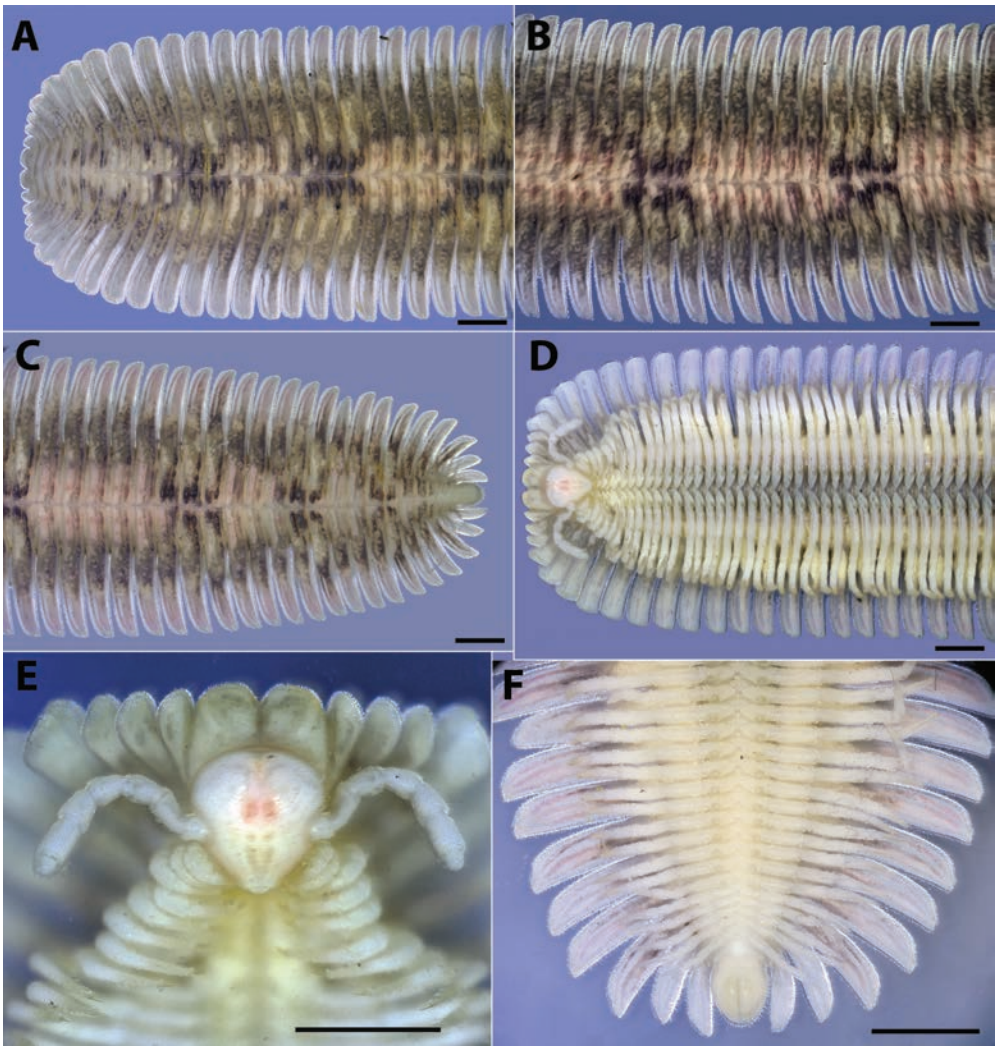

Figure 11. *Pseudodesmus karstomus* sp. nov. Holotype (IEBR-Myr 959H), under white light. **A.** Anterior part of body, dorsal view; **B.** Midbody body rings, dorsal view; **C.** Posterior part of body, dorsal view; **D.** Anterior part of body, ventral view; **E.** Head and collum, ventral view; **F.** Posteriormost part of body, ventral view. Scale bars: 1 mm.

Tergum 2 with a row of 1+1 large, subtriangular tubercles, those tubercles reducing to rather small ones on subsequent terga. Terga 2–5 with one row, from 6th onward with two rows of tubercles, anterior row with 7–8+7–8 tubercles, reaching the middle of paraterga, posterior row with only 2+2, never extending to paraterga; the 1+1 median tubercles (both anterior and posterior) transversally enlarged, elongated, oval (Figs 11A–C, 12A–C).

Paraterga in general very wide (Figs 11, 12). Paraterga 2–3 (Figs 11D, E, 12D, E) anterad directed; paraterga 3–5 extending slightly lateroanterad, paraterga 6–58 laterad, 59–61 lateroposteriad, 62–63 posteriad. Paraterga 1–13 rectangular, from 14th onwards tapering laterad, anterior edge increasingly bending backwards.

Telson (Figs 11C, F, 12C, F) short, caudal margin rounded; epiproct with 3+3 setiferous tubercles at caudal margin (Figs 11C, F, 12C, F). Paraproct and hypoproct semi-circular (Figs 11F, 12F).

Legs slender, shorter than paraterga, terminating before lateral paratergal margins. Claws normal. Coxal sacs present ventrally on body rings 3–59 (Figs 11F, 12F).

Gonopods (Figs 13, 14): Two pairs of gonopods directed mesoanteriad. Anterior gonopods (Figs 13A, 14A, B, F) 6-segmented, covered with long setae; coxite (*co*) broad, basal part sparsely covered with microgranulations; podomeres 2–5, short and stout; podomere 6 slightly longer than other podomeres, distally carrying macrosetae (*mse*). Posterior gonopods (Figs 13B, 14C, D, E) 6-segmented, covered with sparse long setae; coxite (*co*) broad, basal part sparsely covered with microgranulations; podomeres 2–5 short and stout; ultimate podomere (*po6*) longest, with two apical stylets and two lateroapical stylets (*sty*).

Variation. ***Male paratypes*** have 62–63 plus telson, length about 17.76–17.92 mm, length of midbody metazoan ca. 0.29–0.33 mm, width of midbody metazona ca. 2.90–2.94 mm, width of midbody prozona ca. 1.37–1.45 mm; average ratio of width of head and width of collum = 0.89 (width of collum: 0.61 mm, width of head: 0.68 mm).

Female paratype. 66 body rings plus telson; length about 22.36 mm, length of midbody metazoan ca. 0.42 mm, width of midbody metazona ca. 4.06 mm, width

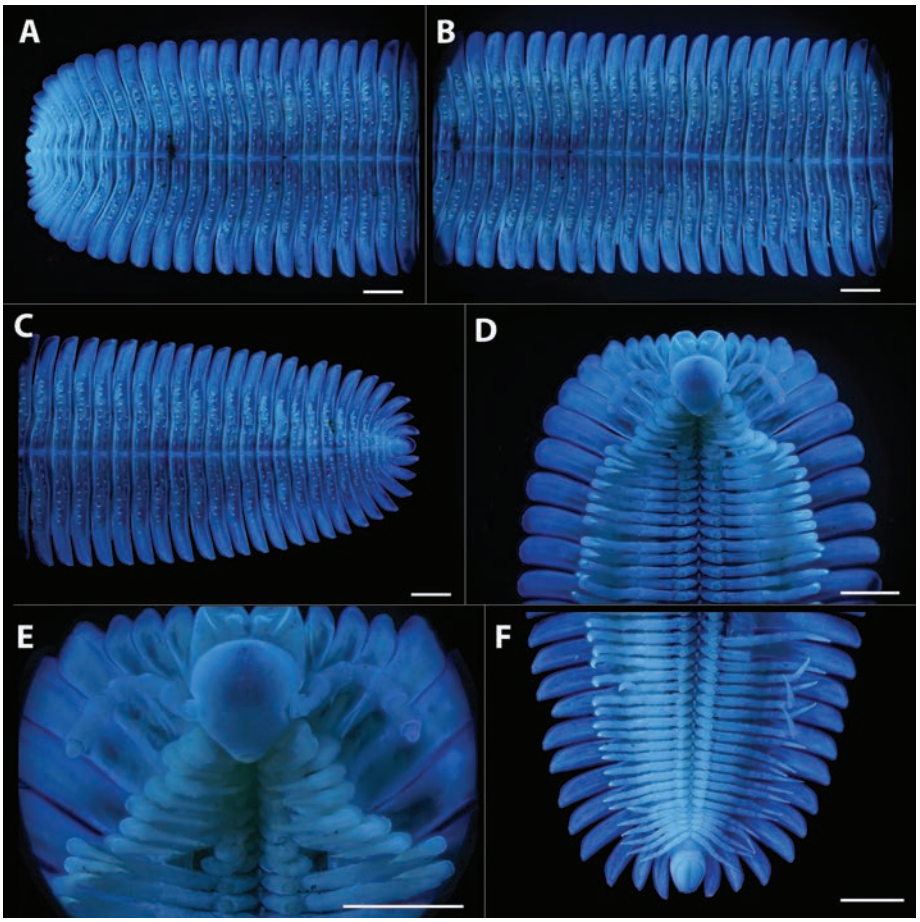

Figure 12. *Pseudodesmus karstomus* sp. nov. Holotype (IEBR-Myr 959H), under UV light. **A.** Anterior part of body, dorsal view; **B.** Midbody body rings, dorsal view; **C.** Posterior part of body, dorsal view; **D.** Anterior part of body, ventral view; **E.** Head and collum, ventral view; **F.** Posterior part of body, ventral vie. Scale bars: 1 mm.

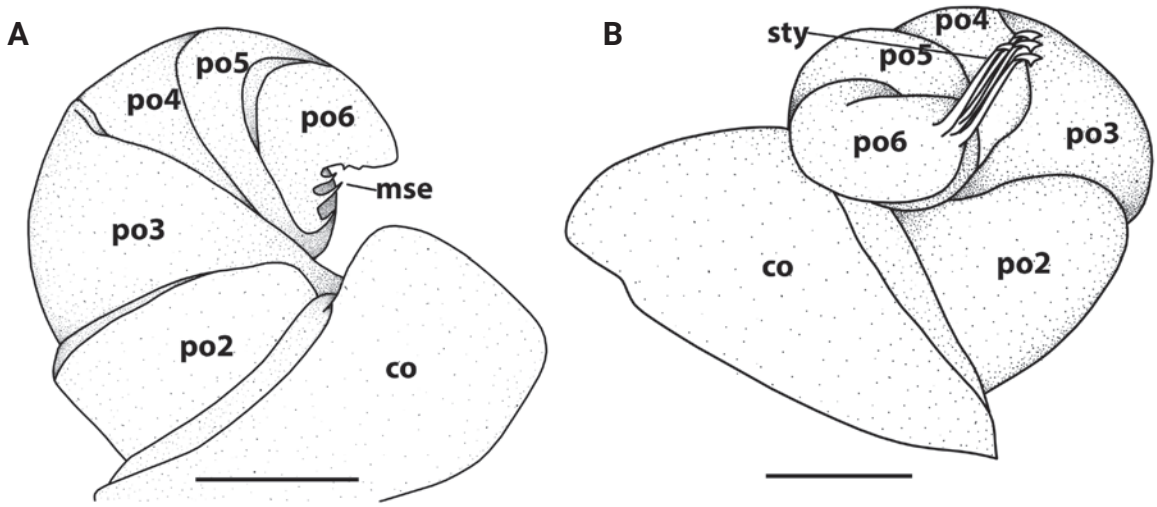

Figure 13. *Pseudodesmus karstomus* sp. nov. Holotype (IEBR-Myr 959H), gonopods. **A.** Left anterior gonopods, anterior view. **B.** Right posterior gonopods, anterior view. *Abbreviations*: co = coxite = podomere 1; po2 = podomere 2; po3 = podomere 3; po4 = podomere 4; po5 = podomere 5; po6 = podomere 6 (ultimate podomere); mse = macrosetae; sty = stylet. Scale bars: 0.1 mm.

of midbody prozona ca. 1.75 mm; ratio of width of head and width of collum = 0.9 (width of collum: 0.72 mm, width of head: 0.65 mm). Nonsexual characters as in male.

Etymology. Named to emphasize the type locality, karst areas. Noun in apposition.

Distribution. The species was found in limestone mountain in Cao Bang Province, northern Vietnam.

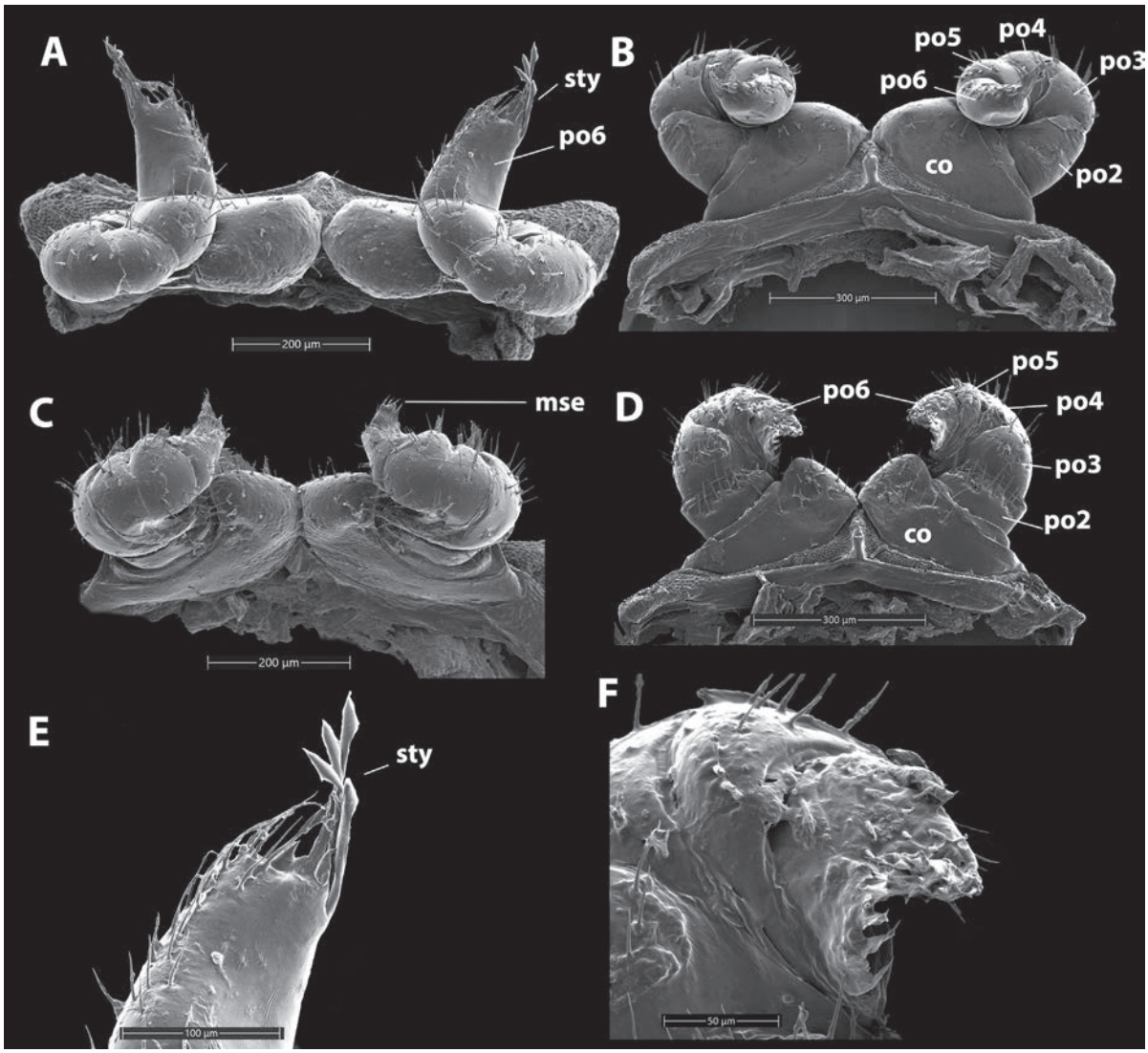

Figure 14. *Pseudodesmus karstomus* sp. nov. Holotype (IEBR-Myr 959H), gonopods. SEM. **A, B.** Posterior gonopods, ventral view (**A**), anterior view (**B**); **C, D.** Anterior gonopods, ventral view (**C**), anterior view (**D**); **E.** Apical stylets of posterior gonopod, ventral view; **F.** Distal part of anterior gonopod, anterior view. *Abbreviations*: co = coxite = podomere 1; po2 = podomere 2; po3 = podomere 3; po4 = podomere 4; po5 = podomere 5; po6 = podomere 6 (ultimate podomere); mse = macrosetae; sty = stylet.

DNA barcoding. A fragment of the COI gene is accessioned at NCBI GenBank with the following accession numbers: PQ423224–PQ423225. The new species has a close COI gene similarity with *Gosodesmus claremontus* (JX962723) of 85.14% in the BLAST search.

Pseudodesmus condao sp. nov.

https://zoobank.org/CE1AD5B1-0A85-447A-91FF-1B490A38097D
Figs 15–20

Material examined. ***Holotype.*** Vietnam • 1 male; Ba Ria-Vung Tau Province, Con Dao NP, on the way to Ong Dung Beach; 08.70528°N, 106.59158°E, 37 m a.s.l., 7 Nov. 2019; A.D. Nguyen leg.; natural forest; IEBR-Myr 982H.

Paratypes. Vietnam • 2 males, 2 females; same data as the holotype; IEBR-Myr 982P • 3 males, 1 female Ba Ria-Vung Tau Province, Con Dao NP, on the way to Ong Dung beach, 08.70528°N, 106.59158°E, 37 m a.s.l., 7 November 2019, leg. Nguyen A.D.; natural forest; IEBR Myr 821 • 8 males, 5 females; Ba Ria-Vung Tau Province, Con Dao NP, on the way to Ong Dung beach, 08.70528°N, 106.59158°E, 37 m a.s.l.; 8 Nov. 2023; A.D. Nguyen leg.; natural forest; IEBR-Myr 977 • 2 males, 2 females; same data as for sample IEBR-Myr 977; HNHM.

Diagnosis. Color dark yellow, little darker in the middle. Head distinctly smaller than collum. Collum bilobed, each with three anterior lobes, no tubercles. Midbody terga with two rows, 3–4 + 3–4 large and 4– 5 + 4– 5 large tubercles in anterior and posterior rows, respectively. Posterior gonopods 6-segmented, with two apical stylets.

Diagnosis remarks. The new species is very similar with *P. camptotrichus* by coloration (dark yellow vs earth brown), but it differs from *P. variegatus* in body coloration (dark yellow vs yellow-brown with black spots).

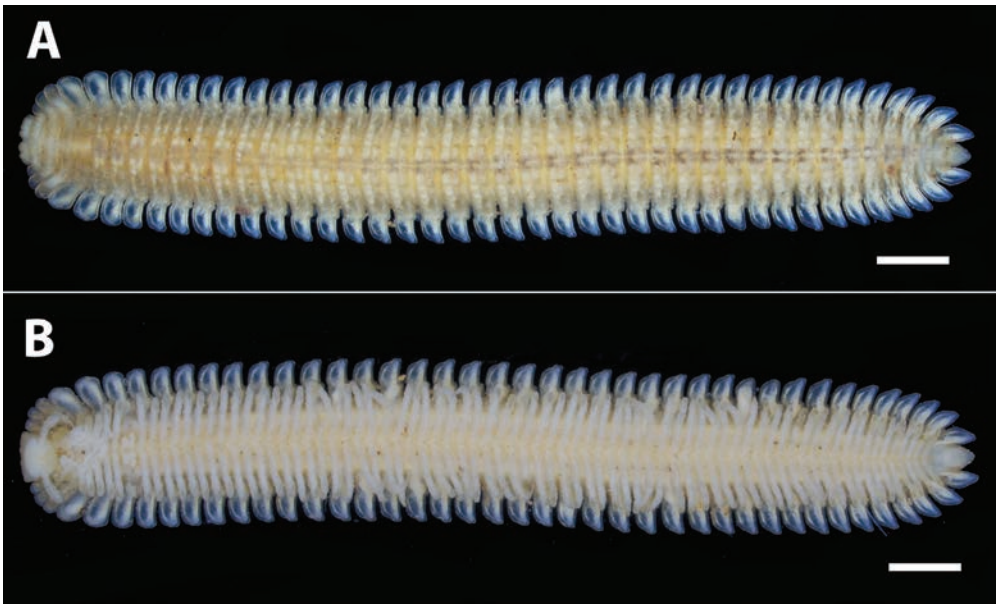

Figure 15. *Pseudodesmus condao* sp. nov. Holotype (IEBR-Myr 982H), under white light. **A, B.** Habitus, dorsal view (**A**), ventral view (**B**). Scale bars: 1 mm.

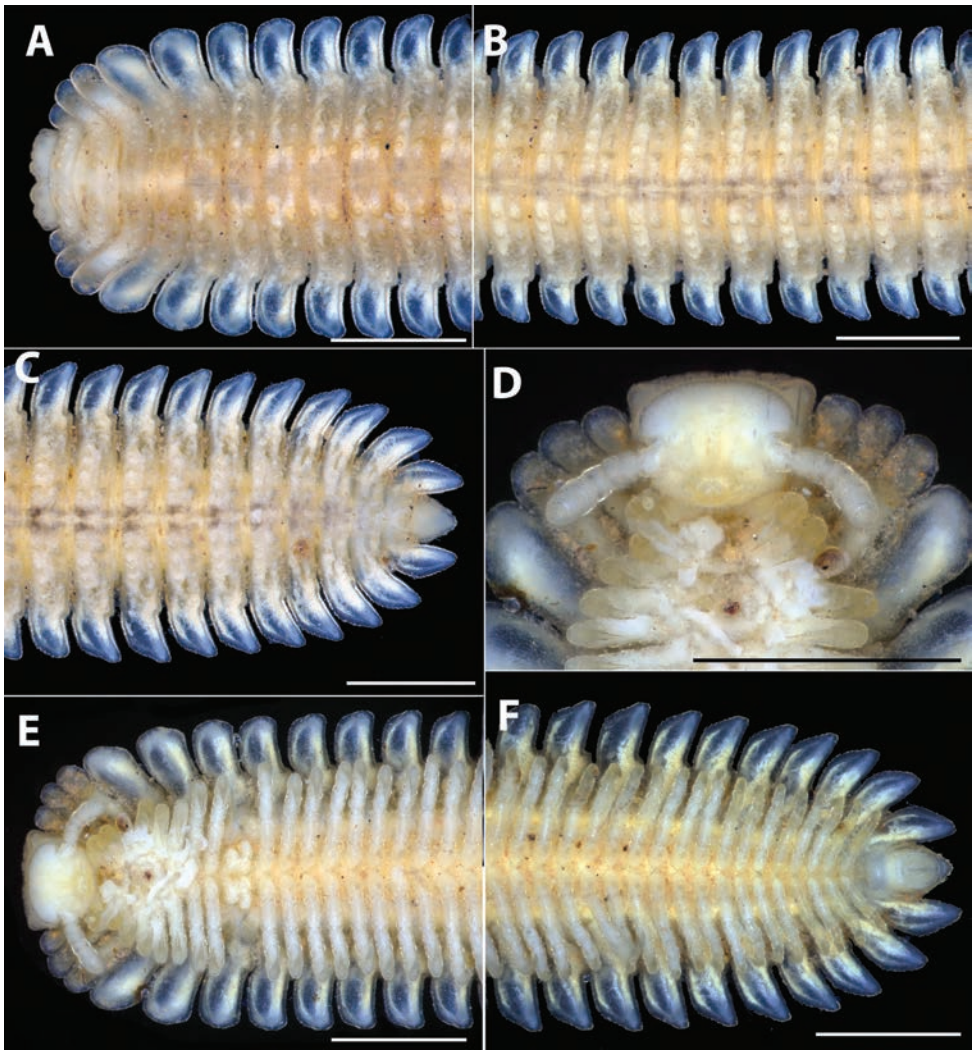

Figure 16. *Pseudodesmus condao* sp. nov. Holotype (IEBR-Myr 982H), under white light. **A.** Anterior part of body, dorsal view; **B.** Midbody body rings, dorsal view; **C.** Posterior part of body, dorsal view; **D.** Head and collum, ventral view; **E.** Anterior part of body, ventral view; **F.** Posterior part of body, ventral view. Scale bars: 1 mm.

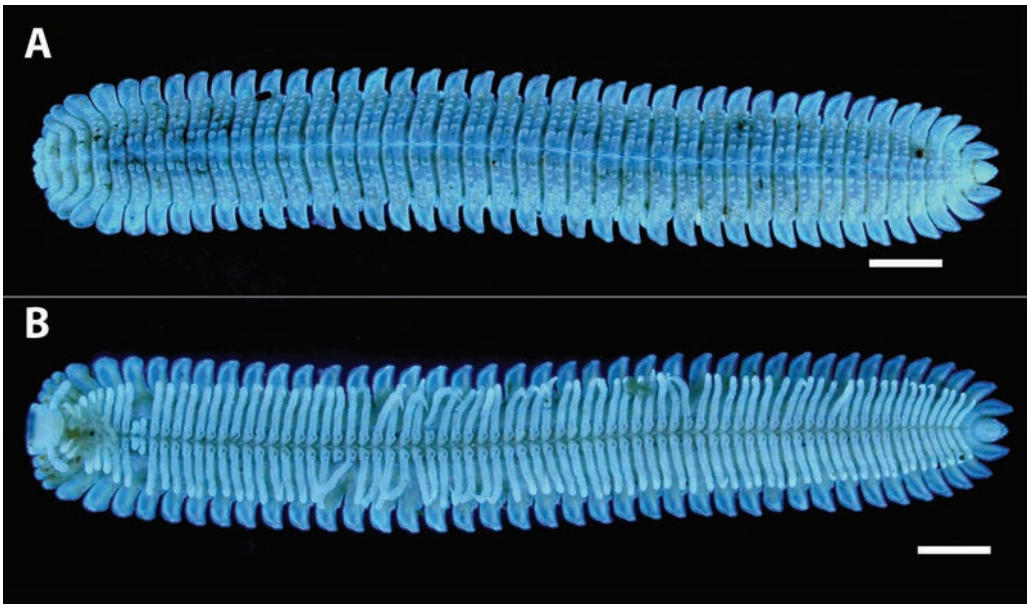

Figure 17. *Pseudodesmus condao* sp. nov. Holotype (IEBR-Myr 982H), under UV light. **A, B.** Habitus, dorsal view (**A**), ventral view (**B**). Scale bars: 1 mm.

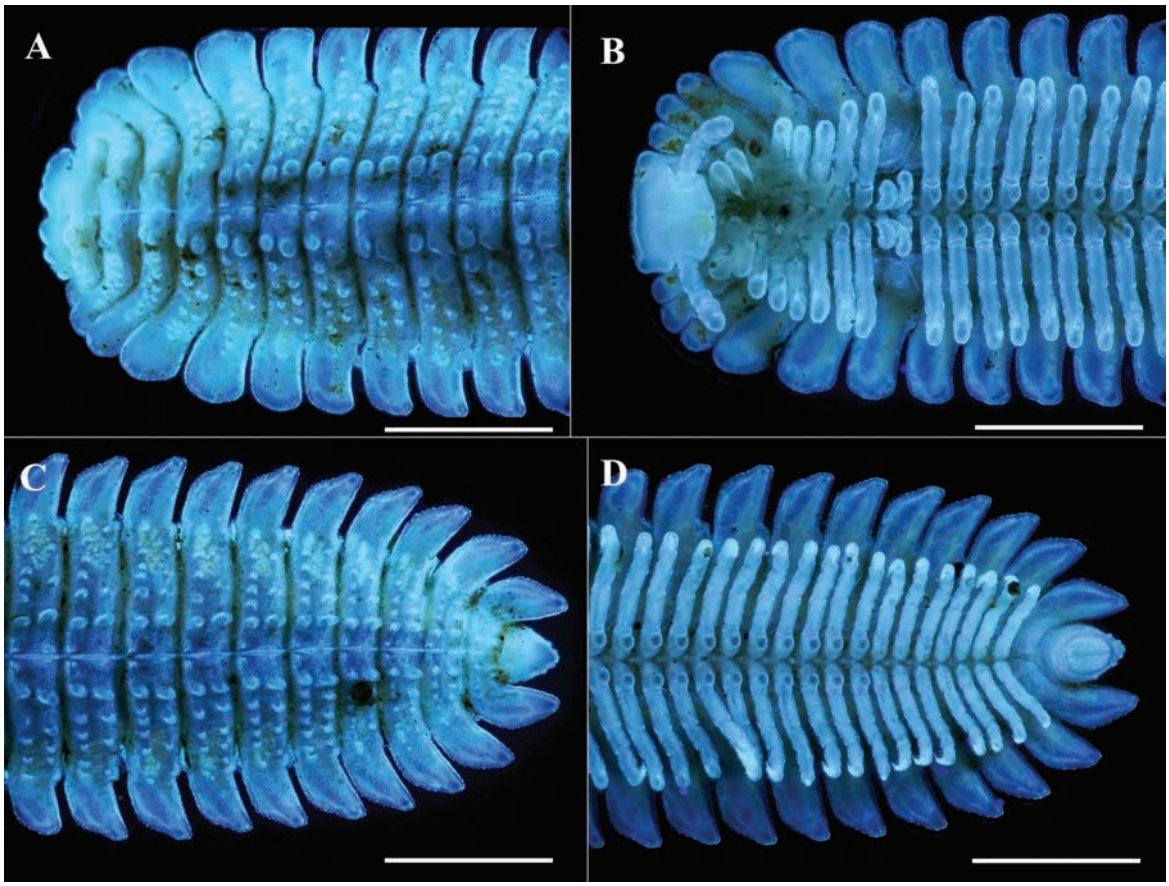

Figure 18. *Pseudodesmus condao* sp. nov. Holotype (IEBR-Myr 982H), under UV light. **A, B.** Anterior part of body, dorsal view (**A**), ventral view (**B**); **C, D.** Posterior part of body, dorsal view (**C**), ventral view (**D**). Scale bars: 1 mm.

In addition, it is smaller than *P. variegatus* and *P. camptotrichus* (length: 9.33 mm vs 32 mm and 14 mm; width: 1.57 mm vs 5.8 mm and 2.0 mm, respestively), having less number of male body rings (42 vs 53–56 and 37–42), and number of metazonal tubercles (two rows of 3–4 + 3–4 and 4–5 + 4–5 tubercles vs two rows of 8–15 + 8–15 and 5–7 + 5–7, and two rows of 6–9 + 6–9 each row, respectively).

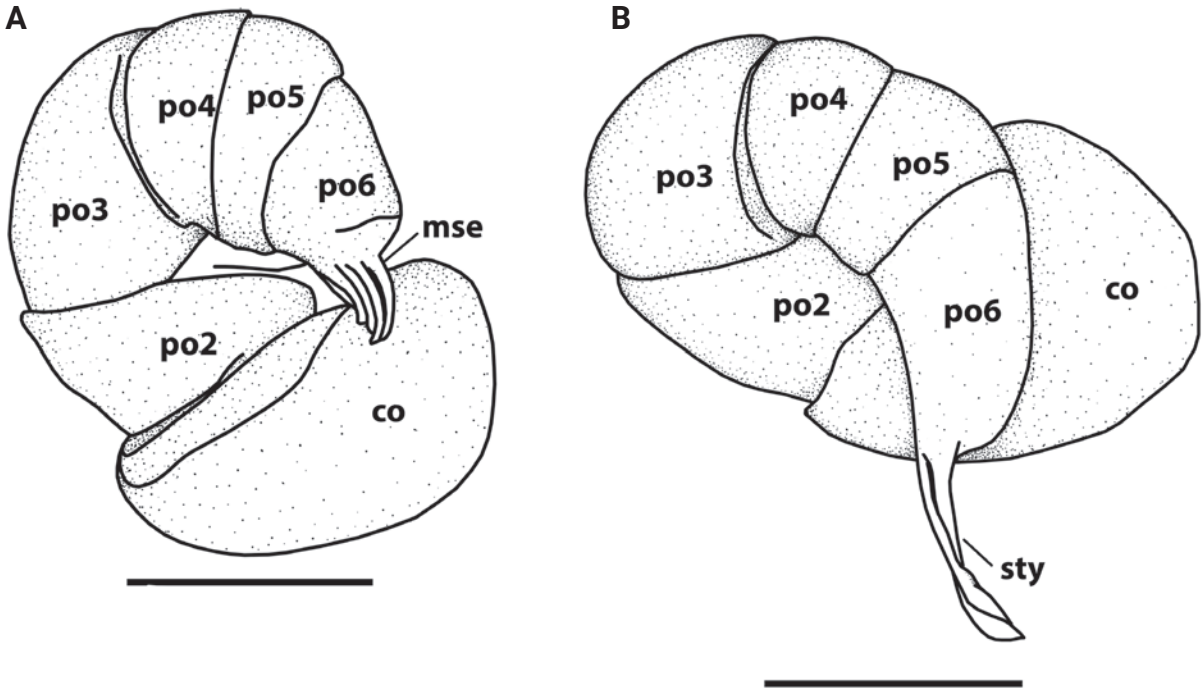

Figure 19. *Pseudodesmus condao* sp. nov. Holotype (IEBR-Myr 982H), gonopods. **A.** Left anterior gonopods, anterior view; **B.** Left posterior gonopod, subventral view. *Abbreviations*: co = coxite = podomere 1; po2 = podomere 2; po3 = podomere 3; po4 = podomere 4; po5 = podomere 5; po6 = podomere 6 (ultimate podomere); mse = macrosetae; sty = stylet. Scale bars: 0.1 mm.

Pseudodesmus condao sp. nov. is differentiated from above three new species, *P. bidoup* sp. nov., *P. ngoclinh* sp. nov and *P. karstomus* sp. nov. in body coloration of generally uniformly dark yellow, smaller body size and number of stylets (two vs four, two and four, respectively).

Description. Male holotype.

Measurements: 42 body rings plus telson, length about 9.33 mm, length of midbody metazona ca. 0.24 mm, width of midbody metazona ca. 1.57 mm, width of midbody prozona ca. 0.63 mm; ratio of width of head and width of collum = 0.89.

Coloration of ethanol-preserved specimens: dark yellow, little darker in the middle.

Head distinctly smaller than collum. Antenna stout, clavate, *in situ* extending to body ring 4; antennomere 6 > 5 >3 > 4 = 2 > 7=1 in length. Collum (Figs 15A, 16A, 17A, 18A) bilobed, each with three anterior lobes, no tubercles. Body rings 2–4 one row of tubercles, then each body ring with 2 rows, body rings 5–8 with 1+1 larger in the middle, then 2+2 larger tubercles, both in anterior and posterior rows (Figs 15A, 16A–C, 17A, 18A, C). Additionally, 2–3 small tubercles in both rows laterally, but only on tergites, not extending to paraterga (Figs 15A, 16A–C, 17A, 18A, C).

Paraterga (Figs 15–18) smooth, almost transparent, wider than in the other species, a little bit spoon form (the distal part is wider than the proximal part), especially in the anterior body ring (up to 10th), later tapering towards the edge, anterior edge is bending backwards, posterior edge remains transverse. Anterior and lateral margin of paraterga serrated (Figs 17A, 18).

Telson (Figs 16C, F, 17C, D) short, caudal margin rounded; epiproct with 2+2 small/tiny tubercles at caudal margin. Paraprocts and hypoproct semi-circular.

Legs slender, shorter than width of body ring together with paraterga, terminating before lateral paratergal margins. Claws normal. Coxal projections present until leg 71 (body ring 38) (Figs 17B, 18D).

Gonopods (Figs 19, 20): Two pairs of gonopods directed anteriad. Anterior gonopods (Figs 19A, 20C, D) 6-segmented, covered with long setae; coxite (*co*) broad, basal part sparsely covered with microgranulations; podomeres 2–5, short and stout; podomere 6 slightly longer than other podomeres, distally carrying macrosetae (*mse*). Posterior gonopods (Figs 19B, 20A, B, E) 6-segmented, covered with sparse long setae; coxite (*co*) broad, basal part sparsely covered with microgranulations; podomeres 2–5 short and stout; ultimate podomere (*po6*) longest, with two apical stylets.

Variation. ***Male paratypes:*** 46–47 body rings plus telson, length about 10.81–11.19mm, length of midbody metazona ca. 0.25–0.28 mm, width of midbody metazona ca. 1.70–1.77 mm, width of midbody prozona ca. 0.75–0.96 mm; ratio of width of head and width of collum = 0.83–0.88. (width of collum: 0.64–0.74 mm, width of head: 0.53–0.65 mm).

Female paratypes: 48–49 body rings plus telson, length about 12.22–12.50 mm, length of midbody metazoan ca. 0.26 mm, width of midbody metazona ca. 1.75–1.77 mm, width of midbody prozona ca. 0.96–0.98 mm; ratio of width of head and width of collum = 0.84. (width of collum: 0.56–0.80 mm, width of head: 0.47–0.67 mm).

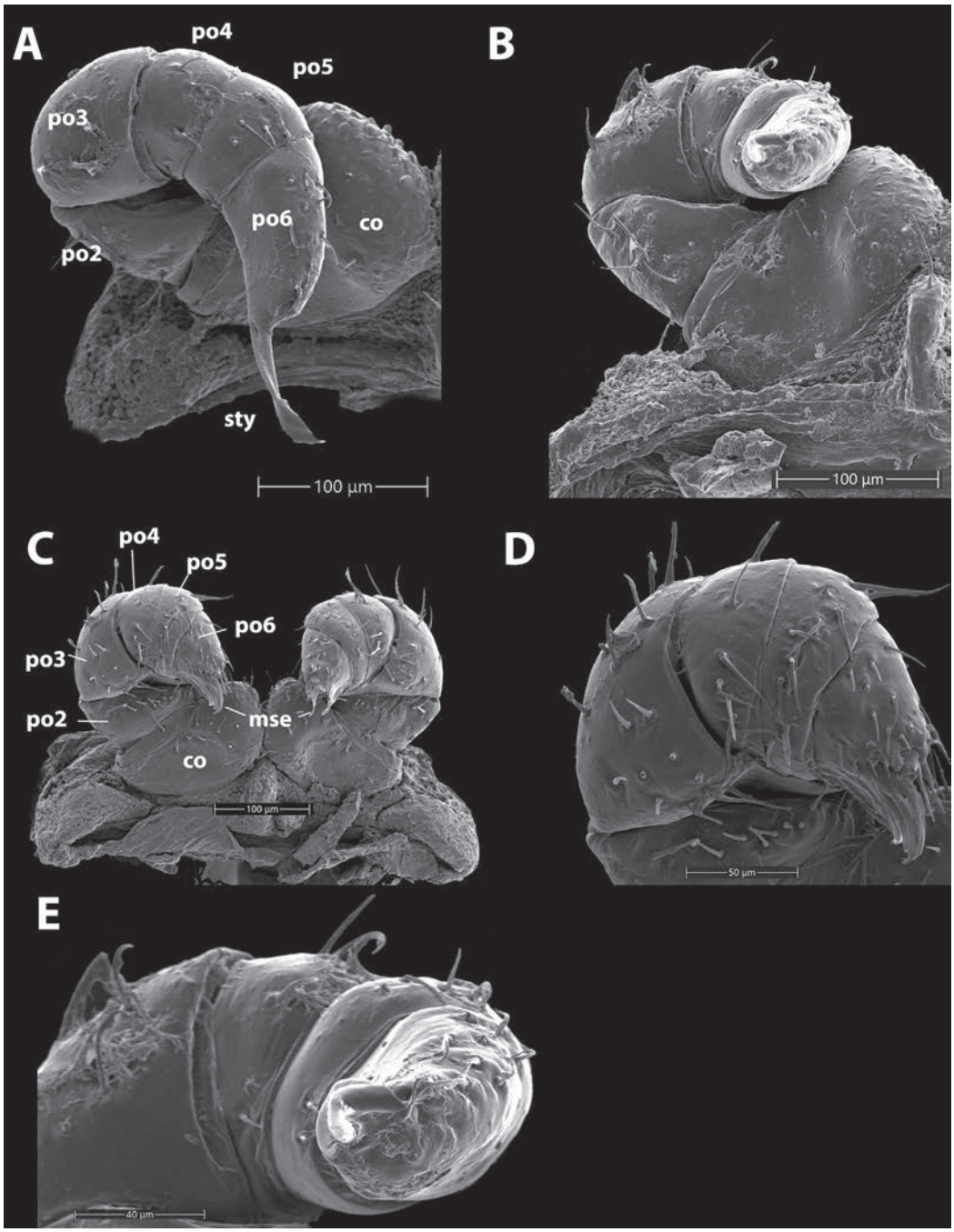

Figure 20. *Pseudodesmus condao* sp. nov. Holotype (IEBR-Myr 982H), gonopods. SEM. **A, B.** Left posterior gonopod, subventral view (**A**), anterior view (**B**); **C.** Anterior gonopods, anterior view; **D.** Left anterior gonopod, anterior view; **E.** Distal part of left posterior gonopod, anterior view. *Abbreviations*: co = coxite = podomere 1; po2 = podomere 2; po3 = podomere 3; po4 = podomere 4; po5 = podomere 5; po6 = podomere 6 (ultimate podomere); mse = macrosetae; sty = stylet.

Etymology. Named after its type locality, Con Dao National Park. Noun in apposition.

Distribution. The species was found in evergreen forests in Con Dao National Park, Ba Ria – Vung Tau Province, southern Vietnam.

DNA barcoding. A fragment of the COI gene is accessioned at NCBI GenBank with the following accession numbers: PQ423226–PQ423227. The new species has a close COI gene similarity with *Gosodesmus claremontus* (JX962723) of 87.46% in the BLAST search.

Pseudodesmus irregularis sp. nov.

https://zoobank.org/2FD3A321-E3F2-419E-A200-4446A132B10A

Figs 21–24

Material examined. ***Holotype.*** Vietnam • 1 male; Khanh Hoa Province, Hon Ba Mt.; 12.11124°N, 108.98426°E; 1,500 m a.s.l.; 15–24 Apr. 2006; A.D. Nguyen leg.; primary forest; IEBR-Myr 958H.

Paratypes. Vietnam • 1 male; same data as for holotype; IEBR-Myr 958P • 1 female; Kon Tum Province,

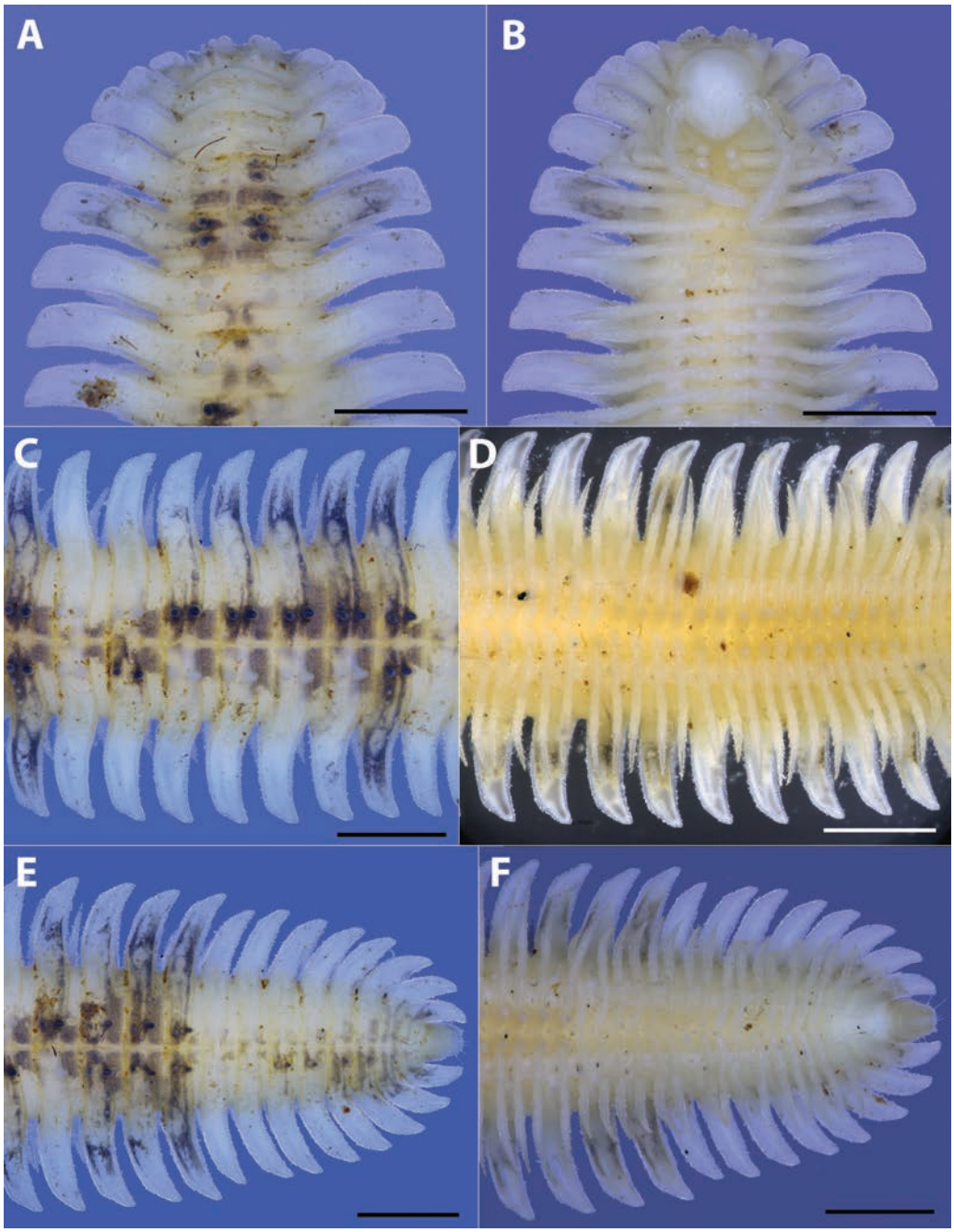

Figure 21. *Pseudodesmus irregularis* sp. nov. Holotype (IEBR-Myr 958H), under normal light. **A, B.** Anterior part of body, dorsal view (**A**), ventral view (**B**); **C, D.** Midbody body rings, dorsal view (**C**), ventral view (**D**); **E, F.** Posterior part of body, dorsal view (**E**), ventral view (**F**). Scale bars: 1 mm.

Ngoc Linh Mt; 15.07071°N, 107.97142°E; 1,700 m a.s.l.; 25 Mar.–11 Apr. 2004, A.D. Nguyen leg.; regenerated forest; IEBR-Myr 960.

Diagnosis. Head narrower than collum. Collum bi-lobed, caudal margin highly elevated with 3+3 tubercles with 3+3 tubercles, and with a row of 1+1 tubercles. Midbody ring with 2 distinct rows of tubercles, anterior row of 6–9+6–9 and posterior of 3+3. Paratergal margins with small/tiny dentations or notches. Posterior gonopods 6-segmented, with three apical stylets.

Diagnosis remarks. The new species is distinguished from *P. camptotrichus* by coloration (irregularly yellow with brown spots vs earth brown), shorter length (12.92 mm vs 14 mm), slightly wider (2.39 mm vs 2.0 mm), having less number of tubercles in posterior metazonal row (3+3 vs 6–9+6–9). The new species is similar to *P. variegatus* regarding body coloration (irregularly yellow with brown spots), but two species can be separated by body size (length: 12.96 mm vs 32 mm; width: 2.39 mm vs 5.8 mm) and and number of metazonal tubercles (two rows of 6–9+6–9 and 3+3 vs two rows of 8–15+8–15 and 5–7+5–7).

Pseudodesmus irregularis sp. nov. is differentiated from above four new species, *P. bidoup* sp. nov., *P. ngo-clinh* sp. nov, *P. karstomus* sp. nov. and *P. condao* sp. nov.

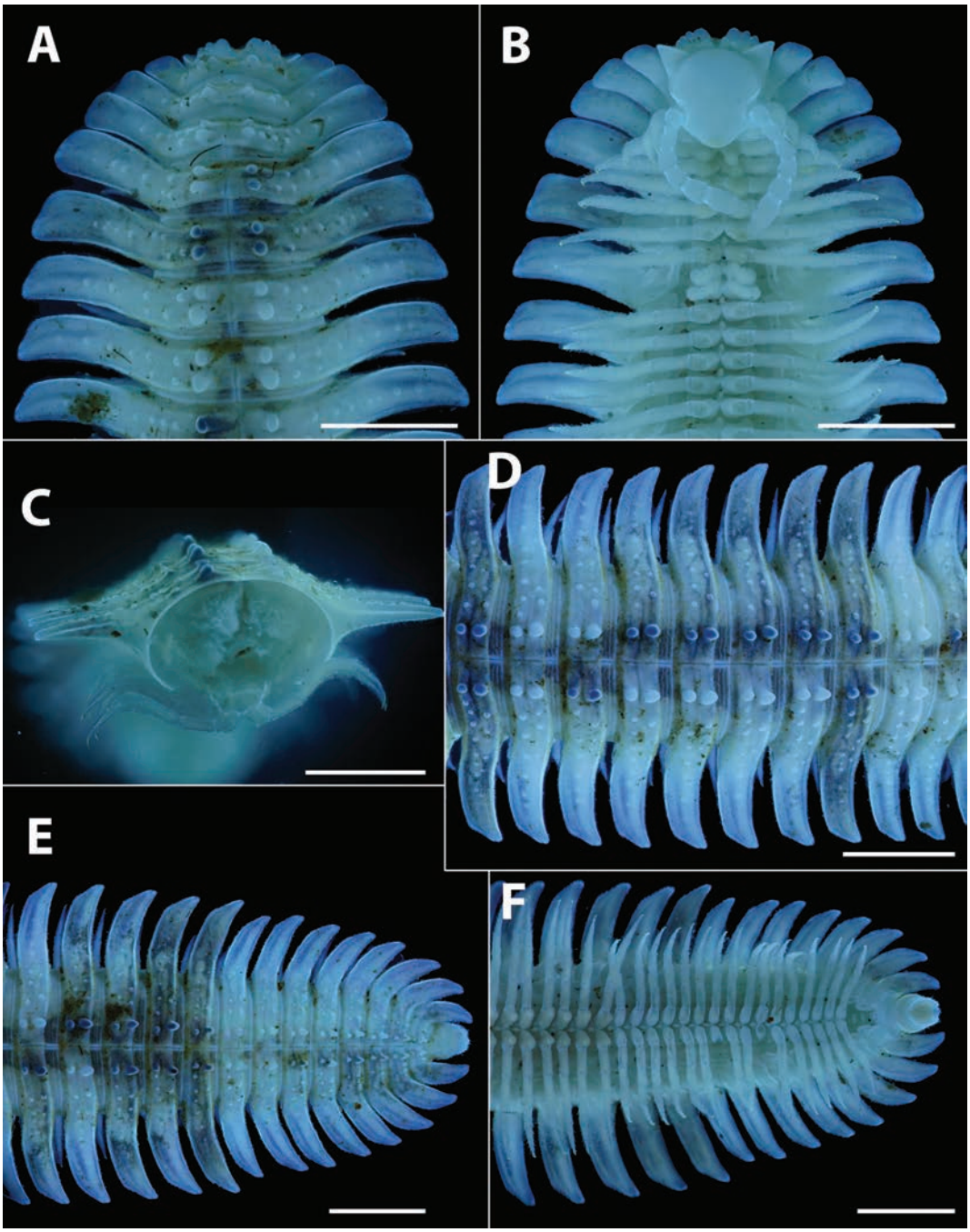

Figure 22. *Pseudodesmus irregularis* sp. nov. Holotype (IEBR-Myr 958H), under UV light. **A, B.** Anterior part of body, dorsal view (**A**), ventral view (**B**); **C.** Cross section of midbody body ring, posterior view; **D.** Midbody body rings, dorsal view; **E, F.** Posterior part of body, dorsal view (**E**), ventral view (**F**). Scale bars: 1 mm.

in body coloration of irregularly yellow with brown spots, body size and number of stylets (three vs four, two, four, and two, respectively).

Description. Male holotype.

Measurements: 42 body rings plus telson, length about 12.96 mm, length of midbody metazona 0.24 mm, width of midbody metazona 2.39 mm, width of midbody prozona 1.08 mm; ratio of width of head and width of collum = 0.74.

Coloration of ethanol-preserved specimens (Fig. 20): complex and irregular: body rings 1–4 with none, body rings 5–7 with 2 brown spots, body ring 8 brown on the right, body ring 9 with two brown spots, body ring 10 brown on the right, body ring 11 brown on the left, body rings 12–13 with two brown spots, body ring 14 none, body ring 15 brown on the left, body rings 16–17 brown on the right, body ring 18 brown on left half, body ring 19 brown on right half, body ring 20 brown on left half, body ring 21 none, body ring 22 with left spot, body ring 23 with two brown spots, body rings 24–26 brown on left half, body rings 27–28 full dark, body ring 29 none, body rings 30–32 brown left, body rings 33–34 brown right,

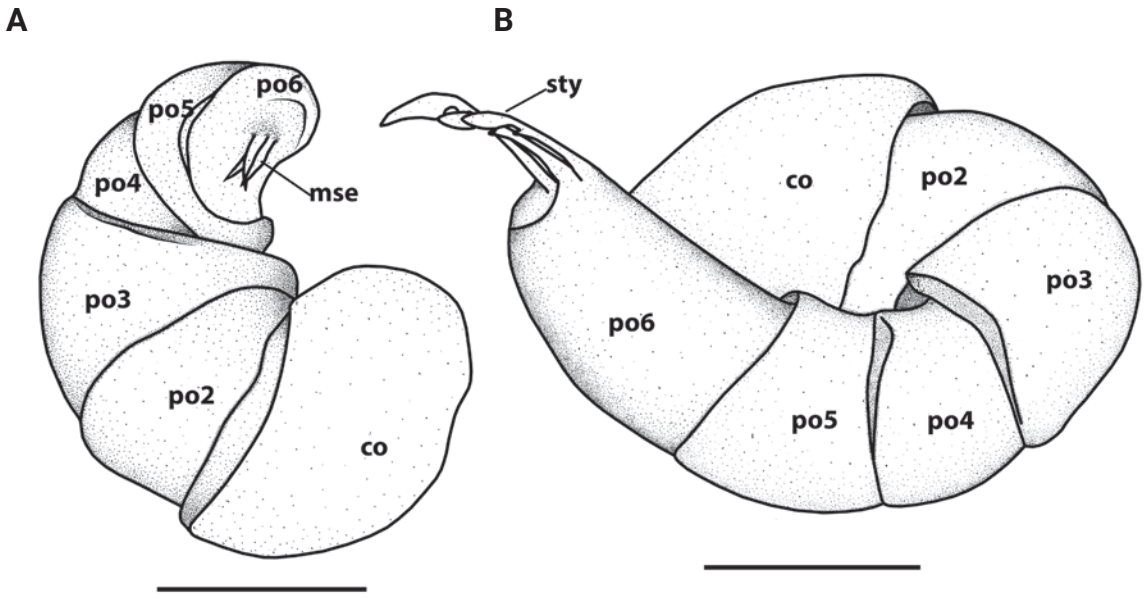

Figure 23. *Pseudodesmus irregularis* sp. nov. Holotype (IEBR-Myr 958H), gonopods. **A.** Left anterior gonopod, anterior view; **B.** Left posterior gonopod, sublateral view. *Abbreviations*: co = coxite = podomere 1; po2 = podomere 2; po3 = podomere 3; po4 = podomere 4; po5 = podomere 5; po6 = podomere 6 (ultimate podomere); mse = macrosetae; sty = stylet. Scale bars: 0.1 mm.

body rings 35–36 full, body rings 37–38 none, body ring 39 brown right, body rings 40–42 light brown.

Head (Figs 21B, 22B) narrower than collum in width, smooth, round-shaped. Antenna stout, clavate, *in situ* extending to body ring 6; antennomere 6 > 5 >3 > 4 = 2 > 7 = 1 in length (Figs 21B, 22B). Collum (Figs 21B, 22B) bilobuled, caudal margin highly elevated with 3+3 tubercles, and with a row of 1+1 tubercles, paramedian one much larger than lateral one.

Body (Figs 21, 22): ring 2 with two rows of 3+3 and 1+1 tubercles; ring 3 with two rows of 3+3 and 3+3 tubercles; other rings with 2 distinct rows of tubercles, anterior row of 6+6 (increasing to (9+9) on midbody rings), and posterior of 2+4 (body ring 4), 3+3 (ring 5), 3+2 (ring 6), 3+3 (on other rings). The last 5 rings with two rows of 3+3 and 3+3 tubercles (Fig. 22E). Anterior rows extending to 2/3 paraterga. Paramedian tubercles on posterior rows much larger than ones on anterior rows.

Paraterga well developed, slightly curved anteriad on body rings 2–3, lateral margins smooth (Figs 21A, B, 22A, B); increasingly less so on the following body rings, slightly curved caudad on body rings 25–27, and strongly curved caudad on body rings 37–40; paraterga of penultimate body ring produced strictly caudad and flanking telson (Figs 21E, F, 22E, F). Lateral margin of paraterga with small/tiny dentations or notches (Figs 21, 22).

Telson (Figs 21E, F, 22E, F) short, caudal margin rounded; epiproct with 2+2 small/tiny tubercles at caudal margin. Paraprocts and hypoproct semi-circular.

Legs slender, shorter than body ring width together with paraterga, terminating before lateral paratergal margins. Claws normal. Coxal sacs strong, present on body rings 3–32 (Fig. 22F).

Gonopods (Figs 23, 24): Two pairs of gonopods directed anteriad. Anterior gonopods (Figs 23A, 24A–C) 6-segmented, covered with long setae; coxite (*co*) broad, basal part sparsely covered with microgranulations; podomeres 2–5, short and stout; podomere 6 slightly longer than other podomeres, distally carrying macrosetae (*mse*). Posterior gonopods (Figs 23B, 24D–F) 6-segmented, covered with sparse long setae; coxite (*co*) broad, basal part sparsely covered with microgranulations; podomeres 2–5 short and stout; ultimate podomere (*po6*) longest, with three apical stylets (*sty*).

Variation. ***Male paratype*** **(IEBR-Myr 958P)**: 36 body rings plus telson, length about 9.75 mm, length of midbody metazoan ca. 0.14 mm, width of midbody metazona ca. 1.72 mm, width of midbody prozona ca. 0.82 mm; ratio of width of head and width of collum = 0.85.

The female from Ngoc Linh Mts (**IEBR-Myr 960**) has 41 body rings plus telson; midbody width 2.1 mm, length about 10.11 mm. Coloration with widening pattern repeated between 7–12, 13–17, 18–24, 25–31, 32–36 body rings (see also Enghoff 2011). Tubercles are small: on collum only one row, on 2–4 two weak rows (reaching only one row on paraterga), from body ring 5 onwards two rows, each 1+1 large tubercles in the middle, then anterior row 10–13 small tubercles reaching edge of paraterga, in posterior row only 3–4 small tubercles, on the last five body rings anterior row is weaker but still with 8–10 small tubercles, in posterior row the median tubercles larger, with 4 small tubercles laterally.

Etymology. To emphasize the irregular pattern of terga. Noun in apposition.

Distribution. The species has been only known from Khanh Hoa and Kon Tum Province, southcentral Vietnam.

DNA barcoding. Sequencing a fragment of the COI gene failed.

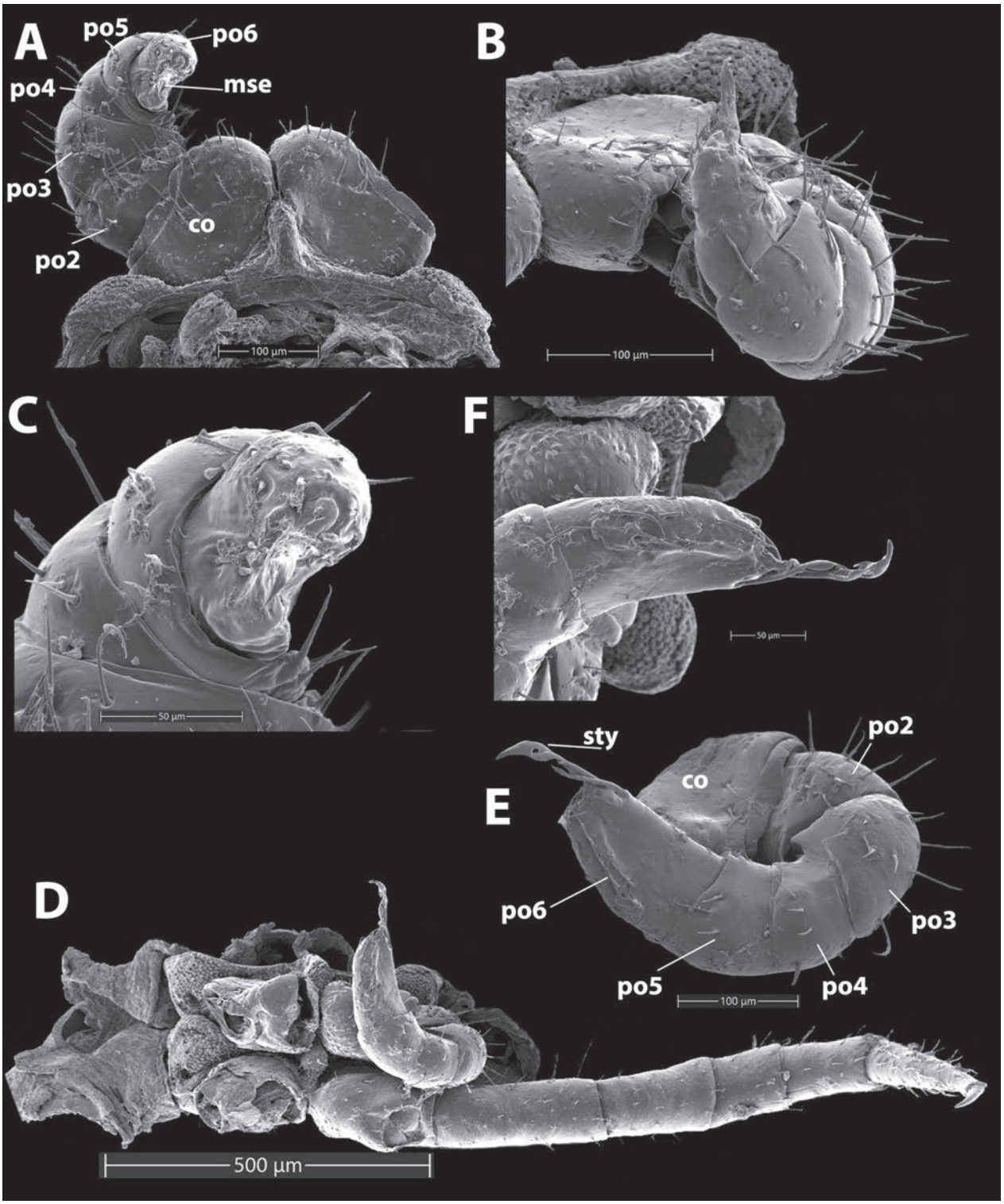

Figure 24. *Pseudodesmus irregularis* sp. nov. Holotype (IEBR-Myr 958H), gonopods. SEM. **A, B.** Left anterior gonopod, anterior view (**A**), ventral view (**B**); **C.** Distal part of left anterior gonopod, anterior view; **D, E.** Posterior gonopod and leg 11, ventral view (**D**), sublateral view (**E**); **F.** Distal part of posterior gonopod, ventral view. *Abbreviations*: co = coxite = podomere 1; po2 = podomere 2; po3 = podomere 3; po4 = podomere 4; po5 = podomere 5; po6 = podomere 6 (ultimate podomere); mse = macrosetae; sty = stylet.

Pseudodesmus spp.

The following specimens have peculiar body shape and color pattern, but because we have only females, we refrained to describe them as new species.

Pseudodesmus sp. 1

Fig. 25

Material examined. Vietnam • 02 females; Daklak, Mdrak, Chu Mur; 12.71233°N, 108.86092°E, 478 m

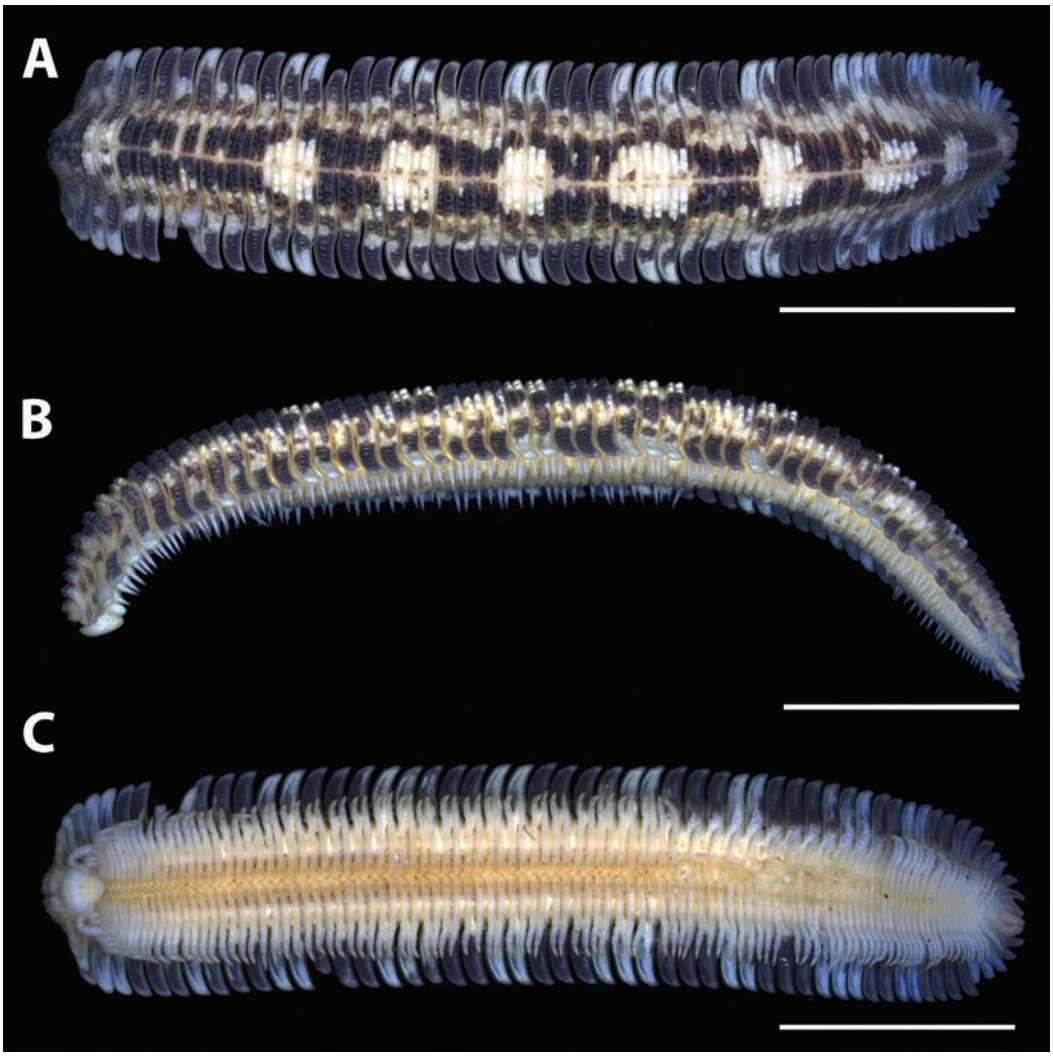

Figure 25. *Pseudodesmus* sp.1. Female (IEBR-Myr 875). **A–C.** Habitus, dorsal view (**A**), lateral view (**B**), ventral view (C). Scale bars: 5 mm.

a.s.l., 15 Jul. 2019; Hoang Quang Duy leg.; under decaying wood along a trail; IEBR-Myr 875.

Description. ***Measurements:*** 57 and 64 body rings (midbody width of the larger one 3.9 mm).

Collum is unique, bilobed, but also divided to anterior and posterior ridges with 5–6+5–6 small tubercles in both rows. Legs with small coxal sacs. Tubercles in two rows, medially widely separated, 2+2 median tubercles not especially large, anterior row with 5–6+5–7 tubercles extending to the middle/edge or paraterga, posterior row with 5–6 small tubercles.

Coloration of ethanol-preserved specimens: very strong pattern, symmetric dark brown (almost black) color extends to the paraterga as well. Dark paraterga: 2–5, 8–10, 14, 18–19, 23, 26–29, 33–34, 36–38, 41–43, 46, 50–51, 53–54, 57–58, 61–64.

Pseudodesmus sp. 2

Fig. 26

Material examined. Vietnam • 1 female; Quang Binh Province, Bo Trach Dist., Son Doong cave, outside cave, back entrance; 17.48667°N, 106.28500°E; 16 Jan. 2023; A.D.Nguyen leg.; IEBR-Myr 987.

Description. ***Measurements:*** 55 body rings plus telson, length ca. 10.9 mm, midbody width 2.7 mm.

Quite convex body, almost cylindrical (without paraterga).

Collum bilobed, narrow, a little bit narrower than head, 2 pair of tubercles, posterior ones stronger.

Tergite tubercles on body rings 2–7 strong and wide, but from there onwards decreasingly inconspicuous, from 8th backwards terga are clearly divided in anterior and posterior parts, also by coloration: light anterior part wider, light posterior part a bit narrower, tubercles disappearing, only weak transversal ridges appear. Telson, including para- and hypoproct dark brown. Coxal sacs on legs small, weak.

Color of ethanol-preserved specimens unique: dark thin median line, terga broadly light, almost white, base of all paraterga dark brown, edge of paraterga light yellow: in general looks like three longitudinal dark stripes, one thin median line and two wider parallel brown stripes. Head color is different: two white bumps (almost like large compound eyes), frontale and mandibulae dark brown, antennae dark brown.

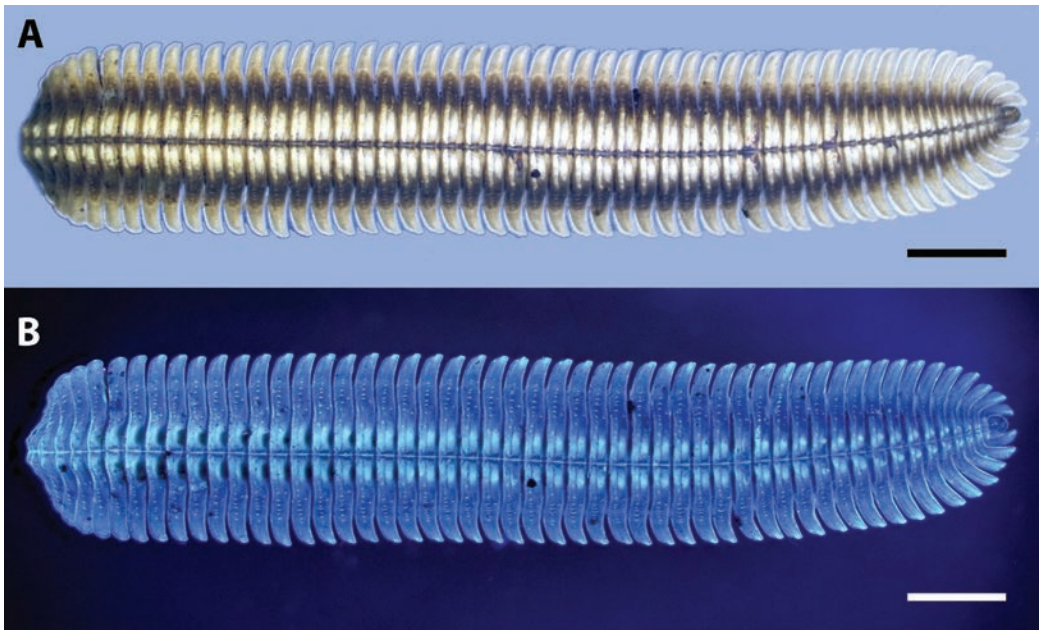

Figure 26. *Pseudodesmus* sp.2. Female (IEBR-Myr 987). **A, B.** Habitus, dorsal view, under normal light (**A**), dorsal view, under UV light (**B**). Scale bars: 1 mm.

Molecular analysis

Dataset

Because of length variation and noisy ends, the final aligned COI dataset comprised a 573 bp fragment from 15 platydesmidan specimens including an outgroup specimen, *Andrognathus corticarius* Cope, 1869 (Table 1). The nucleotide frequencies of A, T, G, and C were 31.1%, 38.5%, 14.6%, and 15.8%, respectively. The GC content was 30.4%. The dataset contained 186 (32.5%) parsimony informative and 251 (43.8%) variable sites.

Genetic distance

The average K2P distance between the 15 platydesmidan samples was 18.0% ± 1%. The genetic distance between the outgroup (*Andrognathus corticarius*) and other andrognathid species was from 22.9% to 32.0%. The distance between platydesmid genera varied between 13.8% (*Pseudodesmus* and *Gosodesmus*) to 27.3% (*Pseudodesmus* and *Brachycybe*). The interspecific distance varied from 1.6% (*P. karstomus* sp. nov.) to 3.6% (*P. ngoclinh* sp. nov.) (Table 2). The genetic distance between new species varied from 14.4%–14.6% (*P. condao* sp. nov. and *P. karstomus* sp. nov.) to 15.1%–17.7% (*P. ngoclinh* sp. nov. and *P. karstomus* sp. nov.).

Phylogenetic relationship

A phylogenetic tree was reconstructed for the 573 bp dataset using maximum likelihood analysis (Fig. 27). The tree supports the separation of two new species, *P. ngoclinh* and *P. karstomus*, from their congeners, with bootstrap values (97% and 88%, respectively). The other new species, *P. condao*, is clustered within a clade consisting of *Brachycybe*, *Gosodesmus*, and *Yamasinaium*, with a low bootstrap value (49%). However, the relationship between those three genera is poorly supported (51–57%). Perhaps, the 573 bp fragment of the COI is too short to accurately estimate phylogenetic relationships.

A key to *Pseudodesmus* species in Vietnam

1 Head slightly broader than collum (ratio of width of head and width of collum = 1.05) ..... *P. ngoclinh* sp. nov.
– Head narrower than collum 2
2 Head significantly narrower than collum (ratio of width of head and width of collum = 0.74–0.89) 3
– Head slightly narrower than collum (ratio of width of head and width of collum = 0.93–0.98) 4
3 Body smaller (length about 9.33 mm, width of midbody metazona ca. 1.57 mm); midbody metazonae with two rows of 3–4+3–4 large and 4–5+4–5 large tubercles; posterior gonopod with two distal stylets ..... *P. condao* sp. nov.
– Body larger (length about 12.96 mm, width of midbody metazona 2.39 mm); midbody metazonae with two rows of 6–9+6–9 and 3+3 tubercles; posterior gonopod with three distal stylets ..... *P. irregularis* sp. nov.
4 Body coloration rather uniformly earth brown ..... *P. camptotrichus*
– Body coloration not uniform, somewhat irregular distribution of yellow-brown and black spots) 5

5 Body larger (length about 32.0 mm, width of midbody metazona 5.8 mm); midbody metazonae with two rows of 8–15+8–15 and 5–7+5–7 ..... *P. variegatus*
– Body smaller; midbody metazonae with two rows of tubercles, but different in number..... 6
6 Ratio of body length and midbody width about 4.6; midbody metazonae with two rows of 7–8+7–8 and 2+2 tubercles *P. karstomus* sp. nov.
– Ratio of body length and midbody width about 5.7; midbody metazonae with two rows of 5+5 and 3+3 tubercles .... *P. bidoup* sp. nov.

Table 1. Voucher specimens and GenBank accession numbers.

No	Species	Species code	Locality	GenBank Accession Number	Sources
1	*Pseudodesmus* sp.1	IEBR-Myr 875	Vietnam, Daklak Province, Mdrak, Chu Mur	PQ423228	This study
2	*Pseudodesmus condao* sp. nov.	IEBR-Myr 982	Vietnam, Ba Ria–Vung Tau Province, Con Dao NP	PQ423226	
3	*Pseudodesmus condao* sp. nov.	IEBR-Myr 977	Vietnam, Ba Ria–Vung Tau Province, Con Dao NP	PQ423227	
4	*Pseudodesmus ngoclinh* sp. nov.	IEBR-Myr 986a	Vietnam, Kon Tum Province, Ngoc Linh Mts,	PQ423222	
5	*Pseudodesmus ngoclinh* sp. nov.	IEBR-Myr 986b	Vietnam, Kon Tum Province, Ngoc Linh Mts,	PQ423223	
6	*Pseudodesmus karstomus* sp. nov.	IEBR-Myr 959a	Vietnam, Cao Bang Province, Tra Linh District	PQ423224	
7	*Pseudodesmus karstomus* sp. nov.	IEBR-Myr 959b	Vietnam, Cao Bang Province, Tra Linh District	PQ423225	
8	*Yamasinaium* sp.	IEBR-HNMH	Japan, Okinawa	PQ423229	
9	*Brachycybe producta*	MIL0021	U.S.A.	JX962721	Marek et al. (2012)
10	*Brachycybe lecontii*	–	U.S.A.	JX437064	Brewer et al. (2013)
11	*Brachycybe rosea*	MIL0025	U.S.A.	JX962722	Marek et al. (2012)
12	*Gosodesmus claremontus*	SPC000941	U.S.A.	JX962723	Marek et al. (2012)
13	Andrognathidae sp.	FLMNH 42128	Myanmar	MF983566	GenBank (direct submission)
14	Andrognathidae sp.	FLMNH 42103	Myanmar	MF983567	GenBank (direct submission)
15	*Andrognathus corticarius*	VTEC MPE01938	U.S.A.	MH282831	Shorter et al. (2018)

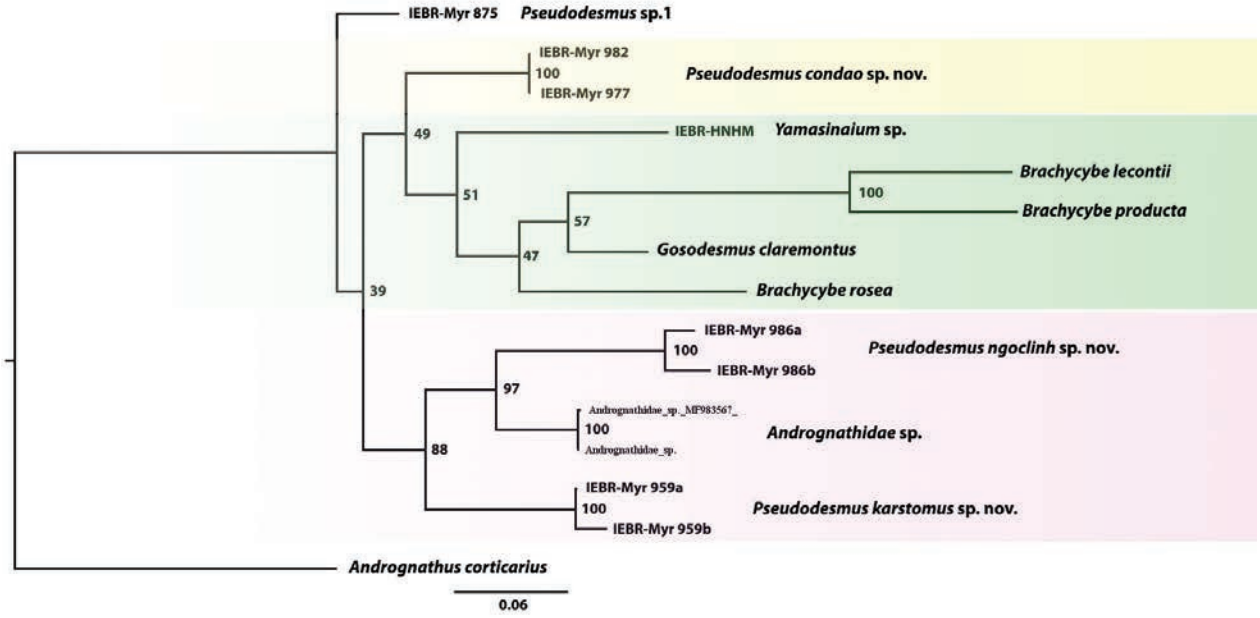

Figure 27. Phylogenetic diagram inferred from a 573bp fragment of the COI gene using maximum likelihood analysis. Numbers at node are bootstrap values.

Table 2. Pairwise nucleotide difference (Kimura 2-parameter model) over sequence pairs between species. Numbers in bold are intraspecific divergences.

Species	(1)	(2)	(3)	(4)	(5)	(6)	(7)	(8)	(9)	(10)	(11)	(12)	(13)	(14)
(1) *Pseudodesmus ngoclinh* sp. nov. (IEBR-Myr 986a)														
(2) *Pseudodesmus ngoclinh* sp. nov. (IEBR-Myr 986b)	**0.036**													
(3) *Pseudodesmus karstomus* sp. nov. (IEBR-Myr 959a)	0.170	0.151												
(4) *Pseudodesmus karstomus* sp. nov. (IEBR-Myr 959b)	0.177	0.158	**0.016**											
(5) *Pseudodesmus condao* sp. nov. (IEBR-Myr 982)	0.177	0.170	0.144	0.146										
(6) *Pseudodesmus condao* sp. nov. (IEBR-Myr 977)	0.177	0.170	0.144	0.146	**0.000**									
(7) *Pseudodesmus* sp.1 (IEBR-Myr 875)	0.168	0.159	0.123	0.127	0.101	0.101								
(8) Andrognathidae sp. (MF983567)	0.121	0.117	0.127	0.131	0.144	0.144	0.125							
(9) Andrognathidae sp. (MF983566)	0.119	0.115	0.125	0.131	0.142	0.142	0.125	0.002						
(10) *Yamasinaium* sp. (IEBR-HMNH)	0.227	0.220	0.179	0.179	0.150	0.150	0.131	0.185	0.185					
(11) *Gosodesmus claremontus* (JX962723)	0.199	0.192	0.165	0.172	0.138	0.138	0.142	0.152	0.150	0.161				
(12) *Brachycybe rosea* (JX962722)	0.213	0.213	0.181	0.190	0.165	0.165	0.161	0.179	0.176	0.155	0.140			
(13) *Brachycybe producta* (JX962721)	0.268	0.273	0.248	0.260	0.208	0.208	0.234	0.248	0.246	0.246	0.185	0.215		
(14) *Brachycybe lecontii* (JX437064)	0.273	0.273	0.248	0.263	0.212	0.212	0.236	0.246	0.243	0.222	0.187	0.210	0.133	
(15) *Andrognathus corticarius* (MH282831)	0.320	0.312	0.258	0.263	0.258	0.258	0.229	0.248	0.246	0.266	0.263	0.283	0.294	0.301

Discussion

Located in tropical regions, Vietnam is expected to have a great diversity of millipedes (Enghoff et al. 2004). Like other millipede taxa e.g. Callipodida (Nguyen et al. 2023), Polydesmida (Nguyen et al. 2024), the Platydesmida have been poorly known, with a little information since 1953. The discoveries of five new species are remarkable for the millipede fauna of Vietnam, but the number of platydesmidan species (seven) does not reflect the true diversity of millipedes in Vietnam. More intensive surveys, especially in caves, will reveal more new species.

The relation or position of *Pseudodesmus* within Andrognathidae was previously discussed several times but no detailed study has been carried out so far. In the gonopods, Carl (1912) didn't find any differences between *Pseudodesmus tuberculatus* and the species of *Platydesmus* and *Brachycybe*, and he proposed *Brachycybe* to be an intermediate form between *Platydesmus* and *Pseudodesmus*.

Gardner (1975) in his Nearctic revision of the family Andrognathidae stated that the species can be superficially divided into two main groups. The first group has broad body (up to 4 mm in width) including *Brachycybe*, *Sinocybe* and *Pseudodesmus*, and the second one has more vermiform bodies comprising of four (North American) genera *Ischnocybe*, *Mitocybe*, *Gosodesmus* and *Andrognathus*. These two groups formally belong to two subfamilies Bazillozoniinae and Dolisteninae, respectively (Hoffman 1980). Hoffman (1980) kept *Pseudodesmus* and *Sinocybe* separate, but he also said "I am by no means assured that *Sinocybe* can be distinguished from *Pseudodesmus*" (Hoffman 1980: p. 117). Also, he wrote that "it is difficult to distinguish *Platydesmus* from *Brachycybe*", even though he classified them into different families (Platydesmidae *vs* Andrognathidae (Hoffman 1980).

Later, Shelley et al. (2005) considered *Sinocybe* to be a junior synonym of *Brachycybe*. Furthermore, they said that there are few if any structural differences between *Brachycybe* and *Pseudodesmus*, and the two genera could be synonymized, and *Yamasinaium* can also be a candidate under *Brachycybe* (Shelley et al. 2005).

Decker (2014) in a conference presentation tentatively suggested synonymy of *Brachycybe* and *Pseudodesmus*, but his detailed reasons are still in manuscript (Decker pers. comm.). He generally said: "Due to the similarity and the mosaic like pattern of morphological characters (incl. gonopods) sharing with North American *Brachycybe*, all Southeast Asian members of Andrognathidae were placed for the present under *Brachycybe*" (Decker 2014). His classificatory acts should be invalid as it was presented only in a conference poster.

Phylogenetically, members of the genera, *Brachycybe* and *Pseudodesmus*, are not monophyletic and occur in distinct clades, but the tree is poorly supported (39%, Fig. 27). In the tree, *Brachycybe* is more closely related to *Gosodesmus*, however, this result should be contrasted with the phylogeny of Rodriguez et al. (2018) who reported that *Brachycybe* was related to *Platydesmus*, and the non-monophyly of the family Andrognathidae. The position of *Yamasinaium* and *Gosodesmus* on the tree, however, is a little bit strange, considering that with they have long and slender body shapes and belong to the subfamily Dolisteninae. Additionally, the geographical distribution of the three genera may also be viewed as problematic: the monotypic *Gosodesmus* (*G. claremontus* Chamberlin, 1922) is from the western U.S.; *Brachycybe* has a northern temperate distribution mainly in southeastern and western United States (6 species), but it has also species in Japan, South Korea, central China, and Taiwan (3 species) (Shelley et al. 2005; Mikhaljova et al. 2010; Shelley and Golovatch 2011; Brewer et al. 2012); *Yamasinaium*, on the other hand, is confined to East Asia: the Korean Peninsula, southern Japan, and Taiwan (3 species).

Pseudodesmus species are only recorded in tropical habitats of Southeast Asia (Brewer et al. 2012). Due to the geographical distribution and the weak molecular supports, it may be better to keep all these genera, especially *Brachycybe* and *Pseudodesmus*, separate. The synonymy of those two genera needs to be confirmed with more morphological and molecular evidence.

As mentioned above, the used fragment of the COI may be too short for phylogenetic analysis. It may not suitable for the reconstruction of relationship between species and genera solely based on the COI, as it is not able to resolve deeper nodes/early splits. However, it is a great tool to identify species and the phylogeny nicely shows clusters of specimens belonging to the same species and visualizes the genetic distances (Fig. 26).

Acknowledgements

The work is supported by the Vietnam Academy of Science and Technology under the project NCXS01.04/23-25 "Developing the first-class research team on the discovery of diversity and application potential of hymenopterans, myriapods and soil nematodes in the limestone mountains of northeastern Vietnam". We thank Dr. Nesrine Akkari (NHMW) for providing data about Attems' types in NHMW. Two reviewers, Paul Marek (USA) and Leif Moritz (Germany) are acknowledged for their constructive comments to improve the manuscript.

References

Attems C (1938) Die von Dr. C. Dawydoff in französisch Indochina gesammelten Myriopoden. Mémoires du Muséum national d'histoire naturelle, N. S. 6: 187–353.

Attems C (1951) Revision systématique des Colobognata (Myriapodes Diplopodes) et description d'espèces nouvelles. Mémoires du Muséum national d'histoire naturelle, N. S., série A 3: 193–231.

Attems C (1953) Myriopoden von Indochina. Expedition von Dr. C. Dawydoff (1938–1939). Mémoires du Muséum national d'histoire naturelle, N. S., série A 5: 133–230.

Brewer MS, Spruill CL, Rao NS, Bond JE (2012) Phylogenetics of the millipede genus Brachycybe Wood, 1864 (Diplopoda: Platydesmida: Andrognathidae): Patterns of deep evolutionary history and recent speciation. Molecular Phylogenetics and Evolution 64: 232–242. https://doi.org/10.1016/j.ympev.2012.04.003

Brewer MS, Swafford L, Spruill CL, Bond JE (2013) Arthropod Phylogenetics in Light of Three Novel Millipede (Myriapoda: Diplopoda) Mitochondrial Genomes with Comments on the Appropriateness of Mitochondrial Genome Sequence Data for Inferring Deep Level Relationships. PLoS ONE 8: e68005. https://doi.org/10.1371/journal.pone.0068005

Carl J (1912) Sur quelques colobognathes du Muséum du Genève. Revue suisse de Zoologie 20: 507–518.

Chamberlin RV (1945) On some Diplopods from the Indo-Australian Archipelago. American Museum Novitates 1282: 1–43.

Chamberlin RV, Wang Y-HM (1953) Records of millipeds (Diplopoda) from Japan and other oriental areas, with descriptions of new genera and species. American Museum Novitates 1621: 1–13.

Decker P (2014) Revision of the family Andrognathidae in Southeast Asia (Diplopoda: Platydesmida) with descriptions of six new species. In: Tuf IH, Tajovský K (Eds) 16th International Congress of Myriapodology. Book of Abstracts 17.

Enghoff H (2011) Trans-segmental serial colour patterns in millipedes and their developmental interpretation (Diplopoda). International Journal of Myriapodology 6: 1–27. https://doi.org/10.3897/ijm.6.1949

Enghoff H, Golovatch SI, Nguyen DA (2004) A review of the millipede fauna of Vietnam. Arthropoda Selecta 13: 25–43.

Folmer O, Black M, Hoeh W, Lutz R, Vrijenhoek R (1994) DNA primers for amplification of mitochondrial cytochrome c oxidase subunit I from diverse metazoan invertebrates. Molecular marine biology and biotechnology 3: 294–299.

Gardner MR (1975) Revision of the millipede family Andrognathidae in the Nearctic region. Memoirs of the Pacific Coast Entomological Society 5: 1–61.

Hoffman RL (1980) Classification of the Diplopoda. Muséum d'Histoire Naturelle, Genève, 1–237 pp.

Jeekel CAW (2001) A bibliographic catalogue of the Siphonophorida (Diplopoda). Myriapod Memoranda 3: 44–71.

Kumar S, Stecher G, Tamura K (2016) MEGA7: Molecular Evolutionary Genetics Analysis Version 7.0 for Bigger Datasets. Molecular Biology and Evolution 33: 1870–1874. https://doi.org/10.1093/molbev/msw054

Larkin MA, Blackshields G, Brown NP, Chenna R, McGettigan PA, McWilliam H, Valentin F, Wallace IM, Wilm A, Lopez R, Thompson JD, Gibson TJ, Higgins DG (2007) Clustal W and Clustal X version 2.0. Bioinformatics 23: 2947–2948. https://doi.org/10.1093/bioinformatics/btm404

Likhitrakarn N, Golovatch SI, Panha S (2014) A checklist of the millipedes (Diplopoda) of Laos. Zootaxa 3754: 473–482. https://doi.org/10.11646/zootaxa.3754.4.8

Loomis HF (1942) *Sinocybe* a new genus of colobognath millipeds from China. Journal of the Washington Academy of Sciences 32: 270–273.

Marek P, Shear W, Bond J (2012) A redescription of the leggiest animal, the millipede *Illacme plenipes*, with notes on its natural history and biogeography (Diplopoda, Siphonophorida, Siphonorhinidae). ZooKeys 241: 77–112. https://doi.org/10.3897/zookeys.241.3831

Mikhaljova EV, Golovatch SI, Korsós Z, Chen C-C, Chang H-W (2010) The millipede order Platydesmida (Diplopoda) in Taiwan, with descriptions of two new species. Zootaxa 2718: 51–63. https://doi.org/10.11646/zootaxa.2718.1.4

Minelli A (2014) 2 Treatise on Zoology: Anatomy, Taxonomy, Biology. The Myriapoda. Vol. 2. Brill, Leiden, 1–482. https://doi.org/10.1163/9789004188273_002

Miyosi Y (1953) Beiträge zur Kenntnis japanischer Myriopoden. 7. Aufsatz. Zoological Magazine 62: 23–26.

Moritz L, Wesener T (2019) The first known fossils of the Platydesmida – an extant American genus in Cretaceous amber from Myanmar (Diplopoda: Platydesmida: Andrognathidae). Organisms Diversity & Evolution 19: 423–433. https://doi.org/10.1007/s13127-019-00408-0

Nguyen AD, Korsós Z, Jang K-H, Hwang U-W (2017) A revision and phylogenetic analysis of the millipede genus *Oxidus* Cook, 1911 (Polydesmida, Paradoxosomatidae). European Journal of Taxonomy 2017. https://doi.org/10.5852/ejt.2017.293

Nguyen AD, Stoev P, Nguyen LTP, Vu TT (2023) A new species of *Paracortina* from a Vietnamese cave, with remarkable secondary sexual characters in males (Callipodida, Paracortinidae). ZooKeys 1149: 181–195. https://doi.org/10.3897/zookeys.1149.99651

Nguyen AD, Vu TTT, Eguchi K (2024) The millipede family Polydesmidae Leach, 1816 (Diplopoda, Polydesmida) from Vietnam, with a description of a new cavernicolous species. ZooKeys 1190: 259–280. https://doi.org/10.3897/zookeys.1190.114958

Pocock RI (1887) Description of a new genus and species of Polyzonidae. Annals and Magazine of Natural History ser. 5: 1–222. https://doi.org/10.1080/00222938709460038

Rodriguez J, Jones TH, Sierwald P, Marek PE, Shear WA, Brewer MS, Kocot KM, Bond JE (2018) Step-wise evolution of complex chemical defenses in millipedes: a phylogenomic approach. Scientific Reports 8: 3209. https://doi.org/10.1038/s41598-018-19996-6

Shear WA (2011) Class Diplopoda de Blainville in Gervais, 1844. Animal biodiversity: An outline of higher-level classification and survey of taxonomic richness. Zootaxa 3148: 159–164. https://doi.org/10.11646/zootaxa.3148.1.32

Shelley RM, Golovatch SI (2011) Atlas of myriapod biogeography. I. Indigenous ordinal and supra-ordinal distributions in the Diplopoda: Perspectives on taxon origins and ages, and a hypothesis on the origin and early evolution of the class. Insecta Mundi 0158: 1–134.

Shelley RM, McAllister CT, Tanabe T (2005) A synopsis of the milliped genus *Brachycybe* Wood, 1864 (Platydesmida: Andrognathidae). Fragmenta Faunistica 48: 137–166. https://doi.org/10.3161/00159301FF2005.48.2.137

Shorter PL, Hennen DA, Marek PE (2018) Cryptic diversity in *Andrognathus corticarius* Cope, 1869 and description of a new Andrognathus species from New Mexico (Diplopoda, Platydesmida, Andrognathidae). ZooKeys 786: 19–41. https://doi.org/10.3897/zookeys.786.27631

Sierwald P, Decker P, Spelda J (2024) MilliBase. *Pseudodesmus* Pocock, 1887. https://www.millibase.org/aphia.php?p=taxdetails&id=892428 [on 2024-10-16]

Silvestri F (1899) Diplopodes de l'Archipel Malais. Revue suisse de zoologie 7: 331–334. https://doi.org/10.5962/p.318254

Sinclair FG (1901) On the myriapods collected during the "Skeat Expedition", to the Malay Peninsula 1899–1900. Proceedings of the Zoological Society of London 2: 505–533. https://doi.org/10.1111/j.1469-7998.1902.tb08186.x

Tömösváry Ö (1885) Myriapoda a Joanne Xanthus in Asia orientali collecta. Ennumeravit speciesque novas descripsit. Természentrajzi Füzetek 9: 63–72.

Trifinopoulos J, Nguyen L-T, von Haeseler A, Minh BQ (2016) W-IQ-TREE: a fast online phylogenetic tool for maximum likelihood analysis. Nucleic Acids Research 44: W232–W235. https://doi.org/10.1093/nar/gkw256

Verhoeff KW (1935) Neue ostasiatische Colobognathen. 140. Diplopden-Aufsatz. Zoologischer Anzeige 112: 62–73.

Verhoeff KW (1939) Diplopoden von der Ryukyu-Insel Okinawa. Transactions of Biogeographical Society of Japan 3: 118–122.

Wesener T (2015) Subterclass Colobognatha Brandt, 1834. In: Minelli A (Ed.) The Myriapoda. Vol. 2. Treatise on Zoology – Anatomy, Taxonomy, Biology. Brill, Leiden, 382–482.

Wood HC (1864) Description of new genera and species of North American Myriapoda. Proceedings of the Academy of natural Science of Philadelphia 1864: 186–187.

Zhang Z, Schwartz S, Wagner L, Miller W (2000) A Greedy Algorithm for Aligning DNA Sequences. Journal of Computational Biology 7: 203–214. https://doi.org/10.1089/10665270050081478

Zoosyst. Evol. 100 (4) 2024, 1543–1556 | DOI 10.3897/zse.100.136428

PENSOFT

für Natur MUSEUM FÜR NATURKUNDE BERLIN

Idiopyrgus Pilsbry, 1911 (Gastropoda, Tomichiidae): a relict genus radiating into subterranean environments

Rodrigo Brincalepe Salvador[1,2], Maria Elina Bichuette[3]

1 *Zoology Unit, Finnish Museum of Natural History, University of Helsinki, Helsinki, Finland*

2 *The Arctic University Museum of Norway, UiT – The Arctic University of Norway, Lars Thørings veg 10, 9006, Tromsø, Norway*

3 *Laboratório de Estudos Subterrâneos, Universidade Federal de São Carlos, Rodovia Washington Luís km 235, Caixa Postal 676, 13565-905, São Carlos, SP, Brazil*

https://zoobank.org/DC99B66D-5862-44E4-B699-0A9CEFE8738F

Corresponding author: Rodrigo Brincalepe Salvador (salvador.rodrigo.b@gmail.com)

Academic editor: Frank Köhler ♦ **Received** 5 September 2024 ♦ **Accepted** 17 October 2024 ♦ **Published** 8 November 2024

Abstract

The freshwater gastropod fauna in Brazil presently consists of circa 180 known species, though this is deemed an underestimate. The little-studied cavern faunas have been considered a potential source of undescribed species, particularly regarding the Truncatelloidea. Here, based on new collection efforts in caves in Bahia state, Brazil, we describe two new troglobitic species of *Idiopyrgus* (Tomichiidae): *Idiopyrgus eowynae* **sp. nov.** and *Idiopyrgus meriadoci* **sp. nov**. We improve upon the previous molecular phylogeny of this genus and take the opportunity to reclassify *Spiripockia umbraticola* Simone & Salvador, 2021, as *Idiopyrgus umbraticola* (Simone & Salvador, 2021), **comb. nov.** The genus *Idiopyrgus* now contains ten species, reinforcing the presence of Tomichiidae in Brazil as a relict lineage that largely radiated into cave environments. Furthermore, considering that so far only snapshots of their biology are known, we have collated all the information currently available from the literature and field observations on the cavernicolous species of *Idiopyrgus*. Notably, due to human action in the area where the two new species have been found, they can already be considered vulnerable.

Key Words

Brazil, Caenogastropoda, Gondwana, molecular phylogenetics, *Spiripockia*, troglofauna, Truncatelloidea

Introduction

The freshwater gastropod fauna in Brazil presently consists of circa 180 known species. However, this number is probably an underestimate due to the dearth of taxonomic studies focusing on this fauna when compared to their marine and terrestrial counterparts (Machado et al. 2023). Most studies on freshwater gastropods in Brazil focus, somewhat understandably, on invasive species and public health issues, the latter representing the vast majority of published papers (Simone 2006; Machado et al. 2023).

Among Brazilian freshwater snails, the poorly known cave faunas have been considered as a potential source of undescribed species (Salvador et al. 2022b). That is expected to be particularly important for members of the superfamily Truncatelloidea (Salvador et al. 2022b; Machado et al. 2023). Some truncatelloidean cave species displaying striking shell morphology have recently been discovered (e.g., Simone 2012; Simone and Salvador 2021).

In a recent phylogenetic study, Salvador et al. (2022a) recognised the family Tomichiidae as a clade comprised of one relict genus from each of three continents: South America (genus *Idiopyrgus* Pilsbry, 1911, restricted to Brazil), Africa (*Tomichia* Benson, 1851), and Australia (*Coxiella* Smith, 1894). Salvador et al. (2022a) also reassessed the diversity of *Idiopyrgus* and described two new species in the genus from caves in eastern Brazil.

Here, based on new collections in caves in Bahia State, Brazil, we describe two additional species of *Idiopyrgus* and reassess the classification of one species of *Spiripockia* Simone, 2012. We also briefly review the current knowledge of the biology of cave-dwelling members of the genus.

Materials and methods

Collections were conducted in a small subterranean drainage at Gruna do Pedro Cassiano, a limestone cave located in the Serra do Ramalho karst area, Bahia state, northeastern region of Brazil (Fig. 1). The drainage is over 1.5 km long but shallow, reaching just about 80 cm depth at most (pools in the distal part of the cave). The area where specimens occur has many submerged roots and lentic waters, formed by silt, with depths of 10–15 cm. Temperature and pH measured on-site varied from 21.3–22.4 °C and 7.5–8.2; the pH values are typical of karst drainages. The Serra do Ramalho karst area comprises plateaus within the Bambuí geomorphological group. Moreover, the limestone in the region forms outcrops that extend parallel to the Middle São Francisco River (Gallão and Bichuette 2018). The climate is tropical dry (=semiarid) ("Aw"), with low annual precipitation of about 640 mm (Bedek et al. 2018). Vegetation consists of mesophytic and xeromorphic forests interspersed with "Cerrado" (savannah-like vegetation). Fig. 2 shows details of the cave environment, microhabitat, threats, and coexisting species of the two new *Idiopyrgus* spp. Common threats in the region are related to human occupation (Gallão and Bichuette 2018), including: water exploitation for agriculture, land use lacking sustainable planning, and reduction in subterranean water bodies likely due to climate change, representing an alarming concern (MEB, pers. obs). Future mining projects are also expected for the region, which should cause severe impacts.

The collections were conducted in November 2021, under permission from Sistema de Autorização e Informação em Biodiversidade (SISBIO #28992). The collected specimens were euthanised, fixed, and preserved in 95% ethanol and deposited in the following collections: Laboratório de Estudos Subterrâneos, Universidade Federal de São Carlos (LES; São Carlos, SP, Brazil), Museu de Zoologia da Universidade de São Paulo (MZSP; São Paulo, SP, Brazil), and Museu Nacional (MNRJ; Rio de Janeiro, RJ, Brazil). Registration numbers of the specimen lots are given below in the entry for each species.

Molecular data

Selected specimens were used for DNA extraction, which was conducted using the QIAGEN DNEasy® Blood & Tissue Kit generally following the manufacturer's standard protocol, but with a modification to the final step to increase yield and concentration, which is helpful for such small freshwater snails. The modification of the final step consisted of initially using one-quarter of the suggested amount of the buffer solution (i.e., 50 µL of buffer AE) and then repeating the elution step using the extract.

A total of six specimens were chosen for DNA extraction. Five of them were from the collection efforts in Gruna Pedro Cassiano (see above), as follows: 2 specimens of the larger-sized *Idiopyrgus* sp. nov. (a typical specimen and a dark morph) (from lots LES 29796 and LES 29797), 3 specimens of the smaller-sized *Idiopyrgus* sp. nov. (from lot LES 29820). The sixth specimen was an individual of *Idiopyrgus souleyetianus* Pilsbry, 1911, stemming from local survey efforts in Minas Gerais state and kindly provided to us by Paulo Ricardo Coelho from the Federal University of Minas Gerais (UFMG, Brazil), included in the present study to improve the phylogenetic analysis. The extraction process failed for the three of the smaller-sized *Idiopyrgus* sp. nov., which were consumed in the process. So, we refrained from spending any additional specimens of it for DNA extraction, considering it better to preserve the scarce specimens with soft parts available for the future, when better options might become available.

We selected three genetic markers to target based on those used in previous phylogenetic studies done on the group (e.g., Kameda and Kato 2011; Wilke et al. 2013; Salvador et al. 2022a; Lawrie et al. 2023): (1) the barcoding region of the mitochondrial COI gene (primers LCO and HCO of Folmer et al. 1994); (2) the mitochondrial 16S rRNA gene (primers 16SarL and 16SbrH of Simon et al. 1994); (3) a stretch of nuclear DNA containing the 3′ end of the 5.8S rRNA gene, the entire ITS2 region, and a large portion of the 5′ end of the 28S rRNA gene, sequenced in two parts (primers LSU-1 and LSU-3 for the first part and primers LSU-2 and LSU-5 for the second part; Wade and Mordan 2000; Wade et al. 2006).

The same PCR protocol was used for amplification of COI and 16S, consisting of an initial denaturation step of 3 min at 95 °C, 35 cycles of denaturation at 95 °C for 30 s, annealing at 48 °C for 1 min, and extension at 72 °C for 2 min; a final extension step of 5 min at 72 °C. The PCR protocol for the ITS2+28S section was as follows: initial denaturation step of 3 min at 95 °C; 40 cycles of denaturation at 95 °C for 30 s; annealing at either 50 °C (ITS2 portion) or 45 °C (28S portion) for 1 min; and extension at 72 °C for either 5 min (ITS2 portion) or 2 min (28S portion); final extension step of 4 min at 72 °C.

Success of PCR was assessed visually via agarose gel electrophoresis. The PCR products were then cleaned with ExoSAP-IT™ (Affymetrix Inc.) following the manufacturer's protocol, and the samples were sent to Macrogen Europe (Amsterdam, The Netherlands) for Sanger sequencing. The resulting sequences were quality-checked and assembled using the software Geneious Prime (v.2023.2.1, Biomatters Ltd.). Consensus sequences were extracted and uploaded to GenBank; the accession numbers can be seen in Table 1.

Phylogenetic analysis

Our initial morphological assessment of the specimens suggested a placement in the genus *Spiripockia*, as they seemed closely related to the species *Spiripockia umbraticola* Simone & Salvador, 2021, previously described from another cave in Bahia state in the same area. To test that hypothesis, we included the new species into a phylogenetic framework focusing on the families of freshwater truncatelloidean snails present in

Brazil (Tateidae and Tomichiidae), as well as those families in which Brazilian species have been previously or tentatively classified (Pomatiopsidae and Cochliopidae). To that end, we relied on genetic data available from our previous studies and those of other authors. The taxa used in the phylogenetic analysis are listed in Table 1, including information on GenBank accession numbers and references.

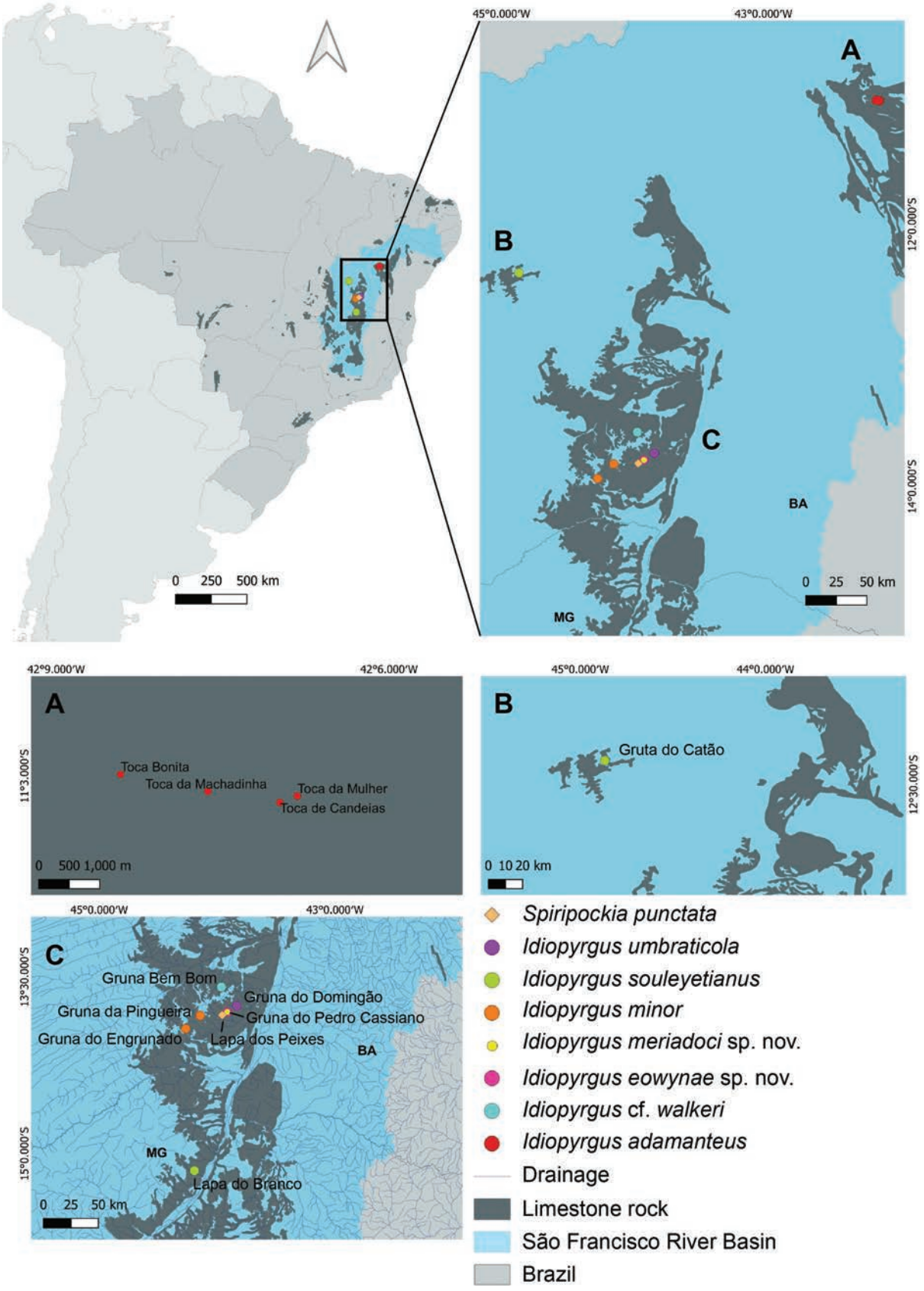

Figure 1. Distribution map of *Idiopyrgus* spp. (and *Spiripockia punctata*) in caves of the state of Minas Gerais and Bahia, Brazil.

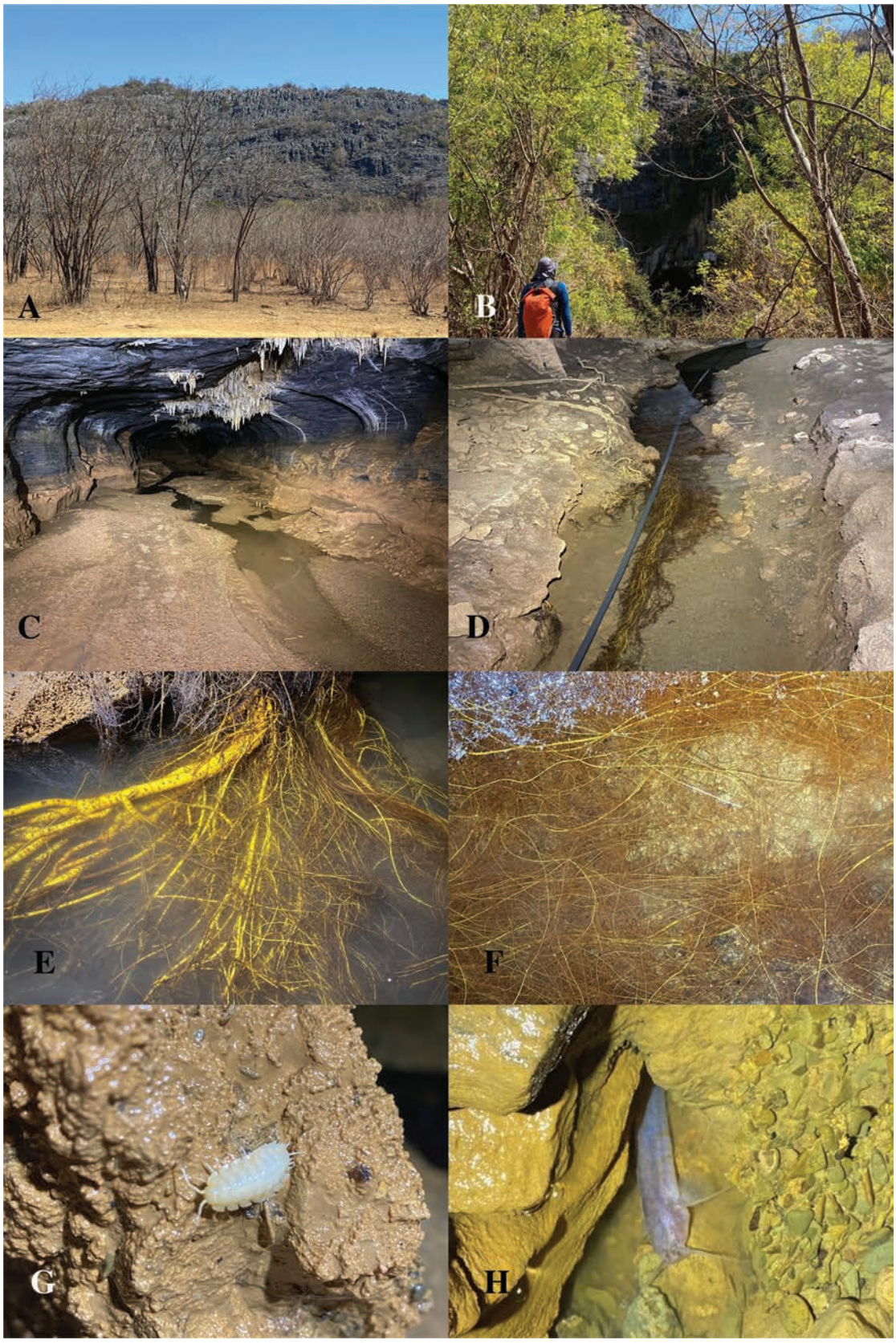

Figure 2. Gruna do Pedro Cassiano ("Pedro Cassiano cave"), Serra do Ramalho karst area, Carinhanha municipality, Bahia state, Brazil; **A.** Cave surroundings showing the limestone outcrops and the dried vegetation, sparse and altered by human impacts; **B.** Cave entrance.; **C.** Cave gallery showing the small subterranean drainage; **D.** Detail of the drainage with the apparatus of water extraction; **E.** Submerged roots, microhabitat of *Idiopyrgus* spp.; **F.** Detail of the microhabitat of *Idiopyrgus* spp., showing thinner roots; **G.** *Xangoniscus* aff. *aganju*, an amphibious troglobitic isopod that co-exists with *Idiopyrgus* spp.; **H.** *Trichomycterus rubbioli*, a cave catfish that co-exists with *Idiopyrgus* spp.

Table 1. Species used in the phylogenetic analysis, with GenBank registration number of each genetic marker, locality data, and reference to the original publication. An asterisk after a species' name indicates that it is the type species of its genus.

Taxon	COI	16S	28S	Locality	References
Amnicolidae					
Akiyoshia kobayashii Kuroda & Habe, 1958	AB611823	AB611822	AB611821	Japan, Shiga, Taga	Kameda and Kato 2011
Amnicola limosus (Say, 1817)	AF213348	AF212903	—	USA, Michigan, Blind Lake	Wilke et al. 2001
Assimineidae					
Assiminea grayana Fleming, 1828*	HQ623170	HQ623153	—	Germany, Lower Saxony, Varel	Wilke et al. 2013
Paludinellassiminea japonica (Pilsbry, 1901)*	AB611811	AB611810	AB611809	Japan, Ehime, Hiburi Is.	Kameda and Kato 2011
Cochliopidae					
Eupaludestrina stagnorum (Gmelin, 1791)	JQ973024	JX970535	—	The Netherlands, Zeeland, Zierikzee	Kroll et al. 2012; Wilke et al. 2013
Heleobops carrikeri Davis & McKee, 1989	AF213347	AF212902	—	USA, Maryland, Dorchester	Wilke et al. 2000
Mexipyrgus carranzae Taylor, 1966*	AF129325	JX970534	—	Mexico, Coahuila, Mojarral Oeste	Hershler et al. 1999; Wilke et al. 2013
Onobops jacksoni (Bartsch, 1953)	AF367645	EU573990	—	USA, Maryland, Dorchester	Wilke et al. 2001; Ponder et al. 2008
Spurwinkia salsa (Pilsbry, 1905)*	AF367633	EU573991	—	USA, Maryland, Dorchester	Wilke et al. 2001; Ponder et al. 2008
Pomatiopsidae					
Blanfordia japonica (Adams, 1861)*	AB611727	AB611726	AB611725	Japan, Niigata, Sado	Kameda and Kato 2011
Cecina manchurica Adams, 1861*	AB611743	AB611742	AB611741	Japan, Ishikawa, Nanao	Kameda and Kato 2011
Fukuia kurodai Abbott & Hunter, 1949*	AB611767	AB611766	AB611765	Japan, Fukui, Takeda	Kameda and Kato 2011
Gammatricula shini (Habe, 1961)	AB611799	AB611798	AB611797	Japan, Okinawa, Yonaguni Is.	Kameda and Kato 2011
Neotricula aperta (Temcharoen, 1971)*	AF531541	AF531556	AY207034	Mekong River (28S Thailand, 16S/COI Laos)	Attwood et al. 2003
Tricula bollingi Davis, 1968	AF531553	AF531551	AY207039	Thailand, Chiang-Mai	Attwood et al. 2003
Tateidae					
Potamolithus ribeirensis Pilsbry, 1911	JX970618	JX970549	—	Brazil, São Paulo, Iporanga	Wilke et al. 2013
Potamopyrgus antipodarum (Gray, 1843)	AY631102	AY314009	AY014159	undetermined	Guan et al. 2008
Potamopyrgus estuarinus Winterbourn, 1970	AB930485	—	AB930357	New Zealand, Auckland, Orewa	Takano and Kano 2014
Tatea huonensis (Tenison Woods, 1876)*	JX970619	JX970550	—	Australia, New South Wales, Manly Lagoon	Wilke et al. 2013
Tomichiidae					
Coxiella exposita (Iredale, 1943)	ON426511	ON455985	ON456011	Australia, Western Australia, Cranbrook	Lawrie et al. 2023
Coxiella gilesi (Angas, 1877) sensu lato	ON426653	ON455993	ON456021	Australia, Western Australia, Lake Carnegie	Lawrie et al. 2023
Coxiella glabra Macpherson, 1957	ON426716	ON455989	ON456030	Australia, Western Australia, Three Springs	Lawrie et al. 2023
Coxiella glauerti Macpherson, 1957	ON426565	ON456001	ON456014	Australia, Western Australia, Esperance	Lawrie et al. 2023
Coxiella cf. *minima* Macpherson, 1954	ON426698	ON455991	ON456027	Australia, Western Australia, Lake Shaster	Lawrie et al. 2023
Coxiella pyrrhostoma (Cox, 1868)	ON426604	ON455998	ON456016	Australia, Western Australia, Esperance	Lawrie et al. 2023
Coxiella striata (Reeve, 1842)	ON426791	ON455990	ON456034	Australia, Victoria, Willaura	Lawrie et al. 2023
Coxiella striatula (Menke, 1843)*	ON426634	ON456004	ON456018	Australia, Western Australia, Esperance	Lawrie et al. 2023
Idiopyrgus adamanteus Salvador, Silva & Bichuette, 2022	ON323464	ON359913	ON324828	Brazil, Bahia, Central	Salvador et al. 2022
Idiopyrgus minor Salvador, Silva & Bichuette, 2022	ON720330	ON720564	ON720562	Brazil, Bahia, Feira da Mata	Salvador et al. 2022
Idiopyrgus souleyetianus Pilsbry, 1911*	—	PQ461199	PQ481827	Brazil, Minas Gerais, Baldim	this paper
Spiripockia eowynae sp. nov. (typical morph)	PQ462606	—	PQ481828	Brazil, Bahia, Carinhanha	this paper
Spiripockia eowynae sp. nov. (black morph)	PQ462605	—	PQ481826	Brazil, Bahia, Carinhanha	this paper
Tomichia sp.	ON426742	ON456007	ON456023	South Africa, Western Cape, c. Quoin Point	Lawrie et al. 2023
Tomichia differens Connolly, 1939	ON426746	ON456009	ON456024	South Africa, Western Cape, Bredasdrop	Lawrie et al. 2023
Tomichia ventricosa (Reeve, 1842)*	ON426774	ON456006	ON456026	South Africa, Western Cape, Soetendalsvlei	Lawrie et al. 2023
Truncatellidae					
Truncatella pfeifferi Martens, 1860	AB611819	AB611818	AB611817	Japan, Ishikawa, Nanao	Kameda and Kato 2011
Truncatella subcylindrica (Linnaeus, 1767)*	—	KC110035	KC109982	Italy, Sicily, Trapani	Criscione and Ponder 2013
Littorinidae (OUTGROUP)					
Littoraria pallescens (Philippi, 1846)	AB611831	AB611830	AB611829	Japan, Okinawa, Nago	Kameda and Kato 2011

Alignment of genetic sequences of each marker was conducted in Geneious Prime using the MAFFT plugin (Katoh et al. 2002; Katoh and Standley 2013) with default settings. The resulting alignments were visually proofed for inconsistencies and then run through Gblocks (Castresana 2000; Talavera and Castresana 2007) to eliminate poorly aligned or data-deficient positions that could affect the analysis. The resulting post-Gblocks alignments were concatenated (1779 bp in total: COI 638 bp, 16S 515 bp, ITS2+28S 626 bp) for a Bayesian inference phylogenetic analysis.

The analysis was conducted with MrBayes (v.3.2.7, Ronquist et al. 2012) through the CIPRES Science Gateway (Miller et al. 2015) with two concurrent runs, each with four Markov chains of 80 million generations (the first 20% discarded as 'burn-in'), the default priors, nst = 6, rates = invgamma, temperature parameter = 0.1, sampling every 1,000 generations, and with substitution model parameters unlinked across the markers (COI, 16S, ITS+28S). MCMC convergence was assessed by examining the standard deviation of split frequencies (<0.001) and the potential scale reduction factor (PSRF ~1.0), as well as trace plots in Geneious (Ronquist et al. 2009).

Results

The resulting tree from the Bayesian analysis (Fig. 3) shows well-supported clades at the family level, as expected. It corroborates recent studies (Salvador et al. 2022a; Lawrie et al. 2023) that joined three relict genera from three different continents in the family Tomichiidae (Fig. 3: posterior probability PP = 1). Likewise, a sister taxon relationship was recovered between the African *Tomichia* and the Brazilian *Idiopyrgus*, albeit with low support (Fig. 3: PP = 0.72), as in the study of Lawrie et al. (2023). Within *Idiopyrgus*, *I. souleyetianus* is sister to a clade that includes all its sequenced congeners, all of which are cavern-dwelling species (Fig. 3: PP = 1 for the genus and all subclades). The latter includes the two specimens of the larger-sized *Idiopyrgus* sp. nov.: the typical morph and the dark morph. This new species and the related smaller-sized *Idiopyrgus* sp. nov. are described below as *Idiopyrgus eowynae* sp. nov. and *Idiopyrgus meriadoci* sp. nov. Unique and consistent sets of diagnostic conchological features are provided.

Pairwise sequence identity for the COI marker of *Idiopyrgus* spp. was extracted from the marker's alignment in Geneious Prime, ignoring eventual terminal gaps.

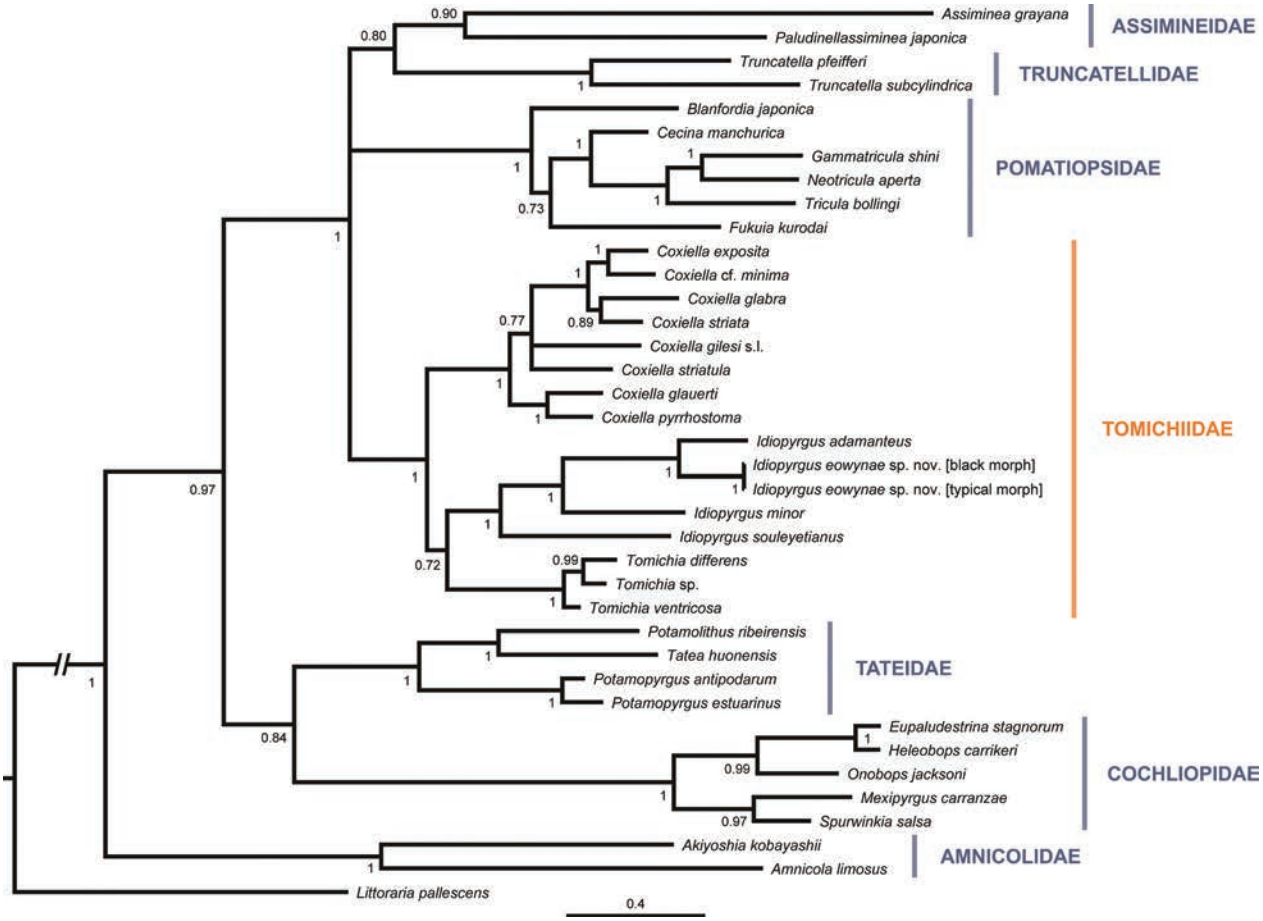

Figure 3. Bayesian inference phylogenetic tree based on concatenated but unlinked markers, highlighting the family Tomichiidae and showing the position of the new species in the genus *Idiopyrgus* and its relationship to its congeners. Posterior probabilities are shown on the nodes. Scale bar is substitutions per site.

The identity between the sequences of the typical and dark morphs of *I. eowynae* sp. nov. was 100%; between both morphs of *I. eowynae* sp. nov. and *I. adamanteus*, 90.8%; and between both morphs of *I. eowynae* sp. nov. and *I. minor*, 89.5%. No good-quality COI sequence could be obtained for *I. souleyetianus* despite repeated attempts.

Systematics

Family Tomichiidae
Genus *Idiopyrgus* Pilsbry, 1911

Idiopyrgus eowynae sp. nov.

https://zoobank.org/733E29CA-FF4B-4138-A3A9-05396C501716
Fig. 4

Type material. LES 29795 (holotype), LES 29796 (4 paratypes), LES 29797 (2 dark morphs paratype), MNRJ 37168 (3 paratypes), MZSP 168419 (3 paratypes). All specimens collected on 10.ix.2021 (M.E. Bichuette & J.E. Gallão leg.); all paratypes from type locality (except dark morphs, which are from the same cave but from the entrance zone).

Type locality. Brazil, Bahia state, Carinhanha municipality, Gruna do Pedro Cassiano ("Pedro Cassiano Cave"), 13°47'48.0"S, 43°54'50.0"W.

Etymology. The species is named in honour of Éowyn, from J.R.R. Tolkien's "The Lord of the Rings." Éowyn exemplifies courage, resilience, and resistance against darkness, both internal and external, standing against Gríma Wormtongue and the Witch-king of Angmar.

Diagnosis. Shell conical to turriform and relatively tall in comparison to congeners. Body whorl is translucent yellow; previous whorls are slightly darker and brownish. Teleoconch sculpture consisting of few (4–7) radial rows of thorn-like hairs on the apical portion of whorl and a multitude of fine irregular spiral lines below them, reaching all the way to the umbilicus. Aperture large, rounded.

Description. Shell conical to turriform, 5–5¼ whorls, 4.5–4.6 mm high, ~2.7 mm wide. Colour pale beige or yellowish on body whorl, but slightly darker and brownish on earlier whorls; body whorl translucent; early whorls typically with flaked off periostracum. Protoconch of 1¼ whorl, rounded, smooth (Fig. 4G, I). Suture deep. Whorls increasing uniformly in width but more rapidly in height. Teleoconch sculptured by minute triangular thorn-like 'periostracal hairs' arranged in equidistantly spaced spiral rows (4 to 7 rows) and restricted to apical portion of body whorl (Fig. 4A–D, H). Below the rows of periostracal hairs, there is a multitude of fine, irregular spiral lines, reaching all the way to the umbilicus (Fig. 4H). Periostracal hairs can be worn out in older specimens (Fig. 4C, D), particularly in the early whorls. Peristome complete, not covering penultimate whorl, expanded, wider in abapical region, narrower in columellar region, of same colour as body whorl or slightly whiter. Aperture rounded, with light apical angulation, but with smooth, rounded contour. Umbilicus rimate, nearly closed. Operculum oval, paucispiral; corneous, thin, and translucent, of same colour as body whorl. Soft body completely white in colour.

Dark morph (Fig. 4E, F) differs from the above-described typical morph by having a black shell with thicker walls, in which the teleoconch sculpture is nearly invisible: a few remnants of the spiral rows of hairs are visible in the adapical portion of the whorls; traces of the sculpture can also be seen through the shell wall of the aperture (Fig. 4E).

Distribution. Known only from type locality (Fig. 1), the twilight and dark (aphotic) zones of the cave (typical morph) and at the cave entrance (dark morph).

Remarks. *Idiopyrgus eowynae* sp. nov. can be easily distinguished from most of its congeners (including the type species *I. souleyetianus*) by its much wider shell and the presence of teleoconch sculpture. It closely resembles *I. meriadoci* sp. nov. (see below) and *I. umbraticola*. It differs from *I. meriadoci* sp. nov. by a much larger size and larger number of whorls, as well as by having a different teleoconch sculpture, which includes periostracal hairs. Conchologically, *I. eowynae* sp. nov. is most similar to *I. umbraticola* comb. nov., from which it can be distinguished by its smaller size (~4.5 mm vs. ~5.0 mm in *I. umbraticola*), higher whorls with a more strongly convex outline, a larger and rounder aperture, and by having a different teleoconch sculpture. In *I. eowynae* sp. nov., there are few spiral rows of the triangular thorn-like hairs, restricted to the apical portion of the whorl, and which are then replaced by irregular spiral lines that continue towards the umbilicus (also visible in juveniles). In *I. umbraticola*, there is a larger number of rows of hairs, stretching the median portion of the whorl; the spiral lines are absent. Notably, a dark morph has also been observed in *I. adamanteus* Salvador, Silva & Bichuette, 2022, and *I.* cf. *walkeri* Pilsbry, 1924 (Salvador et al. 2022a).

Except for the existence of two morphs (typical and black), there is little variation in shell shape, form, and proportions among the presently available specimens of *I. eowynae* sp. nov. (Fig. 4A–F). Notably, the sequences of the COI barcoding gene fragment of the two morphs were 100% identical, while the sequences of both morphs had a pairwise identity of around 90% in relation to *I. adamanteus* and *I. minor*. According to the results of the phylogenetic analysis (Fig. 3), *I. eowynae* sp. nov. is sister to *I. adamanteus*; both species together are sister to *I. minor*.

Idiopyrgus meriadoci sp. nov.

Fig. 5
https://zoobank.org/B70A02D0-9ABD-42F4-89FD-DE52950C7E44

Type material. LES 29798 (holotype), LES 29820 (4 paratypes), MZSP 168420 (2 paratypes). All specimens collected on 10.ix.2021 (M.E. Bichuette & J.E. Gallão leg.); all paratypes from type locality.

Type locality. Brazil, Bahia state, Carinhanha municipality, Gruna do Pedro Cassiano ("Pedro Cassiano Cave"), 13°47'48.0"S, 43°54'50.0"W.

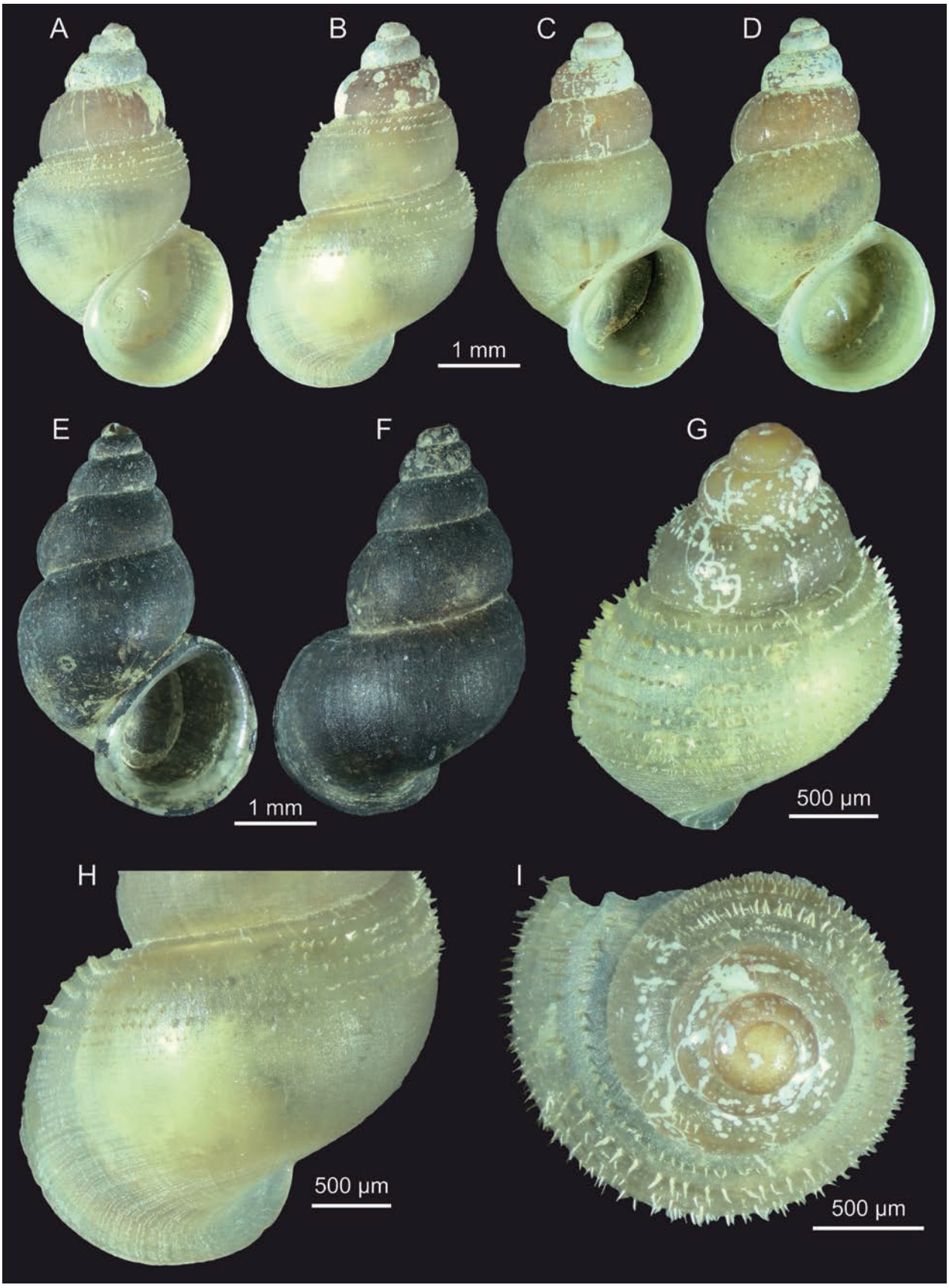

Figure 4. *Idiopyrgus eowynae* sp. nov. **A, B.** Holotype LES 29795;. **C.** Paratype (typical morph) #1 LES 29796; **D.** Paratype (typical morph) #2 LES 29796; **E, F.** Paratype (dark morph) LES 29797; **G.** Paratype (typical morph) #3 LES 29796, juvenile, showing the protoconch in greater detail as well as the sculpture of the first teleoconch whorls; **H.** Detail of the body whorl of holotype in dorsal view, showing the teleoconch sculpture, in particular the multitude of spiral lines; **I.** Paratype #3 in apical view, showing the protoconch.

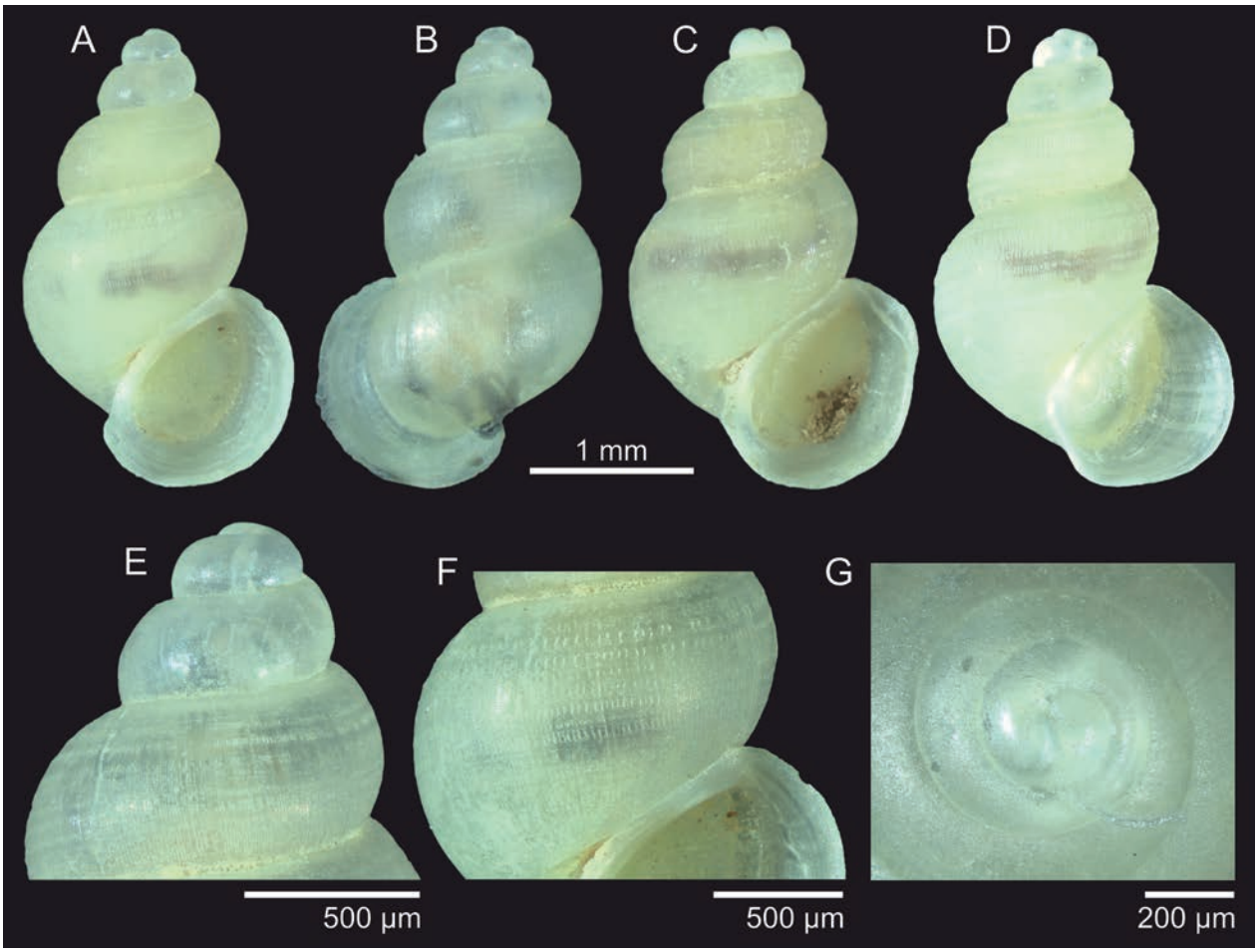

Figure 5. *Idiopyrgus meriadoci* sp. nov. **A, B.** Holotype LES 29798; **C.** Paratype #1 LES 29820; **D.** Paratype #2 LES 29820; **E.** Detail of the spire of the holotype in apertural view, showing the teleoconch sculpture in the early whorls; **F.** Detail of the body whorl of holotype in apertural view, showing the teleoconch sculpture; **F.** Detail of the protoconch of the holotype.

Etymology. The species is named in honour of Meriadoc "Merry" Brandybuck, from J.R.R. Tolkien's "The Lord of the Rings." Besides standing with Éowyn against the Witch-king in the Battle of the Pelennor Fields, Merry is also an example of the fight for nature conservation in Middle-earth, pushing the Ents into action and ultimately ending Saruman's threat to Fangorn Forest.

Diagnosis. Shell minute, whitish, entirely translucent. Teleoconch sculptured by numerous spiral rows of minute vertical pustulae, arranged roughly equidistantly from one another, which do not form thorn-like periostracal hairs. Aperture oval, adapically and abapically angulated.

Description. Shell conical, 4½–4¾ whorls, 2.8–2.9 mm high, 1.6–1.8 mm wide. Colour pale yellow to white; shell entirely translucent. Protoconch of 1¼–1½ whorl (transition to teleoconch not easily observable), rounded, smooth (Fig. 5E,G). Suture deep. Whorls increasing uniformly in height and width. Teleoconch sculptured by numerous spiral rows of minute vertical pustules, arranged roughly equidistantly from one another (Fig. 5E,F); they do not develop thorn-like periostracal hairs as seen in some of its congeners (e.g., *I. eowynae* sp. nov.), though a few pustules on the body display what seem to be minute truncated hairs in two of the more apically-positioned rows (Fig. 5F). Peristome complete, not covering penultimate whorl, expanded, wider in abapical region, narrower in columellar region, of same colour as body whorl. Aperture oval, adapically and abapically angulated, but with smooth, rounded contour. Umbilicus rimate, nearly closed. Operculum oval, paucispiral; corneous, thin, and translucent, of same colour as body whorl. Soft body completely white in colour.

Distribution. Known only from type locality (Fig. 1).

Remarks. *Idiopyrgus meriadoci* sp. nov. is easily distinguished from all its congeners by its unique teleoconch sculpture and much smaller shell; it is smaller than even *Idiopyrgus minor* Salvador, Silva & Bichuette, 2022, which was previously the species with the smallest body size in the genus. The whitish and entirely translucent shell, along with the smaller number of whorls, is likewise useful to easily distinguish it from *Idiopyrgus eowynae* sp. nov. (see above) and *I. umbraticola*. The latter two species also display a teleoconch sculpture that seems to be homologous to that of *I. meriadoci* sp. nov.; the latter, however, lacks the periostracal hairs observed in the former two species.

As for *I. eowynae* sp. nov. above, there is little variation in shell shape and proportions among the presently available specimens of *I. meriadoci* sp. nov. (Fig. 5A–D).

***Idiopyrgus umbraticola* (Simone & Salvador, 2021), comb. nov.**

Spiripockia umbraticola Simone & Salvador, 2021: 3123, figs. 2, 3; Salvador et al. 2022b: 2, figs. 8, 9.

Remarks. *Spiripockia umbraticola* is known only from the type locality, Gruna do Domingão cave (Carinhanha municipality, Serra do Ramalho region, Bahia state). When Simone and Salvador (2021) described that species, we still did not have the understanding of *Idiopyrgus* and of the family Tomichiidae in Brazil that we have today (Salvador et al. 2022a). Hence, those authors classified the new species in *Spiripockia*, heavily influenced by the presence of periostracal hairs on the teleoconch and by the fact that the animals were cavernicolous. Nevertheless, the overall shell shape of *Spiripockia umbraticola* was very different from *Spiripockia punctata* Simone, 2012, the type species of the genus and, at that point, the only species within it. The anatomical similarities between those two species are within expectations in Truncatelloidea, and some meaningful differences in the reproductive trait were observed by Simone and Salvador (2021).

Spiripockia umbraticola is morphologically very similar to *I. eowynae* sp. nov. (see above), which the present phylogenetic analysis has placed with full support within *Idiopyrgus* (Fig. 3). Thus, based on the new morphological and phylogenetic evidence, *Spiripockia umbraticola* is here reclassified as *Idiopyrgus umbraticola* (Simone & Salvador, 2021), comb. nov.

The genus *Spiripockia*, therefore, returns to being monotypic, including only *Spiripockia punctata*. However, considering the newly recognised Gondwanan family Tomichiidae in Brazil (Salvador et al. 2022a; Lawrie et al. 2023) and the new findings presented here, the family-level classification of *Spiripockia* (formerly Pomatiopsidae, presently Cochliopidae; Simone and Salvador 2021) and its status as a distinct genus needs to be reassessed. Previous attempts to obtain genetic sequences from this species failed (Simone and Salvador 2021), and new specimens must be obtained to that end. Furthermore, we lack a consensus of what the anatomical features of Brazilian Cochliopidae and Tomichiidae are, i.e., which are pleiomorphic and which are apomorphic, and more importantly, which can be used as diagnostic features (a confusion already noted by Simone and Salvador 2021 in relation to Cochliopidae in general and other truncatelloid clades as well). That will only be achieved by a thorough anatomical study of both families in Brazil, alongside a solid phylogenetic backbone built on genetic data.

Discussion

Including the present findings, the genus *Idiopyrgus* now counts with ten species, half of which are restricted to or closely related to cave environments. Thus, *Idiopyrgus* is in an odd position of being a relict South American genus of a Gondwanan family (Salvador et al. 2022a; Lawrie et al. 2023) but also having radiated into caves, where several different species arose. Undoubtedly, as the numerous caves in Brazil are explored (karsts are typical hotspots for subterranean biodiversity; Culver and Sket 2000; Sket 2016), more species are bound to come to light (Salvador et al. 2022b; Machado et al. 2023).

Troglomorphisms

In view of the presently available information, the new species described herein are endemic to a single cave (they have not been found in collections in other caves). *Idiopyrgus meriadoci* sp. nov. can be found in the twilight zone and dark (aphotic) zone of the cave; the typical morph of *I. eowynae* sp. nov. is found in the twilight and dark zones, while the dark morph is found closer to the cave entrance.

Considering the classification of subterranean organisms (Romero 2009; Christiansen 2012; Trajano and Carvalho 2017), we identify both *I. eowynae* sp. nov. and *I. meriadoci* sp. nov. as troglobitic species. Besides their endemicity, there are other morphoanatomical features to support this, some of which are of particular importance for freshwater gastropods (Grego et al. 2020; Gladstone et al. 2018, 2021; Salvador et al. 2022b, 2024) as follows. *Idiopyrgus meriadoci* sp. nov. has a white translucent and fragile shell and unpigmented body; it also has a minute size, smaller than all other congeners. These are features typical of specialised cave fauna (Gladstone et al. 2018, 2021; Grego et al. 2020). Likewise, *I. eowynae* sp. nov. has an unpigmented body, and its typical morph has a translucent and fragile shell.

The dark morph of *I. eowynae* sp. nov. displays a sturdier black shell, which has also been observed in *I. adamanteus* and *I.* cf. *walkeri* (Salvador et al. 2022a). While the significance of this is yet unknown, similar colour polymorphism is also known in other troglobitic animals, particularly in gastropods of the genus *Potamolithus* and in fish (Bichuette and Trajano 2004, 2005, 2018). Considering that there is negligible genetic distance between the two morphs in their mitochondrial markers (Fig. 3), we can only hypothesise that would be true for the rest of the genome and that the morphological differences observed in the shell are likely due to phenotypic plasticity and/or have direct environmental causes.

Both *I. eowynae* sp. nov. and *I. meriadoci* sp. nov. have a unique teleoconch sculpture (i.e., rows of periostracal hairs), so far unknown in surface-dwelling freshwater snails in Brazil but known from other cave-dwelling snails in the country: *I. umbraticola* and *Spiripockia punctata* (Simone 2012; Simone and Salvador 2021; Salvador et al. 2022b). However, we are presently unable to say whether this is somehow related to life in a cave environment or not, but the fact that only cave snails display it might be an indication of that. Other members of *Idiopyrgus*, including cave- and surface-dwelling species, lack the sculpture (Salvador et al. 2022a), so future studies

could, for instance, show that the sculpture is a feature related to a clade within the genus (e.g., *I. eowynae* sp. nov. + *I. meriadoci* sp. nov. + *I. umbraticola*). Even so, according to our present phylogenetic analysis (Fig. 3), the cave-dwelling species *I. eowynae* sp. nov., *I. adamanteus*, and *I. minor* form a single clade. While this apparently could indicate that cave species are closely related and descend from a common ancestor, it should be noted that our coverage of the genus is still quite reduced, and future studies with a better sampling across more species and populations could paint a different picture.

The facts that *Idiopyrgus* is a relict genus and that it has radiated into caves, alongside the intraspecific (and potentially non-genetic) differences in shell morphology, make species in this genus good models for studies that go beyond phylogenetics and biogeography and into evolutionary ecology. Thus, we hope that our account will bring more attention to these intriguing animals.

Geographic distribution and natural history

The genus *Idiopyrgus* has a reasonable geographic range throughout Brazil, occurring mostly in the eastern part of the country (except for *I. brasiliensis* (Rey, 1959) in the west) and across five different hydrographic regions: São Francisco (where most diversity and records are), East Northeast Atlantic, Southeast Atlantic, Tocantins-Araguaia, and Paraguay (Salvador et al. 2022a: fig. 4). There is little data on the distribution of most species, but they seem to have restricted ranges, often known only from their type localities (Salvador et al. 2022a). The exception is *I. souleyetianus*, which is a widespread species, distributed across three states (Bahia, Minas Gerais, and Espírito Santo) and two hydrographic regions (São Francisco and Southeast Atlantic) (Salvador et al. 2022a).

Three of the previously known species (*I. adamanteus*, *I. minor*, and *I. umbraticola*) are so far known only from caves, while *I. souleyetianus* and potentially *I. walkeri* have wider distributions and have also been recorded from caves (Salvador et al. 2022a). Notably, *I. umbraticola* and *I. minor* occur in the Serra do Ramalho region near the municipality of Carinhanha, in which both new species described herein (as well as *Spiripockia punctata*) can be found (Fig. 2). The region of Central, to the north of Carinhanha and where *I. adamanteus* can be found, is dominated by the Caatinga biome with a dry vegetation type, and the caves have been hypothesised as refuges for these animals (Salvador et al. 2022a).

Considering the difficulty of accessing the caves and conducting detailed observations of live animals, so far only snapshots of their biology are known. We collated here all the information currently available from the literature and from field observations by MEB.

Idiopyrgus umbraticola occurs only in the aphotic zone of Gruna do Domingão cave, attached to hard surfaces such as rocks and logs in the water (Simone and Salvador 2021). This species co-occurs with (and uses the same microhabitat as) *Xangoniscus aganju* Campos-Filho, Araujo & Taiti, 2014 (Campos-Filho et al. 2014), an amphibious troglobitic isopod.

Both *I. eowynae* sp. nov. and *I. meriadoci* sp. nov. were found side by side in a small stream inside the Gruna do Pedro Cassiano cave, attached to the small roots of plants (e.g., "gameleiras") that penetrate the caves from the surface in search of water; the deep of the small lentic drainage is formed by silt and has a depth of 10 to 15 cm. Values of pH and temperature measured on site varied, respectively, from 7.5 to 8.2 and from 21.3 to 22.4 °C. Both snail species occur in the cave's twilight zone and dark (aphotic) zones; however, the dark morph of *I. eowynae* sp. nov. lives close to the cave entrance. It is interesting that both species also co-occur with a species of the isopod genus *Xangoniscus*, probably *X. aganju* (Fig. 1G), and the cave catfish species *Trichomycterus*, probably *T. rubbioli* (Bichuette & Rizzato, 2012) (Fig. 1H).

Idiopyrgus minor lives in small pools resulting from infiltration water in the aphotic zone of two close-by caves (Gruna da Pingueira cave and Gruna do Engrunado cave) in Feira da Mata municipality and is apparently restricted to this type of habitat (Salvador et al. 2022a). *Idiopyrgus adamanteus* occurs in four close-by caves in Central municipality (Toca Bonita cave, Toca da Mulher cave, Toca de Candeias cave, and Toca da Machadinha cave) (Salvador et al. 2022a); individuals of this species were always found in phreatic waters, in twilight and aphotic zones of the caves, attached to rocks and submerged logs.

Spiripockia punctata lives attached to rocks inside a small stream in the aphotic zone in the Lapa dos Peixes cave (Simone 2012), also co-occurring with the isopod *X. aganju* and a species of cave catfish, *Trichomycterus rubbioli*. Both the isopod and catfish are troglobites (Bichuette and Rizzato 2012; Campos-Filho et al. 2014).

The repeated co-occurrence of *Idiopyrgus* and the isopod *Xangoniscus aganju* is interesting. The genus *Xangoniscus* is composed only by troglobitic species with high endemicity (Campos-Filho et al. 2014; Cardoso et al. 2020), and the somewhat more widespread *X. aganju* is suspected of being a cryptic species complex (MEB, pers. obs.). This partially parallels the story of *Idiopyrgus* in the region (Salvador et al. 2022a). Also, the observation that *Idiopyrgus* spp. and *Xangoniscus* spp. share the same microhabitats begs the investigation of other potential relationships between these species, such as modes of dispersal and cave colonisation.

Conservation concerns

Considering the co-occurrence of two species in the same cave and sharing the same microhabitat, the threats observed regionally and locally such as water use, deforestation in the cave surroundings, and the progressively decreasing recharge of water to the cave likely due to climate changes (Fig. 1A; Gallão and Bichuette 2018), we can consider both species to be in a vulnerable situation.

Some impacts are specific, such as the extraction of water (Fig. 1D) for use in villages and plantations, but they are nonetheless worrying (Gallão and Bichuette 2018). The fact that both species are endemic to the same locality already makes them fragile to any environmental disturbance. In addition, the cave is about 2 km long, considering the mapped passageways (Fig. 1C, cave gallery of Gruna do Pedro Cassiano; Grupo Bambuí de Pesquisas Espeleológicas, pers. comm.), reaching a potential extension area, for both species, of 2,000 m^2. However, from a small-scale perspective, despite the high abundance observed, with population densities reaching an average of 30 individuals/m^2 (estimated *in loco* during fieldwork), both species use specific microhabitats with a high concentration of roots (Fig. 1E, F), which implies a small area of occupation not exceeding 20 m^2 and which further increases their risk of extinction.

Conclusion

Based on our results, we described two new troglobitic species of *Idiopyrgus* and transferred a third species from *Spiripockia* to it. This reinforces the presence of the family Tomichiidae in Brazil, representing a relict genus that largely radiated into cave environments. Thus, building upon the revision of Salvador et al. (2022a), the genus *Idiopyrgus* now contains the following ten species:

- *Idiopyrgus souleyetianus* Pilsbry, 1911 [type species];
- *Idiopyrgus adamanteus* Salvador, Silva & Bichuette, 2022;
- *Idiopyrgus brasiliensis* (Rey, 1959);
- *Idiopyrgus eowynae* sp. nov.;
- *Idiopyrgus meriadoci* sp. nov.;
- *Idiopyrgus minor* Salvador, Silva & Bichuette, 2022;
- *Idiopyrgus pilsbryi* Baker, 1914;
- *Idiopyrgus rudolphi* (Haas, 1938);
- *Idiopyrgus umbraticola* (Simone & Salvador, 2021), comb. nov.;
- *Idiopyrgus walkeri* Pilsbry, 1924 [taxon inquirendum].

Acknowledgements

We thank Paulo Ricardo S. Coelho (UFMG, Brazil) for providing the sample of *Idiopyrgus souleyetianus*; the Department of Arctic and Marine Biology (UiT, Norway) for the support with the genetic analyses; CNPq (Conselho Nacional de Desenvolvimento Científico e Tecnológico) for financial support and productivity fellowship to MEB (#313332/2023-1); SISBIO (Sistema de Autorização e Informação em Biodiversidade) for collection permit to MEB (#28992); ICMBio/CECAV (Instituto Chico Mendes para Conservação da Biodiversidade/Centro Nacional de Pesquisa e Conservação de Cavernas) for financial support from environmental compensation funds through the TCCE Vale and ICMBio agreement to the projects "Estudos para definição de áreas prioritárias para a Conservação de Proteção Espeleológico na Serra do Ramalho – BA", executed by the GBPE (Grupo Bambuí de Pesquisas Espeleológicas) and "Teste de metodologias propostas em legislação ambiental relacionadas à fauna subterrânea e proposição de novas áreas prioritárias para conservação de cavernas" under execution by MEB; and to the three reviewers for their comments and suggestions (even though Reviewer 3 was a LOTR "hater"). We especially thank Jonas E. Gallão for all support in the field trips and collections in Serra do Ramalho region, and to Jessica S. Gallo for confection of the map of Fig. 2. Open access funded by Helsinki University Library.

References

Attwood SW, Ambu S, Meng XH, Upatham ES, Xu FS, Southgate VR (2003) The phylogenetics of triculine snails (Rissooidea, Pomatiopsidae) from south-east Asia and southern China: historical biogeography and the transmission of human schistosomiasis. Journal of Molluscan Studies 69(3): 263–271. https://doi.org/10.1093/mollus/69.3.263

Bedek HE, Zimmermann NE, McVicar TR, Vergopolan N, Berg A, Wood EF (2018) Present and future Köppen-Geiger climate classification maps at 1-km resolution. Scientific Data 5: e180214. https://doi.org/10.1038/sdata.2018.214

Bichuette ME, Rizzato PP (2012) A new species of cave catfish from Brazil, *Trichomycterus rubbioli* sp.n., from Serra do Ramalho karstic area, São Francisco River basin, Bahia State (Siluriformes, Trichomycteridae). Zootaxa 3480: 48–66. https://doi.org/10.11646/zootaxa.3480.1.2

Bichuette ME, Trajano E (2004) Three new subterranean species of *Ituglanis* from Central Brazil (Siluriformes, Trichomycteridae). Ichthyological Exploration of Freshwaters 15(3): 243–256.

Bichuette ME, Trajano E (2005) A new cave species of *Rhamdia* Bleeker, 1858 (Siluriformes, Heptapteridae) from Serra do Ramalho, northeastern Brazil, with notes on ecology and behavior. Neotropical Ichthyology 3(4): 587–595. https://doi.org/10.1590/S1679-62252005000400016

Bichuette ME, Trajano E (2018) Diversity of *Potamolithus* (Littorinimorpha, Truncatelloidea) in a high-diversity spot for troglobites in southeastern Brazil: role of habitat fragmentation in the origin of subterranean fauna, and conservation status. Subterranean Biology 25: 61–88. https://doi.org/10.3897/subtbiol.25.23778

Campos-Filho IS, Araujo PB, Bichuette ME, Trajano E, Taiti S (2014) Terrestrial isopods (Crustacea, Isopoda, Oniscidea) from Brazilian caves. Zoological Journal of the Linnean Society 172(2): 360–425. https://doi.org/10.1111/zoj.12172

Cardoso GM, Bastos-Pereira R, Souza LA, Ferreira RL (2020) New troglobitic species of *Xangoniscus* (Isopoda, Styloniscidae) from Brazil, with notes on their habitats and threats. Zootaxa 4819: 84–108. https://doi.org/10.11646/zootaxa.4819.1.4

Castresana J (2000) Selection of conserved blocks from multiple alignments for their use in phylogenetic analysis. Molecular Biology and Evolution 17(4): 540–552. https://doi.org/10.1093/oxfordjournals.molbev.a026334

Christiansen K (2012) Morphological adaptations. In: Culver DC, White WB (Eds) Encyclopedia of Caves. Elsevier Academic Press, Amsterdam, 2nd ed., 517–528. https://doi.org/10.1016/B978-0-12-383832-2.00075-X

Criscione F, Ponder WF (2013) A phylogenetic analysis of rissooidean and cingulopsoidean families (Gastropoda, Caenogastropoda). Molecular Phylogenetics and Evolution 66(3): 1075–1082. https://doi.org/10.1016/j.ympev.2012.11.026

Culver DC, Sket B (2000) Hotspots of subterranean biodiversity in caves and wells. Journal of Cave and Karst Studies 62: 11–17.

Folmer O, Black M, Hoeh W, Lutz R, Vrijenhoek R (1994) DNA primers for amplification of mitochondrial cytochrome c oxidase subunit I from diverse metazoan invertebrates. Molecular Marine Biology and Biotechnology 3: 294–299.

Gallão JE, Bichuette ME (2018) Brazilian obligatory subterranean fauna and threats to the hypogean environment. Zookeys 746: 1–23. https://doi.org/10.3897/zookeys.746.15140

Gladstone NS, Carter ET, McKinney ML, Niemiller ML (2018) Status and distribution of the cave-obligate land snails in the Appalachians and interior Low Plateau of the eastern United States. American Malacological Bulletin 36: 62–78. https://doi.org/10.4003/006.036.0107

Gladstone NS, Niemiller ML, Hutchins B, Schwartz B, Czaja A, Slay ME, Whelan NV (2021) Subterranean freshwater gastropod biodiversity and conservation in the United States and Mexico. Conservation Biology 36(1): e13722. https://doi.org/10.1111/cobi.13722

Grego J, Mumladze L, Falniowski A, Osikowski A, Rysiewska A, Palatov DM, Hofman S (2020) Revealing the stygobiotic and crenobiotic molluscan biodiversity hotspot in Caucasus: Part I. The phylogeny of stygobiotic Sadlerianinae Szarowska, 2006 (Mollusca, Gastropoda, Hydrobiidae) from Georgia with descriptions of five new genera and twenty-one new species. ZooKeys 955: 1–77. https://doi.org/10.3897/zookeys.955.51983

Guan F, Niu AO, Attwood SW, Li YL, Zhang B, Zhu YH (2008) Molecular phylogenetics of triculine snails (Gastropoda, Pomatiopsidae) from southern China. Molecular Phylogenetics and Evolution 48(2): 702–707. https://doi.org/10.1016/j.ympev.2008.04.021

Hershler R, Liu H-P, Mulvey M (1999) Phylogenetic relationships within the aquatic snail genus *Tryonia*: implications for biogeography of the North American Southwest. Molecular Phylogenetics and Evolution 13: 377–391. https://doi.org/10.1006/mpev.1999.0659

Kameda Y, Kato M (2011) Terrestrial invasion of pomatiopsid gastropods in the heavy-snow region of the Japanese Archipelago. BMC Evolutionary Biology 11(1): e118. https://doi.org/10.1186/1471-2148-11-118

Katoh K, Standley DM (2013) MAFFT Multiple Sequence Alignment Software Version 7: Improvements in performance and usability. Molecular Biology and Evolution 30(4): 772–780. https://doi.org/10.1093/molbev/mst010

Katoh K, Misawa K, Kuma K, Miyata T (2002) MAFFT: A novel method for rapid multiple sequence alignment based on fast Fourier transform. Nucleic Acids Research 30(14): 3059–3066. https://doi.org/10.1093/nar/gkf436

Kroll O, Hershler R, Albrecht C, Terrazas EM, Apaza R, Fuentealba C, Wolff C, Wilke T (2012) The endemic gastropod fauna of Lake Titicaca: correlation between molecular evolution and hydrographic history. Ecology and Evolution 2: 1517–1530. https://doi.org/10.1002/ece3.280

Lawrie AD, Chaplin J, Kirkendale L, Whisson C, Pinder A, Mlambo MC (2023) Phylogenetic assessment of the halophilic Australian gastropod *Coxiella* and South African Tomichia resolves taxonomic uncertainties, uncovers new species and supports a Gondwanan link. Molecular Phylogenetics and Evolution 184: 107810. https://doi.org/10.1016/j.ympev.2023.107810

Machado FM, Miranda MS, Salvador RB, Pimenta AD, Côrtes MO, Gomes JAJ, Miyahira IC, Agudo-Padrón I, Oliveira CDC, Caetano CHS, Coelho PRS, D'ávila S, Arruda EP, Almeida SM, Gomes SR, Alvim J, Filho HG, Ferreira-Júnior AL, Marques RC, Martins I, Souza LS, Arruda JO, Cavallari DC, Santos SB, Pedro NC, Salles ACA, Dornellas APS, Lima TC, Amaral VS, Silva FS, Passos FD, Thiengo SS, Leite TS, Simone LRL (2023) How many species of Mollusca are there in Brazil? A collective taxonomic effort to reveal this still unknown diversity. Zoologia 40: e23026. https://doi.org/10.1590/s1984-4689.v40.e23026

Miller MA, Schwartz T, Pickett BE, He S, Klem EB, Scheuermann RH, Passarotti M, Kaufman S, O'Leary MA (2015) A RESTful API for access to phylogenetic tools via the CIPRES Science Gateway. Evolutionary Bioinformatics Online 11: 43–48. https://doi.org/10.4137/EBO.S21501

Ponder WF, Wilke T, Zhang W-H, Golding RE, Fukuda H, Mason RAB (2008) *Edgbastonia alanwillsi* n. gen & n. sp. (Tateinae, Hydrobiidae s.l., Rissooidea, Caenogastropoda); a snail from an artesian spring group in western Queensland, Australia, convergent with some Asian Amnicolidae. Molluscan Research 28: 89–106. https://doi.org/10.11646/mr.28.2.1

Romero A (2009) Cave Biology: Life in Darkness. Cambridge University Press, Cambridge, 306 pp. https://doi.org/10.1017/CBO9780511596841

Ronquist F, van der Mark P, Huelsenbeck JP (2009) Bayesian phylogenetic analysis using MrBayes. In: Lemey P, Salemi M, Vandamme A-M (Eds) The Phylogenetic Handbook: a Practical Approach to Phylogenetic Analysis and Hypothesis Testing. Cambridge University Press, Cambridge, 210–266. https://doi.org/10.1017/CBO9780511819049.009

Ronquist F, Teslenko M, van der Mark P, Ayres DL, Darling A, Höhna S, Larget B, Liu L, Suchard MA, Huelsenbeck JP (2012) MrBayes 3.2: Efficient Bayesian phylogenetic inference and model choice across a large model space. Systematic Biology 61(3): 539–542. https://doi.org/10.1093/sysbio/sys029

Salvador RB, Silva FS, Bichuette ME (2022a) Phylogenetic position of the relict South American genus *Idiopyrgus* Pilsbry, 1911 (Gastropoda, Truncatelloidea), with the description of two new cave species. Zoosystematics and Evolution 98(2): 365–375. https://doi.org/10.3897/zse.98.90797

Salvador RB, Silva FS, Cavallari DC, Cunha CM, Bichuette ME (2022b) Cave-dwelling gastropods (Mollusca, Gastropoda) of Brazil: state of the art and conservation. Zoologia (Curitiba) 39: e21033. https://doi.org/10.1590/s1984-4689.v39.e21033

Salvador RB, Silva FS, Cavallari DC, Cunha CM, Bichuette ME (2024) Cave-dwelling gastropods of Brazil: a reply to Ferreira et al. (2023). Zoologia 41: e23099. https://doi.org/10.1590/s1984-4689.v41.e23099

Simon C, Frati F, Beckenbach A, Crespi B, Liu H, Flook P (1994) Evolution, weighting, and phylogenetic utility of mitochondrial gene sequences and compilation of conserved Polymerase Chain Reaction primers. Annals of the Entomological Society of America 87: 651–701. https://doi.org/10.1093/aesa/87.6.651

Simone LRL (2006) Land and freshwater Molluscs of Brazil. Fapesp, São Paulo, 390 pp.

Simone LRL (2012) A new genus and species of cavernicolous Pomatiopsidae (Mollusca, Caenogastropoda) in Bahia, Brazil. Papeis Avulsos de Zoologia 52(40): 515–524. https://doi.org/10.1590/S0031-10492012022000001

Simone LRL, Salvador RB (2021) A new species of *Spiripockia* from eastern Brazil and reassignment to Cochliopidae (Gastropoda, Truncatelloidea). Journal of Natural History 54(47–48): 3121–3130. https://doi.org/10.1080/00222933.2021.1890850

Sket B (2016) Subterranean (hypogean) habitats in karst and their fauna. In: Finlayson C, Milton G, Prentice R, Davidson N (Eds) The Wetland Book. Springer, Dordrecht, 1–14. https://doi.org/10.1007/978-94-007-6173-5_241-1

Takano T, Kano Y (2014) Molecular phylogenetic investigations of the relationships of the echinoderm-parasite family Eulimidae within Hypsogastropoda (Mollusca). Molecular Phylogenetics and Evolution 79: 258–269. https://doi.org/10.1016/j.ympev.2014.06.021

Talavera G, Castresana J (2007) Improvement of phylogenies after removing divergent and ambiguously aligned blocks from protein sequence alignments. Systematic Biology 56(4): 564–577. https://doi.org/10.1080/10635150701472164

Trajano E, Carvalho MR (2017) Towards a biologically meaningful classification of subterranean organisms: a critical analysis of the Schiner-Racovitza system from a historical perspective, difficulties of its application and implications for conservation. Subterranean Biology 22: 1–26. https://doi.org/10.3897/subtbiol.22.9759

Wade CM, Mordan PB (2000) Evolution within the gastropod molluscs: using the ribosomal RNA gene cluster as an indicator of phylogenetic relationships. Journal of Molluscan Studies 66: 565570. https://doi.org/10.1093/mollus/66.4.565

Wade CM, Mordan PB, Naggs F (2006) Evolutionary relationships among the pulmonate land snails and slugs (Pulmonata, Stylommatophora). Biological Journal of the Linnean Society 87: 593–610. https://doi.org/10.1111/j.1095-8312.2006.00596.x

Wilke T, Davis GM, Gong X, Liu H-X (2000) *Erhaia* (Gastropoda, Rissooidea): phylogenetic relationships and the question of *Paragonimus* coevolution in Asia. American Journal of Tropical Medicine and Hygiene 62: 453–459. https://doi.org/10.4269/ajtmh.2000.62.453

Wilke T, Davis GM, Falniowski A, Giusti F, Bodon M, Szarowska M (2001) Molecular systematics of Hydrobiidae (Mollusca, Gastropoda, Rissooidea): testing monophyly and phylogenetic relationships. Proceedings. Academy of Natural Sciences of Philadelphia 151(1): 1–21. https://doi.org/10.1635/0097-3157(2001)151[0001:MSOHMG]2.0.CO;2

Wilke T, Haase M, Hershler R, Liu H-P, Misof B, Ponder W (2013) Pushing short DNA fragments to the limit: phylogenetic relationships of 'hydrobioid' gastropods (Caenogastropoda, Rissooidea). Molecular Phylogenetics and Evolution 66(3): 715–736. https://doi.org/10.1016/j.ympev.2012.10.025

Zoosyst. Evol. 100 (4) 2024, 1557–1568 | DOI 10.3897/zse.100.135994

PENSOFT

MUSEUM FÜR NATURKUNDE BERLIN

Rediscovery and phylogenetic analysis of *Agnostrup*, a least known genus of Mecistocephalidae (Chilopoda, Geophilomorpha) in China

Jia-bo Fan[1], Chun-Xue You[1], Chao Jiang[2]

1 *Tianjin Key Laboratory of Agricultural Animal Breeding and Healthy Husbandry, College of Animal Science and Veterinary Medicine, Tianjin Agricultural University, Tianjin 300392, China*

2 *State Key Laboratory for Quality Ensurance and Sustainable Use of Dao−di Herbs, National Resource Center for Chinese Materia Medica, China Academy of Chinese Medical Sciences, Beijing 100700, China*

https://zoobank.org/FD65E13C-0E85-49BF-A691-21E351EEF22E

Corresponding authors: Chao Jiang (jiangchao0411@126.com); Chun-Xue You (youchunxue@mail.bnu.edu.cn)

Academic editor: Martin Husemann ♦ **Received** 31 August 2024 ♦ **Accepted** 15 October 2024 ♦ **Published** 13 November 2024

Abstract

The genus *Agnostrup* Foddai, Bonato, Pereira & Minelli, 2003 is one of the least known genera within the family Mecistocephalidae Bollman, 1893. In this study, we rediscovered the genus *Agnostrup* in China and provided a comprehensive redescription of *A. striatus* (Takakuwa, 1949). Additionally, we conducted a molecular phylogenetic analysis using CO1, 16S, and 28S sequence data, revealing a low genetic distance between *Agnostrup* and *Nannarrup* Foddai, Bonato, Pereira & Minelli, 2003. After comparing the morphological characteristics of these two genera, we synonymized the genus *Nannarrup* **syn. nov.** with *Agnostrup*. As a result, three species previously belonging to the genus *Nannarrup* were transferred to *Agnostrup*: *A. hoffmani* (Foddai et al., 2003), **comb. nov.**, *A. innuptus* (Tsukamoto, 2022), **comb. nov.**, and *A. oyamensis* (Tsukamoto, 2022), **comb. nov.**

Key Words

Agnostrup, description, Mecistocephalidae, molecular phylogeny, taxonomy

Introduction

The geophilomorph family Mecistocephalidae Bollman, 1893, recognized as a monophyletic basal clade, comprises approximately 170 species across 11 genera (Bonato et al. 2011). Within this family, three subfamilies are recognized: Mecistocephalinae Bollman, 1893; Dicellophilinae Cook, 1896; and Arrupinae Chamberlin, 1912. The Arrupinae includes four valid genera: *Arrup* Chamberlin, 1912; *Agnostrup* Foddai, Bonato, Pereira & Minelli, 2003; *Partygarrupius* Verhoeff, 1939; and *Nannarrup* Foddai, Bonato, Pereira & Minelli, 2003 (Foddai et al. 2003).

Agnostrup Foddai, Bonato, Pereira & Minelli, 2003, characterized by forcipular trochanteropraefemur with a well-developed tooth and 41 leg-bearing segments, is one of the least-known genera in the family Mecistocephalidae Bollman, 1893 (Foddai et al. 2003). This genus includes only three species recorded from temperate regions of East Asia: *A. striatus* (Takakuwa, 1949) from Shanxi, China; *A. paucipes* (Miyosi, 1955) from Matsuyama, Japan; and *A. striganovae* (Titova, 1975) from the nearby Sikhote-Alin mountains of Russia. Few articles about the morphology, distribution, ecology, or molecular phylogenetics of species from this genus have been documented since its original description. In particular, the type materials of *Taiwanella paucipes* and *Taiwanella striata* are considered to have been lost after examining many collections (Foddai et al. 2003; Uliana et al. 2007). The published accounts of its morphology are incomplete and contain ambiguous details, and the species' distinguishing features have not been thoroughly examined.

Recently, we collected four specimens from Shanxi, China, that obviously belong to the genus *Agnostrup*. Based on a critical evaluation of published information and examination of fresh material, these specimens were identified as *A. striatus*; one of these specimens is selected

and described here as the neotype for *Taiwanella striata*. We also revised the diagnostic characters of the genus *Agnostrup* and established the phylogenetic relationship of the family Mecistocephalidae based on the COI, 16S, and 28S sequence data. Molecular phylogenetics shows a close relationship between the genus *Agnostrup* and *Nannarrup* Foddai, Bonato, Pereira & Minelli, 2003. After comparing the morphological characters of these two genera, we synonymize the genus *Nannarrup* syn. nov. with *Agnostrup*.

Materials and methods

Biological sampling

Two adult male and two adult female specimens of *Agnostrup spp*. were collected from Shanxi Province, China (see additional geographic details below) in November 2023 and June 2024. These specimens were individually preserved in 75% ethanol and deposited in the herbarium of the National Resource Center for Chinese Materia Medica, China Academy of Chinese Medical Sciences (CMMI).

Morphological terminology for external anatomy follows Bonato et al. (2010). Taxonomic characters were examined in lactic acid and photographed using a Leica M205 FCA stereomicroscope (7.8–160×) or an Olympus BX51 microscope (100–400×). The photos were converted into hand-drawn illustrations with SKETCHBOOK 6.0.6.

DNA extractions and fragment amplification

Two body segments from each sample were used for DNA extraction. Following the manufacturer's protocol, DNA was extracted using the DNeasy® Blood & Tissue Kit (QIAGEN GmbH, Germany). The polymerase chain reaction (PCR) was used to amplify the cytochrome c oxidase subunit I (COI), mitochondrial ribosomal gene 16S, and nuclear ribosomal DNA 28S fragments. PCR primers and programs are provided in Table 1.

Genetic distance and molecular phylogenetic analyses

The genetic distance among genera of Mecistocephalidae was calculated using the Kimura 2-parameter model in MEGA X (Kumar et al. 2018).

Maximum-likelihood (ML) tree were constructed using the concatenated dataset with IQ-tree 1.6.12 (Nguyen et al. 2015). GTR+I+G4+F was selected as the preferred substitution model for ML, with 1,000,000 ultrafast bootstrap replicates (Hoang et al. 2018). Bayesian inference (BI) was conducted using MRBAYES 3.2.6 (Ronquist et al. 2012), with 10,000,000 bootstrap replicates. The GTR+F+I+G4 was chosen as the preferred model for BI, sampling every 1,000 generations and using 25% of the trees as burn-in. A split frequency of less than 0.01 was used to determine stationarity, and the consensus tree was constructed from the remaining trees.

Results

Molecular phylogenetic analyses

Sequences from the *Agnostrup striatus*, along with 16 other Mecistocephalidae samples from different genera and a sample from Geophilidae, were aligned. ML and BI analyses were utilized to construct phylogenetic trees for the combined COI+16S+28S dataset (Figs 1, 2). In the family Mecistocephalidae, the genera *Agnostrup*, *Anarrup*, *Arrup*, *Nannarrup*, and *Partygarrupius*, as well as the species *Dicellophilus anomalus* (Chamberlin, 1904), *Dicellophilus pulcher* (Kishida, 1928), and *Dicellophilus praetermissus* Tsukamoto & Eguchi, 2024, from the genus *Dicellophilus*, all have 41 leg-bearing segments. According to the phylogenetic tree, *Agnostrup* is the sister to *Nannarrup* (PP = 1; BS = 99%). While the genus *Arrup* is nested at the base of Mecistocephalidae in both ML and BI analyses (PP = 1). The genus *Dicellophilus* Cook, 1896 forms a clade with *Proterotaiwanella* + *Tygarrup* + *Mecistocephalus* in ML analyses, uncertain in BI analyses. The genus *Proterotaiwanella* Bonato, Foddai & Minelli, 2002 (subfamily Dicellophilinae) forms a clade with *Tygarrup* and *Mecistocephalus* (subfamily Mecistocephalinae) (PP = 1; BS = 85%), which is inconsistent with morphological results.

Genetic distance among *Agnostrup* and other mecistocephalidae genus

In examining genetic distances within the Mecistocephalidae family, we focused on the *Agnostrup* genus and its relationship with other genera, using sequences from COI, 16S, and 28S mitochondrial DNA regions (Table 3). The average K2P genetic distance is 20.0% (COI), 25.9% (16S), and 11.68% (28S). The data showed distinct genetic differentiation, with *Agnostrup* displaying high genetic distances from the *Tygarrup* genus, marked by 22.2% for COI, 26.9% for 16S, and 11.8% for 28S, indicating significant evolutionary divergence. In contrast, genetic distances between *Agnostrup* and *Nannarrup* genera were notably lower at 16.4% for COI, 18.1% for 16S, and 10.6% for 28S. The mean K2P genetic distance between the specimens of *Agnostrup striatus* is 12.7% (COI), 13.3% (16S), and 2% (28S), which is close to the intergeneric genetic distance between *Agnostrup* and *Nannarrup*. These lower distances suggest a close genetic relationship.

Morphological comparison of *Agnostrup* and *Nannarrup*

The genera *Agnostrup* and *Nannarrup* both belong to the subfamily Arrupinae and share the following diagnostic

Table 1. Primers and programs of PCR.

Loci	Primers Sequence 5– 3	Program	References
CO1	LCO1490 GGTCAACAAATCATAAAGATATTGG HCO2198 TAAACTTCAGGGTGACCAAAAAATCA	2min at 94 °C; 35 cycles of 15s at 95 °C, 40s at 45–47 °C and 45s at 72 °C; 10min at 72 °C	Folmer et al. 1994; Joshi and Karanth 2011
16S	16Sar CGCCTGTTTATCAAAAACAT 16Sb CTCCGGTTTGAACTCAGATC	5min at 95 °C; 35 cycles of 30s at 95 °C, 30s at 55 °C and 1min at 72 °C; 3min at 72 °C	Xiong and Kocher 1991
28S	28SD1F GGGACTACCCCCTGAATTTAAGCAT 28SrD4b CCTTGGTCCGTGTTTCAAGAC	3min at 95 °C; 35 cycles of 30s at 95 °C, 30s at 65 °C and 1min at 72 °C; 3min at 72 °C	Boyer and Giribet (2007); Edgecombe and Giribet (2006)

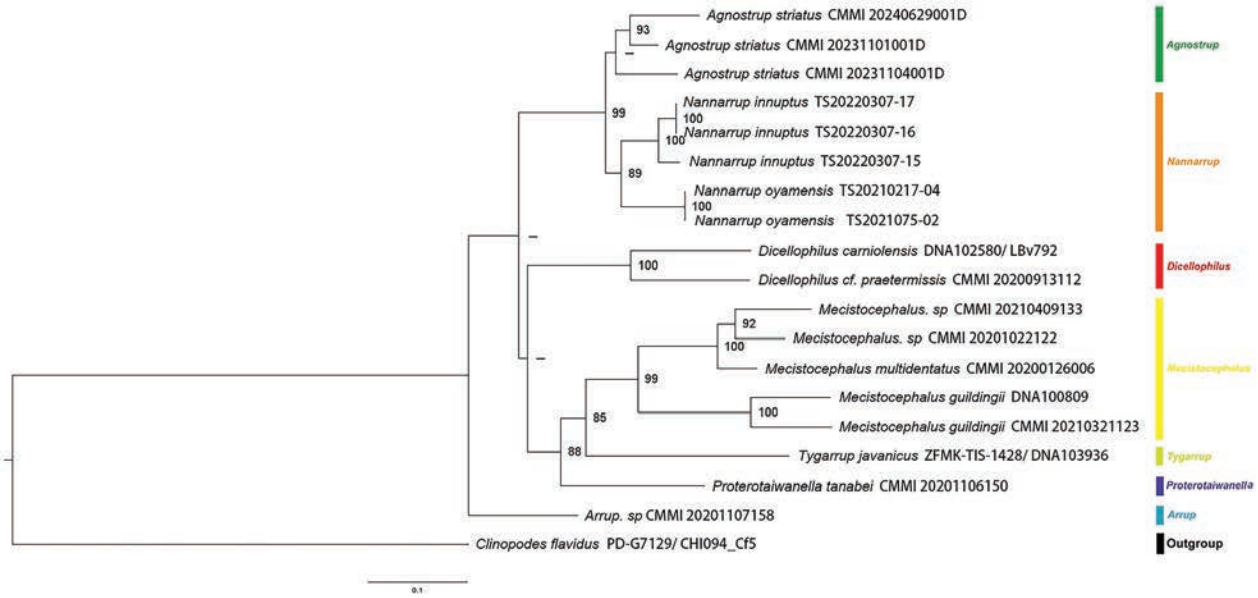

Figure 1. Maximum likelihood phylogenetic tree based on combined data for Mecistocephalidae. Values above the branches represent the bootstrap support (BS); BS < 70% are indicated as hyphens.

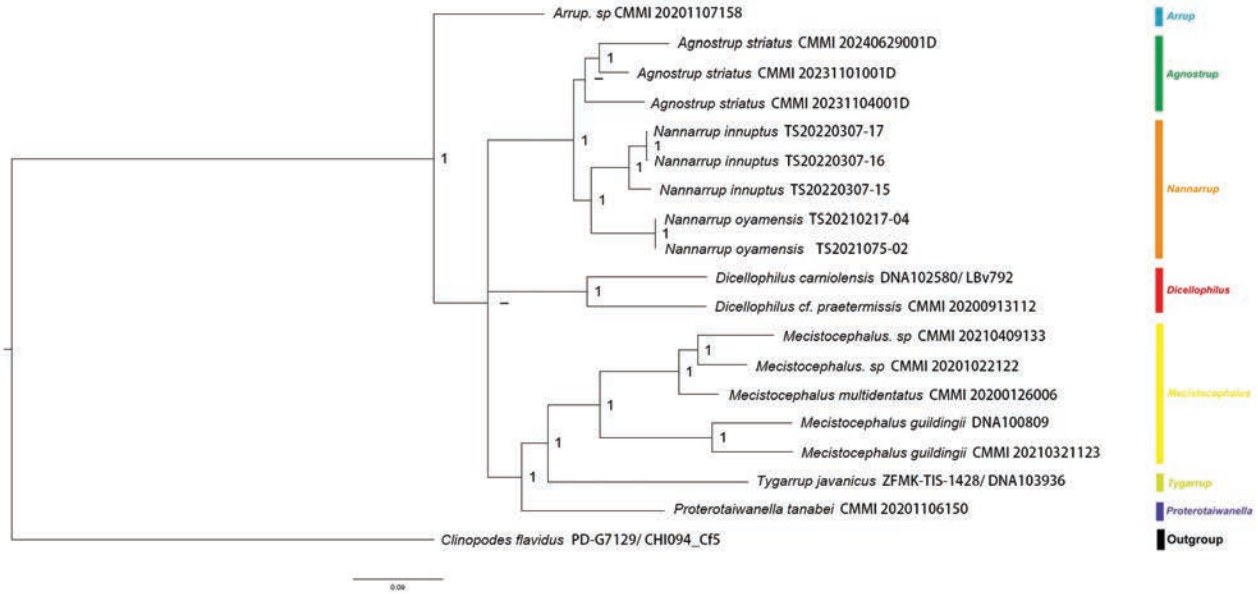

Figure 2. Bayesian inference based on combined data for Mecistocephalidae. Values above the branches represent the posterior probability (PP); PP < 0.9 is indicated as a hyphen.

characters (Foddai et al. 2003): Body inconspicuously tapering backwards; leg-bearing trunk uniform in color, without dark patches; cephalic plate only slightly longer than wide; usually 2 clypeal plagulae divided by a mid-longitudinal stripe, not covering more than posterior half of clypeus; clypeal setae are mainly located in two laterally extended areas; buccae without setae; spiculum absent; internal margin of labral anterior ala reduced to a pointed end; posterior alae without longitudinal stripes; posterior margin of labral sidepiece sinuous, not fringed; coxosternum of first maxil-

Table 2. The list of specimens that were used in the phylogenetic analyses (the new sequences have been uploaded to GenBank).

Species	Voucher	Accession No.			Collection Location	References
		16s	28s	coi		
Dicellophilus cf. *praetermissus* Tsukamoto & Eguchi, 2024	CMMI 20200913112	PP788526	PP750339	PP737183	Huanren, Liao Ning, China	the present study
Proterotaiwanella tanabei Bonato, Foddai & Minelli, 2002	CMMI 20201106150	PP788520	PP750333	PP737177	Lian Yun Gang, Jiang Su, China	the present study
Arrup sp.	CMMI 20201107158	PP788525	PP750338	PP737182	Yan Cheng, Jiang Su, China	the present study
Agnostrup striatus (Takakuwa, 1949)	CMMI 20231104001D	PP788521	PP750334	PP737178	Chang Zhi, Shan Xi, China	the present study
	CMMI 20231101001D	PP788522	PP750335	PP737179	Ning Wu, Shan Xi, China	the present study
	CMMI 20240629001D	PQ213467	–	PQ222662	Ning Wu, Shan Xi, China	the present study
Mecistocephalus sp.	CMMI 20210409133	PP788523	PP750336	PP737180	Jing Shan, Hu Bei, China	the present study
	CMMI 20201022122	PP788527	PP750340	OR864655	Jian Shui, Yun Nan, China	Pan et. al. (2024)
Mecistocephalus multidentatus Takakuwa, 1936	CMMI 20200121006	PP788524	PP750337	PP737181	Heng Yang, Hu Nan, China	the present study
Tygarrup javanicus Attems, 1929	ZFMK-TIS-1428 DNA103936	HM453226	HM453286	KM491598	–	Murienne et al. (2010)
Agnostrup oyamensis (Tsukamoto,2022)	TS20210217-04	LC715630	LC715705	LC715555	Hinata, Isehara-shi, Kanagawa prefecture, Japan	Tsukamoto et al. (2022)
	TS20210725-02	LC715631	LC715706	LC715556	Hinata, Isehara-shi, Kanagawa prefecture, Japan	Tsukamoto et al. (2022)
Agnostrup innuptus (Tsukamoto,2022)	TS20220307-15	LC715484	LC715559	LC715634	Makigawa, Tsushimacho, Uwajima-shi, Ehime prefecture, Japan	Tsukamoto et al. (2022)
	TS20220307-16	LC715483	LC715558	LC715633	Makigawa, Tsushimacho, Uwajima-shi, Ehime prefecture, Japan	Tsukamoto et al. (2022)
	TS20220307-17	LC715482	LC715557	LC715632	Makigawa, Tsushimacho, Uwajima-shi, Ehime prefecture, Japan	Tsukamoto et al. (2022)
Dicellophilus carniolensis (C.L. Koch, 1847)	DNA102580	HM453225	HM453285	KF569305	–	Murienne et al. (2010)
	LBv792	–	–	–	–	Bonato et al. (2014)
Mecistocephalus guildingii Newport, 1843	DNA100809	AY288728	HM453283	AY288747	–	Edgecombe and Giribet (2004); Murienne et al. (2010)
	CMMI 20210321123	PP788528	PP750341	PP737184	Yuan Yang, Yun Nan, China	the present study
Clinopodes flavidus Koch, 1847	PD-G7129 CHI094_ Cf5	MZ427910	EU376008.1	MH816990	–	Peretti et al. (2022)

Table 3. Mean K2P genetic distance between the genus *Agnostrup* and other genera of Mecistocephalidae.

	Tygarrup	*Proterotaiwanella*	*Nannarrup*	*Mecistocephalus*	*Dicellophilus*	*Arrup*
CO11	22.2%	20.5%	16.4%	18.9%	20.3%	21.9%
16S	26.9%	26.6%	18.1%	29.6%	26.8%	27.6%
28S	11.8%	12.0%	10.6%	11.7%	13.4%	10.6%

Table 4. Mean K2P genetic distance between the specimens of *Agnostrup striatus*.

Examined genus	Mean distance (Standard error)		
	CO1	16S	28S
1. *Agnostrup*	13.3% (1.4%)	12.7% (1.5%)	2% (0%)

lae either divided and nonareolate or undivided and areolate, anterolateral corners virtually absent; coxosternum of second maxillae undivided or coxae connected by a membranous isthmus; groove from metameric pore and foraminal process reaching postero-external corner of coxosternum; reduced development of the telopodites of the second maxillae; forcipular tergum evidently wider than long, without a mid-longitudinal sulcus; cerrus absent; forcipular

Table 5. Morphological comparison of six species within the genus *Agnostrup* are based on the description and reference pictures published by Foddai et al. 2003; Tsukamoto et al. 2022; Takakuwa and Takashima 1949; Titova 1975; Uliana et al. 2007.

Characters	*A. paucipes* (Miyosi, 1955)	*A. striatus* (Takakuwa,1949)	*A. striganovae* (Titova, 1975)	*A. hoffmani* Foddai, Bonato, Pereira & Minelli, 2003	*A. innuptus* Tsukamoto, 2022	*A. oyamensis* Tsukamoto, 2022
body length	at least 20 mm	20–35 mm	over 30 mm	10.3 mm	7.0–12.0 mm	8.6 mm
Clypeus: setae on the areolate part (each side)	3	5–8	4–7	7	9	6–7
Clypeus: setae on the plagulae (each side)	8	3–6	5	0	0	0
Clypeus: insulae	absent	present	absent	absent	present	absent
lamellae on mandible	5	5	6	4	at least 4	at least 4
second maxillae: pretarsus	absent	rudimentary truncate claw	absent	short spine	short spine	short spine
Forcipular segment: article I	well-developed distal tooth	large tooth	large and blunt tooth	strong pigmented basal tooth	strong pigmented basal tooth	strong pigmented basal tooth
Forcipular segment: article II	without tooth	without tooth	small sharp tooth	without tooth	without tooth	without tooth
Forcipular segment: articleIII	without tooth	tubercle	small sharp tooth	without tooth	tubercle	tubercle not visible
Forcipular segment: tarsungulum	long basal tooth	large and sharp tooth	large tooth	slightly pigmented basal tooth	well-pigmented basal denticle	well-pigmented basal denticle
Ultimate leg-bearing segment: pretarsus	–	small tubercle	–	small spine	small tubercle	spine

trochanteropraefemur stout, with a distal tooth only; sternal mid-longitudinal sulci not furcate; number of pairs of legs 41. Differences between these two genera include: a frontal line present in *Agnostrup* while absent in *Nannarrup*; two small clypeal plagulae covering approximately one-sixth of the clypeus in *Nannarrup*, whereas the clypeal plagulae of *Agnostrup* cover one-half to most of their clypeus; the mandible in *Nannarrup* is provided with four well-developed pectinate lamellae, whereas 5–6 are present in *Agnostrup*. In contrast to the distinctions observed among other genera within the family Mecistocephalidae, these characters are not significant enough to serve as morphological characters for delineating them as two distinct genera. (The more detailed characteristics of the species within these two genera are presented in Table 5.)

Taxonomic account

Family Mecistocephalidae Bollmann, 1893

Agnostrup Foddai, Bonato, Pereira & Minelli, 2003.
Agnostrup Foddai, Bonato, Pereira & Minelli, 2003: 1254.
Agnostrup: Uliana, Bonato and Minelli 2007: 24.
Nannarrup Foddai, Bonato, Pereira & Minelli, 2003, syn. nov.

Type species. *Krateraspis striganovae* Titova, 1975 – by original designation.

Species included. *Agnostrup hoffmani* (Foddai, Bonato, Pereira & Minelli, 2003), comb. nov., *Agnostrup innuptus* (Tsukamoto, 2022), comb. nov., *Agnostrup oyamensis* (Tsukamoto, 2022), comb. nov., *Agnostrup paucipes* (Miyosi, 1955), *Agnostrup striatus* (Takakuwa, 1949), and *Agnostrup striganovae* (Titova, 1975).

Diagnosis. Mecistocephalids with 41 leg-bearing segments; two clypeal plagulae separated by a mid-longitudinal stripe. Clypeal setae are arranged in a transversal band on the anterior part of the plagulae and on a medial part of the areolate clypeus; spiculum absent. Side-pieces of labrum are divided into anterior and posterior alae; the internal margin of each anterior ala is reduced to a point. Posterior alae with or without longitudinal stripes; posterior margin of labrum is not hairy. Mandible is provided with 4–6 pectinate lamellae. Coxosternum of the first maxillae is divided in the middle; coxosternum of the second maxillae is undivided. Telopodites terminals of the second maxillae with or without a claw. Forcipular trochanteropraefemur with one distal tooth pointing forward; forcipular articles II and III with or without teeth. Basal tooth of tarsungulum well developed. Forcipular tergum without median sulcus; sternal sulcus of trunk segments not furcate. 7–15 pores on the ventral surface of each coxopleuron; anal pores are present.

Remarks. *Agnostrup* differs from other genera of the Mecistocephalidae previously recorded in China due to its unusual forcipular teeth: the trochanteropraefemur with one well-developed distal tooth pointing forward and a well-developed basal tooth of the tarsungulum. *Agnostrup* differs from *Mecistocephalus* by the presence vs. absence of a pair of spicules projecting from the cephalic pleurites. It differs from *Proterotaiwanella* in the pattern of clypeal setae and sensilla and the finger-like processes of the labrum (Bonato et al. 2002). It differs from *Dicellophilus* by the latter having a labrum with longitudinal folds and

fringed by marginal bristles (Bonato et al. 2010). From *Tygarrup*, it differs in having an entire plagula lacking a mid-longitudinal areolate strip (Chao et al. 2020). Finally, it differs from *Arrup* in the unusual teeth of the forcipules and the later having entire coxosternite of the first maxillae, without a mid-longitudinal suture (Foddai et al. 2003).

Agnostrup clearly resembles *Nannarrup* morphologically and in geographical distribution. *Nannarrup* was established for a single species discovered in New York, USA, and is considered to have been introduced from western America or East Asia (Foddai et al. 2003). Nearly twenty years later, Tsukamoto et al. (2022) discovered two new *Nannarrup* species, *N. innuptus* Tsukamoto, 2022, and *N. oyamensis* Tsukamoto, 2022, from Japan based on morphological characteristics and DNA analysis, confirming the East Asian origin of this genus. These two genera both share unique characters of forcipular article I with one well-developed distal tooth and a tarsungulum with one large basal tooth (Foddai et al. 2003; Tsukamoto et al. 2022). Comparisons of the original descriptions of *Agnostrup* and *Nannarrup* reveal several differences between these two genera, such as the presence vs. absence of a frontal line, side-pieces of the labrum fully divided into two alae vs. only incompletely subdivided into an anterior and a posterior ala, the number of setae on the clypeal plagulae, the shape of the pretarsus of the second maxillae, the tooth vs. denticle of the forcipular tarsungulum, the absence vs. presence of claws on the second maxillae, along with different numbers of mandible pectinate lamellae. However, the side-pieces of the labrum are fully divided into two alae in *N. innuptus* and *N. oyamensis* (Tsukamoto et al. 2022), and claws of the second maxillae were confirmed to be present in *A. striatus* after examining the new specimens collected from Shanxi province in China. The size of the teeth on the forcipular tarsungulum is also variable among species within the genus *Nannarrup*; the type species *N. hoffmani* is described as "tarsungulum with a well-developed and slightly pigmented basal tooth," which is quite similar to the *A. striatus* specimen. However, in *N. innuptus* and *N. oyamensis*, this characteristic is described as "tarsungulum with a well-pigmented basal denticle." Additionally, we compared the size of the trochanteroprefemur tooth among the three species within *Nannarrup* and found that *N. innuptus* and *N. oyamensis* have a distal tooth on the trochanteroprefemur that is very similar in size to that of *A. striatus* but significantly larger than that of *N. hoffmani*.

Therefore, the only definite difference between these two genera is the cephalic plate of *Agnostrup*, which has a frontal line, while *Nannarrup* lacks one. However, all three *Nannarrup* species have a smaller body length (ca. 10 mm) compared with the four *Agnostrup* species (ca. 15–30 mm). The frontal line may be absent in small mecistocephalid species. Uliana et al. (2007) also described a small *Arrup* species, *A. lilliputianus* Uliana, Bonato & Minelli, 2007, with a body length of approximately 10 mm that lacks a frontal line. Considering the low genetic distances between *Nannarrup* and *Agnostrup* and the morphologically insignificant characters for delineating them as two distinct genera, we consider *Nannarrup* and *Agnostrup* to be the same genus. Accompanied by these changes, three species previously belonging to the *Nannarrup* genus are transferred to *Agnostrup* as *A. hoffmani* (Foddai, Bonato, Pereira & Minelli, 2003), comb. nov., *A. innuptus* (Tsukamoto, 2022), comb. nov., and *A. oyamensis* (Tsukamoto, 2022), comb. nov.

Agnostrup striatus (Takakuwa, 1949)

Figs 3, 4

Taiwanella striata Takakuwa 1949: 51–69, fig 1.
Taiwanella striata: Wang 1996: 81–99.
Agnostrup striatus: Foddai et al. 2003: 1255.

Material examined. ***Neotype*** (this paper formally assigns): 1 male (CMMI 20231104002D), China, Shanxi Province, Changzhi, Taihang Grand Canyon; 35.9450°N, 113.4520°E; 1280 m a.s.l.; 4 Nov. 2023; coll. Tianyun Chen, Jiabo Fan & Yuan Xiong.

***Non-type specimens*:** 1 female (CMMI 20231104001D), same data as neotype • 1 female (20240629001D), China, Shanxi Province, Ningwu County, Qingren Valley Scenic Area; 38.7980°N, 112.0365°E; 1798 m a.s.l.; 29 Jun. 2024; coll. Jiabo Fan & Yizhan Shi • 1 female (CMMI 20231101001D), China, Shanxi Province, Xinzhou, Mt. Luyashan; 38.9166°N, 112.1031°E; 1910 m a.s.l.; 1 Nov. 2023; coll. Tianyun Chen, Jiabo Fan & Yuan Xiong.

Diagnosis. An *Agnostrup* species with areolate part of the clypeus bearing a smooth insulae on each side. Telopodites of second maxillae with or without a rudimentary truncate claw. Forcipular article I with one large distal tooth, articles II without tooth, articles III with one acute tooth, tarsungulum with one large basal tooth.

Re-description. [The original holotype data from Takakuwa and Takashima (1949) is provided in parentheses]: Body length 20–33 mm (35 mm). Head and forcipule segment dark red in color, rest yellow.

Cephalic plate (Fig. 3A, B): Head 1.5–1.7 times as long as wide, lateral margins slightly convergent backward; frontal line slight protuberance, almost parallel; some setae and punctate depressions in the anterior of back side.

Antennae (Fig. 3C): with 14 articles, the distal end slightly attenuate. Setae are scattered on articles I to VII, while on the remaining articles, the setae are denser and more uniform in size.

Clypeus (Fig. 3D): Clypeal ratio about 1.2; areolate part with 5–8 (5–7) setae, an evident smooth insulae on each side, insulae bearing 2 (1) setae. clypeal plagulae with 3–4 (4–5) setae and an irregular anterior margin.

Labrum (Fig. 3D): anterior ala triangular, medial margin reduced to a vertex; posterior margin of each side-piece straight, not crenulate, and without hair-like projections.

Mandible (Fig. 3E): bearing 5 well-developed lamellae; average intermediate lamella with approximately 5 (7) teeth, all teeth of similar size.

First maxillae (Fig. 3F): coxosternite divided by mid-longitudinal, anterior corners of coxosternum not projecting; each medial projection about 1.2 times as long as wide, with 3 setae, the distal lobe clavate; telopodite about 2–2.1 times as long as wide, without seta, the distal lobe attenuated.

Second maxillae (Fig. 3F): coxosternite medially undivided, without suture; article I of the telopodite about 2.3–2.4 times as long as wide; article III about 2–2.7 times as long as wide, with several setae; telopodites tri-articulate overreaching medial projections; and telopodites of first maxillae. The pretarsus in the form of a rudimentary truncate claw.

Forcipular segment (Fig. 4A–C): The exposed part of the coxosternite is as long as it is wide. anterior margin with shallow medial concavity and with one pair of denticles. Forcipules: the length-to-width ratio of article I is

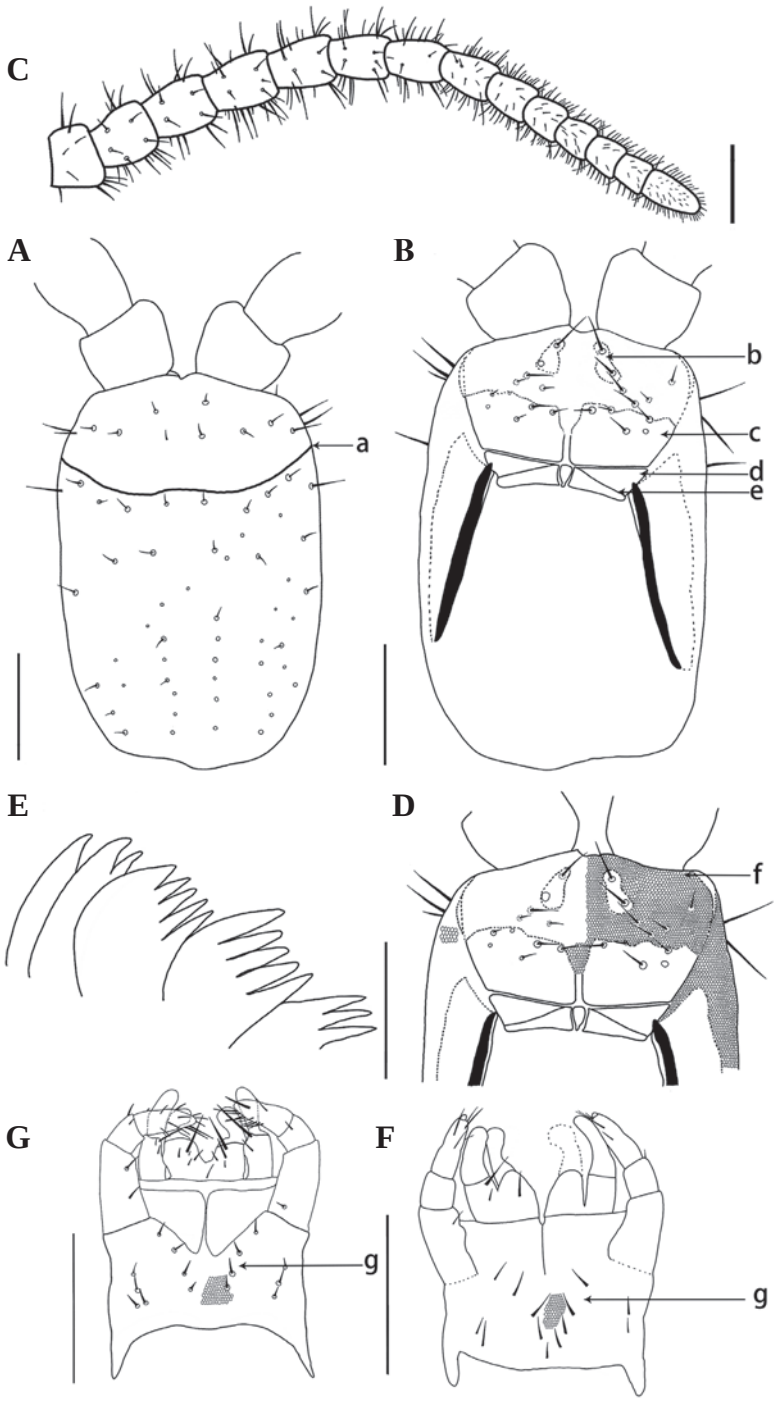

Figure 3. *Agnostrup striatus* (Takakuwa, 1949), (spm. CMMI 20231104002D). **A.** Cephalic plate, dorsal view; **B.** Clypeus, ventral view; **C.** Antenna, dorsal view; **D.** Cephalic plate, ventral view; **E.** Mandible; **F.** Maxillary complex, ventral view; **G.** Maxillary complex, ventral view (spm. CMMI 20231101001D). Arrowheads: a, frontal line; b, insulae; c, plagulae; d, posterior ala; e, transverse thickened line; f, clypeal areolate part; g, second maxillae coxosternite. Scale bar: 250 μm.

greater than one with a well-developed tooth; articles II without tooth; articles III with one acute tooth; tarsungulum with a long basal tooth. Poison calyx only reaching the distal part of forcipular article I.

Leg-bearing segments (Fig. 4D, E): 41 leg-bearing segments; represented by very shallow mid-longitudinal thickening, anterior not furcate; no ventral glandular pores on each metasternite; the first pair of legs much smaller than the rest and the distributed bristles.

Ultimate leg-bearing segment (Fig. 4F–I): sternum sub-triangular, as long as wide; about 15 pores on each coxopleuron. Ultimate legs with or without a small apical tubercle covered with small spines.

Postpedal segments (Fig. 4F–I): The female and male gonopods are both distinct and biarticulate, with a few setae.

Remarks. The type material of the species *Taiwanella striata* (Takakuwa, 1949) is not available and is probably lost (Foddai et al. 2003). Similarly, Takashima (1954,

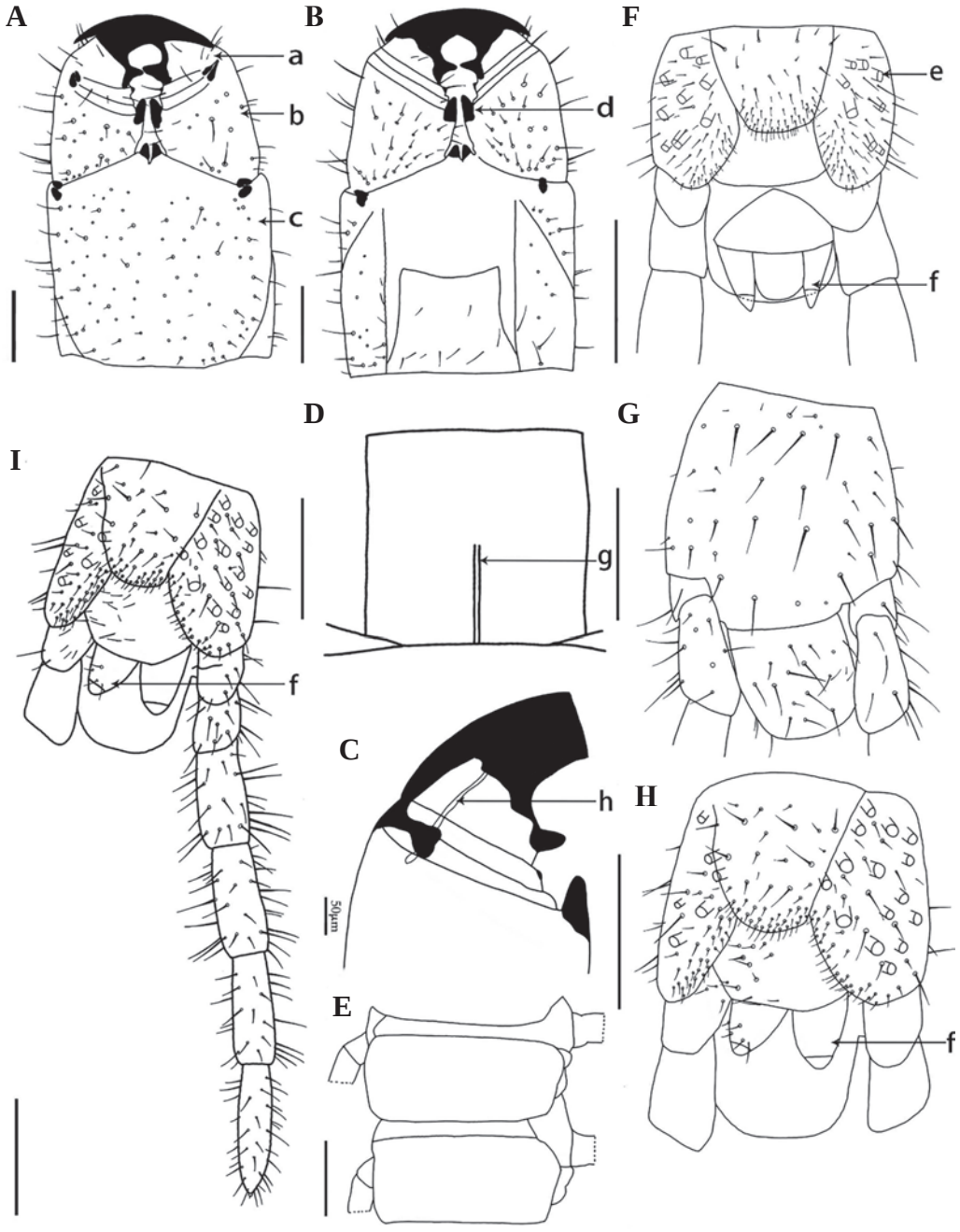

Figure 4. *Agnostrup striatus* (Takakuwa, 1949), (spm. CMMI 20231104002D). **A.** Forcipular segment, ventral view; **B.** Forcipular segment, dorsal view; **C.** A part of left forcipules, ventral view; **D.** Sternum of leg-bearing segment, ventral view; **E.** Tergite of leg-bearing segment, dorsal view; **F.** Ultimate leg-bearing segment, ventral view (spm. CMMI 20231104001D); **G.** Tergite of leg-bearing segment, dorsal view; **H.** Ultimate leg-bearing segment, ventral view; **I.** Ultimate leg-bearing segment and left leg, ventral view; **J.** Ultimate left leg. Arrowheads: a, forcipular tarsungulum; b, forcipular article I; c, forcipular coxosternite; d, tooth of forcipular article I; e, coxal pore; f, gonopod. Scale bar: 250 μm.

1955) conducted a survey of the centipede-type specimens existing in Japan and did not find the holotype of *T. striatus*, speculating that it may have been destroyed during World War II. The type locality of *T. striata* is an unknown locality (Japanese phonetic; it is pronounced near Cinkaiji) of Shanxi, China. We were unable to match it to any present geographical name but collected four fresh specimens morphologically matching this species from Shanxi. Therefore, we designate the specimen that most closely matches the original description as the neotype for this species.

Among these, three specimens had a noticeable rudimentary truncate claw on the telopodites of the second maxillae, while one specimen clearly lacked the claw. The claw of the second maxillae was clearly described by Takakuwa and Takashima (1949), but Foddai et al. (2003) and Uliana et al. (2007) believed that the genus *Agnostrup* lacks claws on the telopodites of the second maxillae. We conducted meticulous morphological examinations, genetic distance, and molecular phylogenetic analyses on these samples, confirming that they all belong to the same species. The differences in this characteristic are identified as minor morphological variations (Fig. 5).

The original description by Takakuwa and Takashima (1949) clearly indicates several smooth insulae on the clypeus, with the third segment of the forcipular article III lacking teeth. This is notably different from the specimens we found in Shanxi: the forcipular article III with one acute tooth in dorsal view, each side of the clypeus bears a smooth insulae, with two setae on each insulae.

Distribution. China (Shanxi).

Discussion

Species recognition based on morphological analysis and DNA barcoding

The genus *Arrup* is nested at the base of Mecistocephalidae in both ML and BI analyses (PP = 1), which is inconsistent with the findings of Bonato et al. (2003, Fig. 4). Bonato et al. (2003, Fig. 4) present an ML tree based on the number of leg-bearing segments, indicating that *Arrup*, *Agnostrup*, and *Nannarrup* belong to the same clade, the subfamily Arrupinae. Meanwhile, the results for *Proterotaiwanella*, which in our trees forms a clade with *Tygarrup* and *Mecistocephalus* (PP = 1; BS = 85%), were also inconsistent with previous morphological findings.

There are too many shared morphological characteristics between *Agnostrup* and *Nannarrup*, and the few differences, including the number of setae on the clypeal plagulae and the size of the forcipular tarsungulum, are too subtle. Compared to other genera in the family Mecistocephalidae, these characters are not significant enough to delineate them as two distinct genera. Additionally, the genetic distance between *Agnostrup* and *Nannarrup* is smaller than the distances between *Agnostrup* and other genera, indicating that they could also be considered the same genera genetically.

In addition to the genera *Nannarrup*, *Agnostrup*, and *Arrup*, *Partygarrupius moiwaensis* (Takakuwa, 1934) also belongs to the Arrupinae Chamberlin, 1912, and is an endemic species of Hokkaido Island, Japan. It has 41 pairs of legs, buccae without setae, and no spiculum. The coxosternum of the first maxillae is divided, while that of the second maxillae is undivided. The forcipular trochanteropraemur has only a distal tooth, and the tarsungulum has only one pointed tooth. The forcipular tergum lacks a median sulcus, and the sternal rhachides are not anteriorly furcate. Based on these similar morphological characteristics, we hypothesize that *Partygarrupius moiwaensis* (Takakuwa, 1934) may form a sister group with *Nannarrup* and *Agnostrup* in the phylogenetic tree. However, unlike *Nannarrup* and *Agnostrup*, it possesses an entire clypeal plagula, without a mid-longitudinal areolate stripe and extending along the lateral margins of the clypeus. This feature is similar to that of *Tygarrup*.

Based on morphological analysis and DNA barcoding, the genus *Agnostrup* now comprises six species. Detailed comparisons of species' morphological characteristics can be found in Table 4.

Distribution of the genus *Agnostrup*

Most species of Arrupinae are confined to specific geographic locations, but the genus *Agnostrup*, with its broad distribution from Shanxi Province and northeastern China to Japan and New York, USA, exhibits a clear dispersal pattern. Specimens of *Agnostrup* spp., which can be as small as 1 cm, are easily transported during the movement of plants (Foddai et al. 2003). The presence of *A. hoffmani* in New York City is confirmed to be a result of human introduction. Another example of human-mediated introduction is *Tygarrup intermedius* Chamberlin, 1914, the type species of *Tygarrup*, originally described from British Guyana but actually taken in Washington in pots of plants imported from British Guyana (Chamberlin, 1914). Similarly, *Tygarrup javanicus* Attems, 1929, a centipede native to Southeast Asia and widely distributed in the Indochinese Peninsula, Java, and other regions, has been found in the Seychelles and Mauritius islands. In recent years, *Tygarrup javanicus* has been recorded in the Hawaiian Islands, suggesting its spread through human activity. This introduction is not unprecedented, as similar cases have been reported in Kew Gardens, London, and Vienna, Austria (Bonato et al. 2004).

The *Agnostrup* genus, distributed in Japan, Shanxi Province in China, and the Sikhote-Alin mountains in Russia, may indicate its adaptation to temperate and subarctic climates. Although these regions are geographically dispersed, they share similar climate zones and ecological environments, particularly forested mountainous

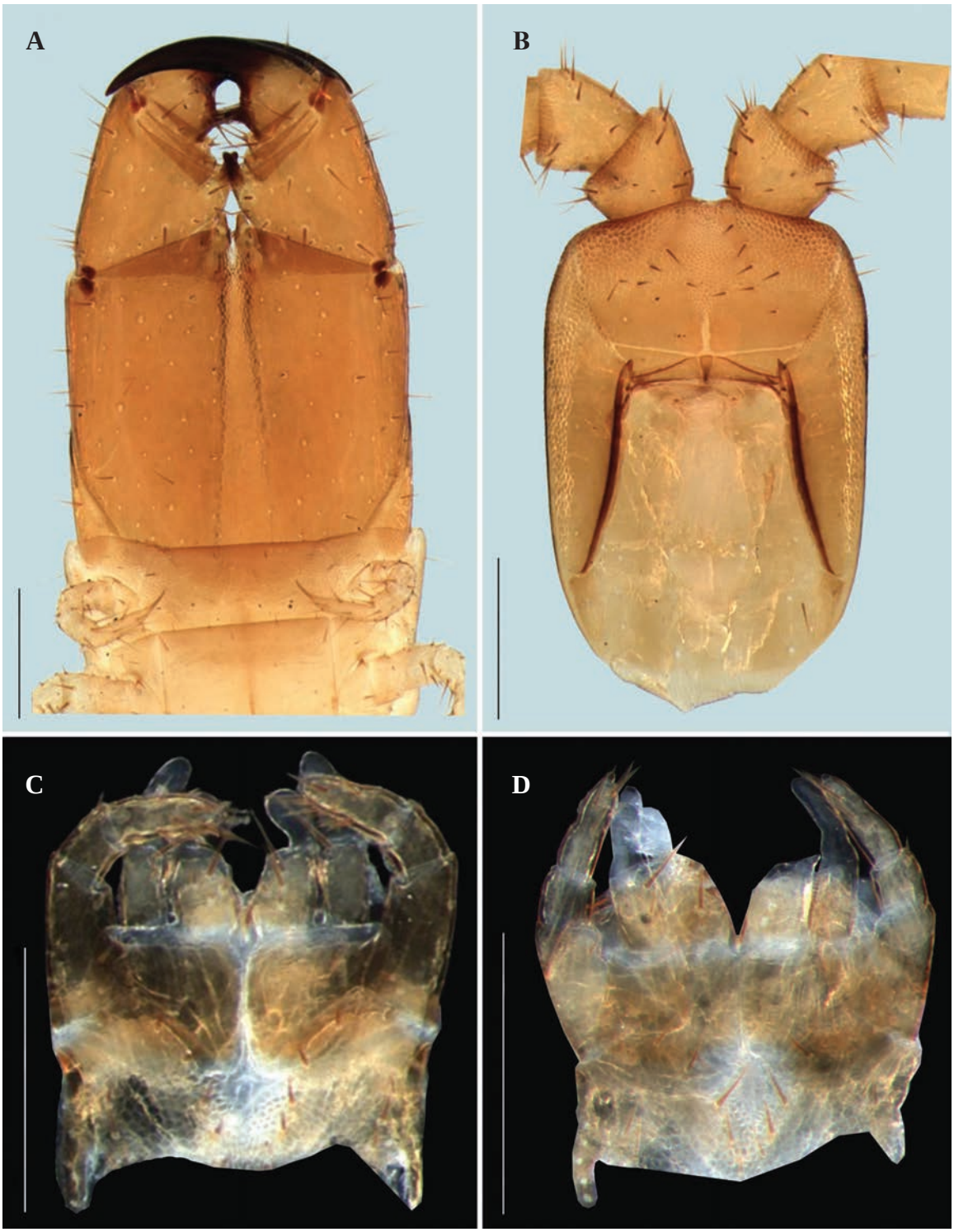

Figure 5. *Agnostrup striatus* (Takakuwa, 1949). **A.** Forcipular segment, ventral view (spm. CMMI 20231104001D); **B.** Clypeus, ventral view (spm. CMMI 20231104001D); **C.** Maxillary complex, ventral view (spm. CMMI 20231101001D); **D.** Maxillary complex, ventral view (spm. CMMI 20231104002D). Scale bar: 250 μm.

terrain. This similarity likely provides stable habitat for the genus, enabling it to survive and thrive in these areas. The distribution of the *Agnostrup* genus extends from Shanxi Province and northeastern China to Japan, further demonstrating its notable geographic dispersal pattern. This wide distribution may be driven by several factors. The climate and ecological environments of Shanxi Province and northeastern China are somewhat similar to those of Japan, particularly within temperate forest ecosystems, which may offer suitable habitats for the natural dispersal of *Agnostrup*. Additionally, the geographic proximity between Japan and northeastern China may facilitate the dispersal of the genus through natural pathways such as wind, river basins, or cross-ocean biological dispersal.

Key to the species of *Agnostrup*

1 With evident smooth insulae on the clypeus 2
– Without evident smooth insulae on the clypeus 3
2 Two large clypeal plagulae covering approximately one-half of the clypeus ..... *A. striatus* (Takakuwa, 1949)
– Two small clypeal plagulae covering approximately one-sixth of the clypeus ..... *A. innuptus* (Tsukamoto, 2022)
3 Clypeal plagulae with additional smooth or weak areolation area along posterior part of paraclypeal sutures ..... *A. hoffmani* (Foddai, Bonato, Pereira & Minelli, 2003)
– Clypeal plagulae without additional smooth or weak areolation area along posterior part of paraclypeal sutures 4
4 Telopodites of second maxillae with a short spine ..... *A. oyamensis* (Tsukamoto, 2022)
– Telopodites of second maxillae without a short spine 5
5 Forcipular articles II and III with a tubercle ..... *A. striganovae* (Titova, 1975)
– Forcipular articles II and III without a tubercle ..... *A. paucipes* (Miyosi, 1955)

Acknowledgements

We sincerely thank Dr. Alessandro Minelli, Dr. Ivan H. Tuf, and Dr. Martin Husemann for their constructive comments and valuable suggestions on the manuscript, which have significantly contributed to improving its quality. We would like to thank Dr. Sho Tsukamoto for providing us with information about the type specimen of *Arrup pauroporus* (Takakuwa, 1936).

This research was supported by the National Natural Science Foundation of China (nos. 82073972 and 82204572), the key project at the central government level: The ability establishment of sustainable use for valuable Chinese medicine resources (nos. 2060302), and the CACMS Innovation Fund (CI2023E002).

References

Bonato L, Foddai D., Minelli A (2002) A new mecistocephalid centipede from Ryukyu Islands and a revisitation of *Taiwanella* (Chilopoda: Geophilomorpha: Mecistocephalidae). Zootaxa 86(1): 1–12. https://doi.org/10.11646/zootaxa.86.1.1

Bonato L, Foddai D, Minelli A (2003) Evolutionary trends and patterns in centipede segment number based on a cladistic analysis of Mecistocephalidae (Chilopoda: Geophilomorpha). Systematic Entomology 28(4): 539–579. https://doi.org/10.1046/j.1365-3113.2003.00217.x

Bonato L, Foddai D, Minelli A, Shelley R (2004) The centipede order Geophilomorpha in the Hawaiian islands (Chilopoda). *Bishop Museum Occasional Papers* 78: 13–32. http://hbs.bishopmuseum.org/fiji/pdf/bonato-etal2004.pdf

Bonato L, Danyi L, Minelli A (2010) Morphology and phylogeny of *Dicellophilus*, a centipede genus with a highly disjunct distribution (Chilopoda: Mecistocephalidae). Zoological Journal of the Linnean Society 158(3): 501–532. https://doi.org/10.1111/j.1096-3642.2009.00557.x

Bonato L, Edgecombe GD, M Zapparoli, Minelli A (2011) Chilopoda – Taxonomic overview: Geophilomorpha. Treatise on Zoology – Anatomy, Taxonomy, Biology. The Myriapoda Volume 1: 407–443. https://doi.org/10.1163/9789004188266_002

Bonato L, Drago L, Murienne J (2014) Phylogeny of Geophilomorpha (Chilopoda) inferred from new morphological and molecular evidence. Cladistics 30: 485–507. https://doi.org/10.1111/cla.12060

Boyer SL, Giribet G (2007) A new model Gondwanan taxon: Systematics and biogeography of the harvestman family Pettalidae (Arachnida, Opiliones, Cyphophthalmi), with a taxonomic revision of genera from Australia and New Zealand. Cladistics 23(4): 337–361. https://doi.org/10.1111/j.1096-0031.2007.00149.x

Chamberlin RV (1914) The Stanford Expedition to Brazil, 1911. John C. Branner, Director. The Chilopoda of Brazil. Bulletin of the Museum of Comparative Zoology at Harvard College 58: 151–221.

Chao JL, Lee KS, Yang ZZ, Chang HW (2020) Two new species of centipedes, *Tygarrup daliensis* sp. nov. (Mecistocephalidae) and *Australobius cangshanensis* sp. nov. (Lithobiidae), from Southwestern China. Opuscula Zoologica (Budapest) 51(S2): 57–67. https://doi.org/10.18348/opzool.2020.S2.57

Edgecombe GD, Giribet G (2004) Adding mitochondrial sequence data (16S rRNA and cytochrome c oxidase subunit I) to the phylogeny of centipedes (Myriapoda: Chilopoda): an analysis of morphology and four molecular loci. Journal of Zoological Systematics and Evolutionary Research 42(2): 89–134. https://doi.org/10.1111/j.1439-0469.2004.00245.x

Edgecombe GD, Giribet G (2006) A century later – a total evidence re-evaluation of the phylogeny of scutigeromorph centipedes (Myriapoda, Chilopoda). Invertebrate Systematics 20(5): 503–525. https://doi.org/10.1071/IS05044

Foddai, D, Bonato L, Pereira LA, Minelli A (2003) Phylogeny and systematics of the Arrupinae (Chilopoda Geophilomorpha Mecistocephalidae) with the description of a new dwarfed species. Journal of Natural History 37(10): 1247–1267. https://doi.org/10.1080/00222930210121672

Folmer O, Black M, Hoeh W, Lutz R, Vrijenhoek R (1994) DNA primers for amplification of mitochondrial cytochrome C oxidase subunit I from diverse metazoan invertebrates. Molecular Marine Biology and Biotechnology 3(5): 294–299. https://www.mbari.org/wp-content/uploads/2016/01/Folmer_94MMBB.pdf

Hoang DT, Chernomor O, Von Haeseler A, Minh BQ, Vinh LS (2018) UFBoot2: Improving the ultrafast bootstrap approximation. Molecular Biology and Evolution 35(2): 518–522. https://doi.org/10.1093/molbev/msx281

Joshi J, Karanth KP (2011) Cretaceous–Tertiary diversification among select scolopendrid centipedes of South India. Molecular Phylogenetics and Evolution 60(3): 287–294. https://doi.org/10.1016/j.ympev.2011.04.024

Kumar S, Stecher G, Li M, Knyaz C, Tamura K (2018) MEGA X: Molecular evolutionary genetics analysis across computing platforms. Molecular Biology and Evolution 35(6): 1547–1549. https://doi.org/10.1093/molbev/msy096

Murienne J, Edgecombe GD, Giribet G (2010) Including secondary structure, fossils and molecular dating in the centipede tree of life. Molecular Phylogenetics and Evolution 57(1): 301–313. https://doi.org/10.1016/j.ympev.2010.06.022

Nguyen LT, Schmidt HA, Von HA, Minh BQ (2015) IQ-TREE: a fast and effective stochastic algorithm for estimating maximum-likelihood phylogenies. Molecular Biology and Evolution 32(1): 268–274. https://doi.org/10.1093/molbev/msu300

Pan YY, Fan JB, Jiang C, You CX (2024) Identification of two new species of *Mecistocephalus* (Chilopoda, Geophilomorpha, Mecistocephalidae) from southern China and the re-description of *Mecistocephalus smithii* Pocock, 1895: Morphological and phylogenetic analyses.[J] ZooKeys [Accepted].

Peretti E, Cecchin C, Fusco G, Gregnanin L, Kos I, Bonato L (2022) Shedding light on species boundaries in small endogeic animals through an integrative approach: species delimitation in the centipede *Clinopodes carinthiacus* (Chilopoda: Geophilidae) in the south-eastern Alps. Zoological Journal of the Linnean Society 196(2): 902–923. https://doi.org/10.1093/zoolinnean/zlac008

Ronquist F, Teslenko M, Mark P, Ayres DL, Darling A, Höhna S, Larget L, Suchard MA, Huelsenbeck JP (2012) MrBayes 3.2: Efficient Bayesian phylogenetic inference and model choice across a large model space. Systematic Biology 61(3): 539–542. https://doi.org/10.1093/sysbio/sys029

Takakuwa Y, Takashima H (1949) Myriapods collected in Shansi, North China. Acta Arachnologica 11(3–4): 51–69. https://doi.org/10.2476/asjaa.11.51

Takashima H (1954) List of the myriapod type specimens existing in Japan (I). Acta Arachnologica 13: 128–131. https://doi.org/10.2476/asjaa.13.128 [In Japanese]

Takashima H (1955) List of the myriapod type specimens existing in Japan (II). Circular of the Japanese Society of Systematic Zoology 9: 128–131. [In Japanese]

Titova LP (1975) Geophilids of the family Mecistocephalidae (Chilopoda) in the fauna of the USSR. Zoologicheskii Zhurnal 54(1): 39–48.

Tsukamoto S, Shimano S, Eguchi K (2022) Two new species of the dwarf centipede genus *Nannarrup* Foddai, Bonato, Pereira & Minelli, 2003 (Chilopoda, Geophilomorpha, Mecistocephalidae) from Japan. ZooKeys 1115: 117–150. https://doi.org/10.3897/zookeys.1115.83946

Uliana M, Bonato L, Minelli A (2007) The Mecistocephalidae of the Japanese and Taiwanese islands (Chilopoda: Geophilomorpha). Zootaxa 1396(1): 1–84. https://doi.org/10.11646/zootaxa.1396.1.1

Wang D (1996) Review and perspective of study on myriapodology of China. Acta Myriapodologica 169: 81–99. https://archive.org/details/biostor-252468

Zoosyst. Evol. 100 (4) 2024, 1569–1584 | DOI 10.3897/zse.100.133632

PENSOFT

für Natur MUSEUM FÜR NATURKUNDE BERLIN

The southernmost record for a symphylan: *Hanseniella guerreroi* sp. nov. (Myriapoda, Scutigerellidae), an inhabitant of the Tierra del Fuego archipelago

Andrés O. Porta[1,2,3], Antonio Parra-Gómez[4], Dante Poy[1], Gaston Kreps[5,6], Roy Mackenzie[7,8], Guillermo Martínez Pastur[9], Leonardo D. Fernández[10]

1 *División Aracnología, Museo Argentino de Ciencias Naturales "Bernardino Rivadavia" – CONICET, Av. Ángel Gallardo 470 C1405DJR, Buenos Aires, Argentina*
2 *Departamento de Biodiversidad y Biología Experimental, Facultad de Ciencias Exactas y Naturales, Universidad de Buenos Aires, Ciudad Autónoma de, Buenos Aires, Argentina*
3 *Departamento de Ciencias Exactas, Universidad Nacional del Oeste, Belgrano 369 C1718, San Antonio de Padua, Buenos Aires, Argentina*
4 *Facultad de Ciencias, Universidad Austral de Chile, Av. Rector Eduardo Morales Miranda 23, Valdivia, Chile*
5 *Departamento de Ciencias de la Atmósfera y de los Océanos, Facultad de Ciencias Exactas y Naturales, Universidad de Buenos Aires, Buenos Aires, Argentina*
6 *Alfred-Wegener-Institut Helmholtz-Zentrum für Meeres - und Polarforschung, Bremerhaven, Germany*
7 *Centro Universitario Cabo de Hornos, Universidad de Magallanes, Puerto Williams Cape Horn International Center CHIC, Puerto Williams 6350000, Chile*
8 *Millennium Institute Biodiversity of Antarctic and Subantarctic Ecosystems (BASE), Las Palmeras, 3425, Santiago 7800003, Chile*
9 *Centro Austral de Investigaciones Científicas (CADIC) – CONICET, Houssay 200, 9410, Ushuaia, Tierra del Fuego, Argentina*
10 *Núcleo de Investigación en Sustentabilidad Agroambiental (NISUA), Facultad de Medicina Veterinaria y Agronomía, Universidad de Las Américas, Manuel Montt 948, Providencia, Santiago, Chile*

https://zoobank.org/669C7F58-9475-4F49-85E8-1B1715135246

Corresponding author: Leonardo D. Fernández (limnoleo@gmail.com)

Academic editor: Martin Husemann ♦ **Received** 1 August 2024 ♦ **Accepted** 15 October 2024 ♦ **Published** 14 November 2024

Abstract

A new species of Symphyla, *Hanseniella guerreroi* **sp. nov.**, is described from specimens collected during expeditions to the Tierra del Fuego archipelago, including Isla Grande de Tierra del Fuego and Isla de los Estados in Argentina, as well as Isla Navarino in Chile. To the best of our knowledge, this new species represents the southernmost record for a myriapod of the class Symphyla. The morphological affinities of this species with other *Hanseniella* species from Gondwanan landmasses are discussed, highlighting its potential for studying the impact of the last Quaternary glaciation on soil arthropods in the far south of the continent. This discovery provides important insights into the biogeographic and evolutionary history of soil arthropods in these remote and climatically challenging regions. *H. guerreroi* **sp. nov.** is an exemplary species adapted to the harsh environmental conditions of subantarctic ecosystems and contributes significantly to our understanding of biodiversity and ecological dynamics in such challenging habitats.

Key Words

Dientes de Navarino, garden centipede, Myriapoda, Navarino Island, *Nothofagus* forests, soil-dwelling arthropod, symphylans, Patagonia, Tierra del Fuego

Introduction

Symphylans, or garden centipedes, are small, soil-dwelling arthropods that belong to the subphylum Myriapoda and the class Symphyla (Minelli and Golovatch 2001). There are only two families within this class: Scutigerellidae and Scolopendrellidae (Jin et al. 2023). These myriapods inhabit organic soils on all continents except Antarctica (Szucsich and Scheller 2011). They have slender and fragile bodies, 5–8 mm long, which allows them to easily move through soil pores where they feed on detritus (Minelli and Golovatch 2001). Some species, particularly within the genera *Scutigerella* and *Hanseniella*, can become agricultural pests by feeding on seeds and plant roots, causing significant damage to crops (Boyle 1981; Murray and Smith 1983).

Argentina and Chile, two neighboring countries in southern South America, are known for their outstanding biodiversity and high rates of endemism of plants, animals, and microbes (Villagrán and Hinojosa 1997; Lamoreux and Lacher 2010; Fernández et al. 2015; Schiaffino et al. 2016; Campello-Nunes et al. 2022; Pérez-Schultheiss et al. 2024). Despite their remarkable diverse ecosystems, these countries have surprisingly low symphylan diversity. In Argentina, only 10 species have been recorded, three of which belong to the family Scutigerellidae and the genus *Hanseniella*, i.e., *Hanseniella angulosa*, *H. chilensis*, and *H. unguiculata* (Scheller 1992). In contrast, only one species, *H. chilensis*, has been recorded in Chile (Vega-Román et al. 2012; Parra-Gómez et al. 2024).

The symphylan diversity of Argentina and Chile is probably much higher than currently known but remains underestimated because no major sampling effort has ever been made to study them. Argentina and Chile have historically lacked Symphyla specialists (Attems 1897; Scheller 1992; Parra-Gómez et al. 2024). Furthermore, the diversity of these and other myriapods has been poorly studied in most of their territories, including remote areas such as the Tierra del Fuego archipelago in the southernmost tip of South America (Minelli and Golovatch 2001; Parra-Gómez and Fernández 2022).

The first records of symphylans in Argentina and Chile were documented by Attems in 1897. Attems (1902) reported the presence of *S. immaculata* in the Argentinean localities of Lapataia and Ushuaia on Isla Grande de Tierra del Fuego, which is divided between Argentina and Chile. He also extended his report to Navarino Island, one of the southernmost Chilean islands of the Tierra del Fuego archipelago. However, Scheller (1998) later questioned Attems' identification, arguing that *S. immaculata* is native to the northern hemisphere. Scheller contended that it is highly unlikely that this species would have established stable populations on these islands given their challenging climatic conditions. This issue, along with the remote origin of the specimens, has led to the suggestion that the symphylans identified by Attems may have belonged to another, perhaps undescribed, species adapted to thrive on the climatically harsh islands of the Tierra del Fuego archipelago (Scheller 1992; Parra-Gómez et al. 2024).

More than a century after Attems' pioneering study, we undertook field expeditions to investigate the arthropod biodiversity of the Tierra del Fuego archipelago. On this archipelago we found a new symphylan species of the genus *Hanseniella* that may correspond to the taxon originally observed by Attems in 1897. To our knowledge, this new species represents the southernmost record for a myriapod of the class Symphyla. Here we describe this species and discuss the similarities between this new species found in the remote, southern islands of Argentina and Chile and other species of the genus *Hanseniella*. We also highlight its significance for studying the effects of the Last Glacial Maximum on the soil mesofauna of extreme southern South America.

Materials and methods

The specimens were collected on Argentinean and Chilean islands of the Tierra del Fuego archipelago (for details see subsection Type material) during three field expeditions conducted by the Museo Argentino de Ciencias Naturales "Bernardino Rivadivia" (**MACN**), the Centro Austral de Investigaciones Científicas (**CADIC**), Argentina and the Universidad de Las Américas (**UDLA**), Chile.

Specimens from the Argentine expeditions were cleared with lactic acid for observation in an open chamber or mounted on slides with Hoyer's medium and examined and measured using an Olympus CH-2 or Wild Heerbrugg M11 compound microscope with phase contrast. For scanning electron microscopy (SEM), specimens were dehydrated through a series of ethanol solutions of increasing concentration in absolute hexamethyldisilazane (Porta and Tricarico 2018) and then air dried, mounted on individual stubs using copper adhesive tape, sputter-coated with gold-palladium, and examined using an FEI XL 30 TMP scanning electron microscope with varying working distance and voltage (15–22 kV).

Specimens collected from Isla Navarino, Chile, were mounted on concave glycerol-filled slides and examined using an N-200M microscope. Two specimens were mounted on copper adhesive tape and dehydrated using a Hitachi HCP-2 critical point dryer. They were then coated with gold and palladium on a Leica EM ACE200 and imaged with a Zeiss EVO M10 SEM at 20 kV. All specimens from both countries are preserved in 80% ethanol.

Descriptions and terminology follow Scheller's descriptions (e.g., Scheller 1961, 1971, 2002, 2007); for some structures, terminology follows Snodgrass (1952) and Domínguez Camacho (2009). Measurements and ratios given here are those of the holotype, followed by the range of other specimens in the type series in parentheses (e.g., 2.1 (2–2.3) vs. (2–) 2.1 (–2.3) in Scheller's notation). The material examined for this study is deposited in the following collections: the Myriapodological Collection of the Museo Argentino de Ciencias Naturales "Bernardino Rivadavia", Buenos Aires (**MACN-My**), the Invertebrate Collection of the Museo Nacional de la Plata (**MLP-Ar**), the Arthropod Collection of the

Centro Austral de Investigaciones Científicas (**CADIC**), Argentina, and the Museo Nacional de Historia Natural (**MNHNC**), Santiago, Chile.

Taxonomy

Scutigelleridae Bagnall, 1913
Hanseniella Bagnall, 1913

Hanseniella guerreroi Porta, Parra-Gómez & Fernández, sp. nov.

https://zoobank.org/2C92A070-37E8-4017-B9F5-530BD35544B3

Figs 2–10

Type material. ***Holotype***, male (MACN-My 69), from Argentina: Provincia de Tierra del Fuego, Antártida e Islas del Atlántico Sur: Tierra del Fuego, Departamento de Ushuaia, Río Irigoyen, 54.62540; -066.70184 (+/-200 m), elev. 230 m, 20–24 Oct. Berlese funnel and hand collected, A. Porta leg., cleared, preserved in ethanol; • same data, 6 paratypes, 4 males and 2 females (MACN-My 70 to 75), cleared, preserved in ethanol; • 10 paratypes, 7 males and 3 females (MACN-My 76 to 85), cleared, preserved in ethanol; • 1 tube with 4 paratypes (MLP-Ar 20497), not cleared, preserved in ethanol; • 1 tube with 4 paratypes (CADIC-My 01), not cleared, preserved in ethanol; • same data, 3 paratypes (MACN-My 86 to 88), mounted for SEM; • Argentina: Provincia de Tierra del Fuego, Antártida e Islas del Atlántico Sur: Isla Grande de Tierra del Fuego, Departamento de Ushuaia, El Martial, 54.790648, -068.391642 (+/- 100 m); elev. 550 MASL. (+/- 50 m); Berlese funnels, A. Porta leg; • 1 paratype, male (MACN-My 89), mounted on slide; • same data, 1 tube with 2 paratypes (MACN-My 90), cleared, preserved in ethanol; Argentina: Provincia de Tierra del Fuego, Antártida e Islas del Atlántico Sur: Isla Grande de Tierra del Fuego: Departamento de Ushuaia: Bahía Buen Suceso, 54.79349, -065.26397; (+/- 20 m); elev. 12 MASL.; Berlese funnels and hand collecting; A. Porta leg., • 1 paratype male (MACN-My 91), cleared, preserved in ethanol; • same data, 1 paratype (MACN-My 96), mounted for SEM; Argentina: Provincia de Tierra del Fuego, Antártida e Islas del Atlántico Sur: Departamento de Ushuaia: Isla de los Estados: Puerto Hoppner; 54.78344, -064.41387 (+/- 200 m); elev. 20 MASL; Berlese funnels and hand collecting, A. Porta leg., • 3 paratypes, 1 male and 2 females (MACN-My 97 to 99), cleared, preserved in ethanol; same data; • same data, 2 paratypes (MACN-My 100 to 101), mounted for SEM; Provincia de Tierra del Fuego, Antártida e Islas del Atlántico Sur: Departamento de Ushuaia: Isla de los Estados: Puerto Parry; 54.81319, -064.37043 (+/- 50 m); elev. 70 MASL; Berlese funnels and hand collecting, A. Porta leg., • 3 paratypes, 2 females and 1 male (MACN-My 104 to 106), mounted; • 3 paratypes, 2 females and 1 male (MACN-My 107 to 109), cleared, preserved in ethanol; • 5 paratypes in 1 vial (MACN-My 110), not cleared, preserved in ethanol; Argentina: Provincia de Tierra del Fuego, Antártida e Islas del Atlántico Sur: Departamento de Ushuaia: Isla de los Estados: Puerto Cook, 54.77711, -064.05438 (+/- 30 m); elev. 40 MASL. (+/-20 m); Berlese funnels and hand collecting, A. Porta leg., • 1 paratype (MACN-My 111), not cleared, preserved in ethanol; Argentina: Provincia de Tierra del Fuego, Antártida e Islas del Atlántico Sur: Departamento de Ushuaia: Isla de los Estados: Puerto de San Juan de Salvamento, 54.753367, -63.889186 (+/- 50 m); elev. 15 MASL; • 2 paratypes, 2 males (MACN-My 112 to 113), cleared, preserved in ethanol; • 4 paratypes in 1 vial (MACN-My 114), not cleared, preserved in ethanol. Chile: Región de Magallanes y de la Antártica Chilena, Provincia de la Antártica Chilena, Isla Navarino, -54.9917, -67.6022, 23 March 2023; hand collecting, under the bark of a dead *Nothofagus pumilio* tree trunk, L. Fernández leg.,• 3 paratypes, 2 females (MNHNC8446 to 8447), mounted for SEM; • 1 paratype, 1 female (MNHNC8448), preserved in ethanol.

Etymology. The specific name is a patronymic in honor of Federico Guerrero, captain of the boat "Ocean Tramp," in recognition of her fundamental contribution to the organization, logistics, and success of the MACN-CADIC 2014 expedition to Península Mitre and Isla de los Estados.

Diagnosis. *H. audax* Clark & Greenslade, 1996 differs from *H. guerreroi* sp. nov. by a greater length (8.7 mm), longer setae on the tergites, both claws of 12 pairs of similar size, and by the morphology of the cerci; *H. conveniens* Clark & Greenslade, 1996 differs by the chaetotaxy and morphology of the cerci; *H. insequens* Clark & Greenslade, 1996 differs by the dorsum of the head with fine pubescence; *H. madecassa* Aubry & Masson, 1953 differs by the chaetotaxy of the first tergite and the apical antennomere with only 2 spined organs; *H. mutila*, Adam & Burtel, 1956 differs by the central rod of the head well-marked behind the ovoid knob, where it is produced forward into 2 lateral branches, claws of leg 12 being of similar size, and by the distribution of the outgrowths (microsetae) in the tergites; *H. nivea* (Scopoli, 1763) differs by the shape of the central rod of the head, the chaetotaxy of the first tergite, and by the relative size of the claws of the 12th leg pair; *H. pluvialis* Clark & Greenslade, 1996 differs by the claws of leg 12 of similar size and the tergal setae being more elongated and of different size; *H. proxima* Adam & Burtel, 1956 differs by the central rod of the head well marked behind the ovoid knob, where it is produced forward into 2 lateral branches and 2 branches delimiting an indistinct posterior area, leg 12 with an elongated anterior seta, and by the first tergite with 2+2 setae; *H. pyrethrata* Clark & Greenslade, 1996, by the cuticle on the posterior part of tergites glabrous and the apical antennomere with only one terminal spined organ; *H. vulgata* Adam & Burtel, 1956 differs by the central rod of the head well-marked before the ovoid knob and behind this where it is produced into 2 branches which delimit a posterior area, the presence of additional setae on the styli (particularly in leg 12), and by the different chaetotaxy on the cerci.

Description. Length of body (Fig. 1) without antennae and cerci 3.4 (3.1–5.4) mm.

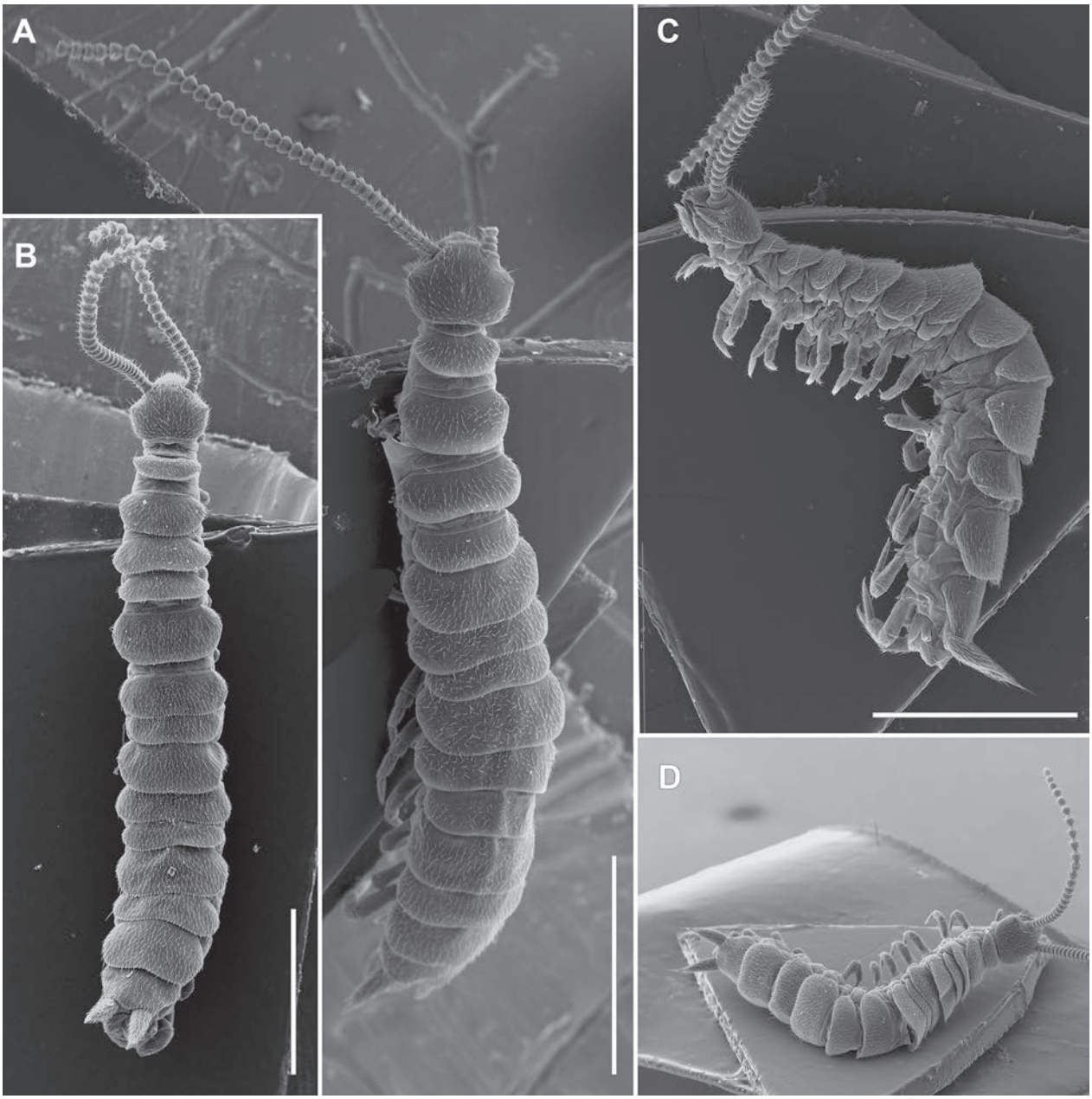

Figure 1. A. *Hanseniella guerreroi* sp. nov., habitus dorsal, paratype (MACN-My 86); **B.** Paratype (MACN-My 96); **C.** Paratype (MACN-My 97), lateral view; **D.** Same, dorsolateral view. Scale bars: 1000 μm (**A–C**).

Head (Fig. 2). Head short, 1.38 (1.05–1.44) broader than long, frontal margin convex with a prominent lateral angle at point of articulation of mandible (Fig. 2A), posterior margin concave with rounded posterolateral angles. Central rod posteriorly ovoid (Fig. 2A, *cr*), 0.24 (0.19–0.36) the length of the head, other parts of the rod and its branches lacking. Dorsal surface of head (Fig. 2A–C) covered with straight, very thin setae of lengths not significantly different. 3+3 distinct large setae near the antennal base. Longest seta of lateral head angles 0.9 (0.8–0.9) of the length of the diameter of the first antennomere and 3.5× longer than shortest setae. Each anterior plate (*m*) of the second maxillae (Fig. 2D) with 3 proximal setae, external side almost straight. External-distal corner of these plates with 5 sets of sensilla with a typical chandelier shape (Fig. 2D, arrow) decreasing in size proximally in addition to 2 elongated setae inserted on conic protuberances, the most posterodistal one with a contiguous small tooth; second-maxillary proximal arms (*pa*) not much wider than anterior plate. Each of the three terminal protuberances (*tp*) (Domínguez Camacho 2009) distal to transversal groove of the second maxilla (*tg*) with a characteristic set composed of 2–4 setae inserted on cylindrical cuticular protuberances plus 1 large distal sensillum, which is contiguous to a small tooth. First maxillary palp (Fig. 2D; *ml* and *p*, 2F) large, conical, and pointed. Head cuticle glabrous (Fig. 2B). Tömösvary organ circular (Fig. 2E, *To*) 30–44 μm wide. Both maxillae bearing several setae on surface.

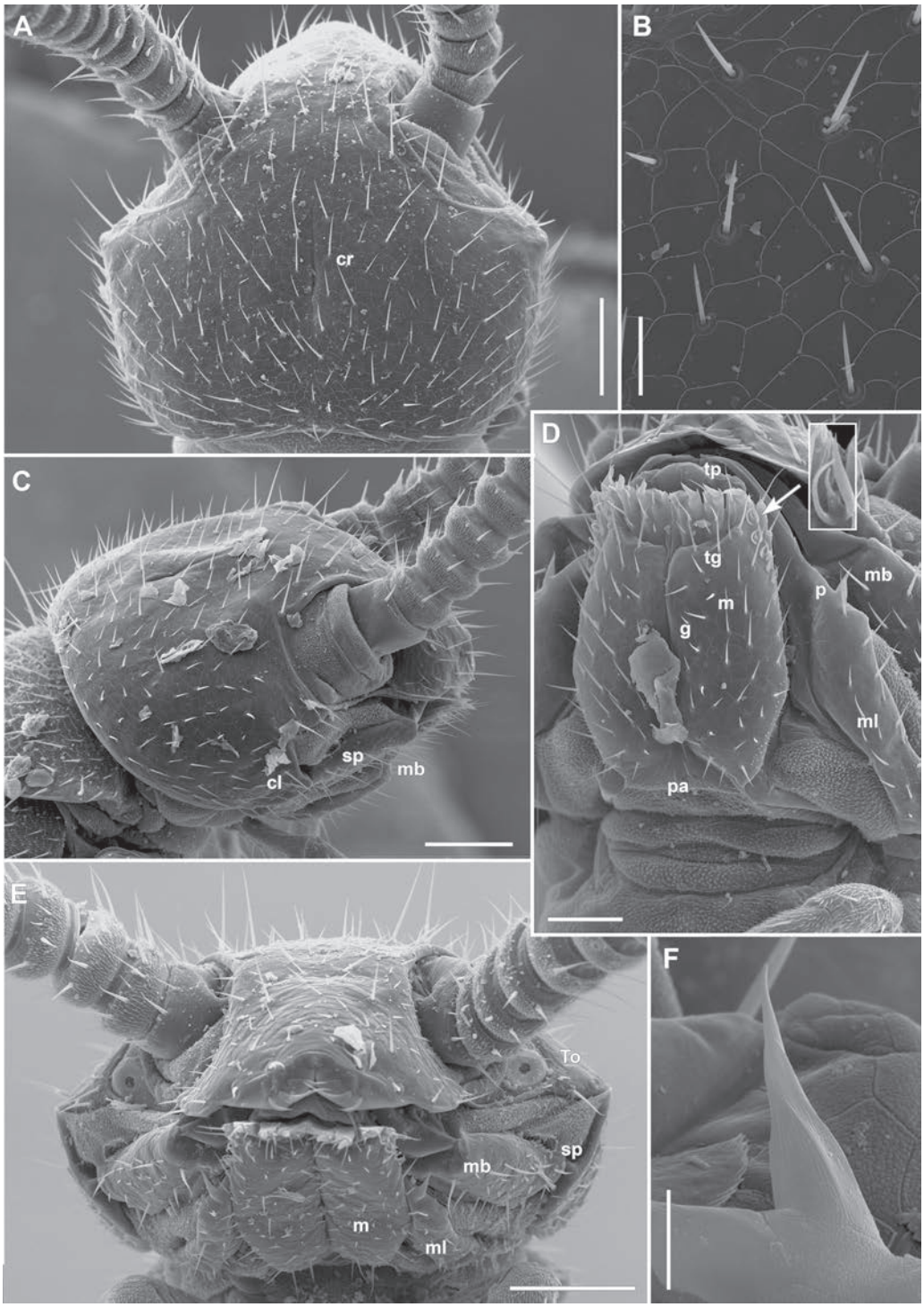

Figure 2. *Hanseniella guerreroi* sp. nov. **A.** Paratype (MACN-My 86), head, dorsal view; **B.** Head dorsal, detail of the cuticle, **C.** Paratype (MACN-My 96), head, lateral view; **D.** Paratype (MACN-My 96), head, ventral view; **E.** Paratype (MACN-My 96), head, anterior view; **F.** Paratype (MACN-My 96), left palp of the first maxillae. Abbreviations: *cl*, cephalic lobe; *cr*, central rod; *g*, median groove of the second maxillae; *m*, anterior plates of the second maxillae; *mb*, mandibular base; *ml*, first maxillae; *p*, first maxillary palp; *pa*, second-maxillary proximal arms; *tg*, transversal ridge of the second maxillae; *tp*, terminal protuberances at this anterior part of the second maxilallae; *sp*, spiracle; *To*, Tömösvary organ. Scale bars: 100 μm (**A, C, E**); 20 μm (**B**); 50 μm (**D**); 10 μm (**F**).

Antennae (Fig. 3). Antennae with (21–38) antennomeres; length (0.37–0.6) of length of body. Distal antennomeres much thinner than proximal antennomeres, diameter of distal antennomere (0.55–0.64) of that of first. First antennomere (Fig. 3A, B) 1.5 (1.4–1.82) × as wide as long with a single apical whorl of 5–6 setae: 2–3 thick-based dorsal setae and 2 inner setae and 0–1 ventral setae. Longest dorsal seta, 0.33 (0.38–0.48) × the diameter of antennomere. Second antennomere (Fig. 3A) 2.16 (1.61–2.6) × as wide as long with 9–10 setae: 6 (5) thick-based setae

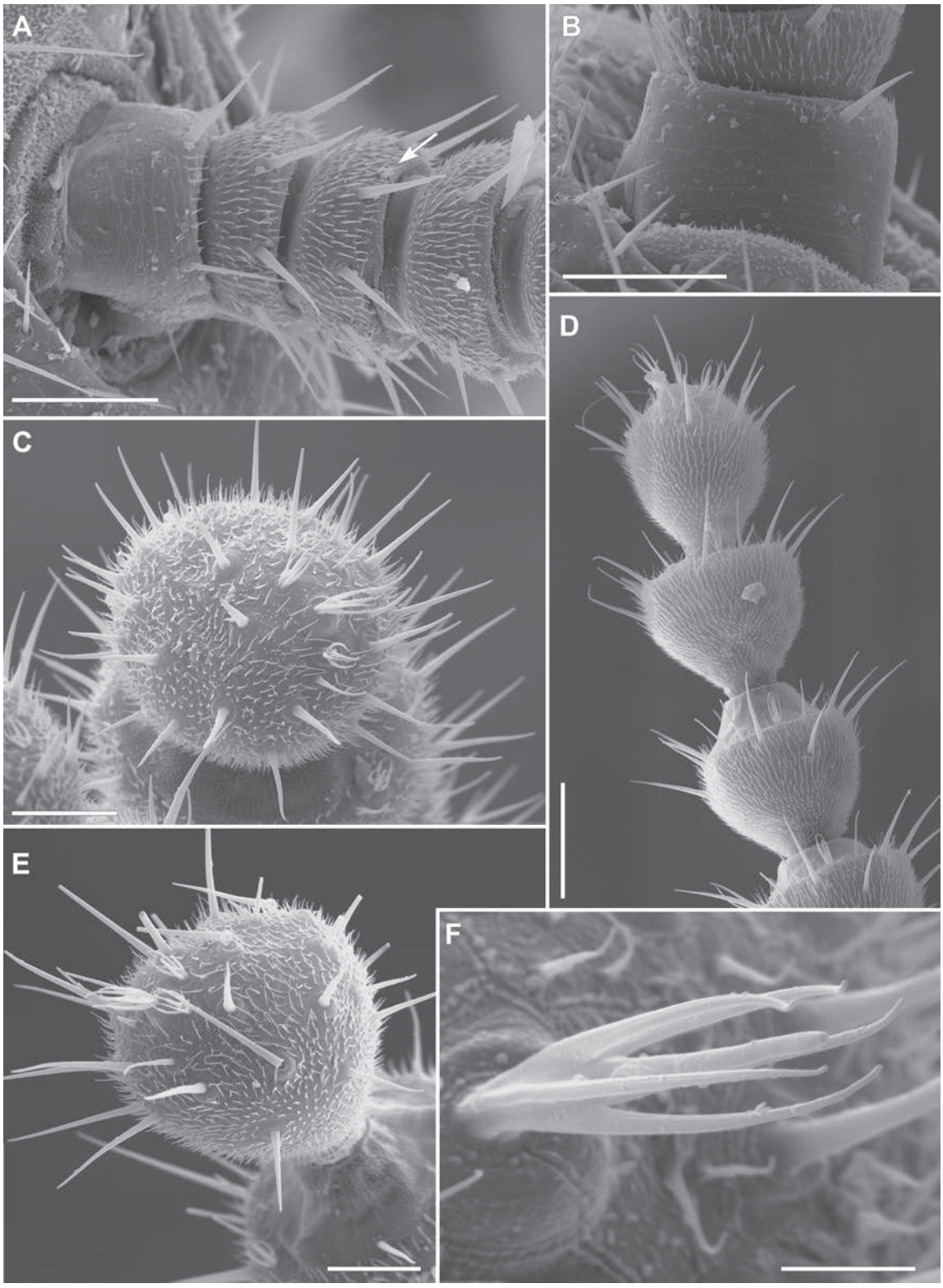

Figure 3. *Hanseniella guerreroi* sp. nov., antenna. **A.** Paratype (MACN-My 96), first four antenal segments, dorsal view; **B.** First antennal segment, dorsal view; **C.** Apical antennal segment, apical view; **D.** Three distal antennal segments, dorsoexternal view; **E.** Apical antennal segment, apical view; **F.** Long-spined apical organ antennal segment. Scale bars: 50 μm (**A, B, D**); 25 μm (**C, E**); 5 μm (**F**).

and 4 thin setae. Third antennomere (Fig. 3A) 1.77 (1.41–1.9) × as wide as long with 8 (6–10) setae; longest seta is dorsal, 0.46 (0.44–0.52) of diameter of antennomere. Small trifid spined organ begins on outer part of the tergal side of the third or fourth antennomere (Fig. 3A, arrow). Second medial whorl of setae begins with 1 seta on inner side of antennomere 4–5 and is complete in antennomere 10 (12–15). Tenth antennomere 1.3 (1.05–1.57) wider than long with 10–20 setae: 8–15 of about the same length, 5–6 very short and thin setae. The antennomere next to the

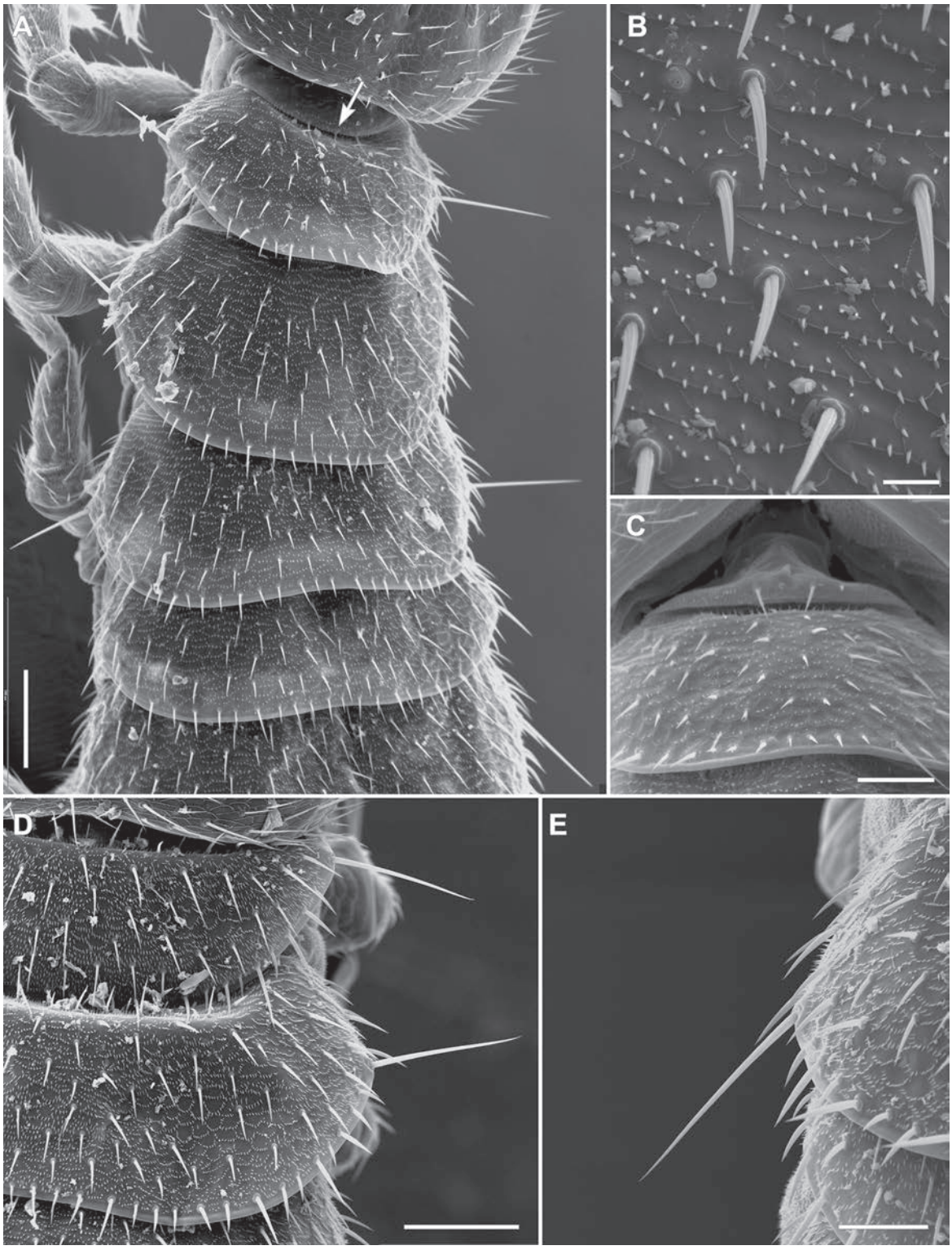

Figure 4. *Hanseniella guerreroi* sp. nov. **A.** Paratype (MACN-My 100), first to sixth terguite; **B.** Detail of the terguite cuticle; **C.** Paratype (MACN-My 87), first segment; **D.** Paratype (MACN-My 87), detail of the macrochaetae of the second and third terguites; **E.** Fourth terguite. Scale bars: 100 μm (**A, D**); 10 μm (**B**); 50 μm (**C, E**).

apical one (Fig. 3D) 1.13 (1.09–1.38) × as long as wide. An additional third whorl never completes, but traces occur from ventral side of 6–12 antennomeres below the apical whorl. Apical antennomere (Fig. 3C–F) 1.1 (1.31–1.5) × as long as wide with 24–28 setae, 2 small spined organs, and one large spined organ. The latter (Fig. 3F) 0.3 (0.21–0.31) of length of antennomere and consisting of a central straight rod surrounded by 5 (4) somewhat curved bracts. First antennomere glabrous with scaly cuticular pattern; distal antennomeres from the second with a sparce, evenly distributed pubescence; apical surface of distal antennomere (Fig. 3C, E) with fine pubescence.

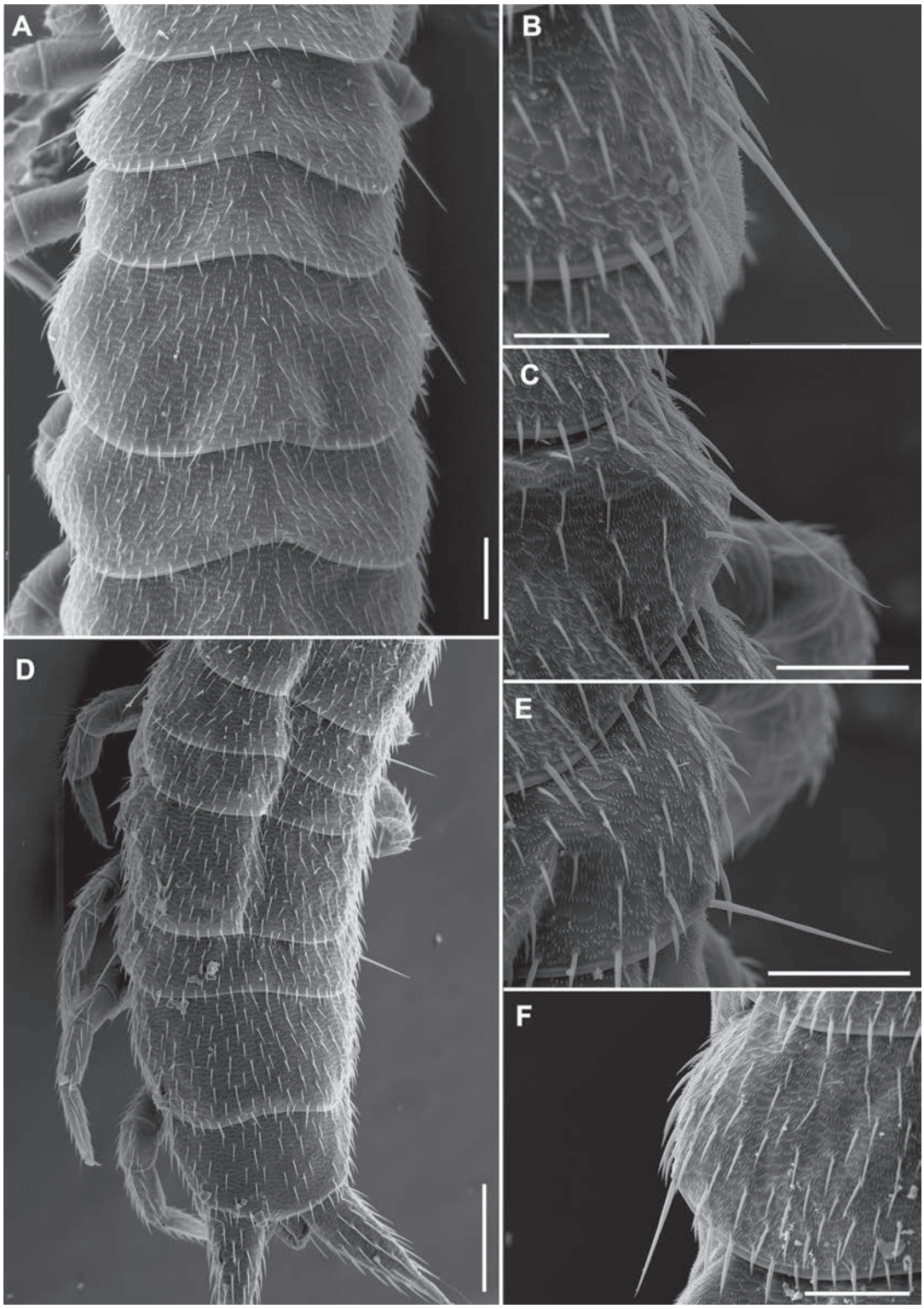

Figure 5. *Hanseniella guerreroi* sp. nov. **A.** Paratype (MACN-My 109), fifth to eighth terguites; **B.** Same, detail of the macrochaeta of the fifth terguite; **C.** Same, detail of the macrochaeta of the ninth terguite; **D.** Paratype (MACN-My 109), tenth to fifteenth terguites; **E.** Paratype (MACN-My 96), detail of the macrochaeta of the tenth terguite; **F.** Same, detail of the macrochaeta of the thirteenth terguite. Scale bars: 100 μm (**A, C, E, F**); 200 μm (**D**); 50 μm (**B**).

Tergites (Figs 1, 4, 5). First tergite (Fig. 4A, C) rudimentary, with 2 distinct lanceolate setae and 0–2 small setae (Fig. 4A, arrow). Second tergite complete (Fig. 4A, C), 2.52 (2.13–2.6) × as broad as long: posterior margin straight in the middle; anterolateral angles distinct with macrochaetae directed outwards and slightly forwards. These macrochaetae are 1.72 (1.25–1.9) of diameter of first antennomere, 21 (16–29) posteromarginal setae; longest posteromarginal seta, 0.5 (0.39–0.57) of the length of anterolateral macrochaetae. Inner setae of tergite short,

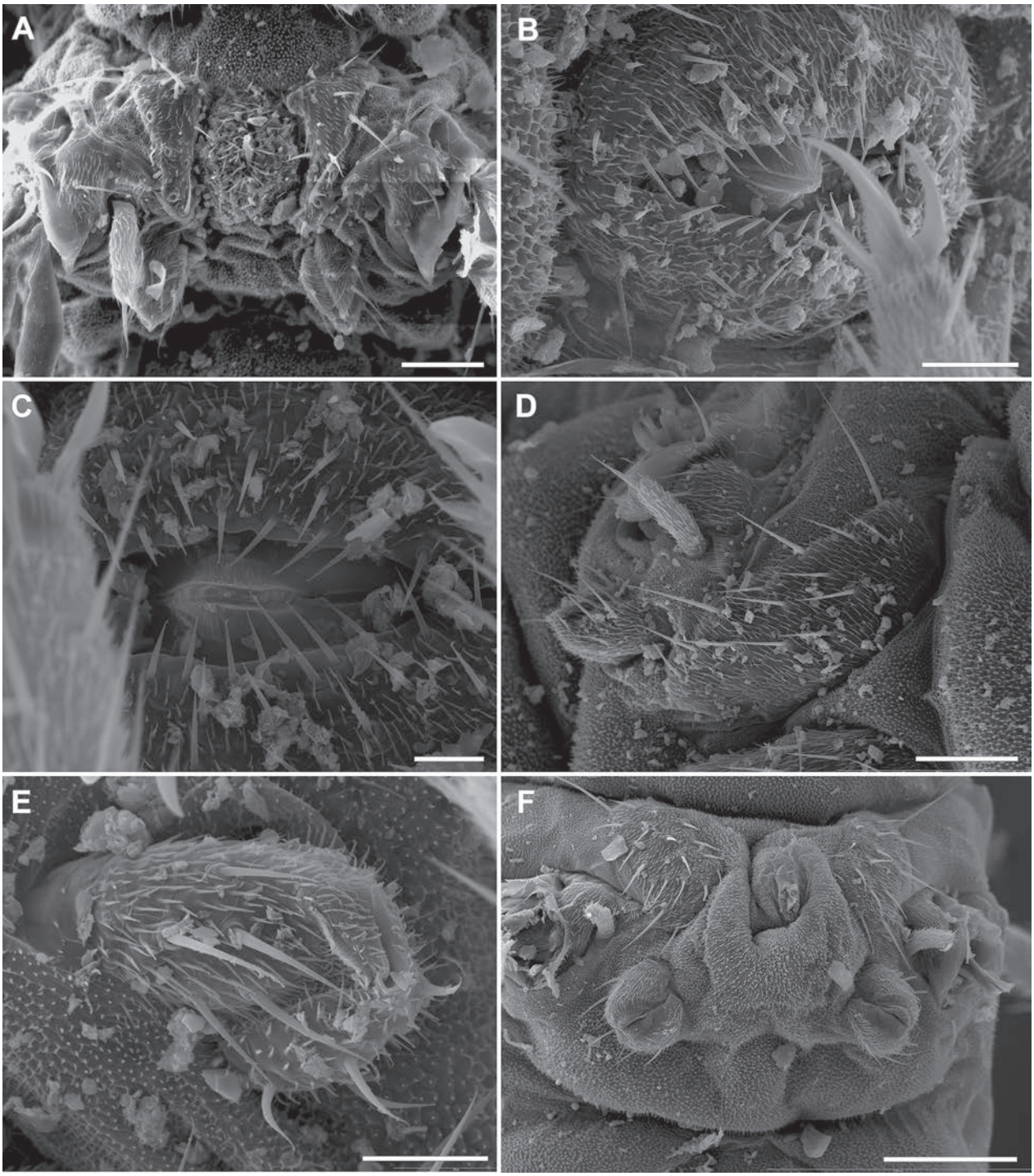

Figure 6. *Hanseniella guerreroi* sp. nov. **A.** Male paratype (MACN-My 88), fourth segment, ventral; **B.** Male paratype (MACN-My 98), detail of the genital opening; **C.** Same, different view; **D.** Same, fourth leg segment, coxal sac and stylus; **E.** Same, detail of the right coxal sac; **F.** Paratype female (MACN-My 99), fourth leg segment. Scale bars: 50 μm (**A, D**); 20 μm (**B, E**); 10 μm (**C**); 100 μm (**F**).

subequal in length, lanceolate, similar to posteromarginal setae. Pubescence short, reaching posterior margin, mostly in short transverse bows (Fig. 4B), reaching up the anteroposterior margins, posterior margin glabrous. Third tergite (Fig. 4A) 2.46 (2–2.85) × as broad as long with straight posterior margin; anterolateral macrochaetae (Fig. 4D) as on preceding tergite, 1.6 (1.31–1.6) of diameter of first antennomere; 30 (22–37) marginal setae between macrochaetae. Posteromarginal setae and pubescence similar to second tergite; longest posteromarginal setae, 0.56 (0.4–0.58) of the length of anterolateral macrochaetae. Fourth tergite (Figs 4A, 5A) much broader than preceding one, 2.81 (2.63–3.68) × as broad as long, posteriorly somewhat emarginate; with anterolateral macrochaetae directed outwards and backwards (Fig. 3E), 1.65 (1.07–1.81) of diameter of first antennomere; 31 (28–34) marginal setae between macrochaetae; inner setae as on third tergite. Tergite fifth to thirteen (Figs 1A, B, 5A, D) emarginated, pubescence as

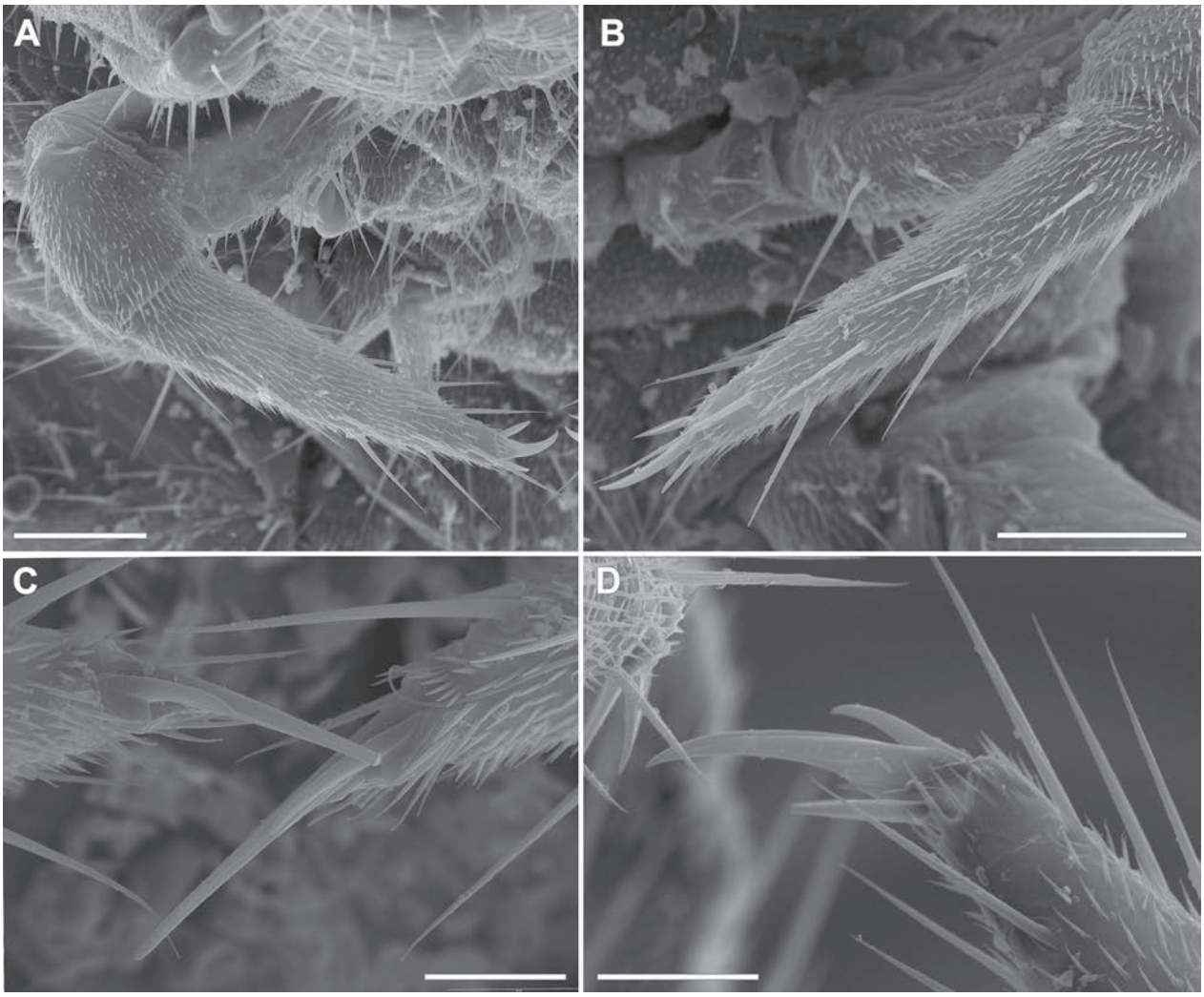

Figure 7. *Hanseniella guerreroi* sp. nov. **A.** Paratype (MACN-My 97), right leg 1; **B.** Left leg 1, tarsus; **C.** Same, detail of the claws, ventral view; **D.** Paratype (MACN-My 99), claws of left leg 1, anterolateral view. Scale bars: 50 μm (**A, B**); 20 μm (**C, D**).

on anterior tergites. Fifth tergite with posterior concavity less pronounced than the preceding one and significantly narrower than the fourth and the sixth (Fig. 1A, B). Penultimate tergite (Fig. 5D) with broad and shallow emargination; setae lanceolate, as on anterior tergites; pubescence as on anterior tergites. Last tergite (Figs 5D, 9B) with a convex posterior margin well projected behind tergal margin bearing 4 recognizable setae, pubescence reaching posterior margin. In addition to macrosetae on tergites 2, 3, and 4, lateral macrochaetae present on tergites 6 (Fig. 5B), 7, 9 (Fig. 5C), 10 (Fig. 5D, E), 12 (absent in populations of State Island), and 13 (Fig. 5D, F).

***Ventral surface*.** Mainly covered by microsetae born from small knobs, last segment surface with longer pubescence born at the posterior end of scale-like cuticular structures. Male genital segment (Fig. 6A–D) with sternal plates with 9–13 setae, 2 of which are 2 (1.45–2.1) × longer than the rest. Female genital segment (Fig. 6F) with sternal plate with 13–18 setae, 2 or 3 of which are longer than the rest, 1.65–2.7 longer than the other setae.

***Coxal sacs*.** Typical for the genus, fully developed at bases of legs 3–9, usually bearing 7–10 setae (Fig. 6E).

Male organs. Genital opening (Fig. 6A–C) valves with 7–10 setae on each of the internal borders and 7 (4–13) setae, which are subequal in length to those of the border.

Legs (Figs 7, 8). Tarsus of first pair of legs (Fig. 7A, B) 3.85 (3.38–4.53) × as long as wide, strongly tapering distally. Longest dorsal row with 5 (4–6) setae, longest ventral row with 4 (4–5) setae; distal setae longer than proximal ones; the longest one most distally on dorsal side, 0.9 (0.81–1.19) × as long as greatest diameter of tarsus. Anterior claw acuminates (Fig. 7C, D), almost straight, its length 0.21 (0.19–0.29) of the length of tarsus and 1.93 (1.7–2.5) × as long as posterior claw. Posterior claw basally suddenly thicker (Fig. 7D); frontal seta lanceolate and subequal in length to posterior claw. Pubescence short but distinct; trochanter with 13–23 setae subequal in length, the longest seta 2× longer than the shortest; coxa with (2–4) setae. Tarsus of 12th leg pair (Fig. 8A–F) 5.5 (4.3–5.6) × as long as wide, slowly tapering distally. Setae (Fig. 8B) arranged in rows lengthways, longest dorsal row with 6 (5–7) setae, longest ventral one with 7 (5–7) setae. Dorsal setae longer,

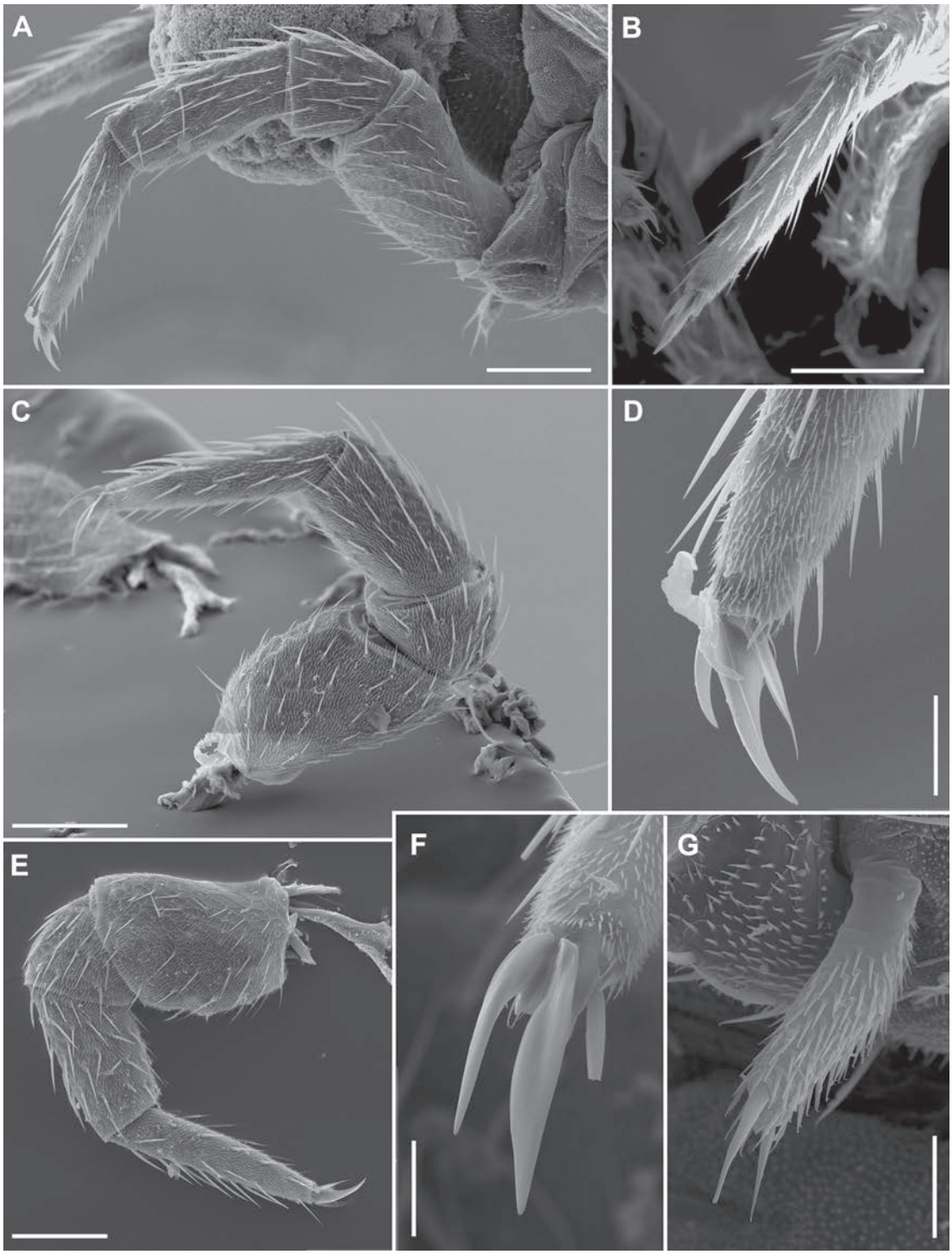

Figure 8. *Hanseniella guerreroi* sp. nov., leg 12. **A.** Paratype (MACN-My 97), right leg 12; **B.** Paratype (MACN-My 88), right leg 12, dorsal view of the tarsus; **C.** Paratype (MACN-My 99), left leg 12; **D.** Paratype (MACN-My 97), right leg 12, detail of the claws; **E.** Paratype (MACN-My 99), right leg 12, dorsal view of the tarsus; **F.** Paratype (MACN-My 96), right leg 12, frontal view of the claws; **G.** Paratype (MACN-My 96), stylus associated with the right leg 12. Scale bars: 100 μm (**A, C, E**); 25 μm (**D, F**); 20 μm (**G**).

longest of these 0.85 (0.61–0.95) of greatest diameter of tarsus. Anterior claw slender, somewhat curved, 0.14 (0.18–0.29) of the length of tarsus; length of posterior claw 0.52 (0.63–0.84) of the length of anterior claw, basally suddenly thicker; frontal seta (Fig. 8D) lanceolate and longer than posterior claw, with an aristate tip. Tibia (Fig. 8A, C, E) 2.23 (1.9–2.71) × as long as wide, its length 0.75 (0.72–0.83) of the length of tarsus; longest row of dorsal side with 5 (4–6) setae, the one on ventral side with 4 (2–5) setae; length of setae decreasing in

length proximally but inconsiderably; posterior side with few, 6 (4–7), setae. Femur very short with 5 (2–5) rows of 2–5 setae on dorsal and anterior sides; 0–1 ventral and 0–1 posterior seta. Trochanter with 22–35 thin subequal setae on dorsal and anterior sides only. Pubescence on tarsus, tibia, and femur short but distinct, sparser in the posterior facies of femur and tibia.

Styli. 3.2 (2.5–3.8) longer than wide, with 2 terminal setae, the larger 2.14 (1.71–2.33) longer than the shorter. On 12 leg well developed, elongated, 3.3 (2.91–4) × longer than wide, their length 1.42 (1.1–1.5) of the width of tarsus and densely covered with a short pubescence, basally glabrous; with 2 apical setae, the longer 1.5 (1.4–2.66) longer than the other, and 0.53 (0.33–0.57) the length of the stylus (Fig. 8G).

Sense calicles. Typical for the genus (Domínguez Camacho 2009) (Fig. 9F).

Cerci (Fig. 9A–E). Conical, proportionately short, 0.12 (0.75–0.12) of the length of body and 3.1 (2.75–4.5) × as long as wide. They have a moderate number of somewhat arched setae, the most distal ones longer than proximal ones; longest distal setae 0.43 (0.37–0.63) of greatest diameter of cercus. Longest dorsal row with 7 (6–9) setae (Fig. 9C), ventral 8 (5–9) (Fig. 9E), longest inner row with 8 (4–9), outer (Fig. 9A), with 9 (5–10) setae. The proximal 0.81 (0.7–0.84) of the tergal side covered with dense pubescence, as in tergites, mainly in short transverse bows following posterior borders of scale-like cuticular structures. Apical end glabrous. 2 apical setae (Fig. 9C, D) of different lengths, the longer one being (0.19–0.29) × the length of the cerci and (1.8–2.75) × the length of shorter seta.

Distribution. We found this species on three islands of the Tierra del Fuego archipelago, which is divided between Argentina and Chile. On the Argentinean side, we found it in the south of the Isla Grande de Tierra del Fuego and in the Isla de Los Estados. On the Chilean side, we found it on the Isla Navarino, one of the southernmost islands of the archipelago. This species seems to be common in the Argentinean islands explored, but less common in Navarino.

Remarks. *H. guerreroi* inhabits the *Nothofagus* forests of the Argentine and Chilean parts of the Tierra del Fuego archipelago (Fig. 10). This species could correspond to the previous records attributed to *S. immaculata* by Attems (1897) from Navarino and Ushuaia, and most probably also from Lapataia.

Affinities. Twelve species of the genus *Hanseniella* have macrochaetae on tergites 2, 3, 4, 6, 7, 9, 10, and 13, putatively on 12, but not on 5, 8, 11, and 14 (Soesbergen 2019): *H. audax* Clark & Greenslade, 1996; *H. conveniens* Clark & Greenslade, 1996; *H. insequens* Clark & Greenslade, 1996; *H. madecassa* Aubry & Masson, 1953; *H. mutila*, Adam & Burtel, 1956; *H. nivea* (Scopoli, 1763); *H. pluvialis* Clark & Greenslade, 1996; *H. proxima* Adam & Burtel, 1956; *H. pyrethrata* Clark & Greenslade, 1996; and *H. vulgata* Adam & Burtel, 1956.

Discussion

In this study, we have described a new species of Symphyla, *H. guerreroi* sp. nov. We have recorded this species on islands of the Tierra del Fuego archipelago, which is divided between Argentina and Chile. On the Argentine side, we found it in the south of Isla Grande de Tierra del Fuego and Isla de Los Estados. On the Chilean side, we found it on Navarino Island, one of the southernmost islands of the archipelago. To our knowledge, *H. guerreroi* sp. nov. represents the southernmost record ever reported for a myriapod of the class Symphyla.

The new species, *H. guerreroi* sp. nov., shows interesting relationships with its congeners; nine of the eleven species that share a similar macrochaetotaxy are distributed on other Gondwanan landmasses, such as Tasmania (six species) and New Zealand (three species). It is well known that many of the endemic taxa from the southern end of the South American continent are phylogenetically more closely related to other taxa from other Gondwanan regions than to the rest of South America (e.g., Giribet and Edgecombe 2006; Giribet and Boyer 2010; Harvey 1996a, 1996b; Swenson et al. 2001; Sanmartín and Ronquist 2004). Further research on the phylogenetic relationships among *Hanseniella* species may reveal interesting relationships among species distributed in Tasmania, New Zealand, Argentina, Chile, and other countries located in areas related to the supercontinent Gondwana.

Symphyla are a diverse and abundant taxon in tropical and temperate climates (Scheller 1992; Minelli and Golovatch 2001; Parra-Gómez and Fernández 2022). However, the Tierra del Fuego archipelago has a subpolar oceanic climate. This suboptimal climate is a challenge for most South American taxa, including myriapods (Parra-Gómez and Fernández 2022). This is because many modern taxa exhibit tropical or temperate niche conservatism, i.e., evolutionary constraints to adapt to extremely hot or cold climates (Wiens et al. 2010; Fernández et al. 2016). The few modern representatives that are able to colonize suboptimal climates are usually taxa that have evolved recent evolutionary novelties that allow them to thrive, for example, in cooler climates (Wiens et al. 2010; Fernández et al. 2022). Except for "Isla de Los Estados", we found *H. guerreroi* sp. nov. at islands that were partially covered by the Patagonian Ice Sheet during the Last Glacial Maximum (LGM) (Davies et al. 2020). Therefore, *H. guerreroi* sp. nov. could be a glacial relict that survived the LGM in a glacial refuge or in ice-free areas east of the Tierra del Fuego archipelago (e.g., at the southeastern end of Isla Grande de Tierra del Fuego or in the Islas de los Estados). In this refuge, *H. guerreroi* sp. nov. probably evolved in isolation from other *Hanseniella* populations and adapted to the climatic conditions that prevail in the Tierra del Fuego archipelago today. Probably, at the end of the LGM, some of its representatives were passively dispersed to the west of Isla Grande de Tierra del Fuego and Isla Navarino, where they established stable populations. A recent analysis of the population genetic structure

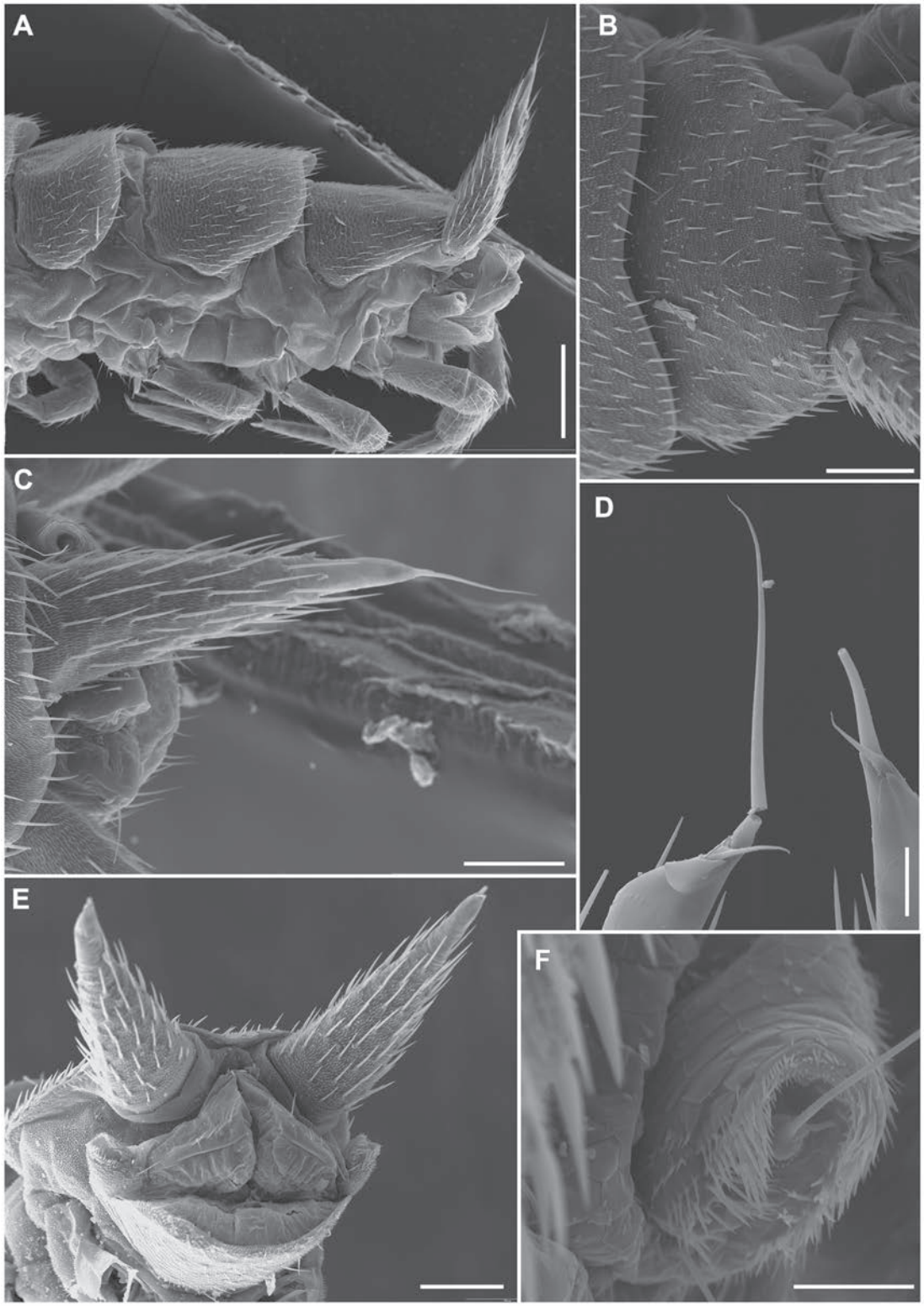

Figure 9. *Hanseniella guerreroi* sp. nov., cerci. **A.** Paratype (MACN-My 97), last trunk segments and left cercus, lateral view; **B.** Paratype (MACN-My 96), fifteenth terguite; **C.** Paratype (MACN-My 88), right cercus, dorsal view; **D.** Paratype (MACN-My 99), apical setae of the left cercus, ventral side; **E.** Paratype (MACN-My 97), posterior view of the trunk showing anus and ventral side of the cerci; **F.** Paratype (MACN-My 96), right sensory calicle. Scale bars: 200 μm (**A**); 100 μm (**B, C, E**); 25 μm (**D, F**).

of a microalga suggests that haplotypes from the western side of Isla Grande de Tierra del Fuego originated from a relict population that survived the LGM on the eastern side of the Tierra del Fuego archipelago (Fernández et al. 2017). Therefore, the populations of *H. guerreroi* sp. nov. from the western and southern regions of the Tierra del Fuego archipelago probably also originated from the eastern side of the archipelago. If this hypothesis is

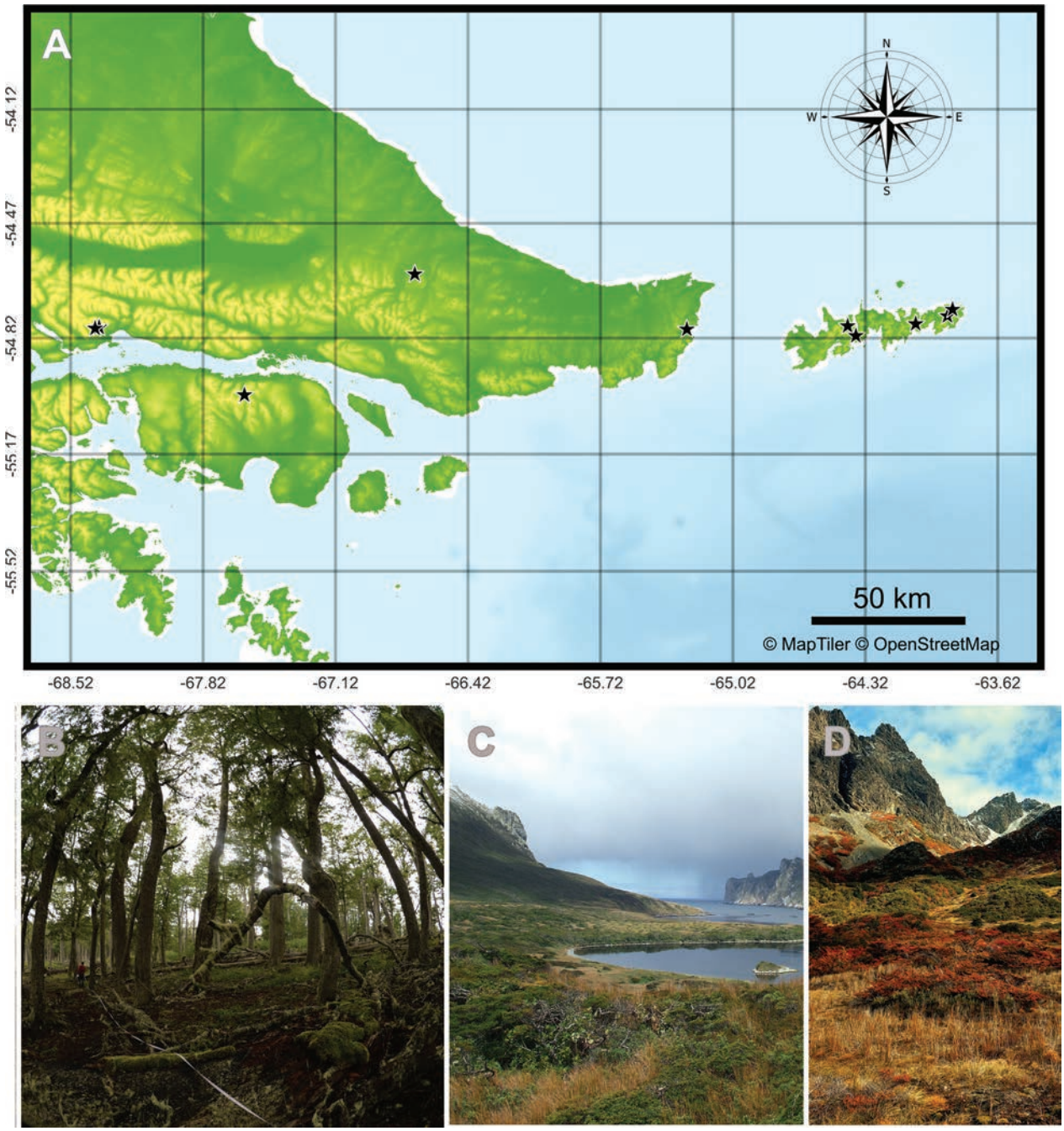

Figure 10. A. Collecting localities of *Hanseniella guerreroi* sp. nov.; **B.** Type locality, Río Irigoyen, Isla Grande de Tierra del Fuego, forest environment dominated by *N. pumilio* (Poepp. & Endl.) Krasser 1896 (Fagales: Nothofagaceae); **C.** Puerto Cook, Isla de los Estados, Argentina, panoramic view; **D.** Navarino Island, Chile (in the background is the Dientes de Navarino mountain range), panoramic view.

correct, the populations in the west and south of the archipelago should consist of a few recent haplotypes, while the populations in the east of the archipelago should have more and older haplotypes.

H. guerreroi sp. nov. may be an exception to the tropical and temperate niche conservatism, and so it is an excellent model organism to study the role of the LGM on the diversity and distribution of arthropods of the southern tip of South America. For instance, it might be useful for testing phylogeographical hypotheses on myriapods and other arthropods. In fact, phylogeographical studies regarding Argentine and Chilean arthropods are very scarce and do not consider taxa from the southern tip of the continent (e.g., Rosseti and Remis 2012; Zúñiga-Reinoso et al. 2016; Ceccarelli et al. 2017; Alfaro et al. 2018; Campos-Soto et al. 2020; Sosa-Pivatto et al. 2020; López-López et al. 2021). Moreover, studying the relations between *H. guerreroi* sp. nov. and a putatively new *Hanseniella* species in the Malvinas Islands (Pugh 2013) could help understand the origins and links of the Malvinas Islands fauna, as it has been discussed that the fauna from these islands has a close relationship with the rest of the austral Gondwanic South America fauna (Ringuelet 1955).

Acknowledgements

We wish to thank, particularly, the Argentine Navy personnel in Puerto Parry and Bahía Buen Suceso stations for their fundamental assistance during the collecting trips. Dr. Miguel Domínguez Camacho, Dr. Luis Pereira (MLP), and Bibl. Roberto Uguet (INTA-Castelar) for providing bibliographic materials. Field work in Argentina was supported by Foncyt grant PICT-2015-0283 to Martín J. Ramírez. Finally, both expeditions in Argentina were possible only because of the constant support of Federico Guerrero and Laura Smith of "Quijote Expeditions." L.D. Fernández and the expedition to Isla Navarino, located in the southern part of the Tierra del Fuego Archipelago, Chile, were funded by the ANID FONDECYT 1220605 project. R. Mackenzie thanks the support of the ANID/BASAL FB210018 y ANID – Millennium Science Initiative Program – ICN2021_002. L.D. Fernández and Roy Mackenzie thank Javier Estay (Wild Navarino Tourism Agency) and the "Watamericonsu" research team for their support during the fieldwork on Navarino Island, Chile. A.O. Porta thanks Ivan Fiorini de Magalhaes (MACN-Conicet) for his support during the collecting trip on Staten Island, Argentina. Valuable edits that helped improve this study were provided by Miguel Domínguez Camacho and Christopher James Dourte. Special thanks go to Martin Husemann, the subject editor, for his valuable assistance with this manuscript.

References

Adam MO, Burtel J (1956) A contribution to the study of the New Zealand Symphyla. Records of the Canterbury Museum 7(2): 61–88.

Alfaro MI, Muñoz-Ramírez, CP, Zúñiga-Reinoso, A, Trewick SA, Méndez MA (2018) Phylogeography of the Chilean red cricket *Cratomelus armatus* (Orthoptera, Anostostomatidae) reveals high cryptic diversity in central Chile. Biological Journal of the Linnean Society 123(4): 712–727. https://doi.org/10.1093/biolinnean/bly019

Attems CG (1897) Myriopoden. In Ergebnisse der Hamburger Magalhaensischen Sammelreise 1892/93. Friederichsen L & Co, Hamburg, 1–8.

Attems CG (1902) Myriopodes. Résultats du voyage du S.Y.Belgica en 1897–1898–1899 sous le commandement de A. de Gerlache de Gomery. Rapports Scientifiques, 3–5.

Aubry MJ, Masson C (1953) Contribution à la faune endogée de Madagascar. Symphyles. Mémoires de l'Institut Scientifique de Madagascar Série A 8: 43–66.

Bagnall RS (1913) On the classification of the order Symphyla. Journal of the Linnean Society of London, Zoology 32(216): 195–199. https://doi.org/10.1111/j.1096-3642.1913.tb01775.x

Boyle H (1981) Symphyla control in young plant cane. The Cane Growers' Quarterly Bulletin 44: 115–116.

Campello-Nunes PH, Woelfl S, da Silva-Neto ID, Paiva T da S, Fernández LD (2022) Checklist, diversity and biogeography of ciliates (Ciliophora) from Chile. European Journal of Protistology 84: 125892. https://doi.org/10.1016/j.ejop.2022.125892

Campos-Soto R, Díaz-Campusano G, Rives-Blanchard N, Cianferoni F, Torres-Pérez F (2020) Biogeographic origin and phylogenetic relationships of *Mepraia* (Hemiptera, Reduviidae) on islands of northern Chile. PLoS ONE 15(6): e0234056. https://doi.org/10.1371/journal.pone.0234056

Ceccarelli FS, Pizarro-Araya J, Ojanguren-Affilastro AA (2017) Phylogeography and population structure of two *Brachistosternus* species (Scorpiones, Bothriuridae) from the Chilean coastal desert – the perils of coastal living. Biological Journal of the Linnean Society 120(1): 75–89. https://doi.org/10.1111/bij.12877

Clark S, Greenslade P (1996) Review of Tasmanian *Hanseniella* Bagnall (Symphyla, Scutigerellidae). Invertebrate Taxonomy 10(1): 189–212. https://doi.org/10.1071/IT9960189

Davies BJ, Darvill CM, Lovell H, Bendle JM, Dowdeswell JA, Fabel D, García J-L, Geiger A, Glasser NF, Gheorghiu DM, Harrison S, Hein AS, Kaplan MR, Martin JRV, Mendelova M, Palmer A, Pelto M, Rodés Á, Sagredo EA, Smedley RK, Smellie JL, Thorndycraft VR (2020) The evolution of the Patagonian Ice Sheet from 35 ka to the present day (PATICE). Earth-Science Reviews 204: 103152. https://doi.org/10.1016/j.earscirev.2020.103152

Domínguez Camacho M (2009) Phylogeny of the Symphyla. Doctoral Thesis: Department of Biology, Chemistry and Pharmacy. Freie Universität Berlin. https://d-nb.info/1027814468/34 [Accessed 10 Feb 2020]

Fernández LD, Lara E, Mitchell EA (2015) Checklist, diversity and distribution of testate amoebae in Chile. European Journal of Protistology 51(5): 409–424. https://doi.org/10.1016/j.ejop.2015.07.001

Fernández LD, Fournier B, Rivera R, Lara E, Mitchell EAD, Hernández CE (2016) Water-energy balance, past ecological perturbations and evolutionary constraints shape the latitudinal diversity gradient of soil testate amoebae in south-western South America. Global Ecology and Biogeography 25: 1216–1227. https://doi.org/10.1111/geb.12478

Fernández LD, Hernández CE, Schiaffino MR, Izaguirre I, Lara E (2017) Geographical distance and local environmental conditions drive the genetic population structure of a freshwater microalga (Bathycoccaceae, Chlorophyta) in Patagonian lakes. FEMS Microbiology Ecology 93(10): fix125. https://doi.org/10.1093/femsec/fix125

Fernández LD, Seppey CVW, Singer D, Fournier B, Tatti D, Mitchell EAD, Lara E (2022) Niche conservatism drives the elevational diversity gradient in major groups of free-living soil unicellular eukaryotes. Microbial Ecology 83(2): 459–469. https://doi.org/10.1007/s00248-021-01771-2

Giribet G, Boyer S (2010) 'Moa's Ark' or 'Goodbye Gondwana': is the origin of New Zealand's terrestrial invertebrate fauna ancient, recent, or both? Invertebrate Systematics 24(1): 1–8. https://doi.org/10.1071/IS10009

Giribet G, Edgecombe GD (2006) The importance of looking at small-scale patterns when inferring Gondwanan biogeography: a case study of the centipede *Paralamyctes* (Chilopoda, Lithobiomorpha, Henicopidae). Biological Journal of the Linnean Society 89(1): 65–78. https://doi.org/10.1111/j.1095-8312.2006.00658.x

Harvey MS (1996a) Small arachnids and their value in Gondwanan biogeographic studies. In: Hopper SD (Eds) Gondwanan Heritage: Past, Present and Future of Western Australian Biota. Surrey Beatty & Sons: Chipping Norton, 155–162.

Harvey MS (1996b) The biogeography of Gondwanan pseudoscorpions (Arachnida). Revue suisse de Zoologie hors série 1, 255–264.

Jin Y-L, Nunes Godeiro N, Bu Y (2023) Description of the first species of Scutigerella (Symphyla, Scutigerellidae) from China, with mitogenomic and genetic divergence analysis. ZooKeys 1157: 145–161. https://doi.org/10.3897/zookeys.1157.99686

Lamoreux JF, Lacher Jr TE (2010) Mammalian endemism, range size and conservation status in the southern temperate zone. Diversity and Distributions 16: 922–931. https://doi.org/10.1111/j.1472-4642.2010.00697.x

López-López A, Acosta V, Rataj L, Galián J (2021) Evolution and diversification of the Southern Chilean genus *Ceroglossus* (Coleoptera, Carabidae) during the Pleistocene glaciations. Systematic Entomology 46(4): 856–869. https://doi.org/10.1111/syen.12494

Minelli A, Golovatch SI (2001) Myriapods. In: Levin SA (Ed.) Encyclopedia of Biodiversity. Academic Press, Amsterdam, 291–303. https://doi.org/10.1016/B0-12-226865-2/00204-2

Murray DAH, Smith D (1983) Effect of Symphyla, *Hanseniella* sp., on establishment of pineapples in south-east Queensland. Queensland Journal of Agricultural Science 40: 121–123.

Parra-Gómez A, Fernández LD (2022) Filling gaps in the diversity and biogeography of Chilean millipedes (Myriapoda, Diplopoda). Arthropod Systematics & Phylogeny 80: 561–573. https://doi.org/10.3897/asp.80.e86810

Parra-Gómez A, Pérez-Schultheiss J, Fernández LD (2024) Redescription of the enigmatic myriapod *Hanseniella chilensis* (Hansen, 1903) (Symphyla, Scutigerellidae) based on scanning electron microscope images of Chilean specimens. ZooKeys 1198: 1–15. https://doi.org/10.3897/zookeys.1198.119723

Porta A, Tricarico F (2018) Secado de muestras de ácaros de suelo para SEM usando hexamethyldisilazane (HDMS) Memorias del V congreso argentino de Microscopia SAMIC 2018. http://samic2018.congresos.unc.edu.ar/ [last accessed 29 May 2019]

Pugh PJA (2013) Why are there so few "far southern" myriapods? Journal of Natural History 47(43–44): 2769–2784. https://doi.org/10.1080/00222933.2013.791890

Ringuelet RA (1955) Ubicación zoogeográfica de las Islas Malvinas (in spanish). Editor Olivieri y Domínguez, 46 pp.

Rosetti N, Remis MI (2012) Spatial genetic structure and mitochondrial DNA phylogeography of Argentinean populations of the grasshopper *Dichroplus elongatus*. PLoS ONE 7(7): e40807. https://doi.org/10.1371/journal.pone.0040807

Sanmartín I, Ronquist F (2004) Southern hemisphere biogeography inferred by event-based models: Plant versus animal patterns. Systematic Biology 53(2): 278–298. https://doi.org/10.1080/10635150490423430

Scheller U (1961) A review of the Australian Symphyla (Myriapoda). Australian Journal of Zoology 9(1): 140–172. https://doi.org/10.1071/ZO9610140

Scheller U (1971) Symphyla from Ceylon and Peninsular India. Entomologica Scandinavica, Supplementum 1: 98–187.

Scheller U (1992) A study of Neotropical Symphyla (Myriapoda): List of species, keys to genera and description of two new Amazonian species. Amazoniana 12(2): 169–180.

Scheller, U (1998) Symphyla. In: Morrone JJ Coscaron S (Eds.). Biodiversidad de artrópodos argentinos: una perspectiva biotaxonómica, Volumen 1. Ediciones SUR, La Plata, 488–490.

Scheller U (2002) A new species of *Hanseniella* Bagnall (Myriapoda, Symphyla) found in a hothouse. Zoosystematics and Evolution 78(2): 269–273. https://doi.org/10.1002/mmnz.20020780206

Scheller U (2007) New records of Pauropoda and Symphyla (Myriapoda) from Brazil with descriptions of new species in *Allopauropus*, *Hanseniella* and *Ribautiella* from the northern Pantanal wetland and from Mato Grosso of Brazil. Amazoniana 19(3/4): 63–75.

Schiaffino MR, Lara E, Fernández LD, Balagué V, Singer D, Seppey CC, Massana R, Izaguirre I (2016) Microbial eukaryote communities exhibit robust biogeographical patterns along a gradient of Patagonian and Antarctic lakes. Environmental Microbiology 18(12): 5249–5264. https://doi.org/10.1111/1462-2920.13566

Schultheiss-Pérez J, Fernández LD, Bezerra Ribeiro F (2024) Two new genera of coastal Talitridae (Amphipoda: Senticaudata) from Chile, with the first record of Platorchestia Bousfield, 1982 in the southeastern Pacific coast. Zootaxa 5477(2): 195–218. https://doi.org/10.11646/ZOOTAXA.5477.2.5

Scopoli JA (1763) Entomologia carniolica exhibens insecta Carnioliae indigena et distributa in ordines, genera, species, varietates. Methodo Linnaeana. Vindobonae [=Vienna]: J. Trattner, xxxvi + 420 pp. https://doi.org/10.5962/bhl.title.119976

Snodgrass RE (1952) A textbook of arthropod anatomy. Cornell University Press, Ithaca, New York.

Soesbergen M (2019) *Hanseniella lanceolata* sp.n. (Myriapoda, Symphyla) found in a European hothouse. Arthropoda Selecta 28(1): 27–36. https://doi.org/10.15298/arthsel. 28.1.04

Sosa-Pivatto M, Camps GA, Baranzelli MC, Espíndola A, Sérsic AN, Cosacov A (2020) Connection, isolation and reconnection: Quaternary climatic oscillations and the Andes shaped the phylogeographical patterns of the Patagonian bee *Centris cineraria* (Apidae). Biological Journal of the Linnean Society 131(2): 396–416, https://doi.org/10.1093/biolinnean/blaa116

Swenson U, Hill R., Mcloughlin S (2001) Biogeography of *Nothofagus* supports the sequence of Gondwana break-up. Taxon 50(4): 1025–1041. https://doi.org/10.2307/1224719

Szucsich N, Scheller U. (2011) Symphyla. In: Minelli A (Ed.) Treatise on Zoology - Anatomy, Taxonomy, Biology. The Myriapoda, Volume 1. Brill, Leiden, The Netherlands, 445–466. https://doi.org/10.1163/9789004188266

Vega-Román E, Ruiz VH, Soto R, Díaz G (2012) Notas sobre el conocimiento de Symphyla de Chile. Dugesiana 19(1): 21–22.

Villagrán C, Hinojosa LF (1997) Historia de los bosques del sur de Sudamérica, II: análisis fitogeográfico. Revista Chilena de Historia Natural 70: 241–267.

Wiens JJ, Ackerly DD, Allen AP, Anacker BL, Buckley LB, Cor-nell HV, Damschen EI, Jonathan Davies T, Grytnes JA, HarrisonSP, Hawkins BA, Holt RD, McCain CM, Stephens PR (2010) Niche conservatism as an emerging principle in ecology and conservation biology. Ecology Letters 13: 1310–1324. https://doi.org/10.1111/j.1461-0248.2010.01515.x

Zúñiga-Reinoso A, Jerez V, Avaria-Llautureo J, Hernández CE (2016) Consequences of the last glacial maximum on *Nyctelia confusa* (Coleoptera, Tenebrionidae) in Patagonia. Biological Journal of the Linnean Society 117(4): 705–715. https://doi.org/10.1111/bij.12700

Zoosyst. Evol. 100 (4) 2024, 1585–1598 | DOI 10.3897/zse.100.125042

PENSOFT

für Natur MUSEUM FÜR NATURKUNDE BERLIN

Two new species of Schizorhynchia (Kalyptorhynchia, Rhabdocoela, Platyhelminthes) from Japan

Naoto Jimi[1,2], Natsumi Hookabe[3], Satoshi Imura[4,5], Yander L. Diez[6,7]

1 *Sugashima Marine Biological Laboratory, Graduate School of Science, Nagoya University, 429-63 Sugashima, Toba, Mie, 517-0004, Japan*
2 *Centre for Marine & Coastal Studies, Universiti Sains Malaysia, 11800 USM, Penang, Malaysia*
3 *Research Institute for Global Change (RIGC), Japan Agency for Marine-Earth Science and Technology (JAMSTEC), 2-15 Natsushima-cho, Yokosuka, Kanagawa 237-0061, Japan*
4 *National Institute of Polar Research, 10-3, Midoricho, Tachikawa 190-8518, Japan*
5 *Polar Science Program, The Graduate University for Advanced Studies, SOKENDAI, Tachikawa 190-8518, Japan*
6 *Museum of Nature Hamburg –Zoology, Leibniz Institute for the Analysis of Biodiversity Change (LIB), Martin-Luther-King-Platz 3, 20146, Hamburg, Germany*
7 *Research Group Zoology: Biodiversity and Toxicology, Centre for Environmental Sciences, Hasselt University, Universitaire Campus Gebouw D, B-3590 Diepenbeek, Belgium*

https://zoobank.org/5E91BC1B-10CD-4E10-8B3A-0300757562D9

Corresponding author: Naoto Jimi (beniimo7010@gmail.com)

Academic editor: Tom Artois ♦ **Received** 9 April 2024 ♦ **Accepted** 17 October 2024 ♦ **Published** 15 November 2024

Abstract

Schizorhynchia is a group of free-living interstitial flatworms within Kalyptorhynchia, characterized by possessing a split proboscis. To date, only seven species of Schizorhynchia have been recorded from Japan. Here, we describe two new species of schizorhynchs, *Proschizorhynchella quadricaudata* **sp. nov.** and *Cheliplana izuensis* **sp. nov.**, based on specimens collected from the intertidal zone of Japanese waters. We also explored the phylogenetic position of the new taxa based on partial sequences of the nuclear 18S rRNA and 28S rRNA genes. *Proschizorhynchella quadricaudata* **sp. nov.** is characterized by (*i*) proboscis lips with a row of glands; (*ii*) a simple cone-shaped stylet; and (*iii*) a caudal end with four finger-shaped projections. *Cheliplana izuensis* **sp. nov.** can be distinguished from its congeners by (*i*) two strong hooks with bifurcate tips, encircling the distal part of the spiny cirrus; (*ii*) the fact that the proximal 20% of the cirrus length is unarmed; (*iii*) proboscis' sidepieces lacking needles; (*iv*) paired seminal vesicles; and (*v*) the presence of a vagina. The phylogenetic analyses support the position of *P. quadricaudata* **sp. nov.** within Schizorhynchidae and the position of *C. izuensis* **sp. nov.** in a clade containing all species of *Cheliplana* within Cheliplanidae.

Key Words

Cheliplanidae, interstitial, meiofauna, Pacific Ocean, Schizorhynchidae, Turbellaria

Introduction

Schizorhynchia is a group of free-living interstitial flatworms within Kalyptorhynchia with worldwide distribution (Tessens et al. 2014; Diez et al. 2019; Smith III et al. 2020). To date, 192 species of Schizorhynchia have been described (Diez et al. 2019; Gobert et al. 2020; Armonies 2023; Velásquez-Rodriguez et al. 2023; WoRMS 2024). Schizorhynchs are characterized by possessing a split proboscis (a pair of finger-like and dorsoventrally opposed tongues) (Smith III et al. 2015), except for species of *Typhlorhynchus* Laidlaw, 1902, which lack a proboscis. Subsequently, schizorhynchs can be subdivided into two groups by the presence or absence of proboscis hooks (not constituting taxonomic categories). The former belong to Cheliplanidae Schilke, 1970; Diascorhynchidae Meixner, 1928; Karkinorhynchidae Meixner, 1928; and Nematorhynchidae Schilke, 1969; and the latter to

Schizorhynchidae Graff, 1905 (Tessens et al. 2014; Smith et al. 2015). In Schizorhynchidae, species of *Carcharodorhynchus* Meixner, 1938, and *Serratorhynchus* Noldt, 1988, and a few species of *Thylacorhynchus* de Beauchamp, 1927, have a proboscis armed with denticles (Smith et al. 2015).

The Japanese microturbellarian fauna and rhabdocoels in general are poorly known, and only seven schizorhynch species have been recorded in the country, including *Freddius tricaudatus* Takeda & Kajihara, 2018, *Proschizorhynchella pacifica* (Evdonin, 1969) Noldt, 1985, *P. caudociliata* Takeda & Kajihara, 2018, *P. magnoliae* Takeda & Kajihara, 2018, *P. shibazakii* Takeda & Kajihara, 2018, and *P. shuttlecock* Takeda & Kajihara, 2018. *Cheliplana setosa* Evdonin, 1971 was also recorded to Japan by Ax (2008); however, Gobert et al. (2021) considered that the specimens described by Ax probably belong to *C. hawaiiensis* Gobert, Reygel, Van Steenkiste & Artois, 2021 or *C. evdonini* Karling, 1983. Therefore, it is not currently possible to establish the identity of the species of *Cheliplana* recorded from Japan.

Recently, Van Steenkiste et al. (2023) recorded the eighth Japanese schizorhynch *Cheliplana terminalis* Brunet, 1968. In the latter paper, an undescribed species of *Carcharodorhynchus* Meixner, 1938, the eukalyptorhynch *Parautelga* sp., and the dalytyphloplanid *Trigonostomum vanmecheleni* Artois, Schockaert, Beenaerts & Reygel, 2013 were also recorded from Japan. Seven other marine or brackish water species of Rhabdocoela are documented from Japan: *Palladia nigrescens* (Evdonin, 1971) Evdonin, 1977, *Phonorhynchoides japonicus* Ax, 2008, *Utelga monodon* Ax, 2008, *Pogaina japonica* Ax, 2008, *P. scypha* Ax, 2008, *Promesostoma teshirogii* Ax, 1992, and *Ptychopera japonica* Ax, 2008 (see Ax 1992, 2008).

During faunal surveys on interstitial marine flatworms in Japan, eight specimens belonging to two species of Schizorhynchia were collected, of which we herein describe two new species. Furthermore, we estimated their phylogenetic relationships based on partial sequences of the nuclear 18S rRNA and 28S rRNA genes.

Material and methods

The specimens examined in the present study were collected from intertidal sand at five localities in Japan (Fig. 1): Yoichi (fine-grained sand, lower intertidal; 43°12'00.1"N, 140°46'55.4"E) on 15 May 2019, Manazuru (coarse sand with rocks, lower intertidal, 35°09'42.9"N, 139°08'25.0"E) on 29 October 2019 and 19 March 2021, Imaihama (fine-grained sand, lower intertidal, 34°45'01.0"N, 139°00'15.3"E) on 30 October 2019, Mihama (fine-grained sand, lower intertidal, 34°58'25.6"N, 138°45'50.9"E) on 29 October 2019, and Ishibu (fine-grained sand, lower intertidal, 34°43'58.8"N, 138°45'21.7"E) on 29 October 2019. Sediment samples were agitated with tap water to extract meiobenthic animals. The suspended water was filtered with a 62-µm mesh net. The residue was subsequently transferred into seawater and sorted under a dissecting microscope. Live

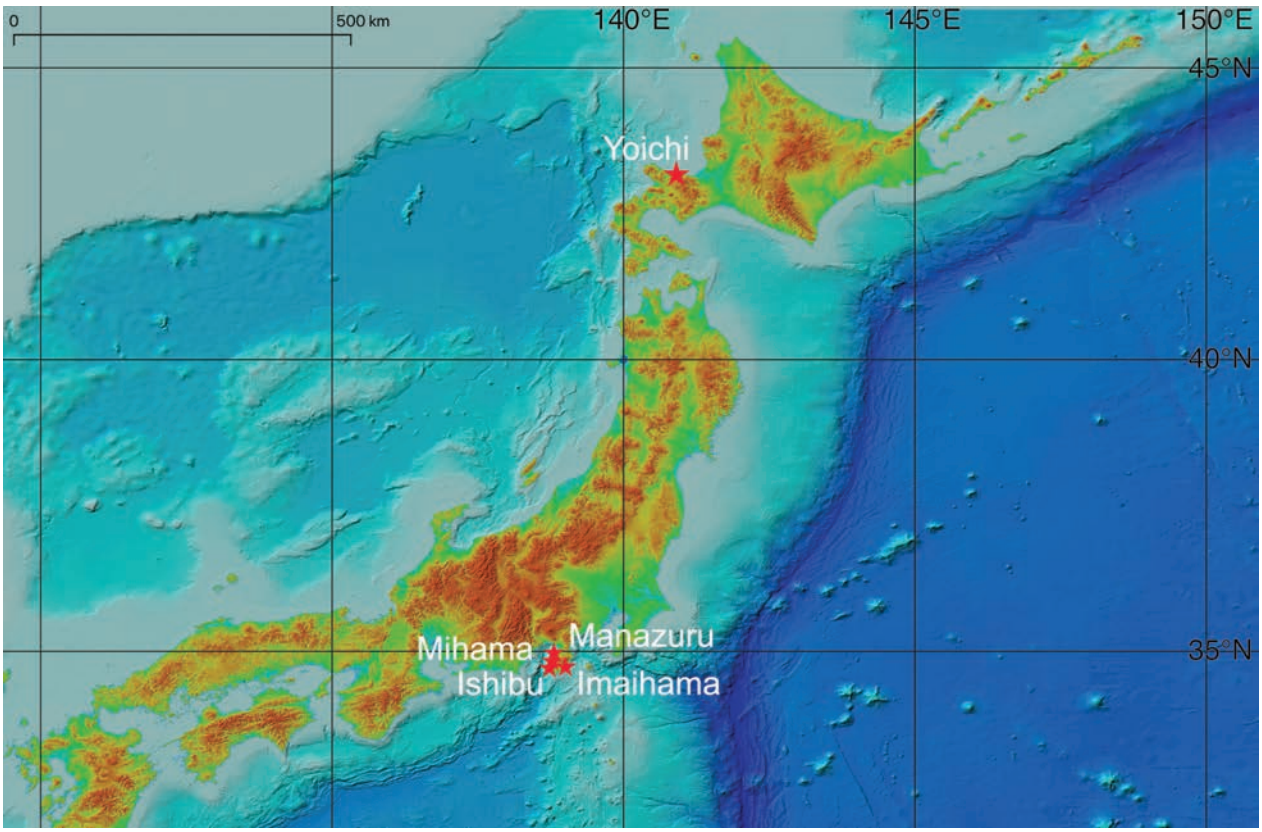

Figure 1. Map of Japan indicating the sampled localities.

specimens were studied, squeezed with seawater, and later fixed in 10% buffered formaldehyde. The holotypes were mounted in glycerol and subsequently sealed with nail polish around the edges of the coverslip. Fresh specimens were photographed using an Olympus E-5 digital SLR camera, observed under Nikon SMZ1500 and Olympus BX51 stereomicroscopes, and photographed using a Nikon D5200 digital camera. The drawings were made based on photographs of fresh specimens using the application Celsys CLIP STUDIO and a pen tablet, Wacom Intuos. Type specimens of the two new species were deposited in the National Museum of Nature and Science, Tsukuba (**NSMT**), Japan.

For morphological observations by scanning electron microscopy (**SEM**), specimens fixed in formaldehyde were washed in deionized water, dehydrated in a graded ethanol series, dried in a Hitachi HCP-2 critical-point dryer using liquid CO_2, coated with gold in a Hitachi E-1045 ion sputter, and observed using a Hitachi S-3000N scanning electron microscope at an acceleration voltage of 15–30 kV.

For the purposes of phylogenetic analyses, total DNA was extracted using a DNeasy Tissue Kit (Qiagen) for one specimen of each species. A reaction mixture [0.2 µl TaKaRa Ex Taq (Takara, Japan), 2 µl of 10× Ex Taq Buffer (Takara, Japan), 1.8 µl dNTP mixture (Takara, Japan), 1 µl of each primer pair (10 µM), 1 µl of extracted DNA, and 14 µl of distilled water] was used for PCR amplification. PCR amplification was performed in an Applied Systems 2720 thermal cycler using the primer pairs 1F/9R (Giribet et al. 1996) for 18S and LSU5/rd5b (Littlewood 1994; Schwendinger and Giribet 2005) for 28S and the following protocol: preheating at 94 °C for 2 min; 35 cycles of 94 °C for 40 s, 52 °C for 75 s, and 72 °C for 60 s; and a final extension at 72 °C for 7 min. Nucleotide sequencing was performed using internal primers in addition to the aforementioned primer pairs with an ABI BigDye Terminator ver. 3.1 Cycle Sequencing Kit and an ABI 3100 Avant Genetic Analyzer (Applied Biosystems). The internal primers used in the present study were as follows: 3F/5R (Giribet et al. 1996) and 18Sbi/S2.0 (Whiting et al. 1997) for 18S, and LSU3/D2F (Littlewood 1994), 28Z (Hillis and Dixon 1991), and Sa (Whiting et al. 1997) for 28S. Newly obtained sequences were deposited in GenBank (https://www.ncbi.nlm.nih.gov/genbank) under the accession numbers listed in Table 1.

A total of 60 sequences (38 for 18S, 22 for 28S; representing 43 species) were used for molecular phylogenetic analyses. Three sequences were obtained from specimens collected for this study, and the remaining 57 sequences were downloaded from GenBank. All sequences were aligned with MAFFT ver. 7.205 using the E-INS-i strategy (Katoh and Standley 2013). Ambiguous positions were removed using trimAL with the gappyout method (Capella-Gutiérrez et al. 2009). The trimmed alignments of the two genes 18S (1558 bp) and 28S (502 bp) were concatenated using Kakusan program (Tanabe 2007), which recommended a GTR+G evolutionary model for each of the genes. A phylogenetic tree was constructed using the maximum likelihood (ML) method in the RAxML-VI-HPC program (Stamatakis 2006). The robustness of the ML tree was evaluated by 1,000 bootstrap pseudo-replicates (F option). Bayesian Inference (BI) analysis was conducted using Mr. Bayes 3.2.2 (Ronquist et al. 2012), with Markov chains of 10 million generations. Model choice for each partition was also based on the Kakusan

Table 1. List of species included in the phylogenetic analyses, together with the respective GenBank accession numbers. Species names are referred to by Rundell and Leander (2014) and Smith et al. (2015).

Species	18S	28S
Cicerina tetradactyla	KJ887465	KJ887520
Paracicerina laboeica	KJ887408	JN852888
Carcharodorhynchus sp. 1 JPS-2015	KR339017	–
Carcharodorhynchus flavidus	KJ887457	KJ887563
Carcharodorhynchus sp. 2 JPS-2015	KR339018	KR339047
Carcharodorhynchus sp. 3 JPS-2015	KR339019	–
Carcharodorhynchus sp. TJ-2014	KJ887472	–
Carcharodorhynchus sp. 4 JPS-2015	KR339020	–
Carcharodorhynchus sp. 1 NVS-2023	OR490851	OR490867
Carcharodorhynchus sp. 2 NVS-2023	OR490850	OR490866
Carolinorhynchus follybeachensis	KR339021	KR339048
Cheliplana sp. 1 JPS-2015	KR339022	KR339049
***Cheliplana izuensis* sp. nov.**	–	**LC512875**
Cheliplana sp. 2 JPS-2015	KR339023	–
Cheliplana sp. 3 JPS-2015	KR339024	–
Cheliplanilla caudata	KJ887449	KJ887502
Cheliplanilla sp. 1 JPS-2015	KR339025	–
***Proschizorhynchella quadricaudata* sp. nov.**	**LC512873**	**LC512874**
Diascorhynchus rubrus	AJ012508	–
Diascorhynchus serpens	KJ887439	–
Karkinorhynchus bruneti	AY775740	–
Lehardyia alleithoros	KR339032	JF340473
Linguabana tulai	JN205121	–
Proschizorhynchella sp. 1 JPS-2015	KR339042	–
Proschizorhynchus sp. 2 JPS-2015	KR339036	KR339054
Proschizorhynchus sp. 3 JPS-2015	KR339037	KR339055
Proschizorhynchus gullmarensis	–	KJ887532
Proschizorhynchus tricingulatus	KJ887423	KJ887503
Proschizorhynchus trductibus	AY775744	–
Proschizorhynchus sp. 5 JPS-2015	KR339039	–
Proschizorhynchus sp. 6 JPS-2015	KR339040	KR339056
Schizorhynchidae sp. 2 JPS-2015	KR339041	AY340463
Schizorhynchidae sp. 3 JPS-2015	KR339043	–
Schizochilus caecus	AY775745	–
Schizochilus chorius	AY775746	–
Schizochilus sp. 1 JPS-2015	KR339044	KR339059
Schizochilus marcusi	AY775747	–
Schizorhinos vancouverensis	JN205120	–
Schizorhyncoides canaliculatus	AY775748	–
Thylacorhynchus ambronensis	AY775749	–
Thylacorhynchus sp. 1 JPS-2015	KR339045	KR339060
Thylacorhynchus conglobatus	KJ887448	KJ887534
Thylacorhynchus sp. 2 JPS-2015	KR339046	–
Thylacorhynchus sp.	–	KJ887508
Undicola toefinoensis	JN205119	–

results. Run convergence was analyzed using Tracer v1.6 (Rambaut et al. 2018); we assessed convergence by examining the trace plots for each parameter to ensure stationarity and proper mixing and confirmed that the effective sample sizes (ESS) for all parameters were above 200, indicating adequate sampling from the posterior distributions. The first one million generations were discarded as burn-in. Two species of Eukalyptorhynchia, *Cicerina tetradactyla* Giard, 1904, and *Paracicerina laboeica* Meixner, 1928, were used as outgroup taxa.

Results

Systematic account

Platyhelminthes Claus, 1887
Rhabditophora Ehlers, 1985
Rhabdocoela Ehrenberg, 1831
Kalyptorhynchia Graff, 1905
Schizorhynchia Meixner, 1928
Schizorhynchidae Graff, 1905
***Proschizorhynchella* Schilke, 1970**

***Proschizorhynchella quadricaudata* sp. nov.**

https://zoobank.org/29B3324A-5D36-4B51-93E0-A0792BB3BAE0

Figs 2–4

(New Japanese name: Yotsuo-kuchibashi-mushi)

Video material. Video of male copulatory organ of *Proschizorynchella quadricaudata* (https://doi.org/10.6084/m9.figshare.25568148.v1).

Type material. ***Holotype*** • (NSMT-Pl 6475): adult, intertidal sands, Imaihama Beach, 30 Nov. 2019, collected by NJ and NH; • one reference specimen (NSMT-Pl 6476): intertidal sands, Ishibu Beach, 30 Oct. 2019, collected by NJ and NH; • one reference specimen (NSMT-Pl 6477): intertidal sands, Manazuru, 29 Oct. 2019, collected by NJ and NH; • one reference specimen (NSMT-Pl 6478): intertidal sands, Yoichi, 15 May 2019, collected by NJ and NH; • additional specimen: intertidal sands, Mihama, 29 Oct. 2019, collected by NJ and NH; • additional specimen: intertidal sands, Imaihama Beach, 30 Nov. 2019, collected by NJ and NH, used for DNA extraction.

Description. Body 2.2 mm long (1.7–2.3 mm, n = 4), 0.4 mm at its widest point (0.4–0.5 mm, n = 4). Live specimens yellowish and translucent (Fig. 2). Two pairs of short bristles (Figs 3A, 4A: br) and two pairs of small globular papillae (Figs 3A, 4A: gp) at anterior end. Proboscis consisting of two elongated lips, 360 μm in length, 100 μm at the widest part (Figs 2A, B, 3A–C, 4A: pr); a row of glands with 27–37 apertures in the four studied specimens on inner side of proboscis lips (Fig. 3A, B, C: indicated by white arrow, Fig. 4A); gland apertures rectangular; glands measuring 14–16 μm long and 6–8 μm in width in the four studied specimens. Pair of black eyes situated posterior to the proboscis (Figs 2, 4A). Pharynx located at midbody, 160–240 μm in length and 200–260 μm in width in the four studied specimens (Figs 2B, 3G).

One adhesive girdle located at the level of the pharynx, composed of six adhesive papillae arranged at regular intervals (Fig. 3D: indicated by black arrows). Tail with four finger-like projections presents at the posterior end (Figs 3H, 4B: fp), each projection similar in size, 40–50 μm in length and 20–30 μm in width in the four studied specimens, muscles strongly developed at their middle part (Fig. 3H: mc).

Pair of testes, each 180 μm in diameter (Figs 2, 4A), located anterior to the pharynx. Seminal ducts widen and form a pair of seminal vesicles posterior to the pharynx (Figs 3E, 4A, B: sv), each 160 μm in length (150–170 μm, n = 4) and 40 μm in width (40–60 μm, n = 4). Seminal ducts (Fig. 4B: sd) fuse in a single duct just before entering the male copulatory bulb. Male copulatory organ comprising a proximal prostate vesicle and a distal stylet. Prostate vesicle globular, 80 μm both in length and width (60–120 μm, n = 4) (Figs 3E, 4B), separated in two packages; necks of the extracapsular prostate glands enter the copulatory bulb proximally. Stylet enclosed by the male genital duct, cone-shaped, 100–150 μm in length and 20–30 μm in width in the four studied specimens (Fig. 4B: st, mgd). Male genital duct opens into the common atrium (Fig. 3E, F: ca), and the latter leads to the exterior through the common genital pore. Common atrium brownish pigmented due to the secretions of atrial glands.

Female genital system consisting of a vitellarium (Fig. 2A: v) extending between the proboscis and the posterior end of the body, a single ovary (Figs 3E, 4B: ov), and bursa located behind the common genital atrium.

Diagnosis. Species of *Proschizorhynchella* with its tail end exhibiting four finger-like projections. Proboscis with a well-developed row of glands on each lip. Cone-shaped stylet ~100 μm long.

Etymology. The specific name is derived from a Latin prefix "*quadri*" + adjective "*caudata*", referring to the tail with four finger-like projections of the new species.

Distribution and habitat. Northern Japan: Yoichi, on fine-grained sand, lower intertidal. Central Japan: Manazuru, on coarse sand with rocks, lower intertidal; Imaihama (type locality), on fine-grained sand, lower intertidal; Mihama, on fine-grained sand, lower intertidal; and Ishibu, fine-grained sand, lower intertidal.

Remarks. The studied specimens show characteristics that, provisionally, allow us to include them within *Proschizorhynchella*. Species of *Proschizorhynchella* are schizorhynchids characterized by a simple male copulatory bulb forming a spiny cirrus and/or one or two stylets. The stylets are simple funnel structures, spiralized plates, or bear ridges (Schilke 1970; Takeda and Kajihara 2018). The diagnostic characteristics provided by Schilke (1970) are shared by a group of species that likely belong to different genera (Noldt 1985; Karling 1989). As noted by Noldt (1985), the only character differentiating species of *Proschizorhynchella* from species of *Proschizorhynchus* Meixner, 1928, is the lack of the curved stylet in the

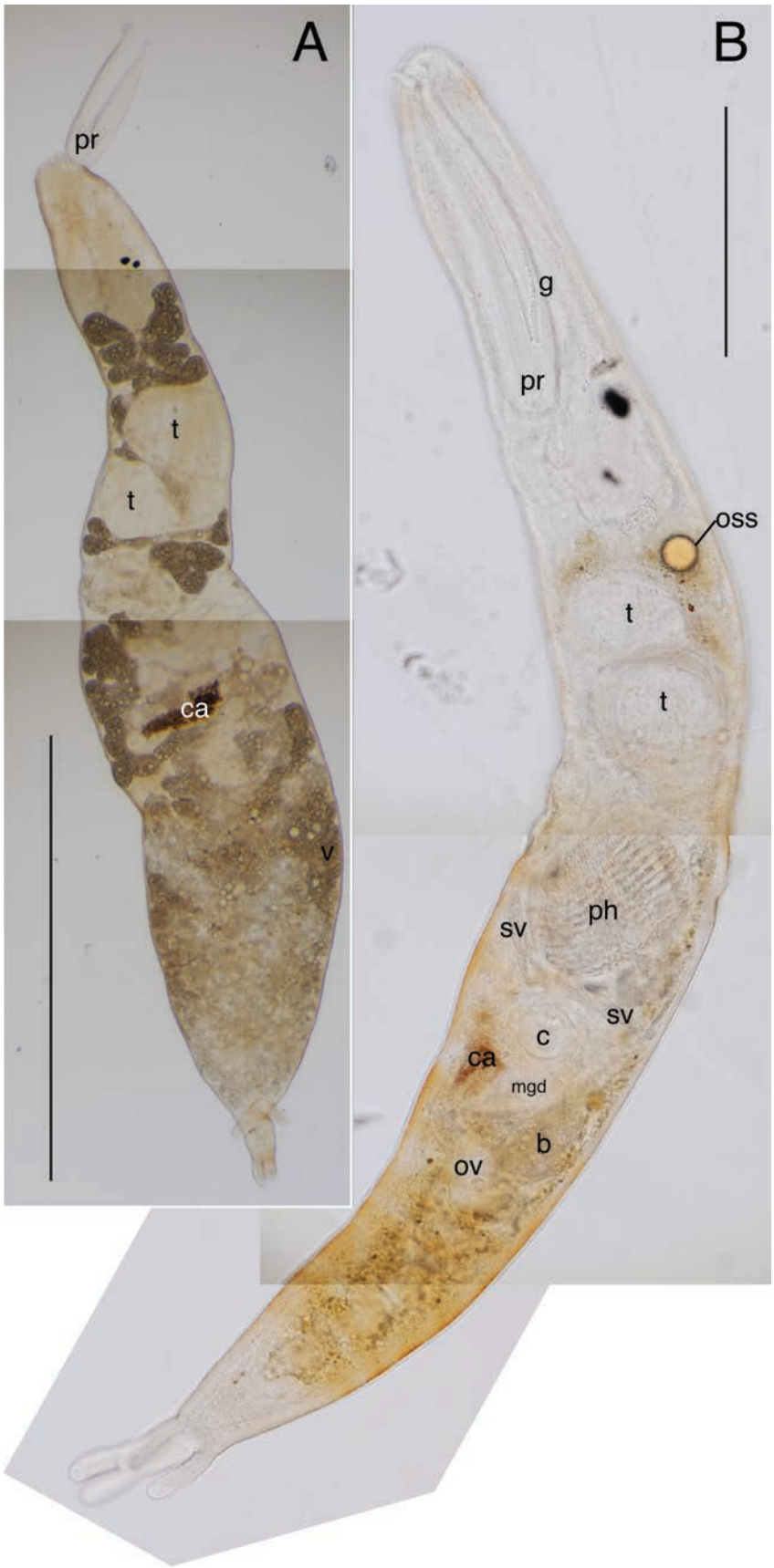

Figure 2. *Proschizorhynchella quadricaudata* sp. nov., live specimen. **A.** Holotype (NSMT-Pl 6475); **B.** Reference specimen (NSMT-Pl 6478). **A.** Whole specimen, dorsal view, pharynx discharged; **B.** Whole specimen, latero-dorsal view. Scale bars: 1 mm (**A**); 0.3 mm (**B**). Abbreviations: b, bursa; c, male copulatory organ; ca, common atrium; g, glands; oss, orange spherical structure; mgd, male genital duct; ov, ovary; ph, pharynx; s, stylet; sv, seminal vesicle; t, testis; v, vitellarium.

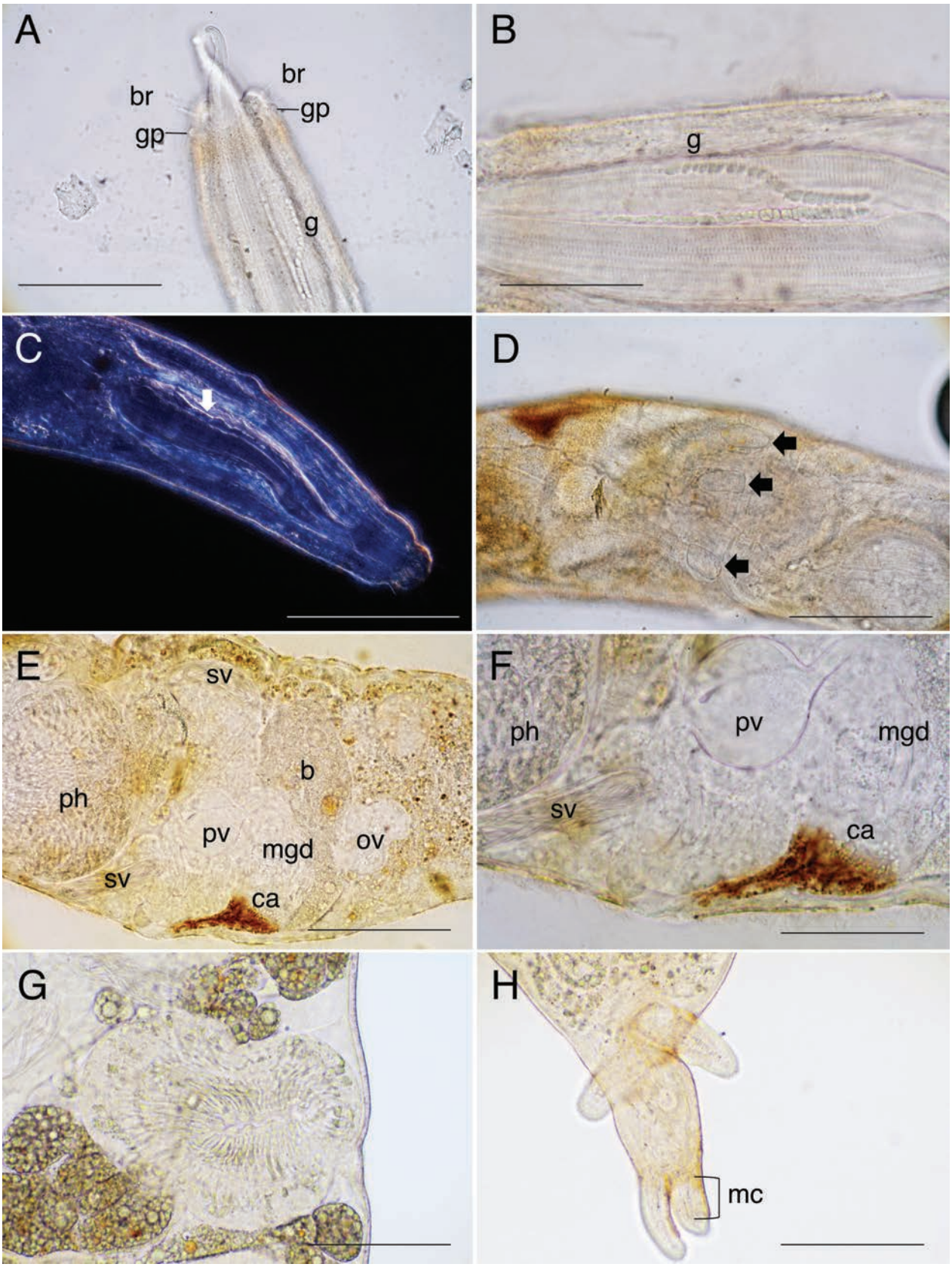

Figure 3. *Proschizorhynchella quadricaudata* sp. nov., live specimen, (**A–F**) reference specimen (NSMT-Pl 6478), (**G, H**) holotype (NSMT-Pl 6475). **A.** Anterior end; **B.** Proboscis with glands row; **C.** DIC view of proboscis with glands row (indicated by arrow); **D.** Midbody area; adhesive papillae are indicated by dashed lines (indicated by arrow); **E.** Overview of reproductive organs; **F.** Copulatory organ and common atrium; **G.** Pharynx; **H.** Tail with four finger-like projections. Scale bars: 200 μm (**A**); 100 μm (**B**); 200 μm (**C–E**); 100 μm (**F–H**). Abbreviations: br, bristles; ca, common atrium; g, glands; gp, globular papillae; mc, muscles; mgd, male genital duct; ov, ovary; ph, pharynx; pv, prostate vesicle; s, stylet; sv, seminal vesicle; t, testis.

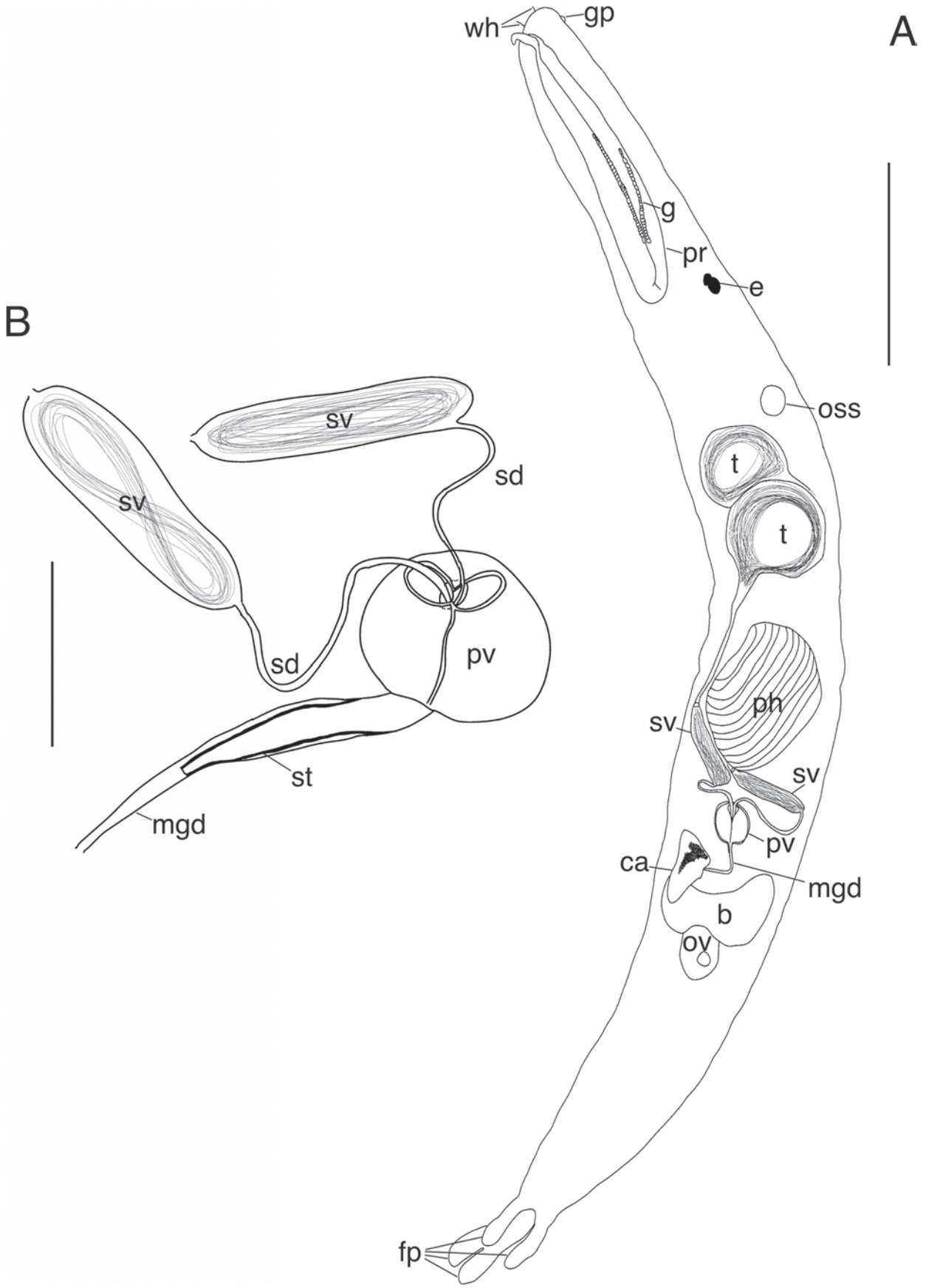

Figure 4. *Proschizorhynchella quadricaudata* sp. nov., drawing based on a reference specimen (NSMT-Pl 6478). **A.** Whole body; **B.** Male copulatory organ with stylet. Scale bars: 300 μm (**A**); 100 μm (**B**). Abbreviations: b, bursa; c, cirrus; ca, common atrium; e, eye; g, glands; gb, globular papillae; mgd, male genital duct; oss, orange spherical structure; ov, ovary; ph, pharynx; pr, proboscis; pv, prostate vesicle; sd, seminal duct; st, stylet; sv, seminal vesicle; t, testis; v, vitellarium; w, whisker.

former. However, the presence of a sclerotized mouthpiece in the bursa of species of *Proschizorhynchus* easily allows their differentiation from species of *Proschizorhynchella* (Armonies 2023).

Karling (1989) elaborated more on the idea that *Proschizorhynchella* includes a paraphyletic group of species and questioned the use of the pharynx position and testes number to differentiate among schizorhynchid genera. However, these authors and posterior ones (Takeda and Kajihara 2018) did not refine the diagnosis of *Proschizorhynchella* or make other taxonomical changes. Unfortunately, the morphological disparities among species of *Proschizorhynchella* have not been tested through molecular phylogenetic analyses, and none of the 18 previously known species of the genus has been molecularly tested (see Discussion). Therefore, we refrain from updating the diagnosis of *Proschizorhynchella* until more molecular and morphological data are available to elaborate a comprehensive reclassification of this taxon.

Among the other 18 known species of *Proschizorhynchella*, *P. quadricaudata* sp. nov. can easily be differentiated because of the four finger-like projections of its posterior end, a characteristic not present in its congeners. The row of glands that opens along its proboscis lips is also unique in this species, and this character has only been reported for an undescribed species of *Proschizorhynchella* (see Smith III et al. 2015: Fig. 3A).

Other characteristics are very variable among species of *Proschizorhynchella* (see Takeda and Kajihara 2018). Most species have two eyes, two testes, and one gonopore. However, the number of adhesive belts varies from 0 to 3. *Proschizorhynchella quadricaudata* sp. nov. exhibits a single adhesive belt at the level of the pharynx. Only three other species of *Proschizorhynchella* present a single belt: *P. bivaginata* Schilke, 1970; *P. robusta* Noldt, 1989; and *P. schilkei* Karling, 1989. *Proschizorhynchella bivaginata* is unique among these species because it has a cirrus in the copulatory bulb, whereas the other species have a stylet. *Proschizorhynchella schilkei* has two pairs of testes, and its stylet is a curved, comma-shaped hook, while *P. robusta* has a spiralized stylet (Karling 1989; Noldt 1989). In contrast, the stylet of *P. quadricaudata* sp. nov. is a simple and more or less straight tube.

Cheliplanidae Schilke, 1970

Cheliplana izuensis sp. nov.

https://zoobank.org/9DC8EDB8-D1D7-4F49-8885-EDE52FE571FE

Figs 5–7

(New Japanese name: Izu-kuchibashi-mushi)

Video material. Video of male copulatory organ of *Cheliplana izuensis* (https://doi.org/10.6084/m9.figshare.25568256.v1).

Type material. ***Holotype*** • (NSMT-Pl 6479): intertidal sands, Imaihama Beach, 30 Oct. 2019 collected by NJ. Two reference specimens were collected together with the holotype, one used for SEM observation (NSMT-Pl 6480) and the other for DNA extraction.

Description. Body 2 mm long and 0.38 mm at its widest point. Live animals brownish and translucent (Fig. 5A), without eyes. Proboscis 100 μm long and 50 μm at its widest point (Fig. 5A, B: pr), with one pair of hooks and one pair of sidepieces (Figs 6A, 7A: h & sp, respectively). Proboscis hooks 15 μm long, 3 μm wide at the base, smooth and curved. Sidepieces straight, cylindrical in shape, not bifurcated. Pharynx 350 μm long and 150 μm wide (Figs 5A, B, 6A). Prepharyngeal cavity with spines (Fig. 6A: cp). One adhesive ring with duo-adhesive glands, without papillae located in the subcaudal body end (Fig. 6A: dashed line indicated by black arrow Fig. 7B: ar).

One testis located anterolaterally to the pharynx, 690 μm long and 70 μm wide (Figs 5A, 6A: t). Atrial organs and ovary located in the caudal body fourth. Seminal ducts form a pair of seminal vesicles at the beginning of the caudal body fourth, each 100 μm long and 20 μm wide (Fig. 6A, B: sv). Seminal vesicles fuse in a single duct just before entering the male copulatory bulb. Male copulatory bulb comprising a prostate vesicle and a cirrus. Prostate vesicle pear-shaped, 100 μm long and 65 μm wide. Male duct forms in its distal half a cirrus, which separates by a sphincter (Fig. 5D: sph, Fig. 6B: ed, sp). Cirrus 65 μm long, 20 μm wide, consisting of three sections (Fig. 6B): (*i*) proximal unarmed region (approximately proximal 20% of its length), (*ii*) armed part with fine spines (approximately 15 μm long), and (*iii*) rhomboid area at distal end of cirrus, armed with fine spines (approximately 20 μm long) and two strong hooks (22 μm long) with bifurcate tips (encircling most distal part of cirrus).

Vitellarium extending from posterior region of pharynx to the caudal body end (Figs 5A, 6A: v). Ovary located posterior to the male copulatory bulb. Common gonopore located just caudally to the male copulatory bulb. Vagina present, a ring of circular muscles surrounding its aperture to the outside.

Etymology. The specific name is derived from a Latin adjective referring to the type locality in the Izu Peninsula.

Distribution and habitat. The new species is only known from the type locality (Imaihama, Izu Peninsula, Shizuoka), fine-grained sand in the lower intertidal.

Remarks. At present, the genus *Cheliplana* contains 49 species (Gobert et al. 2021). *Cheliplana izuensis* sp. nov. is placed in the genus *Cheliplana* due to having a pair of curved proboscis hooks, soft proboscis sidepieces, a single adhesive girdle, and a cylindrical, barrel-shaped pharynx with a long pre-pharyngeal cavity (de Beauchamp 1927; Schilke 1970; Gobert et al. 2017, 2021). It is distinguished from its congeners by the following combination of characteristics: (*i*) two strong hooks with bifurcate tips, encircling the distal part of the cirrus; (*ii*) a cirrus with the proximal 20% of its length unarmed, posteriorly armed with 15-μm-long and fine spines; (*iii*) proboscis sidepieces lacking bristles; (*iv*) paired seminal vesicles; and (*v*) the presence of a vagina.

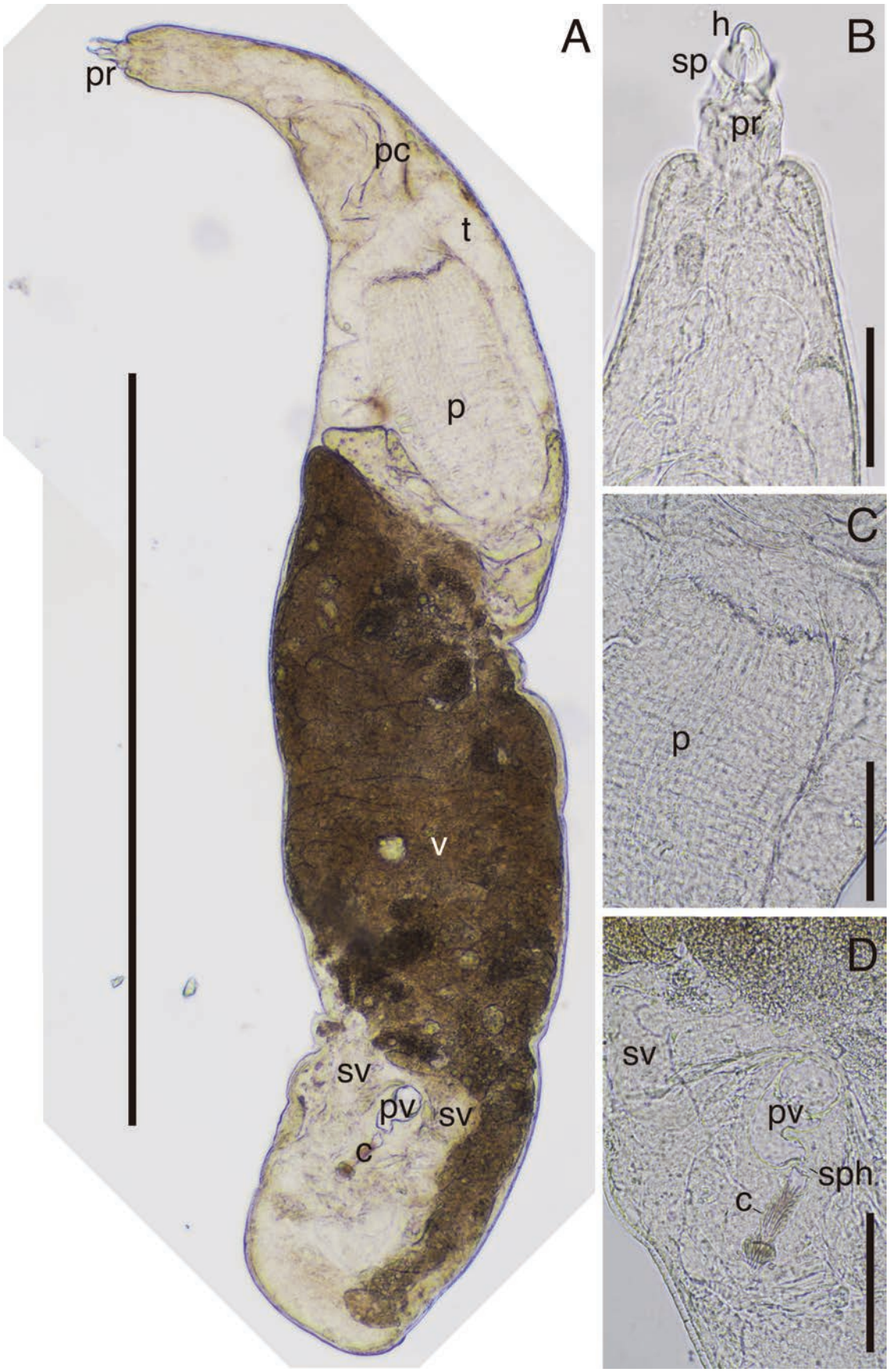

Figure 5. *Cheliplana izuensis* sp. nov., live specimen, holotype (NSMT-Pl 6479). **A.** Whole specimen, dorsal view; **B.** Anterior end; **C.** Pharynx; **D.** Overview of internal organs. Scale bars: 1 mm (**A**); 100 μm (**B**–**D**). Abbreviations: c, cirrus; h, hook; pr, proboscis; pc, proboscis cavity; t, testis; p, pharynx; pv, prostate vesicle; sp, side piece; sph, sphincter; sv, seminal vesicle; v, vitellarium.

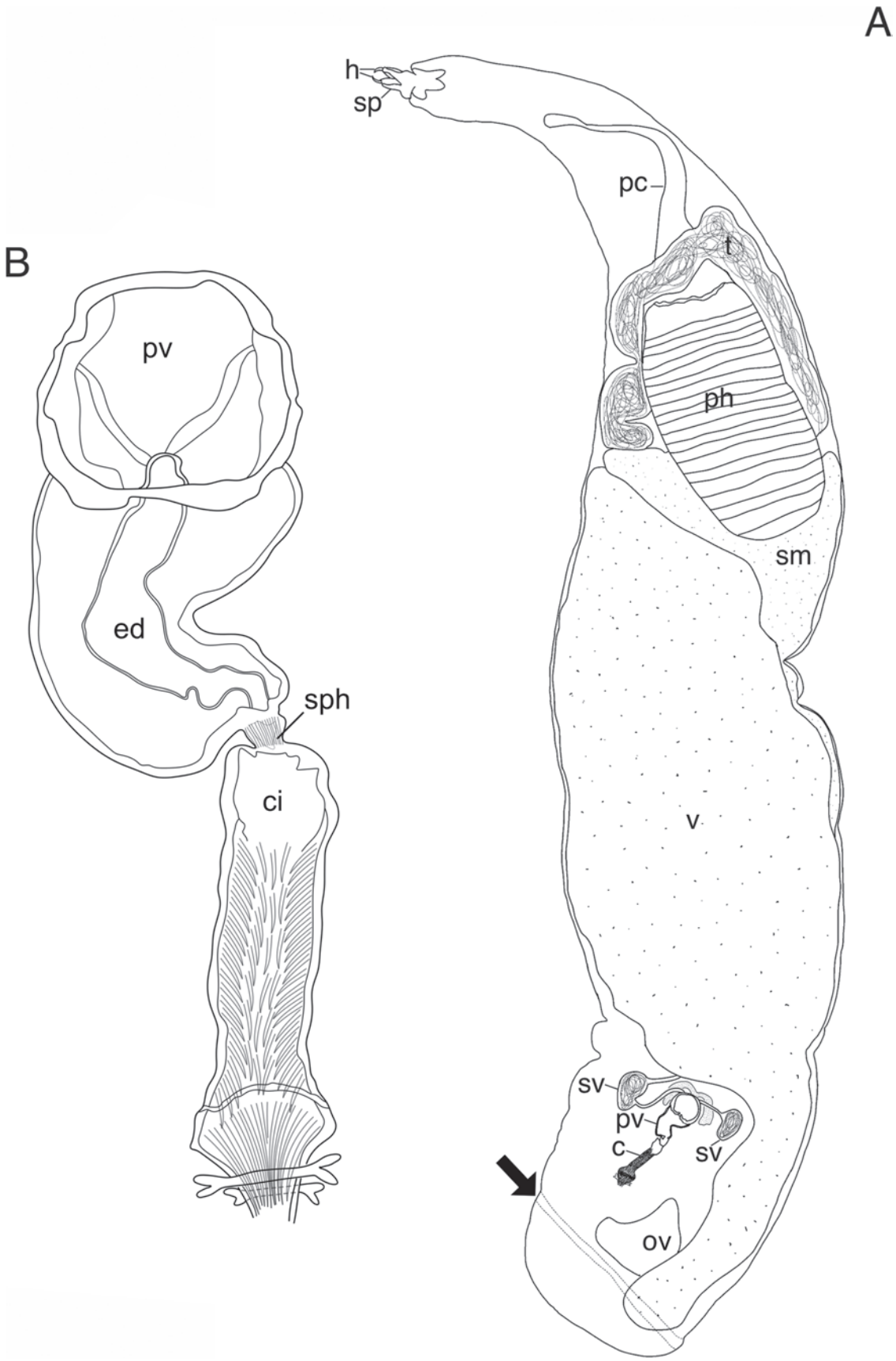

Figure 6. *Cheliplana izuensis* sp. nov., drawing based on holotype (NSMT-Pl 6479). **A.** Whole body; **B.** Male prostate vesicle and cirrus. Scale bars: 5 mm (**A**); 100 μm (**B**). Abbreviations: c, cirrus; cp, cuticular pockets; ed, ejaculatory duct; h, hook; pr, proboscis; pc, proboscis cavity; pv, prostate vesicle; t, testis; p, pharynx; sp, side piece; sm, stomach; sph, sphincter; sv, seminal vesicle; ov, ovary; v, vitellarium. Break line indicates adhesive girdle.

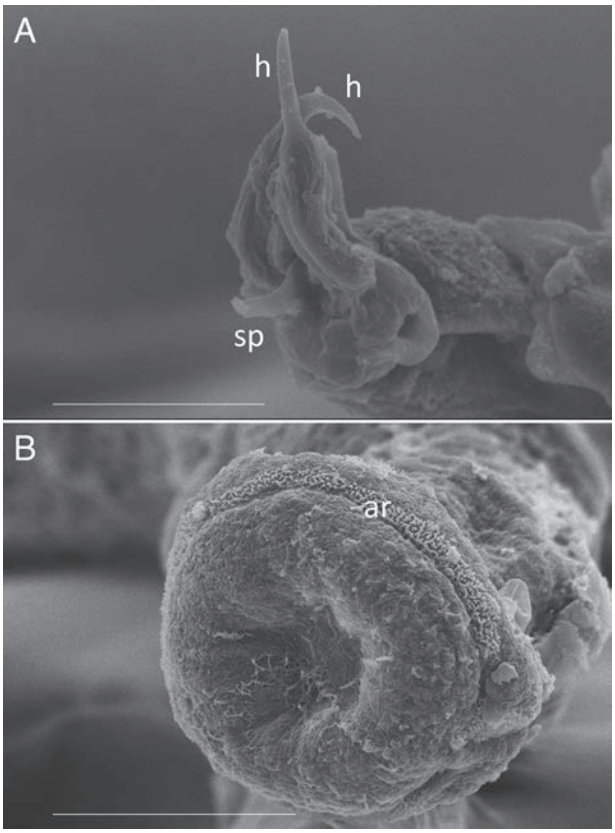

Figure 7. SEM observation of *Cheliplana izuensis* sp. nov., reference specimen (NSMT-Pl 6480). **A.** Proboscis; **B.** Posterior end. Scale bars: 30 μm (**A**); 50 μm (**B**). Abbreviations: ar, adhesive ring. Arrows indicate hooks. Arrowheads indicate sidepieces.

The morphology of the cirrus of *C. izuensis* sp. nov. allows us to state that the new species is related to *C. evdonini* Karling, 1983, and *C. setosa* Evdonin, 1971. This morphological similarity was tested using the identification key provided by Gobert et al. (2021), and, indeed, the three species have a convergent morphology of the cirrus. Therefore, we will mainly compare the new species with the other two morphologically similar ones. The cirrus in these three species has differentiated regions (unarmed or armed with spines differing in size) and includes hooks (*C. evdonini* and *C. izuensis* sp. nov.) or well-differentiated spines (*C. setosa*) more or less organized in a ring. In *C. izuensis* sp. nov., two hooks occur subterminally in the cirrus, whereas six hooks occur about the midlength of the cirrus in *C. evdonini* (Karling 1983), and 5–6 strong spines are present at the beginning of the distal third of the cirrus in *C. setosa* (Gobert et al. 2021). The hooks are distally pointing in *C. evdonini* and *C. setosa* but rounded and bifurcate at both ends in *C. izuensis* sp. nov. Furthermore, the proximal unarmed part of the cirrus distinguishes *C. izuensis* sp. nov. from the other two related species that have the cirrus armed of spines over its whole length. Another possible related species, *C. pusilla* Brunet, 1968, shows a multi-part cirrus; however, it was considered to belong to a different morphological species group due to the lack of hooks in the cirrus as occurs in the previously mentioned species (Gobert et al. 2021). Moreover, *C. izuensis* sp. nov. is differentiable from *C. pusilla* because in the latter species the cirrus shows two distinct spiny regions, a proximal curved area armed with very fine spines and a distal asymmetric one displaying larger spines (Brunet 1968).

The number and morphology of the seminal vesicles are also important to differentiate species of *Cheliplana* (see Diez et al. 2019; Gobert et al. 2021). *Cheliplana izuensis* sp. nov. presents two seminal vesicles, as is the case in *C. setosa*, whereas there is only one in *C. evdonini*. However, it was not clearly observed if both seminal vesicles are connected to the testis in *C. izuensis* sp. nov., while one of the vesicles is blind in *C. setosa*. Nevertheless, both seminal vesicles contain sperm in *C. izuensis* sp. nov., and, therefore, we can suppose that, indeed, they are connected to the testis. Among these three species, *C. izuensis* sp. nov. is also unique by the fact that the proboscis sidepieces do not bear bristles.

Phylogenetic analyses

The phylogenetic analysis, based on concatenated sequences of 18S and 28S rDNA genes, is convergent with those previously performed by Tessens et al. (2014) and Smith III et al. (2015) and evidences the poorly known and defined relationships within Schizorhynchia. Both the Bayesian and ML topologies were congruent (Fig. 8). *Proschizorhynchella quadricaudata* sp. nov. is included in a poorly supported clade including most species of Schizorhynchidae, Diascorhynchidae, and Karkinorhynchidae (pp = 0.98; BS = 52). *Cheliplana izuensis* sp. nov. is included in a clade containing all species of *Cheliplana* (pp = 0.98; BS = 51).

Discussion

Considering the results of our phylogenetic analysis, it is not possible to address the phylogenetic relationships of the taxa within Schizorhynchidae, except for the well-supported clade, including species of *Schizochilus* Boaden, 1963. Tessens et al. (2014) also found this limitation, suggesting that more species of Schizorhynchidae need to be included in molecular phylogenetic analyses (they remain underrepresented) and/or other, maybe more informative, molecular markers need to be used. Indeed, we did not find support for the monophyly of *Proschizorhynchella* due to *P. quadricaudata* sp. nov. not forming a clade with *Proschizorhynchella* sp. We expected that these two species would form a clade because of shared morphological characteristics, such as the belt of glands in the proboscis lips. Considering the morphological variability among species of *Proschizorhynchella* (see a detailed comparison in Takeda and Kajihara 2018), we can suspect that the genus is not monophyletic (see previous remarks on *P. quadricaudata* sp. nov.). On the other hand, species of *Cheliplana*, including *C. izuensis* sp. nov., form a monophyletic group, which is sister to species of *Cheliplanilla*. Therefore, we were able to resolve the relationships between these two genera, a question elusive in previous studies (Smith III et al. 2015).

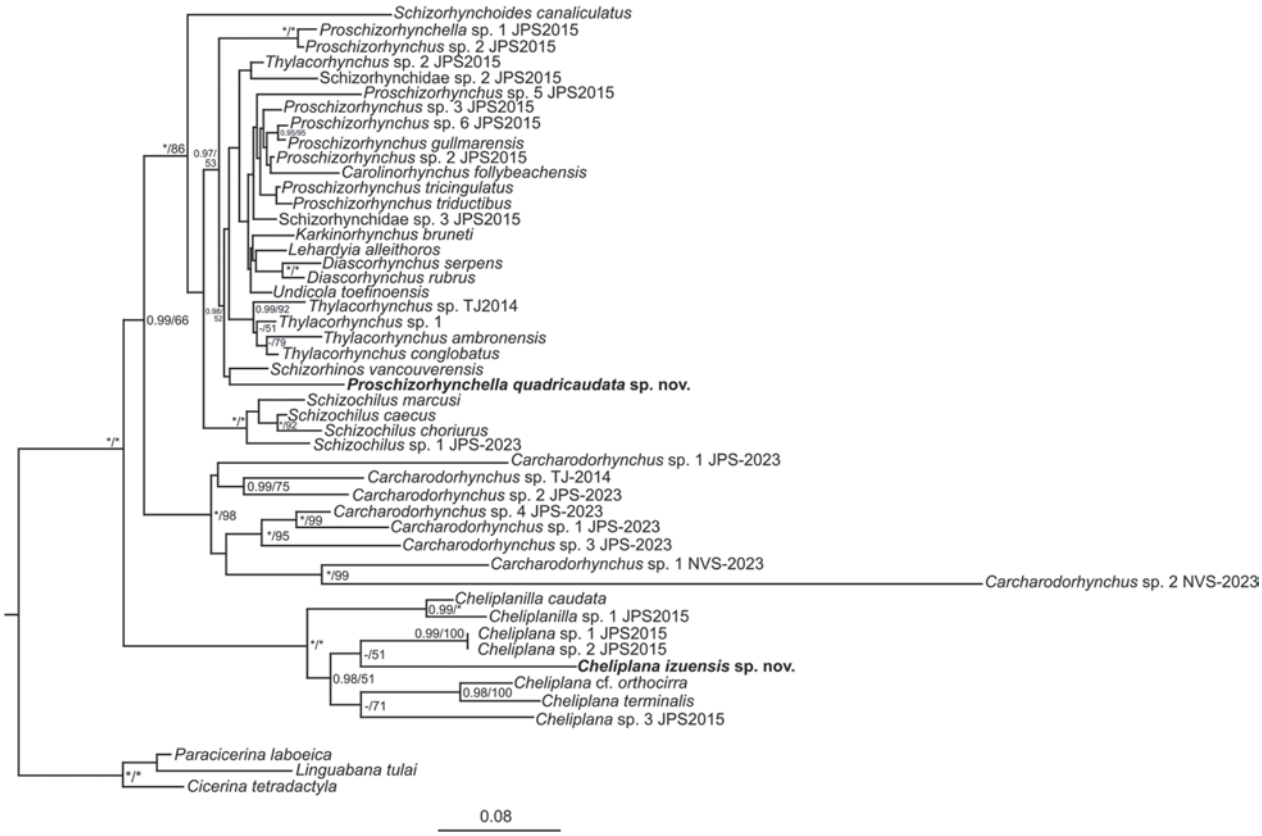

Figure 8. Maximum-likelihood phylogenetic tree of Schizorhynchia based on concatenated 18S and 28S rDNA sequences. The posterior probability of each branch is shown, followed by the bootstrapping values. More than 50% are indicated for each branch.

As of now, nine of the 20 rhabdocoel species recorded from Japan (see Tsuyuki et al. 2024), including the two new species here described, belong to Schizorhynchia. We suspect that the richness of this taxon in this region is higher, as in other recently studied archipelagos (Gobert et al. 2017; Diez et al. 2019, 2023). Most probably, the species richness of its sister taxon 'Eukalyptorhynchia' and microturbellarians as a whole is as high as in other areas of the world. While the macroturbellarian Polycladida have been well documented from Japan (e.g., Oya et al. 2022; Tsuyuki et al. 2022, 2023), major efforts will be necessary in the future to sample and conduct broad taxonomical studies on microturbellarians in this region. Understanding the diversity of free-living flatworms, particularly microturbellarians, is crucial to understanding relevant ecosystem processes. These little animals play important roles as predators and biomass producers, and their study is relevant not only for taxonomical purposes but also to address species and ecosystem conservation.

Acknowledgements

We thank the staff of the Shimoda Marine Research Center, University of Tsukuba, and members of the Department of Biodiversity I, Hokkaido University, for assistance in sampling. This study was partially supported by the Izu Peninsula Geopark 2019 to NH. YLD is supported by a Georg Forster Research Fellowship (Alexander von Humboldt Foundation, Germany, grant number 3.2 - CUB - 1226121 - GF-P). We would like to thank Editage (https://www.editage.com) for English language editing. This study was performed using facilities of the National Institute of Polar Research (NIPR).

References

Armonies W (2023) Platyhelminth fauna of the Island of Sylt: a meta-analysis of distributional patterns and description of 19 new species. Marine Biodiversity 53(1): 17. https://doi.org/10.1007/s12526-022-01309-w

Ax P (1992) *Promesostoma teshirogii* n. sp. (Platyhelminthes, Rhabdocoela) aus Brackgewassern von Japan. Microfauna Marina 7: 159–165.

Ax P (2008) Plathelminthes aus Brackgewässern der Nordhalbkugel. Akademie der Wissenschaft und der Literatur Mainz, Franz Steiner Verlag, Stuttgart, 696 pp.

Beauchamp PD (1927) Rhabdocoeles des sables a diatomees d'Arcachon I. Coup d'oeil sur l' association Schizorhynchidae. Bulletin de la societe zoologique de France 52: 351–359.

Brunet M (1968) Turbellariés Karkinorhynchidae de la région de Marseille. Les genres *Cheliplana* et *Cheliplanilla*. Cahiers de Biologie Marine 9: 421–440.

Capella-Gutiérrez S, Silla-Martínez JM, Gabaldón T (2009) trimAL: a tool for automated alignment trimming in large-scale phylogenetic analysis. Bioinformatics 25: 1972–1973. https://doi.org/10.1093/bioinformatics/btp348

Claus C (1887) Lehrbuch der Zoologie. 4. Auflage. N. G. Elwertsche Verlagsbuchhandlung, Marburg, Leipzig, 1279 pp.

Diez YL, Reygel P, Artois T (2019) Schizorhynchia (Platyhelminthes, Rhabdocoela) from eastern Cuba, with the description of fifteen new species. Zootaxa 4646(1): 1–30. https://doi.org/10.11646/zootaxa.4646.1.1

Diez YL, Sanjuan C, Bosch C, Catalá A, Monnens M, Curini-Galletti M, Artois T (2023) Diversity of free-living flatworms (Platyhelminthes) in Cuba. Biological Journal of the Linnean Society 140(3): 423–433. https://doi.org/10.1093/biolinnean/blad041

Ehlers U (1985) Cytoskelette bei freilebenden Plathelminthen. Verhandlungen der Deutschen Zoologischen Gesellschaft 78: 161.

Ehrenberg CG (1831) Animalia evertebrata exclusis insectis recensuit C.G. Ehrenberg. Series prima cum Tabularum decade prima. In: Hemprich FG, Ehrenberg CG (Eds) Symbolae Physicae 2. Phytozoa Turbellaria. Officina Academica, Berolina, 1–15.

Evdonin LA (1969) Novyi predstavitel' interstitial'nykh Kaliptorinlhii (Turbellaria, Neorhabdcoela, Kalyptorhynchia) ostrova Kunashir. Vestnik Leningradskogo Universiteta 15: 7–14.

Evdonin LA (1971) The interstitial Kalyptorhynchia (Turbellaria, Neorhabdocoela) from the bay of Great Peter of the Sea of Japan. Investigations on the Marine Faunas 8: 55–71. [In Russian]

Giard A (1904) Sur une faunule caractéristique des sables à Diatomées d'Ambleteuse Pas-de-Calais. Comptes rendus des séances de la Société de Biologie, Ser. 10, 56: 295–298.

Giribet G, Carranza S, Baguñà J, Riutort M, Ribera C (1996) First molecular evidence for the existence of a Tardigrada + Arthropoda clade. Molecular Biology and Evolution 13: 76–84. https://doi.org/10.1093/oxfordjournals.molbev.a025573

Gobert S, Reygel P, Artois T (2017) Schizorhynchia (Platyhelminthes Rhabdocoela) of Lanzarote (Canary Islands), with the description of eight new species. Marine Biodiversity 49: 2089–2107. https://doi.org/10.1007/s12526-017-0736-x

Gobert S, Monnens M, Eerdekens L, Schockaert E, Reygel P, Artois T (2020) Schizorhynchia Meixner, 1928 (Platyhelminthes, Rhabdocoela) of the Iberian Peninsula, with a description of four new species from Portugal. European Journal of Taxonomy 595: 1–17. https://doi.org/10.5852/ejt.2020.595

Gobert S, Diez YL, Monnens M, Reygel P, Steenkiste NWL, Leander BS, Artois T (2021) A revision of the genus *Cheliplana* de Beauchamp, 1927 (Rhabdocoela: Schizorhynchia), with the description of six new species. Zootaxa 4970: 453–494. https://doi.org/10.11646/zootaxa.4970.3.2

Graff L von (1905) Marine Turbellarien Orotavas und der Küsten Europas. Teil II. Rhabdocoela. Zeitschrift fur wissenschaftlige Zoologie 83: 68–154.

Hillis DM, Dixon MT (1991) Ribosomal DNA: molecular evolution and phylogenetic inference. Quality Review of Biology 66: 411–453. https://doi.org/10.1086/417338

Karling TG (1983) Structural and systematic studies on Turbellaria Schizorhynchia (Platyhelminthes). Zoologica Scripta 12: 77–89. https://doi.org/10.1111/j.1463-6409.1983.tb00552.x

Karling TG (1989) New taxa of Kalyptorhynchia (Platyhelminthes) from the N. American Pacific coast. Zoologica Scripta 18(1): 19–32. https://doi.org/10.1111/j.1463-6409.1989.tb00120.x

Katoh K, Standley DM (2013) MAFFT multiple sequence alignment software version 7: improvements in performance and usability. Molecular Biology and Evolution 30: 772–780. https://doi.org/10.1093/molbev/mst010

Littlewood DTJ (1994) Molecular phylogenetics of cupped oysters based on partial 28S rRNA gene sequences. Molecular Phylogenetics and Evolution 3: 221–229. https://doi.org/10.1006/mpev.1994.1024

Meixner J (1928) Aberrante Kalyptorhynchia (Turbellaria, Rhabdocoela) aus dem Sande der Kieler Bucht. Zoologischer Anzeiger 77: 229–253.

Meixner J (1938) 4. Turbellaria (Strudelwürmer). Die Tierwelt der Nord- und Ostsee 33: 1–146.

Noldt U (1985) *Typhlorhynchus syltensis* n. sp. (Schizorhynchia, Plathelminthes) and the Adelphotaxa-relationship of *Typhlorhynchus* and *Proschizorhynchus*. Microfauna Marina 2: 347–370.

Noldt U (1988) *Serratohynchus stellatus*, a new schizorhynchid species (Platyhelminthes) with sawblade-like proboscis hard structures. Forts Zoology 36: 385–390.

Noldt U (1989) Kalyptorhynchia (Platyhelminthes) from sublittoral coastal areas near the island of Sylt (North Sea). I. Schizorhynchia. Microfauna Marina 5: 7–85.

Oya Y, Tsuyuki A, Kajihara H (2022) Descriptions of two new species of Armatoplana (Polycladida, Stylochoplanidae) from the coasts of Japan, with their phylogenetic positions in Leptoplanoidea. Zootaxa 5178(5): 433–452. https://doi.org/10.11646/zootaxa.5178.5.2

Rambaut A, Drummond AJ, Xie D, Baele G, Suchard MA (2018) Posterior summarisation in Bayesian phylogenetics using Tracer 1.7. Systematic Biology 67(5): 901–904. https://doi.org/10.1093/sysbio/syy032

Ronquist F, Teslenko M, van der Mark P, Ayres DL, Darling A, Höhna S, Larget B, Liu L, Suchard MA, Huelsenbeck JP (2012) MRBAYES 3.2: Efficient Bayesian phylogenetic inference and model selection across a large model space. Systematic Biology 61: 539–542. https://doi.org/10.1093/sysbio/sys029

Rundell RJ, Leander B (2014) Molecular examination of kalyptorhynch diversity (Platyhelminthes: Rhabdocoela), including descriptions of five meiofaunal species from the north-eastern Pacific Ocean. Journal of the Marine Biological Association of the United Kingdom 94: 499–514. https://doi.org/10.1017/S0025315413001471

Schilke K (1969) Zwei neuartige Konstruktionstypen des Rüsselappartes der Kalyptorhynchia (Turbellaria). Zeitschrift fü Morphologie der Tiere 65: 287–314. https://doi.org/10.1007/BF00765290

Schilke K (1970) Kalyptorhynchia (Turbellaria) aus dem Eulitoral der deustschen Nordseeküste. Helgoländer Meeresuntersuchungen 21: 143–265. https://doi.org/10.1007/BF01630522

Schwendinger PJ, Giribet G (2005) The systematics of the southeast Asian genus *Fangensis* Rambla (Opiliones, Cyphophthalmi, Stylocellidae). Invertebrate Systematics 19: 297–323. https://doi.org/10.1071/IS05023

Smith III JP, Litvaitis MK, Gobert S, Uyeno T, Artois T (2015) Evolution and functional morphology of the proboscis in Kalyptorhynchia (Platyhelminthes). Integrative and Comparative Biology 55: 1–12. https://doi.org/10.1093/icb/icv056

Smith III JP, Van Steenkiste N, Artois T (2020) Platyhelminthes. In: Schmidt-Rhaesa A (Ed.) Guide to the Identification of Marine Meiofauna. Verlag Dr. Friedrich Pfeil, München, 54–103.

Stamatakis A (2006) RAxML-VI-HPC: maximum likelihood-based phylogenetic analyses with thousands of taxa and mixed models. Bioinformatics 22: 2688–2690. https://doi.org/10.1093/bioinformatics/btl446

Takeda N, Kajihara H (2018) A new genus and five new species of Kalyptorhynchia (Platyhelminthes, Rhabdocoela) discovered in northern Japan. Species Diversity 23: 1–11. https://doi.org/10.12782/specdiv.23.1

Tanabe AS (2007) Kakusan: a computer program to automate the selection of a nucleotide substitution model and the configuration of a mixed model on multilocus data. Molecular Ecology Notes 7: 962–964. https://doi.org/10.1111/j.1471-8286.2007.01807.x

Tessens B, Janssen T, Artois T (2014) Molecular phylogeny of Kalyptorhynchia (Rhabdocoela, Platyhelminthes) inferred from ribosomal sequence data. Zoologica Scripta 43: 519–530. https://doi.org/10.1111/zsc.12066

Tsuyuki A, Oya Y, Kajihara H (2022) Reversible shifts between interstitial and epibenthic habitats in evolutionary history: Molecular phylogeny of the marine flatworm family Boniniidae (Platyhelminthes, Polycladida, Cotylea) with descriptions of two new species. PLOS ONE 17(11): e0276847. https://doi.org/10.1371/journal.pone.0276847

Tsuyuki A, Oya Y, Kajihara H (2023) A new species of slender flatworm in the genus *Eucestoplana* and a record of *E.* cf. *cuneata* (Platyhelminthes, Polycladida) from the Okinawa Islands, Japan, with an inference of their phylogenetic positions within Cestoplanidae. Zoosystematics and Evolution 99(2): 363–373. https://doi.org/10.3897/zse.99.102604

Tsuyuki A, Reyes J, Oya Y, Wakeman KC, Leander BS, Van Steenkiste NWL (2024) Marine microturbellarians from Japan, with descriptions of two new species of Reinhardorhynchus (Platyhelminthes, Rhabdocoela, Koinocystididae). Zoosystematics and Evolution 100(3): 877–895. https://doi.org/10.3897/zse.100.120244

Van Steenkiste NWL, Wakeman KC, Söderström B, Leander BS (2023) Patterns of host-parasite associations between marine meiofaunal flatworms (Platyhelminthes) and rhytidocystids (Apicomplexa). Scientific Reports 13: 21050. https://doi.org/10.1038/s41598-023-48233-y

Velásquez-Rodriguez K, Reyes J, Steenkiste NV, Severino R, Brusa F (2023) First records of marine microturbellarians (Platyhelminthes, Rhabdocoela, Fecampiida, and Prolecithophora) from Peru, with the description of a new species. Zootaxa 441: 501–523. https://doi.org/10.11646/zootaxa.5258.5.1

Whiting MF, Carpenter JM, Wheeler QD, Wheeler WC (1997) The Strepsiptera problem: phylogeny of the holometabolous insect orders inferred from 18S and 28S ribosomal DNA sequences and morphology. Systematic Biology 46: 1–68. https://doi.org/10.1093/sysbio/46.1.1

WoRMS (2024) Schizorhynchia. https://www.marinespecies.org/aphia.php?p=taxdetails&id=155663